WAVES 2015

The 12th International Conference on Mathematical and Numerical Aspects of Wave Propagation

July 20-24, 2015

held at:

Karlsruhe Institute of Technology
Germany

Book of Abstracts

The 12th International Conference on Mathematical and Numerical Aspects of Wave Propagation

Local Organizing Committee

Tilo Arens
Willy Dörfler
Marlis Hochbruck
Andreas Kirsch
Wolfgang Reichel

Scientific Committee

Mark Ainsworth
Xavier Antoine
Alex Barnett
Héléne Barucq
Eliane Bécache
Abderrahmane Bendali
Marc Bonnet
Anne-Sophie Bonnet-Bendhia
Liliana Borcea
Oscar Bruno
Anna-Lisa Buffa
Fioralba Cakoni
Simon Neil Chandler-Wilde
Francis Collino
Martin Costabel
Laurent Demanet
Julien Diaz
Rabia Djellouli
Josselin Garnier
Dan Givoli
Nabil Gmati
Houssem Haddar
Thomas Hagstrom
Laurence Halpern
Christophe Hazard
Jan Hesthaven
Ralf Hiptmair
Patrick Joly
Manfred Kaltenbacher
Andreas Kirsch
Olivier Lafitte
Armin Lechleiter
Eric Lunéville
Paul Martin
Peter Monk
Jean-Claude Nédélec
David Peter Nicholls
Nilima Nigam
Naoshi Nishimura
George C. Papanicolaou
Joseph E. Pasciak
Roland Potthast
Jeffrey Rauch
Jerónimo Rodríguez García
Olof Runborg
Dominik Schoetzau
Geza Seriani
Chrysoula Tsogka
Ricardo Weder

Conference Homepage
`http://waves2015.math.kit.edu`

Editor Book of Abstracts: Tilo Arens

Preface

The 12th International Conference on Mathematical and Numerical Aspects of Wave Propagation is organized at Karlsruhe Institute of Technology, jointly by members of the Institute of Analysis and the Institute of Applied and Numerical Mathematics. The organizers gratefully acknowledge support from a variety of institutions, most importantly from the

Deutsche Forschungsgemeinschaft (DFG).

We are also grateful for support from

INRIA
the KIT-Department of Mathematics
CRC 1173 *Wave phenomena: analysis and numerics* at KIT (DFG funded)

This book contains summaries of the contributions that were selected for presentation at the conference. We start with the plenary lectures, followed by minisymposia and finally other contributed talks. These presentations span the whole width of the field of analytical or numerical studies of wave phenomena. Subjects include direct and inverse scattering problems for acoustic, electro-magnetic or elastic waves, waves in waveguides, water waves, waves in non-linear media, finite and boundary element methods, absorbing boundary conditions and both time-harmonic and transient wave propagation problems.

The organizational committee would like to express their thanks to all those that have helped behind the scenes to make this conference a successful event. Special thanks go to Sonja Becker and Marion Ewald for their administrative support. Proofreading of this book was carried out by Elena Dontcheva and Thomas Rösch.

Karlsruhe, June 2015

Tilo Arens
Willy Dörfler
Marlis Hochbruck
Andreas Kirsch
Wolfgang Reichel

Contents

Plenary Lectures

Discontinuous Petrov Galerkin (DPG) Method with Optimal Test Functions for Wave Propagation Problem. An Overview

Leszek Demkowicz[1,*], Jay Gopalakrishnan[2]
[1]ICES, University of Texas at Austin, USA
[2]Fariborz Maseeh Department of Mathematics & Statistics, Portland State University, USA
*Email: leszek@ices.utexas.edu

Abstract

We review the main facts about the DPG method: possibility of different variational formulations, the paradigm of broken test spaces, different interpretations of the abstract DPG method, stability and dispersion analysis, and preliminary results on iterative solvers. Contrary to standard Galerkin, the DPG method does not suffer from any preasymptotic stability problems, and enables adaptivity starting with coarse meshes that do not satisfy the Nyquist criterion. The DPG method automatically reproduces stability of the continuous problem and enables solution of problems that may not be stable when discretized with standard Galerkin, e.g. metamaterials or cloaking problems. The main points of the discussion will be illustrated with time-harmonic acoustics, Maxwell and elastodynamics equations.

Keywords: acoustics, electromagnetics, elastodynamics, DPG method
Acknowledgment: The work has been supported with AFOSR grant FA9550-12-1-0484.

1 Introduction. Different variational formulations

It may not be widely known that a boundary-value (BV) problem can be formulated using different variational formulations [1]. The formulations differ in functional setting and imply convergence in different norms when discretized with finite elements. Consider, e.g. the "mathematician's version" of time-harmonic acoustics equations with the impedance boundary condition (BC):

$$\left\{\begin{array}{rrll} i\omega p & +\mathrm{div} u & = f & \text{in } \Omega \\ i\omega u & +\boldsymbol{\nabla} p & = g & \text{in } \Omega \\ & p & = u\cdot n & \text{on } \Gamma \end{array}\right. \tag{1}$$

Here $\Omega \subset \mathbb{R}^N$ is a Lipschitz domain with boundary Γ, p, u denote pressure and velocity, f, g are data, ω stands for the angular frequency, and i is the imaginary unit. Assuming $(f,g) \in L^2(\Omega)\times(L^2(\Omega))^N$, we can rewrite the equations in the operator language,

$$\left\{\begin{array}{l} p\in H^1(\Omega),\ u\in H(\mathrm{div},\Omega),\ p = u\cdot n \text{ on } \Gamma \\ A(p,u) = (f,g) \end{array}\right. \tag{2}$$

where $A(p,u) = (i\omega p + \mathrm{div} u, i\omega u + \boldsymbol{\nabla} p)$.

The strong formulation (2) is equivalent to what we might call the *trivial* variational formulation,

$$\left\{\begin{array}{lll} p\in H^1(\Omega),\ u\in H(\mathrm{div},\Omega),\ p = u\cdot n \text{ on } \Gamma & & \\ i\omega(p,q) + (\mathrm{div} u, q) & = (f,q) & q\in L^2(\Omega) \\ i\omega(u,v) + (\boldsymbol{\nabla} p, v) & = (g,v) & v\in (L^2(\Omega))^N \end{array}\right. \tag{3}$$

obtained by multiplying equations (1) with test functions q, v and integrating over Ω. As usual, $(\cdot,\cdot)$ denotes the $L^2(\Omega)$ inner product with the corresponding L^2-norm denoted by $\|\cdot\|$. Again, we can write the equation in a more compact form as:

$$\left\{\begin{array}{l} p\in H^1(\Omega),\ u\in H(\mathrm{div},\Omega),\ p = u\cdot n \text{ on } \Gamma \\ (A(p,u),(q,v)) = (f,q) + (g,v) \\ \qquad\qquad q\in L^2(\Omega), v\in (L^2(\Omega))^N \end{array}\right. \tag{4}$$

Each of the the two equations can now be *relaxed*, i.e. integrated by parts with the BC built in. If we relax both equations, we obtain the *ultraweak* variational formulation,

$$\left\{\begin{array}{l} p\in L^2(\Omega), v\in (L^2(\Omega))^N \\ -((p,u), A(q,v)) = (f,q) + (g,v) \\ q\in H^1(\Omega),\ v\in H(\mathrm{div},\Omega),\ q = -v\cdot n \text{ on } \Gamma \end{array}\right. \tag{5}$$

Note that the (formal) adjoint $A^* = -A$, and that the sign in the impedance BC for the test functions has changed.

If we relax only one of the equations, we obtain two *mixed* formulations. For instance, relaxing the conservation of mass equation and keeping the momentum equations in the strong

form, we get,

$$\left\{\begin{array}{l} p\in H^1(\Omega),\ u\in (L^2(\Omega))^N \\ i\omega(p,q)-(u,\boldsymbol{\nabla} q)+\langle p,q\rangle_\Gamma \quad =(f,q) \\ i\omega(u,v)+(\boldsymbol{\nabla} p,v) \qquad\qquad\quad =(g,v) \\ \qquad\qquad q\in H^1(\Omega),\ v\in (L^2(\Omega))^N \end{array}\right. \tag{6}$$

Notice that the impedance BC has been built into the first formulation by replacing normal velocity $u\cdot n$ with pressure p. Brackets denote duality pairing between $H^{-1/2}(\Gamma)$ and $H^{1/2}(\Gamma)$ that, due to the regularity of traces of p,q on Γ, reduces to the L^2-product on Γ.

If we use the second equation to express u in terms of $\boldsymbol{\nabla} p$, substitute it into the first equation, and multiply it side-wise by $i\omega$, we obtain the classical variational formulation for the Helmholtz equation,

$$\left\{\begin{array}{l} u\in H^1(\Omega) \\ (\boldsymbol{\nabla} p,\boldsymbol{\nabla} q)+i\omega\langle p,q\rangle_\Gamma=(i\omega f+g,v) \\ \qquad\qquad\qquad\qquad v\in H^1(\Omega) \end{array}\right. \tag{7}$$

The second mixed formulation is obtained by relaxing the momentum equations,

$$\left\{\begin{array}{l} p\in L^2(\Omega),\ u\in V \\ i\omega(p,q)+(\mathrm{div} u,q) \qquad\qquad\quad =(f,q) \\ i\omega(u,v)-(p,\mathrm{div} v)+\langle u\cdot n,v\cdot n\rangle_\Gamma \quad =(g,v) \\ \qquad\qquad\qquad\qquad q\in L^2(\Omega),\ v\in V \end{array}\right. \tag{8}$$

where the energy space for the velocity has now to incorporate an extra regularity assumption resulting from building in the impedance BC,

$$V:=\{v\in H(\mathrm{div},\Omega)\ :\ v\cdot n\in H^{1/2}(\Gamma)\} \tag{9}$$

As before, we can eliminate now the pressure to obtain a variational formulation in terms of the velocity only,

$$\left\{\begin{array}{l} u\in V \\ (\mathrm{div} u,\mathrm{div} v)-\omega^2(u,v)+i\omega\langle u\cdot n,v\cdot n\rangle_\Gamma \\ \qquad\qquad\qquad =(f+i\omega g,v),\quad v\in V \end{array}\right. \tag{10}$$

The mixed formulations and their reduced counterparts use symmetric functional settings and can be discretized with the classical Galerkin method.

It can be proved [1] that all formulations are simultaneously well (ill) posed with related corresponding inf-sup constants[1]. A critical tool in proving it are the two versions of the Closed Range Theorem, for continuous and for closed operators. Similar results hold for the other two model problems: Maxwell equations and elastodynamics.

2 The paradigm of breaking test functions

Each of discussed variational formulations admits a corresponding variational formulation with *broken test spaces*. In a Finite Element (FE) "slang", we can say that we can "break the test functions". More precisely, we do two things: we eliminate the boundary condition for test functions (if present), and we replace the test spaces with their corresponding "broken" counterparts. The *trivial* formulation stays without any change, the L^2 space does not present any conforming requirements. In the remaining three formulations, and the two reduced formulations the price we pay for breaking test functions is the introduction of extra unknowns: (pressure) traces $\hat{p}\in H^{1/2}(\Gamma_h)$ and (velocity) traces[2] $\hat{u}\cdot n\in H^{-1/2}(\Gamma_h)$. The two trace spaces are defined on mesh skeleton $\Gamma_h:=\bigcup_{K\in\mathcal{T}_h}\partial K$ and can be viewed as traces of functions from $H^1(\Omega)$ and $H(\mathrm{div},\Omega)$ to the mesh skeleton [2] equipped with quotient (minimum energy extension) norms.

The formulations with broken test spaces corresponding to the classical and ultraweak formulations are as follows.
Classical formulation:

$$\left\{\begin{array}{l} u\in H^1(\Omega),\hat{u}\cdot n\in \tilde{H}_0^{-1/2}(\Gamma_h) \\ (\boldsymbol{\nabla} p,\boldsymbol{\nabla}_h q)+i\omega\langle p,q\rangle_\Gamma-\langle\hat{u}\cdot n,q\rangle_{\Gamma_h} \\ \qquad =(i\omega f+g,v),\quad v\in H^1(\Omega_h) \end{array}\right. \tag{11}$$

where

$$\begin{array}{rl} \tilde{H}^{1/2}(\Gamma_h) & :=\mathrm{tr}_{\Gamma_h} H_0^1(\Omega) \\ \tilde{H}^{-1/2}(\Gamma_h) & :=\mathrm{tr}_{\Gamma_h} H_0(\mathrm{div},\Omega) \end{array}$$

In other words, the additional unknowns vanish on domain boundary Γ.
Ultraweak formulation:

$$\left\{\begin{array}{l} p\in L^2(\Omega),\ u\in (L^2(\Omega))^N \\ \hat{p}\in H^{1/2}(\Gamma_h),\ \hat{u}\cdot n\in H^{-1/2}(\Gamma_h) \\ \hat{p}=\hat{u}\cdot n \text{ on } \Gamma \\ -(p,i\omega q+\mathrm{div}_h v)-(u,i\omega v+\boldsymbol{\nabla}_h q) \\ =(f,q)+(g,v)\quad q\in H^1(\Omega_h),\ v\in H(\mathrm{div},\Omega_h) \end{array}\right. \tag{12}$$

[1] They are of the same order.

[2] Also called "fluxes".

Above, $\boldsymbol{\nabla}_h, \mathrm{div}_h$ define element-wise defined operators, and sub-index h in $H^1(\Omega_h), H(\mathrm{div}, \Omega_h)$ indicates broken energy spaces.

The remaining formulations with broken test spaces are introduced in a similar way. We can show [2] that all formulations with broken test spaces are well posed with inf-sup constants of the same order as those corresponding to "unbroken" test spaces. In particular, the stability constants are mesh independent.

3 The ideal and practical DPG methods

The (ideal) DPG method can be viewed from three angles.

DPG is a Petrov-Galerkin scheme with optimal test functions. The test functions are computed by inverting the Riesz operator corresponding to the test inner product. More precisely, if $b(u,v)$, $u \in U, v \in V$ denotes the bilinear form corresponding to any of the discussed formulations, u denotes the (group) unknown, and v stands for the (group) test functions, the optimal test functions $v = v_{\delta u}$ corresponding to a trial (basis, shape) function $\delta u_h \in U_h \subset U$ solves the variational problem

$$\left\{ \begin{array}{l} v_{\delta u_h} \in V \\ (v_{\delta u_h}, \delta v)_V = b(\delta u, \delta v) \quad \delta v \in V \end{array} \right. \tag{13}$$

In the case of broken test spaces and *localizable test norm*,

$$v = \{v_K\}_{K \in \mathcal{T}_h} \quad \|v\|_V^2 := \sum_K \|v_K\|_{V(K)}^2 \tag{14}$$

with $\|v_K\|_{V(K)}$ being a norm of the local, element K test space $V(K)$, the inversion of the Riesz product in (13) is done *element-wise*. In other words, the computation of optimal test functions increases the local but not the global cost of the FE method. The test functions are termed to be *optimal* since, with such test functions, the discrete method automatically inherits stability properties of the continuous one.

DPG is a minimum residual method with the residual measured in the dual norm.

$$\begin{array}{rl} u_h & = \arg\min_{u_h \in U_h} \|b(u_h, \cdot) - l(\cdot)\|_{V'} \\ & = \arg\min_{u_h \in U_h} \|R_V^{-1}(b(u_h, \cdot) - l(\cdot))\|_V \end{array} \tag{15}$$

Above $l(\cdot)$ denotes the antilinear "load functional". Again the practical way to compute the dual norm is to use the fact that the Riesz operator R_V for the test space is an isomorphic isometry, and replace the dual norm in V' with the test norm in V at the expense of inverting R_V.

DPG is a mixed method where one solves simultaneously for the approximate solution $u_h \in U_h$ and the *error representation function* (Riesz representation of the residual),

$$\psi = R_V^{-1}(b(u_h, \cdot) - l(\cdot)) \tag{16}$$

$$\left\{ \begin{array}{lll} u_h \in U_h,\ \psi \in V & & \\ (\psi, v)_V - b(u_h, v) & = -l(v) & v \in V \\ b(\delta u_h, \psi) & = 0 & \delta u_h \in U_h \end{array} \right. \tag{17}$$

This is a weird mixed problem as one solves for the approximate solution u_h coming from the finite-dimensional approximate trial space, and for ψ coming from the broken but still infinite-dimensional test space.

The first two interpretations were proposed in [3], the third one in [4]. Each of the interpretations of DPG implies important properties of the method: DPG stiffness matrix is always Hermitian and positive definite (minimum residuals), DPG is a Ritz method and as such, contrary to standard Galerkin, does not suffer from any preasymptotic behavior (minimum residuals), DPG automatically guarantees stability for any well posed problem (optimal test functions), and DPG comes with an a-posteriori error estimation[3] ($\|\psi\|_V$ = residual) built in.

Inversion of the Riesz operator can be done only approximately. This is done by by replacing the test space V in all three interpretations above with an *enriched test space* $\tilde{V} \subset V$ with higher dimension than the trial space, $\mathrm{dim}\tilde{V} >> \mathrm{dim}U_h$. In practice we define $\tilde{V}$ by raising the order of approximation used to approximate u_h. If u_h is approximated using elements of order p, then the optimal test functions $v_{\delta u_h}$ and ψ, are approximated with polynomials of order[4] $r = p + \Delta p$. Typically $\Delta p = 2$.

The error caused by the approximate inversion of the Riesz operator can be estimated using appropriately defined Fortin operators [2,5].

[3] *Evaluation* really.

[4] We use the exact sequence elements to discretize $p, u, \hat{p}, \hat{u} \cdot n$. The order of approximation refers always to the H^1-conforming elements. This guarantees that best approximation errors corresponding to different components of the group unknown u, converge with the same rates.

4 Discussion

It should be clear by now that it is more appropriate to talk about a DPG methodology rather than a single DPG method. Not only we have different choices of a variational formulation but, given a particular functional setting, we *can choose* different test norms. With different test norms, we minimize the residual in different dual norms and obtain different convergence properties. For any of the discussed DPG methods, we can claim the following convergence result:

$$\|u-u_h\|_U \leq \underbrace{\frac{MC}{\gamma}}_{\text{stability constant}} \inf_{w_h \in U_h} \|u-w_h\|_U \tag{18}$$

where M, C are the continuity constants for bilinear form $b(u,v)$ and the Fortin operator mentioned above, and γ is the inf-sup constant. Remember that u represents here a group unknown, and the error comprises of errors corresponding to different components of u measured in different norms.

In context of problems with large frequency ω, two formulations stand out: strong (trivial) formulation with L^2 test norm leading to the First Order Least Squares (FOSL) method, and ultraweak formulation with test graph norm,

$$\|(q,v)\|_V^2 := \|A(q,v)\|^2 + \|(q,v)\|^2 \tag{19}$$

Both of these formulations are *robust* in ω, i.e. the corresponding stability constants *are independent* of ω. This is reflected in the spectral structure of the corresponding stiffness matrix. Fig. 1 presents spectrum for the stiffness matrix for the 1D version of the discussed model problem obtained after condensation of all internal degrees of freedom (d.o.f.). The number of interface d.o.f. for all DPG formulations is the same and it is roughly doubled compared with the standard Galerkin. As illustrated in Fig.1, the spectrum of the stiffness matrix for Galerkin method is complex. Being a minimum residual method, any DPG method delivers always a positive-definite Hermitian matrix with a real and positive spectrum. Except for a couple of outliers, spectra for the ultraweak DPG and least squares methods are the same whereas the spectrum for the primal DPG method is much more spread out. As expected, the Conjugate Gradient (CG) method converges with the same number of iterations which is essentially smaller than for the primal DPG method.

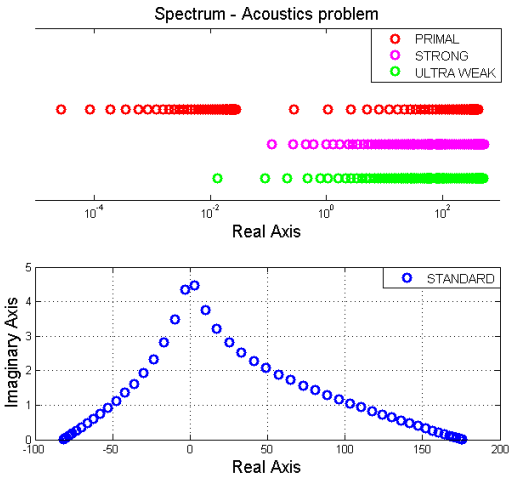

Figure 1: Spectrum of stiffness matrix corresponding to classical Galerkin, least squares, primal and ultraweak DPG methods.

Same spectral properties of the stiffness matrix do not imply that least squares and ultraweak DPG deliver the same quality results. The two methods deliver convergence in different norms. For the ultraweak formulation, the error in p, u is measured in L^2-error, for the strong formulation in the graph norm. The L^2-projection is pollution free [5] whereas the projection in the graph norm is not. In 1D, traces and fluxes are just numbers and the corresponding best approximation error (measured in any norm) is zero. Consequently, the 1D ultraweak DPG method is pollution free, whereas the least squares exhibit very diffusive behavior [6]. The different behavior of different methods for the discussed 1D model problem is illustrated in Fig. 2.

DPG enables automatic adaptivity starting with coarse meshes. We conclude the presentation with an example of an adaptive solution. With guaranteed stability, lack of pre-asymptotic behavior, and the a-posteriori error estimate built in, the DPG methodology provides a very natural framework for adaptive methods, including *hp*-adaptivity. With the DPG adaptive technology we aim at prob-

[5] Keeping number of elements per wavelength fixed guarantees the same L^2 error in percent of the L^2-norm.

lems for which the adaptivity matters: high frequency and coupled problems with localized solutions, and low and medium frequency problems with singular solutions. To illustrate the points we present an adaptive solution to a 2D Gaussian beam problem with 45 wavelengths in the domain. We use the ultraweak formulation starting with an initial 4×4 mesh of quadratic elements that clearly does not satisfy the Nyquist criterion. Fig. 3 presents three meshes selected from a series of 44 *hp*-adaptive meshes along with the corresponding solutions. We "grow" the solution with the mesh, with the final solution supported by a mesh refined only where it is needed. The presented *hp* meshes were obtained using a standard greedy method based on element contributions to the global residual and a simplified *hp* strategy: we proceed with h refinements until we reach an element size smaller than half-wavelength, and then switch to p-refinements.

Remark. The enriched space methodology guarantees the resolution of optimal test functions (residual) with a negligible error *provided* the element length is of the order of half-wavelength. With the use of the graph test norm (essential for optimal stability properties of ultraweak DPG), the condition is not satisfied for coarse meshes (large elements). We circumvent the problem by adjusting the frequency in graph test norm (19) to element size, i.e. we replace ω in (19) with

$$\min(\omega, \frac{6}{h}) \tag{20}$$

where h is the element size. As we resolve the wavelength, the test norm eventually converges to the optimal one. With a fixed test norm, the residual *must decrease monotonically* with refinements. Not surprisingly perhaps, the same behavior is observed in our case as well, as illustrated in Fig.4. Contrary to the residual, the L^2 error does not decrease monotonically.

5 More about the presentation.

We will illustrate the points made in this note with additional examples for Maxwell and elastodynamics problems including wave propagation in metamaterials and cloaking. We will also outline our current work on preconditioning [7]. Finally, we will flash a few examples showing application of the DPG technology to inverse problems.

References

[1] L. Demkowicz, Various Variational Formulations and Closed Range Theorem, *ICES Report* **15–03** .

[2] L. Demkowicz, C. Carstensen and J. Gopalakrishnan, The Paradigm of Broken Test Functions in DPG Discretizations of Elliptic Second–Order PDEs, *in preparation.*

[3] L. Demkowicz and J. Gopalakrishnan, A Class of Discontinuous Petrov-Galerkin Methods. Part II: Optimal Test Functions, *Numer. Meth. Part. D. E.*, **27**: 70-105, 2011, see also *ICES Report 9–16.*

[4] W. Dahmen, Ch. Huang, Ch Schwab, and G. Welper, Adaptive Petrov Galerkin Methods for first order transport equations, *SIAM J. Num. Anal.*, **50(5):** 2420-2445, 2012, see also Institut fuer Geometrie und Praktische Mathematik, *Technical Report 2011/321.*

[5] J. Gopalakrishnan and W. Qiu, An Analysis of the Practical DPG Method, *Math. Comp.*, **83(286):** 537–552, 2014.

[6] J. Gopalakrishnan, I. Muga and N. Olivares, Dispersive and Dissipative errors in the DPG Method with Scaled Norms for Helmholtz Equation, *Comput. Math. Appl.*, 2015, to appear.

[7] J. Gopalakrishnan and J. Schöberl, Degree and Wavenumber InDependence of Schwarz Preconditioner for the DPG Method, *in preparation.*

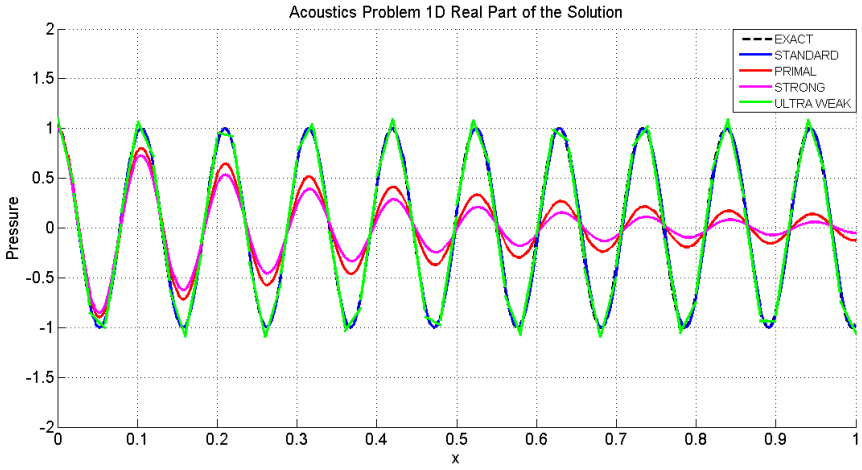

Figure 2: 1D acoustics problem. Real part of pressure obtained with standard Galerkin, least squares, primal and ultraweak DPG methods.

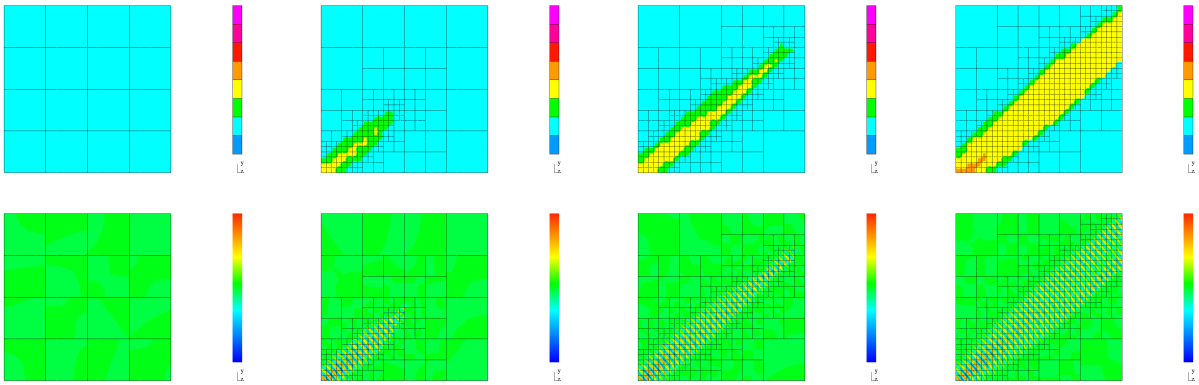

Figure 3: Gaussian beam problem, $\omega = 60\pi$. First, 11th, 21st and 31st *hp*-adaptive mesh and the corresponding numerical solution (imaginary part of pressure).

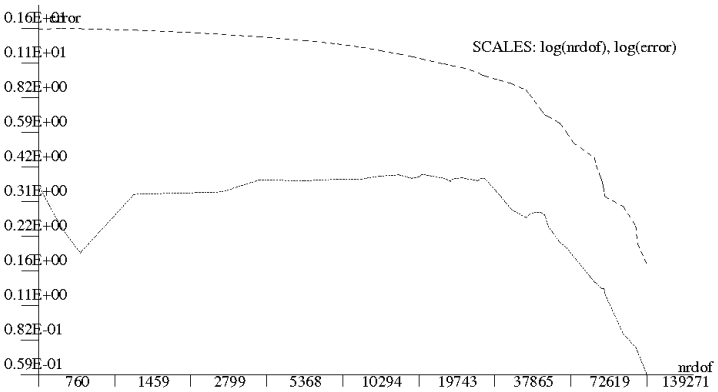

Figure 4: Gaussian beam problem. Convergence history for residual and L^2 error.

Hardy Space Infinite Elements

Thorsten Hohage[1,*]

[1]Institut für Numerische und Angewandte Mathematik, Universität Göttingen, Germany

*Email: hohage@math.uni-goettingen.de

Abstract

In this talk we review the solution of time-harmonic wave equations on unbounded domains using Hardy space infinite elements. These elements exhibit spectral order of convergence, they fit naturally into the finite element context and are easy to implement, and they can be used for the computation of resonances as they preserve the eigenvalue structure of the problem. The starting point is a reformulation of the radiation condition as a pole condition, which leads to a stable – often orthogonal – decomposition of the space of exterior solutions into a Hardy spaces of incoming solutions and a Hardy space of outgoing solution. This approach offers considerable flexibility, and in particular it allows to treat backpropagating modes, i.e. modes with different signs of group and phase velocity as they appear for example in elastic wave guides.

Keywords: transparent boundary conditions, spectral convergence, backpropagating modes

1 Introduction

In this note we consider the solution of time-harmonic wave equations in unbounded domains $\Omega \subset \mathbb{R}^d$. For a given elliptic differential operator L on Ω and a given trace operator B on $\partial\Omega$ we study the *scattering problem*

$$\begin{cases} Lu - \omega^2 u = f_1 & \text{in } \Omega, \\ Bu = f_2 & \text{on } \partial\Omega, \\ u \text{ outgoing} \end{cases} \tag{1}$$

for a given angular frequency $\omega > 0$ and given compactly supported right hand sides f_1 and f_2. The property "u outgoing", also referred to as radiation condition, physically means that energy is transported to infinity and ensures uniqueness. Mathematical definitions of radiation conditions will be discussed in the next section. We will have to assume that both Ω and L are sufficiently "well behaved" outside of some bounded region of interest.

Moreover, we will consider resonance problems

$$\begin{cases} Lu = \omega^2 u & \text{in } \Omega, \\ Bu = 0 & \text{on } \partial\Omega, \\ u \text{ outgoing} \end{cases} \tag{2}$$

where both the solution u and the frequency ω are unknown. As opposed to scattering problems the frequency ω is typically complex-valued, and the resonance function u may grow exponentially at infinity.

To compute the solution of scattering and resonance problems numerically by finite elements, Ω has to be truncated to some bounded domain of interest $\Omega_0 \subset \Omega$. On the artificial boundary $\Sigma := \partial\Omega_0 \setminus \partial\Omega$ of Ω_0 some boundary condition has to be imposed. Such boundary conditions are called *transparent* if they lead to solutions which are close to the solutions of (1) or (2) restricted to Ω_0.

In the following we will discuss the construction of transparent boundary conditions using Hardy Space Infinite Elemenets (HSIE). Competing methods include Perfectly Matched Layers (PML), boundary element methods, other infinite element methods, and local absorbing boundary conditions. Some advantages of HSIE have already been pointed out in the abstract. For a comparision with the PML method we refer to the discussion at the end of the note.

2 Pole condition as radiation condition

Let us first look at the case of a half-line $\Omega = (0, \infty)$. We will consider the Laplace transform

$$(\mathcal{L}u)(s) := \int_0^\infty e^{-sr} u(r)\,\mathrm{d}r, \qquad \Re s \geq 0$$

of the solution. For the Helmholtz equation

$$u''(x) + (n\omega)^2 u(x) = 0 \qquad x > 0$$

with some parameter $n \in \mathbb{C}$ (e.g. a refractive index) satisfying $\Re n > 0$, $\Im n \geq 0$ the general solution is of the form

$$u(x) = C_1 e^{in\omega x} + C_2 e^{-in\omega x}.$$

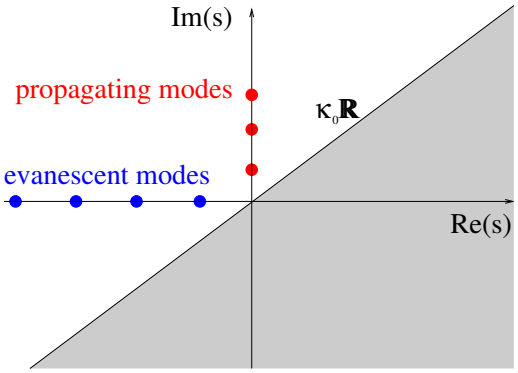

Figure 1: Illustration of the pole condition. The dots show poles of the Laplace transform of an outgoing solution. It is holomorphic in the shaded region and decays at infinity. Hence it belongs to the Hardy space $H^-(\kappa_0\mathbb{R})$.

The second term proportional to C_2 describes a wave moving from right to left if time dependence is given by $e^{-i\omega t}$. Moreover, this term grows exponentially at infinity if $\Im n > 0$. Therefore, u is considered outgoing if $C_2 = 0$. In this case

$$(\mathcal{L}u)(s) = \frac{C_1}{s - in\omega}.$$

More generally, we consider a function u on $(0,\infty)$ as outgoing if it is a linear superposition of exponentials $e^{i\kappa r}$ with $\Re\kappa > 0$ and $\Im\kappa \geq 0$. If the superposition weights are decaying sufficiently rapidly, $\mathcal{L}u$ is holomorphic on $\{s \in \mathbb{C} : \Re s > 0 \text{ or } \Im s < 0\}$ whereas it has poles or other types of singularities in the quadrant $\{s \in \mathbb{C} : \Re s \leq 0 \text{ and } \Im s \geq 0\}$. This is the *pole condition* as first suggested by Frank Schmidt [10]. Again assuming sufficient decay, the restriction of u to a diagonal line $\kappa_0\mathbb{C}$ with $\Re\kappa_0, \Im\kappa_0 > 0$ belongs to the Hardy space $H^-(\kappa_0\mathbb{R})$ defined below.

Definition 1 (Hardy spaces on half spaces) *Let $\kappa_0\mathbb{C}$ with $\Re\kappa_0, \Im\kappa_0 > 0$. Then $H^\pm(\kappa_0\mathbb{R})$ is the set of all functions $f \in L^2(\kappa_0\mathbb{R})$ for which there exists a holomorphic function $\tilde{f}$ on $\{\kappa_0 s : s \in \mathbb{C}, \pm\Im s < 0\}$ and*

$$\sup_{t<0} \int_{-\infty}^{\infty} |\tilde{f}((\sigma+it)/\kappa_0)|^2 \,\mathrm{d}\sigma < \infty,$$
$$\lim_{t\nearrow 0} \int_{-\infty}^{\infty} |\tilde{f}((\sigma+it)/\kappa_0) - f(\sigma/\kappa_0)|^2 \,\mathrm{d}\sigma = 0.$$

It is well-known that $H^\pm(\kappa_0\mathbb{R})$ is a Hilbert space equipped with the L^2 inner product and $L^2(\kappa_0\mathbb{R}) = H^+(\kappa_0\mathbb{R}) \oplus H^-(\kappa_0\mathbb{R})$. We will enforce the radiation condition

$$\mathcal{L}u \in H^-(\kappa_0\mathbb{R})$$

by a Galerkin ansatz. κ_0 will play the role of a tuning parameter of the method.

For higher dimensional problems we connect each point of the artificial boundary Σ by a ray to infinity, and require as radiation condition that the Laplace transform of the solution along each of these rays belongs to $H^-(\kappa_0\mathbb{R})$. Usually this has to be accompanied by some type of uniformity assumption with respect to the points of Σ. The equivalence of this type of pole condition to the Sommerfeld radiation conditiion has been shown in [5], and the equivalence to the Upward Propagating Radiation Condition in half planes was addressed in [1].

3 Hardy space infinite elements

To apply HSIE we first have to transform a variational formulation of the differential equation to a variational formulation in the Hardy space. The basic identity for this purpose is

$$\begin{aligned} \int_0^\infty u(x)v(x)\,\mathrm{d}x &= q(\mathcal{L}u, \mathcal{L}v), \\ q(U,V) &:= \frac{-i}{2\pi}\int_{\kappa_0\mathbb{R}} U(s)V(-s)\,\mathrm{d}s \end{aligned} \tag{3}$$

for a suitable dense set of test functions v (see [3, Lemma A.1]). In higher dimensions integrals over the exterior domain are split using Fubini's theorem into integrals over the boundary Σ and integrals over the rays connecting Σ to infinity.

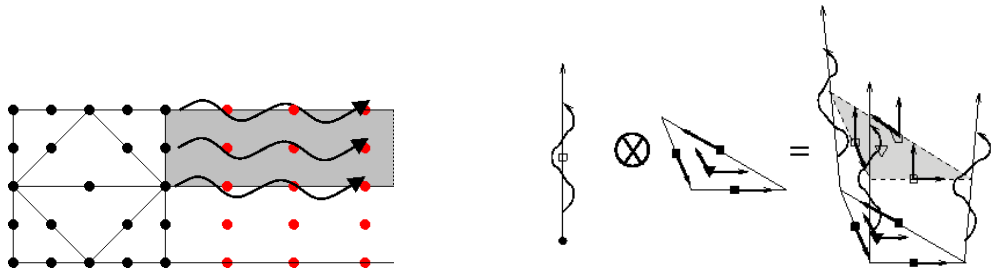

Figure 2: Two examples of Hardy space infinite elements: Left panel: H^1-conforming HSIE for waveguide geometry. Right panel: Tensor product construction of an $H(\mathrm{curl})$-conforming HSIE in a spherical geometry.

For coupling the exterior domain to the interior domain it is convenient to have the boundary value $u_0 := u(0)$ as a degree of freedom. Recall that it can be recovered from $\mathcal{L}u$ be the limit identity $u_0 = \lim_{s\to\infty} s(\mathcal{L}u)(s)$. Moreover, we need the transformation of the derivative operator to the Laplace domain. For these purposes we introduce the operators $\mathcal{S}_\mathrm{m}, \mathcal{S}_\mathrm{s} : \mathbb{C} \times H^-(\kappa_0\mathbb{R}) \to H^-(\kappa_0\mathbb{R})$ by

$$\left(\mathcal{S}_\mathrm{m}\left(\begin{smallmatrix} u_0 \\ U \end{smallmatrix}\right)\right)(s) := \frac{u_0 + U(s)}{s - i\kappa_0},$$
$$\left(\mathcal{S}_\mathrm{s}\left(\begin{smallmatrix} u_0 \\ U \end{smallmatrix}\right)\right)(s) := \frac{u_0 i\kappa_0 + sU(s)}{s - i\kappa_0}.$$

It is easy to see that $\mathcal{L}u$ for smooth, bounded functions u belongs to the range of $\mathcal{S}_\mathrm{m}$ and that

$$\mathcal{L}(u') = \mathcal{S}_\mathrm{s}\mathcal{S}_\mathrm{m}^{-1}\mathcal{L}u. \tag{4}$$

Together with (3) this is the basic identity for transforming variational formulations of differential equations to the Hardy space. In one space dimension we choose $\mathbb{X} : \mathbb{C} \times H^-(\kappa_0\mathbb{R})$ as underlying Hilbert space. For example, if u satisfies the variational equation

$$\int_0^\infty u'(x)v'(x) - \omega^2 u(x)v(x)\,\mathrm{d}x = u(0)f$$

and the pole condition, it follows by (3) and (4) that $\left(\begin{smallmatrix} u_0 \\ U \end{smallmatrix}\right) := \mathcal{S}_\mathrm{m}^{-1}\mathcal{L}u$ satisfies the variational equation

$$q\left(\mathcal{S}_\mathrm{s}\left(\begin{smallmatrix} u_0 \\ U \end{smallmatrix}\right), \mathcal{S}_\mathrm{s}\left(\begin{smallmatrix} v_0 \\ V \end{smallmatrix}\right)\right) + \omega^2 q\left(\mathcal{S}_\mathrm{m}\left(\begin{smallmatrix} u_0 \\ U \end{smallmatrix}\right), \mathcal{S}_\mathrm{m}\left(\begin{smallmatrix} v_0 \\ V \end{smallmatrix}\right)\right) = u(0)f$$

for all $\left(\begin{smallmatrix} v_0 \\ v \end{smallmatrix}\right) \in \mathbb{X}$. By looking for a solution $\left(\begin{smallmatrix} u_0 \\ U \end{smallmatrix}\right)$ to this equation in $\mathbb{X}$, the radiation condition is automatically satisfied.

To construct a basis of $\mathbb{X}$, recall that the Möbius transform $M(z) := i\kappa_0\frac{z+1}{z-1}$ maps $\mathbb{S}^1\backslash\{1\}$ to $\kappa_0\mathbb{R}$, and that $\mathcal{M} : H^-(\kappa_0\mathbb{R}) \to H^+(\mathbb{S}^1)$,

$$(\mathcal{M}U)(z) := \frac{\sqrt{-2i\kappa_0}}{z-1}U(M(z))$$

is unitary. Here $H^+(\mathbb{S}^1)$ denotes the Hardy space of all L^2-boundary values of holomorphic functions on the complex unit disk equipped with the L^2-norm. It has the natural orthogonal basis z^m, $m = 0, 1, 2, \ldots,$. Therefore,

$$\varphi_m := \mathcal{M}^{-1}z^m$$

is an orthogonal basis of $H^-(\kappa_0\mathbb{R})$. We have

$$q(\varphi_m, \varphi_n) = 2\delta_{n,m},$$

and with respect to this basis the operators $\mathcal{S}_\mathrm{m}$ and $\mathcal{S}_\mathrm{s}$ are represented by bidiagonal matrices. As finite dimensional subspace we will choose $\mathrm{span}\{\varphi_0, \ldots, \varphi_N\} \subset H^-(\kappa_0\mathbb{R})$. Since for solutions u to wave equations $\mathcal{M}\mathcal{L}u$ is typically infinitely smooth, these subspaces have the superalgebraic approximation properties of spaces of trigonometric polynomials.

In higher space dimensions HSIE are tensor products of finite elements on the coupling boundary Σ and the one-dimensional infinite elements sketched above. Two examples are illustrated in Figure 2. The local element matrices are typically sums of Kronecker products of local element matrices on the coupling boundary and explicitely given matrices for the infinite direction. Thus they are easy to implement in a finite element package, in which new (in)finite elements can be added.

A contruction of HSIE for the Helmholtz equation on the complement of a bounded domain in $\mathbb{R}^d$ together with a partial convergence

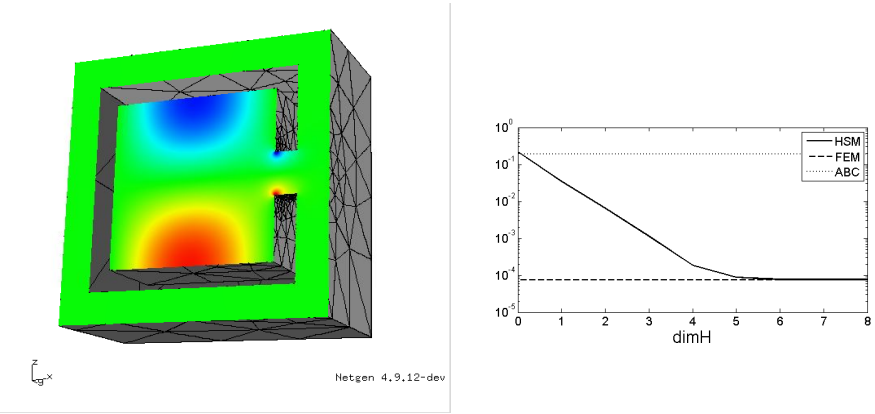

Figure 3: Computation of a resonance for the time-harmonic Maxwell equation. Left panel: First cartesian component of the computed resonance function. Right panel: Convergence as the number of degrees of freedom in the Hardy space tends to infinity. (courtesy of L. Nannen)

analysis is described in [3]. A full convergence analysis of HSIE for wave-guide geometries has been derived in [4]. An exact sequence of HSIE including $H(\mathrm{curl})$ and $H(\mathrm{div})$-conforming elements and applications to Maxwell's equations are described in [8], see also Figure 3.

4 pole condition revisited: backpropagating modes

The standard pole condition as well as the PML method select modes of positive phase velocity. However, physically outgoing modes are characterized by a positive group velocity $\frac{\partial \kappa}{\partial \omega}$ rather than a positive phase velocity κ/ω. This does not pose a problem as long as the signs of phase and group velocities coincide, which is the case for the Helmholtz equation and Maxwell's equations. However, for many other wave equation, for example the linearized elasticity equations in a strip, modes with different signs of phase and group velocity, so-called backpropagating modes exist. In this case both the standard HSIE and the PML method produce stable, but wrong solutions.

As a simple example for backpropagating modes we consider the following fourth order ordinary differation equation:

$$\left(\left(-\partial_x^2 - I\right)^2 + I\right) u(x) = \omega^2 u(x), \quad x > 0 \quad (5)$$

A function of the form $u(x) = e^{ik(\omega)x}$ solves (5) if and only if $k(\omega)$ satisfies the *dispersion relation*

$$(\kappa^2 - 1)^2 + 1 = \omega^2,$$

i.e.

$$\kappa = \pm\sqrt{1 \pm \sqrt{\omega^2 - 1}}. \quad (6)$$

These four solution curves are illustrated in Figure 4 showing that (5) has propagating modes with positive group and negative phase velocity if $\zeta \in (1, \sqrt{2})$. The difficulty is that the set of wavenumbers of outgoing solutions (marked red) cannot be separated from the set of wavenumbers of incoming solution (marked blue) by a straight line.

As a way out the use of Hardy space $H^-(\Gamma)$ with a curved domain Γ^- was suggested in [7]. The curved boundary Γ is chosen to separate the incoming from the outgoing wave numbers. A main challenge was the construction of a stable basis of such curved Hardy spaces. For given complex parameters κ_0 and κ_1 consider the functions

$$\Psi_n(s) := \frac{i\kappa_0 + i\kappa_1}{s - i\kappa_1} \left(\frac{s + i\kappa_0}{s - i\kappa_0}\right)^{\lfloor (n+1)/2 \rfloor} \left(\frac{s + i\kappa_1}{s - i\kappa_1}\right)^{\lfloor n/2 \rfloor}$$

for $n \in \mathbb{N}_0$ where $\lfloor x \rfloor := \max\{m \in \mathbb{Z} : m \le x\}$. Γ has to be chosen as a certain smooth algebraic curve defined in terms of κ_0 and κ_1. The geometric properties of this curve, and in particular its intersection points with the real and imaginary axis can be characterized explicitely. As a

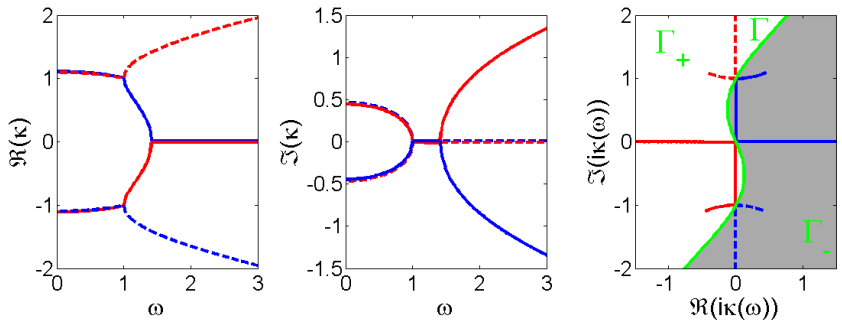

Figure 4: The first two panels show the real and imaginary parts of the dispersion curves (6) of the model problem (5). Modes with positive group velocity $\frac{\partial \kappa}{\partial \omega}$ are drawn in red and modes with negative group velocity in blue. The right panel shows a separating curve Γ and the domain Γ^- of the corresponding Hardy space.

main result it was shown in [7] that these functions form a Riesz basis of $H^-(\Gamma)$, and that the condition number is small for reasonable choices of the parameters κ_0 and κ_1. Based on this result exponential convergence of curved HSIE for the model equation (5) could be shown.

In [2] curved HSIE have been successfully applied to an elastic wave guide (see Figure 5). However, so far no complete convergence analysis is available for this case.

5 Discussion and conclusions

Hardy space infinite elements are a flexible tool for constructing transparent boundary conditions for solving time harmonic wave equations and computing resonances. A close relation of the standard pole condition and hence standard HSIE to the PML method has been shown in [6]. As opposed to PML, HSIE do not boil down to solving some modified PDE in the exterior domain and hence they cannot be implemented within a blackbox finite element code. However, if new finite elements can be added to a finite element code, the implementation of HSIE is not difficult. Advantages of HSIE are the spectral order of convergence and the fact that only the parameter κ_0 (corresponding to choice of the PML path in the complex plane) and the polynomial degree in the Hardy space have to be chosen whereas for PML the width of the PML layer, a mesh in the PML layer, and the order of the finite elements must be selected. For some practical advice on the choice of κ_0 we refer to [8]. Some numerical comparisons of PML and HSIE can be found in [9].

For wave equations with backpropagating modes for which the wave numbers of outgoing and incoming modes cannot be separated by a straight line, both PML and standard HSIE fail. However, in certain relevant cases including elastic wave guides incoming and outgoing wave numbers can still be separated by a suitable curved line. Such equations can be solved in a stable and spectrally accurate manner by HSIE based on curved Hardy spaces.

References

[1] T. Arens and T. Hohage. On radiation conditions for rough surface scattering problems. *IMA J. Applied Math.*, 70:839–847, 2005.

[2] M. Halla and L. Nannen. Hardy space infinite elements for time-harmonic two-dimensional elastic waveguide problems. Technical report, TU Vienna, 2014.

[3] T. Hohage and L. Nannen. Hardy space infinite elements for scattering and resonance problems. *SIAM J. Numer. Anal.*, 47:972–996, 2009.

[4] T. Hohage and L. Nannen. Convergence of infinite element methods for scalar waveguide problems. *BIT Numer. Math.*, 55(1):215–254, 2015.

[5] T. Hohage, F. Schmidt, and L. Zschiedrich. Solving time-harmonic scattering problems based on the pole condition. I: Theory. *SIAM J. Math. Anal.*, 35:183–210, 2003.

[6] T. Hohage, F. Schmidt, and L. Zschiedrich. Solving time-harmonic scattering problems

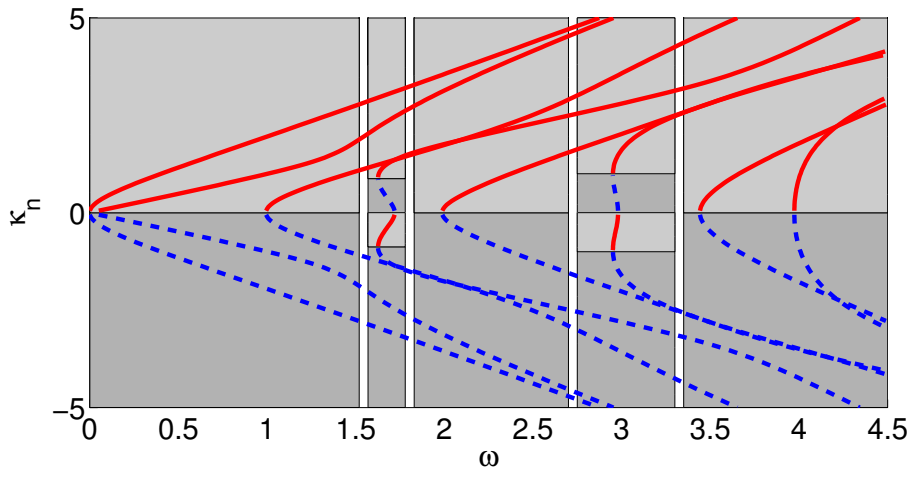

Figure 5: The first eight dispersion curves for an elastic wave guide. Positive group velocity is indicated by red solid lines, negative group velocity by dashed blue lines. In the first, third, and fifth frequency interval standard HSIE can be used whereas in the second and forth frequency interval HSIE based on a curved domain as shown in Fig. 4 have to be used to properly treat backpropagating modes. (courtesy of M. Halla)

based on the pole condition. II: Convergence of the PML method. *SIAM J. Math. Anal.*, 35:547–560, 2003.

[7] T. H. Martin Halla and L. Nannen. Hardy space infinite elements for time harmonic wave equations with phase and group velocities of different signs. *Numerische Mathematik*, to appear.

[8] L. Nannen, T. Hohage, A. Schädle, and J. Schöberl. Exact sequences of high order Hardy space inifinite elements for exterior Maxwell problems. *SIAM J. Sci. Comput.*, 35(2):A1024–A1048, A1024–A1048 2013.

[9] L. Nannen and A. Schädle. Hardy space infinite elements for Helmholtz-type problems with unbounded inhomogeneities. *Wave Motion*, 48(2):116 – 129, 2011.

[10] F. Schmidt and P. Deuflhard. Discrete transparent boundary conditions for the numerical solution of Fresnel's equation. *Computers Math. Appl.*, 29:53–76, 1995.

Can one hear the heat of a body?

Peter Kuchment[1,*]

[1]Department of Mathematics, Texas A&M university, USA

[*]Email: kuchment@math.tamu.edu

Abstract

Medical / industrial / geophysical imaging has been for decades an amazing area of applications of mathematics, providing a bonanza of beautiful and hard problems with real world applications. One can find almost any area of math being involved there. In this talk, I will survey a recent trend of designing the so called coupled physics (or hybrid, or multi-wave) imaging methods and mathematical problems arising there. No prior background in imaging is assumed.

Keywords: tomography, coupled-physics, hybrid

The number of tomographic techniques in use and being developed is very large, one can mention for instance X-ray CT, Ultrasound (UT), Emission tomography (SPECT, PET), Magnetic resonance imaging (MRI), Optical tomography (OT), Electrical impedance tomography (EIT), and quite a few others. Why do we need that many? One obvious reason is that they "see" different physical parameters: tissue density, electrical conductivity, optical absorption, blood oxygenation, etc. Clearly, cost and safety also differ. However, here we are interested mostly in the following two parameters: tissue contrast and image resolution. For instance, some tumors have electrical conductivity and optical absorption drastically higher than the surrounding healthy tissues. Thus, electrical impedance or optical tomography seem to be highly appropriate. Unfortunately, both have dismal resolution. On the other hand, for the same types of tumors ultrasound might offer dismal contrast, but sub-millimeter resolution. This conflict between contrast and resolution is rather common. So, what can one do? The idea is to somehow combine, say, optical irradiation with the ultrasound one, to get the best of both. This leads to the so called **hybrid** methods. The definition of such a technique is too broad, and we will discuss what is more appropriately called **coupled physics** methods.

Let us recall that every tomographic technique contains the following three main steps:

1. irradiating the non-transparent object with some penetrating waves (e.g., acoustic or electromagnetic) or particles, to trigger a response;
2. collecting the response data and processing them mathematically;
3. producing a picture, **tomogram**.

Combining (hybridising) can happen at any of these steps. For instance, one can do this at the 3rd step, correctly overlapping (**registering**) the two independent pictures. This is a very well developed technique, which we will not discussed (it does not improve the contrast or resolution of each individual tomogram).

Combination at the 2nd step is also rather common: feeding the data of two scans into a joint algorithm. For instance, X-ray scan data is needed for the good reconstruction in SPECT.

The coupled-physics methods, on the other hand, are based on the physical interaction (transfer energy) between the two irradiations. In other words, here one wave either physically triggers, or modifies the other one.

Among such techniques, the most developed is Thermo / Photo / Opto-acoustic tomography (TAT, PAT), which leads to beautiful and challenging mathematics. A variety of other coupled physics techniques are being developed, e.g. Ultrasound modulated optical tomography (UOT, UMOT), Magnetic resonance elastography (MRE), Magnetic resonance electrical impedance tomography (MREIT), Current density imaging (CDI).

An interesting observation is that in all these cases, hybridisation stabilizes (improves resolution) formerly unstable (low resolution) techniques, like EIT or OT. Surprisingly, a simple microlocal explanation of this effect exists.

One can find a more detailed survey and references in [1].

References

[1] P. Kuchment, *The Radon Transform and Medical Imaging*, SIAM 2014.

Acoustic Invisibility and Causality

Andrew N. Norris[1,*], **Alexey S. Titovich**[1]
[1]Department of Mechanical and Aerospace Engineering, Piscataway, USA
*Email: norris@rutgers.edu

Abstract

Recent progress on acoustic cloaking and scattering reduction has focused on design of metamaterials without consideration of the consequences in the widest broadband sense. We start from a top down look at a measure of the scattering over all frequencies, the integrated extinction (IE). New properties are derived, including the recognition that broadband cloaking places restraints on the material parameters, specifically, the scatterer must radiate a wavefront in the forward direction that precedes the incident wavefront. This is a uniquely acoustic requirement, there is no electromagnetic counterpart to this *non-causal* (but certainly physical!) condition. Examples of scatterers satisfying the *neutral acoustic inclusion* condition are described, and are related to broadband cloaking. Time permitting, new results in *active cloaking* will be described.

Keywords: Acoustics, invisibility, causality

1 Introduction

The *integrated extinction*, (IE), an integral of the scattering cross-section over all wavelengths [1], is a natural metric for measuring reduction in scattering using physical mechanisms [2, 3]. The IE is proportional to a linear combination of the monopole and dipole amplitudes if the scattering is *causal* [4], that is, the scattered wavefront in the forward direction arrives after an equivalent plane wavefront in the background medium. Causal scattering is the default for electromagnetics, but there is no such limitation in acoustics. Many scattering situations of interest in acoustics are non-causal, such as metal objects in water or air, for which the IE expression of [4] does not apply.

Our first objective is an expression for the acoustic integrated extinction that is valid under all circumstances, and can provide new interpretations for reduction of acoustic scattering. In contrast to the electromagnetic situation, it is possible to have the formal IE expression for causal acoustic scattering to zero. We show that this is possible iff the acoustic scatterer is non-causal. An important example of such a scatterer is the *neutral acoustic inclusion*, which by definition has zero monopole and dipole scattered amplitudes. Based upon the IE results derived in this paper we explore the relationships between integrated extinction, neutral acoustic inclusions, cloaking and causality.

The paper proceeds as follows. In §2 the scattering cross-section and integrated extinction are defined and the result of [4], originally given for 3-dimensional scattering is presented for causal acoustic scattering in 1, 2 and 3 dimensions. The main result for the IE is derived in §2.2. Examples are given in §3 for one dimensional scattering for which the IE can be found in explicit form. Neutral acoustic inclusions are introduced in §4 as canonical scatterers for which the purely causal scattering term vanishes, and they therefore have unique transparency qualities. Practical examples and potential realizations are described in §5. Some of the results presented here can be found in [5,6].

2 Integrated Extinction

2.1 Scattering Cross Section and Causal IE

Consider the Helmholtz equation for the acoustic pressure $p(\mathbf{x}) \in \mathbb{C}$ outside of a finite region Ω, the scatterer,

$$\nabla^2 p + k^2 p = 0, \quad \mathbf{x} \in \mathbb{R}^d/\Omega. \tag{1}$$

Here $k = \omega/c$, ω is frequency and c is the sound speed, with $c = (C\rho)^{-1/2}$ where the uniform exterior acoustic medium has mass density ρ and compressibility C. Time harmonic dependence is considered with the factor $e^{-i\omega t}$ understood and omitted. The system may be one, two or three-dimensional, $d = 1, 2$ or 3. The total field is an incident plane wave plus the scattered pressure p_s,

$$p = e^{ikx} + p_s(\mathbf{x}). \tag{2}$$

The far-field scattering amplitude $S(\theta, \omega)$ is

$$p_s = S(\theta, \omega) \left(\frac{k}{i2\pi r}\right)^{\frac{d-1}{2}} e^{ikr} \left[1 + \mathcal{O}(\frac{1}{kr})\right] \tag{3}$$

as $r = |\mathbf{x}| \to \infty$, where θ is the scattering direction, $\theta = 0$ corresponding to the direction of incidence $\hat{\mathbf{k}}$. The *scattering cross section*, also known as the extinction, is

$$\sigma(\omega) = \int |p_s|^2 \mathrm{d}s \tag{4}$$

where the integral is around a surface enclosing the scatterer. The *integrated extinction* (IE),

$$\Sigma \equiv \int_0^\infty \frac{\sigma(\omega)}{\omega^2}\,\mathrm{d}\omega \;\geq 0, \tag{5}$$

defines the total scattering over all frequencies.

The scattering cross section typically tends to a finite non-zero value as $\omega \to \infty$ while $\sigma = \mathcal{O}(\omega^2)$ for $\omega \to 0$. Hence the only integer value n for which the integral $\mathrm{I} = \int_0^\infty \omega^{-n}\sigma \mathrm{d}\omega$ is bounded, and therefore meaningful, is $n = 2$, i.e. $\mathrm{I} = \Sigma$. Dirichlet boundary conditions on $\partial\Omega$ presents an exceptional limit; for instance, the scattering cross-section of a sphere tends to a non-zero constant as $\omega \to 0$ and the IE of eq. (5) is then undefined. The present results are therefore not applicable to scatterers with pressure-release boundaries. However, such boundary conditions are not strictly physical since a fluid with a pressure-release inclusion is not stable under static pressure perturbation. The IE can also be expressed

$$\Sigma = \int_0^\infty \frac{\mathrm{d}\sigma}{\mathrm{d}\omega}\,\frac{\mathrm{d}\omega}{\omega} = \frac{1}{2\pi c}\int_0^\infty \sigma\,\mathrm{d}\lambda \tag{6}$$

where $\lambda = 2\pi c/\omega$ is wavelength and $\lim_{\omega\to 0}\sigma/\omega = 0$ has been used in the first identity.

Conservation of energy requires zero total energy flux across the closed surface, which implies the well known *optical theorem*

$$\sigma = -2\,\Re S(\omega) \;\text{ where } S(\omega) \equiv S(0,\omega) \tag{7}$$

is the forward scattering amplitude. Equation (3) is exact in $d = 1$ for $\mathbf{x} \notin \Omega$, where $T = 1 + S(0,\omega)$ and $R = S(\pi,\omega)$ are the transmission and reflection coefficients and the optical theorem is the familiar identity $|R|^2 + |T|^2 = 1$.

Causality for forward scatter is here defined such that wave motion in the forward direction does not precede signals from the otherwise uniform medium. This implies that $S(\omega)$ is analytic in the upper half of the complex $\omega-$plane. The transform $f(\omega)$ of a causal function satisfies the Sokhotski-Plemelj relations for real values of ω [7, eq. (1.6.11)]

$$f(\omega) = \frac{1}{i\pi}\fint_{-\infty}^{\infty} \frac{f(\omega')\mathrm{d}\omega'}{\omega' - \omega}, \tag{8}$$

where $\fint$ denotes principal value integral. Setting $f(\omega) = \mathrm{d}S(\omega)/\mathrm{d}\omega$, and using $\sigma(-\omega) = \sigma(\omega)$, it follows from $(6)_1$, (7) and (8) that

$$\Sigma = \Sigma_{\mathrm{pc}} \quad \text{where} \quad \Sigma_{\mathrm{pc}} \equiv \pi\Im\frac{\mathrm{d}S(0)}{\mathrm{d}\omega} \tag{9}$$

and "pc" is included to emphasize that this result is strictly limited to *purely causal* forward scattering. Equation (9) for $d = 3$ was derived by Purcell [1] for electromagnetics and was first used in acoustics by [4]. The identity (9) also follows from the fact that $-iS(\omega)$ is a Herglotz function [8] ($h(z)$ is a Herglotz function if $\mathrm{Im}\,h(z) \geq 0$ for $\mathrm{Im}\,z > 0$).

The zero frequency limit in (9) allows us to interpret Σ_{pc} in terms of quasistatic properties. If the scatterer is a volume V with compressibility $C'(\mathbf{x})$ and uniform density ρ', then [4]

$$\Sigma_{\mathrm{pc}} = \frac{\pi}{2c}\Big(\big(\frac{\langle C'\rangle}{C} - 1\big)V - \hat{\mathbf{k}}\cdot\boldsymbol{\gamma}\Big(\frac{\rho}{\rho'}\Big)\cdot\hat{\mathbf{k}}\Big) \tag{10}$$

where $\boldsymbol{\gamma}$ is the polarizability dyadic [9] proportional to V and $\langle C'\rangle$ is the spatial average.

2.2 IE for Non-Causal Scattering

Acoustic forward scattering is not necessarily causal. We distinguish the causal and anti-causal components $s_+(t)$ and $s_-(t)$, respectively, by

$$\begin{aligned} s(t) &\equiv \frac{1}{2\pi}\int_{-\infty}^{\infty} S(\omega)e^{-i\omega t}\mathrm{d}\omega \\ &= s_-(t) + s_+(t), \quad s_\pm(t) = 0 \text{ for } t \lessgtr 0. \end{aligned} \tag{11}$$

Hence $s(t) = 0$ for $t < 0$ if the scattering is causal, and or non-causal scattering there is some finite time before $t = 0$ for which $s(t) \neq 0$. The time dependent function $s(t)$ can be identified as a forward scattered "impulse-response" function corresponding to an incident delta pulse $p_{\mathrm{inc}}(x,t) = \delta(t - x/c)$. Subscripts $+(-)$ denote functions that are causal (anti-causal) with Fourier transforms analytic in the upper and lower half planes, respectively. The forward scattering function decomposes as

$$\begin{aligned} S(\omega) &= S_-(\omega) + S_+(\omega), \\ S_\pm(\omega) &= \int_0^\infty s_\pm(\pm t)e^{\pm i\omega t}\mathrm{d}t. \end{aligned} \tag{12}$$

For causal scattering $s_-(t) = 0$, $S_-(\omega) = 0$; in the non-causal case s_-, S_- are non-zero.

We note the generalization of the Sokhotski-Plemelj relations (8),

$$f_\pm(\omega) = \frac{\pm 1}{i\pi}\fint_{-\infty}^{\infty} \frac{f_\pm(\omega')\mathrm{d}\omega'}{\omega' - \omega} \tag{13}$$

for ω real. Hence, $(6)_1$, (7) and (13) give us the first form of our main result

$$\Sigma = \pi\Im\left(\frac{\mathrm{d}S_+}{\mathrm{d}\omega}(0) - \frac{\mathrm{d}S_-}{\mathrm{d}\omega}(0)\right). \tag{14}$$

The identity (14) does not have an obvious interpretation in terms of quasi-static quantities, unlike its causal version eqs. (9) and (10). However, converting (14) to the time domain,

$$\Sigma = \pi\int_{-\infty}^{\infty} |t|\, s(t)\mathrm{d}t. \tag{15}$$

This result applies for causal and non-causal scattering. Note the appearance of $|t|$ in (15). The same integral with $|t|$ replaced by t is simply $\Im\,\mathrm{d}S(0)/\mathrm{d}\omega$. Hence, eqs. (9) and (15) imply

$$\boxed{\Sigma = \Sigma_{\rm pc} - 2\pi\int_{-\infty}^{0} t\, s(t)\mathrm{d}t.} \tag{16}$$

This generalizes the causal-only result (9). Since the non-causal response is zero for some $t_- < 0$, i.e. $s(t) = 0$, $t < t_-$, the integral in (16) is only over a finite interval of time from t_- to 0.

3 Examples

3.1 One Dimensional Medium

Consider a 1D system with non-uniform properties $\rho'(x)$, $C'(x)$ restricted to $\Omega = [0, a]$. Define the non-dimensional travel time

$$\mathrm{T} = \langle c/c'(x)\rangle \tag{17}$$

where $\langle\cdot\rangle = \frac{1}{a}\int_0^a \cdot\mathrm{d}x$ is the slab average. T is the ratio of the travel time across the inhomogeneity to the travel time across an equivalent uniform slab. Hence the scatterer is causal if $\mathrm{T} \geq 1$, and non-causal otherwise.

For causal scattering ($\mathrm{T} \geq 1$) the integrated extinction of eq. (9) becomes [6]

$$\begin{aligned}\Sigma_{\rm pc} &= \frac{\pi}{2}\frac{a}{c}\Big(\frac{\langle C'\rangle}{C} + \frac{\langle\rho'\rangle}{\rho} - 2\Big)\\ &= \pi\frac{a}{c}\left(\frac{1}{2}\Big\langle\frac{c}{c'}\Big(\sqrt{\frac{z'}{z}} - \sqrt{\frac{z}{z'}}\Big)^2\Big\rangle + \mathrm{T} - 1\right)\end{aligned} \tag{18}$$

where $z = \rho c$ is the background impedance and $z'(x) = \rho' c'$. Since the scatterer is causal this means that $\Sigma_{\rm pc} \geq 0$ with equality iff $\mathrm{T} = 1$ and the local impedance is constant and equal to the uniform impedance, i.e. $z' = z$. In summary, it is possible that the total IE of eq. (18) can vanish, but only if the slab has (i) uniform impedance and (ii) travel time equivalent to the uniform medium. Condition (i) is expected, it guarantees no reflection/backscattering, while (ii) ensures that the phase of the transmitted wave is the same as that for the uniform medium.

It does not appear to be possible to find an expression for the IE under both causal and non-causal conditions, with the exception of slabs with constant impedance $z' = z$. In that case it is not difficult to show that

$$\Sigma = \pi\frac{a}{c}\,|\,\mathrm{T} - 1| \quad \text{for constant impedance.} \tag{19}$$

The specific example next helps us understand how non-causal scattering effects the IE.

3.2 A Uniform Layer

A layer with uniform properties c', z' occupies $x \in [0, a]$ in the otherwise uniform background. The forward scattering impulse response is

$$s(t) = -\delta(t) + \big(R^{-2} - 1\big)\sum_{n=1}^{\infty} R^{2n}\delta(t - t_n) \tag{20}$$

where $R = \frac{z'-z}{z'+z}$, $t_n = (2n-1)\frac{a}{c'} - \frac{a}{c}$. Define $N \geq 0$ to be the number of non-causal pulses, i.e. $N = 0$ for causal scattering $c' \leq c$ and $N > 0$ for non-causal scattering with $t_N = \max t_n$, $t_n < 0$. It can then be shown that [6]

$$\Sigma = 2\pi\frac{a}{c'}\Big[\Big(\frac{1+R^2}{1-R^2} - \frac{c'}{c} + 2N\Big)\big(R^{2N} - \tfrac{1}{2}\big) + N\Big] \tag{21}$$

The simpler result for causal scattering, i.e. eq. (18), is evident from eq. (21) with $N = 0$. The parameter N is a positive integer for non-causal scattering, and even though it is discontinuous it can be shown that Σ is a continuous though not necessarily smooth function of the layer parameters. Figure 1 shows the IE for a uniform slab with impedance thrice the background as a function of slab wave speed. Also shown is the *magnitude* of the purely causal IE (eq. (18) or (21) with $N = 0$). Clearly, $\Sigma = \Sigma_{\rm pc}$ for $c' \leq c$ as expected. It is also evident that $\Sigma \approx -\Sigma_{\rm pc}$

for $c' > 5c$ with better approximation for larger c'. This can be understood from the mathematical form of Σ in eq. (21). The number N increases approximately linearly with the slab speed $c'$when all other slab parameters are held fixed. The quantity R^{2N} therefore decreases with increasing c', so that $\Sigma \to -\Sigma_{\rm pc}$.

Figure 2 shows the same phenomenon for a larger slab impedance ($z'/z = 8$). The limiting behavior $\Sigma \approx -\Sigma_{\rm pc}$ is again observed, this time at larger values of c' since the quantity R^{2N} decreases less rapidly than for Figure 1.

3.3 Two and Three Dimensions

Consider plane wave incidence on a uniform circular or spherical inhomogeneity of radius a and properties ρ', c'. The IE for causal scattering follows from the low frequency forward scattering amplitude using standard methods [6], as

$$\Sigma_{\rm pc} = \eta \frac{a^d}{c} \frac{\rho}{\rho'} \left(\frac{\left(\frac{\rho'}{\rho} - 1\right)^2}{(d-1)\frac{\rho'}{\rho} + 1} + \mathrm{T}^2 - 1 \right) \qquad (22)$$

where $\mathrm{T} = c'/c$ is the ratio of travel times and $\eta = \pi^2(d-1)/d$. It is interesting to compare this with the analogous 1D result eq. (18). Since $\mathrm{T} \geq 1$ for causal scattering, eq. (22) shows that $\Sigma_{\rm pc}$ vanishes iff $\rho' = \rho$, $c' = c$, implying that there is no combination of ρ', $c' \leq c$ that is transparent except for the trivial case when the scatterer is identical with the background fluid. Despite the fact that there is no known example of a 2- or 3-dimensional non-causal scatterer for which Σ can be found in closed form, we can make some general statements, next.

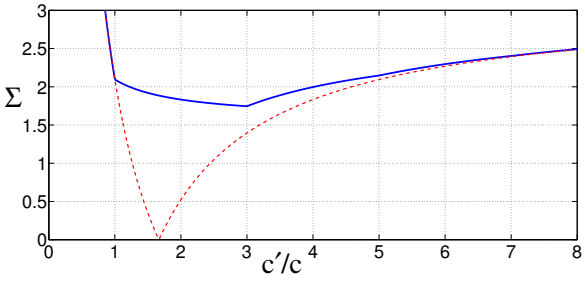

Figure 1: The solid curve shows Σ as a function of c'/c for a uniform slab $z'/z = 3$, $a/c = 1$. The dashed curve shows the magnitude of the causal integrated extinction $\Sigma_{\rm pc}$.

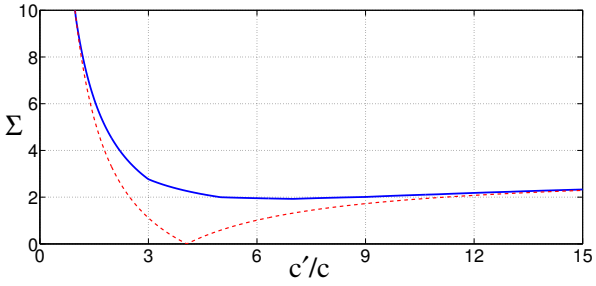

Figure 2: The curves are the same as in Figure 1 except that the slab impedance is $z' = 8z$.

3.4 Discussion

The general form of the IE, eq. (16), is

$$\Sigma = \Sigma_{\rm pc} + 2\,\Sigma^{(-)} = -\Sigma_{\rm pc} + 2\,\Sigma^{(+)} \qquad (23)$$

$$\text{where } \Sigma^{(\pm)} = \pi \int_0^{\pm\infty} t\, s(t) \mathrm{d}t. \qquad (24)$$

$\Sigma^{(+)}$ and $\Sigma^{(-)}$ can be considered as causal and non-causal parts of the IE since $\Sigma = \Sigma^{(+)} + \Sigma^{(-)}$. The purely causal result [1, 4] in eq. (9) follows from the first identity in (23) with $\Sigma^{(-)} = 0$. At the other extreme, the scattering can be *mainly* non-causal in the sense of the examples in Figures 1 and 2. This can occur in one, two or three dimensions if the scatterer supports very fast waves relative to the background, e.g. metallic scatterers in air. Most of the energy is scattered before $t = 0$, implying $|\,\Sigma^{(-)}\,| \gg |\,\Sigma^{(+)}\,|$ and

$$\Sigma \approx -\Sigma_{\rm pc} \qquad (25)$$

which is essentially the opposite of the causal identity (9). The quasistatic quantity $\Sigma_{\rm pc}$ which seemed to be only relevant to causal scattering, is also important for very non-causal scattering, but in the opposite manner, i.e. a sign change!

The 1D case of the constant impedance layer, eq. (19), provides the only example the authors have found for which $\Sigma = -\Sigma_{\rm pc}$. In fact, in this example $\Sigma = \pm\Sigma_{\rm pc}$ with no other possibility. For general scatterers, as the above 1D examples show, it is possible for Σ to differ significantly from $|\,\Sigma_{\rm pc}\,|$. Further understanding of this divergence is essential if we are to achieve truly broadband cloaking. We next consider a first step in this direction, by considering scatterers for which $\Sigma_{\rm pc}$ vanishes.

4 Neutral acoustic inclusions

A *neutral acoustic inclusion* (NAI) has, by definition, zero monopole and dipole scattered am-

plitudes. The two terms in the expression (10) for $\Sigma_{\rm pc}$ correspond to the monopole and dipole contribution to the forward scatter. Both terms vanish for a NAI, implying $\Sigma_{\rm pc}=0$. Hence, *a neutral acoustic inclusion is a non-causal scatterer*. The following identities are easily shown,

$$\left.\begin{aligned}&\int_{-\infty}^{\infty} t\,s(t)\mathrm{d}t=0,\\ &\Sigma=-2\pi\int_{-\infty}^{0} t\,s(t)\mathrm{d}t,\end{aligned}\right\}\quad\text{for a NAI.}\qquad(26)$$

The IE for a NAI is therefore defined completely by the non-causal part of the forward scatter. For electromagnetic scattering, which is causal, the IE equals $\Sigma_{\rm pc}$ and must be positive, and so there is no EM analog of the NAI.

The NAI conditions reduce to constraints on the compressibility and density of the scatterer:

$$\langle C'\rangle=C,\quad \langle\rho'\rangle=\rho.\qquad(27)$$

The vanishing of the monopole and dipole amplitudes leads to reduced scattering in the low frequency range, resulting in increased transparency. The notion of causality, i.e. wave speed, is not contained in the quasistatic definition of neutral inclusions. The finding that neutral acoustic inclusions must be non-causal scatterers is therefore remarkable in that a quasistatic effect implies a necessary dynamic property.

Transparency over a wide range of frequencies, known as cloaking, demands at the very least that the object be transparent in the long wavelength regime, which may be achieved by making the cloak and the object being cloaked together satisfy (27). We therefore conclude that *low frequency acoustic cloaking requires non-causal scattering*. In order to achieve perfect cloaking one *only* needs (i) to satisfy the low frequency cloaking conditions (27), and (ii) have the forward signal arrive at $t=0$ for all directions of incidence. The italicized "only" emphasizes the question of whether or not these conditions can be simultaneously satisfied in 2D and 3D apart from the trivial case $C'=C$, $\rho'=\rho$. By comparison, $\Sigma=0$ is possible for non-trivial C', ρ' in 1D, as shown in eq. (19).

A first step towards achieving broadband transparency is to convert the object into a neutral acoustic inclusion, by surrounding it with a "low frequency cloak" or otherwise. Further improvement in broadband transparency is then equivalent to minimizing the integral $(26)_2$, an integral over a finite time span, from the (negative) time of the first forward arrival until $t=0$. This provides a time-domain based metric for broadband transparency that depends only on the part of the signal that arrives before the background wave. The benefit of this approach is that it is restricted to a finite length time domain signal, while it provides a scalar measure of the forward broadband scattering.

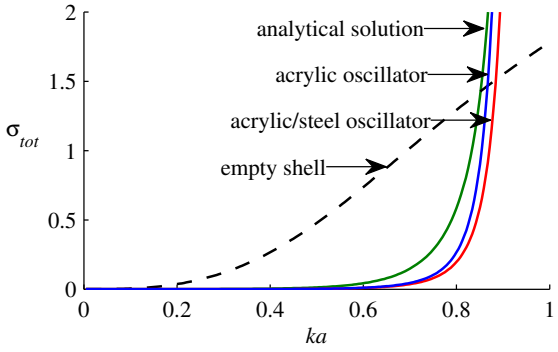

Figure 3: Comparison of the scattering cross section for oscillator designs for an aluminum shell of thickness h to radius a ratio $h/a=0.03$.

5 Neutral acoustic inclusion examples

Specific examples of NAI will be discussed, starting with cylindrical elastic shells in water [5] which provide a practical design for NAIs. Elastic solids have a natural "reservoir" of both stiffness and inertia, and by proper removal of material the scatterer can have the effective properties (27). Adjusting the shell thickness gives the appropriate effective compliance, $\langle C'\rangle=C$, while it simultaneously matches the effective density so that $\gamma=0$. The shell then has reduced total-scattering cross section in the long-wavelength regime [5]. A very limited number of materials can achieve these criteria, so extra measures must be taken, e.g. adding mass. Figure 3 compares the scattering from some designed NAI shells against that for a solid aluminum cylinder of the same radius.

The implications of the possibility for practical NAI designs will be discussed. While the criterion for NAI material design is based on low frequency considerations, numerical simulations show that the low frequency transparency can extend to high frequencies. Figure 3 shows low frequency transparency extending to non-

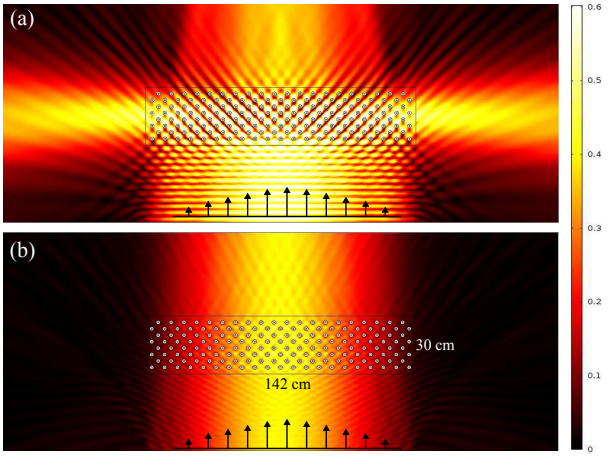

Figure 4: Absolute pressure field for a Gaussian beam incident upon an 8×41 array of acrylic shells in water. Plots (a) and (b) are at 22350 Hz and 27000 Hz, respectively.

dimensionally large frequencies. Figure 4 shows a dramatic example: an array of cylinders that are otherwise transparent exhibit strong and correlated scattering at certain frequencies. The figure illustrates the coöperative scattering effects of the array radiation at a frequency band near a flexural resonance of the individual cylinders, resulting in strong scattering in the direction orthogonal to incidence. This example demonstrates the possibility for an otherwise transparent array to scatter in a preferred direction at certain frequencies.

Other examples will show more general array designs and will also discuss the related topic of *active acoustic cloaking* [10]. The idea is to use a finite set of scatterers each with the ability to radiate in response to insonification. Coherent radiation by several scatterers can annul a finite region of space, allowing cloaking of an arbitrary object without the need to surround it by passive although exceptional materials.

Acknowledgement

This work was supported under ONR MURI Grant No. N000141310631.

References

[1] E. M. Purcell. On the absorption and emission of light by interstellar grains. *Astrophys. J.*, 158:433–440, 1969.

[2] C. Sohl, M. Gustafsson, and G. Kristensson. Physical limitations on broadband scattering by heterogeneous obstacles. *J. Phys. A: Math. Theor.*, 40(36):11165–11182, 2007.

[3] F. Monticone and A. Alù. Do cloaked objects really scatter less? *Phys. Rev. X*, 3:041005+, 2013.

[4] C. Sohl, M. Gustafsson, and G. Kristensson. The integrated extinction for broadband scattering of acoustic waves. *J. Acoust. Soc. Am.*, 122(6):3206–3210, 2007.

[5] A. S. Titovich and A. N. Norris. Tunable cylindrical shell as an element in acoustic metamaterial. *J. Acoust. Soc. Am.*, 136(4):1601–1609, 2014.

[6] A. N. Norris. Acoustic integrated extinction. *Proc. R. Soc. A*, 471(2177):20150008+, 2015.

[7] H. M. Nussenzveig. *Causality and dispersion relations*. Academic, London, 1972.

[8] M. Gustafsson, D. Sjoberg, A. Bernland, G. Kristensson, and C. Sohl. Sum rules and physical bounds in electromagnetic theory. In *Electromagnetic Theory (EMTS), 2010 URSI International Symposium on*, pages 37–40. IEEE, 2010.

[9] G. Dassios and R. Kleinman. *Low frequency scattering*. Oxford: Oxford University Press, 2000.

[10] A. N. Norris, F. A. Amirkulova, and W. J. Parnell. Source amplitudes for active exterior cloaking. *Inverse Problems*, 28 (10) 105002, 2012.

THREE-DIMENSIONAL SOLITARY WATER WAVES

M. D. Groves[1,*]
[1]Fachrichtung Mathematik, Universität des Saarlandes, 66041 Saarbrücken, Germany
*Email: groves@math.uni-sb.de

Abstract

The existence of solitary-wave solutions to the three-dimensional water-wave problem is predicted by the Kadomtsev-Petviashvili (KP) equation in the case of strong surface tension and the Davey-Stewartson (DS) system in the case of weak surface tension. The term *solitary wave* describes any solution which has a pulse-like profile in its direction of propagation, and these model equations admit three types of solitary waves. A *line solitary wave* is spatially homogeneous in the direction transverse to its direction of propagation, while a *periodically modulated solitary wave* is periodic in the transverse direction. A *fully localised solitary wave* on the other hand decays to zero in all spatial directions.

In this talk I outline mathematical results which confirm the existence of the three-dimensional solitary waves for the full gravity-capillary water-wave problem in its usual formulation as a free-boundary problem for the Euler equations; both strong and weak surface tension are treated. The periodically modulated solitary waves are created when a line solitary wave undergoes a dimension-breaking bifurcation, spontaneously losing its spatial homogeneity in the transverse direction; an infinite-dimensional version of the Lyapunov centre theorem is the main ingredient in the existence theorem. The fully localised solitary waves are obtained by finding critical points of a variational functional.

Introduction

The classical *three-dimensional gravity-capillary water wave problem* concerns the irrotational flow of a perfect fluid of unit density subject to the forces of gravity and surface tension. The fluid motion is described by the Euler equations in a domain bounded below by a rigid horizontal bottom $\{y = 0\}$ and above by a free surface $\{y = h + \eta(x, z, t)\}$, where h denotes the depth of the water in its undisturbed state and the function η depends upon the two horizontal spatial directions x, z and time t. *Steady waves* are water waves which are uniformly translating in a distinguished horizontal direction without change of shape; without loss of generality we assume that the waves propagate in the x-direction with speed c and continue to write x as an abbreviation for $x - ct$. In terms of an Eulerian velocity potential $\phi(x, y, z, t)$ the mathematical problem for steady waves is to solve the equations

$$\phi_{xx} + \phi_{yy} + \phi_{zz} = 0, 0 < y < 1 + \eta, \quad (1)$$

$$\phi_y = 0, \qquad y = 0, \quad (2)$$

$$\phi_y = \eta_x\phi_x + \eta_z\phi_z - \eta_x, \qquad y = 1 + \eta \quad (3)$$

and

$$-\phi_x + \frac{1}{2}(\phi_x^2 + \phi_y^2 + \phi_z^2) + \alpha\,\eta - \beta\left[\frac{\eta_x}{\sqrt{1 + \eta_x^2 + \eta_z^2}}\right]_x - \beta\left[\frac{\eta_z}{\sqrt{1 + \eta_x^2 + \eta_z^2}}\right]_z = 0 \quad (4)$$

on $y = 1 + \eta$, in which we have introduced dimensionless variables. The equations involve two physical parameters $\alpha := gh/c^2$ and $\beta := \sigma/hc^2$, where g and σ are respectively the acceleration due to gravity and the coefficient of surface tension. (Nontrivial) steady water waves which satisfy $\eta(x, z) \to 0$ as $x \to \pm\infty$ are called *solitary waves*. A *line solitary wave* is spatially homogeneous in the direction z transverse to its direction of propagation, while a *periodically modulated solitary wave* is periodic in the z-direction. A *fully localised solitary wave* on the other hand satisfies $\eta(x, z) \to 0$ as $|(x, z)| \to 0$.

The steady water-wave problem (1)–(4) is a free boundary-value problem with nonlinear boundary conditions, and in this respect its solution poses considerable mathematical difficulties. At a formal level these difficulties may be overcome by replacing the above equations by a simpler model equation (a 'weakly nonlinear approximation').

Strong surface tension ($\beta > 1/3$): The KP equation

$$\partial_{xx}\left(\zeta_{xx} - \zeta - \frac{3}{2}\zeta^2\right) - \zeta_{zz} = 0, \quad (5)$$

was derived formally by Kadomtsev and Petviashvili [11] as a long-wave approximation for solutions of (1)–(4) in which

$$\beta > 1/3, \qquad \alpha = 1 + \epsilon^2, \quad 0 < \epsilon \ll 1;$$

the variable ζ is supposed to approximate the free surface of the water via the formula

$$\eta(x,z) = \epsilon^2\zeta\left(\epsilon\, x, \epsilon^2 z\right) + O(\epsilon^4)$$

(up to scalings of η, x and z). The KP equation admits explicit line and fully localised solitary-wave solutions, namely

$$\begin{aligned}\zeta_{\rm l}(x) &= -\mathrm{sech}^2\left(\frac{x}{2}\right),\\ \zeta_{\rm f}(x,z) &= -8\frac{3-x^2+z^2}{(3+x^2+z^2)^2},\end{aligned}$$

and explicit formulae for a family of periodically modulated solitary waves are also available (see Tajiri and Murakami [13]). The waves are sketched in Figure 1.

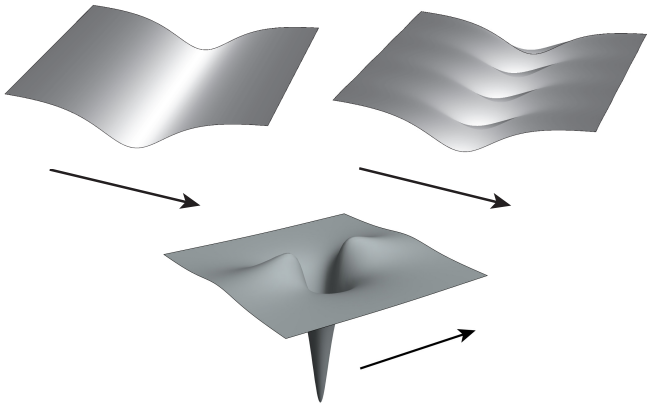

Figure 1: Clockwise from top left: line, periodically modulated and fully localised solitary-wave solutions to the KP system; the arrow shows the x-direction.

Weak surface tension ($\beta < 1/3$): The DS system

$$\begin{aligned}\zeta - \zeta_{xx} - \zeta_{zz} - |\zeta|^2\zeta - \zeta\psi_x &= 0,\\ -\psi_{xx} - \psi_{zz} + (|\zeta|^2)_x &= 0\end{aligned}$$

was derived formally by Djordjevic & Redekopp [4] as a long-wave approximation for solutions of (1)–(4) in which

$$\beta = \beta_0, \qquad \alpha = \alpha_0 + \varepsilon^2, \quad 0 < \epsilon \ll 1$$

and

$$\begin{aligned}\alpha_0 &= \frac{\mu_0^2}{2}\mathrm{cosech}^2\mu_0 + \frac{\mu_0}{2}\coth\mu_0,\\ \beta_0 &= -\frac{1}{2}\mathrm{cosech}^2\mu_0 + \frac{1}{2\mu_0}\coth\mu_0\end{aligned}$$

for some $\mu_0 > 0$; the variable ζ is supposed to approximate the free surface of the water via the formula

$$\eta(x,z) = \frac{\varepsilon}{2}\left(\zeta(\varepsilon x, \varepsilon z)\mathrm{e}^{\mathrm{i}\mu_0 x} + \overline{\zeta(\varepsilon x, \varepsilon z)}\mathrm{e}^{-\mathrm{i}\mu_0 x}\right) + O(\varepsilon^2)$$

(up to scalings of η, x and z). The DS system admits explicit line solitary-wave solutions, namely

$$\zeta_{\rm l}(x) = \pm\mathrm{sech}\, x, \qquad \psi_{\rm lsw}(x) = \tanh x,$$

and there are existence theories for both periodically modulated solitary waves (Groves, Sun & Wahlén [8]) and fully localised solitary waves (Cipolatti [2]). The waves are sketched in Figure 2.

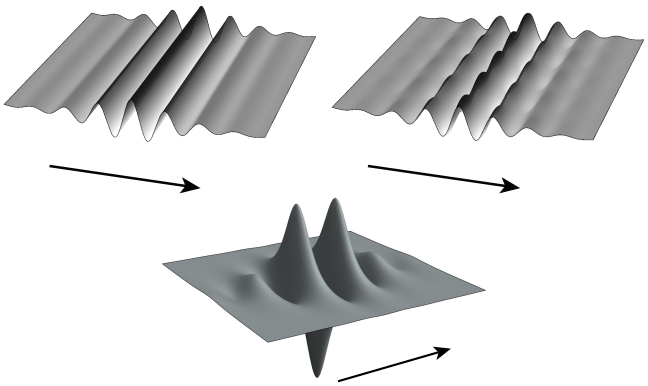

Figure 2: Clockwise from top left: line, periodically modulated and fully localised solitary-wave solutions to the DS system; the arrow shows the x-direction.

The existence of line solitary-wave solutions to (1)–(4) in the KP and DS parameter regimes has been confirmed rigorously by respectively Amick & Kirchgässner [1] and Iooss & Kirchgässner [10], who also showed that the explicit solutions to the model equations accurately describe the asymptotic form of the solitary waves.

Periodically modulated solitary waves

Spatial dynamics

The phrase 'spatial dynamics' refers to an approach where a system of partial differential equations governing a physical problem is formulated as a (typically ill-posed) evolutionary equation in which an unbounded spatial coordinate plays the role of time. We use the method by formulating (1)–(4) as a reversible evolutionary equation

$$w_z = f(w), \tag{6}$$

where u belongs to a space $\mathcal{X}$ of functions which converge to zero as $x \to \pm\infty$, so that all its solutions are solitary waves. In particular, equilibirum and periodic solutions correspond to respectively line and periodically modulated solitary waves. Let $w_{\rm lsw}$ be the solution to (6) corresponding to the KP or DS line solitary wave in the appropriate parameter regime. Using the translation $w(z) = w_{\rm lsw} + u(z)$, we obtain a new evolutionary equation

$$\begin{aligned} u_z &= f^\star(u) \\ &= L^\star u + N^\star(u), \end{aligned} \tag{7}$$

small-amplitude periodic solutions of which correspond to periodically modulated solitary waves emerging from the line solitary wave in a dimension-breaking bifurcation (see Figure 3).

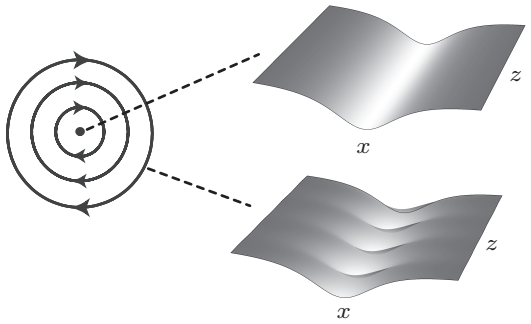

Figure 3: A family of periodic solutions surrounding a nontrivial equilibrium solution to (6) in its phase space (left) corresponds to a dimension-breaking bifurcation of a branch of periodically modulated solitary waves from a line solitary wave (right).

Small-amplitude solutions to (7) are found using a generalisation of the classical Lyapunov centre theorem (for finite-dimensional Hamiltonian or reversible systems) due to Iooss [9].

Theorem Consider a quasilinear, reversible evolutionary equation

$$v_t = Lv + N(v)$$

in the phase space $\mathcal{X}$. Suppose that the linear operator L has a pair $\pm ik$ of simple imaginary eigenvalues, that 0 is contained in its essential spectrum, and that

(H1) all nonzero integer multiples of $\pm ik$ lie in the resolvent set of L;

(H2) L satisfies the estimate $\|(L - i\lambda I)^{-1}\| = O(\lambda^{-1})$ as $\lambda \to \pm\infty$;

(H3) the range of the nonlinearity N lies in the range of L, so that the equation $Lv = -N(u)$ is solvable for each function u in the domain of N.

Under these conditions the above evolutionary equation admits a family of small-amplitude periodic solutions whose frequency is near k.

To apply this technique to the steady water-wave problem it is therefore necessary to formulate (1)–(4) as an evolutionary equation of the form (6) and to confirm the spectral hypotheses in Iooss's theorem for the KP and DS line solitary waves.

Luke's variational principle

The key to obtaining the spatial dynamics formulation (6) of equations (1)–(4) is the observation that they follow from the formal variational principle

$$\delta \int \Bigg(\int_0^{1+\eta} (-\phi_x + \frac{1}{2}(\phi_x^2 + \phi_y^2 + \phi_z^2))\,\mathrm{d}y + \frac{1}{2}\alpha\eta^2 + \beta(\sqrt{1+\eta_x^2+\eta_z^2} - 1)\Bigg)\mathrm{d}(x,z) = 0 \tag{8}$$

(Luke [12]). A more satisfactory version of this variational principle is obtained using the change of variable

$$y = Y(1+\eta(x,z)), \qquad \phi(x,y,z) = \psi(x,Y,z), \tag{9}$$

which transforms the variable fluid domain into the fixed domain $\{0 < Y < 1\}$. One obtains a new variational principle, which we (with a slight abuse of notation) write as

$$\delta\mathcal{F} = 0, \qquad \mathcal{F} = \int \left(\int F(\eta, \psi, \eta_z, \psi_z)\,\mathrm{d}x \right) \mathrm{d}z.$$

This variational principle takes the form of Hamilton's principle for an action functional in which z is the time-like variable, (η, ψ) are the coordinates and (η_z, ψ_z) the corresponding velocities. Following the classical theory, we take the Legendre transform and hence derive the (infinite-dimensional) Hamiltonian system

$$\eta_z = \delta_\omega H, \quad \omega_z = -\delta_\eta H, \quad \psi_z = \delta_\xi H, \quad \xi_z = -\delta_\psi H,$$

where

$$H(\eta, \omega, \psi, \xi) = \int \omega\eta_z\,\mathrm{d}x + \iint \xi\psi_z\,\mathrm{d}Y\,\mathrm{d}x - \int F(\eta, \psi, \eta_z, \psi_z)\,\mathrm{d}x$$

and δ denotes a variational derivative; a solution of this Hamiltonian system defines a steady water wave via the formula (9).

An explicit calculation shows that the above Hamiltonian system is

$$\begin{aligned}
\eta_z &= W\left(\frac{1+\eta_x^2}{\beta^2-W^2}\right)^{1/2},\\
\omega_z &= \frac{W}{(1+\eta)^2}\left(\frac{1+\eta_x^2}{\beta^2-W^2}\right)^{1/2}\int_0^1 Y\psi_Y\xi\,\mathrm{d}Y\\
&\quad-\left[\eta_x\left(\frac{\beta^2-W^2}{1+\eta_x^2}\right)^{1/2}\right]_x+\alpha\,\eta-\psi_x|_{Y=1}\\
&\quad+\int_0^1\left\{\frac{\xi^2-\psi_Y^2}{2(1+\eta)^2}+\frac12\left(\psi_x-\frac{Y\eta_x\psi_Y}{1+\eta}\right)^2\right.\\
&\qquad+\left[\left(\psi_x-\frac{Y\eta_x\psi_Y}{1+\eta}\right)Y\psi_Y\right]_x\\
&\qquad\left.+\left(\psi_x-\frac{Y\eta_x\psi_Y}{1+\eta}\right)\frac{Y\eta_x\psi_Y}{1+\eta}\right\}\mathrm{d}Y,
\end{aligned}$$

$$\begin{aligned}
\psi_z &= \frac{\xi}{(1+\eta)}+\frac{WY\psi_Y}{1+\eta}\left(\frac{1+\eta_x^2}{\beta^2-W^2}\right)^{1/2},\\
\xi_z &= -\frac{\psi_{YY}}{1+\eta}-\left[(1+\eta)\left(\psi_x-\frac{Y\eta_x\psi_Y}{1+\eta}\right)\right]_x\\
&\quad+\left[\left(\psi_x-\frac{Y\eta_x\psi_Y}{1+\eta}\right)Y\eta_x\right]_Y\\
&\quad+\frac{W(Y\xi)_Y}{1+\eta}\left(\frac{1+\eta_x^2}{\beta^2-W^2}\right)^{1/2}.
\end{aligned}$$

This system is reversible with reverser $S(\eta,\omega,\psi,\xi):=(\eta,-\omega,\psi,-\xi)$ and is accompanied by the boundary conditions

$$\begin{aligned}
&\psi_Y|_{Y=0}=0\\
&\eta_x+\left.\frac{\psi_Y}{1+\eta}\right|_{Y=1}\\
&\quad=\eta_x\left(\psi_x-\frac{\eta_x\psi_y}{1+\eta}\right)+\frac{W\xi}{1+\eta}\left(\frac{1+\eta_x^2}{\beta^2-W^2}\right)^{1/2}\Bigg|_{Y=1}
\end{aligned}$$

which emerge as a consequence of the integration by parts necessary to compute the variational derivative with respect to ψ. Note that the boundary condition at $Y=1$ is nonlinear. This difficulty is overcome by a change of variable which converts the Hamiltonian system into an equivalent system with linear boundary conditions (see Groves [5]).

Linear spectral analysis

We now determine the purely imaginary spectrum of the linear operator $L^\star$ appearing in equation (7); an explicit formula for $L^\star$ is obtained from Hamilton's equations and the asymptotic formulae for the line solitary waves. To this end we consider the resolvent equation

$$(L^\star-\mathrm{i}\varepsilon^n kI)u=u^\dagger,\qquad n=\begin{cases}2, & \beta>1/3,\\ 1, & \beta<1/3,\end{cases}$$

where $k\neq0$. Writing $u=(\eta,\omega,\psi,\xi)$, one can solve three of the four components of the resolvent equation to find ω, ψ and ξ as functions of η and $u^\dagger$ and thus reduce the remaining component to a single equation for η of the form

$$g(D)\eta=\mathcal{N}(\eta,u^\dagger),\tag{10}$$

where

$$g(\mu)=\alpha+\beta q^2-\frac{\mu^2}{q}\coth q,\qquad q=\sqrt{\mu^2+\varepsilon^{2n}k^2}$$

and the notation $m(D)$ denotes a Fourier multiplier with respect to x whose symbol is m.

We note that $g(\mu)\geq0$ with equality if and only if $\mu=\mu_0$ (where $\mu_0=0$ for $\beta>1/3$). We therefore write $\eta_1=\chi(D)\eta$, $\eta_2=(1-\chi(D)\eta$, where χ is the characteristic function of the set $(-\mu_0-\delta,-\mu_0+\delta)\cup(\mu_0-\delta,\mu_0+\delta)$ and decompose (10) into two coupled equations for η_1 and η_2. One can solve one equation to find η_2 as a function of η_1 and $u^\dagger$ and thus reduce the other to a single equation

$$\eta_1=\chi(D)\mathcal{N}(\eta_1+\eta_2(\eta_1,u^\dagger),u^\dagger)$$

for η_1.

The next step is to write

$$\eta_1(x,z)=\varepsilon^2\zeta(\varepsilon x)$$

for $\beta>1/3$ or

$$\eta_1(x,z)=\frac{\varepsilon}{2}\left(\zeta(\varepsilon x)\mathrm{e}^{\mathrm{i}\mu_0x}+\overline{\zeta(\varepsilon x)}\mathrm{e}^{-\mathrm{i}\mu_0x}\right)$$

for $\beta<1/3$. Inserting this *Ansatz* into the reduced equation for η_1 yields, after a lengthy calculation, the equation

$$\zeta_{xxxx}-\zeta_{xx}-3(\zeta_1\zeta_x)_x-3(\zeta\zeta_x^\star)_x+O(\varepsilon)+k^2\zeta=\zeta^\dagger(u^\dagger)$$

for $\beta>1/3$ or the system

$$\begin{aligned}
&\zeta-\zeta_{xx}-3(\zeta_1)^2\zeta\\
&\quad-(\zeta_1)^2\overline{\zeta}-\zeta_1\psi_x+O(\varepsilon)+k^2\zeta &&=\zeta^\dagger(u^\dagger),\\
&\quad-\psi_{xx}+2(\operatorname{Re}\zeta_1\zeta)_x+k^2\psi &&=0,
\end{aligned}$$

for $\beta < 1/3$. The left-hand sides of these equations are perturbations of the linearisations of the KP equation or DS system at their line solitary-wave solutions.

We write the reduced equation for ζ as

$$(\mathcal{B}_{\varepsilon,k} + k^2 I)w = w^\dagger,$$

where of course $\mathcal{B}_{0,k}$ is known explicitly (and does not depend upon k). In particular, it is self-adjoint and its spectrum consists of a simple negative eigenvalue and continuous spectrum $[0,\infty)$; standard spectral perturbation theory shows that the same is true of $\mathcal{B}_{\varepsilon,k}$ (see Figure 4).

Figure 4: The spectrum of $\mathcal{B}_{\varepsilon,k}$.

This spectral analysis shows that $\mathcal{B}_{\varepsilon,k} + k^2 I$ has a simple zero eigenvalue if and only if

$$\lambda_{\varepsilon,k} + k^2 = 0 \tag{11}$$

and is invertible if and only if this equation is not satisfied.

Lemma Equation (11) has precisely one positive solution k_ε.

Tracing back the spectral reduction, one finds that $\pm \mathrm{i}\varepsilon^n k_\varepsilon$ are simple eigenvalues of $L^\star$ and $L^\star - \mathrm{i}\varepsilon^n k I$ is invertible for all other values of $k \neq 0$.

Applying the spectral reduction procedure to the equation

$$L^\star(u) = -N^\star(u^\dagger),$$

we arrive at the reduced equation

$$\mathcal{C}_\varepsilon \zeta = \zeta^\dagger(u^\dagger),$$

where

$$\mathcal{C}_\varepsilon \zeta = \zeta_{xx} - \zeta + 3\zeta_1\zeta + O(\varepsilon)$$

for $\beta > 1/3$ or

$$\mathcal{C}_\varepsilon \zeta = \zeta - \zeta_{xx} - 4(\zeta_1)^2\zeta - 2(\zeta_1)^2\overline{\zeta} + O(\varepsilon)$$

for $\beta < 1/3$. Since $\mathcal{C}_0$ is invertible (under the restriction that ζ is symmetric in x), we find that $\mathcal{C}_\varepsilon$ is also invertible.

These observations confirm hypotheses (H1) and (H3) in Iooss's theorem, while (H2) is verified using standard *a priori* estimates. Full details are given by Groves, Haragus & Sun [6] for $\beta > 1/3$ and Groves, Sun & Wahlén [7] for $\beta < 1/3$.

Fully localised solitary waves

The existence theories for fully localised solitary waves are variational in nature, the starting point again being Luke's variational principle (8). Observing that the free-surface elevation $\eta(x,z,t)$ and Dirichlet data at the free surface $\Phi(x,z) = \phi(x,1+\eta(x,z),z)$ completely determine the wave motion, one may formulate the variational principle in terms of these variables as

$$\delta \int_{\mathbb{R}^2} \left\{ \frac{1}{2}\Phi G(\eta)\Phi + \frac{1}{2}\alpha\eta^2 + \beta(\sqrt{1+\eta_x^2+\eta_z^2} - 1) - \eta\Phi_x \right\} \mathrm{d}(x,z) = 0, \tag{12}$$

where $G(\eta)$ is the Dirichlet-Neumann operator defined by $G(\eta)\xi = \nabla\phi.(-\eta_x,-\eta_z,1)|_{y=1+\eta}$ and the potential function ϕ is the harmonic extension of ξ into $\{0 < y < 1+\eta\}$ with Neumann data at $y = 0$. (We specialise to fully localised solitary waves by integrating over the entire plane.) We proceed by reducing (12) to a locally equivalent variational principle using a method analagous to the spectral reduction procedure for periodically modulated solitary waves.

Examining the Euler-Lagrange equations for the variational functional $F(\eta,\Phi)$ appearing in (12), one finds that it is possible to solve one of these equations for Φ as a function of η (in fact $\Phi = G(\eta)^{-1}\eta_x$) and thus reduce the variational principle to

$$\delta J(\eta) = 0, \qquad J(\eta) = F(\eta,\Phi(\eta)).$$

We next write $\eta_1 = \chi(D)\eta$, $\eta_2 = (1-\chi(D)\eta$, where χ is the characteristic function of the set $B_\delta((-\mu_0,0))\cup B_\delta((\mu_0,0))$ (with $\mu_0 = 0$ for $\beta > 1/3$) and the notation $m(D)$ now denotes a Fourier multiplier with respect to (x,z) whose symbol is m. The Euler-Lagrange equation for $J(\eta)$ is correspondingly decomposed into two coupled equations for η_1 and η_2. One can solve one equation to find η_2 as a function of η_1 and thus obtain the reduced variational principle

$$\delta J(\eta_1 + \eta_2(\eta_1)) = 0$$

for the other.

Finally, we write

$$\eta_1(x,z) = \varepsilon^2\zeta(\varepsilon x, \varepsilon^2 z)$$

for $\beta > 1/3$ or

$$\eta_1(x,z) = \frac{\varepsilon}{2}\left(\zeta(\varepsilon x,\varepsilon z)\mathrm{e}^{\mathrm{i}\mu_0 x} + \overline{\zeta(\varepsilon x,\varepsilon z)}\mathrm{e}^{-\mathrm{i}\mu_0 x}\right)$$

for $\beta < 1/3$. Inserting this *Ansatz* into the reduced variational principle for η_1 yields, after a lengthy calculation, the variational principle

$$\delta \tilde{J}_\varepsilon(\zeta) = 0,$$

where

$$\tilde{J}_\varepsilon(\zeta) = \frac{1}{2}\int_{\mathbb{R}^2}\left\{\zeta^2+\zeta_x^2+(\partial_x^{-1}\zeta_z)^2-\zeta^3\right\}\mathrm{d}(x,z)+O(\varepsilon)$$

for $\beta > 1/3$ or

$$\tilde{J}_\varepsilon(\zeta) = \int_{\mathbb{R}^2}\left\{\frac{1}{2}(|\zeta_x|^2+|\zeta_z|^2)+\frac{1}{2}|\zeta|^2 - \frac{1}{4}|\zeta|^4-\frac{1}{4}|\zeta|^2\Delta^{-1}\partial_x^2|\zeta|^2\right\}\mathrm{d}(x,z)+O(\varepsilon)$$

for $\beta < 1/3$. The functional $\tilde{J}_0$ is the variational functional employed to find 'lump' solutions of the KP equation by de Bouard & Saut [3] or the DS system by Cipolatti [2], and critical points of $\tilde{J}_\varepsilon$ are found by correspondingly modifying the methods presented in those references. The main additional technical difficulty is that the $O(\varepsilon)$ remainder term is a superquadratic, nonlocal function of η_1, so that standard applications of methods such as concentration-compactness (for functionals whose superquadratic parts involve only differential operators) are not immediately applicable.

Acknowledgements

The results reported in this this talk are joint endeavours with Boris Buffoni (Lausanne), Mariana Haragus (Besançon) and Erik Wahlén (Lund).

References

[1] C. J. Amick & K. Kirchgässner, "A theory of solitary water waves in the presence of surface tension", Arch. Rat. Mech. Anal., vol. 105, pp. 1–49, 1989.

[2] R. Cipolatti, "On the existence of standing waves for a Devay-Stewartson system", Commun. Partial Diff. Eqns., vol. 17, pp. 967–988, 1992.

[3] A. de Bouard & J.-C. Saut, Solitary waves of generalized Kadomtsev-Petviashvili equations, Ann. Inst. Henri Poincaré Anal. Non Linéaire, vol. 14, pp. 211–236, 1997.

[4] V. D. Djordjevic & L. G. Redekopp, "On two-dimensional packets of capillary-gravity waves", J. Fluid Mech., vol. 79, pp. 703–714, 1977.

[5] M. D. Groves, "An existence theory for three-dimensional periodic travelling gravity-capillary water waves with bounded transverse profiles', Physica D, vol. 152–153, pp. 395–415, 2001.

[6] M. D. Groves, M. Haragus & S. M. Sun, "A dimension-breaking phenomenon in the theory of gravity-capillary water waves", Phil. Trans. Roy. Soc. Lond. A, vol. 360, pp. 2189–2243, 2002.

[7] M. D. Groves, S. M. Sun & E. Wahlén, "A dimension-breaking phenomenon for water waves with weak surface tension", preprint, 2014.

[8] M. D. Groves, S. M. Sun & E. Wahlén, "Periodic solitons for the elliptic-elliptic focussing Davey-Stewartson equations", preprint, 2015.

[9] G. Iooss, "Gravity and capillary-gravity periodic travelling waves for two superposed fluid layers, one being of infinite depth", J. Math. Fluid Mech., vol. 1, pp. 24–63, 1999.

[10] G. Iooss & K. Kirchgässner, "Bifurcation d'ondes solitaires en présence d'une faible tension superficielle", C. R. Acad. Sci. Paris, Sér. 1, vol. 311, pp. 265–268, 1990.

[11] B. B. Kadomtsev & V. I. Petviashvili, "On the stability of solitary waves in weakly dispersing media", Sov. Phys. Dokl., vol. 15, pp. 539–541, 1970.

[12] J. C. Luke, "A variational principle for a fluid with a free surface", J. Fluid Mech., vol. 27, pp. 395–397, 1967.

[13] M. Tajiri & Y. Murakami, "The periodic soliton resonance: solutions to the Kadomtsev-Petviashvili equation with positive dispersion", Phys. Lett. A, vol. 143, pp. 217–220, 1990.

Some new directions in the applications of time-domain boundary integral operators

Lehel Banjai[1,*]
[1]Department of Mathematics, Heriot-Watt University, Edinburgh, UK
[*]Email: l.banjai@hw.ac.uk

Abstract

The use of time-domain boundary integral equations (TDBIE) has gained in popularity in recent years due to the emergence of stable and efficient numerical methods for their discretization and due to the advances in their analysis. Consequently, the scope of their applicability has also increased. For example rigorous approaches to the construction and analysis of coupled formulations with finite element methods have appeared. Working directly in time-domain also allows the treatment of non-linear problems. This is an avenue less explored up to now, but in this paper we consider a simple acoustic scattering problem with a non-linear impedance boundary condition. We present a stability analysis of the time-discretization by convolution quadrature, discuss the implementation and extra cost compared to the linear case, and end with numerical results.

Keywords: time-domain boundary integral equations, non-linear impedance, convolution quadrature

1 Introduction

Consider the scattering problem

$$\begin{aligned} &\ddot{u}^{\mathrm{tot}} - \Delta u^{\mathrm{tot}} = 0, && \text{in } \Omega \times [0,T], \\ &\partial_\nu u^{\mathrm{tot}} = g(\dot{u}^{\mathrm{tot}}), && \text{on } \Gamma \times [0,T], \\ &u^{\mathrm{tot}}(\cdot,t) = u^{\mathrm{inc}}(\cdot,t), && \text{for } t \le 0, \text{ in } \Omega, \end{aligned} \tag{1}$$

where Ω is a bounded domain with boundary Γ, ν is the exterior normal to Γ, u^{inc} satisfies the homogeneous equation in $\mathbb{R}^n$ and $u^{\mathrm{inc}}(\cdot,t)$ is compactly supported in $\mathbb{R}^n \setminus \Omega$ for $t \le 0$. The existence and uniqueness and energy decay of solutions to this type of problem in electromagnetism has been investigated in [7] and a full FEM discretization has been investigated in [12]. The above problem can also be seen as a simplicfication of the wave equation with non-linear damping investigated in [10]. For a more complex system and for the physical background, see also the use of such non-linear boundary damping to stabilise non-linear acoustic boundary conditions [8]. Note that in [10] an extra boundary Γ_0 with homogeneous Dirichlet condition is introduced. We state the problem up to a finite time $T > 0$, so that for a sufficiently distant Γ_0 these problems are equivalent. Instead of stating the properties of g in full generality of [10], let us state the most important properties of g for the present analysis

$$xg(x) \ge 0 \quad \text{and} \quad g'(x) \ge 0.$$

Trivially, linear impedance $g(x) = x$ satisfies these conditions, but also for example

$$g(x) = x + x|x|,$$

i.e., the usual linear impedance together with a non-linear correction term. This is the non-linear impedance condition that will be used in the numerical experiments.

2 Boundary integral representation of the scattered field

As usual we will not be solving for the total field, but for the scattered field

$$u = u^{\mathrm{sc}} = u^{\mathrm{tot}} - u^{\mathrm{inc}}.$$

The scattered field satisfies zero initial conditions and the boundary condition

$$\partial_\nu u = g(\dot{u} + \dot{u}^{\mathrm{inc}}) - \partial_\nu u^{\mathrm{inc}}.$$

The scattered field can be written in terms of boundary potentials as

$$u = S(\partial_t)\varphi + \partial_t^{-1} D(\partial_t)\psi, \tag{2}$$

where $S(\partial_t)$ is the time-domain single layer potential, $D(\partial_t)$ the double layer potential, and the densities are exterior traces $\varphi = -\partial_\nu u$, $\psi = \dot{u}|_\Gamma$.

Remark 1 *Above and for the rest of the paper we make use of the convenient operational notation [11]. In this notation*

$$\left(\mathcal{K}(\partial_t)u\right)(t) = \int_0^t k(t-\tau)u(\tau)d\tau,$$

where $\mathcal{K}(s)$ is the Laplace transform of k. Here we assume

$$|\mathcal{K}(s)| \le C(\sigma)|s|^{\mu}, \quad \operatorname{Re} s > \sigma \ge 0.$$

Note that if $\mu < -1$ then $k(t)$ is a continuous function with $k(0) = 0$. Otherwise $\mathcal{K}(\partial_t)u$ is understood to be the inverse Laplace transform of $\mathcal{K}(s)(\mathscr{L}u)(s)$, where we assume that the Laplace transform of the data u is bounded as

$$|\mathscr{L}u(s)| \le C(\sigma)|s|^{-m}, \quad m > 1 + \mu.$$

If u is m-times continuously differentiable with $u(0) = u^{(1)}(0) = \cdots = u^{(m-1)}(0) = 0$, this condition is satisfied.

The rationale behind the notation can easily be seen from the simple example $\mathcal{K}(s) = s$, where the action is that of differentiation. This explains that in $S(\partial_t)$, $S(s)$ is the frequency domain single layer potential.

Differentiating in time and taking the trace of (2) gives

$$\psi = \partial_t V(\partial_t)\varphi + (K(\partial_t) + \tfrac{1}{2}I)\psi,$$

where V and K are the single and double layer boundary integral operators. Taking the normal trace of (2) and using the boundary condition gives

$$g(\psi + \dot{u}^{\mathrm{inc}}) - \partial_\nu u^{\mathrm{inc}} = (K^{\mathrm{T}}(\partial_t) - \tfrac{1}{2}I)\varphi - \partial_t^{-1} W(\partial_t)\psi,$$

where W is the usual hypersingular boundary integral operator. Combining these two equations gives the boundary integral equation to be solved

$$\begin{aligned} B(\partial_t)\begin{pmatrix}\varphi\\ \psi\end{pmatrix} + \begin{pmatrix}0 & -\frac{1}{2}I\\ \frac{1}{2}I & 0\end{pmatrix}\begin{pmatrix}\varphi\\ \psi\end{pmatrix} \\ + \begin{pmatrix}0\\ g(\psi + \dot{u}^{\mathrm{inc}})\end{pmatrix} = \begin{pmatrix}0\\ \partial_\nu u^{\mathrm{inc}}\end{pmatrix}, \end{aligned} \tag{3}$$

where $B(\partial_t)$ is the Calderón operator

$$B(\partial_t) = \begin{pmatrix}\partial_t V(\partial_t) & K(\partial_t)\\ -K^{\mathrm{T}}(\partial_t) & \partial_t^{-1} W(\partial_t)\end{pmatrix}.$$

We will need the following result expressed in the frequency domain, where we use the definition

$$B_{\mathrm{imp}}(s) = B(s) + \begin{pmatrix}0 & -\frac{1}{2}I\\ \frac{1}{2}I & 0\end{pmatrix}.$$

Lemma 2 *There exists $\beta > 0$ so that*

$$\operatorname{Re}\left\langle \begin{pmatrix}\varphi\\ \psi\end{pmatrix}, B_{imp}(s)\begin{pmatrix}\varphi\\ \psi\end{pmatrix}\right\rangle_{\Gamma} \ge \beta \min(1, |s|^2)\frac{\operatorname{Re} s}{|s|^2}\left(\|\varphi\|^2_{H^{-1/2}(\Gamma)} + \|\psi\|^2_{H^{1/2}(\Gamma)}\right)$$

for $\operatorname{Re} s > 0$ and for all $\varphi \in H^{-1/2}(\Gamma)$ and $\psi \in H^{1/2}(\Gamma)$.

Proof: The same lower bound has been proved for $B(s)$ in [5]. Since the additional operator is skew-symmetric, the result follows. □

We will also need the continuity of the operator $B_{\mathrm{imp}}(s)$ which follows from the continuity of the constituting operators

$$\begin{aligned} \|V(s)\|_{H^{1/2}(\Gamma)\leftarrow H^{-1/2}(\Gamma)} &\le C(\sigma)|s|,\\ \|K(s)\|_{H^{1/2}(\Gamma)\leftarrow H^{1/2}(\Gamma)} &\le C(\sigma)|s|^{3/2},\\ \|K^T(s)\|_{H^{-1/2}(\Gamma)\leftarrow H^{-1/2}(\Gamma)} &\le C(\sigma)|s|^{3/2},\\ \|W(s)\|_{H^{-1/2}(\Gamma)\leftarrow H^{1/2}(\Gamma)} &\le C(\sigma)|s|^{2}. \end{aligned}$$

For a proof of these facts see [2, 3] and for a table with all these properties listed see [9].

3 Time-discretization

For time-discretization we employ convolution quadrature based on an A-stable linear multistep method [11]. As this is the choice used in the numerical experiments let us fix BDF2 as our choice of linear multistep method, that has the generating function

$$\delta(\zeta) = (1 - \zeta) + \tfrac{1}{2}(1 - \zeta)^2.$$

Given a time-step $\Delta t > 0$, the convolution quadrature weights are then defined by the expansion

$$B_{\mathrm{imp}}\left(\delta(\zeta)/\Delta t\right) = \sum_{j=0}^{\infty} B_j \zeta^j.$$

Setting $t_j = j\Delta t$, the time-discretization of (3) is given by

$$\begin{aligned} \left[B_{\mathrm{imp}}(\partial_t^{\Delta t})\begin{pmatrix}\varphi\\ \psi\end{pmatrix}\right]^n + \begin{pmatrix}0\\ g(\psi_n + \dot{u}^{\mathrm{inc}}(t_n))\end{pmatrix} \\ = \begin{pmatrix}0\\ \partial_\nu u^{\mathrm{inc}}(t_n)\end{pmatrix}, \end{aligned} \tag{4}$$

where

$$\left[B_{\mathrm{imp}}(\partial_t^{\Delta t})\begin{pmatrix}\varphi\\ \psi\end{pmatrix}\right]^n = \sum_{j=0}^{n} B_{n-j}\begin{pmatrix}\varphi_j\\ \psi_j\end{pmatrix}$$

is the convolution quadrature approximation of

$$B_{\text{imp}}(\partial_t)\begin{pmatrix}\varphi\\ \psi\end{pmatrix}$$

at time $t = t_n$ and φ_n and ψ_n are approximations of φ and ψ at $t = t_n$.

Remark 3 *Here we are using the discrete operational notation [11]. Again $\mathcal{K}(s) = s$ shows the rationale behind this notation as*

$$\partial_t^{\Delta t} u(t) = \frac{\frac{3}{2}u(t) - 2u(t-\Delta t) + \frac{1}{2}u(t-2\Delta t)}{\Delta t}$$

is the second order backward difference approximation of the derivative.

4 Spatial discretization and Newton iteration

To complete the discretization we perform a spatial Galerkin discretization. This is done by approximating (φ_n, ψ_n) by functions in the space $V_h^0 \times V_h^1 \subset H^{-1/2}(\Gamma) \times H^{1/2}(\Gamma)$ where V_h^0 is the space of piecewise constant functions and V_h^1 the space of continuous, piecewise linear functions. To obtain a fully discrete system, the variational formulation (4) is tested by functions in the space $V_h^0 \times V_h^1$. This gives rise to a fully discrete system

$$\left[\mathbf{B}_{\text{imp}}(\partial_t^{\Delta t})\begin{pmatrix}\boldsymbol{\varphi}\\ \boldsymbol{\psi}\end{pmatrix}\right]^n \tag{5}$$

$$+\begin{pmatrix}0\\ P_h^1 g(\boldsymbol{\psi}_n + P_h^1 \dot{u}^{\text{inc}}(t_n))\end{pmatrix} = \begin{pmatrix}0\\ \mathbf{f}_n\end{pmatrix}, \tag{6}$$

where $\boldsymbol{\varphi}_n \in V_h^0$, $\boldsymbol{\psi}_n \in V_h^1$, P_h^1 is the L^2 projection onto V_h^1, $\mathbf{f}_n = P_h^1 \partial_\nu u^{\text{inc}}(t_n)$ and $\mathbf{B}_{\text{imp}} : V_h^0 \times V_h^1 \to V_h^0 \times V_h^1$.

To solve the non-linear system at each time-step we apply Newton's iteration where the solution of the previous time-step is used as an initial guess. Let

$$\boldsymbol{\psi}_n^0 = \boldsymbol{\psi}_{n-1}.$$

To obtain the Newton method we use the linearization

$$g(\boldsymbol{\psi}_n(x) + P_h^1 \dot{u}^{\text{inc}}(t_n, x)) \approx g(\boldsymbol{\psi}_n^k(x) + P_h^1 \dot{u}^{\text{inc}}(t_n, x)) + g'(\boldsymbol{\psi}_n^k(x) + P_h^1 \dot{u}^{\text{inc}}(t_n, x))(\boldsymbol{\psi}_n(x) - \boldsymbol{\psi}_n^k(x)).$$

Note that in our case $g(x) = x + x|x|$, $g'(x) = 1 + 2|x| \geq 0$. Substituting this linearization gives the Newton iteration

$$\mathbf{B}_0\begin{pmatrix}\boldsymbol{\varphi}_n^{k+1}\\ \boldsymbol{\psi}_n^{k+1}\end{pmatrix} + \begin{pmatrix}0\\ P_h^1 g'(\boldsymbol{\psi}_n^k + P_h^1 \dot{u}^{\text{inc}}(t_n))\boldsymbol{\psi}_n^{k+1}\end{pmatrix} = \tilde{\mathbf{F}}_n + \begin{pmatrix}0\\ \tilde{\mathbf{g}}_n^k\end{pmatrix}, \tag{7}$$

where the right-hand side is given by

$$\tilde{\mathbf{F}}_n = \begin{pmatrix}0\\ \mathbf{f}_n\end{pmatrix} + \sum_{j=0}^{n-1} \mathbf{B}_{n-j}\begin{pmatrix}\boldsymbol{\varphi}_j\\ \boldsymbol{\psi}_j\end{pmatrix}$$

and

$$\begin{aligned}\tilde{\mathbf{g}}_n^k = &- P_h^1 g(\boldsymbol{\psi}_n^k + P_h^1 \dot{u}^{\text{inc}}(t_n)) \\ &+ P_h^1 g'(\boldsymbol{\psi}_n^k + P_h^1 \dot{u}^{\text{inc}}(t_n))\boldsymbol{\psi}_n^k.\end{aligned}$$

Some comments are in order regarding the Newton iteration

- Since $\mathbf{B}_0 = \mathbf{B}_{\text{imp}}(\delta(0)/\Delta t)$, from Lemma 2 it follows that $\mathbf{B}_0$ is coercive. As $g' \geq 0$ we see that each linear system (7) is solvable.
- The expensive part of the numerical method is the computation of the history. As the history need not be recomputed, i.e., $\tilde{\mathbf{F}}_n$ is independent of k, at each iteration, the extra costs due to the Newton iteration as compared with the fully linear problem are low.

5 Stability analysis

To prove the stability of the numerical scheme we require a positivity preservation property of convolution quadrature proved in [5]. Using this and Lemma 2 we can show the following positivity result.

Lemma 4 *Let $T > 0$, then for $\sigma\Delta t > 0$ small enough and with a $\rho = e^{-\sigma\Delta t} + O(\Delta t^2)$ there exists a $\gamma > 0$ depending on T such that*

$$\begin{aligned}\sum_{n=0}^{N} \rho^{2n} \operatorname{Re}\left\langle \begin{pmatrix}\boldsymbol{\varphi}_n\\ \boldsymbol{\psi}_n\end{pmatrix}, \left[\mathbf{B}_{imp}(\partial_t^{\Delta t})\begin{pmatrix}\boldsymbol{\varphi}\\ \boldsymbol{\psi}\end{pmatrix}\right]^n \right\rangle \\ \geq \gamma \sum_{n=0}^{N} \rho^{2n} \big(\|(\partial_t^{\Delta t})^{-1}\boldsymbol{\varphi}_n\|^2_{H^{-1/2}(\Gamma)} \\ + \|(\partial_t^{\Delta t})^{-1}\boldsymbol{\psi}_n\|^2_{H^{1/2}(\Gamma)}\big),\end{aligned}$$

for any sequences of functions $\boldsymbol{\varphi_n} \in V_h^0$ and $\boldsymbol{\psi_n} \in V_h^1$ and with $N = T/\Delta t$.

We will also need continuity in the time-domain which follows directly from estimates in the frequency domain given in Section 2; for a proof see [11].

Lemma 5 *Let $\mathcal{K}(s) : X \to Y$ be a bounded linear operator between two Banach spaces, with*

$$\|\mathcal{K}(s)\|_{Y\leftarrow X} \leq C(\sigma)|s|^{\mu}, \qquad \mathrm{Re}\, s \geq \sigma > 0,$$

for some $\sigma > 0$ and $\mu > 0$. Then for $m > \mu + 1$ and any $w : [0,\infty) \to X$, m times continuously differentiable, with $w(0) = w^{(1)}(0) = \cdots = w^{(m-1)}(0) = 0$, we have

$$\| \left[\mathcal{K}(\partial_t^{\Delta t})w\right]^n \|_Y \leq C(\sigma, t_n) \int_0^{\infty} e^{-\sigma t} \|\partial_t^m w(t)\|_X dt.$$

Using the two lemmas, we can prove the following stability result for (6).

Lemma 6 *For a sufficiently smooth incident wave $\dot{u}^{inc}$, the discrete solution is bounded as*

$$\Delta t \sum_{n=0}^{N} \rho^{2n} \big(\|(\partial_t^{\Delta t})^{-1} \boldsymbol{\varphi}_n\|^2_{H^{-1/2}(\Gamma)} + \|(\partial_t^{\Delta t})^{-1} \hat{\boldsymbol{\psi}}_n\|^2_{H^{1/2}(\Gamma)} \big) \leq const,$$

where the constant depends only on u^{inc} and the final time T.

Proof: To apply Lemma 4, let $\hat{\boldsymbol{\psi}}_n = \boldsymbol{\psi}_n + P_h^1 \dot{u}^{\mathrm{inc}}(t_n)$ giving the system

$$\left[\mathbf{B}_{\mathrm{imp}}(\partial_t^{\Delta t}) \begin{pmatrix} \boldsymbol{\varphi} \\ \hat{\boldsymbol{\psi}} \end{pmatrix}\right]^n + \begin{pmatrix} 0 \\ \mathbf{g}(\hat{\boldsymbol{\psi}}_n) \end{pmatrix} = \hat{\mathbf{F}}_n, \quad (8)$$

where

$$\hat{\mathbf{F}}_n = \begin{pmatrix} 0 \\ \mathbf{f}_n \end{pmatrix} + \left[\mathbf{B}_{\mathrm{imp}}(\partial_t^{\Delta t}) \begin{pmatrix} 0 \\ P_h^1 \dot{u}^{\mathrm{inc}} \end{pmatrix}\right]^n.$$

Next we test this equation with $\begin{pmatrix} \boldsymbol{\varphi}_n \\ \hat{\boldsymbol{\psi}}_n \end{pmatrix}$, multiply by Δt and sum over n. Note that since $\mathbf{g}(\hat{\boldsymbol{\psi}}_n)$ is the L^2 projection of $g(\hat{\boldsymbol{\psi}}_n)$ and $xg(x) \geq 0$ we have that

$$\left\langle \hat{\boldsymbol{\psi}}_n, \mathbf{g}(\hat{\boldsymbol{\psi}}_n) \right\rangle \geq 0.$$

Hence applying Lemma 4

$$\Delta t \sum_{n=0}^{N} \rho^{2n} \Big(\|(\partial_t^{\Delta t})^{-1} \boldsymbol{\varphi}_n\|^2_{H^{-1/2}(\Gamma)} + \|(\partial_t^{\Delta t})^{-1} \hat{\boldsymbol{\psi}}_n\|^2_{H^{1/2}(\Gamma)} \Big) \leq \gamma^{-1} \Delta t \sum_{n=0}^{N} \rho^{2n} \left\langle \begin{pmatrix} \boldsymbol{\varphi}_n \\ \hat{\boldsymbol{\psi}}_n \end{pmatrix}, \hat{\mathbf{F}}_n \right\rangle.$$

Here we would like to complete the proof by continuity, however we have a mismatch, with the discrete integral of $\boldsymbol{\varphi}_n$ and $\hat{\boldsymbol{\psi}}_n$ present on the left but not on the right. This issue can be overcome by placing $(\partial_t^{\Delta t})^{-1}$ on the variables $\boldsymbol{\varphi}_n$ and $\hat{\boldsymbol{\psi}}_n$ and $\partial_t^{\Delta t}$ on $\hat{\mathbf{F}}_n$. The justification of this is based on an argument performed via the frequency domain, as done in the proof of Lemma 6.1 in [5]. Thus we obtain

$$\begin{aligned} &\Delta t \sum_{n=0}^{N} \rho^{2n} \left\langle \begin{pmatrix} \boldsymbol{\varphi}_n \\ \hat{\boldsymbol{\psi}}_n \end{pmatrix}, \hat{\mathbf{F}}_n \right\rangle \\ &\leq \Big[\Delta t \sum_{n=0}^{N} \rho^{2n} \big(\|(\partial_t^{\Delta t})^{-1} \boldsymbol{\varphi}_n\|^2_{H^{-1/2}(\Gamma)} \\ &+ \|(\partial_t^{\Delta t})^{-1} \hat{\boldsymbol{\psi}}_n\|^2_{H^{1/2}(\Gamma)} \big) \Big]^{1/2} \cdot \\ &\left[\Delta t \sum_{n=0}^{N} \rho^{2n} \|\partial_t^{\Delta t} \hat{\mathbf{F}}_n\|^2_{H^{-1/2}(\Gamma)\times H^{1/2}(\Gamma)} \right]^{1/2}. \end{aligned}$$

Using the continuity of $\mathbf{B}_{\mathrm{imp}}(\partial_t^{\Delta t})$ to bound $\hat{\mathbf{F}}_n$ in terms of the data, we have the result of the theorem. □

6 Numerical results

Here we report the results of a numerical experiment. We let the incident wave be a Gaussian plane wave, defined as

$$u^{\mathrm{inc}}(x,t) = p(x-t)$$

where

$$p(x) = \exp(-((x-A)/C)^2)$$

and

$$A = -2, \quad C = 1/5.$$

The domain Ω is the unit circle and the spatial and time discretizations are performed as described in the previous sections. Recall that the scattered wave solves the homogeneous wave equation in $\mathbb{R}^2 \setminus \overline{\Omega}$ with zero initial conditions and impedance boundary condition

$$\partial_\nu u = g(\dot{u} + \dot{u}^{\mathrm{inc}}) - \partial_\nu u^{\mathrm{inc}},$$

where we will compare the results of the linear impedance $g(x) = x$ with the non-linear $g(x) = x(1 + |x|)$.

In the following we have chosen $T = 4$, $N = 120$ and the size of spaces V_h^1 and V_h^0 was $M = 200$. The convolution quadrature was implemented in the recursive, time-stepping way described in [4]. The Newton method needed at

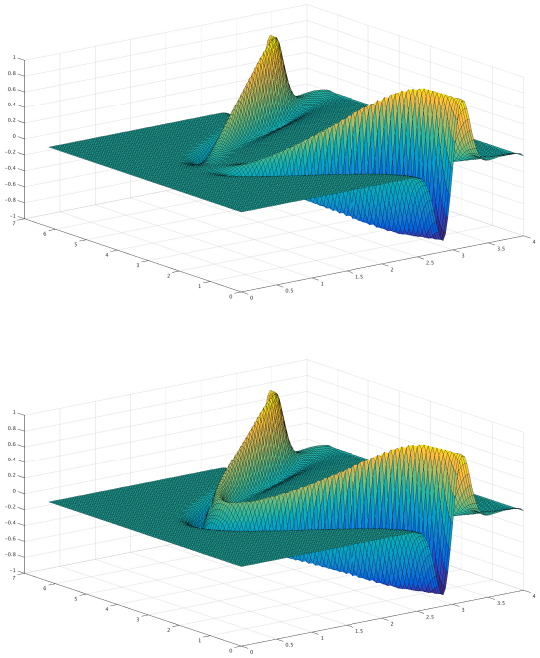

Figure 1: The density $\dot{u}^{\mathrm{sc}}|_\Gamma = \psi$ for the linear impedance on the top and for the non-linear impedance on the bottom.

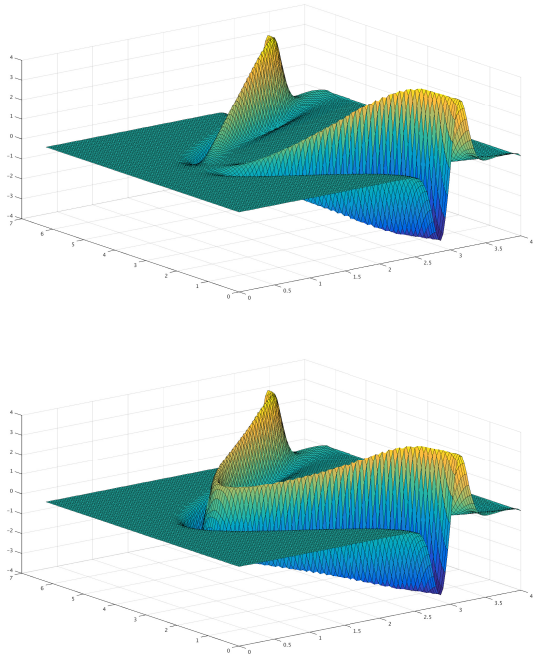

Figure 2: The density $\dot{u}^{\mathrm{sc}}|_\Gamma = \psi$ for the linear (top) and non-linear (bottom) impedance with the four times larger incident wave.

most 4 iterations to converge to a satisfactory accuracy.

In Figure 1 we compare the density of the scattered field $\dot{u}|_\Gamma = \psi$ obtained with the linear and non-linear impedance. When scaling the incident wave to $4 \times u^{\mathrm{inc}}$, the non-linear effects are clearly visible in the changein gshape of the density, see Figure 2.

7 Conclusions

Until recently time-domain boundary integral equations have mostly been used for scattering applications with Dirichlet of Neumann boundary conditions. Recently rigorous stability and convergence analysis of the coupling with finite element methods has been performed [5], see also [1]. Here we show how similar techniques can be used to further expand the applicability of TDBIE and perform rigorous stability analysis of the full discretization of a scattering problem with a non-linear impedance boundary condition. In the future the full convergence analysis will be investigated. We expect that similar techniques will also be applicable to the stabilisation of non-linear [8] or linear [6] acoustic boundary conditions and to similar systems in electromagnetism [7].

References

[1] T. Abboud, P. Joly, J. Rodríguez, and I. Terrasse. Coupling discontinuous Galerkin methods and retarded potentials for transient wave propagation on unbounded domains. *J. Comput. Phys.*, 230(15):5877–5907, 2011.

[2] A. Bamberger and T. H. Duong. Formulation variationnelle pour le calcul de la diffraction d'une onde acoustique par une surface rigide. *Math. Methods Appl. Sci.*, 8(4):598–608, 1986.

[3] A. Bamberger and T. Ha-Duong. Formulation variationelle espace-temps pour le calcul par potentiel retardé d'une onde acoustique. *Math. Meth. Appl. Sci.*, 8:405–435, 1986.

[4] L. Banjai. Multistep and multistage convolution quadrature for the wave equation: Algorithms and experiments. *SIAM J. Sci. Comput.*, 32(5):2964–2994, 2010.

[5] L. Banjai, C. Lubich, and F.-J. Sayas. Stable numerical coupling of exterior and interior problems for the wave equation. *Numer. Math.*, 129(4):611–646, 2015.

[6] J. T. Beale. Spectral properties of an acoustic boundary condition. *Indiana Univ. Math. J.*, 25(9):895–917, 1976.

[7] M. Eller, J. E. Lagnese, and S. Nicaise. Decay rates for solutions of a Maxwell system with nonlinear boundary damping. *Comput. Appl. Math.*, 21(1):135–165, 2002. Special issue in memory of Jacques-Louis Lions.

[8] P. J. Graber. Uniform boundary stabilization of a wave equation with nonlinear acoustic boundary conditions and nonlinear boundary damping. *J. Evol. Equ.*, 12(1):141–164, 2012.

[9] A. R. Laliena and F.-J. Sayas. Theoretical aspects of the application of convolution quadrature to scattering of acoustic waves. *Numer. Math.*, 112(4):637–678, 2009.

[10] I. Lasiecka and D. Tataru. Uniform boundary stabilization of semilinear wave equations with nonlinear boundary damping. *Differential Integral Equations*, 6(3):507–533, 1993.

[11] C. Lubich. On the multistep time discretization of linear initial-boundary value problems and their boundary integral equations. *Numer. Math.*, 67:365–389, 1994.

[12] M. Slodička and S. Durand. Fully discrete finite element scheme for Maxwell's equations with non-linear boundary condition. *J. Math. Anal. Appl.*, 375(1):230–244, 2011.

Topologically protected states in 2D continuous honeycomb structures

C.L. Fefferman[1], J. P. Lee-Thorp[2], Michael I. Weinstein[3,*]

[1]Department of Mathematics, Princeton University, Princeton, NJ USA
[2] Department of Applied Physics & Applied Mathematics, Columbia University, NY, NY USA
[3]Department of Applied Physics & Applied Mathematics, and Department of Mathematics, Columbia University, NY, NY USA

*Email: miw2103@columbia.edu

Abstract

An edge state is a time-harmonic solution of a conservative wave system, *e.g.* Schrödinger, Maxwell, which is propagating (plane-wave-like) parallel to, and localized transverse to, a line-defect or "edge". Topologically protected edge states are edge states which are stable against spatially localized (even strong) deformations of the edge. A theoretical understanding of topological protection has mainly come from discrete (tight-binding) models and direct numerical simulation. In this paper we consider a rich family of continuum PDE models for which we rigorously study regimes where topologically protected edge states exist.

Our model is a class of Schrödinger operators on $\mathbb{R}^2$ with a background two-dimensional honeycomb potential perturbed by an "edge-potential". The edge potential is a domain-wall interpolation, transverse to a prescribed "rational" edge, between distinct periodic structures. General conditions are given for the bifurcation of a branch of topologically protected edge states from *Dirac points* of the background honeycomb structure. The bifurcation is seeded by the zero mode of a one-dimensional effective Dirac operator. A key condition is a spectral no-fold condition for the prescribed edge.

We use this general result to prove the existence of topologically protected edge states along zigzag edges of certain honeycomb structures. Our results are consistent with the physics literature and appear to be the first rigorous results on the existence of topologically protected edge states for continuum 2D PDE systems. We also show that the Hamiltonians we study contain cases where zigzag edge states exist, but which are not topologically protected.

Keywords: Edge state, topological insulator, Schrödinger operator, Dirac operator

1 Introduction

Wave transport in periodic structures with honeycomb symmetry has been an area of intense activity catalyzed by the study of graphene, a single atomic layer two-dimensional honeycomb structure of carbon atoms [1]. The remarkable electronic properties exhibited by graphene have inspired the study of waves in general honeycomb structures or "artificial graphene" in other contexts. One such property, observed in electronic and photonic systems with honeycomb symmetry is the existence of topologically protected *edge states*. Edge states are (i) pseudo-periodic (plane-wave-like or propagating) parallel to a line-defect, and (ii) localized transverse to the line-defect. *Topological protection*, refers to the persistence of these states and their properties, even when the line-defect is subjected to strong local or random perturbations. In applications, edge states are of great interest due to their potential as robust vehicles for channeling energy.

There is an extensive physics literature which explores edge states, in the context of approximate tight-binding (discrete) models or by numerical simulations. First studied in the context of the quantum Hall effect [2,3], protected edge states have attracted huge interest due to their role in the field of topological insulators [4, 5]. The proposed realization of analogous states in the photonic setting was made in [6,7], and studied extensively in linear and nonlinear photonics in [8–11].

We are interested in exploring these phenomena in general energy-conserving wave equations in continuous media. We consider the case of the Schrödinger equation on $\mathbb{R}^2$, $i\partial_t\psi = H\psi$, and study the existence and robustness of edge states of time-harmonic form: $\psi = e^{-iEt}\Psi$. Our model consists of a honeycomb background potential, the "bulk" structure, and a perturbing "edge-potential". The edge-potential inter-

polates between two distinct asymptotic periodic structures, via a *domain wall* which varies transverse to a given line-defect ("edge"). In the context of honeycomb structures, the most frequently studied edges are the "zigzag" and "armchair" edges; see Figure 1. In the context of tight-binding models of graphene, edge states have been shown to localize on zigzag edges but not on armchair edges.

Our goal is to clarify the underlying mechanisms for the existence of topologically protected edge states. Our model of an edge, which breaks spatial inversion symmetry, is motivated by [6, 7], where a domain wall is used to break time-reversal symmetry. In [12, 13] we proved that a one-dimensional variant of such edge-potentials gives rise to topologically protected edge states in periodic structures with symmetry-induced linear band crossings, the analogue in one space dimension of Dirac points (see below). We explore a photonic realization of such states in coupled waveguide arrays in [14].

2 Honeycombs, Dirac points and Edge states

Let $\Lambda_h = \mathbb{Z}\mathbf{v}_1 \oplus \mathbb{Z}\mathbf{v}_2$ denote the regular (equilateral) triangular lattice and $\Lambda_h^* = \mathbb{Z}\mathbf{k}_1 \oplus \mathbb{Z}\mathbf{k}_2$ denote the associated dual lattice, with relations $\mathbf{k}_l \cdot \mathbf{v}_m = 2\pi\delta_{lm}$, $l, m = 1, 2$. The honeycomb structure, $\mathbf{H}$, is the union of two interpenetrating triangular lattices: $\mathbf{A} + \Lambda_h$ and $\mathbf{B} + \Lambda_h$. A *honeycomb lattice potential*, $V(\mathbf{x})$, is a real-valued, smooth function, which is Λ_h- periodic and, relative to some origin of coordinates, inversion symmetric (even) and invariant under a $2\pi/3$ rotation. We take the period cell to be Ω_h, the parallelogram spanned by $\{\mathbf{v}_1, \mathbf{v}_2\}$.

We begin with the Hamiltonian for the unperturbed honeycomb structure: $H^{(0)} = -\Delta + V(\mathbf{x})$. The *band structure* of $H^{(0)}$ is obtained from the family Floquet - Bloch eigenvalue problems, parametrized by $\mathbf{k} \in \mathcal{B}_h$, the Brillouin zone: $(H^{(0)} - E)\Psi = 0$, $\Psi(\mathbf{x}+\mathbf{v}) = e^{i\mathbf{k}\cdot\mathbf{v}}\Psi(\mathbf{x})$, $\mathbf{x} \in \mathbb{R}^2$, $\mathbf{v} \in \Lambda_h$. Equivalently, $\psi = e^{-i\mathbf{k}\cdot\mathbf{x}}\Psi$, satisfies the periodic eigenvalue problem: $\left(H^{(0)}(\mathbf{k}) - E(\mathbf{k})\right)\psi = 0$ and $\psi(\mathbf{x}+\mathbf{v}) = \psi(\mathbf{x})$, where $H^{(0)}(\mathbf{k}) = -(\nabla + i\mathbf{k})^2 + V(\mathbf{x})$. For each $\mathbf{k} \in \mathcal{B}_h$, the spectrum is real and consists of discrete eigenvalues $E_b(\mathbf{k})$, $b \geq 1$, where $E_b(\mathbf{k}) \leq E_{b+1}(\mathbf{k})$. The maps $\mathbf{k} \mapsto E_b(\mathbf{k}) \in \mathbb{R}$ define the dispersion surfaces of $H^{(0)}$. The collection of these surfaces constitutes the *band structure* of $H^{(0)}$. As $\mathbf{k}$ varies over $\mathcal{B}_h$, each map $\mathbf{k} \to E_b(\mathbf{k})$ sweeps out a closed interval in $\mathbb{R}$. The union of these intervals is the $L^2(\mathbb{R}^2)-$ spectrum of $H^{(0)}$.

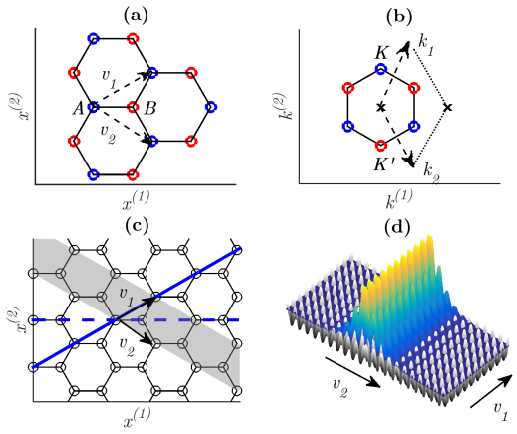

Figure 1: **(a)**: $\mathbf{A} = (0,0)$, $\mathbf{B} = (\frac{1}{\sqrt{3}}, 0)$. The honeycomb structure, $\mathbf{H}$ is the union of two sub-lattices $\Lambda_\mathbf{A} = \mathbf{A} + \Lambda_h$ (blue) and $\Lambda_\mathbf{B} = \mathbf{B} + \Lambda_h$ (red). The lattice vectors $\{\mathbf{v}_1, \mathbf{v}_2\}$ generate Λ_h. **(b)**: Brillouin zone, $\mathcal{B}_h$, and dual basis $\{\mathbf{k}_1, \mathbf{k}_2\}$. $\mathbf{K}$ and $\mathbf{K}'$ are labeled. Other vertices of $\mathcal{B}_h$ are obtained via application of R, rotation by $2\pi/3$. **(c)**: Zigzag edge (solid line), $\mathbb{R}\mathbf{v}_1 = \{\mathbf{x} : \mathbf{k}_2 \cdot \mathbf{x} = 0\}$, armchair edge (dashed line), $\mathbb{R}(\mathbf{v}_1 + \mathbf{v}_2) = \{\mathbf{x} : (\mathbf{k}_1 - \mathbf{k}_2) \cdot \mathbf{x} = 0\}$, and cylinder for the zigzag edge (gray area) are indicated. **(d)**: Edge state propagating parallel to a zigzag edge ($\mathbb{R}\mathbf{v}_1$).

A central role is played by *Dirac points* of $H^{(0)}$. These are quasi-momentum / energy pairs, $(\mathbf{K}_\star, E_\star)$, in the band structure of $H^{(0)}$ at which neighboring dispersion surfaces touch conically at a point [1, 15]. The existence of Dirac points, located at the six vertices of the Brillouin zone, $\mathcal{B}_h$ (regular hexagonal dual cell) for generic honeycomb structures was proved in [15]; see also [13]. The quasi-momenta of Dirac points partition into two equivalence classes; the $\mathbf{K}-$ points consisting of $\mathbf{K}, R\mathbf{K}$ and $R^2\mathbf{K}$, where R is a rotation by $2\pi/3$ and $\mathbf{K}'-$ points consisting of $\mathbf{K}' = -\mathbf{K}, R\mathbf{K}'$ and $R^2\mathbf{K}'$. The time evolution of a wavepacket, with data spectrally localized near a Dirac point, is governed by a massless two-dimensional Dirac system [16].

Associated with the Dirac point $(\mathbf{K}_\star, E_\star)$ is a two-dimensional eigenspace of $\mathbf{K}_\star-$ pseudo-periodic states, $\text{span}\{\Phi_1, \Phi_2\}$: $H^{(0)}\Phi_j = E_\star\Phi_j$, $j = 1, 2$, where $\Phi_j(\mathbf{x}+\mathbf{v}) = e^{i\mathbf{K}_\star\cdot\mathbf{v}}\Phi_j(\mathbf{x})$, $\mathbf{v} \in \Lambda_h$. It is also shown in [15] that a Λ_h- periodic perturbation of $V(\mathbf{x})$, which breaks inversion or time-reversal symmetry lifts the eigenvalue degeneracy; a (local) gap is opened about

the Dirac points and the perturbed dispersion surfaces are locally smooth. The perturbation of $H^{(0)}$ by an edge potential (see (1)) takes advantage of this instability of Dirac points with symmetry breaking perturbations.

To construct our Hamiltonian, perturbed by an edge-potential, we first choose a vector $\mathfrak{v}_1 \in \Lambda_h$, the period lattice, and designate the line $\mathbb{R}\mathfrak{v}_1$ as the "edge". Choose $\mathfrak{v}_2$ such that $\Lambda_h = \mathbb{Z}\mathfrak{v}_1 \oplus \mathbb{Z}\mathfrak{v}_2$. Also introduce dual basis vectors, $\mathfrak{K}_1$ and $\mathfrak{K}_2$, satisfying $\mathfrak{K}_l \cdot \mathfrak{v}_m = 2\pi\delta_{lm},\ l,m = 1,2$. The choice $\mathfrak{v}_1 = \mathbf{v}_1$ is a *zigzag edge*. Introduce the perturbed Hamiltonian:

$$H^{(\delta)} \equiv -\Delta + V(\mathbf{x}) + \delta\kappa(\delta\mathfrak{K}_2 \cdot \mathbf{x})W(\mathbf{x}). \quad (1)$$

Here, δ is real and will be taken to be sufficiently small, and $W(\mathbf{x})$ is Λ_h- periodic and odd. The function κ, defines a *domain wall*. We choose κ to be sufficiently smooth and to satisfy $\kappa(0) = 0$ and $\kappa(\zeta) \to \pm\kappa_\infty \neq 0$ as $\zeta \to \pm\infty$. Without loss of generality, we assume $\kappa_\infty > 0$, *e.g.* $\kappa(\zeta) = \tanh(\zeta)$. We refer to the line $\mathbb{R}\mathfrak{v}_1$ as a $\mathfrak{v}_1-$ edge.

Note that $H^{(\delta)}$ is invariant under translations parallel to the $\mathfrak{v}_1-$ edge, $\mathbf{x} \mapsto \mathbf{x} + \mathfrak{v}_1$, and hence there is a well-defined *parallel quasi-momentum*, denoted $k_\parallel$. $H^{(\delta)}$ transitions adiabatically between asymptotic Hamiltonians $H^{(\delta)}_\pm = H^{(0)} \pm \delta\kappa_\infty W(\mathbf{x})$ as $\mathfrak{K}_2 \cdot \mathbf{x} \to \pm\infty$.

Suppose $H^{(0)}$ has a Dirac point at $(\mathbf{K}_\star, E_\star)$. While $H^{(0)}$ is inversion symmetric, $H^{(\delta)}_\pm$ is not. For $\delta \neq 0$, $H^{(\delta)}_\pm$ does not have Dirac points; its dispersion surfaces are locally smooth and for quasi-momenta $\mathbf{k}$ such that if $|\mathbf{k} - \mathbf{K}_\star|$ is sufficiently small, there is an open neighborhood of $E_\star$ not contained in the $L^2(\mathbb{R}^2/\Lambda_h)-$ spectrum of $H^{(\delta)}_\pm(\mathbf{k})$. This "spectral gap" about $E = E_\star$ may however only be local about $\mathbf{K}_\star$ [15]. If there is a real open neighborhood of $E_\star$, not contained in the spectrum of $H^{(\delta)}_\pm(\mathbf{k}) = -(\nabla + i\mathbf{k})^2 + V \pm \delta\kappa_\infty W$ for *all* $\mathbf{k} \in \mathcal{B}_h$, then $H^{(\delta)}_\pm$ is said to have a (global) omni-directional spectral gap about $E = E_\star$. However it is a "directional spectral gap" (stated in terms of the spectral no-fold hypothesis of Theorem 1) that plays a key role in the existence of edge states.

To formulate the eigenvalue problem in an appropriate Hilbert space, we introduce the cylinder $\Sigma \equiv \mathbb{R}^2/\mathbb{Z}\mathfrak{v}_1$. If $f(\mathbf{x})$ satisfies the pseudo-periodic boundary condition, then $f(\mathbf{x})e^{-i\frac{k_\parallel}{2\pi}\mathfrak{K}_1\cdot\mathbf{x}}$ is well-defined on the cylinder Σ. Denote by $H^s(\Sigma),\ s \geq 0$, the Sobolev spaces of functions defined on Σ. The pseudo-periodicity and decay conditions are encoded by requiring $\Psi \in H^s_{k_\parallel}(\Sigma)$, for some $s \geq 0$, where $H^s_{k_\parallel}(\Sigma)$ consists of f such that $f(\mathbf{x})e^{-i\frac{k_\parallel}{2\pi}\mathfrak{K}_1\cdot\mathbf{x}}$ belongs to $H^s(\Sigma)$.
The edge state eigenvalue problem: Find non-trivial pairs solutions of

$$H^{(\delta)}\Psi = E\Psi, \quad \Psi \in H^2_{k_\parallel}(\Sigma). \quad (2)$$

We next summarize the results of [17].

3 Theorem 1: General conditions for the existence of topologically protected edge states

We formulate hypotheses on the honeycomb potential, $V(\mathbf{x})$, domain wall function, $\kappa(\zeta)$, and asymptotic periodic structure, $W(\mathbf{x})$, which imply the existence of topologically protected $\mathfrak{v}_1-$ edge states, constructed as non-trivial eigenpairs $\delta \mapsto (\Psi^\delta, E^\delta)$ of (2) with $k_\parallel = \mathbf{K}\cdot\mathfrak{v}_1$, defined for all $|\delta|$ sufficiently small. This branch of non-trivial states bifurcates from the trivial solution branch $E \mapsto (\Psi \equiv 0, E)$ at $E = E_\star$. Key among the hypotheses is the *spectral no-fold condition*. At leading order in δ, the edge state, $\Psi^\delta(\mathbf{x})$, is a slow modulation of the degenerate nullspace of $H^{(0)} - E_\star$:

$$\Psi^\delta(\mathbf{x}) \approx \alpha_{\star,+}(\delta\mathfrak{K}_2\cdot\mathbf{x})\Phi_+(\mathbf{x}) + \alpha_{\star,-}(\delta\mathfrak{K}_2\cdot\mathbf{x})\Phi_-(\mathbf{x}),$$
$$E^\delta = E_\star + \mathcal{O}(\delta^2), \quad 0 < |\delta| \ll 1,$$

where $\{\Phi_+, \Phi_-\}$ is an appropriately chosen basis for the kernel of $H^{(0)} - E_\star$. The envelope amplitude-vector, $\alpha_\star(\zeta) = (\alpha_{\star,+}(\zeta), \alpha_{\star,-}(\zeta))^T$, is a zero-energy eigenstate, $\mathcal{D}\alpha_\star = 0$, of the one-dimensional Dirac operator:

$$\mathcal{D} \equiv -i|\lambda_\sharp||\mathfrak{K}_2|\sigma_3\partial_\zeta + \vartheta_\sharp\kappa(\zeta)\sigma_1,$$

where the Pauli matrices σ_j. Here $\lambda_\sharp \in \mathbb{C}$ depends on the unperturbed honeycomb potential, V, and is non-zero for generic V. The constant $\vartheta_\sharp \equiv \langle\Phi_1, W\Phi_1\rangle_{L^2(\Omega_h)}$ is real and is also generically nonzero. $\mathcal{D}$ has a spatially localized zero-energy eigenstate for any $\kappa(\zeta)$ having asymptotic limits of opposite sign at $\pm\infty$. Hence, the zero-energy eigenstate, which seeds the bifurcation, persists for *localized* perturbations of $\kappa(\zeta)$. In this sense, the bifurcating branch of edge states is topologically protected against a class of local perturbations of the edge.

A Corollary of Theorem 1, is the existence of edge states, $\Psi(\mathbf{x};k_\parallel) \in H^2_{k_\parallel}(\Sigma)$ for all $k_\parallel$ in a neighborhood of $k_\parallel = \mathbf{K}\cdot\mathfrak{v}_1$, and by symmetry for all $k_\parallel$ in a neighborhood of $k_\parallel = -\mathbf{K}\cdot\mathfrak{v}_1 = \mathbf{K}'\cdot\mathfrak{v}_1$. It follows that by taking a continuous superposition of these states, one obtains time-dependent states that remain localized about (and dispersing along) the edge for all time.

4 Theorem 2: Existence of topologically protected zigzag edge states

We consider the eigenvalue problem for zigzag edges: $\mathfrak{v}_1 = \mathbf{v}_1$, $\mathfrak{v}_2 = \mathbf{v}_2$, and $\mathfrak{K}_1 = \mathbf{k}_1$, $\mathfrak{K}_2 = \mathbf{k}_2$.

$$H^{(\varepsilon,\delta)}\Psi = E\Psi, \quad \Psi \in H^2_{k_\parallel}(\Sigma) \tag{3}$$
$$H^{(\varepsilon,\delta)} \equiv -\Delta + \varepsilon V(\mathbf{x}) + \delta\kappa(\delta\mathbf{k}_2\cdot\mathbf{x})W(\mathbf{x}).$$

Here, ε and δ are chosen to satisfy

$$0 < |\delta| \lesssim \varepsilon^2 \ll 1. \tag{4}$$

There are two cases, which are delineated by the sign of the distinguished Fourier coefficient, $\varepsilon V_{1,1}$, of the unperturbed (bulk) honeycomb potential, $\varepsilon V(\mathbf{x})$. Here,

$$V_{1,1} \equiv \frac{1}{|\Omega_h|}\int_{\Omega_h} e^{-i(\mathbf{k}_1+\mathbf{k}_2)\cdot\mathbf{y}}\, V(\mathbf{y})\, d\mathbf{y},$$

is assumed to be non-zero. We designate these: **Case (1)** $\varepsilon V_{1,1} > 0$ and **Case (2)** $\varepsilon V_{1,1} < 0$. Explicit families of honeycomb potentials are displayed which can be tuned between Cases 1 and 2, by variation of a lattice scale parameter.

Under the conditions $\varepsilon V_{1,1} > 0$ (Case (1)) and (4), we verify the spectral no-fold condition for the zigzag edge. The existence of zigzag edge states then follows from Theorem 1 and the Corollary. In particular, for all ε and δ satisfying (4) and for each $k_\parallel$ near $\mathbf{K}\cdot\mathbf{v}_1 = 2\pi/3$, the zigzag edge state eigenvalue problem (2) has topologically protected edge states with energies sweeping out a neighborhood of $E^\varepsilon_\star$, where $(\mathbf{K}, E^\varepsilon_\star)$ is a Dirac point. Figures 2 and 3 are illustrative of Cases (1) and (2). Figure 2 displays, for fixed ε, the $L^2_{k_\parallel=2\pi/3}(\Sigma)-$ spectra of $H^{(\varepsilon,\delta)}$ corresponding to a range of δ values (strength / scale of domain wall -perturbation) for Cases (1) $\varepsilon V_{1,1} > 0$ (top panel) and (2) $\varepsilon V_{1,1} < 0$ (middle and bottom panels). Figure 3 displays the $L^2_{k_\parallel}(\Sigma)-$ spectra (plotted vertically) for a range of $k_\parallel$ with δ and ε held fixed.

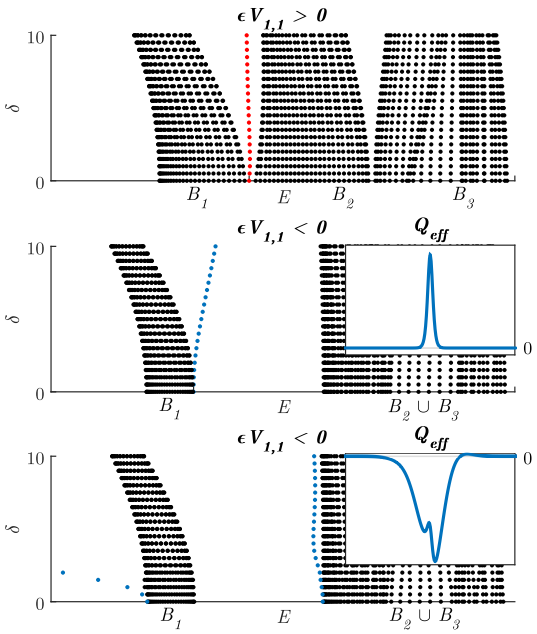

Figure 2: $L^2_{k_\parallel=\mathbf{K}\cdot\mathbf{v}_1}(\Sigma)-$ spectra ($\mathbf{K}\cdot\mathbf{v}_1 = \frac{2}{3}\pi$) of $H^{(\varepsilon,\delta)}$ for the zigzag edge ($\mathbb{R}\mathbf{v}_1$). **Top panel:** Case (1) $\varepsilon V_{1,1} > 0$. Topologically protected bifurcation of edge states, described by Theorem 1 (dotted red curve). The branch of edge states emanates from intersection of first and second bands (B_1 and B_2) at $E = E^\varepsilon_\star$ for $\delta = 0$. **Middle panel:** Case (2) $\varepsilon V_{1,1} < 0$. Spectral no-fold condition does not hold. Bifurcation of zigzag edge states from upper endpoint, $E = \widetilde{E}^\varepsilon$, of the first spectral band. Bifurcation is seeded by bound state of a Schrödinger operator with effective mass $m_{\text{eff}} < 0$ and effective potential $Q_{\text{eff}}(\zeta)$ shown in the inset; bifurcation is *not* topologically protected. **Bottom panel:** Case (2) $\varepsilon V_{1,1} < 0$ with domain wall function $\kappa_\natural$, a localized perturbation of κ, for which the edge state bifurcation from upper endpoint of B_1 (middle panel) is destroyed. Non-protected bifurcations of edge states arise from left endpoints of B_1 and B_2, at which $m_{\text{eff}} > 0$.

In Case (2), where $\varepsilon V_{1,1} < 0$, we do not obtain a bifurcation from the Dirac point. However, we find branches of edge states emanating from the endpoints of spectral band edges. These states are not topologically protected; they are destroyed by appropriate localized perturbations of the edge.

Acknowledgements: This work was supported in part by US NSF grants DMS-1265524 (CF), DMS-1412560, Columbia IGERT DGE-1069420 (JPL-T, MIW), and by a grant from the Simons Foundation (#376319, MIW).

References

[1] A. H. Castro Neto and F. Guinea and N. M. R. Peres and K. S. Novoselov and

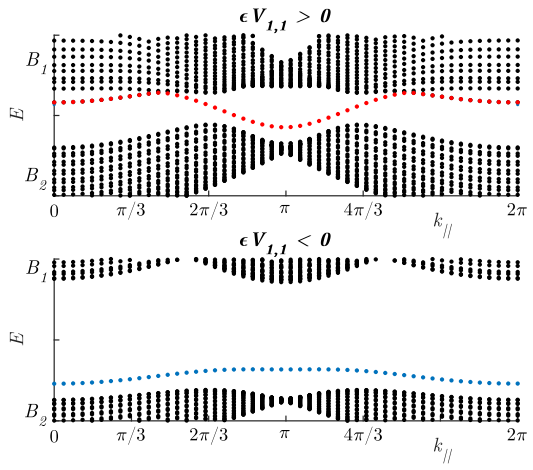

Figure 3: $L^2_{k_\parallel}(\Sigma)-$ spectrum of $H^{(\varepsilon,\delta)}$, for the cases $\varepsilon V_{1,1} > 0$ (**top panel**) and $\varepsilon V_{1,1} < 0$ (**bottom panel**).

A. K. Geim, *The electronic properties of graphene*, Rev. of Mod. Phys. **81** (2009).

[2] B.I. Halperin, *Quantized Hall conductance, current-carrying edge states, and the existence of extended states in a two-dimensional disordered potential*, Phys. Rev. B, **25** 4 (1982) 2185–2190.

[3] X.-G. Wen, *Gapless boundary excitations in the quantum Hall states and in the chiral spin states*, Phys. Rev. B **43** 13 (1991).

[4] C. L. Kane and E. J. Mele, $\mathbb{Z}_2$ *topological order and the quantum spin Hall effect*, Phys. Rev. Lett. **95** (2005) 146802.

[5] J.-M. Graf and M. Porta *Bulk-edge correspondence for two-dimensional topological insulators*, Comm. Math. Phys. **324** 3 (2012) 851-895.

[6] S. Raghu and F. D. M. Haldane, *Analogs of quantum-Hall-effect edge states in photonic crystals*, Phys. Rev. A **78** 3 (2008) 033834.

[7] F. D. M. Haldane, S. Raghu, *Possible realization of directional optical waveguides in photonic crystals with broken time-reversal symmetry*, Phys. Rev. Lett. **100** 1 (2008).

[8] Z. Wang, Y.D. Chong, J. D. Joannopoulos and M. Soljacic, *Reflection-Free One-Way Edge Modes in a Gyromagnetic Photonic Crystal*, Phys. Rev. Lett., **100** (2008) 013905.

[9] Yu, Z. and Veronis, G. and Wang, Z. and Fan, S., *One-Way Electromagnetic Waveguide Formed at the Interface between a Plasmonic Metal under a Static Magnetic Field and a Photonic Crystal*, Phys. Rev. Lett. **100** 2008 023902.

[10] M. C. Rechstman, J. M. Zeuner, Y. Plotnik, Y. Lumer, D. Podolsky, F. Dreisow, S. Nolte, M. Segev and A. Szameit, *Photonic Floquet topological insulators*, Nature **496** (2013) 196.

[11] T. Ma, A.B. Khanikaev, S.H. Mousavi and G. Shvets *Topologically protected photonic transport in bi-anisotropic metawaveguide*, Nature Materials **12** 2013.

[12] C.L. Fefferman, J.P. Lee-Thorp and M.I. Weinstein, *Topologically protected states in one-dimensional continuous systems and Dirac points*, Proceedings of the National Academy of Sciences (2014) 07391.

[13] C.L. Fefferman, J. P. Lee-Thorp and M.I. Weinstein, *Topologically Protected States in One-Dimensional Systems*, Memoirs of the American Mathematical Society, to appear. http://arxiv.org/abs/1405.4569

[14] J. P. Lee-Thorp, I. Vukićević, X. Xu, J. Yang, C. L. Fefferman, C. W. Wong and M. I. Weinstein, *Photonic realization of topologically protected bound states in domain wall modulated waveguide arrays*, submitted.

[15] C. L. Fefferman and M. I. Weinstein, *Honeycomb Lattice Potentials and Dirac Points*, J. Amer. Math. Soc., **25** 4 1169-1220. 2012

[16] C. L. Fefferman and M. I. Weinstein, *Wave Packets in Honeycomb Lattice Structures and Two-Dimensional Dirac Equations* Comm. Math. Phys. **326** (2014) 251–286.

[17] C.L. Fefferman, J. P. Lee-Thorp and M.I. Weinstein, *Edge states in honeycomb structures*, http://arxiv.org/abs/1506.06111.

Transparent boundary conditions for complex media

Sonia Fliss[1]
[1]POEMS, UMR CNRS-ENSTA Paristech-INRIA, Palaiseau, France

Abstract

We are interested in acoustic or elastic wave propagation in time harmonic regime in a two-dimensional medium which is a local perturbation of an infinite anisotropic homogeneous and/or periodic medium. We investigate the question of finding artificial boundary conditions to reduce the numerical computations to a neighborhood of this perturbation. This question is difficult due to the anisotropy and/or the periodicity of the surrounding medium. Our approach consists in coupling several semi-analytical representations of the solution in half-planes surrounding the defect with a FE computation of the solution around the defect. The difficulty is to ensure that all these representations match, in particular in the infinite intersections of the half-planes. It leads to a formulation which couples, via integral operators, the solution in a bounded domain including the defect and its traces on the edge of the half-planes.

Keywords: Transparent boundary conditions, acoustics and elasticity, periodic media

This work is the result of various collaborations with Anne-Sophie Bonnet-Ben Dhia, Julien Coatléven, Patrick Joly and Antoine Tonnoir.

1 Introduction

We consider in this talk a 2D ($\mathbf{x} = (x_1, x_2)$) anisotropic scalar acoustic model

$$\left| \begin{array}{l} \text{Find } u \in H^1(\Omega), \\ -\text{div}(\mathbb{A}\nabla u) - \omega_\varepsilon^2\, \rho\, u = f \quad \text{in } \Omega \end{array} \right. \tag{1}$$

in time-harmonic regime with a small absorption, $\text{Im}(\omega_\varepsilon^2) = \varepsilon > 0$, where $\mathbb{A}$ is a symmetric, positive definite matrix of $(L^\infty(\Omega))^{2\times 2}$ and ρ is a strictly positive function of $L^\infty(\Omega)$.

The domain of propagation Ω is $\mathbb{R}^2$ and the support of the source term is supposed to be compact and strictly included in a bounded region denoted $\Omega_a =]-a, a[^2$ with $a > 0$ (geometrical defects included in Ω_a can also be considered, boundary conditions have to be added to the model). We will consider two situations:

(I) Outside Ω_a, the matrix $\mathbb{A}$ and the coefficient ρ are constant (independent of the space variables). This problem is studied in Section 3.

(II) Outside Ω_a, the matrix $\mathbb{A}$ and the coefficient ρ are (L_1, L_2)-periodic in the two directions. Without loss of generality, we will suppose that $L_x = L_y = 1$. This problem is studied in Section 4.

Our objective is to propose an original numerical method to compute the solution for these two situations. A motivation, in particular for the case (I), is to derive a method for the computation of the solution of the time harmonic anisotropic elastic problem:

$$\left| \begin{array}{l} \text{Find } \mathbf{u} \in H^1(\Omega)^2, \\ -\text{div}\, \sigma(\mathbf{u}) - \omega_\varepsilon^2\, \rho\, \mathbf{u} = \mathbf{f} \quad \text{in } \Omega \end{array} \right.$$

where $\sigma(\mathbf{u})$ is the stress tensor, related to the strain tensor $\epsilon(\mathbf{u}) = 1/2(\nabla\,\mathbf{u} + \nabla^T\,\mathbf{u})$ by Hooke's law : $\sigma(\mathbf{u}) = \mathbb{C} : \epsilon(\mathbf{u})$, $\mathbb{C}$ being the 4th-order elasticity tensor and ρ the mass density.

A natural idea is to reduce the pure numerical computations around the perturbation and try to take advantage of the structure of the medium outside the perturbation. In the case where the surrounding media is homogeneous (Case I), this is a very old problematic and various methods can be used. A first class of methods consists in applying an artificial boundary condition which is transparent or approximately transparent as in: (1) integral equation techniques [1], (2) Dirichlet-to-Neumann (DtN) approaches providing that the boundary is properly chosen to allow separation of variables and (3) local radiation conditions at finite distance [2] constructed as local approximations at various orders of the exact non local condition. However, none of these methods can be applied or extended directly to general exterior periodic media since they use the homogeneous nature of the exterior medium (explicit formulas are used for the Green function or more generally

for the solution of exterior problems). For elasticity problems, when the medium is isotropic, all the methods can be extended [3] – it suffices to use the Helmholtz decomposition of the solution in terms of potential. However when the medium is anisotropic, the extension of these methods is difficult – the computation of the Green tensor is much more costly since the tensor depends not only on the distance between two points but also on the orientation [4] – or impossible – the separation of variables technique does not work anymore to determine the DtN operator.

A second class of methods consists in surrounding the computational domain by an absorbing layer in which the PML technique is applied. Roughly speaking, the PML absorbs the waves with outgoing phase velocity, preventing them to come back in the computational domain, while, in order to catch the physical solution, it should absorb the waves with outgoing group velocities. That is why, in our knowledge, the standard PML technique cannot work for periodic media or anisotropic elasticity where these two velocities differ. In the same spirit, there also exist pole condition techniques [6] that have been extended recently to anisotropic elastic problem but not yet to periodic media.

By contrast, our method can cover all the aforementioned cases. It is based on a simple idea: the solution of –homogeneous or periodic– halfspace problems can be expressed thanks to its trace on the boundary. As several halfspaces surrounding the perturbations are needed to recover the whole domain, they will necessarily overlap. The difficulty is then to find conditions to ensure the compatibility of the representations in the overlapping zones. This method have links with domain decomposition methods with overlap [7], with the specific difficulty that here the overlapping zones are unbounded. For the two cases (I) and (II), the framework of our method is the same and it is described in the next section. Even if the next section may seem technical because of the big amount of notations, the ideas are really simple so never say die! Besides the tools for the two cases differs : the Fourier Transform (FT) is used to solve halfspace problems for the homogeneous case (see Section 3) and analytical representations are derived, whereas the Floquet Bloch Transform (FBT) is used for the periodic case (see Section 4) and only semi-analytical representations are derived. Moreover, the analysis is complete for the homogeneous case and still raises open questions for the periodic case.

2 Description of the method

Let us introduce some notations (see Figure 1) for $b \geq a$

$$\left|\begin{array}{l} \Omega_a =]-a,a[^2 \text{ and } \Sigma_a^{\pm,j} = \partial\Omega_a \cap \{x_j = \pm a\} \\ \Omega_b =]-b,b[^2 \text{ and } \Sigma_b^{\pm,j} = \partial\Omega_b \cap \{x_j = \pm b\} \\ \Omega_H^{\pm,j} = \{(x_1,x_2) \in \Omega,\ \pm x_j \geq a\} \text{ and } \Sigma_H^{\pm,j} = \partial\Omega_H^{\pm,j} \end{array}\right.$$

It is quite obvious to see that if u is solution

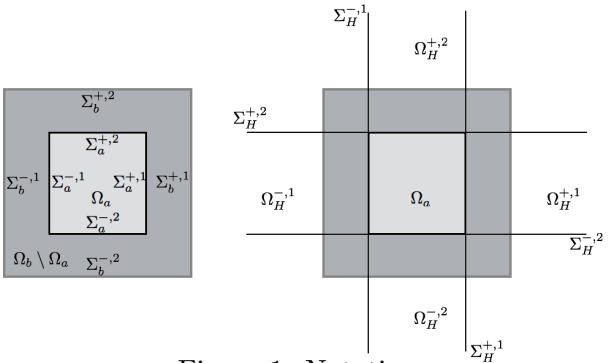

Figure 1: Notations

of (1), then $u|_{\Omega_b}$ is solution of

$$-\mathrm{div}(\mathbb{A}\nabla u_b) - \omega_\varepsilon^2\,\rho\,u_b = f \quad \text{in } \Omega_b, \tag{2}$$

and $u|_{\Omega_H^{\pm,j}}$ for $j \in \{1,2\}$ are solutions of

$$-\mathrm{div}(\mathbb{A}\nabla u_H^{\pm,j}) - \omega_\varepsilon^2\,\rho\,u_H^{\pm,j} = 0 \quad \text{in } \Omega_H^{\pm,j}. \tag{3}$$

Besides, they satisfy, for instance (see Remark 3), the following transmission conditions, for all $j \in \{1,2\}$,

$$\mathbb{A}\nabla u_b \cdot \mathbf{e}_{x_j} = \mathbb{A}\nabla u_H^{\pm,j} \cdot \mathbf{e}_{x_j} \text{ on } \Sigma_b^{\pm,j}, \tag{4}$$

and for all $j \neq k \in \{1,2\}$,

$$\left|\begin{array}{l} u_H^{\pm,j} = u_b \text{ on } \Sigma_a^{\pm,j} \\ u_H^{\pm,j} = u_H^{+,k} \text{ on } \partial(\Omega_H^{\pm,j} \cap \Omega_H^{+,k}), \\ u_H^{\pm,j} = u_H^{-,k} \text{ on } \partial(\Omega_H^{\pm,j} \cap \Omega_H^{-,k}). \end{array}\right. \tag{5}$$

Conversely, using the well posedness of the problems set in the four quadrants and the well posedness of the problem set in the ring $\Omega_b \cap \Omega_a$, we can show the following result.

Theorem 1 *Let $u_b \in H^1(\Omega_b)$ be a solution of* (2) *and $u_H^{\pm,j} \in H^1(\Omega_H^{\pm,j})$ be solutions of* (3) *satisfying the transmission conditions (4-5), then u defined by $u|_{\Omega_b} = u_b$ and $u|_{\Omega_H^{\pm,j}} = u_H^{\pm,j}$ is defined unequivocally and is solution of* (1).

We have then rewritten the problem set in the whole plane as a system of equations coupling 5 unknowns, one defined in the bounded domain Ω^b and 4 defined in each halfspace $\Omega_H^{\pm,j}$. Let us now explain how to eliminate the 4 halfspace unknowns. We can express the solution of any halfspace problem (analytically using the FT if the coefficients are constant or semi-analytically using the FBT if the coefficients are periodic) given its trace on the boundary of the halfspace. Therefore, for any $\varphi \in H^{1/2}(\Sigma_H^{\pm,j})$, we denote by $U_H^{\pm,j}(\varphi)$ the unique solution in $H^1(\Omega_H^{\pm,j})$ of

$$\left| \begin{array}{l} -\mathrm{div}(\mathbb{A}\nabla U_H^{\pm,j}) - \omega_\varepsilon^2\, \rho\, U_H^{\pm,j} = 0 \text{ in } \Omega_H^{\pm,j} \\ U_H^{\pm,j} = \varphi \quad \text{on } \Sigma_H^{\pm,j}, \end{array} \right. \tag{6}$$

Then we introduce the halfspace DtN operator with an overlap, $\Lambda_H^{\pm,j}$, defined by

$$\Lambda_H^{\pm,j}\, \varphi = \mathbb{A}\nabla U_H^{\pm,j}(\varphi) \cdot \mathbf{e}_{x_j}|_{\Sigma_b^{\pm,j}}, \tag{7}$$

and 2 DtD operators $D_+^{\pm,j}$ and $D_-^{\pm,j}$ defined by

$$\left| \begin{array}{l} D_+^{\pm,j}\, \varphi = U_H^{\pm,j}(\varphi)|_{\Sigma_H^{+,k} \cap \Omega_H^{\pm,j}} \\ D_-^{\pm,j}\, \varphi = U_H^{\pm,j}(\varphi)|_{\Sigma_H^{-,k} \cap \Omega_H^{\pm,j}}. \end{array} \right. \tag{8}$$

The expressions of the solutions $U_H^{\pm,j}(\varphi)$ and

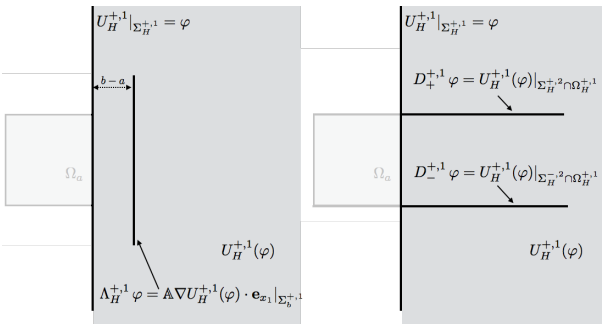

Figure 2: One halfspace problem

the operators $\Lambda_H^{\pm,j}$, $D_+^{\pm,j}$ and $D_-^{\pm,j}$ will be given in Section 3 for homogeneous media and in Section 4 for periodic media.

We can then eliminate the halfspace unknowns and reformulate the problem as a system of coupled equations linking the solution in Ω_b with the traces on each edge of the four halfspaces. More precisely, $u|_{\Omega_b}$ and $(u|_{\Sigma_H^{+,1}}, u|_{\Sigma_H^{+,2}}, u|_{\Sigma_H^{-,1}}, u|_{\Sigma_H^{-,2}})$ satisfy

$$\left| \begin{array}{l} -\mathrm{div}(\mathbb{A}\nabla u_b) - \omega_\varepsilon^2\, \rho\, u_b = f \quad \text{in } \Omega_b \\ A\nabla u_b \cdot \mathbf{e}_{x_j} = \Lambda_H^{\pm,j}\, \varphi_H^{\pm,j} \text{ on } \Sigma_{bb}^{\pm,j} \\ \varphi_H^{\pm,j} = u_b \text{ on } \Sigma_{aa}^{\pm,j} \\ \varphi_H^{\pm,j} = D_\pm^{+,k}\, \varphi_H^{+,k} \text{ on } \Sigma_H^{\pm,j} \cap \Omega_H^{+,k} \\ \varphi_H^{\pm,j} = D_\pm^{-,k}\, \varphi_H^{-,k} \text{ on } \Sigma_H^{\pm,j} \cap \Omega_H^{-,k} \end{array} \right. \tag{9}$$

Conversely, we can prove the following result.

Theorem 2 *Let $u_b \in H^1(\Omega_b)$ and $(\varphi_H^{+,1}, \varphi_H^{+,2}, \varphi_H^{-,1}, \varphi_H^{-,2}) \in H^{1/2}(\mathbb{R})^4$ be a solution of* (9). *Then if $b > a$, u defined by $u|_{\Omega_b} = u_b$ and $u|_{\Omega_H^{\pm,j}} = U_H^{\pm,j}(\varphi_H^{\pm,j})$ is defined unequivocally and is solution of* (1).

This implies existence and uniqueness of the solution of (9) but does not provide stabilities properties. As we will see in the next sections, the equations involving the traces are non standard integral equations. For homogeneous media, this problem is shown to be of Fredholm type but this question remains open for periodic media. In any case, this is this system of equations which is discretized and implemented in practice.

Remark 3 *If $b > a$, other transmission conditions can be imposed instead of (4-5), for example Robin traces instead of Neumann traces in* (4) *and Neumann traces instead of traces in* (5).

If we eliminate, when it is possible, the unknowns $(\varphi_H^{+,1}, \varphi_H^{+,2}, \varphi_H^{-,1}, \varphi_H^{-,2})$ in (9), *we construct a DtN operator linking the trace of u_b on $\partial\Omega_a$ to its normal derivative on $\partial\Omega_b$.*

For homogeneous media, and if Ω_a and Ω_b are triangles, a similar formulation can be derived with only 3 trace unknowns, see [8] for more details. A similar idea applies for hexagonal periodic media involving the traces of the solutions in 3 broken lines, *see [9].*

The case without dissipation ($\varepsilon = 0$) raises challenging open questions : the difficulty comes from the proof of Theorem (1), *more precisely on the well posedness of the associated quadrant problems. However from a numerical point of view, for the homogeneous case, this method seems to work.*

Let us now give a more explicit form of this system, first for homogeneous media and then for periodic media.

3 Case (I) – The locally perturbed homogeneous media

To simplify the presentation, we consider the situation of an isotropic acoustic medium ($\mathbb{A} = \mathbb{I}$) but the method extends easily to any matrix.

To determine the expression of the solution of the halfspace problems (6), it suffices to study the FT of $U_H^{\pm,j}$ which is solution – due to the homogeneity of the medium – of a 1D differential equation set in $L^2(]a,+\infty[)$ or in $L^2(]-\infty,-a[)$, for any dual variable $\xi \in \mathbb{R}$. Using the inverse FT, we obtain for $\pm x_j \geq \pm a,\ x_k \in \mathbb{R}$

$$U_H^{\pm,j}(\varphi) = \frac{1}{\sqrt{2\pi}} \int_{\mathbb{R}} \hat{\varphi}(\xi)\, e^{\mp\sqrt{\xi^2-\omega_\varepsilon^2}\,(x_j \mp a)+\imath\xi x_k}\, d\xi,$$

where $\hat{\varphi}$ is the Fourier transform of φ and $Re\sqrt{\ } > 0$ by convention. The operators $\Lambda_H^{\pm,j}$, $D_+^{\pm,j}$ and $D_-^{\pm,j}$ can then also be expressed analytically by their definition (7) and (8). In particular, we have for p.p. $-b < x_2 < b$

$$\left(\Lambda_H^{+,1}\varphi\right)(x_2) = -\frac{1}{\sqrt{2\pi}} \int_{\mathbb{R}} \sqrt{\xi^2-\omega_\varepsilon^2}\hat{\varphi}(\xi)\, e^{-\sqrt{\xi^2-\omega_\varepsilon^2}\,(b-a)+\imath\xi x_2}\, d\xi, \quad (10)$$

and for p.p. $x_1 > a$

$$\left(D_+^{+,1}\varphi\right)(x_1) = \frac{1}{\sqrt{2\pi}} \int_{\mathbb{R}} \hat{\varphi}(\xi)\, e^{-\sqrt{\xi^2-\omega_\varepsilon^2}\,(x_1-a)+\imath\xi a}\, d\xi. \quad (11)$$

The equations of (9) involving only the trace unknowns are then of integral form. If we consider only the system of the four last equations, given $\psi \in H^{1/2}(\partial\Omega_a)$, find $(\varphi_H^{+,1}, \varphi_H^{+,2}, \varphi_H^{-,1}, \varphi_H^{-,2})$ solution of

$$\left|\begin{array}{l} \varphi_H^{\pm,j} = \psi \text{ on } \Sigma_{aa}^{\pm,j} \\ \varphi_H^{\pm,j} = D_\pm^{+,k}\,\varphi_H^{+,k} \text{ on } \Sigma_H^{\pm,j} \cap \Omega_H^{+,k} \\ \varphi_H^{\pm,j} = D_\pm^{-,k}\,\varphi_H^{-,k} \text{ on } \Sigma_H^{\pm,j} \cap \Omega_H^{-,k} \end{array}\right. \quad (12)$$

we can show the fundamental result

Theorem 4 *The system of equations* (12) *is of Fredholm type and it is well posed in* $L^2(\mathbb{R})^4$.

The proof relies on properties of the Laplace transform, Hilbert-Schmidt operators, explicit computations and analyticity arguments. This result is true for anisotropic media for a suitable choice of $\partial\Omega_a$ and $\partial\Omega_b$. We deduce easily when $b > a$, using the compactness of the halfspace DtN operators, that the problem (9) is also of Fredholm type.

The approximation relies on a truncation and a discretization both in space and Fourier variables (to compute the integrals of type (10) and (11)). The method has been implemented and validated in the scalar acoustic case and in the elastic case.

We represent in Figure 3, for an anisotropic acoustic problem, the solution in the bounded region Ω_b and in two halfspaces $\Omega_H^{1,+}$ and $\Omega_H^{2,+}$. The different reconstructed parts of the solution coincide in the overlapping area because the compatibility conditions on the traces are satisfied.

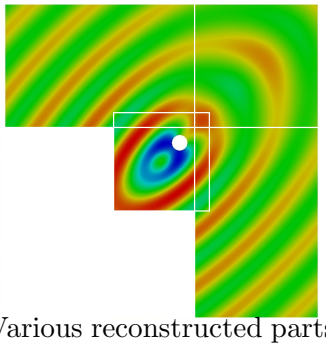

Figure 3: Various reconstructed parts of the solution for an anisotropic acoustic problem

4 Case (II) – The locally perturbed periodic media

We can now cover the case of periodic media. It seems that there are very few works for the simulation of wave propagation in infinite periodic media (or large compared to the wavelength). A first class of methods covers problems where the periodicity can be treated by homogenization techniques [10], typically when the wavelength is much larger than the period. The unboundedness of the homogenized and often anisotropic media can then be handled using classical methods mentioned in Introduction or by the strategy proposed in Section 3. A second class of methods considers the periodicity as such but only for finite media [11] or media which can be reduced to finite domain (for instance the supercell method for the computation of localized modes [12]).

To simplify the presentation, we assume that $a = 1/2$ and $b = 3/2$ but any $a, b \in 1/2\mathbb{Z}^*$ can be considered. Let us now introduce the privileged tool for the study of equations with periodic coefficients.

Definition 5 *The FBT of period* 1 *is defined by (see [13]):*

$$\mathcal{F} : \varphi \in L^2(\mathbb{R}) \mapsto \mathcal{F}\varphi \in L^2(\mathbb{K})$$

where p.p $(x, \xi) \in \mathbb{K} = (-1/2, 1/2) \times (-\pi, \pi)$

$$\mathcal{F}\varphi(x, \xi) = \frac{1}{\sqrt{2\pi}} \sum_{n\in\mathbb{Z}} \varphi(x + n)e^{-\imath n\xi}.$$

Moreover we have the inversion formula: p.p.$x \in [0, 1]$ $\forall n \in \mathbb{Z}$,

$$\varphi(x + n) = \frac{1}{2\pi} \int_{-\pi}^{\pi} \mathcal{F}\varphi(x, \xi)e^{\imath n\xi} d\xi$$

We denote $\mathcal{F}_j u$ the FBT of a function u of $\mathbb{R}^2$ applied in the x_j-direction.

To determine the expression of the solution of the halfspace problems (6), it suffices to study the FBT in the transverse direction $\hat{U}_H^{\pm,j}(\xi_k) = \mathcal{F}_k U_H^{\pm,j}(\cdot; \xi_k)$ of $U_H^{\pm,j}$. Because of the periodicity of the problem, it is solution, for any dual variable $\xi_k \in (-\pi, \pi)$, of the strip problem

$$\begin{cases} -\mathrm{div}(\mathbb{A}\nabla\hat{U}_H^{\pm,j}(\xi_k) - \omega_\varepsilon^2 \rho \hat{U}_H^{\pm,j}(\xi_k) = 0, \text{ in } B_H^{\pm,j} \\ \hat{U}_H^{\pm,j}(\xi_k)|_{x_j=\pm a} = \mathcal{F}_k\varphi(\xi_k)|_{x_j=\pm a}, \\ \hat{U}_H^{\pm,j}(\xi_k)|_{x_k=a} = e^{\imath\xi_k} \hat{U}_H^{\pm,j}(\xi_k)|_{x_k=-a} \\ \mathbb{A}\nabla\hat{U}_H^{\pm,j}(\xi_k) \cdot \mathbf{e}_{x_k}|_{x_k=a} \\ \qquad = e^{\imath\xi_k}\mathbb{A}\nabla\hat{U}_H^{\pm,j}(\xi_k) \cdot \mathbf{e}_{x_k}|_{x_k=-a} \end{cases}$$

where $B_H^{\pm,j} = \Omega_H^{\pm,j} \cap \{-a \le x_k \le a\}$.

As explained in [14], we can characterize and compute periodicity cell by periodicity cell, for every $\xi_k \in (-\pi, \pi)$, the solution of this semi-infinite periodic waveguide thanks to the solutions of two cell problems and a so-called propagation operator $P^{\pm,j}(\xi_k)$. This operator is the unique operator of spectral radius strictly less than 1 to the stationary Ricatti equation

$$T_{10}^{\pm,j}(\xi_k)P^{\pm,j}(\xi_k)^2 + T_{01}^{\pm,j}(\xi_k) + (T_{00}^{\pm,j}(\xi_k) + T_{11}^{\pm,j}(\xi_k))\, P^{\pm,j}(\xi_k) = 0, \quad (13)$$

where the operators $T_{\ell m}^{\pm,j}(\xi_k)$ are local DtN operators defined thanks to the cell problems. Applying the FBT inverse, $U_H^{\pm,j}$ and the operators $\Lambda_H^{\pm,j}$, $D_+^{\pm,j}$ and $D_-^{\pm,j}$ can then be expressed semi-analytically. In particular, we have for all $n \in \{-1, 0, 1\}$, p.p $a + n < x_2 < a + n + 1$,

$$(\Lambda_H^{+,1}\varphi)(x_2) = -\frac{1}{\sqrt{2\pi}} \int_{-\pi}^{\pi} T^{+,1}(\xi_2)P^{+,1}(\xi_2) \mathcal{F}_2\varphi_H^{+,1}(\cdot; \xi_2)e^{\imath n\xi_2} d\xi_2,$$

where $T^{+,1}(\xi_2) = T_{00}^{+,1}(\xi_2) + T_{10}^{+,1}(\xi_2)P^{+,1}(\xi_2)$ and for all $n \in \mathbb{N}$ and p.p $a+n < x_1 < a+n+1$

$$(D_+^{+,1}\varphi)(x_1) = \frac{1}{\sqrt{2\pi}} \int_{-\pi}^{\pi} D^{+,1}(\xi_2)P^{+,1}(\xi_2)^n \mathcal{F}_2\varphi_H^{+,1}(\cdot; \xi_2)\, d\xi_2,$$

where $D^{+,1}(\xi_2) = D_0^{+,1}(\xi_2) + D_1^{+,1}(\xi_2)P^{+,1}(\xi_2)$ and the operators $D_m^{+,1}(\xi_2)$ are defined thanks to the cell problems. Thus, using one of the last equation of (9) for the "+"-case, $j = 2$ and $k = 1$, knowing the FBT of $\varphi_H^{+,1}$, we can recover $\varphi_H^{+,2}$ piece by piece for $x_1 > a$. It is then more natural to rewrite the equations involving the FB transform of the trace unknowns. For example, we find for the "+"-case and $j = 2$

$$\begin{aligned} &2\pi\, \mathcal{F}_1\varphi_H^{+,2}(\cdot; \xi_1) = \sqrt{2\pi}u_b|_{\Sigma_a^{+,2}} \\ &+\int_{-\pi}^{\pi} \Big[e^{\imath\xi_1} D^{-,1}(\xi_2)\,(I - P^{-,1}(\xi_2)e^{\imath\xi_1})^{-1}\mathcal{F}_2\varphi_H^{-,1}(\cdot; \xi_2) \\ &+e^{-\imath\xi_1} D^{+,1}(\xi_2)\,(I - P^{+,1}(\xi_2)e^{-\imath\xi_1})^{-1}\mathcal{F}_2\varphi_H^{+,1}(\cdot; \xi_2)\Big]\, d\xi_2 \end{aligned}$$

The equations of (9) involving only the trace unknowns can be rewritten as integral equations. The properties of the corresponding system of integral equations and then the extension of Theorem 4 are still open questions.

From the numerical point of view, one has to solve first families of decoupled cell problems and stationary Ricatti equations, then discretize the coupled integral equations both in space and in the Floquet variables (ξ_1, ξ_2) and finally construct a discrete FBT inverse for the computation of the halfspaces DtN operators. The method has been implemented and validated in the scalar acoustic case. For instance Figure 4 represents the solution (right figure) for a particular periodic media, whose ρ is represented in the left figure.

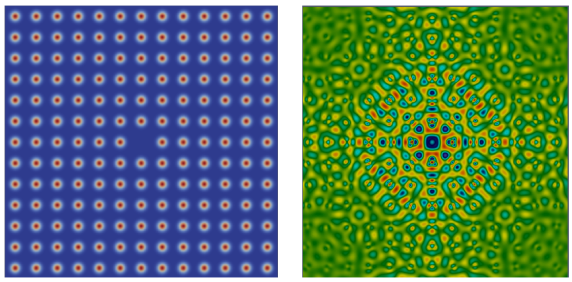

Figure 4: Right figure : Solution of (1) for $\mathbb{A} = \mathbb{I}$ and ρ represented in the left figure.

5 Conclusions and ongoing works

Besides all the open questions already mentioned in this abstract, the case without dissipation is definitely the most challenging and interesting question. It can be summarized as *ensuring an outgoing condition in 4 (or 3?) directions is that sufficient to ensure the radiation condition in all the directions?*

Finally, this original method can be used to deal with time domain wave equations (after semi-discretization in time) or junctions of stratified media (using a generalized Fourier transform to solve the corresponding halfspace problems).

References

[1] C. Johnson and J.C. Nédélec, On the coupling of boundary integral and finite element methods, *Math. Comp.* **152** (1980), pp. 1063-1079.

[2] B. Engquist and A. Majda, Radiation boundary conditions for acoustic and elastic wave calculations, *Comm. Pure Appl. Math.* **32 (3)** (1979), pp 314-358.

[3] D. Givoli and J. B. Keller, Non reflecting boundary conditions for elastic waves, *Wave motion* **12(3)** (1990), pp 261-279.

[4] J. D. Achenbach and C. Y. Wang (1995), Three-dimensional time-harmonic elastodynamic Green's functions for anisotropic solids., *Proc. of the Royal Soc. of London. Math. and Phys. Sc.* **449** (1937), pp 441-458.

[5] J.-P. Berenger, A perfectly matched layer for the absorption of electromagnetic waves, *J. Comput. Phys.* **114 (2)** (1994), pp 185-200.

[6] T. Hohage and F. Schmidt and L. Zschiedrich, Solving time-harmonic scattering problems based on the pole condition. I. Theory, *SIAM J. Math. Anal.* **35 (1)** (2003), pp. 183-210.

[7] N. Gmati and N. Zrelli, Numerical study of some iterative solvers for acoustics in unbounded domains, *ARIMA* **4** (2006), pp. 1-23.

[8] A. Tonnoir, Conditions transparentes pour la diffraction d'ondes en milieu élastique anisotrope, *These de l'Ecole Polytechnique*, 2015.

[9] C. Besse and J. Coatleven and S. Fliss and I. Lacroix-Violet and K. Ramdani, Transparent boundary conditions for locally perturbed infinite hexagonal periodic, *Commun. Math. Sci.* **11(4)** (2013), pp 907-938.

[10] G. Allaire and C. Conca and M. Vanninathan, Spectral asymptotics of the Helmholtz model in fluid-solid structures, *Int. J. Numer. Meth. Engng.* **46** (1999), pp. 1463-1504.

[11] L. Yuan and Y.-Y. Lu, An efficient bidirectional propagation method based on Dirichlet-to- Neumann maps, *IEEE Photonics Technology Letters* **18** (2006), pp. 1967-1969.

[12] S. Soussi, Convergence of the supercell method for defect modes calculations in photonic crystals, *SIAM J. Numer. Anal.* **43 (3)** (2005), pp. 1175-1201.

[13] P. Kuchment, "Floquet theory for Partial differential Equations", *Operator Theory : Advances and applications* **60** (1993), Birkhäuser Verlag, Basel.

[14] S. Fliss and P. Joly and J.-R. Li, Exact boundary conditions for periodic waveguides containing a local perturbation, *CiCP* **1(6)** (2006), pp. 945-973.

[15] A.-S. Bonnet-Ben Dhia and Tillequin A., A generalized mode matching method for scattering problems with unbounded obstacles, *J. Comp. Acous.* **9** (2001), pp. 1611-1631.

Minisymposia

Minisymposium: Advanced Computational Methods for Acoustic and Elastic Wave Propagation

organised by Dan Givoli and Thomas Hagstrom

In recent years there has been an increased interest in advanced computational methods for acoustic and elastic wave problems. Important issues where progress has been made recently include multiscale wave phenomena that require special solution techniques to resolve the various scales, high-order absorbing boundary conditions and Perfectly Matched Layers for wave propagation in unbounded domains, high-order methods for dealing with inhomogeneous anisotropic media, solution of inverse problems based on wave scattering, high order stable and robust methods for time integration, and error estimation for wave problems and adaptive schemes based on error estimates. This minisymposium will address some of these issues, while concentrating on problems in acoustic and elastic waves.

Convergence analysis of leap-frog based local time-stepping for the wave equation

Loredana Gaudio[1], **Marcus J. Grote**[1,*], **Michaela Mehlin**[1]
[1]Department of Mathematics and Computer Science, University of Basel, Switzerland
*Email: marcus.grote@unibas.ch

This paper will be presented in the MS "Advanced Computational Methods for Acoustic and Elastic Wave Propagation" organized by D. Givoli and T. Hagstrom.

Abstract

Local mesh refinement severely impedes the efficiency of explicit time-stepping methods for numerical wave propagation. Local time-stepping (LTS) methods overcome the bottleneck due to a few small elements by allowing smaller time-steps precisely where those elements are located [1]. In [2], leap-frog (LF) type LTS methods of arbitrarily high accuracy were derived, which are fully explicit and conserve an energy. Here we rigorously prove convergence of the LF-LTS method and present numerical experiments with an interior penalty discontinuous Galerkin (IP-DG) spectral element method (SEM) to illustrate their usefulness in the presence of corner singularities.

Keywords: discontinuous Galerkin methods, explicit time integration, multirate methods

1 Introduction

We consider the classical wave equation

$$\begin{cases} u_{tt} - \nabla \cdot (c^2 \nabla u) = f & \text{in } \Omega \times (0,T) \\ u|_{t=0} = u_0 \quad u_t|_{t=0} = v_0 & \text{in } \Omega, \end{cases} \quad (1)$$

where $\Omega \in \mathbb{R}^d$ denotes a bounded domain in $\mathbb{R}^d$, $f \in L^2(0,T;L^2(\Omega))$ a (known) source, and $u_0 \in H_0^1(\Omega)$, $v_0 \in L^2(\Omega)$ prescribed initial conditions. The speed of propagation, $c = c(x)$, is assumed piecewise smooth and strictly positive. At the boundary, $\partial\Omega$, we impose appropriate boundary conditions for well-posedness.

For the spatial discretization of (1), we consider a symmetric IP-DG SEM, which leads to the second-order system of ordinary differential equations:

$$\mathbf{M}\,\frac{d^2U}{dt^2}(t) + \mathbf{K}\,U(t) = F(t)\ , \quad (2)$$

where the mass matrix $\mathbf{M}$ is diagonal. Hence, we can directly compute $\mathbf{M}^{1/2}$ and write (2) as

$$\frac{d^2z}{dt^2}(t) + \mathbf{A}z(t) = R(t), \quad (3)$$

with $z(t) = \mathbf{M}^{\frac{1}{2}}U(t)$, $\mathbf{A} = \mathbf{M}^{-\frac{1}{2}}\mathbf{K}\mathbf{M}^{-\frac{1}{2}}$, $R(t) = \mathbf{M}^{-\frac{1}{2}}F(t)$. The (scaled) stiffness matrix $\mathbf{A}$ is sparse, symmetric and positive semi-definite.

In the absence of forcing and dissipation, the wave equation (1) conserves the total energy. When the standard leap-frog method is used for the time integration of (3), the resulting fully discrete formulation also conserves (a discrete version of) the energy. Due to the CFL stability condition, however, the time-step of any explicit scheme will be dictated by the smallest element in the mesh. In [2], energy conserving LF based LTS methods were derived for (3), which overcome that stringent stability condition without sacrificing explicitness or accuracy.

First, we partition the unknowns in $z(t)$ into a "coarse" and a "fine" subset,

$$z(t) = (\mathbf{I} - \mathbf{P})z(t) + \mathbf{P}z(t)$$

where the partitioning matrix, $\mathbf{P}$, is diagonal: its diagonal entries, equal to zero or one, identify the unknowns associated with the locally refined region, that is where smaller time-steps are needed. Then the LTS-LF algorithm – see [2] for details – proceeds during each time-step $[t_n, t_n + \Delta t]$ as

$$z_{n+1} = -z_{n-1} + 2\,\mathrm{LTS}_2(z_n, -\mathbf{A}(\mathbf{I} - \mathbf{P})z_n), \quad (4)$$

where the function $y_{new} = \mathrm{LTS}_2(y, w)$ is defined as:

1. $y_{new} := y + \frac{1}{2}\left(\frac{\Delta t}{p}\right)^2 (w - \mathbf{A}\mathbf{P}y)$
2. For $m = 1, ..., p-1$
   (i) $y_{old} := y$; $y := y_{new}$
   (ii) $y_{new} := 2y - y_{old} + \left(\frac{\Delta t}{p}\right)^2 (w - \mathbf{A}\mathbf{P}y)$

Here, Δt, p, $\mathbf{A}$ and $\mathbf{P}$ are globally defined. Note that the p multiplications with $\mathbf{A}$ only affect

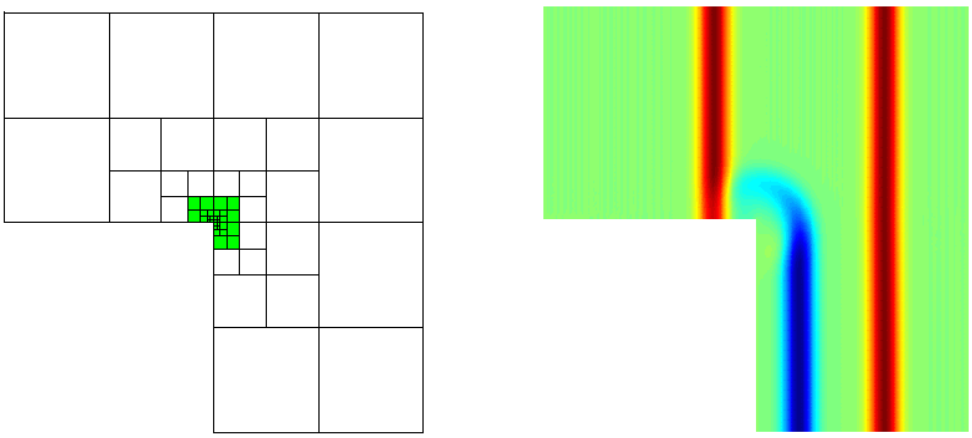

Figure 1: Left: initial mesh with refinement rate $p = 8$ – not drawn to scale. Right: the numerical IP-DG-SEM solution u_h at time $t = 0.4$ with $\ell = 2$.

the unknowns $\mathbf{P}z$, i.e. those located in the refined region, and hence correspond to p local sub-steps each of size $\Delta t/p$.

When the refined region itself contains even finer elements, the recursive application of the above LTS-LF algorithm recently led to a multi-level LTS method, which also conserves a discrete energy [3]. In [4], the multi-level LF-LTS method in time-staggered Newmark form was combined with the well-known spectral element code SPECFEM3D for seismic wave propagation and achieved up to 90% parallel efficiency on the massively parallel supercomputer "Piz Daint" at the Swiss Center for Scientific Computing (CSCS).

Let $u_h(t_n)$ denote the fully discrete numerical FE solution. Under standard smoothness assumptions on the solution u of (1), we can rigorously prove that as $\Delta t, h \to 0$

$$\|u - u_h\|_{L^\infty(0,T;L^2(\Omega))} = O(\Delta t^2 + h^{\ell+1}),$$

where $\ell \geq 1$ denotes the polynomial degree of the underlying spatial discretization. This proof underpins the optimal convergence rates previously observed [2].

2 Numerical Results

To illustrate the usefulness of the LTS-LF methods, we consider (1) with $f = 0$ on a two dimensional L-shaped domain – see Fig. 1. We set homogeneous Neumann conditions on horizontal and homogeneous Dirichlet conditions on vertical boundaries. In (1) we let $v_0 = 0$ and set u_0 to a vertical Gaussian plane wave centered about $x = 0.3$. Towards the re-entrant corner we use a graded locally refined mesh with 1:8 ratio. Since the typical mesh size inside the refined (darker) region is about 8 times smaller than that in the surrounding coarser region, we take $p = 8$ local time-steps in the above LTS-LF algorithm. In Fig. 1, the IP-DG SEM numerical solution with $\ell = 2$ is shown at time $t = 0.4$.

References

[1] F. Collino, T. Fouquet, and P. Joly, A conservative space-time mesh refinement method for the 1-D wave equation. I. Construction, *Numer. Math.*, **95** (2003), pp. 197–221.

[2] J. Diaz and M. J. Grote, Energy conserving explicit local time-stepping for second-order wave equations, *SIAM J. Sci. Comput.*, **31** (2009), pp. 1985–2014.

[3] J. Diaz and M. J. Grote, Multilevel Explicit Local Time-stepping For Second-order Wave Equations, *Comp. Meth. Appl. Mech. Engin., in press.*

[4] M. Rietmann, M. J. Grote, D. Peter, O. Schenk and B. Uçar, Load-Balanced Local Time Stepping for Large-Scale Wave Propagation, *in Proc. of 29th IEEE International Parallel & Distributed Processing Symposium (IPDPS 2015).*

Galerkin Difference Methods from Bandlimited Interpolation Functions

Thomas Hagstrom[1,*], **Jeffrey Banks**[2]
[1]Department of Mathematics, Southern Methodist University, Dallas, TX USA
[2]Department of Mathematical Sciences, Rensselaer Polytechnic Institute, Troy, NY USA
[*]Email: thagstrom@smu.edu

Abstract

We explore the use of bandlimited interpolation functions in place of standard Lagrange interpolants to define wide-stencil difference methods for simulating waves. Experiments are presented indicating that the proposed schemes can be significantly more accurate when broadband signals are propagated. To address the problem of constructing stable boundary closures we propose combining accurate extrapolations with a discontinuous Galerkin construction of the difference schemes. This leads to methods akin to compact difference schemes when exact integration is used, or boundary-corrected explicit differences if mass-lumping is employed.

Keywords: Difference methods, discontinuous Galerkin methods, bandlimited interpolation

1 Introduction

As computational power increases, one hopes to simulate ever more challenging problems. For wave-dominated systems, this challenge often involves the accurate propagation of waves over many wavelengths. As is well-known, due to the effects of dispersion, the optimal approximation order for simple difference approximations, with fixed accuracy, increases with the length of propagation. However, the dispersion error of high-order difference methods is vanishingly small at low frequencies and grows rapidly as the wavelength decreases. For broadband signals, then, much of the spectrum is overresolved.

Following on results presented in [1], we consider an alternative approach which provides uniform accuracy across a predetermined frequncy band. Precisely we base our methods on Knab's bandimited interpolant [2], defined in one dimension via translates of

$$\frac{\sin\frac{\pi x}{h}}{\frac{\pi x}{h}}\cdot\frac{\sinh\left(\pi N\delta\sqrt{1-\left(\frac{x}{Nh}\right)^2}\right)}{\sinh\left(\pi N\delta\right)\cdot\sqrt{1-\left(\frac{x}{Nh}\right)^2}}, \qquad (1)$$

set to zero when $|x| > N$. Here $0 < \delta < 1$ is a parameter which balances the interpolation error, $\frac{1}{\sinh(\pi N\delta)}$, with the resolution, $\frac{2}{1-\delta}$ points-per-wavelength (PPW).

As an example, using exact evolution of the interpolants as in [1], we simulate a turbulent acoustic wave field in two space dimensions with an energy decay in terms of the wave number k

$$E(k) \propto k^{-2}, \qquad (2)$$

and a sharp cutoff at 5 PPW. After a simulation time corresponding to 1000 periods of the shortest wave we find that the relative error using $N = 8$ and a Knab-based scheme is 4.0×10^{-4} while for the same stencil and standard Lagrange interpolation it is 6.2×10^{-3}.

2 DG-based Boundary Closures

As with standard high-order difference methods, some modifications are needed at domain boundaries. Typical approaches are based on algebraic constructions which guarantee stability using either Kreiss determinants [3] or discrete energy estimates [4]. Here we pursue a different approach based on a discontinuous Galerkin formulation, as proposed for Lagrange-based methods in [5]. The basic construction has three parts. Away from boundaries use, as test and trial functions, the Knab functions associated with the grid points as in (1). Near boundaries represent data at "ghost" nodes outside the computational domain via a bandlimited extrapolation procedure. In the Galerkin framework this means that the test and trial functions corresponding to nodes used in the extrapolation procedure are modified. Finally, impose boundary conditions via fluxes.

The stability and accuracy of the resulting method follows directly from standard DG theory [6] combined with the accuracy properties of the interpolation/extrapolation procedures. The only significant bottleneck is the potential for generating a stiff differentiation matrix due to the ill-conditioning of the bandlimited extrapolation - ours is defined through a sinc-

Hilbert matrix which we approximately invert using a truncated SVD.

As a specific example we choose $N = 8$ and $\delta = 3/5$, for which the Knab interpolant has an error tolerance of 5.6×10^{-7} for waves resolved with at least 5 PPW. We extrapolate to the ghost nodes using $3N + 1$ interior nodes. In one space dimension the resulting mass and stiffness matrices have 25×25 nonzero blocks near the boundaries and have 31 nonzero bands in the interior. The spectral radius is $2.46h^{-1}$.

We applied the method to acoustics with wall boundary conditions imposed via an upwind flux in one space dimension. Marching in time using MATLAB's **ode113** and tight error tolerances we simulate a turbulent wave field with spectrum following (2), again for 1000 periods of the shortest wave. The relative error in this case is 1.2×10^{-7}. This is obviously comparable to the interpolation error and much better than what was obtained for an analogous experiment in [1]. We note that the error, plotted in Figure 1, is nearly constant in time, while in [1] we observed linear growth. Thus dispersion error in the DG formulation is negligible.

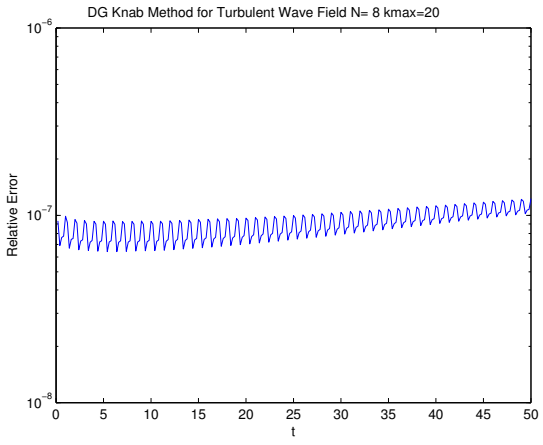

Figure 1: Simulation errors in time

3 Mass-lumping

In order to produce a diagonal mass matrix away from boundaries, and to reduce the bandwidth of the differentiation matrix, we replace the continuous integrals by an appropriate quadrature rule. A seemingly ideal choice is one of Alpert's Gauss-trapezoid rules [7]. We employ a method from this family which, on an interval $[a, b]$, reduces to the standard trapezoid rule at nodes $a+12.88h, \ldots, b-12.88h$, with 15 special nodes and weights at each end. It returns extremely accurate results down to 2 PPW. Using the same values of N, δ and extrapolation matrix as above the boundary blocks are still 25×25, but in the interior the mass matrix reduces to hI and the bandwidth of the differentiation matrix reduces to 17. Applying the mass-lumped method is up to four times cheaper than the standard DG formulation. However, repeating the numerical experiment described above we find that the method is dispersive so the final relative error is much larger, 7.3×10^{-4}. A fairer comparison of lumped and unlumped methods of equal cost would thus be desirable.

4 Acknowledgments

The authors acknowledge the support of DOE Grant DE-AC52-07NA27344. In addition the work of the first author was supported in part by NSF Grant DMS-1418871. Any opinions, findings, and conclusions or recommendations are those of the authors and do not necessarily reflect the views of the DOE or NSF.

References

[1] T. Hagstrom, High-resolution difference methods with exact evolution for multidimensional waves, *Appl. Num. Math.*, **93** (2015), pp. 114–122.

[2] J. Knab, Interpolation of band-limited functions using the approximate prolate series, *IEEE Trans. Inform. Theory* **25** (1979), pp. 717–720.

[3] T. Hagstrom and G. Hagstrom, Grid stabilization of high-order one-sided differencing I: First order hyperbolic systems, *J. Comput. Phys.* **223** (2007), pp. 316–340.

[4] J. Nordström and M. Carpenter, High-order finite-difference methods, multidimensional linear problems, and curvilinear coordinates, *J. Comput. Phys.* **173** (2001), pp. 149–174.

[5] J. Banks and T. Hagstrom, Galerkin finite difference methods, in preparation.

[6] J. Hesthaven and T. Warburton, *Nodal Discontinuous Galerkin Methods*, Springer-Verlag, New York, 2008.

[7] B. Alpert, Efficiency-enhanced hybrid Gauss-trapezoidal rules, in preparation.

Reduced order models for large scale wave propagation

Rob Remis[1,*], **Vladimir Druskin**[2], **Alexander Mamonov**[3], **Mikhail Zaslavsky**[2], **Jörn Zimmerling**[1]

[1]Circuits and Systems Group, Delft, The Netherlands
[2]Schlumberger Doll Research, Cambridge, USA
[3]Department of Mathematics, Houston, USA
[*]Email: r.f.remis@tudelft.nl

Abstract

Reduced order models approximate transfer functions of large-scale linear dynamical systems by small equivalent ones. We discuss some recent applications of this powerful approach to the numerical solution of hyperbolic problems. They include multi-scale elasticity problems and wave propagation in unbounded domains.

Keywords: multi-scale, mimetic model reduction

1 Introduction

We consider the hyperbolic initial-value problem

$$Au+u_{tt}=0, \qquad u|_{t=0}=0,\ u_t|_{t=0}=b, \quad t\geq 0, \tag{1}$$

where A is a selfadjoint nonnegative second order PDE operator on the unbounded domain (e.g., $\mathbb{R}^3$) with absolutely continuous spectrum.

Until now, the method of choice for such problems was the explicit finite-difference time domain (FDTD) method coupled with PML absorbing boundary conditions. Large scale 3D problems (in particular, used in seismic exploration) can be prohibitively expensive even for modern high performance computing. High order and spectral spatial discretizations can significantly reduce computational cost, however, they require special treatment of coefficient discontinuities, e.g., interface conforming elements as in the spectral element method. Such an approach may increase algorithm complexity and often leads to unnecessary restrictive CFL limits. Moreover, it can be practically impossible for complicated models with inhomogeneities spanned in multiple scales. To circumvent the above problems, we suggest here a mimetic multiscale model reduction based discretization.

Another bottleneck of the classical FDTD methods is the upper limitations on the time step, which is particular severe for explicit methods. We address this problem by introducing a reduced order model based on a scattering resonance representation.

2 Multiscale mimetic model reduction

The method presented here is an extension of the techniques from [1, 2], where the so-called optimal (spectrally matched) grids (a.k.a. finite-difference Gaussian qudrature rules) were used to construct the ROMs on the sub-domains. The use of optimal grids relies on the medium being uniform on each sub-domain. The method presented here avoids this limitation and allows for arbitrary sharp discontinuities within the subdomains.

We consider a selfadjoint PDE operator A (e.g., acoustic problem, elasticity or Maxwell's system), that can be described by (1), or by

$$Av+\omega^2 v=b \tag{2}$$

in the frequency domain, assuming that $-\omega^2$ not in the spectrum of A. To outline the idea of our approach, we assume for simplicity that A is defined on a bounded domain Ω, partitioned into two closed non-overlapping subdomains Ω_1, Ω_2, i.e., $\Omega=\Omega_1\cup\Omega_2$ with boundary interface $\Gamma=\Omega_1\cap\Omega_2$. We also assume that b is supported on Γ and it is a single layer charge distribution on that manifold with regular enough density $\mathbf{b}$. We denote operator-valued functions $M_i(\omega^2)$ by the partial NtD maps (a.k.a. impedance or Weyl functions) of the respected subdomains Ω_i on Γ.

Extending results of [2] to operator-valued impedance functions, we obtain spectrally convergent approximation $M(\omega^2)\approx M_n(\omega^2)$ (for the propagative modes) that can be formally presented as operator Stieltjes continued frac-

tion approximations of $M_i(\omega^2)$ in the form

$$M_i^n(\omega^2) = \cfrac{1}{\hat{H}_0^i\omega^2 + \cfrac{1}{H_1^i + \cfrac{1}{\ddots\ + \cfrac{1}{\hat{H}_{n-1}^i\omega^2 + \cfrac{1}{H_n^i}}}}} \tag{3}$$

where $\hat{H}_i, H_i$ are Hermitian nonnegative low rank operators (with the inverse understood as the pseudo-inverse). By extending 1D results of [4], this allows us to represent $M_n(\omega^2)$ via a 'three-point finite-difference scheme' with operator coefficients by introducing fictitious variables $\mathbf{u}_j^i$ for $i = 1, 2$ and $j = 1, \ldots, n-1$ via

$$(H_1^i)^{-1}\left(\mathbf{u}_1^i - \mathbf{u}_0^i\right) + \mathbf{q}^{\mathbf{i}} = -\omega^2\hat{H}_0^i\mathbf{u}_0^i, \tag{4}$$

$$\begin{aligned}(H_{j+1}^i)^{-1}\left(\mathbf{u}^{\mathbf{i}}{}_{j+1} - \mathbf{u}^{\mathbf{i}}{}_j\right) \ &- \ (H_j^i)^{-1}\left(\mathbf{u}_j^i - \mathbf{u}_{j-1}^i\right) \\ &= \ -\omega^2\hat{H}_j^i\mathbf{u}_j^i,\end{aligned} \tag{5}$$

so $M_n(\omega^2)\mathbf{q}^i = \mathbf{u}_0^i$. The conjugation conditions at Γ can be written as $\mathbf{u}_0^1 = \mathbf{u}_0^2 = \mathbf{u}_0 = v|_\Gamma$, $\mathbf{q}^1 + \mathbf{q}^2 = \mathbf{b}$. They allow us to substitute equations (4) for $i = 1, 2$ by the single equation

$$\begin{aligned}(H_1^1)^{-1}\left(\mathbf{u}_1^1 - \mathbf{u}_0\right) + (H_1^2)^{-1}\left(\mathbf{u}_2^i - \mathbf{u}_0\right) \\ = -\omega^2(\hat{H}_0^1 + \hat{H}_0^2)\mathbf{u}_0 - \mathbf{b}.\end{aligned} \tag{6}$$

In the time domain, we replace $-\omega^2$ with $\frac{d^2}{dt^2}$ in (6-5). That system mimics a *second order finite-difference scheme with block-tridiagonal stencil*, and this the reason we call it mimetic. However, similar to the above mentioned optimal grid approach, it yields *spectral* convergence of $\mathbf{u}_0$. It can be solved by standard FDTD algorithm or the model reduction approach described in the following section. Advantage of the the block-tridiagonal stencil is low communication cost. To compute M_i^n (so-called offline preprocessing), we use fine discretization grid of subdomains Ω_i. Its cost grows very rapidly with grid size, so in practice we split the computational domain into a large number of subdomains of moderate sizes. It also helps that the offline preprocessing is independent for every subdomain, i.e., it is an 'embarrassingly' parallel procedure.

The described approach is the most suitable for modern high performance computing, in particular, for graphic processing units (GPUs), however, even its serial implementation is already competitive for complex elastic models with multiple scales.

3 Stability-corrected exponential propagation in unbounded domains

To avoid spurious resonances, the reduced order model should *preserve spectral continuity* of the original problem, i.e., it should not contain poles on the main Riemann sheet. This can be achieved by using (non-Hermitian) complex symmetric discretized operators A_N dumped by perfectly matched layers and a so-called stability-corrected time-domain exponential (SCTDE) matrix function $\Im\left(A_N^{-1/2}e^{\mathrm{i}\sqrt{A_N}t}\right)b_N$, approximation exact solution given by $u = A^{-1/2}\sin(A^{1/2}t)b$ [3].

The SCTDE matrix function is approximated by the Krylov subspace projection algorithm, based on the re-normalized Lanczos method. With the same cost per step as FDTD, it overperforms the latter for large propagation times.

References

[1] S. Asvadurov, V. Druskin and L. Knizhnerman, *Application of the difference Gaussian rules to solution of hyperbolic problems*, J. Comp. Phys. 158 (2000), 116-135.

[2] V. Druskin and L. Knizhnerman, *Gaussian spectral rules for the three-point second differences: I. A two-point positive definite problem in a semiinfinite domain*, SINUM, 37, No 2 (1999), pp. 403–422.

[3] V. Druskin and R. Remis, *A Krylov Stability-Corrected Coordinate-Stretching Method to Simulate Wave Propagation in Unbounded Domains*, SISC, 35 No 2 (2013), pp. 313–357.

[4] I. S. Kac and M. G. Krein, *On the spectral functions of the string*, Amer. Math. Soc. Transl., 103 (1974), pp. 19–102.

Polarized traces: a scalable solver for 2D Helmholtz

Leonardo Zepeda-Núñez[1,*], **Laurent Demanet**[1]
[1]MIT, Department of Mathematics, Cambridge MA, USA
*Email: lzepeda@math.mit.edu

This paper will be presented in the MS "Advanced Computational Methods for Acoustic and Elastic Wave Propagation" organized by D. Givoli and T. Hagstrom.

Abstract

We propose a solver for the 2D high-frequency Helmholtz equation in heterogeneous acoustic media, with online parallel complexity that scales sublinearly as $O\left(\frac{N}{L}\right)$, where N is the number of volume unknowns, and L is the number of processors, as long as L is a small fractional power of N. The solver decomposes the domain into L layers, and uses transmission conditions in boundary integral form to explicitly define "polarized traces", i.e., directional waves sampled at interfaces. The favorable scalability owes to the availability of fast algorithms for the integral kernels. This note is a summary of [**?**].

1 Introduction

Solving the Helmholtz equation with a scalable algorithm in the high frequency regime is a question of great interest for applications in geophysical imaging. Direct methods often run out of memory in realistic applications and they do not scale well in distributed memory environments. Iterative methods require a large number of iterations to converge and standard algebraic preconditioners often fail to improve the convergence rate to tolerable levels [**?**]. Domain decomposition methods also fail because of internal reverberations [**?**]. Only recently, a new type of preconditioners have been developed that achieve linear complexity; however, they are often difficult to parallelize [**?**, **?**, **?**].

2 Method

Define the global Helmholtz equation in a bounded domain $\Omega \subset \mathbb{R}^2$, with frequency ω and squared slowness $m(\mathbf{x}) = 1/c^2(\mathbf{x})$, by

$$\left(-\triangle - m(\mathbf{x})\omega^2\right) u(\mathbf{x}) = f(\mathbf{x}) \qquad (1)$$

with absorbing boundary conditions. For the results that follow, Eq 1 is discretized with a 5-point stencil, and the absorbing boundary conditions are implemented via a perfectly matched layer (PML). This leads to a linear system of the form $\mathbf{Hu} = \mathbf{f}$. Let N be the total number of unknowns of the linear system and $n = N^{1/2}$ the number of points per dimension. There is an important distinction between:

- the offline stage, which consists of any precomputation involving $\mathbf{H}$, but not $\mathbf{f}$; and
- the online stage, which involves solving $\mathbf{Hu} = \mathbf{f}$ for many different right-hand-sides $\mathbf{f}$.

By online complexity, we mean the runtime for solving the system once in the online stage. The distinction is important in situations like geophysical wave propagation, where offline precomputations are often amortized over the large number of system solves with the same matrix $\mathbf{H}$.

The method of polarized traces can be seen as a hybrid between direct and iterative: it uses efficient direct solvers locally on large subdomains, and shows how to properly couple those subdomains with transmission conditions in the form of incomplete Green's integrals resulting in a boundary integral equation, which is solved iteratively. The novelty is twofold.

First, we show how to reduce the discrete Helmholtz equation to a discrete integral system at the interfaces, using the Green's representation formula. Simultaneously, we use local Green's functions in order to perform polarization into one-way components. For instance, a wave is polarized as up-going at an interface Γ when

$$0 = -\int_\Gamma G(\mathbf{x}, \mathbf{x}')\partial_{\nu_{\mathbf{x}'}} u^{\uparrow}(\mathbf{x}')dx' + \int_\Gamma \partial_{\nu_{\mathbf{x}'}} G(\mathbf{x}, \mathbf{x}')u^{\uparrow}(\mathbf{x}')dx',$$

as long as x is below Γ. These polarization conditions create cancelations the discrete integral system, resulting in an easily preconditionable

system for the polarized interface traces $\mathbf{u}^{\uparrow}$ and $\mathbf{u}^{\downarrow}$ such that $\mathbf{u} = \mathbf{u}^{\uparrow} + \mathbf{u}^{\downarrow}$.

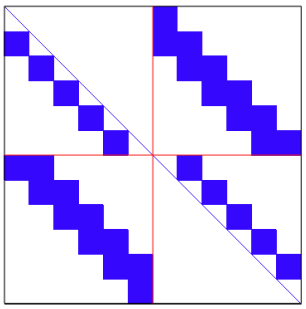

Figure 1: Sparsity pattern of the discrete integral system. The polarized traces preconditioner consists in inverting the triangular upper-left and lower-right blocks, corresponding to the idea of sweeping for computing transmitted waves. The precoditioned system is then solved by GMRES.

Second, we show how to use an adaptive $\mathcal{H}$-matrix fast algorithm for the application of integral kernels, in expressions such as the one above. Empirically, it is shown that one such matrix-vector application can be done in $O(N^{5/8})$ complexity. (Theoretically, we only have the bound $O(N^{3/4})$. The difference owes to discretization effects.) The implementation details are in [**?**].

The method reduces to a sweeping preconditioner when there are as many layers as grid points in one direction ($L = n \sim N^{1/2}$); and it reduces to an efficient direct method when there is no layering ($L = 1$). In both those limits, the online complexity reaches $\mathcal{O}(N)$ up to log factors. The polarized traces solver has online complexity $\mathcal{O}(N/L)$ as long as $L \lesssim N^{1/8}$, asymptotically, hence it is only when the number of layers L obeys $1 \ll L \ll N$ that the method's online complexity is strictly better than $\mathcal{O}(N)$.

3 Numerical results

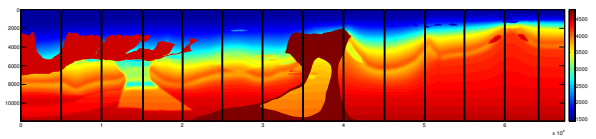

Figure 2: Geophysical benchmark BP 2004 model [**?**].

N	$\omega/2\pi$	$L = 64$	$L = 128$
136×354	1.4	**(8)** 0.84	**(9)** 1.52
269×705	2.7	**(9)** 1.10	**(9)** 2.14
540×1411	5.5	**(9)** 3.06	**(12)** 6.22
1081×2823	11.2	**(10)** 5.75	**(12)** 12.7

Table 1: Number of GMRES iterations (bold) required to reduce the relative residual to 10^{-7}, along with average execution time (in seconds) of one GMRES iteration for different N and L. The frequency is scaled such that $\omega \sim n$. The wavespeed was given by the BP2004 model (Fig. 2).

An $\mathcal{H}-$matrix based direct solver for the Boundary Element Method in 3D elastodynamics

S. Chaillat[1,*], **P. Ciarlet Jr.**[1], **L. Desiderio**[1]

[1]Laboratoire POEMS (UMR CNRS-INRIA-ENSTA 7231), ENSTA Paristech, France

[*]Email: stephanie.chaillat@ensta.fr

Abstract

The main advantage of the Boundary Element Method (BEM) is that only the domain boundaries are discretized leading to a drastic reduction of the total number of degrees of freedom. In traditional BE implementation the dimensional advantage with respect to domain discretization methods is offset by the fully-populated nature of the BEM coefficient matrix. In the present work, we propose a fast method to solve the BEM system in 3-D frequency-domain elastodynamics. Using the $\mathcal{H}$-matrix arithmetic and low-rank approximations (performed with Adaptive Cross Approximation), we derive a fast direct solver. We assess the numerical efficiency and accuracy on the basis of numerical results obtained for problems having known solutions. In particular, we study the efficiency of low-rank approximations when the frequency is increased. The efficiency of the method is also illustrated to study seismic wave propagation in 3-D domains.

Keywords: $\mathcal{H}$-matrix, Boundary Element Method, Direct solver, 3D Elastodynamics.

1 Context

The development of efficient approaches to simulate the propagation of seismic waves in a complex media is crucial for many topics going from understanding the geodynamics of the Earth, the management of underground resources as well as the mitigation of seismic risks. The main advantage of the Boundary Element Method (BEM) is that only the domain boundaries (and possibly interfaces) are discretized leading to a drastic reduction of the total number of degrees of freedom (DOFs). In traditional BE implementation the dimensional advantage with respect to domain discretization methods is offset by the fully-populated nature of the BEM coefficient matrix, with set-up and solution times rapidly increasing with the problem size.

The Fast Multipole Method (FMM) allows one to overcome the drawback of the fully-populated matrix by introducing a fast, reliable and approximate method to compute the linear integral operator. The efficiency of the method has been demonstrated in various fields including in 3D elastodynamics [1]. The FMM requires analytic closed-form expression of the fundamental solution to approximate the integral operator and is defined together with the use of an iterative solver. In 3D elastodynamics, the iteration count becomes the main limitation to use the Fast Multipole accelerated BEM (FM-BEM) on realistic seismological problems [2] (even though algebraic preconditioners can be developed to accelerate the convergence of the iterative solver).

2 Methodology

Other accelerated BEMs, based on hierarchical matrices ($\mathcal{H}$-matrices), have been proposed in the literature [4]. $\mathcal{H}$-matrices permits to approximate the fully-populated BEM matrix by a data-sparse matrix. When used in conjunction with an efficient rank revealing algorithm (for example Adaptive Cross Approximation, ACA) it leads to a data-sparse and memory efficient approximation of the original fully-populated BEM matrix. Contrary to the FM-BEM it is a purely algebraic tool which does not require *a priori* knowledge of the closed-form expression of the fundamental solutions. Such fast BEMs can be used in conjunction with an iterative solver. In computational mechanics, the method has successfully been applied to various problems. For example Coulier et al. [3] have applied the method to the layered half-space elastodynamic fundamental solutions to study soil-structure interaction. Milazzo et al. [5] have applied the method to study anisotropic elastodynamic media.

Recent works (for example [6]) have proposed the development of fast direct solvers based on $\mathcal{H}$-matrices. In the present work, we propose a direct solver based on $\mathcal{H}$-matrices and

ACA for 3-D frequency-domain elastodynamic BEMs (based on the full-space fundamental solutions).

3 Numerical efficiency of the fast BEM

The numerical efficiency and accuracy of the method are assessed on the basis of numerical results obtained for problems having known solutions. In particular, a study of the efficiency of low rank approximations when the frequency is increased is presented: the number of unknowns N is a square function of the frequency (Fig. 1). Finally, the efficiency of the method to study seismic wave propagation in 3-D is demonstrated.

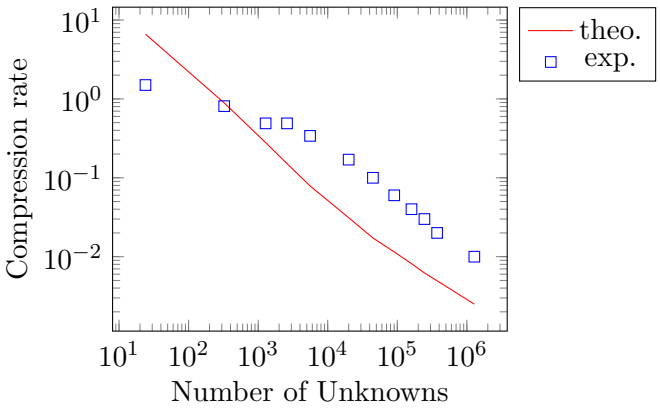

Figure 1: Comparison between the theoretical $N \log N$ and experimental compression rate of the system matrix.

Ongoing work concerns on one hand the study of the efficiency of the method to simulate other configurations like an elastic half-space, layered elastic half-space or anisotropic media and on the other hand the capabilities of such $\mathcal{H}$-matrix based BEMs to define efficient preconditioners for the FM-BEM.

References

[1] S. Chaillat, M. Bonnet, J.F. Semblat. A multi-level fast multipole BEM for 3-D elastodynamics in the frequency domain. *Computer Methods in Applied Mechanics and Engineering*, Vol. **197**, 4233–4249, 2008.

[2] S. Chaillat, J.F. Semblat, M. Bonnet. A preconditioned 3-D multi-region fast multipole solver for seismic wave propagation in complex geometries. *Communications in Computational Physics*, Vol. **11**, 594–609, 2012.

[3] P. Coulier, S. François, G. Lombaert, G. Degrande. Application of hierarchical matrices to boundary element methods for elastodynamics based on Green's functions for a horizontally layered halfspace. *Engineering Analysis with Boundary Elements*, Vol. **37**, 1745–1758, 2013.

[4] W. Hackbusch. A Sparse Matrix Arithmetic Based on $\mathcal{H}$-Matrices. Part I: Introduction to $\mathcal{H}$-Matrices. *Computing*, Vol. **62**, 89–108, 1999.

[5] A. Milazzo, I. Benedetti, M.H. Aliabadi. Hierarchical fast BEM for anisotropic time-harmonic 3-D elastodynamics. *Computers & Structures*, Vol. **96**, 9–24, 2012.

[6] J. Shaeffer. Direct solve of electrically large integral equations for problem sizes to 1M unknowns. *IEEE Transactions on Antennas and Propagation*, Vol. **56**, 2306–2313, 2008.

The Double Absorbing Boundary (DAB) Method

Dan Givoli[1,*], **Daniel Rabinovich**[1], **Daniel Baffet**[2], **Thomas Hagstrom**[3], **Jacobo Bielak**[4]

[1]Dept. of Aerospace Engineering, Technion, Haifa, Israel
[2]Dept. of Mathematics, EPFL, Lausanne, Switzerland
[3]Dept. of Mathematics, Southern Methodist University, Dallas, TX, USA
[4]Dept. of Civil Eng., Carnegie-Mellon University, Pittsburgh, PA, USA
[*]Email: givolid@technion.ac.il

Abstract

A new approach, called the Double Absorbing Boundary (DAB) is presented. DAB is devised for solving wave problems in unbounded domains. It has common features to high-order ABC and to PML. However, it is different from both methods and enjoys relative advantages with respect to both.

Keywords: Double Absorbing Boundary, Absorbing Boundary Condition, Non-Reflecting Boundary Condition, Perfectly Matched Layer, Acoustic Waves, Elastic Waves

1 Introduction

The need for artificial computational boundaries in the solution of exterior wave problems, called "absorbing boundaries" among other names, arises quite often in various fields of application. In solid-earth geophysics they are needed for practically every simulation. Since the mid 90's two classes of methods have emerged as especially powerful: the Perfectly Matched Layer (PML) method [1, 2] and the method of using high-order Absorbing Boundary Conditions (ABCs), which are local and involve no high derivatives [3, 4]. The use of ABCs has been very popular already since the early 70's, but the term "high-order ABCs" relates to the ability to implement ABCs of an arbitrarily high order. High-order derivatives are eliminated by introducing auxiliary variables which are discretized on the boundary.

Most of the high-order ABCs proposed thus far have been devised for the acoustic (scalar) wave equation. Until recently, the only ABCs proposed for elastic waves were that devised by Tsogka and Joly and that devised by Rabinovich et al. Both turned out to be unstable for long times.

2 The DAB Approach

In this presentation a new approach is reported that has been devised for solving wave problems in unbounded domains. It has common features to high-order ABC and to PML. However, it is different from both and enjoys relative advantages with respect to both. The new method, called the Double Absorbing Boundary (DAB) method, is based on truncating the unbounded domain to produce a finite computational domain, and on applying a local high-order ABC on two parallel artificial boundaries, which are a small distance apart, and thus form a thin non-reflecting layer. Auxiliary variables are defined on the two boundaries and inside the layer bounded by them, and participate in the numerical scheme.

The DAB method is first introduced in general terms, and then it is applied to the scalar wave equation in a wave guide, and to elastodynamics problems in homogeneous and heterogeneous media. Standard finite element discretization in space and dissipative time stepping are employed. The computational aspects of the method are discussed, showing its advantages over using a single ABC or a PML. A stability proof is also provided. Numerical experiments demonstrate the performance of the new method.

Fig. 1 shows the "ladder" structure of the DAB equations, for the case of acoustics. The figure shows the flow of information on each of the two artificial boundaries. The termination condition on the outer boundary is the Lysmer-Kuhlemeyer condition, which is responsible to the stability of the ABC, as was proved in [5].

In [6], the new method was applied to the scalar wave equation. We incorporated the DAB in a fully explicit finite difference scheme in 1D, and in a Finite Element (FE) scheme in 2D. In [7] the DAB was applied to problems in 2D isotropic elastodynamics, written in first-order

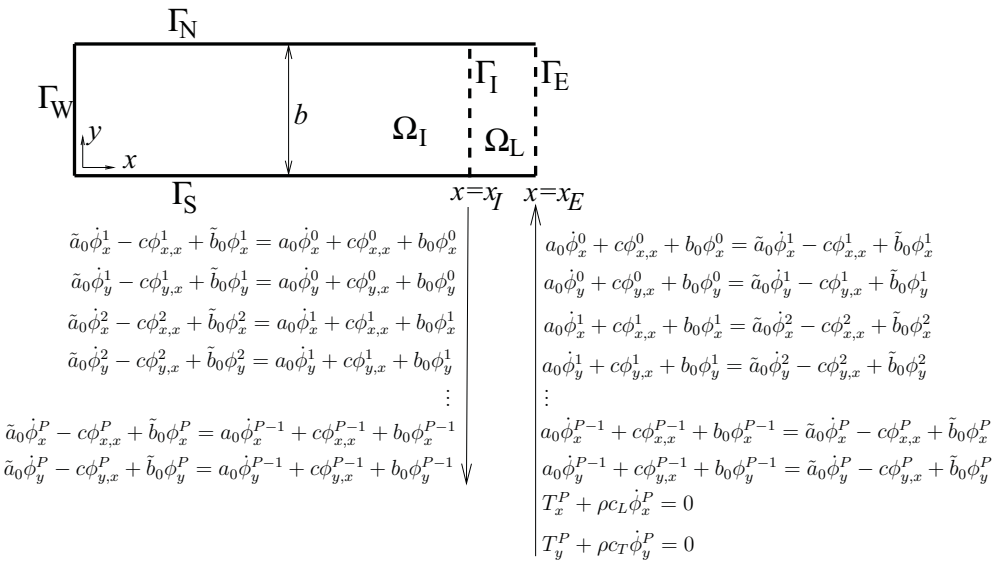

Figure 1: The "ladder" structure of the DAB, showing the flow of information on the two boundaries bounding the layer.

conservation form. The problem was discretized using the Lax–Wendroff finite difference scheme. In [8] we apply DAB to problems in elastodynamics in a homogeneous and layered medium using FEs in space and Newmark time-stepping. In the entire study the problem is solved with a waveguide geometry.

3 Stability

In [7], a well-posedness proof was provided for the DAB scheme for the acoustics problem written in second-order form. The energy method was employed to obtain uniform-in-time estimates of the norm of the solution and the auxiliary functions, thus establishing the well-posedness and asymptotic stability of the DAB formulation.

In the elastic case, our formulation and numerical examples assume periodic boundary conditions along the boundaries perpendicular to the artificial DAB boundaries. This choice is made since some stability issues arise when the periodic conditions are replaced by some physical boundary conditions (e.g., traction free conditions). Attempts to resolve these issues are underway. No such difficulties occur in the acoustic case.

Acknowledgement

This work was supported by the US-Israel Binational Science Foundation (BSF), grant number 890020 (Technion number 2011303). The work of DG was also supported by the fund provided through the Lawrence and Marie Feldman Chair in Engineering; that of TH by NSF grant DMS-1418871 and ARO grant W911NF-09-1-0344; and that of JB by the U.S. National Science Foundation Award No. NSF OCI-0749227. Any conclusions or recommendations in the paper are those of the authors and do not necessarily represent the views of the BSF, NSF or ARO.

References

[1] J.P. Bérenger, A Perfectly Matched Layer for the Absorption of Electromagnetic Waves, *Journal of Computational Physics* **114** (1994), pp. 185–200.

[2] A. Bermudez, L. Hervella-Nieto, A. Prieto and R. Rodriguez, Perfectly Matched Layers for Time-Harmonic Second Order Elliptic Problems, *Archives Comput. Meth. in Engng.* **17** (2010), pp. 77–107.

[3] F. Collino, High Order Absorbing Boundary Conditions for Wave Propagation Models. Straight Line Boundary and Corner Cases, in *Proc. 2nd Int. Conf. on Mathematical & Numerical Aspects of Wave Propagation, R. Kleinman et al., Eds., SIAM, Delaware, USA, 1993,* pp. 161–171.

[4] D. Givoli, High-Order Local Non-Reflecting Boundary Conditions: A Review, *Wave Motion* **39** (2004), pp. 319–326.

[5] D. Baffet, J. Bielak, D. Givoli, T. Hagstrom and D. Rabinovich, Long-Time Stable High-Order Absorbing Boundary Conditions for Elastodynamics, *Computer Methods in Applied Mechanics and Engineering* **241–244** (2012), 20–37.

[6] T. Hagstrom, D. Givoli, D. Rabinovich and J. Bielak, The Double Absorbing Boundary Method, *Journal of Computational Physics* **259** (2014), 220–241.

[7] D. Baffet, T. Hagstrom and D. Givoli, Double Absorbing Boundary Formulations for Acoustics and Elastodynamics, *SIAM J. on Sci. Comput.* **36** (2014), A1277–A1312.

[8] D. Rabinovich, D. Givoli, J. Bielak and T. Hagstrom, The Double Absorbing Boundary Method for Elastodynamics in Homogeneous and Layered Media, *Advanced Modeling and Simulation in Engineering Sciences*, under review.

A new discontinuous Galerkin formulation for wave equations in second order form

Daniel Appelö[1,*], **Thomas Hagstrom**[2]
[1]Department of Mathematics and Statistics, The University of New Mexico
[2]Department of Mathematics, Southern Methodist University
[*]Email: appelo@math.unm.edu

Abstract

We develop and analyze a new strategy for discontinuous Galerkin discretization of wave equations in second order form. The method features a direct, parameter-free approach to defining interelement fluxes. Both upwind and energy-conserving discretizations can be devised. We derive a priori error estimates in the energy norm for certain fluxes and present numerical experiments showing that optimal convergence in L^2 is obtained.

Keywords: Discontinuous Galerkin, Second order wave equation

We consider, in general, wave equations associated with a nonnegative energy functional or Hamiltonian

$$E(t) = \int_\Omega \frac{1}{2} \left| \frac{\partial \mathbf{u}}{\partial t} \right|^2 + G(\mathbf{u}, \nabla \mathbf{u}, \mathbf{x}). \quad (1)$$

Here $\Omega \subset \mathbb{R}^d$, $\mathbf{u}(\mathbf{x}, t) \in \mathbb{R}^m$. The system of wave equations we aim to solve, which can be identified as the Euler-Lagrange equations derived from the action principle associated with the Lagrangian $\frac{1}{2} \left| \frac{\partial \mathbf{u}}{\partial t} \right|^2 - G - \mathbf{u} \cdot \mathbf{f}$, is given by

$$\frac{\partial^2 u_i}{\partial t^2} = \sum_k \frac{\partial}{\partial x_k} \left(\frac{\partial G}{\partial u_{i,k}} \right) - \frac{\partial G}{\partial u_i} + f_i, \quad (2)$$

where we define $u_{i,k} = \frac{\partial u_i}{\partial x_k}$. Then introducing as a new variable, $v_i = \frac{\partial u_i}{\partial t}$, we find that the change of energy on an element Ω_j is given by the source term and a boundary contribution

$$\frac{d}{dt} \int_{\Omega_j} \frac{1}{2} |\mathbf{v}|^2 + G = \int_{\Omega_j} \mathbf{v} \cdot \mathbf{f} + \int_{\partial \Omega_j} \sum_{i,k} v_i \frac{\partial G}{\partial u_{i,k}} n_k, \quad (3)$$

where $\mathbf{n}$ denotes the outward unit normal.

To discretize on a simplicial element we require that the components of $(\mathbf{u}^h, \mathbf{v}^h)$ restricted to Ω_j be polynomials of degree s and q respectively; that is elements of $(\Pi^s)^m \times (\Pi^q)^m$. Typically we choose $s = q + 1$ corresponding to the role of v_i^h as an approximate derivative of u_i^h, but the stability theory allows independent choice of approximation spaces.

Now specialize to the linear case; that is, assume that G depends quadratically on $\mathbf{u}$. We seek approximations to the system

$$\frac{\partial u_i}{\partial t} - v_i = 0, \quad (4)$$

$$\frac{\partial v_i}{\partial t} - \sum_k \frac{\partial}{\partial x_k} \left(\frac{\partial G}{\partial u_{i,k}} \right) + \frac{\partial G}{\partial u_i} = f_i, \quad (5)$$

satisfying a discrete energy identity analogous to (3). To motivate our choice consider the time derivative of the discrete energy in Ω_j:

$$\frac{dE_j^h}{dt} = \sum_i \int_{\Omega_j} v_i^h \frac{\partial v_i^h}{\partial t} + \sum_k \frac{\partial G}{\partial u_{i,k}} \frac{\partial^2 u_i^h}{\partial x_k \partial t} + \frac{\partial G}{\partial u_i} \frac{\partial u_i^h}{\partial t}. \quad (6)$$

To develop a weak form compatible with the discrete energy we test (4) with

$$-\sum_k \frac{\partial}{\partial x_k} \frac{\partial G}{\partial u_{i,k}} (\phi_u, \nabla \phi_u, \mathbf{x}) + \frac{\partial G}{\partial u_i} (\phi_u, \nabla \phi_u, \mathbf{x}),$$

$\phi_u \in (\Pi^s)^m$, and (5) by $\phi_{v,i} \in \Pi^q$. In addition we impose corrections based on boundary states

$$v_i^* \approx v_i, \qquad w_{i,k}^* \approx \frac{\partial G}{\partial u_{i,k}}. \quad (7)$$

This results in the equations for $i = 1, \ldots, m$:

$$\int_{\Omega_j} \left(-\sum_k \frac{\partial}{\partial x_k} \frac{\partial G}{\partial u_{i,k}} (\phi_u) + \frac{\partial G}{\partial u_i} (\phi_u) \right) \left(\frac{\partial u_i^h}{\partial t} - v_i^h \right) = \int_{\partial \Omega_j} \sum_k n_k \frac{\partial G}{\partial u_{i,k}} (\phi_u) \left(v_i^* - \frac{\partial u_i^h}{\partial t} \right), \quad (8)$$

$$\int_{\Omega_j} \phi_{v,i} \frac{\partial v_i^h}{\partial t} + \phi_{v,i} \left(-\sum_k \frac{\partial}{\partial x_k} \frac{\partial G}{\partial u_{i,k}} (\mathbf{u}^h) + \frac{\partial G}{\partial u_i} (\mathbf{u}^h) \right) - \phi_{v,i} f_i = \int_{\partial \Omega_j} \phi_{v,i} \sum_k n_k \left(w_{i,k}^* - \frac{\partial G}{\partial u_{i,k}} (\mathbf{u}^h) \right). \quad (9)$$

Note that we have suppressed the dependence on the gradient and the spatial coordinate.

Although, by construction, solutions of (8)-(9) will satisfy an energy identity, these equations are often insufficient to uniquely determine the time derivatives within an element. In particular, in many cases G is invariant with respect to certain transformations of $\mathbf{u}$. In the linear case the transformations are generated by null vectors, $u_{i,k} = \frac{\partial \tilde{\phi}_{u,i}}{\partial x_k}$, $u_i = \tilde{\phi}_{u,i} \in \mathcal{N}$ associated with equation (8) and we must supplement it by

$$\sum_i \int_{\Omega_j} \tilde{\phi}_{u,i} \left(\frac{\partial u_i^h}{\partial t} - v_i^h \right) = 0. \qquad (10)$$

Fluxes

To complete the problem specification we must prescribe the states $\mathbf{w}^*$, $\mathbf{v}^*$ both at interelement and physical boundaries. Label two elements sharing an internal boundary by 1 and 2. Then their net contribution to the energy derivative can be shown to be the integral of

$$J^h = \sum_{i,k} \left(v_{i,1}^h n_k^{(1)} + v_{i,2}^h n_k^{(2)} \right) w_{i,k}^* + \left(v_i^* - v_{i,1}^h \right) \frac{\partial G}{\partial u_{i,k}} (\mathbf{u}_1^h) n_k^{(1)} + \left(v_i^* - v_{i,2}^h \right) \frac{\partial G}{\partial u_{i,k}} (\mathbf{u}_2^h) n_k^{(2)}.$$

This contribution can be controlled by choosing the fluxes according to the general parametrization

$$\begin{aligned} v_i^* &= \left(\alpha_i v_{i,1}^h + (1-\alpha_i) v_{i,2}^h \right) - \tau_i [[D_{\nabla u_i} G^h]], \\ w_{i,k}^* &= -\beta_i [[v_i^h]]_k \\ &\quad + \left((1-\alpha_i) \frac{\partial G}{\partial u_{i,k}} (\mathbf{u}_1^h) + \alpha_i \frac{\partial G}{\partial u_{i,k}} (\mathbf{u}_2^h) \right). \end{aligned}$$

Then

$$J^h = -\sum_i \left[\beta_i \left| [[v_i^h]] \right|^2 + \tau_i [[D_{\nabla u_i} G^h]]^2 \right],$$

leading to an energy stable method for β_i, $\tau_i \geq 0$. Some examples are:

Central flux : $\alpha_i = 1/2$, $\beta_i = \tau_i = 0$.

Alternating flux : $\alpha_i = 0, 1$, $\beta_i = \tau_i = 0$.

Sommerfeld flux : $\alpha_i = 1/2$, $\beta_i = \frac{1}{2}$, $\tau_i = \frac{1}{2}$.

The flux specification at boundaries is similarly straightforward and will be discussed in the talk.

Error estimates

For the scalar wave equation we present error estimates in the energy norm for all flux choices considered. Optimal convergence is proven in one space dimension for flux parameters satisfying a certain algebraic relation, which covers both the energy-conserving alternating flux and the dissipative upwind Sommerfeld flux. Simple numerical experiments with the scalar wave equation lead to the observation that the convergence in L^2 is one order higher than in the energy norm, and that optimal convergence with the alternating or upwind flux is maintained for a non-Cartesian grid of quadrilaterals.

Applications

We will present applications of the general formulation to the scalar wave equation as well as to the elastic wave equation (see also [1,2]). For the elastic wave equation we will demonstrate the approximation properties of the method by solving a sequence of classical benchmark problems.

References

[1] D. Appelö and T. Hagstrom, A new discontinuous Galerkin formulation for wave equations in second order form, *SINUM, in press* (2015).

[2] D. Appelö and T. Hagstrom, An energy-based discontinuous Galerkin discretization of the elastic wave equation in second order form, *in preparation* (2015).

Acknowledgement

DA was supported in part by NSF Grant DMS-1319054. Any conclusions or recommendations expressed in this paper are those of the author and do not necessarily reflect the views of NSF. TH was supported in part by ARO Contract W911NF-09-1-0344 and NSF Grant OCI-0904773. Any conclusions or recommendations expressed in this paper are those of the author and do not necessarily reflect the views of ARO or NSF.

A FEM-BEM coupling for wave scattering problems with rotating obstacles

Silvia Falletta[1,*], **Giovanni Monegato**[1]

[1]Dipartimento di Scienze Matematiche, Politecnico di Torino, Italy

*Email: silvia.falletta@polito.it

Abstract

We consider the problem of a wave scattered by a moving obstacle $\mathcal{O} \subset \mathbb{R}^2$ having a sufficiently smooth boundary Γ. The fictitious domain method ([2]), or embedding method, consists in extending artificially the solution inside the obstacle and in imposing the boundary condition on Γ weakly, by means of lagrange multipliers. The main point is that the mesh for the solution on the enlarged domain can be chosen independently of the geometry of the obstacle. In order to obtain a finite computational domain, we further need to truncate the infinite external domain by an artificial boundary $\mathcal{B}$ and to impose on it transparent boundary conditions. We choose a Non Reflecting Boundary Condition (NRBC) based on a space-time integral equation and defining a relationship between the solution of the differential problem and its normal derivative on $\mathcal{B}$ (see [1]). We analyze the coupled problem and we apply it to the scattering of waves by moving (rotating) rigid bodies. In this case the method avoids the complexity of constructing at each time step a new finite element computational mesh.

Keywords: fictitious domain, absorbing boundary conditions

1 Introduction

Let $\mathcal{O} \subset \mathbb{R}^2$ be an open bounded domain, which in general may be subject to a rigid motion, with a sufficiently smooth boundary Γ . We consider, in the time domain, the wave propagation problem in $\mathbb{R}^2 \setminus \bar{\mathcal{O}}$ and, for its solution by a finite element method, we introduce an artificial boundary $\mathcal{B}$ where we impose transparent conditions (see [1]). In particular, we introduce the single and double layer integral operators

$$\boldsymbol{\mathcal{V}}\psi(\mathbf{x},t) = \int_0^t \int_{\mathcal{B}} G(\mathbf{x}-\mathbf{y}, t-\tau)\psi(\mathbf{y},\tau) d\mathcal{B}_{\mathbf{y}} d\tau,$$

and

$$\boldsymbol{\mathcal{K}}\varphi(\mathbf{x},t) = \int_0^t \int_{\mathcal{B}} \partial_{\mathbf{n}_{\mathcal{D}}} G(\mathbf{x}-\mathbf{y}, t-\tau)\varphi(\mathbf{y},\tau) d\mathcal{B}_{\mathbf{y}} d\tau,$$

where $G(\mathbf{x},t) = H(t-\|\mathbf{x}\|)/(2\pi\sqrt{t^2-\|\mathbf{x}\|^2})$ denotes the fundamental solution of the wave equation (being $H(\cdot)$ the Heaviside function). We consider the following problem in the finite computational domain Ω, which is bounded internally by Γ and externally by $\mathcal{B}$:

$$\begin{cases} u_{tt} - \Delta u & = f & \text{in } \Omega \\ u & = 0 & \text{on } \Gamma \\ \frac{1}{2}u - \boldsymbol{\mathcal{V}}\partial_n u + \boldsymbol{\mathcal{K}} u & = 0 & \text{on } \mathcal{B} \\ u(\mathbf{x},0) & = u_0 & \text{in } \Omega \\ u_t(\mathbf{x},0) & = v_0 & \text{in } \Omega. \end{cases} \qquad (1)$$

2 The fictitious domain approach

In order to describe the fictitious domain approach, we introduce the larger and simpler domain $\widetilde{\Omega}$ that includes $\mathcal{O}$ and is bounded by the artificial boundary $\mathcal{B}$. The main idea of the fictitious domain method (or domain embedding method) consists in extending artificially the solution of the exterior problem inside the obstacle, and to solve the new problem in the whole extended domain $\widetilde{\Omega}$. The main advantage of this approach is the possibility of solving the problem in a simpler domain by treating the Dirichlet boundary conditions on Γ by lagrange multipliers, and of choosing the mesh of the enlarged domain independent of the geometry of the obstacle, thus allowing to use structured, regular meshes over the extended domain.

For a generic function w, we set $w(t)(\mathbf{x}) := w(\mathbf{x},t)$. Then, the problem defined in the domain of interest $\widetilde{\Omega}$ consists in:

find the unknown functions $u(t) \in H^1(\widetilde{\Omega})$, $\lambda_\Gamma(t) \in H^{-1/2}(\Gamma)$, $\lambda_{\mathcal{B}}(t) \in H^{-1/2}(\mathcal{B})$ such that the following generalized saddle-point evolution problem

$$\begin{cases} (\ddot{u}(t), v)_{\widetilde{\Omega}} + a(u(t), v) + \\ \qquad + < \lambda_\Gamma(t), v >_\Gamma + < \lambda_{\mathcal{B}}(t), v >_{\mathcal{B}} = (f(t), v)_{\widetilde{\Omega}} \\ \\ < \varphi, u(t) >_\Gamma = 0 \\ \\ 2 < \boldsymbol{\mathcal{V}} \lambda_{\mathcal{B}}(t), \mu >_{\mathcal{B}} - < \mu, u(t) >_{\mathcal{B}} \\ \qquad\qquad -2 < \mu, \boldsymbol{\mathcal{K}} u(t) >_{\mathcal{B}} = 0 \\ u(0) = u_0 \\ \frac{du}{dt}(0) = v_0. \end{cases} \tag{2}$$

holds in the distributional sense in $(0, T)$, where $a : H^1(\widetilde{\Omega}) \times H^1(\widetilde{\Omega}) \to \mathbb{R}$ is the bilinear form

$$a(v, w) = \int_{\widetilde{\Omega}} \nabla v \cdot \nabla w,$$

and $(v, w)_{\widetilde{\Omega}} = \int_{\widetilde{\Omega}} vw$. The bilinear forms $< \lambda_\Gamma(t), v >_\Gamma$ and $< \lambda_{\mathcal{B}}(t), v >_{\mathcal{B}}$ denote the duality pairing between $H^{-1/2}(\Gamma)$ and $H^{1/2}(\Gamma)$, and $H^{-1/2}(\mathcal{B})$ and $H^{1/2}(\mathcal{B})$, respectively.

We discretize the space-time integral equation on $\mathcal{B}$ by combining a second order (in time) BDF convolution quadrature and a Galerkin (or a collocation) method in space. Such a discretization is then coupled with an uncoditionally stable ODE time integrator and a FEM in space. The finite element mesh for the solution in the enlarged domain $\widetilde{\Omega}$ is chosen independently of the geometry of the obstacle, and the constraint on Γ is imposed by a matrix B_h that represents a discrete trace operator.

A particularly useful application of this approach is the scattering of a wave by moving rigid bodies. In this case the method avoids the complexity of constructing at each time step a new finite element computational mesh and requires only the construction of the discrete trace operator B_h. We have applied the proposed method to problems of waves generated by non trivial data and scattered by rotating bodies. In Figure 1 we show the snapshots of a wave that, starting from a initial value u_0 with initial null velocity v_0 , impinges upon an ellipsoidal scattering that rotates with constant velocity around the origin. In Figure 2 we show the behavior of the solution at a point $P \approx (10, 0)$ that belongs to the artificial boundary (left plot) and the energy behavior of the system with respect to time (right plot). The wave bumps the rotating obstacle around $t = 3.5$, and the energy is preserved up to the time instant $t \approx 5$, when the wave reaches the transparent boundary and leaves the computational domain.

Figure 1: Snapshots of the solution with a non trivial initial datum u_0, at different times.

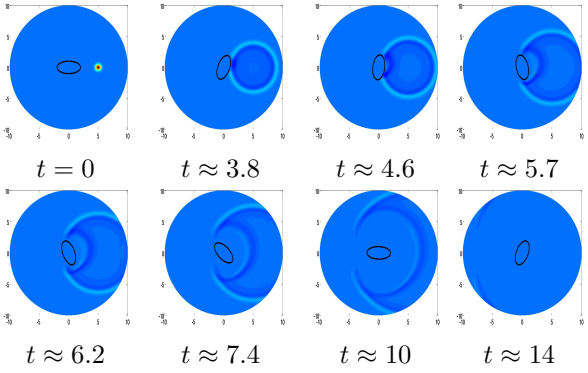

Figure 2: Behavior of the solution at $P \approx (10, 0)$ (left plot) and energy dissipation (right plot).

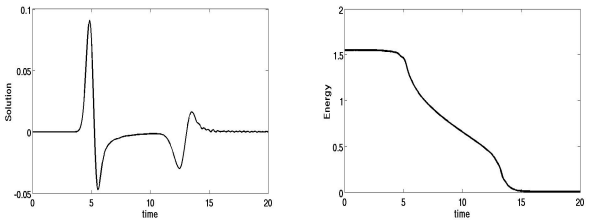

References

[1] S. Falletta, G. Monegato, An exact non reflecting boundary condition for 2D time-dependent wave equation problems. Wave Motion 51 (2014), no. 1, 168–192.

[2] V. Girault, R. Glowinski, Error analysis of a fictitious domain method applied to a Dirichlet problem. Japan J. Indust. Appl. Math 12 (1995), 487–524.

Minisymposium: Boundary Integral Equations for Time Harmonic Scattering

organised by Xavier Claeys and Euan Spence

This minisymposium will focus on the derivation and numerical analysis of computationally efficient boundary element methods for time harmonic wave propagation problems, both from theoretical and practical point of view. Several talks will concern intrinsically well conditioned boundary integral formulations discussing the Generalized Combined Field Integral Equation strategy in the context of elastodynamics (S.Chaillat) or for transmission problems (C.Turc). Another important topic will concern integral formulations for geometrically complex problems such as scattering by fractal planar screens (D.Hewett), or multi-subdomain diffraction treated by means of a first kind multi-trace formulation (C.Jerez) or a second kind single-trace formulation (E.Spindler). Other aspects of boundary element methods discussed in this minisymposium will include high frequency adapted quadrature techniques (V.Dominguez) and a posteriori error analysis and adaptative mesh refinement strategy in the context of integral equations (M.Bakry).

A Well-Conditioned Fast Multipole Boundary Element Method for 3-D Elastodynamics

S. Chaillat[1,*], **M. Darbas** [2], **F. Le Louër**[3]

[1]Laboratoire POEMS (UMR CNRS-INRIA-ENSTA 7231), ENSTA Paristech, FRANCE
[2]LAMFA (UMR CNRS 7352), Université de Picardie Jules Verne, FRANCE
[3]LMAC, Université de Technologie de Compiègne, FRANCE
[*]Email: stephanie.chaillat@ensta-paristech.fr

Abstract

The fast multipole accelerated boundary element method (FM-BEM) is a possible approach to deal with scattering problems of time-harmonic elastic waves by a three-dimensional rigid obstacle. In 3D elastodynamics, the FM-BEM has been shown to be efficient with solution times of order $O(N \log N)$ per iteration (where N is the number of BE degrees of freedom). However, the number of iterations in GMRES can significantly hinder the overall efficiency of the FM-BEM. To reduce the number of iterations, we propose a clever integral representation of the scattered field which naturally incorporates a regularizing operator. When considering Dirichlet boundary value problems, the regularizing operator is a high-frequency approximation to the Dirichlet-to-Neumann operator, and is constructed in the framework of the On-Surface Radiation Condition (OSRC) method. This OSRC-like preconditioner is successfully applied to Dirichlet exterior problems in 3D elastodynamics.

Keywords: Analytic Preconditioner, fast BEM, approximate Dirichlet-to-Neumann operator, OSRC, 3D Elastodynamics

1 Motivations

When considering the solution of scattering problems of time-harmonic elastic waves by a three-dimensional rigid obstacle, the main difficulty in the numerical simulation comes from the unbounded characteristic of the computational domain. The boundary element method (BEM) is one possible approach to overcome this issue. The method results from the discretization of boundary integral equations (BIE). In traditional boundary element (BE) implementations, the dimensional advantage with respect to domain discretization methods is offset by the fully-populated nature of the BEM coefficient matrix. The Fast Multipole Method (FMM) permits to overcome the drawback of the fully-populated matrix by introducing a fast and approximate method to compute the linear integral operator in conjunction with the use of an iterative solver (e.g. GMRES). In 3D elastodynamics the FM-BEM has been shown to be efficient [1] with solution times of order $O(N \log N)$ per iteration (where N is the number of BE degrees of freedom). However, the number of iterations in GMRES can significantly hinder the overall efficiency of the FM-BEM even though an algebraic preconditioner is applied [2]. Preconditioning the FM-BEM is therefore an important practical issue. A possible approach consists in exploiting mathematical properties of the relevant continuous integral operators.

2 Methodology

In [3], Darbas *et al.* present the successful combination of an On-Surface Radiation Condition (OSRC)-based preconditioner and a FM-BEM to define an efficient solver for 3-D acoustic scattering by sound-hard obstacles at high frequencies. The idea is to consider a clever integral representation of the scattered field which naturally incorporates a regularizing operator. The objective is to force the boundary integral operator arising from this representation to become a compact perturbation of the identity operator. When considering Dirichlet boundary value problems, the regularizing operator is a high-frequency approximation to the Dirichlet-to-Neumann (DtN) operator, and is constructed in the framework of the On-Surface Radiation Condition (OSRC) method. This approximate method has been successfully proposed and applied in acoustics and electromagnetism but its extension to 3D elastodynamics is involved. A preparatory theoretical work has been proposed by Darbas and Le Louër [4] to derive an OSRC-

like preconditioner to solve Dirichlet exterior scattering problems in 3D elasticity. We propose here a first extension of the OSRC method to 3D elastodynamic problems and its application as a preconditioner of the FM-BEM. The preconditioned Combined field integral equation for an incident field u^{inc} reads:
Find $\boldsymbol{\varphi} = -\gamma_1^+(\mathbf{u} + \mathbf{u}^{inc})$ solution to

$$(\frac{I}{2} + D' - \boldsymbol{\Lambda}'_\varepsilon S)\boldsymbol{\varphi} = -(\gamma_1^+\mathbf{u}^{inc} - \boldsymbol{\Lambda}'_\varepsilon\gamma_0^+\mathbf{u}^{inc})$$

where S and D' are the classical boundary integral operators; γ_0^+ and γ_1^+ are respectively the Dirichlet and Neumann traces; and Λ'_ε is the approximation of the DtN.

3 Results

This communication is organized as follows. First, the approximation of the DtN proposed in [4] and its application in the OSRC context is presented. The low costs of the ORSC method to construct an approximate solution of the exterior Navier problem at high frequencies is demonstrated for different obstacles (see for example Fig. 1). Then, the proposed approximation of the DtN is used to precondition the FM-BEM in a black box framework. Finally, the numerical efficiency of the combination of the OSRC-based preconditioner with a FM-BEM solver is presented on high-frequency 3-D cases. The independence of the iteration counts with respect to the mesh density and frequency is confirmed on numerical examples. The additional computational cost of the preconditioner is shown to be negligible compared to the cost of a FMM accelerated matrix-vector product.

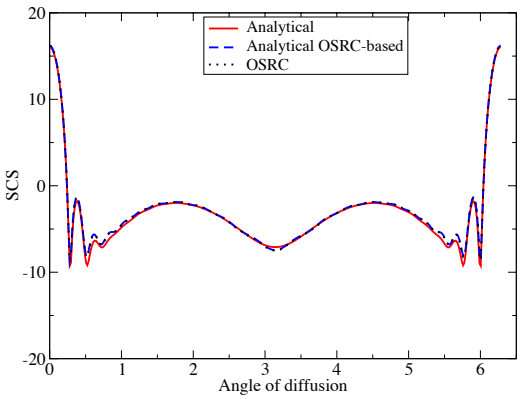

Figure 1: Diffraction of plane P-waves by a unit sphere ($\kappa_s = 8\pi$): comparison of the SCS for the analytical solution, the analytical OSRC-based solution and the OSRC-based solution.

References

[1] S. Chaillat, M. Bonnet, J.F. Semblat. A multi-level fast multipole BEM for 3-D elastodynamics in the frequency domain. *Computer Methods in Applied Mechanics and Engineering*, Vol. **197**, 4233–4249, 2008.

[2] S. Chaillat, J.F. Semblat, M. Bonnet. A preconditioned 3-D multi-region fast multipole solver for seismic wave propagation in complex geometries. *Communications in Computational Physics*, Vol. **11**, 594–609, 2012.

[3] M. Darbas, E. Darrigrand, Y. Lafranche. Combining analytic preconditioner and Fast Multipole Method for the 3D Helmholtz equation. *Journal of Computational Physics*. Vol. **236**, 289–316, 2013.

[4] M. Darbas, F. Le Louër. Analytic preconditioners for the iterative solution of elasticity scattering problems. *Mathematical Methods in the Applied Sciences*, Vol. **38**, 1705-1733, 2015.

Comparisons of integral equations formulations for high-frequency two-dimensional Helmholtz transmission problems in domains with corners

Catalin Turc[1,*], **Víctor Domínguez**[2], **Mark Lyon**[3]

[1]Department of Mathematics New Jersey Institute of Technology, Newark, USA
[2]Ingeniería Matemática e Informática E.T.S.I.I.T. Universidad Pública de Navarra, Spain
[3]Department of Mathematics University of New Hampshire, Durham, USA
[*]Email: catalin.c.turc@njit.edu

Abstract

We present comparisons between the performance of high-order Nyström solvers based on various boundary integral formulations of transmission Helmholtz problems in Lipschitz domains in the high-frequency regime. The main formulations under considerations are: (1) the first kind formulation of Costabel and Stephan [4]; (2) the second kind formulations of Kress and Roach [1]; (3) the single integral formulation of Kleinman and Martin [2]; (4) the Multiple Trace Formulation of Claeys, Jerez-Hanckes and Hiptmair [3]; and (5) a *direct* regularized combined field formulation recently introduced by some of the authors [5]. We also establish the well-posedness of some of the formulations above.

Keywords: Helmholtz transmission problems, High-frequency, Lipschitz domains

1 Introduction

We consider the transmission Helmholtz problem involving two time-harmonic fields u^1 and u^2 that result as an incident field u^{inc} impinges upon the boundary Γ of a homogeneous dielectric scatterer D_2. We assume that both media occupying the bounded region D_2 and its exterior are nonmagnetic, and the electric permitivity of the dielectric material inside the domain D_2 is denoted by ϵ_2 while that of the medium occupying the exterior of D_2 is denoted by ϵ_1. We seek a radiating field u^1 and a field u^2 such that

$$\begin{aligned} \Delta u^2 + k_2^2 u^2 &= 0, \qquad \text{in } D_2, \\ \Delta u^1 + k_1^2 u^1 &= 0, \qquad \text{in } D_1 = \mathbb{R}^2 \setminus \overline{D_2}, \end{aligned} \tag{1}$$

given an incident field u^{inc}, where the wavenumbers $k_i, i = 1, 2$ are defined as $k_i = \omega\sqrt{\epsilon_i}, i = 1, 2$ in terms of the frequency ω. In addition, the fields u^1, u^{inc}, and u^2 are related on the boundary Γ by the following boundary conditions

$$\begin{aligned} \gamma_D^1 u^1 + \gamma_D^1 u^{inc} &= \gamma_D^2 u^2 \qquad \text{on } \Gamma \\ \gamma_N^1 u^1 + \gamma_N^1 u^{inc} &= \nu \gamma_N^2 u^2 \qquad \text{on } \Gamma. \end{aligned} \tag{2}$$

In equations (2) and what follows $\gamma_D^i, i = 1, 2$ denote exterior and respectively interior Dirichlet traces, whereas $\gamma_N^i, i = 1, 2$ denote exterior and respectively interior Neumann traces taken with respect to the exterior unit normal on Γ. We assume that the boundary Γ is a closed Lipschitz curve in $\mathbb{R}^2$. In what follows we denote by S_j, K_j, $K_j^\top$, and N_j the boundary integral operators corresponding to the wavenumber K_j that feature in the Calderón calculus.

We present next the main integral formulation we consider. We start with the CFIEFK formulation [4] and the CFIESK formulation [1] posed in terms of the total field $u = u^1 + u^{inc}$ and its normal derivative on Γ taken with respect to the unit normal pointing into D_1:

$$\begin{aligned} -(K_1 + K_2)[u] + (\nu^{-1} S_2 + S_1)[\partial_n u] &= u^{inc} \\ -(N_1 + \nu N_2)[u] + (K_1^\top + K_2^\top)[\partial_n u] &= \partial_n u^{inc}, \end{aligned} \tag{3}$$

$$\begin{pmatrix} (K_2 - \nu^{-1} K_1) & \nu^{-1}(S_1 - S_2) \\ N_2 - N_1 & (K_1^\top - \nu^{-1} K_2^\top) \end{pmatrix} \begin{pmatrix} u \\ \partial_n u \end{pmatrix} + \frac{\nu^{-1} + 1}{2} \begin{pmatrix} u \\ \partial_n u \end{pmatrix} = \begin{pmatrix} u^{inc} \\ \partial_n u^{inc} \end{pmatrix} \tag{4}$$

The *single* integral equation [2] (SCFIE) is given by

$$-(1+\nu)/2\mu + \mathbf{K}\mu - i\eta \mathbf{S}\mu = \partial_n u^{inc} - i\eta u^{inc} \tag{5}$$

where μ is an *unphysical* density defined on Γ, $\eta \in \mathbb{R}$, $\eta \neq 0$ and $\mathbf{K} = -K_2^\top(\nu I - 2K_2^\top) - \nu K_1^\top(I + 2K_2^\top) + 2(N_1 - N_2)S_2$ and $\mathbf{S} = -\nu S_1(I + 2K_2^\top) - (I - 2K_1)S_2$.

The Multiple Trace Formulation (MTF) is [3]

$$\begin{pmatrix} K_1 & -S_1 & -I/2 & 0 \\ N_1 & -K_1^\top & 0 & -I/2 \\ -I/2 & 0 & -K_2 & S_2 \\ 0 & -I/2 & -N_2 & K_2^\top \end{pmatrix} \begin{pmatrix} \gamma_D^1 u^1 \\ \gamma_N^1 u^1 \\ \gamma_D^2 u^2 \\ \gamma_N^2 u^2 \end{pmatrix} \tag{6}$$
$$= -1/2 \left(\gamma_D^1 u^{inc} \ \gamma_N^1 u^{inc} \ -\gamma_D^1 u^{inc} \ -\gamma_N^1 u^{inc}\right)^\top.$$

Finally the direct regularized formulation (CFIER) is given by

$$\mathcal{R} \begin{pmatrix} -(K_1+K_2) & S_1 + \nu^{-1} S_2 \\ -(N_1 + \nu N_2) & K_1^\top + K_2^\top \end{pmatrix} \begin{pmatrix} u \\ \partial_n u \end{pmatrix} \tag{7}$$
$$+ \begin{pmatrix} I/2 + K_2 & -\nu^{-1} S_2 \\ \nu N_2 & I/2 - K_2^\top \end{pmatrix} \begin{pmatrix} u \\ \partial_n u \end{pmatrix}$$
$$= \mathcal{R} \begin{pmatrix} u^{inc} \\ \partial_n u^{inc} \end{pmatrix},$$

where

$$\mathcal{R} := \begin{pmatrix} \frac{1}{1+\nu} I & \frac{2}{1+\nu} S_\kappa \\ -\frac{2\nu}{1+\nu} N_\kappa & \frac{1}{1+\nu} I \end{pmatrix}, \ \Im(\kappa) > 0.$$

The well posedness of the CFIEFK, CFIESK, and MTF formulations has been established in the literature. Furthermore

Theorem 1 *In the case* Γ *is Lipschitz and* $k_j > 0$ *the SCFIE are well posed in* $L^2(\Gamma)$ *and the CFIER are well posed in* $H^1(\Gamma) \times L^2(\Gamma)$.

2 Numerical Results

We use polynomially graded meshes based on sigmoid transforms and we construct weighted versions of the integral equations presented above. The weights are simply the arclengths of parametrizations of Γ that incorporates piece-wise sigmoid transforms—the weights vanish polynomially at corners. The new weighted unknowns are more regular than the original ones. We used a Nyström method based on global trigonometric interpolation of the weighted unknowns and logarithmic kernel splitting.

We present in Figure 2 the numbers of iterations needed by the five formulations considered to reach GMRES relative residuals of 10^{-4} in the case of a transmission of a plane wave by a unit square. We used Calderón preconditioning for both the CFIEFK and MTF formulations. We considered a high-contrast case with $\epsilon_1 = 1$ and $\epsilon_2 = 16$, frequencies $\omega = 2^i, i = 1, \ldots, 7$, and corresponding discretizations that produce results accurate to four digits in the far-field. As it can be seen from Figure 2, in the high-contrast, high-frequency regime the formulations SCFIE and CFIER outperform the other three formulations.

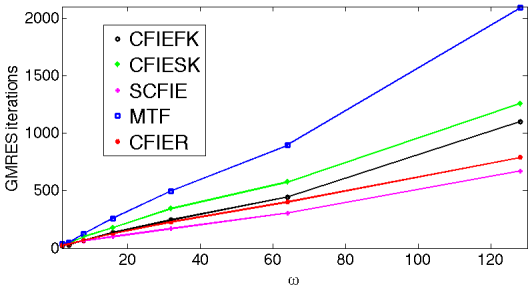

Figure 1: Numbers of iterations to 10^{-4} GMRES residuals for the CFIEFK, CFIESK, SCFIE, MTF, and CFIER formulations, unit square under plane wave incidence, $\epsilon_1 = 1$ and $\epsilon_2 = 16$, frequencies $\omega = 2^i, i = 1, \ldots, 7$.

References

[1] R. Kress, and G. Roach, *Transmission problems for the Helmholtz equation*, J. Math. Phys., **19** (1978), 1433-1437.

[2] R. Kleinman, P. Martin, *On single integral equations for the transmission problem of acoustics*, SIAM J. Appl. Math., Vol. 48, **2**, (1998), 307-325.

[3] X. Claeys, R. Hiptmair, C. Jerez-Hanckes, *Multi-trace boundary integral equations*, Direct and Inverse 51 Problems in Wave Propagation and Applications, (2012).

[4] M. Costabel, and E. Stephan, *A direct boundary integral equation method for transmission problems*, J. Math. Anal. Appl. **106** (1985), 367-415

[5] Y. Boubendir, V. Dominguez, D. Levadoux, and C. Turc, *Regularized combined field integral equations for acoustic transmission problems*, in press, SIAM (2015).

Well-Conditioned Boundary Element Formulation for Scattering at Partly Impenetrable Objects

E. Spindler[1,*], **X. Claeys**[2], **R. Hiptmair**[3]
[1]Seminar for Applied Mathematics, ETH Zurich, Switzerland
[2]Laboratoire Jacques-Louis Lions, Paris VI, France
[3]Seminar for Applied Mathematics, ETH Zurich, Switzerland
[*]Email: elke.spindler@sam.math.ethz.ch

Abstract

We consider acoustic scattering of time-harmonic waves at partly impenetrable composite objects. Using so-called multi-potentials, we cast the scattering problem into a second-kind boundary integral equation for the Cauchy trace of the total field on the union of the material interfaces. The new formulation is *intrinsically well-conditioned* and allows to use any kind of L^2-stable, also discontinuous, trial and test functions in the framework of a Ritz-Galerkin discretization.

In this respect it is superior to the first-kind formulation proposed by T. von Petersdorff, which is the most popular boundary integral equation method to solve this kind of problem. Galerkin boundary element discretization with low-order piecewise polynomials leads to ill-conditioned linear systems on fine meshes.

We obtain competitive solutions by applying an inexpensive post-processing procedure to the traces computed through the second-kind formulation.

Keywords: Acoustic scattering, second-kind boundary integral equations, Galerkin boundary element methods

1 New Formulation

We treat acoustic scattering in the case of piecewise constant wave numbers attaining the constant value $\kappa_i \in \mathbb{R}_+$ on each subdomain Ω_i, where $\bigcup_{i=0}^n \overline{\Omega}_i = \mathbb{R}^d$, $d = 2, 3$. Ω_0 denotes the unbounded exterior domain.

We propose a new formulation, whose unknowns are both, the Dirichlet and Neumann traces on the skeleton $\Sigma := \bigcup_{i=0}^n \partial\Omega_i$. Sound-soft and sound-hard boundary conditions can be handled.

We arrive at a second-kind boundary integral equation of the form

$$(\mathrm{Id} - \mathrm{T})\mathrm{u} = \mathrm{b}\,,$$

where in the absence of boundary conditions, T is a compact operator mapping $L^2(\Sigma)$ into $L^2(\Sigma)$.

The operator T encodes the cross-coupling of all subdomains, also of those that are not sharing a common interface. However, these far-field interactions are amenable to low-rank compression.

We have analyzed and implemented the new Ritz-Galerkin boundary element method based on a discretization with merely $L^2(\Sigma)$-conforming piecewise polynomial boundary element spaces.

2 Numerical Tests

As a numerical example we consider a ball B in $\mathbb{R}^3$ of radius $r = 0.5$ centered at the origin. It is partitioned into two halves by the plane $z = 0$. The exterior domain $\Omega_0 := \mathbb{R} \setminus \overline{\mathrm{B}}$ is characterized by the wave number $\kappa_0 = 4$, the lower half ball Ω_1 is impenetrable and the upper half ball Ω_2 has wave number $\kappa_2 = 10$. As incident field, we take the plane wave from direction $d = (0, \frac{1}{\sqrt{2}}, \frac{1}{\sqrt{2}})^\top$. For a visualization, see Figure 1a. As ansatz and test space we use discontinuous piecewise constant boundary elements for the second-kind approach. We compare our results with the classical first-kind approach called PMCHWT (see [3]), discretized with continuous piecewise linear and discontinuous piecewise constant boundary elements for Dirichlet and Neumann traces, respectively. The tests confirm the excellent conditioning of the Galerkin matrices of our second-kind approach (see Figure 2b), resulting in fast convergence of iterative solvers like GMRES (see Figure 2a).

The convergence results for the Galerkin solutions in $L^2(\Sigma)$-norm, can be found in Figure 1b, where the post-processed Dirichlet trace is denoted by "Dirichlet proj. second-kind". It is obtained by projecting the discontinuous piecewise constant Dirichlet trace onto the continuous piecewise linear boundary element space

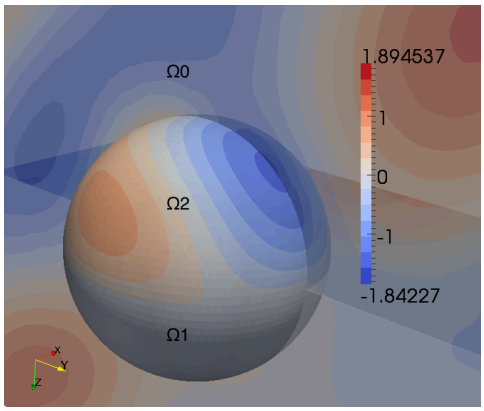

(a) **Visualization of the geometry used in the given numerical experiment.** The plotted data corresponds to the real part of the Galerkin solution U_h.

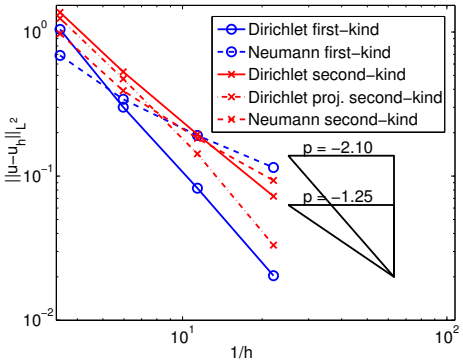

(b) **Convergence of the error of the computed Galerkin solutions u_h in relative $L^2(\Sigma)$-norm** wrt. to the inverse of the mesh size. As a reference solution we use the Galerkin solution u calculated on a mesh of high resolution (11264 mesh-elements and mesh size $h = 0.023$).

Figure 1: Convergence studies for the numerical example.

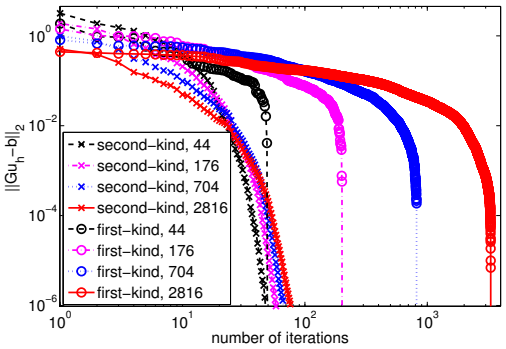

(a) **Convergence of the iterative solver GMRES.** The residuum $||\mathbf{G}\mathbf{u}_h - \mathbf{b}||_2$ is plotted wrt. to the number of iterations. The numbers listed in the legend of the figure denote the number of mesh-elements used for the computation of the Galerkin matrix $\mathbf{G}$ and the right hand side $\mathbf{b}$.

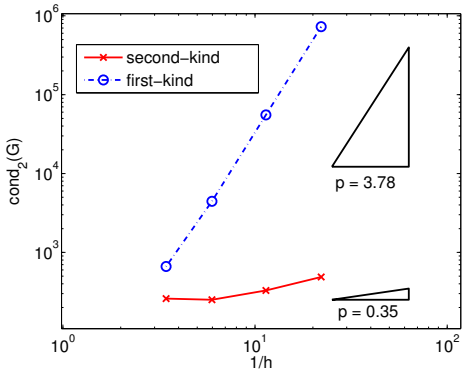

(b) **Euclidean condition numbers** plotted wrt. to the inverse of the mesh size.

Figure 2: Convergence of GMRES and condition numbers for the numerical example.

in the L^2-sense. In contrast to the widely held belief that the accuracy of second-kind formulations is inferior to that of the first-kind approach, the numerical results show competitive accuracy.

References

[1] X. Claeys. A single trace integral formulation of the second kind for acoustic scattering. *Technical Report No. 14, ETH Zürich, 2011.*

[2] X. Claeys, and R. Hiptmair, and E. Spindler, A second-kind Galerkin boundary element method for scattering at composite objects, *BIT Numerical Mathematics, Springer Netherlands*, 55(1):33–57, 2014.

[3] T. von Petersdorff. Boundary integral equations for mixed Dirichlet, Neumann and transmission problems. *Mathematical methods in the applied sciences*, 11(2):185–213, 1989.

Local Multiple Traces Modeling for High-Frequency Scattering

Carlos Jerez-Hanckes[1,*], **José Pinto**[1], **Simon Tournier**[1]
[1]School of Engineering, Pontificia Universidad Católica de Chile, Santiago, Chile
[*]Email: cjerez@ing.puc.cl

Abstract

We tackle high-frequency Helmholtz scattering by heterogenous penetrable objects in 2D via the local *Multiple Traces Formulation*. By weakly imposing transmission conditions and boundary integral equations per subdomain, we obtain a Galerkin-Petrov formulation employing weighted Chebyshev polynomials. FFT and regularization techniques are employed for quick matrix computations. Numerical results for a wide frequency sweeps and general structures confirm the robustness of the formulation.

Keywords: Boundary integral equations, wave scattering, multiple traces formulations

1 Introduction

We consider so-called *high frequency* scattering problems, i.e. whenever wavelengths are much smaller than the scatterer's size. Available solution methods are mostly based on: fast multipoles [1]; geometrical or physical optics [2]; Nyström approach [3]; and, hybrid numerical asymptotic [4]. Still, questions arise as to when and how these techniques should be applied and what to do in situations that require accommodating different ranges of frequencies as in heterogenous scatterers.

In this work, we propose a solution method capable of dealing with 2D composite scatterers with largely varying wavenumbers following the *Multiple Traces Formulations* (MTFs) [5, 6]. In particular, we will focus on a variant dubbed *local* since all unknown boundary traces are locally defined on subdomain boundaries and transmission conditions per interface are enforced weakly by local operators using suitable test functions, i.e. functions that allow interface duality pairings. On the continuous level, the resulting first-kind Fredholm equation possesses unique solutions with a block diagonal structure hinting at its amenability to parallelization and operator preconditioning. Numerical analysis and results in two and three dimensions validate this for low-order elements. However, and as expected, such discretization bases are not sufficient for high frequency regimes, and so we will explore a purely *spectral* or p-element approximation for boundary unknowns. In doing so, we will further extend the formalism provided for the local MTF to account for piecewise Cauchy data.

2 Generalized Local Multiple Traces Formulation

Following [5], we consider a bounded scatterer Ω composed of two different materials with wavenumbers κ_i and such that $\overline{\Omega} := \overline{\Omega}_1 \cup \overline{\Omega}_2$ with exterior domain $\Omega_0 := \mathbb{R}^2 \setminus \overline{\Omega}$ and boundaries $\partial\Omega_i$. From the integral representation formulas, we retrieve weak Calderón identities on each subdomain boundary :

$$\langle \boldsymbol{\lambda}^i \, , \boldsymbol{\varphi}^i \rangle_\times = \left\langle \left(\frac{1}{2}\mathrm{Id} + \mathsf{A}_i \right) \boldsymbol{\lambda}^i \, , \boldsymbol{\varphi}^i \right\rangle_\times \tag{1}$$

wherein $\times$ denotes the cross duality pairing, the standard boundary integral operators are condensed into A_i:

$$\mathsf{A}_i := \begin{pmatrix} -\mathsf{K}_i & \mathsf{V}_i \\ \mathsf{W}_i & \mathsf{K}_i' \end{pmatrix} : \mathbb{V}_i \to \mathbb{V}_i, \tag{2}$$

and $\mathbb{V}_i := H^{1/2}(\partial\Omega_i) \times H^{-1/2}(\partial\Omega_i)$. Transmission conditions are weakly enforced across each interface Γ_{ij}. This is done via local restriction, normal orientation and extension-by-zero operators $\widetilde{\mathsf{X}}_{ij} : \mathbb{V}_i \to \mathbb{V}_{\mathrm{pw},i}$, where "pw" denotes piecewise per interface. The dual of $\mathbb{V}_{\mathrm{pw},i}$ is $\widetilde{\mathbb{V}}_i := \widetilde{H}^{1/2}_{\mathrm{pw}}(\partial\Omega_i) \times \widetilde{H}^{-1/2}_{\mathrm{pw}}(\partial\Omega_i)$. With this, the system of equations takes the form:

$$\langle \mathsf{M}\boldsymbol{\lambda} \, , \boldsymbol{\varphi} \rangle \;\; = \langle \mathbf{g} \, , \boldsymbol{\varphi} \rangle_\times \tag{3}$$

where $\boldsymbol{\lambda} = (\boldsymbol{\lambda}^0, \boldsymbol{\lambda}^1, \boldsymbol{\lambda}^2)$ belongs to p.w.-interface Cauchy functions, $\boldsymbol{\varphi} = (\boldsymbol{\varphi}^0, \boldsymbol{\varphi}^1, \boldsymbol{\varphi}^2)$ in p.w.- interface dual spaces, and

$$\mathsf{M} := \begin{pmatrix} \mathsf{A}_0 & -\frac{1}{2}\widetilde{\mathsf{X}}_{01} & -\frac{1}{2}\widetilde{\mathsf{X}}_{02} \\ -\frac{1}{2}\widetilde{\mathsf{X}}_{10} & \mathsf{A}_1 & -\frac{1}{2}\widetilde{\mathsf{X}}_{12} \\ -\frac{1}{2}\widetilde{\mathsf{X}}_{20} & -\frac{1}{2}\widetilde{\mathsf{X}}_{21} & \mathsf{A}_2 \end{pmatrix}. \tag{4}$$

Observe that due to the local character of the $\widetilde{\mathsf{X}}_{ij}$, the matrix is dense only along the diagonal blocks.

3 Discretization by Spectral Elements

Define a canonical interface $\hat{\Gamma} : [-1, 1]$ and set the weight function $\omega(t) := \sqrt{1 - t^2}$. Based on Tchebyshev polynomials of the first and second kind, T_n, U_n, respectively, we construct two sets of bases provable dense in the associated test and trial functional spaces. With them, we proceed to build the Petrov-Galerkin matrices arising from (3).

Particular attention is made to approximation properties of the BI kernels and their acceleration via FFT. Specifically, we compute integrals of the canonical form:

$$I_{\mathsf{L}} = \int_{\hat{\Gamma}} \int_{\hat{\Gamma}} F_{\mathsf{L}}(s,t) T_m(s) \omega(t) U_l(t) ds dt,$$

where L is any of the BIOs and F_{L} represents the associated kernel together with the mappings required to push the interfaces Γ_{ij} onto $\hat{\Gamma}$.

First, we approximate the kernel F_{L} as a degenerate kernel using Chebyshev polynomials so one can make use of the FFT to compute coefficients $g_n(t)$ such that

$$F(s,t) \approx \sum_{n=0}^{N_c} g_n(t) U_n(s),$$

for a suitable choice of N_c. Secondly, by applying the orthogonality properties of U_n, one can quickly obtain expressions of the form:

$$I_{\mathsf{L}} \approx \frac{\pi}{2} \int_{-1}^{+1} g_l(t) T_m(t) dt,$$

which can be easily obtained by Gauss–Legendre quadrature.

4 Numerical Results

The geometry considered three domains such that, $\Omega_0 = \{\mathbf{x} \in \mathbb{R}^2, \|\mathbf{x}\|_2 > 1\}$, $\Omega_1 = \{\mathbf{x} \in \mathbb{R}^2, \|\mathbf{x}\|_2 < 1, x_1 < 0\}$, $\Omega_2 = \{\mathbf{x} \in \mathbb{R}^2, \|\mathbf{x}\|_2 < 1, x_1 > 0\}$. This geometry contains all the difficulties portraying Lipschitz domains with sharp corners.

Fig. 1 shows two error measurements for the solution traces of the scattered field –Dirichlet jump and compliance with Calderón identity– for a frequency sweep for fixed material parameters with $\kappa_i = \kappa_0 \sqrt{\epsilon_i}$. The number of terms for convergence follows the rule $N = 1.4 \max k_i + 7$. Quadrature rules, N_c and matrix computations proved to be the most critical points when improving approximation errors.

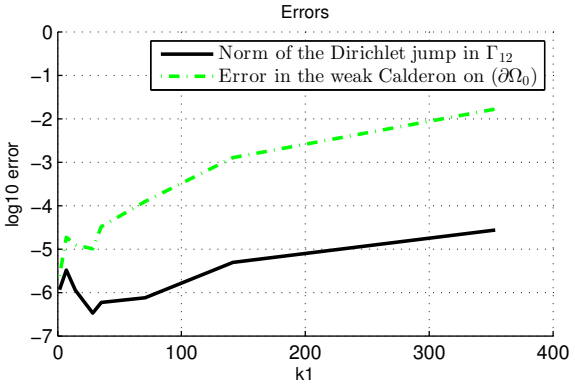

Figure 1: Errors for $\epsilon_0 = 1$, $\epsilon_1 = 2$, $\epsilon_2 = 3$.

5 Conclusions and Future Prospects

Numerical results validate our claims. Furthermore, the formulation is amenable to operator-type preconditioning with future developments focused on improving computational accuracy.

References

[1] E. Darve, P. Havé, Efficient fast multipole method for low-frequency scattering, *J. Comput. Phys.* **197** (2004), pp. 341–363.

[2] P. D. Lin, *New computation methods for geometrical optics*, Vol. 178 of Springer Series in Optical Sciences, Springer, Singapore, 2014.

[3] O. P. Bruno, S. K. Lintner, A high-order integral solver for scalar problems of diffraction by screens and apertures in three-dimensional space, *J. Comput. Phys.* **252** (2013), pp. 250–274.

[4] S. L. Samuel P. Groth, David P. Hewett, Hybrid numerical-asymptotic approximation for high frequency scattering by penetrable convex polygons, *IMA J Appl Math* **80** (2015), pp. 324–353.

[5] R. Hiptmair, C. Jerez-Hanckes, Multiple traces boundary integral formulation for Helmholtz transmission problems, *Advances in Computational Mathematics* **37** (2012), pp. 39–91.

[6] C. Jerez-Hanckes, J. Pinto, S. Tournier, Local multiple traces formulation for high-frequency scattering problems, *J. Computational and Applied Mathematics* **289** (2015), pp. 306–321.

Function spaces for integral equations on fractal domains

Simon N. Chandler-Wilde[1], **David P. Hewett**[2,*], **Andrea Moiola**[1]
[1]Department of Mathematics and Statistics, University of Reading, UK
[2]Mathematical Institute, Oxford, UK
*Email: hewett@maths.ox.ac.uk

Abstract

We report some results arising from our investigations into boundary integral equation formulations of acoustic scattering problems involving planar screens with fractal boundaries. Our focus is on determining the correct Sobolev space setting in which to pose the integral equations. This is well understood when the screen is smooth (Lipschitz). But for non-Lipschitz (e.g. fractal) screens the situation is less clear, because many of the equivalences and relations between the standard definitions of Sobolev spaces on subsets of Euclidean space (e.g. restriction, completion of spaces of smooth functions, interpolation...) that hold in the Lipschitz case, fail to hold in general. We point to concrete counterexamples for which the standard equivalences fail, as well as discussing the implications of this failure for the well-posedness (or otherwise) of the classical screen scattering problem.

Keywords: Integral equations, Sobolev spaces, Screen problems, Non-Lipschitz domains

1 Motivation

This paper concerns properties of Sobolev spaces relevant to the study of integral equations on non-Lipschitz domains. Our motivating example is time-harmonic acoustic scattering in $\mathbb{R}^{d+1}$ by a planar screen $\Gamma \times \{0\}$, where Γ is a non-empty bounded open subset of $\mathbb{R}^d$, $d = 1$ or 2. Such problems could represent simplified models for the performance of fractal antennas in electrical engineering applications [1].

The Sobolev spaces we study are derived from the Bessel potential spaces $H^s(\mathbb{R}^d)$, $s \in \mathbb{R}$. Following the notation of [2], let $H^s(\Gamma) := \{U|_\Gamma : U \in H^s(\mathbb{R}^d)\}$, where $|_\Omega$ denotes the (distributional) restriction to Γ. Let $\tilde{H}^s(\Gamma)$ denote the closure of $C_0^\infty(\Gamma)$ in $H^s(\mathbb{R}^d)$; we note that $H^s(\Gamma)$ is the dual space of $\tilde{H}^{-s}(\Gamma)$. For compact $K \subset \mathbb{R}^d$ let $H^s_K := \{u \in H^s(\mathbb{R}^d) : \operatorname{supp} u \subset K\}$.

For the screen scattering problem with Neumann boundary conditions, the scattered wave satisfies the following boundary value problem: Given $g_{\mathsf{N}} \in H^{-1/2}(\Gamma)$ (arising from the incident wave), find $u \in W^1_{\mathrm{loc}}(\mathbb{R}^{d+1} \setminus (\overline{\Gamma} \times \{0\}))$ such that $\Delta u + k^2 u = 0$ in $\mathbb{R}^{d+1} \setminus (\overline{\Gamma} \times \{0\})$, u is outgoing at infinity, and $\partial u/\partial \mathbf{n} = g_{\mathsf{N}}$ on Γ. (The latter condition can be written more precisely as $(\partial^{\pm}_{\mathbf{n}}(\chi u))|_\Gamma = g_{\mathsf{N}}$, where $\partial^+_{\mathbf{n}}$ and $\partial^-_{\mathbf{n}}$ are Neumann trace operators onto $\mathbb{R}^d \times \{0\}$ from the half spaces $x_{d+1} > 0$ and $x_{d+1} < 0$ respectively, and $\chi \in \mathbb{C}_0^\infty(\mathbb{R}^d)$ is any cut-off function which equals one in a neighbourhood of $\Gamma \times \{0\}$.)

This problem is well-posed whenever Γ is a Lipschitz subset of $\mathbb{R}^d$. In [3] it is shown that to ensure well-posedness (specifically, uniqueness) for arbitrary Γ one has to impose the following two additional conditions (with χ as above, and $\gamma^{\pm}$ denoting Dirichlet traces):

$$[\partial u/\partial \mathbf{n}] := \partial^+_{\mathbf{n}}(\chi u) - \partial^-_{\mathbf{n}}(\chi u) = 0, \quad (1)$$

$$[u] := \gamma^+(\chi u) - \gamma^-(\chi u) \in \tilde{H}^{1/2}(\Gamma). \quad (2)$$

Condition (1) ensures that u can be represented as a double layer potential $u = \mathcal{D}[u]$ (with no single layer potential component). A priori (from the Helmholtz equation and boundary condition) $[\partial u/\partial \mathbf{n}] \in H^{-1/2}_{\partial\Gamma}$, so (1) is required whenever Γ is rough enough that $H^{-1/2}_{\partial\Gamma} \neq \{0\}$.

Condition (2) ensures that the resulting first-kind boundary integral equation on Γ, involving the hypersingular operator, has a unique solution: as shown in [3], this operator is invertible between $\tilde{H}^{1/2}(\Gamma)$ and $H^{-1/2}(\Gamma)$. A priori, $[u] \in H^{1/2}_{\overline{\Gamma}} \supset \tilde{H}^{1/2}(\Gamma)$, so (2) is required whenever Γ is rough enough that $\tilde{H}^{1/2}(\Gamma) \subsetneq H^{1/2}_{\overline{\Gamma}}$.

We want to understand the how the geometry of Γ affects whether or not these additional conditions are required. We might also ask the question: Given two screens Γ_1, Γ_2, under what conditions are the solutions u_1, u_2 for the respective scattering problems equal? It turns out that, under appropriate assumptions on the form of the incident wave, this holds for every incident wave if and only if $\tilde{H}^{1/2}(\Gamma_1) = \tilde{H}^{1/2}(\Gamma_2)$.

2 Function space results

Motivated by the above considerations, we pose the following general questions, with $s \in \mathbb{R}$.

Q1: When is $H^s_K = \{0\}$ for a compact set K?

Q2: When is $\tilde{H}^s(\Gamma) = H^s_{\overline{\Gamma}}$ for an open set Γ?

Q3: When is $\tilde{H}^s(\Gamma_1) = \tilde{H}^s(\Gamma_2)$ for $\Gamma_1 \neq \Gamma_2$?

Q1 concerns the "negligibility" of the set K in terms of Sobolev regularity. It is straightforward to show that for every non-empty compact K there exists $s_K \in [-d/2, d/2]$ such that $H^s_K = \{0\}$ for $s > s_K$ and $H^s_K \neq \{0\}$ for $s < s_K$.

If K has zero Lesbegue measure then s_K can be expressed in terms of Hausdorff dimension. (Some partial results for sets with positive measure will be reported in the talk.)

Theorem 2.1 *Let K be non-empty, compact, and have zero Lesbegue measure. Then* $s_K = (\dim_{\mathrm{H}}(K) - d)/2$.

Theorem 2.2 *(i) If Γ is C^0 then $s_{\partial\Gamma} \in [-1/2, 0]$, and furthermore $H^0_{\partial\Gamma} = L^2(\partial\Gamma) = \{0\}$. (ii) If Γ is $C^{0,\alpha}$ for some $0 < \alpha < 1$ then $s_{\partial\Gamma} \in [-1/2, -\alpha/2]$. (iii) If Γ is Lipschitz then $s_{\partial\Gamma} = -1/2$, and furthermore $H^{-1/2}_{\partial\Gamma} = \{0\}$.*

These theorems provide open sets Γ for which $H^{-1/2}_{\partial\Gamma} \neq \{0\}$; for $d = 2$ this will hold whenever $\dim_{\mathrm{H}}(\partial\Gamma) > 1$. For instance, one can take Γ to be the interior of the Koch snowflake ($\dim_{\mathrm{H}}(\partial\Gamma) = \log 4/\log 3$), or the open set formed by removing from a unit equilateral triangle the points of the Sierpinski triangle ($\dim_{\mathrm{H}}(\partial\Gamma) = \log 3/\log 2$). A further example is $\Gamma = ((0,1) \setminus C_\lambda)^2$, for $1/4 < \lambda < 1/2$. Here $C_\lambda := \cap_{n=0}^{\infty} C_{\lambda,n}$ is the Cantor set where $C_{\lambda,0} = [0,1]$ and, for $n > 0$, $C_{\lambda,n}$ is formed by removing an open interval from the middle of each interval in $C_{\lambda,n-1}$ to leave two subintervals of length λ^n (see figure below).

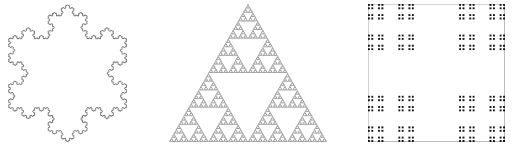

Concerning **Q2**, it is well-known (see e.g. [2]) that if Γ is C^0 then $\tilde{H}^s(\Gamma) = H^s_{\overline{\Gamma}}$ for all $s \in \mathbb{R}$. However, this equality fails in general. The following result relates **Q2** to **Q1** and provides a way of constructing counterexamples.

Theorem 2.3 *If $\exists$ a compact set $K \subset \mathrm{int}(\overline{\Gamma})\backslash\Gamma$ for which $H^{-s}_K \neq \{0\}$, then $\tilde{H}^s(\Gamma) \subsetneqq H^s_{\overline{\Gamma}}$.*

Q3 is also intimately related to **Q1**.

Theorem 2.4 *For $\Gamma_1 \neq \Gamma_2$, $\tilde{H}^s(\Gamma_1) = \tilde{H}^s(\Gamma_2)$ iff $H^{-s}_K = \{0\}$ for every compact $K \subset \Gamma_1 \ominus \Gamma_2$.*

We end with a remark on interpolation. For Lipschitz Γ, both $H^s(\Gamma)$ and $\tilde{H}^s(\Gamma)$ are interpolation scales over $s \in \mathbb{R}$. But for general open Γ this can fail - see the counterexamples in [4]. It would seem that interpolation is a somewhat unstable way of defining spaces on rough domains.

References

[1] D. H. Werner and S. Ganguly, An overview of fractal antenna engineering research, *IEEE Antenn. Propag. M.* **45** (2003), pp. 38–57.

[2] W. McLean, *Strongly Elliptic Systems and Boundary Integral Equations*, CUP, 2000.

[3] S. N. Chandler-Wilde and D. P. Hewett, Acoustic scattering by fractal screens: mathematical formulations and wavenumber-explicit continuity and coercivity estimates, University of Reading preprint MPS-2013-17, 2013.

[4] S. N. Chandler-Wilde, D. P. Hewett, and A. Moiola, Interpolation of Hilbert and Sobolev spaces: quantitative estimates and counterexamples, Mathematika, 61(2), 414-443, 2015.

Computation of highly oscillatory double integrals and application to Boundary Element Methods in high frequency domain

V. Domínguez[1,*], **I.G. Graham**[2], **T. Kim**[2]

[1]Dep. of Mathematics and Computing Engeenering, Universidad Pública de Navarra, Tudela, Spain
[2]Dep. of Mathematical Sciences, University of Bath, Bath, UK

[*]Email: victor.dominguez@unavarra.es

Abstract

In this work we propose and provide theoretical support to a novel method for approximating highly oscillatory double integrals. This kind of integrals arises in intermediate calculations in a wide variety of numerical algorithms, for instance in high frequency scattering problems (see [2] and references therein). The method consists basically in: (a) a change of variables which makes the oscillatory behavior depend in a very simple form on only one variable; (b) a combination of classical and Clenshaw-Curtis product integration rules (for the oscillatory variable) for handing the one-dimensional integrals. The theoretical analysis identifies possible singularities in the integrands (either because these were already in the original integral or appear as a result of the change of variables), and adjusts the underlying grids of the quadrature rules accordingly to improve the performance of the algorithm.

Keywords: Numerical integration, Oscillatory integrals, High frequency scattering problems.

1 Introduction

This work is concerned with the numerical approximation of integrals as

$$I_{D,k}(F,G) = \iint_D F(s,t)\exp(ikG(s,t))\mathrm{d}s\,\mathrm{d}t$$

where F,G are smooth, G real, $k \in \mathbb{R}$ (possibly large) and $i^2 = -1$. We assume

- A1 $D := \{(s,t) \ : \ s \in (a,b),\ \varphi^-(s) < t < \varphi^+(s)\}$, with $\varphi^\pm$ smooth;
- A2 $\partial_t G(s,t) \neq 0$, for all $(s,t) \in \overline{D}$;
- A3 The first derivatives of $\psi^\pm(s) := G(s,\varphi^\pm(s))$ can vanish only at a or b.

It is simple to check that the assumptions listed above are not very restrictive in practice and that problems on more complex domains can be split into several integrals satisfying A1-A3.

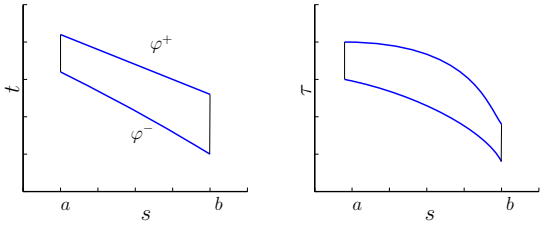

Figure 1: Original and transformed domain

2 A change of variables

Our approach starts with the change of variables (see Figure 1)

$$(s,\tau) = (s, G(s,t)). \tag{1}$$

Condition A2 ensures not only that the change of variables is applicable but the Jacobian is in fact a smooth function. The integral in the new variables can be then written as a sum of, at most, three new integrals of the form

$$I(m,k) := \int_{\tau_m}^{\tau_{m+1}} \underbrace{\left[\int_{\ell_m(\tau)}^{u_m(\tau)} \mathcal{F}(s,\tau)\mathrm{d}s\right]}_{=:f_m(\tau)} \exp(ik\tau)\mathrm{d}\tau.$$

Clearly $\tau_m, \tau_{m+1} \in \{\psi^\pm(a), \psi^\pm(b)\}$ and functions ℓ_m, u_m are either constant functions ($\equiv a, b$) or the inverse of $\psi^\pm$ (see Figure 2).

The first result at this point is that $\mathcal{F}$ is also smooth. Therefore, the evaluation of $f_m(\tau)$, the inner integral, can be carried out using classical methods (eg. Gaussian rules, Gauss-Lobatto, Clenshaw-Curtis, etc).

However, some singularities in $f_m(\tau)$ can arise at the ends points if $\tau_{\{m,m+1\}}$ corresponds to a turning point of the domain (see Figure 2). The correct description of such singularities is one of the contributions in this work. We have then two possibilities:

If f_m is **smooth**, we use the (product integration or modified) Clenshaw-Curtis rule:

$$I_N(m,k) := \int_{\tau_m}^{\tau_{m+1}} f_{m,N}(\tau)\exp(ik\tau)\mathrm{d}\tau \approx I(m,k).$$

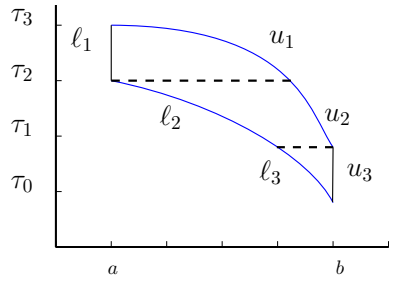

Figure 2: Integration in (s, τ)

In the expression above, $f_{m,N} \in \mathbb{P}_N$ and interpolates f_m at the Chebyshev nodes on $[\tau_m, \tau_{m+1}]$. The benefit of using this rule has been well established (see [1] and references therein):

The rule can be implemented rapidly, with cost independent of k, and it converges superalgebraically as $N \to \infty$ (actually exponentially if f_m is analytic) and both, the relative and absolute error decay, for fixed N as $k \to \infty$.

If f_m is **singular**, say at τ_m, we apply the same rule but in a compound manner on the graded grid

$$\tau_m + \left(\frac{j}{M}\right)^q (\tau_{m+1} - \tau_m), \quad j = 0, \ldots, M, \; q > 1.$$

This strategy concentrates nodes close to τ_m and leads to a new approximation which will be denoted by $I_{M,N,q}(m,k)$. The exponential convergence of the error is lost but it still converges quickly provided that the grading parameter q is suitably chosen.

3 Convergence of the rule

Theorem 1 *Assume that f_m, the inner integral, is evaluated within error ε.*

If τ_m, τ_{m+1} do not correspond to a turning point then

$$|I_N(m,k) - I(m,k)| \lesssim \left[\varepsilon + N^{-r+4} k^{-2}\right] \|F\|_{\mathcal{C}^r(D)}.$$

If either τ_m or τ_{m+1} is a turning point of order n then taking $q > nN$ as grading parameter, it holds for all $r \leq N - 1$

$$|I_{M,N,q}(m,k) - I(m,k)| \lesssim \left[\varepsilon + M^{-N} k^{-1}\right] \|F\|_{\mathcal{C}^r(D)}.$$

With "$\lesssim$" we mean that the omitted constants in the bounds above are independent of k and f as well as of N in the first case and M in the second one. Therefore, the accuracy of the rule improves as k grows to infinity.

4 Some extensions

The results described here can be extended to handle stationary points, i.e., domains where $\partial_t G$ vanishes. It can be assumed that this happens at the boundary of the domain, which makes the change of variables (1) still valid. However the Jacobian introduces a stronger, but integrable, singularity for which the same method applies cf [2].

The adaptation of these ideas to functions F with singularities is more straightforward. For instance, a common case in BEM is $F(s,t) \approx A(s,t) \log|s-t|$ which leads to integrals with a singularity on the lower (or upper) part of the boundary. It is easy to see that, in absence of stationary points, function f_m, has the same singularity which can be handled in a similar way, using the same graded meshes.

References

[1] V. Domínguez, I.G. Graham, and T. Kim. Filon-Clenshaw-Curtis rules for highly-oscillatory integrals with algebraic singularities and stationary points, *SIAM J. Numer. Anal.* **51** (2013), pp 1542–1566.

[2] S.N. Chandler-Wilde, I.G. Graham, S. Langdon and E.A. Spence, Numerical-asymptotic boundary integral methods in high-frequency acoustic scattering. *Acta Numer.* **21** (2012), pp. 89–305.

Formulation and solution of wave scattering problems in BEM++

Timo Betcke[1,*], **Simon Arridge**[2], **Samuel Groth**[3], **Nicolas Salles**[1], **Matthew Scroggs**[1], **Elwin van't Wout**[2]

[1]Department of Mathematics, University College London, UK
[2]Department of Computer Science, University College London, UK
[3]Department of Mathematics and Statistics, University of Reading, UK
[*]Email: t.betcke@ucl.ac.uk

Abstract

BEM++ is a C++/Python based library for the solution of a variety of boundary element problems. In this talk we give an overview of the BEM++ features for the solution of acoustic and electromagnetic wave scattering problems. Various applications will be presented in which BEM++ is currently being used.

Keywords: BEM software, acoustics, electromagnetics

1 An overview of BEM++

BEM++ (`www.bempp.org`) [1] is a project to develop a comprehensive Galerkin boundary element library for the solution of Laplace, Helmholtz and electromagnetic problems in bounded and unbounded domains. Development has started at the end of 2010 at University College London and is ongoing. BEM++ is based on a fast C++ core library and offers a comprehensive Python interface. It implements the standard single-layer, double-layer, adjoint double-layer and hypersingular operators for Laplace and Helmholtz, and the electric field and magnetic field integral operators for Maxwell. Supported function spaces include polynomial, discontinuous polynomial and Raviart-Thomas elements on triangular surface meshes. Fast boundary element methods are enabled by built-in support for H-Matrix compression.

While BEM++ does not yet have optimized solvers for high-frequency wave problems it is very capable for problems in the low to medium frequency range. In the following we give an overview of existing and in development features of BEM++ for wave problems and demonstrate some current applications of BEM++.

2 OSCRC preconditioners

Preconditioning based on OSRC (On-surface Radiation Condition) formulations is a very effective tool to reduce the number of GMRES iterations necessary for the solution of high-frequency Helmholtz problems [2]. OSRC preconditioners require the assembly and solution of surface PDEs with shifted Laplace-Beltrami operators. OSRC preconditioners have been implemented in BEM++ and will become officially part of version 3.0. An example application of OSRC is scattering from ribcages in High-Intensity Focused Ultrasound (see Figure 2 and the corresponding talk by Elwin van't Wout).

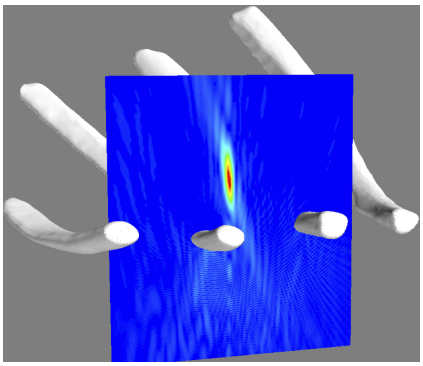

Figure 1: HIFU simulation with BEM++

3 FEM/BEM coupled wave problems

Coupling interfaces to
FEniCS (`www.fenicsproject.org`)
and to
DUNE (`www.dune-project.org`)
are in development. This allows the implementation of coupled FEM/BEM formulations for waves scattering through inhomogeneous media. We will demonstrate the progress of these efforts and show first example applications.

4 Maxwell transmission problems

BEM++ is able to solve a wide range of Maxwell problems, including screen and transmission problems. We will review the Maxwell functionality of BEM++ and demonstrate the application to transmission problems in the simulation

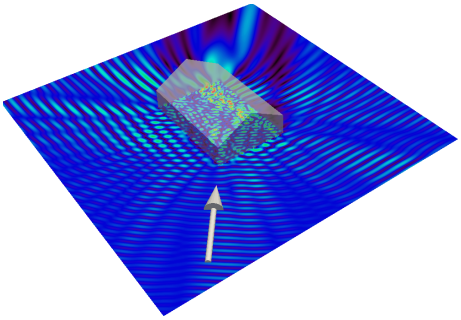

Figure 2: Light scattering from an ice crystal

of light scattering from ice crystals (see Figure 4) [4].

5 Time-domain problems via Convolution Quadrature

We have implemented parallel CQ methods with BEM++. These will be eventually made available as part of BEM++ [3], and we will give a brief update on these developments (see also talk by N. Salles).

6 Support for fast solvers

Development is ongoing for built-in support of hierarchical matrices in BEM++ and we will present first results demonstrating the performance of the BEM++ H-Matrix code. Support for FMM via external libraries is in planning.

7 Summary

BEM++ offers a range of features for the solution of low to medium frequency wave problems, making it simple to solve a wide area of realistic applications. Many of the mentioned developments are already included in the current preview release and will be included in the final 3.0 version. BEM++ is open-source and can be downloaded from `www.bempp.org`.

References

[1] Wojciech Śmigaj, Timo Betcke, Simon Arridge, Joel Phillips and Martin Schweiger, *ACM Transactions on Mathematical Software* **41** (2015), pp. 6:1–6:40.

[2] Xavier Antoine and Marion Darbas, Generalized combined field integral equations for the iterative solution of the three-dimensional Helmholtz equation, *ESAIM: Mathematical Modelling and Numerical Analysis* **41** (2007), pp. 147–167.

[3] Timo Betcke, Nicolas Salles and Wojciech Śmigaj, Exponentially accurate evaluation of time-stepping methods for the wave equation via convolution quadrature type schemes, *to be submitted*.

[4] S. P. Groth, A. J. Baran, T. Betcke, S. Havemann and W. Śmigaj, The boundary element method for light scattering by ice crystals and its implementation in BEM++, *submitted*.

A NEW A POSTERIORI ERROR ESTIMATE FOR THE BEM IN 2D-ACOUSTICS

Marc Bakry[1,*], **Sébastien Pernet**[2], **Francis Collino**[3]
[1]ONERA/DTIM/M2SN, Toulouse & CNRS/POEMS, Palaiseau, France
[2]ONERA/DTIM/M2SN, Toulouse, France
[3]CNRS/POEMS, Palaiseau, France
*Email: marc.bakry@onera.fr

Abstract

We extend some existing *a posteriori* error estimates for the Boundary Element Method for the 2-dimensional Laplace equation to 2D-acoustic wave propagation problems. We try to bypass their efficiency constant issues by introducing a new efficient and reliable *a posteriori* error estimate. It is constructed by a new localization technique of the residual from $H^{\pm 1/2}$ into L^2 which leads to an efficiency constant almost equal to 1.

Keywords: *a posteriori* error estimate, boundary element method

1 Introduction

The Boundary Element Method is a widely used tool, based on boundary integral formulation, for the resolution of wave propagation problems. It features strong advantages since it requires only the meshing of the boundary Γ of the scattering object and the radiation condition is automatically taken into account. Its main disadvantages are a difficult implementation and, in its "raw form" the manipulation of fully populated matrices. However, the BEM in general lack reliable, efficient and automatic tools for the control of the error. Such tools are called *a posteriori* error estimates and are an equivalent norm of the error. They can be used to build the *optimal approximation space*. In other words, we would like to ensure that the error on the solution is below a certain value, and this process should be automatic.
Let us denote by η such an estimate, then

$$\exists\ \{c, C\} > 0,\ c\,\eta \leq \text{error} \leq C\,\eta. \qquad (1)$$

The right inequality is named *reliability* and guarantees that the error converges *at least* as fast as the estimate when the mesh size goes to 0. The left one is called *efficiency* and means that the error converges at much as fast as the estimate. We eventually require from η that it has a *local* property, i.e. that if $\mathcal{T}_h$ is a discretization of Γ, then $\eta^2 = \sum_{\tau\in\mathcal{T}_h} \eta_\tau^2$ where η_τ is a local computable value. Unfortunately, the "natural" norm on the involved functional spaces are not local, and once the estimate has been expressed in terms of this norm, localization techniques are used to map it into $L^2(\Gamma)$. We propose a different point of view where we will use an operator to transport the values of interest into L^2. We will eventually show that it gives us control over the efficiency constant and the Galerkin norm of the error.

2 The Λ-based *a posteriori* estimation

We study the propagation of a 2-dimensional acoustic wave. Standard estimates such as the one which can be found in [1], [2], [3] are based on space reconstruction on polynomial spaces of higher order, or on the localization of the residual (the norm of the residual is, under inf-sup condition, an equivalent norm of the error). However, the localization makes us lose control over the efficiency constant which may be geometry-dependent. Our goal is then to design an estimate for which its value will be as close as possible to a reference, for example the Galerkin norm of the error $|||e|||$. We will base it on the computation of the residual which is a value we can "easily" access.
Instead of a standard localization of the norm of the residual, we will try to transport it into $L^2(\Gamma)$. Let us suppose there exists an operator Λ which is an isomorphism from the space V where the residual r_h of the equation (not the iterative resolution !) "lives" into some subspace W of $L^2(\Gamma)$. Let

$$\eta_\Lambda = \|\Lambda r_h\|_{L^2}, \qquad (2)$$

then η_Λ is reliable, efficient and local (this result is immediate). Much better, by carefully choosing Λ, one can show that the estimate will behave as

$$\eta_\Lambda \simeq \alpha\, |||e||| \qquad (3)$$

where α is a strictly positive constant, independent from Γ (or at least weakly dependent for non regular geometries), *eventually equal to 1.* It remains the question on how to build such Λ. We give here a hint on its construction. Let $\mathcal{A}_k$ the operator of the equation which was solved, k being the wave number. We suppose that $\mathcal{A}$ can be decomposed in a coercive part and a compact part, i.e. $\mathcal{A}_k = \mathcal{A}_0 + \mathcal{A}_{\mathcal{C},k}$. Using the definition of $\|\Lambda r_h\|_{L^2}$,

$$\begin{aligned}\|\Lambda r_h\|_{L^2}^2 &= \langle \Lambda\mathcal{A}\, e, \Lambda\mathcal{A}\, e\rangle \\ &= \langle \mathcal{A}^\star\Lambda^\star\Lambda\mathcal{A} e, e\rangle \\ &= \langle \mathcal{A}_0^\star\Lambda^\star\Lambda\mathcal{A}_0 e, e\rangle + \text{higher order}\end{aligned}$$

If we can choose Λ such that $\mathcal{A}_0^\star\Lambda^\star\Lambda = \alpha\mathbb{I} +$ compact perturbation, then

$$\|\Lambda r_h\|_{L^2}^2 \simeq \alpha|||e|||^2 + \text{ higher order terms.}$$

It appears that the most natural choice will be to choose Λ as the square root of the inverse of $\mathcal{A}_0$. We start by isolating the principal symbol of $\mathcal{A}_0$, then we take the square root of its inverse which allows us to build the kernel of Λ. We adjust $\alpha = 1$ by scaling a multiplicative constant. In the case of the 2D Helmholtz equation, the Λ associated with the single layer potential is

$$\Lambda^D : H^{1/2}(\Gamma)/\mathbb{C} \to V = \{p \in L^2(\Gamma), \int_\Gamma p\, d\gamma = 0\}$$

$$(\Lambda^D u)(x) = \frac{2}{\sqrt{\pi}}\nabla_\Gamma \int_\Gamma \sqrt{|x-y|}\nabla_\Gamma u(y)\, d\gamma_y$$

The single layer potential is of order -1 and Λ^D is of order $1/2$. Similarly, we have the Λ^N associated with the normal derivative of the double layer potential

$$\Lambda^N : H^{-1/2}(\Gamma) \to L^2(\Gamma)$$

$$(\Lambda^N u)(x) = \frac{1}{\sqrt{\pi}} \int_\Gamma \frac{u(y)}{\sqrt{|x-y|}}\, d\gamma_y$$

Λ^N performs a "half-integration".

3 Simulation

Different simulations have been made for both smooth and polygonal contours Γ. We present on Figure 1 the convergence for a square with side 1 and $k = 15$. Even though the theoretical results hold only (at this time) on smooth boundaries for the Λ-based estimation, one can see in Figure 1 that our new estimate behaves well on singular geometries since we retrieve with autoadaptive refinement the expected convergence rate ($\mathcal{O}(N^{-3/2})$) and we get an efficiency constant really close to 1.

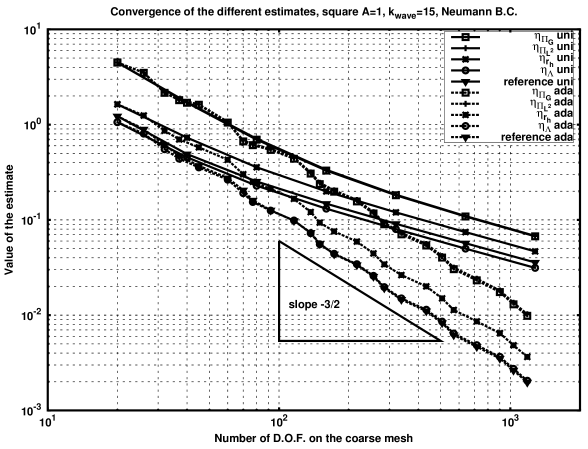

Figure 1: Convergence of different estimates for a square with sides of length 1 and $k = 15$. η_Λ and the reference overlap.

4 Acknowledgement

This work is supported by the *Agence Nationale de la Recherche* and the *Ministère français de la Défense - Délégation Générale de l'Armement.*

References

[1] C. Carstensen and D. Praetorius, Averaging techniques for the effective numerical solution of Symm's integral equation of the first kind, *SIAM J. Sci. Comp.* (2006), Vol. 27, No. 4, pp. 1226-1260

[2] C. Carstensen and D. Praetorius, Averaging techniques for the a posteriori BEM error control for a hypersingular integral equation in two dimensions, *SIAM J. Sci. Comp.* (2007), Vol. 29, No. 2, pp. 782-810

[3] C. Carstensen, An A posteriori error estimate for a first-kind integral equation, *Mathematics of Computation* (1997), Vol. 66, No. 217, 1997

Minisymposium: Fast Solvers for the Helmholtz Equation
organised by Wim Vanroose, Domenico Lahaye and Chris Stolk

This mini symposium presents an overview of recent advances in solvers for large scale Helmholtz problems. The problems appear in many scientific and industrial problems ranging from scattering in quantum systems to seismic inversion. The numerical solution of the equation poses serious challenges for numerical solvers. In this mini symposium we present the latest advances in using shifted Laplacians, deflation, sweeping, domain-decomposition, boundary integrals and other preconditioners to accelerate the solution of the Helmholtz equation.

Combination of multilevel methods and Krylov subspace methods for acoustic full waveform inversion in seismics

Henri Calandra[1], Youssef Diouane[2], Serge Gratton[3], Xavier Vasseur[4,*]

[1]TOTAL, E&P Research and Technology USA, llc 1201 Lousiana, Suite 1800, Houston, TX 77002-4397, USA

[2]ISAE, 10 avenue Edouard Belin, BP 54032, 31055 Toulouse Cedex 4, France

[3]ENSEEIHT, INPT, rue Charles Camichel, B.P. 7122 31071, Toulouse Cedex 7, and CERFACS, 42 avenue Gaspard Coriolis, 31057 Toulouse Cedex 01, France

[4]CERFACS, 42 Avenue Gaspard Coriolis, 31057 Toulouse Cedex 01, France

*Email: vasseur@cerfacs.fr

Abstract

We present a combination of multilevel methods and Krylov subspace methods to address the different challenges related to the solution of acoustic full waveform inversion in seismics. A specific focus is first given on a geometric multilevel preconditioner for the efficient solution of heterogeneous Helmholtz problems. Secondly recent block Krylov subspace methods that allow the use of a variable preconditioner for the solution of linear systems with multiple right-hand sides given simultaneously are detailed. Their use in both forward and inverse problems in the context of full waveform inversion is presented. Numerical experiments on three-dimensional public domain applications in seismics are shown to illustrate the efficiency of the proposed combination. This talk is part of the minisymposium "Fast solvers for the Helmholtz equation" organized by Wim Vanroose, Domenico Lahaye and Chris Stolk.

Keywords: Acoustic full waveform inversion, complex shifted Laplace preconditioner, flexible Krylov subspace methods, Helmholtz equation, heterogeneous media, variable preconditioning.

1 Introduction

In this talk, we address the solution of three-dimensional heterogeneous Helmholtz problems discretized with second-order or fourth-order finite difference methods with application to acoustic waveform inversion in geophysics [11, 12]. In this setting, the numerical simulation of wave propagation phenomena requires the approximate solution of possibly very large indefinite linear systems of equations. This task is known to be challenging for iterative methods [6] and the design and analysis of efficient and scalable multilevel preconditioners (e.g. of multigrid or domain decomposition type) to be used on massively parallel computing platforms is a current open issue.

2 A multilevel preconditioner

For that purpose, we present an iterative two-grid method proposed in [4]. This method is acting on the original Helmholtz operator where the coarse grid problem is solved inaccurately. A geometric multigrid method applied to a complex shifted Laplace operator [7, 9] is used as a preconditioner for the approximate solution of the coarse problem. A single cycle of this novel method is then used as a variable preconditioner of a flexible Krylov subspace method such as flexible GMRES [10]. We review the properties of the preconditioned operator. We show numerical results that confirm the theory and demonstrate the usefulness of the algorithm on three-dimensional public domain applications related to heterogeneous media (EAGE/SEG Salt dome [1]). The proposed numerical method allows us to solve successfully three-dimensional wave propagation problems even at high frequencies on a reasonable number of cores of a massively parallel distributed memory computer. Both weak- and strong scalability properties of the numerical method will be presented.

3 Application to the full waveform inversion problem

It is known that full waveform inversion requires the solution of linear systems with multiple right-hand sides given simultaneously. Due to the large size of the linear systems, block Krylov subspace methods [8] are found to be relevant candidates in this setting. We present recent developments related to block Krylov subspace methods to allow the use of a variable mul-

tilevel preconditioner for the solution of such systems [2, 3]. The numerical performance of this combination is shown on realistic public domain applications in seismics and scalability with respect to the number of right-hand sides is discussed. A new globally convergent stochastic algorithm has been recently applied to the acoustic full waveform inversion on parallel distributed memory platforms [5]. In such formulation linear systems with both multiple right- and left-hand sides naturally appear. To conclude this presentation we will discuss possible strategies to design efficient preconditioned Krylov subspace methods in this setting.

References

[1] F. Aminzadeh, J. Brac, and T. Kunz, 3D Salt and Overthrust models, SEG/EAGE modeling series I, Society of Exploration Geophysicists, 1997.

[2] H. Calandra, S. Gratton, R. Lago, X. Vasseur, and L. Carvalho, A modified block flexible GMRES method with deflation at each iteration for the solution of non-Hermitian linear systems with multiple right-hand sides, *SIAM J. Sci. Comput.* **35(5)**, (2013), pp. S345-367.

[3] H. Calandra, S. Gratton, J. Langou, X. Pinel, and X. Vasseur, Flexible variants of block restarted GMRES methods with application to geophysics, *SIAM J. Sci. Comput.*, **34(2)**, (2012), pp. A714–A736.

[4] H. Calandra, S. Gratton, X. Pinel, and X. Vasseur, An improved two-grid preconditioner for the solution of three-dimensional Helmholtz problems in heterogeneous media, *Numer. Linear Algebra Appl.* **20**, (2013), pp. 663–688.

[5] Y. Diouane, *Globally Convergent Evolution Strategies with Application to an Earth Imaging Problem in Geophysics*, PhD thesis, Institut National Polytechnique de Toulouse, 2014.

[6] O. Ernst and M. J. Gander, Why it is difficult to solve Helmholtz problems with classical iterative methods, In O. Lakkis I. Graham, T. Hou and R. Scheichl, editors, *Numerical Analysis of Multiscale Problems*, Springer, 2011.

[7] Y. A. Erlangga, C. W. Oosterlee, and C. Vuik, A novel multigrid based preconditioner for heterogeneous Helmholtz problems, *SIAM J. Scientific Computing*, **27**, (2006), pp. 1471–1492.

[8] M. H. Gutknecht, Block Krylov space methods for linear systems with multiple right-hand sides: an introduction, In A.H. Siddiqi, I.S. Duff, and O. Christensen, editors, *Modern Mathematical Models, Methods and Algorithms for Real World Systems*, pages 420–447, New Delhi, India, 2006.

[9] B. Reps, W. Vanroose, and H. bin Zubair, On the indefinite Helmholtz equation: complex stretched absorbing boundary layers, iterative analysis, and preconditioning, *J. Comp. Phys.*, **229**, (2010), pp. 8384–8405.

[10] Y. Saad, A flexible inner-outer preconditioned GMRES algorithm, *SIAM J. Sci. Statist. Comp.*, **14**, (1993), pp. 461–469.

[11] A. Tarantola, *Inverse Problem Theory and Methods for Model Parameter Estimation.* SIAM, Philadelphia, 2005.

[12] J. Virieux and S. Operto, An overview of full waveform inversion in exploration geophysics, *Geophysics*, **74(6)**, (2009), pp. WCC1–WCC26.

On efficiency and pollution error in Helmholtz solvers

Christiaan C. Stolk[1,*]

[1]Korteweg-de Vries Institute for Mathematics, University of Amsterdam, Amsterdam, The Netherlands

[*]Email: C.C.Stolk@uva.nl

Abstract

We consider the numerical solution of the Helmholtz equation in an inhomogeneous medium in the high-frequency regime in two and three dimensions. As problems of increasing size are being treated the dispersion errors associated with the discretization must be very small, while the discretization should use as few points per wavelength as possible on grounds of efficiency. From this viewpoint we compare several existing regular mesh discretizations and a new optimized finite difference method. The latter yields very good results in both two and three dimensions, e.g. a relative phase slowness error of $7 \cdot 10^{-6}$ using just five points per wavelength in two dimensions. We discuss the implications of using such methods for some recently developed solvers.

Keywords: Helmholtz equation, high-frequency limit, pollution effect, multigrid solver

1 Introduction

We consider the Helmholtz equation

$$-\Delta u - k(x)^2 u = f$$

on unbounded domains in two and three dimensions, assuming that the computational domain is a rectangle, and some form of absorbing layer (a perfectly matched layer or a conventional damping layer) is present near the boundary. As usual, $k(x) = \frac{\omega}{c(x)}$, with $c(x)$ the velocity of the medium. Due to developments in algorithms and computer equipment, these systems can be solved for increasingly large values of k, using domains whose size is on the order of several hundred wavelenghts. To have accurate solutions, it is important that numerical dispersion errors, closely related to pollution errors [1], are tightly controlled. This means that the differences between the phase slownesses (or phase velocities) of the numerical scheme and that of the continuous equation must be sufficiently small.

There are many different discretizations. Here we assume a regular mesh is used and we denote by G the minimum number of points per wavelength. Second order finite differences with $G = 10$ are often used as a testcase for solvers. However, it is well known that this is insufficient. In the geophysical literature, optimized finite difference methods have been proposed for use with G as small as 4 [3]. In the mathematical literature, higher order finite element methods have been recommended. Also, certain tailored finite element/finite difference methods have been studied, in particular the quasi-stabilized FEM method (QS-FEM) of [1]. For this latter method we are, however not aware of a three dimensional generalization. In this work we will study these schemes (except second order FD) and then discuss a new optimized finite difference method for which very small phase errors are obtained in both two and three dimensions, comparable to QS-FEM. We will then discuss how the use of these schemes affects the performance of certain solvers compared to second order finite differences at $G = 10$.

2 Phase slowness errors and optimized finite differences

Phase slownesses are related to the plane wave solutions of the Helmholtz equation $-\Delta u - k^2 u = 0$ with constant $k = \frac{\omega}{c}$. When $e^{ix\cdot\xi}$ is a solution, then the phase slowness vector is $p = \omega^{-1}\xi$. It is easily seen that the phase slownesses are precisely the vectors with $\|p\| = c$. For numerical schemes phase slownesses can be defined using Fourier modes or Bloch waves on the mesh. The numerical phase slownesses are in general different from c, the relative difference will be called the phase slowness error and denoted by Δp_{rel}. This error depends on the angle and on G.

The phase slowness errors directly translate to errors in the solution. In a first approximation these are phase errors, that can be estimated by $2\pi\Delta p_{\text{rel}}$ times the distance from the source that the wave is observed measured in wavelengths. While the required accuracy of

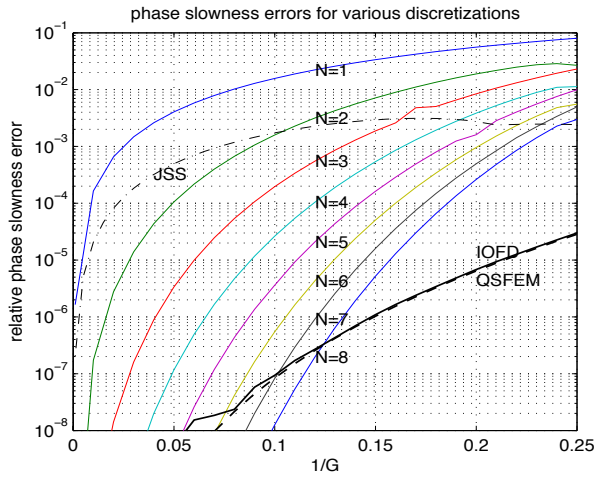

Figure 1: Phase slowness errors vs. $1/G$.

course depends on the application, the requirement

$$\Delta p_{\text{rel}} \lesssim 10^{-4} \tag{1}$$

appears reasonable in our setting.

In Figure 1 we give the relative phase slowness errors for several methods in two dimensions as a function of $1/G$. Results for finite element methods using tensor products of polynomials of order $N = 1$ to $N = 8$ are given. These can satisfy the criterion (1), but are quite demanding in terms of order N and value of G. The results for the method of [3] are marked with the text JSS. This method does not satisfy (1). The QS-FEM method has very small error, e.g. $< 7 \cdot 10^{-6}$ for $G \geq 5$.

Generalizing ideas of [3] and [4] we will present a new, compact stencil optimized finite difference method, called interpolated optimized finite differences (IOFD). Omitting the details we present the phase slowness errors in the figure. The relative phase slowness errors are very similar to those of QS-FEM. The advantage is that this method is easily generalized to 3-D.

3 Solvers using QS-FEM or IOFD

Solvers for high-frequency Helmholtz problems are an active area of research, see e.g. [2,5] and references. Many of these solvers are tested using second order finite differences (often at $G = 10$). The results will be different when the QS-FEM of IOFD discretization is used. Various issues play a role here. The larger stencils will affect the cost per degree of freedom, an effect that should be offset by the smaller value of G. Other factors also play a role, for example multigrid performance in general decays for smaller values of G. In the talk we will show examples how some of these solvers perform when used with IOFD or QS-FEM discretization on coarse grids.

4 Conclusions

To conclude, QS-FEM (in two dimensions) and our new IOFD method are the most efficient discretizations in the regime under consideration. They lead to very small phase slowness errors at quite coarse grids. The extent to which efficient solvers, such as those of [2,5] can be used with these methods will be discussed in the talk.

References

[1] I. Babuška, F. Ihlenburg, E.T. Paik and S.A. Sauter, A generalized finite element method for solving the Helmholtz equation in two dimensions with minimal pollution, *Comput. Methods Appl. Mech. Engrg.* **128**(1995), pp. 325–359.

[2] H. Calandra, S. Gratton, X. Pinel and X. Vasseur, An improved two-grid preconditioner for the solution of three-dimensional Helmholtz problems in heterogeneous media, *Numer. Linear Algebra Appl.*, **20**(2013), pp. 663–688.

[3] C.-H. Jo, C. Shin and J.H. Suh, An optimal 9-point, finite-difference, frequency-space, 2-D scalar wave extrapolator, *Geophysics* **61**(1996), pp. 529–537.

[4] C.C. Stolk, M. Ahmed, and S.K. Bhowmik, A multigrid method for the helmholtz equation with optimized coarse grid corrections, *SIAM J. Sci. Comput.* **36**(2014), pp. A2819-A2841.

[5] C.C. Stolk, A two-grid accelerated sweeping preconditioner for the Helmholtz equation, arxiv.org/abs/1412.0464

Toward a scalable solver for 2D resonant cavities

Leonardo Zepeda-Núñez[1,*], **Laurent Demanet**[1]
[1]MIT, Department of Mathematics, Cambridge MA, USA
*Email: lzepeda@math.mit.edu

Abstract

We present a compressed direct solver for the Helmholtz equation with medium featuring resonant cavities and sharp interfaces, in the high frequency regime. The online runtime scales sublinearly with respect to the number of unknowns in a distributed memory environment, with constants empirically independent of the features of the medium. The offline complexity (precomputation of the compressed factorization) is however still quite large.

1 Introduction

A new class of highly efficient iterative algorithms for solving the Helmholtz equation in heterogeneous media was recently proposed [**?**, **?**,**?**,**?**]. However, the performance of these methods often degrades when dealing with media featuring resonant cavities and sharp contrasts. In this note we explore a variant of [**?**], with a more thorough offline precomputation, but a practically identical online parallel complexity: sublinear in N when the number L of cores scales like a small fractional power of N.

The method may be called "compressed boundary reduction". Its ingredients (such as adaptive $\mathcal{H}$-matrices) are not particularly novel by themselves, but the documentation of the online complexity claim seems to be new. The method is potentially attractive in situations where the precomputation is amortized over many right-hand sides. Such applications range from optimizing the shape of waveguides and ring resonators in nanophotonics, to optimal survey design for seismic prospection, and to optimal focusing for intracraneal treatments using high intensity ultrasound.

2 Method

Consider a rectangular domain $\Omega \subset \mathbb{R}^2$ and consider the symmetric formulation of the Helmholtz equation with absorbing boundary conditions for a velocity field $c(\mathbf{x})$ and frequency ω (see Eq. 107 in [**?**]), discretized using Q1 finite elements (see [**?**]). To compute the mass matrix, the integrals are computed using an adaptive quadrature resulting in a second order accurate discretization, even in the presence of sharp interfaces and high contrasts. Let N for the total number of volume unknowns, n the number of unknowns in each dimension, and we suppose that $\omega \sim \sqrt{n}$.

We decompose Ω in L non-overlapping layers $\{\Omega^\ell\}_{\ell=1}^L$. We consider local Helmholtz problems in each layer, with artificial absorbing boundary conditions at the interfaces between layers. Following [**?**], we build a discrete integral system internal for interface unknowns $\mathbf{u}$ from an application of Green's representation formula (GRF):

$$\mathbf{M}\mathbf{u} = \mathbf{f}. \tag{1}$$

For the offline stage, a block LU factorization of $\mathbf{M}$ is computed (without pivoting), giving $\mathbf{LU} = \mathbf{M}$. The diagonal blocks of the LU factors are inverted explicitly. The blocks of the modified LU factors are then compressed in adaptive partitioned low rank form (PLR; a special case of $\mathcal{H}$-matrices, see Section 5 in [**?**]). For the online step, the back-substitution routine relies only on fast matrix vector products, allowing to solve the system in Eq. 1 in empirical $\mathcal{O}(LN^{5/8})$ time.

Following [**?**], the source $\mathbf{f}$ is assembled from local solves. After $\mathbf{u}$ is computed, the field u in the volume is obtained from another set of local solves.

3 Complexity

The offline stage of this algorithm is comprised of the LU factorization of the local problems, the computation of the local Green's functions to assemble $\mathbf{M}$, its factorization, the inversion of the diagonal blocks of the LU factors of $\mathbf{M}$ and the compression in PLR form of the blocks of the modified LU factors. The overall offline complexity is dominated by the factorization of the discrete integral system, which is $\mathcal{O}(LN^{3/2})$.

The online stage is composed of the local solves at each local layer ($\mathcal{O}(N/L)$), the solve of Eq. 1 ($\mathcal{O}(LN^{5/8})$) and the local reconstruction

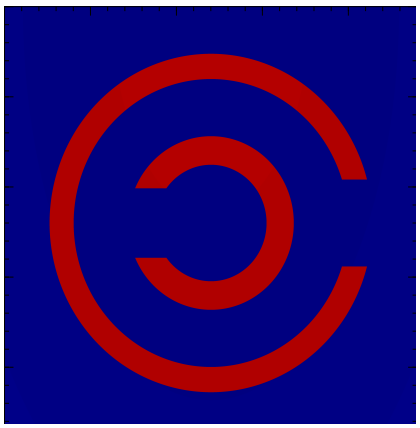

Figure 1: Resonant wave-guide.

in the volume ($\mathcal{O}(N/L)$). As in [**?**], the online runtime is sublinear ($O(N^{13/16})$) if L is chosen to grow as a small fractional power of N.

4 Numerical Experiments

The model in Fig. 4 was used for the numerical experiments. The shape is kept constant, with a background speed $c_{\text{blue}} = 1$. The results for $L = 10$ layers, different contrasts, frequencies, and problem sizes, are shown in Fig.2. We observe that the runtimes are independent of the contrast at high frequency. The complexity of [**?**] would severely deteriorate with high contrasts.

Fig. 2, bottom, shows the runtime for a fixed constrast ($c_{\text{red}} = 100$) and shows the scaling for the fast solve of Eq. 1. We obtain the same scaling as in [**?**] for the cavity-free problem.

If we apply the same compressed LU technique to solve a Schur complement system associated to a layered partitioning, rather than the GRF-based Eq. 1, we empirically obtain the same scalings.

In principle, the cost of the of offline computation of the boundary-reduced LU factors and their compression can be decreased by using $\mathcal{H}$-matrix algebra to perform the pivoting (see [**?**]).

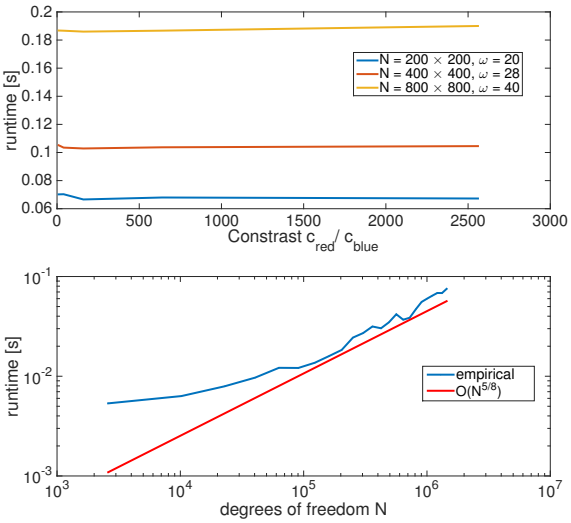

Figure 2: Top: online runtime for different constrasts and problem sizes. Bottom: runtime for a fixed constrast. L is fixed throughout.

A Parallelized DDM Sweeping Preconditioner for the Solution of High-Frequency Helmholtz and Maxwell Equations

A. Vion[1], **C. Geuzaine**[1,*]

[1]Montefiore Institute, University of Liège, Belgium

[*]Email: cgeuzaine@ulg.ac.be

Abstract

We propose an improvement of the double sweep preconditioner for the solution of Helmholtz and Maxwell problems by an optimized Schwarz method. It consists in reducing the sweeping range in order to perform several shorter sweeps in parallel, thereby alleviating a major drawback of the sweeping preconditioner—its sequential nature. This modification leads to small to moderate increase in the iteration count, which is largely counterbalanced by the gain in time-to-solution and better resource usage; pipe-lining multiple right-hand sides is a complementary option for maximizing throughput.

Keywords: Domain Decomposition Methods; Sweeping preconditioners; Parallel solvers

Introduction

The idea of sweeping for helping the solution of wave propagation problems has recently gained interest [5, 6]. It is indeed quite natural since it somehow accompanies the propagation of the wave in the medium. An inherent problem of this approach however is the sequential nature of the sweeping process, that prevents the efficient implementation of such methods on massively parallel architectures and makes the algorithm quite slow, especially in the case of many subdomains.

1 Non-Overlapping Optimized Schwarz Domain Decomposition Method

Consider a domain Ω with boundary $\partial\Omega$. We decompose Ω into N non-overlapping slices $\Omega_{i,1\leq i\leq N}$, with artificial boundaries Σ_{ij} between Ω_i and Ω_j. (This is a layered partitioning, not a general 2D partitioning.) For the Helmholtz equation with wavenumber k, the iterative scheme, detailed in [1, 2], uses impedance-matching boundary conditions on Σ_{ij} and recasts the problem in terms of the set of interface data $g = \{g_{ij}, 1 \leq i \neq j \leq N, |i-j| = 1\}$. An iteration amounts to solving the following subproblems in parallel:

$$\begin{aligned} -(\Delta + k^2)u_i^{(m+1)} &= 0 && \text{in } \Omega_i \\ (\partial_n + \mathcal{S})u_i^{(m+1)} &= (-\partial_n + \mathcal{S})u_j^{(m)} && \text{on } \Sigma_{ij} \\ &= g_{ij}^{(m)}, \end{aligned}$$

and then performing the update

$$\begin{aligned} g_{ij}^{(m+1)} &= -\partial_n u_j^{(m+1)} + \mathcal{S}u_j^{(m+1)} && \text{on } \Sigma_{ij} \\ &= -g_{ji}^{(m)} + 2\mathcal{S}u_j^{(m+1)}. \end{aligned}$$

(A similar formulation can be derived for the time-harmonic Maxwell equations.) Boundary conditions on $\partial\Omega_i \cap \partial\Omega$ are conserved from the original problem. This procedure can be rewritten as a fixed point iteration on the unknowns g:

$$Fg = b, \tag{1}$$

where applying the operator F amounts to solving the subproblems and updating g. The solution of problem (1) can be accelerated using GMRES.

The choice of operator $\mathcal{S}$ is critical for the rate of convergence. It was shown in [4] that the optimum is obtained if $\mathcal{S}$ is the DtN map for the complementary of the subdomain of interest. Different local approximations of the DtN map have been proposed [2, 3]; non-local approximations have also been proposed that make use of PMLs [1, 6]. This last idea has proved particularly efficient in the non-homogeneous case, where currently available local approximations are less efficient.

In [1], we preconditioned system (1) by an approximate inverse $\tilde{F}^{-1}$ of operator F, expressed as a sparse matrix made of transfer operators. We showed that it can be implemented as a double (forward/backward) sequence of subproblem solves, or double sweep; a sweep can be interpreted as the process of collecting and transporting data over the full span of the domain, therefore similar to the action of a coarse grid.

By construction, such a preconditioner works best for accurate approximations of the DtN

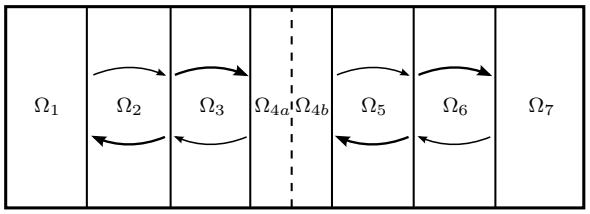

Figure 1: Introducing cuts in the sequence (here Ω_4) leads to smaller and independent sweeps, reducing the preconditioner application time when done in parallel.

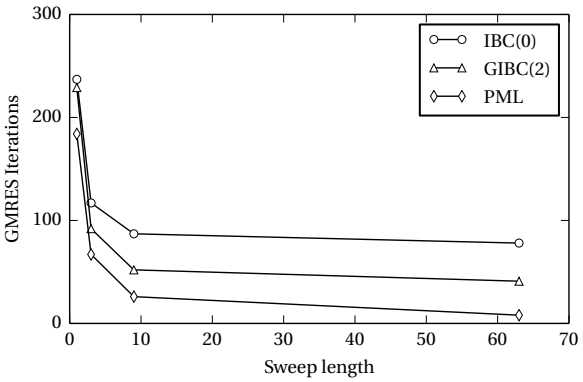

Figure 2: Iteration count for the marmousi model, with 64 subdomains. Both the choice of the transmission condition and the number of cuts have an influence on the convergence; performing a few cuts however has moderate impact, while enabling better parallelization.

map. The resulting method makes the convergence rate virtually independent of the number of subdomains N and wavenumber k, the drawback being the sequential nature of the sweeps, leading to long application time in the case of many subdomains, and long processor idleness in the case where one CPU is assigned to each subdomain. Similar findings were obtained using variations in the sweeping process [5, 6].

2 Parallelization of the Double Sweep

Here we propose to introduce cuts in the sequence of solves, in order to perform smaller sweeps over groups of subdomains, as illustrated on Figure 1. Since they are independent of each other, they can be performed in parallel, thereby partially re-enabling the parallelism of the original Schwarz algorithm.

Of course, this block-Jacobi-type modification of the preconditioner can be expected to cause a degradation of its performance, since information is no longer shared between all the subdomains.

However, in practice, the degradation is limited once "not-too-short" sweeping lengths are used. For example, on the standard marmousi underground wave propagation benchmark with 64 subdomains, a sweeping length of 10 brings quasi-optimal iteration counts (see Figure 2). Remaining processor idleness can be exploited for the solution of multiple right-hand sides, in a pipe-lining fashion [7].

References

[1] A. Vion and C. Geuzaine, *Double Sweep Preconditioner for Optimized Schwarz Methods Applied to the Helmholtz Problem*, J. Comp. Phys., **231** (2012), pp. 262–280.

[2] Y. Boubendir, X. Antoine and C. Geuzaine, *A quasi-optimal non-overlapping domain decomposition algorithm for the Helmholtz equation*, J. Comp. Phys., **266** (2014), pp. 171–190.

[3] M. El Bouajaji, X. Antoine and C. Geuzaine, *Approximate local magnetic-to-electric surface operators for time-harmonic Maxwell's equations*, J. Comp. Phys., **279** (2014), pp. 241–260.

[4] F. Nataf, *Interface Connections in Domain Decomposition Methods*, NATO Science Series II, **75** (2001), pp 323–364.

[5] B. Engquist, L. Ying, *Sweeping Preconditioner for the Helmholtz equation: Moving Perfectly Matched Layers*, SIAM MMS, **9** (2011).

[6] C. Stolk, *A rapidly converging domain decomposition method for the Helmholtz equation*, J. Comp. Phys., **241** (2013), pp. 240–252.

[7] A. Vion and C. Geuzaine, *Improved DDM sweeping algorithm for high-frequency Helmholtz and Maxwell problems in non-homogeneous media*, in preparation.

Deflating the Shifted Laplacian for the Helmholtz Equation

Abdul Sheikh Hannan[1], **Domenico Lahaye**[1,*], **Kees Vuik**[1]
[1]Delft Institute of Applied Mathematics, Delft, The Netherlands
*Email: d.j.p.lahaye@tudelft.nl

Abstract

The Shifted Laplace preconditioned for the Helmholtz equation is slower to converge for large wave numbers. This can be explained by the increase of small eigenvalues of the preconditioned systems. In this work we look into deflating these small eigenvalues by multigrid vectors. These vectors are constructed by standard coarsening a uniform mesh. We consider two algorithmic variants. The first deflates the preconditioned operator and requires some form of approximation to become computationally viable. The second variant deflates the original Helmholtz operator and can be applied directly. The extension of both algorithms to multiple levels of coarsening requires the deployment of a Krylov subspace acceleration on each level. This gives raise to so-called multilevel Krylov algorithms. A Rigorous Fourier analysis confirms that the use of deflation results in a tighter cluster of eigenvalues. This clustering favors the convergence of the outer Krylov method. Numerical results give evidence of a speedup of the computations. Problems that were previously too large can now instead be solved.

Keywords: Helmholtz equation, preconditioning, shifted Laplacian, deflation

1 Introduction

In [2] the authors propose to combine the shifted Laplacian preconditioner for the Helmholtz equation with a deflation method. First the deflation is applied to the preconditiond operator. Subsequently the preconditioner and the deflation operator are combined multiplicatively resulting in a composite preconditioner. The deflation operator attempts to remove near-kernel eigenmodes that hampers the convergence of the Krylov method. Multigrid vectors are selected as deflation vectors. The multilevel extension of the algorithm proposed requires a Krylov acceleration at each level and a multilevel Krylov method is arrived at.

In this work we propose a variant of the method put forward in [2]. Instead of applying the deflation to the preconditioned Helmholtz operator, we apply the deflation to the Helmholtz operator directly. Other algorithmic components carry over from [2]. We perform a rigorous Fourier two-grid analysis of a one-dimensional problem with Dirichlet boundary conditions assuming both the preconditioner (or smoother) and the coarse grid correction operator be inverted exactly. This analysis reveals that the deflation operator transforms the spectrum into a spectrum that is more favorable for the convergence of the outer Krylov acceleration. Numerical results confirm a reduction in the number of outer Krylov iterations that in turn yields a decrease in CPU time for sufficiently large problems. More details can be found in [1].

2 Spectral Analysis

In Figure 1 we plotted the spectrum resulting from a Rigorous Fourier analysis of the two-level composite deflated preconditioned operator for wavenumbers $k = 100$ (top) and $k = 1000$ (bottom). The figure shows for $k = 100$ a tight cluster of eigenvalues around $(1, 0)$ in the complex plane. For $k = 1000$ however the clusters smears out in both directions of the real axis. Despite of this smearing, the use of deflation turns out to be beneficial as shown by numerical experiments.

3 Numerical Results

In Table 1 we tabulated the number of outer FGMRES iterations required to solve the Helmholtz equation on a unit square as a function of the meshwidth and the number of gridpoints in each direction. We listed the iterations count for both the algorithm with and without deflation. The boxed numbers on the diagonal correspond to the use of ten grid points per wavelength. The numbers clearly show the reduction in iteration count for the algorithm with deflation.

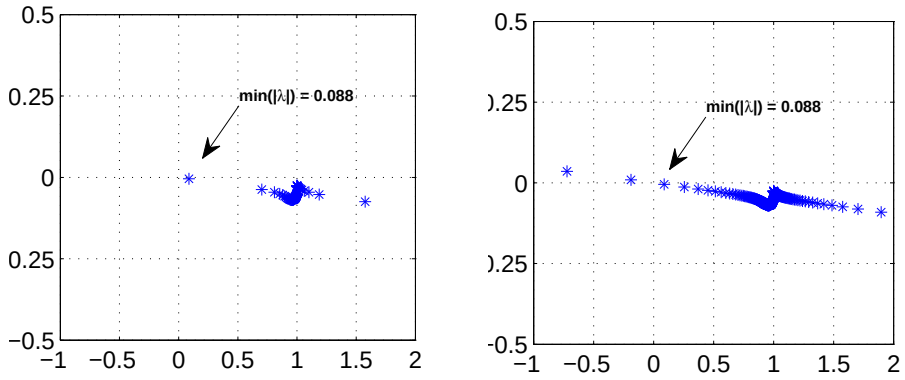

(a) k=100 (b) k=1000

Figure 1: Spectrum of the deflated preconditioned operator for two wavenumbers.

	Wavenumber				
Grid	$k = 10$	$k = 20$	$k = 30$	$k = 40$	$k = 50$
$n = 32$	5/10	8/17	14/28	26/44	42/70
$n = 64$	4/10	6/17	8/28	12/36	18/45
$n = 96$	3/10	5/17	7/27	9/35	12/43
$n = 128$	3/10	4/17	6/27	7/35	9/43
$n = 160$	3/10	4/17	5/27	6/35	8/43

Table 1: Number of outer FGMRES iterations with and without deflation for unit square domain problem

References

[1] A. H. Sheikh, D. Lahaye, and C. Vuik. On the convergence of shifted Laplace preconditioner combined with multilevel deflation. *Numerical Linear Algebra with Applications*, 20(4):645–662, 2013.

[2] Y.A. Erlangga and R. Nabben. On a multilevel Krylov method for the Helmholtz equation preconditioned by shifted Laplacian. *Electronic Transactions on Numerical Analysis (ETNA)*, 31:403–424, 2008.

Domain decomposition methods combined with absorption for the Helmholtz equation

P.N.Childs[1], I.G. Graham[2,*], J.D. Shanks[2], E.A. Spence[2], E. Vainikko[3]

[1]Emerson Process Management, Northbrook House, Oxford Science Park, OX4 4GA, UK
[2]Dept of Mathematical Sciences, University of Bath, Bath BA2 7AY, UK
[3]University of Tartu, Tartu, Estonia
[*]Email: I.G.Graham@bath.ac.uk

Abstract

There has been much recent research on preconditioning (discretisations of) the Helmholtz operator $\Delta + k^2$ using the (approximate) inverse of a discrete version of the so-called "shifted Laplacian" $\Delta + (k^2 + \mathrm{i}\epsilon)$ for some $\epsilon > 0$. Recent work [5] has provided a theory of this, giving estimates on the rate of convergence of GMRES explicit in k and ϵ, based on the assumption that the discrete shifted Laplacian problem is inverted exactly. To make this method practical this inverse should be replaced by a cheaper approximation. In the literature a multigrid V-cycle is a popular choice but there is no rigorous theory for the use of such approximations and this appears to be a fairly hard theoretical problem. The theoretical part of this talk describes recent results on domain decomposition methods, with and without coarse grids for solving the shifted problem. Their use in solving the unshifted problem is then investigated experimentally. Practical illustrations are given for model homogeneous and heterogeneous problems in $2D$ and a few more substantial $3D$ problems motivated by applications in seismic inversion. In the work we also include results on using domain decomposition as an inner solver in the implementation of sweeping preconditioners.

Keywords: High frequency Helmholtz, Preconditioning, Domain Decomposition, GMRES .

1 Introduction

In this talk we present some recent results on solvers for the high-frequency Helmholtz equation

$$\Delta u + k^2 u = f \qquad (1)$$

posed on some $2D$ or $3D$ domain Ω and discretised by conventional low order finite element methods. While these methods suffer from the pollution effect, they still form the first discretisation widely used in practice, for which the development of efficient iterative solvers is of wide interest. The resulting linear systems for high wavenumber k are notoriously hard to solve and the analysis of Krylov space-based iterative solvers such as GMRES is also hard, since the corresponding system matrices are complex, non-Hermitian and usually highly non-normal and so information about spectra and condition numbers of the system matrices generally does not give much information about the convergence rate of iterative methods. We consider preconditioners for this system built from suitable approximations of the corresponding problem with absorption - an approach which has been explored in many papers, e.g. [3], [1], but for which there remain many open questions. Our approach is both theoretical - to explain as rigorously as possible properties of the solvers which are observed in practice, and also practical - to obtain new methods based on this understanding. In the theoretical part of the talk we restrict to the case where Ω is a bounded domain, the wavenumber k is constant, and the problem is subject to the first order absorbing boundary condition $\partial u/\partial n - \mathrm{i}ku = g$ on $\partial\Omega$. Numerical experiments will be given for this case and also for more general boundary conditions and cases when k is highly variable. Let A, A_ϵ denote, respectively, the system matrices for discretizations of (1) and the corresponding "shifted problem", obtained by replacing k^2 by $k^2 + \mathrm{i}\epsilon$, $\epsilon > 0$. Let B_ϵ^{-1} denote any (efficient to compute) approximate inverse for A_ϵ which we shall use as a (left or right) preconditioner for A. Thus we will be interested in the convergence of GMRES for solving systems with coefficient matrix either $B_\epsilon^{-1}A$ or AB_ϵ^{-1}. Restricting to left preconditioning (right is similar), and applying the classical convergence theory for GMRES [2], sufficient conditions for good convergence are that (i) the matrix $B_\epsilon^{-1}A$ is not too large in norm and (ii) the distance of the field of values of $B_\epsilon^{-1}A$ can be bounded well away from the

origin. Since we may trivially write

$$B_\epsilon^{-1}A = B_\epsilon^{-1}A_\epsilon(I + \delta_\epsilon),$$

where $\delta_\epsilon = A_\epsilon^{-1}(A - A_\epsilon)$, it is easy to see that the required conditions for $B_\epsilon^{-1}A$ will follow provided (a) analogous conditions on $B_\epsilon^{-1}A$ could be established and (b) the "perturbation" term δ_ϵ is sufficiently small. Such conditions can be established by delicate balances between the choice of ϵ and the performance of B_ϵ^{-1} as a preconditioner for A_ϵ. This justifies the analysis of preconditioners for the shifted problem A_ϵ as a useful first step in finding good preconditioners for A. The talk describes research along these lines in the cases when B_ϵ^{-1} is constructed using classical additive Schwarz algorithms with coarse grids [6] or by novel Schwarz methods with optimised interface conditions [7], [8]. The latter method is also used as an inner approximate solver in a hybrid variant [4] of the sweeping preconditioner, and is used for some substantial 2D and 3D problems motivated by seismic inversion in [7].

References

[1] S. Cools and W. Vanroose. Local Fourier Analysis of the complex shifted Laplacian preconditioner for Helmholtz problems. *Numerical Linear Algebra with Applications*, **20**:575 - 597, 2013.

[2] S.C. Eisenstat, H.C. Elman and M.H. Schultz, Variational iterative methods for nonsymmetric systems of linear equations, *SIAM J. Numer. Anal.*, **20**:345-357, 1983.

[3] Y. A. Erlangga, C. W. Oosterlee, and C. Vuik. A novel multigrid based precconditioner for heterogeneous Helmholtz problems. *SIAM J. Sci. Comp.*, **27**:1471 - 1492, 2006.

[4] P.N. Childs, I.G. Graham and J.D. Shanks, Hybrid sweeping preconditioners for the Helmholtz equation, Proceedings of WAVES 2013.

[5] M. Gander, I.G.Graham and E.A. Spence, Applying GMRES to the Helmholtz equation with shifted Laplacian preconditioning: What is the largest shift for which wavenumber-independent convergence is guaranteed? *Numer. Math.* DOI: 10.1007/s00211-015-0700-2, Published online, 25th January 2015.

[6] I.G. Graham, E.A. Spence and E. Vainikko, Domain Decomposition preconditioning for high-frequency Helmholtz problems using absorption, submitted for publication.

[7] J.D. Shanks, P.N. Childs, and I.G Graham, A hybrid sweeping domain decomposition method for the Helmholtz equation, in preparation.

[8] J.D. Shanks, Robust solvers for large indefinite systems in seismic inversion, PhD Thesis, University of Bath, 2015.

A scalable solver for the far- and near-field maps of Helmholtz and Schrödinger equations.

Siegfried Cools[1,*], **Wim Vanroose**[1]

[1]Department of Mathematics and Computer Science, University of Antwerp, Belgium

[*]Email: siegfried.cools@uantwerp.be

Keywords: Helmholtz equation, Schrödinger equation, iterative methods, multigrid, far field and near field map.

Helmholtz equation. The Helmholtz equation plays an important role in many areas of science and engineering. It describes the propagation of waves through an object in the frequency domain. The equation is

$$\left(-\Delta - k^2(\mathbf{x})\right) u(\mathbf{x}) = f(\mathbf{x}), \quad \mathbf{x} \in \Omega \subset \mathbb{R}^d \quad (1)$$

where $k(\mathbf{x})$ is the wave number that describes how the wave speed changes through the object, $u(\mathbf{x})$ is the scattering solution, and $f(\mathbf{x})$ represents the source. The equation is defined on a domain $\Omega \subset \mathbb{R}^d$, where d is the dimension of the problem. Many physical problems typically require outgoing wave boundary conditions on the boundary of Ω. Here we assume that $k(\mathbf{x})$ only differs from a constant background, denoted by k_0, inside a compact subset of the domain Ω.

After discretization of the equation (1) and the absorbing boundary conditions one obtains a large scale linear system $Ax = b$, which is indefinite due the wave number and non-normal due to the absorbing boundary conditions. Moreover, equation (1) is known to be hard to solve using traditional iterative methods. In particular the failure of multigrid as a Helmholtz solver is well-documented, see [1, 2].

Far- and near-field. In many applications the scattered wave solution $u(\mathbf{x})$ is not required *inside* but rather *outside* the numerical domain Ω. This is, for example, the case when one is interested in calculating the near- or far field scattered wave solution. The solution can then be written as a integral over the numerical domain

$$u(\mathbf{x}) = \int_\Omega G(\mathbf{x},\mathbf{s}) \left[f(\mathbf{s}) - \left(k_0^2 - k^2(\mathbf{s})\right) u^n(\mathbf{s}) \right] d\mathbf{s} \quad (2)$$

for any $\mathbf{x} \in \mathbb{R}^d$, where $G(\mathbf{x},\mathbf{s})$ is the Green's function of the operator $-\Delta - k_0^2$, and u^n is the numerical solution of Eq. (1) on a domain that covers the compact subdomain in which $k(\mathbf{x})$ deviates from the constant background, with outgoing wave boundary conditions.

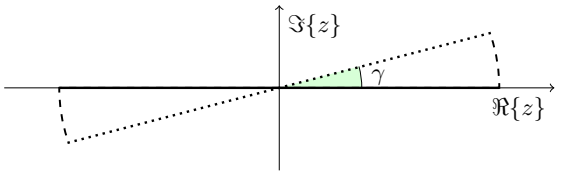

Figure 1: *Schematic representation of the complex contour for the far field integral calculation* (3) *illustrated in 1D. The full line represents the real-valued computational domain* Ω*, the dotted and dashed lines represent the complex contour* $Z \subset \mathbb{C}$*.*

When $k(\mathbf{x})$ is an analytical function, the contour of the volume integral, Eq. (2), can be deformed into the complex domain without affecting the value of the integral, as was shown in [3]. Hence, the value of u outside the domain can alternatively be calculated as an integral over the solution u^n of the Helmholtz equation on a complex valued domain $Z \subset \mathbb{C}^d$, i.e.

$$u(\mathbf{x}) = \int_Z G(\mathbf{x},\mathbf{z}) \left[f(\mathbf{z}) - \left(k_0^2 - k^2(\mathbf{z})\right) u^n(\mathbf{z}) \right] d\mathbf{z} \quad (3)$$

Equivalence to complex shifted Laplacian. One easily observes that the Helmholtz equation along the deformed contour is equivalent to a complex shifted Laplacian problem. Indeed, consider the complex shifted Helmholtz problem

$$\left(-\Delta - (1+i\beta)k^2(\mathbf{x})\right) u(\mathbf{x}) = g(\mathbf{x}), \quad \mathbf{x} \in \Omega, \quad (4)$$

with Dirichlet boundary conditions $u(\mathbf{x}|_{\partial\Omega}) = 0$ and a complex shift parameter $\beta \in \mathbb{R}$. After finite difference discretization on a d-dimensional Cartesian grid with fixed grid distance h in every spatial dimension, one typically obtains a linear system

$$-\left(\frac{1}{h^2}L + (1+i\beta)k^2\right) u_h = g_h, \quad (5)$$

where L is the matrix operator expressing the stencil structure of the Laplacian. Dividing both

	$n_x \times n_y \times n_z$	16^3	32^3	64^3	128^3	256^3
k_0	1/4	**10** (10)	**9** (59)	**9** (560)	**9** (4456)	**9** (35165)
		0.24	0.20	0.21	0.20	0.20
	1/2	12 (12)	**10** (63)	**10** (611)	**10** (4937)	**9** (35405)
		0.31	0.24	0.22	0.23	0.21
	1	7 (8)	13 (83)	**11** (691)	**10** (4899)	**10** (38975)
		0.13	0.32	0.27	0.24	0.24
	2	2 (4)	8 (54)	13 (809)	**11** (5418)	**10** (38051)
		0.01	0.14	0.33	0.27	0.24
	4	1 (3)	2 (17)	7 (457)	13 (6337)	**11** (41848)
		0.01	0.01	0.12	0.33	0.26

Table 1: *3D Helmholtz problem solved on a full complex grid rotated by $\theta = \pi/6$ using a series of multigrid V(1,1)-cycles with GMRES(3) smoother up to residual reduction tolerance `1e-6`. Displayed are the number of V-cycle iterations, number of work units and average convergence factor for various wavenumbers k_0 and different discretizations. 1 WU is calibrated as the cost of 1 V(1,1)-cycle on the 16^3-points grid $k_0 = 1/4$ problem. Discretizations respecting the $k_0 h < 0.625$ criterion for a minimum of 10 grid points per wavelength are indicated by a bold typesetting.*

sides in (5) by $(1+i\beta)$, we obtain the equivalent system

$$-\left(\frac{1}{(1+i\beta)h^2}L + k^2\right) u_h = \frac{g_h}{1+i\beta}. \qquad (6)$$

The left-hand side matrix operator of this equation is a discretization of the original Helmholtz operator $-\Delta - k^2$ using a complex grid distance $\tilde{h} = \sqrt{1+i\beta}\, h$. Hence, (6) is the discrete representation of the Helmholtz equation on a complex grid Z, i.e. the operator $\big(-\Delta - k^2(\mathbf{z})\big)$.

Recalling the integral (2), it clear that a shifted problem needs to be solved in the first step of the far field map calculation to obtain the scattered wave u^n along the complex contour Z. In Table 1 we show convergence results for multigrid applied to the problem along the contour. Note that the multigrid scheme is used as a solver, contrary to its use as a preconditioner in e.g. [4].

Comments on the contour approach. Although the value of the integral is theoretically independent of the choice of the contour, the contour can in practice not be defined arbitrarily. Choosing the complex part of $\tilde{h}$ very large corresponds to a large complex shift β, which implies fast multigrid convergence. However, a large shift (or rotation angle) makes the far field integral harder to calculate, since the integrand is typically a product of an exponentially decaying with a exponentially increasing function, and a larger angle implies an increased rate of decay and/or growth.

In [5] we have illustrated the effectiveness of the method for the solution of high-dimensional Schrödinger equations. The dependence on the complex shift was analyzed and an additional coarse grid correction was proposed to further accelerate the method.

References

[1] H. C. Elman and O. G. Ernst and D. P. O'Leary, *A multigrid method enhanced by Krylov subspace iteration for discrete Helmholtz equations.* SIAM Journal on scientific computing 23(4) (2001) 1291-1315.

[2] O. G. Ernst and M. J. Gander, *Why it is difficult to solve Helmholtz problems with classical iterative methods*, Numerical Analysis of Multiscale Problems. Springer Berlin Heidelberg, (2012) 325-363.

[3] S. Cools, B. Reps and W. Vanroose, *An efficient multigrid method calculation of the far field map for Helmholtz problems*, SIAM journal on Scientific Computing 36(3) B367-B395 (2014).

[4] Y. A. Erlangga, C. W. Oosterlee, and C. Vuik, *A novel multigrid based preconditioner for heterogeneous Helmholtz problems*, SIAM Journal on Scientific Computing 27.4 (2006) 1471-1492.

[5] S. Cools and W. Vanroose, *A fast and robust computational method for the ionization cross sections of the driven Schrödinger equation using an O(N) multigrid-based scheme* Submitted, arxiv:1412.1953.

Minisymposium: Low Frequency Electromagnetic Imaging and Eletrical Impedance Tomography

organised by Bastian v. Harrach and Roland Griesmaier

Low frequency inverse scattering and electrical impedance tomography have been very active fields of research in recent years. New trends have emerged that have allowed to obtain further insights and encouraging results for these well established and fascinating inverse problems. The minisymposium focuses on innovative contributions in this direction, considering both theoretical results and numerical algorithms.

A MUSIC scheme for impedance imaging using multiple AC frequencies

Martin Hanke[1,*]

[1]Institut für Mathematik, Johannes Gutenberg-Universität, 55099 Mainz, Germany

[*]Email: hanke@math.uni-mainz.de

Abstract

We investigate a multifrequency impedance imaging technique that has recently been suggested for mammography screenings. This MUSIC type technique uses boundary voltages generated by time harmonic (AC) boundary currents with the same spatial distribution but different driving frequencies.

We prove that the method will always find a single small focal lesion in two or three space dimensions. Concerning the two dimensional case we also discuss the potential of the method to find and separate multiple inclusions. Generically, the given measurements not only allow to locate the lesions but also to determine their conductivities and permittivities to facilitate their classification. It might also be possible to extract shape information from these data.

Keywords: Electrical impedance tomography, MUSIC method, polarization tensor

1 Introduction

We consider the conductivity equation for biological tissues given exciting AC currents with small frequencies in the kHz regime. Assuming a homogeneous background we search for tiny inclusions with frequency dependent complex admittivity. In the applications we have in mind (like, e.g., breast cancer detection using the TransScan TS2000 device [5]) it is only possible to impose a single spatial boundary current distribution, and the only option for generating multiple data sets is by varying the driving AC frequency.

For this setting Scholz [5] suggested a variant of the well-known MUSIC algorithm to localize malign lesions within the breast. Ammari, Boulier, and Garnier [2] provided a theoretical justification, restricting themselves to small inclusions with the shape of a disk in $\mathbb{R}^2$.

Together with Roland Griesmaier we recently have shown [4] that the method finds an inclusion of arbitrary shape, as long as it is small and the number of driving frequencies is sufficiently large. These results are based on a detailed investigation [3] of the so-called polarization tensor affiliated with the domain that is taken by the inclusion, considered as a meromorphic function of the admittivity contrast. The overall technique is strongly tied to two space dimensions.

In this paper we extend the analysis of the method to the more relevant setting in $\mathbb{R}^3$. We prove that the method will always locate a small single inclusion.

2 Problem Formulation

Let $D \subset \mathbb{R}^3$ be a bounded and simply connected domain with boundary ∂D, and $\Omega \subset \overline{\Omega} \subset D$ be the domain taken by an obstacle within D. Imposing a (nontrivial) AC boundary current

$$F(x,t) \,=\, f(x)e^{\mathrm{i}\omega t}\,, \quad x \in \partial D\,,\ t \in \mathbb{R}\,,$$

with driving frequency $\omega > 0$ and fixed spatial distribution $f \in L^2(\partial D)$ with vanishing mean, a time-harmonic potential $U(x,t) \,=\, u(x;\omega)e^{\mathrm{i}\omega t}$ is generated in D, and under suitable physical assumptions its spatial component satisfies the boundary value problem

$$\begin{aligned} -\nabla\cdot(\gamma\nabla u) \,&=\, 0 \qquad \text{in } D\,,\\ \partial_\nu u \,&=\, f \qquad \text{on } \partial D\,, \end{aligned}$$

with u having vanishing mean over ∂D. Here, the frequency dependent complex admittivity γ is assumed to be $\gamma = 1$ in $D \setminus \overline{\Omega}$ and $\sigma + \mathrm{i}\varepsilon$ in Ω, where the constant quantities $\sigma > 0$ and $\varepsilon > 0$ are the conductivity and permittivity of the obstacle, respectively. Our aim is to determine the obstacle Ω from measurements of

$$g_n \,=\, u(\,\cdot\,;\omega_n)\big|_{\partial D}$$

for infinitely many frequencies $\omega_n > 0$. To this end we compare g_n with the reference potential $g_0 \,=\, u_0|_\Gamma$ for the case $\Omega = \emptyset$; note that g_0 is independent of the driving frequencies.

3 Theoretical Results

Our theoretical results treat the case when the obstacle Ω within $D \subset \mathbb{R}^3$ is small. We assume

that such an obstacle is located in a point x_0 and has the shape of a reference domain $\mathcal{O}$, and that its size is determined by a scaling parameter $\delta > 0$, i.e.,

$$\Omega = x_0 + \delta\mathcal{O}\,.$$

Then a known asymptotic formula (cf., e.g., [1] asserts that

$$\frac{1}{\delta^3}(g_n - g_0) \longrightarrow h_n\,, \quad \delta \to 0\,,$$

where h_n is the trace of a dipole potential located in x_0 with dipole moment $p_n \in \mathbb{R}^3$ and with homogeneous Neumann boundary condition on ∂D. the dipole moment p_n depends analytically on the frequency ω_n and on the shape $\mathcal{O}$ and the reference potential u_0 near x_0.

To retrieve the location of a small obstacle we sample the points $z \in D$ and use a MUSIC scheme to check whether the trace ϕ_z on ∂D of a corresponding dipole potential located in z with dipole moment $p = \nabla u_0(z)$ is spanned by the relative data $g_n - g_0$. This is based on the following result.

Theorem 1 *Assume that* $\nabla u_0(x_0) \neq 0$ *and* $z \in \Omega$. *Then there exists* $(a_n) \in \ell^1$, *such that*

$$\phi_z = \sum_{n=1}^{\infty} a_n h_n\,,$$

if and only if $z = x_0$.

4 Numerical Results

When there is more than one obstacle, this version of the MUSIC scheme should be modified by testing more than one dipole moment for each test point $z \in D$, as this will increase the robustness of the method. In $\mathbb{R}^2$ we have provided in [4] a list of exceptional shapes and orientations of two given inclusions where even the stabilized method will fail. However, in the generic situation the method will find all obstacles present and may even be used to determine their material parameters. This is illustrated in the numerical reconstruction below.

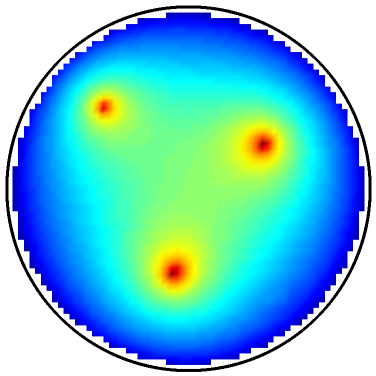

Figure 1: Reconstruction of three obstacles

References

[1] H. Ammari and H. Kang, *Polarization and Moment Tensors with Applications to Inverse Problems and Effective Medium Theory*, Springer, New York, 2007.

[2] H. Ammari, T. Boulier, and J. Garnier, Modeling active electrolocation in weakly electric fish, *SIAM J. Imaging Sci.* **6** (2013), pp. 285–321.

[3] R. Griesmaier and M. Hanke, Polarization tensors of planar domains as functions of the admittivity contrast, Preprint, arXiv:1410.4916 [math.AP] (2014), submitted.

[4] R. Griesmaier and M. Hanke, Multifrequency impedance imaging with multiple signal classification, *SIAM J. Imaging Sci.*, to appear.

[5] B. Scholz, Towards virtual electrical breast biopsy: Space frequency MUSIC for trans-admittance data, *IEEE Trans. Med. Imaging* **21** (2002), pp. 588–595.

Imaging of Dielectric Objects Via Monotonicity of the Transmission Eigenvalues

A. Tamburrino[1,2,*], **L. Barbato**[1], **D. Colton**[3], **P. Monk**[3]

[1]DIEI, Università di Cassino e del Lazio Meridionale, Cassino, Italy
[2]ECE, Michigan State University, East Lansing, MI, USA
[3]Department of Mathematical Sciences, University of Delaware, Newark, NJ, USA
[*]Email: tamburrino@unicas.it

Abstract

In the past years monotonicity has been recognized as a key property for developing real-time imaging methods for inverse medium or obstacle problems such as Electrical Resistance Tomography (governed by an elliptic PDE) or Eddy Current Testing (governed by a parabolic PDE). Recently, monotonicity has been found also for transmission eigenvalues in wave propagation problems. In this work we propose a monotonicity based imaging method relying on this property of transmission eigenvalues.

Keywords: Inverse Problems, Non-Iterative Imaging, Monotonicity, Transmission Eigenvalues

1 Introduction

In the recent years a new class of Non-Iterative Imaging Methods have been introduced that are based on some monotonicity property associated with quantities/operators appropriate for the problem. Monotonicity (based) Imaging Method (MIM) was introduced initially in the context of the inverse obstacle problem for Electrical Resistance Tomography (ERT) [1] and, then, extended to Eddy Current Testing (ECT) [2, 3] where experimental results are also available [4]. The objective of such papers was to find the shape of an object in an otherwise homogeneous material (the inverse obstacle problem). The key feature in MIM is the existence of a proper criterion (based on monotonicity) for establishing if a test anomaly (prescribed in terms of shape and position) is part of the unknown object or not. By considering many different test anomalies, one can reconstruct/approximate the shape of the unknown object. This approach provides upper and lower bounds for the unknown object in the case of a finite number of measurements (limited aperture data) [1]. In ERT, it provides the exact shape in case of an infinite number of measurements (full aperture data) [5]. Moreover, its computational cost is linear with the number of test anomalies (i.e. voxels or pixels used to discretize the region of interest).

Recently, it has also been found that wave propagation problems, governed by a different underlying physics, have a type of monotonicity. Specifically, it has been proved that transmission eigenvalues depend in a monotonic way on the refractive index [6]. Our contribution provides the description of an imaging algorithm based on this monotonicity property together with a first numerical example.

The research of David Colton and Peter Monk was supported in part by a grant from the Air Force Office of Scientific Research.

2 Transmission Eigenvalues and Monotonicity Property

Transmission eigenvalues arise from the interior transmission problem [7, 8]:

$$\nabla^2 v + k^2 v = 0 \text{ in } \Omega \quad (1a)$$
$$\nabla^2 u + k^2 n^2 u = 0 \text{ in } \Omega \quad (1b)$$
$$v = u \text{ on } \partial\Omega \quad (1c)$$
$$\partial_n v = \partial_n u \text{ on } \partial\Omega \quad (1d)$$

where k is the wavenumber, n the refraction index, Ω the support of a scatterer and ∂_n the normal derivative operator. Transmission eigenvalues are those values of k such that (1) admits a non-trivial solution. Transmission eigenvalues form a discrete sequence; hereafter we focus on the real ones and we assume they are ordered in increasing order.

In this work we focus on the inverse obstacle problem where the goal is to retrieve the shape of an anomalya scattereran object (equivalently, the refraction index n_I) in an otherwise homogeneous background material (refraction index n_{BG}, $n_I < n_{BG}$) occupying domain Ω. Let $n_D(r) = n_{BG} + (n_I - n_{BG})\,\chi_D(r)$ be the refractive index related to an anomaly in the subset $D \subset \Omega$. From [6] it follows that:

$$D_a \subseteq D_b \Rightarrow \tau_a^i \leq \tau_b^i, \forall i \in \mathbb{N}, \quad (2)$$

where τ_a^i and τ_b^i are the transmission eigenvalues associated to the refractive indices n_{Da} and n_{Db}, respectively.

3 Inversion algorithm

The inversion algorithm is based on (2). Indeed, the following proposition holds:

$$\text{if } \exists\ i \text{ s.t. } \tau_a^i > \tau_b^i \Rightarrow D_a \not\subseteq D_b. \qquad (3)$$

Proposition (3) is nothing but a simple test for evaluating if an anomaly D_a is contained in another anomaly D_b starting from the knowledge of the transmission eigenvalues. Assuming Ω is partitioned as $\Omega = \cup_{n=1}^{N} V_n$, we have the following (basic) imaging algorithm: take as reconstructed anomaly object the union of all the V_n's such that $\tau_n^i \leq \tau^i\ \forall i \in \mathbb{N}$, where τ_n^i is related to a (known!) test anomaly in V_n and τ^i is related to the unknown object.

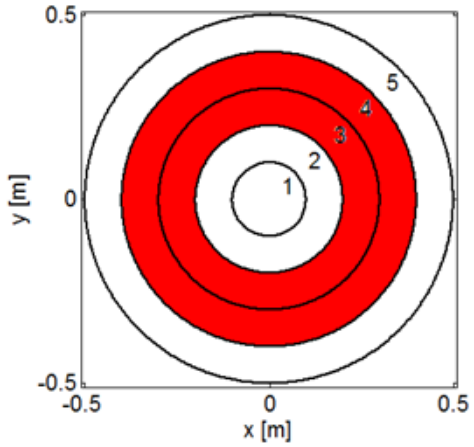

Figure 1: The domain Ω and its partitioning. Regions 3 and 4 represent the unknown anomaly.

4 Inversion algorithm

The simple test case considered here is a 2D axisymmetric problem: a dielectric cylinder illuminated by a TM wave ($n_{BG} = \sqrt{10}$, $n_I = \sqrt{3}$). The domain, a circle of radius 0.5m, is partitioned in five regions ($V_1, \ldots, V_5$) and the unknown anomaly object is $V_3 \cup V_5$ (see Figure 1). The following Table reports the first five (numerically computed) transmission eigenvalues for the target "unknown" object and for each test anomaly $V_1, \ldots, V_5$. In this case, the reconstruction algorithm of Section 3 provide an error free image of the unknown object.

Tr. Eig.	τ^1	τ^2	τ^3	τ^4	τ^5
Object	2.772	3.930	5.509	7.211	7.947
Test 1	2.825	3.386	4.123	4.860	5.614
Test 2	3.018	3.754	4.333	4.965	5.649
Test 3	2.667	3.860	4.982	5.702	6.000
Test 4	2.719	3.386	4.333	5.386	6.053
Test 5	3.088	3.930	4.737	5.509	6.228

References

[1] A. Tamburrino and G. Rubinacci, A New Non-Iterative Inversion Method for Electrical Resistance Tomography, *Inverse Problems* (2002), pp. 1809–1829.

[2] A. Tamburrino and G. Rubinacci, Fast Methods for Quantitative Eddy Current Tomography of Conductive Materials, *IEEE Trans. on Magnetics* **42** (2006), pp. 2017–2028.

[3] A. Tamburrino, S. Ventre and G. Rubinacci, Recent developments of a Monotonicity Imaging Method for Magnetic Induction Tomography in the small skin-depth regime, *Inverse Problems* **26** (2010) pp. 074016 (21pp).

[4] A. Tamburrino, F. Calvano, S. Ventre and G. Rubinacci, Non-iterative imaging method for experimental data inversion in eddy current tomography, *NDT & E International* **47** (2012), pp. 26—34.

[5] B. Harrach and M. Ullrich, Monotonicity-based shape reconstruction in Electrical Impedance Tomography, *Siam J. Math. Anal.* **45** (2013), pp. 3382–3403.

[6] F. Cakoni and H. Haddar, Transmission Eigenvalues in Inverse Scattering Theory, *Inside Out II*, MSRI Publications, **60** (2012), pp. 529–580.

[7] D. Colton and P. Monk, The inverse Scattering Problem for Time-Harmonic Acoustic Waves in an Inhomogeneous Medium, *Quart. J. Mech. Appl. Math.* **41:1** (1988), 97–125.

[8] A. Kirsch, The densness of the far field patterns for the transmission problem, *IMA J. Appl. Math.* **37:3** (1986), pp. 213–225.

Model-aware Newton-type Inversion for Electrical Impedance Tomography

Robert Winkler[1,*], **Andreas Rieder**[1]

[1]Institute for Applied and Numerical Mathematics , Karlsruhe Institute of Technology, Germany

[*]Email: robert.winkler@kit.edu

Abstract

The inverse problem of electrical impedance tomography (EIT) with electrodes is delicate as it is nonlinear, ill-posed, highly under-determined, and entails uncertainties about the setting. Each respect needs to be addressed carefully for successful inversion. The presented reconstruction scheme estimates unknown model parameters from the measurements before solving the full nonlinear problem. Therein, nonlinearity is reduced with a parameter transformation, underdetermination is resolved by a scheme promoting non-oscillatory conductivities, and regularization is applied with an inexact Newton method. The reconstruction procedure is free of design parameters and requires no calibration data. Numerical results demonstrate the performance of this concept.

Keywords: electrical impedance tomography, inverse problem, complete electrode model, regularization, inexact Newton method

1 Problem and Model

The purpose of EIT is to determine a conductivity $\sigma \in L^\infty_+(\Omega)$ on a domain $\Omega \in \mathbb{R}^{\{2,3\}}$ from measurements on its boundary. The realistic complete electrode model (Somersalo et al. 1992) describes the injection of currents $I \in \mathbb{R}^L_\diamond = \{x \in \mathbb{R}^L \colon \sum x_i = 0\}$ and the measurement of corresponding potentials $U \in \mathbb{R}^L_\diamond$ through $L \in \mathbb{N}_{\geq 2}$ electrodes $E_1, \dots, E_L \subset \partial\Omega$ with contact impedances $z_{1,\dots,L} > 0$. Recovering σ from the *discrete* Neumann-Dirichlet map $\mathcal{R}_\sigma \colon I \mapsto U$ inherits the severe nonlinearity and ill-posedness of its continuum counterpart (Alessandrini 1988), and moreover is highly under-determined as $\mathcal{R}_\sigma$ is finite-dimensional.

For a set of $M \in \mathbb{N}$ currents $\mathcal{I} \coloneqq \{I^1, \dots, I^M\} \in \mathbb{R}^{L \times M}$ we measure a set of noisy potentials $\mathcal{U}^v \coloneqq \mathcal{R}_\sigma \mathcal{I} + N^v$, with each entry of the noise $N^v \in \mathbb{R}^{L \times M}$ being $\overset{\text{iid}}{\sim} \mathcal{N}(0, v)$ with unknown variance v. The inverse conductivity problem reads

$$\text{Find} \quad \sigma \quad \text{given} \quad \mathcal{U}^v. \tag{1}$$

For iterated Newton-type methods, an estimate of the contact impedances $z_{1,\dots,L}$ and an initial conductivity σ_0 are required for evaluating the forward operator $F \colon \sigma \mapsto \mathcal{R}_\sigma$, and a good estimate of the noise level $\delta \coloneqq \|N^v\|_{\text{Fro}}$ is valuable for applying regularization. Moreover, we need a strategy to resolve the underdetermination and possibly to reduce the nonlinearity of (1).

2 Initialization

The contact impedances, background conductivity and data noise level are usually unknown. However, they can be estimated directly from $\mathcal{U}^v$. Assume that all contact impedances are approximately constant, $z_{1,\dots,L} \approx z$, and denote by $\mathcal{V} = \{V^1, \dots, V^M\}$ a set of simulated potentials for currents $\mathcal{I}$, conductivity $1\chi_\Omega$, and an arbitrary contact impedance $\omega > 0$. Using Green's identity, we get an approximation for z and the background $\sigma_0 \chi_\Omega$ by setting $\rho = \sigma_0^{-1}$ and solving the $M \times 2$ linear regression problem

$$a_m \rho + b_m z = c_m, \quad m = 1, \dots, M,$$

with $b_m = \sum_{l=1}^L |E_l|^{-1} (I_l^m)^2$, $c_m = \sum_{l=1}^L (U^v)_l^m I_l^m$ and $a_m = \sum_{l=1}^L \left(V_l^m - w|E_l|^{-1} I_l^m\right) I_l^m$; see [1].

Moreover, knowing δ is valuable when applying Newton's method with a discrepancy principle. If $\mathcal{I}$ forms a generating set of $\mathbb{R}^L_\diamond$ and $\mathcal{I}^+$ denotes its pseudo-inverse, then δ can be estimated from $\mathcal{U}^v$ by exploiting the symmetry of $\mathcal{R}_\sigma$. Denoting by

$$e_v \coloneqq \left\| \mathcal{U}^v \mathcal{I}^+ - \left(\mathcal{U}^v \mathcal{I}^+\right)^\top \right\|^2_{\text{Fro}}$$

the symmetry error caused by noise of variance v, it can be shown that $\mathbb{E} e_v = 2(L-1)\|\mathcal{I}^+\|^2_{\text{Fro}} v$,

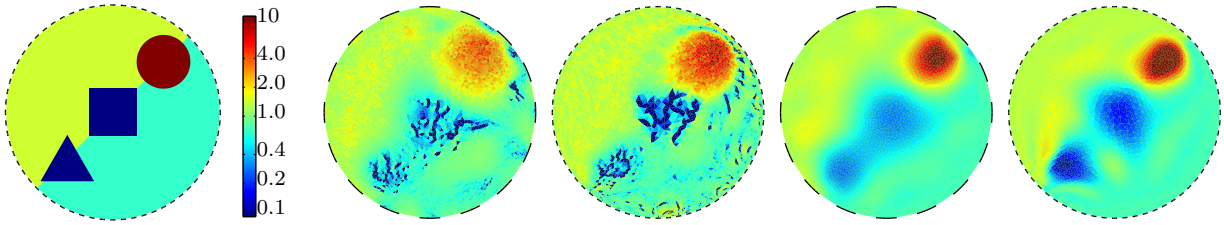

Fig.1 (a) Conductivity (b) $L{=}16,\eta^+$ (c) $L{=}64,\eta^+$ (d) $L{=}16,\eta^{+W},t_\alpha$ (e) $L{=}64,\eta^{+W},t_\alpha$

and moreover $\mathbb{E}\delta \approx \sqrt{MLv}$. Combining both, we obtain the noise estimate

$$\delta^{\mathrm{CEM}} := \sqrt{\tfrac{MLe_v}{2(L-1)}}\left\|\mathcal{I}^+\right\|_{\mathrm{Fro}}^{-1} \approx \mathbb{E}\delta,$$

a computable quantity even if v is unknown. The quality of these estimates has been verified numerically, even for inhomogeneous conductivities, varying contact impedances and different current patterns, in [1].

3 Nonlinearity considerations

Problem (1) is constrained ($\sigma > 0$) and highly nonlinear, which can lead to several problems for Newton-type methods solving unconstrained problems by linearization. Both issues are addressed simultaneously by performing a conductivity transformation, $\sigma \mapsto t_*(\sigma) := t$, and considering the transformed operator $F_* : t \mapsto \mathcal{R}_{t_*^{-1}(t)}$. A well-known example is $t_*(\sigma) = \log(\sigma)$, which has an unconstrained parameter space $t \in L^\infty(\Omega)$ and reduces nonlinearity in particular at small constants. We suggest another transformation, namely $t_\alpha(\sigma) := (1-\alpha)\sigma^{-1} - \alpha\sigma$ for $\alpha \in (0,1)$, which is also unconstrained and has limited nonlinearity for all constant conductivities [1].

4 Newton-type inversion

When applying Newton's method in EIT, the evaluation of the forward operator and its Fréchet derivative are usually done numerically by finite elements, which requires a discretization of the domain $\Omega = \Omega_1 \cup \ldots \cup \Omega_P$, $P \in \mathbb{N}$. The Jacobian $\mathcal{S} \in \mathbb{R}^{LM \times P}$ at t is then assembled column-wise by $\mathcal{S}_p = \mathrm{col}(F_*'(t)[\chi_{\Omega_p}])$, $p = 1,\ldots,P$, and the linearized problem

$$\mathcal{S}\eta = d, \quad d = \mathrm{col}(\mathcal{U}^v - F_*(t)\mathcal{I}), \qquad (2)$$

is solved in each Newton iteration to compute the Newton update η. Usually, $LM \ll P$ and (2) is highly under-determined and ill-posed. The naïve pseudo-inverse attempt

$$\eta^+ = \mathcal{S}^+ d = \operatorname*{arg\,min}_{\eta \in \mathcal{N}(\mathcal{S})^\perp} \|\mathcal{S}\eta - d\|_2, \qquad (3)$$

resolves underdetermination, but is undesired as it heavily depends on the local discretization geometry. However, the dependence can be lifted using a weighted inner product $\langle\cdot,\cdot\rangle_W := \langle\cdot, W\cdot\rangle$ with weight matrix $W = \mathrm{diag}(w_1,\ldots,w_P)$, $w_p = (t_*^{-1})'(t_*(\sigma))\|S_p\|_2\sigma^{-1}$ on Ω_p, and picking a solution in the W-orthogonal complement of $\mathcal{N}(\mathcal{S})$,

$$\eta^{+W} := \operatorname*{arg\,min}_{\eta \in \mathcal{N}(\mathcal{S})^{\perp_W}} \|\mathcal{S}\eta - d\|_2. \qquad (4)$$

This choice is unique and almost independent of the discretization. Moreover, it promotes non-oscillatory conductivity updates. Finally, ill-posed- ness is addressed using an inexact Newton method which approximates each Newton update η^{+W} by a regularized version. It terminates by the discrepancy principle $\|F_*(t)\mathcal{I} - \mathcal{U}^v\| < 1.1 \cdot \delta^{\mathrm{CEM}}$.

5 Numerical examples

To investigate the capability of reconstructing both low and high contrasts and multiple backgrounds, we consider the test conductivity shown in Fig. 1(a) and $\delta = 1\%$. Reconstructions are performed for $L = 16$ (b) and for $L = 64$ (c) with the proposed initializations, but without transformation and using updates η^+. The results when using transformation t_α and updates η^{+W} in the same setting are shown in (d) and (e), respectively. We observe that the reconstruction of high and low contrasts and multiple background succeeds from noisy EIT data, without fine-tuning any parameters. For more examples and tank experiments, see [1].

References

[1] R Winkler and A Rieder, *Model-aware Newton-type inversion scheme for electrical impedance tomography*, Inverse Problems **31**(2015), no. 4, 045009.

A FFT-based numerical method to convert intensity maps into conductivity contrast maps

Cédric Bellis[1,*], **Hervé Moulinec**[1]
[1]LMA CNRS, Marseille, France
[*]Email: bellis@lma.cnrs-mrs.fr

Abstract

Within the framework of the periodic scalar conductivity equation, this work focuses on a FFT-based numerical method to convert full-field measurements of intensity fields into maps of associated conductivity distributions. The proposed algorithm aims at solving a Lippmann-Schwinger equation for the unknown material conductivity field by the method of successive approximations. A set of numerical results is presented to illustrate the performances of the approach.

Keywords: Inverse problems, Full-field measurements, Conductivity equation

1 Introduction

Consider a periodic medium with representative volume element $\mathcal{V} \subset \mathbb{R}^d$ and the associated conductivity problem

$$\begin{aligned} &\operatorname{div}\Big(\gamma(\boldsymbol{x})\big(\boldsymbol{\nabla} u(\boldsymbol{x}) + \mathbf{E}\big)\Big) = 0 \quad \text{in } \mathbb{R}^d \\ &u \text{ is } \mathcal{V}\text{-periodic,} \end{aligned} \tag{1}$$

where $\gamma \in L^\infty_{\text{per}}(\mathcal{V}, \mathbb{R}_+\backslash\{0\})$ denotes the $\mathcal{V}$-periodic map of material conductivity while u is a scalar potential. The corresponding intensity field is defined as $\boldsymbol{e} = \boldsymbol{\nabla} u + \mathbf{E}$ while the angular brackets $\langle\cdot\rangle$ denote the spatial average over $\mathcal{V}$

$$\langle \boldsymbol{e} \rangle = \frac{1}{|\mathcal{V}|} \int_{\mathcal{V}} \boldsymbol{e}(\boldsymbol{x}) \, \mathrm{d}\boldsymbol{x},$$

so that $\mathbf{E}$ denotes the mean intensity that is prescribed in the problem (1). There exists a solution $u \in H^1_{\text{per}}(\mathcal{V}, \mathbb{R})$ to (1) that is unique up to an additive constant.

The framework adopted in this study relies on the assumption that a number N of experiments can be performed by varying the imposed mean intensity as $\mathbf{E} = \mathbf{E}_\ell$ with $\ell = 1, \dots, N$ in the problem (1), while we consider available some internal measurements, or maps, of the corresponding set of intensity field solutions [1], i.e. $\boldsymbol{e}_\ell(\boldsymbol{x}) = \boldsymbol{\nabla} u_\ell(\boldsymbol{x}) + \mathbf{E}_\ell$ for all $\boldsymbol{x} \in \mathcal{V}$. In this context, this study focuses on a numerical method that makes use of these full-field images of measured intensity fields $\boldsymbol{e}_\ell(\boldsymbol{x})$ in order to reconstruct the conductivity distribution $\boldsymbol{x} \mapsto \gamma(\boldsymbol{x})$ of the material within $\mathcal{V}$ or alternatively the corresponding contrast map associated with the mean value $\langle\gamma\rangle$.

2 Integral formulation

The first step is to establish a Lippmann-Schwinger equation for the sought conductivity function $\gamma(\boldsymbol{x})$. For all $k = 1, \dots, d$, let $\bar{\boldsymbol{e}}_k \in \mathbb{R}^d$ and $\ell_k \in \{1, \dots, N\}$ denote a companion label, so that, given $\bar{\gamma} \in \mathbb{R}_+\backslash\{0\}$, the original problem (1) with prescribed mean $\mathbf{E}_{\ell_k}$ and associated solution $\boldsymbol{e}_{\ell_k}$ can be recast as the following auxiliary problems which unknown is the conductivity field $\gamma(\boldsymbol{x})$:

$$\begin{aligned} &\operatorname{div}(\gamma(\boldsymbol{x})\, \bar{\boldsymbol{e}}_k) = -\operatorname{div} \boldsymbol{\tau}_k(\boldsymbol{x}) \quad \text{in } \mathcal{V} \\ &\langle\gamma\rangle = \bar{\gamma} \qquad\qquad\qquad\qquad \gamma \text{ is } \mathcal{V}\text{-periodic} \end{aligned}$$

where the right-hand side term is given by

$$\boldsymbol{\tau}_k(\boldsymbol{x}) = \gamma(\boldsymbol{x})\, \delta\boldsymbol{e}_k(\boldsymbol{x}) \text{ with } \delta\boldsymbol{e}_k(\boldsymbol{x}) = \boldsymbol{e}_{\ell_k}(\boldsymbol{x}) - \bar{\boldsymbol{e}}_k.$$

Defining the periodic Fourier transform as

$$\hat{f}(\boldsymbol{\xi}) = \frac{1}{|\mathcal{V}|} \int_{\mathcal{V}} f(\boldsymbol{x}) e^{-2\pi \mathrm{i}\, \boldsymbol{x}\cdot\boldsymbol{\xi}} \, \mathrm{d}\boldsymbol{x},$$

and assuming that $\{\bar{\boldsymbol{e}}_k\}_k$ constitutes an orthogonal basis of $\mathbb{R}^d$, yet not necessarily normalized, then the above set of d auxiliary problems can be used to obtain in Fourier-space

$$\begin{aligned} &\hat{\gamma}(\boldsymbol{\xi}) = -\hat{\boldsymbol{\Gamma}}(\boldsymbol{\xi}) : \sum_{k=1}^{d} \frac{\bar{\boldsymbol{e}}_k \otimes \hat{\boldsymbol{\tau}}_k}{|\bar{\boldsymbol{e}}_k|^2} \qquad \forall\, \boldsymbol{\xi} \neq \mathbf{0} \\ &\hat{\gamma}(\mathbf{0}) = \bar{\gamma} \end{aligned} \tag{2}$$

where $\hat{\boldsymbol{\Gamma}}$ is the periodic Green's operator for the conductivity problem which reads for all $\boldsymbol{\xi} \neq \mathbf{0}$

$$\hat{\boldsymbol{\Gamma}}(\boldsymbol{\xi}) = \frac{\boldsymbol{\xi} \otimes \boldsymbol{\xi}}{|\boldsymbol{\xi}|^2}.$$

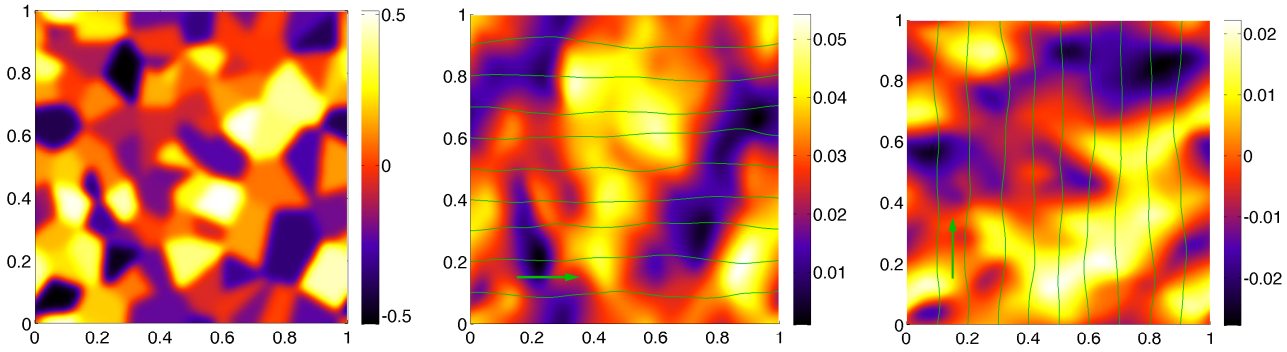

(a) True conductivity contrast $\bar{\delta}\gamma(\boldsymbol{x})$ (b) Experience 1: $u_1(\boldsymbol{x})$ (c) Experience 2: $u_2(\boldsymbol{x})$

Figure 1: (a) 2D configuration considered to compute synthetic data. (b–c) Scalar potential fields u_k solutions of (1) computed using the F.E. method with arrows corresponding to prescribed average fields $\mathbf{E}_k$ and streamlines of intensity fields $\boldsymbol{e}_k(\boldsymbol{x})$.

Therefore, one readily obtains from (2) the sought Lippmann-Schwinger equation for the field γ as

$$\gamma(\boldsymbol{x}) + \frac{1}{|\mathcal{V}|}\left[\boldsymbol{\Gamma} \underline{\underline{*}} \sum_{k=1}^{d} \frac{\bar{\boldsymbol{e}}_k \otimes (\,\gamma\,\delta\boldsymbol{e}_k\,)}{|\bar{\boldsymbol{e}}_k|^2}\right](\boldsymbol{x}) = \bar{\gamma} \quad (3)$$

where $\underline{\underline{*}}$ denotes the spatially convoluted doubly contracted product.

3 Iterative reconstruction algorithm

An integral equation such as (3) is commonly encountered in scattering theory. When the terms $\delta\boldsymbol{e}_k$, for $k = 1, \ldots, d$, can be assumed to be small then the unknown conductivity map can be approximated by a series expansion. The corresponding Neumann series reads

$$\gamma(\boldsymbol{x}) = \sum_{n\geqslant 0}\left(-\frac{1}{|\mathcal{V}|}\boldsymbol{\Gamma} \underline{\underline{*}} \sum_{k=1}^{d} \frac{\bar{\boldsymbol{e}}_k \otimes (\,\cdot\,\delta\boldsymbol{e}_k\,)}{|\bar{\boldsymbol{e}}_k|^2}\right)^n \bar{\gamma}$$

where the operator raised to the power n is to be interpreted as the in-parenthesis operator applied n times. If it exists, computing the solution γ from the above series expansion is achieved in this work using the method of successive approximations [2]. To avoid using any a priori information such as knowledge of the mean conductivity $\langle\gamma\rangle = \bar{\gamma}$, the proposed algorithm is recast in terms of the conductivity contrast normalized by the mean conductivity, a term we denote by

$$\bar{\delta}\gamma(\boldsymbol{x}) = \frac{\gamma(\boldsymbol{x}) - \bar{\gamma}}{\bar{\gamma}}. \quad (4)$$

The approach discussed here is derived from FFT-based numerical methods [3] for computing the response of non-linear composite materials.

Our aim is to analyse and discuss this iterative algorithm that alternates between real-space and Fourier-space to circumvent the costly computation of convolution terms. A set of numerical results is discussed, see the example of Figure 1 with the associated computed reconstruction of Figure 2.

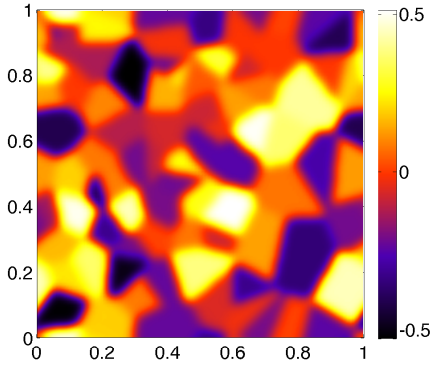

Figure 2: Reconstructed conductivity contrast after 50 iterations of the algorithm.

References

[1] G. Bal. *Hybrid inverse problems and internal functionals*, Inside Out II, MSRI Publications, 2012.

[2] R. Kress. *Linear Integral Equations*, Springer, 2014.

[3] H. Moulinec, P. Suquet. *A numerical method for computing the overall response of nonlinear composites with complex microstructure*, Comput. Meth. Appl. Mech. Engrg, 69–94, 1998.

A conformal mapping method in inverse obstacle scattering

Houssem Haddar[1], **Rainer Kress**[2,*]
[1]CMAP, Ecole Polytechnique, Palaiseau, France
[2]Institut für Numerische und Angewandte Mathematik, University of Göttingen, Germany
[*]Email: kress@math.uni-goettingen.de

Abstract

Over the last decade, Akduman, Haddar and Kress [1, 2, 4] have analyzed a conformal mapping technique for the inverse problem to reconstruct a perfectly conducting inclusion in a homogeneous background medium from Cauchy data for electrostatic imaging. We propose an extension of this approach to inverse obstacle scattering for time-harmonic waves. The main idea is to use the conformal mapping algorithm in an iterative procedure to obtain Cauchy data for a Laplace problem from the given Cauchy data for the Helmholtz problem. In the talk, we present the foundations of the method together with a convergence result and exhibit the feasibility of the method via numerical examples.

Keywords: conformal mapping, low frequency iterations

1 The inverse problems

Assume that D_0 and D_1 are two simply connected bounded domains in $\mathbb{R}^2$ with C^2 smooth boundaries $\Gamma_0 := \partial D_0$ and $\Gamma_1 := \partial D_1$ such that $\overline{D}_0 \subset D_1$ and denote by D the doubly connected domain $D := D_1 \setminus \overline{D}_0$. The inverse problems we are concerned with is to determine the unknown interior boundary curve Γ_0 from the Cauchy data

$$f := u|_{\Gamma_1} \quad \text{and} \quad g := \frac{\partial u}{\partial \nu}\Big|_{\Gamma_1} \tag{1}$$

on Γ_1 of a solution $u \in H^1(D)$ of the Laplace equation $\Delta u = 0$ or the Helmholtz equation $\Delta u + k^2 u = 0$ with wave number $k > 0$ satisfying the homogeneous Dirichlet condition

$$u = 0 \tag{2}$$

on Γ_0. Here, the unit normal ν to Γ_1 is directed into the exterior of D_1 and the functions f and g are assumed to be complex valued.

2 The Laplace case

To describe the conformal mapping method we will identify $\mathbb{R}^2$ and $\mathbb{C}$ in the usual manner and introduce the annulus B bounded by two concentric circles C_0 with radius $\rho < 1$ and C_1 with radius one centered at the origin. By the Riemann conformal mapping theorem for doubly connected domains there exists a uniquely determined radius ρ and a holomorphic function Ψ that is unique up to rotations and that maps B bijectively onto D such that the boundaries C_0 and C_1 are mapped onto Γ_0 and Γ_1, respectively. We parameterize the exterior boundary $\Gamma_1 = \{\gamma(t) : t \in [0, 2\pi)\}$ and fix the freedom in rotating B by prescribing $\Psi(1) = \gamma(0)$. For the unit circle C_1 we use the canonical parametrization $C_1 = \{c(t) : t \in [0, 2\pi)\}$ where $c(t) := e^{it}$.

Now we define the boundary correspondence function $\varphi : [0, 2\pi] \to [0, 2\pi]$ by setting

$$\varphi := \gamma^{-1} \circ \Psi \circ c. \tag{3}$$

Clearly the function φ uniquely determines Ψ as the solution to the Cauchy problem with $\Psi|_{C_1} = \gamma \circ \varphi \circ c^{-1}$.

The main ingredient of the conformal mapping method is the nonlocal and nonlinear ordinary differential equation

$$\frac{\mathrm{d}\varphi}{\mathrm{d}t} = \mathrm{Re}\, \frac{\overline{g \circ \gamma \circ \varphi}\, A_\rho(f \circ \gamma \circ \varphi)}{|g \circ \gamma \circ \varphi|^2} \tag{4}$$

for φ together with the boundary conditions

$$\varphi(0) = 0, \quad \varphi(2\pi) = 2\pi. \tag{5}$$

Here $A_\rho : H^{1/2}[0, 2\pi] \to H^{-1/2}[0, 2\pi]$ denotes the Dirichlet-to-Neumann operator for the annulus B that maps functions h onto the normal derivative

$$A_\rho h := \frac{\partial v}{\partial \nu} \circ c \tag{6}$$

of the harmonic function $v \in H^1(B)$ with boundary values $v = h \circ c^{-1}$ on C_1 and $v = 0$ on C_0. The differential equation (4) is complemented by the equation

$$\rho = \exp\left(- \mathrm{Re}\, \frac{\int_{\Gamma_1} \overline{g}\, \mathrm{d}s \int_0^{2\pi} f \circ \gamma \circ \varphi\, \mathrm{d}t}{\left| \int_{\Gamma_1} g\, \mathrm{d}s \right|^2} \right). \tag{7}$$

Though we only have the local result that (4) and (7) can be solved by successive approximations provided that D is sufficiently close to B and f sufficiently close to a constant, numerical examples exhibit convergence for a much larger class of domains D and functions f (see [1, 2]). Once φ and ρ are available the highly ill-posed Cauchy problem to determine the holomorphic function Ψ in the annulus B from its boundary values $\Psi|_{C_1} = \gamma \circ \varphi \circ c^{-1}$ can be solved by a Laurent expansion that need to be stabilized, for example, by a Tikhonov type regularization.

Finally, the interior boundary Γ_0 is obtained by $\Gamma_0 = \Psi(C_0)$. Summarizing, the conformal mapping method for the Laplace case defines a solution operator R taking the Cauchy data (f, g) on Γ_1 onto the interior boundary curve Γ_0, that is,

$$\Gamma_0 = R(f, g). \tag{8}$$

Its regularized version R_α with regularization parameter $\alpha > 0$ leads to a regularized solution $\Gamma_{0,\alpha} = R_\alpha(f, g)$.

3 The Helmholtz case

Given incident fields $u_{i,0}$ and $u_{i,k}$ by solutions to the Laplace and Helmholtz equation in an open set containing $\mathbb{R}^2 \setminus D_0$, respectively, we now consider the scattering problems for solutions u_0, u_k in $H^1_{\mathrm{loc}}(\mathbb{R}^2 \setminus \bar{D}_0)$ to the Laplace equation $\Delta u_0 = 0$ or the Helmholtz equation $\Delta u_k + k^2 u_k = 0$ in $\mathbb{R}^2 \setminus \bar{D}_0$ satisfying the Dirichlet boundary conditions

$$u_0 = -u_{i,0} \quad \text{and} \quad u_k = -u_{i,k} \quad \text{on } \Gamma_0 \tag{9}$$

together with an appropriate radiation condition at infinity. The solutions of these two exterior Dirichlet problems define operators F_0 and F_k that for fixed incident fields $u_{i,0}$ and $u_{i,k}$ map the interior boundary Γ_0 onto the Cauchy data (f_L, g_L) and (f_H, g_H) of the total fields $u_0^{\mathrm{tot}} := u_0 + u_{i,0}$ and $u_k^{\mathrm{tot}} := u_k + u_{i,k}$ on Γ_1, respectively. Then, subtracting $F_k(\Gamma_0)$ from $F_0(\Gamma_0)$ and inserting (8) for Γ_0 we arrive at the fixed point equation

$$(f_L, g_L) = (f_H, g_H) + (F_0 - F_k)(R(f_L, g_L)) \tag{10}$$

for the Cauchy data (f_L, g_L) for the Laplace solution u_0^{tot}, given the Cauchy data (f_H, g_H) for the Helmholtz solution u_k^{tot}. It can be shown (see [3]) that for sufficiently small wave numbers k and incident fields given by plane waves (10) can be solved via successive approximations

$$(f_{n+1}, g_{n+1}) := (f_H, g_H) + (F_0 - F_k)(R_\alpha(f_n, g_n))$$

for $n = 0, 1, 2, \ldots$ starting with the given Helmholtz data as initial guess $(f_0, g_0) = (f_H, g_H)$ and using the regularized version R_α of the solution operator with an appropriate choice of α (provided D is close to B). Numerical examples exhibit the feasibility of this approach for more general domains (see [3]).

Each iteration step consists of two parts: In the first part the two steps of the conformal mapping algorithm for the Laplace case is applied with Cauchy data (f_n, g_n) to obtain an approximation $\Gamma_n = R_\alpha(f_n, g_n)$ for the interior boundary curve. Then in the second part both boundary value problems (9) are solved for the interior boundary Γ_n to obtain both $F_0(R_\alpha(f_n, g_n))$ and $F_k(R_\alpha(f_n, g_n))$ in order to update the Cauchy data.

References

[1] I. Akduman and R. Kress, Electrostatic imaging via conformal mapping. *Inverse Problems* **18** (2002), pp. 1659–1672.

[2] H. Haddar and R. Kress, Conformal mappings and inverse boundary value problems. *Inverse Problems* **21** (2005), pp. 935–953.

[3] H. Haddar and R. Kress, A conformal mapping method in inverse obstacle scattering. *Complex Variables and Elliptic Equations* **59** (2014), pp. 863–882 .

[4] R. Kress, Inverse problems and conformal mapping. *Complex Variables and Elliptic Equations* **57** (2012), pp. 301–316.

Recovering Multiscale Buried Anomalies in a Two-layered Medium

Jingzhi Li[1], Peijun Li[2], Hongyu Liu[3], Xiaodong Liu[4,*]

[1]Faculty of Science, South University of Science and Technology of China, 518055 Shenzhen, P. R. China

[2]Department of Mathematics, Purdue University, West Lafayette, IN 47907, United States.

[3]Department of Mathematics, Hong Kong Baptist University, Kowloon, Hong Kong SAR.

[4]Institute of Applied Mathematics, Academy of Mathematics and Systems Science, Chinese Academy of Sciences, 100190 Beijing, P. R. China

*Email: xdliu@amt.ac.cn

Abstract

We develop an inverse scattering scheme of recovering impenetrable anomalies buried in a two-layered medium. The recovery scheme works in a rather general setting and possesses several salient features. It makes use of a single far-field measurement in the half-space above the anomalies, and works independently of the physical properties of the anomalies. There might be anomalous components of multiscale sizes presented simultaneously. Moreover, the proposed scheme is of a totally direct nature without any inversion involved, and hence it is very fast and robust against measurement noise. Both theoretical foundation and numerical experiments are presented.

Keywords: Inverse scattering, locating, single far-field measurement, limited aperture data, indicator functions.

1 Motivation and background

In this work, we consider the recovery of anomalies buried in a two-layered medium; see Fig. 1 for a schematic illustration. Suppose the space is delimited by a flat plane Γ_0 into two half-spaces: the upper one and the lower one. The two half-spaces are occupied by two different (homogeneous) mediums. It is further supposed that some inhomogeneous anomalies are buried or immersed in the lower half-space. We are interested in recovering the anomalies by wave detection made in the upper half-space, which is proceeded as follows. One sends a certain wave field from the upper half-space, and then measures the perturbed wave field caused by the anomalies together with the ambient lower-space medium. The detecting wave field is referred to as the incident wave field and the perturbed wave field is referred to as the scattered wave filed. The inverse problem that we are concerned with is to recover the anomalies by knowledge of the scattered wave field. Practical scenarios of our current study include the underground mineral prospection, mines locating in the battlefield, and anti-submarine detection.

The inverse scattering problem described above can be abstractly formulated as an operator equation,

$$F(\mathrm{O}) = \mathcal{M}, \tag{1}$$

where O denotes the anomalous object, and $\mathcal{M}$ denotes the wave measurement data. F is an operator which sends the anomaly to the corresponding measurement, defined by the forward wave scattering system. As a typical feature for various inverse scattering problems, (1) is nonlinear by noting that generally one has $F(\mathrm{O}_1 \cup \mathrm{O}_1) \neq F(\mathrm{O}_1) + F(\mathrm{O}_2)$, where O_1 and O_2 are two different anomalies. This is mainly due to the multiple wave scattering interaction between O_1 and O_2. Moreover, it is easily seen that the inverse problem (1) is ill-posed in the sense of Hadamard.

In order to tackle the nonlinearity of various inverse problems, a salient technique that has been widely investigated in the literature is the so-called sampling. A variety of schemes have been developed in this category, including the linear sampling method [3], the factorization method [5] and the MUSIC-type methods [2], among others. The cores of these methods are certain imaging functionals, which are used to indicate a space point belonging to the interior or the exterior of the scattering anomaly. The process of calculating those imaging functionals is linear and hence the nonlinearity of the inverse problem is reduced to the determination of the belongingness of any given space point, that can be easily visualized. In order to tackle the ill-posedness, various regularizations

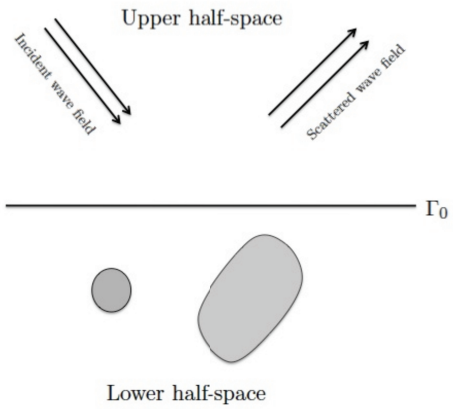

Figure 1: Schematic illustration of the anomalies detection in a two-layered medium.

are incorporated into those schemes. Recently, a novel sampling scheme was proposed for the inverse scattering problem of locating inhomogeneities embedded in a homogeneous space in [6]. The approach also relies on certain properly designed imaging functionals, whose calculations are totally direct without any inversion involved. More notably, the method makes use of only a single far-field measurement, which is much fewer than the existing methods in the literature. Hence, the method is very efficient and robust against measurement noise, and easy to implement as well. In this work, we extend the method to the practical and interesting case of recovering the multiscale anomalies buried in a two-layered medium as described earlier. The major novelty and difficulty of the current study are the inhomogeneous two-layered background medium.

Following a similar spirit to the study in [6], we develop the new recovery scheme in three steps. First, we consider the recovery of anomalies with small size compared to the detecting wavelength. This is based on linearizing the inverse problem (1). To that end, we derive the asymptotic expansion of scattered wave field in terms of the small diameter parameter of the underlying anomalies. Second, we consider the recovery of multiple regular-size anomalies. In this case, we need require that the anomalies are from an admissible class, which is known in advance. The recovery is based on projecting the measured far-field pattern into a space of far-field patterns generated by the admissible scatterers. Finally, by concatenating the above two procedures via a local tuning technique, one can recover multiple multiscale buried anomalies. We would like to mention in passing that similar inverse problems of recovering buried objects were also considered in [1, 4] with different methods.

References

[1] H. Ammari, E. Iakovleva and D. Lesselier, *A music algorithm for locating small inclusions buried in a half-space from the scattering amplitude at a fixed frequency*, SIAM Multiscale Model. Simul. , **3** (2005), 597-628.

[2] M. Cheney, *The linear sampling method and the MUSIC algorithm*, Inverse Problems, **17** (2001), 591.

[3] D. Colton and A. Kirsch, *A simple method for solving inverse scattering problems in the resonance region*, Inverse Problems, **12** (1996), 383.

[4] F. Delbary, K. Erhard, R. Kress, R. Potthast and J. Schulz, *Inverse electromagnetic scattering in a two-layered medium with an application to mine detection*, Inverse Problems, **24** (2008), 015002.

[5] A. Kirsch and N. Grinberg, *The Factorization Method for Inverse Problems*, Oxford Univ. Press, Oxford, 2008.

[6] J. Li, H. Liu and J. Zou, *Locating multiple multiscale acoustic scatterers*, SIAM Multiscale Model. Simul., **12** (2014), 927–952.

Source Supports from Sparse Measurements in Electric Impedance Tomography

Stefanie Hollborn[1,*], **Martin Hanke**[1], **Nuutti Hyvönen**[2]

[1]Institut für Mathematik, Johannes Gutenberg-Universität Mainz, 55099 Mainz, Germany

[2]Department of Mathematics and Systems Analysis, Aalto University, 00076 Aalto, Finland

[*]Email: sh@math.uni-mainz.de, birth name: Stefanie Reusswig

Abstract

Electric impedance tomography seeks to visualize an object's interior by means of current-voltage-measurements at the object's boundary. In many situations it is of practical interest not to completely recover the interior conductivity but rather to detect the shape and location of possible inhomogeneities hidden inside the object. The convex source support extracts information about the support of such inclusions from only one current-voltage-measurement. In this talk, I will present this concept and demonstrate its applicability to measurements taken with a single pair of electrodes moved along the boundary. Numerical experiments with both - simulated data and measurements obtained from a specially designed tomograph - may illustrate the theoretical findings.

Keywords: electric impedance tomography, inverse source problem, anomaly detection, backscatter

1 Introduction

Electric impedance tomography aims to extract information on the interior electrical properties by means of current-voltage-measurements on an object's boundary. However, the recovery of the conductivity distribution inside the object is an extremely ill-posed problem. The careful investigation of the information content of a single electrostatic measurement is therefore of vital importance.

Inspired by an approach of Kysiak and Sylvester in the scattering context [5], we introduced the notion of the so-called *convex source support* to electrostatics, cf. [1]. This concept is applicable to a variety of different data types in impedance tomography including sparse data collected by a single pair of electrodes as demonstrated in Sections 3 and 4.

2 Source Supports

Let us consider the inverse boundary value problem of impedance tomography in a bounded and simply connected domain $D \subset \mathbb{R}^2$. We focus on applications where the investigated object has a known background conductivity but may be contaminated by inhomogeneities. Thus, we assume that the conductivity $\sigma \in L^\infty(D)$ is strictly positive and equal to one near the boundary. We seek to recover the location and shape of $\Omega = \operatorname{supp}(1-\sigma)$, which we will call *inclusion* hereafter. Given a boundary current f on ∂D, the resulting electrostatic potential u satisfies

$$\nabla \cdot (\sigma \nabla u) = 0 \ \text{ in } D, \quad \frac{\partial}{\partial \nu} u = f \text{ on } \partial D, \tag{1}$$

supplemented with a normalization condition to ensure uniqueness. The Dirichlet potential $u|_{\partial D}$ is registered, and the Cauchy-pair $(f, u|_{\partial D})$ constitutes one measurement.

With the help of the reference potential u_0 that satisfies (1) with σ replaced by one, we rephrase above problem to an inverse source problem for the Poisson equation. The relative potential $w = u - u_0$ is harmonic outside Ω, and it satisfies

$$\Delta w = F \text{ in } D, \qquad \frac{\partial}{\partial \nu} w = 0 \text{ on } \partial D \tag{2}$$

with a distributional source $F = \nabla \cdot (1-\sigma)\nabla u$. In this manner, the inhomogeneity Ω is characterized as the support of the source F that gives rise to the potential w with $w|_{\partial D} = (u-u_0)|_{\partial D}$. An intuitive idea for recovery is to harmonically extend the data $g = (u-u_0)|_{\partial D}$ as far as possible into the domain D and luckily find Ω where the harmonic extension comes to a halt. Unfortunately, the non-uniqueness of the harmonic extension thwarts this attempt. We consider instead the set $\mathcal{U}_g$ of all distributional sources F for which the solution w of (2) satisfies $w|_{\partial D} = g$ on the boundary.

Definition 1 *The* convex source support $\mathcal{C}g$ *is the intersection of the convex hull of the support of all sources* F *generating* g*, i.e.*

$$\mathcal{C}g = \bigcap_{F \in \mathcal{U}_g} \operatorname{ch}(\operatorname{supp} F)$$

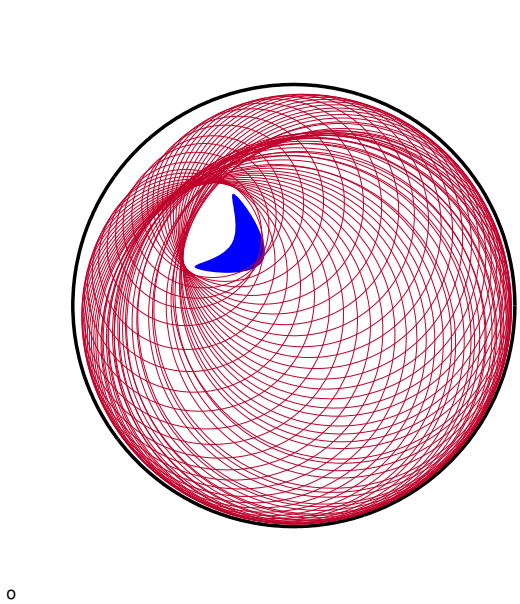

Figure 1: The convex source support for backscatter data from an insulating inclusion.

In the talk, I will argue that the convex source support indeed provides useful information on the true inclusion Ω, for it is nonempty as long as $g \neq 0$, and it is a subset of the convex hull of Ω. Moreover, it can be numerically approximated in a efficient manner, see Section 4.

3 Backscatter data & locked angle data

The convex source support complies well with data evoked and measured simultaneously by a single pair of electrodes. The electrodes are either kept very close to each other or in a fixed distance, and they are moved along the boundary ∂D collecting data at different positions. The first data type are so-called *backscatter data*, cf. [3], the second may be termed *locked angle data*, cf. [4]. Both are sparse as not the whole Dirichlet potential is registered but only its value at the electrodes' position. The theory of the convex source support applies here since backscatter as well as locked angle data are the boundary value of an harmonic function outside Ω. Thus, their convex source support may be computed.

4 Numerical Results

The convex source support can be computed numerically as we demonstrate for the case that D is the unit disk in $\mathbb{R}^2$. Given the Fourier coefficients (α_n) of the data on ∂D one determines the largest annulus $A_R = \{x \in D : \|x\| > R\}$ on which the Laurent series of (α_n) converges. This procedure is repeated under different conformal coordinate transformation, i.e. Moebius transforms, of the data. They all yield different disks, and their overall intersection is an approximation of the convex source support, see Figure 1. We present reconstructions from simulated backscatter data as in Figure 1. Furthermore, we apply the algorithm to locked angle data that were measured by a specially designed tomograph.

References

[1] M. Hanke, N. Hyvönen, M. Lehn, and S. Reusswig, Source supports in electrostatics, *BIT* **48** (2008), 245-264.

[2] M. Hanke, N. Hyvönen, and S. Reusswig, Convex source support and its application to electric impedance tomography, *SIAM J. Img. Sci.* **1** (2008), 364-378.

[3] M. Hanke, N. Hyvönen, and S. Reusswig, Convex backscattering support in electric impedance tomography, *Numer. Math.* **117** (2011), 373-396.

[4] M. Hanke, S. Hollborn, and M. Simon, Sparse-data-reconstructions from a specially designed tomograph, in preparation.

[5] S. Kusiak, and J. Sylvester, The scattering support, *Comm. Pure Appl. Math* **56** (2003), 1525-1548.

Spectral approximations for iterative inversion methods: A parabolic case

Lauri Mustonen[1,*]

[1]Department of Mathematics and Systems Analysis, Aalto University, Finland

[*]Email: lauri.mustonen@aalto.fi

Abstract

In the context of nonlinear inverse problems, we present an efficient way to construct the linear subproblems of a Gauss–Newtonian iteration. The method is based on solving the forward problem in a high-dimensional parameter domain by using spectral methods, resulting in a numerical solution that depends explicitly on the parameters. The computational cost of evaluating the solution and its derivatives as multivariate polynomials is analyzed. As an example we study the inverse boundary value problem of a parabolic PDE, but the method is also applicable in, e.g., electrical impedance tomography.

Keywords: inverse problems, spectral methods, least squares

1 Introduction

Iterative methods for nonlinear inverse problems typically require a forward PDE solver to be available. The computational cost of solving forward problems and constructing the associated Jacobian matrices can be significant. Here, we take another approach and solve the forward problem for a large family of parameter values before the actual inverse problem is even touched. This is done by approximating the parameter dependence with a spectral method, i.e., by using orthogonal multivariate polynomials.

These methods have been studied in the field of uncertainty quantification, where the motivation is to propagate the uncertainty from the input parameters to the solution [3]. For example, statistics such as mean and variance can be approximated almost trivially once the stochastic dependence is explicitly visible in the solution as polynomial coefficients. The polynomial also allows a direct evaluation of the solution for *any* given parameter vector. This property can be exploited when an inverse problem is iteratively solved.

The parameter domain often lies in a very high-dimensional space. Single-domain spectral methods have turned out to be computationally efficient discretization strategies, at least if the parameter dependence is smooth enough. Both Galerkin and collocation approaches can be used; here we concentrate on the former. In addition to choosing the parametrization and the polynomial basis, the parametric forward problem naturally requires spatial and temporal discretizations as well.

The presented method is versatile and can be utilized for different types of inverse problems. Also, classical regularization techniques and Bayesian paradigm with maximum a posteriori estimate can both benefit from the spectral solution. Here, we study an inverse parabolic problem related to thermal tomography [4], but similar method has already been utilized for electrical impedance tomography in [1].

2 Parametric parabolic equation

As a model problem we consider the diffusion equation

$$\begin{cases} \partial_t u - \nabla \cdot (a \nabla u) = 0 & \text{in } \Omega \times (0,T) \times \Theta, \\ a \nabla u \cdot \hat{\boldsymbol{n}} = g & \text{on } \partial\Omega \times (0,T) \times \Theta, \\ u = u_0 & \text{in } \Omega \times \{0\} \times \Theta, \end{cases}$$

where $\Omega \subset \mathbb{R}^d$, $d = 2, 3$, is the spatial domain, $T > 0$ is the final time and $\Theta \subseteq \mathbb{R}^P$ is the high-dimensional parameter domain. We assume that $a \colon \Theta \to L^\infty_+(\Omega)$ has time-independent realizations that are bounded away from zero and resort to a parametrization of the form

$$a(\boldsymbol{\vartheta}) = \sum_{p=1}^{P} \vartheta_p \psi_p, \qquad \boldsymbol{\vartheta} \in \Theta,$$

where $\{\psi_p\}_{p=1}^P \subset L^\infty(\Omega)$.

The variational form, followed by discretizations of the spaces $H^1(\Omega)$ and $L^2(\Theta)$ with a finite element method and a spectral Galerkin method, respetively, yields an ODE

$$\partial_t \boldsymbol{M} \hat{\boldsymbol{u}} + \boldsymbol{A} \hat{\boldsymbol{u}} = \hat{\boldsymbol{g}},$$

where $\boldsymbol{M}, \boldsymbol{A} \in \mathbb{R}^{MN \times MN}$ and $\hat{\boldsymbol{u}}, \hat{\boldsymbol{g}} \in \mathbb{R}^{MN}$. Here, M denotes the number of degrees of freedom of the finite element space and N is the

number of P-variate orthogonal polynomials. The latter can be very large if polynomials of high degree are used. However, due to the smooth parameter dependence shown in [2], it may be sufficient to use a surprisingly low degree. An efficient time integration scheme, which requires little or no additional storage, was proposed in [5].

3 Inverse boundary value problem

Let us assume that we have a measurement vector $\tilde{\boldsymbol{U}} \in \mathbb{R}^Q$, which corresponds to given physical coordinates. The inverse problem of determining the diffusivity a can be recast as a regularized nonlinear least squares problem

$$\arg\min_{\boldsymbol{\vartheta}\in\Theta} \left\{ \|\boldsymbol{U}(\boldsymbol{\vartheta}) - \tilde{\boldsymbol{U}}\|_2^2 + \|\boldsymbol{R}(\boldsymbol{\vartheta})\|_2^2 \right\},$$

where $\boldsymbol{U}\colon \Theta \to \mathbb{R}^Q$ is a polynomial mapping and $\boldsymbol{R}$ is some differentiable function. For simplicity, we assume that $\boldsymbol{R}$ is easy to evaluate and differentiate (e.g., $\boldsymbol{R}$ is a linear operator) and thus ignore it in what follows.

Gauss–Newton based methods for nonlinear least squares problems require evaluating the objective function and its Jacobian

$$\boldsymbol{J}_{\boldsymbol{U}}(\boldsymbol{\vartheta})\colon \Theta \to \mathbb{R}^{Q\times P},$$

as well as computing the solution for a linearized least squares problem. The linear problem is usually solved with the QR factorization of the Jacobian and generally takes $\mathcal{O}(QP^2)$. We show that if the parameter dependence is approximated by quadratic polynomials, the complexity of evaluating $\boldsymbol{U}$ and its Jacobian is $\mathcal{O}(QP^2)$ as well. In particular, the workload of the inverse problem is completely independent on spatial and temporal discretizations of the forward problem.

In a nutshell, the proposed method seems feasible if the parameter dependence is smooth, and if there is enough time to solve the parametric forward problem before doing the measurements.

We consider the case where the measurements are done on the spatial boundary $\partial\Omega \times (0,T)$, although the algorithm can handle interior measurements equally well. Numerical examples with simulated noisy boundary data are provided in the unit square $\Omega \subset \mathbb{R}^2$. Diffusivity reconstructions indicate that the method works, even though the optimal measurement settings (e.g., boundary fluxes and measurement locations) have not been studied yet.

References

[1] H. Hakula, N. Hyvönen and M. Leinonen, Reconstruction algorithm based on stochastic Galerkin finite element method for electrical impedance tomography, *Inverse Problems* **30** (2014), pp. 065006.

[2] V. H. Hoand and Ch. Schwab, Sparse tensor Galerkin discretization of parametric and random parabolic PDEs—analytic regularity and generalized polynomial chaos approximation, *SIAM Journal on Mathematical Analysis* **45** (2013), pp. 3050–3083.

[3] O. P. Le Maître and O. M. Knio, *Spectral Methods for Uncertainty Quantification: With Applications to Computational Fluid Dynamics*, Springer, 2010.

[4] J. M. Toivanen, T. Tarvainen, J. M. J. Huttunen, T. Savolainen, H. R. B. Orlande, J. P. Kaipio, V. Kolehmainen, 3D thermal tomography with experimental measurement data, *International Journal of Heat and Mass Transfer* **78** (2014), pp. 1126–1134.

[5] D. Xiu and J. Shen, Efficient stochastic Galerkin methods for random diffusion equations, *Journal of Computational Physics* **228** (2009), pp. 266–281.

Minisymposium: Numerical Bottlenecks in Helioseismology
organised by Juliette Chabassier and Damien Fournier

The goal of helioseismology is to recover internal properties of the Sun (density, meridional circulation, ...) via the analysis and the inversion of acoustic waves propagating through the Sun using surface observations. This topic is closely related to Earth-seismology but numerical difficulties are different as the Sun is not a solid body but a rotating heterogeneous fluid, subject to magnetic and gravitational fields. Moreover the acoustic sources, mostly due to convective turbulence, are not well characterized. The aim of this mini-symposium is to present the state-of-the-art in numerical methods for helioseismology and to gather people from different communities who could give new insights in the topic.

If the full 3D modeling of the solar interior is still out of reach, simplified models (Helmholtz or Galbrun's equations with realistic physical coefficients) that represent most of the propagating aspect of the physics can be used. A coupling with the magnetic field should then be added because of their strong influence on the fluid dynamics, a problem closely related to electroseismic coupling in geophysics. Coupling with gravitational waves is still an open issue.

Once a forward model is chosen and can be solved efficiently, an inversion can be performed. An interesting and powerful approach coming from geophysics is the full-waveform inversion. First attempt in this direction has also been done in helioseismology. A characteristic of helioseismology is that, due to convection, the observations are stochastic. Adequate modeling of the underlying noise leads to satifying results but care must be taken to treat the inverse and forward problems.

Solving the Forward Problem of Helioseismology in the Frequency Domain

Laurent Gizon[1,*], Hélène Barucq[2], Marc Duruflé[2], Aaron C. Birch[1], Juliette Chabassier[2], Damien Fournier[3], Cristopher Hanson[1], Michaël Leguebe[1]

[1]Max-Planck-Institut für Sonnensystemforschung, Göttingen, Germany and Institut für Astrophysik, Georg-August-Universität Göttingen, Göttingen, Germany
[2]Magique-3D, INRIA Bordeaux Sud-Ouest, Pau, France
[3]Institut für Numerische und Angewandte Mathematik, Georg-August-Universität Göttingen, Göttingen, Germany
*Email: gizon@mps.mpg.de

Abstract

Solar acoustic waves are continuously excited by turbulent convection (a random process). The forward problem of local helioseismology was specified at the Waves 2013 conference: computing the cross-covariance of the wave field between any two locations on the solar surface. Here we solve the problem in the frequency domain using the finite element solver *Montjoie*. One of the specificities of wave propagation problems in the Sun is the very sharp decrease of sound speed and density with radius near the surface. We show that the problem simplifies considerably under the assumption that the covariance function of the source of excitation is proportional to the attenuation.

Keywords: acoustics, forward problem, local helioseismology

1 Scalar Acoustics

Rather than solving the forward problem in all its complexity, we neglect gravity, assume that the medium is steady, and consider linear adiabatic waves only. Under these approximations the linearized equations of motion reduce to a single equation for the scalar quantity

$$\psi = c\,\mathrm{div}\boldsymbol{\xi}, \tag{1}$$

where $\boldsymbol{\xi}$ is the wave displacement vector and c is the sound speed. If we further assume that waves are excited by a stationary random process (source function s), we only need to solve the problem one frequency ω at a time:

$$L\psi = s \tag{2}$$

with the wave operator

$$L = -\omega^2 - 2\mathrm{i}\omega\gamma - 2\mathrm{i}\omega\boldsymbol{u}\cdot\nabla + H \tag{3}$$

$$H\psi = -c\,\mathrm{div}\left(\frac{1}{\rho}\nabla(\rho c\psi)\right), \tag{4}$$

where ρ is density, $\gamma > 0$ is the attenuation, and $\boldsymbol{u}$ is the background flow. The factor c in the definition of ψ is chosen such that the spatial operator H is Hermitian symmetric under free surface boundary conditions ($\psi = 0$ on ∂V). Since mass is conserved the advection operator is also Hermitian, while the attenuation operator is anti-Hermitian. Note that the computational domain V ends approximately 500 km above the solar photosphere, i.e. above the observation height.

2 Cross-Covariance Function

Consider ψ measured at positions $\boldsymbol{r}_1$ and $\boldsymbol{r}_2$ near the solar surface (inside the computational domain). At frequency ω, the cross-covariance function is

$$C(\boldsymbol{r}_1,\boldsymbol{r}_2,\omega) = \mathbb{E}[\psi^*(\boldsymbol{r}_1,\omega)\psi(\boldsymbol{r}_2,\omega)], \tag{5}$$

as defined by Duvall et al. (1993) [1]. We study the forward problem, i.e. how a change in solar structure,

$$\begin{aligned} &c(\boldsymbol{r}) \to c(\boldsymbol{r}) + \delta c(\boldsymbol{r}),\\ &\rho(\boldsymbol{r}) \to \rho(\boldsymbol{r}) + \delta\rho(\boldsymbol{r}),\\ &\boldsymbol{u}(\boldsymbol{r}) \to \boldsymbol{u}(\boldsymbol{r}) + \delta\boldsymbol{u}(\boldsymbol{r}), \end{aligned} \tag{6}$$

will affect the cross-covariance function,

$$C \to C + \delta C. \tag{7}$$

Using the first-order Born approximation and the assumption that sources are spatially uncorrelated, Gizon (2013) [2] wrote

$$\begin{aligned} \delta C(\boldsymbol{r}_1,\boldsymbol{r}_2) = &-\int_V G(\boldsymbol{r}_2,\boldsymbol{r})\,\delta L[C(\boldsymbol{r}_1,\boldsymbol{r})]\,\rho d\boldsymbol{r}\\ &-\int_V G^*(\boldsymbol{r}_1,\boldsymbol{r})\,\delta L^*[C^*(\boldsymbol{r}_2,\boldsymbol{r})]\,\rho d\boldsymbol{r}, \end{aligned} \tag{8}$$

where δL is the perturbation to the wave operator L caused by the perturbations to the

medium, and G is the Green's function defined by

$$LG(\boldsymbol{r}, \boldsymbol{r}', \omega) = \frac{1}{\rho}\delta(\boldsymbol{r} - \boldsymbol{r}'). \tag{9}$$

Thus the two quantities that really matter in local helioseismology are the functions C and G computed in the reference model.

3 Convenient Source of Excitation

It is well known that under appropriate conditions the expectation value of the cross-covariance is related to the imaginary part of the Green's function. If we could write such a simple relationship, our problem would simplify considerably. In particular, for all practical purposes, the problem would become deterministic and the Green's function would be the only remaining quantity in our problem.

Starting from the definition of the Green's functions $G(\boldsymbol{r}, \boldsymbol{r}_1)$ and $G(\boldsymbol{r}, \boldsymbol{r}_2; -\boldsymbol{u})$, where the latter is for a medium with opposite background flow, one can show

$$G(\boldsymbol{r}_2, \boldsymbol{r}_1) - G^*(\boldsymbol{r}_2, \boldsymbol{r}_1; -\boldsymbol{u}) = 4\mathrm{i}\omega \int_V \gamma(\boldsymbol{r}) G^*(\boldsymbol{r}_1, \boldsymbol{r}) G(\boldsymbol{r}_2, \boldsymbol{r})\, \rho d\boldsymbol{r}. \tag{10}$$

In order to obtain this result, generalized seismic reciprocity was used:

$$G(\boldsymbol{r}, \boldsymbol{r}') = G(\boldsymbol{r}', \boldsymbol{r}; -\boldsymbol{u}). \tag{11}$$

Note that an extra surface integral should be included above if the boundary condition is not Dirichlet. By identification with equation (10), we see that the choice of source covariance

$$\mathbb{E}[s^*(\boldsymbol{r}, \omega) s(\boldsymbol{r}', \omega)] = P_s(\omega) \frac{\gamma(\boldsymbol{r})}{\rho(\boldsymbol{r})} \delta(\boldsymbol{r} - \boldsymbol{r}') \tag{12}$$

implies

$$C(\boldsymbol{r}_1, \boldsymbol{r}_2) = \frac{P_s}{4\mathrm{i}\omega} \left[G(\boldsymbol{r}_2, \boldsymbol{r}_1) - G^*(\boldsymbol{r}_2, \boldsymbol{r}_1; -\boldsymbol{u}) \right]. \tag{13}$$

Thus the cross-covariance can be written as a sum of causal and anti-causal Green's functions. The volume sources must be proportional to the local attenuation to enforce energy equipartition between the modes (see Snieder *et al.* 2007 [4] for a discussion).

4 2.5D FEM Forward Solver

To check if equation (13) is a good approximation, we compute the Green's function for a standard solar model (Model S) using the FEM direct solver *Montjoie* from INRIA Pau, and compare the cross-covariance and oscillation power spectra with observations from the Solar Dynamics Observatory (NASA). The results are very encouraging.

To speed up the computations, we consider a solar background model that is symmetric about an axis. The computational domain is a 2D generating section of the geometry, which is meshed in quadrilateral elements.

5 Inverse Problem

The inverse problem consists of inferring the properties of the medium (ρ, c and $\boldsymbol{u}$) from measurements of the cross-covariance function (or travel times). An iterative inversion is possible since all the tools are in place to compute the perturbation to the cross-covariance starting from a completely general background medium. Damien Fournier et al. will discuss the inverse problem of local helioseismology at the conference.

References

[1] T. L. Duvall Jr. *et al.*, Time-distance helioseismology, *Nature* **362**, 430-432 (1993)

[2] L. Gizon, Seismology of the Sun, Waves 2013, Tunisia (2013)

[3] L. Gizon and A. C. Birch, Time-distance helioseismology: the forward problem for random distributed sources, *Astrophys. J.* **571**, 966-986 (2002)

[4] R. Snieder, K. Wapenaar and U. Wegler, Unified Green's function retrieval by cross-correlation; connection with energy principles, *Phys. Rev. E* **75**, 036103 (2007)

Solution of time-harmonic Galbrun's equation in the context of helioseismology

Marc Duruflé[1,*], **Juliette Chabassier**[1]
[1]Magique3D Team, INRIA Bordeaux Sud Ouest, FRANCE
[*]Email: marc.durufle@inria.fr

Abstract

Galbrun's equations are solved with different formulations. Problems of convergence are observed for the tested formulations for moderate Mach numbers. Simplified Galbrun's equations are proposed without this problem of convergence. Numerical results are presented for the sun's configuration.

Keywords: Galbrun's equation, Discontinuous Galerkin, Helioseismology

1 Introduction

When gravitational and magnetic forces are neglected, the propagation of waves inside the sun can be modelled with Galbrun's equation (in time-harmonic domain):

$$\begin{aligned}\rho_0\left(-i\omega+\sigma+M\cdot\nabla\right)^2 u-\nabla\left(\rho_0\, c_0^2\,\mathrm{div}\, u\right)\\ +(\mathrm{div}\, u)\,\nabla p_0-(\nabla u)^T\nabla p_0 \;=\; f\end{aligned} \tag{1}$$

where ρ_0, c_0, p_0 are the background density, sound speed and pressure, σ is a damping coefficient. For a quiet sun, the flow $M=(m_x,m_y)$ is null, but is non-null in the general case. In this talk, we will explore different formulations in order to solve Galbrun's equations in 2-D and for an axisymmetric geometry.

2 Equivalent formulations

Equation (1) will be solved directly with SIPG (Symmetric Interior Penalty Galerkin) method. An equivalent first-order formulation can be easily obtained

$$\begin{cases}\rho_0\left(-i\omega+\sigma+M\cdot\nabla\right)u-\rho_0 v=0\\ \rho_0\left(-i\omega+\sigma+M\cdot\nabla\right)v-\nabla(\rho_0\, c_0^2\, p)\\ \qquad\qquad +p\nabla p_0-(\nabla u)^T\nabla p_0=f\\ p-\mathrm{div}\, u=0\end{cases}$$

This formulation will be solved with LDG (Local Discontinuous Galerkin) method. The last equation of this formulation is similar to a constraint. In order to obtain a formulation close to an hyperbolic system, we have introduced the following first-order formulation

$$\begin{cases}\rho_0\left(-i\omega+\sigma+M\cdot\nabla\right)u-\nabla p-\rho_0\, q=0\\ \rho_0\left(-i\omega+\sigma+M\cdot\nabla\right)q-(\nabla\sigma)\,p-(\nabla M)^T\nabla p\\ \quad -\frac{M\cdot\nabla\rho_0}{\rho_0}\nabla p+(\mathrm{div}\, u)\nabla p_0-(\nabla u)^T\nabla p_0=f\\ \rho_0\left(-i\omega+\sigma+M\cdot\nabla\right)p-\rho_0^2\, c_0^2\,\mathrm{div}\, u=0\end{cases}$$

This equivalent formulation will be solved with LDG as well. Finally, a H^1 formulation (coupled with discontinuous Galerkin) [1] has been considered. All these formulations are equivalent and should provide the same solution.

3 Linearized Euler Equations

Linearized Euler Equations are also considered

$$\begin{cases}(-i\omega+\sigma+M\cdot\nabla)p+\mathrm{div}(c_0^2\, u)\\ \qquad +(\gamma-1)(\mathrm{div}M)\,p-\frac{(\gamma-1)}{\rho_0}u\cdot\nabla p_0=0\\ (-i\omega+\sigma+M\cdot\nabla)\rho+\rho\,\mathrm{div}\, M+\mathrm{div}\, u=0\\ (-i\omega+\sigma+M\cdot\nabla)u+\nabla p+\nabla M(u+\rho\, M)=\dfrac{g}{\rho_0}\end{cases}$$

They give the same solution as Galbrun's equations for an uniform flow and when

$$f \;=\; (-i\omega+\sigma+M\cdot\nabla)g$$

4 Convergence study

When the flow is uniform (or null), the different formulations converge correctly in a similar fashion. Tests have been conducted on a square $[-4,4]^2$ with periodic coefficients:

$$\begin{cases}m_x=\mathrm{coeff}\times\left(0.3+0.1\cos\left(\frac{\pi y}{4}\right)\right)/\rho_0(x,y)\\ m_y=\mathrm{coeff}\times\left(0.2+0.08\sin\left(\frac{\pi x}{4}\right)\right)/\rho_0(x,y)\\ \rho_0=1.5+0.2\cos\left(\frac{\pi x}{4}\right)\sin\left(\frac{\pi y}{2}\right)\\ p_0=1.44\rho_0+0.08\rho_0^2\;,\;\; c_0^2=1.44+0.16\rho_0\\ \omega=0.78\times 2\,\pi,\quad \sigma=0.1\end{cases}$$

When the coefficient coeff is small, the different formulations seem to converge correctly (see Fig. 1), but it is no longer the case for larger values of this coefficient (see Fig. 2). r is the order of approximation used. This default of convergence is not observed for Linearized Euler Equations.

Figure 1: Relative L^2 error versus h/r for quadrilateral elements and non-uniform flow coeff $= 0.1$ with different formulations ($r = 5$).

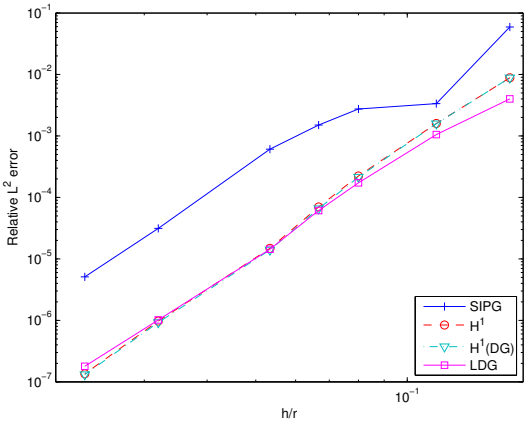

5 Application for the sun

Simplified Galbrun's equations are proposed such that they are equivalent to Galbrun's equation when M is null, and converge correctly:

$$\begin{cases} \rho_0(-i\omega + \sigma + M\cdot\nabla)\, p + \rho_0^2\, c_0^2 \operatorname{div} u = 0 \\ \rho_0(-i\omega + \sigma + M\cdot\nabla)\, u + \nabla p + \\ \qquad \frac{1}{-i\omega+\sigma}\left((\operatorname{div} u)\nabla p_0 - (\nabla u)^T \nabla p_0\right) = g \end{cases}$$

They are solved for realistic coefficients of the sun with a rotating flow, see figure 3. It can be seen in figure 4, that original Galbrun's equations exhibits curious oscillations that are not converged.

References

[1] A. S. Bonnet-Ben Dhia, J. F. Mercier, F. Millot, S. Pernet, A low Mach model for time harmonic acoustics in arbitrary flows, *Journal of Computational and Applied Mathematics* **234(6)** (2010), pp. 1868–1875.

Figure 2: Relative L^2 error versus h/r for quadrilateral elements and non-uniform flow for LDG formulation ($r = 10$) and different values of coeff.

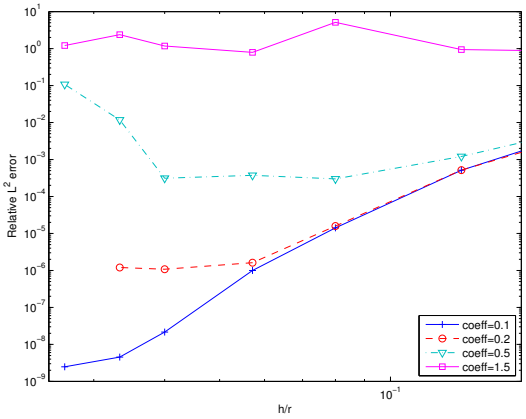

Figure 3: Real part of u_x for the sun (simplified Galbrun's equations).

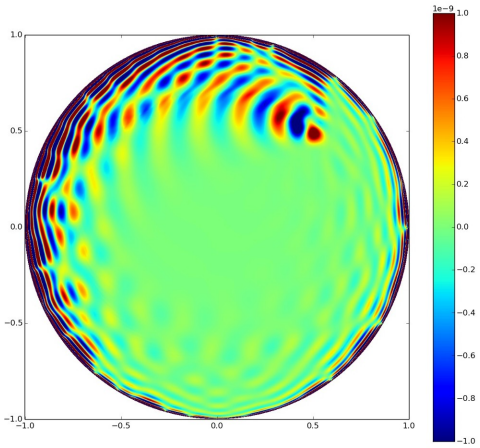

Figure 4: Real part of u_x for the sun (original Galbrun's equations).

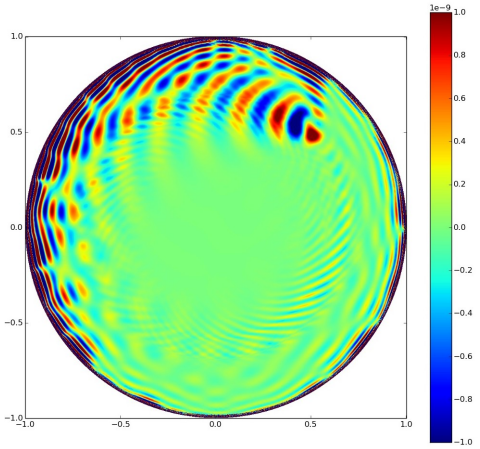

Statistical interpretation of seismic observations

Laura Cobden[1,*], **Jeannot Trampert**[1], **Ralph de Wit**[1]
[1]Department of Earth Sciences, Utrecht University, Utrecht, The Netherlands
*Email: l.j.cobden@uu.nl

Over 90% of the global seismic data available for the Earth can be represented by one-dimensional, radially symmetric wave speed models. Such models, e.g., PREM [5] and AK135 [6], form the basis for 3-D seismic tomography, in which lateral variations in wave speed are measured as a percentage difference, or anomaly, relative to the chosen 1-D reference model. As technological advances allow increasingly higher resolution of 3-D structures in seismic tomography, there is a greater impetus to interpret these structures quantitatively in terms of dynamically relevant parameters [9]. However, seismic models themselves do not tell us about the underlying dynamic behaviour of the Earth's interior — for this we need to know a range of physical variables, most importantly chemical composition and temperature, and we need to know exactly which temperature and chemical composition corresponds to a particular wave speed or density. Such information is available through mineral physics, and an intelligent interpretation of seismic tomography requires us to make a quantitative comparison between the seismic and mineralogical data, taking into account the uncertainties in both [1]. However, quantifying model uncertainties presents a challenge in traditional seismological inverse problems; consequently, most existing techniques are pragmatic and based upon linear approximations. An assessment of model uncertainty is natural in a Bayesian framework, in which all inferences are probabilistic. Any inference made about a model is the result of the conjunction of our current (prior) knowledge and the ability of the model to explain the observations, e.g. [10]. The posterior knowledge on the model, i.e. the knowledge after observing the data, represents the updated degree of belief in the model, expressed by a probability density function (PDF). In this talk we will present a synopsis of Bayesian techniques that have been employed in terrestrial seismology in order to interpret seismic data.

1 Uncertainties in seismic observations

Seismic tomography on the Earth is both an ill-posed and an ill-conditioned inverse problem. Due to the irregular distributions of earthquakes and seismic receivers, there are always parts of the Earth which are under-determined by the data and parts which are over-determined. This results in significant null spaces in the tomographic model, and small errors in the data can produce large errors in the model.

One technique for addressing these problems is probabilistic tomography [12]. Instead of producing one solution for the 3-D wave speed structure, the wave speed at each point in the tomographic model is represented by a probability density function (PDF). Visually this is usually shown by two maps: the mean of the PDF in one map, and the standard deviation in another (Fig 1). Probabilistic tomography models can be obtained via the Neighborhood Algorithm, where a Monte Carlo approach is used to infer all the possible information from data [7, 11].

Since 3-D tomography models are expressed as perturbations from a 1-D reference model, then in isolation they can only be interpreted in terms of lateral variations in physical properties. In order to determine the absolute values of physical properties, we must also refer to the 1-D reference model and map its uncertainties. Some methods which have been applied to explore these uncertainties are the Reversible Jump Markov Chain Monte Carlo Algorithm [2] and machine learning techniques [4].

2 Uncertainties in mineral physics

Mineral physics forms the basis for any quantitative interpretation of seismic observations, because it allows us to link seismic velocities seen in the Earth with the physical properties of candidate rock-forming minerals. On the one hand, phase equilibria tell us which minerals will be thermodynamically stable at a given temperature (T) and pressure (P) for a chosen chemical composition. On the other, the mineral elastic parameters – namely, bulk modulus (K),

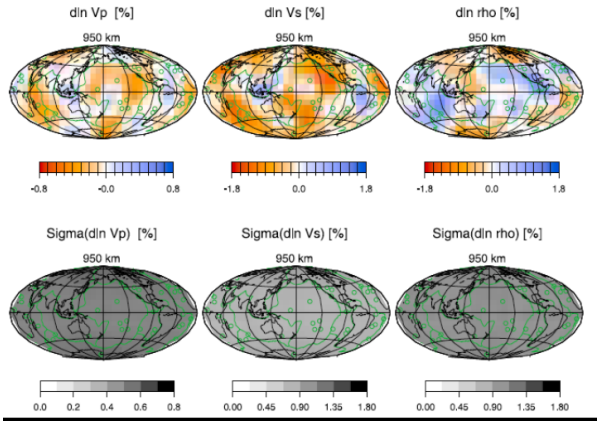

Figure 1: Probabilistic tomography model of the wave speed and density structure at 950 km depth in the Earth [7]. Continents are shown in black and plate boundaries and hotspots in green.

shear modulus (G) and density (ρ) – allow us to compute the aggregate seismic velocities of a mineral assemblage. However, K, G and ρ vary significantly as a function of temperature and pressure. At the same time, experimental limitations mean that both elastic parameters and phase equilibria are only measured at a finite number of P, T conditions, and thus not for all depths in the Earth. Additionally, each datum is subject to measurement errors, and studies of the same minerals by different methods are not always compatible. Subsequently, we rely on Equations of State (EoS) to define continuous relations between the elastic parameters and P and T. These equations are typically derived through ad-hoc curve-fitting and thermodynamic reasoning. The further we extrapolate from the surface of the Earth, the more uncertain the equations become, especially in the lower mantle. Simple Monte-Carlo forward modelling [1, 2] can be used to explore the seismic manifestation of mineral physics uncertainties.

An added complication when interpreting seismic data for the Earth's mantle is that seismic structures are likely generated by both thermal and chemical effects, which can be indistinguishable from each other when we study only one type of seismic observable. Inverting for two or more variables, e.g. P-wave speed, S-wave speed, ratios of P to S –wave speed, or density, can help to distinguish between thermal and chemical structures. When these observables have been probabilistically determined, we can simultaneously fit their distributions with corresponding distributions of temperature and mineralogy, using techniques such as the Metropolis-Hastings Algorithm [3, 7, 8].

References

[1] L. Cobden et al., Geophys. J. Int. 175 (2), 627–648 (2008)

[2] L. Cobden et al., J. Geophys. Res.: Solid Earth 114 (B11) (2009)

[3] L. Cobden et al., Phys. Earth planet. Inter., 210–211, 21–35 (2012)

[4] R.W.L. de Wit et al, Phys. Earth planet. Inter., 237, 1-17 (2014)

[5] Dziewonski, A.M. and Anderson, D.L., Phys. Earth planet. Inter., 25, 297–356 (1981)

[6] Kennett, B.L.N., Enghdahl, E.R. and Buland, R., Geophys. J. Int., 122, 108–124 (1995)

[7] I. Mosca et al., J. geophys. Res.-Solid Earth, 117, B06304 (2012)

[8] Mosegaard, K., Tarantola, J. Geophys. Res. 100, 12431–12447 (1995)

[9] Trampert, J. and Van Der Hilst, R.D., eds Van der Hilst, R.D., Bass, J.D., Matas, J. and Trampert, J. American Geophysical Union,Washington, DC (2005)

[10] Tarantola, A., Valette, B., J. Geophys. 50, 159–170 (1982)

[11] Sambridge, M., Geophys. J. Int., 138, 479–494 (1999)

[12] J. Trampert et al., Science, 306, 853–856 (2004)

Parameter identification for the acoustic wave equation in helioseismology

Damien Fournier[1,*], **Thorsten Hohage**[1], **Laurent Gizon**[2]
[1]Institute for Applied Mathematics, Göttingen, Germany
[2]Max-Planck Institute for Solar Sytem, Göttingen, Germany
[*]Email: d.fournier@math.uni-goettingen.de

Abstract

The goal of helioseismology is to infer properties of the Sun interior using observations of solar oscillations on its surface. It requires a good knowledge of the wave propagation inside the Sun (forward model), of the noise properties of the observations and a reliable inversion method. In this paper, a simplified model (scalar acoustic wave equation) that captures most of the propagating aspects of the physics will be used. The goal is then to identify some parameters of this PDE that characterize the medium (density, sound speed) by using linear and nonlinear inversions.

Keywords: inverse problem, helioseismology, acoustic wave equation

1 Introduction

Helioseismology aims at recovering some properties of the solar interior from observations of the line-of-sight velocity $\psi(\mathbf{r}, t)$ where $\mathbf{r}$ are points on the surface and t is the time. From this time-serie, one generally computes the time $\tau(\mathbf{r}_1, \mathbf{r}_2)$ it takes for the wave to go between two points $\mathbf{r}_1$ and $\mathbf{r}_2$ at the solar surface. These quantities are the basic input of time-distance helioseismology [1]. In order to recover some properties q of the solar interior, they have to be linked to the observations. A simplified forward model that represents wave propagation in the Sun (PDE satisfied by ψ) is presented in Section 2. The observation operator that links travel-time to ψ is given in Section 3 and finally different inversion methods are compared in Section 4.

2 Forward problem

We consider that ψ satisfies an acoustic wave equation in the Sun Ω with homogeneous Dirichlet boundary conditions on $\partial\Omega$. The medium is assumed to be steady and is characterized by its density ρ and sound speed c. The source S is stationary and stochastic with zero mean and known covariance. The problem decouples for all frequencies ω and is given by

$$\begin{cases} \mathcal{L}\psi := -\sigma^2\psi - 2\mathrm{i}\omega\mathbf{u}\cdot\nabla\psi + H\psi = S \quad \text{in } \Omega \\ \psi = 0 \quad \text{on } \partial\Omega, \end{cases} \tag{1}$$

with $\sigma = \omega + \mathrm{i}\gamma$ and

$$H\psi = -c\nabla\cdot\left(\frac{1}{\rho}\nabla(\rho c\psi)\right). \tag{2}$$

The waves are damped by γ and are subject to a flow $\mathbf{u}$. Without flow and if the coefficients ρ and c are constant, then Eq. 1 is simply the Helmholtz equation. In the Sun, these coefficients vary strongly close to the boundary (several orders of magnitude) and care has to be taken in the numerical resolution. We use the Montjoie code [1] that solves Eq. 1 with finite elements. Details about the numerical scheme can be found in [3] where it is also shown that even if Eq. 1 is highly simplified, it captures most of the propagating aspects of the physics.

3 Observation operator

In order to link travel-time to the observations, let us first define the cross-covariances $C_{12}(\omega) = C(\mathbf{r}_1, \mathbf{r}_2, \omega)$ in the Fourier space between pairs of points $(\mathbf{r}_1, \mathbf{r}_2)$ on the solar surface by

$$C_{12}(\omega) = \psi^*(\mathbf{r}_1, \omega)\psi(\mathbf{r}_2, \omega). \tag{3}$$

The travel times are linearly dependent of the cross-covariance

$$\tau_{12} = \int W_{12}(\omega)^*\Big(C_{12}(\omega) - C_{12}^{\mathrm{ref}}(\omega)\Big)d\omega \tag{4}$$

with C^{ref} representing a reference cross-covariance that can come from a solar model or averaged observations [2] and W is a given function that depends on C^{ref}. We denote T the (quadratic) operator that maps the observations to ψ

$$\tau = T(\psi). \tag{5}$$

[1]montjoie.gforge.inria.fr

4 Inversion

The observations τ are linked to some internal properties of the Sun q by a nonlinear inverse problem

$$F(q) = \tau, \tag{6}$$

where F is defined implicitely by $F(q) = (T \circ \mathcal{L}_q^{-1})\psi$ with $\mathcal{L}_q$ given by Eq. 1 and the observation operator T by Eq. 5. Then the inverse problem can be stated:

The inverse problem (IP). *Knowing the observations τ^{obs}, the problem is to find the optimal parameter q solution of the nonlinear inverse problem (Eq. 6).*

4.1 Linear inversion

A classical approach to solve (IP) in helioseismology is to consider only first order perturbations by using the first Born approximation (single scattering approximation). In this case the perturbations are linearly linked to the observations

$$\mathbb{E}[\tau] = \sum_q \int_\Omega K_q(\mathbf{r})\delta q(\mathbf{r}) dV. \tag{7}$$

The kernels are obtained by differentiating Eq. 4 and computing $\delta\psi$ at first order

$$\mathcal{L}_q[\delta\psi] = -\delta\mathcal{L}_q[\psi] + \delta S, \tag{8}$$

with $\delta\mathcal{L}_q$ computed by deriving formally Eq. 1. For the different perturbations q, the sensitivity kernels K_q can be written as a function of G, C and of the operators H and σ. The exact expression of the kernels can be found in [3].

Eq. 7 can be solved for example by Tikhonov regularization

$$\min_{\delta q} \left(\|K_q\delta q - \mathbb{E}[\tau]\|^2 + \|L\delta q\|^2 \right), \tag{9}$$

where L can be the identity or a discrete version of a gradient or a Laplacian in order to impose smoothness of the solution. (IP) can also be solved by the adjoint method [4] which employs techniques close to nonlinear inversions.

4.2 Nonlinear inversion

In order to find the optimal q by nonlinear methods, we need to be able to evaluate the forward operator $F(q_k)$, its derivative $F'[q_k]\delta q$ and the adjoint of the derivative $F'[q_k]^\dagger \delta C$. These three ingredients are required for all types of nonlinear inversions and can be computed by solving the same PDEs (the forward operator and its adjoint) but with different right hand side. For example, the update $\psi_{k+1} = \psi_k + \delta\psi$ is obtained from $F'[q_k]\delta q = T'[\psi_k]\delta\psi$ where $\delta\psi$ is the solution of

$$\mathcal{L}_q[\delta\psi] = -\delta\mathcal{L}_q[\psi_k](\delta q). \tag{10}$$

An efficient method to solve (IP) is to use the conjugate gradient applied to the normal equation. We solve a quadratic least square problem to find δq_k that minimizes

$$\left\| F'[q_k]\delta q + F(q_k) - \tau^{\text{obs}} \right\|^2, \tag{11}$$

and the regularization is made by choosing an early stopping criterion at each iteration [5].

A comparison of the inversion methods will be presented showing which types of perturbations can be recovered with linear inversions and when nonlinear methods become necessary.

References

[1] T. L. Duvall, S. M. Jefferies, J. W. Harvey and M. A. Pomerantz, Time-Distance Helioseismology, *Nature*, **362** (1993), 430-432

[2] L. Gizon and A. C. Birch, Time-Distance Helioseismology: the Forward Problem for Random Distributed Sources, *The Astrophysical Journal*, **571** (2002), 966-986

[3] L. Gizon et al., Framework for computational local helioseismology, *Astronomy and Astrophysics*, to be submitted

[4] S. M. Hanasoge, A. C. Birch, L. Gizon and J. Tromp, The Adjoint Method Applied to Time-Distance Helioseismology, *The Astrophysical Journal*, **738** (2011), 100-120

[5] M. Hanke, Conjugate gradient type methods for ill-posed problems (1995) (Vol. 327). CRC Press.

Viscoacoustic full waveform inversion for spatially uncorrelated problems

R. Shigapov[1], A. Kurzmann[2,*], T. Bohlen[2]

[1]Saint Petersburg State University, Saint Petersburg, Russia

[2]Karlsruhe Institute of Technology (Geophysical Institute), Karlsruhe, Germany

[*]Email: kurzmann@kit.edu

Abstract

Seismic attenuation contains valuable information about the subsurface. In this work we investigate the applicability of 2D viscoacoustic full waveform inversion (FWI) to synthetic marine reflection data. Viscoacoustic FWI is a multiparameter inverse problem, and suffers from the cross-talk between different parameter classes. We investigate the cross-talk using spatially uncorrelated models of velocity and attenuation. Our results show a good reconstruction of the velocity model and satisfactory recovery of Q only in shallow areas. With increasing depth we observe a stronger footprint of the velocity model. This can be interpreted either as low sensitivity of the synthetic data to attenuation properties in deep parts or as cross-talk with explanation of attenuation-related data misfit by the velocity model. We find that the investigation of multiparameter inverse problems with spatially uncorrelated parameters has to be considered as a necessary step to verify the reliability of inversion strategies.

Keywords: marine seismics, full waveform inversion, attenuation, viscoacoustic

1 Introduction

Attenuation and dispersion of seismic waves play important role and need to be taken into account. However, our understanding of attenuation mechanisms and ability to get reliable Q estimates [4] are still limited. The main research question of our study is: Can spatial distributions of velocity and intrinsic attenuation be accurately inverted by applying full waveform inversion (FWI) to reflection data? Since the first numerical implementations of viscoacoustic FWI [8] until the most recent ones both the modeling and inversion were mostly developed in the frequency domain – exploiting its benefits, such as easy implementation of attenuation, computation of gradients for velocity and Q without extra-cost, and natural use of a multi-scale strategy with sequential inversion from low to high frequencies. Time-domain FWI in attenuative media is less popular [1]. First, implementation of strictly constant Q within a wide frequency band is not so easy. To get approximately constant Q for a given frequency band, we have to consider a sum of relaxation mechanisms [6]. From other side, an advantage of time-domain implementations is efficient parallelizability. In this work we investigate the applicability of time-domain viscoacoustic FWI on synthetic marine reflection data. We show numerical results using spatially uncorrelated models of velocity and attenuation.

2 Methodology

In time domain a general linear viscoacoustic equation of motion consists of a convolutional kernel representing Bolzmann's superposition principle. This integro-differential equation can be reformulated as a system of differential equations with a new "memory variable". Then, the conventional constant Q_P model, i.e., $Q_\mathrm{P}(\omega) = const.$ with frequency ω, can be approximated by the generalized standard linear solid (GSLS) with L relaxation mechanisms [2] and within the given frequency band. The viscoacoustic medium is defined by density ρ, the relaxed bulk modulus κ_r and the relaxation parameter τ_P related to relaxation mechanisms and Q_P, e.g., for one mechanism $\tau_\mathrm{P} = 2/Q_\mathrm{P}$. For a 2D viscoacoustic medium, we have to solve a system of $3 + L$ differential equations (pressure field, field of particle velocities and L memory variables) using a time-domain finite-difference time-stepping method [3, 5]. The inverse problem of finding the vector $\mathbf{m}(\mathbf{x}) = [\mathbf{v}_\mathrm{p}(\mathbf{x}), \mathbf{Q}_\mathrm{p}(\mathbf{x})]$ of model parameters is formulated as a minimization problem using the conventional L_2-norm of a misfit between the modelled and observed pressure fields. Although the parameters of interest are velocity v_P and quality factor Q_P, our implementation of viscoacoustic equations requires parameter τ_P rather Q_P. However, since Q_P ranges over

few orders of magnitude, we prefer to invert for $\log(\tau_\mathrm{P})$. We derived gradients of the misfit function using the adjoint-state method (e. g., [7]):

$$g_{[v_\mathrm{P}]} = \int \left(v_\mathrm{P} \rho \left(1 + L\ \tau_\mathrm{P}\right) \nabla \cdot \mathbf{w} + \frac{r}{v_\mathrm{P}} \right) \hat{p}\ \mathrm{d}t,$$

$$g_{[\log(\tau_\mathrm{P})]} = \int \left(v_\mathrm{P}^2\ \rho\ L\ \tau_\mathrm{P}\ \nabla \cdot \mathbf{w} + r \right) \hat{p}\ \mathrm{d}t,$$

where $\hat{p} = \hat{p}\,(\mathbf{x}, t)$ denotes adjoint pressure field, $\mathbf{w} = \mathbf{w}\,(\mathbf{x}, t)$ represents the forward field of particle velocities and $r = r\,(\mathbf{x}, t)$ denotes the sum of all L forward memory variables (due to clarity in equations, spatial and temporal dependences are omitted). We minimize the misfit function using the preconditioned conjugate gradient method. The iterative model updates of v_P and $\log(\tau_\mathrm{P})$ comprise independently computed step lengths using a parabolic line search algorithm.

3 Synthetic FWI experiment

We apply viscoacoustic inversion to the 2D Marmousi model and investigate its impact on spatially uncorrelated models of v_P and Q_P. Density model, source signal (Ricker wavelet with a dominant frequency $f_s = 9$ Hz) and parameters in the water layer are assumed to be correct. The acquisition geometry is a marine streamer consisting of 32 explosive sources as well as a maximum number of 300 hydrophones. To consider the relevant frequency content, we use three relaxation mechanisms. The true Q_P (Fig. 1d) model is derived from v_P (Fig. 1a) and turned upside down to avoid spatial correlation. The initial models for FWI can be found in Fig. 1b,e. The sequential inversion of both parameters (i.e., first inverting for v_P, then both v_P and Q_P) recovers a satisfactory v_P model (Fig. 1c). The Q_P model shows significant artefacts (Fig. 1f). However, we can distinguish a quite good Q_P reconstruction in shallow areas and the unreliable footprint of v_P in deeper areas due to the cross-talk between both model parameters and insensitivity of seismic data to attenuation.

4 Conclusions

In this work we implemented time-domain viscoacoustic full waveform inversion based on the generalized standard linear solid. We tested its applicability on synthetic reflection marine data using the 2D Marmousi model. In contrast to the most of existing studies, we considered spatially uncorrelated models of v_P and Q_P. While v_P is recovered very well, Q_P is inverted satisfactorily only in shallow parts. The excellent fit of recorded and modelled seismograms can be interpreted either as low sensitivity of the synthetic data to deeper parts or a cross-talk effect where the Q_P-related data misfit is explained by the v_P model. The Marmousi experiment illustrates the improvement of the velocity reconstruction by the satisfactory Q_P recovery in shallow areas and even by artificial quality factors in deeper parts. In viscoacoustic inversion, the conventional assumption of correlated velocity and attenuation subsurface structures might induce an incorrect interpretation. On the one hand, the preliminary Q_P result in this work makes clear that further development of inversion strategies is necessary to extract the desired attenuation information from seismic data. On the other hand, the investigation of multiparameter inverse problems with (highly) spatially uncorrelated parameters has to be considered as a necessary step to verify the reliability of these strategies.

References

[1] A. Askan, V. Akcelik, J. Bielak and O. Ghattas, Full Waveform Inversion for Seismic Velocity and Anelastic Losses in Heterogeneous Structures, *Bulletin of the Seismological Society of America* **97** (2007), pp. 1990–2008.

[2] J. Blanch, J. Robertsson and W. Symes, Modeling of a constant Q: Methodology and algorithm for an efficient and optimally inexpensive viscoelastic technique, *Geophysics* **60** (1995), pp. 176–184.

[3] T. Bohlen, Parallel 3D viscoelastic finite difference seismic modelling, *Computers and Geosciences* **28** (2002), pp. 887–899.

[4] R. Kamei and R. G. Pratt, Inversion strategies for visco-acoustic waveform inversion, *Geophysical Journal International* **194** (2013), pp. 859–884.

[5] A. Kurzmann, A. Przebindowska, D. Köhn and T. Bohlen, Acoustic full waveform tomography in the presence of attenuation: a sensitivity analysis, *Geophysical Journal International* **195** (2013), pp. 985–1000.

[6] H.-P. Liu, D. L. Anderson and H. Kanamori, Velocity dispersion due to

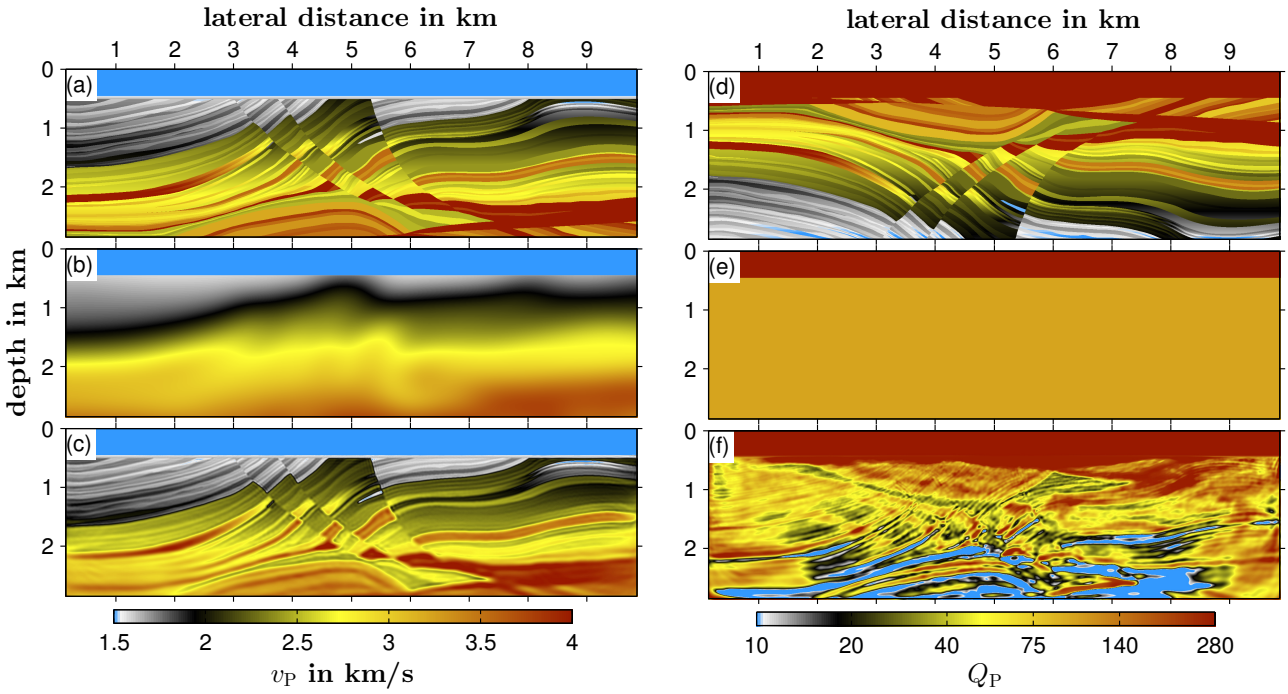

Figure 1: v_P model: true (a), initial (b), final (c); Q_P model: true (d), initial (e), final (f)

anelasticity; implications for seismology and mantle composition, *Geophysical Journal International* **47** (1976), pp. 41–58.

[7] R.-E. Plessix, A review of the adjoint-state method for computing the gradient of a functional with geophysical applications, *Geophysical Journal International* **167** (2006), pp. 495–503.

[8] Z. Song, P. Williamson and R. Pratt, Frequency-domain acoustic-wave modeling and inversion of crosshole data: Part II – Inversion method, synthetic experiments and real-data results, *Geophysics* **60** (1995), pp. 796–809.

Waveform inversion across the scales: A terrestrial perspective

Andreas Fichtner[1,*]

[1]Department of Earth Sciences, ETH Zurich, Zurich, Switzerland

[*]Email: andreas.fichtner@erdw.ethz.ch

Abstract

We present a method for the joint full waveform inversion for small-scale shallow-layer structure and deeper larger-scale heterogeneities. The simultaneous inversion of higher-frequency data within smaller submodels and lower-frequency data in the surrounding domain overcomes the numerical bottleneck that arises from the need to mesh high-resolution subregions very densely. Following a brief description of the methodology, we present examples with terrestial seismic waveform data.

Keywords: full waveform inversion, multiscale methods, homogenisation

1 Introduction

Seismic tomography on the Sun and the Earth is a multiscale problem where the resolution of detailed structure affects the reconstruction of large-scale features, and vice versa. The interdependence of scales is particularly pronounced in the relation between hardly resolvable near-surface layers and large-scale deeper structure. On the Earth, the shallow layer corresponds to the thin crust, with thickness varying between 0 and $\sim$ 70 km; that is hardly more than 1 % of the Earth's radius. Resolution of crustal structure requires denser networks and higher-frequency seismic data than resolution of deeper mantle structure. The fine grid spacing needed locally to image details of the shallow crust creates a numerical bottleneck in traditional waveform inversion techniques.

Here we present a novel approach to multiscale full seismic waveform inversion based on the simultaneous inversion within subvolumes of variable scale, ranging from few hundreds of kilometres to the globe [1]. Following a condensed outline of the method, we present a real-data application to the crust and mantle of the Eurasian continent.

2 Multi-scale full waveform inversion

Our method rests on the decomposition of the structural model domain into smaller subvolumes for which more densely sampled higher-frequency data are available. Typically, on the Earth, these subvolumes are defined by regions with high seismicity and deployments of dedicated seismometer arrays with an inter-station spacing much less than the global average.

Within each subdomain, we perform traditional full seismic waveform inversions based on the combination of spectral-element wave propagation and adjoint techniques [2, 3].

Inversions in differently sized subdomains are coupled with the help of non-periodic homogenisation [4]. Following, for instance, an inversion of higher-frequency data within a smaller subdomain, the obtained high-resolution model is upscaled such that it can be meshed with a grid size similar to the one in the surrounding lower-resolution domain. Subsequently, the larger-scale domain is updated by a full waveform inversion that uses lower-frequency data from less densely spaced receivers. This procedure is repeated until the data in all submodels, including the largest-scale base model, are explained to within the noise.

Our domain decomposition strategy circumvents the numerical bottleneck that arises from the requirement of a dense mesh in high-resolution regions, and it can be applied to an arbitrary number of subvolumes on any scale where suitable data are available.

3 Application

We illustrate our method with a multi-scale full waveform inversion of the Eurasian continent. Embedded high-resolution subregions include Anatolia and the western Mediterranean. On the continental scale we used 14, 525 recordings from 84 earthquakes in the period range from 30-200 s, meaning that these data mostly constrain upper-mantle structure. This was complemented by 2, 312 regional recordings from 29 earthquakes in Turkey with periods from 8-50 s that provide additional information on crustal heterogeneities. Furthermore, we added 13, 089 recordings with periods from 12-120 s from 52 earthquakes in the western Mediterranean region.

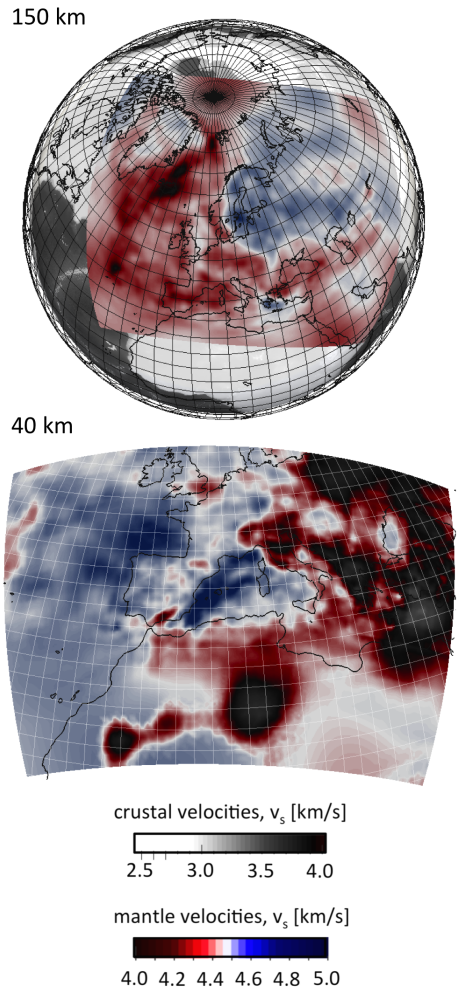

Figure 1: Shear velocity structure beneath Eurasia. **Top**: Mantle structre at 150 km depth. **Bottom**: Zoom into the shallow (crustal) structure in the Mediterranean region at 40 depth.

Our final model shown in figure 1 is distinguished by the joint resolution of shallow crustal structure and the underlying mantle to depths of nearly $1,500$ km. This indicates that multi-scale full waveform inversion is capable of bridging the classical gap between crustal and mantle tomography.

Acknowledgements

The author acknowledges M. Afanasiev, Y. Capdeville, P. Cupillard, A. Gokhberg, E. Saygin and A. Villaseñor, as well as the Swiss National Supercomputing Center (projects CH1 and GeoScale).

References

[1] A. Fichtner, J. Trampert, P. Cupillard, E. Saygin, T. Taymaz, Y. Capdeville and A. Villaseñor, Multi-scale full waveform inversion, *Geophysical Journal International* **194** (2013), pp. 534-556.

[2] C. Tape, Q. Liu, A. Maggi and J. Tromp, Seismic tomography of the southern California crust based upon spectral-element and adjoint methods, *Geophysical Journal International* **180** (2010), pp. 433-462.

[3] A. Fichtner, B. L. N. Kennett, H. Igel and H.-P. Bunge, Full seismic waveform tomography for upper-mantle structure in the Australasian region using adjoint methods, *Geophysical Journal International* **179** (2009), pp. 1703-1725.

[4] Y. Capdeville, L. Guillot and J. J. Marigo, 2-D nonperiodic homogenization to upscale elastic media for P-SV waves, *Geophysical Journal International* **182** (2010), pp. 903-922.

Minisymposium: Wave-based Discretizations
organised by David Hewett and Andrea Moiola

Wave propagation problems are notoriously difficult to solve numerically in the high frequency regime when the wavelength is short compared to the size of the scatterer or the propagation domain. Conventional numerical methods such as the finite element method or the boundary element method, based on piecewise polynomial approximations, suffer from the limitation that a fixed number of degrees of freedom per wavelength is required in each spatial dimension in order to represent the oscillations in the solution, which leads to high computational cost at high frequencies. A promising and rapidly developing methodology for reducing this cost is to use wave-based discretisations, which use approximation spaces built from oscillatory functions (often solutions of the homogeneous wave equation under consideration) which can more efficiently approximate the wave solution than can piecewise polynomials. The wave-based approach has been developed in many contexts, in standard FEM, DG and BEM, both in the frequency domain, and recently in the time domain. It has been successfully applied to problems in acoustics, electromagnetics and structural mechanics. This minisymposium will bring together experts in wave-based discretisations selected from these areas, with the aim of fostering communication, collaboration and the exchange of novel analytical and computational techniques.

Asymptotic Solution of High-Frequency Multiple Scattering Problems

Samuel Groth[1], **Daan Huybrechs**[2,*], **Peter Opsomer**[2]
[1]Department of Mathematics, University of Reading, United Kingdom
[2]Department of Computer Science, University of Leuven, Belgium
*Email: daan.huybrechs@cs.kuleuven.be

Abstract

Waves propagating in a configuration with multiple scattering obstacles at high frequency can be seen as a collection of rays bouncing back and forth. We show how to derive the asymptotic expansion of each of these rays to high order, including after several reflections, for the two-dimensional Helmholtz equation based on an integral equation formulation. It is known that rays can get trapped in a finite number of periodic orbits in the scene, corresponding to quasi-resonance modes. This is discouraging for phase extraction methods in a raytracing scheme for solving the integral equation. However, we show that these rays quickly settle down to an asymptotic regime after a few reflections, possibly enabling phase extraction for the entire mode at once.

Keywords: high-frequency scattering, asymptotic analysis, ray tracing

1 Introduction

It is well known that high-frequency solutions to the Helmholtz equation

$$\Delta u + k^2 u = 0$$

exhibit asymptotic behaviour. The asymptotic analysis is typically localized, in the sense that the path of a ray through a scene is determined by local properties of the medium and any obstacles in its way. A prime example is the principle of reflection of light: a light ray that hits an obstacle reflects in a direction such that incoming and outgoing directions make equal angles with the normal at the surface in the contact point. Higher order terms depend on the local curvature of the obstacle.

We are interested in a full expansion of the solution, in the form

$$u(x) \sim \sum_{j=0}^{\infty} u_j(x)\, k^{-j}. \qquad (1)$$

Typically, the phase of the asymptotic solution is determined from the governing PDE via the *eikonal equation*, and subsequent terms in an expansion of the form (1) can be found recursively by solving *transport equations* [1].

More specifically, we wish to obtain the asymptotic expansion of a related integral equation, explicitly and to high order. Consider the integral equation of the first kind

$$\int_\Gamma K(x,y)v(y)\mathrm{d}s_y = -u^i(x), \qquad x \in \Gamma \quad (2)$$

where $u^i(x)$ is an incoming wave field, $\Gamma = \partial\Omega$ is the boundary of a scattering obstacle Ω and

$$K(x,y) = \frac{i}{4} H_0^{(1)}(k|x-y|)$$

is the Green's function of the 2D Helmholtz equation. The asymptotic expansion of the density function $v(y)$ was derived for a similar setting in [2], and subsequent work focused on 3D and other wave equations.

Furthermore, we aim for the asymptotic expansion of $v(y)$ after several reflections, and an analysis of the periodic orbits of trapped rays in a configuration with multiple scattering obstacles. Details of the derivation are found in [4].

2 Single reflections

The key to an asymptotic expansion for $v(y)$ in (2), is to plug in an appropriate ansatz for $v(y)$. We assume a right hand side of the form

$$-u^i(x) = -u_s^i(x) e^{ikg(x)}, \qquad x \in \Gamma$$

where $u_s^i(x)$ is a non-oscillatory function on at least a part of Γ, which furthermore satisfies

$$u_s^i(x) \sim \sum_{i=0}^{\infty} u_{s,j}^i(x)\, k^{-j}. \qquad k \to \infty \quad (3)$$

Locally near a point of reflection x, an incoming ray induces a reflecting ray corresponding to a density with the same phase $g(x)$. The ansatz for v is

$$v(y) \sim e^{ikg(y)} \sum_{i=-1}^{\infty} v_j(y)\, k^{-j}. \qquad k \to \infty \quad (4)$$

The coefficient functions $v_j(y)$ can be determined recursively by plugging (3) and (4) into equation (2), expanding the integrals in the left hand side asymptotically, and equating terms of equal asymptotic order in k in left and right hand sides. The integrals are expanded analytically using the steepest descent method in terms of the values and derivatives of a smooth parameterization $\kappa(t) : [a, b] \to \Gamma$. Similar integrals were evaluated analytically in [2] using known expressions involving Hankel functions.

3 Multiple reflections

The solution to (2) can be determined asymptotically, with high order terms, at a point x on the boundary. This results in a reflected wave at points $z \in \mathbb{R}^2$ in the field, along the ray bouncing off the point x. The phase at the point z is $g(x) + |z - x|$, and the direction of the reflected ray is such that x is a stationary point for the oscillatory integral formally written as

$$\int_\Gamma K(z, y) e^{ikg(y)} \left(\sum_{i=-1}^{\infty} v_j(y)\, k^{-j} \right) \mathrm{d}s_y. \quad (5)$$

This integral, too, can be expanded asymptotically using the known expansion of the Hankel function for large argument and by localizing the integral around the stationary point x – which is precisely where the expansion of v is valid.

It is reasonably straightforward to follow the path of a ray throught a scene. A more complicated problem is the inverse, namely to determine which rays will leave the scene in a certain direction. Indeed, several rays passing through the scene may end up leaving in the same direction. Infinitely many, in fact, since rays can stay within the configuration arbitrarily long close to the periodic orbits, before leaving. For the forward problem, experiments indicate that a small number of iterations are sufficient for an accurate solution, using higher order terms. Furthermore, it appears possible to compute the tail of the iterations in one go by solving for quasi-resonance modes.

4 Quasi-resonance modes

We end with a few observations regarding the rays that are trapped indefinitely in a multiple scattering configuration, travelling in periodic orbits along the paths that minimize the distance between two or more of the obstacles in the scene [3]. These orbits are independent of the incoming wave. The phases of the subsequently reflected waves quickly settle down to an asymptotic limit. Moreover, the corresponding amplitudes settle down to an asymptotic distribution also, decreasing by a fixed constant factor after each orbit due to the constant loss of energy in rays leaving the scene.

Rays in such an orbit have the same phase, up to a constant phase shift, each time they hit one of the obstacles along their path. This means that these phases can be extracted for all iterations at once. The remaining smooth amplitude functions can conceivably be solved from a coupled integral equation formulation.

References

[1] V. M. Babich and V. S. Buldyrev, *Short-wavelength diffraction theory*, Springer-Verlag, Berlin, 1991.

[2] O. Bruno and M. Caponi and A. Sei, High-order high-frequency solutions of rough surface scattering problems, *Radio Science* **37** (2002), pp. 1049–1061.

[3] F. Ecevit and F. Reitich, Analysis of multiple scattering iterations for high-frequency scattering problems. I: The two-dimensional case, *Numerische Mathematik* **114** (2009), pp. 271–354.

[4] S. Groth and D. Huybrechs, High order terms in the ray expansion for high frequency scattering by single and multiple obstacles, *in preparation.*

Hybrid numerical asymptotic approximation for multiple scattering problems

A. Gibbs[1,*], **S.N. Chandler-Wilde**[1], **S. Langdon**[1], **A. Moiola**[1]
[1]Department of Mathematics and Statistics, University of Reading, UK
*Email: a.j.gibbs@pgr.reading.ac.uk

Abstract

Standard numerical schemes for scattering problems have a computational cost that grows at least in direct proportion to the frequency of the incident wave. For many problems of scattering by single obstacles, it has been shown that a careful choice of approximation space, utilising knowledge of high frequency asymptotics, can lead to numerical schemes whose computational cost is independent of frequency. Here, we extend these ideas to multiple scattering configurations, focusing in particular on the case of two scatterers, with one much larger than the other.

Keywords: Multiple scattering, BEM, high frequency, Helmholtz equation, Hybrid Numerical Asymptotic method

1 Introduction

We consider the problem of scattering of a time-harmonic incident wave $u^i(\mathbf{x}) := \exp(ik\mathbf{x}\cdot\mathbf{d})$ propagating in direction $\mathbf{d}$ with wavenumber $k>0$, by multiple sound-soft scatterers in two-dimensions. For simplicity, here we consider the case of two scatterers as shown in Figure 1. We assume the larger scatterer is a convex polygon with boundary Γ and denote the boundary of the smaller scatterer by γ. What follows may also be applied to more general cases where γ is the union of many scatterers, which are not required to be convex or polygonal. Our boundary value problem is: Find $u \in H^1_{\text{loc}}(D)\cap C^2(D)$, such that

$$(\Delta + k^2)u = 0 \text{ in } D, \quad u = 0 \text{ on } \Gamma\cup\gamma, \qquad (1)$$

where $D\subset\mathbb{R}^2$ is the complement of the scatterers and the scattered field $u^s := u - u^i$ satisfies the Sommerfeld radiation condition.

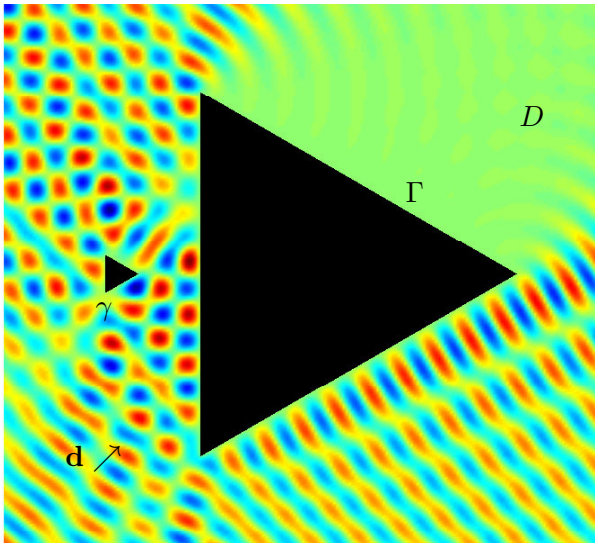

Figure 1: $\text{Re}(u)$ in D, scattering by two triangles. $|\Gamma| = 6\pi$, $|\gamma| = 3\pi/5$, $k = 10$, $\mathbf{d} = 2^{-1/2}(1,1)^T$.

Using the standard Green's representation formula (see e.g. [3]), the problem reduces to finding $\partial u/\partial n$ on $\Gamma\cup\gamma$. We use a direct formulation

$$\mathcal{A}\left[\frac{\partial u}{\partial n}\right] = f \quad \text{on } \Gamma\cup\gamma, \qquad (2)$$

where $\mathcal{A}$ is the standard combined layer integral operator as in (for example) [1] and f consists of known boundary data. For problems with a low wavenumber k, a standard BEM can approximate $\partial u/\partial n$ with piecewise polynomials φ_ℓ:

$$\frac{\partial u}{\partial n}(\mathbf{x}) \approx \sum_{i=1}^{M_\gamma} \beta_i\varphi_i(\mathbf{x}) \quad \text{on } \gamma, \quad \alpha_i\in\mathbb{C}. \qquad (3)$$

With this approach, the number of degrees of freedom M_γ must increase at least linearly with k to maintain accuracy.

2 HNA ansatz for a convex polygon Γ

For a single convex scatterer, the Hybrid Numerical Asymptotic (HNA) method [3] is used to enrich the approximation space with carefully chosen oscillatory basis functions, designed

to capture the oscillations of the diffracted waves. The HNA approximation is

$$\frac{\partial u}{\partial n}(\mathbf{x}) \approx \Psi(\mathbf{x}) + \sum_{\ell=1}^{M_\Gamma} \alpha_\ell \phi_\ell(\mathbf{x}) \mathrm{e}^{\mathrm{i}k\psi_\ell(\mathbf{x})}, \quad \mathbf{x} \in \Gamma,$$

where Ψ is the geometrical optics approximation which represents the reflected wave. The phases ψ_ℓ are chosen a priori, only the (non-oscillatory) amplitudes of these oscillations are approximated by the piecewise polynomials ϕ_ℓ with M_Γ degrees of freedom.

3 Extension of the HNA ansatz to multiple scatterers

The HNA ansatz can be extended to account for multiple scatterers [2], with an additional term representing the contribution to the solution on Γ from the solution on γ. The approximation on Γ becomes

$$\frac{\partial u}{\partial n}\Big|_\Gamma(\mathbf{x}) \approx \Psi(\mathbf{x}) + \sum_{\ell=1}^{M_\Gamma} \alpha_\ell \phi_\ell(\mathbf{x}) \mathrm{e}^{\mathrm{i}k\psi_\ell(\mathbf{x})} + \sum_{i=1}^{M_\gamma} \beta_i \mathcal{G}\varphi_i(\mathbf{x}) \tag{4}$$

where $\mathcal{G} : H^{-1/2}(\gamma) \to H^{-1/2}(\Gamma)$ is defined by

$$\mathcal{G}\varphi(\mathbf{x}) := -2 \int_{\gamma \cap U_j} \frac{\partial \Phi(\mathbf{x}, \mathbf{y})}{\partial n(\mathbf{x})} \varphi(\mathbf{y}) \, \mathrm{d}s(\mathbf{y}), \quad \mathbf{x} \in \Gamma_j,$$

for each side Γ_j of Γ. Here Φ is the fundamental solution to the Helmholtz equation and U_j is the half-plane with Γ_j situated along its boundary, such that $\Gamma \not\subset U_j$ (as in Figure 2). The term $\mathcal{G}[\partial u/\partial n|_\gamma]$ represents the contribution from the solution on γ to the solution on Γ.

4 Numerical results

We solve for the unknown on the large obstacle Γ and small obstacle γ simultaneously, approximating $\partial u/\partial n$ using (4) on Γ and (3) on γ, with piecewise polynomials φ_i and ϕ_ℓ on a graded mesh. A Galerkin method is used with the BIE (2) as in [1]. For each k we observe exponential convergence as the number of degrees of freedom increases, whilst the error does not appear to grow with k for fixed degrees of freedom.

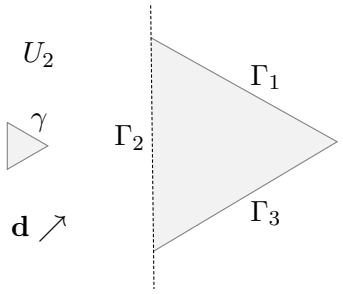

Figure 2: The half-plane U_2 relative to the side Γ_2 for configuration of Figure 1 is the area to the left of the dotted line. Notice that $\operatorname{supp}\{\mathcal{G}[\partial u/\partial n|_\gamma]\} = \Gamma_2$, as the analogous half-planes U_1 and U_3 do not contain γ.

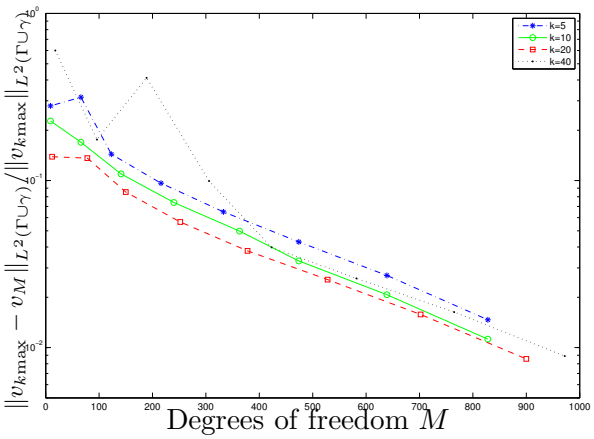

Figure 3: L^2 convergence results. $M := M_\Gamma + M_\gamma$ is the total number of degrees of freedom, whilst $v_{k\max}$ denotes a reference solution for each k, computed with higher M.

References

[1] S. N. Chandler-Wilde and S. Langdon, A Galerkin boundary element method for high frequency scattering by convex polygons *SIAM J. Numer. Anal.* **45**, pp. 610–640.

[2] A. Gibbs et al., HNA BEM for multiple scattering, (in preparation)

[3] S. N. Chandler-Wilde, et al. Numerical-asymptotic boundary integral methods in high-frequency acoustic scattering *Acta Numer.* **21**, pp. 89–305.

A high-frequency boundary element method for a transmission scattering problem

Samuel P. Groth[1,*], **David P. Hewett**[2], **Stephen Langdon**[1]

[1]Department of Mathematics and Statistics, University of Reading, UK

[2]Department of Mathematics, University of Oxford, UK

[*]Email: s.groth@pgr.reading.ac.uk

Abstract

We consider time-harmonic scattering by penetrable polygonal obstacles in 2D. We present a boundary element method (BEM) based on a hybrid numerical-asymptotic (HNA) approximation space built from oscillatory basis functions. The basis functions are carefully chosen to capture the leading order terms in the high-frequency asymptotic behaviour of the boundary solution. Numerical experiments suggest that the method can achieve fixed accuracy using a small (and frequency-independent) number of degrees of freedom, even at high frequencies.

Keywords: Helmholtz, high-frequency scattering, transmission, boundary element method

1 Introduction

It is well-known that conventional numerical methods for time-harmonic scattering problems become computationally expensive when the size of the scattering obstacle is large relative to the wavelength of the incident wave. The HNA boundary element approach (see [1] and the references therein) aims to address this by building the high-frequency oscillatory behaviour of the solution directly into the approximation space.

This is done by making a high-frequency ansatz for the boundary solution of the form

$$V(\mathbf{x}) = V_{go}(\mathbf{x}, k) + \sum_{m=1}^{M} V_m(\mathbf{x}, k) \exp(ik\psi_m(\mathbf{x})), \tag{1}$$

where V_{go} is the geometrical optics (GO) approximation and the summation term represents the diffracted field. The phases ψ_m are chosen by referring to asymptotic methods, such as the Geometrical Theory of Diffraction (GTD). If the phases are chosen correctly, the amplitudes V_m will be slowly varying and hence may be efficiently approximated by low-order polynomials at all frequencies. To date, HNA methods have been applied successfully to problems for which the asymptotics are known and (1) requires only a small number of terms. In particular, to scattering by impenetrable convex, as well as a class of non-convex, polygons.

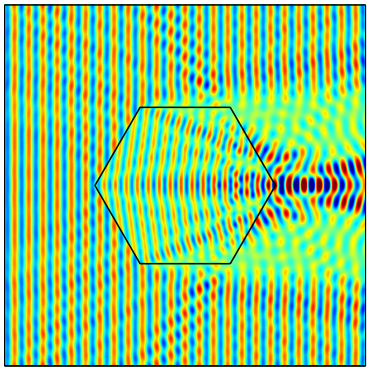

Figure 1: Hexagonal scatterer with $\mu = 1.31$.

The present work extends the HNA methodology to a transmission problem. In this problem, the GO and diffracted components are considerably more complicated owing to internal reflections. In fact, both components comprise infinitely many terms. Furthermore, the relevant canonical problem of scattering by an infinite penetrable wedge has, as yet, no known closed form or asymptotic solution.

In [2] the construction of a HNA approxmation space for this problem, using a heuristic adaptation of classical GTD, was discussed. A beam-tracing algorithm was employed to calculate V_{go} and, in the summation in (1), only the leading order diffracted waves were considered, i.e. both head waves and internal reflections of diffracted waves were ignored. Here we present the implementation of this approximation space within a Galerkin BEM.

2 The transmission problem

Consider the 2D problem of scattering of a time-harmonic wave u^i by a penetrable polygon Ω, as illustrated in Figure 1. We wish to determine the field u_1 in the exterior domain D and the

field u_2 within Ω such that

$$\begin{aligned} &\Delta u_1 + k_1^2 u_1 = 0, \quad \text{in } D := \mathbb{R}^2 \backslash \Omega, \\ &\Delta u_2 + k_2^2 u_2 = 0, \quad \text{in } \Omega, \\ &u_1 = u_2 \text{ and } \frac{\partial u_1}{\partial \mathbf{n}} = \alpha \frac{\partial u_2}{\partial \mathbf{n}}, \quad \text{on } \partial\Omega, \end{aligned} \tag{2}$$

in addition to an outgoing radiation condition for the scattered field $u^s := u_1 - u^i$ at infinity. Here $\alpha \in \mathbb{C}$, k_1, k_2 are the wavenumbers in the exterior and interior domains respectively. We shall write $k_2 = \mu k_1$, μ being the complex refractive index of the scatterer with $\mathrm{Im}(\mu) \geq 0$.

We may employ Green's representation theorem to reformulate (2) as a system of boundary integral equations, for example as

$$AV = f,$$

where $V = (u_1, \partial u_1/\partial \mathbf{n})^T$, $f = \left(u^i, \partial u^i/\partial \mathbf{n}\right)^T$,

$$A = \begin{pmatrix} \frac{1}{2}(I+\alpha) - (D_1 - \alpha D_2) & S_1 - S_2 \\ -\alpha(H_1 - H_2) & \frac{1}{2}(I+\alpha) + (\alpha D_1' - D_2') \end{pmatrix},$$

and S_i, D_i, D_i' and H_i, for $i = 1, 2$, are the single, double, adjoint-double and hypersingular integral operators.

3 HNA for the transmission problem

Our HNA ansatz for V on each side is (as in [2])

$$\begin{aligned} V(\mathbf{x}) \approx V_{go} &+ V_1^+ e^{ik_1 s} + V_1^- e^{-ik_1 s} \\ &+ V_2^+ e^{ik_2 s} + V_2^- e^{-ik_2 s} + \sum_{j=1}^{n-2} V_j^r e^{ik_2 r_j}, \end{aligned}$$

where s is the arc-length along the side, n is the number of corners, and $r_1, \ldots, r_{n-2}$ are the distances between $\mathbf{x}$ and the $n-2$ corners not adjacent to the side. Therefore, this ansatz aims to capture the "primary" diffraction on each side arising from all the corners of the polygon. By primary, we mean that we are excluding the effects of diffracted waves which have undergone at least one internal reflection, and head waves.

Numerically, we aim to approximate the amplitudes $V_i^{\pm}$ by low-order piecewise polynomials on overlapping meshes graded towards the corners. The amplitudes V_j^r are approximated by polynomials on a mesh with elements dictated by discontinuities in V_{go}.

4 Numerical results

The table below presents results for scattering by an equilateral triangle with $\alpha = 1$ at different size parameters ak_1, where a is the radius of the smallest circle which circumscribes the triangle. The maximum polynomial degree in the approximation space is 3. The scattered field u^s is calculated on a circle of radius $3a/2$ with its centre coinciding with that of the triangle. We also calculate the Kirchhoff approximation (KA) on this circle which is obtained by replacing u_1 and $\partial u_1/\partial \mathbf{n}$ in Green's representation formula by their GO approximations on $\partial\Omega$. The errors shown are relative errors calculated in the L^2-norm and the reference solutions are obtained using a standard BEM at high resolution (to ensure an accuracy of $\sim 1e-6$ relative error on Γ).

ak_1	$u_1\|_{\partial\Omega}$ error	u^s error	u_{KA} error	# DOF per λ
20	4.1e-3	2.9e-4	6.2e-2	5.5
40	2.5e-3	1.7e-3	4.6e-2	2.8
80	7.9e-4	4.0e-4	3.2e-2	1.4
160	3.0e-3	1.4e-3	2.3e-2	6.9e-1
320	1.2e-3	5.0e-4	1.64e-2	3.4e-1

We observe that an error of ∼0.4% or less is maintained in both the field on the boundary $u_1|_{\partial\Omega}$ and the scattered field u^s as the size parameter is increased. The number of degrees of freedom (DOF) in the approximation space was fixed at 138 for all ak_1. We note that even with this relatively small number of DOF (corresponding to only 0.34 DOF per wavelength in the case $ak_1 = 320$) we gain a significant improvement over the KA, which is a widely employed asymptotic approach. Moreover, the error in the HNA method appears to be bounded independently of the size parameter.

References

[1] S. N. Chandler-Wilde, I. G. Graham, S. Langdon and E. A. Spence, Numerical-asymptotic boundary integral methods in high-frequency acoustic scattering, *Acta Numer.* **21** (2012), pp. 89–305.

[2] S. P. Groth, D. P. Hewett and S. Langdon, Hybrid numerical-asymptotic approximation for high-frequency scattering by penetrable convex polygons, *IMA J. Appl. Math.* (2013) doi: 10.1093/imamat/hxt040.

BEM-based Finite Element Methods with PDE-adapted basis functions on polygonal and polyhedral meshes

Steffen Weißer[1,*]

[1]Universität des Saarlandes, FR 6.1 – Mathematik, 66123 Saarbrücken, Germany

[*]Email: weisser@num.uni-sb.de

Abstract

In the development of numerical methods for solving boundary value problems the requirement of flexible mesh handling gains more and more importance. The BEM-based Finite Element Method is one of the new promising strategies which yields conforming approximations on polygonal and polyhedral meshes. This flexibility is obtained by special trial functions which are defined implicitly as solutions of local boundary value problems related to the underlying differential equation. Due to this construction, the approximation space already inherits some properties of the unknown solution. These implicitly defined trial functions are treated by means of Boundary Element Methods (BEM) in the numerical realization.

Keywords:
BEM-based FEM, local Trefftz method, nonstandard FEM, polygnoal/polyhedral meshes

1 Introduction and Formulation

Let $\Omega \subset \mathbb{R}^d$, $d = 2, 3$ be a bounded domain and $\mathcal{K}_h$ its decomposition into polygonal and polyhedral subdomains, respectively. We consider the boundary value problem

$$Lu = f \text{ in } \Omega, \quad u = 0 \text{ on } \partial\Omega,$$

where L is an elliptic, second order differential operator with piecewise constant coefficients on the decomposition $\mathcal{K}_h$. The Galerkin formulation reads

$$\text{Find } u \in V: \quad a(u, v) = \varphi(v) \quad \forall v \in V$$

with corresponding bilinear form a, right hand side φ and $V = H_0^1(\Omega)$.

For the discretization, a Trefftz-like approximation space is chosen, which enables the application on polygonal and polyhedral meshes, see Figure 1. The finite dimensional space $V_h \subset V$ for the discrete Galerkin formulation is given via its basis functions $\psi \in \Psi$. Every $\psi \in \Psi$ is defined piecewise on each subdomain $K \in \mathcal{K}_h$

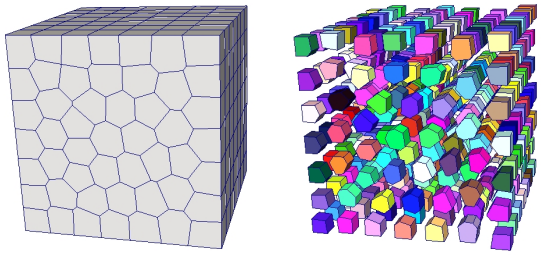

Figure 1: Polyhedral mesh

as solution of a local boundary value problem, cp. Figure 2,

$$L_K\psi = p \text{ in } K, \quad \psi = q \text{ on } \partial K,$$

where L_K is the restriction of L onto K with constant coefficients. In 2D, p and q are suitably chosen polynomials, see [4], whereas a hierarchical construction is proposed in 3D, see [3]. The 3D construction makes use of boundary value problems related to the underlying operator L on faces and edges of the polyhedral subdomains. Due to the global continuity, a conforming approximation space is obtained on general meshes. Its approximation order depends on the choice of p and q. Furthermore, the hierarchical construction yields stabilizing effects in numerical simulations, see [2].

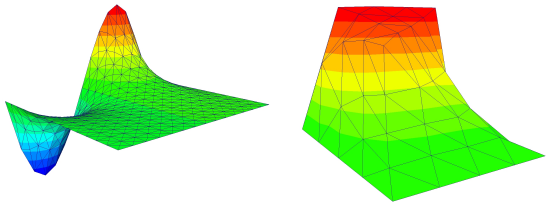

Figure 2: Approximation of third order basis function for $L_K = \Delta$ (left), and of first order basis function for $L_K = \Delta + b \cdot \nabla$ (right) over rectangular element

2 BEM-based approximation

The implicitly defined basis functions are treated by means of Boundary Element Methods. This is possible due to the existence of a fundamental

solution of L_K. For simplicity let $p = 0$, then $\psi \in \Psi$ has the representation

$$\psi(x) = \left(\mathbf{V}_K \gamma_1^K \psi\right)(x) - \left(\mathbf{W}_K \gamma_0^K \psi\right)(x)$$

for $x \in K$, where $\gamma_0^K \psi = q$ and $\gamma_1^K \psi$ is the so called conormal derivative. $\mathbf{V}_K$ and $\mathbf{W}_K$ are boundary integral operators, namely the single and double layer potentials. Obviously, it is sufficient to know the Dirichlet and Neumann traces $\gamma_0^K \psi$ and $\gamma_1^K \psi$, respectively, for the treatment of the basis functions. The unknown trace $\gamma_1^K \psi$ can be expressed by the Steklov-Poincaré operator $\gamma_1^K \psi = \mathbf{S}_K \gamma_0^K \psi$ with

$$\mathbf{S}_K = \mathbf{D}_K + \left(\tfrac{1}{2}\mathbf{I} + \mathbf{K}_K'\right) \mathbf{V}_K^{-1} \left(\tfrac{1}{2}\mathbf{I} + \mathbf{K}_K\right),$$

which employs further boundary integral operators. In the numerical realization, these operators are discretized by Galerkin schemes involving only integrals over the boundary ∂K. Consequently, the dimension of the comparatively small local problems is additionally reduced by one.

In the setup of the global system of linear equations arising from the FEM formulation, it is possible to proceed as usual. In a loop over all elements, the system matrix is assembled by adding the local contributions of the bilinear form. Let a_K be the restriction of a to the element $K \in \mathcal{K}_h$. Thus, Green's first identity yields

$$a_K(u, v) = (L_K u, v)_{L_2(K)} + (\gamma_1^K u, \gamma_0^K v)_{L_2(\partial K)},$$

where the volume integral vanishes for the basis functions with $p = 0$ and the boundary integral can be approximated with the help of the discretized Steklov-Poincaré operator, which serves as local stiffness matrix in the assembling process.

3 Enhancements

The BEM-based FEM has its roots in domain decomposition methods via boundary integral equations and was originally designed for elliptic equations. However, the ideas are transfered into varies directions.

The first results on time dependent problems were presented in [5], where a time stepping scheme was applied to resolve the dependence in the time variable.

Beside of scalar valued approximation, there are results for vector valued problems. In [1], a conforming approximation space for $\mathbf{H}(\mathrm{div})$ was proposed, which benefits from the idea of local, Trefftz-like basis functions treated by means of Boundary Element Methods.

References

[1] Y. Efendiev, J. Galvis, R. Lazarov and S. Weißer, Mixed FEM for second order elliptic problems on polygonal meshes with BEM-based spaces, in: I. Lirkov, S. Margenov, J. Waśniewski (Eds.), *Large-Scale Scientific Computing*, Vol. 8353 of *Lecture Notes in Computer Science*, pp. 331–338, Springer, Berlin Heidelberg, 2014.

[2] C. Hofreither, U. Langer and S. Weißer, Convection adapted BEM-based FEM, *ArXiv e-prints*, arXiv:1502.05954 (2015).

[3] S. Rjasanow and S. Weißer, FEM with Trefftz trial functions on polyhedral elements, *Journal of Computational and Applied Mathematics* **263** (2014), pp. 202–217.

[4] S. Weißer, Arbitrary order Trefftz-like basis functions on polygonal meshes and realization in BEM-based FEM, *Computers & Mathematics with Applications* **67:7** (2014), pp. 1390–1406.

[5] S. Weißer, BEM-based Finite Element Methods with Prospects to Time Dependent Problems, in: *Proceedings of WCCM XI, ECCM V, ECFD VI, Barcelona, Spain, July 2014*, pp. 4420–4427.

Generalized plane waves for variable coefficients.

Lise-Marie Imbert-Gérard[1,*]

[1]Courant Institute of Mathematical Sciences, NYU, New York, NY, USA.

[*]Email: imbertgerard@cims.nyu.edu

Abstract

In order to take into account variable coefficients in a wave-like discretization, Generalized Plane Waves (GPWs) are proposed as basis functions. Their design, properties and use will be discussed in this work.

Keywords: variable coefficients, generalized plane waves, interpolation

1 Introduction

In mathematical models, density fluctuations appear as variable coefficients. Approximating these variable coefficients by piecewise constant functions and use classical plane waves could provide a discretization procedure for such problems. Such plane wave methods are used in the p regime, i.e. using a larger number of basis functions per element for a fixed size of mesh. However this process requires a very refined mesh to obtain a good approximation in a variable coefficient, and therefore ruins the advantages of this type of method. This work proposes to develop wave-like basis functions adapted to variable coefficients. These basis functions, namely the GPWs, are designed locally so that they would be approximated solutions of the adjoint equation, see [2].

2 General Plane Wave design

The design process is based on a local Taylor expansion. Consider the general equation $Lu = 0$ where

$$\begin{aligned} Lu = \nabla \cdot (\mathbf{A}\nabla u) + \alpha(x,y)\partial_x u \\ +\beta(x,y)\partial_y u + \gamma(x,y)u, \end{aligned}$$

with $\mathbf{A} = \begin{pmatrix} A_{11} & A_{12} \\ A_{21} & A_{22} \end{pmatrix} = \mathbf{A}^*$. A GPW φ is defined locally at (x_G, y_G) as a function $\varphi = \exp P(x-x_G, y-y_G)$, $P = \sum_{0\le i+j\le \deg P} \lambda_{i,j} X^i Y^j$.

In order for a GPW to be an approximated solution of the adjoint equation $L^*\varphi = 0$, consider the Taylor expansion of each differential operator applied to the GPW, for instance: denoting for simplicity $(\tilde{x}, \tilde{y}) = (x_G, y_G)$

$$\begin{aligned} \partial_x^2\varphi &= (\partial_x^2 P(\tilde{x},\tilde{y}) + (\partial_x P(\tilde{x},\tilde{y}))^2)\varphi \\ &= \left(\sum_{0\le i+j\le \deg P-2} (i+2)(i+1)\lambda_{i+2,j}\tilde{x}^i\tilde{y}^j \right. \\ &\quad \left. + \left(\sum_{0\le i+j\le \deg P-1} (i+1)\lambda_{i+1,j}\tilde{x}^i\tilde{y}^j \right)^2 \right) \varphi. \end{aligned}$$

To approximate the adjoint equation $L^*\varphi = 0$, we set the lowest order coefficients of the Taylor expansion to zero so that $L^*\varphi = O(|(\tilde{x},\tilde{y})|^q)$. It is equivalent to a nonlinear system with

- $N_u = \frac{(\deg P+1)(\deg P+2)}{2}$ unknowns, the $\lambda_{i,j}$s,
- $N_e = \frac{q(q+1)}{2}$ equations.

For instance the first equation reads

$$\begin{aligned} -2A_{11}\lambda_{2,0} - (A_{12}+A_{21})\lambda_{1,1} - 2A_{22}\lambda_{0,2} \\ -2A_{11}\lambda_{1,0}^2 - (A_{12}+A_{21})\lambda_{0,1}\lambda_{1,0} - 2A_{22}\lambda_{0,1}^2 \\ +\overline{\alpha(x_G,y_G)}\lambda_{1,0} + \overline{\beta(x_G,y_G)}\lambda_{0,1} + \overline{\gamma(x_G,y_G)} = 0. \end{aligned}$$

An explicit method to solve this system will be discussed, based on first a convenient choice for $\deg P$ to ensure that the system is invertible, then a careful study of the linear terms of the system to obtain a systematic resolution algorithm. Moreover this design provides a number of free coefficients $\lambda_{i,j}$, which can be used to build a set of linearly independent GPWs at a given point for the operator L.

3 Interpolation properties

Interpolation properties of the GPWs are extended from interpolation properties of classical plane waves. For the operator $L = -\Delta + \gamma(x,y)$ where γ is any $\mathcal{C}^\infty$ function. Consider a set of p GPWs defined at a given point $\overrightarrow{g} = (x_G, y_G)$, and an order of approximation q such that $L^*\varphi = O(|(\tilde{x},\tilde{y})|^q)$ for each GPW φ. The following interpolation result states a sufficient condition on p and q to get a given order of approximation of u by GPWs.

Theorem 1 *Assume $\Omega \subset \mathbb{R}^2$ is a bounded domain, $n \in \mathbb{N}$ is such that $n > 0$, $q \geq n+1$, $p = 2n+1$. Consider that u is a solution of scalar wave equation $Lu = 0$ which belongs to $\mathcal{C}^{n+1}$. Then there are a linear combination of plane waves u_a depending on γ and n, and a constant $C(\Omega, n)$ depending on γ and n such that for all $\overrightarrow{m} \in \mathbb{R}^2$*

$$\begin{cases} |u(\overrightarrow{m}) - u_a(\overrightarrow{m})| \\ \qquad \leq C(\Omega,n)\,|\overrightarrow{m} - \overrightarrow{g}|^{n+1}\,\|u\|_{\mathcal{C}^{n+1}(\Omega)}\,, \\ \|\nabla u(\overrightarrow{m}) - \nabla u_a(\overrightarrow{m})\| \\ \qquad \leq C(\Omega,n)\,|\overrightarrow{m} - \overrightarrow{g}|^{n}\,\|u\|_{\mathcal{C}^{n+1}(\Omega)}\,. \end{cases} \tag{1}$$

The proof of such a result strongly relies on properties of the polynomial coefficients $\lambda_{i,j}$ that stem from the design process described in the previous paragraph. This proof will be outlined to emphasize the design's importance.

These interpolation properties can be validated numerically as displayed in Figure 1. The numerical orders of convergence match perfectly the theorem's predictions.

4 Applications

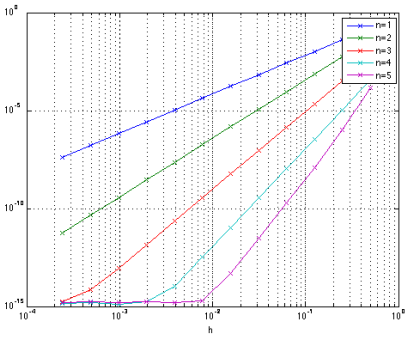

Figure 1: Numerical validation of Theorem 1, showing the relative L^∞ error with respect to $h = \max|(\tilde{x}, \tilde{y})|$, for different values of n.

We incorporated the GPWs in a discretization scheme, by coupling them with the Ultra-Weak Variational Formulation (UWVF). The UWVF was introduced in [1], while the idea of the coupling was proposed in [3].

Some examples of applications will be presented, including a convergence study and plasma oriented simulations. For instance, in order to model what is called an O-mode wave propagating toward a plasma and reflected at a certain cut-off density, consider the operator $L = -\Delta + \gamma(x,y)$ where

$$\gamma(x,y) = \begin{cases} -\kappa^2 & x \leq 2, \\ -\kappa^2(4-x)/2 & x \geq 2. \end{cases}$$

In this model the cut-off is the line along which $\gamma(x,y) = 0$. Figure 2 displays the behavior of a wave sent from an antenna toward a cut-off.

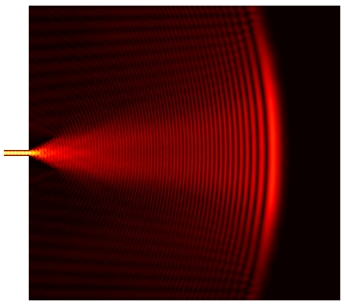

Figure 2: Waves propagating toward and reflected by a cut-off, defined by $\gamma(x,y) = 0$.

References

[1] Després, B. (1994) Sur une formulation variationnelle de type ultra-faible, *C. R. Acad. Sci. Paris Sér. I Math.* **318** no. 10, 939–944.

[2] Imbert-Gérard, Lise-Marie Interpolation properties of generalized plane waves *Numerische Mathematik* (2015) doi:10.1007/s00211-015-0704-y

[3] Imbert-Gerard, L.-M. & Despres, B. A generalized plane-wave numerical method for smooth nonconstant coefficients *IMA Journal of Numerical Analysis*, (2014) **34** (3): 1072-1103.

Study of damping in locally resonant metamaterials through unit cell modelling

Lucas Van Belle[1,*], **Claus Claeys**[1], **Elke Deckers**[1], **Wim Desmet**[1]
[1]KU Leuven, Department of Mechanical Engineering, Division PMA, Leuven, Belgium
*Email: lucas.vanbelle@kuleuven.be

Abstract

Recently, locally resonant metamaterials have shown great potential for noise and vibration control engineering [1]. Understanding the influence of damping is important, as it impacts the performance of these materials. Damping is included in a unit cell modelling technique, the results are studied and are in agreement with earlier findings and measurements.

Keywords: locally resonant metamaterials, stop band, damping, unit cell modelling

1 Introduction

Through the addition of resonant structures to a host structure, sound transmission loss can be improved in specific frequency bands, called stop bands, around their resonant frequency [1].

Periodic structure theory can be used for stop band prediction for the considered structures [1]. Application of Bloch-Floquet periodicity conditions to a finite element unit cell (UC) model yields an eigenvalue problem in the frequency f and propagation constants (μ_x, μ_y). Assuming free wave propagation, thus imaginary propagation vectors $\boldsymbol{\mu} = (\mu_x, \mu_y) = j(\epsilon_x, \epsilon_y)$, this eigenvalue problem can be solved for f. Stop bands emerge as frequency zones for which no free wave propagation is found. Due to periodicity and symmetry of the considered rectangular UC, only solutions along the irreducible Brillouin contour $(\epsilon_x, \epsilon_y) : \mathrm{O} - \mathrm{A} - \mathrm{B} - \mathrm{O} \mapsto (0,0), (\pi,0), (\pi,\pi), (0,0)$ need to be analyzed, leading to dispersion curves as shown in figure 1: for the sake of clarity, only the acoustically relevant out-of-plane bending waves are shown [1].

The resonance based stop band can, however, influence the radiation efficiency of the structure [1]. This is indicated in figure 1, where a stop band below the coincidence frequency creates an additional zone of efficient radiation just above the stop band. Also damping has an important effect, as this increases the frequency range of attenuation, at the expense of peak performance [1]. The introduction of damping and its possible contribution to radiation efficiency is studied.

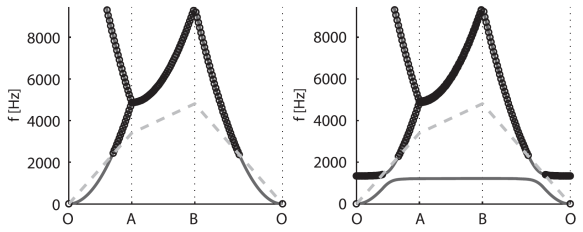

Figure 1: Bending wave dispersion curves along the irreducible Brillouin contour $\mathrm{O}-\mathrm{A}-\mathrm{B}-\mathrm{O} \mapsto (0,0), (\pi,0), (\pi,\pi), (0,0)$ of the structure (——), efficiently radiating free propagating structural waves (∘) and the dispersion curve of air (- - -) for an infinite 5 mm thick steel plate without (left) and with (right) spring-mass resonators tuned at 1171 Hz [1].

2 Dispersion relations with damping

When damping is introduced, previous procedure no longer applies. For real f, the solutions for μ_x and μ_y are complex, implying spatial decay. From observations in [1], the Brillouin contour might no longer contain all necessary information. The eigenvalue problem can be reformulated as a polynomial eigenvalue problem in case f and the direction of wave propagation θ are known, and the ratio $\frac{\mu_y}{\mu_x} = \frac{L_y}{L_x}\tan(\theta)$ is real [2]. This procedure allows calculating complex dispersion relations for various propagation directions.

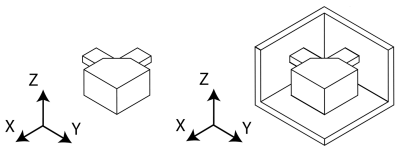

Figure 2: Resonator and UC design from [1] with Z denoting the out-of-plane direction.

In [1] resonant structures were added to a periodic host structure, both polyamide components ($E = 1.65$ GPa, $\rho = 950$ kg/m^3, $\nu = 0.4$), to obtain a stop band between 1065 Hz and 1226 Hz. For the UC, as shown in figure 2, the solutions are calculated along the $\mathrm{O} - \mathrm{A}$ $(= x)$

direction ($\theta = 0$) without damping and with 2% structural damping. The undamped solutions show good agreement, however, now also solutions emerge inside the stop band (figure 3). From figure 4 it is seen that these are complex $\boldsymbol{\mu}$-solutions, in agreement with the solutions for a 1D problem in [1]. These complex solutions represent mainly damped motion of the resonators and strongly damped motion of the host structure, corresponding well to the findings and measurements in [1].

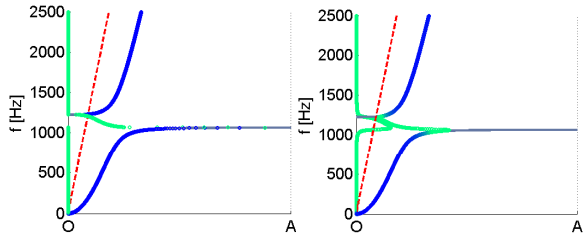

(a) No structural damping(b) 2% structural damping

Figure 3: Bending wave dispersion results for the UC from [1] (free propagating (∘), damped (∘)) without (left) and with (right) 2% structural damping for the $\mathrm{O}-\mathrm{A} \mapsto (0,0),(\pi,0)$ direction, results assuming free wave propagation (——) and dispersion curve of air (- - -).

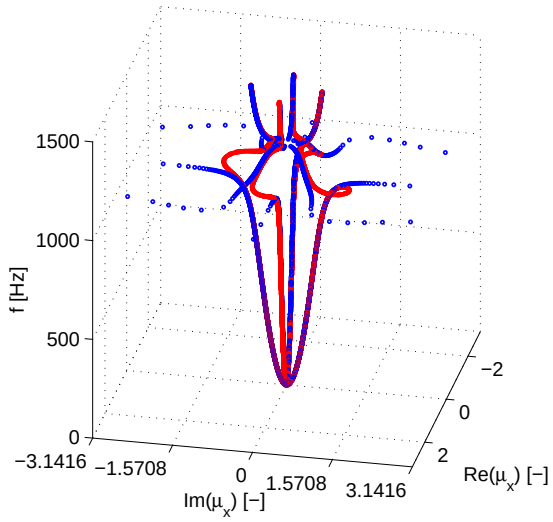

Figure 4: Bending wave dispersion results for the UC from [1] without (∘) and with (∘) 2% structural damping for the $\mathrm{O}-\mathrm{A} \mapsto (0,0),(\pi,0)$ direction: propagating and attenuated part versus frequency.

When damping is added, the definition of a stop band fades, since the dispersion curves seem to close and no longer cover the entire Brillouin contour (figure 3b), as was also found for the 1D problem in [1]. As shown in figure 4, the addition of damping leads to the formation of loops in the complex $\boldsymbol{\mu}$-space. Previously purely propagating solutions become damped, while purely decaying solutions become partly propagating.

Similar to [1], the size of the complex solution loops varies with the amount of damping. Depending on the distance from the air dispersion curve, location of the stop band and magnitude of the real part of the propagation vector, the presence of damping could strongly impact the effectiveness of the metamaterial by causing a larger zone of efficient radiation. Consequently, the presence of damping might result in an even bigger zone of efficient radiation than can be expected by assuming free wave propagation.

3 Conclusions

A procedure is implemented for calculating complex dispersion relations for locally resonant metamaterial UC models with damping. Good agreement is found with solution procedures for free propagating waves and earlier results and measurements. It becomes clear that a thorough understanding of damping phenomena is important for accurate prediction of the acoustic behaviour of resonant metamaterial based stop bands.

Acknowledgements

Lucas Van Belle is a doctoral fellow and Elke Deckers is a postdoctoral fellow of the Fund for Scientific Research Flanders (F.W.O.). The European Commission is acknowledged for their support through the ENLIGHT project (http://www.project-enlight.eu/) and the KU Leuven for their support through an IOF-Leverage project.

References

[1] C. Claeys. *Design and Analysis of Resonant Metamaterials for Acoustic Insulation.* PhD thesis, KU Leuven - Faculty of Engineering Science, 2014.

[2] B. Mace and E. Manconi. Modelling wave propagation in two-dimensional structures using finite element analysis. *Journal of Sound and Vibration*, 318(4-5):884–902, 2008.

The space-time Trefftz discontinuous Galerkin method for the wave equation

Fritz Kretzschmar[1], **Andrea Moiola**[2,*], **Ilaria Perugia**[3], **Sascha M. Schnepp**[4]

[1]Graduate School of Computational Engineering, TEMF, TU Darmstadt Germany
[2]Department of Mathematics and Statistics, University of Reading, UK
[3]Faculty of Mathematics, University of Vienna, Austria
[4]Institute of Geophysics, Department of Earth Sciences, ETH Zürich, Switzerland
[*]Email: a.moiola@reading.ac.uk

Abstract

We consider a space-time DG scheme for the scalar wave equation in which the basis functions are (polynomial) piecewise solutions of the same equation. We show well-posedness and quasi-optimality. In one space dimension, we prove high order, fully explicit, *hp* error bounds in L^2 norm.

Keywords: Trefftz method, discontinuous Galerkin method, space-time finite elements, linear wave equation, a priori error analysis.

1 The model problem

We consider the initial boundary value problem for the homogeneous wave equation with Dirichlet boundary conditions, written as a first-order system as follows:

$$\begin{aligned}
&\nabla v + \frac{\partial \boldsymbol{\sigma}}{\partial t} = \mathbf{0} && \text{in } Q, \qquad (1)\\
&\nabla \cdot \boldsymbol{\sigma} + \frac{1}{c^2}\frac{\partial v}{\partial t} = 0 && \text{in } Q,\\
&v(\cdot,0) = v_0, \quad \boldsymbol{\sigma}(\cdot,0) = \boldsymbol{\sigma}_0 && \text{on } \Omega,\\
&v(\mathbf{x},\cdot) = g, && \text{on } \partial\Omega \times [0,T],
\end{aligned}$$

where $\Omega \subset \mathbb{R}^n$ is a bounded Lipschitz domain with outward unit normal $\mathbf{n}$, $n \geq 1$, $Q := \Omega \times (0,T)$ with $T > 0$; $v_0, \boldsymbol{\sigma}_0, g$ are the problem data; $c>0$ is the wave speed, which is assumed to be piecewise constant and independent of t. The nabla symbol ∇ represents derivation in the space variable $\mathbf{x}$ only. The equations in (1) may be derived from the wave equation $-\Delta U + c^{-2}\frac{\partial^2}{\partial t^2}U = 0$ setting $v = \frac{\partial U}{\partial t}$ and $\boldsymbol{\sigma} = -\nabla U$.

2 Space-time DG and Trefftz methods

Among the countless numerical schemes devised for the approximation of problem (1), the *space-time discontinuous Galerkin* (DG) methods offer high-order accuracy, great flexibility, ease of implementation, space-time *hp*-refinement.

To reduce the number of degrees of freedom needed to achieve a given accuracy and to incorporate the wave speed into the trial space, we propose a *Trefftz method*, namely a scheme in which all the discrete basis functions, when restricted to a mesh element, are solution of the PDE to be discretised. Trefftz methods have been successfully used and analysed for time-harmonic waves, see e.g. [1] and references therein, while in time-domain they appeared only recently in [3–5], where the acoustic and the electromagnetic wave equations are considered.

3 Mesh assumptions and DG notation

We introduce a mesh $\mathcal{T}_h$ on Q, such that its elements are Cartesian products of Lipschitz polytopes in $\mathbb{R}^n$ and time intervals. We assume that the parameter c is constant in each element. We call "space-like" the faces lying in a constant-time hyperplane and "time-like" those orthogonal to them. We denote with $\mathcal{F}_h := \bigcup_{K\in\mathcal{T}_h} \partial K$ the mesh skeleton, $\mathcal{F}_h^{\text{space}}$ the union of the internal space-like faces, $\mathcal{F}_h^{\text{time}}$ the union of the internal time-like faces, $\mathcal{F}_h^0 := \Omega \times \{0\}$, $\mathcal{F}_h^T := \Omega \times \{T\}$ and $\mathcal{F}_h^\partial := \partial\Omega \times [0,T]$.

On a time-like interface between two elements K_1 and K_2, with outward unit normal vectors $\mathbf{n}^x_{K_1} = -\mathbf{n}^x_{K_2}$, we define the averages and the normal jumps of piecewise-continuous scalar (w) and vector ($\boldsymbol{\tau}$) fields in the standard DG fashion:

$$\begin{aligned}
&\{\!\{w\}\!\} := \frac{w_{|_{K_1}} + w_{|_{K_2}}}{2}, \quad \{\!\{\boldsymbol{\tau}\}\!\} := \frac{\boldsymbol{\tau}_{|_{K_1}} + \boldsymbol{\tau}_{|_{K_2}}}{2},\\
&[\![w]\!]_x := w_{|_{K_1}}\mathbf{n}^x_{K_1} + w_{|_{K_2}}\mathbf{n}^x_{K_2},\\
&[\![\boldsymbol{\tau}]\!]_x := \boldsymbol{\tau}_{|_{K_1}} \cdot \mathbf{n}^x_{K_1} + \boldsymbol{\tau}_{|_{K_2}} \cdot \mathbf{n}^x_{K_2}.
\end{aligned}$$

On $\mathcal{F}_h^{\text{space}}$, we denote by w^- and w^+ the traces of the function w from the adjacent elements at lower and higher times, respectively.

Seek $(v_{hp}, \boldsymbol{\sigma}_{hp}) \in \mathbf{V}(\mathcal{T}_h)$ such that $\quad a(v_{hp}, \boldsymbol{\sigma}_{hp}; w, \boldsymbol{\tau}) = \ell(w, \boldsymbol{\tau}) \quad \forall (w, \boldsymbol{\tau}) \in \mathbf{V}(\mathcal{T}_h)$, where

$$a(v_{hp}, \boldsymbol{\sigma}_{hp}; w, \boldsymbol{\tau}) := \int_{\mathcal{F}_h^{\text{space}}} \big(c^{-2} v_{hp}^-(w^- - w^+) + \boldsymbol{\sigma}_{hp}^- \cdot (\boldsymbol{\tau}^- - \boldsymbol{\tau}^+)\big)\mathrm{d}\mathbf{x} + \int_{\mathcal{F}_h^T} (c^{-2} v_{hp} w + \boldsymbol{\sigma}_{hp} \cdot \boldsymbol{\tau})\mathrm{d}\mathbf{x}$$

$$+ \int_{\mathcal{F}_h^{\text{time}}} \big(\{\!\{v_{hp}\}\!\}[\![\boldsymbol{\tau}]\!]_x + \{\!\{\boldsymbol{\sigma}_{hp}\}\!\} \cdot [\![w]\!]_x + \alpha [\![v_{hp}]\!]_x \cdot [\![w]\!]_x + \beta [\![\boldsymbol{\sigma}_{hp}]\!]_x [\![\boldsymbol{\tau}]\!]_x\big)\mathrm{d}S + \int_{\mathcal{F}_h^\partial} \big(\boldsymbol{\sigma} \cdot \mathbf{n} + \alpha v_{hp}\big) w \mathrm{d}S,$$

$$\ell(w, \boldsymbol{\tau}) := \int_{\mathcal{F}_h^0} (c^{-2} v_0 w + \boldsymbol{\sigma}_0 \cdot \boldsymbol{\tau})\mathrm{d}\mathbf{x} + \int_{\mathcal{F}_h^\partial} g(\alpha w - \boldsymbol{\tau} \cdot \mathbf{n})\mathrm{d}S.$$

4 The Trefftz-DG method

We define the Trefftz space

$$\mathbf{T}(\mathcal{T}_h) := \Big\{(w, \boldsymbol{\tau}) \in L^2(Q)^{1+n}, \text{ s.t.}$$
$$(w|_K, \boldsymbol{\tau}|_K) \in H^1(K)^{1+n},$$
$$\nabla w + \frac{\partial \boldsymbol{\tau}}{\partial t} = \mathbf{0}, \nabla \cdot \boldsymbol{\tau} + c^{-2} \frac{\partial w}{\partial t} = 0 \; \forall K \in \mathcal{T}_h\Big\},$$

and fix a finite-dimensional subspace $\mathbf{V}(\mathcal{T}_h) \subset \mathbf{T}(\mathcal{T}_h)$ (arbitrary at this stage). Extending the derivation of [2] (which in turn extends [3]) we obtain the Trefftz-DG variational formulation displayed in the box. Here $0 \le \alpha \in L^\infty(\mathcal{F}_h^{\text{time}} \cup \mathcal{F}_h^\partial)$ and $0 \le \beta \in L^\infty(\mathcal{F}_h^{\text{time}})$ are penalisation parameters. We use upwind fluxes on space-like faces and centred fluxes with jump penalisation on time-like faces.

5 A priori error analysis

Assume that the penalisation parameters α and β are uniformly positive. After defining two mesh-dependent norms on $\mathbf{T}(\mathcal{T}_h)$, which we denote $|||\cdot|||_{DG}$ and $|||\cdot|||_{DG^+}$, proceeding again as in [2, §4.1] we can prove that the bilinear form is continuous and coercive, thus the method is well-posed and quasi-optimality holds:

$$|||(v, \boldsymbol{\sigma}) - (v_{hp}, \boldsymbol{\sigma}_{hp})|||_{DG} \le 3 \inf_{(w,\boldsymbol{\tau}) \in \mathbf{V}(\mathcal{T}_h)} |||(v, \boldsymbol{\sigma}) - (w, \boldsymbol{\tau})|||_{DG^+}.$$

It is easy to show that for $g = 0$ (homogeneous boundary conditions) the method is dissipative and that energy is dissipated through the jumps of the discrete solution across mesh interfaces. Numerical tests show that the amount of dissipation is small, decreases for "high order" discrete spaces, and has a stabilising effect; it may be further reduced using non-penalised methods ($\alpha = \beta = 0$).

In one space dimensions, if the wave speed c is constant, we show that the $L^2(Q)$ norm of the error is controlled by the DG norm [2, §4.2].

6 Discrete Trefftz spaces

Given $p \in \mathbb{N}$, the discrete Trefftz space $\mathbf{V}(\mathcal{T}_h)$ can be chosen as $\prod_{K \in \mathcal{T}_h} \mathbf{V}_p(K)$, where $\mathbf{V}_p(K)$ is the space of the solutions $(w, \boldsymbol{\tau})$ of the wave equation in K that are polynomials of degree at most p. The space $\mathbf{V}_p(K)$ has dimension of order $\mathcal{O}_{p\to\infty}(p^n)$, thus for high polynomial degrees it is much smaller than the full (space-time) polynomial space $\mathbb{P}^p(\mathbb{R}^{n+1})^{1+n}$, which has dimension $\mathcal{O}_{p\to\infty}(p^{n+1})$.

A basis of the Trefftz space can be constructed using "transport polynomials" in the form $(\mathbf{x} \cdot \mathbf{d}_j - ct)^\ell$ for $0 \le \ell \le q$, where the propagation directions $\mathbf{d}_j \in \mathbb{R}^n$, $|\mathbf{d}_j| = 1$, are suitably chosen.

In one space dimension we prove *hp* best approximation estimates for this space. This leads to a priori, fully explicit, high order, *hp*-error bounds for the Trefftz-DG method [2, §6].

Future work includes the extension of the scheme to general meshes and of the L^2 stability and approximation results to higher dimensions.

References

[1] R. Hiptmair, A. Moiola, and I. Perugia, *Appl. Num. Math.* **79** (2014), pp. 79–91.

[2] F. Kretzschmar, A. Moiola, I. Perugia and S. M. Schnepp, *arXiv:1501.05253* (2015).

[3] F. Kretzschmar, S. M. Schnepp, I. Tsukerman, and T. Weiland, *J. Comput. Appl. Math.* **270** (2014), pp. 211–222.

[4] S. Petersen, C. Farhat, and R. Tezaur, *Internat. J. Numer. Methods Engrg.* **78** (2009), pp. 275–295.

[5] D. Wang, R. Tezaur, and C. Farhat, *Internat. J. Numer. Methods Engrg.* **99** (2014), pp. 263–289.

A Trefftz time-space discontinuous Galerkin method for the second-order wave equation

Lehel Banjai[1], **Emmanuil Georgoulis**[2], **Oluwaseun F Lijoka**[3]

[1]Maxwell Institute, Department of Mathematics, Heriot-Watt University
[2]Department of Mathematics, University of Leicester
[3]Department of Mathematics, Heriot-Watt University

Abstract

We develop a time-space discontinuos Galerkin method that allows the use of local solutions of the homogeneous wave equation as basis functions of the discrete space. The method gives rise to an implicit, dissipative time-scheme. Numerical experiments show excellent accuracy for few degrees of freedom of the scheme.

Keywords: Trefftz methods, wave equation, time-space dG methods

1 Introduction

In recent years there has been much interest in using Trefftz methods for solving medium to high frequency wave problems in the frequency domain. Lately this interest has spread to the time domain. Our formulation is most similar to [1], that uses Lagrange multiplyer technique unlike our method based on interior penalty dG.

We will consider the wave equation

$$\begin{aligned} \frac{1}{c(x)^2}\ddot{u} - \Delta u &= 0 && \text{in } \Omega\times[0,T],\\ u &= 0 && \text{on } \partial\Omega\times[0,T],\\ u(x,0) = u_0(x),\ \dot{u}(x,0) &= v_0(x), && \text{in } \Omega, \end{aligned} \tag{1}$$

where Ω is a bounded domain in $\mathbb{R}^d$ and $\partial\Omega$ is its boundary. For simplicity in this paper we only consider the homogeneous Dirichlet boundary condition, however impedance condition can be dealt with similarly.

We aim to discretize this problem by a time-space dG method. In principle this could be done on a general time-space mesh, however for the simplicity of presentation (and implementation) we construct a time discretization $0 = t_0 < t_1 < \cdots < t_N = T$ and a spatial-mesh $\mathcal{T}$ of Ω consisting of open simplices such that $\Omega = \cup_{K\in\mathcal{T}}\overline{K}$. Therefore the space-time mesh consists of time-slabs $\mathcal{T}\times I_n$, where $I_n = [t_n, t_{n+1}]$. We will denote the spatial meshwidth h by $h = \max_{K\in\mathcal{T}}\operatorname{diam}(K)$.

Next we define some notation. The *skeleton* of the mesh is defined by $\Gamma := \cup_{K\in\mathcal{T}}\partial T$ and the interior skeleton by $\Gamma_{\text{int}} = \Gamma\setminus\partial\Omega$. Let K^+ and K^- be two elements sharing a face $e = K^+\cap K^- \in \Gamma_{\text{int}}$ with respective outward normal vectors $\mathbf{n}^+$ and $\mathbf{n}^-$ on e. For $u:\Omega\to\mathbb{R}$ and $\mathbf{v}:\Omega\to\mathbb{R}^d$ let $u^\pm : e\to\mathbb{R}$ and $\mathbf{v}^\pm : e\to\mathbb{R}^d$ be the traces on e with limits taken from $K^\pm$. The we set

$$\begin{aligned} \{u\}|_e &= \frac{1}{2}(u^+ + u^-), \qquad \{\mathbf{v}\}|_e = \frac{1}{2}(\mathbf{v}^+ + \mathbf{v}^-),\\ [u]|_e &= u^+\mathbf{n}^+ + u^-\mathbf{n}^-, \quad [\mathbf{v}]|_e = \mathbf{v}^+\cdot\mathbf{n}^+ + \mathbf{v}^-\cdot\mathbf{n}^-, \end{aligned}$$

and finally if $e\in K^+\cap\partial\Omega$, we set $\{\mathbf{v}\}|_e = \mathbf{v}^+$ and $[u]|_e = u^+\mathbf{n}^+$. We will also require the jump in time

$$[\![u(t_n)]\!] = u(t_n^+) - u(t_n^-), \qquad [\![u(t_0)]\!] = u(t_0^+).$$

As the local discrete test and trial space we will use the space of local Trefftz polynomials $S^p_{n,\text{Trefftz}}$. For example in 1-D this space contains functions $1, (x\pm t), (x\pm t)^2, \ldots, (x\pm t)^p$.

2 Derivation of a time-space discontinuous Galerkin method

To derive the weak form suitable for dG discretization we start with the standard symmetric interior penalty discontinuous Galerkin formulation on the time-slab I_n

$$\begin{aligned} \int_{I_n}\Big[\int_\Omega \ddot{u}\dot{v} + \nabla u\cdot\nabla\dot{v}\,dx \\ - \int_\Gamma \{\nabla u\}\cdot[\dot{v}]\,ds - \int_\Gamma [u]\cdot\{\nabla\dot{v}\}\,ds \\ + \sigma\int_\Gamma [u]\cdot[\dot{v}]\,ds\Big]dt = 0, \end{aligned}$$

where note that we have tested with $\dot{v}$. This leads to the following definition of energy at time t

$$\begin{aligned} E(t) = \frac{1}{2}\|\dot{u}(t)\|^2_{L^2(\Omega)} + \frac{1}{2}\|\nabla u(t)\|^2_{L^2(\Omega)} \\ + \frac{1}{2}\sigma\|\,[u(t)]\,\|^2_{L^2(\Gamma)} - \int_\Gamma\{\nabla u\}\cdot[u]\,ds. \end{aligned}$$

Note that the energy is non-negative if the penalisation parameter σ is chosen in the standard

way. Choosing as test function $v = u$ and summing over n we obtain the energy identity

$$0 = E(t_N^-) - E(t_0^+) - \sum_{n=1}^{N-1} [\![E(t_n)]\!].$$

In order to allow for discontinuities in time, the formulation needs to be modified in order to control the terms $[\![E(t_n)]\!]$ that have no sign. In this way we arrive at the fully discrete formulation: For $n = 0, \dots, N-1$

$$a_n(u^n, v) = b_n(u^{n-1}, v) + (f, v)_{L^2(\Omega \times I_n)},$$

for all $v \in S^p_{n,\text{Trefftz}}$, where u^{-1} is obtained from the initial data and

$$\begin{aligned} a_n(u,v) = &\int_{t_n}^{t_{n+1}} \Big[\int_\Omega \ddot{u}\dot{v} + \nabla u \cdot \nabla \dot{v} dx \\ &- \int_\Gamma \{\nabla u\} \cdot [\dot{v}]\, ds - \int_\Gamma [u] \cdot \{\nabla \dot{v}\}\, ds \\ &+ \sigma \int_\Gamma [u] \cdot [\dot{v}]\, ds \Big] dt \\ &+ \int_\Omega \dot{u}(t_n^+)\dot{v}(t_n^+) dx + \int_\Omega \nabla u(t_n^+) \cdot \nabla v(t_n^+) dx \\ &- \int_\Gamma \{\nabla u(t_n^+)\} \cdot [v(t_n^+)]\, ds \\ &- \int_\Gamma [u(t_n^+)] \cdot \{\nabla v(t_n^+)\}\, ds \\ &+ \sigma \int_\Gamma [u(t_n^+)] \cdot [v(t_n^+)]\, ds, \end{aligned}$$

$$\begin{aligned} b_n(u,v) = &\int_\Omega \dot{u}(t_n^-)\dot{v}(t_n^+) dx + \int_\Omega \nabla u(t_n^-) \cdot \nabla v(t_n^+) dx \\ &- \int_\Gamma \{\nabla u(t_n^-)\} \cdot [v(t_n^+)]\, ds \\ &- \int_\Gamma [u(t_n^-)] \cdot \{\nabla v(t_n^+)\}\, ds \\ &+ \sigma \int_\Gamma [u(t_n^-)] \cdot [v(t_n^+)]\, ds. \end{aligned}$$

3 Stability and existence of solution

The following energy relation can be shown for the above derived method

$$\begin{aligned} E(t_N^-) = E(t_1^-) &- \sum_{n=1}^{N-1} \frac{1}{2} \int_\Omega [\![\dot{u}(t_n)]\!]^2 + [\![\nabla u(t_n)]\!]^2 dx \\ &- \sum_{n=1}^{N-1} \int_\Gamma [\![\{\nabla u(t_n)\}]\!] \cdot [\![[u(t_n)]]\!] \\ &+ \frac{1}{2}\sigma [\![[u(t_n)]]\!] \cdot [\![[u(t_n)]]\!] ds \end{aligned} \tag{2}$$

which shows that the method is dissipative. We can further show that the natural dG norm is in fact a norm and not just a semi-norm. From this the uniqueness of solution follows. Further, it can be shown that adding another term to the formulation allows a convergence analysis as well.

4 Numerical results

Here we compute the error in time-space L^2 norm for Trefftz spaces of degree $p = 2, 3, 4$ with $\Omega = (0, 1)$ and $T = 1$. The initial data is

$$u_0(x) = e^{-(x-5/8)^2/\sigma}, \quad v_0(x) = 0, \quad \sigma = 5 \times 10^{-4}.$$

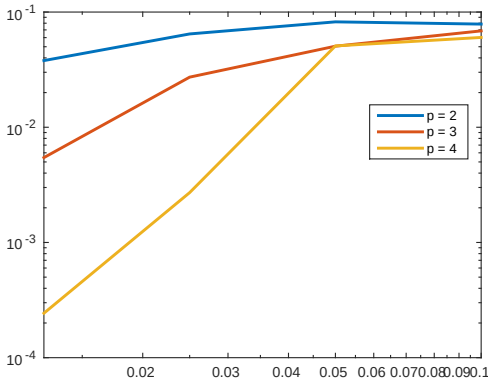

Figure 1: Convergence of the Trefftz method.

References

[1] S. Petersen, C. Farhat, and R. Tezaur, A space-time discontinuous Galerkin method for the solution of the wave equation in the time domain, *Internat. J. Numer. Methods Engrg.*, **78** (2009), pp. 275–295.

Minisymposium: Wave Motions of Fluid-Loaded Structures and Multiple Scattering

organised by Hyuck Chung and Malte Peter

The topic of the minisymposium is the wave motion of structures, e.g., plates and cylinders, which are surrounded by water or air, and multiple scattering involving such structures. The existence of the fluid, either incompressible or compressible, increases the complexity of the mathematics required to study the waves. The speakers have been active in both theoretical researches and practical applications. The research methods used by the speakers are both analytical and numerical, and make full use of various numerical computation techniques.

The primary aim of the minisymposium is to exchange ideas about the current state of play in the mathematical techniques for wave motions of fluid-loaded structures and multiple scattering. In particular, we will see various ways how the analytical methods, which used to be able to deal only with highly idealized model, can now be used for more complex models with the increase of computing power. For example, a purely numerical method such as the finite element method is now used in combination with an analytical technique such as Fourier series or transform methods. Conversely, analytical methods have evolved to take advantage of computing power (e.g., parallel & cluster computing), which has become easily accessible. During this minisymposium, we will discuss such methods and explore their current limits.

Effective versus individual waves for water wave and thin plate problems

Sebastian Rupprecht[1,*], **Malte A. Peter**[1], **Luke G. Bennetts**[2], **Hyuck Chung**[3]
[1]Institute of Mathematics, University of Augsburg, Germany
[2]School of Mathematics, University of Adelaide, Australia
[3]School of Computer and Mathematical Sciences, Auckland University of Technology, NZ
[*]Email: sebastian.rupprecht@math.uni-augsburg.de

Abstract

Numerical results are presented to show that, for small-amplitude roughness, individual wave elevations attenuate at a far slower rate than the corresponding effective wave elevation for both ocean waves travelling over a rough seabed in intermediate depth and waves in a thin plate in vacuo. Use of the effective wave elevation, therefore, results in misleading predictions of attenuation.

Keywords: Wave attenuation, random media, effective wave field, multiple scattering

1 Introduction

Ocean surface waves attenuate with distance travelled into the sea-ice covered ocean. Wave propagation in the ice-covered ocean is conventionally modelled using linear potential-flow theory for the water and thin-plate theory for the ice cover. Bennetts & Peter [1] conducted a preliminary investigation of wave attenuation in the ice-covered ocean due to ice roughness. They modelled the roughness as random variations in stiffness and mass of the ice and derived a semi-analytic expression for the attenuation rate of the effective wave field, i.e. the mean wave field with respect to realisations.

In a recent paper, Bennetts et al. [2] showed that individual wave fields attenuate far slower than the effective wave field for the related problem of free-surface waves over a rough seabed in intermediate depth, originally considered by Mei & Hancock [3]. They used large ensembles of numerical solutions for randomly generated realisations of the bed profile. Further, they review the existing literature on wave propagation over a rough seabed.

Here, we extend the study of Bennetts et al. [2] to problems involving thin plates, with the aim of establishing whether effective media theory is valid to study wave propagation in the ice-covered ocean. We summarise the method and results of [2] in §2 and apply the method to a rough thin plate in vacuo in §3.

2 Free-surface/rough-bed problem

Consider a linear monochromatic wave propagating in the positive x-direction. In open water, the wavenumber, k, is related to the angular frequency, ω, via the dispersion relation $k\tanh(kh) = K$, where $K = \omega^2/g$, h is the fluid depth and g is the gravitational acceleration.

The seabed fluctuates about $z = -\bar{h}$, where $\bar{h}$ is an intermediate depth, i.e. $k\bar{h} = \mathrm{O}(1)$. The fluctuations have a known correlation length, l, and root-mean-square amplitude, $\varepsilon \ll 1$. The function $z = -h(x)$, where $h(x) = \bar{h} - \varepsilon p(x)$ and $p = \mathrm{O}(1)$ is an autocorrelated random function, denotes the location of the bed.

The water velocity field is defined as the gradient of $\mathrm{Re}\{(g/\mathrm{i}\omega)\phi(x,z)\mathrm{e}^{-\mathrm{i}\omega t}\}$. The velocity potential, ϕ, satisfies

$$\partial_x^2\phi + \partial_z^2\phi = 0 \qquad (-h < z < 0), \tag{1a}$$

$$\partial_z\phi + h'(\partial_x\phi) = 0 \qquad (z = -h), \tag{1b}$$

and is coupled to the wave elevation, denoted $z = \mathrm{Re}\{\eta(x)\mathrm{e}^{-\mathrm{i}\omega t}\}$, via

$$\phi = \eta \quad \text{and} \quad \partial_z\phi = K\eta \quad (z = 0). \tag{1c}$$

Consider the problem in which the roughness extends over a long, finite interval $x \in (0, L)$. For given $h(x)$, we approximate the rough bed profile by a piece-wise constant function on $M \gg 1$ sub-intervals and solve for the velocity potential using an iterative algorithm.

Wave elevations are calculated for a large ensemble of randomly generated realisations of the bed profile, cf. [2]. Two measures of the attenuation rate are obtained from the ensemble of wave elevations. First, an attenuation rate, $Q_{\mathrm{eff}}^{(\mathrm{rs})}$, is extracted from the effective wave elevation via

$$|\langle\eta\rangle| \asymp \mathrm{e}^{-Q_{\mathrm{eff}}^{(\mathrm{rs})}x} \quad (0 < x < L). \tag{2}$$

Second, an attenuation rate, $Q_{\mathrm{ind}}^{(\mathrm{rs})}$, is calculated as the ensemble average of attenuation rates

of individual wave elevations. The attenuation rate is defined as $Q_{\text{ind}}^{(\text{rs})} = \langle Q_i \rangle$, where Q_i is extracted from the individual wave elevation $\eta = \eta_i$, i.e.

$$|\eta_i| \propto \mathrm{e}^{-Q_i x} \quad (0 < x < L). \tag{3}$$

It turns out that both rates are proportional to the bed amplitude squared but differ by orders of magnitude for a large range of parameters [2].

Figure 1 shows example individual wave elevations and corresponding effective wave elevations for $\bar{k}l = 0.9$ and 5. The wavenumber $\bar{k}$ corresponds to the mean depth $\bar{h}$, and $\bar{k}\bar{h} = 1$ is set. The smaller correlation length is chosen to produce visible (though weak) attenuation of the individual wave elevation. The corresponding effective wave elevation attenuates slightly more rapidly than the individual wave elevation. The largest correlation length is chosen to produce maximal attenuation of the effective wave elevation. The corresponding individual elevation does not attenuate (on the scale shown). Attenuation of the effective elevation is, therefore, not related to the individual elevations.

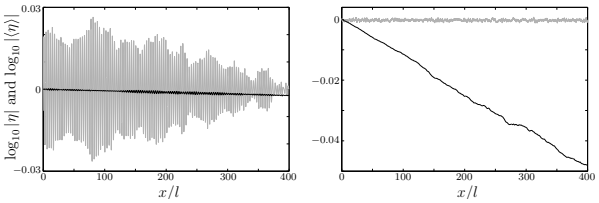

Fig. 1: Example individual wave elevations (grey) and corresponding effective wave elevations (black), for $\bar{k}\varepsilon = 10^{-2}$ and $\bar{k}l = 0.9$ (left) and 5 (right).

3 In vacuo plate problem

Next, we consider an infinitely long rough thin plate in vacuo. The problem is one-dimensional in the horizontal coordinate x. The spatial part $u(x)$ of the plate deflection $\mathrm{Re}\{u(x)\mathrm{e}^{-\mathrm{i}\omega t}\}$ satisfies the thin plate equation

$$\beta \partial_x^4 u - \gamma \omega^2 u = 0 \quad (-\infty < x < \infty), \tag{4}$$

where β is the constant plate stiffness and $\gamma(x)$ is its varying mass.

We use an analogous iterative algorithm together with a step approximation as in the rough bed problem, where the local wavenumber κ_m is $\kappa(x) = (\omega^2\gamma(x)/\beta)^{\frac{1}{4}}$, evaluated at the midpoint of the mth sub-interval.

Again, solutions are calculated for large ensembles of different realisations of the varying wavenumber function, which share a common correlation length and roughness amplitude. Figure 2 shows the results for the in vacuo plate, in analogy to figure 1 for the rough bed. As can be seen, the behaviour is very similar and the analogous conclusions are drawn.

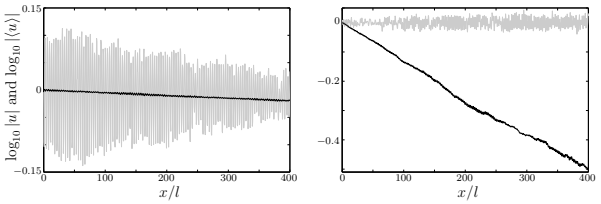

Fig. 2: As in Fig. 1 but for in vacuo plate problem.

Acknowledgements

This work was supported by the Group of Eight, Australia, and German Academic Exchange Service (DAAD) Joint Research Co-operation Scheme. LB acknowledges funding support from the Australian Research Council (DE130101571) and the Australian Antarctic Science Grant Program (Project 4123).

References

[1] L. G. Bennetts and M. A. Peter, Approximations of wave propagation in one-dimensional multiple scattering problems with random characteristics, In: Proc. 27th IWWWFB, Copenhagen, pp. 9–12 (2012).

[2] L. G. Bennetts, M. A. Peter, and H. Chung, Absence of localisation in ocean wave interactions with a rough seabed in intermediate water depth *Q. J. Mech. Appl. Math.* **68**(1) (2015) 97–113.

[3] C. C. Mei and M. J. Hancock, Weakly nonlinear surface waves over a random bed, *J. Fluid Mech.* **475** (2003) 247–268.

Transmission of ocean waves through a row of randomly perturbed circular ice floes

Fabien Montiel[1,*], **Vernon A. Squire**[1]
[1]Department of Mathematics and Statistics, University of Otago, Dunedin, New Zealand
[*]Email: fmontiel@maths.otago.ac.nz

Abstract

A method is described to compute the transmission matrix of a finite array of ice floes under ocean wave forcing. We discuss the behaviour of the transmission matrix when the floes are regularly spaced and randomly positioned. The scattering angles of the regular array are gradually filtered out under increasing disorder.

Keywords: ocean waves, directional spectra, scattering angles, random arrays

1 Introduction

We consider the multiple scattering of time-harmonic ocean waves by a finite array of ice floes floating at the surface of a fluid domain with constant depth and infinite horizontal extent. Our goal is to model wave attenuation and directional spreading due to scattering in inhomogeneous ice-covered seas. In particular, we seek to understand better the effect of randomly perturbed arrays on these properties, which can be extracted from the scattering matrix of the array. We use the method proposed in [2] and extend the analysis of [1] for acoustic waves to discuss the effect of introducing random perturbations in a regular array of ice floes on the scattering properties of the array.

2 Preliminaries

Cartesian coordinates $\mathbf{x} = (x, y, z)$ are used in the fluid domain Ω with $z = 0$ and $z = -h$ coinciding with the undisturbed free surface and seabed, respectively. Let M denote the number of floes. All floes are circular (with radius a), have uniform thickness D and experience flexural motion when perturbed from rest. For each floe j, $1 \leq j \leq M$, we define the coordinates (x_j, y_j) of its centre and the local polar coordinates (r_j, θ_j). We assume that the centres of all floes are contained in the slab $0 \leq x \leq L$.

Within the framework of time-harmonic linear water wave and thin elastic plate theories, the potential $\Phi(\mathbf{x}, t) = \mathrm{Re}\{(g/\mathrm{i}\omega)\phi(\mathbf{x})\mathrm{e}^{-\mathrm{i}\omega t}\}$ is used to describe the fluid motion, where ω is the radian frequency and g acceleration due to gravity. The (reduced) potential ϕ then satisfies

$$\left(\nabla^2 + \partial_z^2\right)\phi = 0 \ (\mathbf{x} \in \Omega) \quad (1)$$

$$\partial_z\phi = 0 \ (z = -h) \quad (2)$$

$$\partial_z\phi = \alpha\phi \ (r_j > a,\, z = 0) \quad (3)$$

$$\left(\beta\nabla^4 + 1 - \alpha d\right)\partial_z\phi = \alpha\phi \ (r_j < a,\, z = -d) \quad (4)$$

$$\partial_{r_j}\phi = 0 \ (r_j = a,\, -d < z < 0). \quad (5)$$

We have introduced the parameters $\alpha = \omega^2/g$, $\beta = ED^3/12(1-\nu^2)\rho g$, where $E \approx 6\,\mathrm{GPa}$ and $\nu \approx 0.3$ are ice Young's modulus and Poisson's ratio, respectively, $\rho \approx 1025\,\mathrm{kg\,m^{-3}}$ is the fluid density and $d = (\rho_i/\rho)D$ is the floe draught, with $\rho_i \approx 922.5\,\mathrm{kg\,m^{-3}}$ the ice density. Free edge conditions are further imposed at the floe edges, and the scattered field obeys a radiation condition in the far-field to ensure its decay.

3 Transmission matrix

We consider a wave forcing of the form

$$\phi^{\mathrm{In}}(\mathbf{x}) = \psi(z)\int_{-\pi/2}^{\pi/2} A(\tau)\mathrm{e}^{\mathrm{i}k(x\cos\tau + y\sin\tau)}\,\mathrm{d}\tau, \quad (6)$$

where $\psi(z) = \cosh k(z+h)/\cosh kh$ describes the vertical motion and k is the wavenumber related to frequency ω through the free surface dispersion relation $gk\tanh kh = \omega^2$. The incident field is a superposition of plane waves travelling at angle $\tau \in (-\pi/2, \pi/2)$ with amplitudes $A(\tau)$. The wave field transmitted through the slab is given in the form

$$\phi^{\mathrm{T}}(\mathbf{x}) = \psi(z)\int_{-\pi/2}^{\pi/2} B(\chi)\mathrm{e}^{\mathrm{i}k((x-L)\cos\chi + y\sin\chi)}\,\mathrm{d}\chi, \quad (7)$$

for $x > L$, such that the unknown transmitted spectrum $B(\chi)$ is related to the incident spectrum $A(\tau)$ through

$$B(\chi) = \int_{-\pi/2}^{\pi/2} \mathcal{T}(\chi : \tau)A(\tau)\,\mathrm{d}\tau. \quad (8)$$

The solution to the transmission problem is fully described by the transmitted kernel $\mathcal{T}(\chi : \tau)$. Similar relations exist for the reflected field, but are not discussed here.

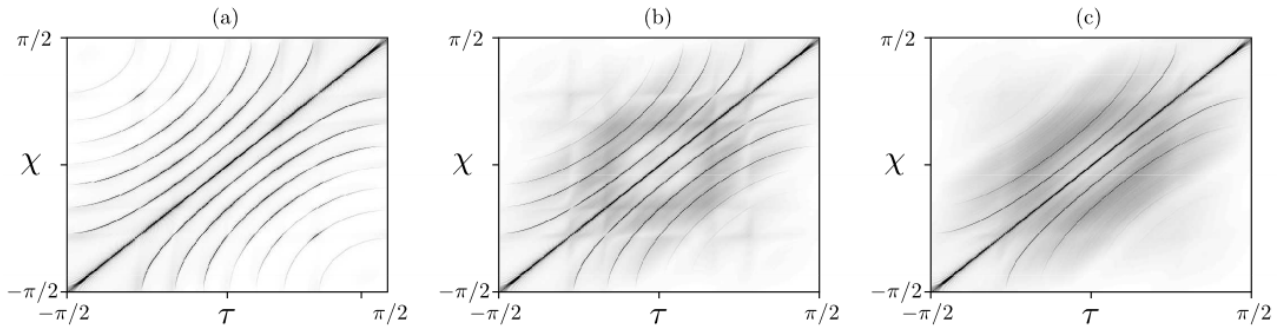

Figure 1: Magnitude of the transmission matrix for (a) $\mu = 0$, (b) 0.5 and (c) 1.

A solution method was developed in [2] which provides semi-analytical expressions for the transmitted (and reflected) kernels. The method is summarised as follows:

1. derive a self-consistent multiple scattering solution using cylindrical multipole expansions to represent the field near each floe (based on Graf's addition theorem);

2. transform the multipole expansions into integrals of plane waves using Sommerfeld's integral representation of Hankel functions.

A numerical solution is then obtained by discretising $A(\tau)$, $B(\chi)$ and $\mathcal{T}(\chi : \tau)$ in (8) at N regular angular samples τ_i and χ_i, $1 \leq i \leq N$. Using the trapezoidal rule for numerical integration (8) becomes

$$\mathbf{b} = \mathbf{S}^T \mathbf{a}, \tag{9}$$

where $\mathbf{S}^T$ is the transmission matrix, and $\mathbf{a}$ and $\mathbf{b}$ are discrete versions of A and B, respectively.

4 Results

We analyse the magnitude $\mathbf{S}^T$. The entry corresponding to $\mathcal{T}(\chi_i : \tau_j)$ describes the transmitted wave amplitude at angle $\chi = \chi_i$ due to an impulse incident at angle $\tau = \tau_j$, i.e. $A(\tau) = \delta(\tau - \tau_j)$ with δ denoting the Delta function. We consider an array of 51 floes regularly positioned along the y-axis with spacing $s = 300\,\mathrm{m}$, such that $y_j = \tilde{y}_j = s(j - 26)$, for $1 \leq j \leq 51$. We set $h = 200\,\mathrm{m}$, $a = 100\,\mathrm{m}$, $D = 1.5\,\mathrm{m}$ and the wave period $T = 7\,\mathrm{s}$. We then introduce a random perturbation on the position of each floe, such that $(x_j, y_j) = (50\varepsilon\mu, \tilde{y}_j + 50\varepsilon\mu)$, where $0 \leq \mu \leq 1$ and ε is a random variable with uniform distribution in $[-1, 1]$.

Figure 1 shows a grayscale image of the magnitude of the entries of $\mathbf{S}^T$ for $\mu = 0$, 0.5 and 1. For the two latter cases, the entries are averaged over 100 random realisations of the array. The grayscale image shows clearly the existence of the scattering angles in the regular case ($\mu = 0$), which arise from scattering by regular gratings and satisfy $\sin\chi = \sin\tau + 2n\pi/ks$ for n integer. When perturbations are introduced ($\mu > 0$) and increase, the scattering angles are gradually filtered out and the energy is redistributed across the directional range (shaded areas). The dominant diagonal corresponds to a transmitted wave travelling in the same direction as the incident wave. With sufficient disorder, waves are expected to transmit with directionality unaffected but reduced amplitudes. These results are consistent with the findings of [1] for acoustic waves.

References

[1] F. Montiel, Squire, V. A. and Bennetts, L. G., Evolution of directional wave spectra through finite regular and randomly-perturbed arrays of scatterers *SIAM J. Appl. Math.*, **75** (2015), pp. 630–651.

[2] F. Montiel, Squire, V. A. and Bennetts, L. G., Reflection and transmission of ocean wave spectra by a band of randomly distributed ice floes *Ann. Glaciol.: sea ice in a changing environment*, **56(69)** (2015), pp. 315–322.

A model for small oscillations of a pressurised, elastic, spherical shell

K. A. Kuo[1,*], **H. E. M. Hunt**[1], **J. R. Lister**[2]

[1]Department of Engineering, University of Cambridge, Cambridge, UK.

[2]Department of Applied Mathematics and Theoretical Physics, University of Cambridge, Cambridge, UK

[*]Email: Kirsty.Kuo@kuleuven.be

Abstract

This paper presents a novel model for the small oscillations of a pressurized, elastic, spherical shell. The shell has three features: a pressure difference across the skin; a thin, tensioned membrane; and a double curved interfacial surface. An analytical solution for the natural frequencies and mode shapes, incorporating the inertia both of the shell and of the surrounding fluid, is derived. When the membrane tension is set to zero, the results converge to the analytical solution for a spherical shell, and when the skin elasticity is neglected, the results converge to the constant-tension solution of a bubble.

Keywords: pressurised shell, elastic membrane, vibration modes

1 Introduction

This paper describes a new model that combines consideration of an elastic spherical shell, the influence of skin pre-tension, and the inertial effect of internal and external fluids. Example of such shells are sports balls, biological organs, airbags and balloons. There is a long tradition of analytical models of spherical shell vibrations, and the approach taken in this paper builds on some established models.

2 Existing Models

A well-known model of elastic spherical shell vibrations is based on Love's deep-shell equations [1] and Lamb's study on a thin spherical shell [2]. This model is unsuitable for application to the vibrations of pressurized, elastic, spherical shells as it does not account for: (a) the pre-tension in the skin that results from the pressure difference across the surface, that is, the initial stressed state; and (b) the influence of the inertia of the internal and external fluids on the radial momentum of the balloon. These two effects are present in Grinfeld's model of the small oscillations of a spherical soap bubble [3], which extends Lamb's solution [4] for the oscillation of a fluid drop to include the inertia of the soap film. This model is, however, unsuitable for the vibration of an elastic shell, as it assumes constant uniform and isotropic skin tension (surface tension) in line with Laplace's classical model of capillarity. This means that the changes in stress state in the shell due to elastic deformation are neglected. For this reason, a new model is developed that draws on elements of these two existing models.

3 Model Formulation

This formulation considers linearized, axisymmetric, normal modes that are harmonic in time with angular frequency ω. There is no loss of generality in focussing on axisymmetric modes for convenience, since a non-axisymmetric normal mode can be written as a linear combination of rotations of an axisymmetric mode of the same frequency.

For simplicity, we assume that the fluids inside and outside the shell are incompressible and inviscid. The effect of compressibility is negligible provided that $\omega \ll c/R$, where c is the acoustic wavespeed and R is the shell radius. The effect of fluid viscosity is negligible provided that the Reynolds number is much greater than one. Euler's equations for incompressible, inviscid flow then apply, and axisymmetric solutions in spherical coordinates are assumed. The kinematic condition at the fluid-shell interfaces requires that the shell's normal velocity component is equal to both the internal fluid's normal velocity component and the external fluid's normal velocity component.

The motion of the thin, spherical shell results from the combination of three effects: elastic thin-shell deformations; the pre-tension in the shell that results from the initial pressure difference across the surface; and the influence of the inertia of the internal and external fluids on the momentum of the shell. The elastic shell deformations are captured in [1,2], and we

now consider how to incorporate the tensile and inertial effects into these equations.

The shell is considered to be under an initial state of isotropic tension T. When the shell deforms from its equilibrium position, the effect of this tension is a radial restoring stress proportional to the tension and the change in curvature due to deformation. As the tension is isotropic, no force occurs in the meridional direction. As the fluids are assumed inviscid, there are no fluid inertia effects in the meridional direction; this influence is only in the radial direction. The radial restoring stress due to the fluid inertia is simply the difference in pressure between the internal and external fluids.

The small displacements in the radial and meridional directions, u and v respectively, are assumed to be of the form $u = UP_n(\cos\phi)\mathrm{e}^{\mathrm{i}\omega t}$ and $v = VQ_n(\cos\phi)\mathrm{e}^{\mathrm{i}\omega t}$, where $P_n(\cos\phi)$ and $Q_n(\cos\phi)$ are the Legendre functions of the first and second kind, respectively. Then the governing equations of a shell of thickness h, density ρ, Young's modulus E and Poisson's ratio ν are:

$$\frac{Eh}{(1-\nu)R^2}\left(-n(n+1)V + 2U\right) + \frac{(n^2+n-2)TU}{R^2} = A\rho h\omega^2 U \tag{1a}$$

$$\frac{Eh}{(1-\nu^2)R^2}\left[-n(n+1)V + (1-\nu)V + (1+\nu)U\right] = -\rho h\omega^2 V \tag{1b}$$

where $n = 0, 1, 2, ...$ is the mode number. The non-dimensional parameter A represents the effective shell inertia:

$$A = 1 + \frac{\rho_e R}{\rho h(n+1)} + \frac{\rho_i R}{\rho h n} \tag{2}$$

where ρ_e and ρ_i are the densities of the external and internal fluids, respectively.

The natural frequencies of the shell are then the (positive) solutions of ω. For each value of n, two natural frequencies exist. These natural frequencies correspond to different mode shapes with varying ratios U/V of radial and meridional motion of the skin. The lower branch has more radial motion and the upper branch less, but both branches involve elastic coupling between the two directions of motion.

Setting the skin tension to zero ($T = 0$) and removing the effects of the internal and external fluids ($A = 1$) recovers the solution for an elastic shell given in [1,2]. The solution for a pre-tensioned elastic shell with no surrounding fluids is found by setting $A = 1$. Removing the elasticity in the skin ($E = 0$) results in a single governing equation, which can be rearranged to obtain Grinfeld's solution for the natural frequencies of a soap bubble. The removal of the elasticity term results in only one natural frequency per modenumber n, with the corresponding modeshapes consisting of purely radial skin motion.

4 Conclusions

This paper has described the formulation of a model for the vibrations of an elastic, spherical shell, subject to internal pressure. The model formulation draws on elements of two existing models: the well-known elastic shell model based on Love's deep shell equations and Lamb's study on a thin spherical shell; and a model for soap-bubble vibrations that incorporates fluid effects.

References

[1] A. E. H. Love, On the small free vibrations and deformations of thin elastic shells, *Philosophical Transactions of the Royal Society A* **179** (1888).

[2] H. Lamb, On the vibrations of a spherical shell, *Proceedings of the London Mathematical Society* **XIV** (1883).

[3] P. Grinfeld, Small oscillations of a soap bubble, *Studies in Applied Mathematics* **128** (2011), pp.30–39.

[4] H. Lamb, *Hydrodynamics*, Dover Publications, New York, 1993.

Scattering by a Cage

P. A. Martin[1,*]

[1]Department of Applied Mathematics and Statistics, Colorado School of Mines, USA

[*]Email: pamartin@mines.edu

Abstract

Acoustic scattering by a ring comprising a large number of equally spaced small circles is considered, using a combination of Foldy-type approximations, circulant matrices and asymptotics.

Keywords: multiple scattering, acoustics, asymptotics

1 Introduction

Time-harmonic acoustic waves are scattered by N obstacles. Such multiple scattering problems can be solved exactly, in principle, by reducing them to integral equations or to infinite systems of linear algebraic equations [2].

In this paper, we are interested in the scattering of an incident wave by N identical parallel circular cylinders arranged in a particular way: in a cross-sectional plane, there are N circles (radius a) with their centres located on, and equally spaced around, a larger circle (radius b). We call this geometrical configuration a *ring* or a *cage*, the latter word being used because we can consider the configuration as giving a simple model of a Faraday cage.

Exact (numerical) methods have been applied to scattering by a cage. However, we are especially interested when N is large, so that we have many small circles around the ring with small gaps between them.

Intuitively we expect that, in the limit (when there are no gaps), we should approach the solution for scattering by a single large cylinder (with cross-section of radius b). Can this be shown, and, if so, how fast is the limit achieved?

In a recent paper [3], we gave an analysis of cage problems. The cylinders comprising the cage were assumed to be small, both geometrically ($a \ll b$) and acoustically ($ka \ll 1$, where $2\pi/k$ is the incident wavelength). For the scattering itself, we used *Foldy's method* [1], [2, §8.3]. This is an approximate theory, in which the scattering by each circular cylinder is represented by a single term (proportional to $H_0(kr)$, see below) instead of the usual infinite separation-of-variables series. However, all multiple scattering effects are taken into account. The result is an $N \times N$ linear algebraic system. This reduction works for N scatterers at more-or-less arbitrary locations. However, for a ring of equally-spaced identical scatterers, the matrix occurring has a special structure: it is a *circulant* matrix. This means that it can be inverted explicitly, using a discrete Fourier transform, and then the behaviour of the solution as N grows can be analysed. It turns out that the expected limit is achieved but the limit is approached slowly, at best as N^{-1}.

So far, we have not mentioned the boundary condition on each cylinder. Most exact methods can accommodate any choice, such as Dirichlet (sound-soft) or Neumann (sound-hard) conditions.

For the Foldy-type analysis described above, the underlying assumption is that each cylinder scatters *isotropically*: note the presence of $H_0(kr)$ with no dependence on the polar angle. This is entirely appropriate for Dirichlet problems: we know that small ($ka \ll 1$) sound-soft circles really do scatter like a monopole. However, sound-hard circles do not scatter isotropically: monopole and dipole contributions are equally important and both must be retained. The dipole gives a directional dependence to the waves scattered by one circle, and this must be incorporated into the calculation of the multiply scattered waves when there are N circles. Foldy's method can be extended to cover sound-hard scatterers, leading to a $3N \times 3N$ linear algebraic system. We can use this extension to study scattering by a sound-hard cage.

2 Foldy approach

Foldy's method, when applied to a cage of soft circles, leads to an $N \times N$ system,

$$\sum_{j=1}^{N} K_{n-j} A_j = f_n, \quad n = 1, 2, \ldots, N, \qquad (1)$$

where $f_n = -u_{\text{in}}(\mathbf{r}_n)$, u_{in} is the incident wave, $K_0 = -g^{-1}$, $g = -[J_0(ka)]/[H_0(ka)]$,

$$K_j = H_0(2kb\,|\sin(j\pi/N)|), \quad j \neq 0 \bmod N$$

and K_j is N-periodic: $K_{j+mN} = K_j$ for all integers m. The nth circle is centred at $\mathbf{r}_n$, $r = b$, $\theta = nh$, where $h = 2\pi/N$ is the angular spacing between adjacent circles.

The unknown coefficients A_n appear in our representation of the total field,

$$u(\mathbf{r}) = u_{\rm in}(\mathbf{r}) + \sum_{j=1}^{N} A_j H_0(k|\mathbf{r} - \mathbf{r}_j|). \qquad (2)$$

The circulant structure means that we can solve (1) explicitly, using discrete Fourier transforms. Then all properties of the wavefield can be found. In particular, it is possible to extract asymptotic properties as N grows.

3 Extended Foldy approach

Sound-hard scatterers always generate a dipole field. Foldy's method can be generalized to cover these situations [2, §8.3.3]. Thus, we add

$$\sum_{j=1}^{N} \mathbf{q}_j \cdot \mathbf{g}(\mathbf{r} - \mathbf{r}_j)$$

to the right-hand side of (2), where $\mathbf{q}_j$ is an unknown vector (dipole strength and direction), $\mathbf{g}(\mathbf{r}) = \hat{\mathbf{r}}\, H_1(kr)$, $\hat{\mathbf{r}} = \mathbf{r}/r$ and $r = |\mathbf{r}|$.

For a cage, it is convenient to write $\mathbf{q}_j$ in terms of its radial and tangential components with respect to the cage. Let $\hat{\mathbf{i}}$ and $\hat{\mathbf{j}}$ be unit vectors in the x and y directions, respectively. Then $\hat{\mathbf{r}}_j = \mathbf{r}_j/b = \hat{\mathbf{i}}\cos\theta_j + \hat{\mathbf{j}}\sin\theta_j$ with $\theta_j = jh$. Let $\hat{\boldsymbol{\theta}}_j = \hat{\mathbf{j}}\cos\theta_j - \hat{\mathbf{i}}\sin\theta_j$ be a unit tangent vector, so that $\hat{\mathbf{r}}_j \cdot \hat{\boldsymbol{\theta}}_j = 0$. Write

$$\mathbf{q}_j = B_j \hat{\mathbf{r}}_j + C_j \hat{\boldsymbol{\theta}}_j,$$

so that the $3N$ unknowns are A_j, B_j and C_j, for $j = 1, 2, \ldots, N$. These satisfy the system

$$\sum_{j=1}^{N} \mathbf{K}_{n-j} \mathbf{x}_j = \mathbf{f}_n, \quad n = 1, 2, \ldots, N, \qquad (3)$$

with $\mathbf{f}_n = (-u_{\rm in}(\mathbf{r}_n),\ -\hat{\mathbf{r}}_n \cdot \mathbf{v}_{\rm in}(\mathbf{r}_n),\ \hat{\boldsymbol{\theta}}_n \cdot \mathbf{v}_{\rm in}(\mathbf{r}_n))^T$, $\mathbf{x}_j = (A_j, B_j, C_j)^T$ and $\mathbf{v}_{\rm in}(\mathbf{r}) = k^{-1}\mathrm{grad}\, u_{\rm in}$. $\mathbf{K}_j$ is a symmetric 3×3 matrix; in detail,

$$\mathbf{K}_0 = \mathbf{K}_N = \begin{pmatrix} Z_0^{-1} & 0 & 0 \\ 0 & (2Z_1)^{-1} & 0 \\ 0 & 0 & -(2Z_1)^{-1} \end{pmatrix},$$

$Z_n = J_n'(ka)/H_n'(ka)$, and, for $j \neq 0 \bmod N$,

$$\mathbf{K}_j = \begin{pmatrix} K_{11} & K_{12} & K_{13} \\ K_{12} & K_{22} & K_{23} \\ K_{13} & K_{23} & K_{33} \end{pmatrix},$$

with entries as follows:

$$\begin{aligned} K_{11} &= H_0, \quad K_{12} = -(2b)^{-1} R_j H_1, \\ K_{13} &= b R_j^{-1} H_1 \sin\theta_j, \\ K_{22} &= \frac{H_1}{kR_j}\cos\theta_j + H_2 \frac{R_j^2}{4b^2}, \\ K_{23} &= \frac{H_1}{kR_j}\sin\theta_j - \frac{1}{2} H_2 \sin\theta_j, \\ K_{33} &= -\frac{H_1}{kR_j}\cos\theta_j + H_2 \frac{b^2}{R_j^2}\sin^2\theta_j. \end{aligned}$$

All Hankel functions have argument kR_j with $R_j = 2b|\sin(j\pi/N)|$. Clearly, $\mathbf{K}_j$ is N-periodic: $\mathbf{K}_{j+mN} = \mathbf{K}_j$, $m = \pm 1, \pm 2, \ldots$.

The system (3) gives $3N$ equations for $3N$ unknowns. Application of the discrete Fourier transform breaks the system into N 3×3 systems, one for each $\mathbf{x}_j$, thus permitting further analysis.

References

[1] L. L. Foldy, The multiple scattering of waves. I. General theory of isotropic scattering by randomly distributed scatterers. *Phys. Rev.* **67** (1945) 107–119.

[2] P. A. Martin, *Multiple Scattering*, Cambridge University Press, 2006.

[3] P. A. Martin, On acoustic and electric Faraday cages. *Proc. Roy. Soc.* A **470** (2014) 20140344.

Scattering of water waves by thin floating plates

Richard Porter[1,*]

[1]School of Mathematics, University of Bristol, Bristol, BS8 1TW, UK

[*]Email: richard.porter@bris.ac.uk

Abstract

This work centres on problems involving the interaction of water waves with thin rigid or flexible plates which can either be fixed or freely-floating on the surface of the fluid. A Fourier transform method is key to developing integral equations can subsequently be efficiently solved numerically using a Galerkin approach. A large class of problems can be considered using this approach, including scattering by rectangular and rhomboidal-shaped plates and eigenvalue problems for sloshing modes in ice holes.

Keywords: Water waves, floating plates, Integral equations

1 Introduction

The reflection and transmission of surface gravity waves by a rigid plate or 'dock' on the surface of a fluid is a classical problem in the study of linearised water waves. For example, when the plate covers the half-plane – the so-called semi-infinite dock problem – an explicit expression for the reflection coefficient can be found using the Wiener-Hopf technique (see [1]). For a plate that is infinitely-long and of uniform constant width – the so-called 'finite dock problem' – exact solutions are no longer possible and various techniques have been employed all leading to approximations of the reflection and transmission. See for example, [2], [3].

In §2 we outline how a Fourier transform method may be applied to this two-dimensional scattering problem that results efficient and accurate numerical results. We do not claim that this approach is superior to existing methods, but it does allow a number of extensions to be considered and some of these are outlined in §3 and §4. Further extensions will be presented in the talk.

2 A two-dimensional scattering problem and its solution

To illustrate the main features of the approach, we consider scattering of obliquely-incident plane waves by a rigid thin plate fixed in the free surface of water of infinite depth.

Cartesian coordinates are used with $z = 0$ in the mean free surface and the fluid extending into $z < 0$. A rigid horizontal plate is placed on the surface, $z = 0$, and extends uniformly in the y-direction with $-a < x < a$.

Assuming time-harmonic incident waves of angular frequency ω making an angle θ_0 with respect to the positive x direction, the velocity field components are found from the gradient of $\Re\{\phi(x,z)\mathrm{e}^{\mathrm{i}(\beta_0 y-\omega t)}\}$ where the velocity potential $\phi(x,z)$ satisfies

$$(\nabla^2 - \beta_0^2)\phi(x,z) = 0, \qquad z < 0, \tag{1}$$

with $\beta_0 = K\sin\theta_0$, $K = \omega^2/g$ and

$$\phi_z(x,0) - K\phi(x,0) = 0, \tag{2}$$

on the free surface and $|\nabla\phi| \to 0$ as $z \to -\infty$. The zero-velocity condition to be applied on the plate is

$$\phi_z(x,0) = 0, \qquad |x| < a. \tag{3}$$

and at the ends of the plate (as x approaches $\pm a$) the potential should be bounded. Finally radiation conditions are required and we write

$$\phi(x,z) \sim \begin{cases} \phi_i(x,z) + R\phi_i(-x,z), & x \to -\infty \\ T\phi_i(x,z), & x \to \infty \end{cases} \tag{4}$$

where R and T are the complex reflection and transmission coefficients and $\phi_i(x,z) = \mathrm{e}^{\mathrm{i}\alpha_0 x}\mathrm{e}^{Kz}$ with $\alpha_0 = K\cos\theta_0$.

The Fourier transform of the scattered part of the potential is defined by

$$\overline{\phi}(\alpha,z) = \int_{-\infty}^{\infty} (\phi(x,z) - \phi_i(x,z))\mathrm{e}^{-\mathrm{i}\alpha x}\,dx \tag{5}$$

and the contour of integration in the inverse transform will be defined in order to satisfy the radiation condition.

The application of the Fourier transform yields the following integral equation for the unknown function $\phi(x,0)$

$$\phi(x,0) + (\mathcal{K}_0\phi)(x) = \mathrm{e}^{\mathrm{i}\alpha_0 x} \tag{6}$$

for $|x| < a$ where

$$\mathcal{K}_0\phi = \frac{K}{2\pi}\int_{-\infty}^{\infty}\frac{\mathrm{e}^{\mathrm{i}\alpha x}}{k_0 - K}\int_{-a}^{a}\phi(x',0)\mathrm{e}^{-\mathrm{i}\alpha x'}\,dx'\,d\alpha.$$

and $k_0^2 = \alpha^2 + \beta_0^2$. R and T can be expressed in terms of simple integral relations of ϕ.

The unknown in (6) is expanded in terms of a set of prescribed functions,

$$\phi(x,0) = \tfrac{1}{2}\sum_{n=0}^{\infty}\mathrm{i}^n a_n P_n(x/a), \quad |x| \le a \qquad (7)$$

with unknown complex-valued coefficients a_n where P_n are orthogonal Legendre polynomials.

The expansion (7) is substituted into (6) which is multiplied through by $p_m^*(x/a)$ and integrated over $-a < x < a$. This Galerkin procedure results in the following infinite system of equations for the unknown coefficients a_n:

$$\frac{a_m}{2(2m+1)} + \sum_{n=0}^{\infty} a_n K_{m,n} = j_m(\alpha_0 a), \qquad (8)$$

$m = 0, 1, 2, \ldots$ where

$$K_{m,n} = \frac{Ka}{2\pi}\int_{-\infty}^{\infty}\frac{j_n(\alpha a)j_m(\alpha a)}{k_0 - K}\,d\alpha. \qquad (9)$$

and $j_m(x)$ is the spherical Bessel function. The integral passes under the pole at $k_0 = K$.

Numerical results show that a truncation to just 1 term works well over a large range of Ka and accuracy increases rapidly with increasing truncation size.

3 Extensions to three-dimensional scattering by finite docks

The main focus of the talk will be on using extensions of this method for 3-dimensional scattering problems. The figures illustrate examples of the results one can obtain. We show maximum surface amplitudes for monochromatic plane incident wave (left to right) scattering by rectangular rigid plates and rhomboidal plates.

4 Eigenvalue problems

A second extension of the approach is in solving geometrically complementary problems where the surface is covered by a rigid plate apart from a, say, rectangular section in which the fluid forms a free surface. Mathematically we have an eigenvalue problem in which the sloshing modes and their frequencies can be determined from a homogenous system of equations.

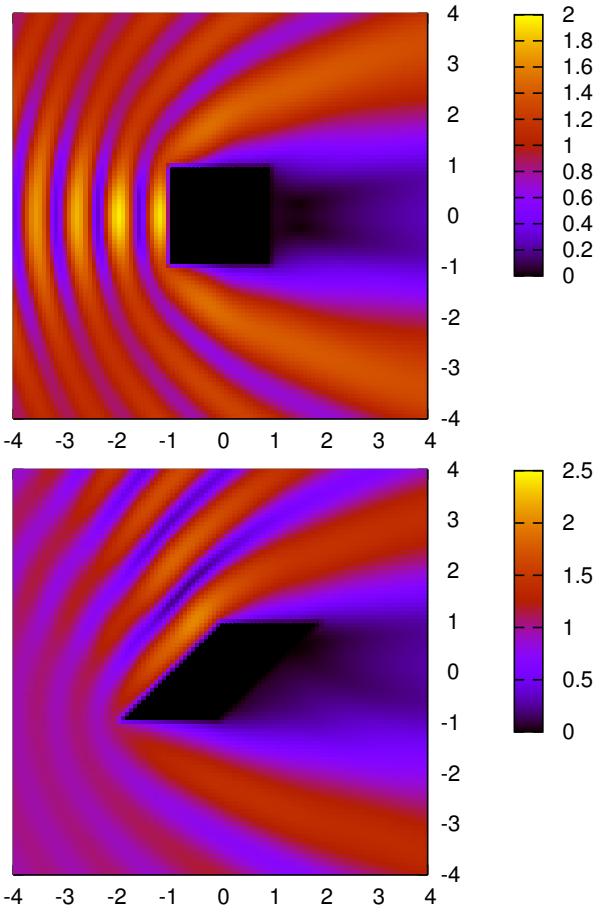

Figure 1: Wave amplitudes for left-right incident wave scattering by rigid plates in the surface.

References

[1] A. E. Heins, Water waves over a channel of finite depth with a dock. *American Journal of Mathematics* **70** (1948), pp. 730–748.

[2] F. G. Leppington, On the scattering of short surface waves by a finite dock. *Proc. Camb. Phil. Soc.* **64** (1968), 1109–1129.

[3] C. M. Linton, The finite dock problem. *Z. angew. Math. Phys.* **52** (2001), pp. 640–656.

Minisymposium: Waves and Plasmas
organised by Bruno Despres and Lise-Marie Imbert-Gerard

The mini symposium "Waves and plasmas" intends to make a tour on recent advances on the mathematical and numerical theory (on the broad sense) of waves in magnetic plasmas [7]. This is physically motivated by the fusion program on Tokamaks [6] for which waves propagation will play an important role either for heating or for reflectometry purposes. It has motivated the development of new mathematical and numerical tools and this mini symposium will be the place to discuss these advances.

A mathematical model is the so-called cold plasma model

$$\operatorname{curl}\operatorname{curl} E - \frac{\omega^2}{c^2}\,\epsilon E = 0$$

where the dielectric tensor $\epsilon \in C^0(M^{3\times 3}(C))$ is non standard with respect to the standard mathematical theory [2], and is representative of the anisotropy of the wave propagation due to the strong background magnetic field B_0 . Indeed the eigenvalues of ϵ change sign continuously. One can refer to [4] where the solution E is shown to be a Dirac mass plus a principle value in the case of the hybrid resonance. It has deep impact of numerical methods, a preliminary work to be found in [5].

The mathematical theory of such problem is quite close to the one of metamaterials [1], a topic that will be discussed at KIT in other mini symposia. Therefore we expect strong interactions with our colleagues expert in the metamaterial mathematical theory.

References

[1] A.S. Bonnet-Ben Dhia, L. Chesnel, P. Ciarlet Jr., T-coercivity for scalar interface problems between dielectrics and metamaterials, Math. Mod. Num. Anal., 18 (2012) 1363-1387.

[2] P. Monk, Finite element for Maxwell's equations, Clarendon Press, Oxford, 2003.

[3] F. da Silva, S. Heuraux, E. Z. Gusakov, and A. Popov, A Numerical Study of Forward- and Backscattering Signatures on Doppler-Reflectometry Signals IEEE Transactions on Plasma Science 38, 9 (2010) 2144.

[4] B. Després, L.-M. Imbert-Gerard and R. Weder, Hybrid resonance of Maxwell's equations in slab geometry, Journal de Mathématiques Pures et Appliqu ées Volume 101, Issue 5, May 2014, Pages 623-659.

[5] A generalized plane-wave numerical method for smooth nonconstant coefficients, Lise-Marie Imbert-Gérard and Bruno Després, IMA 2013.

[6] ITER organization web page, `http://www.iter.org/`

[7] D. G. Swanson, Plasma Waves, 2nd Edition, 2003, Series in Plasma Physics.

Discretization of Maxwell's equations in a magnetic plasma with non uniform density

Felipe da Silva[1], Martin Campos Pinto[2], Bruno Després[3,*], Stéphane Heuraux[4]

[1]Instituto de Plasmas e Fusão Nuclear, Instituto Superior Técnico, Universidade de Lisboa, 1049-001 Lisboa, Portugal

[2]CNRS, UMR 7598, Laboratoire Jacques-Louis Lions, F-75005, Paris, France

[3]Sorbonne Universités, UPMC Univ Paris 06, UMR 7598, Laboratoire Jacques-Louis Lions, F-75005, Paris, France

[4]Institut Jean Lamour, UMR 7198 CNRS-University Lorraine, Vandoeuvre, France

*Email: despres@ann.jussieu.fr

Abstract

This work analyzes the stability of the Yee scheme for non stationary Maxwell's equations coupled with a linear current model with density fluctuations. Indeed the usual procedure may yield unstable scheme for physical situations that correspond to strongly magnetized plasmas in X-mode (TE) polarization. We propose to use **first order clustered discretization** of the vectorial product that gives back a stable coupling. We validate the schemes on some test cases representative of direct numerical simulations of X-mode in a magnetic fusion plasma including turbulence at level relevant to simulate the experiments.

Keywords: Maxwell's equation, fusion plasma, stable scheme, FDTD, linear current model.

1 Introduction

The general model problem considered in this work is the non stationary Maxwell system

$$\begin{cases} -\varepsilon_0 \partial_t \mathbf{E} + \mathrm{curl}\mathbf{H} = \mathbf{J} \\ \mu_0 \partial_t \mathbf{H} + \mathrm{curl}\mathbf{E} = 0 \end{cases} \tag{1}$$

coupled with a linear equation for the electronic current density $\mathbf{J} = eN_e\mathbf{u}_e$,

$$m_e \partial_t \mathbf{u}_e = e\left(\mathbf{E} + \mathbf{u}_e \wedge \mathbf{B}_0\right). \tag{2}$$

The unknowns are the electromagnetic field $(\mathbf{E}, \mathbf{H})$, with the usual notation that $\mathbf{H} = \frac{\mathbf{B}}{\mu_0}$, and the electronic current is $\mathbf{J}$. Equation (2) is the linearized Newton law for electrons where the Lorentz force on the right hand side is obtained by linearization [4] of the full Newton law in a strongly magnetized medium with bulk magnetic field $\mathbf{B}_0 \neq 0$, and vanishing electric field and current $\mathbf{E}_0 = \mathbf{J}_0 = 0$. The coefficients are the mass m_e and charge $e < 0$ of the electron, the permittivity ε_0 and permeability μ_0 of vacuum. The electronic density $N_e = N_e(t, \mathbf{x})$ is a prescribed function of the space and time variables. The background magnetic field could as well be dependent of the space and time variables $\mathbf{B}_0 = \mathbf{B}_0(t, \mathbf{x})$. The plasma frequency and cyclotron frequency are defined by

$$\omega_p = \sqrt{\frac{e^2 N_e}{m_e \varepsilon_0}} \quad \text{and} \quad \omega_c = \frac{|e\mathbf{B}_0|}{m_e}. \tag{3}$$

At any time, the total energy of the system is naturally the sum of the electromagnetic energy and the kinetic energy of electrons

$$\mathcal{E} = \int_\Omega \left(\frac{\varepsilon_0 |\mathbf{E}|^2}{2} + \frac{|\mathbf{B}|^2}{2\mu_0} + \frac{m_e |\mathbf{J}|^2}{2|e|^2 N_e} \right) \mathrm{d}\mathbf{x}. \tag{4}$$

The standard method to compute a numerical approximation of (1)-(2) on a Cartesian grid consists of coupling the Yee scheme with a linear discretization of the current, see [5]. The problem is that it easily yields unstable numerical solutions if the electronic density is highly non uniform. This behavior is somehow non intuitive, since the basic numerical scheme was the well-known Yee scheme and the linear current equation is "only" a ordinary differential equation. However the characteristic frequencies ω_p and ω_c of the problem are comparable to the frequency of the incoming wave ω. The reason is the strong interaction between the linear current equation and the scheme for the Maxwell part, which may induce extremely strong numerical instability at long time in particular with resonances [3].

2 A solution

The proposed solution exploits the energy identity (4). Let n denote the time step ($t_n = n\Delta t$). In the standard approach of [1,5], the electrical field is discretized on the integer time steps n, $n+1$ ... , while the other fields are on the half

time steps $n-\frac{1}{2}$, $n+\frac{1}{2}$ ... The algorithmic structure of the standard method reads then

$$\left\{\begin{array}{ll} \varepsilon_0\dfrac{\mathbf{E}^{n+1}-\mathbf{E}^n}{\Delta t} & = \mathrm{curl}\mathbf{H}^{n+\frac{1}{2}}-\mathbf{J}^{n+\frac{1}{2}}, \\ \mu_0\dfrac{\mathbf{H}^{n+\frac{1}{2}}-\mathbf{H}^{n-\frac{1}{2}}}{\Delta t} & = -\mathrm{curl}\mathbf{E}^n, \\ \dfrac{\mathbf{J}^{n+\frac{1}{2}}-\mathbf{J}^{n-\frac{1}{2}}}{\Delta t} & = \varepsilon_0\omega_p^2\mathbf{E}^n \\ & +\omega_c\mathbf{b}\wedge\dfrac{\mathbf{J}^{n+\frac{1}{2}}+\mathbf{J}^{n-\frac{1}{2}}}{2}. \end{array}\right. \tag{5}$$

The equation for $\mathbf{J}_h$ can be obtained as the limit for small friction of the one from [5].

The key point is to use a clustered discretization of the vectorial product as depicted in figure 1. This is counter-intuitive since this procedure is first -order accurate and the rest of the scheme is second-order accurate. The proof of stability relies on proving the discrete energy estimate $\widehat{\mathcal{E}}_h^{n+1}\leq\widehat{\mathcal{E}}_h^n$ with

$$\widehat{\mathcal{E}}_h^n=\|\widehat{\mathbf{E}}_h^n\|_h^2+\|\widehat{\mathbf{B}}_h^{n-\frac{1}{2}}\|_h^2+\|\widehat{\mathbf{J}}_h^n\|_h^2-\Delta t\langle\widehat{\mathbf{E}}_h^n,cR\widehat{\mathbf{B}}_h^{n-\frac{1}{2}}\rangle_h.$$

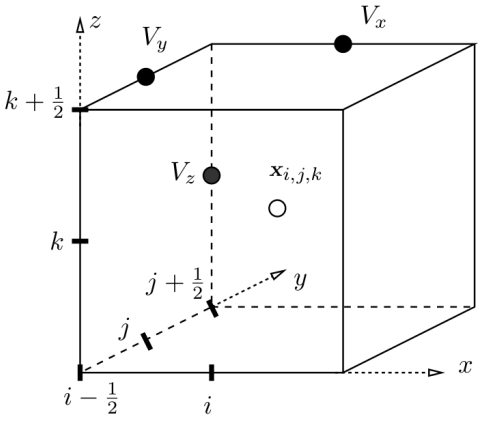

Figure 1: Graphical depiction of a (bulleted) cluster of staggered degrees of freedom.

The structure of the scheme is as follows

$$\left\{\begin{array}{lll} \mathbf{H}_h^{n+\frac{1}{2}} & = & \mathbf{H}_h^{n-\frac{1}{2}}-\frac{\Delta t}{\mu_0}R^t\mathbf{E}_h^n \\ \mathbf{J}_h^{n+\frac{1}{2}} & = & \Big(I+S\big(\frac{\theta}{1+\theta^2}\big)(\mathbf{b}\wedge_h) \\ & & +S\big(\frac{\theta^2}{1+\theta^2}\big)(\mathbf{b}\wedge_h)^2\Big)\mathbf{W}_h^n \\ \mathbf{E}_h^{n+1} & = & \mathbf{E}_h^n+\frac{\Delta t}{\varepsilon_0}(R\mathbf{H}_h^{n+\frac{1}{2}}-\mathbf{J}_h^{n+\frac{1}{2}}) \end{array}\right. \tag{6}$$

with $\theta=\frac{\Delta t\omega_c}{2}$ and $\mathbf{W}_h^n=\Delta t\varepsilon_0 S(\omega_p^2)\mathbf{E}_h^n+(I+\frac{\Delta t}{2}S(\omega_c)\mathbf{b}\wedge_h)\mathbf{J}_h^{n-\frac{1}{2}}$.

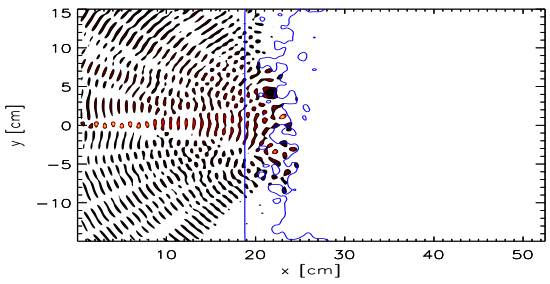

Figure 2: Snapshot of $\max(H_z,0)$.

3 Conclusion

Many numerical simulations [2] confirm the uniform stability of the new method which can now be used for some simulations that were not possible before. Further researches will be devoted to some optimization needed for time varying density profiles like $N_e(\mathbf{x}-\mathbf{a}t)$.

References

[1] Matthias Ulrich Bohner,

[2] da Silva, Campos Pinto, Després and Heuraux, Stable explicit coupling of the Yee scheme with a linear current model in fluctuating magnetized plasmas, Hal preprint 2014.

[3] Després, Imbert-Gérard and Weder, Hybrid resonance of Maxwell's equations in slab geometry, JMPA, 2014.

[4] Stix, The theory of plasma waves, 1962.

[5] Xu and Yuan, FDTD Formulations for Scattering From 3-D Anisotropic Magnetized Plasma Objects, IEEE, 2006.

Stable Perfectly Matched Layers for a Simplified Anisotropic Model of Cold Plasma

Éliane Bécache[1,*], Patrick Joly[1,*], Maryna Kachanovska[1,*]
[1]POEMS, INRIA, ENSTA ParisTech, Palaiseau, France
*Email: maryna.kachanovska@ensta-paristech.fr

Abstract

This work deals with the construction of stable perfectly matched layers (PMLs) for the wave propagation in cold plasmas. This phenomenon is described by Maxwell equations with an anisotropic tensor of dielectric permittivity that depends on frequency. Traditional PMLs exhibit instabilities for this model, due to the presence of backward propagating modes. In this work we demonstrate how this difficulty can be overcome for the case of cold plasma under infinitely large background magnetic field. Namely, in 2D we use of the anisotropic frequency-dependent absorption rate inside the PML. In 3D we split the Maxwell equations into two systems, one of which presenting no difficulties for the traditional PMLs, and another one being treated in a manner similar to the 2D system. We present theoretical and numerical evidence to support our arguments.

Keywords: perfectly matched layers, plasma, Maxwell equations

1 Introduction

We consider electromagnetic wave propagation in a cold collisionless plasma under a uniform background magnetic field $\mathbf{B}_0 = (0,\ 0,\ B_0)$. For simplicity, we assume that the plasma is composed of particles of a single species, with mass m and charge q, whose density N is constant. As $B_0 \to +\infty$, the electromagnetic field satisfies (c.f. [1])

$$\begin{aligned} \frac{1}{c}\partial_t \mathbf{E} - \mathbf{curl}\,\mathbf{B} &= -\frac{4\pi}{c} qNv\mathbf{e}_3, \\ \frac{1}{c}\partial_t \mathbf{B} + \mathbf{curl}\,\mathbf{E} &= 0, \\ m\partial_t v &= qE_3, \end{aligned} \tag{1}$$

where c is the light speed, $\mathbf{E}$ is an electric field, $\mathbf{B}$ is a magnetic field, $\mathbf{e}_3 = (0,\ 0,\ 1)$ and v is a particle velocity.

To perform simulations in free space, we make use of the PML technique. In this method the computational domain is surrounded by a layer (in practice of a finite width), within which the original equations are modified so that their solutions decay in space. A perfect matching property ensures that there is no reflection between the computational and artificial domain. The PMLs are typically constructed via introducing an anisotropic absorption into the original equations. On the external boundary of the PML the choice of zero boundary conditions results in a numerically insignificant reflection. However, such PMLs are known [2, 3] to be unstable in the presence of the backward propagating waves defined as below.

Definition 1 *A mode $\omega(\mathbf{k})$, $\mathbf{k} \in \mathbb{R}^d$, is called backward propagating in the direction $\mathbf{n} \in \mathbb{R}^d$ if*

$$\left(\frac{d\omega}{d\mathbf{k}} \cdot \mathbf{n}\right)\left(\frac{\omega}{k}\frac{\mathbf{k}}{k} \cdot \mathbf{n}\right) < 0.$$

For plasmas the presence of such waves was noticed in [5], however, no PML was proposed in this work.

In this abstract we concentrate on the model (1). It appears that already this simple situation gives rise to instabilities of the PML.

2 Stable Perfectly Matched Layers in 2D

In 2D, for solutions independent of x, the problem (1) can be split into the TM (for variables B_y, B_z, E_x) and TE (E_y, E_z, B_x) modes. We study the dispersion relation of the TE mode [4]

$$F_{2D}(\omega, k_y, k_z) = \frac{k_z^2}{\omega^2} + \frac{k_y^2}{\omega^2\left(1 - \frac{\omega_p^2}{\omega^2}\right)} - 1 = 0,$$

where we used the scaling $c = 1$. Here $\omega_p^2 = \frac{4\pi q^2 N}{m}$. In the sense of Definition 1 in the direction $\mathbf{n} = \mathbf{e}_z$ all modes are forward propagating. In the direction $\mathbf{e}_y$ the situation is different: for $\omega < \omega_p$ all respective modes are backward propagating, and for $\omega \geq \omega_p$ all modes are forward propagating. Then stable PMLs can be constructed following the strategy:

1. in the direction $\mathbf{e}_z$ use Bérenger's PML;

2. in the direction $\mathbf{e}_y$ employ the technique of [3]. The PML absorption rate is multiplied by a function $\psi(\omega)$ chosen so that $\psi(\omega)$ is negative for $\omega < \omega_p$ (i.e. in the presence of backward propagating modes), and $\psi(\omega)$ is positive for $\omega > \omega_p$ (i.e. when the standard PML is stable).

3 Stable Perfectly Matched Layers in 3D

In 3D the problem (1) has the dispersion relation of the form

$$F(\omega, k_x, k_y, k_z) = F_w F_{2D}(\omega, \sqrt{k_x^2 + k_y^2}, k_z),$$
$$F_w = F_w(\omega, k_x, k_y, k_z) = k_x^2 + k_y^2 + k_z^2 - \omega^2.$$

Like in 2D case, for all ω in the direction $\mathbf{e}_z$ and for $\omega > \omega_p$ in directions $\mathbf{e}_{x,y}$ there exist only forward propagating modes. However, in the directions $\mathbf{e}_{x,y}$ for frequencies $\omega < \omega_p$ there exist both forward and backward propagating modes **for the same frequency**. To deal with this difficulty, we split the Maxwell system (1) into two systems, one with the dispersion relation $F_{2D}(\omega, \sqrt{k_x^2 + k_y^2}, k_z)$, and another one with the dispersion relation $F_w(\omega, k_x, k_y, k_z)$ (perhaps with additional modes that would not present difficulties for the PML treatment). This splitting is done based on the analysis of the eigenspaces of (1) written in Fourier (in time and spatial variables) space. Importantly, this can be done only for the homogeneous problem (and we assume that all coefficients are constant outside of a bounded domain, inside the domain where the PML is constructed).

Then the PML is constructed as follows:

1. for the system with the dispersion relation $F_w(\omega, k_x, k_y, k_z)$ a standard PML appears to be stable;

2. for the system with the dispersion relation $F_{2D}(\omega, \sqrt{k_x^2 + k_y^2}, k_z)$ the behaviour is similar to the 2D case. Thus in the directions $\mathbf{e}_x$, $\mathbf{e}_y$ the PML absorption rate is modified as described in Section 2, and in the direction $\mathbf{e}_z$ the standard PML absorption is used.

The resulting systems are discretized with the help of the Yee scheme. Inside the PML the split system is used, and inside the physical domain the original Maxwell system is solved. The coupling between two systems is done *on a discrete, FDTD level*, through a thin layer.

4 Outline and Future Work

We have constructed stable PMLs for Maxwell equations in plasmas under very strong background magnetic fields. In the future work we aim to study the following questions:

1. stable variational formulation (*on a continuous level*) for the coupling of the Maxwell system with the new split system;

2. construction of stable PMLs for Maxwell equations in plasmas for arbitrary magnetic fields.

References

[1] T.H. Stix, *Waves in Plasmas*, American Institute of Physics, New York, 1992.

[2] É. Bécache, S. Fauqueux and P. Joly, Stability of perfectly matched layers, group velocities and anisotropic waves. *J. Comput. Phys.*, **188** (2003), no. 2, pp. 399–433.

[3] É. Bécache, P. Joly and V. Vinoles, On the analysis of perfectly matched layers for a class of dispersive media. Application to negative index metamaterials. *In preparation.*

[4] É. Bécache, P. Joly, M. Kachanovska and V. Vinoles, Perfectly matched layers in negative index metamaterials and plasmas. *ESAIM: Proc.*, vol. **50** (2015), pp. 113-132

[5] J. Jacquot, L. Colas, F. Clairet, M. Goniche, S. Heuraux, J. Hillairet, G. Lombard and D. Milanesio, 2D and 3D modeling of wave propagation in cold magnetized plasma near the Tore Supra ICRH antenna relying on the perfectly matched layer technique. *Plasma Physics and Controlled Fusion*, **55(11)** (2013), 115004 (17pp)

Numerical Solution of the Wave Kinetic Equation in Tokamak Plasmas

Hannes Weber[1], **Omar Maj**[1,*], **Emanuele Poli**[1]

[1] Max Planck Institute for Plasma Physics, Boltzmannstraße 2, D-85748 Garching.

*Email: Omar.Maj@ipp.mpg.de

Abstract

In this paper we report on the mathematical theory and the numerical scheme at the basis of the `WKBeam` code, which describes the propagation of electromagnetic wave beams in the hot, magnetized plasma of a tokamak machine, the primary candidate for a fusion energy reactor. The code solves the wave kinetic equation in the appropriate (toroidal) geometry and it accounts for beam diffraction, absorption, and scattering by turbulent fluctuations of the plasma density.

Keywords: Wave kinetic equation, turbulent media, tokamak plasmas.

1 Introduction and wave equation

In plasma physics, beams of electron cyclotron waves [1, 2] have frequency in the microwave region of the spectrum. The problem therefore exhibits a large separation of scales: a millimeter wave, propagating over distances of meters, in an inhomogeneous plasma equilibrium with scale length of several centimeters. Therefore, semiclassical methods are ideal to solve efficiently the relevant equation for the wave electric field $E(\omega, x)$ for a large frequency ω.

Let the electric field be given on a plane Σ, which represents a mirror of the wave launcher system and is typically located in vacuum, away from the plasma. In normalized form, we can consider the field $u(h, x) = E(\omega, x)/E_0$, where $h = \frac{c}{\omega L} \ll 1$ is the ratio of the typical wave length to the typical scale L of variation of the plasma equilibrium and E_0 is a reference normalization, e.g., the peak value of $|E|$ on Σ.

The problem for the wave electric field reads

$$\mathrm{Op}_h(D)u(h, x) = 0, \quad u_{|\Sigma} = u_a, \qquad (1)$$

where $u_{|\Sigma}$ denotes an appropriately defined restriction of u to the plane Σ, and u_a is the boundary condition on the mirror. (Uniqueness of the solution requires an additional condition on the direction of propagation which we do not specify in this note.) The linear operator $\mathrm{Op}_h(D)$ is the semiclassical Weyl quantization [3] of the symbol

$$D_{ij}(h, x, \xi) = \xi^2\delta_{ij} - \xi_i\xi_j - \varepsilon_{ij}(h, x, \xi), \qquad (2)$$

and $\varepsilon(h, \cdot, \cdot)$ is the plasma dielectric tensor [1] given as a function of both position $x \in \mathbb{R}^d$ and refractive index vector $\xi \in \mathbb{R}^d$.

All the information on the plasma dynamics is encoded in the dielectric tensor $\varepsilon(h, x, \xi)$. We adopt the common approximation

$$\varepsilon(h, x, \xi) \approx \varepsilon_0(x) + ih\varepsilon_1(x, \xi),$$

where $\varepsilon_0(x)$ is the Hermitian part of the cold-plasma limit of the dielectric tensor [1], while $\varepsilon_1(x, \xi)$ is the anti-Hermitian part of the exact plasma dielectric tensor. In fact, we replace the Hermitian part of ε with the much simpler cold-plasma approximation.

For a weakly turbulent plasma, the electron density can be represented as a smooth background $n(x)$ plus a perturbation $\sqrt{h}\delta n(x)$, with $\delta n(x)$ being a random field independent of h and satisfying $\mathbb{E}\big(\delta n(x)\big) = 0$. The factor $\sqrt{h}$ is introduced in order to express the fact that fluctuations are weak, $\delta n(x)$ being understood as an $O(1)$ quantity. This particular scaling with the frequency of the beam can only be justified *a posteriori* [4]. In view of the particular structure of the cold-plasma dielectric tensor, one has

$$\varepsilon(h, x, \xi) \approx \varepsilon_0(x) + ih\varepsilon_1(x, \xi) + \sqrt{h}\big(I - \varepsilon_0(x)\big)\frac{\delta n(x)}{n(x)}. \qquad (3)$$

In presence of fluctuations, the solution $u(h, x)$ is also a random field.

2 The wave kinetic equation for beams

Following McDonald's work [5], we consider the Wigner matrix of the two-point correlation function $\rho(h, x, y) = \mathbb{E}\big(u(h, x)u^*(h, y)\big)$, i.e.,

$$W(h, x, \xi) = \int e^{-\frac{i}{h}\xi\cdot s}\rho\big(h, x + \tfrac{s}{2}, x - \tfrac{s}{2}\big)ds.$$

From equation (1), formal semiclassical asymptotics is obtained in the form [5]

$$W(h, x, \xi) \approx \sum\nolimits_\alpha w_\alpha(h, x, \xi)e_\alpha(x, \xi)e_\alpha^*(x, \xi).$$

This shows that, the leading-order Wigner matrix is diagonal on the basis of the eigenvectors $e_\alpha(x,\xi)$ of the cold-plasma dispersion tensor $D_0 = \xi^2 - \xi\otimes\xi - \varepsilon_0(x,\xi)$; the index α runs over all wave modes supported by the medium: a polarization e_α is included in the sum if the eigenvalue $H_\alpha = e_\alpha^* D_0 e_\alpha$ vanishes on a non-empty set $\mathcal{C}_\alpha$. For electron cyclotron waves, one finds $\mathcal{C}_\alpha = \{(x,\xi) : \xi_\perp = n_\alpha(x,\xi_\parallel)\}$, where $\xi_\perp = |\xi - \pi_b(x)\xi|$ and $\xi_\parallel = b(x)\cdot\xi$, whereas $\pi_b = b\otimes b$ and b is the unit vector in the direction of the local magnetic field.

The Wigner functions w_α are determined by a boundary value problem for the steady state wave kinetic equation, namely,

$$\begin{aligned} &\{H_\alpha, w_\alpha\} = -2\gamma_\alpha w_\alpha + \sum\nolimits_\beta S_{\alpha\beta}(\Gamma, w_\alpha, w_\beta),\\ &H_\alpha w_\alpha = 0, \quad w_{\alpha|\Sigma} = w_{\alpha,a}, \end{aligned} \tag{4}$$

where $\{\cdot,\cdot\}$ are canonical Poisson brackets, $\gamma_\alpha = e_\alpha^*\varepsilon_1 e_\alpha$ is the absorption coefficient, and $S_{\alpha\beta}$ is a matrix of scattering operators accounting for the effects of turbulent density fluctuations and depending on the Wigner matrix $\Gamma(h,x,\xi)$ of the density correlation $\mathbb{E}(\delta n(x)\delta n(y))$.

The constraint $H_\alpha w_\alpha = 0$ implies that w_α is a singular distribution supported on $\mathcal{C}_\alpha$. In view of the specific form of the latter, however, we can consider distributions w_α that are smooth in position x, so that the restriction $w_{\alpha|\Sigma}$ is well-defined. The boundary value $w_{\alpha,a}$ is obtained from the Wigner transform of u_a in equation (1).

3 Numerical solution

Due to the high dimensionality of the problem which is formulated in phase space and the constraint which forces distributional solutions, the natural choice of a numerical method for the wave kinetic equation (4) falls on Monte Carlo techniques.

We consider the auxiliary Cauchy problem (neglecting cross-polarization terms that means $S_{\alpha\beta}\approx 0$, when $\alpha\neq\beta$)

$$\begin{aligned} &\partial_t f_h + \{H_\alpha, f_h\} = -2\gamma_\alpha + S_{\alpha\alpha}(\Gamma, f_h, f_h),\\ &f_h(t,x,\xi) = |n\cdot\nabla_\xi H_\alpha| w_{\alpha,a}\otimes\delta_\Sigma,\\ &\qquad\qquad \text{for } (t,x,\xi)\in\{0\}\times\Sigma\times\mathbb{R}^d, \end{aligned} \tag{5}$$

where n is the unit normal to Σ and δ_Σ is the Dirac's delta on the plane Σ (given by $\delta(X_1)$ in coordinates $(X_1,\ldots,X_d)$ such that the X_1-axis is directed along n).

When Σ is located in vacuum and u_a corresponds to a Gaussian beam, this choice of the initial datum guarantees that f_h is a positive measure and $w(h,x,\xi) = \int f_h(t,x,\xi)dt$ satisfies the wave kinetic equation (4) for the single polarization α.

Equation (5) is solved by Monte Carlo ray tracing in the code `WKBeam`. First results for a fully realistic tokamak geometry demonstrate the validity of the method. A further quantitative analysis shows that scattering from density fluctuations has detrimental effects for electron cyclotron wave heating and current drive in large tokamaks.

References

[1] M. Bornatici, R. Cano, O. D. Barbieri and F. Engelmann, *Nuclear Fusion* **23** (1983), pp. 1153–1257.

[2] R. Prater, *Physics of Plasmas* **11** (2004), pp. 2349–2376.

[3] A. Martinéz, *An Introduction to Semiclassical and Microlocal Analysis*, Springer, New York, 2002.

[4] L. Ryzhik, G. Papanicolaou and J. Keller, *Wave Motion* **24** (1996), pp. 327–370.

[5] S. W. McDonald, *Physical Review A* **43** (1991), pp. 4484–4499.

Plasma and electromagnetic waves interaction: study of the hybrid resonance.

Olivier Lafitte[1,*], **Bruno Despres**[2], **Lise-Marie Imbert-Gerard**[3]

[1]Université Paris 13, Sorbonne Paris Cité, LAGA (UMR 7539) 93430 - Villetaneuse, France, and DM2S/STMF, CEA Saclay, 91191 Gif sur Yvette cedex

[2]Sorbonne Universités, UPMC Univ Paris 06, UMR 7598, Laboratoire Jacques-Louis Lions, F-75005, Paris, France

[3]Courant Institue of Mathematical Sciences, New York University, 251 Mercer Street, New York, NY 10012-1185.

*Email: lafitte@math.univ-paris13.fr

Abstract

The cold plasma model studied here is a simple model describing a plasma as a one species fluid, namely electrons, neglecting the ions motion. (24) This model includes different types of formal singularities, called resonances in the physics literature. We are interested in describing the behavior of the solutions in the neighborhood of the cyclotron resonance and the hybrid resonance, thanks to a limit absorption principle. A singular behavior appears only in the neighborhood of the hybrid resonance. It can be explicitly described thanks to a careful analysis based on Bessel functions.

Keywords: plasma physics, Bessel functions

1 Introduction

We consider a linearized model of interaction of a plasma with an electromagnetic wave. This model is associated with Tokamak studies, hence one studies an applied magnetic field, orientated along the vertical axis $\vec{e}_z$, depending on an horizontal coordinate x. The physical quantities of interest are $n_0(x)$, density of the plasma of electrons, and $B_0(x)$ the intensity of the applied magnetic field. From these two quantities, one defines usually two frequencies $\omega_c(x) = \frac{eB_0(x)}{m}$ (cyclotron frequency) and $\omega_p(x) = (\frac{4\pi e^2 n_0(x)}{m})^{\frac{1}{2}}$ (plasma frequency). A traditional analysis of the coupled system of equations relies on the definition of an equivalent dielectric tensor $\underline{\underline{\varepsilon}}(x,\omega)$, such that the resulting equation on the electric field $\vec{E}$ writes

$$\nabla \wedge (\nabla \wedge \vec{E}) = \omega^2 c^{-2} \underline{\underline{\varepsilon}}(x,\omega)\vec{E}. \qquad (1)$$

The equivalent dielectric tensor is singular at $\omega = \omega_c(x)$ (namely $(\omega - \omega_c(x))\underline{\underline{\varepsilon}}(x,\omega)$ has non zero limit when $\omega - \omega_c(x) \to 0$, and its diagonal term $\epsilon_{11}(x) = \epsilon_{22}(x)$ vanishes for $\omega = (\omega_p^2(x) + \omega_c^2(x))^{\frac{1}{2}} = \omega_h(x)$, which is called the upper hybrid singularity. This second singularity has been studied in a model case under the name of 'Budden' problem.

Our aim in this paper is to write a new formulation of the interaction problem, in which on one hand the cyclotron singularity does not give rise to a singular behavior of the electromagnetic field, and on the other hand, the upper hybrid frequency (X mode in the literature) gives rise to a singular behavior of the electromagnetic field (namey $||(\omega - \omega_h(x))\vec{E}(x)|| \geq c > 0$ in the neighborhood of the point x where $\omega = \omega_h(x)$). This difference will be emphasized through a physical quantity, called the heating of the plasma (introduced in [1]).

2 The electromagnetic model

Recall the classical electromagnetic equations with dissipation for the plasma of electrons characterized by ν

$$\nabla \wedge E = -\partial_t B, c^2 \nabla \wedge B = \partial_t E - \varepsilon_0^{-1} J$$
$$\partial_t J + \nu J = \varepsilon_0 (\omega_p(x))^2 E - \omega_c(x) J \wedge e_z$$

Assume that all fields depend only on (x,y,t), that the dependency on y,t is characterized by the phase $i\frac{\omega}{c}(\sin\theta_0 y - ct)$. One obtains the system (1), where $\underline{\underline{\varepsilon}}(x,\omega)$ is replaced by $\underline{\underline{\varepsilon}}^{\nu}(x,\omega)$. This system is not singular when $\nu > 0$ and the singularities appear when $\nu \to 0_+$. To study them, instead of obtaining an ODE on $\vec{E}$, we calculate (E_1, J_1, J_2) in terms of E_2, B_3, and use the result in

$\frac{dE_2}{dx} = i\omega B_3 + \frac{\omega}{c}\sin\theta_0 E_1, \quad c^2 \frac{dB_3}{dx} = i\omega E_2 - J_2.$

The resulting system is ($W = c^2 B_3$, the coefficients a_ν, b_ν, c_ν being explicit from $\varepsilon_{11}(x)$ and $\varepsilon_{12}(x) = -\varepsilon_{21}(x)$)

$$\frac{d}{dx}\begin{pmatrix} E_2 \\ W \end{pmatrix} = \begin{pmatrix} a_\nu(x,\omega) & b_\nu(x,\omega) \\ c_\nu(x,\omega) & -a_\nu(x,\omega) \end{pmatrix}\begin{pmatrix} E_2 \\ W \end{pmatrix}. \qquad (2)$$

The above matrix, called M_ν, has a finite limit when $\nu \to 0$ for x in a neighborhood of x_c, unique solution for a given frequency ω of the equation $\omega_c(x) = \omega$ where ω_c is the cyclotron frequency, and is singular at the unique x_h such that $\omega = \omega_h(x)$.
Our analysis is thus valid only when, in the neighborhood of the point that is considered, the coefficients are analytic with respect to x and to ν. This system (2) is equivalent to the system:

$$\begin{array}{l} \frac{d}{dx}(\frac{1}{c_\nu}(x)\frac{dW}{dx}) = \frac{1}{c_\nu}(a_\nu^2 + b_\nu c_\nu - c_\nu(\frac{a_\nu}{c_\nu})')W, \\ E_2 = c_\nu^{-1}(\frac{dW}{dx} + a_\nu W). \end{array} \tag{3}$$

The ordinary differential equation on W is regular for all ν in a neighborhood of x_c, and has a regular singular point at $x = x_h$ for $\nu = 0$. This regular singular point corresponds to a Bessel-type behavior(identical to the one studied in [2]), that we shall outline.

3 Bessel equation and solution

It is enough to recall that the Bessel equation (equivalent to the classical one through a change of unknown and variable) $\frac{dh}{dX} = (-\frac{1}{4X^2} - \frac{\lambda}{4X})h$ has $\sqrt{X}J_0(\lambda\sqrt{X})$ and $\sqrt{X}Y_0(\lambda\sqrt{X})$ as solutions. We shall use that $J_0(z)$ has an analytic expansion in powers of z^2, and that $T_0(z) = J_0(z) - \frac{2}{\pi}\ln z Y_0(z)$ has the same property.
Let us introduce the **eikonal equation**:

$$\frac{(\rho')^2(1+\rho)}{4\rho^2} = c_\nu(\frac{a_\nu}{c_\nu})' - a_\nu^2 - b_\nu c_\nu + \sqrt{-c_\nu}(\frac{1}{\sqrt{-c_\nu}})'' \tag{4}$$

Under the assumption that $\epsilon_{11}(x)$ has an isolated zero at x_h, one proves that there exists $X_\nu \in \mathbb{C}$ such that $|(x - X_\nu)c_\nu(x)| \geq a > 0$ in a neighborhood of $(x_h, 0)$. This leads to the existence of $\sigma_\nu(x)$, $\sigma_\nu(X_\nu) = 1$, such that the unique bounded solution in the neighborhood of x_h of (4) is $\rho_\nu(x) = (x - X_\nu)\sigma_\nu(x)$. One can then define approximate solutions of (3) in the neighborhood of X_ν as $U_\nu(x) = \sqrt{\frac{\rho_\nu'(x)}{\rho_\nu(x)}}J_0(\sqrt{\rho_\nu(x)})$ and $V_\nu(x) = \sqrt{\frac{\rho_\nu'(x)}{\rho_\nu(x)}}Y_0\sqrt{\rho_\nu(x)})$.
With these notations, there exists A_ν and B_ν, smooth in a neighborhood of X_ν uniformly in ν, such that (thanks to a Volterra integral equation, non singular), any solution of (3) write

$$W(x) = A_\nu(x)U_\nu(x) + B_\nu(x)V_\nu(x)$$

uniformly in a neighborhood of $(x_h, 0)$ in $\mathbb{C}^2$.

4 Resonant heating

It has been introduced previously the following quantity

$$\begin{array}{l} Q^\nu(a,b) = \Im\int_a^b(\underline{\underline{\varepsilon}}^\nu(x)\vec{E}^\nu(x), (\vec{E}^\nu)^*(x))dx \\ = -\Im(W^\nu(b)(E_2^\nu)^*(b)) + \Im(W^\nu(b)(E_2^\nu)^*(a)) \end{array}$$

where a and b are fixed.
In the case of the cyclotron singularity $x = x_c$, as the solution has a finite bounded limit when $\nu \to 0$, the limits of $W^\nu(b)(E_2^\nu)^*(b)$ and of $W^\nu(a)(E_2^\nu)^*(a)$ are real, hence the limit of the resonant heating for the cyclotron singularity is zero.
This proves that the so-called fluid model of the interaction of the plasma and the electromagnetic field has no singularity at the cyclotron frequency.
On the other hand, when a and b belong to the neighborhood on which all quantities are extendable, and such that $a \leq \Re X_\nu - \delta_0 \leq \Re X_\nu + \delta_0 \leq b$ for all admissible values of ν.
There limit value for vanishing ν is the resonant heating, and one gets

$$\begin{array}{c} \lim_{\nu\to 0_+} Q^\nu(a,b) \\ = \\ \frac{1}{\pi}|B_0(x_h)|^2|\epsilon_{12}^0(x_h)|^2(\mathrm{sign}(\partial_\nu\epsilon_{11}^\nu)|_{\nu=0}(x_h)). \end{array}$$

5 References

References

[1] B. Després, L.-M. Imbert-Gerard and R. Weder, Hybrid resonance of Maxwell's equations in slab geometry, J. Math. Pures App. **101** (5), 2014, 623-659.

[2] O. Lafitte, M. Williams and K. Zumbrun, High-frequency stability of multidimensional ZND detonations, 2013, to be published in Siam J. Math. Anal. arxiv preprint http://arxiv.org/abs/1312.6906.

The electromagnetic wave propagation in magnetized plasmas of Tokamaks

A. Back[1,*], **T. Hattori**[1], **S. Labrunie**1, **J-R Roche**[1], **P. Bertrand**[2]
[1]Université de Lorraine, Institut Elie Cartan, Nancy, France
[2]Université de Lorraine, Institut Jean Lamour, Nancy, France
[*]Email: aurore.back@univ-lorraine.fr

Abstract

Tokamaks plasmas must be heated to very high temperatures to undergo fusion reactions. To this end, many techniques exist such as Joule effect, injection of neutrals, and electromagnetic waves. We will focus on the last one. The waves are emitted by an antenna located on the wall of the tokamak; the choice of the frequency selects the region of the plasma which will be heated by absorbing some of the wave energy. Thus, we derive a model [1] for the propagation and the absorption of electromagnetic waves in a magnetized plasma. We refer to [2, 5] for the finite element discretization. The numerical results show where the absorption of waves takes place.

Keywords: Magnetised plasma, Maxwell's equations, Finite Element method

1 Introduction

Let us denote by Ω the domain representing the tokamak and $\mathbf{B}_{ext}$ the strong, external, static magnetic field. The wave propagation and absorption in the plasma is described by the equations [1, 2, 4, 5]

$$\begin{aligned} \mathbf{curl}\,\mathbf{curl}\,\mathbf{E} - \frac{\omega^2}{c^2}\underline{\boldsymbol{K}}\mathbf{E} &= 0 \quad \text{in } \Omega, \quad (1)\\ \operatorname{div}(\underline{\boldsymbol{K}}\mathbf{E}) &= 0 \quad \text{in } \Omega, \quad (2)\end{aligned}$$

where $\omega > 0$ is the wave frequency and c the speed of light satisfying $\epsilon_0\,\mu_0\,c^2 = 1$ with ϵ_0 and μ_0 the electric permittivity and magnetic permeability of vacuum. If we use the Stix coordinates, i.e., the third coordinate parallel to $\mathbf{B}_{ext}$, the (complex and non-Hermitian) tensor $\underline{\boldsymbol{K}}(\mathbf{x})$ has the following form:

$$\underline{\boldsymbol{K}}_S(\mathbf{x}) = \begin{pmatrix} S(\mathbf{x}) & -iD(\mathbf{x}) & 0 \\ iD(\mathbf{x}) & S(\mathbf{x}) & 0 \\ 0 & 0 & P_L(\mathbf{x}) \end{pmatrix}. \quad (3)$$

The expressions of the entries S, D and P_L involve the plasma and cyclotron frequencies of each species (ion and electron), and the collision frequency. The boundary conditions are defined as follows: we split the boundary of the domain Ω in two parts, Γ_A being the antenna and Γ_C the rest of the boundary. We can consider a Neumann boundary condition on Γ_A and a perfectly conducting condition on Γ_C:

$$\begin{aligned} \mathbf{curl}\,\mathbf{E}\times\mathbf{n} &= i\omega\mu_0\boldsymbol{j}_s \quad \text{on } \Gamma_A\\ \mathbf{E}\times\mathbf{n} &= \mathbf{0} \quad \text{on } \Gamma_C.\end{aligned}$$

or This boundary-value problem admits a *mixed augmented* variational formulation [1] where the the divergence condition (2) is taken as a constraint. For a numerical approach, we reduce the 3D problem to a series of 2D ones [3] by using cylindrical coordinates (R, Z, ϕ) and by expanding all functions as Fourier series in the angular coordinate ϕ. The modal variational formulation is then discretized using a Taylor–Hood P2-iso-P1 finite element in (R, Z) [2, 5]. The equations (1)-(2) being valid in any coordinate system, we derive from (3) the expression of the matrix $\underline{\boldsymbol{K}}$ in cylindrical coordinates:

$$\underline{\boldsymbol{K}}(\mathbf{x}) = \mathbb{P}(\mathbf{x})\underline{\boldsymbol{K}}_S(\mathbf{x})\mathbb{P}^\top(\mathbf{x}). \quad (4)$$

where $\mathbb{P}$ is the change of basis matrix from the Stix to the cylindrical coordinates. In the following we assume that the external magnetic field, and the electron and ion density and temperature are independent of ϕ. This implies that $\underline{\boldsymbol{K}}$ is independent of ϕ, thus the div $\underline{\boldsymbol{K}}$ operator can be expanded in Fourier series without a convolution product.

2 Accessibility conditions

We look for a solution to (1) in the form $\mathbf{E} = \tilde{\mathbf{E}}e^{i\mathbf{k}\cdot\mathbf{x}}$. Plugging this ansatz in (1), we obtain a linear system $\underline{\boldsymbol{M}}\tilde{\mathbf{E}} = 0$, with:

$$\underline{\boldsymbol{M}} = \begin{pmatrix} S - n_\parallel^2 & -iD & n_\perp n_\parallel \\ iD & S - n_\perp^2 - n_\parallel^2 & 0 \\ n_\perp n_\parallel & 0 & P - n_\perp^2 \end{pmatrix}$$

and $\mathbf{n} = \frac{c}{\omega}\mathbf{k} = \left(n_\perp, 0, n_\parallel\right)^\top$ in the Stix frame. The plasma is accessible, i.e., the waves can

propagate in it, if there exists $\mathbf{n} \in \mathbb{R}^3$ such that $\det \underline{\boldsymbol{M}} = 0$. One finds: $\det \underline{\mathbf{M}} = Q(\mathbf{n}_\perp^2)$, where:

$$Q(X) = S\,X^2 - ((S+P)r - D^2)\,X + P(r^2 - D^2),$$

and $r = S - n_\parallel^2$. The discriminant of Q writes as a function of r as:

$$\Delta_Q(r) = (S-P)^2 r^2 - 2D^2(S+P)r + D^2(D^2 + 4SP).$$

To find the sign of $\Delta_Q(r)$ we study its discriminant in r:

$$\Delta_{\Delta_Q} = 16 D^2 SP(D^2 - (S-P)^2).$$

Under conditions which are generally satisfied in practice, one can show that the plasma is accessible under either one of the following conditions:

- $\Delta_{\Delta_Q} \leqslant 0$, with $|r| \geqslant D$ or $-D \leqslant r \leqslant r' = \frac{D^2}{S+P}$
- $\Delta_{\Delta_Q} > 0$ and $r \notin]r_-, r_+[$ with

$$r_\pm = \frac{2D^2(S+P) \pm \sqrt{\Delta_{\Delta_Q}}}{2(S-P)^2},$$

and, again, $|r| \geqslant D$ or $-D \leqslant r \leqslant r'$.

3 Numerical results

We consider an external magnetic field with the following expression

$$\mathbf{B}_{ext}(R,Z) = \frac{B_0 R_0}{R}\left(\frac{-Z}{d(r)\,q(r)}, \frac{R-R_0}{d(r)\,q(r)}, 1\right)^\top$$

with B_0 a constant, R_0 the major radius of the torus, $d(r) = \sqrt{R_0^2 - r^2}$, $r = \sqrt{(R-R_0)^2 + Z^2}$, and $q(r) = \left(\frac{r}{r_0}\right)^2 (q_b - q_c) + q_c$ is the "safety factor", with r_0 the minor radius of the torus.

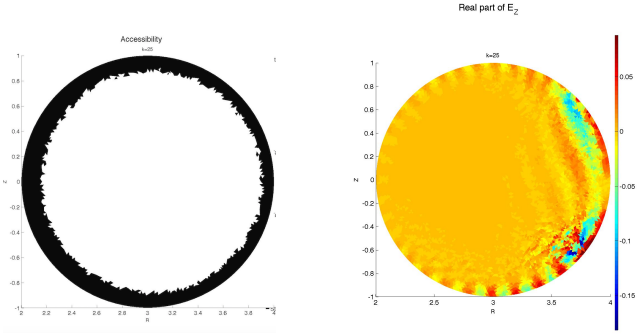

The first picture shows the accessibility of the plasma (black where accessible, white elsewhere), and the second the real part of the third component of the electric field.

References

[1] A. Back, T. Hattori, S. Labrunie, J-R Roche and P. Bertrand, Electromagnetic wave propagation and absorption in magnetized plasmas: variational formulations and domain decomposition, *M2AN* (2015), https://hal.archives-ouvertes.fr/hal-01075137 .

[2] T. Hattori, *Décomposition de domaine pour la simulation Full-Wave dans un plasma froid*. Ph.D. Thesis, Université de Lorraine (2014). (In French.)

[3] P. Ciarlet Jr, S. Labrunie, Numerical solution of Maxwell's Equations in axisymmetric domains with the Fourier Singular complement method, Differential Equations and Applications 3, (2011), pp. 113-155.

[4] E. Sébelin, Développement des méthodes numériques pour la résolution de la propagation et de l'absorption de l'onde hybride dans les tokamaks. Phd 1997. (In French.)

[5] Y. Peysson, J.R. Roche, P. Bertrand, J.H. Chatenet, C. Kirsch, A. Mokrani and S. Labrunie, Mixed augmented formulation (MAVF) for lower hybrid full-wave calculations, in *RF: The 18th Topical Conference on Radio Frequency Power in Plasmas*, V. Bobkov, J.M. Noterdaeme Eds., AIP Conf. Proc. **1187** (2009) 633–636.

Structure-preserving Maxwell solvers with particles: conforming and non-conforming schemes

Martin Campos Pinto[1,*], **Mathieu Lutz**[2], **Eric Sonnendrücker**[3]

[1]CNRS, UMR 7598, Laboratoire Jacques-Louis Lions, F-75005, Paris, France

[2]Univ. de Toulouse, UMR 5219, Institut de Mathématiques de Toulouse, F-31062 Toulouse, France

[3]Max-Planck Institute for plasma physics, Boltzmannstr. 2, D-85748 Garching, Germany

[*]Email: campos@ann.jussieu.fr

Abstract

This talk describes a unified approach to design conforming and non-conforming Galerkin schemes for the time-dependent Maxwell system that preserve a proper discrete Gauss law when coupled with a particle method for the Vlasov equation, or even when considered alone. Our approach consists of identifying structure relations that should be satisfied by the discrete divergence involved in the Gauss law and the associated discrete continuity equation. After reviewing the case of curl-conforming finite elements we indicate how to extend the method to non-conforming schemes, and we provide numerical illustrations.

Keywords: Maxwell-Vlasov system, compatible Gauss law, charge-conserving method, discrete continuity equation.

1 Introduction

In plasma physics the Maxwell evolution system

$$\begin{cases} \partial_t \boldsymbol{E} - \mathbf{curl}\, B = -\boldsymbol{J} \\ \partial_t B + \operatorname{curl} \boldsymbol{E} = 0 \end{cases} \tag{1}$$

is often coupled to the Vlasov equation

$$\partial_t f + \mathbf{v} \cdot \boldsymbol{\nabla}_{\mathbf{x}} f + (\boldsymbol{E} + \mathbf{v} \times \boldsymbol{B}) \cdot \boldsymbol{\nabla}_{\mathbf{v}} f = 0 \tag{2}$$

where $f = f(t, \mathbf{x}, \mathbf{v})$ is the phase-space distribution of a charged particles gas. Here the current density is $\boldsymbol{J} := \int \mathbf{v} f \, \mathrm{d}\mathbf{v}$ and if (1) is considered alone, it is a given source term.

The problem of charge conservation is related to the fact that numerical schemes for (1) should preserve a discrete analog of Gauss's law

$$\operatorname{div} \boldsymbol{E} = \rho \tag{3}$$

where $\rho := \int f \, \mathrm{d}\mathbf{v}$ is the charge density. It is indeed the case at the continuous level, thanks to the continuity equation

$$\partial_t \rho + \operatorname{div} \boldsymbol{J} = 0 \tag{4}$$

satisfied by the sources. However for a given discretization of (1)-(2) there is no reason that a proper discrete continuity equation holds. This leads to the development of small errors which accumulate to large deviations for long simulation times, see e.g., [6]

2 Structure preserving discretizations

At the continuous level, we see that the Gauss law (3) is preserved by taking the divergence of the Ampere equation and using the continuity equation (4). Here we have also used that the divergence of a curl always vanishes, i.e.,

$$\operatorname{div} \mathbf{curl} = 0. \tag{5}$$

The idea of structure-preserving discretizations is to get a discrete version of (4) and (5). Thus, we shall look for approximations of the form

$$\begin{cases} \partial_t \boldsymbol{E}_h - \mathbf{curl}_h\, B_h = -\boldsymbol{J}_h \\ \partial_t B_h + \operatorname{curl}_h \boldsymbol{E}_h = 0 \end{cases} \tag{6}$$

with the following properties:

a) the approximated sources satisfy a discrete continuity equation analog to (4),

$$\partial_t \rho_h + \operatorname{div}_h \boldsymbol{J}_h = 0 \ ; \tag{7}$$

b) with underlying discrete operators that satisfy an analog to (5),

$$\operatorname{div}_h \mathbf{curl}_h = 0. \tag{8}$$

The resulting field will then preserve the corresponding Gauss law,

$$\operatorname{div}_h \boldsymbol{E}_h = \rho_h \tag{9}$$

and a similar procedure can be applied for B.

This program gives satisfactory results for several classes of solvers. For Finite Differences schemes, conservative methods to compute $\boldsymbol{J}_h$

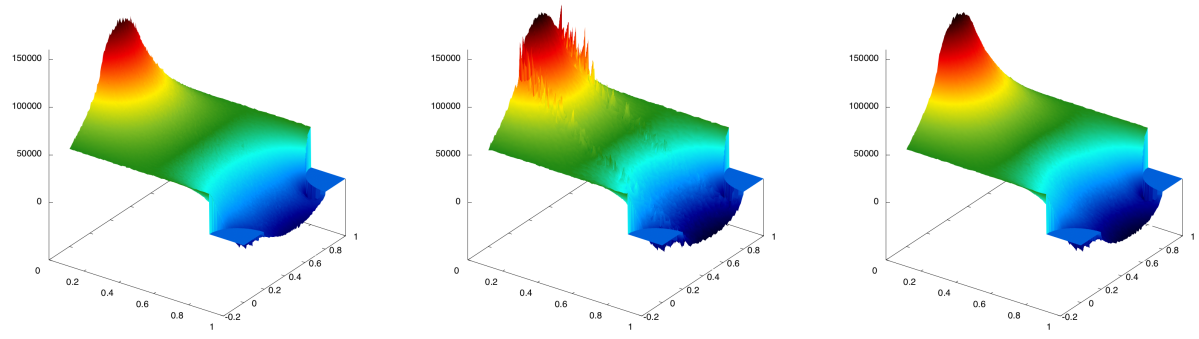

Figure 1: Beam test case. Numerical fields E_x computed with a curl-conforming scheme (left) and DG schemes using either a standard current deposition method (center) or a compatible one (right).

have been introduced in [7] and later improved by other authors. In the scope of curl-conforming finite elements, deposition schemes have been proposed in [4] and generalized to arbitrary orders and unstructured meshes in [1].

However, for non-conforming schemes this procedure fails to provide stable solutions, because (8) does not suffice to guarantee that the preserved Gauss law is strong enough. Indeed to ensure long-time stability (9) should allow to characterize the fields in $\ker \operatorname{curl}_h$, since their temporal growth is not controlled in the evolution equation (6). If one considers the case of metallic boundary conditions for simplicity, relation (8) should then be replaced by the stronger

$$\ker \operatorname{div}_h = (\ker \operatorname{curl}_h)^{\perp} \qquad (10)$$

as is the case for the continuous operators. For curl-conforming schemes, (10) is typically guaranteed by an exact sequence property satisfied by the discrete finite element spaces [3]. To design charge-conserving schemes for non-conforming Maxwell solvers we thus need to find exact sequences that hold in the corresponding non-conforming spaces. We will describe how this approach can be applied to DG schemes, leading to "source correction" methods.

References

[1] M. Campos Pinto, S. Jund, S. Salmon and E. Sonnendrücker, Charge conserving FEM-PIC schemes on general grids, *C.R. Mécanique* **342** (2014), pp. 570–582.

[2] M. Campos Pinto and E. Sonnendrücker, Gauss-compatible Galerkin schemes for time-dependent Maxwell equations, (2014), `http://hal.upmc.fr/hal-00969326`.

[3] M. Costabel and M. Dauge, Computation of resonance frequencies for Maxwell equations in non-smooth domains, in *Topics in computational wave propagation 2003,* Springer, Berlin, pp. 125–161.

[4] J.W. Eastwood, The virtual particle electromagnetic particle-mesh method, *Computer Physics Comm.* **64** (1991), pp. 252–266.

[5] P. Monk and L. Demkowicz, Discrete compactness and the approximation of Maxwell's equations in $\mathbb{R}^3$, *Math. of Computation* **70** (2001), pp. 507–523.

[6] C.-D. Munz, R. Schneider, E. Sonnendrücker and U. Voß, Maxwell's equations when the charge conservation is not satisfied, *C.R. Mathématique* **328** (1999), pp. 431–436.

[7] J. Villasenor and O. Buneman, Rigorous charge conservation for local electromagnetic field solvers, *Computer Physics Comm.* **69** (1992), pp. 306–316.

Contributed Talks

Monday, July 20
Morning Session
10:45 – 12:45

High-fidelity numerical simulation of the dynamic beam equation

Ken Mattsson[1,*], **Vidar Stiernström**[1]
[1]Department of Information Technology, Uppsala University, Sweden
[*]Email: ken.mattsson@it.uu.se

Abstract

A high-fidelity finite difference approximation of the dynamic beam equation is derived. Different types of well-posed boundary conditions are analysed. The boundary closures are based on the summation-by-parts (SBP) framework and the boundary conditions are imposed using a penalty (SAT) technique, to guarantee linear stability. The resulting SBP-SAT approximation leads to fully explicit time integration. The accuracy and stability properties of the newly derived SBP-SAT approximations are demonstrated for both 1-D and 2-D problems.

Keywords: finite difference methods, high-order derivative, high-order accuracy, stability, boundary treatment, dynamic beam equation

1 Introduction

The dynamic beam equation (DBE), also known as the Euler-Bernouilli beam equation, is a standard model of flexible body dynamics and is thus of interest in many engineering applications where beams are used as the basis of supporting structure or as axles, e.g when studying vibrations of buildings or railway structures. The DBE is derived from Euler-Bernoulli beam theory, one of the simplest beam theories dating back to the 18th century.

To capture the dispersive nature of the DBE efficiently it is essential that high-order (i.e. higher than second order) spatially accurate numerical methods are used to capture the high-frequency parts of the solution. Since the wave speed scales as the frequency the physics require $\mathrm{d}t \simeq \mathrm{d}x^2$. In the literature, numerical analysis of the DBE in time-domain is very scarce, in particular concerning higher-order methods. In the present study we analyse and solve the DBE in time-domain using an explicit time-symmetric finite difference method, with a CFL condition similar to the physical time-step requirement. The dispersive nature of the DBE makes a high-fidelity numerical simulation computationally demanding. A well-proven approach to reduce the computational cost is to employ a high-order accurate finite-difference method. The major difficulty with higher-order finite difference methods is to obtain a stable boundary treatment, which has received considerable past attention.

The SBP-SAT method is a robust and well-proven high-order finite difference methodology that ensures stability of time-dependent partial differential equations (PDE). The SBP-SAT approach has so far been developed for problems involving first and second derivatives in space (see for example [1, 3]). Recently, high-order accurate SBP operators for third and fourth derivatives were derived [2].

2 The dynamic beam equation

For a beam of length L with its axis along the x-direction, denote the deflection of the beam from its axis as u. The governing equation of the 1-D DBE is given by,

$$\mu u_{tt} = -(E\,I\,u_{xx})_{xx} + F\ ,\ 0 \le x \le L,\ t \ge 0\ ,$$

where $F = F(x,t)$ is a forcing function, E the elastic modulus of the beam, I the second moment of area of the cross section of the beam and μ the mass per unit length.

A few of the most commonly used and well-posed boundary conditions (BC) for the DBE are listed below,

$$\begin{array}{llll} u = 0, & u_x = 0, & \text{'Clamped'}, \\ u_{xx} = 0, & u_{xxx} = 0, & \text{'Free'}, \\ u = 0, & u_{xx} = 0, & \text{'Hinged'}, \\ u_x = 0, & u_{xxx} = 0, & \text{'Sliding'}\ . \end{array} \tag{1}$$

Next to each of the BC in (1) the physical interpretation of the BC imposed on a homogeneous beam is stated. By specifying the ingoing characteristic variables (here referred to as the *characteristic* BC) we obtain the most dissipative set of well-posed BC,

$$\begin{array}{llll} u_{xt} - u_{xx} = 0, & u_t + u_{xxx} = 0, & x = 0\ , \\ u_{xt} + u_{xx} = 0, & u_t - u_{xxx} = 0, & x = L\ . \end{array} \tag{2}$$

This will introduce damping through the boundaries (, i.e., nonreflecting BC). In the present study the clamped BC is of special interest as they are particularly difficult to impose using the SBP-SAT method.

m	$\log l^{2^{(2nd)}}$	$q^{(2nd)}$	$\log l^{2^{(6th)}}$	$q^{(6th)}$
51	-1.43		-3.09	
101	-1.67	0.82	-4.58	4.93
201	-2.32	2.15	-6.32	5.80
401	-2.69	1.66	-8.02	5.81

Table 1: $log(l^2 - errors)$ and convergence q.

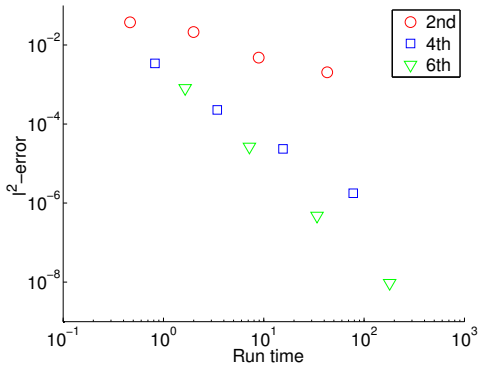

Figure 1: The l^2-error as a function of runtime.

3 Computations

The accuracy and efficiency properties of the SBP-SAT approximations are verified against analytic solutions in 1-D. In Table 1 we present the convergence results (with clamped BC) using the second- and sixth-order accurate SBP-SAT approximations. The convergence rate is calculated as

$$q = \log_{10}\left(\frac{\|u - v^{(m_1)}\|_h}{\|u - v^{(m_2)}\|_h}\right) / \log_{10}\left(\frac{m_1}{m_2}\right) , \quad (3)$$

where u is the analytic solution, and $v^{(m_1)}$ the corresponding numerical solution with m_1 unknowns.
$\|u - v^{(m_1)}\|_h$ is the discrete l^2 norm of the error. In Figure 1 we compare the efficiency for different orders of accuracy. We plot the $l^2 - error$ as a function of runtime (where the unit is seconds).

A 2-D extension of the DBE with clamped BC is also presented. In Figure 2 a sixth-order accurate simulation using 401×401 grid-points is presented. The initial data is a Gaussian pulse, and at $t = 0.003$ the dispersive waves have reached the boundaries.

A detailed convergence and efficiency analysis (not shown in this short abstract) for the 2-D simulations were performed and showed similar results as presented in Figure 1 and Table 1.

Figure 2: A high-fidelity simulation of the 2-D DBE with clamped BC. Initial data (Gaussian) and the solution at $t = 0.003$.

References

[1] M. Almquist, K. Mattsson, and T. Edvinsson. High-fidelity numerical solution of the time-dependent Dirac equation. *J. Comput. Phys.*, 262:86–103, 2014.

[2] Ken Mattsson. Diagonal-norm summation by parts operators for finite difference approximations of third and fourth derivatives. *J. Comput. Phys.*, 274(0):432 – 454, 2014.

[3] Kristoffer Virta and Ken Mattsson. Acoustic wave propagation in complicated geometries and heterogeneous media. *J. Scient. Comput.*, pages 1–29, 2014.

High-fidelity numerical simulation of solitons in the nerve axon

Ken Mattsson[1], **Jonatan Werpers**[1,*]

[1]Department of Information Technology, Uppsala University, Uppsala, Sweden

*Email: jonatan.werpers@it.uu.se

Abstract

We derive high-order accurate finite difference schemes for a non-linear soliton model of nerve signal propagation in axons. Two types of well-posed boundary conditions are analysed. The boundary closures are based on the summation-by-parts (SBP) [4] framework and the boundary conditions are imposed weakly using a penalty technique [3], to guarantee linear stability. The resulting finite difference approximations lead to fully explicit time integration. The accuracy and stability properties of the newly derived finite difference approximations are demonstrated for a 1-D soliton solution.

Keywords: finite difference methods, high-order derivative, high-order accuracy, stability, boundary treatment, nerve signals, solitons

1 Introduction

Commonly, nerve signals in the axon are modeled using the Hodgkin and Huxley model [1]. However, it has been suggested that the HHM does not accurately describe certain phenomena observed in experiments. Some examples are the effects of anesthesia, temperature induced nerve pulses and thickness changes with pulse propagation. Trying to address these discrepancies, researchers are looking for new ways to describe the propagation of nerve signals. In a series of recent publications by Heimburg *et al.* [2] an alternative thermodynamic model is proposed in which nerve pulses are described as a localized density pulse (soliton) in the axon membrane. This model will be referred to as the nerve soliton model (NSM) in the present study.

2 The equation

The NSM is a partial differential equation in time and one dimension of space. It's foundation is the the wave equation for area density changes,

$$\frac{\partial^2}{\partial \tau^2}\Delta\rho^A = \frac{\partial}{\partial z}\left[c^2\frac{\partial}{\partial z}\Delta\rho^A\right], \tag{1}$$

where τ is time, z is position, c is the speed of sound and $\Delta\rho^A$ is the density offset from the equilibrium. The sound velocity in the lipid membrane is considered a function of density, and is represented by a truncated power series,

$$c^2 = c_0^2 + p\Delta\rho^A + q\left(\Delta\rho^A\right)^2, \tag{2}$$

where p and q are parameters determined by measurements and c_0 is the velocity of small amplitude sound. To account for dispersion observed in experiments an extra term $-h\frac{\partial^4}{\partial z^4}\Delta\rho^A$ is added. We finally arrive at the following mathematical model for the density of the lipid membrane in the axon,

$$\frac{\partial^2}{\partial \tau^2}\Delta\rho^A = \frac{\partial}{\partial z}\left[B(\Delta\rho^A)\frac{\partial}{\partial z}\Delta\rho^A\right] - h\frac{\partial^4}{\partial z^4}\Delta\rho^A, \tag{3}$$

where

$$B(\Delta\rho^A) = c_0^2 + p\Delta\rho^A + q\left(\Delta\rho^A\right)^2 \tag{4}$$

By introducing the variable changes

$$\begin{aligned} &u = \frac{1}{\rho_0^A}\Delta\rho^A, \quad x = \frac{c_0}{h}z, \quad t = \frac{c_0^2}{\sqrt{h}}\tau, \\ &\gamma_1 = \frac{\rho_0}{c_0^2}p, \qquad \gamma_2 = \frac{\rho_0^2}{c_0^2}q, \end{aligned} \tag{5}$$

we obtain the following dimensionless version of (3),

$$u_{tt} = \left(b(u)u_x\right)_x - u_{xxxx}, \tag{6}$$

where

$$b(u) = 1 + \gamma_1 u + \gamma_2 u^2, \tag{7}$$

and subscripts denote differentiation.

Remark 1 *The empirical values of γ_1 and γ_2 guarantees that $b(u) > 0$ for all u.*

In the present study we analyse two kinds of well-posed boundary conditions, characteristic BC,

$$\begin{aligned} &u_{xt} - u_{xx} = g_0^{(1)}(t), && x = 0\,, \\ &\sigma u_t - bu_x + u_{xxx} = g_0^{(2)}(t), && x = 0\,, \\ &u_{xt} + u_{xx} = g_L^{(1)}(t), && x = L\,, \\ &\sigma u_t + bu_x - u_{xxx} = g_L^{(2)}(t), && x = L\,, \end{aligned} \tag{8}$$

m	$\log l^{2(4th)}$	$q^{(4th)}$	$\log l^{2(6th)}$	$q^{(6th)}$
51	-1.51		-1.49	
101	-2.01	1.66	-2.71	4.03
201	-3.56	5.15	-4.46	5.81
401	-4.99	4.77	-5.91	4.83

Table 1: $log(l^2 - errors)$ and convergence rates comparing the fourth- and sixth-order accurate SBP-SAT approximations (10).

and Dirichlet-Neumann BC

$$\begin{array}{llll} u = g_0^{(1)}(t) & u_x = g_0^{(2)}(t) & x = 0 \\ u = g_L^{(1)}(t) & u_x = g_L^{(2)}(t) & x = L \end{array} . \tag{9}$$

3 The semi-discrete problem

Utilizing the SBP-SAT framework write the semidiscrete version of (6) with BC in (9) as

$$\begin{aligned} v_{tt} = D_1 B D_1 v - D_4 v &+ H^{-1}\tau_l^{(1)}\left\{e_1^T v - g_0^{(1)}\right\} \\ &+ H^{-1}\tau_l^{(2)}\left\{d_{1;1} v - g_0^{(2)}\right\} \\ &+ H^{-1}\tau_r^{(1)}\left\{e_m^T v - g_L^{(1)}\right\} \\ &+ H^{-1}\tau_r^{(2)}\left\{d_{1;m} v - g_L^{(2)}\right\} . \end{aligned} \tag{10}$$

where $\tau_i^{(j)}$ are penalty paramters. We show that by choosing the penalty parameters correctly and letting the operators satisfy a compatibility condition we achieve stability for the frozen coefficient problem.

4 Computations

We present a convergence study where we compare the numerical solution to an analyitical soliton solution. The analytical solution is imposed at the boundaries. The results are shown in Table 1. Figure 1 shows a soliton reflecting off of a homogenouse Dirichlet-Neumann BC.

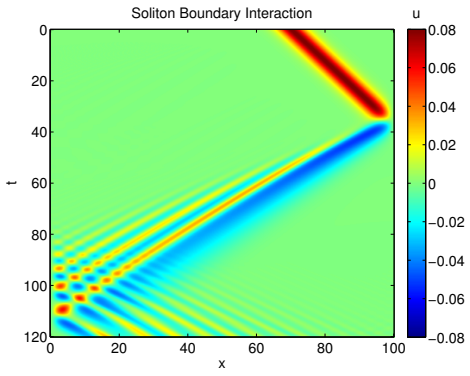

Figure 1: Soliton interaction with homogeneous Dirichlet-Neumann BC.

References

[1] A.L. Hodgkin and A.F. Huxley. A quantitative description of membrane current and its application to conduction and excitation in nerve. *J. Physiol.*, 117:500–544, 1952.

[2] T. Heimburg and A.D. Jackson. On soliton propagation in biomembranes and nerves. *Proc. Natl Acad. Sci. USA*, 102:9790–9795, 2005.

[3] M. H. Carpenter, D. Gottlieb, and S. Abarbanel. Time-stable boundary conditions for finite-difference schemes solving hyperbolic systems: Methodology and application to high-order compact schemes. *J. Com- put. Phys.*, 111(2), 1994.

[4] H.-O. Kreiss and G. Scherer. Finite element and finite difference methods for hyperbolic partial differential equations. *Mathematical Aspects of Finite Elements in Partial Differential Equations., Academic Press, Inc.*, 1974.

Uniformly optimised wavenumber approximations by central finite difference operators

Viktor Linders[1,*], **Jan Nordström**[1]

[1]Department of Mathematics, Computational Mathematics, Linköping University, SE-581 83 Linköping, Sweden

[*]Email: viktor.linders@liu.se

Abstract

We construct accurate central difference schemes for problems involving high frequency waves or multi-frequency solutions over long time intervals, with a relatively coarse spatial mesh, and with an easily obtained error bound. It is demonstrated that the problem of constructing central difference stencils that have minimal dispersion error in the L^∞-norm can be recast into a problem of approximating a continuous function from a finite dimensional subspace with a basis forming a Chebyshev set. In this new formulation, characterising and numerically obtaining optimised schemes can be done using established theory.

Keywords: Dispersion relation, wavenumber approximation, finite differences.

1 Introduction

Numerical schemes that preserve dispersion relations have received considerable attention in the past few decades. Among the early comprehensive treatments are [1, 2]. The motivation comes from problems involving wave propagation, where one must consider errors stemming from inexact approximations of wave speed. In particular, waves with high wavenumbers require small spatial increments, Δx, in order to be properly resolved. Over sizeable intervals the dispersion error may dominate the error in the approximation, which restricts the size of Δx. Such problems are common in computational fluid dynamics, aeroacoustics and electromagnetism.

We will henceforth consider centered finite difference stencils. Traditionally such stencils have been constructed by optimising the approximation accuracy with respect to the bandwidth of the scheme. However, it can be shown that these *classical* stencils underestimate the phase and group speeds of propagating waves, which stems from poor preservation of the dispersion relation of the governing problem.

We present a new family of central spatial discretisation that mimic the dispersion properties of the governing problem by minimising the dispersion error in the L^∞-sense.

2 Improved dispersion preservation

Consider a central difference stencil approximating a first derivative of the function $u(x,t)$:

$$\left(\frac{\partial u}{\partial x}\right)_i + \mathcal{O}(\Delta x^{2p}) = \frac{1}{\Delta x}\sum_{k=1}^{p+n} a_k(u_{i+k} - u_{i-k}).$$

Such a scheme uses $(p+n)$ points on either side of x_i to approximate the derivative, however the formal accuracy is $\mathcal{O}(\Delta x^{2p})$. Here a_k are the coefficients of the stencil. Only p of the coefficients are required to fulfil the accuracy requirements. We are thus left with n degrees of freedom that we shall use to minimise the dispersion error.

The *numerical wavenumber* corresponding to this scheme is (see e.g. [2])

$$\bar{\xi} = 2\sum_{k=1}^{p+n} a_k \sin(k\xi).$$

Here $\xi = \kappa\Delta x$, where κ denotes the exact or *analytic wavenumber*. Let $\tilde{\mathbf{a}} = (a_1, \dots, a_{p+n})$. Our goal may be formulated as: Find

$$\underset{\tilde{\mathbf{a}}\in\mathbb{R}^{p+n}}{\operatorname{argmin}} \|\xi - \bar{\xi}\|_\infty \tag{1}$$

ensuring that the stencil has accuracy $\mathcal{O}(\Delta x^{2p})$.

It is known (see e.g. [3]) that a unique solution to problem (1) exists if, for any choice of $\tilde{\mathbf{a}}$, the function $\bar{\xi}$ has at most $n-1$ zeros in some finite interval. Unfortunately this cannot be guaranteed for any $n \geq 1$. We are thus forced to reformulate the problem. The following theorem is useful:

Theorem 1 *The numerical wavenumber of the $2p^{th}$ order central difference stencil can be equivalently written as*

$$\bar{\xi} = \bar{\xi}_c + \psi(\xi, \mathbf{a})$$

where $\bar{\xi}_c$ *is the numerical wavenumber of the* $2p^{th}$ *order classical central difference stencil and*

$$\psi(\xi, \mathbf{a}) = \sum_{j=1}^{n} a_{p+j}\phi_j(\xi),$$

$$\phi_j(\xi) = 2\sin\left((p+j)\xi\right) + 2\sum_{k=1}^{p} \alpha_k^{(j)} \sin\left(k\xi\right).$$

Here, the vector $\mathbf{a} = (a_{p+1}, \ldots, a_{p+n})$ *and the coefficients* $\alpha_k^{(j)}$ *are independent of* $\mathbf{a}$ *and* ξ*.*

The functions ϕ_j are linearly independent and thus span some n-dimensional vector space Ξ_n. Hence, we may reformulate problem (1) in terms of the equivalent problem: Find

$$\underset{\mathbf{a}\in\mathbb{R}^n}{\operatorname{argmin}} \|E_c - \psi(\xi, \mathbf{a})\|_\infty \tag{2}$$

where E_c is the dispersion error of the classical $2p^{\text{th}}$ order stencil and $\psi \in \Xi_n$.

We can show the following theorem:

Theorem 2 *The functions* ϕ_j *form a Chebyshev set on the interval* $\xi \in (0, \pi)$*. Equivalently, any non-trivial function* $\psi(\xi, \mathbf{a}) \in \Xi_n$ *has at most* $n - 1$ *zeros in this interval.*

This is sufficient to guarantee the existence and uniqueness of a solution to problem (2) and thus also to problem (1) [3].

Conveniently, due to Remez [4], there is a convergent algorithm for finding the desired vector $\mathbf{a}$. Thus, in principle we may find new central differences stencils of arbitrary accuracy and with n free parameters that minimise the dispersion error in the L^∞-sense.

A toy example is presented in Fig. 1. Here the dispersion error of a 31 point wide stencil of formal accuracy $\mathcal{O}(\Delta x^2)$ is shown. The stencil is optimal in the L^∞-sense for wavenumbers in the interval $\xi \in [0, \pi/2]$. This particular stencil has a dispersion error of the order $\mathcal{O}(10^{-12})$.

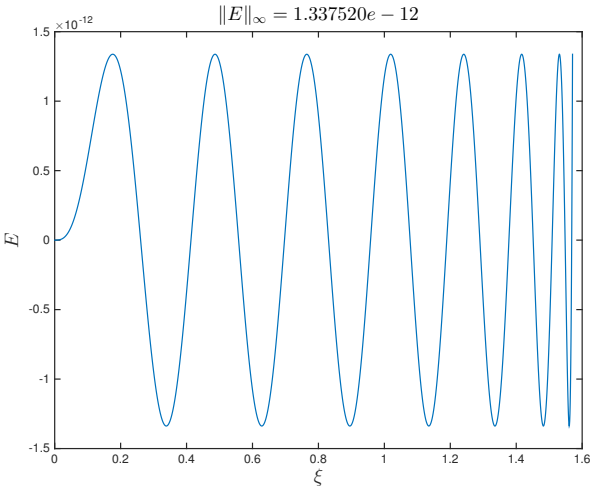

Figure 1: Toy example of a central difference stencil with minimal dispersion error in the L^∞-sense. The stencil is optimised for wavenumbers in the interval $\xi \in [0, \pi/2]$. Here, $p = 1$ and $n = 14$, i.e. the stencil has formal accuracy $\mathcal{O}(\Delta x^2)$ and is 31 points wide.

References

[1] S. K. Lele, Compact finite difference schemes with spectral-like resolution, *Journal of Computational Physics* **103** (1992), pp. 16–42.

[2] C. Tam and J. Webb, Dispersion-relation-preserving finite difference schemes for computational acoustics, *Journal of Computational Physics* **107** (1993), pp. 262–281.

[3] G. A. Watson, *Approximation Theory and Numerical Methods*, John Wiley & Sons Ltd., 1980

[4] E. Remez, Sur le calcul effectif des polynomes d'approximation de Tchebichef, *Comptes Rendues* **199** (1934), pp. 174–181.

Adaptive Eigenspace Inversion for the Helmholtz Equation

Marcus J. Grote[1], **Uri Nahum**[1,*]
[1]Department of Mathematics and Computer Science, University of Basel, Basel, Switzerland
*Email: uri.nahum@unibas.ch

Abstract

An adaptive inversion method was presented in [1] for time-dependent inverse scattering problems set in a (known) constant background medium. Here we extend that approach to a general varying background in the frequency domain, while dispensing with the need for an open observational subset. The resulting adaptive eigenspace inversion (AEI) method not only proves more accurate and robust to missing data, but also incurs only a fraction of the computational cost of a standard grid-based truncated Gauss-Newton approach.

Keywords: Full wave-form inversion, time harmonic scattering, inverse medium problem.

1 Inverse medium problem

We consider a time-harmonic scattering problem in unbounded space. Given N_E sources f_k inside a bounded region $\Omega \subset \mathbb{R}^d$, $d \leq 3$, and corresponding measurements at the boundary $\partial\Omega$, we wish to reconstruct the (unknown) velocity $u(x)$ inside Ω. Outside Ω, the velocity $u_0(x)$ is known and may vary. Then, for each source f_k, the scattered field y_k satisfies the Helmholtz equation:

$$\begin{cases} -\nabla\cdot(u^2\nabla y_k) - \omega^2 y_k = f_k & \text{in } \Omega\,, \\ \dfrac{\partial y_k}{\partial n} = \dfrac{i\omega}{u_0} y_k & \text{on } \partial\Omega. \end{cases} \tag{1}$$

Here ω is the time frequency and we impose a Sommerfeld boundary condition on $\partial\Omega$, for simplicity. Next, we let $q = u^2$ and discretize (1) with second-order finite differences on an equispaced Cartesian grid. This yields the linear systems

$$\boldsymbol{A}(q)\boldsymbol{y}_k = \boldsymbol{f}_k\,, \quad k = 1, \ldots, N_E. \tag{2}$$

Given measurements $\hat{\boldsymbol{y}}_k$, $k = 1, \ldots, N_E$, different methods from PDE-constrained optimization can be used to retrieve q by minimizing the misfit, stated either in the full-space [2] or in the reduced-space [3] formulation.

Here, we opt for the reduced-space approach and thus seek q, which minimizes

$$\min_{q\in S} L(q) = \frac{1}{2}\sum_{k=1}^{N_E} \left\| \boldsymbol{V}\boldsymbol{A}(q)^{-1}\boldsymbol{f}_k - \hat{\boldsymbol{y}}_k \right\|^2\,, \tag{3}$$

where $\boldsymbol{V}$ is the evaluation matrix at the sensor positions. To solve (3), we use a standard truncated Gauss-Newton (G-N) method and solve the linear systems inexactly using a fixed number of CG iterations [4,5], which avoids the need for extra regularization.

To reduce the risk of convergence to a false local minimum, we use frequency stepping, that is we solve (3) for a sequence of increasing ω, initializing each optimization run with the solution q_ω obtained from the previous lower frequency.

2 Adaptive eigenspace basis

Usually q is described by grid-based point values and hence expanded in a nodal basis. In the AEI method, we instead expand q as

$$q(x) = q_0(x) + \sum_{m=1}^{K} \beta^m \phi^m(x)\,, \tag{4}$$

where ϕ^m are the first K eigenfunctions of

$$\begin{cases} -\nabla\cdot(\mu(x)\nabla\phi^m(x)) = \lambda^m\phi^m(x) & x \in \Omega\,, \\ \phi^m(x) = 0 & x \in \partial\Omega\,, \end{cases}$$

and μ is defined as

$$\mu(x) = \frac{1}{|\nabla q_\omega(x)|^p + \varepsilon}\,, \quad \varepsilon > 0\,. \tag{5}$$

In (5) we set $p = 0$ for the initial frequency, ω_0, and $p = 1$ otherwise. To handle the varying surrounding medium, we determine q_0 in (4) from the solution of

$$\begin{cases} -\nabla\cdot(\mu(x)\nabla q_0(x)) = 0 & \text{in } \Omega\,, \\ q_0(x) = u_0^2(x) & \text{on } \partial\Omega\,, \end{cases} \tag{6}$$

We start with a small number of eigenfunctions K and as ω increases, we also increase K.

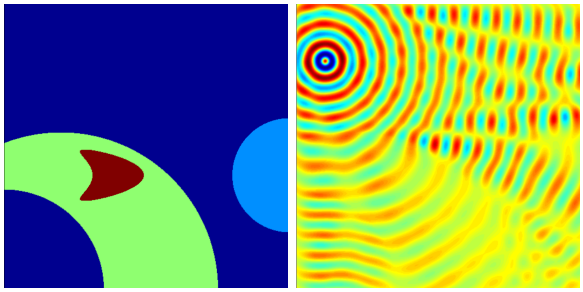

Figure 1: Left: true profile q; Right: real part of y_k with f_k at $(0.1, 0.8)$ and $\omega = 90$.

Numerical Experiments

We consider the true profile, q, shown in Figure 1, which mimics a layered material with regions of different wave speed. The receivers are located on the four lateral boundaries of $\Omega = (0,1) \times (0,1)$. Moreover, nine Gaussian sources are located at $(0.1, 0.8), \ldots, (0.9, 0.8)$ and one additional source at $(0.15, 0.15)$. We use a 500×500 mesh and set the initial profile $q = 1$. To avoid any inverse crime, we calculated the reference solution on a 1024×1024 mesh. Starting at the lowest frequency $\omega_0 = 8$, we use frequency stepping at the frequencies $\omega = 10, 12, 14, \ldots, 90$. The reconstructed profiles are shown in the top of Figure 2 either for a nodal basis (left) or the adaptive eigenspace basis (right).

	Full data		Partial data	
Basis	Err	N_q	Err	N_q
Nodal	15.91%	501,000	30.24%	501,000
AEI	4.65%	≤ 360	4.80%	≤ 360

Next, we repeat the previous experiment, but now omit the receivers at the lower boundary of Ω together with the tenth source located at $(0.15, 0.15)$. As shown in the bottom of Figure 2, the AEI method is still able to recover q, unlike the standard grid-based approach, while using only a small fraction of the number of control variables N_q. Thus, we dramatically reduce the number of control variables, while the reconstructions are more accurate and more tolerant to missing data.

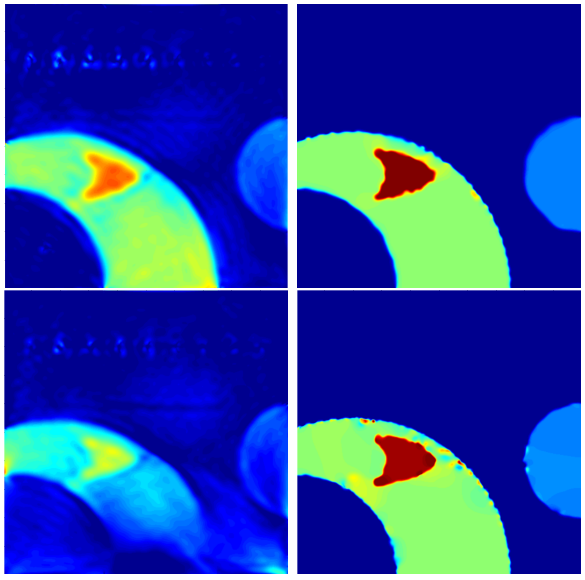

Figure 2: Top, full boundary data: nodal basis (left), AEI (right); Bottom, partial boundary data: nodal basis (left), AEI (right).

References

[1] M. de Buhan, M. Kray. A new approach to solve the inverse scattering problem for waves: combining the TRAC and the Adaptive Inversion methods. *Inv. Probl.* **29** (2013) 085009.

[2] M. J. Grote, J. Huber K. Drosos, O. Schenk: Inexact Interior-Point Method for PDE-Constrained Nonlinear Optimization. *SIAM J. Sci. Comp.* **36** (2014) A1251-1276.

[3] E. Haber, U. Ascher and D. Oldenburg: On Optimization Techniques for Solving Nonlinear Inverse Problems. *Inv. Probl.* **16** (2000), 1263-1280.

[4] J. Nocedal, S. J. Wright. *Numerical Optimization*, 2nd edition, Springer (2000).

[5] R. S. Dembo, T. Steihaug. Truncated-Newton Algorithms for Large-Scale Unconstrained Optimization. *Math. Progr.* **26** (1983) 190-212.

Absence of trapped modes for a class of unbounded propagative media

A.-S. Bonnet-Ben Dhia[1], **S. Fliss**[1], **C. Hazard**[1,*], **A. Tonnoir**[1,2]
[1]POEMS (CNRS / ENSTA-ParisTech / INRIA), Palaiseau, France
[2]ANEDP, Orsay, France
*Email: christophe.hazard@ensta-paristech.fr

Abstract

We propose a new approach to prove that there are no square-integrable nonzero solutions to the two-dimensional Helmholtz equation in a homogeneous conical domain with a vertex angle greater than π. This shows that for a medium filling the whole plane, there can be no trapped modes if all the inhomogeneities (penetrable or not) are concentrated in a conical domain with a vertex angle less than π.

Keywords: Helmholtz equation, Rellich type theorem

1 Introduction

We are interested in the question of existence of square-integrable solutions to the Helmholtz equation in a non-homogeneous unbounded domain in the absence of source. Such solutions are often called *trapped modes*, for their energy remains confined in a bounded region despite the unboundedness of the propagative medium. Trapped modes are known to occur for local perturbations of *closed* uniform infinite waveguides [3] but not *open* uniform waveguides [2], that is, when the transverse section becomes unbounded (e.g., optical fibers). Our aim here is to prove the absence of trapped modes for 2D inhomogeneous media filling the whole plane as soon as all the inhomogeneities (penetrable or not) are concentrated in a conical domain with a vertex angle less then π. This follows from the following theorem and the unique continuation principle.

Theorem 1 *Let $k > 0$, $\theta \in (0, \pi/2)$ and $\Omega := \{(x, y) \in \mathbb{R}^2;\ y > -|x| \tan\theta\}$. If $u \in L^2(\Omega)$ satisfies the Helmholtz equation*

$$\Delta u + k^2 u = 0 \quad \text{in } \Omega \tag{1}$$

in the distributional sense, then $u = 0$.

This theorem is optimal in the sense that it becomes false if $\theta = 0$. Indeed it is easy to construct solutions to the Helmholtz equation which are square-integrable in a half-plane.

We present below the main steps of the proof, where the functional details are omitted for clarity. Following [1, 2] (inspired by the pioneering work of Weder [4]), the main ingredients are a *modal representation* of the acoustic field and an *analyticity property*. The latter property derives here from an original idea which consists in using the modal representation in two oblique directions.

2 Elements of the proof

Our basic tool can be formulated as follows.

Lemma 2 *Let $\Pi := \mathbb{R} \times (0, +\infty)$. If $u \in L^2(\Pi)$ satisfies the Helmholtz equation (1) in Π, then*

$$u(\mathrm{x}, \mathrm{y}) = \frac{1}{\sqrt{2\pi}} \int_{|\xi|>k} \widehat{\varphi}(\xi)\, \mathrm{e}^{\mathrm{i}\mathrm{x}\xi - \mathrm{y}\sqrt{\xi^2-k^2}}\, \mathrm{d}\xi \tag{2}$$

for all $(\mathrm{x}, \mathrm{y}) \in \Pi$, where

$$\widehat{\varphi}(\xi) := \frac{1}{\sqrt{2\pi}} \int_{\mathbb{R}} u(\mathrm{x}, 0)\, \mathrm{e}^{-\mathrm{i}\mathrm{x}\xi}\, \mathrm{dx}$$

is the Fourier transform of $u(\cdot, 0)$ along the x-direction, which satisfies $\widehat{\varphi}(\xi) = 0$ if $|\xi| < k$.

The proof of this lemma is easy : we simply have to apply the Fourier transform to the Helmholtz equation and solve the resulting differential equation by taking into account the assumption $u \in L^2(\Pi)$. Formula (2) then follows from the inverse Fourier transform.

This formula appears as a modal representation of u in the sense that it can be interpreted as a superposition of the waves $\exp(\mathrm{i}\mathrm{x}\xi - \mathrm{y}\sqrt{\xi^2 - k^2})$ where $\widehat{\varphi}(\xi)$ stands for the amplitude of the superposition. These waves are propagative in the x-direction and evanescent in the y-direction (since $|\xi| > k$ in (2)). The fact that $\widehat{\varphi}(\xi) = 0$ if $|\xi| < k$ expresses actually the absence of propagative waves in the y-direction, which results from the assumption $u \in L^2(\Pi)$.

The proof of Theorem 1 is based on three uses of Lemma 2. Let $u = u(x, y)$ a L^2-solution

to the Helmholtz equation (1) in Ω. First notice that the conclusions of the lemma hold true in the half plane $\{y > 0\}$ (i.e., with $(\mathrm{X}, \mathrm{Y}) = (x, y)$). In particular, $\widehat{\varphi}(\xi) = 0$ if $|\xi| < k$. Then the main argument consists in proving that $\widehat{\varphi}(\xi)$ extends to an analytic function of ξ in a complex vicinity of the real axis. As $\widehat{\varphi}$ vanishes on the interval $(-k, +k)$, analyticity implies that it must vanish everywhere: $\widehat{\varphi}(\xi) = 0$ for all ξ. The modal representation (2) tells us that u vanishes in the half-plane $\{y > 0\}$, so also in the whole domain Ω by virtue of the unique continuation principle. This completes the proof of Theorem 1.

It remains to prove the analyticity of $\widehat{\varphi}(\xi)$. To do this, the key idea is to split the definition of $\widehat{\varphi}$ in the form

$$\widehat{\varphi}(\xi) = \frac{1}{\sqrt{2\pi}} \sum_{\pm} \int_{\mathbb{R}^{\pm}} u(x, 0)\, \mathrm{e}^{-\mathrm{i}x\xi}\, \mathrm{d}x \qquad (3)$$

and to express $u(\cdot, 0)|_{\mathbb{R}^{\pm}}$ by using again Lemma 2 in two half-planes contained in Ω and defined respectively by the equations $y > \mp x \tan\theta$. Using both changes of variables

$$\begin{aligned} \mathrm{X} &= x\cos\theta \mp y\sin\theta, \\ \mathrm{Y} &= \pm x\sin\theta + y\cos\theta, \end{aligned}$$

we obtain the following modal representations:

$$u(x, 0) = \int_{|\eta|>k} \widehat{\varphi}^{\pm}(\eta)\, \mathrm{e}^{\mathrm{i}\eta x\cos\theta \mp \sqrt{\eta^2 - k^2}\, x\sin\theta}\, \frac{\mathrm{d}\eta}{\sqrt{2\pi}}$$

for $x \in \mathbb{R}^{\pm}$. Hence, substituting these expressions in (3) and using Fubini's theorem, we obtain

$$\widehat{\varphi}(\xi) = \frac{1}{2\pi} \int_{|\eta|>k} F(\eta, \xi)\, \mathrm{d}\eta,$$

where

$$F(\eta, \xi) := \sum_{\pm} \frac{\widehat{\varphi}^{\pm}(\eta)}{\mp\mathrm{i}(\eta\cos\theta - \xi) + \sqrt{\eta^2 - k^2}\,\sin\theta}.$$

For almost every η, this function extends to an analytic function of ξ in any complex domain in which both denominators do not vanish. The complex values of ξ for which there exists a $\eta \in \mathbb{R} \setminus (-k, +k)$ such that one of the denominators vanishes is the hyperbola defined by

$$\frac{(\mathrm{Re}\,\xi)^2}{\cos^2\theta} - \frac{(\mathrm{Im}\,\xi)^2}{\sin^2\theta} = k^2,$$

which crosses the real axis at points $\pm k\cos\theta$. Hence, for almost every η, $F(\eta, \xi)$ is an analytic function of ξ in the three connected components of the complex plane delimited by this hyperbola. By the Lebesgue's dominated convergence theorem, we deduce that the same holds true for $\widehat{\varphi}(\xi)$. As we already know that $\widehat{\varphi}$ vanishes on $(-k, +k)$, the analyticity in these components implies that $\widehat{\varphi}(\xi)$ vanishes everywhere, in particular for $\xi \in \mathbb{R} \setminus (-k, +k)$, which is the desired result.

3 Consequences and possible extensions

One interesting consequence of our result concerns the case of curved open waveguides (e.g., bended optical fibers). Unlike *closed* waveguides for which trapped modes confined near the bend may occur, Theorem 1 implies that trapped modes cannot exist if the core of the waveguide is located in a cone with vertex angle less than π. More generally, this result holds true regardless this cone is composed of (provided the unique continuation principle applies).

Theorem 1 holds true for higher space dimensions and can be extended for some situations which involve non-homogeneous media (using a generalized Fourier transform instead of the usual one, see [1, 2]). Works on these subjects are in progress.

References

[1] A.-S. Bonnet-Ben Dhia, G. Dakhia, C. Hazard and L. Chorfi, Diffraction by a defect in an open waveguide : a mathematical analysis based on a modal radiation condition, *SIAM J. Appl. Math.* **70** (2009), pp. 677–693.

[2] C. Hazard, On the absence of trapped modes in locally perturbed open waveguides, *IMA J. Appl. Math.* (2014), doi: 10.1093/imamat/hxu046.

[3] C.M. Linton and P. McIver, Embedded trapped modes in water waves and acoustics, *Wave Motion* **45** (2007), pp. 16–29.

[4] R. Weder, *Spectral and Scattering Theory for Wave Propagation in Perturbed Stratified Media*, Springer-Verlag, 1991.

Sharp high-frequency estimates for the Helmholtz equation

Euan A. Spence[1,*], **Dean Baskin**[2], **Jared Wunsch**[3]
[1]Department of Mathematical Sciences, University of Bath, UK
[2]Department of Mathematics, Texas A&M University, USA
[3]Department of Mathematics, Northwestern University, USA
[*]Email: E.A.Spence@bath.ac.uk

Abstract

We prove sharp bounds on the exterior Dirichlet-to-Neumann and Neumann-to-Dirichlet maps for the Helmholtz equation in nontrapping domains. We also prove a sharp bound on the solution of the interior impedance problem for the Helmholtz equation.

Keywords: Helmholtz, wavenumber-explicit bounds, Dirichlet-to-Neumann map, Neumann-to-Dirichlet map, interior impedance problem.

1 Introduction

Proving bounds on solution of the Helmholtz equation

$$\Delta u + k^2 u = -f \tag{1}$$

(where $k > 0$) has a long history. Nevertheless, the following problems remain open (see, e.g., the discussion in [4, §1].

1. There do not exist sharp bounds on the *Dirichlet-to-Neumann (DtN)* or *Neumann-to-Dirichlet (NtD)* maps for the homogeneous Helmholtz equation (i.e. (1) with $f = 0$) in exterior nontrapping domains.

2. There do not exist sharp bounds on the solution of the *interior impedance problem (IIP)* for general domains, where this boundary value problem (BVP) consists of (3) posed in a bounded domain with the boundary condition

$$\frac{\partial u}{\partial n} - \mathrm{i}\eta u = g \tag{2}$$

where g is a given function and $\eta \in \mathbb{R}\backslash\{0\}$.

This paper fills these gaps in the literature.

The motivation for studying the exterior DtN and NtD maps for the Helmholtz equation is fairly clear, since these are natural objects in the study of scattering problems. The motivation for studying the IIP is two-fold.

(i) It has become a standard model problem used when designing numerical methods for solving the Helmholtz equation, and to prove error estimates one needs bounds on the solution of the BVP.

(ii) The integral equations used to solve the exterior Dirichlet, Neumann, and impedance problems can also be used to solve the IIP; therefore, to prove bounds on the inverses of these integral operators, one needs to have bounds on the solution of the IIP (see, e.g., [4, §1.3] and the references therein).

2 Statement of the main results

Let $\Omega_- \subset \mathbb{R}^d$, $d = 2, 3$, be a bounded, Lipschitz open set with boundary $\Gamma := \partial\Omega_-$, such that the open complement $\Omega_+ := \mathbb{R}^d \setminus \overline{\Omega_-}$ is connected. Let $\gamma_\pm$ denote the trace operators from $\Omega_\pm$ to Γ, let $\partial_n^\pm$ denote the normal derivative trace operators, and let ∇_Γ denote the surface gradient operator on Γ.

Theorem 1 (Exterior DtN map bounds) *Let $u \in H^1_{\mathrm{loc}}(\Omega_+)$ satisfy the Helmholtz equation*

$$\Delta u + k^2 u = 0 \quad \text{in } \Omega_+, \tag{3}$$

and the Sommerfeld radiation condition

$$\frac{\partial u}{\partial r} - \mathrm{i}ku = o\left(\frac{1}{r^{(d-1)/2}}\right) \tag{4}$$

as $r := |x| \to \infty$, uniformly in $\hat{x} := x/r$. If either Ω_+ *is nontrapping* or Ω_- *is a nontrapping polygon (in the sense of [2, §5])* or Ω_- *is Lipschitz and star-shaped, then, given $k_0 > 0$,*

$$\left\|\partial_n^+ u\right\|_{H^{-1/2}(\Gamma)} \lesssim k \left\|\gamma_+ u\right\|_{H^{1/2}(\Gamma)}, \tag{5}$$

for all $k \geq k_0$. Furthermore, if $\gamma_+ u \in H^1(\Gamma)$ then $\partial_n^+ u \in L^2(\Gamma)$ and, given $k_0 > 0$,

$$\left\|\partial_n^+ u\right\|_{L^2(\Gamma)} \lesssim \left\|\nabla_\Gamma(\gamma_+ u)\right\|_{L^2(\Gamma)} + k \left\|\gamma_+ u\right\|_{L^2(\Gamma)} \tag{6}$$

for all $k \geq k_0$.

Theorem 2 (Bounds on the NtD map) *Let Ω_+ be nontrapping and let $u \in H^1_{\mathrm{loc}}(\Omega_+)$ satisfy the Helmholtz equation* (3) *and the Sommerfeld radiation condition* (4)*. Let $\beta = 2/3$ in the case when Γ has strictly positive curvature, and $\beta = 1/3$ otherwise. Then, given $k_0 > 0$,*

$$\|\gamma_+ u\|_{H^{1/2}(\Gamma)} \lesssim k^{1-\beta} \left\|\partial_n^+ u\right\|_{H^{-1/2}(\Gamma)}, \qquad (7)$$

for all $k \geq k_0$. Furthermore, if $\partial_n^+ u \in L^2(\Gamma)$ then $\gamma_+ u \in H^1(\Gamma)$ and, given $k_0 > 0$,

$$\|\nabla_\Gamma(\gamma_+ u)\|_{L^2(\Gamma)} + k \|\gamma_+ u\|_{L^2(\Gamma)} \lesssim k^{1-\beta} \left\|\partial_n^+ u\right\|_{L^2(\Gamma)}, \qquad (8)$$

for all $k \geq k_0$.

By considering the specific examples of Γ the unit circle (in 2-d) and the unit sphere (in 3-d) and using results about the asymptotics of Bessel and Hankel functions, it was shown in [4, Lemmas 3.10, 3.12] that the bounds (5) and (6) are sharp, and that (7) and (8) are sharp in the case of strictly positive curvature.

Theorem 3 (Interior impedance bound) *Let Ω be a bounded C^∞ domain in 2- or 3-d with boundary Γ. Let a, b be real-valued C^∞ functions on Γ and assume that $b \geq 0$ and there exists an $a_- > 0$ such that* either

$$a(x) \geq a_- > 0 \quad \text{for all } x \in \Gamma$$

or

$$-a(x) \geq a_- > 0 \quad \text{for all } x \in \Gamma.$$

Let $\eta(x) := a(x) + \mathrm{i}b(x)$. Given $g \in L^2(\Gamma)$, $f \in L^2(\Omega)$, and η defined as above, let $u \in H^1(\Omega)$ be be the solution to the interior impedance problem

$$\Delta u + k^2 u = -f \quad \text{in } \Omega$$

and

$$\partial_n u - \mathrm{i}\eta\gamma u = g \quad \text{on } \Gamma.$$

Then, given $k_0 > 0$,

$$\|\nabla u\|_{L^2(\Omega)} + k \|u\|_{L^2(\Omega)} \lesssim \|f\|_{L^2(\Omega)} + \|g\|_{L^2(\Gamma)} \qquad (9)$$

for all $k \geq k_0$.

Note that the allowed values of η in Theorem 3 include the common choices $\eta = \pm k$.

3 Outline of how these results were obtained

The DtN bounds in Theorem 1 are obtained using an argument first introduced in [3] (and then further used in [4]) which obtains (non-sharp) DtN bounds from (i) the resolvent estimate for the problem and (ii) bounds on the DtN map for the modified Helmholtz equation (i.e. the equation $\Delta u - k^2 u = 0$). Instead of using bounds on the modified Helmholtz equation, we use bounds on the equation $\Delta u + (k^2 + \mathrm{i}k)u = 0$, and this change in the argument yields the sharp Helmholtz DtN bounds.

The NtD bounds in Theorem 2 are obtained using a collection of estimates proved by [5] for solutions to the wave equation with Neumann (or indeed many other) boundary conditions.

The IIP bound in Theorem 3 is obtained from the results of [1] about the wave equation with damping boundary condition.

References

[1] C. Bardos, G. Lebeau, and J. Rauch. Sharp sufficient conditions for the observation, control, and stabilization of waves from the boundary. *SIAM Journal on Control and Pptimization*, 30(5):1024–1065, 1992.

[2] D. Baskin and J. Wunsch. Resolvent estimates and local decay of waves on conic manifolds. *Journal of Differential Geometry*, 95(2):183–214, 2013.

[3] E. Lakshtanov and B. Vainberg. A priori estimates for high frequency scattering by obstacles of arbitrary shape. *Communications in Partial Differential Equations*, 37(10):1789–1804, 2012.

[4] E. A. Spence. Wavenumber-explicit bounds in time-harmonic acoustic scattering. *SIAM J. Math. Anal.*, 46(4):2987–3024, 2014.

[5] D. Tataru. On the regularity of boundary traces for the wave equation. *Ann. Scuola Norm. Sup. Pisa Cl. Sci.(4)*, 26(1):185–206, 1998.

A high-order Nyström solver for electromagnetic scattering from orthotropic media

Akash Anand[1], **Awanish Kumar Tiwari**[1,*], **Ambuj Pandey**[1]
[1]Indian Institute of Technology Kanpur
*Email: awanisht@iitk.ac.in

Abstract

We present a high-order Nyström solver for the time-harmonic electromagnetic wave scattering problem where the bounded material inhomogeneity is anisotropic and penetrable. The high-order convergence of this integral equation based procedure is attained through a combination of changes of parametric variables to resolve the singularities of the Green function and use of specialized weighted Clenshaw-Curtis quadratures to effectively deal with near singular integrals. A brief account of the main algorithmic components of the scheme are presented, together with some numerical results that exemplify its performance.

Keywords: Electromagnetic scattering, Nyström method, High-order method

1 Introduction

We consider the scattering of time-harmonic electromagnetic wave by a penetrable anisotropic medium of compact support. The electric field E and the magnetic field H satisfy the *Maxwell's equations* $\nabla \times E - ikH = 0, \nabla \times H + ik\mathcal{N}E = 0$, with the wave number $k > 0$ and the refractive index, independent of the x_3 coordinate, is assumed to have the form $\mathcal{N} = \mathcal{N}(x) = \begin{bmatrix} n_{11}(x) & n_{12}(x) & 0 \\ n_{21}(x) & n_{22}(x) & 0 \\ 0 & 0 & n_{33}(x) \end{bmatrix}$, where $\mathrm{Re}(\mathcal{N})$ is positive definite, $\mathrm{Im}(\mathcal{N})$ semi-positive definite and $\mathcal{N}-\mathcal{I}$ has compact support $\Omega \subset \mathbb{R}^2$, for the 3×3 identity matrix $\mathcal{I}$. The TM scattering problem is modeled by *Lippmann Schwinder* integral equation that can be solved to high-order by employing available numerical techniques (e.g., [1]). The TE scattering problem, on the other hand, with $u = H_3$ satisfies $\nabla \cdot (N\nabla)u + k^2 u = 0$ where $N = N(x) = \frac{1}{n_{11}(x)n_{22}(x)-n_{12}(x)n_{21}(x)} \begin{bmatrix} n_{11}(x) & n_{21}(x) \\ n_{12}(x) & n_{22}(x) \end{bmatrix}$. The integral equation formulation for this problem is given by [3], $u(x) - (Au)(x) = u^i(x), x \in \Omega$ where $(Au)(x) = \int_\Omega \nabla\Phi(x,x').(M(x')\nabla u(x'))dx'$ with kernel $\Phi(x,x') = \frac{i}{4}H_0^1(k|x-x'|)$ and $M(x) = I - N(x)$, I being the 2×2 identity matrix.

We note that the singularity present in the kernel $\nabla\Phi$ of the integral operator A is more severe that what occurs in the integral equation for the TM case, and require a more careful numerical treatment if a high-order accuracy is to be achieved. This text proposes a high-order Nyström scheme for solution of the TE scattering problem that we present next.

2 Numerical Method

We begin by constructing a finite overlapping cover $\{\Omega_\ell : \ell = 1, \ldots, L\}$ of the scattering media Ω where each patch Ω_ℓ is homeomorphic to $(0,1)^2$ via a smooth invertible parameterization $x_\ell = x_\ell(s,t)$. With the help of a partition of unity $\{\psi_\ell : \ell = 1, \ldots, L\}$ subordinate to this cover, we rewrite the integral operator A as $(Au)(x) = \sum_{\ell=1}^{L}(A_\ell u)(x)$, where $(A_\ell u)(x) = \int_0^1\int_0^1 \nabla\Phi(x, x_\ell(s',t')) \cdot (Vu)(s',t')\, ds'\, dt'$, with $(Vu)(s,t)$ is given by $\psi_\ell(x_\ell(s,t))j_\ell(s,t)M(x_\ell(s,t))\nabla u(x_\ell(s,t))$, j_ℓ being the Jacobian of the transformation x_ℓ.

The $\mathcal{O}(1/|x-x'|)$ singularity present in the kernel of the integral operator needs to be resolved for accurate evaluation of A_ℓ. One can overcome this difficulty by moving to polar variables centered around the target point $(s,t) = (x_\ell)^{-1}(x)$. The integration in polar coordinates is localized with the help of a smooth cut-off function $\eta = \eta(\rho)$ satisfying $\eta(\rho) = 0$ for $\rho > \rho_0$ and $\eta(\rho) = 1$ for $\rho < \alpha\rho_0$ for a suitable choice of $\alpha < 1$. Indeed, $(A_\ell u)(x) = (A_\ell^R u)(x) + (A_\ell^S u)(x)$ where $(A_\ell^R u)(x) =$

$$\int_0^1\int_0^1 \Phi_\ell^R(x; s', t') \cdot (Vu)(s', t')\, ds'\, dt' \qquad (1)$$

with a smooth kernel $\Phi_\ell^R(x; s', t') = (1 - \eta(|(s,t) - (s',t')|))\nabla\Phi(x, x_\ell(s',t'))$ and

$$\int_{[0,1]^2\cap D_{\rho_0}(s,t)} \Phi_\ell^S(x;\rho,\theta) \cdot (\widetilde{Vu})(\rho,\theta)\, d\rho\, d\theta, \quad (2)$$

with $\Phi_\ell^S(x;\rho,\theta) = \rho\nabla\Phi(x, x_\ell(s+\rho\cos\theta, t+\rho\sin\theta))$, $(\widetilde{Vu})(\rho,\theta) = \eta(\rho)(Vu)(s+\rho\cos\theta, t+\rho\sin\theta)$

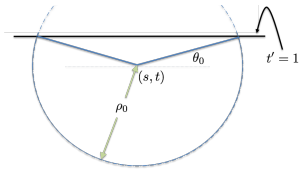

Figure 1: Splitting of angular integration

yields $(A_\ell^S u)(x)$. In (2), $D_{\rho_0}(s,t)$ denotes the disc centered at (s,t) of radius ρ_0.

For ℓ corresponding to interior patches on which ψ^ℓ vanish to high order in all directions, the integral in (1) of a smooth and compactly supported integrand is approximated to high-order using trapezoidal rule in both variables. The computation of (2), where integration domain can be extended to all of $D_{\rho_0}(s,t)$ can be carried out in a manner similar to the one introduced in [2].

On edge patches, where ψ_ℓ vanish to high order only in s' variable, we obtain high-order approximations of (1) by using trapezoidal rule for s' integration and Chenshaw-Curtis quadrature in t' variable. The accurate evaluation of (2), particularly when $D_{\rho_0}(s,t)$ does not completely lie within $[0,1]^2$, demand splitting of the angular integration into multiple pieces. The example in Figure 1 depicts a typical scenario, where

$$\int_{[0,1]^2 \cap D_{\rho_0}(s,t)} \cdots = \int_{-\pi-\theta_0}^{\theta_0} \int_0^{\rho_0} \cdots + \int_{\theta_0}^{\pi-\theta_0} \int_0^{\frac{1-t}{\sin\theta}} \cdots .$$

Both angular and radial integrals are handled accurately by Clenshaw-Curtis quadrature. An additional difficulty in the form of near singular behavior of the θ-integrand presents itself when t is very close to 1. We employ a weighted Chenshaw-Curtis quadrature that explicitly resolves the near singular scenarios to obtain rapidly convergent approximations.

N	Relative Error	Order
$3 \times 16 \times 16$	1.22×10^{-2}	-
$3 \times 32 \times 32$	9.24×10^{-4}	3.72
$3 \times 64 \times 64$	1.46×10^{-5}	5.98
$3 \times 128 \times 128$	3.90×10^{-7}	5.22

Table 1: Convergence for Disc shape scatterer.

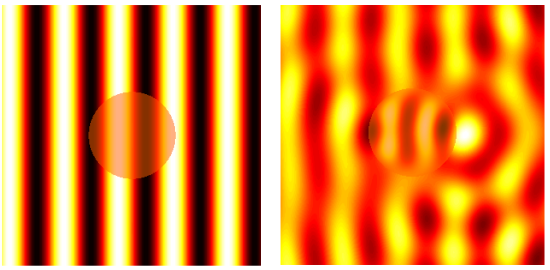

(a) Plane wave incidence (b) Total field

Figure 2: Scattering of a plane wave by an orthotropic penetrable disc of size $ka = 10$ — numerical approximation on a $3 \times 64 \times 64$ grid with 0.077% error compared to the Mie series solution.

3 Numerical Results

We present, in Table 1, a convergence study for scattering of a plane wave with wavenumber $k = 1$, by an anisotropic penetrable unit disc. The refractive index matrix N is chosen to have entries $n_{11} = 2, n_{12} = 1, n_{21} = -1$, and $n_{22} = 2$. This study clearly show the high-order nature of our integral equation solver. In Figure 2, we depict the incident and total wave from the same anisotropic penetrable disc when the wave number $k = 5$.

References

[1] A. Anand, A. Pandey and J. Paul, *A high-order Nyström scheme for acoustic scattering by inhomogeneous penetrable media in two dimensions*, Proceedings of the 11th International Conference on Mathematical and Numerical Aspects of Waves, 2013, pp. 269-270.

[2] O. P. Bruno and L. A. Kunyansky, *A Fast, High-Order Algorithm for the Solution of Surface Scattering Problems: Basic Implementation, Tests, and Applications*, Journal of Computational Physics, **169**, 2001, pp. 80–110.

[3] R. Potthast, Electromagnetic scattering from an orthotropic medium, Journal of Integral Equation and Applications, **11**(2), 1999, pp. 197-215.

A High-Order Integral Equation Solver for Problems of Electromagnetic Scattering by Three-Dimensional Open Surfaces

Carlos Pérez-Arancibia[1,*], **Oscar P. Bruno**[1]

[1]Computing & Mathematical Sciences, California Institute of Technology, Pasadena, USA

[*]Email: cperezar@caltech.edu

Abstract

We present a computational methodology for accurate solution of problems of electromagnetic scattering by three-dimensional smooth open surfaces. Our integral equation solver is a generalization of the Nyström method for acoustic scattering problems by open smooth surfaces introduced in [1]. High-order discretization of the EFIE is obtained by i) introducing an appropriate ansatz that accounts for the edge singularity of the densities and, ii) an overlapping-patch representation of the open surface which allows for the use of high-order trapezoidal rule integration and FFT differentiation/interpolation of the unknown smooth densities. The use of an appropriate preconditioner that yields a significant reduction of the number of iterations of the Krylov-subspace iterative linear-algebra solvers is discussed. The method exhibits spectral convergence for the examples considered.

Keywords: open PEC surface scattering, integral equation methods, high-order methods

1 Introduction

We consider the problem of scattering of an electromagnetic plane-wave $\mathbf{E}^{\rm inc}$ by a perfect electric conductor (PEC) open surface $\Gamma \subset \mathbb{R}^3$, which is assumed of class $\mathcal{C}^\infty$. The surface is assumed to be covered by a finite number of overlapping patches, each one of them parametrized by a bijective smooth mapping $\mathbf{r}(u,v)$, where u and v are the local coordinates of the patch (see [1, 2] for details). In the classical electric field integral equation (EFIE) setting, the scattered electric field is represented as

$$\mathbf{E}^s = ik\mathcal{S}_k\,[\mathbf{J}] + \frac{i}{k}\nabla\mathcal{S}_k[\,\mathrm{div}\,_\Gamma\mathbf{J}] \quad \text{in} \quad \mathbb{R}^3\setminus\Gamma$$

in terms of an unknown current density $\mathbf{J}$, where $\mathcal{S}_k$ denotes the single-layer potential. By imposing the boundary conditions on the PEC surface, we arrive to the EFIE:

$$ik\mathbf{n}\times S_k[\mathbf{J}] + \frac{i}{k}\mathbf{n}\times\mathbf{N}_k[\mathbf{J}] = -\mathbf{n}\times\mathbf{E}^{\rm inc} \quad \text{on} \quad \Gamma,$$

where

$$\begin{aligned} S_k[\mathbf{J}](\boldsymbol{x}) &= \int_\Gamma G_k(\boldsymbol{x},\boldsymbol{y})\mathbf{J}(\boldsymbol{y})\,\mathrm{d}s \\ \mathbf{N}_k[\,\mathrm{div}\,_\Gamma\mathbf{J}] &= \nabla\int_\Gamma G_k(\boldsymbol{x},\boldsymbol{y})\,\mathrm{div}\,_\Gamma\mathbf{J}(\boldsymbol{y})\,\mathrm{d}s. \end{aligned}$$

The unknown density $\mathbf{J}$ can be obtained by solving the EFIE, however, as is well-known, the components of $\mathbf{J}$ along the edge of Γ behaves asymptotically as $1/\omega$ where $\omega=\sqrt{d}$, d denoting the distance to the to edge, while the normal components of the density behaves like ω (see [3]). The surface divergence $\mathrm{div}\,_\Gamma\mathbf{J}$ on the other hand, behaves like $1/\omega$.

In order to deal with the edge singularity of the density we introduce the ansatz $\mathbf{J} = W\mathbf{j}$, where, for a current density $\mathbf{j} = j_u\mathbf{r}_u + j_v\mathbf{r}_v$ defined inside an edge patch, $W\mathbf{j}$ is given by

$$W\mathbf{j} = \frac{1}{\omega}j_u\mathbf{r}_u + \omega j_v\mathbf{r}_v.$$

The regularized electric field integral equation (REFIE) is then given by $\mathcal{T}_W[\mathbf{j}] = -\mathbf{n}\times\mathbf{E}^{\rm inc}$ where

$$\mathcal{T}_W[\mathbf{j}] = ik\mathbf{n}\times S_k[W\mathbf{j}] + \frac{i}{k}\mathbf{n}\times\mathbf{N}_k[\,\mathrm{div}\,_\Gamma(W\mathbf{j})].$$

In order to improve the spectral properties of the integral operator $\mathcal{T}_W$, and consequently, improve the convergence of the Krylov-subspace linear algebra solver, we introduce an analytic preconditioner given by [4]

$$\mathcal{T}_\omega[\mathbf{j}] = ik\mathbf{n}\times S_k[W\mathbf{j}] + \frac{i}{k}\mathbf{n}\times\mathbf{N}_k[\omega\,\mathrm{div}\,_\Gamma\mathbf{j}],$$

so that we look for solutions of the integral equation

$$\mathcal{T}_\omega\circ\mathcal{T}_W[\mathbf{j}] = -\mathcal{T}_\omega[\mathbf{E}^{\rm inc}] \quad \text{on} \quad \Gamma.$$

The operators in the integral equation above are applied in a successive manner. The high-order quadrature rules we use for these operators resolve the multiple Green function and

N	E_x	E_y	E_z
$16^2 + 2 \times 20 \times 16$	1.62e-2	3.20e-2	2.08e-2
$32^2 + 2 \times 40 \times 32$	5.12e-4	1.07e-3	6.45e-4
$64^2 + 2 \times 80 \times 64$	1.14e-5	1.04e-5	8.42e-6

Table 1: Convergence test: Error for various grid refinements.

edge singularities and thus give rise to super-algebraically fast convergence as the discretization sizes are increased. Tangential derivatives of single-layer potentials are obtained by accurate evaluation of Cauchy principal-value integrals [1], while the surface divergence of the density in the application of $\mathcal{T}_W$ is obtained by FFT differentiation [2].

2 Numerical Results

The proposed algorithm produces highly accurate solutions of electromagnetic scattering problem by smooth open surfaces. Table 1 below shows the results of a convergence test for the problem of scattering of a plane-wave with wavenumber $k = 1$ by a disc of unit radius. The disc is represented by three overlapping patches; one interior patch and two edge patches. The total number of discretization points N is given by $N = n^2 + 2 \times m \times n$, where the first term denotes the number of points in the interior patch while the second term account for the points in the edge patches. The resulting linear system of equations is solved iteratively by using the GMRES algorithm with a tolerance of `tol` =1.0e-4. The electric field $\mathbf{E} = (E_x, E_y, E_z)$ is then evaluated at a plane one diameter away from the disc, and the error is estimated by comparing the different components of the electric field with the field obtained by solving the discretized integral equation using the grid $N = 128^2+2\times160\times128$. Finally, Figure 1 shows the magnitude of the electric field obtained by solving the problem of scattering by a disc of diameter 10λ. Its solution required 37 GMRES interactions. Remarkably, the Poisson spot is visible at the center of the shadow region under the disc.

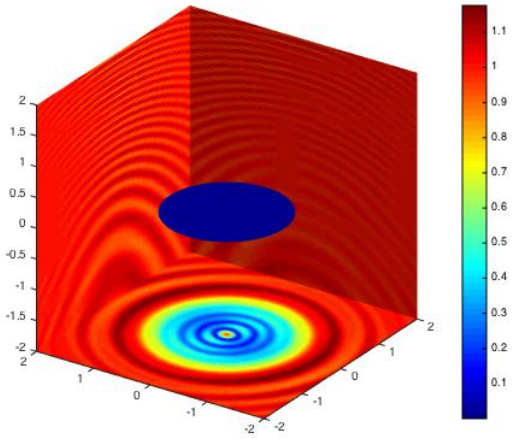

Figure 1: Diffraction by disc under normal incidence.

References

[1] O. P. Bruno and S. Lintner, A high-order integral solver for scalar problems of diffraction by screens and apertures in three-dimensional space, *Journal of Computational Physics* **252** (2013), pp. 250–274.

[2] O. P. Bruno, T. Elling, R. Paffenroth and C. Turc, Electromagnetic integral equations requiring small numbers of Krylov-subspace iterations, *Journal of Computational Physics* **228** (2009), pp. 6169–6183.

[3] A. Ya. Povzner and I. V. Suharevskii, Integral equations of the second kind in problems of diffraction by an infinitely thin screen, *Soviet Physics. Dokl.*, **4** (1960), pp. 798–801.

[4] C. Turc, A. Anand, O. P. Bruno and J. Chaubell, Efficient solution of three-dimensional problems of acoustic and electromagnetic scattering by open surfaces, in Proceedings of WAVES 2011.

First order estimates in integral equations on stochastic boundaries

B.L. Michielsen[1,*]

[1]Onera, Department of Electromagnetism and Radar, Toulouse, France

[*]Email: Bastiaan.Michielsen@Onera.fr

Abstract

We study boundary integral equation methods for electromagnetic scattering by impenetrable obstacles with uncertain geometry. The uncertainty in the geometry is accounted for by means of the flow of a stochastic vector field defining a stochastic deformation. A first order perturbation approximation is developed which, under conditions derived in the paper, allows for efficient estimates.

Keywords: Boundary integral equations, stochastic surfaces, electromagnetic scattering

1 Introduction

In order to obtain useful information from numerical computations, one has to provide more than the results for just one numerical model for a physical configuration. There are many reasons why significant differences may appear between the computational results for the chosen numerical representation and what would be observed in the physical situation being modelled. Besides the inevitable discretisation errors there are uncertainties in both the geometrical realisation and the physical constitution of the objects playing a role in the process. One of the approaches to capture this, is to refine the deterministic numerical models into probabilistic models in which such uncertainties are modelled as well. What we essentially want to do is to find as detailed as possible characterisations of the statistics of observable quantities (i.e. which can be put into correspondence with the outcome of measurements). In all but the most trivial situations, we will have to be satisfied with computing the dominant moments: the average, i.e., the conventional deterministic computation, the standard deviation, capturing the sensitivity to fluctuations around the average, and the higher order moments like skewness and kurtosis, which provide more and more structure information of the probability distribution of the observables.

In this contribution, we develop the example of the electromagnetic plane wave scattering operator. It maps incident plane-waves, characterised by a polarisation vector $e^-(\vartheta^-)$ orthogonal to the propagation direction $\vartheta \in S_1^2$, to asymptotic scattered-field polarisations

$$e^+(\vartheta^+) = \int_{\vartheta^- \in S_1^2} S(\vartheta^+, \vartheta^-) e^-(\vartheta^-)$$

The scattering coefficients $S(\vartheta^+, \vartheta^-)$ are vector-valued linear forms on the (complexified) tangent spaces of the unit sphere. They have the following integral representation

$$S_{pq}(\vartheta^+, \vartheta^-) = j\omega\mu_0 \int_{\partial\Omega} \psi_{-\vartheta^+} e_p(\vartheta^+) \wedge H_{e_q(\vartheta^-)}$$

where $e_p(\vartheta)$ is a basis polarisation of a co-tangent frame in (ϑ), $\psi_\vartheta(x) = \exp(-jk\vartheta\cdot x)$ and $H_{e_q(\vartheta^-)}$ is the surface current density induced by an incident plane wave defined by (e_q, ϑ^-).

The scattering coefficients are our observables and we consider $\partial\Omega$ the boundary of the obstacle to be a stochastic deformation of an average surface. We first explain how we model these stochastic fluctuations and then study the boundary integral equation over this surface to characterise the the stochastic distribution. (The final step, i.e. to compute the variances of the scattering coefficients will be shown in the presentation only.)

2 Modelling stochastic geometries

In order to let all realisations of the stochastic surface be "realistic" we have to warrant that the stochastic deformations have a convenient spatial covariance. We can achieve this by taking the deformation as the flow of a stochastic vector field on the embedding space and fix the spatial covariances of this vector field. A simple stochastic linear combination of vector fields can be sufficient.

$$v_\alpha = \sum_p \alpha_p v_p$$

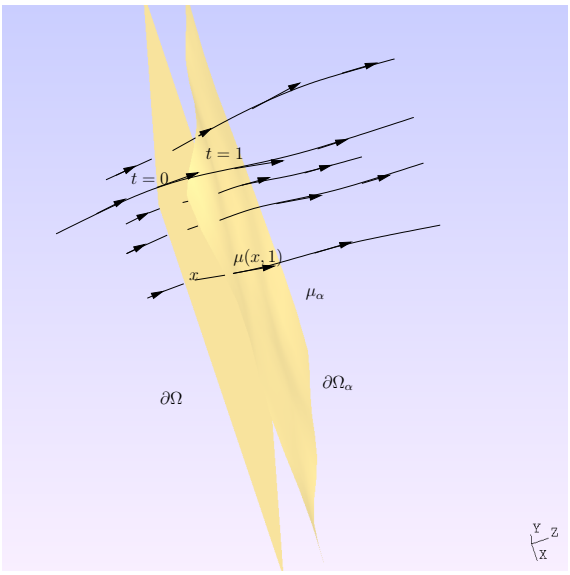

Figure 1: Illustrating the deformation of a surface using the flow of a stochastic vector field

with α_p centred random reals. The flow μ_α of the vector field is defined by

$$\partial_t \mu_\alpha(x,t) = v_\alpha(\mu_\alpha(x,t))$$

The stochastic boundary is a deformation

$$\partial\Omega_0 \ni x \mapsto \mu_\alpha(x,1) \in \partial\Omega_\alpha$$

of the nominal or average boundary $\partial\Omega_0$.

3 Stochastic integral equation

We consider the Electric Field Integral Equation (EFIE) on deformed boundaries

$$\Big[\int_{y\in\partial\Omega_\alpha} G_x^{eh}(y) \wedge H(y)\Big]_{\partial\Omega_\alpha} = -\big[E^i\big]_{\partial\Omega_\alpha}(x)$$

This is pulled-back to the nominal boundary

$$\int_{y\in\partial\Omega} (\mu_\alpha^* \times \mu_\alpha^* G^{eh})(x,y) \wedge \mu_\alpha^* H(y) \\ = -(\mu_\alpha^* E^i)(x)$$

Written formally as $Bj = e$, with B a stochastic operator and e a stochastic field on a fixed surface $\partial\Omega$.

4 First order asymptotics

Let $j^1 = j_0 + j_1\alpha$ be the first-order asymptotic solution of the stochastic integral equation. Its coefficients satisfy

$$B_0 j_0 = e_0$$
$$B_0 j_1 = e_1 - B_1 j_0$$

where of $B_{0,1}$ are the first two terms of the expansion of the operator B. The kernel distribution of B_1 is a function of the distance between two points on $\partial\Omega_\alpha$ expressed in coordinates on $\partial\Omega$. For scattering by obstacles in free space, the first order perturbation of the Green function

$$G_1(x,y) = -G_0(x,y) \\ \frac{\theta(x,y)\cdot(v(x)-v(y))(1+jk\|x-y\|)}{\|x-y\|}$$

fixes the kernel of B_1. In the presentation, we shall develop the consequences of the observation that this kernel vanishes locally near the "diagonal" $(x \to y)$ when the deformations are orthogonal to the surface.

5 Conclusion

In this contribution, it is shown that when the fluctuations of a stochastic boundary surface, which is locally flat on the scale of the correlation length, are along the normal an interesting simplification is obtained in boundary integral equations on stochastic surfaces.

References

[1] B. L. Michielsen, Probabilistic modelling of stochastic interactions between electromagnetic fields and systems, *Comptes Rendus de l'Académie des Sciences: Physique*, **7** (2006), pp. 543–559.

[2] B. L. Michielsen, O.O. Sy and M.C. van Beurden, Estimates in first order approximations to electromagnetic boundary integral equations on stochastic surfaces, *Proceedings ICEAA, Torino, 2013*

Curious energy losses at corners of metallic inclusions.

A.-S. Bonnet-Ben Dhia[1,*], **C. Carvalho**[1], **C. Chambeyron**[1], **L. Chesnel**[2], **P. Ciarlet Jr.**[1], **A. Nicolet**[3], **F. Zolla**[3]

[1]POEMS (CNRS - ENSTA ParisTech - INRIA), Palaiseau, France.
[2]CMAP (CNRS - Ecole Polytechnique), Palaiseau, France.
[3]Institut FRESNEL (CNRS - Université d'Aix-Marseille), Marseille, France.
[*]Email: Anne-Sophie.Bonnet-Bendhia@ensta-paristech.fr

Abstract

We consider a Transverse Magnetic time-harmonic scattering problem. The scatterer is a metallic object whose cross-section has corners and whose permittivity is a function of the frequency, typically given by Drude's law. When the dissipation effects in the metal are neglected, it has been proved in [2] that there is a range of frequencies where some energy is trapped by the corners, due to the so-called plasmonic black-hole waves. The purpose of this work is to show that a similar phenomenon can be observed when considering a realistic dissipative metal, like silver.

Keywords: electromagnetic scattering, Drude's model, singularities, black-hole waves, energy balance

1 The scattering problem

For simplicity, let us suppose that the cross-section Ω of the metallic scatterer has the shape of a droplet (see figure 1), with a single corner, located at the origin. The relative dielectric permittivity in the metal obeys the following law, known as the Drude's model

$$\varepsilon_\gamma(\omega) = 1 - \frac{\omega_p^2}{\omega^2 + i\omega\gamma}, \qquad (1)$$

where $\omega > 0$ is the pulsation, $\gamma \geq 0$ (for a harmonic regime in $e^{-i\omega t}$) characterizes the dissipative effects, and $\omega_p > 0$ is the plasma frequency (for silver $\gamma = 0.113\,10^{15}$ Hz and $\omega_p = 13.3\,10^{15}$ Hz [1]). We are interested in a frequency range $\omega < \omega_p$ below the plasma frequency, where the real part of $\varepsilon_\gamma(\omega)$ is negative while its imaginary part is positive (see figure 1). We consider the following scattering problem: find $u_\gamma = u^{\text{inc}} + u_\gamma^{\text{sca}}$ such that $\text{div}\left(\varepsilon_\gamma^{-1}\nabla u_\gamma\right) + \omega^2 c^{-2} u_\gamma = 0$ in $\mathbb{R}^2$ and

$$\lim_{\xi\to+\infty} \int_{|\mathbf{x}|=\xi} \left| \frac{\partial u_\gamma^{\text{sca}}}{\partial r} - i\omega c^{-1} u_\gamma^{\text{sca}} \right|^2 d\sigma = 0,$$

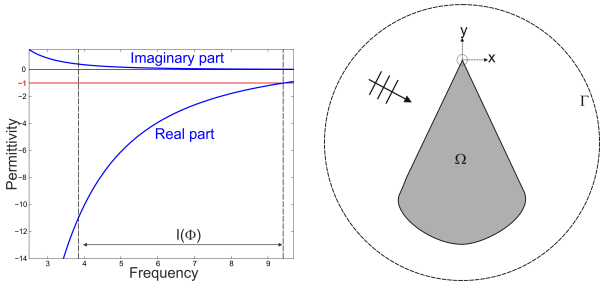

Figure 1: Permittivity of silver and geometry

where u_γ represents the transverse component of the magnetic field, u^{inc} is a plane wave, c denotes the light speed and ε_γ is a function defined by $\varepsilon_\gamma = 1$ in $\mathbb{R}^2 \setminus \Omega$ and $\varepsilon_\gamma = \varepsilon_\gamma(\omega)$ in Ω.

For $\gamma > 0$, thanks to the imaginary part of $\varepsilon_\gamma(\omega)$, one can prove with standard arguments that this problem is well-posed in $H^1_{\text{loc}}(\mathbb{R}^2)$, and if Γ is a circle enclosing the droplet, we have:

$$-\Im m\left(\int_\Gamma \frac{\partial u_\gamma}{\partial r}\overline{u_\gamma}\right) = \Im m\left(\frac{-1}{\varepsilon_\gamma(\omega)}\right)\int_\Omega |\nabla u_\gamma|^2.$$

This quantity, denoted in the sequel by $J_\gamma(\omega)$, is strictly positive and corresponds to the energy dissipated during one time period in the metallic inclusion.

2 The non-dissipative case $\gamma = 0$

If γ is small compared to ω_p, there is a range of frequencies between γ and ω_p where it may be relevant to neglect the dissipation in the metal by taking $\gamma = 0$ (see figure 1). Then the permittivity ε_0 is a real-valued function, negative in the metal and positive elsewhere. The well-posedness of such a sign-changing transmission problem has been extensively studied and the results for the scattering problem depend on the value of ω (see [2] for the details). If we denote by Φ the angle at the corner, we define the fre-

quency interval $I(\Phi)$ by the following property:

$$\omega \in I(\Phi) \Leftrightarrow \varepsilon_0(\omega) \in \left]-\frac{2\pi-\Phi}{\Phi}, -1\right[.$$

If $\omega \notin \overline{I(\Phi)}$, the scattering problem is well-posed in $H^1_{\text{loc}}(\mathbb{R}^2)$ and there is no energy dissipation ($J_0(\omega) = 0$). On the contrary, if $\omega \in I(\Phi)$, the scattering problem is not well-posed in $H^1_{\text{loc}}(\mathbb{R}^2)$. However the well-posedness can be recovered in a different functional framework [3]. The solution u_0 (which is the limit of u_γ when $\gamma \to 0$) may be very singular at the corner, it behaves like $a \exp(i\kappa \log r)$ (in polar coordinates) with $\kappa \in \mathbb{R}$, where the constant $a \in \mathbb{C}$ depends on the incident wave. When $a \neq 0$, this so-called black-hole wave carries energy towards the corner, which results in a dissipation of energy ($J_0(\omega) > 0$), even if the dissipation in the material has been neglected.

3 The slightly dissipative case

From a physical point of view, the relevance of this strange phenomenon (dissipation of energy in a non dissipative material) is discussed in the literature [4]. Indeed one could suspect that it is due to idealized non-realistic hypotheses, like the perfect corner and the non dissipative material ($\gamma = 0$). Our objective here is to show that the phenomenon of leakage at the corner is still present in a realistic dissipative material.

We have computed $J_\gamma(\omega)$ as a function of ω for the case of silver for two different incidences and for two inclusions, a droplet-shaped one as described above, with an angle $\Phi = \pi/6$, while the second one has the shape of a disk. For the comparison, the two shapes have the same perimeter as losses are due to the plasmonic surface wave propagating at the surface of the metal (the wave does not propagate inside the metal because the real part of ε and μ have opposite signs). Obviously, for the disk, the two incidences give the same result represented by the black dashed curve. For the droplet, the first incidence in red is such that the black-hole wave is excited while it is not for the second incidence in blue.

As expected, the energy losses for the droplet are much larger than for the disk in the interval $I(\Phi)$ when the black-hole wave is excited.

Let us mention that a refined mesh near the interface would be necessary for the frequencies at the right end of $I(\Phi)$, which correspond to the almost ill-posed case $\Re e(\varepsilon_\gamma(\omega)) = -1$.

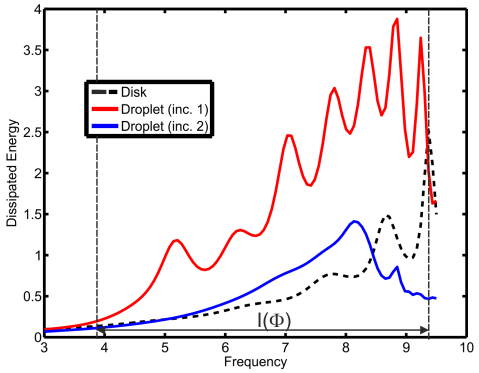

Figure 2: Energy dissipation for a droplet and a disk inclusions, for two directions of incidence

The computations are done with the code Xlife++ [5].

References

[1] Palik, E.D., *Handbook of Optical Constants of Solids*, Elsevier (1997).

[2] Bonnet-Ben Dhia, A. S., Carvalho, C., Chesnel, L. and Ciarlet, P. Jr, *On the use of Perfectly Matched Layers at corners to capture plasmonic black-hole waves*, preprint.

[3] Bonnet-Ben Dhia, A. S., Chesnel, L. and Claeys, X., *Radiation condition for a non-smooth interface between a dielectric and a metamaterial*, Math. Models Meth. App. Sci., vol. 3, (2013).

[4] Li, L., *Hypersingularity, electromagnetic edge condition, and an analytic hyperbolic wedge model*, J. Opt. Soc. Am. A 31, 808-817 (2014).

[5] http://uma.ensta-paristech.fr/soft/XLiFE++/

Finite Element Heterogeneous Multiscale Method for Maxwell's Equation in Frequency Domain

Patrick Ciarlet Jr.[1], **Sonia Fliss**[1], **Christian Stohrer**[1,*]
[1]POEMS (CNRS/ENSTA ParisTech/INRIA), Palaiseau, France
[*]Email: christian.stohrer@ensta-paristech.fr

Abstract

To solve numerically Maxwell's equations, describing electromagnetic phenomena, one usually uses Nédélec's first family of edge finite elements. If the medium, where the electromagnetic wave is propagating through, oscillates on a microscopic length scale, this approximation becomes infeasible since the mesh must resolve all details of the medium. We propose a multiscale scheme to overcome this difficulty following the framework of the finite element heterogeneous multiscale method (FE-HMM). We prove convergence to the homogenized solution in the periodic case, and show some numerical experiments.

Keywords: Maxwell's Equations, heterogeneous multiscale methods, Nédélec finite element

1 Model problem

Let Ω be a bounded polyhedral domain of $\mathbb{R}^3$, and denote by $V := H_0(\mathrm{curl};\Omega)$ the Sobolev space of functions in $L^2(\Omega)$ whose curl is in $L^2(\Omega)$ with vanishing tangential trace on $\partial\Omega$. We assume that within Ω the electric permittivity ε^η and the inverse of the magnetic permeability ν^η are admissible quasi-periodic tensors, i.e. they are given almost everywhere by

$$\varepsilon^\eta(x) = \varepsilon(x,\eta^{-1}x) \text{ and } \nu^\eta(x) = \nu(x,\eta^{-1}x),$$

where η is a small parameter, and ε and ν are uniformly bounded and coercive matrix-valued functions, which are $Y = (-1/2,1/2)^3$-periodic in their second variable.

We consider the model problem corresponding to Maxwell's equations in frequency domain

$$\begin{cases} \text{Find } u^\eta \in V, \text{ such that } \forall v \in V \\ B^\eta(u^\eta, v) - \omega^2 \left(u^\eta, v\right)_\eta = (f, v)\,, \end{cases} \tag{1}$$

where $(\cdot,\cdot)$ is the standard L^2 inner product, $(v,w)_\eta := (\varepsilon^\eta v, w)$, and

$$B^\eta(v,w) := (\nu^\eta \nabla\times v, \nabla\times w)\,.$$

To ensure the well-posedness of equation (1) for small η we assume that there is $\gamma > 0$ such that for a threshold value $\tilde\eta$ we have

$$\inf_{0<\eta\le\tilde\eta}\inf_{\lambda^\eta\in\Lambda^\eta}\left(\left|\omega^2-\lambda^\eta\right|\right) \ge \gamma > 0.$$

Here, Λ^η denotes the discrete set of the eigenvalues of the eigenproblem associated to (1).

2 Homogenization theory

Under the assumptions mentioned above, the sequence of solutions of (1) converges weakly in $L^2(\Omega)$ as $\eta \to 0$ to u^0, the solution of the homogenized problem

$$\begin{cases} \text{Find } u^0 \in V, \text{ such that } \forall v \in V \\ B^0(u^0, v) - \omega^2 \left(u^0, v\right)_0 = (f, v)\,, \end{cases} \tag{2}$$

where $(v,w)_0 = (\mathcal{H}_{\mathrm{div}}(\varepsilon)v, w)$ and

$$B^0(v,w) = (\mathcal{H}_{\mathrm{curl}}(\nu)\nabla\times v, \nabla\times w)\,.$$

The homogenized permittivity $\mathcal{H}_{\mathrm{div}}(\varepsilon)$ and the homogenized inverse permittivity $\mathcal{H}_{\mathrm{curl}}(\nu)$ display no oscillation on the micro scale of order η. Both operators $\mathcal{H}_{\mathrm{div}}$ and $\mathcal{H}_{\mathrm{curl}}$ map a quasi-periodic tensor to its homogenized counterpart. The operator $\mathcal{H}_{\mathrm{div}}$ is the usual homogenization operator appearing in homogenization of a second order elliptic equation and given by

$$\mathcal{H}_{\mathrm{div}}(\varepsilon) = \int_Y \varepsilon(x,y)\big(I + D_y^T\chi^\varepsilon(x,y)\big)\,dy,$$

where $\chi^\varepsilon = (\chi_1^\varepsilon, \chi_2^\varepsilon, \chi_3^\varepsilon)^T$ and χ_i^ε solves

$$\begin{cases} \text{Find } \chi_i^\varepsilon : \Omega \to H^1_{\mathrm{per}}(Y), \text{ such that} \\ \displaystyle\int_Y \varepsilon(x,y)(e_i + \nabla\chi_i^\varepsilon)\cdot\nabla z\,dy = 0, \\ \text{for all } z \in H^1_{\mathrm{per}}(Y). \end{cases}$$

On the other hand, the operator $\mathcal{H}_{\mathrm{curl}}$ is designed for Maxwell's equation. It is given by

$$\mathcal{H}_{\mathrm{curl}}(\nu) = \int_Y \nu(x,y)\big(I + \nabla\times X^\nu(x,y)\big)\,dy,$$

where $X^\nu = (X_1^\nu, X_2^\nu, X_3^\nu)$ and X_i^ν solves

$$\begin{cases} \text{Find } X_i^\nu : \Omega \to H_{\text{per}}(\text{curl}, Y), \text{ such that} \\ \displaystyle\int_Y \nu(x,y)(e_i + \nabla \times X_i^\nu) \times (\nabla \times z)\, dy = 0, \\ \text{for all } z \in H_{\text{per}}(\text{curl}, Y). \end{cases}$$

Convergence of u^η to the homogenized solution u^0 can be proven using two-scale convergence, cf. [2]. The multiscale scheme proposed next reflects the specific structure of the homogenization operators involved.

3 Multiscale method

Let V_H be the finite dimensional space of lowest order Nédélec elements on a macroscopic triangulation $\mathcal{T}_H$ of Ω into simplices K. This triangulation does not need to resolve the fine scale structure, i.e. mesh sizes $H \gg \eta$ are allowed. Our FE-HMM scheme is given by

$$\begin{cases} \text{Find } u_H \in V_H, \text{ such that } \forall v_H \in V_H \\ B_H(u_H, v_H) - \omega^2 (u_H, v_H)_H = (f, v_H)\,. \end{cases} \tag{3}$$

The FE-HMM bilinear form is defined as follows

$$B_H(v_H, w_H) = \sum_{K,j} \frac{\omega_{K,j}}{|Y_{K,j}^\eta|} \int_{Y_{K,j}^\eta} \nu^\eta(x)(\nabla \times v_h) \cdot (\nabla \times w_h)\, dx,$$

where $Y_{K,j}^\eta := x_{K,j} + \eta Y$, $(x_{K,j}, \omega_{K,j})_{j=1}^J$ are the nodes and weights of a quadrature formula on the simplex K and v_h (resp. w_h) are the FE solution of

$$\begin{cases} \nabla \times \big(\nu^\eta(x)(\nabla \times v_h)\big) = 0 \text{ in } Y_{K,j}^\eta, \\ \nabla \cdot v_h = 0 \text{ in } Y_{K,j}^\eta, \ \displaystyle\int_{Y_{K,j}^\eta} v_h\, dx = 0, \\ v_h(x) - v_{H,\text{curl}}(x) \text{ is } \eta Y\text{-periodic.} \end{cases}$$

We use the linear function $v_{H,\text{curl}}$ given by

$$v_{H,\text{curl}}(x) = v_H(x_{K,j}) + \frac{1}{2}\big(\nabla \times v_H(x_{K,j})\big) \times (x - x_{K,j}).$$

to couple the macro and micro scales. By construction, $v_{H,\text{curl}}(x) = v_H(x_{K,j})$ and

$$\nabla \times v_{H,\text{curl}}(x_{K,j}) = \nabla \times v_H(x_{K,j}),$$

which are the important properties.

The FE-HMM scalar product is given by

$$(v_H, w_H)_H = \sum_{K,j} \frac{\omega_{K,j}}{|Y_{K,j}^\eta|} \int_{Y_{K,j}^\eta} \varepsilon^\eta(x)(\nabla \varphi_h) \cdot (\nabla \psi_h)\, dx,$$

where φ_h (resp. ψ_h) are the FE solution of

$$\begin{cases} -\nabla \cdot \big(\varepsilon^\eta(x)(\nabla \varphi_h)\big) = 0 \text{ in } Y_{K,j}^\eta, \\ \displaystyle\int_{Y_{K,j}^\eta} \varphi_h\, dx = 0, \\ \varphi_h(x) - v_H(x_{K,j}) \cdot (x - x_{K,j}) \ \eta Y\text{-periodic.} \end{cases}$$

The FE-HMM scalar product is closely related to standard FE-HMM schemes, see e.g. [1]. In contrast, the use of curl-curl micro problems for the FE-HMM bilinear form is a novelty.

4 A priori error estimate

The following theorem can be proven combining classical arguments of numerical analysis with the discretized version of T-coercivity [3].

Theorem. *Under sufficient regularity assumptions, we have for H small enough*

$$\begin{aligned} \big\|u^0 - u_H\big\|_V \lesssim \inf_{v_H \in V_H} \Bigg(& \big\|u^0 - v_H\big\|_V \\ & + \sup_{w_H \in V_H \setminus \{0\}} \frac{\big|B^0(v_H, w_H) - B_H(v_H, w_H)\big|}{\|w_H\|_V} \\ & + \sup_{w_H \in V_H \setminus \{0\}} \frac{\big|\,(v_H, w_H)_0 - (v_H, w_H)_H\,\big|}{\|w_H\|_V} \Bigg). \end{aligned}$$

The consistency error terms on the second and third line can be bounded further.

Acknowledgement

This work is financially supported by the ANR project METAMATH (ANR-11-MONU-016) and the SNSF (Early Postdoc.Mobility 151906).

References

[1] A. Abdulle, W. E, B. Engquist, and E. Vanden-Eijnden, The Heterogeneous Multiscale Method, *Acta Numer.* **21** (2012), pp. 1–87

[2] N. Wellander and G. Kristensson, Homogenization of the Maxwell equations at fixed frequency, *SIAM J. Appl. Math.* **64** (2003), pp. 170–195.

[3] P. Ciarlet Jr., T-coercivity: Application to the discretization of Helmholtz-like problems, *Comput. Math. Appl.* **64** (2012), pp. 22–34.

Analysis of Multiscale Methods for Long Time Wave Propagation in Locally Periodic Media

Doghonay Arjmand[1], **Olof Runborg**[1]
[1]Department of Mathematics and Swedish e-Science Research Center, KTH, Sweden

Abstract

In the present work, we give an analysis of the upscaling error for a multiscale method approximating long time effective solutions of the multiscale scalar wave equation. In particular, we consider a multi-dimensional locally-periodic media and prove that the long time effects are accurately captured by the method.

Keywords: multiscale methods, multiscale wave propagation, homogenization

1 Introduction

We consider the scalar wave equation in locally-periodic media

$$\partial_{tt}u^\varepsilon(t,x) = \nabla\cdot\Big(A(x,x/\varepsilon)\nabla u^\varepsilon(t,x)\Big), \qquad (1)$$
$$u^\varepsilon(0,x) = g(x), \quad \partial_t u^\varepsilon(0,x) = h(x).$$

We assume that $(x,t)\in\Omega\times[0,T^\varepsilon]$ where $\Omega\subset\mathbb{R}^d$ and $T^\varepsilon = O(\varepsilon^{-1})$. Moreover, $A = A(x,y)$ is a bounded symmetric positive-definite matrix function in $\mathbb{R}^{d\times d}$. We denote the d-dimensional unit cube by $Y=[0,1]^d$ and assume that A is Y-periodic in the y variable and $A_{ij}\in C^\infty(\Omega\times Y)$. Here $\varepsilon\ll 1$ represents the size of microscopic variations in the media.

When $\varepsilon\ll 1$, a numerical simulation of (1) becomes expensive since the small scales must be resolved over the entire Ω. To decrease the cost one can resort to *multiscale methods*, where the idea is to avoid resolving small scales everywhere at the expense of targeting only the coarse part of u^ε.

The coarse part of u^ε is related to the theory of homogenization where effective equations are obtained by mixing the heterogeneities infinitely, achieved in the limit as $\varepsilon\longrightarrow 0$. In locally-periodic media and in addition when the final time $T=O(1)$ is independent of ε, the homogenized solution u^0 solves

$$\partial_{tt}u^0(t,x) = \nabla\cdot\Big(\hat{A}(x)\nabla u^0(t,x)\Big), \qquad (2)$$

where $\hat{A}$ is the homogenized coefficient. $\hat{A}$ is computed by solving another set of non-oscillatory problems over Y.

One of the limitations of homogenization theory is that in general it is not possible to find explicit expressions for $\hat{A}$. Another drawback of (2) is that it does not describe the effective properties over long time scales. In the present study we consider a multiscale method which, unlike homogenization, does not assume any knowledge about A and still give a good approximation of the effective properties for the long time setting as well. We first assume a locally-periodic setting and derive an effective equation accurate up to $O(\varepsilon^{-1})$ time scales. We then present a multiscale method and show that the long time effects are accurately captured by the method.

2 Effective Equations

There has been a great interest in finding effective equations describing the long time behaviour of the scalar wave equation. In purely periodic media, when A is constant in x, the following effective equation was derived in [1]:

$$\partial_{tt}\hat{v}(t,x) = \sum_{i,j}\hat{A}_{ij}\partial_{x_ix_m}\hat{v} + \varepsilon^2 L[\hat{v}], \qquad (3)$$

where $L := \sum_{i,j,\ell,m} C_{ij\ell m}\partial_{x_ix_jx_\ell x_m}$, and C is a fourth order tensor which can be computed using A, and $\hat{A}$ is the standard constant homogenized coefficient. Similar effective equations were derived later in [2] as well.

The effective equation (3) is valid in purely-periodic media and accurate up to $O(\varepsilon^{-2})$ time scales. In locally-periodic media, using asymptotic expansions, we have derived the effective equation

$$\partial_{tt}\hat{v}(t,x) = \nabla\cdot\Big(\Big(\hat{A}(x)+\varepsilon B(x)\Big)\nabla\hat{v}(t,x)\Big) + \varepsilon\sum_{j,m,\ell=1}^{d}\partial_{x_j}\left(D_{jm\ell}(x)\partial_{x_mx_\ell}\hat{v}(t,x)\right), \qquad (4)$$

where $\hat{A}$ is again the homogenized coefficient and B, and D can be computed by solving a set of non-oscillatory cell problems over Y.

Note the difference between (4) and (3). When the medium is locally-periodic, and when $d\geq 2$,

the non-trivial effects show up in much shorter time scales, i.e., $T^\varepsilon = O(\varepsilon^{-1})$. This is the case also for system of wave equations, see e.g. [4]. Therefore, the study of locally-periodic setting better uncovers the generic behaviour of long time waves.

3 Multiscale Method

We introduce a finite difference heterogeneous multiscale method (FD-HMM) from [3] for numerical approximation of (1). For similar approaches in the finite element setting see e.g. [5]. The FD-HMM has a macro- and a micro model. The macro model is

$$\partial_{tt} U(t,x) - \nabla \cdot F = 0. \tag{5}$$

Here U is the macroscopic solution and the flux F is the missing data in the model. A numerical approximation of the macro model (5) by a standard finite difference (FD) method would require values for F at discrete points in Ω. Let r_0 be an arbitrary grid point in Ω. To compute $F(r_0)$ we first solve

$$\begin{aligned} &\partial_{tt} u^\varepsilon - \nabla \cdot (A(x, x/\varepsilon)\nabla u^\varepsilon) = 0, \\ &u^\varepsilon(0,x) = \bar{u}(x), \quad \partial_t u^\varepsilon(0,x) = 0, \end{aligned} \tag{6}$$

over a microscopic box $\Omega_\eta \times [0,\tau]$, where $\tau = O(\varepsilon)$ is a microscopic time and $\Omega_\eta := r_0 + [-L_\eta, L_\eta]^d$ where $L_\eta \geq \eta + \tau\sqrt{|A|_\infty}$ and $\eta = O(\varepsilon)$. The flux $F(r_0)$ is then computed by

$$F(r_0) = \int_{-\tau}^{\tau} \int_{\Omega_\eta} K_\eta(x - r_0) K_\tau(t) A(x, x/\varepsilon) \nabla u^\varepsilon(t,x) dx dt, \tag{7}$$

where $K_\eta(x) := 1/\eta K(x/\eta)$, and K is an averaging kernel such that $K^{(q+1)} \in BV(\mathbb{R})$ and

$$\int_{\mathbb{R}} K(t) t^r dt = \begin{cases} 1 & r = 0, \\ 0 & r \leq p. \end{cases}$$

Moreover, let $\hat{u}(x)$ be a piecewise polynomial interpolant of the macroscopic solutions. Then the initial data $\bar{u}(x)$ is chosen such that the local average in time and space of u^ε agrees with $\hat{u}(x)$.

4 Analysis

Assume that the initial data in (6) is linear and given by $\bar{u} = \hat{u} = s \cdot (x - r_0)$, where $s \in \mathbb{R}^d$ is the slope of the macro solutions. With this choice the FD-HMM captures the effective coefficients $\hat{A}$ and B in (4). To capture D as well, the micro problem (6) should be provided with atleast a second order polynomial. Here we consider only linear initial data and prove the following theorem.

Theorem 1 *Let F and K be given as above. Then with $\eta = \tau$ and $\eta = \varepsilon^{1-\beta}$ for $0 < \beta < 2/7$ we have*

$$\begin{aligned} &\left| F(x) - \left(\hat{A}(x)\nabla\hat{u} + \varepsilon B(x)\nabla\hat{u} \right) \right| \\ &\qquad \leq C \left(\varepsilon^{\beta(q-2)} + \varepsilon^{2-7\beta} \right) |\nabla \hat{u}|_\infty . \end{aligned} \tag{8}$$

where C does not depend on x, ε, η but may depend on K, p, q, d or A.

The first term in the right hand side of (8) accounts for the averaging error in FD-HMM while the second term is due to the higher order effects of waves. The estimate (8) shows that the FD-HMM captures the right long time effects up to $O(\varepsilon^2)$ accuracy upon choosing an arbitrarily small β and a large q, e.g. $q = k/\beta$. Note that small values for β imply lower computational cost as $\eta = O(\varepsilon^{1-\beta})$. Moreover, q can be taken arbitrarily large without further increasing the computational cost.

References

[1] F. Santosa, W. W. Symes, *Siam J. Appl. Math.* **51** (1991), pp. 984–1005.

[2] T. Dohnal, A. Lamacz, B. Schweizer, *arXiv* 1302.4865, (2013).

[3] B. Engquist, H. Holst, and O. Runborg, *in Lect. Notes Comput. Sci. Eng., Springer Verlag*, 2006.

[4] L. Guillot, Y. Capdeville, J. J. Marigo, *Geophys. J. Int.*, **182** (2010), pp. 1438–1454.

[5] A. Abdulle, M. Grote, and C. Stohrer, *Multiscale Model. Simul.*, **12** (2014), pp. 1230–1257.

Interaction of seismic waves with the microstructure of cavernous-fractured reservoirs

Vladimir Tcheverda[1,*], **Vadim Lisitsa**[2], **Maksim Protasov**[3], **Galina Reshetova**[4], **Anastasiya Merzlikina**[5]

[1]Dept. of Comp. Geoph., IPGG SB RAS, Novosibirsk, Russia and Kazakh-British Technical University, Almaty, Kazakhstan

[2]Math. Depth. of Novosibirsk State University, Novosibirsk, Russia and Dept. of Comp. Geoph., IPGG SB RAS, Novosibirsk, Russia

[3]Dept. of Comp. Geoph., IPGG SB RAS, Novosibirsk, Russia and Math. Depart. of Novosibirsk State University

[4]Math. Geoph. Dept., Inst. of Comp. Math. and Math Geoph. SB RAS, Novosibirsk, Russia and Kazakh-British Technical University, Almaty, Kazakhstan

[5]RN KrasnoyarskNIPIneft, Krasnoyarsk, Russia

[*]Email: cheverdava@ipgg.sbras.ru

Abstract

The interaction of seismic waves with fractured reservoirs is analyzed on the base of finite-difference simulation with locally refined grids. The necessity to use such grids is caused by significantly differing scale of heterogeneities in the background (coarse grid) and reservoir (fine grid). Computations for subdomain with coarse and fine grids are carried out in parallel by a group of processor units. The data exchange between these groups is done simultaneously with coupling the coarse and fine grids by spatial interpolation on the base of Fast Fourier Transform.

To understand peculiarities of seismic waves' propagation through the fractured reservoir we construct the generalized realistic digital seismic model on the base of real seismic and well log data for some East Siberian oil field (YUrubchen). The data obtained are used to connect azimuth distribution of scattered energy and fracture orientation. The results are justified by the data of a downhole fracture monitor.

Keywords: seismic waves, multiscale media, scattering, fractures, finite-difference simulation, parallel computations

1 Introduction

Over the last decade the use of scattered waves won a significant place among the wide range of seismic processing techniques. But so far the main area of their application is narrowed to spatial localization of micro heterogeneities clusters, like cracked and fractured areas, cavities and so on. In other words these waves are used just to say "yes" or "no" to the presence of a microstructure. At the same time more detailed knowledge about fine structure of hydrocarbon reservoirs, like orientation of fracture corridors is extremely important.

Recently the finite-difference techniques for seismic waves' simulation in multiscale 3D heterogeneous media is developed and justified (Kostin et al., 2015). Let us stress, that the necessity to use locally refined in time and space grids is caused by significantly different scales of heterogeneities in the background (coarse grid) and reservoir (fine grid).

On this base special software for supercomputers with parallel architecture is implemented. Therefore the people has got the unique possibility for the *in situ* studying of processes of waves' propagation in realistic 3D heterogeneous multiscale models of geological media. We apply this software to simulate seismic waves' propagation through realistic digital model developed for some East Siberian oil field (Yurubchen).

2 Model description and numerical experiments

The general view of the model of fractured carbonate reservoir is presented in Fig.1 together with the classification of fractures following (Petit and Bazalgette, 2002).

The software with local grid refinement is applied to generate the full synthetic wave field. Next we split specular reflection and scattering by means of the Gaussian beam decomposition and spectral filtration of the images obtained (Protasov et al., 2015). The Fig.2 represents the azimuth distribution of the scattered energy extracted from the full wave field for a central point of acquisition. There are two global max-

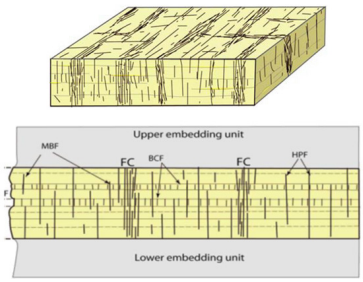

Figure 1: Top: general view of a fractured layer. Bottom: fractures classification. FC - fracture corridors, HPF - high persistent fractures, MBF - multibed fractures, BCF - bed controlled fractures.

ima corresponding to azimuths 90° and 270° coinciding with orientations of the most intensive fracture corridor. At the same time there is some secondary maximum corresponding to the direction of the orthogonal set of fractures.

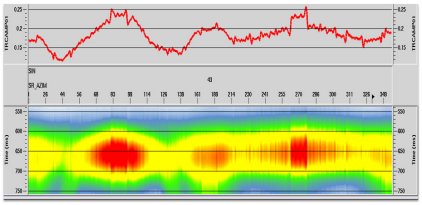

Figure 2: Fracture energy azimuth distribution (horizontal direction). Zero corresponds to west-east direction in the Fig.1, top.

3 Comparison with real data

To verify the approach of estimation of fracture orientation the real data processing was done. Results can be seen in Fig.3. Here the azimuth distribution of the scattered energy (green) is compared with distribution of fractures obtained with the help of a downhole fracture monitor at the depth corresponding to the fractured layer (red). Correlation coefficient between the shapes of two these curves is equal to 0.79, which confirms the reliability of the approach proposed.

4 Conclusion

On the base of the finite-difference technique with local refinement in time and space the approach to estimate orientation of fractures is proposed and justified by real field data.

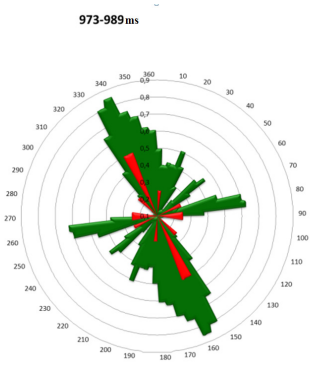

Figure 3: Green: azimuth distribution of a scattered energy at the time slice 973 - 989 ms.

5 Acknowledgements

The research described in this publication was partially supported by Russian Foundation for Basic Research, grants no. 13-05-00076, 14-05-00049, 14-01-00180, 14-05-93090. Vladimir Tcheverda and Galina Reshetova are supported by the Ministry of Education and Science of the Republic of Kazakhstan under grants 0981/GF4 and 1771/GF4. The simulations were performed on the Siberian Supercomputer Center, Joint Supercomputer Center of RAS and Supercomputer Lomonosov of Moscow State University.

References

[1] V.Kostin, V.Lisitsa, G.Reshetova, V.Tcheverda, Local time-space mesh refinement for simulation of elastic wave propagation in multi-scale media, *Journal of Computational Physics* **281** (2015), pp. 669–689.

[2] J.P.Petit and Bazalgette, Fracture corridors: What are they? in *Inaugural Meeting of SFERA, Pescara, Italy, 2002.*

[3] M.Protasov, G.Reshetova, V.Tcheverda, Fracture detection by Gaussian beam imaging of seismic data and image spectrum analysis, *Geophysical Prospecting* **accepted** (2015).

Eliminating the pollution effect in Helmholtz problems by local subscale correction

Dietmar Gallistl[1], **Daniel Peterseim**[1,*]
[1]Institute for Numerical Simulation, Bonn University, Bonn, Germany
*Email: peterseim@ins.uni-bonn.de

Abstract

We introduce a new Petrov-Galerkin multiscale method for the numerical approximation of the Helmholtz equation with large wave number κ in bounded domains in $\mathbb{R}^d$. The discrete test spaces are generated from standard mesh-based finite elements by local subscale corrections in the spirit of numerical homogenization. The precomputation of the corrections involves the solution of coercive cell problems on localized subdomains of size ℓH; H being the mesh size and ℓ being the oversampling parameter. If the mesh size and the oversampling parameter are such that $H\kappa$ and $\log(\kappa)/\ell$ fall below some generic constants, the method is stable and its error is quasi-minimal; pollution effects are eliminated in this regime.

Keywords: pollution effect, Helmholtz problem, finite element, multiscale method, numerical homogenization

This talk concerns the numerical solution of the Helmholtz equation by the finite element method or related schemes in the regime of large wave numbers. The highly oscillatory nature of the solution plus a wave number dependent pollution effect puts very restrictive assumptions on the smallness of the underlying mesh. Typically, this condition is much stronger than the minimal requirement for a meaningful representation of highly oscillatory functions from approximation theory, that is, to have at least $5-10$ degrees of freedom per wave length and coordinate direction.

The wave number dependent preasymptotic effect denoted as pollution or numerical dispersion is well understood by now and many attempts have been made to overcome or at least reduce it. However, for many standard methods, this is not possible in 2d or 3d [1].

Inspired by the numerical homogenization of diffusion problems with rough and highly oscillatory diffusion tensor [4] , this talk introduces a novel Petrov-Galerkin multiscale method of to cure pollution in the numerical approximation of the Helmholtz problem. The discrete trial and test spaces of the method are generated from standard mesh-based finite elements by local subscale corrections. The precomputation of the corrections involves the solution of H^{-d} coercive cell problems on localized subdomains of size ℓH; H being the mesh size and ℓ being the adjustable oversampling parameter. If the data of the problem (domain, boundary condition, force term) allows for polynomial-in-κ bounds of the solution operator and if the mesh size and the oversampling parameter of the method are such that the resolution condition $H\kappa \lesssim 1$ and the oversampling condition $\log(\kappa)/\ell \lesssim 1$ are satisfied, then the method is stable and satisfies the error estimate

$$\kappa\|u-u_{\mathrm{msPG}}\|_{L^2(\Omega)} + \|\nabla(u-u_{\mathrm{msPG}})\|_{L^2(\Omega)} \leq C(H+\beta^\ell)$$

with generic constants $C>0$ and $\beta<1$ independent of κ. For a fairly large class of Helmholtz problems, including the acoustic scattering from convex non-smooth objects, this result shows that pollution effects can be suppressed under the quasi-minimal resolution condition $H\kappa \leq \mathcal{O}(1)$ at the price of a moderate increase of the inter-element communication, i.e., logarithmic-in-κ oversampling. The complexity overhead due to oversampling is comparable with that of [5, 6], where instead of increasing the inter-element communication, the number of degrees of freedom per element is increased via the polynomial degree which is coupled to $\log\kappa$ in a similar way. While [1] shows that pollution cannot be avoided with a fixed stencil, our results show that already a logarithmic-in-κ growths of the stencil can suffice to eliminate pollution.

Although the results are constructive, their practical relevance for actual computations is not immediately clear in any case. The multiscale method requires accurate precomputations on sufficiently fine subgrids. These precomputations are both local and independent, but the worst-case (serial) complexity of the method can exceed the cost of a direct numerical simulation on a global fine mesh. In this

context, this talk also shows how, in a structured mesh, the number of cell problems can be reduced from $\mathcal{O}(H^{-d})$ to $\mathcal{O}(\ell^d)$, where the hidden constant depends only on the number of geometric feature of the computational domain. This complexity reduction turns the approach into a feasible and competitive numerical method for acoustic scattering problems. Several numerical experiments will demonstrate the practical performance of the method.

This talk is based on the recent preprints [7] and [2].

References

[1] I. M. Babuška and S. A. Sauter, Is the pollution effect of the FEM avoidable for the Helmholtz equation considering high wave numbers?, *SIAM Rev.*, **42**(3):451–484, 2000.

[2] D. Gallistl and D. Peterseim, Multiscale Petrov-Galerkin method for acoustic scattering, *ArXiv e-prints*, 1503.04948, 2015.

[3] P. Henning and D. Peterseim, Oversampling for the Multiscale Finite Element Method, *Multiscale Model. Simul.*, **11**(4):1149–1175, 2013.

[4] A. Målqvist and D. Peterseim, Localization of Elliptic Multiscale Problems, *Mathematics of Computation*, **83**(290):2583-2603, 2014.

[5] J. M. Melenk and S. Sauter, Convergence analysis for finite element discretizations of the Helmholtz equation with Dirichlet-to-Neumann boundary conditions, *Math. Comp.*, **79**(272):1871–1914, 2010.

[6] J. M. Melenk and S. Sauter, Wavenumber explicit convergence analysis for Galerkin discretizations of the Helmholtz equation, *SIAM J. Numer. Anal.*, **49**(3):1210–1243, 2011.

[7] D. Peterseim, Eliminating the pollution effect in Helmholtz problems by local subscale correction, *ArXiv e-prints*, 1411.1944, 2014.

Monday, July 20
First Afternoon Session
15:30 – 17:00

A high frequency boundary element method for scattering by three-dimensional screens

J. A. Hargreaves[1], D. P. Hewett[2], Y. W. Lam[1], S. Langdon[3,*]
[1]School of Computing, Science and Engineering, University of Salford, U.K.
[2]Mathematical Institute, University of Oxford, U.K.
[3]Department of Mathematics and Statistics, University of Reading, U.K.
*Email: s.langdon@reading.ac.uk

Abstract

We propose a numerical-asymptotic boundary element method for time-harmonic acoustic scattering of an incident plane wave by sound-soft three-dimensional (3D) screens. Standard numerical schemes require the number of degrees of freedom to grow rapidly in order to maintain accuracy as frequency increases. Here, we enrich our approximation space away from the edges of the screen with oscillatory basis functions carefully designed to capture the high frequency behaviour of the solution. We show that reasonable accuracy can be achieved for a range of frequencies using relatively few degrees of freedom.

Keywords: Helmholtz, high frequency, hybrid numerical-asympotic boundary element method

1 Problem statement

We consider the 3D problem of scattering of the time harmonic incident plane wave $u^i(\mathbf{x}) = \mathrm{e}^{\mathrm{i}k\mathbf{x}\cdot\mathbf{d}}$, where $\mathbf{x} = (x_1, x_2, x_3) \in \mathbb{R}^3$, $k > 0$ is the wavenumber and $\mathbf{d}$ is a unit direction vector, by a sound soft screen $\Gamma := \{(x_1, x_2, 0) \in \mathbb{R}^3 : (x_1, x_2) \in (0, 2\pi) \times (0, 2\pi)\}$. The boundary value problem (BVP) we wish to solve is: given u^i, determine $u \in C^2(D) \cap W^1_{loc}(D)$ such that

$$\Delta u + k^2 u = 0 \text{ in } D := \mathbb{R}^3 \backslash \bar{\Gamma},\ u = 0 \text{ on } \Gamma,$$

and the scattered field $u^s := u - u^i$ satisfies the Sommerfeld radiation condition. For the solution of the above BVP, a form of Green's representation theorem holds:

$$u(\mathbf{x}) = u^i(\mathbf{x}) + \int_\Gamma \Phi_k(\mathbf{x}, \mathbf{y}) \left[\frac{\partial u}{\partial \mathbf{n}}\right](\mathbf{y})\, \mathrm{d}\mathbf{y},\ \mathbf{x} \in D,$$

where $\Phi_k(\mathbf{x}, \mathbf{y}) = \exp(\mathrm{i}k|\mathbf{x} - \mathbf{y}|)/4\pi|\mathbf{x} - \mathbf{y}|$ and $[\partial u/\partial \mathbf{n}] =: \phi$ is the jump in the normal derivative $\partial u/\partial \mathbf{n}$ across Γ. Then ϕ satisfies the boundary integral equation (see, e.g., [1, §7.6])

$$S_k\phi(\mathbf{x}) := \int_\Gamma \Phi_k(\mathbf{x}, \mathbf{y})\phi(\mathbf{y})\, \mathrm{d}\mathbf{y} = u^i(\mathbf{x}),\ \mathbf{x} \in \Gamma. \tag{1}$$

2 Approximation space

The key idea of our approach is to adapt our approximation space for the solution of (1) to the high frequency asymptotic behaviour of the solution. Specifically, for $\mathbf{x} \in \Gamma$ we write

$$\phi(\mathbf{x}) = \Psi(\mathbf{x}) + \sum_{m=1}^{M} V_m(\mathbf{x}, k) \exp(\mathrm{i}k\psi_m(\mathbf{x})), \tag{2}$$

where $\Psi := 2\partial u^i/\partial \mathbf{n}$ represents the Geometrical Optics approximation, and our aim is to choose the phase functions ψ_m, $m = 1, \ldots, M$, in such a way that the corresponding amplitudes $V_m(\cdot, k)$ are (relatively) non-oscillatory. For the equivalent 2D problem (see [2]) it is sufficient to take $M = 2$, in which case V_1 and V_2 are provably non-oscillatory (i.e. all of the oscillations are captured completely by a small number of phase functions). For the 3D problem this is not the case, since the waves diffracted by the edges and corners of the screen are rediffracted infinitely often by the other edges and corners of the screen, taking a different direction of travel after each rediffraction. However, it turns out that with a judicious choice of ψ_m in (2) we can represent ϕ to a reasonable degree of accuracy away from the edges of the screen (where the solution is singular and a standard approximation space is used) using only a small value of M. Specifically, we choose $M = 8$, and ψ_m, $m = 1, \ldots, 8$, so that $\exp(\mathrm{i}k\psi_m(\mathbf{x}))$, $m = 1, \ldots, 4$, represent plane waves propagating in the direction of the singly-diffracted rays predicted by the Geometrical Theory of Diffraction (see [1, §7.6]), with one such wave associated to each of the four edges of the screen, and $\exp(\mathrm{i}k\psi_m(\mathbf{x}))$, $m = 5, \ldots, 8$, represent their reflections by other edges (this being sufficient to

capture all rereflections from edges, due to the regular nature of the screen). Using (2) we can design an appropriate approximation space to represent $\varphi := \phi - \Psi$, the difference between $[\partial u/\partial \mathbf{n}]$ and its Geometrical Optics approximation. Precisely: within a tenth of a wavelength of each edge of the screen we use a standard (piecewise polynomial) approximation space on an appropriate graded mesh (in order to capture the singular behaviour near the edges); away from the edge of the screen we divide the screen into nine elements, and on each element our approximation space consists of piecewise polynomials (of maximum order p) multiplied by each of the four plane waves described above, as shown in Figure 1.

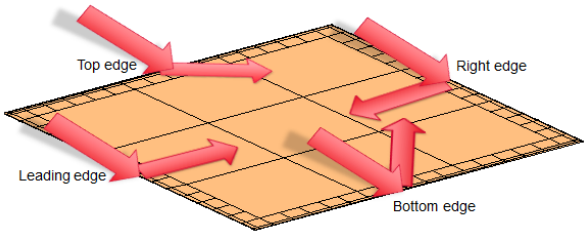

Figure 1: Coarse mesh away from edges, standard (graded) mesh near edges

3 Numerical results

We use a Galerkin method to select an element from our approximation space, denoted by $V_{p,k}$. That is, we seek $\varphi_p \in V_{p,k}$ such that

$$\langle S_k \varphi_p, v\rangle_\Gamma = \left\langle u^i - S_k\Psi, v\right\rangle_\Gamma, \forall v \in V_{p,k}, \quad (3)$$

where the duality pairings in (3) are L^2 inner products. With $\mathbf{d} = (3,1,1)/\sqrt{11}$ we solve (3) for $p = 0,1,2$, giving up to $1,4,9$ polynomials respectively on each coarse element. So, with eight wave directions and nine coarse elements, we have, for $p = 0,1,2$, respectively 72, 288, and 648 total degrees of freedom on our coarse mesh, and we keep this value fixed for each different value of k tested. Note that this central part of the screen covers $k - 0.2$ wavelengths in each direction, so a standard scheme requiring, say, 10 degrees of freedom per wavelength, might require of the order of $100(k-0.2)^2$ degrees of freedom on this region in order to represent the solution to "engineering accuracy". In Figure 2 we plot on a logarithmic scale the relative L^2 errors in ϕ on this central section (we restrict attention here to this central portion because we are primarily interested in understanding how well we can represent the oscillatory behaviour), against k, for $p = 0,1,2$, demonstrating that we can achieve a reasonable level of accuracy using this approach with a very small number of degrees of freedom compared to standard methods.

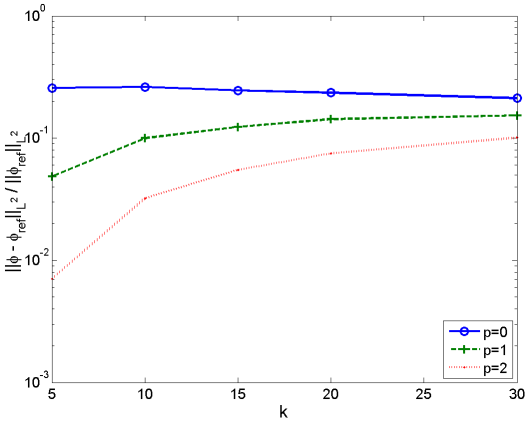

Figure 2: Convergence results

Acknowledgements

The authors gratefully acknowledge support for this work from EPSRC grants EP/J022071/1 and EP/K000012/1.

References

[1] S. N. Chandler-Wilde, I. G. Graham, S. Langdon and E. A. Spence, Numerical-asymptotic boundary integral methods in high-frequency acoustic scattering, *Acta Numer.*, **21** (2012), pp. 89–305.

[2] S. N. Chandler-Wilde, D. P. Hewett and S. Langdon, A frequency-independent boundary element method for scattering by two-dimensional screens and apertures, *IMA J. Numer. Anal.*, published online 2014, doi:10.1093/imanum/dru043.

High-frequency asymptotic compression of dense BEM matrices

Peter Opsomer[1], **Daan Huybrechs**[1]
[1]Department of Computer Science, University of Leuven, Belgium

Abstract

A Boundary Element Method (BEM) discretization matrix for a high-frequency scattering problem is typically large and dense. A matrix-vector product is very costly, unless accelerated by FMM. We introduce an alternative, and relatively simple technique to reduce the cost of a matrix-vector product by introducing sparsity. The matrix represents the action of an oscillatory integral operator on an oscillatory function, and at high frequencies this action is essentially local in nature. We show how to exploit this locality by modifying the Green's function using well-chosen windowing functions in an otherwise standard BEM implementation. We present proof-of-concept results to illustrate that asymptotic compression can be achieved even for near-trapping domains and multiple scattering obstacles.

Keywords: BEM, oscillatory integration, high-frequency scattering, compression

1 Introduction

In sound simulations, one converts the Helmholtz equation into a Boundary Integral equation. The scattered field by an obstacle with boundary Γ can be represented via Green 's theorem by the single layer potential

$$u^{\mathrm{s}}(\vec{x}) = \int_{\Gamma} K(\vec{x},\vec{y})v(\vec{y})ds(\vec{y}), \qquad (1)$$

where $K(\vec{x},\vec{y})$ represents the Green's function. For a sound-soft obstacle, we have

$$u^{\mathrm{s}}(\vec{x}) = -u^{\mathrm{inc}}(\vec{x}), \forall \vec{x} \in \Gamma, \qquad (2)$$

with incident wave $u^{\mathrm{inc}}(\vec{x})$. A collocation approach solves the linear system $Ax = b$, where b represents the right hand side of (2) at the collocation points $\vec{x}_i$, x the density $v(\vec{y})$ at $\vec{x}_i$ and Ax approximates the integral in (1).

We have chosen an incident plane wave in Figure 1, for a slightly non-convex obstacle with wave number $k = 256$. We have used $N = 1,536$ degrees of freedom in the discretization. There are no multiple reflections in this scene, but results for other domains are included further on.

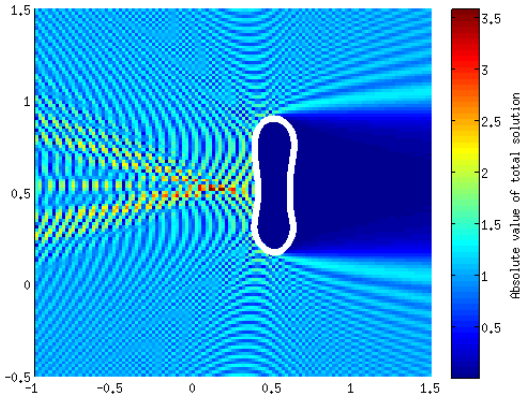

Figure 1: Scattering simulation for a near-convex obstacle using $k = 256$ and $N = 6k$.

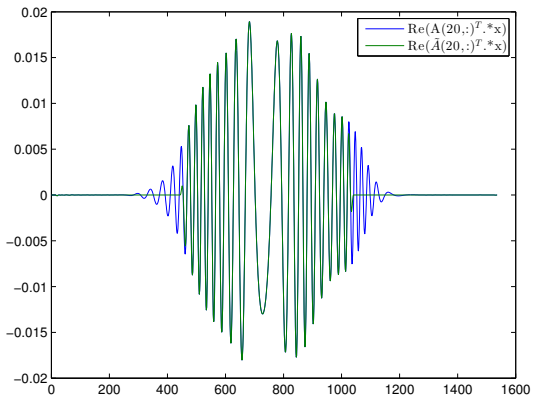

Figure 2: Real part of the 20-th row of A (blue), resp $\tilde{A}$ (green), times x for $k = 256$ and $N = 6k$.

2 Oscillatory integration

In Figure 2, we have shown the real part of the vector $A[20,:]^T . * x$, which sums to $b[20]$. This approximates the oscillatory integrand in (1). Most of the oscillations cancel out when summing, and even more so when k increases.

This agrees with results in asymptotic analysis: contributions to the integral originate in points of singularity, or in so-called stationary points. The latter are points where the derivative of the phase of the integrand vanishes, which renders the integrand locally non-oscillatory.

The singularity is present everywhere along the diagonal of the matrix and *self-reflections correspond to stationary points* at the correspond-

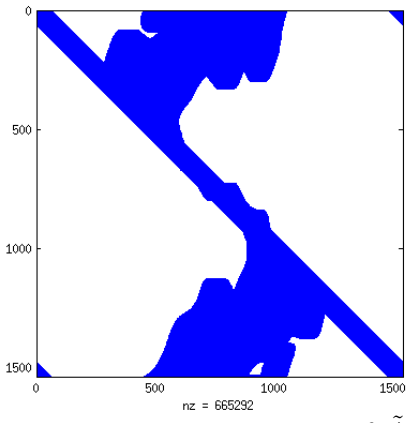

Figure 3: Nonzero pattern of $\tilde{A}$.

ing location in A. First order compression could be based on a simple visibility condition.

In order to assess the possible rate of compression, we follow a crude but fully automatic technique to locate stationary points. We multiply each row of the matrix A with a sliding C^∞ window and compute correlations with the exact solution vector x. Small correlation means there is no contributing point inside the support of the window. After thresholding and enforcing adding the singularity along the diagonal, this results in a pattern shown in Figure 3. For collocation points inside the shadow region, there is a stationary point in the illuminated region.

3 Method and results

The exact phase of the solution is known only for simple convex obstacles [2]. However, when the Green's function is multiplied by a smooth cut-off function around each stationary point, the resulting integral is asymptotically the same, even if the phase is not known explicitly.

This C^∞ window is based on our correlation test, resulting in a compressed matrix $\tilde{A}$ which avoids approximating zero. Note that it is not sufficient to simply discard entries of A. Similar patterns were seen in [1, 3], based on phase extraction which we do not employ here.

Results are shown in Table 1 for $k = 2^8$ and 2^{10}, using the windows found at the former also for the larger wavenumber, since stationary points are independent of frequency. One could also use increasingly smaller windows for rising frequencies, thus reducing computational complexity but still with an increasing N.

Results are included for a self-reflecting obstacle and a near-trapping domain. Here, the support of the window functions is rather large

Obstacle	% nnz	Error at 2^8	Error at 2^{10}
Ellipse	25%	5.0%	0.22%
Figure 1	28%	6.2%	0.14%
Self-reflecting	51%	12%	1.9%
Near-trapping	52%	5.1%	0.63%
3 ellipses	31%	14%	12%

Table 1: Pct. of nonzeros and $||\tilde{x}-x||/||x||$ for 5 domains at different k, using $N = 6k$.

and compression deteriorates. However, the method remains applicable in principle, and results improve with increasing frequency. A scene with 3 scattering ellipses can also be asymptotically compressed, although our preliminary implementation exhibits higher errors.

References

[1] E. Giladi, Asymptotically derived boundary elements for the Helmholtz equation in high frequencies, *J. Comput. Appl. Math.* **198** (2007), pp. 52–74.

[2] S. Chandler-Wilde, I. Graham, S. Langdon and E. Spence, Numerical-asymptotic boundary integral methods in high-frequency acoustic scattering, *Acta Numer.* (2012), pp. 89-–305.

[3] D. Huybrechs and S. Vandewalle, A sparse discretization for integral equation formulations of high frequency scattering problems, *SIAM J. Sci. Comput.* **29(6)** (2007), pp. 2305–2328.

A high-frequency preconditioner for the boundary element method applied to high-intensity focused ultrasound

Elwin van 't Wout[1,*], **Pierre Gélat**[2], **Timo Betcke**[3], **Simon Arridge**[1]

[1]Centre for Medical Image Computing, University College London, United Kingdom
[2]Department of Mechanical Engineering, University College London, United Kingdom
[3]Department of Mathematics, University College London, United Kingdom

*Email: e.wout@ucl.ac.uk

Abstract

Medical therapies with high-intensity focused ultrasound have promising applications in the non-invasive treatment of cancer. Yet, their clinical use is limited when the diseased tissue is located behind a rib cage. Numerical methods can play an important role in the treatment planning. This necessitates the computation of acoustic scattering at MHz frequencies. Modern boundary element methods provide fast and accurate computation of large-scale scattering, but quick convergence is difficult to achieve at high frequencies. This paper presents the use of an operator preconditioner based on on-surface radiation conditions that effectively improves convergence in the high-frequency range. The feasibility for medical applications is demonstrated with scattering analysis of a human rib cage by focused ultrasound of 1 MHz.

Keywords: boundary element method, medical physics, acoustic scattering, preconditioning

1 Introduction

The convential medical treatments of liver cancer are surgical resection and transplantation. These invasive procedures pose severe health risks to the patients. As a non-invasive alternative, high-intensity focused ultrasound (HIFU) can be used to ablate tumours by heating a localised region of tissue. Although HIFU treatment has been demonstrated to be feasible for a range of different cancers, there are a number of significant challenges which currently hinder its more widespread clinical use. In particular, the scattering of ultrasound by ribs can result in overheating of the bone and abberations at the focal region. The patient-specific planning for transcostal HIFU treatment is likely to rely on numerical modelling to optimise the multi-element array of ultrasound transducers.

The boundary element method (BEM) has shown great promise relative to other numerical schemes because of its ability to solve large-scale scattering problems [1]. However, the applicability of BEM is limited by the large demand for computational resources, the weak convergence and the presence of spurious resonance modes for simulation of high-frequency scattering. In this paper, we will use a Burton-Miller formulation with a high-frequency preconditioner based on on-surface radiation conditions (OSRC) [2]. The improvement that such techniques can bring to the effectiveness of BEM for HIFU simulations will be demonstrated.

2 Methodology

Let us consider a bounded domain $\Omega \subset \mathbb{R}^3$ representing a rib cage, with a Lipschitz smooth boundary $\Gamma = \partial\Omega$. The time-harmonic scattering of acoustic waves on a rigid surface can be modelled with the Helmholtz exterior boundary value problem

$$\begin{cases} \Delta p + k^2 p = 0, \\ \partial_n (p + p_{\text{inc}})|_\Gamma = 0, \\ \lim_{|\mathbf{x}|\to\infty} |\mathbf{x}| \left(\nabla p \cdot \frac{\mathbf{x}}{|\mathbf{x}|} - \mathrm{i}kp \right) = 0 \end{cases}$$

where p denotes the unknown pressure field and k the wavenumber. The scattered field can be rewritten in terms of the double-layer potential $\varphi = (p_{\text{inc}} - p)|_\Gamma$ on the surface. To avoid spurious resonances, a Burton-Miller formulation with coupling parameter $\eta \in \mathbb{C}$ will be used:

$$\left(\tfrac{1}{2} I + M - \eta D\right) \varphi = -p_{\text{inc}}|_\Gamma + \eta \partial_n p_{\text{inc}}|_\Gamma$$

where I, M and D denote the identity, double-layer and hypersingular boundary operators. The convergence of the Galerkin discretised Burton-Miller formulation deteriorates at high frequencies, where the wavelength is small compared with the dimension of the scatterer. Preconditioning of the unbounded hypersingular boundary operator is necessary to achieve fast convergence. A regularising operator $\tilde{V} : H^{-\frac{1}{2}}(\Gamma) \to$

$H^{\frac{1}{2}}(\Gamma)$ will be used as preconditioner and included as $\eta = \tilde{V}$ in the Burton-Miller formulation. Specifically, we use a high-frequency approximation of the Neumann-to-Dirichlet map with the OSRC technique [2], given by

$$\tilde{V} = \frac{1}{\mathrm{i}k}\left(1 + \frac{\Delta_\Gamma}{(k+\mathrm{i}\epsilon)^2}\right)^{-\frac{1}{2}}$$

where Δ_Γ denotes the Laplace-Beltrami operator. Singularities are prevented with a damped wavenumber $k + \mathrm{i}\epsilon$, $\epsilon > 0$. After approximating this pseudo-differential operator with a Padé series, Galerkin discretisation results in a sparse set of linear equations and thus fast computations. The preconditioner is particularly accurate for high-frequency scattering and therefore results in quick convergence for HIFU simulations. Moreover, it can be combined with fast multipole methods or $\mathcal{H}$-matrix compression.

3 Numerical experiments

The OSRC preconditioned Burton-Miller formulation for acoustic scattering of rigid surfaces has been implemented in the open-source software package `BEM++` [3]. Test problems on a sphere confirm the improved convergence for high frequencies; in fact, the number of iterations for the GMRES algorithm remains almost constant for increasing wavenumber. To demonstrate the applicability to HIFU simulation, we use a model of four ribs with a length of approximately 12 cm from a human rib cage, embedded in water. A transducer array that has already been optimised for focusing behind a rib cage will be used as excitation [1]. The 256 piston sources have a common frequency of 1 MHz. The triangular surface mesh results in 78 297 degrees of freedom for piecewise continuous linear test and basis functions. The OSRC preconditioned BEM converges in 94 iterations and 2 minutes on a desktop computer with 12 cores and 80 GB RAM. This is a considerable improvement compared to the 4741 iterations and 69 minutes required for the Burton-Miller formulation. Furthermore, the realistic pressure field, depicted in Figure 1, demonstrates the applicability of OSRC preconditioned BEM to transcostal HIFU simulation.

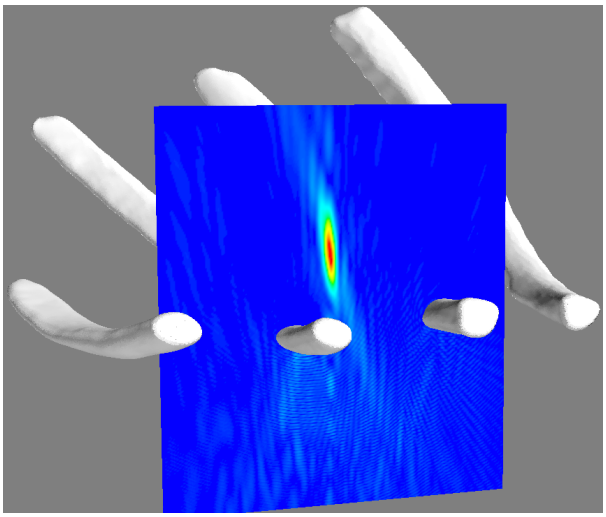

Figure 1: Simulation of the focusing of a HIFU field behind a rib cage, performed with the OSRC preconditioned BEM.

References

[1] P. Gélat, G. ter Haar and N. Saffari, A comparison of methods for focusing the field of a HIFU array transducer through human ribs, *Physics in Medicine and Biology* **59** (2014), pp. 3139–3171.

[2] M. Darbas, E. Darrigand and Y. Lafranche, Combining analytic preconditioner and Fast Multipole Method for the 3-D Helmholtz equation, *Journal of Computational Physics* **236** (2013), pp. 289–316.

[3] W. Śmigaj, S. Arridge, T. Betcke, J. Phillips and M. Schweiger, Solving Boundary Integral Problems with BEM++, accepted for publication in *ACM Transactions on Mathematical Software* (2015).

Inverse Scheme for Acoustic Source Localization based on Microphone Array Measurements

Manfred Kaltenbacher[1,*], **Barbara Kaltenbacher**[2]

[1]Institute of Mechanics and Mechatronics, Vienna University of Technology, Austria
[2]Institute of Applied Analysis, Alpen-Adria-Universität Klagenfurt, Austria

[*]Email: manfred.kaltenbacher@tuwien.ac.at

Abstract

In the last years, considerable improvements have been achieved in acoustic source localization using microphone arrays. However, main restrictions include simplified source models and using Green's function for free radiation as the transfer function between source and microphone signal. To overcome these limitations, we aim to solve the corresponding partial differential equation (Helmholtz equation) with the actual boundary conditions as given in the measurement setup.

Keywords: Acoustic source localization, inverse method, Helmholtz equation

1 Introduction

Acoustic beamforming is used to determine source locations and distributions, measure acoustic spectra for complete models and subcomponents, and project results from the array to far field points. The fundamental processing method, Frequency Domain Beamforming (FDBF) [**?**] is robust, fast, and renders continuous source distributions as continuous images. Here, the beamforming map is computed by

$$a(\boldsymbol{g}) = \boldsymbol{g}^* \boldsymbol{C} \boldsymbol{g} \tag{1}$$

with $\boldsymbol{g}$ the steering vector, * the complex conjugate, and $\boldsymbol{C}$ the cross spectral matrix (CSM) of the array. The CSM is computed out of the measured microphone signals and is modeled by

$$\boldsymbol{C} = \sum_{j=1}^{M} \sigma_j \boldsymbol{g}\boldsymbol{g}^* \tag{2}$$

with M the number of assumed sound sources. Assuming that only the source σ_k is nonzero, we obtain

$$\boldsymbol{C} = \sigma_k \boldsymbol{g}_k \boldsymbol{g}_k^* \tag{3}$$

and the source map results in

$$a(\boldsymbol{g}) = \sigma_k \boldsymbol{g}_k^* \boldsymbol{g}_k \boldsymbol{g}_k^* \boldsymbol{g}_k \,. \tag{4}$$

By forcing $\boldsymbol{g}_j^* \boldsymbol{g}_j = 1$, we obtain the correct source location with strength σ_k. The resolution is limited by the Rayleigh limit [**?**], and the dynamic range to about 20 dB by the finite aperture of the microphone array and further reduced to 7-12 dB by the sparse array design that is necessary for high frequency operation with a limited number of microphones. A second processing step is required to convert a raw FDBF map into a source density map. This can be done by application of an overall scaling factor, known as the integration technique [**?**] or deconvolution by, e.g., CLEAN [**?**], DAMAS [**?**] or CLEANSC [**?**]. A main restriction is currently that the sources are modeled as monopoles or/and dipoles and the steering vector $\boldsymbol{g}$ describing the transfer function between source and microphone signal is modeled by Green's function for free radiation. To overcome these limitations, we plan to solve the corresponding PDE with the actual boundary conditions as given, e.g., in aeroacoustic wind tunnels, where such measurements are often performed.

2 Physical Model

We assume that we have the original geometry of the setup and Fourier-transformed acoustic pressure signals $p_{\mathrm{m}i}(\omega)$ (ω being the angular frequency, $i = 1, ..., M$) measured by microphones at positions $\boldsymbol{x}_i$. Therefore, our physical model is the Helmholtz equation

$$\Delta p + k^2 p = \sigma \tag{5}$$

with the wave number k and the searched for acoustic sources $\sigma(\boldsymbol{x}, \omega)$. Since we will do the identification separately for each frequency ω_j, we will neglect dependence on ω in the following. For the acoustic sources, we may write

$$\sigma(\boldsymbol{x}) = \sum_{j=1}^{N} a_j e^{i\varphi_j} \delta_{\boldsymbol{x}_j} \tag{6}$$

with delta pulses $\delta_{\boldsymbol{x}_j}$ located at N grid points $\boldsymbol{x}_j$, the searched for amplitudes $a_1, a_2, ..., a_N \in$

$\boldsymbol{R}$ and phases $\varphi_1, \varphi_2, ..., \varphi_N \in [-\pi/2, \pi/2]$. Our goal is to minimize the following term

$$\frac{1}{2}\sum_{i=1}^{M} |p_i(\boldsymbol{x}_i) - p_{\mathrm{m}i}|^2 + \alpha \left(\sum_{j=1}^{N} \left| a_j \right|^q + \gamma \sum_{j=1}^{N} \varphi_j^2 \right) \tag{7}$$

(with a small regularization factor $\alpha > 0$ and a fixed value γ) such that (5) is fulfilled. The exponent $q > 1$ is chosen close to one to enhance sparsity [**?**], i.e. to pick the few true source locations from a large number N of trial sources. Here, the L^q norm is used as a smooth approximation of the L^1 norm. According to the discrepancy principle, we choose $\alpha = 2^{-m}$ $(m = 0, 1, 2,)$ such that

$$\sqrt{\sum_{i=1}^{M} \left(p_i(\boldsymbol{x}_i) - p_{\mathrm{m}i}\right)^2} \sim \varepsilon \tag{8}$$

with ε the measurement errror.

3 Numerical Scheme

According to our model, we define the following Lagrange functional $\mathcal{L}(a_1, .., a_N, \varphi_1, .., \varphi_N, p, z)$

$$\frac{1}{2}\sum_{i=1}^{M} |p_i(\boldsymbol{x}_i) - p_{\mathrm{m}i}|^2 + \alpha \left(\sum_{j=1}^{N} \left| a_j \right|^q + \gamma \sum_{j=1}^{N} \varphi_j^2 \right) + \mathrm{Re}\left(\int_\Omega \left(k^2 p z - \nabla p \cdot \nabla z - \sum_{j=1}^{N} a_j e^{i\varphi_j} \delta_{\boldsymbol{x}_j} z \right) \mathrm{d}\Omega \right) .$$

In a next step, we perform the directional derivatives of our Lagrange functional w.r.t. the arguments. Starting with the searched for amplitudes a_j, we obtain the first defining equation

$$0 = \frac{\partial \mathcal{L}}{\partial a_j}[z] = \alpha q \left| a_j \right|^{q-1} \mathrm{sign}(a_j) - \mathrm{Re}\left(e^{i\varphi_j} z(\boldsymbol{x}_j) \right) . \tag{9}$$

For the searched for phases, we get

$$0 = \frac{\partial \mathcal{L}}{\partial \varphi_j}[z] = 2\alpha\gamma\varphi_j + a_j \mathrm{Im}\left(e^{i\varphi_j} z(\boldsymbol{x}_j) \right) . \tag{10}$$

For the directional derivative w.r.t. the acoustic pressure p, we perform a linearization in the direction of v and finally arrive at

$$\Delta z + k^2 z = \sum_{l=1}^{M} \left(p(\boldsymbol{x}_l) - p_{\mathrm{m}}(\boldsymbol{x}_l) \right)^* \delta_{\boldsymbol{x}_l} \tag{11}$$

with $*$ the conjugate complex operation. The last directional derivative w.r.t z results in the state equation (5).

Thereby, our scheme is based on interatively solving (9) to (11) and (5).

4 Outlook

In the talk, we will provide details of our inverse scheme and its application to real world problems to demonstrate the additional benefit of our scheme as compared to the classical approach.

The generalized linear sampling method for limited aperture data

Lorenzo Audibert[1,*], **Houssem Haddar**[2], **Alexandre Girard**[3]
[1]EDF R&D, Chatou, France
[2]INRIA Saclay & CMAP, Palaiseau, France
[3]EDF R&D, Chatou, France
[*]Email: lorenzo.audibert@edf.fr

Abstract

In [1] we propose and analyse a new formulation of the Linear Sampling Method, the Generalized Linear Sampling Method that gives an exact characterization of the target's shape in terms of the so-called farfield operator (at a fixed frequency). In this paper we present an extension of this method to the case of limited aperture data. This case has only been studied in the restricted situation where the direction of the incident plane waves and the measured farfield patterns are the same (this situation corresponds to measure in transmission). We extend the theoretical justification of the Generalized Linear Sampling method to any set of direction of incidence and measurement.

Keywords: Inverse scattering, Qualitative method, Limited aperture

1 Introduction

We are interested in extending the result from [1] to the case of limited aperture data. We will restrict ourselves to the case of scalar acoustic waves and penetrable obstacle. First we will recall the equations that defines the farfield operator and its factorization. Secondly we will recall the result of the GLSM that applied in the case of full aperture (and when the direction of incidence and measurement are the same. Finally we will give the modification that one should applied to GLSM in order to have an exact characterization of the support of the obstacle in term of the limited aperture farfield operator.

2 Direct problem

We restrict ourselves to the case of scalar time harmonic waves and we focus on farfield measurements associated to incident plane waves. For a wave number $k > 0$, the total field solves the Helmholtz equation:

$$\Delta u + k^2 n u = 0 \text{ in } \mathbb{R}^d$$

for $d = 2$ or 3 and n the refractive index, where $\Im(n) \geq 0$. We denote by $\bar{D}$ the support of $n-1$ and assume that D is a bounded domain with Lipschitz boundary and connected complement. We are interested in the case where u is generated by an incident plane wave, $u^i(\theta, x) := e^{ikx\cdot\theta}$ for $x \in \mathbb{R}^d$ and $\theta \in \Gamma_s$, where $\Gamma_s \subset \mathbb{S}^{d-1}$ is the set of angles of the incident plane waves. We also introduce the scattered field u^s defined by:

$$\begin{cases} u^s(\theta, \cdot) := u - u^i(\theta, \cdot) \text{ in } \mathbb{R}^d, \\ \lim\limits_{r\to\infty} \int\limits_{|x|=r} \left| \frac{\partial u^s}{\partial r} - iku^s \right|^2 ds = 0. \end{cases} \quad (1)$$

We introduce the farfield $u^\infty(\theta, \hat{x})$ defined through the following expansion:

$$u^s(\theta, x) = \frac{e^{ik|x|}}{|x|^{(d-1)/2}}(u^\infty(\theta, \hat{x}) + O(1/|x|))$$

for $|x| \to \infty$ and for all $(\theta, \hat{x}) \in \Gamma_s \times \Gamma_m$, where $\Gamma_m \subset \mathbb{S}^{d-1}$ is the set of angles of the measured farfield pattern (.

Leading to the farfield operator:

$$Fg(\hat{x}) := \int_{\Gamma_s} u^\infty(\theta, \hat{x}) g(\theta) ds(\theta).$$

It is well known [3] that the farfield operator admits the factorization $F = H_m^* T H_s$. The compact operator $H_s : L^2(\Gamma_s) \to L^2(D)$ is defined by :

$$H_s g := \int_{\Gamma_s} e^{ikx\cdot\theta} g(\theta) ds(\theta), \ g \in L^2(\Gamma_s), \ x \in D, \quad (2)$$

and is dense in $\{v \in L^2(D) \ s.t. \ \Delta v + k^2 v = 0 \text{ in } D\}$. We can define H_m the same way and its adjoint: $H^* : L^2(D) \to L^2(\Gamma_m)$ is defined by :

$$H_m^* \varphi(\hat{x}) := \int_D e^{-iky.\hat{x}} \varphi(y) dy, \ \varphi \in L^2(D), \ \hat{x} \in \Gamma_m.$$

Finally we define T: $L^2(D) \to L^2(D)$ by:

$$Tu^i := -k^2(1-n)u, \quad (3)$$

The operator T satisfies (under hypothesis 1) :

$$|(Th,\, h)| \geq \mu \left\|h\right\|^2 \quad \forall\, h \in \mathcal{R}(H), \qquad (4)$$

where $\mu > 0$ is a constant independent of h.

Hypothesis 1 *The index of refraction n and the domain D satisfy $n \in L^\infty(\mathbb{R}^d)$, $\mathrm{supp}(n-1) = \overline{D}$, $\Im(n) \geq 0$ and there exist a constant $n_* > 0$ such that $\Re(n(x)-1) \geq n_*$ for a.e. $x \in D$.*

3 The GLSM

In this subsection we suppose that $\Gamma_i = \Gamma_m = \Gamma$ which is the case in full aperture or transmission measurement. This implies that F has a symmetric factorization $F = H^*TH^*$. We introduce the farfield pattern of the Green function:

$$\phi_z(\hat{x}) := e^{-ik\hat{x}\cdot z}$$

and the key ingredient of the GLSM:

Theorem 1 *Assume that k is not an interior transmission eigenvalue [2]. Then $G = H^*T$ is compact, injective with dense range and $\phi_z \in \mathcal{R}(G)$ if and only if $z \in D$.*

We outline the main results of the GLSM in the case of noisy data (see [1]). The noisy operator, F^δ is such that $\left\|F^\delta - F\right\| \leq c\delta$ where c is a real constant.Let $g_z^{\alpha,\delta} \in L^2(\mathbb{S}^{d-1})$ be the minimizer of

$$J_\alpha^\delta(\phi_z; g) := \alpha(|\left(F^\delta g,\, g\right)| + \delta \left\|g\right\|^2) + \left\|F^\delta g - \phi_z\right\|^2, \qquad (5)$$

for $\alpha > 0$, $\delta > 0$ and $\phi_z \in L^2(\Gamma)$. The functional

$$\mathcal{A}^{\alpha,\delta}(g) := |\left(F^\delta g,\, g\right)| + \delta \left\|g\right\|^2 \qquad (6)$$

gives a characterization of D through the following result.

Theorem 2 *Under the aforementioned hypothesis on k and n we have:*

- *$z \in D$ implies $\limsup_{\alpha\to 0} \limsup_{\delta\to 0} \mathcal{A}^{\alpha,\delta}(g_z^{\alpha,\delta}) < \infty$,*
- *$z \notin D$ implies $\liminf_{\alpha\to 0} \liminf_{\delta\to 0} \mathcal{A}^{\alpha,\delta}(g_z^{\alpha,\delta}) = \infty$.*

4 The limited aperture case

We now suppose that $\Gamma_s \neq \Gamma_m$ and we suppose that D is included in a larger domain E. From the definition of H_s (and H_m) it is obvious that they can be extended to operator from $L^2(\Gamma_s)$ to $L^2(E)$.

Let $g_{s,z}^{\alpha,\delta} \in L^2(\Gamma_s)$ and $g_{m,z}^{\alpha,\delta} \in L^2(\Gamma_s)$ be the couple that minimizes the modified cost functional (5) :

$$J_\alpha^\delta(\phi_z; g_s, g_m) := \alpha(|\left(F^\delta g_s,\, g_m\right)| + \delta(\left\|g_s\right\|^2 + \left\|g_m\right\|^2)) + \left\|H_s g_s - H_m g_m\right\|_{L^2(E)}^2 + \left\|F^\delta g_s - \phi_z\right\|^2, \qquad (7)$$

for $\alpha > 0$, $\delta > 0$ and $\phi_z \in L^2(\Gamma_m)$. The functional

$$\mathcal{A}^{\alpha,\delta}(g_s, g_m) := |\left(F^\delta g_s,\, g_m\right)| + \delta(\left\|g_s\right\|^2 + \left\|g_m\right\|^2) \qquad (8)$$

gives a characterization of D through the following result.

Theorem 3 *Under the aforementioned hypothesis on k and n we have:*

- *$z \in D$ implies $\limsup_{\alpha\to 0} \limsup_{\delta\to 0} \mathcal{A}^{\alpha,\delta}(g_{s,z}^{\alpha,\delta}, g_{m,z}^{\alpha,\delta}) < \infty$,*
- *$z \notin D$ implies $\liminf_{\alpha\to 0} \liminf_{\delta\to 0} \mathcal{A}^{\alpha,\delta}(g_{s,z}^{\alpha,\delta}, g_{m,z}^{\alpha,\delta}) = \infty$.*

References

[1] L. Audibert and H. Haddar, A generalized formulation of the linear sampling method with exact characterization of targets in terms of farfield measurements, *Inverse Problems* **30** (2014), 035011.

[2] F. Cakoni and D. Colton, *A Qualitative Approach to Inverse Scattering Theory*, Springer-Verlag, Berlin, 2006.

[3] A. Kirsch and N. Grinberg, *The factorization method for inverse problems*, Oxford University Press, Oxford, 2008.

Computing Interior Eigenvalues of Domains from Far Fields

Zixian Jiang[1,*], **Armin Lechleiter**[2]
[1]DÉFI Team, INRIA Saclay, Palaiseau, France
[2]Center for Industrial Mathematics, University of Bremen, Bremen, Germany
*Email: zixian.jiang@inria.fr

Abstract

Interior eigenvalues of bounded scattering objects can be rigorously characterized from multistatic and multi-frequency far field data. This characterization, the so-called inside-outside duality, holds for various types of penetrable and impenetrable scatterers and is based on the behavior of a particular eigenvalue of the far field operator. It naturally leads to a numerical algorithm for computing interior eigenvalues of a scatterer that does not require shape or physical properties of the scatterer as input. Since the non-linear inverse problem to compute such interior eigenvalues from far field data is ill-posed, we propose a regularizing algorithm that is shown to converge as the noise level of the far field data tends to zero. We illustrate feasibility and accuracy of our algorithm by numerical experiments where we compute Robin eigenvalues of the Laplacian in three-dimensional domains from scattering data of these domains due to plane incident waves.

Keywords: time-harmonic scattering, interior eigenvalue, inside-outside duality, regularization.

1 Introduction

We consider the time-harmonic scattering at wave number $k > 0$ from a impenetrable scatterer $D \subset \mathbb{R}^3$ (bounded Lipschitz domain with connected complement). The total field u is governed by

$$\Delta u + k^2 u = 0 \qquad \text{in } \mathbb{R}^3 \setminus \overline{D}, \tag{1}$$
$$\partial_\nu u|_{\partial D} + \tau\, u|_{\partial D} = 0 \qquad \text{on } \partial D, \tag{2}$$

where $\tau \in L^\infty(\partial D, \mathbb{R})$ is real-valued. It is well-known [1,2] that for an incident plane wave $u^i : x \mapsto \exp(\mathrm{i}k\,\theta \cdot x)$ of direction $\theta \in \mathbb{S}^2$ there exists a unique total field $u \in H^1_{\mathrm{loc}}(\mathbb{R}^3)$ solving (1)–(2) such that the scattered field $u^s = u - u^i$ satisfies the Sommerfeld radiation condition,

$$\left(\frac{\partial u^s}{\partial |x|} - \mathrm{i}k u^s\right) = \mathcal{O}\left(\frac{1}{|x|^2}\right) \text{ as } |x| \to \infty. \tag{3}$$

Hence, u^s behaves like an outgoing spherical wave as $|x| \to \infty$,

$$u^s(x,\theta) = \frac{\exp(\mathrm{i}k|x|)}{4\pi|x|}\left(u^\infty(\hat{x},\theta) + \mathcal{O}\left(\frac{1}{|x|}\right)\right),$$

with a far field pattern $u^\infty(\cdot,\theta) \in L^2(\mathbb{S}^2)$. The far field operator F on $L^2(\mathbb{S}^2)$ is defined by

$$Fg(\hat{x}) := \int_{\mathbb{S}^2} u^\infty(\hat{x},\theta) g(\theta)\, \mathrm{d}S(\theta). \quad \hat{x} \in \mathbb{S}^2, \tag{4}$$

For problem (1)–(3) F is compact and normal. There exists a complete orthonormal eigensystem $(\lambda_j, g_j)_{j\in\mathbb{N}}$ with $\lambda_j \to 0$ as $j \to \infty$ such that

$$Fg = \sum_{j\in\mathbb{N}} \lambda_j (g, g_j) g_j \qquad \text{for all } g \in L^2(\mathbb{S}^2).$$

The eigenvalues can be ordered according to their magnitude, i.e. $|\lambda_1| \geq |\lambda_2| \geq \ldots$. It is well-known [2] that each eigenvalue λ_j lies on a circle of radius $8\pi^2/k$ centered at $8\pi^2\mathrm{i}/k$ in the complex plane. In polar coordinates it writes

$$\lambda_j = r_j \exp(\mathrm{i}\vartheta_j) \quad \text{with } r_j \geq 0,\ \vartheta_j \in [0,\pi). \tag{5}$$

We set $\nu_j = 0$ if $\lambda_j = 0$. Since $\mathrm{Re}\,(\lambda_j) > 0$ for all $j > N$ large enough [4], the phases $\vartheta_j \to 0$ as $j \to \infty$. Hence the largest phase $\vartheta^* = \max_{j\in\mathbb{N}} \vartheta_j$ of the eigenvalues is well defined and attained by some eigenvalue $\lambda^* \neq 0$.

Theorem 1 (Th. 13 in [4]) *$k_0^2 > 0$ is a Robin eigenvalue of $-\Delta$ in D, i.e. $-\Delta v = k_0^2 v$ in D and $\partial_\nu v + \tau v = 0$ on ∂D hold for some non-trivial $v \in H^1(D)$, if and only if*

$$\lim_{k \searrow k_0} \vartheta^*(k) = \pi.$$

To construct a numerical algorithm computing interior Robin eigenvalues of D based on Theorem 1 we first compute the eigenvalues of a finite-dimensional approximation $F_N(k)$ to the far field operator $F(k)$ gained from discrete far field data $u^\infty(\theta_j, \theta_\ell)$ at finitely many directions

$\theta_{j,\ell} \subset \mathbb{S}^2$, and repeat this for sufficiently many wave numbers k in a given interval of interest (or a sufficiently dense grid K of wave numbers in that interval). Secondly, check at which wave numbers the largest phase of these eigenvalues jumps to π; these numbers approximate square roots of interior Robin eigenvalues.

Since the essential spectrum of F is the origin, F_N may have many eigenvalues inside a small ball around zero whose radius equals the approximation error $\varepsilon = \|F_N - F\|$. These eigenvalues in general possess arbitrary phases in $[0, 2\pi)$. Thus, a crucial regularization step consists in neglecting eigenvalues of F_N that are smaller in magnitude than, roughly speaking, the approximation error. The maximal phase of the remaining eigenvalues of $F_N(k)$ is called the largest regularized discrete phase and denoted by $\vartheta^{\divideontimes}(k, N)$.

2 Main results

Assume that the approximation error $\varepsilon \to 0$ as $N \to \infty$ and that the sequence of wave numbers $k_i \in K$ tends from above to k as $i \to \infty$. Then k^2 is an interior Robin eigenvalue if and only if the largest regularized discrete phase $\vartheta^{\divideontimes}(k_i, N_i) \to \pi$ as $i \to \infty$ at least for some subsequence $\{N_i\}_{i\in\mathbb{N}} \subset \mathbb{N}$.

As the error between the largest regularized discrete phase $\vartheta^{\divideontimes}(k, N)$ of F_N and the exact largest phase $\vartheta^*(k)$ of F tends to zero as $N \to \infty$, numerically checking for jumps of $\vartheta^{\divideontimes}$ thus yields approximations to the square roots of interior Robin eigenvalues of D. The accuracy of these approximations of course depends on the step size of the grid K and the approximation error of $F_N(k)$ for $k \in K$.

3 Numerical examples

We choose D to be the unit cube $(0, 1)^3$, such that the exact interior Robin eigenvalues can be analytically computed. $\tau = 1$ in the Robin boundary condition. The approximation F_N to F is gained from discrete far field data of $N = 120$ equally distributed directions for incident waves and observations $(\theta_j, \theta_l)_{j,l=1}^N$ on the sphere $\mathbb{S}$. Reconstruction results of interior Robin eigenvalues are shown in Figure 1.

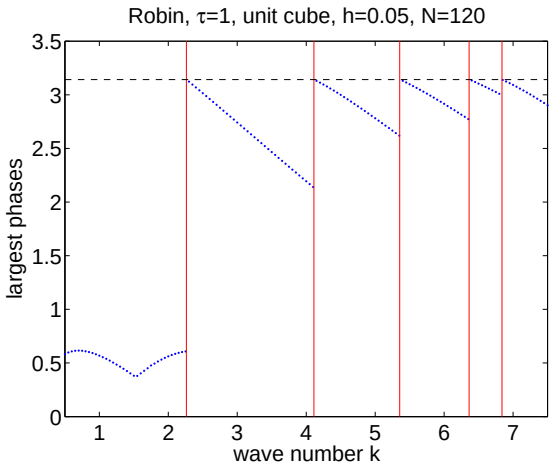

(a) no art. noise

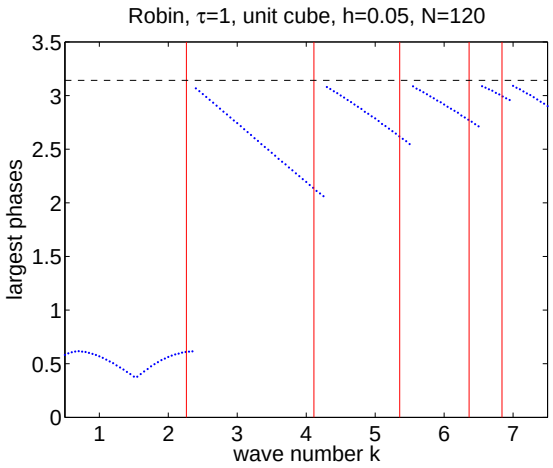

(b) 5% art. noise

Figure 1: The largest regularized discrete phases for the artificial noise levels 0% (up) and 5% (down). Red vertical lines mark the location of the square roots of the exact Robin eigenvalues.

References

[1] D. L. Colton and R. Kress. *Inverse acoustic and electromagnetic scattering theory.* Springer, 2013.

[2] A. Kirsch and N. I. Grinberg. *The Factorization Method for Inverse Problems.* Oxford University Press, Oxford, 2008.

[3] A. Kirsch and A. Lechleiter. The inside-outside duality for scattering problems by inhomogeneous media. *Inverse Probl.*, 29:104011, 2013.

[4] A. Lechleiter and S. Peters. Analytical characterization and numerical approximation of interior eigenvalues for impenetrable scatterers from far fields. *Inverse Probl.*, 30:045006, 2014.

Hydrodynamic model for surface plasmon polaritons in metallic nanostructures

Giuseppe Toscano[1,*], **Jakob Straubel**[2], **Carsten Rockstuhl**[1]

[1]Institute of Theoretical Solid State Physics, Karlsruhe Institute of Technology (KIT), D-76131 Karlsruhe, Germany

[2]Institute of Theoretical Solid State Physics and Institute of Nanotechnology, Karlsruhe Institute of Technology (KIT), D-76131 Karlsruhe, Germany

[*]Email: giuseppe.toscano@kit.edu

Abstract

We study the optical response of metal nanoparticles by using the hydrodynamic model of the electron gas, that can be derived from its classical Hamiltonian. By applying a perturbation expansion, we calculate the linear response of the electron fluid to an exciting electromagnetic field of low intensity. The resulting system of linear equations is coupled to Maxwell's wave equation, and implemented in a finite element method numerical scheme. Computational details as well as properties of the algorithm are discussed and selected results are presented.

Keywords: plasmonics, hydrodynamic equations, electrodynamics

1 Introduction

The optical response of metallic nanoparticles to an electromagnetic fields is usually described in classical electrodynamics by means of a model known as Drude model. However, this model fails to properly predict the effects that are encountered for metallic nanoparticles of critical dimensions comparable to the characteristic dimension of the electron gas in a metal. The latter length scale is known as the *Fermi wavelength* λ_F. The usual value of λ_F is about 0.1 nm for noble metals such as Au and Ag, that are employed in the plasmonic applications. This limitation can be mitigated by introducing more refined models to describe the electron gas, that take into account its wave nature. We propose here to use the Hydrodynamic Model (HDM) [1], that describes the electron gas as a fluid exposed to electromagnetic radiation. The HDM is a semiclassical model that reproduces the quantum effects of the electron-electron interactions with a low computational complexity and high accuracy. A simplified version of this model, that does not describe surface effects such as the electron spill-out in free space, has been extensively used in the recent years [2], and has proven to give accurate results for isolated or coupled systems of nanoparticles made of noble metals where the spill-out effects can be neglected. Here, we will consider the general formulation of the model, that can be used to fully describe the spill-out and electron tunneling effects.

2 Methodology

The Bloch Hamiltonian for the electron gas can be written as:

$$H[n(\mathbf{r},t),\mathbf{p}(\mathbf{r},t)] = \tag{1}$$
$$G[n(\mathbf{r},t)] + \int \frac{(\mathbf{p}(\mathbf{r},t) - e\mathbf{A}(\mathbf{r},t))^2}{2m} n(\mathbf{r},t) d\mathbf{r}$$
$$+e\int \phi(\mathbf{r},t) n(\mathbf{r},t) d\mathbf{r} + e\int V_{\text{back}}(\mathbf{r}) n(\mathbf{r},t) d\mathbf{r},$$

where $n(\mathbf{r},t)$ is the electron density and $\mathbf{p}(\mathbf{r},t) = m\mathbf{v}(\mathbf{r},t) + e\mathbf{A}(\mathbf{r},t)$ its conjugate momentum, with e being the electron charge and m the electron mass. The electrons are coupled to the electromagnetic field expressed by the retarded potentials $\phi(\mathbf{r},t)$ and $\mathbf{A}(\mathbf{r},t)$. The electrostatic potential $V_{\text{back}}(\mathbf{r})$ is a confining background potential, that is generated by the positive ions in a metal, i.e. $\nabla^2 V_{\text{back}}(\mathbf{r}) = -\rho^+(\mathbf{r})/\varepsilon_0$, where $\rho^+(\mathbf{r})$ is the positive charge density of the metal ions. The term $G[n(\mathbf{r},t)]$ is the internal energy of the electron gas, which is given by the sum of a kinetic energy and exchange-correlation functional:

$$G[n(\mathbf{r},t)] = T[n(\mathbf{r},t)] + F_{\text{xc}}[n(\mathbf{r},t)].$$

The kinetic-energy functional is given by the sum of the Thomas–Fermi functional and the von Weizsäcker functional,

$$T_{\text{TFW}}[n] = T_{\text{TF}}[n] + T_{\text{W}}[n] =$$
$$\frac{3}{10}\frac{\hbar^2}{m}(3\pi^2)^{2/3}\int n^{5/3}(\mathbf{r},t)\, d\mathbf{r} +$$
$$+\frac{1}{72}\frac{\hbar^2}{m}\int \frac{|\nabla n(\mathbf{r},t)|^2}{n(\mathbf{r},t)}\, d\mathbf{r}. \tag{2}$$

The equations of motion can be obtained from Eq. 1 by means of the methods of the Hamiltonian formulation of fluid dynamics [3].

The force balance on a fluid element is stated by the Euler equation

$$mn\Big(\frac{\partial \mathbf{v}}{\partial t} + \mathbf{v}\cdot\nabla\mathbf{v}\Big) = -n\nabla\frac{\delta G}{\delta n} + ne(\mathbf{E} + \mathbf{v}\times\mathbf{B}), \tag{3}$$

where the density n satisfies the charge continuity equation

$$\frac{\partial n}{\partial t} = -\nabla\cdot(n\mathbf{v}). \tag{4}$$

Equations 3 and 4 can be linearized for small perturbations of the electron density $n_1(\mathbf{r},t)$ respect to the equilibrium density $n_0(\mathbf{r})$. It can be shown [4] that $n_0(\mathbf{r})$ satisfies

$$\Big(\frac{\delta G}{\delta n}\Big)_0 + e(\phi_0 + V_{\text{back}}) = \mu, \tag{5}$$

where ϕ_0 is the potential generated by the equilibrium charge density $\rho_0 = en_0$. Thus ϕ_0 and ρ_0 are related by Poisson's equation $\nabla^2\phi_0(\mathbf{r}) = -\rho_0(\mathbf{r})/\varepsilon_0$. The quantity $\big(\frac{\delta G}{\delta n}\big)_0$ is the the functional derivative evaluated at the equilibrium density n_0, and μ represents the (constant) chemical potential of the electron gas. The equation 5 has been extensively studied [5–7], and it is known as Thomas-Fermi-Dirac-von Weizsäcker equation.

The linearized versions of both Eq. 3 and Eq. 4 can be written in terms of the electric-charge density perturbation $\rho_1 = en_1$, and the electric current-density vector $\mathbf{J}_1 = \rho_0\mathbf{v}_1$,

$$\frac{\partial \mathbf{J}_1}{\partial t} = -\frac{\rho_0}{m}\nabla\Big(\frac{\delta G}{\delta n}\Big)_1 + \omega_{\text{p}}^2\varepsilon_0\mathbf{E}_1, \tag{6}$$

while the linearized continuity equation becomes

$$\nabla\cdot\mathbf{J}_1 = -\frac{\partial\rho_1}{\partial t}. \tag{7}$$

The quantity $\big(\frac{\delta G}{\delta n}\big)_1$ in Eq. 6 is the first order term of the perturabative expansion of $\big(\frac{\delta G}{\delta n}\big)$, and $\omega_{\text{p}} = [e^2n_0/(m\varepsilon_0)]^{1/2}$ is the plasma frequency of the electron gas. The vector fields $\mathbf{E}_1$ and $\mathbf{J}_1$ satisfy Maxwell's wave equation

$$\nabla\times\nabla\times\mathbf{E}_1 + \frac{1}{c^2}\frac{\partial^2\mathbf{E}_1}{\partial t^2} = -\mu_0\frac{\partial\mathbf{J}_1}{\partial t}. \tag{8}$$

The linear system given by Eqs. 6, 7, and 8 is closed, and can be solved once the density $\rho_0(\mathbf{r})$ has been calculated by means of Eq. 5.

Both the Eq. 5 and the system (6, 7, 8) can be easily rewritten in a weak form, and included in a finite element scheme. In our case, we implemented these equations in COMSOL Multiphysics, and we studied the impact of the surface effects on the plasmonic response of systems of isolated particles, such as Na and Ag cylinders and spheres. We found that the HDM provides accurate results, that can be compared with those obtained with more refined quantum models such as TD-DFT. This allows to study metallic nanoparticles of bigger size, and can be applied to arbitrary nanoplasmonic systems of much larger sizes than accessible with TD-DFT methods.

References

[1] F. Bloch, *Zeitschrift für Physik*, 1933, **81, 363**.

[2] K. R. Hiremath, L. Zschiedrich, F. Schmidt, *J. Comput. Phys.*, 2012, **231, 5890**

[3] P. J. Morrison, J. M. Greene, *Phys. Rev. Lett.*, 1980, **45, 790**.

[4] G. Toscano, J. Straubel, A. Kwiatkowski, C. Rockstuhl, F. Evers, H. Xu, N. A. Mortensen, M. Wubs, *Nat. Commun.*, 2015, **6, 7132**.

[5] P. Gombas, R. Gaspar, *Nature*, 1951, **168, 122**

[6] R. Benguria, H. Brezis, E. H. Lieb *Commun. Math. Phys.*, 1981, **79, 167**.

[7] E. H. Lieb *Commun. Math. Phys.*, 1982, **85, 15**.

Numerical study of dispersion models for nanophotonics.

S. Lanteri[1], C. Scheid[2], N. Schmitt[3], J. Viquerat[1]

[1]INRIA Sophia Antipolis, Nachos project-team 2004 Route des Lucioles, BP 92, 06902 Sophia Antipolis Cedex, France

[2]INRIA Sophia Antipolis, Nachos project-team 2004 Route des Lucioles, BP 92, 06902 Sophia Antipolis Cedex, France, & Univ. Nice Sophia Antipolis, CNRS, LJAD, UMR 7351, 06100 Nice, France.

[3]TU-Darmstadt, Institut für Theorie Elektromagnetischer Felder Schloßgartenstr. 8 64289 Darmstadt, Germany

Abstract

Nanophotonics is a field of physics that allows for observing unusual phenomena, through the illumination of nanometric structures. Their exploitation is at the basis of a lot of striking applications. In this context, computational nanophotonics is essential. The physical characteristics and scales of the media considered are complex and give rise to problems in terms of modelling and numerical efficient simulations. The mathematical modelling relies on the time dependent Maxwell's equations, describing the propagation of waves, coupled to a model of dispersion of the media. In this work, we study different types of dispersion models, propose and analyze a discretization framework (Discontinuous Galerkin) that is adapted to the specific requirements of nanophotonics. Academic and realistic numerical simulations illustrate the results.

Keywords: Maxwell's equations, Dispersion models, Discontinuous Galerkin, Nanophotonics

1 Modelling aspects in Nanophotonics

Nanophotonics finds its power in the ability of controlling and exploiting the interaction of light with nanometer scaled devices. Metals are especially interesting, leading to a special branch of nanophotonics, called nanoplasmonics. At optical frequencies and nanometer scales, matter starts to exhibit peculiar features that allow for numerous applications such as sub-wavelength imaging, perfect lenses, plasmonics resonators and plasmonics waveguides, to cite but just a few.

The modelling of these phenomena rely on characterizing the interaction of electromagnetic waves with media at the nanometer scales. In this precise context, dispersion effects can not be neglected anymore: the electrons present in the metal do not react instantaneously to the applied electric field, leading to the existence of a polarization. In terms of modelling, this is rendered via a coupling between the time-domain Maxwell's equations and an ordinary differential equation describing the evolution of the polarization, as in the so-called Drude model:

$$\begin{cases} \mu \dfrac{\partial \mathbf{H}}{\partial t} + \operatorname{curl} \mathbf{E} = 0, \\ \varepsilon_0 \varepsilon_r \dfrac{\partial \mathbf{E}}{\partial t} - \operatorname{curl} \mathbf{H} = \mathbf{J} - \sigma \mathbf{E}, \\ \dfrac{\partial \mathbf{J}}{\partial t} = -\mathbf{J} + \varepsilon_0 \omega_d^2 \mathbf{E}. \end{cases} \tag{1}$$

where σ, μ, ε_0, ε_r denote respectively the conductivity, the permeability, the vacuum permittivity and the relative permittivity. $\mathbf{J}$ denotes the polarization current due to dispersion and ω_d the plasma frequency. In the frequency domain, this is expressed as a frequency dependent permittivity entering Maxwell's equations. We will detail this model and some other classical models for this kind of dispersion and explain their derivation.

We intend in addition to go further in the modelling. Indeed, by reaching even smaller scales (namely close to the Fermi distance of interaction of the electrons), experimenters start to discover new effects that could not be rendered with the latter type of models. Thus one has to enrich the classical dispersion models. One has to take into account that the reaction of the electrons in the metal depend on the electric field, not only at the precise position of the electron, but also in its neighborhood. This is qualified as a *non local* behavior (in space) expressed via both a frequency and wave-vector dependent permittivity. In the time domain, that is our main concern in this work, this is modelled via a coupling between Maxwell's equation

and a partial differential equation describing the evolution of the polarization (rather than an ordinary differential equation as in (1)). We will present and study one type of *non local* model and discuss some of its properties.

2 Numerical approximation and results

Beyond experiments, there is a need of efficient simulation tools able to deal with all the specific challenges of nanophotonics. There are indeed several types of complexity arising from: the geometry of the domain, its scale and the physical characteristics of the media. That's why, one needs accurate numerical methods able to capture fine phenomena such as high field enhancement with regards to this complexity level.

Finite Differences Time Domain methods, based on Yee's scheme, are the most popular in the nanophotonics community. They have a lot of advantages, but present also several serious limitations in terms of accuracy when dealing with the above mentioned difficulties. Thus Finite Elements type methods based on unstructured meshes begin to have their own place in this context. Among these, we choose to concentrate in this work on Discontinuous Galerkin approaches. These types of methods proved to be robust and flexible enough to treat the type of problems encountered in nanophotonics (see e.g. [1]).

We more precisely propose to study a Time Domain Discontinuous Galerkin scheme of high order, specially designed for dispersion models (from *local* ones to *non local* ones). Stability and convergence properties are studied in the context of *local* dispersion models, and a first insight through the analysis of the *non local* models will be presented. We concentrate on the full tri-dimensional case for *local* dispersion models and the two-dimensional (TE modes) case for *non local* ones. Some standard (see figure 1) and more realistic test cases such as plasmonic waveguides will illustrate the results (see [3] and [2]).

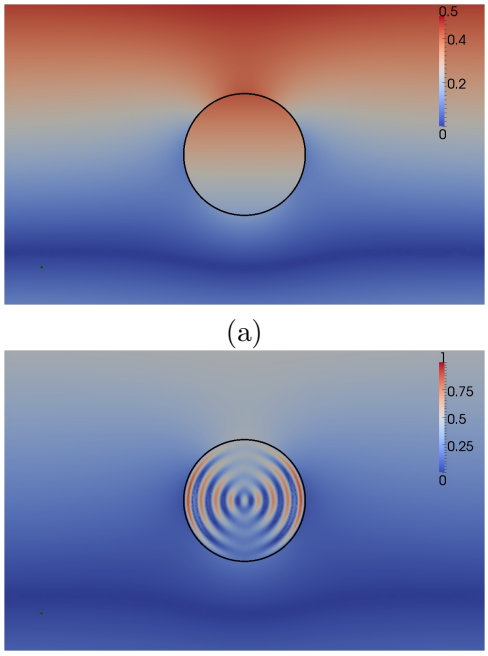

Figure 1: Illumination of a metallic sphere. Comparison between (a) *local* and (b) *non local* models. Visualization in the Fourier space at a given frequency.

References

[1] J. Niegemann K. Busch, M. König. Discontinuous Galerkin methods in nanophotonics. Laser Photonics Rev. 5, No. 6, 773-809, 2011. v, 23, 24

[2] N. Schmitt, C. Scheid, S. Lanteri, J. Viquerat, A. Moreau, A DGTD method for the numerical modelling of the interaction of light with nanometer scale metallic structures taking into account non-local dispersion effects, RR INRIA (2015).

[3] J. Viquerat, M. Klemm, S. Lanteri, C. Scheid, Theoretical and numerical analysis of local dispersion models coupled to a discontinuous Galerkin time-domain method for Maxwell's equations, RR INRIA (2014).

An efficient integral equation solver for two-dimensional simulations in nanoplasmonics

H. Kurkcu[1,*], **F. Reitich**[2], **A. Ortan**[2]

[1]Gulf University for Science and Technology, Mishref, Kuwait

[2]School of Mathematics, University of Minnesota, Minneapolis, Mn 55455, USA

[*]Email: kurkcu@math.umn.edu

Abstract

Nanoplasmonics forms a major part of the field of nanophotonics, which explores how electromagnetic fields can be confined over dimensions on the order of or smaller than the wavelength. Here, we present an integral-equation formulation of the mathematical model that delivers accurate solutions in small computational times for surface plasmons coupled by periodic corrugations of flat surfaces.

Keywords: nanoplasmonics, integral equations

1 Introduction

Nanoplasmonics forms a major part of the field of nanophotonics, which explores how electromagnetic fields can be confined over dimensions on the order of or smaller than the wavelength. Initiated in 1902 by R.W. Wood [1] with the discovery of grating anomalies, this phenomenon has attracted significant attention over the last hundred years [2, 3]. Mie in 1908 gave a mathematical description of light scattering from spherical particles of sizes comparable to the wavelength [2], describing an effect that would come to be known as localized surface plasmons in the context of nanoplasmonics. It is based on interaction processes between electromagnetic radiation and conduction electrons at metallic interfaces or in small metallic nanostructures, leading to an enhanced optical near-field at subwavelength dimension. In 1899, Sommerfeld had described surface waves (waves propagating at the surface of metals) mathematically, and in 1902 Wood observed anomalous drops in the intensity of light reflected by a metallic grating [2]. But theory and observation would not be linked until 1941, by Fano [4]. Further experimental validation came in 1968, when Kretschmann and Raether used prism coupling to excite surface waves with visible light [5]. Other forms of coupling to surface plasmons have been thoroughly investigated since then. All of the phenomena mentioned above are based entirely on classical electromagnetics, and thus can be mathematically described by Maxwell's equations. In this paper, an integral-equations formulation is given for an infinitely periodic metal surface whose period d is on the nanometer scale. The metal is assumed to extend infinitely below this surface, while a dielectric material extends infinitely above the surface. Some details of the numerical implementation and the results of a few numerical experiments are also given in Sec. 2 and 3.

2 Formulation and Algorithm

In this section, a system of integral equations for the total exterior field u ($u = E_z$ in Transverse Electric –TE– and $u = H_z$ in Transverse Magnetic –TM– polarizations) and its normal derivative $\frac{\partial u}{\partial n}$ on the surface ∂D are given. The metal surface ∂D is infinitely thick and periodic and satisfies $f(x + d, y) = f(x, y)$. These fields $[u, \frac{\partial u}{\partial n}]$ satisfy [5];

$$u^i(r) = \int_P G_i(r, r')\frac{\partial u^i(r')}{\partial n(r')} - \frac{\partial G_i}{\partial n(r')}(r, r')u^i(r')ds(r'),$$

$$u^e(r) = \int_P u^e(r')\frac{\partial G_e}{\partial n(r')}(r, r') - G_e(r, r')\frac{\partial u^e(r')}{\partial n(r')}ds(r'),$$

for $x \in D$, and for $x \in D^c$, respectively where n is the unit normal to ∂D directed into the exterior of D and P is a single period of the surface ∂D. Here, $G(r, r')$ is the quasi-periodic Green's function [6] given by

$$G_Q(r, r') = \frac{i}{4}\sum_{n=-\infty}^{\infty} e^{i\alpha n d}H_0^{(1)}(kr_n)$$

where $\alpha = k\sin(\theta)$ and θ is incidence angle.

As $x \to \partial D$ and using the boundary conditions, the surface integral equations become

$$u^{\text{inc}}(r) = \psi(r) + \int_P \frac{\partial(G_i - G_e)}{\partial n(r')}(r, r')\psi(r')dr' - \int_P (\nu G_i - G_e)(r, r')\frac{\partial \psi(r')}{\partial n(r')}dr',$$

$$\frac{\partial u^{\text{inc}}(r)}{\partial n(r)} = \frac{\nu + 1}{2}\frac{\partial \psi(r)}{\partial n(r)} + \int_P \frac{\partial^2(G_i - G_e)}{\partial n(r)\partial n(r')}(r, r')\psi(r')dr' - \int_P \frac{\partial(\nu G_i - G_e)}{\partial n(r)}(r, r')\frac{\partial \psi(r')}{\partial n(r')}dr',$$

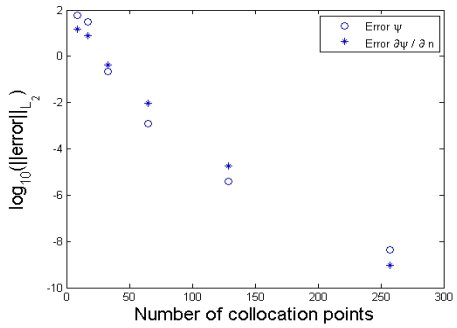

Figure 1: The error in the total field and its normal derivative as a function of the number of collocation points for the sinusoidal grating. The error is shown on a logarithmic scale for where a plasmon is generated.

for $r \in \partial D$ with the unknowns $\psi(r) = u_e(r) + u^{\text{inc}}(r)$ and $\partial\psi(r)/\partial n(r)$. Here $u^{\text{inc}}(r)$ denotes the incoming incident wave and $\nu = 1$ for TE polarization and $\nu = k_i/k_e$ for TM polarization.

Our numerical algorithm depends on seeking the unknowns on the surface of the grating, and the matrix elements are evaluated through the derivation of a careful decomposition that allows for explicit evaluation of the singular and non-singular parts of the kernels [7].

3 Numerical Results

In this section, we provide numerical experiments for the algorithm described above implemented in MATLAB. The test cases in the simulations that follow correspond to ("two-dimensional") infinitely periodic metal gratings that invariant in the z direction. To investigate the existence of plasmonic resonances, we concentrate on the analysis at length scales where these do appear, namely

$$h << \lambda \sim d$$

where d is the period, h is the height of the rough surface and λ is the wavelength. The grating profile consists of a (Fejér-smoothed) approximation to a semi-elliptical profile represented with 51 Fourier modes (See Fig. 4). The "linewidth" (size of the major axis of the ellipse) is 400 nm, and the period is $d = 630$nm. Here we present results of the integral solver for heights $h = 20$nm and $h = 30$nm, and display a specific verification against the high-order perturbation method introduced in [8] (See Fig. 5).

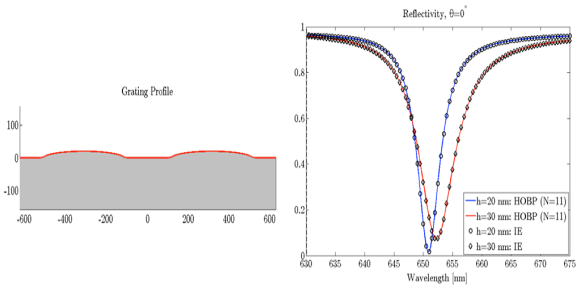

Figure 2: A semi-elliptical grating. Comparison of IE solver and HOPM of [10] for the profile in Fig. 4. Results for incident angles $\theta = 0^o$, and heights of $h = 20$nm and $h = 30$nm.

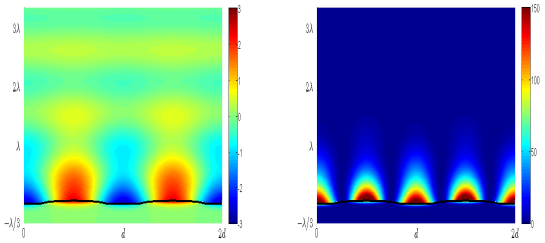

Figure 3: The real part (left) and intensity (right) of the field above and below the surface of the semi-elliptical grating for $h = 30$nm, $\lambda = 652$nm and for an angle of incidence of $\theta = 0^o$.

References

[1] R. W. Wood, *On a remarkable case of uneven distribution of light in a diffraction grating spectrum*, Philos. Mag. 4, 396-402 (1902).

[2] G. Mie, *Contributions to the optics of turbid media, particularly of colloidal metal solutions,* 25, no. 3, Annal. der Physik, pp. 377–445, 1908.

[3] M. I. Stockman, *Nanoplasmonics: The physics behind the applications,* Physics Today, vol. 64.

[4] Fano U., *The theory of anomalous diffraction gratings and of quasi-stationary waves on metallic surfaces (Sommerfeld's waves)*, J. Opt. Soc. Amer. 31, 213-222 1941.

[5] Colton D. and Rainer K., *Inverse Acoustic and Electromagnetic Scattering Theory*, Springer-Verlag, 1992.

[6] Kurkcu H. and Reitich F., *Stable and efficient evaluation of periodized Green's functions for the Helmholtz equation at high frequencies*, in Journal of Comp. Physics, 228, 2009 pp. 75-95.

[7] Kurkcu H., *An efficient algorithm for the solution of high-frequency scattering by infinite rough surfaces*, PhD Thesis 2008.

[8] Reitich F., Johnson T., Oh S., and Meyer G., *A fast and high-order accurate boundary perturbation method for nanoplasmonic simulations: basic concepts, analytic continuation and applications*, in J. Opt. Soc. Amer. A, Vol. 30, Issue 11, 2013 pp. 2175-2187.

Uniqueness and stability results on the gravity water waves with vorticity

Evgeniy Lokharu[1,*], **Vladimir Kozlov**[2], **Nikolay Kuznetsov**[2]
[1]Department of Mathematics, Linköping University, Sweden
[2]Russian Academy of Sciences, Russian Federation.
[*]Email: evgeniy.lokharu@liu.se

Abstract

We consider the two-dimensional nonlinear problem describing steady gravity water waves with vorticity in a channel of a finite depth. The water motion is assumed to be unidirectional and the surface tension is neglected. For small-amplitude waves we prove a stability estimate that imply uniqueness with a prescribed Cauchy data of the profile at some point and provide a parametrization by the height for waves of small amplitude. This allows to verify the so-called Benjamin and Lighthill conjecture for steady water waves for waves with near-critical values of the Bernoulli's constant.

Keywords: nonlinear water waves.

Let an open channel of uniform rectangular cross-section be bounded below by a horizontal rigid bottom and let water occupying the channel be bounded above by a free surface not touching the bottom. In appropriate Cartesian coordinates (x, y), the bottom coincides with the x-axis and gravity acts in the negative y-direction. We use the non-dimensional variables proposed by Keady and Norbury; namely, lengths and velocities are scaled to $(Q^2/g)^{1/3}$ and $(Qg)^{1/3}$ respectively. Here Q and g are the dimensional quantities for the rate of flow and the gravity acceleration respectively, whereas $(Q^2/g)^{1/3}$ is the depth of the critical uniform stream in the irrotational case.

The steady water motion is supposed to be two-dimensional and rotational; the surface tension is neglected on the free surface of the water, where the pressure is constant. These assumptions and the fact that water is incompressible allow us to seek the velocity field in the form $(\psi_y, -\psi_x)$, where $\psi(x, y)$ is referred to as the *stream function*. The vorticity distribution ω is supposed to be a prescribed continuous function depending on ψ.

We choose the frame of reference so that the velocity field is time-independent as well as the unknown free-surface profile. The latter is assumed to be the graph of $y = \eta(x)$, $x \in \mathbb{R}$, where η is a positive continuous function, and so the longitudinal section of the water domain is $D = \{x \in \mathbb{R},\ 0 < y < \eta(x)\}$. The following non-dimensional free-boundary problem for ψ and η which describes all kinds of waves has long been known:

$$\begin{cases} \psi_{xx} + \psi_{yy} + \omega(\psi) = 0, \quad (x, y) \in D; \\ \psi(x, 0) = 0, \quad x \in \mathbb{R}; \\ \psi(x, \eta(x)) = 1, \quad x \in \mathbb{R}; \\ |\nabla\psi(x, \eta(x))|^2 + 2\eta(x) = 3r, \quad x \in \mathbb{R}. \end{cases}$$

In the last condition (Bernoulli's equation), r is a constant considered as the problem's parameter and referred to as Bernoulli's constant/the total head. In what follows, we suppose that ψ is a strictly monotonic function of y, say

$$\psi_y(x, y) > 0 \quad \text{for all } (x, y) \in \bar{D},$$

which means that the flows we are going to study are unidirectional.

In 1954, Benjamin and Lighthill made a conjecture concerning irrotational steady gravity waves on water of finite depth. According to this conjecture, all steady water waves with zero vorticity may be parametrized by points in some cusped region on the (r, s)-plane (r and s are the non-dimensional Bernoulli's constant and the flow force, respectively) and any point of the region corresponds to some steady wave motion. The flow force s is defined by

$$s(x) = \left[r + \frac{2}{3}\Omega(1)\right]\eta(x) - \frac{1}{3}\left[\eta(x)^2 + \int_0^t \left((\Psi_x)^2 - (\Psi_y)^2 + 2\Omega(\Psi)\right) dy\right]$$

and is independent of $x \in \mathbb{R}$. We prove this conjecture for steady waves in the presence of vorticity when the Bernoulli's constant is around its critical value. Our proof is based on the following stability estimate

$$\int_{\mathbb{R}} |\eta^{(1)}(x) - \eta^{(2)}(x)|^2 e^{-\nu|x-x_0|} dx \leq$$

$$C\left[|\eta^{(1)}(x_0)-\eta^{(2)}(x_0)|^2+|\eta_x^{(1)}(x_0)-\eta_x^{(2)}(x_0)|^2\right]$$

which is valid for any two small-amplitude solutions of the problem with constants C and η independent of x. A similar stability estimate is valid for solitary type waves that allows to prove that in the absence of surface tension no solitary waves of depression exist (even with vorticity).

Entropy Stable Approximations for Shallow Water Models

Andrew R. Winters[1,*], **Gregor J. Gassner**[1]
[1]Mathematical Institute, University of Cologne, Cologne, Germany
[*]Email: awinters@math.uni-koeln.de

Abstract

We outline a provably entropy stable approximation for the shallow water magnetohydrodynamic (SWMHD) equations. In the absence of magnetic fields the SWMHD model becomes the classical shallow water equations. The method incorporates two source terms, one to account for non-constant bottom topographies and another to guarantee that the scheme is entropy stable. A specific discretization of the bottom topography contribution guarantees the method is well-balanced, an attribute property that an approximation preserves a steady-state solution of constant water height.

Keywords: entropy stability, shallow water magnetohydrodynamics, discontinuous Galerkin

1 Introduction

The SWMHD equations comprise a nonlinear hyperbolic system and may be written in a conservative form with an additional divergence-free constraint on the magnetic field quantities. For the SWMHD system the issue of entropy conservation and satisfaction of the divergence-free condition are inextricably linked. To derive an entropy conservative numerical flux function we weaken the divergence-free condition and incorporate a source term [4,5] (analogous to the Janhunen source term for the ideal MHD equations) and find the augmented one dimensional model

$$\frac{\partial}{\partial t}\begin{bmatrix} h \\ hv_1 \\ hv_2 \\ hB_1 \\ hB_2 \end{bmatrix} + \frac{\partial}{\partial x}\begin{bmatrix} hv_1 \\ hv_1^2 + \frac{g}{2}h^2 - hB_1^2 \\ hv_1v_2 - hB_1B_2 \\ 0 \\ hv_1B_2 - hv_2B_1 \end{bmatrix} = -\frac{\partial b}{\partial x}\begin{bmatrix} 0 \\ gh \\ 0 \\ 0 \\ 0 \end{bmatrix} - \frac{\partial (hB_1)}{\partial x}\begin{bmatrix} 0 \\ 0 \\ 0 \\ v_1 \\ v_2 \end{bmatrix},$$

where g is the gravitational constant, we denote the vector of conserved variables by $\mathbf{u} = (h, hv_1, hv_2, hB_1, hB_2)^T$, and the bottom topography $b(x)$.

In Sec. 2 we present the main results of the discrete entropy analysis and skew-symmetric high-order discontinuous Galerkin (DG) approximation described by the authors in [4,5]. Then in Sec. 3 we give brief remarks regarding our entropy stable approximation.

2 Entropy Stable DG Approximation for SWMHD

We summarize a high-order entropy stable DG approximation for the SWMHD equations in Thm. 1. Generally, we denote vectors by lowercase bold and matrices by uppercase bold letters. Complete details and derivations are provided by the authors in [4,5]:

Theorem 1 (ESDGSEM) *An element-wise, entropy stable, discontinuous Galerkin spectral element approximation for the SWMHD equations is given by*

$$\begin{aligned}
\mathcal{J}\partial_t \mathbf{u}_1 + \mathbf{D}\mathbf{f}_1 &= \mathbf{S}\left[\mathbf{f}_1^* - \mathbf{f}_1\right], \\
\mathcal{J}\partial_t \mathbf{u}_2 + \mathbf{D}\mathbf{f}_2 + \mathbf{s}_{hv^2} + \mathbf{s}_{h^2} - \mathbf{s}_{hB_1^2} &= \mathbf{S}\left[\mathbf{f}_2^* - \mathbf{f}_2\right] - g\mathbf{H}\mathbf{D}\mathbf{b} \\
&\quad - \frac{1}{2}\left(\frac{\{\!\{h\}\!\}_L [\![b]\!]_L}{\omega_0}\mathbf{e}_0 + \frac{\{\!\{h\}\!\}_R [\![b]\!]_R}{\omega_N}\mathbf{e}_N\right), \\
\mathcal{J}\partial_t \mathbf{u}_3 + \mathbf{D}\mathbf{f}_3 + \mathbf{s}_{hv_1v_2} - \mathbf{s}_{hB_1B_2} &= \mathbf{S}\left[\mathbf{f}_3^* - \mathbf{f}_3\right], \\
\mathcal{J}\partial_t \mathbf{u}_4 + \mathbf{D}\mathbf{f}_4 + \mathbf{s}_{hv_1B_1} - \mathbf{s}_{hB_1v_1} &= \mathbf{S}\left[\mathbf{f}_4^* - \mathbf{f}_4\right] - \mathbf{V}_1\mathbf{D}\mathbf{H}\mathbf{B}_1 \\
&\quad - \frac{1}{2}\left(\frac{\{\!\{v_1B_1\}\!\}_L}{\{\!\{B_1\}\!\}_L}\frac{[\![hB_1]\!]_L}{\omega_0}\mathbf{e}_0 + \frac{\{\!\{v_1B_1\}\!\}_R}{\{\!\{B_1\}\!\}_R}\frac{[\![hB_1]\!]_R}{\omega_N}\mathbf{e}_N\right), \\
\mathcal{J}\partial_t \mathbf{u}_5 + \mathbf{D}\mathbf{f}_5 + \mathbf{s}_{hv_1B_2} - \mathbf{s}_{hB_1v_2} &= \mathbf{S}\left[\mathbf{f}_5^* - \mathbf{f}_5\right] - \mathbf{V}_2\mathbf{D}\mathbf{H}\mathbf{B}_1 \\
&\quad - \frac{1}{2}\left(\frac{\{\!\{v_2B_2\}\!\}_L}{\{\!\{B_2\}\!\}_L}\frac{[\![hB_1]\!]_L}{\omega_0}\mathbf{e}_0 + \frac{\{\!\{v_2B_2\}\!\}_R}{\{\!\{B_2\}\!\}_R}\frac{[\![hB_1]\!]_R}{\omega_N}\mathbf{e}_N\right),
\end{aligned}$$

where $\mathcal{J} = \frac{\Delta x}{2}$, $\mathbf{D}$ is the standard polynomial derivative matrix, $\mathbf{S} = diag\left(\frac{1}{\omega_0}, 0, \ldots, 0, -\frac{1}{\omega_N}\right)$ is the surface matrix scaled by the Gauss-Lobatto quadrature weights [2], $\{\!\{\cdot\}\!\}$ is the arithmetic mean, and $[\![\cdot]\!]$ is the linear jump. Further there are the discrete flux components

$$\begin{aligned}
\mathbf{f}_1 &= \mathbf{H}\mathbf{v}_1, \\
\mathbf{f}_2 &= \mathbf{H}\mathbf{v}_1^2 + \frac{g}{2}\mathbf{h}^2 - \mathbf{H}\mathbf{B}_1^2, \\
\mathbf{f}_3 &= \mathbf{H}\mathbf{V}_1\mathbf{v}_2 - \mathbf{H}\mathbf{B}_1\mathbf{B}_2, \\
\mathbf{f}_4 &= \mathbf{0}, \\
\mathbf{f}_5 &= \mathbf{H}\mathbf{V}_1\mathbf{B}_2 - \mathbf{H}\mathbf{V}_2\mathbf{B}_1,
\end{aligned}$$

with, for example, $\mathbf{H} = \mathrm{diag}(\mathbf{h})$*, and nonlinear correction terms in the discrete product rule*

$$\begin{aligned}
\mathbf{s}_{hv_1^2} &= \frac{1}{2}\left[-\mathbf{DHv}_1^2 + \mathbf{HV}_1\mathbf{Dv}_1 + \mathbf{V}_1\mathbf{DHv}_1\right], \\
\mathbf{s}_{h^2} &= \frac{g}{2}\left[-\mathbf{Dh}^2 + 2\mathbf{HDh}\right], \\
\mathbf{s}_{hB_1^2} &= \frac{1}{2}\left[-\mathbf{DHB}_1^2 + \mathbf{HB}_1\mathbf{DB}_1 + \mathbf{B}_1\mathbf{DHB}_1\right], \\
\mathbf{s}_{hv_1v_2} &= \frac{1}{2}\left[-\mathbf{DHV}_1\mathbf{v}_2 + \mathbf{HV}_1\mathbf{Dv}_2 + \mathbf{V}_2\mathbf{DHv}_1\right], \\
\mathbf{s}_{hB_1B_2} &= \frac{1}{2}\left[-\mathbf{DHB}_1\mathbf{B}_2 + \mathbf{HB}_1\mathbf{DB}_2 + \mathbf{B}_2\mathbf{DHB}_1\right], \\
\mathbf{s}_{hv_1B_1} &= \frac{1}{2}\left[-\mathbf{DHV}_1\mathbf{B}_1 + \mathbf{HV}_1\mathbf{DB}_1 + \mathbf{B}_1\mathbf{DHv}_1\right], \\
\mathbf{s}_{hB_1v_1} &= \frac{1}{2}\left[-\mathbf{DHB}_1\mathbf{v}_1 + \mathbf{HB}_1\mathbf{Dv}_1 + \mathbf{V}_1\mathbf{DHB}_1\right], \\
\mathbf{s}_{hv_1B_2} &= \frac{1}{2}\left[-\mathbf{DHV}_1\mathbf{B}_2 + \mathbf{HV}_1\mathbf{DB}_2 + \mathbf{B}_2\mathbf{DHv}_1\right], \\
\mathbf{s}_{hB_1v_2} &= \frac{1}{2}\left[-\mathbf{DHB}_1\mathbf{v}_2 + \mathbf{HB}_1\mathbf{Dv}_2 + \mathbf{V}_2\mathbf{DHB}_1\right].
\end{aligned}$$

Finally we compute an entropy stable numerical flux

$$\mathbf{f}^{*,es} = \mathbf{f}^{*,ec} - \frac{1}{2}\mathbf{R}|\mathbf{\Lambda}|\mathbf{T}\mathbf{R}^T[\![\mathbf{q}]\!],$$

where we use the entropy conserving flux derived in [4] as a base

$$\mathbf{f}^{*,ec} = \begin{bmatrix} \{\!\{h\}\!\}\{\!\{v_1\}\!\} \\ \{\!\{h\}\!\}\{\!\{v_1\}\!\}^2 + \frac{g}{2}\{\!\{h^2\}\!\} - \{\!\{hB_1\}\!\}\{\!\{B_1\}\!\} \\ \{\!\{h\}\!\}\{\!\{v_1\}\!\}\{\!\{v_2\}\!\} - \{\!\{hB_1\}\!\}\{\!\{B_2\}\!\} \\ \{\!\{h\}\!\}\{\!\{v_1\}\!\}\{\!\{B_1\}\!\} - \{\!\{hB_1\}\!\}\{\!\{v_1\}\!\} \\ \{\!\{h\}\!\}\{\!\{v_1\}\!\}\{\!\{B_2\}\!\} - \{\!\{hB_1\}\!\}\{\!\{v_2\}\!\} \end{bmatrix},$$

define the vector of entropy variables

$$\mathbf{q} = \left(g(h+b) - \tfrac{1}{2}\left(v_1^2 + v_2^2 + B_1^2 + B_2^2\right), v_1, v_2, B_1, B_2\right)^T,$$

the matrices

$$\mathbf{R} = \begin{bmatrix} 1 & 0 & 1 & 0 & 1 \\ v_1 - c_g & 0 & v_1 & 0 & v_1 + c_g \\ v_2 & 1 & v_2 & 1 & v_2 \\ 0 & 0 & \frac{c_g^2}{B_1} & 0 & 0 \\ B_2 & 1 & B_2 & -1 & B_2 \end{bmatrix},$$

$$\mathbf{T} = diag\left(\frac{c^2}{2gc_g^2}, \frac{c^2}{2g}, \frac{B_1}{gc_g^2}, \frac{c^2}{2g}, \frac{c^2}{2gc_g^2}\right),$$

and the diagonal matrix of eigenvalues

$$\mathbf{\Lambda} = diag(v_1 - c_g, v_1 - B_1, v_1, v_1 + B_1, v_1 + c_g),$$

with wave celerity $c^2 = gh$ *and magnetogravity wave celerity* $c_g^2 = gh + B_1^2$*.*

Remark 2 (Well-Balancedness) *The surface contributions of the bottom topography component are analogous to the discretization developed by Fjordholm et. al. [1]. A complete proof of entropy conservation, high-order accuracy, and well-balancedness for a skew-symmetric DG approximation for the shallow water equations can be found for one and two dimension spatial dimensions in [2, 3] respectively.*

3 Concluding Remarks

We summarized a high-order, entropy stable DG approximation for the SWMHD equations. In the absence of magnetic fields the scheme becomes an entropy stable approximation for the classical shallow water model. We note that the dissipation in $\mathbf{f}^{*,es}$ is the amount necessary for stability, but is not enough to guarantee an overshoot free approximation in the presence of shocks. We present the ESDGSEM as a baseline scheme to which additional artificial viscosity can be added to control overshoots.

References

[1] U. S. Fjordholm, S. Mishra, and E. Tadmor, Well-Balanced and Energy Stable Schemes for the Shallow Water Equations with Discontiuous Topography, Journal of Computational Physics **230** (2011), pp. 5587–5609.

[2] G. J. Gassner, A. R. Winters, and D. A. Kopriva, A Well Balanced and Entropy Conservative Discontinuous Galerkin Spectral Element Method for the Shallow Water Equations, *under revision.*

[3] N. Wintermeyer, A. R. Winters, G. J. Gassner, and D. A. Kopriva, An Entropy Stable Discontinuous Galerkin Method for the Two Dimensional Shallow Water Equations with Discontinuous Bathymetry, *in preparation.*

[4] A. R. Winters and G. J. Gassner, An Entropy Stable Finite Volume Scheme for the Equations of Shallow Water Magnetohydrodynamics, *submitted.*

[5] A. R. Winters and G. J. Gassner, Entropy Stable Discontinuous Galerkin Spectral Element Approximations for the Shallow Water Magnetohydrodynamic Equations, *submitted.*

An asymptotic technique for computing travelling water waves

Konstantinos Kalimeris[1,*]
[1]RICAM, Austrian Academy of Sciences, Linz, Austria
*Email: konstantinos.kalimeris@ricam.oeaw.ac.at

Abstract

In this talk we consider the classical water wave problem described by the Euler equations with a free surface under the influence of gravity over a flat bottom. We restrict our attention to two-dimensional, finite-depth periodic water waves with general vorticity. This is joint work with Adrian Constantin and Otmar Scherzer and is triggered by a penalization method for computing large amplitude water waves.

Keywords: water waves, asymptotics

1 Introduction

Starting from the Euler equations, we formulate a free boundary problem with the presence of a parameter in the boundary conditions, [1]. This parameter is the so-called Bernoulli's constant which represents the total mechanical energy on the free boundary and here is treated as a bifurcation parameter, for details see [3]. Next, we transform this problem to a fixed boundary value problem, however nonlinear. An asymptotic technique is applied to approximate the solutions of this problem that correspond to non-laminar flows, see [2].

We denote by (u, v), η and P the velocity field, the free surface and the pressure of the fluid, respectively. Assuming that the water is inviscid and incompressible the Euler equations [3] that govern the flow take the form

$$\begin{aligned} &u_x + v_y = 0,\\ &-cu_x + uu_x + vu_y = -P_x,\\ &-cv_x + uv_x + vv_y = -P_y - g, \quad \text{in } \mathcal{D}, \end{aligned}$$

with boundary conditions

$$\begin{aligned} &P = P_{atm} \text{ on } S,\\ &v = (u-c)\eta_x \text{ on } S,\\ &v = 0 \text{ on } B, \end{aligned}$$

where
$\mathcal{D} = \{(x, y) : -\pi < x < \pi \text{ and } -d < y < \eta(x)\}$,

which is bounded from above by the free curve
$S = \{(x, y) : -\pi < x < \pi \text{ and } y = \eta(x)\}$,

and from below by the flat bottom
$B = \{(x, y) : -\pi < x < \pi \text{ and } y = -d\}$.

Here d is the depth, g is the gravitational constant and P_{atm} is the atmospheric pressure.

2 The free boundary problem

Define the *relative mass flux* by

$$p_0 := \int_{-d}^{\eta(x)} (u - c)dy < 0.$$

Define the stream function ψ by

$$\begin{aligned} &\psi_x = -v, \qquad \psi_y = u - c \qquad \text{in } \overline{\mathcal{D}},\\ &\psi(x, -d) = -p_0\ . \end{aligned}$$

Define the vorticity function

$$\gamma := u_y - v_x.$$

The constants g (gravitational constant), p_0 (relative mass flux), Q (hydraulic head) and the function $\gamma : [p_0, 0] \mapsto \mathbb{R}$ (vorticity) are given.

Moreover, for given η, which we assume to be normalized to satisfy $\int_{-\pi}^{\pi} \eta(x)dx = 0$, let $\psi = \psi[\eta]$ be the solution of

$$\Delta\psi = \gamma(\psi),$$

with boundary conditions

$$\psi(x, -d) = -p_0, \text{ on } B \quad \text{and} \quad \psi = 0 \text{ on } S,$$

$$\psi(\pi, y) = \psi(-\pi, y) \quad \text{and} \quad \psi_x(\pm\pi, y) = 0,$$

for $y \in [-d, \eta(x)]$.

For given η this *linear* PDE is overdetermined by imposing the non-linear boundary condition, known as the Bernoulli's law

$$\mathcal{B}_B[\psi] := |\nabla\psi|^2 + 2g(\eta(x) + d) = Q, \text{ on } S.$$

The free boundary problem consists in using the over-determinacy to determine η.

Definition 1 *The free boundary value problem can also be viewed as solving an operator equation*

$$\mathcal{G}(\eta) = 0\,,$$

where $\mathcal{G} : \eta \mapsto \mathcal{B}_B[\psi[\eta]]$.

3 Dubreil-Jacotin transformation

Since, ψ is constant both on the bottom and the free surface, we now introduce the Dubreil-Jacotin transformation

$$q = x, \qquad p = -\psi,$$

which transforms the domain $\mathcal{D}$ to the rectangle

$$R = \{(q,p); -\pi < q < \pi \text{ and } p_0 < p < 0\}\ .$$

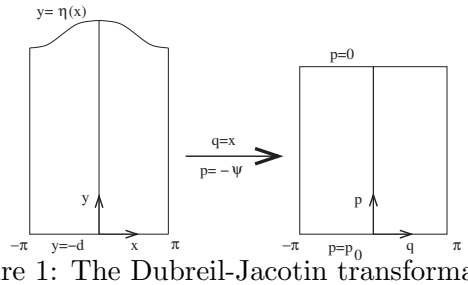

Figure 1: The Dubreil-Jacotin transformation.

Define the height above the flat bottom by

$$h(q,p) = y + d.$$

Then the constitutive equations for the height function, which is even and 2π-periodic in q, are

$$\begin{aligned}\mathcal{H}[h] &:= (1+h_q^2)h_{pp} - 2h_p h_q h_{pq} \\ &\quad + h_p^2 h_{qq} - \gamma(-p)h_p^3 = 0 \quad \text{ on } R,\\ \mathcal{B}_0[h] &:= 1 + h_q^2(q,0) + (2gh - Q)h_p^2(q,0) = 0,\\ \mathcal{B}_1[h] &:= h(q,p_0) = 0.\end{aligned}$$

In the new formulation the free boundary $\eta(x)$ is given by $h(q,0)$.

4 Approximation of non laminar flows

For $\gamma(-p)$ =constant, we consider a parametrized family of functions, see [2], of the form

$$\hat{h}(q,p) = h_0(p) + bh_1(q,p) + b^2 h_2(q,p), \qquad \text{for } b \in \mathbb{R}\,,$$

where h_0 is the laminar flow, i.e the q-independent solution. We analytically determine the explicit formulas for h_1 and h_2 such that

$$\mathcal{H}[\hat{h}](p,q) = \mathcal{O}(b^3)\,,\ \mathcal{B}_0[\hat{h}](q) = \mathcal{O}(b^3)$$

and

$$\mathcal{B}_1[\hat{h}](q) = 0\ .$$

Below, we depict the height function $\hat{h}(q,p)$ along the streamlines (p=constant) for the values of vorticity $\gamma = 1$ and $\gamma = -2$, respectively.

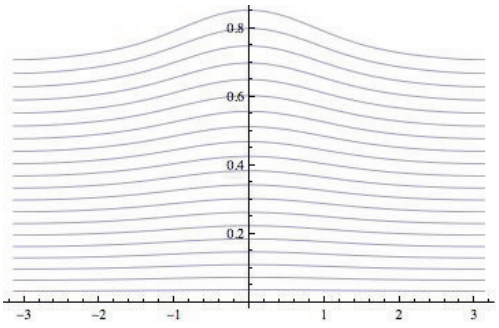

Figure 2: $\gamma = 1$

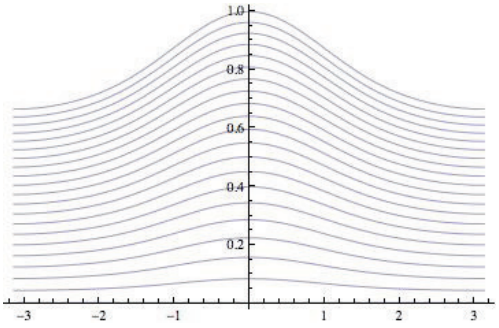

Figure 3: $\gamma = -2$

References

[1] A. Constantin, K. Kalimeris and O. Scherzer, A penalization method for calculating the flow beneath travelling water waves of large amplitude, submitted.

[2] A. Constantin, K. Kalimeris and O. Scherzer, Approximations of steady periodic water waves in flows with constant vorticity, in preparation.

[3] A. Constantin and W. Strauss, Exact steady periodic water waves with vorticity, *Comm. Pure Appl. Math.* **57** (2004), 481-527.

Monday, July 20
Second Afternoon Session
17:15 – 18:15

A discretisation method with the H_{div} scalar product for the electric field integral equation

Kazuki Niino[1,*], **Sho Akagi**[1], **Naoshi Nishimura**[1]

[1]Graduate school of Informatics, Kyoto University

[*]Email: niino@i.kyoto-u.ac.jp

Abstract

A discretisation method with the H_{div} scalar product for the EFIE (Electric Field Integral Equation) is proposed. The EFIE with the conventional Galerkin discretisation show bad accuracy for problems with a small frequency and this problem is known as a low-frequency problem. The discretisation method proposed in this paper utilises the H_{div} scalar product with a scalar coefficient for the Galerkin discretisation and overcomes the low-frequency problem by choosing an appropriate value of the coefficient. The efficiency of this method is verified through some numerical examples.

Keywords: Boundary element method, Maxwell's equations, Galerkin method

1 introduction

Boundary element methods (BEMs) are efficient numerical methods for electromagnetic problems. It is, however, well known that BEMs show bad accuracy for electromagnetic problems in low frequencies. This problem is called "low-frequency problem" and various methods which remedy this problem have been suggested [1,2]. In this paper, we will propose a new method which accurately solves a electric field integral equation (EFIE) in low frequencies by utilizing a H_{div} scalar product for discretisation.

2 formulation

We consider a simple connected scatterer $\Omega^- \in \mathbb{R}^3$ enclosed by a smooth boundary Γ. We denote $\mathbb{R}^3 \backslash \overline{\Omega^-}$ by Ω^+ and the outward normal vector defined on the surface Γ by $\boldsymbol{n}$. We are interested in solving the following boundary value problem:

$$\nabla \times \boldsymbol{E} = \mathrm{i}\omega\mu\boldsymbol{H},\ \nabla \times \boldsymbol{H} = -\mathrm{i}\omega\varepsilon\boldsymbol{E} \quad \text{in } \Omega^+$$
$$\boldsymbol{m} := \boldsymbol{E}^+ \times \boldsymbol{n} = 0 \quad \text{on } \Gamma$$

subjecting to the raditation conditions for the scattering fields ($\boldsymbol{E}^{\mathrm{sca}}$, where $\boldsymbol{E}$ and $\boldsymbol{H}$ are unknown electric and magnetic fields, ω is the frequency, ε and μ are the permittivity and permeability of Ω and the scattering fields are defined by $(\boldsymbol{E}^{\mathrm{sca}}, \boldsymbol{H}^{\mathrm{sca}}) = (\boldsymbol{E} - \boldsymbol{E}^{\mathrm{inc}}, \boldsymbol{H} - \boldsymbol{H}^{\mathrm{inc}})$ with the incident waves denoted by $\boldsymbol{E}^{\mathrm{inc}}$ and $\boldsymbol{H}^{\mathrm{inc}}$ in the exterior domain Ω^+, respectively.

For solving this problem, we will use the EFIE:

$$\mathrm{i}\omega\mu\boldsymbol{n} \times \Phi_{ij} j_j = E_i^{\mathrm{inc}} \times \boldsymbol{n} \tag{1}$$

where

$$\Phi_{kl} = \left(\delta_{kl} + \frac{1}{k^2}\partial_k\partial_l\right) G(x),$$
$$G(x) = \frac{\mathrm{e}^{\mathrm{i}k\|x\|}}{4\pi\|x\|}.$$

Note that we use the summation convention to repeated indices in these formulae.

3 discretisation

The Galerkin method is widely used for discretising equation (1). In general, the Rao-Wilton-Glisson (RWG) basis functions $\boldsymbol{t}_i$ [3] is applied as the testing function with the $L^2(\Gamma)$ scalar product:

$$(\boldsymbol{n} \times \boldsymbol{t}_i,\ \mathrm{i}\omega\mu\boldsymbol{n} \times \boldsymbol{\Phi}\boldsymbol{j})_{L_T^2(\Gamma)}$$
$$= (\boldsymbol{n} \times \boldsymbol{t}_i,\ \boldsymbol{E}^{\mathrm{inc}} \times \boldsymbol{n})_{L_T^2(\Gamma)} \tag{2}$$

This equation is numerically ill-conditioned for small frequency since, in the LHS of equation (2), the term $1/k^2 \int \partial_k\partial_l G \boldsymbol{j}_l$ is dominant and this term vanishes for any functions with $\mathrm{div}_S \boldsymbol{j} = 0$

For solving this problem, we utilise the H_{div} scalar product

$$(\boldsymbol{u}, \boldsymbol{v})_{H_{\mathrm{div}}(\Gamma)} := (\boldsymbol{u}, \boldsymbol{v})_{L_T^2(\Gamma)} + c(\mathrm{div}_S \boldsymbol{u}, \mathrm{div}_S \boldsymbol{v})_{L^2(\Gamma)}$$

for discretising the boundary integral equations in (1) as

$$(\boldsymbol{s}_i,\ \mathrm{i}\omega\mu\boldsymbol{n} \times \boldsymbol{\Phi}\boldsymbol{j})_{H_{\mathrm{div}}(\Gamma)}$$
$$= (\boldsymbol{s}_i,\ \boldsymbol{E}^{\mathrm{inc}} \times \boldsymbol{n})_{H_{\mathrm{div}}(\Gamma)} \tag{3}$$

where c is a positive constant and $\boldsymbol{s}_i$ is a testing function. For the functions $\boldsymbol{s}_i$, the Buffa-Christiansen (BC) basis function [4] is used if

we expand the unknown function $\boldsymbol{j}$ with the RWG basis function since the testing function does not include the term $\boldsymbol{n}\times$, which is different from equation (2). Equation (3) can be calculated as follows:

$$
\begin{aligned}
&(\boldsymbol{s}_i,\, \mathrm{i}\omega\mu\boldsymbol{n}\times\boldsymbol{\Phi}\boldsymbol{j})_{L^2_T(\Gamma)} - c(\mathrm{div}_S\boldsymbol{s}_i,\, \boldsymbol{n}\cdot\mathrm{i}\omega\mu\boldsymbol{\Psi}\boldsymbol{j})_{L^2(\Gamma)} \\
&= (\boldsymbol{s}_i,\, \boldsymbol{E}^{\mathrm{inc}}\times\boldsymbol{n})_{L^2_T(\Gamma)} \\
&- \mathrm{i}\omega\mu^{+}c(\mathrm{div}_S\boldsymbol{s}_i,\, \boldsymbol{n}\cdot\boldsymbol{H}^{\mathrm{inc}})_{L^2(\Gamma)} \qquad (4)
\end{aligned}
$$

where $\Psi_{kl} = \mathrm{e}_{kjl}\partial_j G(x)$. Hence the EFIE discretised with the H_{div} inner product is equal to the sum of the tangiential component of the EFIE and the normal component of the magnetic field integral equation (MFIE).

Equation (4) is numerically well-conditinoed due to the second term, the normal component of MFIE. The value of the constant c is, therefore, set so that this term does not vanish for small frequency as shown in the next section.

4 Numerical examples

We consider a spherical scatterer with a 0.25 radius illuminated by the plane wave:

$$\boldsymbol{E}^{\mathrm{inc}}(\boldsymbol{x}) = \boldsymbol{E}^{\mathrm{inc}}_0\mathrm{e}^{\mathrm{i}\boldsymbol{k}\cdot\boldsymbol{x}}$$

where $\boldsymbol{k} = (0,0,k)^T$, $\boldsymbol{E}^{\mathrm{inc}}_0 = (1,0,0)^T$.

We test the discretidsation methods with the $H_{\mathrm{div}}(\Gamma)$ and $L^2(\Gamma)$ scalar product for equation (1). In the discretisation method with the $H_{\mathrm{div}}(\Gamma)$ scalar product, we set the constant $c = \omega^{-1}, \omega^{-}2$ and 1. The surface of the spherical scatterer is decomposed with 2000 triangular meshes, and we utilise the RWG basis function for expanding the unknown function $\boldsymbol{j}$, and the BC basis function as a testing function. The linear equations obtained with the discretisation methods are solved with the generalised minimul residual method (GMRES) with error tolerance 10^{-5}.

Figure1 shows the L^2 relative error of the numerical methods for several frequencies. The error of the conventional $L^2(\Gamma)$ scalar product becomes large for small frequencies. The $H_{\mathrm{div}}(\Gamma)$ scalar products with $c = \omega^{-1}$ and ω^{-2}, however, show good accuracy for any frequencies.

5 Conclusion

A new discretisation method with the H_{div} scalar product for the EFIE is investigated. This discretisation method improves the accuracy of BEMs for the low-frequency problems.

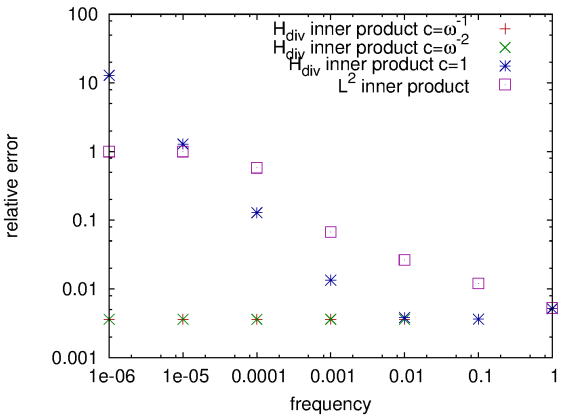

Figure 1: $L^2(\Gamma)$ relative error.

Acknowledgment

This research was supported by Grants-in-Aid for Young Scientists Grant Number 26790078.

References

[1] Francesco Andriulli, Kristof Cools, Ignace Bogaert, and Eric Michielssen. *IEEE Transactions on Antennas and Propagation*, Vol. **61**, No. 4, pp. 2077–2087, 2013.

[2] Zhi Guo Qian and Weng Cho Chew. *Microwave and Optical Technology Letters,* Vol. **50**, No. 10, pp. 2658–2662, 2008.

[3] S. Rao, D. Wilton, and A. Glisson. *IEEE Transactions on Antennas and Propagation,* Vol. **30**, No. 3, pp. 409–418, 1982.

[4] A. Buffa and S.H. Christiansen. *Mathematics of Computation,* Vol. **76**, pp. 1743–1769, 2007.

Boundary Integral Formulations for Modeling Eddy Current Testing

Marc Bonnet[1,*], **Edouard Demaldent**[2,*], **Audrey Vigneron**[2]
[1]POEMS (UMR 7231 CNRS-INRIA-ENSTA), ENSTA, 91762 Palaiseau Cedex, France
[2]CEA LIST, Imaging, Simulation and Control Department, Saclay, 91191 Gif-sur-Yvette, France
[*]Email: edouard.demaldent@cea.fr

Abstract. We propose a simple block-SOR solution method for the PMCHWT-type Maxwell integral formulation, that is well suited for the low-frequency, high-conductivity limit typical of eddy current (EC) testing methods. We also derive an asymptotic expansion of the Maxwell integral formulation in powers of the relevant (small) non-dimensional number γ_1 and show its relation to Hiptmair's EC integral formulation. Both aspects are validated on 3D numerical experiments.

Keywords: Boundary element method, Eddy current approximation, non destructive testing

Background. Eddy current (EC) non-destructive testing (NDT) aims to assess the presence of defects (cut, corrosion ...) in a conductive, and possibly magnetic, medium. Such testing is typically done on highly conductive parts and at low frequencies, i.e. in situations where $\gamma_1 := (\varepsilon_0\omega/\sigma)^{1/2}L \ll 1$ and $\gamma_2 := (\mu_0\omega\sigma)^{1/2}L \sim 1$ (σ: conductivity, L: characteristic part diameter, ω: angular frequency). It proceeds by creating a magnetic current in the probed part using a nearby electromagnetic source. The presence of a defect perturbs this current and induces an impedance variation in a receiver coil. As the latter may be small relative to the complete signal, such tests are often modeled by determining a primary field in the defect-free part and then computing the response of an assumed defect. For time-harmonic excitations, and since the considered media are usually piecewise-homogeneous, the primary field may be computed using boundary integral equations for either the harmonic Maxwell equations or their EC approximation [1].

For a conductive part in air, Maxwell integral formulations (e.g. the PMCHWT formulation) result from taking weighted combinations of inner and outer (tangential or rotated-curl) traces of the Stratton-Chu identity written for the conductive medium or the air, and setting them in Galerkin form, see [4]. The main unknowns are the tangential parts $\mathbf{J}$ and $\mathbf{M}$ of the electric and magnetic fields on the air-part interface Γ.

Block-SOR Maxwell integral formulation. We focused on a Maxwell-based approach, in order to be able to model testing either (i) within the EC approximation (for which $\gamma_1 \ll 1$) or (ii) using higher frequencies for poorly conductive media (where $\gamma \ll 1$ no longer holds).

Maxwell integral formulations suffer from a well-known low-frequency breakdown if $\gamma \ll 1$ [2]. While the latter can be circumvented by applying a Helmholtz ("loop-tree") decomposition to the approximation space (see [3] for EC NDT), the resulting global linear system remains highly ill-conditioned. The normalization method proposed in [2] for circumventing ill-conditioning at low frequencies is not applicable here, as it relies on a low-wavenumber expansion of the fundamental solution for a non-conductive body.

Instead, the loop-tree decomposition applied to the electric and magnetic current densities on the air-part interface is used to partition the global system into a 4×4 block system, whose diagonal blocks are found empirically to have a stable condition number over the physical parameter range of interest for NDT modeling, and in particular as $\gamma \to 0$. The system is then solved by means of a block-SOR (successive over-relaxation) method.

Several test cases allowed to validate the approach. For example, we considered a truncated tube ($\sigma = 10\,\mathrm{MS/m}$, inner and outer diameters 19.68 mm and 22.22 mm, height 10 mm, either non-magnetic or magnetic with $\mu_r = 100$), excited by a coaxial coil (inner and outer diameters 15.66 mm and 17 mm, height 2 mm). The condition numbers of the global matrix $\mathbf{Z}$ and of each diagonal block $\mathbf{Z}^{\beta\beta}_{\alpha\alpha}$ produced by the loop-tree decomposition are shown (Fig. 1) against the frequency for a fixed mesh (2640 Raviart-Thomas quadrilateral boundary elements). The block SOR algorithm is seen in Fig. 2 to converge within a reasonable number of iterations,

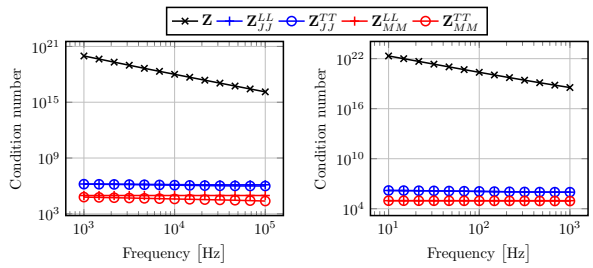

Figure 1: Condition number against frequency for non-magnetic (left) and magnetic (right) tubes. $\mathbf{Z}$ is the global BEM matrix; indices J, M, L and T indicate partitioning into electric, magnetic, solenoidal (loop) and non-solenoidal (tree) components.

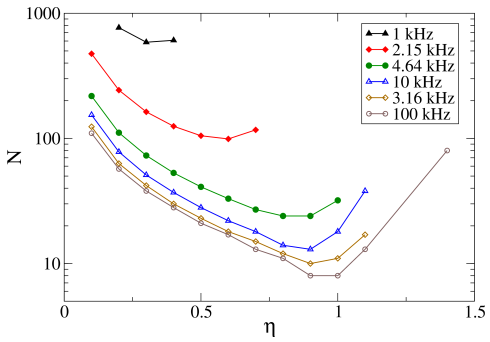

Figure 2: SOR iteration count N (with stopping criterion defined by relative residual less than 10^{-6}) against the SOR relaxation parameter η (non-magnetic tube).

except for the lowest two frequencies which in fact are not physically relevant (the skin depth then exceeding the tube thickness).

Eddy current asymptotics. To gain insight into links between Maxwell and EC integral formulations, we derived an asymptotic expansion of the former about $\gamma_1 = 0$ in powers of γ_1, assuming power series expansions of the loop and tree components $\mathbf{J}^L, \mathbf{J}^T, \mathbf{M}^L, \mathbf{M}^T$ of the surface unknowns and expanding in powers of γ_1 the Green's functions involved in the integral operators and right-hand sides. This approach in particular differs from [5], where the leading behavior of low-frequency expansions of Maxwell and EC models are shown to coincide. The leading asymptotic behaviour of the unknowns is obtained as

$$\mathbf{J}^L = \mathbf{J}^L_0 + o(1), \qquad \mathbf{J}^T = \gamma_1^2 \mathbf{J}^L_2 + o(\gamma_1^2),$$
$$\mathbf{M}^L = \gamma_1 \mathbf{M}^L_1 + o(\gamma_1), \quad \mathbf{M}^T = \gamma_1 \mathbf{M}^L_1 + o(\gamma_1),$$

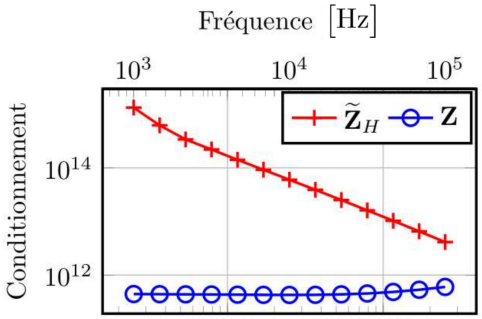

Figure 3: Condition number of integral operators $\mathbf{Z}$ (governing the leading unknowns $\mathbf{J}^L_0$, $\mathbf{M}^L_1$, $\mathbf{M}^L_1$) and $\mathbf{Z}_H$ of Hiptmair's EC formulation.

and the resulting integral problem for the leading unknowns ($\mathbf{J}^L_0$, $\mathbf{M}^L_1$, $\mathbf{M}^L_1$) is found to coincide with the EC integral formulation of [1] up to blockwise normalization by powers of γ_1, i.e. defines a better-conditioned version of the latter for $\gamma_1 \ll 1$ (see Fig. 3). Higher-order expansions in powers of γ_1 of the Maxwell integral problem may moreover be defined to extend the validity of the EC approximation.

References

[1] R. Hiptmair, Boundary element methods for eddy current computation, *Boundary element analysis. Mathematical aspects and applications* (pp. 213–248), Springer (2007).

[2] S. Chen, W. C. Chew, J. Song, J.-S. Zhao, Analysis of low frequency scattering from penetrable scatterers, *IEEE Trans. Geosc. Remote Sensing*, **39**:726–735 (2001).

[3] A. Vigneron, E. Demaldent, M. Bonnet, Surface integral equations for electromagnetic testing : the low-frequency and high contrast case, *IEEE Trans. Magn.*, **50**:117–120 (2014).

[4] A. Buffa, R. Hiptmair, T. von Petersdorff, C. Schwab, Boundary element methods for Maxwell transmission problems in Lipschitz domains. *Numer. Math.*, **95**:459–495 (2003).

[5] H. Ammari, A. Buffa, J. C. Nedelec, A justification of eddy currents model for the Maxwell equations. *SIAM J. Appl. Math.*, **60**:1805–1823 (2000).

Computational method for exact frequency dependent ray tracing

Maxim Protasov[1,*], **Kirill Gadylshin**[2]
[1]NSU, Novosibirsk, Russia; IPGG SB RAS, Novosibirsk, Russia
[2]IPGG SB RAS, Novosibirsk, Russia
[*]Email: protasovmi@ipgg.sbras.ru

Abstract

A computational method is presented which enables one to trace exact frequency dependent rays when a solution to the Helmholtz equation is already available. In this paper also is provided the analysis of the properties of exact frequency dependent rays and compare them with the standard ray-tracing and time domain finite-difference modelling.

Keywords: frequency dependent ray, Hemholtz solver

1 Introduction

There were several attempts to account band limited nature of seismic energy while remaining within the framework of ray tracing scheme. In the paper [1] author uses an approximation to the Helmholtz equation. There are calculated frequency dependent slowness fields where conventional ray tracing is performed. This approach suffers from the fact that the solution of lower frequencies relies on the solution of higher frequencies. An alternative frequency-dependent ray-tracing method that captures the band-limi- ted structure of wave propagation was presented in the paper [3] as the wavelength-smoothing (WS) method. The WS method averages the velocity model within the plane perpendicular to the ray by a weighting function whose width is proportional to the wavelength.

One more way to capture the band-limited wave propagation property of finite-difference me- thods with the least compromise is to do frequency dependent ray tracing. In the paper [2], frequency dependency of rays was visualized by looking at the phase of the solution of the Helm- holtz equation. This approach requires a Helm- holtz solver which is computationally more demanding than ray tracing. But this approach gives exact frequency dependent rays while all other approaches give different approximations. Therefore in this paper we developed computational method to extract those rays. Also we provide the analysis of their properties and compare them with the standard ray-tracing and time domain finite-difference modelling.

2 Method

Whenever a solution of the Helmholtz equation is known, it is possible to determine what the ray path trajectories *would* be if a ray theory approximation is not invoked. To see how this comes about, let us suppose that a solution Ψ to the Helmholtz equation

$$\triangle\Psi + k^2\Psi = f(\omega)\delta(x - x_s) \tag{1}$$

is known for some particular source configuration ($f(\omega)$ - source singature, x_s - point source position) and wave number k(x) in a lossless medium. After computing the gradient of the defining equation for A and Ψ, namely $\Psi = A\mathrm{e}^{\imath\Phi}$, one obtains

$$\frac{\nabla\Psi}{\Psi} = \frac{\nabla A}{A} + \imath\mathrm{K}. \tag{2}$$

Since A and $\mathrm{K} = \nabla\Phi$ are real, evidently

$$\frac{\nabla A}{A} = Re\frac{\nabla\Psi}{\Psi}, \tag{3}$$

and

$$\mathrm{K}\frac{\mathrm{d}\mathrm{r}}{\mathrm{d}s} = Im\frac{\nabla\Psi}{\Psi}. \tag{4}$$

The latter is a first order differential equation for the ray path. It is desirable for computational reasons to Eliminate K from the ray path equation by defining a new path parameter σ for such that $\mathrm{K}\mathrm{d}\sigma = \mathrm{d}s$. Then equation (4) becomes

$$\frac{\mathrm{d}\mathrm{r}}{\mathrm{d}\sigma} = Im\frac{\nabla\Psi}{\Psi}. \tag{5}$$

One traces a ray by integrating equation (5), usually by numerical methods. One also can calculate K by

$$\mathrm{K} = \left| Im\frac{\nabla\Psi}{\Psi} \right|, \tag{6}$$

which results in achieved by computing $\mathrm{K}\cdot\mathrm{K}$ using (4). Also available is the amplitude A, by way $A^2 = \Psi\Psi^*$.

That the ray path (5) is a first order differential equation has several remarkable consequences, two having to do with the computational process of solving ray path equations, or tracing rays, and another having to do with the qualitative behaviour of the paths themselves. Only one initial condition is required in order to solve a first order differential equation, while a second order equation requires two initial or boundary conditions for its solution. Another peculiar consequence of the exact ray equation being first order is that eigenrays for arbitrary points can often be found by tracing the ray *backwards* from an observation point to the source. This is accomplished by requiring the numerical integrator to solve (5) for decreasing, rather then increasing, values of σ. The resulting ray trace will proceed from the observation point right back to the source.

3 Examples

Let the acoustic velocity field be a linear gradient with depth $v(z) = a*z+b$. The parameter a and b are as follows $a = 3.1$ and $b = 1600$ m/s. In this case it is easy to construct analytical solution to the classical ray theory. On the Fig.1 one can observe the convergence of the exact rays to the classical rays, as we increase the frequency for in the Helmholtz equation.

4 Conclusions

A computational method is presented which enables one to trace exact frequency dependent rays when a solution to the Helmholtz equation is already available. Some of the properties of the exact rays which distinguish them from their classical counterparts are: the ray trajectories depend on the source frequency and on the boundaries, the exact frequency dependent rays intrude into shadow zones impenetrable by classical rays, the field is finite at caustics, the exact frequency dependent rays never exhibit multipathing, which is the hallmark of classical rays diagrams.

5 Acknowledgements

The research described in this publication was supported by RFBR grants 14-05-93090, 14-05-31257, 15-35-20015 and grant no.MK-2909.2014.5 of Russian Government.

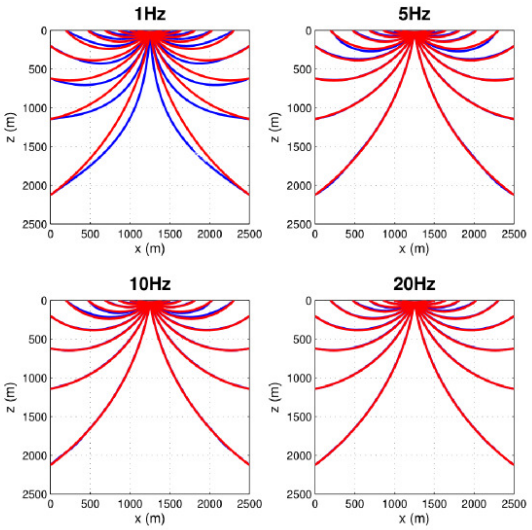

Figure 1: The corresponding classical ray trajectories (red) vs. exact ray paths (blue) are shown on each plot.

References

[1] Biondi, B., Solving the frequency dependent eikonal equation, *72nd Annual International Meeting, SEG, Expanded Abstracts, 11, 1992,* pp.1315-1319.

[2] Foreman, T., A frequency dependent ray theory, *PhD thesis, The University of Texas at Austin, 1987.*

[3] Lomax, A., The wavelength-smoothing method for approximating broad-band wave propagation through complicated velocity structures, *Geophysical Journal International, 117, 1994,* pp.313-334.

Multilevel Monte Carlo method for Helmholtz equation with random coefficients

Myoungnyoun Kim[1,*], Imbo Sim[1,*]
[1] National Institute for Mathematical Sciences, Daejeon, Republic of Korea
*Email: gmnkim,imbosim@nims.re.kr

Abstract

We apply the multilevel Monte Carlo method [1] to Helmholtz equation with random coefficients. The mean of the solutions at the fixed wave number is more accurate than the usual Monte Carlo method, or the computational complexity is less for the same order of error.

Keywords: multilevel Monte Carlo, Helmholtz equation, random coefficient

1 Monte Carlo Approximation

For simplicity, we consider an elliptic problem with a random coefficient under homogeneous Dirichlet boundary condition on a spatial domain D. Let $V = H_0^1(D)$ be a Sobolev space of square integrable functions with square integrable first derivatives and null trace on the boundary of D. Shape regular simplicial *triangulations* $\mathcal{T}_l$ of D with mesh size h_l form a collection of the *hierarchical* triangulation on D when all nodes of $\mathcal{T}_{l-1}$ belong to those in $\mathcal{T}_l$, for $0 \le l \le L$. Let V_l be the space of piecewise linear functions on simplices in $\mathcal{T}_l$, i.e.,

$$V_l = \Big\{ v \in V \,:\, v\big|_K \in \mathcal{P}_1(K),\ ^\forall K \in \mathcal{T}_l \Big\},$$

where $\mathcal{P}_1(K)$ is a linear polynomial space on a simplex $K \in \mathcal{T}_l$. Let $\{u_{l,k}\}_{k=1}^{M_l} \subset V_l$ be Galerkin approximations in V_l corresponding to the realizations of the random variable $\omega \in \Omega$. Then the *Monte Carlo* (MC) estimator $E_{M_l}(u_l)$ of solutions u_l in V_l is defined by

$$E_{M_l}(u_l) = \frac{1}{M_l} \sum_{k=1}^{M_l} u_{l,k}.$$

Assume the boundedness of the coefficient and the regularities of the coefficient and forcing term. There exist a constant $C_f = C\|f\|_{L^2(\Omega;L^2(D))}$ such that

$$\|u - u_l\|_{L^2(\Omega;V)} \le C_f h_l. \tag{1}$$

Here, the square of the Bochner norm $\|\cdot\|_{L^2(\Omega;V)}$ is $\|u\|^2_{L^2(\Omega;V)} = \mathbb{E}[\|u\|_V^2]$ for the mean operator $\mathbb{E}$, which is an integration of a function defined on Ω with a probability measure $\mathbb{P}$, or $\mathbb{E}[u] = \int_\Omega u(\omega)\, d\mathbb{P}(\omega)$. For a given tolerance $\varepsilon > 0$, let $C_f^2 h_l^2 = 2^{-1}\varepsilon^2$ and $C_f^2 M_l^{-1} = 2^{-1}\varepsilon^2$. Then the mean square error is less than or equal to ε^2. We obtain $h_l = \mathcal{O}(\varepsilon)$ and $M_l = \mathcal{O}(\varepsilon^{-2})$. Since the complexity of solving a sparse linear system in the spatial dimension d is of the same order of the degree of freedom $N_l = \mathcal{O}(h_l^{-d})$, the complexity of the MC method in V_l is

$$\begin{aligned} \mathcal{C}(E_{M_l}(u_l)) &= \mathcal{O}(\varepsilon^{-3}), \quad d = 1, \\ &= \mathcal{O}(\varepsilon^{-4}), \quad d = 2, \\ &= \mathcal{O}(\varepsilon^{-5}), \quad d = 3. \end{aligned}$$

2 Multilevel Monte Carlo Method

The *Multilevel Monte Carlo (MLMC)* estimator $\mathcal{E}_L(u)$ is defined by

$$\mathcal{E}_L(u) = \sum_{l=0}^{L} E_{M_l}(u_l - u_{l-1}), \quad u_{-1} = 0.$$

Under (1) for all $l \ge 0$, we set $C_f^2 h_L^2 = 2^{-1}\varepsilon^2$, $C_f^2 (h_l + h_{l-1})^2 {M_l}^{-1} = 2^{-1}(L+1)^{-1}\varepsilon^2$ for $l \ge 1$, and $C_f^2 {M_0}^{-1} = 2^{-1}(L+1)^{-1}\varepsilon^2$. By imposing $h_{l-1} = 2h_l$, for $l \ge 1$, we have $h_L = \mathcal{O}(\varepsilon)$, and $M_l = 4^{-l}\mathcal{O}(\varepsilon^{-2})$. Since $N_l = \mathcal{O}(h_l^{-d})$, the complexity of the MLMC method is

$$\begin{aligned} \mathcal{C}(\mathcal{E}_L(u)) &= \mathcal{O}(\varepsilon^{-2}), \quad d = 1, 2, \\ &= \mathcal{O}(\varepsilon^{-2} + \varepsilon^{-3}), \quad d = 3. \end{aligned}$$

The MLMC method reduces the computational complexity by at least one power factor compared to that by the MC method.

3 Model Problem

For a wave number k, the Helmholtz problem with a random coefficient is

$$-\nabla \cdot (a \nabla u) - k^2 u = f, \text{ in } D,$$

and

$$u = g, \text{ on } \Gamma_1, \quad a\frac{\partial u}{\partial \nu} - iku = 0, \text{ on } \Gamma_2,$$

where $\partial D = \Gamma_1 \cup \Gamma_2$. The random coefficient a is a truncated Karhunen-Loève (KL) expansion up to mode N_{KL}, see [1–4].

The assumption (1) takes the form of

$$\|u - u_l\|_{L^2(\Omega;V)} \leq C_f(\tilde{k}h_l + \tilde{k}^3 h_l^2), \qquad (2)$$

where $\tilde{k}^2 = k^2/a_{\min}$ for the minimum $a_{\min}$ of the coefficient a. By setting $\tilde{k}h_L + \tilde{k}^3 h_L^2 \approx \varepsilon$, we obtain $h_L \approx \tilde{k}^{-1.5}\varepsilon^{0.5}$. The complexity of the MLMC method for the Helmholtz equation is

$$\mathcal{C}(\mathcal{E}_L(u)) \quad = \quad \mathcal{O}(\varepsilon^{-2} + \tilde{k}^6\varepsilon^{-2}), \quad d = 1, 2, 3.$$

We impose $kh_L = 0.0156$ for the finest grid size and use a covariance operator of $\sigma = 1$ and $\lambda = 0.3$ to generate eigen pairs for a truncated KL expansion up to $N_{\mathrm{KL}} = 1000$ modes. We regard a mean of solutions in the fine grid for $900,000$ samples as an ideal mean for a fixed wave number $k = 10$. In Figure 1, relative errors versus computational complexities for the MC and MLMC methods are depicted in log-log scale.

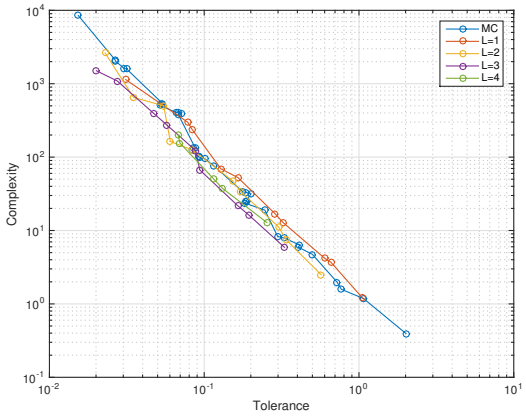

Figure 1: Complexity versus tolerance

4 Conclusion

The MC method needs quadruple samplings to reduce the error in half, which is expressed as the order of convergence being $1/2$. The MLMC method uses the solutions at the coarse grid and saves the computational cost by decreasing samples at the fine grid. Since the MLMC method is one of the variance reduction method, we show the same order of convergence as the MC method. Thus the same property of the MC method holds for the MLMC method, i.e., we need quadruple samples to reduce the error in half.

The MLMC method is a variant of the MC method and inherits the property of convergence. It improves the computational complexity and saves the computational effort by using coarse grid solutions. The error easily gets worse due to the uncertainty of the random coefficient and always increases the complexity to keep the same order of convergence.

References

[1] K. A. Cliffe, M. B. Giles, R. Scheichl and A. L. Teckentrup, Multilevel Monte Carlo methods and applications to elliptic PDEs with random coefficients, *Comput. Visual Sci.* **14** (2011), pp. 3–15.

[2] M. Loève, Probability Theory. I, *Grad. Texts in Math.* **45** (1977)

[3] M. Loève, Probability Theory. II, *Grad. Texts in Math.* **46** (1978)

[4] George Stefanou, The stochastic finite element method: Past, present and future, *Comput. Methods Appl. Mech. Engrg.* **198** (2009) pp. 1031–1051.

Convergence and Inherent Oscillations within a Method-of-Auxiliary-Sources Solution to a Problem of Potential Theory

G. Fikioris[1], **N. L. Tsitsas**[2,*]

[1]School of Electrical and Computer Engineering, Athens, Greece
[2]Department of Informatics, Thessaloniki, Greece

*Email: ntsitsas@csd.auth.gr

Abstract

We investigate the numerical solution of a simple magnetostatic problem by the method of auxiliary sources (MAS) and show analytically (by proving a certain asymptotic formula) that it is possible for the vector potential to converge to the correct potential function even in the case when the auxiliary currents diverge.

Keywords: method of auxiliary sources, convergence of numerical methods, Laplace's equation, oscillations

1 Introduction

Several wave scattering problems are modeled by the method of auxiliary sources (MAS) [1]. The MAS approximates the solution of a boundary value problem by a superposition of fields of auxiliary sources located outside the problem's domain and being proportional to the fundamental solution of the governing PDE. The boundary conditions on the physical boundary determine the fields amplitudes.

Investigations of scattering problems for the Helmholtz equation have revealed that the MAS *field* can converge to the correct scattered field even when the MAS *currents* diverge [2]. This MAS currents divergence is accompanied by unphysical oscillations which are similar but unrelated to matrix ill-conditioning oscillations.

The purpose of this paper is to investigate the corresponding Laplace problem. The motivation comes from engineering applications like crack singularities [3] and inductance calculations [4]. We prove an asymptotic formula for the oscillating currents in the static case and show that the magnetostatic vector potential converges to the correct potential function even in the case when the auxiliary currents diverge.

2 Statement of the Problem

We consider a simple 2-D magnetostatic problem. An infinitely long z-directed current I, located at $(\rho, \phi) = (\rho_{fil}, 0)$, illuminates a perfectly conducting circular cylinder of radius ρ_{cyl} ($\rho_{cyl} < \rho_{fil}$). The cylinder acts as a current return path, so that its total current is $-I$. The *total* magnetostatic vector potential $A_z(\rho_{obs}, \phi_{obs})$ satisfies Laplace's equation for $\rho_{obs} > \rho_{cyl}$ and $(\rho_{obs}, \phi_{obs}) \neq (\rho_{fil}, 0)$. Appropriate boundary conditions are: (i) A_z is constant on the conducting surface, $A_z(\rho_{cyl}, \phi_{cyl}) = C$ and (ii) A_z vanishes at $\rho_{obs} = \infty$. The latter is consistent with that the current on the cylinder is $-I$.

3 Application of the MAS

Application of the MAS to magnetostatic problems requires caution because the *total* potential vanishes at $\rho_{obs} = \infty$, while that due to I and each individual potential due to a MAS current are logarithmically infinite at $\rho_{obs} = \infty$ [3].

The N MAS currents I_l and the N collocation points are located at $(\rho_{aux}, \phi_A + 2\pi l/N)$ and $(\rho_{cyl}, \phi_C + 2\pi p/N)$, where $\rho_{aux} < \rho_{cyl}$ and $-\frac{\pi}{N} < \phi_A, \phi_C \leq \frac{\pi}{N}$. Then, by the Biot-Savart law, the total vector potential takes the form

$$A_{z,N}(\rho_{obs}, \phi_{obs}) = -\frac{\mu_0}{2\pi}\left[I \ln\left(\frac{R_{fil,obs}}{d_{ref}}\right) + \sum_{l=0}^{N-1} I_l \ln\left(\frac{R_{l,obs}}{d_{ref}}\right)\right] \quad (1)$$

where $d_{ref} > 0$ and

$$R_{fil,obs} = \left(\rho_{obs}^2 + \rho_{fil}^2 - 2\rho_{obs}\rho_{fil}\cos\phi_{obs}\right)^{\frac{1}{2}}$$

$$R_{l,obs} = \left(\rho_{obs}^2 + \rho_{aux}^2 - 2\rho_{obs}\rho_{aux}\times \cos\left(\phi_A + 2\pi l/N - \phi_{obs}\right)\right)^{\frac{1}{2}}$$

For $A_{z,N}$ to vanish, we demand that (1) presents no logarithmic singularity at $\rho_{obs} = \infty$, or that

$$\sum_{l=0}^{N-1} I_l = -I \quad (2)$$

Now enforcing the boundary condition

$$A_{z,N}(\rho_{cyl}, \phi_C + 2\pi p/N) = C \quad (3)$$

gives the N equations (for $p = 0, 1, \ldots, N-1$)

$$\sum_{l=0}^{N-1} I_l \ln\left(\frac{b_{l-p}}{d_{ref}}\right) = I_C - I \ln\left(\frac{d_p}{d_{ref}}\right), \quad (4)$$

in which $I_C = -2\pi C/\mu_0$ is yet unknown and

$$b_l = \big(\rho_{cyl}^2 + \rho_{aux}^2 - 2\rho_{cyl}\rho_{aux} \cos\left(\phi_A - \phi_C + 2\pi l/N\right)\big)^{\frac{1}{2}}$$

$$d_p = \big(\rho_{cyl}^2 + \rho_{fil}^2 - 2\rho_{cyl}\rho_{fil}\cos\left(\phi_C + 2\pi p/N\right)\big)^{\frac{1}{2}}$$

Eqs. (2) and (4) are a $(N+1) \times (N+1)$ system with unknowns $I_0, I_1, \ldots, I_{N-1}$, and I_C.

4 Exact and Asymptotic Expressions for Magnetostatic Currents

The MAS currents I_l are determined from their DFT's $I^{(m)}$ which are given by

$$I^{(m)} = -\frac{I}{N} e^{im\phi_A} \frac{f^{(m)}\left(\rho_{cyl}, \rho_{fil}, \phi_C\right)}{f^{(m)}\left(\rho_{aux}, \rho_{cyl}, \phi_C - \phi_A\right)} \quad (5)$$

with (for $m \neq 0$ and $0 < \rho_1 < \rho_2$)

$$f^{(m)}(\rho_1, \rho_2, \phi) = -\frac{1}{2} \sum_{q=-\infty}^{\infty} \frac{1}{|qN+m|} \left(\frac{\rho_1}{\rho_2}\right)^{|qN+m|} e^{iqN\phi}, \quad (6)$$

while

$$I^{(0)} = -I/N\,. \quad (7)$$

As $N \to \infty$, from (6) we get

$$f^{(m)}(\rho_1, \rho_2, \phi) \sim -\frac{1}{2}\frac{1}{|m|}\left(\frac{\rho_1}{\rho_2}\right)^{|m|}, \quad (8)$$

and hence obtain

$$I^{(m)} \sim -\frac{I}{N}\left(\frac{\rho_{cri}}{\rho_{aux}}\right)^{|m|} e^{im\phi_A}, \quad m \neq 0\,, \quad (9)$$

where the critical radius is defined by

$$\rho_{cri} \equiv \rho_{cyl}^2/\rho_{fil}\,. \quad (10)$$

Since $\rho_{aux} < \rho_{cri}$, it can be shown that the I_l oscillate and do not converge to a continuous surface current density.

5 Convergence/Divergence of MAS Vector Potential

We examine the convergence of the MAS vector potential $A_{z,N}^{scatt}(\rho_{obs}, \phi_{obs})$ for $N \to \infty$, $\rho_{obs} > \rho_{cyl} > \rho_{aux}$. We replace $I^{(m)}$ $(m \neq 0)$ by its large-N expression (9) and use (7) to find

$$A_{z,\text{limit}}^{scatt}(\rho_{obs}, \phi_{obs}) = \frac{\mu_0 I}{2\pi}\left[\ln\left(\frac{\rho_{obs}}{d_{ref}}\right) - \frac{1}{2}\sum_{m\neq 0}\frac{1}{|m|}\left(\frac{\rho_{cri}}{\rho_{obs}}\right)^{|m|} e^{im\phi_{obs}}\right] \quad (11)$$

which is independent of all MAS parameters (N, ρ_{aux}, ϕ_A, and ϕ_C). Eq. (11) is simplified as

$$A_{z,\text{limit}}^{scatt}(\rho_{obs}, \phi_{obs}) = \frac{\mu_0 I}{2\pi}\ln\left(\frac{R_{cri,obs}}{d_{ref}}\right) \quad (12)$$

where

$$R_{cri,obs} = \left(\rho_{obs}^2 + \rho_{cri}^2 - 2\rho_{obs}\rho_{cri}\cos\phi_{obs}\right)^{\frac{1}{2}}.$$

Eq. (12) gives the potential at (ρ_{obs}, ϕ_{obs}) due to an image at $(\rho, \phi) = (\rho_{cri}, 0)$ and carrying a current $-I$. Consequently, this limit equals (even when $\rho_{aux} < \rho_{cri}$) the true scattered vector potential and when added to the incident field, the result in (12) becomes independent of d_{ref} and vanishes at $\rho_{obs} = \infty$. For $\rho_{aux} < \rho_{obs} < \rho_{cyl}$, the series in (11) converges when $\rho_{cri} < \rho_{obs} < \rho_{cyl}$, diverges when $\rho_{aux} < \rho_{obs} < \rho_{cri}$, and has a singularity at $(\rho_{obs}, \phi_{obs}) = (\rho_{cri}, 0)$.

References

[1] D. I. Kaklamani and H. T. Anastassiu, Aspects of the Method of Auxiliary Sources (MAS) in computational electromagnetics, *IEEE Antennas Propagat. Magazine.* **44** (2002), pp. 48–64.

[2] G. Fikioris, On two types of convergence in the Method of Auxiliary Sources, *IEEE Trans. Antennas Propagat.* **54** (2006), pp. 2022–2033.

[3] Z.-C. Li, T.-T. Lu, and G. Q. Xie, The method of fundamental solutions and its combinations for exterior problems, *Engineering Analysis with Boundary Elements* **36** (2012), pp. 394–403.

[4] E. E. Nigussie, *Variation Tolerant on-Chip Interconnects*, Springer, New York, 2012.

Impedance Transmission Conditions for the Electric Potential across a Highly Conductive Casing

A. Erdozain[1,*], **V. Péron**[1,2]
[1]INRIA Bordeaux Sud-Ouest, Team magique 3D
[2]Université de Pau et des Pays de l'Adour
[*]Email: aralar.erdozain@inria.fr

Abstract

We present Impedance Transmission Conditions (ITCs) for the electric potential in the framework of borehole through-casing resistivity measurements. Such ITCs substitute the part of the domain corresponding to a highly conductive casing. The naturally small thickness of the casing makes it ideal for exhibiting ITCs. We numerically observe the delivered order of accuracy.

Keywords: Impedance Conditions, Electric Potential, Borehole, Casing, Resistivity.

1 Introduction

Borehole resistivity measurements are commonly used when trying to obtain a better characterization of the earth's subsurface. Often a metallic casing is employed to surround the well, which allows to protect the well and avoid possible collapses. The use of such casing highly complicates the analysis due to large contrast between the conductivities of the casing and the rock formations.

This work is motivated by realistic configurations [2] where the conductivity of the casing is $\sigma_{\mathrm{c}} \approx \varepsilon^{-3}$ when ε denotes the thickness of the casing. In this framework, our aim is to derive ITCs for the electromagnetic field across such a casing. As a first approach we derive ITCs for the electric potential.

We refer to [1] where the authors derive ITCs for eddy current models with a conductivity parameter of a thin sheet of the form $\sigma \approx \varepsilon^{-2}$.

We first introduce the mathematical model. Then, we explicit two asymptotic models of order two and four. Finally, we numerically analyse the performance and order of accuracy of the ITCs.

2 The Mathematical Model

We consider a transmission problem for the static case of the electric potential, the governing equations read as follows

$$\begin{cases} \sigma_{\mathrm{i}}\Delta u_{\mathrm{i}} = f_{\mathrm{i}} & \text{in} \quad \Omega_{\mathrm{i}}^{\varepsilon} \\ \sigma_{\mathrm{e}}\Delta u_{\mathrm{e}} = f_{\mathrm{e}} & \text{in} \quad \Omega_{\mathrm{e}}^{\varepsilon} \\ \sigma_{\mathrm{c}}\Delta u_{\mathrm{c}} = 0 & \text{in} \quad \Omega_{\mathrm{c}}^{\varepsilon} \\ u_{\mathrm{i}} = u_{\mathrm{c}} & \text{on} \quad \Gamma_{\mathrm{i}}^{\varepsilon} \\ u_{\mathrm{c}} = u_{\mathrm{e}} & \text{on} \quad \Gamma_{\mathrm{e}}^{\varepsilon} \\ \sigma_{\mathrm{i}}\partial_n u_{\mathrm{i}} = \sigma_{\mathrm{c}}\partial_n u_{\mathrm{c}} & \text{on} \quad \Gamma_{\mathrm{i}}^{\varepsilon} \\ \sigma_{\mathrm{c}}\partial_n u_{\mathrm{c}} = \sigma_{\mathrm{e}}\partial_n u_{\mathrm{e}} & \text{on} \quad \Gamma_{\mathrm{e}}^{\varepsilon} \\ u = 0 & \text{on} \quad \partial\Omega \end{cases} \tag{1}$$

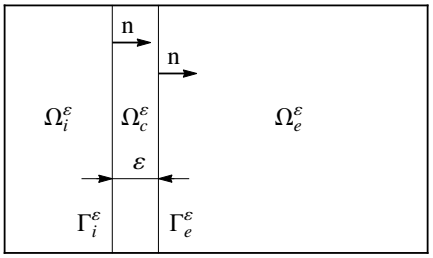

Figure 1: Domain of interest.

The considered domain $\Omega \subset \mathbb{R}^2$ is formed by three subdomains $\Omega_{\mathrm{i}}^{\varepsilon}$, $\Omega_{\mathrm{c}}^{\varepsilon}$, $\Omega_{\mathrm{e}}^{\varepsilon}$, which are characterized by different conductivities σ_{i}, σ_{e}, σ_{c}. These subdomains have rectangular shape and $\Omega_{\mathrm{c}}^{\varepsilon}$ is a thin layer of uniform thickness ε, as shown in Figure 1. In (1), f_{i}, f_{e}, σ_{i}, σ_{e} and σ_{c} are known data and u corresponds to the unknown, whose restrictions to the different subdomains are denoted as $u|_{\Omega_{\mathrm{i}}^{\varepsilon}} = u_{\mathrm{i}}$, $u|_{\Omega_{\mathrm{e}}^{\varepsilon}} = u_{\mathrm{e}}$, $u|_{\Omega_{\mathrm{c}}^{\varepsilon}} = u_{\mathrm{c}}$.

In this framework, we address the issue of ITCs for u (as $\varepsilon \to 0$) when the conductivity of the casing is $\sigma_{\mathrm{c}} = \alpha\varepsilon^{-3}$ ($\alpha \in \mathbb{R}$).

3 Main Results

For developing ITCs, we perform a formal expansion of the solution u in power series of ε. This leads to a collection of problems which can be solved successively. Then truncating the series we build asymptotic models by obtaining ITCs between $\Gamma_{\mathrm{i}}^{\varepsilon}$ and $\Gamma_{\mathrm{e}}^{\varepsilon}$.

Definition 1 *Let u be the solution of problem (1). We say that $u^{[k]}$ satisfies an asymptotic model of order $k+1$ when (for ε small enough)*

$$||u - u^{[k]}||_{L^2(\Omega_i^\varepsilon \cup \Omega_e^\varepsilon)} \leq C\varepsilon^{k+1}, \quad C \in \mathbb{R}.$$

We derive two asymptotic models of order two and four.

Order 2 model

$$\begin{cases} \sigma_{\mathrm{i}} \Delta u_{\mathrm{i}}^{[1]} &= f_{\mathrm{i}} \quad \text{in} \quad \Omega_{\mathrm{i}}^\varepsilon \\ u_{\mathrm{i}}^{[1]} &= 0 \quad \text{on} \quad \partial\Omega_{\mathrm{i}}^\varepsilon \end{cases}$$

$$\begin{cases} \sigma_{\mathrm{e}} \Delta u_{\mathrm{e}}^{[1]} &= f_{\mathrm{e}} \quad \text{in} \quad \Omega_{\mathrm{e}}^\varepsilon \\ u_{\mathrm{e}}^{[1]} &= 0 \quad \text{on} \quad \partial\Omega_{\mathrm{e}}^\varepsilon \end{cases}$$

Order 4 model

$$\begin{cases} \sigma_{\mathrm{i}} \Delta u_{\mathrm{i}}^{[3]} &= f_{\mathrm{i}} \quad \text{in} \quad \Omega_{\mathrm{i}}^\varepsilon \\ \sigma_{\mathrm{e}} \Delta u_{\mathrm{e}}^{[3]} &= f_{\mathrm{e}} \quad \text{in} \quad \Omega_{\mathrm{e}}^\varepsilon \\ \left[u^{[3]}\right] &= 0 \\ \left[\sigma \partial_n u^{[3]}\right] &= -\frac{\alpha}{\varepsilon^2} \Delta_\Gamma \left\{u^{[3]}\right\} \\ u_{\mathrm{i}}^{[3]} &= 0 \quad \text{on} \quad \partial\Omega_{\mathrm{i}}^\varepsilon \backslash \Gamma_{\mathrm{i}}^\varepsilon \\ u_{\mathrm{e}}^{[3]} &= 0 \quad \text{on} \quad \partial\Omega_{\mathrm{e}}^\varepsilon \backslash \Gamma_{\mathrm{e}}^\varepsilon \end{cases}$$

Here, the jump and mean value of a function u across the domain $\Omega_{\mathrm{c}}^\varepsilon$ are

$$[u] := u_{\mathrm{e}}|_{\Gamma_{\mathrm{e}}^\varepsilon} - u_{\mathrm{i}}|_{\Gamma_{\mathrm{i}}^\varepsilon}$$
$$\{u\} := \frac{1}{2}\left(u_{\mathrm{e}}|_{\Gamma_{\mathrm{e}}^\varepsilon} + u_{\mathrm{i}}|_{\Gamma_{\mathrm{i}}^\varepsilon}\right).$$

The validation of these models consists in proving estimates for $u - u^{[k]}$ (see Definition 1). Hereafter, we present numerical validations for each asymptotic model.

4 Numerical Results

We developed a finite element code to solve problem (1) and the two asymptotic models. We consider $f_{\mathrm{i}} = 1$, $f_{\mathrm{e}} = 1$ as right hand sides and we select $\sigma_{\mathrm{i}} = 3$, $\sigma_{\mathrm{e}} = 5$, $\sigma_{\mathrm{c}} = \varepsilon^{-3}$ as the different conductivities.

We compute the L^2 error between the solution of problem (1) and the solution of each asymptotic model for different values of ε by using triangular elements and degree five Lagrange polynomials. We observe these results in Figure 2 and the corresponding slopes of the graphics in Table 1. Each numerical convergence rate converges to the formal order of accuracy.

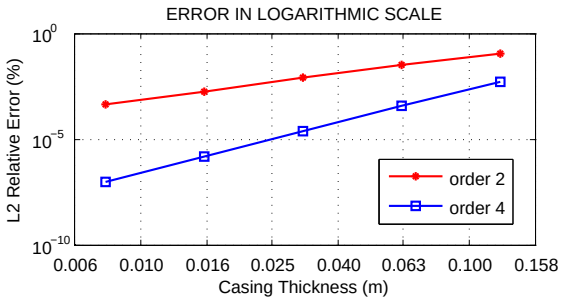

Figure 2: L^2 error of the order 2 and order 4 model for different values of ε

Casing Thickness ε	0.0117	0.0234	0.0469	0.0938
Order 2 Slopes	1.9944	1.9848	1.9537	1.8456
Order 4 Slopes	3.9906	3.9699	3.8962	3.6430

Table 1: Slopes corresponding to the curves of Figure 2

5 Perspectives

Among the future perspectives, we would like to derive asymptotic models for different configurations including the non-static case of the electric potential and electromagnetic field. We plan to perform mathematical proofs to validate these asymptotic models.

References

[1] K. Schmidt, A. Chernov, Robust transmission conditions of high order for thin conducting sheets in two dimensions, *IEEE Trans. Magn.*, **50** (2014), pp. 41–44.

[2] D. Pardo, C. Torres-Verdin, Z. Zhang, Sensitivity study of borehole-to-surface and crosswell electromagnetic measurements acquired with energized steel casing to water displacement in hydrocarbon-bearing layers, *Geophysics*, **73** (2008), pp. F261–F268.

Limiting amplitude principle for a two-layered medium composed of a dielectric material and a metamaterial

Maxence Cassier[2,1,*], Christophe Hazard[2], Patrick Joly[2]

[1]Department of mathematics, University of Utah, Salt Lake City, United States
[2]POEMS, CNRS-ENSTA-INRIA, Palaiseau, France

*Email: cassier@math.utah.edu

Abstract

For wave propagation phenomena, the limiting amplitude principle (LAP) holds if the time-harmonic regime represents the large time asymptotic behavior of the solution of the evolution problem with a time-harmonic excitation. Considering a two-layered medium composed of a dielectric material and a Drude metamaterial separated by a plane interface, we prove that the LAP holds except for a critical situation related to a surface resonance phenomenon.

Keywords: Maxwell's equations, metamaterials, spectral theory.

1 Introduction

In the frequency domain, the permittivity and permeability of a non-dissipative dispersive material $\varepsilon(\omega)$ and $\mu(\omega)$ are real-valued functions of the frequency ω. For metamaterials, these coefficients may become negative in particular frequency ranges, which raises theoretical and numerical difficulties. In [1], the authors proved that for a transmission problem between a dielectric material and a metamaterial separated by a smooth interface, the time-harmonic problem is well-posed except when both ratios of ε and μ across the interface are equal to -1 (which is the case of the "perfect lens" [3]). Nevertheless, the associated time-dependent problem remains well-posed. What is the link between both problems, in particular when the harmonic problem is ill-posed? We answer here the question in the case of a planar transmission problem which involves a Drude metamaterial.

2 Formulation of the problem

We consider a two-layered medium composed of a standard dielectric material and a Drude material, both homogeneous and non-dissipative, which fill respectively the half planes $\mathbb{R}^3_- = \{\boldsymbol{x} = (x,y,z) \in \mathbb{R}^3 \mid x < 0\}$ and $\mathbb{R}^3_+ = \{\boldsymbol{x} = (x,y,z) \in \mathbb{R}^3 \mid x > 0\}$. $(\boldsymbol{e_x}, \boldsymbol{e_y}, \boldsymbol{e_z})$ will refer to the canonical basis of $\mathbb{R}^3$. We denote by $\boldsymbol{E}$ and $\boldsymbol{H}$ the electric and magnetic fields and by $\boldsymbol{D}$ and $\boldsymbol{B}$ the electric and magnetic inductions. In the presence of a source current density $\boldsymbol{J_s}$, the evolution of $(\boldsymbol{E}, \boldsymbol{D}, \boldsymbol{H}, \boldsymbol{B})$ is governed by Maxwell's equations:

$$\begin{aligned} \partial_t \boldsymbol{D} - \mathbf{Curl}\, \boldsymbol{H} &= -\boldsymbol{J_s} \\ \partial_t \boldsymbol{B} + \mathbf{Curl}\, \boldsymbol{E} &= 0, \end{aligned}$$

(where the usual transmission conditions at the interface $x = 0$ are implicitly understood). These equations must be supplemented by the constitutive laws of each material. In the dielectric material, they are simply expressed by

$$\boldsymbol{D} = \varepsilon_0\, \boldsymbol{E} \quad \text{and} \quad \boldsymbol{B} = \mu_0\, \boldsymbol{H},$$

for two positive constants ε_0 and μ_0. In a dispersive media, these laws involve two additional unknowns, the electric and magnetic polarizations $\boldsymbol{P}$ and $\boldsymbol{M}$:

$$\boldsymbol{D} = \varepsilon_0 \boldsymbol{E} + \boldsymbol{P} \quad \text{and} \quad \boldsymbol{B} = \mu_0 \boldsymbol{H} + \boldsymbol{M}.$$

For the Drude model, the fields $\boldsymbol{P}$ and $\boldsymbol{M}$ are related to $\boldsymbol{E}$ and $\boldsymbol{H}$ through

$$\begin{aligned} \partial_t \boldsymbol{P} = \boldsymbol{J} \quad &\text{and} \quad \partial_t \boldsymbol{J} = \varepsilon_0\, \Omega_e^2\, \boldsymbol{E} \\ \partial_t \boldsymbol{M} = \boldsymbol{K} \quad &\text{and} \quad \partial_t \boldsymbol{K} = \mu_0\, \Omega_m^2\, \boldsymbol{H}, \end{aligned}$$

where Ω_e and Ω_m are positive parameters. By eliminating $\boldsymbol{D}$, $\boldsymbol{B}$, $\boldsymbol{P}$ and $\boldsymbol{M}$ in the above equations, we obtain

$$(P) \quad \begin{cases} \varepsilon_0\, \partial_t \boldsymbol{E} - \mathbf{Curl}\, \boldsymbol{H} + \boldsymbol{\Pi}\, \boldsymbol{J} = -J_s & \text{in } \mathbb{R}^3, \\ \mu_0\, \partial_t \boldsymbol{H} + \mathbf{Curl}\, \boldsymbol{E} + \boldsymbol{\Pi}\, \boldsymbol{K} = 0 & \text{in } \mathbb{R}^3, \\ \partial_t \boldsymbol{J} = \varepsilon_0\, \Omega_e^2\, \boldsymbol{E} & \text{in } \mathbb{R}^3_+, \\ \partial_t \boldsymbol{K} = \mu_0\, \Omega_m^2\, \boldsymbol{H} & \text{in } \mathbb{R}^3_+, \end{cases}$$

where $\boldsymbol{\Pi}$ denotes the operator of extension by 0 of a vectorial field defined on $\mathbb{R}^3_+$ to $\mathbb{R}^3$.

When looking for time-harmonic solutions of (P): $(\boldsymbol{\mathcal{E}}(\boldsymbol{x}), \boldsymbol{\mathcal{H}}(\boldsymbol{x}), \boldsymbol{\mathcal{J}}(\boldsymbol{x}), \boldsymbol{\mathcal{K}}(\boldsymbol{x}))\, e^{-i\omega t}$ for a periodic current density $\boldsymbol{\mathcal{J}_s}(\boldsymbol{x}) e^{-i\omega t}$, we can eliminate $\boldsymbol{\mathcal{J}}(\boldsymbol{x})$ and $\boldsymbol{\mathcal{K}}(\boldsymbol{x})$. In the half-plane $\mathbb{R}^3_+$ filled by the Drude material, we obtain

$$\begin{aligned} i\,\omega\varepsilon(\omega)\, \boldsymbol{\mathcal{E}} + \mathbf{Curl}\, \boldsymbol{\mathcal{H}} &= \boldsymbol{\mathcal{J}_s} \\ -i\,\omega\mu(\omega)\, \boldsymbol{\mathcal{H}} + \mathbf{Curl}\, \boldsymbol{\mathcal{E}} &= 0, \text{ where} \end{aligned}$$

$$\varepsilon(\omega) = \varepsilon_0 \left(1 - \frac{\Omega_e^2}{\omega^2}\right) \text{ and } \mu(\omega) = \mu_0 \left(1 - \frac{\Omega_m^2}{\omega^2}\right).$$

In the half-plane $\mathbb{R}^3_-$ filled by the dielectric material, we obtain the same equations with $\varepsilon(\omega)$ and $\mu(\omega)$ replaced by ε_0 and μ_0. Note that in the Drude material, $\varepsilon(\omega)$ and $\mu(\omega)$ become negative at low frequencies (which justifies the word "metamaterial"). Moreover, both ratios $\varepsilon(\omega)/\varepsilon_0$ and $\mu(\omega)/\mu_0$ are simultaneously equal to -1 at the same frequency if and only if $\Omega_e = \Omega_m$ ($:= \Omega^*$) and $\omega = \pm\Omega^*/\sqrt{2}$ ($:= \pm\omega^*$), where ω_* is called the *plasmonic frequency*.

3 Main results

We are interested in the long-time behavior of the solution of the transverse magnetic (TM) version of (P) for a time-harmonic source term $J_s(\boldsymbol{x}, t) = \mathcal{J}_s(x, y)\, e^{-i\omega t}\boldsymbol{e_z}$ with $\omega > 0$ and zero initial conditions. In this case, we have $\boldsymbol{E} = (0, 0, E_z)$ and $\boldsymbol{H} = (H_x, H_y, 0)$ where E_z, H_x and H_y do not depend on z, as well as the same properties for $\boldsymbol{J}$ and $\boldsymbol{K}$. We express below our main result in terms of the electrical field E_z but the same results hold for the other unknowns H_x, H_y, J_z, K_x, K_y.

Theorem 1 (i) *If $\Omega_e \neq \Omega_m$, the LAP holds at all frequencies, in the sense that for all $\omega > 0$, there exists a function $\mathcal{E}_z$ (related to the time-harmonic problem) such that*

$$E_z(\cdot, t) = \mathcal{E}_z(\cdot)\, e^{-i\,\omega t} + o(1) \text{ as } t \to +\infty,$$

where $o(1)$ stands for a function which tends to 0 in $L^2_{loc}(\mathbb{R}^2)$.

(ii) *If $\Omega_e = \Omega_m$, the LAP never holds. More precisely, with the same notations as above,*
• *if $\omega \neq \omega_*$, then there exists functions $\mathcal{E}^*_{z,\pm}$ and $\mathcal{E}_z$ such that*

$$E_z(\cdot, t) = \sum_{\pm} \mathcal{E}^*_{z,\pm}(\cdot)\, \mathrm{e}^{\mp i\omega_*\, t} + \mathcal{E}_z(\cdot)\, \mathrm{e}^{-i\omega t} + o(1);$$

• *If $\omega = \omega_*$, then there exists functions $\mathcal{E}^*_z$ and $\mathcal{E}_z$ such that*

$$E_z(\cdot, t) = t\, \mathcal{E}^*_z(\cdot)\, \mathrm{e}^{-i\omega_* t} + \mathcal{E}_z(\cdot)\, \mathrm{e}^{-i\omega_* t} + o(1).$$

4 Method of Analysis

The (very technical) proof follows from standard arguments (see, e.g., [4]). The main difficulty here is related to the dependence of $\varepsilon(\omega)$ and $\mu(\omega)$ with respect to ω (see [2] for details). We first rewrite the original problem (P) as an abstract Schrödinger equation

$$\frac{d\boldsymbol{U}}{dt} + i\,\mathbb{A}\boldsymbol{U} = \boldsymbol{F}\, e^{-i\,\omega t} \text{ with } \boldsymbol{U}(0) = 0,$$

where $\mathbb{A}$ is an unbounded self-adjoint operator in an appropriate Hilbert space $\mathcal{H}$. The key of the analysis is the spectral theory of the operator $\mathbb{A}$. This permits a quasi-explicit representation of the solution via the (generalized) diagonalization of $\mathbb{A}$. This is achieved by combining a partial Fourier transform along the interface with Sturm-Liouville type techniques in the orthogonal direction. For $\Omega_e = \Omega_m$, the resonance phenomenon is linked to the fact that $\mathbb{A}$ admits at the plasmonic frequency ω_* an eigenvalue of infinite multiplicity.

References

[1] A.-S. Bonnet-Bendhia and L. Chesnel and P. Ciarlet Jr, T-coercivity for the Maxwell problem with sign-changing coefficients, Communications in Partial Differential Equations, 39 (2014), 1007–1031.

[2] M. Cassier, Étude de deux problèmes de propagation d'ondes transitoires: (1) Focalisation spatio-temporelle en acoustique; (2) Transmission entre un diélectrique et un métamatériau (French) (Ph.D. thesis), Ecole Polytechnique, 2014, available online at https://pastel.archives-ouvertes.fr/pastel-01023289.

[3] J. B. Pendry, Negative refraction makes a perfect lens, Physical review letters 85(18) (2000), 3966.

[4] R. Weder, Spectral and scattering theory for wave propagation in perturbed stratified media, Applied mathematical sciences 50, Springer-Verlag New York, 1991.

Mathematical analysis and modeling of time-domain cloaking with metamaterials

Yunqing Huang[1], **Jichun Li**[2,*]

[1] Hunan Key Lab. for Computation and Simulation in Sci. and Eng., Xiangtan University, China
[2]Department of Mathematical Science, University of Nevada Las Vegas, USA

*Email: jichun@unlv.nevada.edu

Abstract

In this talk, we will present some of our recent works on mathematical analysis and finite element modeling of cloaking devices constructed by metamaterials. Our talk will focus on the cloaking simulation in time-domain.

Keywords: Cloak, metamaterial, finite element

1 Introduction

In June 23, 2006's issue of Science magazine, Pendry et al and Leonhardt independently published their works on electromagnetic cloaking. In Nov.10, 2006's Science, Pendry et al demonstrated the first practical realization of such a cloak with the use of artificially structured metamaterials. Since then, there is a growing interest in using metamaterials to construct invisibility cloaks cf. [1, Ch.9].

In recent years, mathematicians have started investigating this fascinating subject, but most works are still limited to frequency-domain or the quasi-static regime by mainly solving the Helmholtz equation, and the time-harmonic Maxwell's equations. In this talk, we will focus on our recently published work on time-domain carpet cloak [2].

2 The carpet cloak model

A triangular carpet cloak shown in Fig.1 (Left) can be achieved with spatially homogeneous anisotropic dielectric materials. The cloaked region is the bottom triangle with vertices $(0, H_1)$, $(-d, 0)$ and $(d, 0)$. The cloaking region is the quadrilateral region formed by vertices $(-d, 0)$, $(0, H_1)$, $(d, 0)$ and $(0, H_2)$, where $H_1, d > 0$. In order to make the hiden objects inside the cloaked region invisible to outside observer, the permittivity and permeability in the cloaking region need to be specially designed:

$$\varepsilon = \begin{bmatrix} a & b \\ b & c \end{bmatrix} = \begin{bmatrix} \frac{H_2}{H_2-H_1} & -\frac{H_1H_2}{(H_2-H_1)d}\mathrm{sgn}(x) \\ -\frac{H_1H_2}{(H_2-H_1)d}\mathrm{sgn}(x) & \frac{H_2-H_1}{H_2} + \frac{H_2}{H_2-H_1}(\frac{H_1}{d})^2 \end{bmatrix},$$

$$\mu = \frac{H_2}{H_2 - H_1},$$

where $\mathrm{sgn}(x)$ is the standard sign function. By construction, it is assumed that $H_2 > H_1 > 0$.

Denote

$$\lambda_1 = \frac{a + c - \sqrt{(a-c)^2 + 4b^2}}{2},$$

$$\lambda_2 = \frac{a + c + \sqrt{(a-c)^2 + 4b^2}}{2},$$

$$p_1 = \sqrt{\frac{\lambda_2 - a}{\lambda_2 - \lambda_1}}, \quad p_2 = \sqrt{\frac{a - \lambda_1}{\lambda_2 - \lambda_1}} \cdot \mathrm{sgn}(x),$$

$$p_3 = -\sqrt{\frac{\lambda_2 - c}{\lambda_2 - \lambda_1}} \cdot \mathrm{sgn}(x), \quad p_4 = \sqrt{\frac{c - \lambda_1}{\lambda_2 - \lambda_1}},$$

and matrices M_A and M_B:

$$M_A = \begin{pmatrix} p_1^2\lambda_2 + p_2^2 & p_2p_4 + p_1p_3\lambda_2 \\ p_2p_4 + p_1p_3\lambda_2 & p_3^2\lambda_2 + p_4^2 \end{pmatrix},$$

$$M_B = \begin{pmatrix} p_2^2 & p_2p_4 \\ p_2p_4 & p_4^2 \end{pmatrix} \omega_p^2,$$

where ω_p is the plasma frequency. We can obtain the governing equations for the carpet cloak:

$$\boldsymbol{D}_t = \nabla \times H, \tag{1}$$

$$\varepsilon_0\lambda_2 \left(\boldsymbol{E}_{t^2} + \omega_p^2 \boldsymbol{E}\right) = M_A \boldsymbol{D}_{t^2} + M_B \boldsymbol{D}, \tag{2}$$

$$\mu_0\mu H_t = -\nabla \times \boldsymbol{E}, \tag{3}$$

where H denotes the magnetic field, and $\boldsymbol{D}$ and $\boldsymbol{E}$ represent 2D electric displacement and electric field. The curl operators are in 2D sense. To make the model complete, we assume that (1)-(3) satisfy the initial conditions

$$\boldsymbol{D}(\boldsymbol{x}, 0) = \boldsymbol{D}_0(\boldsymbol{x}), \quad \boldsymbol{E}(\boldsymbol{x}, 0) = \boldsymbol{E}_0(\boldsymbol{x}),$$
$$H(\boldsymbol{x}, 0) = H_0(\boldsymbol{x}), \quad \forall\, \boldsymbol{x} \in \Omega, \tag{4}$$

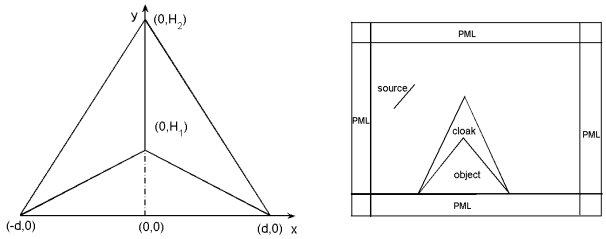

Figure 1: The physical space of the carpet cloak.

and the PEC boundary condition:

$$\boldsymbol{n} \times \boldsymbol{E} = \boldsymbol{0} \quad \text{on } \partial\Omega, \tag{5}$$

where $\boldsymbol{D}_0, \boldsymbol{E}_0$ and H_0 are some properly given functions, $\boldsymbol{n}$ is the unit outward normal vector to $\partial\Omega$, and Ω denotes the cloaking region.

The well-posedness of this model and the following stability is proved.

Theorem 1 *For solution $(\boldsymbol{D}, \boldsymbol{E})$ of (1)–(5) and any $t \in [0, T]$, the following stability holds true:*

$$\begin{aligned} & (||\sqrt{M_A}\boldsymbol{D}_t||^2 + ||\sqrt{M_B}\boldsymbol{D}||^2 + ||\boldsymbol{E}_{t^2}||^2 \\ & +||\boldsymbol{E}_t||^2 + ||\boldsymbol{E}||^2 + ||\sqrt{M_A}\nabla \times \boldsymbol{E}_t||^2)(t) \\ \leq\ & C(||\sqrt{M_A}\boldsymbol{D}_t||^2 + ||\sqrt{M_B}\boldsymbol{D}||^2 + ||\boldsymbol{E}_{t^2}||^2 \\ & +||\boldsymbol{E}_t||^2 + ||\boldsymbol{E}||^2 + ||\sqrt{M_A}\nabla \times \boldsymbol{E}_t||^2)(0), \end{aligned}$$

where the constant $C > 0$ depends on the physical parameters $\varepsilon_0, \mu_0, d, H_1, H_2$ and ω_p.

A leap frog type scheme with edge elements is developed for our model and many simulations are carried out. Due to page limit, here we show one example by choosing $H_1 = 0.05m, H_2 = 0.2m, d = 0.2m$, and $\Omega = [-0.3, 0.3]\ m \times [0, 0.3]\ m$, which is partitioned by a uniform triangular mesh with a mesh size $h = 0.00625$. The PML region surrounding Ω is partitioned by a uniform rectangular mesh. Our final mesh yields 53330 total edges, 26960 total triangular elements, and 6258 total rectangular elements. In the test, we choose the time step size $\tau = 2 * 10^{-13}$ s, and the total number of time steps 15000, i.e., the final simulation time $T = 3.0$ nanosecond (ns).

The incident wave is generated by a plane wave source $H_z = 0.1\sin(\omega t)$ imposed at line $x = -0.3$, where $\omega = 2\pi f$ with frequency $f = 3.0$ GHz. The numerical electric fields E_y at different time steps are presented in Fig.2, which shows clearly that the plane wave pattern is recovered very well after passing through the cloaking region, which makes any objects hiden inside the cloaked region invisible to observers at the far end.

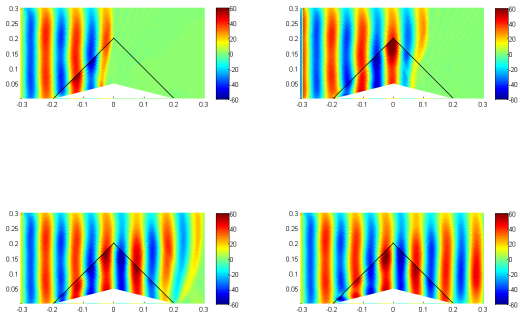

Figure 2: The E_y fields at 5000, 7000, 10000, and 15000 time steps.

References

[1] J. Li and Y. Huang, *Time-Domain Finite Element Methods for Maxwell's Equations in Metamaterials*, Springer, 2013.

[2] J. Li, Y. Huang, W. Yang and A. Wood, Mathematical analysis and time-domain finite element simulation of carpet cloak, *SIAM J. Appl. Math.* **74 (4)** (2014), pp. 1136–1151.

Tuesday, July 21
Morning Session
10:30 – 12:30

Homogenization for the one-dimensional wave equation with periodic coefficients in a bounded domain.

Thi Trang Nguyen[1,*], **Michel Lenczner**[2], **Matthieu Brassart**[3]

[1]University of Franche-Comté, FEMTO-ST institute, UMR CNRS 6174, Besancon, France

[2]Technology University of Belfort-Montbeliard, FEMTO-ST institute, UMR CNRS 6174, Besancon, France

[3]University of Franche-Comté, Laboratoire de Mathématiques de Besancon, France

[*]Email: thitrang.nguyen@femto-st.fr

Abstract

We present a method for periodic homogenization of the one-dimensional wave equation in a bounded domain. It allows modelling both low and high frequency waves. In this presentation, we focus mainly on the high frequency model part. It includes oscillations at the microscopic scale with amplitudes governed by a well-posed hyperbolic system constituting the macroscopic equations. This model was already presented in [1] but only for the entire n-dimensional space. The formulation of the boundary conditions were left as an open problem. Numerical simulations are provided to corroborate the theory.

Keywords: Homogenization, Bloch waves, Wave equation, Two-scale convergence

1 Introduction

For a one-dimensional bounded open set $\Omega = (0, \alpha) \subset \mathbb{R}^+$ and a finite time interval $I = (0, T) \subset \mathbb{R}^+$, we establish a homogenized model for the wave equation,

$$\begin{aligned} &\rho^\varepsilon \partial_{tt} u^\varepsilon - \partial_x \left(a^\varepsilon \partial_x u^\varepsilon \right) = f^\varepsilon \text{ in } I \times \Omega, \\ &u^\varepsilon \left(t = 0, x \right) = u_0^\varepsilon, \, \partial_t u^\varepsilon \left(t = 0, x \right) = v_0^\varepsilon \text{ in } \Omega, \end{aligned} \tag{1}$$

with homogeneous Dirichlet boundary conditions. The coefficients are positive, and given $\varepsilon > 0$ a small parameter, they are ε-periodic. Namely $a^\varepsilon = a\left(\frac{x}{\varepsilon}\right)$ and $\rho^\varepsilon = \rho\left(\frac{x}{\varepsilon}\right)$ where $a(y)$ and $\rho(y)$ are 1-periodic in $\mathbb{R}$. An asymptotic analysis of this problem is carried out when ε tends to zero.

The homogenization of the wave equation has been studied in various works. The construction of homogenization and corrector results for the low frequency waves has been published in [3], [4]. These works were taking into account only a small part of fast time oscillations, so these models reflect only a part of physical solutions. In [1], an asymptotic analysis of the solution $u^\varepsilon(t, x)$, that exhibit time and space oscillations occurring both at low and high frequencies in a bounded domain, has been introduced. It is derived from a formulation of the wave equation as a first order system and uses a decomposition over Bloch modes. The resulting asymptotic model includes separated parts for low and high frequency waves respectively. The latter is comprised with a microscopic equation and with a first order macroscopic equation which boundary conditions are missing. A similar result has been obtained in [2] for an unbounded domain, based on the second order formulation of the wave equation, which homogenized solution is periodic in space because it does not include a decomposition on Bloch modes. In this presentation, we synthesize these ideas in a model, based on the second order formulation of the wave equation, using the Bloch wave decomposition of the solution and more importantly including boundary conditions. Moreover, for the sake of comparison, the homogenization is also presented for the first order formulation as in [1], enriched by the boundary conditions. This work is a part of the thesis work [5].

The model derivation method is based on the modulated two-scale transform defined in [1] for both the time and space variable, and the Bloch wave decomposition consists in an expansion over a family of the eigenfunctions solution to the spectral problem

$$\partial_y \left(a \partial_y \phi^k \right) = -\lambda^k \phi^k$$

posed in the reference cell $Y \subset \mathbb{R}$ equipped with k-quasi-periodic boundary conditions for $k \in [-\frac{1}{2}, \frac{1}{2})$. The homogenization process starts with a very weak formulation of the wave equation. Applying our method yields two-scale models including the expected high frequency parts but also a low frequency part.

2 Homogenization results

Considering a subsequence ε such that the sequence $\frac{\alpha k}{\varepsilon} - \left[\frac{\alpha k}{\varepsilon}\right]$ converges to a limit l^k, the approximation of the solution u^ε is

$$u^\varepsilon(t,x) \approx u^0(t,x) + \varepsilon\theta\left(\frac{x}{\varepsilon}\right)\partial_x u^0(t,x) \quad (2)$$
$$+\varepsilon\sum_k\sum_{n\in\mathbb{Z}^*} u_n^k(t,x)\, e^{sign(n)i\sqrt{\lambda_{|n|}^k}t/\varepsilon}\phi_{|n|}^k\left(\frac{x}{\varepsilon}\right).$$

where u^0 and $\theta\left(\frac{x}{\varepsilon}\right)\partial_x u^0$ represent the classical low frequency solution and its usual elliptic corrector not detailed here. The remaining sum is the high frequency corrector and is made with Bloch waves. The amplitudes $(u_n^k)_{n\in\mathbb{Z}^*}$ are solution of the high frequency macroscopic problem, a first order system of differential equations. In particular, for $k \notin \left\{0, -\frac{1}{2}\right\}$ and for each n, the high frequency macroscopic model has the form

$$b(k,n,n)\,\partial_t u_n^k + c(k,n,n)\,\partial_x u_n^k = F_n^k \quad (3)$$
$$b(-k,n,n)\,\partial_t u_n^\sigma + c(-k,n,n)\,\partial_x u_n^{-k} = F_n^{-k}$$

in $I\times\Omega$, with some initial conditions not precise here, and boundary conditions on the form

$$u_n^k\phi_{|n|}^k(0)\, e^{\frac{2i\pi l^k x}{\alpha}} + u_n^{-k}\phi_{|n|}^{-k}(0)\, e^{-\frac{2i\pi l^k x}{\alpha}} = 0 \quad (4)$$

on $I\times\partial\Omega$. The two partial differential equations in (3) are coupled by their boundary conditions only. The coefficients $c(.,.,.)$, $b(.,.,.)$ and the right-hand sides $F_n^{\pm k}$ are defined from the Bloch eigenelements and with the function f^ε. For $k \in \left\{0, -\frac{1}{2}\right\}$ the Bloch eigenvalues are double and the macroscopic model statement has a similar form.

Moreover, the homogenization of the wave equation expressed as a first order system yields a first order formulation of the Bloch modes but a similar form of the macroscopic equation. The figures below represent a numerical example issued from the homogenized model of the first order system which unknown is the vector of first order derivatives $\left(\sqrt{a^\varepsilon}\partial_x u^\varepsilon, \sqrt{\rho^\varepsilon}\partial_t u^\varepsilon\right)$.

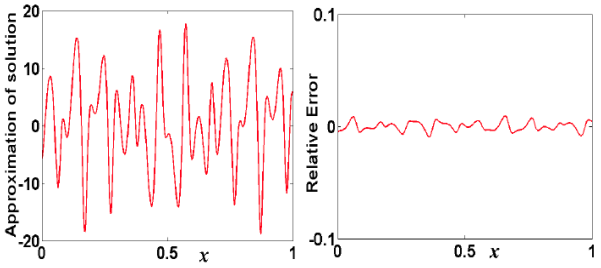

Figure 1: Left: The component $\sqrt{a^\varepsilon}\partial_x u^\varepsilon$ for $x \in \Omega$ at a prescribed time step. Right: The corresponding relative error between $\sqrt{a^\varepsilon}\partial_x u^\varepsilon$ and its approximation which $L^2(\Omega)$-norm is equal to $3.5e-3$.

Acknowledgements

This work is funded by the Labex ACTION program (contract ANR-11-LABX-01-01).

References

[1] M. Brassart and M. Lenczner, A two-scale model for the periodic homogenization of the wave equation, *Journal de mathématiques pures et appliquées* **93** (2010), pp. 474–517.

[2] J. Casado-Díaz, J. Couce-Calvo, F. Maestre and J. Martín Gómez, Homogenization and correctors for the wave equation with periodic coefficients, *Mathematical Models and Methods in Applied Sciences* **24** (2013), pp. 1–46.

[3] S. Brahim-Otsmane, GA. Francfort and F. Murat, Correctors for the homogenization of the wave and heat equations, *Journal de mathématiques pures et appliquées* **71** (1992), pp. 197–231.

[4] GA. Francfort and F. Murat, Oscillations and energy densities in the wave equation, *Communications in partial differential equations* **17** (1992), pp. 1785–1865.

[5] TT. Nguyen, *Contributions to periodic homogenization of a spectral problem and of the wave equation*, PhD thesis, University of Franche-Comté, Besançon, France, 2014.

On the homogenization of a transmission problem

Fioralba Cakoni[1], **Bojan Guzina**[2,*], **Shari Moskow**[3]

[1]Dept. of Mathematical Sciences, University of Delaware, Newark, US
[2]Dept. of Civil, Environmental & Geo-Engineering, University of Minnesota, Minneapolis, US
[3]Dept. of Mathematics, Drexel University, Philadelphia, US

*Email: guzin001@umn.edu

Abstract

This study deals with the homogenization of a transmission problem for bounded scatterers with periodic coefficients in $\mathbb{R}^d$ ($d = 2, 3$). The focus is on the Helmholtz equation where the index of refraction and its companion "matrix" coefficient are C^∞ functions over the unit cell with characteristic size ϵ. By way of multiple scales expansion, the analysis aims to unveil the $O(\epsilon^k)$, $k = 1, 2$ bulk and boundary corrections of the (leading-order) homogenized transmission problem. The analysis in particular provides the H^1 and L^2 estimates of the error committed by the first-order-corrected solution considering i) bulk correction only, and ii) boundary and bulk correction. The study also establishes the $O(\epsilon^2)$-bulk correction for the mean motion inside the scatterer, and an explicit treatment of the $O(\epsilon)$ boundary correction when the scatterer is a unit square.

Keywords: homogenization, Helmholtz equation, transmission problem

1 Introduction

Consider the transmission problem for a bounded scatterer $D \subset \mathbb{R}^d$ ($d = 2, 3$) with periodically varying coefficients, namely

$$\begin{aligned} \nabla \cdot \big(a(x/\epsilon)\nabla u_\epsilon\big) + k^2 n(x/\epsilon) u_\epsilon &= 0 \text{ in } D \\ \Delta u_\epsilon + k^2 u_\epsilon &= 0 \text{ in } \mathbb{R}^d \setminus \overline{D} \\ u_\epsilon^+ - u_\epsilon^- &= f \text{ on } \partial D \\ (\nabla u_\epsilon \cdot \nu)^+ - (a(x/\epsilon)\nabla u_\epsilon \cdot \nu)^- &= g \text{ on } \partial D \end{aligned} \quad (1)$$

where u_ϵ satisfies the Sommerfeld radiation condition at infinity. Here ν is the outward unit normal on ∂D, while superscripts "+" and "−" denote the respective limits on ∂D from the exterior and interior of D. The matrix coefficient function $a(y)$ and its scalar companion $n(y)$ are assumed to be C^∞-periodic functions of $y \in Y$, where $Y = [0, 1]^d$ is the unit cell in d dimensions. We are interested in developing the asymptotic theory for this problem as $\epsilon \to 0$, as was done previously for Dirichlet and Neumann problems [2, 3] on bounded domains. One expects the homogenized problem to read

$$\begin{aligned} \nabla \cdot A\nabla u_0 + k^2 \overline{n} u_0 &= 0 \text{ in } D \\ \Delta u_0 + k^2 u_0 &= 0 \text{ in } \mathbb{R}^d \setminus \overline{D} \\ u_0^+ - u_0^- &= f \text{ on } \partial D \\ (\nabla u_0 \cdot \nu)^+ - (A\nabla u_0 \cdot \nu)^- &= g \text{ on } \partial D \end{aligned} \quad (2)$$

where u_0 satisfies the Sommerfeld radiation condition; $\overline{n}$ is the unit cell average of n, i.e.

$$\overline{n} = \int_Y n(y) dy,$$

and A is a constant-valued matrix given by the weighted averages

$$A_{ij} = \int_Y \left(a_{ij}(y) - a_{ik}(y) \frac{\partial \chi^j}{\partial y_k}(y) \right) dy, \quad (3)$$

which make use of the Einstein's summation convention. Here $\chi^j(y)$ are the cell functions [1] which represent the Y-periodic solutions to

$$\frac{\partial}{\partial y_i} \left(a_{ij}(y) - a_{ik}(y) \frac{\partial \chi^j}{\partial y_k}(y) \right) = 0. \quad (4)$$

The additive constant for χ^j is chosen so that

$$\bar{\chi} := \int_Y \chi^j \, \mathrm{d}y = 0,$$

whereby the solutions to (4) are unique in $H^1_\#(Y)$, the space of H^1 functions on the d-dimensional torus, and are themselves C^∞ due to the smoothness of a. To derive this asymptotic limit and prove convergence, we will use the standard technique [1] which regards the solution as that depending on a "slow" variable x, and a "fast" variable $y = x/\epsilon$. Following [2], we further write the equation for u_ϵ inside D as a first-order system

$$\begin{aligned} a(x/\epsilon)\nabla u_\epsilon - v_\epsilon &= 0 \\ \nabla \cdot v_\epsilon + k^2 n(x/\epsilon) u_\epsilon &= 0 \end{aligned} \quad (5)$$

which allows us to obtain (lower regularity) L^2-based estimates of the error. In this setting, an ansatz for the bulk expansions inside D reads

$$\begin{aligned} u_\epsilon &= u_0(x, x/\epsilon) + \epsilon u^{(1)}(x, x/\epsilon) + \dots \\ v_\epsilon &= v_0(x, x/\epsilon) + \epsilon v^{(1)}(x, x/\epsilon) + \dots \end{aligned} \quad (6)$$

For the bulk expansion in $\mathbb{R}^d \backslash \overline{D}$, on the other hand, it suffices to use

$$u_\epsilon = u_0(x), \qquad v_\epsilon = v_0(x),$$

since there is no microstructure in the exterior. We note however that the boundary corrector functions are completely different story and, as is frequently the case with homogenization problems involving compact support, they must be accounted for both in D and $\mathbb{R}^d \backslash D$ in order to obtain higher-order convergence estimates. Such corrector functions solve problems which are substantially more difficult than our original; none- theless they are necessary for full understanding of the behavior of the solution.

2 Main results

The first-order bulk correction in (6) can be computed as

$$u^{(1)} = -\chi^j(y) \frac{\partial u_0}{\partial x_j}. \quad (7)$$

Next, let $q(x, y)$ be the solution to

$$\mathrm{rot}_y(q) = v_0 - A \nabla u_0, \quad (8)$$

and define

$$\hat{v}^{(1)} = \mathrm{rot}_x\,(q) + k^2 a(y) \nabla_y \beta(y) u_0 \quad (9)$$

where β is unique zero-mean solution to

$$\nabla_y \cdot (a \nabla_y \beta(y)) \;=\; \overline{n} - n(y). \quad (10)$$

With such definitions, the first-order boundary correction $(\hat{\theta})$ of the transmission problem can be shown to solve

$$\begin{aligned} \nabla \cdot a(x/\epsilon) \nabla \hat{\theta}_\epsilon + k^2 n(x/\epsilon) \hat{\theta}_\epsilon &= 0 \text{ in } D \\ \Delta \hat{\theta}_\epsilon + k^2 \hat{\theta}_\epsilon &= 0 \text{ in } \mathbb{R}^d \setminus \overline{D} \\ \hat{\theta}_\epsilon^+ - \hat{\theta}_\epsilon^- &= u^{(1)} \text{ on } \partial D \\ (\nabla \hat{\theta}_\epsilon \cdot \nu)^+ - (a(x/\epsilon) \nabla \hat{\theta}_\epsilon \cdot \nu)^- &= \\ = \left(\frac{v_0 - \overline{v}_0}{\epsilon} + \hat{v}^{(1)} \right) \cdot \nu \text{ on } \partial D. & \end{aligned} \quad (11)$$

Theorem 1 *Let u_ϵ be the solution to (1), u_0 the solution to (2), and let the bulk correction $u^{(1)}$ be given by (7) in the interior of D and zero on the exterior of D. Then for any ball B_R of radius $R > 0$ which contains D,*

$$\|u_\epsilon - (u_0 + \epsilon u^{(1)})\|_{H^1(B_R)} \leqslant C_R\, \epsilon^{1/2}$$

and

$$\|u_\epsilon - u_0\|_{L^2(B_R)} \leqslant C_R\, \epsilon \left(1 + \|\hat{\theta}_\epsilon\|_{L^2(B_R)}\right)$$

where the boundary correction $\hat{\theta}$ solves (11) and constant C_R is independent of ϵ.

Remark 2 *While the bulk correction is necessary to obtain the H^1 convergence, it does not in general improve upon the L^2 estimate. That is, unless the boundary correction approaches zero (which is not true in general), or is somehow accounted for,*

$$\|u_\epsilon - (u_0 + \epsilon u^{(1)})\|_{L^2(B_R)} \leqslant C_R\, \epsilon$$

is the best that one can obtain.

In the remainder of this work, we continue with the asymptotic expansion of the transmission problem in terms of higher powers of ϵ.

References

[1] J. Dupond and M. Smith, A Good Paper, *Journal of Important Papers* **44** (2006), pp. 2408–2431.

[2] J. Dupond, A. Dupont and M. Smith, A Good Conference Proceedings, in *Proceedings of the Mathematical Conference, Paris, France, 8-9 December 1978,* pp. 2047–2078.

[3] M. Smith, *A Good Book*, 2nd edition, Important Editions, London, 2006.

High order transmission conditions between homogeneous and homogenized periodic half-spaces

Xavier Claeys[1], **Sonia Fliss**[2], **Valentin Vinoles**[2,*]

[1]Jacques-Louis Lions laboratory, Pierre and Marie Curie University, Paris, France
[2]POEMS (CNRS/ENSTA Paristech/INRIA), Palaiseau, France
*Email: valentin.vinoles@ensta-paristech.fr

Abstract

Using matched asymptotics, we construct high order transmission conditions between an homogeneous and an homogenized periodic half space, since classical homogenization theory poorly takes into account interfaces. The analysis is based on an original combination of Floquet-Bloch transform and a periodic version of Kondratiev techniques. The obtained conditions involve Laplace-Beltrami operators at the interface and requires to solve "cell" problems in infinite strips.

Keywords: homogenization, periodic media, matched asymptotics

1 Problem statement

We want to solve the transmission problem between an homogeneous and a periodic half space ($\mathbf{x} = (x_1, x_2) \in \mathbb{R}^2$):

$$-\nabla \cdot \left[a\left(\frac{\mathbf{x}}{\varepsilon}\right) \nabla u_\varepsilon(\mathbf{x}) \right] - \omega^2 u_\varepsilon(\mathbf{x}) = f(\mathbf{x}) \quad (1)$$

where $\varepsilon > 0$ is a small parameter, ω the frequency with $\operatorname{Im} \omega^2 > 0$, $f \in L^2(\mathbb{R}^2)$ a source term whose support is compactly supported in $\Omega^- := \{x_1 < 0\}$, and a is an uniformly bounded and coercive function such that, in Ω^-, a is a constant $a_0 > 0$, and in $\Omega^+ := \{x_1 > 0\}$, a is 1-periodic in the two directions.

2 Classical homogenization results

The aim of periodic homogenization is to derive an effective homogeneous media from a periodic one when $\varepsilon \to 0$. A classical method is the two scale asymptotic expansion [1] which consists in expanding the solution u_ε of (1) as

$$u_\varepsilon(\mathbf{x}) = \begin{cases} \sum_{n\geq 0} \varepsilon^n u_n^-(\mathbf{x}) & \text{in } \Omega^- \\ \sum_{n\geq 0} \varepsilon^n u_n^+(\mathbf{x}, \mathbf{x}/\varepsilon) & \text{in } \Omega^+ \end{cases} \quad (2)$$

where the functions u_n^+ are 1-periodic w.r.t. the fast variables $\mathbf{y} := \mathbf{x}/\varepsilon$.

For the zeroth order, we obtain the homogenized transmission problem

$$\begin{cases} -\nabla \cdot (A^* \nabla u_0) - \omega^2 u_0 = f \quad \text{on } \mathbb{R}^2 \setminus \Gamma \\ [u_0]_\Gamma = 0, \ [A^* \nabla u_0 \cdot \mathbf{n}]_\Gamma = 0 \end{cases} \quad (3)$$

where $A^* = a_0$ on Ω^- and $A^* = a^*$ on Ω^+. Here, $a^* \in \mathcal{M}_2(\mathbb{R})$ is the homogenized tensor

$$a^*_{ij} := \int_Y a(\mathbf{y}) \left[\partial_{y_j} w_i(\mathbf{y}) + \delta_{ij} \right] \mathrm{d}\mathbf{y}$$

where $W = (w_1, w_2) \in (H^1_{\text{per}}(Y))^2$, $Y := (0,1)^2$, are the solutions of the 2 cell problems

$$\begin{cases} -\nabla \cdot [a(\mathbf{y}) \nabla w_j] = \partial_{y_j} a(\mathbf{y}) \quad \text{on } Y \\ \int_Y w_j = 0. \end{cases} \quad (4)$$

For the next order, in Ω^+, u_1^+ is given by

$$u_1^+(\mathbf{x}, \mathbf{y}) = \nabla_{\mathbf{x}} u_0(\mathbf{x}) \cdot W(\mathbf{y}) + \widehat{u_1}(\mathbf{x})$$

where $\widehat{u_1}$ does not depend on $\mathbf{y}$. Each function u_1^- and $\widehat{u_1}$ solves respectively the same volumic equation of (3) in Ω^- and Ω^+.

However, the expansions (2) does not lead to coherent transmission conditions for $(u_1^-, \widehat{u_1})$; they would have to depend on the fast variables $\mathbf{y}$. This is a well-known problem linked to the presence of boundary layers [1]. A common choice in the literature to avoid this difficulty is to take $u_1^- = \widehat{u_1} = 0$, but this leads to quite disappointing error estimates: defining

$$v := \begin{cases} u_0^- & \text{in } \Omega^- \\ u_0^+ + \varepsilon \nabla_{\mathbf{x}} u_0^+(\mathbf{x}) \cdot W(\mathbf{x}/\varepsilon) & \text{in } \Omega^+, \end{cases}$$

gives the following non-optimal error estimates

$$\begin{cases} \|u_\varepsilon - v\|_{H^1(\mathbb{R}^2)} = \mathcal{O}\left(\sqrt{\varepsilon}\right) \\ \|u_\varepsilon - v\|_{L^2(\mathbb{R}^2)} = \mathcal{O}(\varepsilon). \end{cases} \quad (5)$$

3 Matched asymptotics

We want to enrich the homogenized transmission problem (3) by deriving higher order transmission conditions which better take into account the phenomenon near the interface. We employ for this purpose a method which combines the techniques of matched asymptotics [3] and periodic homogenization [1].

We make different expansions on each area. Far from the interface Γ, we expand u_ε as in (2) and obtain the same volumic equations for the so-called far fields $u_n^\pm$. Near the interface, we look for a different asymptotic expansions of u_ε

$$u_\varepsilon(\mathbf{x}) = \sum_{n\geq 0} \varepsilon^n U_k\left(\frac{x_1}{\varepsilon}, x_2, \frac{x_2}{\varepsilon}\right) \tag{6}$$

where the so-called near fields U_k are 1-periodic w.r.t. $y_2 = x_2/\varepsilon$ **but not w.r.t.** $y_1 = x_1/\varepsilon$. The expansion (6) leads to a family of problems on the infinite strip $\mathcal{B} = \mathbb{R}\times(0,1)$ of the form

$$\begin{cases} -\nabla\cdot[a(\mathbf{y})\nabla U_n] = L(U_{n-1}, U_{n-2}) & \text{on } \mathcal{B} \\ U_n \text{ 1-periodic w.r.t. } y_2. \end{cases} \tag{7}$$

In order to match the behaviour of the far and near fields at the interface, we need to allow polynomial growing at $y_1 = \pm\infty$ of the near fields U_n. Without entering into details, to justify the well-posedness of these problems, we adapt Kondratiev techniques [2] in a periodic framework via the Floquet-Bloch transform.

4 Approximate problem

From all these expansions, we can finally build an approximate problem of order 1 by matching the behaviour of the near fields when $y_1 \to \pm\infty$ with the behaviour of the far fields when $x_1 \to 0^\pm$ (using Taylor expansions). We are able to construct a problem whose solution v_ε is close to the first non oscillating 2 terms of the far fields expansion, namely $v_\varepsilon = u_0^- + \varepsilon u_1^-$ on Ω^- and $u_0^+ + \varepsilon\widehat{u_1}$ on Ω^+. We obtain the (first order) homogenized transmission problem

$$\begin{cases} -\nabla\cdot(A^*\nabla v_\varepsilon) - \omega^2 v_\varepsilon = f \quad \text{on } \mathbb{R}^2\setminus\Gamma \\ [v_\varepsilon]_\Gamma = \varepsilon\mathcal{P}(v_\varepsilon) \\ [A^*\nabla v_\varepsilon\cdot\mathbf{n}]_\Gamma = \varepsilon\mathcal{Q}(v_\varepsilon) \end{cases} \tag{8}$$

where $\mathcal{P}$ is the operator

$$\mathcal{P}(u) = C_1\partial_{x_1}\langle u\rangle_* + C_2\partial_{x_2}\langle u\rangle$$

with $\langle\cdot\rangle$ the average over Γ and $\langle\cdot\rangle_*$ the weighted average $\langle u\rangle_* = (a_0 u|_{\Gamma^-} + a_{11}^* u|_{\Gamma^+})/2$, and where $\mathcal{Q}$ is a Laplace-Beltrami operator defined as

$$\mathcal{Q}(u) = C_3\partial^2_{x_1x_2}\langle u\rangle_* + C_4\partial^2_{x_2x_2}\langle u\rangle + \omega^2 C_5\langle u\rangle.$$

The coefficients C_j are constants computed from the so-called profil functions, which are solution of problems of type (7). In particular they are defined on the infinite strip $\mathcal{B} = \mathbb{R}\times(0,1)$ and have polynomial growth at infinity. From a numerical point of view, the profil functions and the C_j can be determined restricting the computational domain around the interface by using Dirichlet-to-Neuman operators (see [4] for the construction of such operators in periodic waveguides).

Moreover, if we add the oscillating part to v_ε on Ω^+:

$$\widetilde{v_\varepsilon} := \begin{cases} v_\varepsilon & \text{in } \Omega^- \\ v_\varepsilon + \varepsilon\nabla_{\mathbf{x}} v_\varepsilon(\mathbf{x})\cdot W(\mathbf{x}/\varepsilon) & \text{in } \Omega^+, \end{cases}$$

we obtain the expected error estimates

$$\begin{cases} \|u_\varepsilon - \widetilde{v_\varepsilon}\|_{H^1(\Omega)} = \mathcal{O}(\varepsilon) \\ \|u_\varepsilon - \widetilde{v_\varepsilon}\|_{L^2(\Omega)} = \mathcal{O}(\varepsilon^2). \end{cases} \tag{9}$$

for any $\Omega\subset\mathbb{R}^2$ such that $\overline{\Omega}\cap\Gamma = \emptyset$.

Numerical results will be shown during the presentation.

References

[1] G. Papanicolau, A. Bensoussan and J. L. Lions, *Asymptotic analysis for periodic structures*, Elsevier, 1978.

[2] V.A. Kozlov, V.G. Maz'ja and J. Rossmann, *Elliptic boundary value problems in domains with point singularities*, (vol. 52) American Mathematical Society, 1997.

[3] A.M. Il'in, *Matching of asymptotic expansions of solutions of boundary value problems*, American Mathematical Society, 1992.

[4] P. Joly, J.R. Li and S. Fliss, *Exact boundary conditions for periodic waveguides containing a local perturbation*, Commun. Comput. Phys. 1(6) 945-973, 2006.

Homogenized model of vibro-acoustic transmission on multi-plate panels

Eduard Rohan[1,*], **Vladimír Lukeš**[2]

[1]Department of Mechanics, Faculty of Applied Sciences, University of West Bohemia, Pilsen, Czech Republic

[2]European Centre of Excellence, NTIS New Technologies for Information Society, Faculty of Applied Sciences, University of West Bohemia, Pilsen, Czech Republic

[*]Email: rohan@kme.zcu.cz

Abstract

We consider problems of the acoustic wave propagation through panels consisting of several vibrating periodically perforated Reissner-Mindlin plates. The proposed model of the wave transmission through a layer involving the acoustic fluid and the panel is derived using the homogenization method. This provides homogenized transmission conditions which are prescribed on a flat interface representing the panel, so that the computational complexity of the vibroacoustic problem is reduced, although the geometrical arrangement of pores in the panel is respected in a detail. For a suitable mutual arrangement of holes in two, or more parallel plates there is a coupling between transverse and surface acoustic waves propagating along the panel.

Keywords: Acoustic transmission, porous panel, Reissner-Mindlin plate, homogenization

1 Introduction

Usually the models of the acoustic impedance are based on semi-empirical formulae which are tuned by experiments. To treat the vibroacoustic problem in a rigorous and efficient way, we derive a reduced model of the acoustic transmission which is based on the two-scale homogenization [1].For this we extend the approach developed in [2], where homogenization of rigid plates was pursued to derive effective nonlocal transmission conditions.

2 Vibroacoustic interaction on plates

We consider a layer $\Omega \subset \mathbb{R}^3$, see Fig. 1, with the thickness δ bounded by surfaces Γ_δ^+ and Γ_δ^- parallel to the midplane Γ_0 (defined by $x_3 = 0$), so that $\Omega_\delta = \Gamma_0 \times]-\delta/2, \delta/2[\subset \mathbb{R}^3$. ε is the characteristic size of the perforation of plates, whereby $\delta = \varkappa\varepsilon$ for a given $\varkappa > 0$, see Fig. 1.

The layer contains two elastic perforated plates Σ_K^ε, $K = I, II$, whereby ε is the characteristic size of the perforation; for a given $\varkappa > 0$, $\delta = \varkappa\varepsilon$.

Each elastic plate Σ_K^ε is represented by the perforated domain $\Gamma_K^\varepsilon \subset \Gamma_K$, the thickness $h_K^\varepsilon = \varepsilon\bar{h}_K$. Its vibration is described using the Reissner-Mindlin (R-M) plate model. The following equations in Γ_K^ε govern the plate displacements $\mathbf{u}^K = (\boldsymbol{u}^{\varepsilon,K}, w^{\varepsilon,K})$ and rotations $\boldsymbol{\theta}^{\varepsilon,K}$ (below the suffix K is omitted) as the harmonic response the acoustic pressure acting on the plate surface

$$\left\{\begin{array}{rcl} -\omega^2 h^\varepsilon \rho \boldsymbol{u}^\varepsilon - h^\varepsilon \mathrm{div}[\mathbb{C}\overline{\nabla}^S(\boldsymbol{u}^\varepsilon)] &=& \boldsymbol{t}^\varepsilon\,, \\ -\omega^2 h^\varepsilon \rho w^\varepsilon - h^\varepsilon \mathrm{div}[\gamma(\nabla w^\varepsilon - \boldsymbol{\theta}^\varepsilon)] &=& f^\varepsilon\,, \\ -\omega^2 \frac{(h^\varepsilon)^3}{12}\rho\boldsymbol{\theta}^\varepsilon - \frac{(h^\varepsilon)^3}{12}\mathrm{div}[\mathbb{C}\overline{\nabla}^S(\boldsymbol{\theta}^\varepsilon)] & & \\ -h^\varepsilon\gamma(\overline{\nabla}w^\varepsilon - \boldsymbol{\theta}^\varepsilon) &=& \overline{\boldsymbol{m}}^\varepsilon\,, \end{array}\right. \tag{1}$$

where $\overline{\nabla} = (\partial_\alpha)$ is the in-plane gradient, $\mathbb{C}, \gamma$ are elastic coefficients, ω is the frequency and the generalized loads $\boldsymbol{t}^\varepsilon = (\bar{b}_\alpha)$, $\alpha = 1, 2$, $f^\varepsilon = \bar{b}_3$, and $\overline{\boldsymbol{m}}^\varepsilon$, as well as the Neumann conditions prescribed on the holes $\partial\Gamma_K^\varepsilon \setminus \partial\Gamma_K$, are derived from the boundary traction forces $\boldsymbol{b}^\varepsilon = \mathrm{i}\omega\rho_0\boldsymbol{n}p^\varepsilon$, where ρ_0 is the fluid density, acting on free surfaces $\partial_f\Sigma_K^\varepsilon$ of the plate and involving the acoustic potential p^ε. The plates are clamped on $\partial\Gamma_K$ and the Neumann conditions expressed in terms of p^ε are prescribed on the holes $\partial\Gamma_K^\varepsilon \setminus \partial\Gamma_K$.

The total acoustic potential, p^ε satisfies the following equalities in Ω^ε and on $\partial\Omega^\varepsilon$,

$$c^2\nabla^2 p^\varepsilon + \omega^2 p^\varepsilon = 0 \quad \text{in } \Omega^\varepsilon\,,$$
$$\frac{\partial p^\varepsilon}{\partial n} = \left\{\begin{array}{ll} -\mathrm{i}\omega g^{\varepsilon\pm} & \text{on } \Gamma^{\pm\delta}\,, \\ -\mathrm{i}\omega\boldsymbol{n}\cdot\mathbf{u}^\varepsilon & \text{on } \partial\Sigma^\varepsilon\,, \\ 0 & \text{on } \partial\Omega \setminus (\Gamma_\delta^+ \cup \Gamma_\delta^-)\,, \end{array}\right. \tag{2}$$

where c is the speed of sound propagation, $\boldsymbol{n}$ is the normal vector, and $g^{\varepsilon\pm}$ represents the transverse acoustic velocity.

3 Homogenized transmission conditions

The homogenization procedure which consists in the asymptotic analysis $\varepsilon \to 0$ of the system (2)-(1) reduces the 3D vibroacoustic interaction problem to a 2D problem involving

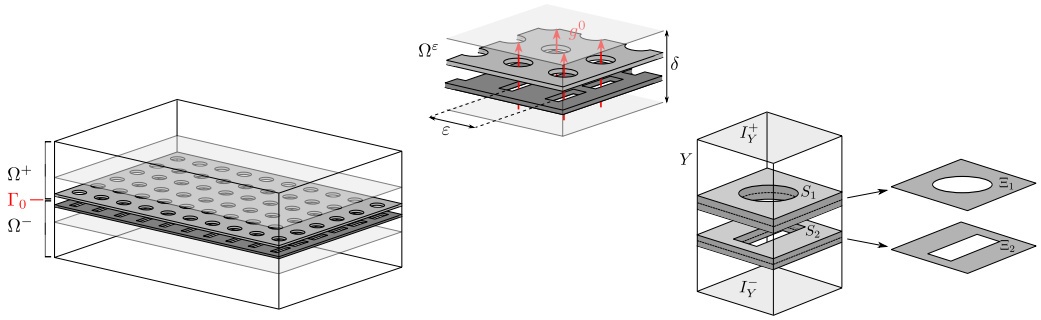

Figure 1: A Schematic view of the transmission layer with 2 plates of different perforation design. The layer thickness $\delta = \varkappa\varepsilon$, the plate thickness $h_K^\varepsilon = \varepsilon\bar{h}_K$.

limit acoustic potential p^0, transverse velocity (represented by g^0) and limit plate displacements $\mathbf{u}^K = (\boldsymbol{u}^{0,K}, w^{0,K})$. The following set of equations imposed in Γ_0 constitutes an implicit form of the Dirichlet-to-Neumann operator which couples the jump in external acoustic fields $(p^+_{\rm ext} - p^-_{\rm ext})/\varepsilon_0$, whereby $\varepsilon_0\bar{h}_K$ is the actual plate thickness, with the transverse acoustic velocity $\approx g^0$ and its mean fluctuation Δg^1,

$$
\begin{aligned}
&-\omega^2 m^K \mathbf{u}^K - \omega^2 \sum_{L=I,II} \mathbb{M}^{KL}\mathbf{u}^L - \overline{\nabla}\cdot\mathbb{D}^K\overline{\nabla}\mathbf{u}^K \\
&\qquad + \mathrm{i}\omega\mathbb{P}^K\overline{\nabla}p^0 - \omega^2\mathbb{N}^K g^0 = \boldsymbol{0}\ , \\
&\mathrm{i}\omega \sum_{L=I,II} \mathbb{P}^L\overline{\nabla}\mathbf{u}^L - \omega^2\Big(\frac{\varkappa}{c^2} + \rho_0 T_K\Big)p^0 \\
&\qquad - \varkappa\overline{\nabla}\cdot\boldsymbol{A}\overline{\nabla}p^0 - \mathrm{i}\omega\boldsymbol{B}\cdot\overline{\nabla}g^0 = -\Delta g^1\ , \\
&-\omega^2 \sum_{L=I,II} \mathbb{N}^L\cdot\mathbf{u}^L + \mathrm{i}\omega\boldsymbol{B}\cdot\overline{\nabla}p^0 + \omega^2 F g^0 \\
&\qquad = \frac{\mathrm{i}\omega}{\varepsilon_0}(p^+_{\rm ext} - p^-_{\rm ext})\ ,
\end{aligned}
$$

where $m^K, \mathbb{M}^{KL}, \mathbb{N}^K, \mathbb{D}^K, \mathbb{P}^K, \boldsymbol{B}, F, \boldsymbol{A}$ are the homogenized parameters; to compute them, local problems for characteristic responses must be solved in the representative periodic cell Y consisting of the fluid part and solid parts $\Xi_{1,2}$ representing the plates, see Fig. 1. The coefficients $\boldsymbol{B}$ are responsible for coupling the transverse and tangential acoustic waves; they do not vanish when different perforations of the two plates are used.

4 Conclusion

The obtained model represents implicit transmission conditions involving g^0 and other internal variables, p^0, $(\mathbf{u}^K)$, whereby $\frac{\partial p^\pm_{\rm ext}}{\partial n} = \pm\mathrm{i}\omega g^0$ is prescribed on Γ_0 representing the perforated panel. Due to the scaling of the plate thicknesses, the homogenized bending stiffness of the panel vanishes in the limit. As the main advantage, this homogenization based modelling approach reduces significantly the computational complexity of solving the acoustic wave transmission through the panel numerically. In the paper report numerical aspects of the model and compare its response with the one on the rigid panel, see [2]. Our further research is focused on the optimal perforation design problem, see [3].

The research is supported by the grant project GACR P101/12/2315.

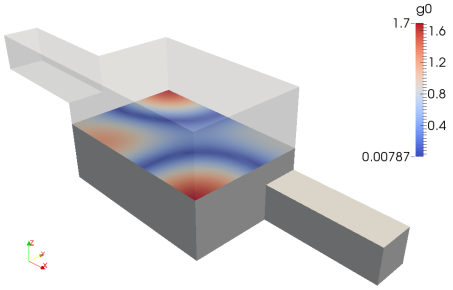

Figure 2: Transversal acoustic velocity g^0.

References

[1] D. Cioranescu, P. Donato, *An introduction to homogenization*. Oxford University Press, Oxford, 1999.

[2] E. Rohan, V. Lukeš, Homogenization of the acoustic transmission through perforated layer, *J. of Comput. and Appl. Math.* **234** (2010), pp. 1876–1885.

[3] E. Rohan, V. Lukeš, Homogenized perforated interface in acoustic wave propagation – modeling and optimization, in *Z. D. et.al. (Ed.), Proc. of ICOVP 2013, Lisbon, Portugal, 2013,* pp. 1–10.

Far field investigation in the presence of substrate

Sahar Sargheini[1,*], **Ralf Hiptmair**[2]
[1]Institute of Electromagnetic Fields, ETH Zurich, Switzerland
[2]Seminar for Applied Mathematics, ETH Zurich, Switzerland
[*]Email: sargheini@ethz.ch

Abstract

The near-field to far-field mapping is a tool used to describe radiation at far distances from scatterers. We consider the geometric setting of a bounded scatterer mounted on a substrate, and investigate the contribution of different asymptotic terms in the far-field functional. A closed form representation is given in term of both volume and boundary integrals. When finite element methods are used to solve Maxwell's equations approximately, the volume based expression is more accurate than the boundary integral. We confirmed the validity of our results by performing several numerical experiments and compared them with other numerical and experimental results.

Keywords: far-field mapping, asymptotic analysis, scattering, substrate.

1 Introduction

In many electromagnetic scattering problems, the key quantity of concern is the radiation pattern at far distances. However, numerical methods like Finite Elements or Finite Differences provide the solution to Maxwell's equations within some finite computational domain.
Field values at far distances can be obtained using a post-processing procedure called near-field to far-field mapping. The mapping is a linear operator on the near-field solution. Formulas for far-field calculations for structures in free space are well known. However, for structures located above a substrate, the calculations are more challenging [1, 2].
We present an asymptotic analysis for outgoing electromagnetic waves and derive a closed form expression for the field of a dipole over a substrate at far distances. Then, far-field functionals are stated in terms of a boundary integral over a surface surrounding the scatterer. Since boundary integrals are not well-defined on the natural variational space, we reformulate the far-field mapping in terms of a volume integral.

2 Theory

Electromagnetic field components can be represented in terms of vector and scalar potentials.The vector potential is the solution of the vector Helmholtz equation [3, Section 2.2]. In Cartesian coordinates, the vector Helmholtz equation can be decomposed into three scalar Helmholtz equations. The Green's function for scalar Helmholtz equation $g_0(\mathbf{r}, \mathbf{r}')$ at point $\mathbf{r} = (x, y, z)$ is obtained by considering a point source at $\mathbf{r}' = (x', y', z')$

$$\Delta g_0(\mathbf{r}, \mathbf{r}') + k^2\, g_0(\mathbf{r}, \mathbf{r}') = \delta(\mathbf{r} - \mathbf{r}') \qquad (1)$$

where k is the wave number.
The solution of (1) in free space can be expanded in terms of plane waves and cylindrical waves using Weyl and Sommerfeld identities, respectively. In the presence of a substrate, reflected and transmitted waves must be added to the expansions.
The asymptotic analysis of improper radiation integrals in the complex plane consists of examining following additive contributions:

- Saddle point contribution
  The stationary phase method is used to derive it [4].
- Critical points contribution
  There are three types of critical points:
  - branch point singularity
  - pole singularity
  - integration end points.

  The far-field asymptotics of each contribution can be determined using the method of steepest descent [4].

We analyze each of these contributions asymptotically and show that [3, Section 3]

- The saddle point contribution $g_s(\mathbf{r}, \mathbf{r}')$ in the presence of a substrate comprises a direct wave, reflected wave, and transmitted wave. $g_s(\mathbf{r}, \mathbf{r}')$ decays according to $\frac{1}{r}$ ($r = |\mathbf{r}|$) for $r \to \infty$.

- The branch point contribution decays according to $\frac{1}{r^2}$ for $r \to \infty$.
- The pole contribution plays a role only under the condition that the substrate is highly lossy and the observation point is located on the substrate. Under these conditions, a term with decay rate of $\frac{1}{\sqrt{r}}$ occurs for $r \to \infty$. This term resembles surface waves. However, investigating other terms in the final formula reveals that at far distances the pole contribution does not play any significant role due to fast exponential decays.
- No contribution arises from the end point at far distances.

As soon as we obtain the asymptotic form of the Green's function at $r \to \infty$, we can use the Huygens principle to derive field values for scattering problems at far distances [1].
Yet, the boundary integrals, which are traditionally used to calculate the far-field pattern, are not well-defined on the natural variational space. We reformulate the far-field mapping in terms of a volume integral

$$\begin{aligned}\mathbf{E}_\infty(\hat{\mathbf{r}}) \cdot \hat{\ell} = &\int_{\Omega_f} \nabla^{\mathbf{r}'} \times \mathbf{E}(\mathbf{r}') \cdot \\ &\nabla^{\mathbf{r}'} \times \left(\Psi(\mathbf{r}')\mathbf{G}_\infty(\mathbf{r},\mathbf{r}',\hat{\ell})\right) \\ -&\int_{\Omega_f} \nabla^{\mathbf{r}'} \times \mathbf{G}_\infty(\mathbf{r},\mathbf{r}',\hat{\ell}) \cdot \\ &\nabla^{\mathbf{r}'} \times \left(\Psi(\mathbf{r}')\mathbf{E}(\mathbf{r}')\right)\, d\mathbf{r}'\end{aligned} \tag{2}$$

where $\mathbf{E}_\infty(\hat{\mathbf{r}})$ is the far-field pattern and $\hat{\ell}$ is the direction of the observed field. $\mathbf{G}_\infty(\mathbf{r},\mathbf{r}',\hat{\ell}) = g_0(\mathbf{r},\mathbf{r}')\hat{\ell}$ as $r \to \infty$. Ω_f is a subregion between two closed path Γ_i and Γ_o around the scatterer and $\Psi(\mathbf{r}') \in H^1(\Omega_f)$ is a cut-off function such that

$$\Psi(\mathbf{r}')|_{\Gamma_i} \equiv 1 \text{ , and } \quad \Psi(\mathbf{r}')|_{\Gamma_0} \equiv 0 \tag{3}$$

3 Numerical results

We analyze the plasmon resonances of gold nanoparticles (NP) in the presence of a glass substrate. The far-field pattern is calculated within a finite aperture and compared with optical measurements reported in [5]. The NPs are elliptical gold cylinders. The Three principal axes of the cylinder are a, b, and h where a and b are in-plane axes and h is the height of the NP. λ_a is the resonance frequency of the NP when the incident electric field is parallel to the a axis. Figure 1 shows how λ_a depends on the size of a axis when b and h are kept constant.

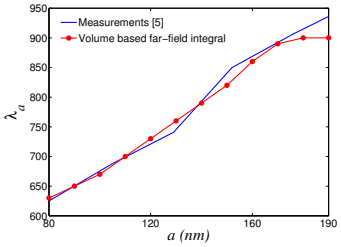

Figure 1: Dependence of the resonance frequency λ_a on the size of principle axis a.

References

[1] W. C. Chew, *Waves and fields in inhomogeneous media*, Van Nostrand Reinhold , New York, 1990.

[2] L. B. Felsen, *Radiation and scattering of waves*, Prentice-Hall, Englewood Cliffs-New Jersey, 1973.

[3] R. Hiptmair, S. Sargheini, Scatterers on Substrate: Far field formulas, *SAM-Report* **2015-02** (2015).

[4] J. D. Murray, *Asymptotic analysis* Springer-Verlag, New York, 1984.

[5] R. Giannini, *Shape dependence of LSPRs and their applications in nanoemitters*, PhD. thesis, ETH University of Zurich, in preparation.

Transmission and Scattering of Waves by General Shapes with High Order Accuracy Using the Difference Potentials Method

Michael Medvinsky[1,*], **Eli Turkel**[2], **Semyon Tsynkov**[3]

[1]Department of Mathematics,University of Utah, Salt Lake City, Utah, USA
[2]School of Mathematical Sciences, Tel Aviv University, Tel Aviv, Israel
[3]Department of Mathematics, North Carolina State University, Raleigh, NC, USA
[*]Email: medvinsky.michael@gmail.com

Abstract

In the talk we consider propagation of waves across various star-shaped, not necessarily convex, interfaces and inhomogeneous media. We develop numerical approach based on Calderon's operators and the Difference Potentials Method [1]. Our methodology provides high order accuracy and at the same time employs only simple structured grids, e.g., Cartesian or polar, regardless of the shape of the interfaces or external boundaries. Therefore the computational complexity of the developed algorithms is that of a finite-difference schemes on a simple grid. We will illustrate the accuracy and robustness of developed methods on several numerical tests in 2D.

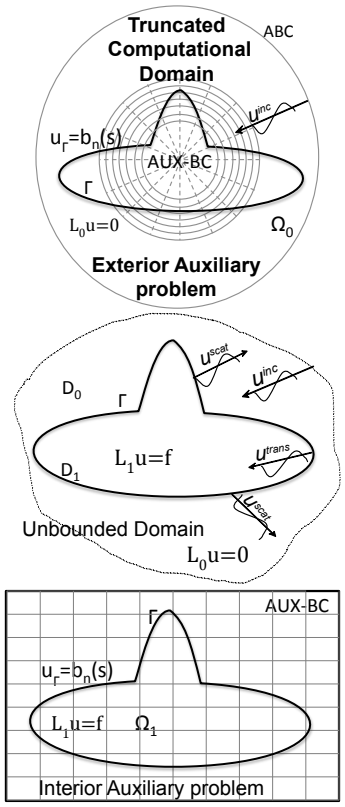

Figure 1: Schematic

Keywords: Difference potentials, Boundary projections, Calderon's operators, Curvilinear / non-conforming boundaries / interfaces on regular grids, Variable coefficients, High order accuracy, Exterior problems,

We consider high order numerical solution of the Helmholtz equation for the domains where the interfaces do not necessarily conform to the mesh. The general formulation involves a geometrically large region of space separated by several arbitrarily shaped interfaces. The material properties are assumed smooth between the interfaces, whereas at the interfaces they may undergo jumps. Examples include scattering about complex shapes (see Figure 1) and bodies with multiple layers or several (non-homogeneous) media. Smooth, but not constant, material characteristics lead to variable coefficient extensions to the wave number in the Helmholtz equation. Due to pollution errors, it is desirable that the solution be approximated with high order accuracy, especially for high frequencies. However, the existence of interfaces typically degrades the accuracy of the scheme.

We focus on a scalar monochromatic wave field, or equivalently, acoustic propagation in the frequency domain. Our goal is to guarantee that the method for solving this class of problems will provide high order accuracy notwithstanding the presence of interfaces. It should match the geometric flexibility of boundary integral methods, yet without singular integrals and without being limited to constant coefficients. At the same time, it should be efficient while not being constrained to regular geometries.

Our new method uses only simple structured grids, e.g., Cartesian or polar, regardless of the shape of the interface. In the regions of smoothness, it employs high order accurate finite differences schemes on compact stencils. The interfaces that are not aligned with the grid, which are usually a major difficulty, are treated by Calderon's operators and the method of difference potentials [1]. This involves no loss of accuracy regardless of the shape of the interface (as long as it is smooth).

Calderon's projections, unlike in the classical potential theory, reduce the differential equation from the domain to the boundary irrespec-

tive of the specific boundary value problem (e.g., Dirichlet or Neumann). Moreover, the discrete counterparts of Calderon's operators doesn't approximate singular integrals, they are built by solving discretized PDEs on a regular grid. The approximation of the continuous potential by the difference potential is then established [1]. The boundary representations inherit the accuracy of the core scheme, and high order accuracy is achieved on regular grids for curved boundaries with no adverse effects due to staircasing. Variable coefficients present no difficulties and the reduced boundary problem is always well-posed as long as the original formulation on the domain is well-posed. The procedure is automatic, and the discrete equations are fully characterized in algorithmic terms. Finally, the extension from interior domains to problems on unbounded domains can be handled in a natural way.

Let $\boldsymbol{L}_j$ be the Helmholtz operator $\boldsymbol{L}_j = \Delta + k_j^2$ on the domain D_j, where $j \in 0, 1$. Consider the following problem:

$$\begin{cases} \boldsymbol{L}_1 u = 0, & \boldsymbol{x} \in D_1, \\ \boldsymbol{L}_0 u = 0, & \boldsymbol{x} \in D_0 = \mathbb{R}^n \setminus D_1, \end{cases} \tag{1}$$

with the geometry depicted in Figure 1, driven by a given impinging wave $u^{(\text{imp})}$. For uniqueness we require the Sommerfeld radiation condition at infinity. We also require that the solution and its first normal derivative be continuous across the interface.

We split problem (1) into two distinct auxiliary problems (AP) according to the sub-domains, see Figure 1 external (top) and internal (bottom) subproblems. The condition on Γ depends on the solution on each side of the interface which is not known ahead of time. Hence, finding the solution and satisfying the interface condition has to be done simultaneously. We implement the interface condition using an expansion in some basis, e.g., Fourier, so the problem is reduced to finding the coefficients of the expansion of the solution u on an interface Γ.

The analytical interface Γ is transformed to a grid interface γ using the intersection of the unification of stencils centered at D_1 with the unification of those centered in D_0. To guarantee n^{th} order accuracy of the numerical solver to be the accuracy of the overall solution one transforms the basis functions from Γ to the grid boundary γ using a Taylor expansion of order $n+1$, see [3]. The truncation of the infinite series in the basis can be experimentally chosen to fit the desired accuracy.

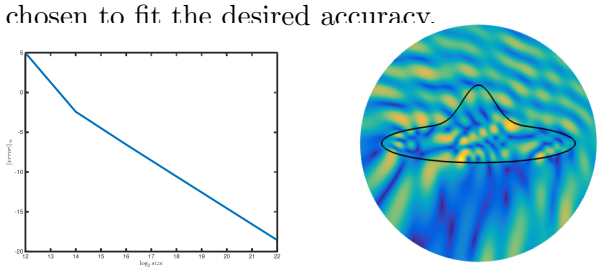

Figure 2: Results.

Preliminary numerical results include the solution of a transmission/scattering problem for D_1 being a submarine-like parametric surface, $k_0 = 10$ and $k_1 = 20e^{-10r^6(r-r_0)^6}$ for $r \leqslant r_0$ and $k = k_0$ for $r > r_0$, where $r_0 = 1.6$. The incident wave is a plane wave impinging at 40°. The interior AP is solved on a rectangular grid, while the exterior AP problem is solved using polar coordinates. In Figure 2 (right), we are showing the absolute value of the solution, and in Figure 2 (left), we are showing the grid convergence on a logarithmic scale. The latter clearly demonstrates fourth order accuracy and thus confirms the theoretical design properties of the method.

References

[1] V. S. Ryaben'kii, "Method of Difference Potentials and Its Applications", *volume 30 of Springer Series in Computational Mathematics, Springer-Verlag, Berlin*, (2002)

[2] M. Medvinsky, "High order numerical simulation of waves using regular grids and non-conforming interfaces", Ph.D. Dissertation Tel Aviv, (2013)

[3] M. Medvinsky, S. Tsynkov, and E. Turkel, "The method of difference potentials for the Helmholtz equation using compact high order schemes", J. Sci. Comput., 53, 150–193, (2012)

Volume integral method for solving scattering problems from locally perturbed periodic layers

H.Haddar[1], **T.P.Nguyen**[1,*]
[1]INRIA Saclay Ile de France/ CMAP, ecole Polytechnique
[*]Email: tpnguyen@cmap.polytechnique.fr

Abstract

We investigate the scattering problem for the case of locally perturbed periodic layer in $\mathbb{R}^2$. Using Floquet-Bloch transform in x_1-direction we reformulate this scattering problem as an equivalent system of coupled volume integral equations. Using periodization in the x_2-direction we apply a spectral method to discretize the problem and compute a numerical approximation of the solution. The convergence of this method is established and numerical validating results are conducted.

Keywords: Floquet-Bloch transform, volume integral formulation, spectral discretization

1 Introduction

The scattering problem that we consider is defined as: Find $u \in H^1(\mathbb{R}^2)$,

$$\Delta u + k^2 n u = f \quad \text{in } \mathbb{R}^2, \tag{1}$$

where $n = n_p$ outside a compact set, $n_p \in L^\infty(\mathbb{R}^2)$ is a periodic function with respect to x_1-variable with period L, $f \in L^2(\mathbb{R}^2)$ is a compactly supported function and the wave number k^2 is complex with positive imaginary part. Some notations will be useful in the sequel: $\Omega_m := [(m-\frac{1}{2})L, (m+\frac{1}{2})L] \times \mathbb{R}$, $H^s_\xi(\Omega_0)$ is closure of C^∞ $\xi-$quasi periodic functions in $\mathbb{R}^2$ with respect to the $H^s(\Omega_0)$ norm. Further assume that $supp(n-n_p) \cup supp(f) \subset \Omega_0 := \mathbb{R} \times [-\frac{1}{2}, \frac{1}{2}]$. Then, after applying the Floquet-Bloch transform to (1) and observing that the Floquet-Bloch transform of $n-n_p$ and f coincide with $n-n_p$ and f (respectively) in Ω_0, we obtain the coupled quasi periodic equations: Find $\tilde{u} \in L^2([-\frac{\pi}{L}, \frac{\pi}{L}], H^1_\xi(\Omega_0))$ such that:

$$\begin{cases} \Delta\tilde{u}(\cdot;\xi) + k^2 n_p \tilde{u}(\cdot;\xi) + k^2(n-n_p)u = f \text{ in } \Omega_0 \\ u = \frac{L}{2\pi}\int_{-\frac{\pi}{L}}^{\frac{\pi}{L}} \tilde{u}(\cdot;\xi)d\xi \end{cases} \tag{2}$$

Thanks to elliptic regularity $\tilde{u}(\cdot;\xi)$ also belongs to $H^2_\xi(\Omega_0)$ and $u(\cdot)$ extended to $\mathbb{R}^2$ by:

$$u(x_1,x_2) := \frac{L}{2\pi}\int_{-\frac{\pi}{L}}^{\frac{\pi}{L}} \tilde{u}(x_1 - mL, x_2; \xi)e^{im\xi L}d\xi$$

$\forall m \in \mathbb{Z}, (x_1,x_2) \in \Omega_m$ is solution to (1).

2 Periodized volume integral equation

We first consider the periodic problem without perturbation ($n = n_p$). Then problem (2) is equivalent to find solution $u_\xi := u(\cdot,\xi) \in H^1_\xi(\Omega_0)$ to:

$$\Delta u_\xi + k^2 n_p u_\xi = f \quad \text{in } \Omega_0. \tag{3}$$

Let $h > 0$ such that $n_p - 1 = f = 0$ in $\{|x_2| > h\}$ and set $\Omega_0^h := [-\frac{L}{2}, \frac{L}{2}] \times [-h, h]$. Let $G_\xi(\cdot) \in L^2(\mathbb{R}^2)$ be the Green's function to the $\xi-$quasi-periodic Helmholtz equation in $\mathbb{R}^2$ and define the volume potential

$$V_\xi f(\cdot) = \int_{\Omega_0^h} G_\xi(\cdot - y)f(y)dy, x \in \mathbb{R}^2. \tag{4}$$

Then V_ξ is bounded from $L^2(\Omega_0^h)$ into $H^2_\xi(\Omega_0)$ and for all $f \in L^2(\Omega_0^h)$, the potential $u := V_\xi f \subset H^2_\xi(\Omega_0)$ is the unique $\xi-$quasi-periodic solution to: $\Delta u + k^2 u = -f$ in Ω_0. Solving (3) is equivalent to solving the following volume integral equation in $L^2(\Omega_0^h)$:

$$u_\xi = k^2 V_\xi((n_p - 1)u_\xi) - V_\xi f_\xi. \tag{5}$$

To find a numerical solution using spectral element method as in [2], we consider G^R_ξ which is $\xi-$quasi periodic in x_1 and $2R-$periodic in x_2, $R > 2h$ such that $G^R_\xi(x) = G_\xi(x)$, $\forall x = (x_1,x_2) \in \mathbb{R} \times (-R, R)$, then define the periodized volume potential $V_{\xi,per}$ as in (4) with G_ξ replaced with G^R_ξ. The solution to the periodized integral equation in $L^2(\Omega_0^R)$, where $\Omega_0^R := [-\frac{L}{2}, \frac{L}{2}] \times [-R, R]$:

$$u_\xi = k^2 V_{\xi,per}((n_p - 1)u_\xi) - V_{\xi,per} f_\xi \tag{6}$$

coincides with the solution to (5) in Ω_0^h. Define the trigonometric orthogonal basis $\{\varphi^j_\xi := \frac{1}{\sqrt{LR}}\exp\left(i\left(\xi + \frac{2\pi}{L}j_1\right)x_1 + i\frac{\pi}{R}j_2x_2\right), j = (j_1,j_2) \in \mathbb{Z}^2\}$ and the finite dimensional space $\mathcal{T}^N_\xi := span\{\varphi^j_\xi, j \in \mathbb{Z}^2_N\}$, where $\mathbb{Z}^2_N := \{j \in \mathbb{Z}^2 | -\frac{N_1}{2}+1 \le j_1 \le \frac{N_1}{2}, -\frac{N_2}{2}+1 \le j_2 \le \frac{N_2}{2}\}$. Then a numerical approximation $u^N_\xi \in \mathcal{T}^N_\xi$ to

problem (6) can be computed using spectral element discretization and FFT based-iterative scheme by solving:

$$\left\langle u_\xi^N - k^2 V_{\xi,per}\left((n_p-1)u_\xi^N\right), v_\xi^N\right\rangle_{L^2(\Omega_0^R)} = \left\langle -V_{\xi,per} g_\xi, v_\xi^N\right\rangle_{L^2(\Omega_0^R)},\ \forall v_\xi^N \in \mathcal{T}_\xi^N.$$

Theorem 1 *There exists an integer $N_0 > 0$ and a positive constant $C > 0$ that are independent of ξ such that, $\forall N > N_0$:*

$$\|u_\xi - u_\xi^N\|_{L^2(\Omega_0^R)} \leq C \inf_{v_\xi^N \in T_\xi^N} \|u_\xi - v_\xi^N\|_{L^2(\Omega_0^R)}.$$

3 Discretization of the locally perturbed periodic problem

We first consider the discretization of problem (2) with respect to the Floquet-Bloch variable using M sub-intervals of size $\Delta\xi = \frac{2\pi}{ML}$. Defining $\xi_j = j\Delta, \xi\ j = -\frac{M}{2}\ \cdots\ \frac{M}{2}$, we obtain the following system of coupled equations: Find $u_{\xi_j,M} \in H^1(\Omega_0^h),\ j = -\frac{M}{2}+1\ \cdots\ \frac{M}{2}$ such that:

$$\begin{cases} u_{\xi_j,M} - k^2 V_{\xi_j}((n_p-1)u_{\xi_j,M}) - \\ k^2 V_{\xi_j}((n-n_p)u_M) = -V_{\xi_j}(f) \text{ in } L^2(\Omega_0^R), \\ u_M = \frac{1}{M}\sum_{j=-\frac{M}{2}+1}^{\frac{M}{2}} u_{\xi_j,M}. \end{cases} \tag{7}$$

One can prove that extending $u_{\xi_j,M}$ by ξ_j- quasi periodicity to $\mathbb{R}^2$ defines through the second equation in (7) a function $u_M \in H^1(\Omega_M)$ which is ML periodic and satisfies equation (1) in Ω_M. Then using the exponential decay of the solution with respect to $|x|$ (see for instance [1]), we have the following theorem.

Theorem 2 *There exists a constant $C > 0$ independent of M and $\tau > 0$ such that*

$$\|u - u_M\|_{H^1(\Omega_M)} \leq Ce^{-\tau ML}\|e^{\tau|x|}u\|_{H^1(\Omega_M)}. \tag{8}$$

Now we discretize the M coupled problems in space using spectral element method as in Section 2, i.e., find $u_{\xi_j,M}^N \in \mathcal{T}_{\xi_j,M}^N$ solution to:

$$\begin{cases} \left\langle u_{\xi_j,M}^N - k^2 V_{\xi_j,per}\left((n_p-1)u_{\xi_j,M}^N\right), v_{\xi_j,M}^N\right\rangle_{L^2} \\ -k^2\left\langle V_{\xi_j,per}\left((n-n_p)(\Delta\xi\sum_l u_{\xi_l,M}^N\right), v_{\xi_j,M}^N\right\rangle_{L^2} \\ = \left\langle -V_{\xi,per} g_\xi, v_\xi^N\right\rangle_{L^2},\ \forall v_\xi^N \in \mathcal{T}_\xi^N, \\ u_N^M := \frac{1}{M}\sum_{l=-\frac{M}{2}+1}^{\frac{M}{2}} u_{\xi_l,M}^N, \end{cases} \tag{9}$$

where $\mathcal{T}_{\xi_j,M}^N$ is defined similarly to $\mathcal{T}_\xi^N$. Then, one can also prove (with involved calculations) that extending $u_{\xi_j,M}^N$ by ξ_j- quasi periodicity to $\mathbb{R}^2$ defines through the second equation of (9) a function u_M^N which is ML periodic. We then prove:

Theorem 3 *For all $M > 0$, there exists $N_0(M) \in \mathbb{N}$ and $C > 0$ independent of M and N such that $\forall N = (N_1, N_2), N_1, N_2 > N_0$:*

$$\|u_M - u_M^N\|_{L^2(\Omega_M^R)} \leq C\left(\frac{1}{MN_1} + \frac{1}{N_2}\right)\|f\|_{L^2(\Omega_0^h)}.$$

4 A numerical example

We just present here a preliminary validating example by comparing the solution obtained by our algorithm (Fig. (b)) with the solution obtained by the Finite Element software FreeFem (Fig. (a)).

The index of refraction inside the squares is $n = 3$, $k = 1 + 0.1i$, $L = 2\pi$. We used $M = 14$, $N_1 = 2^8$ and $N_2 = 2^9$. The incident field is a point source at $x^0 = (0, 5\pi)$.

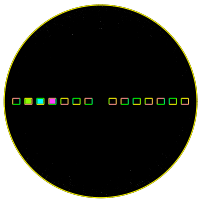

Mesh for FreeFem solution

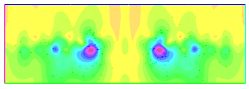

(a)

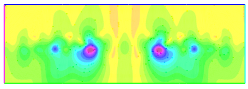

(b)

References

[1] J. Coatléven, Helmholtz equation in periodic media with a line defect, in *J. Comput. Phys.* **231**, 2012, pp. 1675–1704.

[2] A. Lechleiter, D.-L. Nguyen, A trigonometric Galerkin method for volume integral equations arising in TM grating scattering, in *Adv. Comput. Math.* **40**, 2014, pp.1–25.

Improvement of the Foldy-Lax model for three dimensional multiple scattering by small obstacles.

Pierre-Henri Cocquet[1,*], **Abderrahmane Bendali**[2], **Sébastien Tordeux**[3]

[1]PIMENT, Université de la Réunion, 2 rue Joseph Wetzell, 97490 Sainte-Clotilde.

[2]INSA - Département de Génie Mathématique 145, avenue de Rangueil, 31077 Toulouse.

[3]INSA - Département de Génie Mathématique Project-Team Magique 3D, INRIA and University of Pau, Avenue de l'Université, 64013 Pau.

[*]Email: Pierre-Henri.Cocquet@univ-reunion.fr

Abstract

This paper deals with multiple scattering of time-harmonic scalar wave by obstacles whose size is small compared to the wavelength. One way to tackle this problem is to use the heuristic Foldy-Lax model which allows to recast the problem as a linear system. We compute an asymptotic expansion by means of matched asymptotic techniques, with respect to the size of the objects, that gives a justification of this model. Finally, it is shown how this model can be improved.

Keywords: Multi-scattering, Foldy-Lax model.

1 Introduction

Let $\mathcal{O}_j$ be N obstacles, with Lipshitz boundary, whose characteristic size is a small positive adimensional parameter δ. The multiple scattering problem reads as follow:

$$\begin{cases} (\Delta+\kappa^2)u_\delta = 0 \text{ in } \mathbb{R}^3 \setminus \cup_{j=1}^N \overline{\mathcal{O}_j}, \\ u_\delta = 0 \text{ on } \partial\mathcal{O}_j, \\ \left(\partial_{|x|} - i\kappa\right)(u_\delta - u_{\text{inc}}) = o(1/|x|), \end{cases} \tag{1}$$

where $u_{\text{inc}}(x) = \exp(i\kappa \mathbf{d}\cdot x/|x|)$ is a plane wave propagating in the direction of the unit vector $\mathbf{d}$ and κ is the wavenumber.

The Foldy-Lax model (see [4]) consists in replacing u_δ by a superposition of u_{inc} and N unknown monopoles located at a point $c_j \in \mathcal{O}_j$ called the *center of phase*:

$$\begin{array}{l} u_\delta^{\text{FL}}(x) = u_{\text{inc}}(x) + \sum_{l=1}^N A^{(l)} h_0(\kappa|x-c_l|), \\ A^{(j)} = \mathrm{i}\kappa\delta\sigma_0^{(j)}(u_{\text{inc}}(c_j) + \sum_{l\neq j} A^{(l)} h_0(\kappa|c_j-c_l|)), \end{array} \tag{2}$$

where $\sigma_0^{(j)}$ are the so-called scattering coefficient and h_n are the spherical Hankel functions.

The justification of this model has been done using Fourier series in 2D [2], with integral equation in 3D [5] and an extended Foldy-Lax model including dipoles and self-interaction effects can be found in [3]. The main drawback of these works is that the error estimates are based on a 1st-order asymptotic expansion. The multiple scattering effects are thus neglected so only first-order Born approximations are involved and there is no gain solving Foldy's system.

In this paper, we compute a full asymptotic expansion of the multiple scattering problem and next propose an improvement of (2). This allows to set the c_j in a non arbitrary fashion and also introduce self interaction terms. Multiple interactions are then really taken into account leading to an additional order of convergence.

2 Matched asymptotic expansion

To compute an asymptotic expansion of u_δ, we use the method of matched asymptotic expansions [1]. An outer expansion describing the field outside all the small obstacles is then defined

$$u_\delta(x) = u_{\text{inc}}(x) + \delta u_1(x) + \delta^2 u_2(x) + \cdots,\ x \neq c_j.$$

One also needs N inner expansions giving the behavior in the vicinity of each $\mathcal{O}_j$. They depend on the fast variable $X = (x-c_j)/\delta$ and are found through the identification

$$u_\delta(c_j + \delta X) = \Pi_0(X) + \delta\Pi_1(X) + \cdots.$$

Note that the inner fields Π_j are defined on the exterior of a scaled obstacle $\widehat{\mathcal{O}_j}$. The matching conditions are obtained according to the Van Dicke principle saying that the inner and outer expansions are related to the same function. The above expansions are determined by replacing them in (1) and identifing terms having same power of δ.

Theorem 1 *([1] p.32) The matched asymptotic expansion exists at any order. Let $\mathcal{U}$ be a bounded domain such that* $\inf_j \operatorname{dist}(c_j,\mathcal{U}) = \gamma > 0$*, then one has the optimal error estimates*

$$\|u_\delta - u_{\text{inc}} - \sum_{n=1}^{k} u_n\|_{H^1(\mathcal{U})} \leq C\delta^{k+1}.$$

3 Improvement of the Foldy-Lax model

Foldy's model and its improvement are based on the explicit determination of the second order outer expansion. The latter is obtained with the solution to the problems

$$\begin{cases} \Delta\Phi^{(j)} = 0, \text{ in } \widehat{\mathcal{O}_j}^c, \\ \Phi^{(j)} = 0, \text{ on } \partial\widehat{\mathcal{O}_j}^c, \\ \Phi^{(j)}(X) = 1 + o(1) \end{cases} \quad \begin{cases} \Delta\Lambda^{(j)} = 0, \text{ in } \widehat{\mathcal{O}_j}^c, \\ \Lambda^{(j)} = 0, \text{ on } \partial\widehat{\mathcal{O}_j}^c, \\ \Lambda^{(j)}(X) = X + o(1). \end{cases}$$

Using integral representation together with asymptotic expansion of the Laplace Green kernel, one can compute the terms in the expansions

$$\Phi^{(j)}(X) = 1 + \frac{\sigma_0^{(j)}}{|X|} + \frac{\sigma_1^{(j)}}{|X|^3} + O(|X|^{-3}),$$
$$\Lambda^{(j)}(X) = X + \frac{\boldsymbol{S}_0^{(j)}}{|X|} + O(|X|^{-2}).$$

The first outer coefficient is then given by a superposition of monopoles located at c_j [1] p.39

$$u_1(x) = \sum_{j=1}^{N} \mathrm{i}\kappa\sigma_0^{(j)} u_{\mathrm{inc}}(c_j) h_0(\kappa|x - c_j|).$$

$u_{\mathrm{inc}} + \delta u_1$ then coincides with the first order expansion of u_δ^{FL}, see (2). From theorem 1, we infer the justification of the usual Foldy's model with error $O(\delta^2)$.

To improve the Foldy's model, one needs u_2, see [1] p.43. It is given by $u_2(x) =$

$$\sum_{j=1}^{N} [i\kappa^2 u_0(c_j)\, h_1^{(1)}(\kappa|x - c_j|)\, \boldsymbol{\sigma}_1^{(j)} \cdot \tfrac{x-c_j}{|x-c_j|} + i\kappa\sigma_0^{(j)} \left(\begin{array}{c} \sum_{\substack{\ell=1 \\ \ell\neq j}}^{N} i\kappa\sigma_0^{(\ell)} u_0(c_\ell)\, h_0^{(1)}(\kappa\delta|c_j - c_\ell|) \\ + i\kappa\sigma_0^{(j)} u_0(c_j) + \boldsymbol{\nabla} u_0(c_j) \cdot \boldsymbol{S}_0^{(j)} \end{array} \right) \times h_0^{(1)}(\kappa|x - c_j|)].$$

The main idea is to consider a correction of the center of phase, instead of chosing arbitrary c_j , hence replacing them by

$$c_j^{\mathrm{cor}} = c_j + \frac{\delta}{\sigma_0^{(j)}} \sigma_1^{(j)}.$$

Green's identity gives that $\sigma_0^{(j)} \neq 0$ so c_j^{cor} are well-defined. With c_j^{cor}, one gets ([1] p.37)

$$\sigma_0^{(j)} \text{ unchanged, } \sigma_1^{(j)} = 0 \text{ and } \boldsymbol{S}_0^{(j)} = 0. \quad (3)$$

The improved Foldy-Lax model is then

$$u_\delta^{\mathrm{IFL}}(x) = u_{\mathrm{inc}}(x) + \sum_{l=1}^{N} A^{(l)} h_0(\kappa|x - c_l^{\mathrm{cor}}|),$$

$$A^{(j)} = \frac{\mathrm{i}\kappa\delta\sigma_0^{(j)}}{1 - \mathrm{i}\kappa\delta\sigma_0^{(j)}} \times \left(u_{\mathrm{inc}}(c_j^{\mathrm{cor}}) + \sum_{l\neq j} A^{(l)} h_0(\kappa|c_j^{\mathrm{cor}} - c_l^{\mathrm{cor}}|) \right),$$

Using (3), we see that the 2nd order expansion of the u_δ^{IFL} coicides with $u_{\mathrm{inc}} + \delta u_1 + \delta^2 u_2$. Theorem 1 then gives that the error of the improved Foldy's model is $O(\delta^3)$.

References

[1] A. Bendali, P.H. Cocquet, Sébastien Tordeux, *Approximation by multipoles of the multiple scattering by small obstacles in three dimensions and application to the Foldy theory of isotropic scattering*, In revision.

[2] M. Cassier, C. Hazard, *Multiple scattering of acoustic waves by small sound-soft obstacles in two dimensions: mathematical justification of the Foldy–Lax model*, Wave Motion, 50.1, p. 18-28, 2013.

[3] J. Liao, J. Chao, *Extended Foldy–Lax Approximation on Multiple Scattering*, Mathematical Modelling and Analysis, 19.1, p. 85-98, 2014.

[4] P.A. Martin, *Multiple scattering: interaction of time-harmonic waves with N obstacles*, No. 107, Cambridge University Press, 2006.

[5] D.P. Challa, M. Sini, *On the Justification of the Foldy–Lax Approximation for the Acoustic Scattering by Small Rigid Bodies of Arbitrary Shapes*, Multiscale Modeling and Simulation, 12.1, p.55-108, 2014.

Locally Implicit Time Integration for Linear Maxwell's Equations

Marlis Hochbruck[1], **Andreas Sturm**[1,*]

[1] Institute for Applied and Numerical Analysis, Karlsruhe Institute of Technology, Germany

*Email: andreas.sturm@kit.edu

Abstract

An attractive feature of discontinuous Galerkin (DG) spatial discretizations of the Maxwell's equations is their ability to handle complex geometries by using unstructured, possibly locally refined meshes. Furthermore, DG methods lead to block diagonal mass matrices which in combination with an explicit time integrator allow for a fully explicit scheme. However, such explicit approaches require a constraint on the time step size related to the diameter of the smallest mesh element to ensure stability. A natural way to overcome this restriction is to use implicit time integrators. The drawback of such methods is that they require the solution of a large linear system in each time step.

If only a small part of the grid contains tiny elements, the combination of the both upper approaches provides a promising alternative for the time integration. These so called locally implicit methods have been considered in [1,2], for instance.

In this talk we will present an error analysis for the full discretization of locally implicit methods for linear Maxwell's equations based on a variational formulation and energy techniques.

Keywords: Maxwell equations, locally implicit schemes, error analysis, full discretization, discontinuous Galerkin methods

1 Linear Maxwell's Equations

The Maxwell's equations for linear isotropic materials are given by

$$\begin{aligned} \partial_t(\mu\mathbf{H}) &= -\operatorname{curl}\mathbf{E}, & \operatorname{div}(\mu\mathbf{H}) &= 0, \\ \partial_t(\varepsilon\mathbf{E}) &= \operatorname{curl}\mathbf{H} - \mathbf{J}, & \operatorname{div}(\varepsilon\mathbf{E}) &= \rho, \end{aligned} \tag{1}$$

for $x \in \Omega$, $t > 0$. Here, $\mathbf{E}(t,x)$, $\mathbf{H}(t,x) \in \mathbb{R}^3$ denote the electric and magnetic fields, $\mu(x)$ and $\varepsilon(x) \in \mathbb{R}$ denote the electric permittivity and magnetic permeability, respectively. Moreover, $\mathbf{J}(t,x) \in \mathbb{R}^3$ is the electric current density, and $\rho(t,x) \in \mathbb{R}$ is the electric charge density. These equations are complemented with initial conditions $\mathbf{H}_0(x)$, $\mathbf{E}_0(x) \in \mathbb{R}^3$ and metallic boundary conditions $(n \times \mathbf{E})|_{\partial\Omega} = 0$.

2 Space Discretization

We discretize (1) in space using the DG method with central fluxes and with polynomial order k. This leads to the semidiscrete problem

$$\begin{aligned} \partial_t\mathbf{H}_h &= -\mathbf{C}_E\mathbf{E}_h, \\ \partial_t\mathbf{E}_h &= \mathbf{C}_H\mathbf{H}_h - \mathbf{J}_h, \end{aligned} \tag{2}$$

where $\mathbf{C}_E$ and $\mathbf{C}_H$ denote the discretized curl operators. It is well-known that these operators are adjoint w.r.t. the weighted $L^2(\Omega)$-inner products with weights ε and μ, i.e.

$$(\mathbf{C}_H\mathbf{H}_h, \mathbf{E}_h)_\varepsilon = (\mathbf{H}_h, \mathbf{C}_E\mathbf{E}_h)_\mu. \tag{3}$$

3 Time Discretization

In order to obtain a fully discrete scheme we further have to integrate (2) in time. Employing an explicit time integration scheme, e.g., the *leap frog scheme*

$$\begin{aligned} \mathbf{H}_h^{n+1/2} - \mathbf{H}_h^n &= -\tfrac{\tau}{2}\mathbf{C}_E\mathbf{E}_h^n, \\ \mathbf{E}_h^{n+1} - \mathbf{E}_h^n &= \tau\mathbf{C}_H\mathbf{H}_h^{n+1/2} - \tfrac{\tau}{2}(\mathbf{J}_h^{n+1} + \mathbf{J}_h^n), \\ \mathbf{H}_h^{n+1} - \mathbf{H}_h^{n+1/2} &= -\tfrac{\tau}{2}\mathbf{C}_E\mathbf{E}_h^{n+1}, \end{aligned}$$

requires a severe restriction on the time step size τ in order to guarantee stability. In fact, we cannot use step sizes larger than $\tau \sim h_{\min}$, where $h_{\min}$ denotes the diameter of the smallest mesh element (CFL condition).

This constraint can be overcome by using an implicit scheme, for instance the *Crank–Nicolson method*

$$\begin{aligned} \mathbf{H}_h^{n+1/2} - \mathbf{H}_h^n &= -\tfrac{\tau}{2}\mathbf{C}_E\mathbf{E}_h^n, \\ \mathbf{E}_h^{n+1} - \mathbf{E}_h^n &= \tfrac{\tau}{2}\mathbf{C}_H(\mathbf{H}_h^{n+1} + \mathbf{H}_h^n) \\ &\quad - \tfrac{\tau}{2}(\mathbf{J}_h^{n+1} + \mathbf{J}_h^n), \\ \mathbf{H}_h^{n+1} - \mathbf{H}_h^{n+1/2} &= -\tfrac{\tau}{2}\mathbf{C}_E\mathbf{E}_h^{n+1}. \end{aligned}$$

However, this requires the solution of a large linear system for $\mathbf{E}_h^{n+1}$ in each time step.

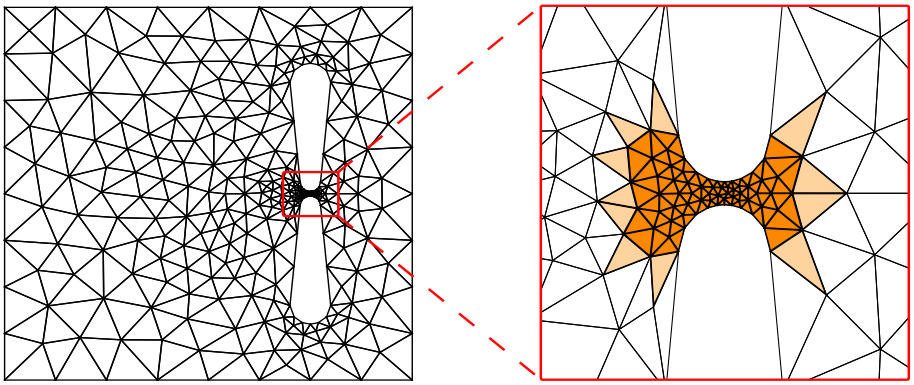

Figure 1: Locally refined mesh. The dark orange elements indicate the fine part of the mesh, the light orange elements their neighbors. Orange elements are treated implicitly, white elements explicitly.

4 Locally Implicit Scheme

We consider the case where the spatial mesh contains only a small number of tiny elements, see Figure 1 for an example. Unfortunately, even one single tiny element requires using very small time steps for the time integration of an explicit scheme. In [1] Verwer suggested to tackle this problem by blending an explicit with an implicit time integration method. In fact, he proposed to apply the Crank–Nicolson method on the tiny elements and to use the leap frog scheme on the coarse elements. His work is based on a matrix formulation of the discretization (treating the problem as a system of ordinary differential equations) and not on a variational approach. Hence it also did not consider meshes or space discretization errors, which turns out to be indispensable for the error analysis of the fully discrete scheme.

In order to realize Verwer's idea in the context of DG methods we use indicator functions χ_i and χ_e to assign the mesh elements to the implicitly and explicitly treated parts, respectively. It turns out that besides the small mesh elements we also have to treat their direct neighbors implicitly, see Figure 1, where the light orange elements belong to the coarse mesh but are treated implicitly.

We define discretized split operators by

$$\mathbf{C}_H^i := \mathbf{C}_H \circ \chi_i, \qquad \mathbf{C}_H^e := \mathbf{C}_H \circ \chi_e,$$
$$\mathbf{C}_E^i := \chi_i \circ \mathbf{C}_E, \qquad \mathbf{C}_E^e := \chi_e \circ \mathbf{C}_E.$$

This decomposition was done such that $\mathbf{C}_H = \mathbf{C}_H^e + \mathbf{C}_H^i$, $\mathbf{C}_E = \mathbf{C}_E^e + \mathbf{C}_E^i$ and that (3) is inherited, i.e.

$$(\mathbf{C}_H^b \mathbf{H}_h, \mathbf{E}_h)_\varepsilon = (\mathbf{H}_h, \mathbf{C}_E^b \mathbf{E}_h)_\mu, \quad b \in \{e, i\}.$$

The resulting *locally implicit time integrator* reads

$$\begin{aligned}
\mathbf{H}_h^{n+1/2} - \mathbf{H}_h^n &= -\tfrac{\tau}{2}\mathbf{C}_E \mathbf{E}_h^n, \\
\mathbf{E}_h^{n+1} - \mathbf{E}_h^n &= \tfrac{\tau}{2}\mathbf{C}_H^i(\mathbf{H}_h^{n+1} + \mathbf{H}_h^n) \\
&\quad + \tau \mathbf{C}_H^e \mathbf{H}_h^{n+1/2} - \tfrac{\tau}{2}(\mathbf{J}_h^{n+1} + \mathbf{J}_h^n), \\
\mathbf{H}_h^{n+1} - \mathbf{H}_h^{n+1/2} &= -\tfrac{\tau}{2}\mathbf{C}_E \mathbf{E}_h^{n+1}.
\end{aligned}$$

This scheme can be implemented very efficiently, see [1, 2] for numerical examples.

Our main result is the following.

Theorem 1 *The locally implicit method is stable under a CFL condition depending on the coarse mesh only. It converges of order k in space and two in time with constants being independent of the mesh sizes of the fine mesh.*

The proof is based on an energy technique [3] and the properties of the splitted operators.

References

[1] J. G. Verwer, Component splitting for semi-discrete Maxwell equations, *BIT*, 51(2), pp. 427–445, 2011.

[2] S. Descombes, S. Lanteri, and L. Moya, Locally implicit time integration strategies in a discontinuous Galerkin method for Maxwell's equations, *J. Sci. Comput.*, 56(1), pp. 190–218, 2013.

[3] M. Hochbruck and T. Pažur, Implicit Runge–Kutta methods and discontinuous Galerkin discretizations for linear Maxwell's equations, *SIAM J. Numer. Anal.*, 53(1), pp. 485–507, 2015.

Fourth order energy-preserving locally implicit discretization for linear wave equations

Juliette Chabassier[1,*], **Sébastien Imperiale**[2]

[1]Magique3D Team, Inria Bordeaux Sud Ouest, University of Pau and Pays de l'Adour, Pau, France.
[2]M3DISIM Team, Inria Saclay, Palaiseau, France

[*]Email: juliette.chabassier@inria.fr

Abstract

A family of fourth order locally implicit schemes is presented as a special case of fourth order coupled implicit schemes for linear wave equations. The domain of interest is decomposed into several regions where different (explicit or implicit) fourth order time discretization are used. The coupling is based on a Lagrangian formulation on the boundaries between the several non conforming meshes of the regions. Fourth order accuracy follows from global energy identities. Numerical results in 1d and 2d illustrate the good behavior of the schemes and their potential for the simulation of realistic highly heterogeneous media or strongly refined geometries, for which using everywhere an explicit scheme can be extremely penalizing. Fourth order accuracy reduces the numerical dispersion inherent to implicit methods used with a large time step, and makes this family of schemes attractive compared to classical approaches.

Keywords: High-order numerical methods, Time discretization, Locally implicit schemes.

1 Continuous system

We want to solve for time $t > 0$, the system (closed with Neumann homogeneous boundary conditions):

$$\begin{cases} \partial_t^2 u_0 - \nabla \cdot c^2(\mathbf{x})\,\nabla u_0 = s_0 \ \text{ in } \Omega_0, & \text{(1a)} \\ c^2(\mathbf{x})\,\nabla u_0 \cdot \mathbf{n}_0 = \lambda \qquad \text{on } \Gamma, & \text{(1b)} \\ \partial_t^2 u_1 - \nabla \cdot c^2(\mathbf{x})\,\nabla u_1 = s_1 \ \text{ in } \Omega_1, & \text{(1c)} \\ c^2(\mathbf{x})\,\nabla u_1 \cdot \mathbf{n}_1 = -\lambda \qquad \text{on } \Gamma, & \text{(1d)} \\ u_0 = u_1 \quad \text{on } \Gamma & \text{(1e)} \end{cases}$$

in a domain Ω composed by disjoint sets $\Omega = \Omega_0 \cup \Omega_1$ separated by $\Gamma = \overline{\Omega_0} \cap \overline{\Omega_1}$. s_0 and s_1 are given source terms, and $c(\mathbf{x}) > c_0 > 0$ is the inhomogeneous velocity of the waves. Any solution to (1) satisfies the energy identity:

$$\frac{d\mathcal{E}_{01}}{dt} = \int_{\Omega_0} s_0\,\partial_t u_0 + \int_{\Omega_1} s_1\,\partial_t u_1, \text{ where}$$
$$\mathcal{E}_{01} = \frac{1}{2}\,\|\partial_t u_0\|^2_{L^2(\Omega_0)} + \frac{1}{2}\,\|\partial_t u_1\|^2_{L^2(\Omega_1)} + \frac{1}{2}\,\|c\,\nabla u_0\|^2_{L^2(\Omega_0)} + \frac{1}{2}\,\|c\,\nabla u_1\|^2_{L^2(\Omega_1)} \quad (2)$$

2 Semi discrete system

We consider spatial meshes of Ω_0 and Ω_1 upon which are based finite dimensional finite element spaces: $\mathcal{V}_{h,0} \subset H^1(\Omega_0)$, $\mathcal{V}_{h,1} \subset H^1(\Omega_1)$ and $\Gamma_h \subset H^{-1/2}(\Gamma)$. One have leeway in the choice of $(\mathcal{V}_{h,0}, \mathcal{V}_{h,1})$ after which Γ_h must be chosen so that an inf-sup type condition is satisfied, see [1, 3, 4]. $(\widetilde{U}_{h,0}, \widetilde{U}_{h,1}, \widetilde{\Lambda}_h)$ is the solution of:

$$\begin{cases} d_t^2 M_{h,0}\widetilde{U}_{h,0} + K_{h,0}\widetilde{U}_{h,0} - {}^tC_{h,0}\widetilde{\Lambda}_h = M_{h,0}\widetilde{S}_{h,0} & \text{(3a)} \\ d_t^2 M_{h,1}\widetilde{U}_{h,1} + K_{h,1}\widetilde{U}_{h,1} + {}^tC_{h,1}\widetilde{\Lambda}_h = M_{h,1}\widetilde{S}_{h,1} & \text{(3b)} \\ C_{h,0}\,\widetilde{U}_{h,0} = C_{h,1}\,\widetilde{U}_{h,1} & \text{(3c)} \end{cases}$$

A semi discrete energy identity can be obtained.

$$\frac{d\mathcal{E}_{01,h}}{dt} = M_{h,0}\widetilde{S}_{h,0} \cdot d_t\widetilde{U}_{h,0} + M_{h,1}\widetilde{S}_{h,1} \cdot d_t\widetilde{U}_{h,1},$$

where

$$\mathcal{E}_{01,h} = \frac{1}{2}\|d_t\widetilde{U}_{h,0}\|^2_{M_{h,0}} + \frac{1}{2}\|d_t\widetilde{U}_{h,1}\|^2_{M_{h,1}} + \frac{1}{2}\|\widetilde{U}_{h,0}\|^2_{K_{h,0}} + \frac{1}{2}\|\widetilde{U}_{h,1}\|^2_{K_{h,1}} \quad (4)$$

where $\|X\|^2_M = MX \cdot X$ for any nonnegative matrix M. In the following, I_h will denote the identity matrix.

3 Discrete system

The proposed numerical discretization is based on the following definitions:

$$D^2_{\Delta t}U^n_h := \left(U^{n+1}_h - 2U^n_h + U^{n-1}_h\right)/\Delta t^2$$
$$\{U_h\}^n_\theta := \theta\,U^{n+1}_h + (1-2\theta)U^n_h + \theta\,U^{n-1}_h$$

The consistency analysis of the fourth order family of schemes [2] applied to each equation of system (3) instigates the following scheme:

$$\begin{cases} M_{h,0} D^2_{\Delta t} U^n_{h,0} + K_{h,0}\{U_{h,0}\}^n_{\theta_0} - {}^tC_{h,0}\Pi^n_h = M_{h,0}\, S^n_{h,0} \\ +\Delta t^2 \alpha_0 K_{h,0} M^{-1}_{h,0} \left[-K_{h,0}\{U_{h,0}\}^n_{\varphi_0} + {}^tC_{h,0}\Pi^n_h\right] \quad (5a) \\ \\ M_{h,1} D^2_{\Delta t} U^n_{h,1} + K_{h,1}\{U_{h,1}\}^n_{\theta_1} + {}^tC_{h,1}\Pi^n_h = M_{h,1}\, S^n_{h,1} \\ +\Delta t^2 \alpha_1 K_{h,1} M^{-1}_{h,1} \left[-K_{h,1}\{U_{h,1}\}^n_{\varphi_1} - {}^tC_{h,1}\Pi^n_h\right] \quad (5b) \\ \\ C_{h,0}\, \dfrac{U^{n+1}_{h,0} - U^{n-1}_{h,0}}{2\Delta t} - C_{h,1}\, \dfrac{U^{n+1}_{h,1} - U^{n-1}_{h,1}}{2\Delta t} = 0 \quad (5c) \end{cases}$$

where $\alpha_i = \theta_i - 1/12$. Any solution to (5) satisfies the energy identity:

$$\frac{\mathcal{E}^{n+1/2}_{01,4,h} - \mathcal{E}^{n-1/2}_{01,4,h}}{\Delta t} = \widetilde{I}^{-1}_{h,0}\, M_{h,0}\, S^n_{h,0} . \frac{U^{n+1}_{h,0} - U^{n-1}_{h,0}}{2\Delta t} + \widetilde{I}^{-1}_{h,1}\, M_{h,1}\, S^n_{h,1} \cdot \frac{U^{n+1}_{h,1} - U^{n-1}_{h,1}}{2\Delta t},$$

where the discrete energy reads

$$\mathcal{E}^{n+1/2}_{01,4,h} = \frac{1}{2}\left\| \frac{U^{n+1}_{h,0} - U^n_{h,0}}{\Delta t} \right\|^2_{\widehat{M}_{h,0}} + \frac{1}{2}\left\| \frac{U^{n+1}_{h,1} - U^n_{h,1}}{\Delta t} \right\|^2_{\widehat{M}_{h,1}} + \frac{1}{2}\left\| \frac{U^{n+1}_{h,0} + U^n_{h,0}}{2} \right\|^2_{K_{h,0}} + \frac{1}{2}\left\| \frac{U^{n+1}_{h,1} + U^n_{h,1}}{2} \right\|^2_{K_{h,1}}$$

where the modified mass matrices $\widehat{M}_{h,i}$ are defined by $\widehat{M}_{h,i} = \widetilde{I}^{-1}_{h,i}\, \widetilde{M}_{h,i}$ where

$$\begin{cases} \widetilde{I}_{h,i} = I_{h,i} + \Delta t^2 \left(\theta_i - \dfrac{1}{12}\right) K_{h,i}\, M^{-1}_{h,i} \\ \widetilde{M}_{h,i} = M_{h,i} + \Delta t^2 \left(\theta_i - \dfrac{1}{4}\right) K_{h,i} \\ \qquad\qquad + \Delta t^4 \left(\theta_i - \dfrac{1}{12}\right)\left(\varphi_i - \dfrac{1}{4}\right) K_{h,i} M^{-1}_{h,i} K_{h,i} \end{cases}$$

The positivity of the energy can be proven under standard CFL condition that depend on the parameters (θ_i, φ_i). Despite the non standard form of this energy, stability in $L2$-norm can be proved in the case $\theta_i \geq 1/4$ and $\varphi_i \geq 1/4$. $L2$-Stability in the other cases is not proven yet but show good numerical behavior.

A 1d numerical experiment is performed where the segment $[0, 1]$ is cut in two intervals $\Omega_0 = [0, 0.5]$ and $\Omega_1 = [0.5, 1]$. Ω_0 and Ω_1 are respectively divided into 7 and 13 elements. Sixth order spectral elements are implemented. A fourth order explicit scheme is used on Ω_0 ($\theta_0 = \varphi_0 = 0$) while an unconditionally stable implicit scheme is used on Ω_1 ($\theta_1 = \varphi_1 = 1/4$). A gaussian initial condition is set on the left interval and crosses the middle point around time 0.3.

Fig. 1 shows that the energy is preserved up to machine precision. Fig. 2 shows that the coupling of second order implicit and explicit schemes only provides second order accuracy (as expected), while our scheme provides fourth order accuracy.

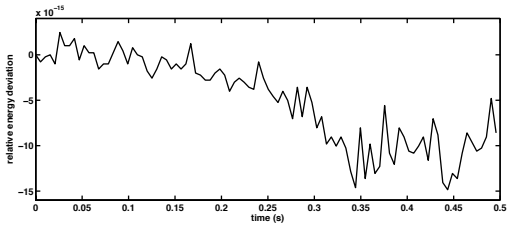

Figure 1: Relative energy deviation

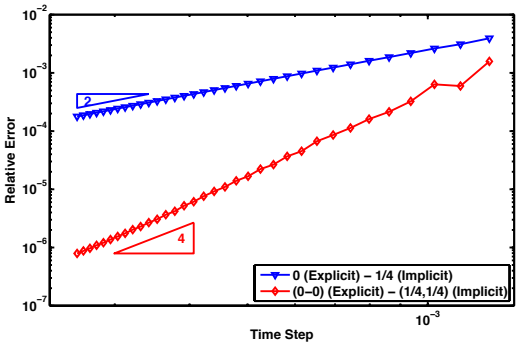

Figure 2: Relative L2 error with the analytical solution as the time step tends to zero.

Numerical illustrations in 2D as well as details about stability and consistency of scheme (5) will be presented at the oral session.

References

[1] E. Becache, P. Joly, J. Rodríguez, Space-time mesh refinement for elastodynamics. Numerical results, *CMAME,* vol. 194 (2-5), pp 355–366, 2005.

[2] J. Chabassier, S. Imperiale. *JCAM*, vol. 245, pp 194–212, 2012.

[3] G. Derveaux, P. Joly, J. Rodriguez Effective computational methods for wave propagation. Chap 13 : Space time mesh refinement methods, *Chapman and Hall/CRC*, 2008.

[4] Y. Maday, C. Mavriplis, A. T. Patera, Nonconforming mortar element methods - Application to spectral discretizations in Domain decomposition methods, *SIAM Philadelphia*, pp 392–418, 1989.

Runge-Kutta type Explicit Local Time-Stepping for Electromagnetics

Marcus J. Grote[1], **Michaela Mehlin**[1,*]
[1]Department of Mathematics and Computer Science, University of Basel, Switzerland
*Email: michaela.mehlin@unibas.ch

Abstract

We propose high-order local time-stepping (LTS) schemes based on explicit Runge-Kutta (RK) methods for the simulation of electromagnetic waves. By using smaller time-steps precisely were the small elements in the mesh are located, these methods overcome the severe stability restrictions caused by local mesh refinement without sacrificing the explicitness, accuracy or efficiency of the original RK method.

Keywords: high-order methods, explicit time integration, local time-stepping, multirate methods, Runge-Kutta methods

1 Introduction

We consider Maxwell's equations

$$\varepsilon\frac{\partial}{\partial t}\mathbf{E} - \nabla\times\mathbf{H} + \sigma\mathbf{E} = \mathbf{j}, \tag{1}$$

$$\mu\frac{\partial}{\partial t}\mathbf{H} + \nabla\times\mathbf{E} = 0, \tag{2}$$

in a linear isotropic medium. Here μ, ε and σ denote the relative magnetic permeability, the relative electric permittivity and the conductivity of the medium, respectively, while the source term $\mathbf{j}$ corresponds to the applied current density. The spatial discretization of (1)-(2) with standard edge finite elements (FE) with mass-lumping or a discontinuous Galerkin (DG) method [5] leads to a system of ordinary differential equations

$$\mathbf{y}'(t) = \mathbf{B}\mathbf{y}(t) + \mathbf{F}(t), \tag{3}$$

where the matrix $\mathbf{B}$ involves the inverse, $\mathbf{M}^{-1}$, of the mass matrix $\mathbf{M}$. Since $\mathbf{M}$ is essentially diagonal, its inverse is explicitly known, and so is $\mathbf{B}$.

Standard explicit numerical methods for the time integration of (3) include explicit Runge-Kutta (RK) and Adams-Bashforth (AB) methods, whose time-step, Δt, is dictated by the smallest elements in the mesh. When mesh refinement is restricted to a small region, using the small time-step Δt on the entire computational domain is generally too high a price to pay.

Various recent methods overcome that geometry induced stability restriction without loss of accuracy by using either smaller time-steps or an implicit scheme, but only where the smallest elements in the mesh are located. Locally implicit methods [1, 6] build on the long tradition of hybrid implicit-explicit (IMEX) algorithms. Unlike locally implicit schemes, multistep based LTS methods [2, 4] remain fully explicit.

2 Time Integration

Here we discuss LTS schemes based on RK methods. Starting from (3) with $\mathbf{F} = 0$ for simplicity, we first split the vector of unknowns $\mathbf{y}$ as

$$\begin{aligned}\mathbf{y}(t) &= (\mathbf{I}-\mathbf{P})\mathbf{y}(t) + \mathbf{P}\mathbf{y}(t)\\ &= \mathbf{y}^{[c]}(t) + \mathbf{y}^{[f]}(t).\end{aligned} \tag{4}$$

In (4), the entries of the diagonal matrix $\mathbf{P}$, equal to zero or one, identify the unknowns associated with the locally refined regions, $\mathbf{y}^{[f]}$; the remaining "coarse" are located in $\mathbf{y}^{[c]}$.

Hence the exact solution of (3) is given by

$$\begin{aligned}\mathbf{y}(t_n+\xi\Delta t) = \mathbf{y}(t_n) &+ \int_{t_n}^{t_n+\xi\Delta t}\mathbf{B}\mathbf{y}^{[c]}(t)\,dt\\ &+ \int_{t_n}^{t_n+\xi\Delta t}\mathbf{B}\mathbf{y}^{[f]}(t)\,dt\,.\end{aligned} \tag{5}$$

To derive an LTS method that overcomes the stringent stability conditions dictated by the smallest elements in the mesh, we shall treat the fine elements differently from the remaining coarser elements. In doing so, we approximate the first integral in (5) by the quadrature formula associated with the RK scheme. In the resulting expression, we approximate the (unknown) values of $\mathbf{y}^{[c]}$ at the quadrature points by Taylor expansion. Differentiation then leads to a modified differential equation, which is solved numerically from t_n to $t_n + \Delta t$ by using a RK method with local time-step $\Delta\tau = \Delta t/p$; here, p denotes the coarse to fine mesh aspect ratio.

In [3] we have proved that the LTS-RK$s(p)$ methods yield the same rate of convergence as the underlying RKs scheme:

Theorem 1 *Starting from a standard explicit RKs method of order k, the corresponding LTS-RKs(p) scheme is k-th order accurate.*

Theorem 2 *For $s = k = 2, 3, 4$ the LTS-RKs(p) scheme is convergent of order k.*

3 Numerical Results

To illustrate the usefulness of LTS-RK methods, we consider (1)-(2) in TM (transverse magnetic) form in two spatial dimensions:

$$\varepsilon \frac{\partial E^z}{\partial t} - \left(\frac{\partial H^y}{\partial x} - \frac{\partial H^x}{\partial y} \right) + \sigma E^z = j,$$
$$\mu \frac{\partial H^x}{\partial t} + \frac{\partial E^z}{\partial y} = 0,$$
$$\mu \frac{\partial H^y}{\partial t} - \frac{\partial E^z}{\partial x} = 0.$$

Next we let the spatial domain Ω be rectangular of size $[0, 3] \times [0, 1]$ adjacent to a roof mounted antenna of thickness 0.01 – see Figure 1. We consider homogeneous source data, PEC boundary conditions, model parameters $\sigma = 0$, $\mu = \varepsilon = 1$ and a Gaussian pulse for E^z as initial condition.

We use $\mathcal{P}^3$ nodal DG FEM [5] in space on a triangular mesh which is highly refined near the antenna, see Figure 1 (top). For the time discretization, we choose the fourth-order LTS-RK4 scheme. Thus, the numerical method is fourth-order accurate both in space and time with respect to the L^2-norm. Since the typical mesh size inside the refined region is about $p = 7$ times smaller than the mesh size in the surrounding coarser region, we take p local time-steps of size $\Delta\tau = \Delta t/p$ for every time-step Δt. In Figure 1 (bottom) we present a snapshot of the electric field E_h^z at time $t = 0.75$.

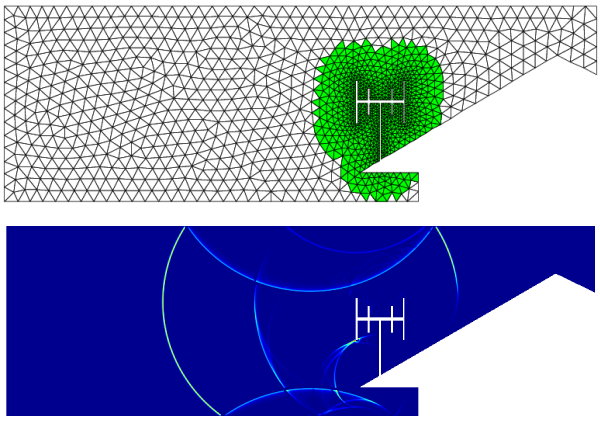

Figure 1: Initial mesh with $h_{fine} \approx h_{coarse}/7$ (top) and E_h^z at time $t = 0.75$ (bottom).

References

[1] S. Descombes, S. Lanteri and L. Moya, Locally implicit time integration strategies in a discontinuous Galerkin method for Maxwell's equations, *J. Sci. Comput.*, **56** (2013), 512–526.

[2] J. Diaz and M. J. Grote, Energy conserving explicit local time-stepping for second-order wave equations, *SIAM J. Sci. Comput.*, **31** (2009), 1985–2014.

[3] M. J. Grote, M. Mehlin and T. Mitkova, Runge-Kutta based explicit local time-stepping methods for wave propagation, *SIAM J. Sci. Comput.*, **37** (2015), A747–A775 .

[4] M. J. Grote and T. Mitkova, High-order explicit local time-stepping methods for damped wave equations, *J. Comput. Appl. Math.*, **239** (2013), 270–289.

[5] J. S. Hesthaven and T. Warburton, *Nodal Discontinuous Galerkin Methods*, Springer, 2008.

[6] A. Kanevsky, M. H. Carpenter, D. Gottlieb and J. S. Hesthaven, Application of implicit-explicit high order Runge-Kutta methods to discontinuous-Galerkin schemes, *J. Comput. Phys.*, **225** (2007), 1753–1781

Multi-Level Runge-Kutta Based Local Time-Stepping for Wave Propagation

Martin Almquist[1,*], **Marcus J. Grote**[2], **Michaela Mehlin**[2]
[1]Department of Information Technology, Uppsala University, Sweden
[2]Department of Mathematics and Computer Science, University of Basel, Switzerland
[*]Email: martin.almquist@it.uu.se

Abstract

Locally refined meshes severely reduce the efficiency of explicit Runge-Kutta (RK) methods for numerical wave propagation, as the maximal time step is dictated by the smallest elements in the mesh. Local time-stepping (LTS) methods circumvent this bottleneck caused by a few small elements by taking small time-steps precisely where the small elements are located. However, when the locally refined region contains a sub-region of even smaller elements, the stability constraint on the local time-step again becomes overly restrictive. To overcome the repeated bottleneck caused by hierarchical mesh refinement, we propose multi-level local time-stepping (MLTS) methods. Starting from classical or low-storage explicit RK methods, we derive explicit MLTS methods of arbitrarily high accuracy. The resulting time-integration schemes retain the high accuracy, stability and efficiency of the underlying RK methods.

Keywords: time-integration, Runge-Kutta methods, multi-level local time-stepping

1 Runge-Kutta based local time stepping

Consider the scalar damped wave equation,

$$u_{tt} + \sigma u_t = \nabla \cdot \left(c^2 \nabla u\right) \qquad \text{in } \Omega \times (0,T), \quad (1)$$
$$u = 0 \qquad \text{on } \partial\Omega \times (0,T)\,, \quad (2)$$

where the damping coefficient $\sigma = \sigma(x)$ is non-negative and the speed of propagation $c = c(x)$ is piecewise smooth and strictly positive. When solving (1)-(2) numerically, local mesh refinement severely decreases the efficiency of explicit time-integration schemes because of the overly small time-step dictated by a few small elements. Local time-stepping (LTS) methods overcome that bottleneck by using smaller time-steps only where the smallest elements are located. In [1], explicit second-order LTS methods for (1)-(2) were derived, which are based on the leap-frog scheme. In the absence of damping, i.e., $\sigma = 0$, these LTS-schemes yield schemes of arbitrarily high order by the modified equation approach. However, when $\sigma > 0$, this approach cannot readily be extended beyond order two. To achieve arbitrarily high accuracy also when damping is present, explicit LTS methods were derived in [2], based on Adams-Bashforth multi-step schemes.

Here, we consider explicit high-order LTS schemes based on classical or low-storage Runge-Kutta (RK) schemes [3]. In contrast to Adams-Bashforth methods, RK methods are one-step methods; hence they do not require a starting procedure and easily accommodate adaptive time-step selection. To facilitate also efficient hierarchical mesh refinement, we propose multi-level LTS-RK (MLTS-RK) methods, which permit the appropriate time-step at each level of mesh refinement.

2 Numerical experiments

To verify the accuracy and stability properties of the MLTS-RK schemes, we consider the 1-D problem defined by (1)-(2) with $\Omega = [0,6]$ and $c = 1$, $\sigma = 0.1$. The initial conditions $u(x,0) = \sin(\pi x)$, $u_t(x,0) = -\frac{\sigma}{2}\sin(\pi x)$ yield the exact solution

$$u(x,t) = e^{-\sigma t/2}\cos\left(\sqrt{\pi^2 - \frac{\sigma^2}{4}}\,t\right)\sin(\pi x)\,.$$

Following the method of lines approach, we discretize (1)-(2) in space using either nodal discontinuous Galerkin, continous finite element, or finite difference methods. In the case of finite difference methods, we opt for Summation-By-Parts–Simultaneous Approximation Term (SBP-SAT) methods [4]. In $\Omega_1 = [0,2]$ we discretize with space-step h. In $\Omega_2 = [2,4]$ and $\Omega_3 = [4,6]$, we refine the grid 2 and 6 times, respectively, such that the space-step is $h/2$ in Ω_2 and $h/6$ in Ω_3. Figure 1 shows the numerical solution obtained with such a grid at time $t = 0.1$. In Ω_1 we choose the time-step Δt as the maximal time-step permitted by the CFL stability condition.

In Ω_2 and Ω_3, we use the local time-steps $\Delta t/2$ and $\Delta t/6$, respectively, i.e., the maximal time-steps allowed by the CFL condition in these regions.

Table 1 shows the L^2-errors compared to the exact solution at the final time $t = 8.7$ for the MLTS methods derived from the classical RK3 and RK4 schemes, here combined with a 4th order SBP-SAT finite difference discretization in space. The expected 3rd and 4th order convergence rates are obtained. Moreover, as the MLTS methods permit the maximal time-step at every level of grid refinement, we conclude that the numerical stability of the underlying RK methods is retained. In that sense, the CFL condition of our MLTS-RK schemes is optimal.

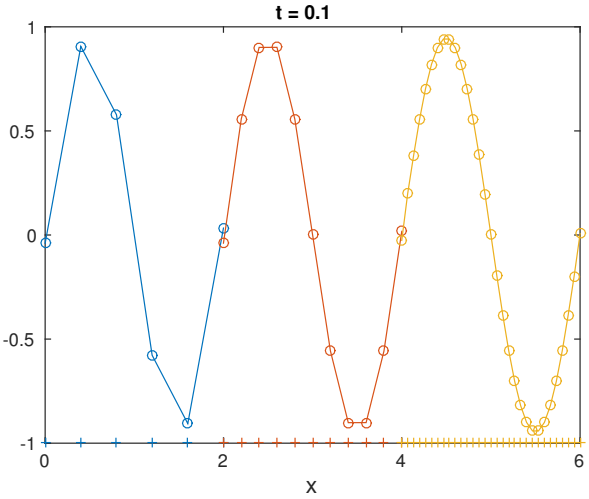

Figure 1: Numerical solution at time $t = 0.1$. The locations of the grid points are marked by vertical bars on the line $y = -1$. In the regions $[0, 2]$, $[2, 4]$ and $[4, 6]$ the space-steps are h, $h/2$ and $h/6$, respectively. Similarly, the local time-steps are Δt, $\Delta t/2$, and $\Delta t/6$.

h	$\log e_{L^2}^{(RK3)}$	$q^{(RK3)}$	$\log e_{L^2}^{(RK4)}$	$q^{(RK4)}$
1/10	-2.70		-2.94	
1/20	-3.64	3.11	-4.21	4.24
1/40	-4.54	3.00	-5.40	3.93
1/80	-5.45	3.01	-6.58	3.95
1/160	-6.35	3.01	-7.78	3.97

Table 1: $\log(L^2$-errors) measured at time $t = 8.7$ and corresponding convergence rates for the MLTS-RK3 and MLTS-RK4 methods, combined with a 4th-order SBP-SAT spatial discretization.

References

[1] J. Diaz and M. J. Grote, Energy Conserving Explicit Local Time Stepping for Second-Order Wave Equations, *SIAM Journal on Scientific Computing* **3** (2009), pp. 1985–2014.

[2] M. J. Grote and T. Mitkova, High-order explicit local time-stepping methods for damped wave equations, *Journal of Computational and Applied Mathematics* **239** (2013), pp. 270–289.

[3] M. J. Grote, M. Mehlin, and T. Mitkova, Runge–Kutta-Based Explicit Local Time-Stepping Methods for Wave Propagation, *SIAM Journal on Scientific Computing* **3** (2015), pp. 1985–2014.

[4] K. Mattsson, F. Ham, and G. Iaccarino, Stable and Accurate Wave-Propagation in Discontinuous Media, *Journal of Computational Physics*, **227** (2008), pp. 8753–8767.

Determining Transmission Eigenvalues of Anisotropic Inhomogeneous Media from Far Field Data

Stefan Peters[1,*]

[1]Department of Inverse Problem, Bremen, Germany

[*]Email: Stefan.Peters@math.uni-bremen.de

Abstract

We characterize interior transmission eigenvalues of penetrable anisotropic acoustic scattering objects by a technique known as inside-outside duality. Under certain conditions on the anisotropic material coefficients of the scatterer, the inside-outside duality allows to rigorously characterize interior transmission eigenvalues from multi-frequency far field data. This theoretical characterization moreover allows to derive a simple numerical algorithm for the approximation of interior transmission eigenvalues.

Keywords: Transmission Eigenvalues, Inside-Outside Duality

1 Determining Interior Transmission Eigenvalues from Far Field Data

In our model the scatterer $D \subset \mathbb{R}^3$ is represented by the material parameter $A = \mathrm{Id} + Q$, which is assumed to be real-valued, symmetric and positive definite in $\mathbb{R}^3$ and the matrix-valued contrast $Q : \mathbb{R}^3 \to \mathbb{R}^{3\times 3}$ is supported and sign-definite in the closure of the scatterer D. We want to determine positive wave numbers $k > 0$ such that k^2 is an interior transmission eigenvalues, i.e. there exists a non-trivial pair (v, w) of functions defined in D such that

$$\begin{aligned} \operatorname{div}(A\nabla v) + k^2 v = 0 \quad &\text{in } D, \\ \Delta w + k^2 w = 0 \quad &\text{in } D, \\ v = w \quad &\text{on } \partial D, \\ \nu^\top A \nabla v = \tfrac{\partial w}{\partial \nu} \quad &\text{on } \partial D, \end{aligned}$$

where ν is the exterior unit normal to the domain D. To determine the eigenvalues we consider the corresponding scattering problem

$$\operatorname{div}(A\nabla u) + k^2 u = 0 \quad \text{in } \mathbb{R}^3.$$

The total wave field u can be split into a sum of an incident plane wave $u^i(x, \theta) = \exp(\mathrm{i}k\,\theta \cdot x)$ with direction $\theta \in \mathbb{S}^2 = \{x \in \mathbb{R}^3, |x| = 1\}$ and a scattered field $u^s(\cdot, \theta)$ that satisfies Sommerfeld's radiation condition. The scattered wave $u^s(\cdot\theta)$ behaves like an outgoing spherical wave, such that it can be represented by its far field $u^\infty(\hat{x}, \hat{\theta})$. In particular the far field operator $F : L^2(\mathbb{S}^2) \to L^2(\mathbb{S}^2)$ can now be defined as

$$Fg(\hat{x}) := \int_{\mathbb{S}^2} u^\infty(\hat{x}, \theta) g(\theta) \mathrm{d}S(\theta), \qquad \hat{x} \in \mathbb{S}^2.$$

The far field operator is compact and normal and its eigenvalues λ_j lie on a circle of radius $8\pi^2/k$ with center $8\pi^2\mathrm{i}/k$ in the complex plane (see e.g. [1]). We represent the eigenvalues in polar coordinates such that

$$\lambda_j = r_j \exp(\mathrm{i}\vartheta_j), \qquad r_j > 0, \quad \vartheta_j \in (0, \pi).$$

It can be shown that the eigenvalues λ_j converge to zero from the left if Q is positive definite and from the right if Q is negative definite. Therefore in the first case the eigenvalue λ_* with the smallest phase ϑ_* is well-defined and in the second case the eigenvalues λ^* with the largest phase ϑ^* is well-defined.

Under certain conditions to the contrast Q our main result is the following (see [3]):

If Q is positive definite, then k_0^2 is an interior transmission eigenvalue if and only if the smallest phase ϑ_* of the eigenvalue λ_* of F converges to zero as k approaches k_0 from below. If Q is negative definite, then k_0^2 is an interior transmission eigenvalue if and only if the largest phase ϑ^* of the eigenvalue λ^* of F converges to π as k approaches k_0 from below.

Crucial tools we use in the proof are the eigenvalue decomposition of the far field operator F, a particular factorization $F = -H^*TH$ we derive for this scattering problem and the properties of the arising operators.

2 Numerical Results

To verify our theoretical results for the case that the constrast $Q = q \cdot \mathrm{Id}$ is either constant negative or constant positive we created far field data using the software package BEM++ (see [2]) to solve the arising boundary integral equations. As domains of computation we chose the

unit ball $B_1(0)$ and the unit cube $C := [0,1]^3$. As a result we obtained a matrix F_N as a numerical approximation to the far field operator F. In particular we obtained numerical approximations λ_j^N and ϑ_j^N to the eigenvalues λ_j and its corresponding phases ϑ_j. Depending on the sign of Q, we are either interested in the behaviour of the smallest phase ϑ_* or the largest phase ϑ^* with varying wavenumber k. Therefore we plottet the phases ϑ_j^N against the wavenumber k. First we use the unit ball as a scattering object with positive constrast $q = 10$ to obtain graph in Figure 1. In this special case, we can analyt-

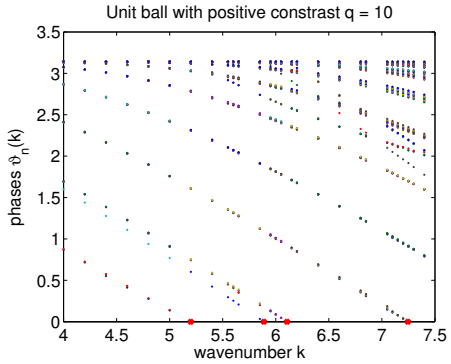

Figure 1: Dots mark the phases $\vartheta_j^N(k)$ of the numerical eigenvalues $\lambda_j^N(k)$. Red dots on the $\{\vartheta = 0\}$-axis mark the extrapolated positions of the transmission eigenvalues.

ically compute the square roots of the first four transmission eigenvalues $k_{0,1}, .., k_{0,4}$ to compare them to the numerically computed values in the following table.

$B_1(0), q = 10$	$k_{0,1}$	$k_{0,2}$	$k_{0,3}$	$k_{0,4}$
computed ITE	5.199	5.888	6.106	7.245
exact ITE	5.204	5.886	6.104	7.244

For the case of Q with negative sign, we use the unit cube as a scattering object and obtain the graph in Figure 2. The square roots of the first three computed transmission eigenvalues are listed in the following table.

$D = [0.1]^3, q = -0.9$	$k_{0,1}$	$k_{0,2}$	$k_{0,3}$
computed ITE	2.863	3.029	3.164

In summary we see that the numerical computations confirm the predicted behaviour of the smallest phase $\vartheta_*(k)$ or the largest phase

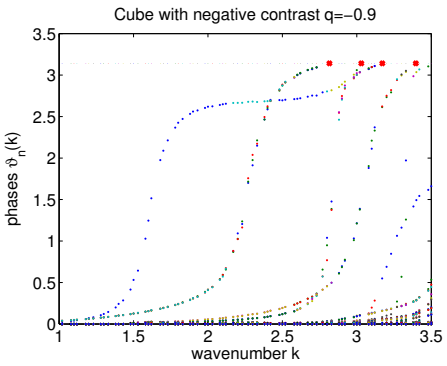

Figure 2: Dots mark the phases $\vartheta_j^N(k)$ of the numerical eigenvalues $\lambda_j^N(k)$. Red dots on the $\{\vartheta = \pi\}$-axis mark the extrapolated positions of the transmission eigenvalues.

$\vartheta^*(k)$ in the proximity of interior transmission eigenvalues.

3 References

References

[1] Andreas Kirsch, An Integral Equation for the Scattering Problem for an Anisotropic Medium and the Factorization Method, *World Sci. Publ., Hackensack, NJ* (2008), pp. 57-70.

[2] Wojciech Śmigaj and Timo Betcke and Simon Arridge and Joel Phillips and Martin Schweiger, Solving Boundary Integral Problems with BEM++, *ACM Transactions on Mathematical Software* **42** (2014).

[3] Armin Lechleiter and Stefan Peters, Determining Transmission Eigenvalues of Anisotropic Inhomogeneous Media from Far Field Data, *To be published in Communications in Mathematical Sciences*, (2015).

Boundary Integral Equations for the Transmission Eigenvalue Problem for Maxwell's Equations

Fioralba Cakoni[1], **Houssem Haddar**[2], **Shixu Meng**[1,*]

[1]Department of Mathematical Sciences, University of Delaware, Newark, Delaware 19716, USA
[2]CMAP, Ecole Polytechnique, Route de Saclay, 91128 Palaiseau Cedex, France
[*]Email: sxmeng@udel.edu

Abstract

We formulate the transmission eigenvalue problem using boundary integral equation. Under the assumption that the contrast is constant near the boundary of the support of the inhomogeneity, we prove that the set of transmission eigenvalues is discrete with positive infinity as the only accumulation point.

Keywords: Transmission eigenvalue problem, boundary integral equations, Maxwell's equations

1 Introduction

Let $D \in \mathbb{R}^3$ be a bounded open and connected region with C^2-smooth boundary $\partial D := \Gamma$ and let ν denotes the outward unit normal vector on Γ. In general we consider a 3×3 matrix-valued function N with $L^\infty(D)$ entries such that $\overline{\xi} \cdot \mathrm{Re}(N)\xi \geq \alpha > 0$ and $\overline{\xi} \cdot \mathrm{Im}(N)\xi \geq 0$ in D for every $\xi \in \mathbb{C}^3$, $|\xi| = 1$. The transmission eigenvalue problem can be formulated as finding $\mathbf{E}, \mathbf{E}_0 \in \mathbf{L}^2(D)$, $\mathbf{E} - \mathbf{E}_0 \in \mathbf{H}(\mathrm{curl}^2, D)$ that satisfy

$$\begin{aligned}
\mathrm{curl}\,\mathrm{curl}\,\mathbf{E} - k^2 N\mathbf{E} = 0 \quad &\text{in} \quad D \quad (1)\\
\mathrm{curl}\,\mathrm{curl}\,\mathbf{E}_0 - k^2\mathbf{E}_0 = 0 \quad &\text{in} \quad D \quad (2)\\
\nu \times \mathbf{E} = \nu \times \mathbf{E}_0 \quad &\text{on} \quad \Gamma \quad (3)\\
\nu \times \mathrm{curl}\,\mathbf{E} = \nu \times \mathrm{curl}\,\mathbf{E}_0 \quad &\text{on} \quad \Gamma \quad (4)
\end{aligned}$$

where

$$\mathbf{L}^2(D) := \left\{\mathbf{u} : \mathbf{u}_j \in L^2(D), j = 1, 2, 3\right\}$$

$$\mathbf{H}(\mathrm{curl}^2, D) := \left\{ \begin{array}{c} \mathbf{u} \in \mathbf{L}^2(D), \mathrm{curl}\,\mathbf{u} \in \mathbf{L}^2(D) \\ \text{and } \mathrm{curl}\,\mathrm{curl}\,\mathbf{u} \in \mathbf{L}^2(D) \end{array} \right\}$$

Definition 1 *Values of $k \in \mathbb{C}$ for which the (1)-(4) has a nontrivial solution $\mathbf{E}, \mathbf{E}_0 \in \mathbf{L}^2(D)$, $\mathbf{E} - \mathbf{E}_0 \in \mathbf{H}_0(\mathrm{curl}^2, D)$ are called transmission eigenvalues.*

2 Boundary Integral Equations for Constant Electric Permittivity

Define the Hilbert spaces of tangential fields defined on Γ:

$$\mathbf{H}^{s_1,s_2}(\mathrm{div}, \Gamma) = \{\mathbf{u} \in \mathbf{H}_t^{s_1}(\Gamma), \mathrm{div}_\Gamma \mathbf{u} \in H^{s_2}(\Gamma)\}$$
$$\mathbf{H}^{s_1,s_2}(\mathrm{curl}, \Gamma) = \{\mathbf{u} \in \mathbf{H}_t^{s_1}(\Gamma), \mathrm{curl}_\Gamma \mathbf{u} \in \mathbf{H}^{s_2}(\Gamma)\}$$

and the boundary layer potentials

$$\mathbf{T}_k(\mathbf{u}) = \frac{1}{k}\gamma_\Gamma \left(\mathrm{curl}^{\,2} \int_\Gamma \Phi_k(\cdot, \mathbf{y})\mathbf{u}(\mathbf{y})\, ds_y \right) ds_y$$

$$\mathbf{K}_k(\mathbf{u}) = \gamma_\Gamma \left(\mathrm{curl} \int_\Gamma \Phi_k(\cdot, y)\mathbf{u}(\mathbf{y})\, ds_y \right)$$

where $\gamma_\Gamma\, \mathbf{u} = \nu \times (\mathbf{u} \times \nu)$. Furthermore we define

$$\mathbf{L}(k) = \begin{pmatrix} k\sqrt{n}\mathbf{T}_{k\sqrt{n}} - k\mathbf{T}_k & \mathbf{K}_{k\sqrt{n}} - \mathbf{K}_k \\ \mathbf{K}_{k\sqrt{n}} - \mathbf{K}_k & \frac{1}{k\sqrt{n}}\mathbf{T}_{k\sqrt{n}} - \frac{1}{k}\mathbf{T}_k \end{pmatrix}$$

To analyse the boundary integral operator we prove the following.

Lemma 2 *Let $\mathbf{u}^t \in \mathbf{H}^{-\frac{1}{2},\frac{1}{2}}(\mathrm{curl}, \Gamma)$ and $\mathbf{u} \in \mathbf{H}^{-\frac{3}{2},-\frac{1}{2}}(\mathrm{div}, \Gamma)$. Then $\langle \mathbf{u}^t, \mathbf{u} \rangle$ is a well-defined duality with respect to $\mathbf{L}^2(\Gamma)$ as a pivot space.*

Lemma 3 *For a fixed k, the linear operator*

$$\begin{aligned}\mathbf{L}(k) : \mathbf{H}_t^{-\frac{1}{2}}(\Gamma) \times \mathbf{H}^{-\frac{3}{2},-\frac{1}{2}}(\mathrm{div}, \Gamma)\\ \to \mathbf{H}_t^{\frac{1}{2}}(\Gamma) \times \mathbf{H}^{-\frac{1}{2},\frac{1}{2}}(\mathrm{curl}, \Gamma)\end{aligned}$$

is bounded. Moreover, the family of operators $\mathbf{L}(k)$ depends analytically on $k \in \mathbb{C}\backslash\mathbb{R}_-$.

Following the work in [1] and representing $\mathbf{E} - \mathbf{E}_0$ using boundary integrals we can prove the following

Theorem 4 *Assume there exists non trivial $\mathbf{E}$, $\mathbf{E}_0 \in \mathbf{L}^2(D)$, $\mathbf{E} - \mathbf{E}_0 \in \mathbf{H}(\mathrm{curl}^2, D)$ such that (1)-(4) holds. Then there exists non trivial $(\mathbf{M}, \mathbf{J}) \in \mathbf{H}_t^{-\frac{1}{2}}(\Gamma) \times \mathbf{H}^{-\frac{3}{2},-\frac{1}{2}}(\mathrm{div}, \Gamma)$ such that*

$$\mathbf{L}(k) \begin{pmatrix} \mathbf{M} \\ \mathbf{J} \end{pmatrix} = \begin{pmatrix} 0 \\ 0 \end{pmatrix}. \quad (5)$$

This theorem will be proved to be true for matrix valued function N where $\mathbf{L}(k)$ is replaced by (6) in Section 3.

Define $\mathbf{H}_0(\Gamma) := \mathbf{H}_t^{-\frac{1}{2}}(\Gamma) \times \mathbf{H}_0^{-\frac{3}{2},-\frac{1}{2}}(\mathrm{div}, \Gamma)$ where $\mathbf{H}_0^{-\frac{3}{2},-\frac{1}{2}}(\mathrm{div}, \Gamma)$ is the space of $\mathbf{u} \in \mathbf{H}^{-\frac{3}{2},-\frac{1}{2}}(\mathrm{div}, \Gamma)$ with $\mathrm{div}_\Gamma \mathbf{u} = 0$. Let $\mathbf{H}^*(\Gamma)$ be the dual space of $\mathbf{H}_0(\Gamma)$. Having defined these spaces we can prove

Lemma 5 *Let $\kappa > 0$. The operator $\mathbf{L}(i\kappa) : \mathbf{H}_0(\Gamma) \to \mathbf{H}^*(\Gamma)$ is strictly coercive.*

Lemma 6 *Let $\gamma(k) := \frac{k_1^2 - k^2}{|k_1|^2 - |k|^2}$ and $k_1 = k\sqrt{n}$ for $k \in \mathbb{C} \setminus \mathbb{R}_-$. Then $\mathbf{L}(k) + \gamma(k)\mathbf{L}(i|k|) : \mathbf{H}_0(\Gamma) \to \mathbf{H}^*(\Gamma)$ is compact.*

Define $\mathbf{H}_1(\Gamma) := \left\{ \nabla_\Gamma p, p \in H^{\frac{3}{2}}(\Gamma) \right\}$, then by Helmholtz decomposition $\mathbf{J} = \mathbf{Q} + \mathbf{P}$ where $\mathbf{Q} \in \mathbf{H}_0^{-\frac{3}{2},-\frac{1}{2}}(\mathrm{div}, \Gamma)$ and $\mathbf{P} \in \mathbf{H}_1(\Gamma)$. The equation (5) is equivalent to

$$\tilde{\mathbf{L}}(k) \begin{pmatrix} \mathbf{M} \\ \mathbf{Q} \\ \mathbf{P} \end{pmatrix} = 0$$

for $(\mathbf{M}, \mathbf{Q}, \mathbf{P}) \in \mathbf{H}_t^{-\frac{1}{2}}(\Gamma) \times \mathbf{H}_0^{-\frac{3}{2},-\frac{1}{2}}(\mathrm{div}, \Gamma) \times \mathbf{H}_1(\Gamma)$. $\tilde{\mathbf{L}}(k)$ is a 3×3 operator and satisfies the following property.

Lemma 7 *The operator $\tilde{\mathbf{L}}(k) : \mathbf{H}_0(\Gamma) \times \mathbf{H}_1(\Gamma) \to \mathbf{H}^*(\Gamma) \times \mathbf{H}^{-\frac{1}{2}}(\Gamma)$ is Fredholm with index zero.*

3 General Inhomogeneous Medium

Let $\mathcal{O}$ be a neighborhood of ∂D in D. Assume that $N = nI$ in $\mathcal{O}$, where $n \neq 1$ is a positive constant. We can express $\mathbf{E}_0$ in D and $\mathbf{E}$ in $\mathcal{O}$ by boundary integrals, and in $D \setminus \overline{\mathcal{O}}$ we can express $\mathbf{E}$ in the form of partial differential equation with Cauchy data connected to $\mathbf{E}$ in $\mathcal{O}$. Hence we can obtain Theorem 4 where the operator $\mathbf{L}(k)$ is written as

$$\mathbf{L}(k) = \mathbf{L}_n(k) - \mathbf{L}^{\Sigma,\Gamma}(k)\mathbf{A}^{-1}(k)\mathbf{L}^{\Gamma,\Sigma}(k) \quad (6)$$

where $\mathbf{L}_n(k)$ is the boundary integral operator corresponding to the transmission eigenvalue problem with constant $n - 1$. Furthermore $\mathbf{L}^{\Sigma,\Gamma}(k)$ and $\mathbf{L}^{\Gamma,\Sigma}(k)$ are compact and $\mathbf{A}(k)$ is invertible. By writing $\mathbf{L}(k)$ as a 3×3 operator $\tilde{\mathbf{L}}(k)$ similar to Lemma 7 we can have the following.

Lemma 8 *The operator $\tilde{\mathbf{L}}(k) : \mathbf{H}_0(\Gamma) \times \mathbf{H}_1(\Gamma) \to \mathbf{H}^*(\Gamma) \times \mathbf{H}^{-\frac{1}{2}}(\Gamma)$ is a Fredholm with index zero.*

4 The existence of non transmission eigenvalue wave numbers

Following the idea of [3] for the scalar case we have

Theorem 9 *Assume $N = nI$ in $\mathcal{O}$, $n \neq 1$ is constant. Then there exists a sufficiently large real $\lambda > 0$ with $k = i\lambda$ such that (1)-(4) has only trivial solutions.*

5 Discreteness of transmission eigenvalues

From Theorem 9 we can prove

Lemma 10 *Assume $N = nI$ in $\mathcal{O}$, $n \neq 1$ is constant. There exists a sufficiently large $k > 0$ such that $\tilde{\mathbf{L}}(ik)$ is injective.*

Combining Theorem 4, Lemma 8, Lemma 10 and using the analytic Fredholm theory yields

Theorem 11 *Assume $N = nI$ in $\mathcal{O}$, $n \neq 1$ is constant, then the set of the transmission eigenvalues in $\mathbb{C}$ is discrete.*

6 References

References

[1] A. Cossonnière and H. Haddar, Surface integral formulation of the interior transmission problem, *J. Integral Equations and Applications* 25 (2013), 1123-1138.

[2] H. Haddar, The interior transmission problem for anisotropic Maxwell's equations and its applications to the inverse problem, *Math. Methods Appl. Sci.* **27**, no. 18, 2111-2129 (2004).

[3] J. Sylvester, Discreteness of transmission eigenvalues via upper triangular compact operator, *SIAM J. Math. Anal.* 44:341-354 (2012).

Weyl law for signed counting function of positive interior transmission eigenvalues

E. Lakshtanov[1], **B. Vainberg**[2,*]
[1]Department of Mathematics, Aveiro, Portugal
[2]Department of Mathematics, UNC Charlotte, USA
*Email: brvainbe@uncc.edu

Abstract

We consider the interior transmission eigenvalue (ITE) problem, which arises when scattering by inhomogeneous media is studied. The ITE problem is not self-adjoint. We show that positive ITEs are observable together with plus or minus signs that are defined by the direction of motion of the corresponding eigenvalues of the scattering matrix (when the latter approach $z = 1$). We obtain a Weyl type formula for the counting function of positive ITEs, which are taken together with ascribed signs.

Keywords: interior transmission eigenvalue, Weyl law

1 Introduction

Let $\mathcal{O} \in R^d$ be an open bounded domain with C^2 boundary ∂O and the outward normal ν. *Interior transmission eigenvalues (ITEs)* are defined as values of $\lambda \in \mathbb{C}$ for which the problem

$$-\Delta u - \lambda u = 0, \quad x \in \mathcal{O}, \quad u \in H^2(\mathcal{O}),$$
$$-\Delta v - \lambda n(x) v = 0, \quad x \in \mathcal{O}, \quad v \in H^2(\mathcal{O}),$$

$$u - v = 0, \quad x \in \partial\mathcal{O},$$
$$\frac{\partial u}{\partial \nu} - \frac{\partial v}{\partial \nu} = 0, \quad x \in \partial\mathcal{O},$$

has a non-trivial solution. Here $n(x) > 0$, $x \in \overline{\mathcal{O}}$, is a smooth positive function, $H^2(\mathcal{O})$ is the Sobolev space.

This spectral problem for a system of two equations in a *bounded* domain $\mathcal{O} \in R^d$ appears naturally when the scattering transmission problem (scattering of plane waves by an inhomogeneous medium) is studied. The scattering problem is stated as

$$-\Delta u - \lambda u = 0, \quad x \in R^d \backslash \mathcal{O},$$
$$-\Delta v - \lambda n(x) v = 0, \quad x \in \mathcal{O},$$

$$u - v = 0, \quad x \in \partial\mathcal{O},$$
$$\frac{\partial u}{\partial \nu} - \frac{\partial v}{\partial \nu} = 0, \quad x \in \partial\mathcal{O},$$

where u is the sum of the incident plane wave and the scattered wave, i.e., $u = e^{ik(\omega,x)} + \psi_{\rm sc}$, $\lambda = k^2$, $\psi_{\rm sc}$ satisfies the radiation conditions as $r = |x| \to \infty$

$$\psi_{\rm sc} = f(k, \theta, \omega) \frac{e^{ikr}}{r^{\frac{d-1}{2}}} + O\left(r^{-\frac{d+1}{2}}\right), \quad \theta = \frac{x}{r}.$$

The main relation between the scattering and ITE problems is due to the following fact: if the far-field operator $F = F(k) : L_2(S^{d-1}) \to L_2(S^{d-1})$:

$$F\phi = \int_{S^{d-1}} f(k, \theta, \omega)\phi(\omega) dS_\omega$$

has zero eigenvalue at the frequency $k = k_0 > 0$, then $\lambda = k_0^2$ is an ITE [3]. This relation between ITEs and operator F is very important in the study of scattering by inhomogeneous media. In particular, it is known that positive ITEs are observable. They have been extensively used in the study of the inverse problem, starting from papers [3], [2], [8].

The transmission problem considered above has a simple analogue, which is scattering by a soft or rigid obstacle $\mathcal{O}$. It is the exterior problem with the Dirichlet or Neumann boundary condition. The corresponding interior problem in the latter case is the eigenvalue problem for the Dirichlet or Neumann (negative) Laplacian in $\mathcal{O}$. Unlike the Dirichlet or Neumann eigenvalues, the ITEs are defined by a much more complicated spectral problem, which is neither symmetric nor elliptic.

One of the important properties of the eigenvalues for the Dirichlet or Neumann negative Laplacian is the Weyl law for the counting function of the eigenvalues. *The goal of this paper is to obtain an analogue of the Weyl law for the signed counting function of positive ITEs and establish an important connection between positive ITEs and the scattering matrix.*

2 Main result

Due to the lack of symmetry (and ellipticity), the discreteness of the spectrum of the ITE problem, the existence of real eigenvalues, and their

asymptotics can not be obtained by soft arguments. Moreover, the existence of non-real ITEs was shown in [7], and an example of an elliptic ITE problem where the set of ITEs is not discrete can be found in [5, Examples 1,2].

There is extensive literature (see the review [1]) on the properties of ITEs and corresponding eigenfunctions. The following results are most closely related to our study. It was shown in [9] that the set of ITEs is discrete if $n(x) \neq 1$ everywhere at the boundary of the domain $\partial\mathcal{O}$. The latter condition (which means that the inhomogeneity has a sharp boundary) will be assumed to hold in our study. It was shown that the standard Weyl estimate holds for the *complex* ITEs located in an arbitrary cone containing the real positive semi-axis when $\lambda \to \infty$:

$$\#\{i : |\lambda_i^T| \leq \lambda\} \sim \frac{\lambda^{\frac{d}{2}}\omega_d}{(2\pi)^d}\left[\mathrm{Vol}(\mathcal{O}) + \int_{\mathcal{O}} n^{\frac{d}{2}}(x)dx\right], \tag{1}$$

where ω_d is the volume of the unit ball in $\mathbb{R}^d$. Earlier we have shown that if

$$\gamma := \mathrm{Vol}(\mathcal{O}) - \int_{\mathcal{O}} n^{\frac{d}{2}}(x)dx \neq 0,$$

then the set of *positive* ITEs (which are the most important for applications) is infinite, and moreover, if $\lambda \to \infty$, then

$$\#\{0 < \lambda_i^T < \lambda\} \;\geq\; \frac{\omega_d}{(2\pi)^d}|\gamma|\lambda^{\frac{d}{2}} + O(\lambda^{\frac{d}{2}-\delta}).$$

Obviously, the coefficient $|\gamma|$ is always smaller than the corresponding coefficient in (1). We plan to show that there are signs that can be naturally ascribed to positive ITEs λ_i^T in such a way that the Weyl law for the signed counting function (that counts the eigenvalues with the ascribed signs) for positive ITEs is valid with the coefficient γ in the first term.

Thus we will ascribe a value $\sigma_i = \pm 1$ to each simple positive ITE. These values are observable and defined by the direction (clockwise or counterclockwise) of the rotation of the eigenvalues of the scattering matrix. In the case of an ITE of geometric multiplicity $n > 1$, we ascribe a coefficient $\sigma_i, |\sigma_i| \leq n$, to the whole group, not to each of ITEs separately. The main result of this paper [6] is formulated as follows.

Theorem 1 *Let $n(x) \neq 1, x \in \partial\mathcal{O}$. The Weyl law holds for the signed counting function for positive eigenvalues of the interior transmission problem as $\lambda \to \infty$:*

$$\sum_{i\,:\,0<\lambda_i^T<\lambda} \sigma_i = \frac{\omega_d}{(2\pi)^d}\gamma\lambda^{\frac{d}{2}} + O(\lambda^{\frac{d}{2}-\delta}), \quad \delta = \frac{1}{2d}.$$

This statement generalizes the standard Weyl law for the Dirichlet/Neumann Laplacian where $\sigma_i = 1,\ i \geq 1$. It was noted in [4] that the sign of σ_i can vary in the transmission problem.

References

[1] F. Cakoni, H. Haddar, Transmission Eigenvalues in Inverse Scattering Theory, Inside Out II, *MSRI Publications*, **60** (2012).

[2] D. Colton, P.Monk, The inverse scattering problem for time harmonic acoustic waves in an inhomogeneous medium, *Quarterly Journal of Mechanics and Applied Mathematics,* **41** (1988), 97-125.

[3] A. Kirsch, The denseness of the far field patterns for the transmission problem, *IMA J. Appl. Math.,* **37** (1986), 213–223.

[4] A. Kirsch, A. Lechleiter, The inside–outside duality for scattering problems by inhomogeneous media, Inverse Problems, **29** (2013), 104011.

[5] E. Lakshtanov, B. Vainberg, Ellipticity in the interior transmission problem in anisotropic media, *SIAM J. Math. Anal.,* **44** (2012), 1165-1174.

[6] E. Lakshtanov, B. Vainberg, Sharp Weyl Law for Signed Counting Function of Positive Interior Transmission Eigenvalues, arXiv:1401.6213.

[7] Y.J. Leung, D. Colton, Complex transmission eigenvalues for spherically stratified media, *Inverse Problems,* **28** (2012), 075005.

[8] B. Rynne, B. Sleeman, The interior transmission problem and inverse scattering from inhomogeneous media, *SIAM J. Math. Anal.,* **22** (1991) 61755–62.

[9] J. Sylvester, Discreteness of Transmission Eigenvalues via Upper Triangular Compact Operators, *SIAM J. Math. Anal.,* **44** No 1, (2011), 341-354.

A numerical method to compute electromagnetic interior transmission eigenvalues

Andreas Kleefeld[1,*]
[1]Brandenburg University of Technology, 03046 Cottbus, Germany
*Email: kleefeld@tu-cottbus.de

Abstract

The numerical calculation of eigenvalues of the interior transmission problem arising in electromagnetic scattering for constant contrast in three dimensions is a challenging task. A new method based on the boundary integral equation method and complex-valued contour integrals is presented which is able to calculate numerically interior transmission eigenvalues for various obstacles with computational cost lower than those of existing methods. Furthermore, the algorithm is capable of finding the multiplicities of the eigenvalues as well as complex-valued eigenvalues. Up until now, the proof of existence of such eigenvalues is still an open question.

Keywords: interior transmission problem, interior transmission eigenvalue, boundary integral equation, contour integral, electromagnetic scattering, Maxwell equations

1 Introduction

Interior transmission eigenvalues play an important role in electromagnetic scattering, since they carry information about material properties. Thus, they might serve to detect abnormalities inside homogeneous media (see for example [2]). They first appear in Kirsch [4] for the acoustic case. The numerical results given in Kleefeld [5] for the acoustic interior transmission problem are extended to the electromagnetic case. He combines the boundary integral equation method recently proposed by Cossonnière [3] and the complex-valued contour integral algorithm by Beyn [1] to provide a new algorithm which is able to calculate interior transmission eigenvalues for various obstacles in three dimensions. Additionally, the multiplicities of such eigenvalues can be provided. Further, the algorithm is capable of finding complex-valued eigenvalues. A proof of existence is still missing.

2 Problem statement

Assume that D is a domain in $\mathbb{R}^3$ with a connected boundary Γ belonging to class C^2. Further, assume that $\mathbb{R}^3\backslash\overline{D}$ is connected. We denote the wavenumber by κ, the normal pointing in the exterior by ν, with $N = n\,I$ the constant contrast, and $\mathbf{E}$ and $\mathbf{H}$ are the electric and magnetic field, respectively. Find a non-trivial solution $(\mathbf{E}, \mathbf{E_0})$ to the electromagnetic interior transmission eigenvalue problem:

$$\begin{aligned}
\operatorname{curl}\operatorname{curl}\mathbf{E} - \kappa^2\, N\,\mathbf{E} &= 0 \quad \text{in } D\,,\\
\operatorname{curl}\operatorname{curl}\mathbf{E_0} - \kappa^2\,\mathbf{E_0} &= 0 \quad \text{in } D\,,\\
\mathbf{E}\times\nu - \mathbf{E_0}\times\nu &= 0 \quad \text{on } \Gamma\,,\\
\operatorname{curl}\mathbf{E}\times\nu - \operatorname{curl}\mathbf{E_0}\times\nu &= 0 \quad \text{on } \Gamma\,.
\end{aligned}$$

Interior transmission eigenvalues are values of κ for which this problem has non-trivial solutions. The system of boundary integral equations is derived by employing the first and second Stratton-Chu formula, using the jump relations, and the given boundary conditions. This yields the system

$$\begin{bmatrix} \mathbf{T}_{\kappa\sqrt{n}} - \mathbf{T}_\kappa & \mathbf{K}_{\kappa\sqrt{n}} - \mathbf{K}_\kappa \\ \mathbf{K}_{\kappa\sqrt{n}} - \mathbf{K}_\kappa & \dfrac{\mathbf{T}_{\kappa\sqrt{n}}}{\kappa^2 n} - \dfrac{\mathbf{T}_\kappa}{\kappa^2} \end{bmatrix} \begin{bmatrix} M \\ J \end{bmatrix} = \begin{bmatrix} 0 \\ 0 \end{bmatrix}$$

with the two boundary integral operators $\mathbf{K}_\kappa$, $\mathbf{T}_\kappa : \mathbf{H}_\times^{-1/2}(\operatorname{div}_\Gamma, \Gamma) \to \mathbf{H}_\times^{-1/2}(\operatorname{div}_\Gamma, \Gamma)$ defined by

$$\begin{aligned}
(\mathbf{K}_\kappa\psi)(x) &= \operatorname{curl}_x\{(\mathbf{A}_\kappa\psi)(x)\}\times\nu(x)\,,\\
(\mathbf{T}_\kappa\psi)(x) &= \operatorname{curl}_x\operatorname{curl}_x\{(\mathbf{A}_\kappa\psi)(x)\}\times\nu(x)\,,\\
(\mathbf{A}_\kappa\psi)(x) &= \int_\Gamma \psi(y)\,\Phi_\kappa(x,y)\,\mathrm{d}s(y)\,,
\end{aligned}$$

where Φ_κ denotes the fundamental solution of the Helmholtz equation. Further, we set

$$M = E\times\nu = E_0\times\nu \in \mathbf{H}_\times^{-1/2}(\operatorname{div}_\Gamma, \Gamma)$$

and

$$J = \operatorname{curl} E\times\nu = \operatorname{curl} E_0\times\nu \in \mathbf{H}_\times^{-1/2}(\operatorname{div}_\Gamma, \Gamma)$$

on the surface Γ. The system above can be written abstractly as $\mathbf{Z}(\kappa)V = 0$ with the obvious definition of the operator $\mathbf{Z}(\kappa)$ and the function V. After discretizing, one has to solve the nonlinear eigenvalue problem

$$\mathrm{Z}(\kappa)v = 0\,, \qquad \kappa\in\Omega\subset\mathbb{C}$$

with $v \in \mathbb{C}^m\,, v \neq 0$ and $\mathrm{Z}(\kappa) \in \mathbb{C}^{m\times m}$, where Ω is some open domain in the complex plane and its boundary is denoted by $\partial\Omega$ assuming that there are $k \ll m$ eigenvalues inside the contour including multiplicities. It is solved with the complex-valued contour algorithm which is based on Keldysh's theorem reducing the original nonlinear eigenvalue problem to a linear eigenvalue problem of size k (see [1]).

3 Numerical results

First, numerical results are presented using the method of Cossonnière to calculate real-valued interior transmission eigenvalues in the interval $[3, 4]$ for a unit sphere centered at the origin, an ellipsoidal surface with semi-axis $(1, 1, 6/5)$ in the interval $[5/2, 4]$, and a peanut-shaped surface in the interval $[5/2, 4]$ given parametrically by $x = \varrho\sin(\phi)\cos(\theta)$, $y = \varrho\sin(\phi)\sin(\theta)$, and $z = \varrho\cos(\phi)$ with ϱ defined by the expression $\varrho^2 = 9\left\{\cos^2(\phi) + \sin^2(\phi)/4\right\}/4$ using $n = 4$. We are able to detect five real-valued interior transmission eigenvalues. We detect eleven and nine interior transmission eigenvalues for the ellipsoidal surface and the peanut-shaped surface, respectively. In Table 1, we report the first four eigenvalues including their multiplicities (listed in square brackets) using the new method, where we used the contour of an ellipse centered at $(7/2, 0)$, $(3, 0)$, and $(3, 0)$ with semi-axis $(1/2, 1/4)$ for the unit sphere, the ellipsoidal obstacle, and the peanut-shaped obstacle, respectively. Note that the new method is

EV	Unit sphere	Ellipsoid	Peanut
1.	3.14 [3]	2.92 [2]	3.00 [2]
2.	3.49 [5]	3.06 [1]	3.04 [2]
3.	3.59 [3]	3.23 [2]	3.37 [1]
4.	3.69 [5]	3.31 [3]	3.42 [1]

Table 1: The four eigenvalues (EV) for the interior transmission problem for $n = 4$.

more than ten times faster and at the same time provides better accuracy. Finally, we use the new method to calculate complex-valued eigenvalues. We use the contour of an ellipse centered at $(5/2, -1/2)$ with semi-axis $(1/2, 1/2)$ for the first two obstacles under consideration. We obtain the two eigenvalues $2.69 - 0.71\mathrm{i}$ and $2.40 - 0.68\mathrm{i}$ with multiplicities three and five for the unit sphere. For the ellipsoidal surface, we get the five eigenvalues $2.19 - 0.55\mathrm{i}$, $2.22 - 0.60\mathrm{i}$, $2.64 - 0.64\mathrm{i}$, $2.50 - 0.70\mathrm{i}$, and $2.32 - 0.71\mathrm{i}$ with multiplicities one, two, one, two, and two, respectively.

4 Summary and outlook

A new method is presented which is able to calculate numerically interior transmission eigenvalues including their multiplicities arising in electromagnetic scattering. Additionally, the method is able to calculate complex-valued interior transmission eigenvalues. Further investigation regarding those is subject of future research.

References

[1] W.-J. Beyn, An integral method for solving nonlinear eigenvalue problems, *Linear Algebra Appl.*, **436** (2012), pp. 3839–3863.

[2] F. Cakoni and H. Haddar, *Transmission eigenvalues in inverse scattering theory*, Inside Out II, G. Uhlmann editor, MSRI Publications, **60** (2012), pp. 527–578.

[3] A. Cossonnière, *Valeurs propres de transmission et leur utilisation dans l'identification d'inclusions à partir de mesures électromagnétiques*, Ph.D. Thesis, Université de Toulouse, December 2011.

[4] A. Kirsch, The denseness of the far field patterns for the transmission problem, *IMA J. Appl. Math.*, **37** (1986), pp. 213–225.

[5] A. Kleefeld, A numerical method to compute interior transmission eigenvalues, *Inverse Problems*, **29** (2013), 104012 (20pp).

Tuesday, July 21
First Afternoon Session
15:30 – 17:00

Resonance Problems in Cylindrical Waveguides with Backward Propagating Modes

Martin Halla[1], **Lothar Nannen**[1,*]

[1]Institute for Analysis and Scientific Computing, Vienna University of Technology, Austria

*Email: lothar.nannen@tuwien.ac.at

Abstract

We consider time-harmonic linear elasticity equations in domains with cylindrical waveguides. Since for such problems there exist modes with different signs of group and phase velocity, standard PML methods fail. We apply an infinite element method based on a pole condition, which characterizes outgoing solutions by the poles of their Laplace transform in propagation direction. Since this condition is frequency independent, it is well-suited for resonance problems.

Keywords: Elastic waveguide, resonance problem, pole condition, Hardy space infinite element

1 Introduction

Let $\Omega = \Omega_{\text{int}} \cup \Omega_{\text{ext}} \cup \Upsilon$ be a Lipschitz domain with a bounded interior domain $\Omega_{\text{int}} \subset \mathbb{R}^d$ ($d = 2, 3$), a bounded interface $\Upsilon = \{0\} \times \tilde{\Upsilon} \subset \partial\Omega_{\text{int}}$ with $\tilde{\Upsilon} \subset \mathbb{R}^{d-1}$, and an unbounded waveguide $\Omega_{\text{ext}} = \mathbb{R}_+ \times \tilde{\Upsilon}$ with $\overline{\Omega_{\text{ext}}} \cap \overline{\Omega_{\text{int}}} = \Upsilon$. We consider the time-harmonic isotropic linear elasticity problem

$$-\operatorname{div} \sigma(\mathbf{u}) - \omega^2 \mathbf{u} = \mathbf{f} \text{ in } \Omega. \qquad (1)$$

Here, $\Re(\mathbf{u}(\mathbf{x})e^{-\mathrm{i}\omega t})$ for $\mathbf{x} \in \Omega$ and time $t > 0$ is the time-harmonic displacement vector, $\omega > 0$ the angular frequency, $\sigma(\mathbf{u})$ the stress tensor, and $\mathbf{f}$ a volumetric force with compact support in Ω_{int}. We assume traction-free boundary conditions $\sigma(\mathbf{u}) \cdot \mathbf{n}$ at $\partial\Omega_{\text{ext}} \setminus \Upsilon$ and a suitable boundary condition with compact support in $\partial\Omega_{\text{int}} \setminus \Upsilon$. Additionally, we need a radiation condition in order to get physically relevant solutions.

2 Elastic Waveguide

The radiation condition for elastic waveguides is constructed out of a modal expansion: The modes

$$\mathbf{u}(\xi, \eta; \omega) = e^{\mathrm{i}\kappa(\omega)\xi}\mathbf{w}(\eta; \omega), \quad (\xi, \eta) \in \mathbb{R}_+ \times \tilde{\Upsilon},$$

are solutions to (1), if and only if the wavenumber $\kappa(\omega) \in \mathbb{C}$ solves a dispersion relation. A mode is called outgoing, if

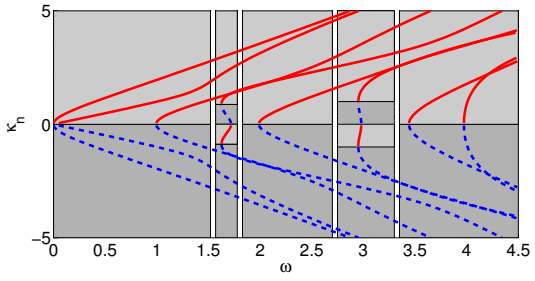

Figure 1: The first eight dispersion curves for a two-dimensional waveguide. Modes corresponding to the red solid part have positive group velocity and modes corresponding to the blue dashed part have negative group velocity.

- it is evanescent, i.e. $\Im(\kappa(\omega)) > 0$, or
- if the group velocity $\partial_\kappa\omega(\kappa)$ and with it the energy transport is positive for $\kappa(\omega) \in \mathbb{R}$.

Fig. 1 shows a typical situation for real wavenumbers: There exist backward propagating modes with positive group and negative phase velocity ω/κ. A standard complex scaling method fails in such cases, since it selects modes with positive phase instead of positive group velocities.

More details for the modal decomposition can be found in [1]. In particular it is shown in [1], that there exists a sequence of positive frequencies $(\omega_j)_{j\in\mathbb{N}}$ such that the traces of outgoing modes are dense in $H^1(\Upsilon)$ for all $\omega \in \mathbb{R}_+ \setminus \{\omega_j, j \in \mathbb{N}\}$. In Fig. 1 there exist eight such frequencies ω_j with vanishing group velocity, six of them with vanishing wavenumbers.

3 Pole Condition

The modal radiation condition is frequency dependent and therefore not well-suited for resonance problems. An alternative radiation condition is the pole condition, which assumes the Laplace transform in propagation direction

$$\mathcal{L}\,\mathbf{u}(\bullet, \eta; \omega)(s) = \frac{\mathbf{w}(\eta; \omega)}{s - \mathrm{i}\kappa(\omega)}, \quad s \in \mathbb{C} \setminus \{\mathrm{i}\kappa(\omega)\},$$

to be holomorphic in some region of the complex plane for all modes, all $\eta \in \tilde{\Upsilon}$ and all frequen-

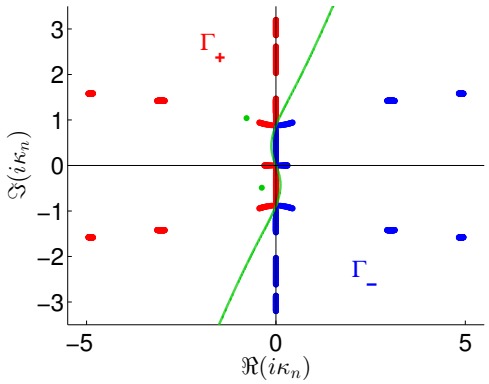

Figure 2: Lowest outgoing (red) and incoming (blue) wavenumbers (multiplied with i) for $\omega \in (1.57, 1.78)$ with separating curve Γ (green).

cies $\omega \in (\tilde{\omega}_1, \tilde{\omega}_2) \setminus \{\omega_j, j \in \mathbb{N}\}$ with $0 < \tilde{\omega}_1 < \tilde{\omega}_2$. For the second interval in Fig. 1 the situation is sketched in Fig. 2: There exist an oriented curve Γ with Γ^+ on the left and Γ^- on the right, such that most of the outgoing poles of $\mathcal{L}\,\mathbf{u}(\bullet, \eta; \omega)$ are separated by Γ from the incoming poles. Only two frequencies exist with vanishing group velocities and poles on Γ.

For the exact definition of the pole condition and the Hardy space infinite element method based on this framework we refer to [2,3]. Note, that the radiation condition is clearly independent of ω in an interval of frequencies.

4 Resonance Problem

(1) leads after discretization to a linear system of the form $(A - \omega^2 B)\mathbf{u}_h = \mathbf{f}_h$ with frequency independent matrices A and B. For the corresponding resonance problem we are looking for resonances $\omega \in \mathbb{C}$ with $\Re(\omega) > 0$ with non-trivial eigenfunction $\mathbf{u}_h$ such that

$$A\mathbf{u}_h = \omega^2 B\mathbf{u}_h.$$

5 Numerics

We study the scattering of a wave signal containing a backward propagating mode by a cavity in a two dimensional waveguide, see Fig. 3

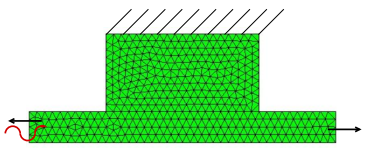

Figure 3: Scattering of an incoming wave by a cavity

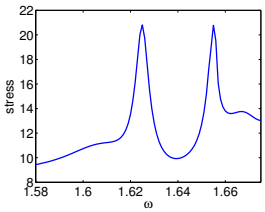

(a) stress in the cavity

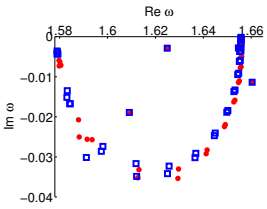

(b) spectrum for two different discretizations

Figure 4: Frequency dependency

for the domain. In Fig. 4(a) the stress in the cavity was measured for different frequencies. The first peak coincides with the resonance with $|\Im(\omega_{\text{res}})|$ most low. The second peak corresponds to a second resonance with small absolute value of imaginary part, which is hidden in Fig. 4(b) behind the discretization of an essential spectrum. A zoom into this region illustrates this resonance.

Hence, the Hardy space method is well-suited for resonance as well as scattering problems even in the case of backward propagating modes.

References

[1] A. G. Kostyuchenko, M. B. Orazov, Problem of oscillations of an elastic half cylinder and related self-adjoint quadratic pencils, *Journal of Soviet Mathematics* **33 (3)** (1986), 1025–1065.

[2] M. Halla, T. Hohage, L. Nannen, and J. Schöberl, Hardy space infinite elements for time-harmonic wave equations with phase velocities of different signs, *ASC Report* **18** (2014).

[3] M. Halla, L. Nannen, Hardy space infinite elements for time-harmonic two-dimensional elastic waveguide problems, *ASC Report* **33** (2014).

New perspectives offered by overlaps to design transparent boundary conditions in waveguides

V. Baronian[1], A.-S. Bonnet-Ben Dhia[2], S. Fliss[2], A. Tonnoir[3,*]

[1]CEA-LIST, Palaiseau, France.

[2]POEMS (CNRS/ENSTA Paristech/INRIA), Palaiseau, France.

[3]POEMS (CNRS/ENSTA Paristech/INRIA), Palaiseau, France, ANEDP, Orsay, France.

*Email: Antoine.Tonnoir@ensta-paristech.fr

Abstract

In this work, we propose new transparent boundary conditions for the time-harmonic diffraction problem in an acoustic or elastic waveguide.
These new conditions use the natural modal decomposition in the waveguide and are said "with overlap" by analogy with the domain decomposition methods. Among their main advantages, they can be implemented in general anisotropic waveguides, for which usual Dirichlet to Neumann maps are not available. Moreover, the traditional benefit of the overlap for iterative resolution is obtained, independently of the size of the overlap.

Keywords: transparent boundary conditions, waveguides, modal decomposition, anisotropic elasticity, iterative methods.

1 Model problem

To present the method, for the seek of simplicity, we consider a diffraction problem in an acoustic isotropic half-guide $\Omega = S\times]-a,+\infty[$ where $S \subset \mathbb{R}^2$ denotes the bounded cross-section of the guide (see figure 1 for notations). At the

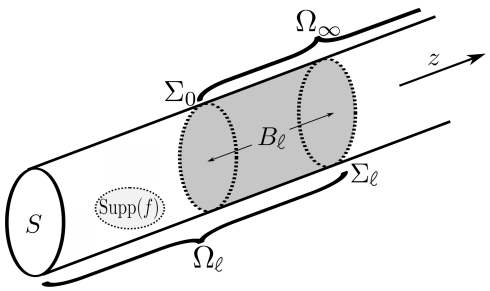

Figure 1: Geometry and notations

frequency ω, the pressure field p satisfies

$$\left| \begin{array}{lll} \Delta p + \omega^2 c^{-2} p = f & \text{in} & \Omega, \\ \partial_\nu p = 0 & \text{on} & \partial\Omega. \end{array} \right. \quad (1)$$

Here ν is the exterior normal to $\partial\Omega$, c the velocity of sound, the source term f is supposed to be compactly supported in $\{z < 0\}$ and we seek for the outgoing solution. We denote by p_ℓ (resp. p_∞) the restriction of p to the subdomain $\Omega_\ell = \Omega \cap \{z < \ell\}$ (resp. $\Omega_\infty = \Omega \cap \{z > 0\}$) and we want to derive transparent boundary conditions for p_ℓ on Σ_ℓ. Looking for the outgoing solution, p_∞ admits the following expression

$$p_\infty(x,y,z) = \sum_{k\geq 0} a_k^\infty \varphi_k(x,y) e^{i\beta_k z} \quad (2)$$

involving the right-going modes $\varphi_k(x,y)e^{i\beta_k z}$ (the φ_k being an orthonormal basis of $L^2(S)$). The a_k^∞ are the unknown modal amplitudes.

In the usual approach, we impose the two following matching conditions on the outer boundary Σ_ℓ:

$$p_\ell|_{\Sigma_\ell} = p_\infty|_{\Sigma_\ell} \quad \text{and} \quad \partial_\nu p_\ell|_{\Sigma_\ell} = \partial_\nu p_\infty|_{\Sigma_\ell}. \quad (3)$$

Then, using the formula (2) and the orthogonality of the φ_k, one can derive a transparent condition for p_ℓ, involving the classical Dirichlet-to-Neumann operator:

$$\frac{\partial p_\ell}{\partial z} = \sum_{k\geq 0} i\beta_k (p_\ell, \varphi_k)_{\Sigma_\ell} \varphi_k \ \text{ on } \ \Sigma_\ell. \quad (4)$$

Let us emphasize that this method requires the orthogonality of the modes, which does not hold for instance in anisotropic acoustic waveguides or in elastic waveguides (even isotropic [2]). We will present now two other approaches.

2 The Dirichlet-to-Neumann operator with overlap

A natural extension (see [1] for more details) of the above approach consists in imposing the matching conditions on two different boundaries:

$$p_\ell|_{\Sigma_0} = p_\infty|_{\Sigma_0} \quad \text{and} \quad \partial_\nu p_\ell|_{\Sigma_\ell} = \partial_\nu p_\infty|_{\Sigma_\ell}. \quad (5)$$

This leads to the following Dirichlet-to-Neumann condition with overlap:

$$\frac{\partial p_\ell}{\partial z} = \sum_{k\geq 0} i\beta_k e^{i\beta_k \ell} (p_\ell, \varphi_k)_{\Sigma_\ell} \varphi_k \ \text{ on } \ \Sigma_\ell \quad (6)$$

which has better mathematical properties than (4) (thanks to the sequence $e^{i\beta_k \ell}$ which decreases exponentially with k, the related term in the variational formulation is compact). This formulation is therefore more suitable for an iterative resolution, and similarly to domain decomposition methods, we can prove that, up to a point, the larger ℓ is, the faster the iterative algorithm is.

The difficulty is that the equivalence with the initial problem is not obvious. This equivalence holds if and only if $v = p_\ell - p_\infty$, defined in $B_\ell = \Omega_\ell \cap \Omega_\infty$ and verifying

$$\left| \begin{array}{lll} \Delta v + \omega^2 c^{-2} v = 0 & \text{in} & B_\ell, \\ v = 0 & \text{on} & \Sigma_0, \\ \partial_\nu v = 0 & \text{on} & \partial B_\ell \setminus \Sigma_0, \end{array} \right. \tag{7}$$

is equal to 0, which is true except when ω is an eigenfrequency of the above homogeneous problem. Let us remark that we easily avoid these "box frequencies" by using for instance a Robin type condition on Σ_ℓ [1].

Again, this approach cannot be generalizable when the orthogonality of the modes does not hold, contrary to the next approach.

3 The "outgoing" to Neumann approach

This last method consists in changing the condition on Σ_0. Since p_ℓ can be decomposed in B_ℓ on the right-going and left-going modes:

$$p_\ell(x,y,z) = \sum_{k\geq 0} \left(a_k^+ e^{i\beta_k z} + a_k^- e^{-i\beta_k z} \right) \varphi_k(x,y),$$

we propose to consider as transmission conditions

$$a_k^+ = a_k^\infty \text{ on } \Sigma_0 \quad \text{and} \quad \partial_\nu p_\ell|_{\Sigma_\ell} = \partial_\nu p_\infty|_{\Sigma_\ell}. \tag{8}$$

On Σ_0, it amounts to match the modal amplitudes of the outgoing modes.

Now to prove that $v = p_\ell - p_\infty = 0$ in B_ℓ, we notice that thanks to the modal condition on Σ_0, we have

$$v(x,y,z) = \sum_{k\geq 0} a_k^- \varphi_k(x,y) e^{-i\beta_k z} \quad \text{in} \quad B_\ell.$$

Then the condition $\partial_\nu v = 0$ on Σ_ℓ directly implies that $v = 0$. In some sense, spurious effects of the box B_ℓ have been eliminated. Numerically, we observe that the rate of convergence of iterative methods of resolution is now independent of the size ℓ of the overlapping.

Finally, we can again eliminate p_∞ to derive a transparent boundary condition for p_ℓ which takes the following form:

$$\frac{\partial p_\ell}{\partial z} = \sum_{k\geq 0} i\beta_k e^{i\beta_k \ell} a_k^+ \varphi_k \text{ on } \Sigma_\ell \tag{9}$$

where

$$a_k^+ = \frac{1}{2} \left(\frac{1}{i\beta_k} (\partial_\nu p_\ell, \varphi_k)_{\Sigma_0} + (p_\ell, \varphi_k)_{\Sigma_0} \right).$$

The normal derivative in the expression of the a_k^+ must be understood in a weak sense and can be eliminated by integrating by part in small volumic domain.

A main advantage of this last approach is that the latter formula can be generalized in the anisotropic case (and in the elastic case) thanks to the general biorthogonality relations verified by the modes [2].

Numerical illustrations will be presented for 2D and 3D waveguides.

References

[1] Gmati, N. and Zrelli, N., Numerical study of some iterative solvers for acoustics in unbounded domains, *ARIMA*, vol. 4, pp. 1-23, (2006).

[2] Baronian, V., Bonnet-BenDhia, A.-S., & Lunéville, E., Transparent boundary conditions for the harmonic diffraction problem in an elastic waveguide, *J. of Comp. and Applied Mathematics*, vol. 234(6), pp. 1945-1952, (2010).

An Infinite Element Method Treating Backward Waves in Unbounded Elastic Plates

Martin Halla[1,*], **Lothar Nannen**[1]
[1]Institute for Analysis and Scientific Computing, Vienna University of Technology, Austria
*Email: martin.halla@tuwien.ac.at

Abstract

We consider time-harmonic wave propagation in unbounded elastic plates. These kind of problems admit waves with different signs of group and phase velocity, leading to numerical difficulties, as standard perfectly matched layer methods fail in these cases. We explain how to construct a transparent boundary condition based on a pole condition and a numerical scheme incorporating the physical radiation condition. The method is based on a transformation to cylindrical coordinates and the Laplace transform in propagation direction. Numerical simulations showing the effectiveness of the method are presented.

Keywords: transparent boundary condition, pole condition, waveguide, backward waves

1 General Setting

We consider plates $P := \mathbb{R}^2 \times (-1,1)$ with local pertubations, i.e. $\Omega := P \setminus K$ with compact scatterer $K \subset \overline{P}$, $0 \in K$. We are looking for solutions $u \in \big(H^1_{\mathrm{loc}}(\Omega)\big)^3$ to the time-harmonic linear isotropic elasticity equation

$$-\operatorname{div}\sigma(u) - \omega^2 u = 0 \text{ in } \Omega, \tag{1a}$$
$$\sigma_n(u) = 0 \text{ on } \partial\Omega \cap \partial P, \tag{1b}$$
$$u = g \text{ on } \partial\Omega \setminus \partial P, \tag{1c}$$
$$u \text{ satisfies a radiation condition}, \tag{1d}$$

with boundary datum $g \in \big(H^{1/2}(\partial\Omega \setminus \partial P)\big)^3$. Outside a cylinder containing K (1a)-(1b) admit solutions in cylindrical coordinates [1]

$$u(r,\theta,z) = e^{\mathrm{i}n\theta} \begin{pmatrix} \kappa f_1(z) H_n'(\kappa r) + f_2(z)\frac{n}{r} H_n(\kappa r) \\ \mathrm{i}\big(f_1(z)\frac{n}{r} H_n(\kappa r) + \kappa f_2(z) H_n'(\kappa r)\big) \\ \kappa f_3(z) H_n(\kappa r) \end{pmatrix},$$

where f_l are known functions depending on ω, κ, H_n are Hankel functions of the first kind and $n \in \mathbb{Z}$ is the circumferential index. $\kappa \in \mathbb{C}$ has to fulfill a symmetric dispersion relation $F_\omega(\kappa) = 0$. The roots κ_j of F_ω are called wave-numbers. The physical radiation condition demands solutions to be either damped, i.e. $\Im(\kappa_j) > 0$, or to have positive group velocity, i.e. $\kappa_j \in \mathbb{R}, \mathrm{d}\omega/\mathrm{d}\kappa_j > 0$. The sign of the latter may not coincide with the sign of the phase velocity ω/κ_j, see Fig. 1. In this case, infinitely many backward modes exist, because the dispersion relation is independent of the circumferential index.

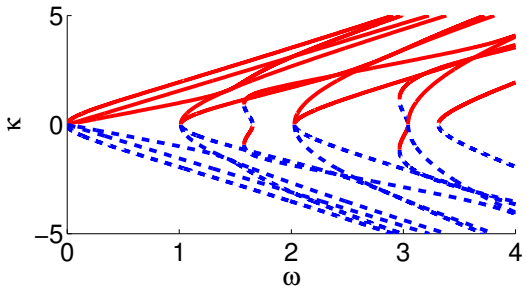

Figure 1: Wave-numbers belonging to red solid/blue dashed dispersion curves yield modes with positive/negative group velocity.

2 Pole Condition

To derive a numerical method we choose a transparent boundary Υ. Let $\hat{x}\colon D \subset \mathbb{R}^2 \to \Upsilon$ be a parametrization. We demand Υ to be of the form $\partial\tilde{\Upsilon} \times (-1,1)$, where $\tilde{\Upsilon} \subset \mathbb{R}^2$ is a convex domain with (piece-wise) smooth boundary, s.t. $K \subset \tilde{\Upsilon} \times [-1,1]$. The exterior domain $\Omega_{\mathrm{ext}} := \Omega \setminus \overline{\tilde{\Upsilon} \times (-1,1)}$ is then parametrized in cylindrical coordinates with

$$T_{\mathrm{cyl}}(r,\alpha,\beta) := \hat{x}(\alpha,\beta) + r\|a(\alpha,\beta)\|^{-1} a(\alpha,\beta),$$

where $e_3 := (0,0,1)^\top$ is the cylindrical axis and $a(\alpha,\beta) := \hat{x}(\alpha,\beta) - e_3\langle e_3, \hat{x}(\alpha,\beta)\rangle$ the direction of propagation. Since the Laplace transforms

$$\big(\mathcal{L}(u \circ T_{\mathrm{cyl}}(\bullet,\alpha,\beta))\big)(s) := \int_0^\infty u \circ T_{\mathrm{cyl}}(r,\alpha,\beta) e^{-sr}\mathrm{d}r$$

of $H_n(\pm\kappa_j \bullet)$ have singularities at $\pm\mathrm{i}\kappa_j$, we proceed as in [2]: We chose a point-symmetric contour Γ, splitting the complex plane in two parts $\Gamma^\pm$, s.t. all (un)physical wave-numbers are contained in $(-\mathrm{i}\Gamma^-)$ $-\mathrm{i}\Gamma^+$, see Fig. 2. Let $H^-(\Gamma) \subset L^2(\Gamma)$ be the Hardy space on Γ, consisting of all L^2-traces of in Γ^- holomorphic functions. We say that u satisfies the pole condition, if

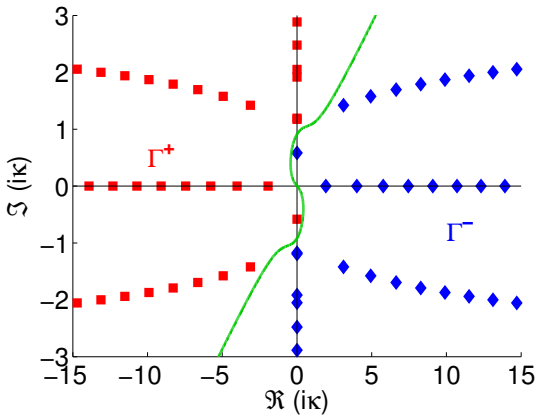

Figure 2: Physical/unphysical wave-numbers κ_j multiplied with i are marked as red squares/blue diamonds. Γ is marked in green.

its Laplace transform has a holomorphic extension in $H^-(\Gamma) \otimes L^2(D)$. For modal solutions the pole condition is equivalent to the radiation condition.

3 Variational Formulation

To obtain a numerical method the weak formulation of (1a)-(1b) in Ω_{ext} is transformed by T_{cyl} to cylindrical coordinates and the identity

$$\int_0^\infty u(r)v(r)\mathrm{d}r = \int_\Gamma (\mathcal{L}u)(s)(\mathcal{L}v)(-s)\mathrm{d}s$$

is applied. This leads to a variational formulation in a subspace of $H^-(\Gamma)\otimes L^2(D)$, similar to the one obtained in [3]. The radiation condition is thereby posed in an essential sense.

Moreover, we show a convenient factorization of the Jacobian $J := \mathrm{D}_{\mathrm{r},\alpha,\beta}\, T_{\text{cyl}}$. This enables the analytic computation of all infinite element matrices arising in the bilinear form.

4 Numerical Results

We couple the method with a high-order finite element discretization of the interior problem and use tensor product basis functions for the discretization of $H^-(\Gamma)\otimes L^2(D)$. For Fig. 3 the boundary datum g was set to be the trace of the sum of a forward and a backward mode. A relative error in the $H^1(\Omega_{\text{int}})$-norm of $4.7e\text{-}3$ is obtained with $3 \times 48\,191$ degrees of freedom for the interior finite element space, 17 d.o.f. for the Hardy space and $3 \times 114\,950$ d.o.f. in total.

5 Conclusion

We showed how the pole condition can be applied to reformulate the physical radiation condition in the context of elastic plates and presented a numerical method to discretize the problem under investigation. The method is capable of treating backward waves and does not require the computation of modal solutions. Essential ingredients for this are the use of cylindrical rather than euclidean coordinates and the crucial scaling by $\|a\|^{-1}$ in T_{cyl}. To our knowledge, this is the first non-modal method for problems with infinitely many backward modes.

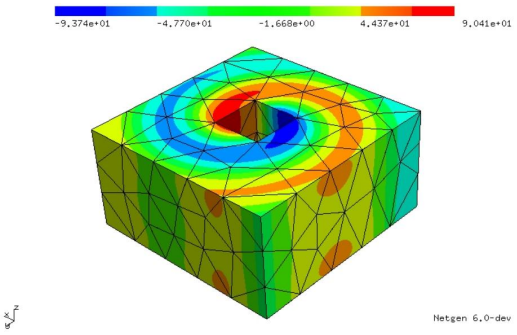

Figure 3: Computed real part of the third Cartesian component.

References

[1] F.K.W. Tso, S.B. Dong and R.B. Nelson, Circular Wave Motions in a Plate of Transversely Isotropic Materials, *Journal of Sound and Vibration* **37**(2) (1974), pp. 149–160.

[2] M. Halla, T. Hohage, J. Schöberl and L. Nannen, Hardy space infinite elements for time-harmonic wave equations with phase velocities of different signs, *ASC Report* **18** (2014).

[3] M. Halla and L. Nannen, Hardy space infinite elements for time-harmonic two-dimensional elastic waveguide problems, *ASC Report* **33** (2014).

MyBEM, a fast boundary element solver by Sparse Cardinal Sine Decomposition

Matthieu Aussal[1,*], **François Alouges**[1]
[1]CMAP - École Polytechnique - Route de Saclay - 91128 Palaiseau CEDEX France
[*]Email: matthieu.aussal@polytechnique.edu

Keywords : SCSD, MyBEM, Green convolution, BEM, NuFFT, fast solver

Abstract

As Fast Multipole Method (FMM), adaptive cross approximation (ACA) or $\mathcal{H}$-matrices, various algorithms for fast convolution on unstructured grids have been developed for many applications (e.g. electrostatics, magnetostatics, acoustics, electromagnetics, etc.). The goal is to reduce the complexity of matrix-vector products, from $O(N^2)$ to $O(N \log N)$.

In [1], we described a new efficient numerical method (SCSD), based on a suitable Fourier decomposition of the Green kernel, sparse quadrature formulae and Type-III Non Uniform Fast Fourier Transform (type-III NUFFT) [5,6]. This talk summarizes the approach and gives results of an application of our new open-source boundary element solver, *MyBEM*.

1 Fast formulation with SCSD

Boundary element formulations lead to the classical single layer potential expression, defined as :

$$\mathcal{S}\lambda(\mathbf{x}) = \int_\Gamma G(\mathbf{x},\mathbf{y})\lambda(\mathbf{y}) d\Gamma_y, \quad \forall \mathbf{x} \in \mathbb{R}^3,$$

where $G(\mathbf{x},\mathbf{y})$ is the Green kernel and Γ the boundary. Using a discrete quadrature of Γ, this convolution product needs a fast computation of discrete sums as :

$$G \star f(\mathbf{x}) \sim \sum_{n=1}^{N} G(\mathbf{x},\mathbf{y}_n) f_n, \qquad (1)$$

where the potential $(f_n)_{1\leq n\leq N}$ is known for all $\mathbf{y}_n$.

In the case of the tridimensional Helmholtz Green kernel, defined as :

$$G(\mathbf{x},\mathbf{y}) = \frac{e^{-ik|\mathbf{x}-\mathbf{y}|}}{4\pi|\mathbf{x}-\mathbf{y}|},$$

the imaginary part can be evaluated on the unit sphere S^2 by spherical integral representation :

$$\mathfrak{Im}\left(G(\mathbf{x},\mathbf{y})\right) = \frac{k}{(4\pi)^2}\int_{S^2} e^{ik\mathbf{s}\cdot\mathbf{x}} e^{-ik\mathbf{s}\cdot\mathbf{y}} d\mathbf{s}.$$

Since in this formula, the variables $\mathbf{x}$ and $\mathbf{y}$ are well separated, the imaginary part of the discrete Green convolution (1) can obtained by a standard quadrature $(\mathbf{s}_m;\sigma_m)_{1\leq m\leq M}$ on S^2 :

$$\begin{aligned} \mathfrak{Im}\left(G\star f(\mathbf{x})\right) &\sim \frac{k}{(4\pi)^2}\sum_{m=1}^{M} e^{ik\mathbf{x}\cdot\mathbf{s}_m} g_m, \\ \text{with} \quad g_m &= \sigma_m \sum_{n=1}^{N} e^{-ik\mathbf{s}_m\cdot\mathbf{y}_n} f_n, \end{aligned}$$

where each sum is fastly and successively computed using a type-III NUFFT (complexity $N \log N$).

For the real part, we have proposed a quadrature rule to approximate the cosine function as sum of (dilated) sine functions (e.g. [1, 2]), enough sparse on a large interval of $k|\mathbf{x}-\mathbf{y}|$. It leads to a final quadrature $(\xi_l;\omega_l)_{1\leq l\leq L}$ of the full space $\mathbb{R}^3$, constructed as concentric spheres. The final formalism for eq. (1) is :

$$\begin{aligned} G\star f(\mathbf{x}) &\sim \frac{k}{(4\pi)^2}\sum_{l=1}^{L} e^{ik\mathbf{x}\cdot\xi_l} h_l, \\ \text{with} \quad h_l &= \omega_l \sum_{n=1}^{N} e^{-ik\xi_l\cdot\mathbf{y}_n} f_n, \end{aligned}$$

where each sum is evaluated by type-III NUFFT. The complexity has been theoretically studied for the Green Laplace kernel in [1], numerically evaluated for Helmoltz kernel in [2], and the final mono-level algorithm goes as $N^{\frac{6}{5}} \log N$.

2 Test case, a Dirichlet problem

To evaluate the approach, a Matlab solver with Galerkin boundary element approximation has been developed, firstly for Helmholtz equation. This library, called MyBEM, provide direct BEM resolution, iterative FMM (from L. Greengard [3, 4]) and new SCSD computation. This library was parallelized, using the Matlab Parallel Toolbox, and an 8-core computer cadenced at 3GHz was used.

For this validation, analytical results from infinite spherical scattering u^∞ is compared to the numerical solution u provided by MyBEM,

SNR (dB)			*BEM*		*FMM*		*SCSD*	
N_{dof}	f (Hz)	$kr_{\max}$	SNR_2	SNR_∞	SNR_2	SNR_∞	SNR_2	SNR_∞
10^3	300	5	0.017	0.032	0.033	0.067	0.016	0.032
10^4	1000	19	0.002	0.008	0.017	0.060	0.009	0.024
10^5	3200	118	-	-	0.011	0.039	0.019	0.073
10^6	10000	368	-	-	0.021	0.120	0.014	0.090

TOTAL TIMES (s)			*BEM*	*FMM*		*SCSD*	
N_{dof}	f (Hz)	$kr_{\max}$	Time (s)	Time (s)	N_{iter}	Time (s)	N_{iter}
10^3	300	5	2.91	1.76	5	1.67	5
10^4	1000	19	162	15.7	7	8.07	7
10^5	3200	118	-	197	9	95.8	9
10^6	10000	368	-	2700	12	1400	12

FIGURE 1 – Time and accuracy comparison beetween direct BEM, FMM and SCSD computation.

and following signal to noise ratio gives the accuracy :

$$SNR_2 = \sqrt{\frac{1}{n}\sum_{i=1}^{n}\left[20\log 10\left(\left|\frac{u_i}{u_i^\infty}\right|\right)\right]^2},$$

$$SNR_\infty = \max_{i\in[1,n]}\left|20\log 10\left(\left|\frac{u_i}{u_i^\infty}\right|\right)\right|.$$

In this case, a piecewise linear approximation with Brackage-Werner formulation was used to solve boundary integral equation. As shown in figure 1, MyBEM provides a good accuracy from 10^3 to 10^6 degrees of freedom N_{dof}. Moreover, the SCSD seems to be significantly faster than the FMM.

3 Conclusion

We provide a new promising fast convolution on unstructured grid method, and first results from concrete implementation in numerical solver gives good matching with well known methods as FMM. Same results obtained by MyBEM, not detailed in this abstract, are obtained for the Maxwell equations.

4 References

Références

[1] Alouges, F., & Aussal, M. (2015). *The sparse cardinal sine decomposition and its application for fast numerical convolution.* Numerical Algorithms, 1-22.

[2] Aussal, M. (2014). *Méthodes numériques pour la spatialisation sonore, de la simulation à la synthèse binaurale.* Doctoral dissertation, Ecole Polytechnique X.

[3] Greengard, L., & Rokhlin, V. (1987). *A fast algorithm for particle simulations.* Journal of computational physics, 73(2), 325-348.

[4] Greengard, L. (1988). *The rapid evaluation of potential fields in particle systems.* MIT press.

[5] Greengard, L., & Lee, J. Y. (2004). *Accelerating the nonuniform fast Fourier transform.* SIAM review, 46(3), 443-454.

[6] Lee, J. Y., & Greengard, L. (2005). *The type 3 nonuniform FFT and its applications.* Journal of Computational Physics, 206(1), 1-5.

A Spectral View On Convolution Quadrature Type Method For The Wave Equation.

Timo Betcke[1], **Nicolas Salles**[1,*]
[1]Department of Mathematics, University College London, London, United-Kingdom
*Email: n.salles@ucl.ac.uk

Abstract

Convolution Quadrature (CQ) methods are Laplace transform type methods for the solution of time-domain problems, usually using Boundary Integral Equations. Several new analytical results on the convergence of the numerical solution of acoustic problems computed using a CQ type method with multistep schemes are presented. We will show that it's possible to achieve exponential convergence of the numerical solution to the exact solution of the underlying time-stepping scheme solution. The rate of convergence relies upon the underlying time-stepping scheme and upon the radii of analyticity of the Laplace-domain boundary condition and solution, and so on the integral formulation. Actually, the integral formulation employed has a big impact on the rate of convergence that can be obtained. Numerical examples computed with the BEM++ library will be presented.

Keywords: convolution quadrature, wave equation, boundary element method

1 Introduction

Convolution Quadrature (CQ) is an efficient technique for the solution of time-domain problems using Boundary Element Methods with an interesting property: independent frequency-domain problems have to be solved [1, 2]. We use this technique to solve the acoustic problem that follows:

$$\begin{cases} \dfrac{\partial^2 u}{\partial t^2}(x,t) - c^2 \Delta_x u(x,t) = 0, \ x \in \Omega_e, \\ u(x,0) = \dfrac{\partial u}{\partial t}(x,0) = 0, \\ u(x,t) = g(x,t) \text{ for } x \in \Gamma, \end{cases} \tag{1}$$

where $\Omega \subset \mathbb{R}^3$ is a compact obstacle, $\Gamma = \partial\Omega$ its boundary and $\Omega_e = \mathbb{R}^3 \backslash \bar{\Omega}$ the exterior domain where we solve the wave equation.

The idea is based on a Z-Transform of the time steps of an underlying time-stepping scheme and a simple (but accurate) trapezoidal rule to approximate the inverse Z-Transform. For the wave equation, this leads to a range of modified Helmholtz problems. The time domain solution is then synthesised by an inverse Z-transform. Typically, the number of frequency problems is chosen to be the same as the number of time steps. However, in contrast to previous presentations we decouple the number of frequency solves from the number of time steps in order to achieve a better accuracy. Actually, an exponential convergence to the solution of the underlying time-stepping scheme is obtained [6].

2 Convolution Quadrature Methods

The time-domain solution, related to a multistep scheme, of (1) is obtained by the inverse Z-transform, that is given as a simple contour integral of the Laplace-domain variable U_d

$$u_d(x, t_n) = \frac{1}{2\pi i} \int_{\mathcal{C}} \frac{U_d(x,z)}{z^{n+1}} dz, \tag{2}$$

where $\mathcal{C}$ is a contour around the origin in the region of convergence of the Z-transform. U_d is the solution of a frequency-domain problem, actually the modified Helmholtz problem:

$$\begin{aligned} &\left(\frac{\gamma(z)}{c\Delta t}\right)^2 U_d(x,z) - \Delta U_d(x,z) = 0, \quad x \in \Omega_e, \\ &U_d(x,z) = G(x,z), \quad x \in \Gamma, \end{aligned} \tag{3}$$

where $\gamma(z)$ is the generating polynomial of the multistep scheme used, Δt is the time step, c is the speed of the sound in Ω_e, and $U_d(x,z) = \sum_{n=0}^{\infty} u_d(x,t_n) z^n$, and $G(x,z) = \sum_{n=0}^{\infty} g(x,t_n) z^n$, are the Z-Transforms of respectively the solution and the Dirichlet data. For example, for Backward Euler it holds that $\gamma(z) = 1 - z$. For the contour integration, we use a circle of radius λ: $\mathcal{C} = \{z \in \mathbb{C} : |z| = \lambda\}$ for some appropriately chosen $\lambda > 0$.

By choosing λ such that the Laplace-domain solution U_d is analytic in the neighborhood of the disk of radius $\lambda > 0$, we can take advantage of the property of the exponential convergence of the trapezoidal rule [4] to approximate (2). The trapezoidal rule is performed with N_f frequencies at the points $z_k = e^{-2\pi i \frac{k}{N_f}}$ with $k = 1, \ldots, N_f$. This leads to

$$u_d^{(N_f)}(x,t_n) := \frac{\lambda^{-n}}{N_f}\sum_{\ell=1}^{N_f}\frac{U_d(x,\lambda z_\ell)}{z_\ell^n}. \qquad (4)$$

The accuracy of computing $u_d^{(N_f)}$ via (4) depends on the number N_f of frequency problems solved and on the ratio $\frac{\lambda}{\lambda_U}$, with λ_U the radius of analyticity of U_d.

3 Integral formulations and Convergence

In [6], we present for $\left|u_d(x,t_n) - u_d^{(N_f)}(x,t_n)\right|$ an estimate and an asymptotic estimate when $N_f \to \infty$ that allow to choose λ and N_f to get a desired accuracy. The error estimate relies upon the radius of analyticity of the Laplace-domain solution U_d of (3) and then on the location of the closest scattering poles [3] and the eigenfrequencies related to the interior problem. These eigenfrequencies, that play a major role in the convergence, are result of the integral formulation chosen. It is new to study the influence of the integral formulation on CQ methods. Several indirect integral formulations (first kind, second kind and combined formulation with different combining coefficients) will be compared. Figure 1 shows the absolute error of the solution obtained with an indirect second kind formulation for several λ (see also [6]).

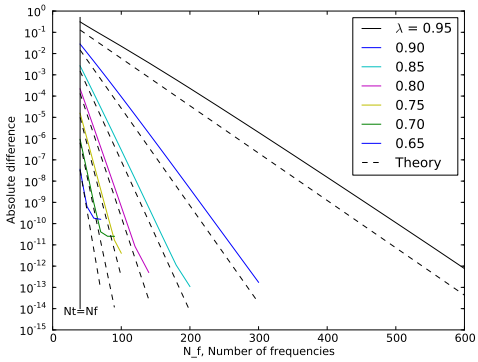

Figure 1: Absolute difference of the solution with a reference solution for the scattering by the unit sphere using indirect second kind formulation for several different λ. The accuracy obtained usually is indicated by $N_t = N_f$.

4 Conclusion

The convergence of CQ methods, actually of (4) to (2), when the number of frequencies increases is studied. The integral formulation used, the number of frequencies and the radius λ of the contour play a major role. Actually, the key point is the location of the resonant poles and the eigenfrequencies of the interior problem relative to the contour. Numerical results obtained using the BEM++ library[1] [5] will be shown.

Acknowledgments. This work was supported by Engineering and Physical Sciences Research Council Grant EP/K03829X/1.

References

[1] Lubich, C., *Convolution quadrature and discretized operational calculus. I*, Numerische Mathematik, (1988).

[2] Banjai, L. and Sauter, S., *Rapid Solution of the Wave Equation in Unbounded Domains*, SIAM J. Num. An., (2008).

[3] Taylor, M. E.,*Partial Differential Equations II: Qualitative Studies of Linear Equations, 2nd Ed.*, Springer, (2010).

[4] Trefethen, L. N. and Weideman, J. A. C., *The exponentially convergent trapezoidal rule*, SIAM Review, (2014).

[5] Śmigaj, W. and al., *Solving Boundary Integral Problems with BEM++*, ACM Trans. Math. Software, Accepted.

[6] Betcke, T., Salles, N. and Śmigaj, W., *Exponentially accurate evaluation of time-stepping schemes for the wave equation via Convolution Quadrature type Methods*, Submitted.

[1] `http://www.bempp.org`

Using impedance transmission conditions in time domain - the application to thin sheets for the eddy current model.

Maxim Felde[1,*], **Kersten Schmidt**[1]

[1]Research center Matheon & Department of Mathematics, TU Berlin, Berlin, Germany

[*]Email: maxim.felde@math.tu-berlin.de

Abstract

Impedance transmission conditions (ITC) are used for the model reduction of eddy current problems with thin conducting sheets. We show how ITC derivated for frequency domain can be applied for problems in time domain. Due to the time convolution, the resulting systems exhibit in general a nonlocal dependency in time. For the time discretisation we use convolution quadrature (CQ) and fast and oblivious convolution quadrature method (FOCQ), developed in [1, 2], see also [3].

Keywords: impedance transmission conditions, convolution quadrature

Model problem

We consider a time dependent eddy current problem in the open bounded domain Ω, consisting of insulating domain Ω^d_{ext} and conducting sheet Ω^d_{int} of thickness d, where $\Omega^d_{\text{ext}} = \Omega \setminus \overline{\Omega}^d_{\text{int}}$,

$$\begin{aligned} \mu\sigma u_t - \Delta u &= 0 && \text{in } \Omega^d_{\text{int}} \times (0,T), \\ -\Delta u &= f && \text{in } \Omega^d_{\text{ext}} \times (0,T), \\ u(\cdot,t) &= 0 && \text{on } \partial\Omega \times (0,T), \\ u(\cdot,0) &= 0 && \text{in } \Omega, \end{aligned} \tag{1}$$

with fixed time $T > 0$ and source term $f \in L^2(0,T;L^2(\Omega))$ with $f(\cdot,0) = 0$. In frequency domain the term u_t in (1) is replaced by $-i\omega\hat{u}$ (or in Laplace domain by $s\hat{u}$). Here, ITC are approximate conditions on the mid-line Γ of Ω^d_{int}, which replace the first equation in (1). In [4, 5] several ITC in the form

$$\begin{aligned} -[\hat{u}] &= \hat{T}_{12}\{\hat{u}\} + \hat{T}_{13}\{\partial_n\hat{u}\}, \\ -[\partial_n\hat{u}] &= \hat{T}_{22}\{\hat{u}\} + \hat{T}_{23}\{\partial_n\hat{u}\}, \end{aligned} \tag{2}$$

are proposed.

In (2), $\hat{u}$ is the Laplace transform of (an approximation to) u, $\hat{T}_{ij}$ some functions, which depend on the choice of the ITC, $[\cdot]$ denotes the jump, and $\{\cdot\}$ the mean value over Γ. With the

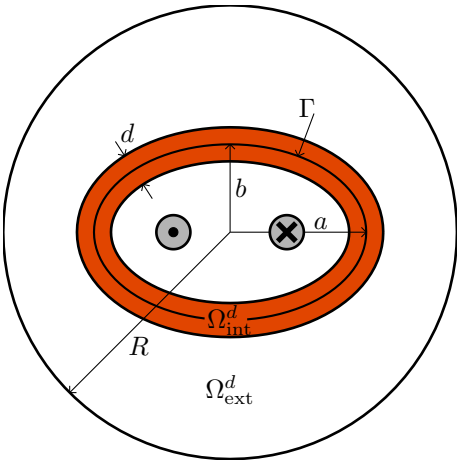

Figure 1: Geometrical setting. Ω^d_{ext} – insulating, Ω^d_{int} - conducting, Γ – interface on which the Ω^d_{int} is reduced.

Laplace inversion formula, we get

$$\begin{aligned} K_{ij}g &:= \int_0^t T_{ij}(t-\tau)g(\tau)\,d\tau \\ &= \frac{1}{2\pi i}\int_\gamma \hat{T}_{ij}(s)\int_0^t e^{s(t-\tau)}g(\tau)d\tau\,ds, \end{aligned} \tag{3}$$

where T_{ij} is the inverse Laplace transform of $\hat{T}_{ij}$. The inner integral is the solution of the initial value problem $y' = sy + g,\ y(0) = 0$, which is solved by time integration, e.g., a Runge-Kutta method.

In case of ITC-1-0, ITC-1-1 and ITC-2-0, for which only $\hat{T}_{22}$ is non zero, the model in the time domain can be written as

$$\begin{aligned} -\Delta u &= f && \text{in } \Omega \times (0,T), \\ [\partial_n u] + K_{22}\{u\} &= 0 && \text{on } \Gamma \times (0,T), \end{aligned} \tag{4}$$

with initial and boundary conditions as in (1). A spatial discretisation of (4) leads then to the mixed system

$$\begin{aligned} \mathbf{B}_{11}\boldsymbol{u}(t) + \mathbf{B}_{12}\boldsymbol{\lambda}(t) &= \boldsymbol{\varphi}(t) && \text{for } t \in (0,T), \\ K_{22}\mathbf{B}_{21}\boldsymbol{u}(t) + \mathbf{B}_{22}\boldsymbol{\lambda}(t) &= 0 && \text{for } t \in (0,T), \end{aligned}$$

where $\boldsymbol{u}(t)$ and $\boldsymbol{\lambda}(t)$ are the coefficient vectors for $u(t)$ and $[\partial_n u](t)$, $\mathbf{B}_{11}$ is the stiffness matrix in Ω, $\mathbf{B}_{12}, \mathbf{B}_{21}$ and $\mathbf{B}_{22}$ are mass matrices on Γ.

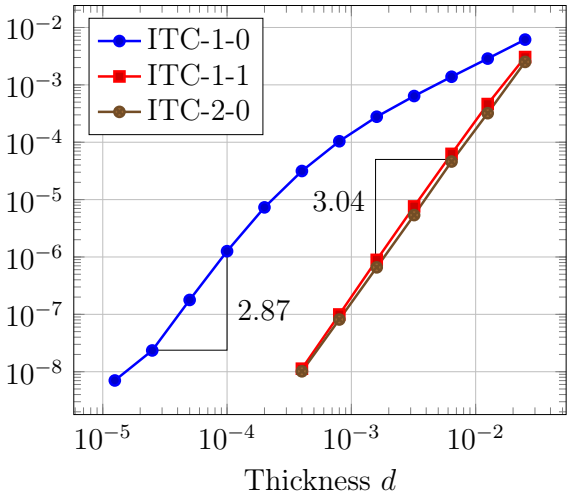

Figure 2: Relative error over thickness d.

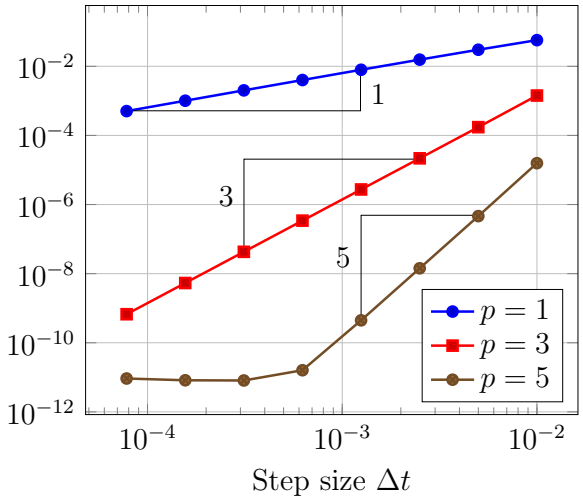

Figure 3: Relative error over the step size Δt for Runge-Kutta of order p.

An approximation to $K_{22}\mathbf{B_{21}}\boldsymbol{u}(t_n)$, for $n = 1 \dots N$, $(N+1)\Delta t = T$, is obtained using Runge-Kutta values $\tilde{\boldsymbol{u}}_j$ and

$$\sum_{j=0}^{n} (\mathbf{W}_{n-j} \otimes \mathbf{B}_{21}) \tilde{\boldsymbol{u}}_j \qquad (5)$$

with weighting matrices $\mathbf{W}_j$, depending on $\hat{T}_{22}$. Using CQ, the evaluation of (5) requires $\mathcal{O}(N^2)$ multiplications.

We use FOCQ for an efficient evaluation of (5). Here, the effort to compute the convolution behaves only like $\mathcal{O}(N \log N)$. Moreover, only logarithmicaly few linear combinations of $\tilde{\boldsymbol{u}}_j$ are kept in memory [2].

Numerical results

ITC in frequency domain improve the accuracy for thinner sheets, which however depend on the frequency. For a time-dependent source, continuous in frequency, we observe a convergence rate of approximately 3 for the ITC-1-0, ITC-1-1 and ITC-2-0 models, see Fig. 2. Numerical experiments show a convergence in step size Δt, which corresponds to the order of underlying Runge-Kutta method, see Fig. 3.

References

[1] C. Lubich, and A. Ostermann, Runge-Kutta methods for parabolic equations and convolution qadrature. In *Math. Comp.* 60 (1993) pp. 105–131.

[2] A. Schädle, M. López-Fernández, and C. Lubich, Fast and Oblivious Convolution Quadrature. In *SIAM J. Sci. Comp.* 28 (2006), Nr. 2, pp. 421–438.

[3] R. Hiptmair, M. López-Fernández, and A. Paganini, Fast Convolution Quadrature Based Impedance Boundary Conditions. In *J. Comp. Appl. Math.* (2013), pp. 500–517.

[4] K. Schmidt, and S. Tordeux, High order transmission conditions for thin conductive sheets in magneto-quasistatics. In *ESAIM: M2AN* 45 (2011), pp. 1115–1140.

[5] K. Schmidt, and A. Chernov, A unified analysis of transmission conditions for thin conducting sheets in the time-harmonic eddy current model. In *SIAM J. Appl. Math* 73 (2013) pp. 1980–2003.

Wave splitting for time-dependent scattered field separation

Marcus Grote[1], **Marie Kray**[1,*], **Frédéric Nataf**[2], **Franck Assous**[3]
[1]Institute of Mathematics, University of Basel, Rheinsprung 21, CH-4051 Basel, Switzerland
[2]CNRS-UPMC Univ Paris 06, UMR 7598, Laboratoire Jacques-Louis Lions, F-75005, Paris, France & INRIA Rocquencourt, Alpines, BP105, 78153 Le Chesnay cedex, France
[3]Department of Computer Sciences and Mathematics, Ariel University, 40700, Ariel, Israel
[*]Email: marie.kray@unibas.ch

Abstract

Starting from classical absorbing boundary conditions, we propose a method for the separation of time-dependent scattered wave fields due to multiple sources or obstacles. In contrast to previous techniques, our method is local in space and time, deterministic, and also avoids a priori assumptions on the frequency spectrum of the signal.

Keywords: Wave splitting, multiple scattering, absorbing boundary conditions

1 Introduction

When an incident wave illuminates a target, it generates a scattered wave which carries information about the obstacle. However, if the location, spatial distribution or time dependence of the original source are not precisely known, or other undesired sources interfere with the signal, extraction of the scattered field by subtraction of the incident wave becomes non-trivial.

In the frequency-domain, various methods are available to extract a single scattered field from the superposition of multiple wave fields [1, 2]. In the time-domain, Potthast *et al.* [4] applied via Fourier transform the point source method, which relies on integral based formulations. Here we propose a different approach, which is local in space and time, deterministic, and also avoids any a priori assumptions on the frequency spectrum of the signal.

2 Wave splitting

We consider wave scattering from two bounded disjoint scatterers in unbounded two- or three-dimensional space, which are well separated, i.e. which can be surrounded by two non-intersecting spheres S_1 and S_2. In the unbounded region Ω outside the two spheres, we assume that the medium is homogeneous, isotropic and source-free. Hence the scattered field u satisfies:

$$\frac{\partial^2 u}{\partial t^2} \; - \; c^2 \Delta u \; = \; 0 \qquad \text{in } \Omega, \quad t > 0, \qquad (1)$$

with constant wave speed $c > 0$. Moreover we assume that u is initially confined to the interior of the two spheres. Hence it splits into two unique wave fields u_1 and u_2 [3]:

$$u \; = \; u_1 \; + \; u_2 \qquad \text{in } \Omega, \quad t > 0, \qquad (2)$$

where each u_k satisfies (1) and is purely outgoing outside of S_k, $k = 1, 2$.

Now, let Γ denote a surface patch in three dimensions or a curve segment in two dimensions, not necessarily closed or connected. Given the measured values of u on Γ, we wish to recover the entire time history of u_1 and u_2. Since each u_k is outgoing, it can be written as a progressive wave expansion in inverse powers of distance. In 1980, Bayliss and Turkel [5] derived a sequence of differential operators that annihilate the leading order terms in that expansion:

$$B_k[u_k] = \; O\left(\frac{1}{r_k^{2m+1}}\right), \quad k = 1, 2, \qquad (3)$$

where k identifies the local spherical coordinate system $(r_k, \theta_k, \varphi_k)$ centered about the origin of the sphere S_k. Neglecting the error term in (3), we thus obtain on Γ for $j = 1, 2$:

$$B_j[u_k] \; = B_j[u_k + u_j] = \; B_j[u], \quad k \neq j. \qquad (4)$$

Since u is known on Γ, equation (4) yields a partial differential equation for the unknown wave field u_k. In general, it will involve tangential, normal and time derivatives. By rewriting the normal derivative as a combination of tangential and radial derivatives, and then using (3) to replace radial by time derivatives, the resulting equation will involve only tangential and time derivatives and thus be restricted to Γ.

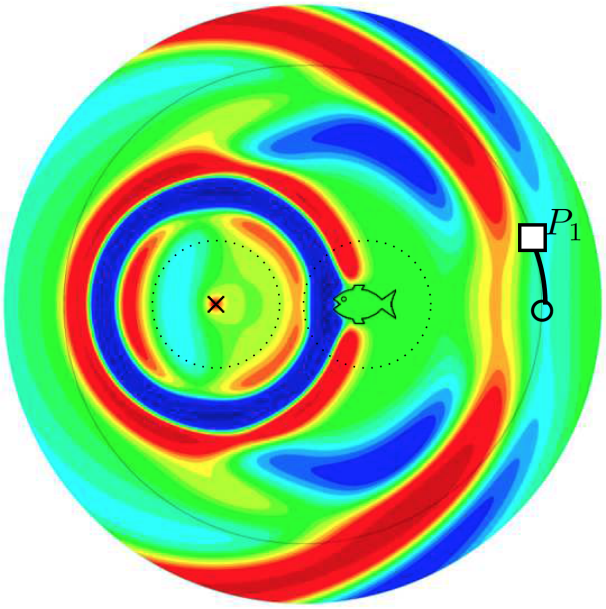

Figure 1: Snapshot of the total field. The incident wave originates from a point source, which impinges on a sound-soft fish-shaped obstacle.

Clearly, appropriate initial and boundary conditions must also be set for well-posedness.

3 Two-dimensional example

We consider a numerical experiment in two-space dimensions with B_j in (4) set to the first-order Bayliss-Turkel boundary condition from (3) with $m = 1$. On a circular arc Γ, after replacing normal by tangential and time derivatives, (4) becomes

$$\left[\alpha_k(\theta_k)\frac{\partial}{\partial t} + \beta_k(\theta_k)\frac{\partial}{\partial \theta_k} + \gamma_k(\theta_k)\right](\sqrt{r_k}u_k) = B_j[u] \tag{5}$$

where $\alpha_k(\theta_k)$, $\beta_k(\theta_k)$ and $\gamma_k(\theta_k)$ can be explicited. Since (5) is hyperbolic, we set boundary conditions according to its characteristics. Moreover we set homogeneous initial conditions, since at the initial time, all fields vanish in Ω.

Now, an incident wave originating from a point source u_1 generates a scattered field u_2 as it impinges upon a sound-soft fish-shaped inclusion, see Fig. 1. To recover u_1 at P_1, we only need to solve (5) on the short arc connecting the two points $\theta_1 = 0$ and P_1, due to the direction of the characteristics, see Fig. 1. In Fig. 2, we display at location P_1 the total field u together with u_1, obtained from (5), and also u_2 obtained by subtraction.

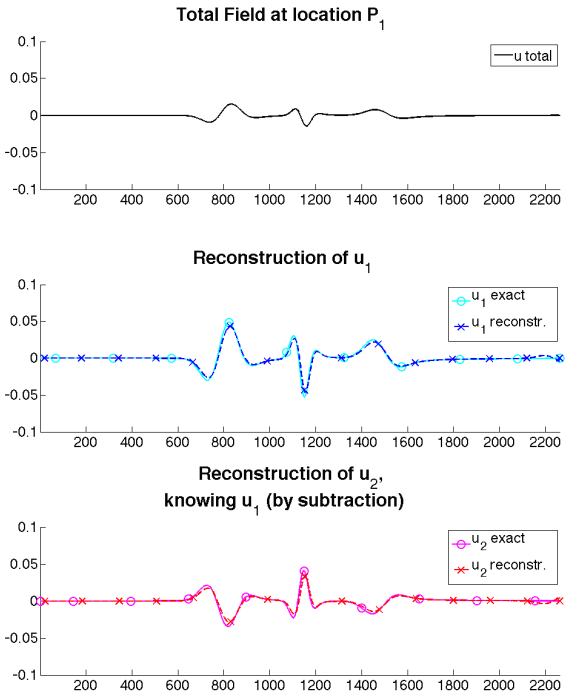

Figure 2: Recovery of wave fields u_1 and u_2 from total field measurements u at location P_1. Top: total field u. Middle: u_1 recovered by solving (5). Bottom: u_2 obtained by subtraction.

References

[1] F. Ben Hassen, J. Liu, and R. Potthast. On source analysis by wave splitting with applications in inverse scattering of multiple obstacles. *J. Comput. Math*, **625**(3) (2007) 266–281.

[2] R. Griesmaier, M. Hanke, and J. Sylvester. Far field splitting for the Helmholtz equation. *SIAM J. Numer. Anal.*, **652**(1) (2014) 343–362.

[3] M. J. Grote and C. Kirsch. Nonreflecting boundary condition for time-dependent multiple scattering. *J. Comput. Phys.*, **6221**(1) (2007) 41–67.

[4] R. Potthast, F. M. Fazi, and P. A. Nelson. Source splitting via the point source method. *Inv. Problems*, **626**(4) (2010) 045002.

[5] A. Bayliss and E. Turkel. Radiation boundary conditions for wave-like equations. *Comm. Pure Appl. Math.*, **33**(6) (1980) 707–725.

Far field splitting by iteratively reweighted ℓ^1 minimization

Roland Griesmaier[1,*], **John Sylvester**[2]
[1]Institut für Mathematik, Universität Würzburg, Germany
[2]Department of Mathematics, University of Washington, Seattle, Washington
[*]Email: roland.griesmaier@uni-wuerzburg.de

Abstract

The aim of far field splitting for time-harmonic acoustic or electromagnetic waves is to decompose the far field of a wave radiated by an ensemble of several compactly supported sources into the individual far field components radiated by each of these sources separately. Without further assumptions this is an ill-posed inverse problem. Observing that far fields radiated by compactly supported sources have nearly sparse representations with respect to certain suitably transformed Fourier bases that depend on the approximate source locations, we reformulate the far field splitting problem as a weighted ℓ^1 minimization problem in the spirit of basis pursuit. To this end we assume that some a priori information on the locations of the individual source components is available. We discuss the equivalence of this minimization problem with the far field splitting problem, consider a numerical algorithm to approximate its unique solution, and we propose an iterative strategy to successively improve the required a priori information on the approximate source locations.

Keywords: Helmholtz equation, far field splitting, source splitting

1 Introduction

Given a compactly supported function $f \in L^2_0(\mathbb{R}^2)$ and a fixed *wave number* $\kappa > 0$ we consider the *source problem* for the Helmholtz equation

$$-\Delta u - \kappa^2 u = f \qquad \text{in } \mathbb{R}^2\,, \tag{1a}$$

$$\lim_{r\to\infty} \sqrt{r}\Big(\frac{\partial u}{\partial r} - \mathrm{i}\kappa u\Big) = 0 \qquad \text{for } |x| = r\,. \tag{1b}$$

It is well known that the unique solution $u \in H^1_{\mathrm{loc}}(\mathbb{R}^2)$ to (1) has the asymptotic behavior

$$u(x) = \frac{e^{\mathrm{i}\pi/4}}{\sqrt{8\pi\kappa}} \frac{e^{\mathrm{i}\kappa|x|}}{\sqrt{|x|}} u^\infty(\widehat{x}) + O\left(|x|^{-3/2}\right)$$

as $|x| \to \infty$, where $\widehat{x} := x/|x|$ and

$$u^\infty(\widehat{x}) = \int_{\mathbb{R}^2} e^{-\mathrm{i}\kappa\widehat{x}\cdot y} f(y)\,\mathrm{d}y\,, \qquad \widehat{x} \in S^1\,. \tag{2}$$

We refer to f as the *source* and to u^∞ as the *far field radiated by* f.

2 Splitting far field patterns radiated from well-separated domains

Suppose next that u^∞ from (2) is the superposition

$$u^\infty = u_1^\infty + \cdots + u_m^\infty \tag{3}$$

of m far fields $u_1^\infty, \ldots, u_m^\infty$ supported in well separated balls $B_{r_1}(z_1), \ldots, B_{r_m}(z_m)$, i.e., $|z_j - z_l| \gg r_j + r_l$ for $1 \le j, l \le m$, $j \ne l$. By this we mean that there exist sources $f_j \in L^2_0(B_{r_j}(z_j))$, $j = 1, \ldots, m$, such that $\mathcal{F}_{B_{r_j}(z_j)} f_j = u_j^\infty$, where the *restricted far field operator* $\mathcal{F}_{B_{r_j}(z_j)} : L^2(\Omega) \to L^2(S^1)$ is given by

$$(\mathcal{F}_{B_{r_j}(z_j)} f)(\widehat{x}) := \int_{B_{r_j}(z_j)} e^{-\mathrm{i}\kappa\widehat{x}\cdot y} f(y)\,\mathrm{d}y\,.$$

The decomposition on the right hand side of (3) is uniquely determined. In fact, it follows immediately from [3, Lemma 6] that

$$\mathcal{R}(\mathcal{F}_{B_{r_j}(z_j)}) \cap \mathcal{R}(\mathcal{F}_{B_{r_l}(z_l)}) = \{0\}\,, \qquad j \ne l\,.$$

On the other hand, the adjoint of the restricted far field operator $\mathcal{F}_{B_{r_j}(z_j)}$, $1 \le j \le m$, is the Herglotz operator $\mathcal{F}^*_{B_{r_j}(z_j)} : L^2(S^1) \to L^2(\Omega)$,

$$(\mathcal{F}^*_{B_{r_j}(z_j)} g)(y) = \int_{S^1} e^{\mathrm{i}\kappa\widehat{x}\cdot y} g(\widehat{x})\,\mathrm{d}s(\widehat{x})\,,$$

and using the one-to-one correspondence between Herglotz wave functions and their kernels (cf. [1, Theorem 3.15]) it follows that $\mathcal{F}^*_{B_{r_j}(z_j)}$ is injective, and thus $\mathcal{F}_{B_{r_j}(z_j)}$ has dense range. In this talk we consider the inverse problem to split the far field u^∞ as in (3) into its individual components $u_1^\infty, \ldots, u_m^\infty$.

Assuming that the approximate locations of the individual source components are known a

priori, we recently discussed in [2] a Galerkin method for this far field splitting problem. More precisely, this algorithm requires the centers and the radii of well separated balls in space

$$B_{r_1}(z_1), \ldots, B_{r_m}(z_m)$$

as above containing the supports of the individual source components. The finite dimensional subspaces used in this Galerkin scheme are spanned by singular vectors of the restricted far field operators $\mathcal{F}_{B_{r_1}(z_1)}), \ldots, \mathcal{F}_{B_{r_m}(z_m)})$ associated with the balls containing the individual source components, and the number of degrees of freedom is directly related to the size of these balls. The Galerkin approach has both advantages and shortcomings: It is very fast and highly accurate as long as the balls containing the individual source components given as a priori information are sufficiently small relative to their distances. However, if this is not the case for whatever reasons (e.g., if the a priori information is not sharp), then the Galerkin scheme becomes ill-conditioned and the reconstructions deteriorate.

The aim of the method presented in this talk is to reduce the dependence of the reconstructed far field components on the accuracy of the given a priori information on the approximate source locations. To this end we replace the Galerkin approach, which may be considered as a finite dimensional least squares best approximation problem, by a weighted ℓ^1 minimization problem in the spirit of basis pursuit. We prove that the unique solution to this weighted ℓ^1 minimization problem coincides with the solution to the far field splitting problem, and we discuss its numerical approximation. Furthermore, we propose an iterative strategy to successively improve the available a priori information by solving a sequence of these weighted ℓ^1 minimization problems, where estimates of the approximate locations of the individual source components that are used as a priori information for the next iteration are computed from the value of the current solution. This also gradually decreases the ill-posedness of the splitting problem, and it significantly improves the quality of the reconstructions. We present a series of numerical examples to demonstrate the performance of this algorithm.

References

[1] D. Colton and R. Kress, *Inverse Acoustic and Electromagnetic Scattering Theory*, 2nd ed., Springer, Berlin, 1998.

[2] R. Griesmaier, M. Hanke, and J. Sylvester, Far field splitting for the Helmholtz equation, *SIAM J. Numer. Anal.*, 52 (2014), 343–362.

[3] J. Sylvester, Notions of support for far fields, *Inverse Problems*, 22 (2006), 1273–1288.

A high-order solver for inhomogeneous penetrable scattering in two dimensions

Jagabandhu Paul[1,*], **Ambuj Pandey**[1], **Akash Anand**[1], **B.V. Rathish Kumar**[1]
[1]Department of Mathematics and Statics, Indian Institute of Technology Kanpur, India
*Email: jagapaul@iitk.ac.in

Abstract

We present a high-order method for solving a volume-surface integro-differential equation, which is used to model the acoustic and electromagnetic scattering problem for penetrable, inhomogeneous media with variable material properties in two-dimensions. The rapid convergence is achieved through suitable changes of variables aimed at analytically resolving the singularities present in the integral operator. This procedure also employs efficient and accurate interpolation schemes for off-grid evaluation of the discrete data needed by quadratures as well as for accurate approximations of differential operators.

Keywords: Wave scattering, High-order methods, Penetrable inhomogeneous media.

Introduction

We present a high-order method to solve an integral equation (1), see [4],

$$\psi(\boldsymbol{r}) = \psi_{inc}(\boldsymbol{r}) + (\mathcal{K}\psi)(\boldsymbol{r}) + (\mathcal{S}\psi)(\boldsymbol{r}), \quad (1)$$

with $(\mathcal{K}\psi)(\boldsymbol{r}) = \int_{\Omega} G_e(\boldsymbol{r},\boldsymbol{r}')(V\psi)(\boldsymbol{r}')\,dv'$, and $(\mathcal{S}\psi)(\boldsymbol{r}) = \int_{\partial\Omega} G_e(\boldsymbol{r}',\boldsymbol{r}')F(\boldsymbol{r}')\,d\sigma'$,
that is equivalent to the scattering problems modeled by Bergmann's equation (2),

$$\rho(\boldsymbol{r})\nabla\cdot\left[\frac{1}{\rho(\boldsymbol{r})}\nabla\psi(\boldsymbol{r})\right] + \kappa(\boldsymbol{r})^2\psi(\boldsymbol{r}) = 0, \quad (2)$$

where ψ is the unknown field, ρ_i, ρ_e and κ_i, κ_e are the densities and the wave-numbers inside the obstacles Ω and exterior to Ω, respectively, while ψ and $(1/\rho)\partial\psi/\partial\boldsymbol{n}$ are continuous across the interface of Ω and $\psi - \psi_{inc}$ satisfies the Sommerfeld radiation condition. The kernel $G_e(\boldsymbol{r},\boldsymbol{r}') = 1/4H_0^1(\kappa_e|\boldsymbol{r}-\boldsymbol{r}'|)$, $V\psi = (\kappa_e^2-\kappa_i^2)\psi + \rho_i^{-1}(\nabla\rho_i)\cdot\nabla\psi$, and $F = \{\rho_e/\rho_i - 1\}\partial\psi/\partial\boldsymbol{n}'$. Recall that (1) models the electromagnetic scattering problem with $\psi = E_z$, $\rho = \mu$ in **TM**-mode, and $\psi = H_z$, $\rho = \epsilon$ in **TE**-mode, in addition to the two-dimensional acoustic scattering problem.

To our knowledge, only limited attempts have been made toward obtaining high-order numerical solution to this problem in its general configuration. One among them is [2], where the authors provide a fast solver for the problem in three dimensions, fails to achieve rapid convergence. The main goal of the present work is to extend the ideas presented in [3] and [1], to produce a high-order method for solution of a general version of the scattering problem where density vary inside the obstacle and is allowed to be discontinuous across the interface $\partial\Omega$.

We begin by splitting the integral domain, using a *fixed* partitions of unity $\{\omega_p(\boldsymbol{r}) : p = 1,\ldots,P_B, P_B+1,\ldots,P = P_B+P_I\}$, into P_B number of *boundary patches* and P_I number of *interior patches*, where boundary patches are homeomorphic to $(0,1)\times(0,1]$ and interior patches are homeomorphic to $(0,1)\times(0,1)$ via a smooth invertible parametrizations $\boldsymbol{r}_p = \boldsymbol{r}_p(s,t)$ for $p = 1,\ldots,P$. This allows us to rewrite the volume operator $\mathcal{K}$ as $(\mathcal{K}\psi)(\boldsymbol{r}) = \sum_{p=1}^{P}(\mathcal{K}_p\psi)(\boldsymbol{r})$, where

$$\mathcal{K}_p\psi)(\boldsymbol{r}) = \int_0^1\int_0^1 G_e(\boldsymbol{r},\boldsymbol{r}')V_p(\boldsymbol{r}')ds'dt',$$

$V_p\psi = (\kappa_e^2-\kappa_i^2(\boldsymbol{r}_p'))\psi(\boldsymbol{r}_p') + \rho_i(\boldsymbol{r}_p')^{-1}(\nabla\rho_i(\boldsymbol{r}_p(s',t')))\cdot\nabla\psi(\boldsymbol{r}_p(s',t'))w_p(\boldsymbol{r}')J_p(\boldsymbol{r}')$, $\boldsymbol{r}_p' = \boldsymbol{r}_p(s',t')$ and J_p is the Jacobian of the transformation $\boldsymbol{r}_p$. We observe that $\{\omega_p(\boldsymbol{r}|_{t=1}), p = 1,\ldots,P_B\}$ serves as a partitions of unity for $\partial\Omega$, which enable us to rewrite the surface operator $\mathcal{S}$ as $(\mathcal{S}\psi)(\boldsymbol{r}) = \sum_{p=1}^{P_B}(\mathcal{S}_p\psi)(\boldsymbol{r})$, where

$$(\mathcal{S}_p\psi)(\boldsymbol{r}) = \int_0^1 G_e(\boldsymbol{r},\boldsymbol{r}')F_p(\boldsymbol{r}')ds', \text{ and } F_p\psi =$$

$\{\rho_e/\rho_i(\boldsymbol{r}_p')-1\}\partial\psi(\boldsymbol{r}_p')/\partial\boldsymbol{n}'(\boldsymbol{r}_p')\omega_p(\boldsymbol{r}'|_{t=1})J_p^B(\boldsymbol{r}')$, where J_p^B is the surface Jacobian.

1 Numerical Schemes

We place our grid in such a way that, it simultaneously conforms to the requirements of the high order quadratures for approximations of volume and surface integral operators. Before discussing the approximation of integral operators, we briefly describe our approach for the computation of differential operators in (1).

Table 1: Convergence study for scattering by a disc centered at (0,0) with radius 1, with $\kappa_i/\kappa_e = \sqrt{2}$ and $\rho_e/\rho_i = 10^{-2}$. N_u^B, N_v^B are number of discretization points in a boundary patch and N_u^I,N_v^I are number of discretization points in an interior patch.

N_u^B	N_v^B	N_u^I	N_v^I	Rel. Err.	Ord. Conv.
16	8	16	16	4.6e-02	-
32	16	32	32	1.7e-02	1.42
64	32	64	64	3.6e-04	5.56
128	64	128	128	3.38e-06	6.77

Differential Operators: We employ an FFT based efficient and accurate two dimensional interpolation scheme, see [1], for off-grid evaluation of the discrete data. This allows us to compute required derivatives using finite difference approach with very fine step size, yielding highly accurate approximations in an efficient manner.

Surface Integral: For computing $S_p\psi$ when $\boldsymbol{r} \in \partial\Omega$ or is close to the boundary, we adopt an approach similar to the one discussed in [1]. As a first step, the singularity in the kernel is localized using a floating partition of unity. In this region, a change of integration variable centered around the point of singularity with vanishing derivatives at the origin, analytically resolves the logarithmic singularity of the kernel. We then use a high-order quadrature rule to integrate accurately. The case when $\boldsymbol{r}$ is sufficiently away from the surface, on the other hand, can be integrated in a straightforward manner owing to the smoothness of the underlying integrand.

Volume Integral: To integrate over an interior patch, we adopt the methodology similar to the one introduced in [3]. Once singularity has been extracted out using a floating partition of unit, the smooth and bi-periodic integrands are integrated using trapezoidal rule. The singular part are handled by changing to polar variables centered around the singularity followed by an application of trapezoidal rule for accurate approximation of the integral.

Our methodology to integrate over boundary patches, on the other hand, follows closely the steps prescribed in [1] where the numerical approach utilizes a change of variable in s' variable that not only resolve the kernel singularity, but also helps overcome the near singular behavior of the integrand. We refer the readers to [1] for a more detailed discussion on this methodology.

2 Numerical Results

In Table 1, we present the convergence of the proposed numerical scheme for the scattering of a plane wave incidence by a disc with constant material properties where a series solution is available for direct comparison.

Figure 1: Incident field and real part of the computed field inside a disc.

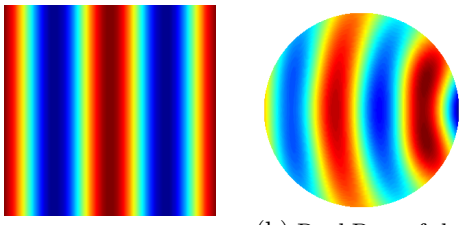

(a) Incident field (b) Real Part of the computed field

In subfigures (a) and (b) of Figure 1, we present the incident field and real part of the field inside of a disc of radius 0.8λ, centered at (0,0) with $\kappa_i/\kappa_e = \sqrt{2}$ and $\rho_e/\rho_i = 10^{-2}$ with a relative error of 10^{-6}.

Acknowledgment: Akash Anand gratefully acknowledges support from SERB-DST through contract No. SERB/F/5152/2013-2014.

References

[1] A. Anand, An Efficient High-Order Algorithm for Scattering from Penetrable Thin Structures, Ph.D. Thesis, University of Minnesota, USA, February 2006.

[2] E. Bleszynski, M. Bleszynski and T. Jaroszewicz, Fast volumetric integral-equation solver for high-contrast acoustic, *Journal of Acoustical Society of America* **124** (6), December 2008.

[3] O. P. Bruno and L. A. Kunyansky A Fast, High-Order Algorithm for the Solution of Surface Scattering Problems: Basic Implementation, Tests, and Applications, *Journal of Computational Physics,* **169** (2001), pp. 80–110.

[4] P. Martin, Acoustic Scattering by Inhomogeneous Obstacles, *SIAM Journal of Applied Mathematics* **64** (2003), No. 1, pp. 297–302.

A Super-Algebraic Convergent Solver for Systems of Biperiodic Integral Equations and Applications to Scattering of Electromagnetic Waves by Biperiodic Gratings

Thomas Rösch[1,*], **Tilo Arens**[1]

[1]KIT, Institue of Applied and Numerical Mathematiks, Karlsruhe, Germany

[*]Email: thomas.roesch@kit.edu

Abstract

We present a numerical solver for electromagnetic scattering in 3D. The solver has super-algebraic convergence rate, provided the surface is smooth enough. From a theoretical point of view, we show the basic ideas – ending up with a formulation of the main convergence theorem. And for illustrating some applications, we give numerical examples for a bounded obstacle and for an obstacle whose surface is biperiodic.

Keywords: scattering, electromagnetic waves, boundary integral equation, collocation method

1 Problem Setting

In the following let $\Omega \subseteq \mathbb{R}^3$ be an unbounded domain with $\partial\Omega = \operatorname{graph}(f)$, where $f \in C^\infty(\mathbb{R}^2, \mathbb{R})$ is assumed to be Q-periodic. We consider Maxwell's equations

$$\begin{aligned} \nabla \times E - \mathrm{i}kH &= 0 \\ \nabla \times H + \mathrm{i}kE &= 0 \end{aligned} \qquad \text{in } \mathbb{R}^3 \setminus \overline{\Omega}$$

with boundary condition $n \times E = 0$ on $\partial\Omega$ for the total field. In addition, appropriate periodicity and radiation conditions have to be posed.

To solve this problem, we make an ansatz

$$\begin{aligned} E(x) &= \nabla \times \int_{\partial\Omega} G(x,y)\, \varphi(y)\, \mathrm{d}s(y), \\ H(x) &= \frac{1}{\mathrm{i}k} \nabla \times E(x), \end{aligned} \qquad x \in \mathbb{R}^3 \setminus \overline{\Omega},$$

with density φ, being a tangential field on $\partial\Omega$, and the quasi-periodic Green's function G for the Helmholtz equation [1,3]. This leads to the boundary integral equation

$$\varphi + M\varphi = \psi \qquad \text{on } \partial\Omega, \tag{1}$$

where ψ is determined by the incident field and

$$M\varphi(x) = 2 \int_{\partial\Omega} n(x) \times \big[\nabla_x \times (G(x,y) P \varphi(y))\big]\, \mathrm{d}s(y), \quad x \in \partial\Omega.$$

P is the orthogonal projection onto the tangential space on $\partial\Omega$ and appears for numerical reasons. It simplifies the required spaces.

Unique solvability of a variational formulation of (1) in Sobolev spaces of quasi-periodic functions is obtained by adapting corresponding ideas in [1].

2 System of Integral Equations

Let $Q = (-\pi, \pi) \times (-\pi, \pi)$. For $s \geq 0$ we denote by H^s_Q the space

$$H^s_Q = \Big\{ \varphi \in L^2(Q) \;\Big|\; \sum_{\mu \in \mathbb{Z}^2} (1 + |\mu|^2)^s |\varphi_\mu|^2 < \infty \Big\},$$

where φ_μ are the Fourier coefficients of φ. Fixing some $n \in \mathbb{N}$, we set $\boldsymbol{H}^s_Q = (H^s_Q)^n$. Problem (1) can be reformulated as a system of Q-periodic integral equations: for given $\boldsymbol{\psi} \in \boldsymbol{H}^s_Q$, find $\boldsymbol{\varphi} \in \boldsymbol{H}^s_Q$ such that

$$\varphi_i(t) - \sum_{j=1}^{n} \int_Q k^{(i,j)}(t,\tau)\, \varphi_j(\tau)\, \mathrm{d}\tau = \psi_i(t) \qquad t \in Q, \quad i = 1, \ldots, n. \tag{2}$$

All integral operators turn out to be at most weakly singular so that Fredholm's theory is applicable. A unique solution to (2) can be shown to exist.

3 Numerical Method

The method is a variant of the method of Bruno and Kunyanski, see [4] and references therein. A convergence analysis of this variant was first given in [1] and subsequently improved by the authors in [2]. This variant is a fully-discrete collocation method in a space of trigonometric polynomials.

First of all, the kernel functions in (2) have a representation $k = \hat{k} + k_{\text{smooth}}$, where $k_{\text{smooth}} \in C^\infty(\mathbb{R}^2 \times \mathbb{R}^2)$ is Q-periodic in both variables while $\hat{k} \in C^\infty((\overline{Q} \times \overline{Q}) \setminus \{(t,t) \mid t \in \overline{Q}\})$ is weakly singular but also Q-periodic with respect to both arguments. Here and in the following we suppress the superscripts and assume $n = 1$ for the moment for simplicity. To remove the weak singularity, we use the substitution $\tau = t + \Pi(p)$, where

$$\Pi(p) = r\, \frac{\varrho}{\pi} \begin{pmatrix} \cos\theta \\ \sin\theta \end{pmatrix}, \qquad p = (r, \theta)^\top \in Q,$$

with some fixed $0 < \varrho < \pi$. Then, for $\varphi \in H^s_Q$ and $t \in Q$, we write $\int_Q k(t,\tau)\,\varphi(\tau)\,\mathrm{d}\tau = J_1\varphi(t) + J_2\varphi(t)$ with the integral operators

$$J_2\varphi = \int_Q k_{\mathrm{smooth}}(\cdot,\tau)\,\varphi(\tau)\,\mathrm{d}\tau \qquad \text{and}$$
$$J_1\varphi = \int_Q k_{\mathrm{polar}}(\cdot,p)\,\chi_1(\Pi(p))\,\varphi(\cdot+\Pi(p))\,\mathrm{d}p$$

and where χ_1 denotes some appropriate cut-off function. Now, k_{polar} can be considered as a smooth and Q-periodic function (in both arguments), too. Denoting by $\mathcal{T}_N$ the space of trigonometric polynomials up to order N and by P_N the projection operator onto $\mathcal{T}_N$ by trigonometric interpolation, we introduce approximations of J_1 and J_2 in the form

$$J_{2,N}\varphi(t) = \int_Q P_N[k_{\mathrm{smooth}}(t,\cdot)\,\varphi](\tau)\,\mathrm{d}\tau$$

and, due to reasons of stability and reduced computational costs,

$$J_{1,M,\tilde{M}}\varphi(t) = \int_Q P_M\big[k_{\mathrm{polar}}(t,\cdot)\, O_M\big[\{\chi_2\,\tilde{O}_{\tilde{M}}[\chi_3\,\varphi(t+\cdot)]\}\circ\Pi\big]\big](p)\,\mathrm{d}p,$$

where O_M is the L^2-orthogonal projection onto $\mathcal{T}_M$, with $\tilde{O}_{\tilde{M}}$ a scaled version of it, and χ_2, χ_3 are again some cut-off functions. The operator $J_{1,M,\tilde{M}}$ is of non-standard form, which requires some effort for the analysis of its approximation behaviour.

For the general case, $n > 1$, we obtain a fully-discrete system

$$(\boldsymbol{I} - \boldsymbol{P}_N\boldsymbol{J}_{1,M,\tilde{M}} - \boldsymbol{P}_N\boldsymbol{J}_{2,N})\,\hat{\boldsymbol{\varphi}} = \boldsymbol{P}_N\boldsymbol{\psi},$$

for $\hat{\boldsymbol{\varphi}} \in \boldsymbol{\mathcal{T}}_N = (\mathcal{T}_N)^n$. By a straightforward procedure we can generalize the following convergence result, see [2, Theorem 3.12].

Theorem 1 *Suppose $I - J_1 - J_2 \in \mathcal{L}(H^s_Q)$ and boundedly invertible for all $s \geq 0$. Let $\alpha \in (0, 1/3)$ and $\varrho = (\pi/N)^\alpha$. Assume $\sigma \geq 0$. Then for sufficiently large $s > 1$, there exists $C, N_0 > 0$ such that*

$$\|\hat{\varphi} - \varphi\|_{H^\sigma_Q} \leq C\,N^{(\sigma-s)(1-3\alpha)/2}\|\varphi\|_{H^s_Q}$$

for all $N \geq N_0$.

Here, φ denotes the exact solution. This super-algebraic convergence rate was verified by several numerical examples in [2].

References

[1] T. Arens, *Scattering by Biperiodic Layered Media: The Integral Equation Approach,* Habilitation Thesis, Karlsruhe Institute of Technology, 2010, `http://digbib.ubka.uni-karlsruhe.de/volltexte/1000016241`.

[2] T. Arens and T. Rösch, *A Collocation Method for Systems of Biperiodic Integral Equations with Super-Algebraic Convergence Rates*, submitted for publication, `www.math.kit.edu/iag1/~arens/seite/publist/en`.

[3] T. Arens, K. Sandfort, S. Schmitt and A. Lechleiter, *Analysing Ewald's method for the evaluation of Green's functions for periodic media*, IMA J. Appl. Math. (2011) `doi:10.1093/imamat/hxr057`.

[4] O.P. Bruno, V. Domínguez, and F.J. Sayas, *Convergence analysis of a high-order Nystrom integral-equation method for surface scattering problems*, Numer. Math. **124**, 603-645 (2013).

A system of boundary integral equations for transient wave-structure interaction

Francisco-Javier Sayas[1,*], **Tonatiuh Sánchez-Vizuet**[2,*]
[1]Department of Mathematical Sciences, University of Delaware
[2]Department of Mathematical Sciences, University of Delaware
[*]Email: tonatiuh@udel.edu

Abstract

In this paper we present a system of time-domain boundary integral equations describing the scattering of acoustic waves by an elastic obstacle. The analysis of well-posedness is done simultaneously at the continuous and semidiscrete level. We use Laplace domain techniques for the analysis of well-posedness and for the study of the error due to Galerkin semidiscretization of the integral system.

Keywords: boundary integral equations, wave-structure interaction, vector-valued distributions

1 The differential system

We will consistently use evolution equation notation for our partial differential equations. Like this, a function of space-and-time variables will be thought as a function of time with values in a vector space of functions of the space variables. Differentiation with respect to the space variables will be written with the usual symbols of vector calculus (gradient, divergence, laplacian) without making any reference to the space variables. Differentiation with respect to time will be written with an upper dot. Time-domain integral operators and potentials will be written in convolutional notation, emphasizing this same effect: considered as vector- or operator-valued distributions of the time variable, they correspond to causal convolution of distributions of a single variable.

Consider a bounded Lipschitz domain (possibly non-connected) $\Omega_- \subset \mathbb{R}^d$ with boundary Γ and exterior Ω_+. Let us assume that a linearly elastic material, subject to small deformations, occupies Ω_-. We characterize the material properties of this object by its two Lamé parameters and its mass density. This means that the displacement field satisfies the elastic wave equation

$$\rho_s \ddot{\mathbf{u}} = \operatorname{div} \boldsymbol{\sigma}(\mathbf{u}), \tag{1}$$

where

$$\boldsymbol{\sigma}(\mathbf{u}) = \mu(\nabla \mathbf{u} + (\nabla \mathbf{u})^\top) + \lambda(\nabla \cdot \mathbf{u})\,\mathrm{I}$$

is the stress tensor for a Hookean material. The normal traction on Γ is denoted $\mathbf{t}(\mathbf{u}) = \boldsymbol{\sigma}(\mathbf{u})\boldsymbol{\nu}$, where $\boldsymbol{\nu}$ is the unit normal vector field on Γ pointing from Ω_- to Ω_+.

An acoustic field is measured on a fluid surrounding Ω_-. The interaction [3] will be triggered by a given incident wave v^{inc}. The total wave $v^{\mathrm{tot}} = v + v^{\mathrm{inc}}$ is decomposed as the sum of the incident wave and a scattered wave, which satisfies the acoustic wave equation

$$c^{-2}\ddot{v} = \Delta v \tag{2}$$

and a radiation–causality condition that can be expressed in simple terms: at every time $t > 0$ the support of v is contained in a ball of radius that grows proportionally to ct. The interaction is mathematically represented by two transmission conditions:

$$\dot{\mathbf{u}} + \nabla v^{\mathrm{tot}} \cdot \boldsymbol{\nu} = 0 \tag{3}$$

and

$$\mathbf{t}(\mathbf{u}) + \rho_f \dot{v}^{\mathrm{tot}} \boldsymbol{\nu} = \mathbf{0}. \tag{4}$$

The parameters c and ρ_f are the speed of waves and density of the acoustic fluid. At time $t = 0$ we assume that the incident wave has not reached the elastic obstacle and therefore the solid is at rest and the only acoustic field is the incident one.

The simplest approach to prove that (1)-(4) is well posed consists of taking Laplace transforms of the equations and write a variational formulation [1]. Assuming that v^{inc} is a tempered causal distribution with values in

$$H^1_\Delta(\mathcal{O}) := \{v \in H^1(\mathcal{O}) \,:\, \Delta v \in L^2(\mathcal{O})\},$$

where $\mathcal{O}$ is an open neighborhood of Γ, we can prove that (1)-(4) has a unique solution $(\mathbf{u}, v)$ which is a causal Laplace transformable distribution with values in $\mathbf{H}^1_\sigma(\Omega_-)^3 \times H^1_\Delta(\Omega_+)$, where

$$\mathbf{H}^1_\sigma(\Omega_-) := \{\mathbf{u} \in H^1(\Omega_-)^3 \,:\, \boldsymbol{\sigma}(\mathbf{u}) \in L^2(\Omega_-)^{3\times 3}\}.$$

2 An equivalent integral system

The layer potentials associated to the acoustic wave equation around Γ can be defined as determining the unique causal $H^1_\Delta(\mathbb{R}^d \setminus \Gamma)$-valued solution $v = \mathcal{S} * \eta - \mathcal{D} * \phi$ of the wave equation

$$c^{-2}\ddot{v} = \Delta v$$

satisfying the transmission conditions

$$\begin{aligned} \gamma^- v - \gamma^+ v &= \phi, \\ \partial_\nu^- v - \partial_\nu^+ v &= \eta, \end{aligned}$$

where the superscripts $\pm$ are used to tag traces and normal derivatives from $\Omega_\pm$. Four retarded integral operators can be defined as follows:

$$\begin{aligned} \mathcal{V} * \eta &:= \gamma^-(\mathcal{S} * \eta) = \gamma^+(\mathcal{S} * \eta), \\ \mathcal{K} * \phi &:= \tfrac{1}{2}\gamma^-(\mathcal{D} * \phi) + \tfrac{1}{2}\gamma^+(\mathcal{D} * \phi), \\ \mathcal{J} * \eta &:= \tfrac{1}{2}\partial_\nu^-(\mathcal{S} * \eta) + \tfrac{1}{2}\partial_\nu^-(\mathcal{S} * \eta), \\ \mathcal{W} * \phi &:= -\partial_\nu^-(\mathcal{D} * \phi) = -\partial_\nu^+(\mathcal{D} * \phi). \end{aligned}$$

Definitions in very much the same spirit can be given for the elastic retarded layer potentials and operators, which we will denote with the same letters in boldface. We finally need two operators related to the normal vector field:

$$\mathrm{N}\boldsymbol{\phi} := \boldsymbol{\phi} \cdot \boldsymbol{\nu}, \quad \mathrm{N}^t\eta := \eta\boldsymbol{\nu}.$$

This work relates the system (1)-(4) with the following system of integral equations:

$$\begin{aligned} &\boldsymbol{\mathcal{W}} * \boldsymbol{\phi} + \rho_f \mathrm{N}^t \mathcal{V} * (\mathrm{N}\ddot{\boldsymbol{\phi}}) \qquad (5) \\ &\quad + \rho_f(\mathrm{N}^t(\mathcal{K} * \dot{\phi}) - \boldsymbol{\mathcal{J}} * (\mathrm{N}\dot{\boldsymbol{\phi}})) \\ &\quad = -\rho_f \mathrm{N}^t \partial_\nu \dot{v}^{\mathrm{inc}} \\ &\qquad + \rho_f(-\tfrac{1}{2}\mathrm{N}^t\gamma\dot{v}^{\mathrm{inc}} + \boldsymbol{\mathcal{J}} * (\mathrm{N}^t\gamma\dot{v}^{\mathrm{inc}})) \\ &\rho_f(\mathrm{N}(\boldsymbol{\mathcal{K}} * \dot{\boldsymbol{\phi}}) - \mathcal{J} * (\mathrm{N}\dot{\boldsymbol{\phi}})) \qquad (6) \\ &\quad + \rho_f^2 \mathrm{N}\boldsymbol{\mathcal{V}} * (\mathrm{N}^t\ddot{\phi}) + \rho_f \mathcal{W} * \phi \\ &\quad = \rho_f(\tfrac{1}{2}\partial_\nu v^{\mathrm{inc}} + \mathcal{J} * \partial_\nu v^{\mathrm{inc}}) \\ &\qquad - \rho_f^2 \mathrm{N}\boldsymbol{\mathcal{V}} * (\mathrm{N}^t\gamma\ddot{v}^{\mathrm{inc}}) \end{aligned}$$

In this work we prove that the wave-structure interaction problem (1)-(4) is equivalent to the system (5)-(6) in the sense that the unknowns of the latter are related to the values of the former by

$$\boldsymbol{\phi} = \gamma^- \mathbf{u}, \qquad \phi = \gamma^+ v.$$

We also show that the system (5)-(6) admits a unique solution, even after Galerkin semidiscretization in space with any discrete pair $\boldsymbol{Y}_h \times Y_h \subset H^{1/2}(\Gamma)^d \times H^{1/2}(\Gamma)$. The study also includes mapping properties for the solution of (5)-(6) and the reconstruction of the solution of (1)-(4) using integral representation formulas. It also incorporates the study of the effect of semidiscretization in space. This is done with techniques developed in a systematic way in [4], but going back to the seminal work [1]. Following [2], the analysis leaves the full discretization with Lubich's Convolution Quadrature ready to be applied and analyzed.

3 Acknowledgment

This research was partially supported by the National Science Foundation, under grant DMS 1216356.

References

[1] A. Bamberger and T. Ha Duong, Formulation variationnelle espace-temps pour le calcul par potentiel retardé de la diffraction d'une onde acoustique. I. *Math. Methods Appl. Sci.* **8** (1986), pp. 405–435.

[2] A.R. Laliena and F.J. Sayas, Theoretical aspects of the application of convolution quadrature to scattering of acoustic waves. *Numer. Math.* **112** (2009), pp. 637–678.

[3] G. Sandberg and R. Ohayon (eds.), Computational Aspects of Structural Acoustics and Vibration, Springer, 2008.

[4] F.J. Sayas, Retarded potentials and time-domain boundary integral equations: a road-map. Submitted.

Spectral properties of selfadjoint rational operator functions and applications to wave propagation in photonic crystals

Christian Engström[1,*]

[1]Department of Mathematics and Mathematical Statistics, Umeå University, Sweden

[*]Email: christian.engstrom@math.umu.se

Abstract

In this paper we analyze operator-valued functions, where frequency dispersive material properties lead to a rational nonlinearity. In particular, the analysis applies to wave propagation in photonic crystals when the λ-dependent permittivity is of Lorentz type and losses are ignored. The corresponding block operator matrix is then selfadjoint with a non-empty essential spectrum.

Keywords: nonlinear eigenvalue problem, block operator matrix

1 Introduction

Block operator matrices are frequently used to study coupled systems of partial differential equations but the theory is also an indispensable tool for analyzing operator functions. The studied rational operator function will be analyzed by considering the corresponding selfadjoint block operator matrix.

2 Operator formulation

Let $\mathcal{H}$, $\widehat{\mathcal{H}}$, and $\widehat{\mathcal{H}}_\ell$ be infinite dimensional Hilbert spaces and let $B_\ell : \widehat{\mathcal{H}}_\ell \to \mathcal{H}$, $\ell = 1, 2, \dots$ denote bounded linear operators. Moreover, assume that $A : \mathcal{H} \to \mathcal{H}$ is a self-adjoint operator with compact resolvent that is bounded from below. In this work we consider rational operator functions in a Hilbert space $\mathcal{H}$ of the form

$$\mathcal{S}(\lambda) = A - \lambda - \sum_{\ell=1}^{L} \frac{B_\ell B_\ell^*}{c_\ell - \lambda}, \ \lambda \in \mathbb{C} \setminus \{c_1, c_2, \dots\} \tag{1}$$

with $c_1 < c_2 < \cdots < c_L$, $\operatorname{dom} \mathcal{S}(\lambda) = \operatorname{dom} A$.

Set $\widehat{\mathcal{H}} := \widehat{\mathcal{H}}_1 \oplus \cdots \oplus \widehat{\mathcal{H}}_L$, then $\mathcal{S}$ is the Schur complement of the operator matrix $\mathcal{A}$ in the Hilbert space $\widetilde{\mathcal{H}} = \mathcal{H} \oplus \widehat{\mathcal{H}}$ given by

$$\mathcal{A} = \begin{pmatrix} A & B \\ B^* & C \end{pmatrix} = \begin{pmatrix} A & B_1 & B_2 & \cdots & B_L \\ B_1^* & c_1 & 0 & \cdots & 0 \\ B_2^* & 0 & c_2 & \cdots & 0 \\ \vdots & \vdots & \vdots & \ddots & \vdots \\ B_L^* & 0 & 0 & \cdots & c_L \end{pmatrix}, \tag{2}$$

where $\operatorname{dom} \mathcal{A} = \operatorname{dom} A \oplus \widehat{\mathcal{H}}$. The block operator matrix $\mathcal{A}$ is selfadjoint and bounded from below with essential spectrum $\{c_1, c_2, \dots, c_L\}$ [1, 8]. Hence, we can apply the classical variational characterisation of the eigenvalues below c_1 [7].

In recent years, it has been an increased interest in numerical analysis of selfadjoint spectral problems with non-empty essential spectrum. Points in the discrete spectrum, which are enclosed in between two points of the essential spectrum are called *non-variational* eigenvalues since the classical min-max principle only applies below the minimum of the essential spectrum. However, variational principles can in some cases also be established above the minimum of the essential spectrum and we will consider such a case. In this work, we establish variational principles in $(c_\ell, c_{\ell+1})$ without postulating that the infimum of the Rayleigh functional exists [6]. Moreover, we apply the new theory to an unbounded operator function with periodic coefficients. The main applications for this operator function are photonic crystals and periodic waveguides. These nano-sized structures can be used to control the flow of light and the rational terms in the function (1) is a consequence of frequency dependent material parameters [2–5]. The block operator matrix is discretised with a high order finite element method and several examples illustrate the general theory. In particular, we show the connection between eigenvalue accumulation at c_ℓ and a numerical approximation of the corresponding singular sequence.

This talk is based on a joint work with Heinz Langer and Christiane Tretter [6].

References

[1] Atkinson, F. V., Langer, H., Mennicken, R., and Shkalikov, A. A., *The essential spectrum of some matrix operators*, Math. Nachr. **167**, 5–20 (1994).

[2] Tip T, Moroz T., and Combes J.M. *Band structure of absorptive photonic crystals* J. Phys. A: Math. Theor. **33**, 6223–6252 (2000).

[3] Sakoda K, Kawai N, Ito T, Chutinan A, Noda S, Mitsuyu T, and Hirao K. *Photonic bands of metallic systems. I. Principle of calculation and accuracy.* Phys. Rev. B 2001; 64(4):045116.

[4] Engström, C., *On the spectrum of a holomorphic operator-valued function with applications to absorptive photonic crystals*, Math. Models Methods Appl. Sci. **20**, 1319–1341 (2010).

[5] Effenberg, C., Kressner, D., and Engström, C., *Linearization techniques for band structure calculations in absorbing photonic crystals*, Int. J. Num. Meth. Eng. **89**, 180–191 (2012).

[6] Engström, C., Langer, H., and Tretter, C., *Nonlinear eigenvalue problems and applications to photonics crystals: spectral theory and numerics*, In preparation.

[7] Reed, M. and Simon, B., *Methods of Modern Mathematical Physics, Volume 4: Analysis of Operators*, New York: Academic Press (1978).

[8] Tretter, C., *Spectral theory of block operator matrices and applications*, Imperial College Press (2008).

Efficient computation of scattering resonances for frequency dependent dielectric resonators

Juan C. Araujo-Cabarcas[1,*], **Christian Engström**[1]

[1]Department of Mathematics and Mathematical Statistics, Umeå University, Sweden

[*]Email: juan.araujo@math.umu.se

Abstract

Dielectric resonators have several applications in photonics that vary from optical switching devices to lasers. The computation of scattering resonances with a finite element method requires an outgoing wave condition. For this, we compare two well known methods: Dirichlet to Neumann maps (DtN) and the perfectly matched layer (PML) [1, 2]. In particular, we study systems where the materials are characterized by a complex permittivity function $\varepsilon(\mathbf{r}, \omega)$. We use the Lorentz-Drude model for the frequency dependent material and discretize the resulting nonlinear eigenvalue problem with a high-order finite element method. The computed eigenvalues show an accumulation towards the poles of the Lorentz-Drude model and we illustrate with numerical examples the behavior of the solutions when the eigenvalues approach these poles. Moreover, we show that the number of spurious eigenvalues can be reduced by using a high-order method.

Keywords: nonlinear eigenvalue problem, perfectly matched layer, non-selfadjoint

Introduction

Metallic and dielectric resonators in unbounded domains are a keystone in photonic circuits. In this work we compute scattering resonances [3], which are closely related to the localization of energy peaks of an incoming plane wave. In disk or sphere-shaped resonators the so-called whispering gallery modes feature extremely high Q-factors, when studying scattering of electromagnetic waves. These resonant modes exhibit energy peaks that can be used as ultra narrow optical filters.

Problem formulation

The use of the DtN for resonance problems of the Helmholtz type posed on exterior domains, will always give raise to a nonlinear eigenvalue problem involving transcendental functions in dimensions 2 and 3. Meanwhile, for frequency independent material parameters the PML results in a linear eigenvalue problem.

Metals and many dielectrics typically show a strong dispersive behavior at optical frequencies and we use the Lorentz-Drude model to take this frequency dependency into account:

$$\varepsilon(\omega) = \varepsilon_\infty + \sum_j^{N_p} \frac{\xi_j^2}{\eta_j^2 - \omega^2 - i\gamma_j\,\omega} \qquad (1)$$

where N_p is the number of poles in the rational model and ε_∞, ξ_j, η_j and γ_j are material dependent coefficients.

The use of the DtN results in a fully nonlinear eigenvalue problem, while the PML method produces a rational eigenvalue problem that can be linearized in different ways [4, 5]. We choose a Schur complement method as it results in a significant reduction of the degrees of freedom of the discrete system.

Using the PML approach the eigenvalue problem for the transverse magnetic (TM) polarization reads

$$\nabla \cdot (A\nabla u) + \omega^2 \alpha\tilde{\alpha}\,\varepsilon(\mathbf{r}, \omega)\,u = 0 \qquad (2)$$

where ω is the spectral parameter, α, $\tilde{\alpha}$ and the matrix A are PML coefficients. The permittivity ε is one outside the scatterer and given by a Lorentz-Drude model (1) inside the scatterer. Note that the operator-valued function used to model the resonances is always non-selfadjoint, where the corresponding problem with quasi-periodic boundary conditions (photonic crystal) is selfadjoint if $\gamma_j = 0$, $j = 1, \ldots, N_p$ [6].

We discretize in space by using a high order finite element method and observe that for both DtN and PML spurious eigenvalues appear if the discretization is not sufficiently good.

References

[1] Peter Monk and Francis Collino, *The Perfectly Matched Layer in Curvilinear Coordinates*, SIAM J. Sci. Comput., **19**, pp. 2061–2090 (1996)

[2] S. Kim and J. E. Pasciak, *The computation of resonances in open systems using a perfectly matched layer*, Math. Comput., **78**, no. 267, pp. 1375–1398 (2009)

[3] M. Lenoir, M. Vullierme-Ledard, and C. Hazard, *Variational formulations for the determination of resonant states in scattering problems*, SIAM J. Math. Anal., **23**, pp. 579–608 (1992)

[4] Y. Su and Z. Bai, *Solving rational eigenvalue problems via linearization*, SIAM J. Matrix Anal. Appl., **32**, pp. 201–216 (2011).

[5] Effenberg, C., Kressner, D., and Engström, C., *Linearization techniques for band structure calculations in absorbing photonic crystals*, Int. J. Num. Meth. Eng. **89**, 180–191 (2012).

[6] Engström, C., Langer, H., and Tretter, C., *Nonlinear eigenvalue problems and applications to photonics crystals: spectral theory and numerics*, In preparation.

Spectral properties of non-selfadjoint rational operator functions and applications to wave propagation in photonic crystals

Christian Engström[1], **Axel Torshage**[2,*]

[1]Department of Mathematics and Mathematical Statistics, Umeå University, Sweden
[2]Department of Mathematics and Mathematical Statistics, Umeå University, Sweden
[*]Email: axel.torshage@math.umu.se

Abstract

Electromagnetic material properties are in general characterized by complex-valued functions, which depend on the frequency ω. The spectral parameter relates often to the frequency, leading to spectral analysis of operator-valued functions. We study problems where the ω-dependent permittivity is of Lorentz type, which implies that the nonlinearity is rational. If losses are ignored the problem can be analyzed by considering the corresponding selfadjoint block operator matrix. However, in this work the losses are included and the block operator matrix is non-selfadjoint. The analysis applies for example to wave propagation in metallic photonics crystals, which are attractive materials for controlling electromagnetic waves.

Keywords: nonlinear eigenvalue problem, block operator matrix, non-selfadjoint operator

1 Introduction

Conservative photonics crystals are considered in the vast majority of publications and considerable mathematical progress has been made [1]. However, dispersion and material losses (absorption) in lossy dielectrics and metals significantly change the wave propagation through the crystal. There are only a few mathematical investigations of the absorbing case [2,3] and, to our knowledge, no detailed investigation of the spectral properties of common material models such as the Lorentz model.

2 Operator formulation

Let $\mathcal{H}$ and $\widehat{\mathcal{H}}$ be infinite dimensional Hilbert spaces and let $B : \widehat{\mathcal{H}} \to \mathcal{H}$ denote a bounded operator. Assume that $A : \mathcal{H} \to \mathcal{H}$ is a self-adjoint operator with compact resolvent that is bounded from below. Let $d \geq 0$ and set $\theta = \sqrt{c - d^2/4}$, in this work we consider for $\omega \in \mathbb{C} \setminus \{\pm\theta - id/2\}$ rational operator functions $\mathcal{T}(\omega) : \mathcal{H} \to \mathcal{H}$ of the form

$$\mathcal{T}(\omega) = A - \omega^2 - B\frac{c - id\omega}{c - id\omega - \omega^2}B^*, \qquad (1)$$

with $c \geq 0$ and $\operatorname{dom}\mathcal{T}(\omega) = \operatorname{dom} A$. If the damping coefficient d is set to 0 it is convenient to study the spectrum problem with spectral parameter $\lambda = \omega^2$ which can be linearized to a selfadjoint block-operator matrix. This spectral problem is studied in [5]. The block operator $\mathcal{A}$ corresponding to the function $\mathcal{T}(\omega)$ is defined as

$$\mathcal{A} = \begin{pmatrix} 0 & A & \frac{\theta - \frac{1}{2}id}{\sqrt{2\theta}}B & \frac{\theta + \frac{1}{2}id}{\sqrt{2\theta}}B \\ I & 0 & 0 & 0 \\ 0 & \frac{\theta - \frac{1}{2}id}{\sqrt{2\theta}}B^* & \theta - \frac{1}{2}id & 0 \\ 0 & -\frac{\theta + \frac{1}{2}id}{\sqrt{2\theta}}B^* & 0 & -\theta - \frac{1}{2}id \end{pmatrix}, \qquad (2)$$

where $\operatorname{dom}\mathcal{A} = \mathcal{H} \oplus \operatorname{dom} A \oplus \widehat{\mathcal{H}} \oplus \widehat{\mathcal{H}}$. The block operator matrix $\mathcal{A}$ is similar to the linearization obtained in [6], where the finite dimensional case was studied. It is then shown that the essential spectrum of $\mathcal{A}$ is given by the two poles of the rational problem and that the discrete part of the spectrum of $\mathcal{A}$ coincides with the spectrum of $\mathcal{T}(\omega)$. The block operator matrix $\mathcal{A}$ is clearly non-selfadjoint for each value of the d. However for $d = 0$, we prove that $\mathcal{A}$ is selfadjoint in a Krein space $\mathcal{K}$ [4,7]. Damped problems, $2\sqrt{c} > d > 0$, can then be studied as a perturbation of a block operator matrix that is selfadjoint in a Krein space. Hence, it possible to write the block-operator matrix as

$$\mathcal{A} = \mathcal{A}_{\Re} + i\mathcal{A}_{\Im}, \qquad (3)$$

where $\mathcal{A}_{\Re}$ is selfadjoint in $\mathcal{K}$ and $i\mathcal{A}_{\Im}$ is a bounded skew-symmetric perturbation growing with d. This is used to show that the imaginary part of the eigenvalues of $\mathcal{A}$ is negative and to obtain a lower bound for the imaginary part. Furthermore, it is shown that as the real part of the

eigenvalues approaches infinity the imaginary part approaches zero in at least quadratically pace.

References

[1] Kuchment, P. *Floquet Theory for Partial Differential Equations* Birkhauser (1993)

[2] Tip T, Moroz T., and Combes J.M. *Band structure of absorptive photonic crystals* J. Phys. A: Math. Theor. **33**, 6223–6252 (2000).

[3] Engström, C., *On the spectrum of a holomorphic operator-valued function with applications to absorptive photonic crystals*, Math. Models Methods Appl. Sci. **20**, 1319–1341 (2010).

[4] Adamjan, V. M. and Langer, H. *Spectral properties of a class of rational operator valued functions*, J. Operator Theory **33**, no. 2, 259–277 (1995)

[5] Engström, C., Langer, H., and Tretter, C. *Nonlinear eigenvalue problems and applications to photonics crystals: spectral theory and numerics*, In preparation.

[6] Effenberg, C., Kressner, D., and Engström, C., *Linearization techniques for band structure calculations in absorbing photonic crystals*, Int. J. Num. Meth. Eng. **89**, 180–191 (2012).

[7] Tretter, C., *Spectral theory of block operator matrices and applications*, Imperial College Press (2008).

Efficient Time Integration of the Maxwell-Klein-Gordon Equation in the Non-Relativistic Limit Regime

Patrick Krämer[1,*], **Katharina Schratz**[1]
[1]KIT, Department of Mathematics, Karlsruhe, Germany
[*]Email: patrick.kraemer3@kit.edu

Abstract

The Maxwell-Klein-Gordon equation (MKG) describes the motion of a charged particle in an electromagnetic field. It is described by a set of coupled nonlinear equations for a complex scalar field $z(t,x)$ and a four-vector potential $(\Phi(t,x), \boldsymbol{\mathcal{A}}(t,x))$. In the Coulomb gauge, i.e. $\operatorname{div} \boldsymbol{\mathcal{A}} \equiv 0$, the MKG equation reads

$$\begin{cases} \left(\frac{\partial_t}{c} + i\frac{\Phi}{c}\right)^2 z - \left(\nabla - i\frac{\boldsymbol{\mathcal{A}}}{c}\right)^2 z + c^2 z = 0, \\ \partial_{tt}\boldsymbol{\mathcal{A}} - c^2\Delta\boldsymbol{\mathcal{A}} = \mathcal{P}\left[c\,\mathrm{Re}\left(iz\nabla\overline{z}\right) - \boldsymbol{\mathcal{A}}|z|^2\right], \\ \Delta\Phi = \mathrm{Re}\left(iz\left(\partial_t - i\Phi\right)\overline{z}\right)/c^2, \end{cases} \tag{1}$$

where $\mathcal{P}[J]$ denotes the projection of $J\colon \mathbb{R}^d \to \mathbb{R}^d$ smooth enough onto its divergence-free part.

Solving this equation in the non-relativistic limit regime $c \gg 1$ is numerically very delicate as the solution becomes highly oscillatory in time. In order to resolve the oscillations, standard numerical time integration schemes require severe time step restrictions.

The idea to overcome this numerical challenge is to filter out the high frequencies explicitly and asymptotically expand the exact solution with respect to the small parameter c^{-2} as in [1] such that the problem reduces to a Schrödinger-Poisson system independent of the large parameter c, which we can solve very efficiently. Finally we obtain an approximation $z_0(t,x)$ which gets closer to the exact solution the larger c gets.

Keywords: highly oscillatory, Maxwell-Klein-Gordon, non-relativistic limit

1 Introduction

In order to get familiar with the ideas of deriving such an approximation, for sake of simplicity we neglect the influence of the vector potential $\boldsymbol{\mathcal{A}}$ at first, i.e. we set $\boldsymbol{\mathcal{A}} \equiv 0$, and we consider periodic boundary conditions.

Hence our starting point in this paper is the Klein-Gordon equation coupled to a scalar real potential Φ on the torus $\mathbb{T}^d$ with smooth initial data, i.e.

$$\begin{cases} \left(\frac{\partial_t}{c} + i\frac{\Phi}{c}\right)^2 z + \langle\nabla\rangle_c^2 z = 0, \\ \Delta\Phi = \mathrm{Re}\left(i\frac{z}{c}\overline{D_0 z}\right), \\ z(0) = \varphi, \quad D_0 z(0) = \langle\nabla\rangle_c^{-1}\psi, \end{cases} \tag{2}$$

where $\langle\nabla\rangle_c := \sqrt{-\Delta + c^2}$, $D_0 z := \frac{1}{c}(\partial_t + i\Phi)z$.

The idea is now to rewrite (2) as a first order system for functions u, v such that

$$\begin{cases} \partial_t \begin{bmatrix} u \\ v \end{bmatrix} = ic\langle\nabla\rangle_c \begin{bmatrix} u \\ v \end{bmatrix} - \frac{i}{2}\Phi^+ \begin{bmatrix} u \\ -v \end{bmatrix} - \frac{i}{2}\Phi^- \begin{bmatrix} \overline{v} \\ -\overline{u} \end{bmatrix}, \\ \Delta\Phi = \frac{1}{4c}\mathrm{Re}\left((u+\overline{v})\langle\nabla\rangle_c(\overline{u}-v)\right), \\ u(0,x) = \varphi - i\psi, \quad v(0,x) = \overline{\varphi} - i\overline{\psi}, \end{cases}$$

where

$$\Phi^{\pm} := \Phi \pm \langle\nabla\rangle_c^{-1}\,\Phi\,\langle\nabla\rangle_c .$$

In particular we have that $z = \frac{1}{2}(u + \overline{v})$.

Applying a Taylor series expansion to $\langle\nabla\rangle_c$ and using the ansatz

$$\begin{bmatrix} u \\ v \end{bmatrix}(t,x) = e^{ic^2 t}\begin{bmatrix} u_0 \\ v_0 \end{bmatrix}(t,x) + \sum_{n=1}^{\infty} c^{-2n} e^{ic^2 t}\begin{bmatrix} u_n \\ v_n \end{bmatrix}(t,x)$$

then yields a Schrödinger-Poisson system for the first terms in the expansion, i.e. u_0, v_0 satisfy

$$\begin{aligned} \partial_t \begin{bmatrix} u_0 \\ v_0 \end{bmatrix} &= -i\frac{1}{2}\Delta\begin{bmatrix} u_0 \\ v_0 \end{bmatrix} - i\Phi_0\begin{bmatrix} u_0 \\ -v_0 \end{bmatrix} \\ \Delta\Phi_0 &= \frac{1}{4}(|u_0|^2 - |v_0|^2), \\ u_0(0,x) &= \varphi - i\psi, \quad v_0(0,x) = \overline{\varphi} - i\overline{\psi}, \end{aligned} \tag{3}$$

which are the so-called *limit equations*, cf. [2].

Note that this Schrödinger Poisson system is independent of the large parameter c. Hence it can be solved numerically very efficiently without time step restrictions by using for instance a Strang splitting method.

The numerical advantage is that now we have an approximation

$$z_0(t,x) = \frac{1}{2}\left(e^{ic^2t}u_0(t,x) + e^{-ic^2t}\overline{v_0}(t,x)\right)$$

such that $z(t,x) = z_0(t,x) + \mathcal{O}\left(c^{-2}\right)$, see Theorem 1 below, where u_0 and v_0 can be computed efficiently.

2 Asymptotic error in H^s

First we state the asymptotic approximation error of z_0.

Theorem 1 *Let $s > \frac{d}{2}$, and let $\varphi, \psi \in H^{s+4}$ the initial data of (2). Then there exists $T > 0$ such that*

$$\|z(t) - z_0(t)\|_s \leq c^{-2} K(T, m_0, m_1, m_2)\, \forall t \in [0,T],$$

where

$$\begin{aligned} m_0 &= \max\{\|\varphi\|_{s+4}, \|\psi\|_{s+4},\}, \\ m_1 &= \max_{t\in[0,T]}(\|u(t)\|_{s+2} + \|v(t)\|_{s+2}), \\ m_2 &= \max_{t\in[0,T]}(\|u_0(t)\|_{s+4} + \|v_0(t)\|_{s+4}). \end{aligned}$$

For the $\mathbb{R}^d$ setting see [2].

Idea of the proof: The error $\|z(t) - z_0(t)\|_s$ can be estimated by applying the triangle inequality and then estimating $\left\|u(t) - e^{ic^2t}u_0(t)\right\|_s$ and $\left\|v(t) - e^{ic^2t}v_0(t)\right\|_s$. In the mild formulation of u and $e^{ic^2t}u_0$ the dominant terms are of type $e^{ic\langle\nabla\rangle_c\xi}u(\xi)$ and $e^{i(c^2-\frac{1}{2}\Delta)\xi}u_0(\xi)$. Then we use that $e^{ic\langle\nabla\rangle_c t}$ as well as $e^{i\Delta t}$ is an isometry in H^s and together with the estimate for some $w_0 \in H^{s+4}$, i.e.

$$\left\|c\langle\nabla\rangle_c w_0 - (c^2 - \frac{1}{2}\Delta)w_0\right\|_s \leq c^{-2} C \|w_0\|_{s+4},$$

after some calculation we find an inequality such that Gronwall's lemma applies. □

3 Error of the method

Next we apply a Strang splitting method with time step size $\tau < 1$ to the system (3), where we solve the kinetic part and the potential part separately. Note that in the potential part Φ_0 is constant. Thus, we can solve both subproblems exactly in time.

Hence for sufficiently smooth initial data the error of $u_0^n \approx u_0(t_n)$, $t_n = n\tau, n = 0,1,2,\ldots$ satisfies $\|u_0(t_n) - u_0^n\|_s \leq C\tau^2$, see [4].

Setting the numerical approximation as $z_0^n := e^{ic^2t_n}u_0^n + e^{-ic^2t_n}\overline{v_0^n} \approx z(t_n)$, we can apply the estimate of section 2 and obtain the main result of the paper, namely that

$$\begin{aligned} \|z(t_n) - z_0^n\|_s &\leq \|z(t_n) - z_0(t_n)\|_s + \|z_0(t_n) - z_0^n\|_s \\ &\leq C\left(\quad c^{-2} \quad + \quad \tau^2 \quad\right). \end{aligned}$$

Note that for large values of c only the time integration error of the splitting scheme is relevant. For more information on splitting methods we refer to [3] and [4].

4 Work in progress

Our aim is to also construct efficient numerical time integrators for the full MKG (1) on $\mathbb{T}^d$. As stated in [2] on $\mathbb{R}^d$, we expect that the corresponding limit equations for $c \to \infty$ read

$$\begin{cases} \partial_t \begin{bmatrix} u_0 \\ v_0 \end{bmatrix} = -i\frac{1}{2}\Delta \begin{bmatrix} u_0 \\ v_0 \end{bmatrix} - i\Phi_0 \begin{bmatrix} u_0 \\ -v_0 \end{bmatrix} \\ \Delta\Phi_0 = \frac{1}{4}(|u_0|^2 - |v_0|^2), \\ \partial_{tt}\boldsymbol{\mathcal{A}}_0 = c^2\Delta\boldsymbol{\mathcal{A}}_0. \end{cases}$$

such that for all $t \in [0,T]$ there holds

$$\begin{aligned} \|z(t) - z_0(t)\|_s &\leq K_1 c^{-2} \\ \|\Phi(t) - \Phi_0(t)\|_s &\leq K_2 c^{-2} \\ \|\boldsymbol{\mathcal{A}}(t) - \boldsymbol{\mathcal{A}}_0(t)\|_s &\leq K_3 c^{-1}. \end{aligned}$$

References

[1] E. Faou and K. Schratz, Asymptotic preserving schemes for the Klein-Gordon equation in the non-relativistic limit regime, *Numer. Math., Vol. 126, 2014, No. 3*, pp. 441–469.

[2] N. Masmoudi and K. Nakanishi, Nonrelativistic limit from Maxwell-Klein-Gordon and Maxwell-Dirac to Poisson-Schrödinger, *Int. Math. Res. Not., 2003, No. 13*, pp. 697–734.

[3] T.Jahnke and C. Lubich, Error Bounds for Exponential Operator Splittings, *BIT Numerical Mathematics,Vol. 40, 2000, No.4*, pp. 735-744

[4] C. Lubich, On splitting methods for Schrödinger-Poisson and cubic nonlinear Schrödinger equations, *Math. Comp., Vol.77, 2008, No.264*, pp. 2141–2153.

Error analysis of hybrid particle-in-cell (PIC) methods for oscillatory Maxwell-like equations

Simone Buchholz[1,*], **Marlis Hochbruck**[1]

[1]Institute for Applied and Numerical Analysis, Karlsruhe Institute of Technology, Germany

[*]Email: simone.buchholz@kit.edu

Abstract

Our aim is to prove error bounds for hybrid particle-in-cell (PIC) methods applied to a coupled system of Maxwell-like equations. We want to achieve second-oder convergence under realistic regularity assumptions and without any severe step size restriction.

Keywords: high-frequency solutions, splitting method, hybrid particle-in-cell (PIC) method, overdense plasma, no step size restriction

1 Introduction

We consider the convergence of a 3-D full electromagnetic relativistic hybrid plasma code developed in [3]. To simulate complex laser-plasma physics this hybrid PIC method combines a PIC method for the low-density hot plasma and a hydrodynamic model for the high-density cold background plasma. As a physical application one can consider electron propagation through solid targets and the resulting target normal sheath acceleration (TNSA).

In the hydrodynamic model we have to deal with the fundamental plasma frequency ω_p, which is the frequency of the plasma electrostatic oscillations. Standard explicit and implicit methods are usually computationally expensive if the frequency is huge. In [3], a splitting method was proposed, which interprets each of the split differential equations exactly. Unfortunately this method suffers from resonances, so filter functions were used to achieve second-order convergence.

Although numerical experiments yields good results, an error analysis was missing in [3]. In an ongoing dissertation project by G.Jansing (Düsseldorf) second-order convergence with strong filter functions is shown in a special case of a single frequency $\omega_p = \omega$.

Our aim is to prove second-order convergence for more general frequencies under realistic assumptions and without any step size restrictions.

2 Hybrid Model

The simplified model considered in [3] consists of the Maxwell equations coupled to a momentum equation for the hydrodynamically treated particles. In dimensionless variables it reads

$$\begin{aligned} \frac{d\boldsymbol{p}}{dt} &= \boldsymbol{E}, \\ \frac{\partial \boldsymbol{E}}{\partial t} &= \nabla \times \boldsymbol{B} - \omega_p^2 \boldsymbol{p}, \\ \frac{\partial \boldsymbol{B}}{\partial t} &= -\nabla \times \boldsymbol{E}, \end{aligned}$$

where $\boldsymbol{E}$ and $\boldsymbol{B}$ denote the electric and magnetic field vectors, respectively, and $\boldsymbol{p}$ is the momentum. The equations on a spatial domain in $\mathbb{R}^d$, $d = 1, 2, 3$ are equipped with appropriate boundary conditions, like periodic boundary conditions in a large simulation box. The scaled plasma frequency is given by

$$\omega_p^2 = \frac{n_h}{\gamma_h}, \qquad \gamma_h = \sqrt{1 + \|\boldsymbol{p}\|^2},$$

where $n_h = n_h(x)$ describes the density of the hybrid particles and γ_h is the relativistic factor. For the error analysis we neglect relativistic effects and set $\gamma_h \equiv 1$, which means that ω_p is a function of the spatial variable only. Moreover the energy is finite, thus a constant K exists such that

$$\|\omega_p \boldsymbol{p}(t)\|^2 + \|\boldsymbol{E}(t)\|^2 + \|\boldsymbol{B}(t)\|^2 \le K\,.$$

3 Numerical Algorithm

After space discretization (with the Yee scheme, finite elements or discontinuous Galerkin methods) we split the system into three parts

$$\begin{aligned} &\dot{\boldsymbol{p}} = \boldsymbol{E}, && \dot{\boldsymbol{E}} = -\Omega^2 \boldsymbol{p}, && \dot{\boldsymbol{B}} = 0, \\ &\dot{\boldsymbol{p}} = 0, && \dot{\boldsymbol{E}} = \nabla_h \times \boldsymbol{B}, && \dot{\boldsymbol{B}} = 0, \\ &\dot{\boldsymbol{p}} = 0, && \dot{\boldsymbol{E}} = 0, && \dot{\boldsymbol{B}} = -\nabla_h \times \boldsymbol{E}, \end{aligned}$$

where $\nabla_h \times$ denotes the discretized $\nabla\times$-operator on a spatial mesh and Ω is a diagonal matrix containing the values $\omega_p(x_j)$ on a spatial grid as

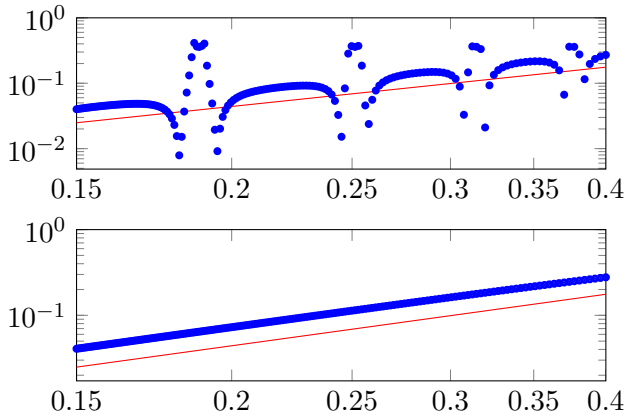

Figure 1: Absolute error in the $\boldsymbol{E}$ field for different step sizes without filter functions (top) and with suitable chosen filter functions (bottom)

diagonal entries. We are now interested in the case $\omega_{max} = \|\Omega\| \gg h^{-1}$, where h is the smallest spatial step size. For the splitting ansatz the three parts are integrated exactly using the flows φ_τ^j, $j = a, b, c$ over the time $\tau > 0$ and combining them in a symmetric way

$$\varphi_\tau = \varphi_{\tau/2}^c \circ \varphi_{\tau/2}^b \circ \varphi_\tau^a \circ \varphi_{\tau/2}^b \circ \varphi_{\tau/2}^c \,.$$

Although the scheme is of classical order two, it suffers from resonances if the density ω_p becomes large (see Fig.1). Similar effects have been observed in [1], where second-order can be retrieved by introducing filter functions ψ and ϕ:

$$\begin{aligned}
\boldsymbol{B}^{n+\frac{1}{2}} &= \boldsymbol{B}^n - \frac{\tau}{2}\nabla_h \times \phi(\tau\Omega)\boldsymbol{E}^n \\
(\boldsymbol{E}^+)^n &= \boldsymbol{E}^n + \frac{\tau}{2}\psi(\tau\Omega)\nabla_h \times \boldsymbol{B}^{n+\frac{1}{2}} \\
\boldsymbol{p}^{n+1} &= \cos(\tau\Omega)\boldsymbol{p}^n + \tau\mathrm{sinc}(\tau\Omega)(\boldsymbol{E}^+)^n \\
(\boldsymbol{E}^-)^{n+1} &= -\Omega\sin(\tau\Omega)\boldsymbol{p}^n + \cos(\tau\Omega)(\boldsymbol{E}^+)^n \\
\boldsymbol{E}^{n+1} &= (\boldsymbol{E}^-)^{n+1} + \frac{\tau}{2}\psi(\tau\Omega)\nabla_h \times \boldsymbol{B}^{n+\frac{1}{2}} \\
\boldsymbol{B}^{n+1} &= \boldsymbol{B}^{n+\frac{1}{2}} - \frac{\tau}{2}\nabla_h \times \phi(\tau\Omega)\boldsymbol{E}^{n+1}
\end{aligned}$$

The numerical solution can be computed very efficiently, since the trigonometric matrix functions are evaluated at diagonal matrices $\tau\Omega$.

4 Error analysis

For our error analysis we eliminate $\boldsymbol{B}$ and $\boldsymbol{p}$ in the coupled Maxwell system and obtain the wave equation

$$\ddot{\boldsymbol{E}} = -\Omega^2\boldsymbol{E} - \nabla_h \times \nabla_h \times \boldsymbol{E}\,.$$

Note that the application we are interested in requires not only $\boldsymbol{E}$ but also $\boldsymbol{B}$ and $\boldsymbol{p}$, so solving the wave equation instead of the Maxwell system is not an option. On the other hand, analyzing the splitting method for the complete system turns out to be very difficult. We thus exploit that the numerical scheme can be shown to be equivalent to the two-step formulation

$$\begin{aligned}
&\boldsymbol{E}^{n+1} - 2\cos(\tau\Omega)\boldsymbol{E}^n + \boldsymbol{E}^{n-1} = \\
&-\tau^2\cos^2(\tfrac{1}{2}\tau\Omega)\psi(\tau\Omega)\nabla_h \times \nabla_h \times \Phi(\tau\Omega)\boldsymbol{E}^n
\end{aligned}$$

with initial steps $\boldsymbol{E}_0$ and an appropriately chosen $\boldsymbol{E}_1$.

Motivated by the convergence analysis of [1] we showed second order convergence for $\boldsymbol{E}^n$, $\boldsymbol{B}^n$, and $\boldsymbol{p}^n$. As in [1], the bounds are independent of the spatial mesh width but require certain assumptions on the filter functions and on the initial values.

As an alternative approach we study the Gautschi-type integrators from [2] with more general filter functions. For second order problems of the form

$$\ddot{\boldsymbol{y}} = -\Omega^2\boldsymbol{y} + \boldsymbol{g}(y)$$

we consider the two-step scheme

$$\boldsymbol{y}_{n+1} - 2\cos(\tau\Omega)\boldsymbol{y}_n + \boldsymbol{y}_{n-1} = \tau^2\vartheta(\tau^2\Omega^2)\boldsymbol{g}_n,$$

where $\boldsymbol{g}_n = \boldsymbol{g}\big(\phi(\tau\Omega)\boldsymbol{y}_n\big)$ for an appropriate filter function ϕ. In [2], various choices of ϕ but a fixed $\vartheta(\xi) = \mathrm{sinc}^2(\xi/2)$ was considered. Motivated by the two-step formulation of the plasma problem above, we now present an error analysis for other filter functions ϑ.

References

[1] V. Grimm and M. Hochbruck, Error analysis of exponential integrators for oscillatory second-order differential equations, *Journal of Physics A: Mathematical and General* **39** (2006), pp.5495–5507.

[2] M. Hochbruck and C. Lubich, A Gautschi-type method for oscillatory second-order differential equations. *Numer. Math.*, 83 (3):403–426, 1999.

[3] T. Tückmantel, A.Pukhov, J.Liljo and M.Hochbruck, Three-dimensional relativistic particle-in-cell hybrid code based on an exponential integrator, *IEEE Transactions on Plasma Science* **38** (2010), pp.2383-2389.

Convergence analysis of a splitting method for laser-plasma interaction simulations

Georg Jansing[1,*], **Achim Schädle**[1,*]
[1]Mathematisches Insititut, Heinrich-Heine Universität, Düsseldorf, Germany
*Email: schaedle@am.uni-duesseldorf.de

Abstract

We analyze and modify a triple splitting method that was proposed by Hochbruck, Liljo, Karmakar, Pukhov and Tückmantel in [1,2] for simulating laser-plasma interactions with over-dense plasmas, where the large density parameter gives rise to numerical stability issues in classical time integration methods. The method contains an exponential integrator in its central component and was specifically designed for systems that describe those interactions. We will analyze a slightly generalized version of the method and identify modifications, which then allow to prove second order convergence.

Keywords: splitting method, laser-plasma interaction, highly oscillatory differential equations

1 Problem Description

We consider the propagation of a short laser pulse in vacuum targeted at a plasma around a thin foil. The electric and magnetic field E and B describing the laser are governed by Maxwell's equations. In this simple model the plasma is modeled as a fluid by the electron number density ρ (number of electrons per volume) and the probability density function of the impulses of the electrons p.

$$\partial_t E = \nabla \times B - e\rho p, \tag{1a}$$
$$\partial_t B = -\nabla \times E, \tag{1b}$$
$$\partial_t p = eE. \tag{1c}$$

Here we make the simplifying assumptions that the positively charged nuclei do not move and hence ρ is constant in time. The electrons however will oscillate, which is reflected by their time-dependent impuls p. Additionally we neglect the influence of the magnetic field on the electrons and do not take into account relativistic effects. Initial values are concentrated away from the plasma and for simplicity, we assume periodic boundary conditions.

$e = -1$ is the electron charge. In (1) space is scaled to the wave number and time to the laser frequency. Due to the high electron density we have a large ρ, say $\rho = 10^5$, in the region of the foil and ρ vanishing elsewhere. A typical simulation of a partially reflected pulse is shown in Fig. 1.

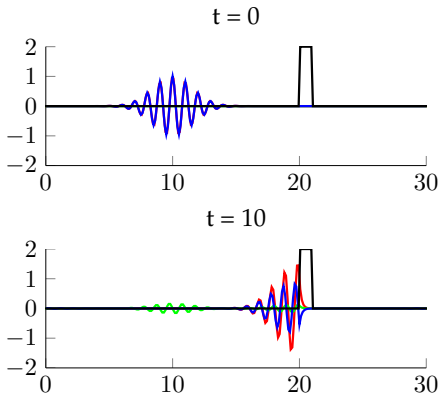

Figure 1: Two snapshots of the laser pulse reflected at a "plasma wall" (black) at $x = 20$. E (blue), B (red), p (green).

2 Time integration scheme

Discretizing in space by the Yee-scheme, we denote by C_E and C_B discretized versions of the curl operator, such that $C_E = C_B^T$ and by

$$\Omega = \begin{bmatrix} 0 & 0 \\ 0 & \omega I \end{bmatrix}, \quad \omega = e\sqrt{\rho}, \quad \rho \gg 1$$

the discretization of the density profile. We have to assume that there is only one fixed ω. For a time step-size τ the explicit time integration scheme proposed in [1,2], which can be interpreted as a certain exponential triple splitting of (1) with filter functions ϕ and ψ, is given

by

$$B_{n+\frac{1}{2}} = B_n - \tfrac{\tau}{2} C_E \phi(\tfrac{\tau}{2}\Omega)\ E_n, \tag{2a}$$

$$E_n^+ = E_n + \tfrac{\tau}{2}\psi(\tfrac{\tau}{2}\Omega) C_B B_{n+\frac{1}{2}}, \tag{2b}$$

$$\begin{bmatrix} p_{n+1} \\ E_{n+1}^- \end{bmatrix} = \begin{bmatrix} \cos(\tau\Omega) & \tau\,\mathrm{sinc}(\tau\Omega) \\ -\frac{1}{\Omega}\sin(\tau\Omega) & \cos(\tau\Omega) \end{bmatrix} \begin{bmatrix} p_n \\ E_n^+ \end{bmatrix}, \tag{2c}$$

$$E_{n+1} = E_{n+1}^- + \tfrac{\tau}{2}\psi(\tfrac{\tau}{2}\Omega) C_B B_{n+\frac{1}{2}}, \tag{2d}$$

$$B_{n+1} = B_{n+\frac{1}{2}} - \tfrac{\tau}{2} C_E \phi(\tfrac{\tau}{2}\Omega) E_{n+1}. \tag{2e}$$

Filter functions to avoid resonances in a numerical schemes for highly oscillatory differential equations are widely used in the literature, cf. [3, Ch. XIII.2].

Numerical experiments in [1] with $\phi(z) = \psi(s) = \mathrm{sinc}(z)$ indicate convergence of second order in τ. A more detailed experiment however reveals that the method in [1] shows only first order convergence in τ.

Our new convergence analysis of the above scheme allows to formulate conditions on the filter functions to obtain second order convergence in τ. We have the following

Theorem 1 *Provided that the initial values $E(0)$ $B(0)$ $p(0)$ are sufficiently smooth and bounded independently of ω and that the fields are initially "small" in the plasma region, i.e. $\Omega E(0)$, $\Omega^2 p(0)$ and $\Omega^2 C_B B(0)$ are bounded independent of ω, choosing $\phi(z) = \mathrm{sinc}(z)$ and $\psi(z) = \mathrm{sinc}^2(z)$, for $\tau\omega > c_0$ the time discretization error is*

$$\|E_n - E(t_n)\| \le C\tau^2$$

$$\|B_n - B(t_n)\| \le C\tau^2$$

$$\|p_n - p(t_n)\| \le C\tau^2$$

where the generic constant C in the estimate depends on the spatial discretization of the curl operators and on $T = n\tau$, but is independent of n, τ and ω.

The idea of the proof is as follows. We view the equation as Hamiltonian system and rewrite (2) as a two step-method for the electric field E. By this the oscillator step (2c) results in a "natural filter". A small modification of the initial step, and we have to prove that the modification is small in some sense, allows to apply Theorem 4.1 from [3, Ch. XIII.4.1]. The estimates for the magnetic flux and the impulse can be done borrowing ideas from [4] and some trigonometric identities.

In fact Theorem 1 can be formulated more generally than it is stated here. We obtain conditions on the filter functions for first order convergence and some more conditions for second order convergence. For the filter functions used in [1] our convergence analysis proves first order convergence.

References

[1] J. Liljo, A. Karmakar, A. Pukhov and M. Hochbruck. One-dimensional electromagnetic relativistic PIC-hydrodynamic hybrid simulation code H-VLPL (hybrid virtual laser plasma lab). *Computer Physics Communications*, 179(6):371 – 379, 2008.

[2] T. Tückmantel, A. Pukhov, J. Liljo, and M. Hochbruck. Three-dimensional relativistic particle-in-cell hybrid code based on an exponential integrator. *IEEE Transactions on Plasma Science*, 38(9):2383–2389, 2010.

[3] E. Hairer, Ch. Lubich, and G. Wanner. *Geometric numerical integration - Structure-preserving algorithms for ordinary differential equations*. Springer Series in Computational Mathematics. Springer-Verlag, Berlin, Heidelberg, 2nd ed. edition, 2006.

[4] V. Grimm and M. Hochbruck. Error analysis of exponential integrators for oscillatory second-order differential equations. *J. Phys. A: Math. Gen.*, 39:5495–5507, 2006.

Tuesday, July 21
Second Afternoon Session
17:15 – 18:15

An FMM for waveguide problems for Helmholtz' equation in 2D

Ryota Misawa[1], **Kazuki Niino**[1], **Naoshi Nishimura**[1,*]
[1]Graduate School of Informatics Kyoto University, Kyoto, Japan
*Email: nchml@i.kyoto-u.ac.jp

Abstract

We present an FMM for solving waveguide problems for Helmholtz' equation in a 2 dimensional infinite strip with homogeneous Neumann B.C. on the sides. Costly evaluation of Green's function for the problem is avoided with the help of the method of images and the FMM. We solve transmission problems for multiple scatterers to observe that even a few scatterers give rise to stopbands in the waveguide.

Keywords: waveguide problems, Green's functions, FMM, stopband

1 Introduction

Waveguide problems are of interest in engineering with various applications. We therefore consider a Boundary Integral Equation Method (BIEM) for waveguide problems for 2 dimensional Helmholtz' equation in an infinite strip using Green's function which satisfies homogeneous Neumann B.C. on the sides of the strip. In BIEM it is important to accelerate the algorithm because a naive BIEM costs $O(N^2)$ computational time where N is the degrees of freedom. This is particularly the case in the present case since the evaluation of Green's function is costly. In this paper, we present an FMM accelerated BIEM for waveguide problems using the method of images and lattice sums as in the case of periodic problems [1]. We show some numerical examples including the stopband phenomena caused by multiple scatterers in the waveguide.

2 Formulation

We consider 2 dimensional Maxwell's equations with the $e^{-\mathrm{i}\omega t}$ time dependence. Let $P \subset \mathbb{R}^2$ be an infinite strip given by $P = [-\frac{1}{2}, \frac{1}{2}] \times \mathbb{R}$, whose sides are denoted by $S_1^{\pm} = \{\boldsymbol{x} \in \mathbb{R}^2 | x_1 = \pm\frac{1}{2}\}$. We assume that P is divided into a bounded open set Ω_2 (scatterer) and the remainder $\Omega_1 = P \setminus \bar{\Omega}_2$. We consider an incident plane wave u^{inc} in the strip P. Our problems is to find u which satisfies the 2 dimensional Helmholtz eq.: $\Delta u(\boldsymbol{x}) + k_i^2 u(\boldsymbol{x}) = 0$, $\boldsymbol{x} \in \Omega_i$ $(i = 1, 2)$, B.C.s on $\partial\Omega_i$: $u_1 = u_2$, $\frac{1}{\epsilon_1}\frac{\partial u_1}{\partial n} = \frac{1}{\epsilon_2}\frac{\partial u_2}{\partial n}$, homogeneous Neumann B.C.s on the sides of the strip: $\frac{\partial u}{\partial x_1}|_{S_1^{\pm}} = 0$, and the outward radiation conditions for the scattered wave $u - u^{\mathrm{inc}}$ as $|x_2| \to \infty$, where k_i, ϵ_i are the wavenumber and permitivity in each domain Ω_i $(i = 1, 2)$, respectively. The symbol u_i stands for the limiting value of u from Ω_i on $\partial\Omega_i$, and $\frac{\partial u_i}{\partial n}$ denotes the similar limit of the normal derivative and n is the unit outward normal from Ω_2 to Ω_1. By using Green's function Γ which satisfies $\Delta\Gamma(\boldsymbol{x}, \boldsymbol{y}) + k_1^2\Gamma(\boldsymbol{x}, \boldsymbol{y}) = -\delta(\boldsymbol{x} - \boldsymbol{y})$ and $\frac{\partial\Gamma(\boldsymbol{x},\boldsymbol{y})}{\partial x_1}|_{S_1^{\pm}} = 0$ $(\boldsymbol{y} \in P)$, we obtain the following boundary integral equation which is well-known as the PMCHWT formulation :

$$\begin{pmatrix} -(D_\Gamma + D_{G_{k_2}}) & \epsilon_1 S_\Gamma + \epsilon_2 S_{G_{k_2}} \\ -(\frac{N_\Gamma}{\epsilon_1} + \frac{N_{G_{k_2}}}{\epsilon_2}) & D_\Gamma^* + D_{G_{k_2}}^* \end{pmatrix} \begin{pmatrix} u \\ q \end{pmatrix} = \boldsymbol{b}^{\mathrm{inc}} \quad (1)$$

where S, D are the single and double layer potentials and D^*, N are their normal derivatives, respectively. The subscripts show the kernel function of the potentials. The discretized equation of (1) converges fast with GMRES [2].

We consider a fast method of computing potentials including Γ. Note that Green's function Γ can be written as the lattice sum of the fundamental solution G_{k_1} for k_1:

$$\Gamma(\boldsymbol{x}, \boldsymbol{y}) = \sum_{l=-\infty}^{\infty} G_{k_1}(\boldsymbol{x}, \boldsymbol{y}_{2l}) + \sum_{l=-\infty}^{\infty} G_{k_1}(\boldsymbol{x}, \boldsymbol{y}'_{2l}), \quad (2)$$

where source points $\boldsymbol{y}_{2l}$ and $\boldsymbol{y}'_{2l}$ are given by $\boldsymbol{y}_{2l} = (y_1 + 2l, y_2)$ and $\boldsymbol{y}'_{2l} = (-y_1 + 2l + 1, y_2)$, respectively. The representation (2) of Γ enables us to regard the potentials as the superposition of contributions from the infinite number of the mirror images of the scatterer (Fig.1), thus leading to a natural extension of the ordinary FMM to our problem. To implement the FMM for Γ, we divide the mirror images into square cells whose side lengths are equal to the width of the strip as shown in Fig.1. We set these cells as level 0 FMM cells. We now focus on the target cell in Fig.1 painted in black where we compute

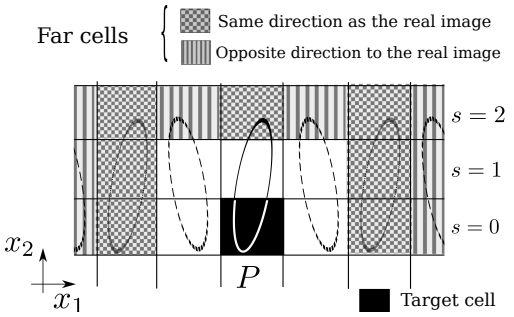

Figure 1: method of images

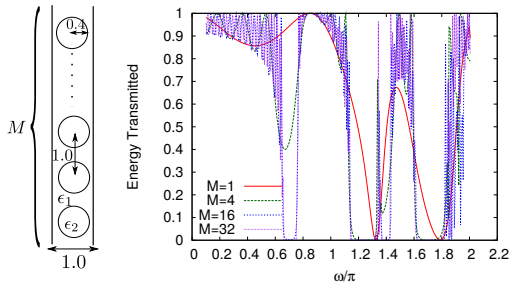

Figure 2: Energy Transmitted

the potentials. We can compute the contributions from white cells around the target cell by using the ordinary FMM. Contributions from other cells in Fig.1 can be evaluated as one uses the following lattice sums as the coefficients for the M2L translations at level 0 in the FMM algorithm:

$$O_n^{\text{even}}(s) = \sum_l O_n(-(2l\boldsymbol{e}_1 + s\boldsymbol{e}_2)) \tag{3}$$

$$O_n^{\text{odd}}(s) = \sum_l O_n(-((2l+1)\boldsymbol{e}_1 + s\boldsymbol{e}_2)) \tag{4}$$

where $\boldsymbol{e}_{1,2}$ are unit vectors in $x_{1,2}$ directions and we set the center of the target cell to be $(0,0)$. Also, O_n is defined by $O_n(\boldsymbol{x}) = \mathrm{i}^n H_n^{(1)}(k_1 r)e^{in\theta}$ with (r,θ) being the polar coordinate of $\boldsymbol{x}$ and H_n the Hankel function of the first kind and the n-th order. Lattice sums in (3) and (4) are used to evaluate the contributions from cells filled with checker and stripe patterns which are $|s|$ units away from the target cell along the x_2 direction, respectively (see Fig.1). Since the series (3-4) converge very slowly, we compute them by using Fourier integrals as in [1] when $|s| < 2$, and by using the Poisson summation formula when $|s| \geq 2$. Since these lattice sums depend only on k_1, we can precompute them once for all in the FMM algorithm. In addition, the rest of the algorithm is exactly the same as the standard FMM. We thus see that the computational complexity of our FMM is the same as that of the ordinary FMM, which is $O(N)$ in low frequency problems.

We note that the Green's function Γ diverges at specific wavenumbers given by $k_1 = p\pi$, $\forall p \in \mathbb{N}$ and the numerical solvers which use Γ give inaccurate results near these wavenumbers in general. We can, however, deal with this problem by modifying our approach using techniques used in [3].

3 Numerical Examples

We consider transmission problems for multiple scatterers. Let Ω_2 consists of M circular scatterers given by $x_1^2 + (x_2 - i)^2 \leq 0.4^2$ $(i = 0, \cdots, -M+1)$ with $\epsilon_2 = 4$ and $\epsilon_1 = 1$. Each circle is discretized with 500 piecewise constant elements. In Fig.2, we plot the transmitted energy for the cases of $M = 1, 4, 16, 32$ and various values of ω. Computational time needed at each ω is 291s at the longest (we used a cluster of Appro GreenBlade 8000, 16 Intel Xeon cores). In Fig.2, we see that the energy transmittance for a single scatterer $(M = 1)$ varies smoothly with ω. In multiple scatterer cases $(M = 4, 16, 32)$, however, we can see sudden changes of the energy transmittance and stopbands which are known in periodic problems [4]. The cases $M = 16$ and $M = 32$ behave similarly, but the change of the energy transmittance for $M = 32$ seems to be sharper. From this example, we can say that more scatterers give rise to clearer stopbands, but we also see that even a few scatterers produce stopbands.

Acknowledgement

This work has been supported by JSPS KAKENHI Grant Number 14J03491.

References

[1] Y. Otani, N. Nishimura, *Int.J. Numer. Meth. Eng.*, **73** (2008), pp. 381–406.

[2] K. Niino, N. Nishimura, *J. Comput. Phys.*, **231** (2012), pp.66–81.

[3] A. Barnett, L. Greengard, *BIT*, **51** (2011), pp. 67–90.

[4] M. A. Haider, S P. Shipman, S. Venakides, *SIAM. J. Appl. Math*, **62** (2002), pp.2129–2148.

Domain Optimization for a Junction of Closed Acoustic Waveguides

Julian Ott[1,*]
[1]Department of Mathematics, Karlsruhe Institute for Technology
[*]Email: julian.ott@kit.edu

Abstract

We study a problem modelling the scattering of a time-harmonic acoustic wave at the junction of two closed waveguides. Our focus lies in an optimal control problem for the domain: We aim to design a junction which optimally transmits an incident wave from one waveguide into the other.

Keywords: scattering problem, Helmholtz equation, optimal control, free boundary problem

1 The Scattering Problem

Let us start by specifying the geometry: We consider two closed acoustic waveguides parallel to each other, having the form $\Omega_- = (-\infty, -b] \times S_-$, $\Omega_+ = [+b, +\infty) \times S_+$, where $S_-, S_+ \subset \mathbb{R}^{N-1}$ are the bounded intersections of the waveguides. Furthermore, let Ω be some domain that connects Ω_- and Ω_+ in a suitable sense (see Figure 3). We then denote the whole waveguide junction by $D = \Omega \cup \Omega_+ \cup \Omega_-$.
For a real wavenumber $k \in \mathbb{R}$ and a given incident field $u_i : \Omega_- \cup \Omega_+ \to \mathbb{C}$, we are interested in the problem of finding $u : D \to \mathbb{C}$ such that

$$(\mathrm{P}) \begin{cases} \Delta u + k^2 u = 0 \text{ in } D, \quad u = 0 \text{ on } \partial D \\ u - u_i \text{ fulfills a MRC on } \Omega_+ \cup \Omega_-. \end{cases}$$

Here MRC denotes a modal radiation condition well known for this type of waveguide scattering problems.
In an appropriate weak formulation this problem is Fredholm. Using Rellich-type integral relations, we derive a bound for the H^1 norm of our solution, which holds under a certain geometric condition for sufficiently smooth D; Of particular importance for the next step is the fact that the bound holds uniformly for all domains fulfilling those conditions.

2 On Existence of Optimal Domains

If we fix the two waveguides Ω_+, Ω_-, can we change the junction Ω such that an incident field on Ω_- is perfectly transmitted to the other waveguide Ω_+?

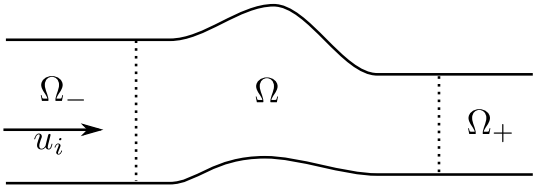

Figure 1: Basic geometrical situation: A wave is incident in the left hand waveguide Ω_- and will in general produce scattered outgoing waves in left *and* right hand waveguides.

To get an existence result for optimal domains, we show that the solution u depends continuously on Ω within a certain class of domains: This is done by extending the uniform bound to a (suitably defined) Hausdorff compact class of junction domains. The proof of continuity is then done with standard tools of optimal shape design for elliptic problems.
This immediately yields the existence of optimal junctions for H^1 continuous figures of merit, since they can be considered as continuous function from the compact metric space of junction domains into $\mathbb{R}$.
However, for practical situations, the geometric condition defining our class of junctions is too restrictive.

3 Transmission Optimization

To construct explicit examples for this optimization problem, we try to maximize the energy transmitted into Ω_+, which can be calculated by

$$E(\Omega) = \int_{\Gamma_+} \mathrm{Im}\left(\frac{\partial u_\Omega}{\partial n}\overline{u}_\Omega\right) \,\mathrm{d}o,$$

over a suitable class of domains (u_Ω denotes the solution on the variable domain Ω, while Γ_+ is an arbitrary intersection of Ω_+).

We use the so called shape derivatives of the scattering problem: The solution u_Ω can be differentiated with respect to some boundary variation a (see Figure 2). This derivative can be represented as the solution v of the scattering

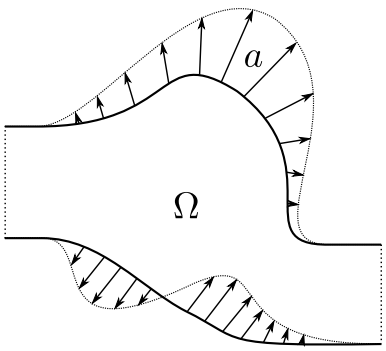

Figure 2: A variation of a reference domain Ω by a vector field a.

problem

$$(\mathrm{dP}_a)\begin{cases} \Delta v + k^2 v = 0 \text{ in } D, \\ v = -(a\cdot n)\dfrac{\partial u}{\partial n} \text{ on } \partial D, \\ v \text{ fulfills MRC on } \Omega_+ \cup \Omega_-. \end{cases}$$

Here n denotes the outward normal on D. Thus, by choosing a suitable finite set of boundary variations $S = \mathrm{span}\{a_1, \ldots, a_M\}$, we can calculate the gradient of E with respect to the boundary variations, allowing us to apply standard nonlinear optimization methods to search for optimal junctions numerically.

4 Numerical Examples

We calculate numerical examples for solutions of P and dP_a by a standard finite element Galerkin's method on the junction domain Ω, which has been extended by transparent (Dirichlet to Neumann) boundary conditions, realizing the coupling with the two waveguides. For the optimization procedure we employed a conjugate gradient method with a line search utilizing the second domain derivatives.
For "nice" situations, the optimization procedure generated junction domains with a nearly perfect energy transmission (see figure 3). For such perfectly transmitting junctions, some interesting scattering relation holds, which we will also illustrate on our numerical examples.

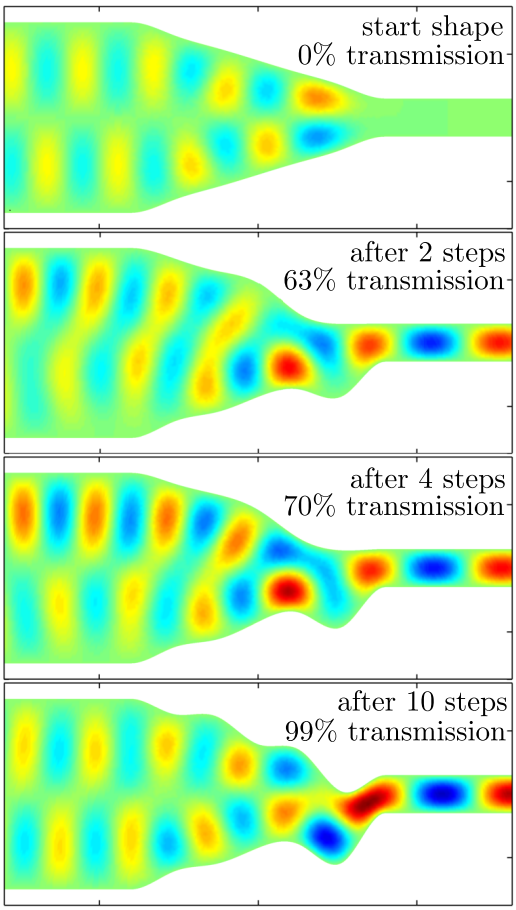

Figure 3: An example optimization history: In all figures, we send in the same incident field (the second guided mode on the left) towards the junction. While the starting junction completely reflects the wave back to the left, we can see that after 10 iterations a near optimal transmission of 99% is obtained.

References

[1] J. Ott, Domain Optimization for an Acoustic Waveguide Scattering Problem, *Applied Mathematics and Optimization* (2014).

Excitation of a Layered Sphere by an Arbitrarily Positioned Point Source: Direct Problem

P. Prokopiou[1], **N. L. Tsitsas**[1,*]

[1]Department of Informatics, Thessaloniki, Greece

*Email: ntsitsas@csd.auth.gr

Abstract

The excitation problem due to a point-source arbitrarily located inside or outside a layered sphere is investigated. A methodology for solving the direct scattering problem is developed. Then, certain far-field approximations in the low-frequency regime are derived which are expected to be effective in inverse scattering algorithms.

Keywords: layered sphere, point-source scattering, low-frequency

1 Introduction

The simplicity of the layered spherical model as well as the possibility of obtaining exact solutions for the associated scattering problems have constituted it a frequently and effectively utilized model in a variety of applications, like e.g. medical imaging.

The low-frequency realm offers an effective environment for the development of inverse scattering algorithms concerning the determination of the sphere's characteristics by using point-source fields [1]. The interior direct and inverse low-frequency excitation of a layered sphere was investigated in [2]. Finding a source inside a homogeneous sphere by using surface field data was studied in [3].

In this work, we consider the excitation of a layered sphere by a point-source lying at an arbitrary position (r_q,θ_q,ϕ_q) inside or outside the sphere. A methodology for solving the direct scattering problem is presented and then certain low-frequency far-field approximations are derived. Previous investigations have considered the point-source lying on the z-axis [1, 2]. The present consideration of an arbitrarily located source is more realistic, particularly with respect to the development of inverse source algorithms.

2 Mathematical Formulation

Consider a layered spherical scatterer V of $\mathbb{R}^3$ with radius a_1. The interior of V is divided into N layers V_j (j=1,...,N), defined by $a_{j+1} < r < a_j$ (j=1,...,$N-1$) and having wavenumbers k_j and densities ρ_j. The core V_N ($0 \leq r < a_N$) is soft; the exterior V_0 has constants k_0 and ρ_0.

The scatterer V is excited by a primary spherical acoustic wave, generated by a point-source at $\mathbf{r}_q \in V_q$ (q=0,...,$N-1$), and expressed by

$$u^{pr}(\mathbf{r};\mathbf{r}_q) = A\frac{\exp(ik_q|\mathbf{r}-\mathbf{r}_q|)}{|\mathbf{r}-\mathbf{r}_q|},\ \mathbf{r} \neq \mathbf{r}_q\,. \quad (1)$$

In V_q, the total field is

$$u^q(\mathbf{r};\mathbf{r}_q) = u^{pr}(\mathbf{r};\mathbf{r}_q) + u^{sec}(\mathbf{r};\mathbf{r}_q),\ \mathbf{r} \in V_q \setminus \{\mathbf{r}_q\};$$

in V_j ($j \neq q$) the total field is the secondary u^j.

The fields u^j satisfy the Helmholtz equations

$$\Delta u^j(\mathbf{r};\mathbf{r}_q) + k_j^2 u^j(\mathbf{r};\mathbf{r}_q) = 0,$$

for $\mathbf{r} \in V_j$ if $j \neq q$ and $\mathbf{r} \in V_q \setminus \{\mathbf{r}_q\}$ if $j = q$, as well as the boundary conditions

$$\begin{aligned} u^{j-1}(\mathbf{r};\mathbf{r}_q) &= u^j(\mathbf{r};\mathbf{r}_q), \quad r = a_j \\ \frac{1}{\rho_{j-1}}\frac{\partial u^{j-1}(\mathbf{r};\mathbf{r}_q)}{\partial r} &= \frac{1}{\rho_j}\frac{\partial u^j(\mathbf{r};\mathbf{r}_q)}{\partial r}, \quad r = a_j \end{aligned} \quad (2)$$

The total field on the core's surface satisfies

$$u^{N-1}(\mathbf{r};\mathbf{r}_q) = 0, \quad r = a_N\,. \quad (3)$$

The total field in V_0 must satisfy, for $r \to \infty$, the Sommerfeld radiation condition as well as

$$u^0(\mathbf{r};\mathbf{r}_q) = g(\hat{\mathbf{r}};\mathbf{r}_q)h_0(k_0 r) + \mathcal{O}(r^{-2})\,, \quad (4)$$

where g is the far-field pattern.

Also, we define the total cross-section

$$\sigma = \frac{1}{k_0^2}\int_{S^2} |g(\hat{\mathbf{r}};\mathbf{r}_q)|^2 \mathrm{d}s(\hat{\mathbf{r}})\,, \quad (5)$$

with $\hat{\mathbf{r}} \in S^2 = \{\mathbf{x} \in \mathbb{R}^3, ||\mathbf{x}|| = 1\}$.

3 Solution of the Direct Problem

We select the spherical coordinate system (r,θ,ϕ) with the origin O at the centre of V, so that the point-source is at (r_q,θ_q,ϕ_q).

For $r > r_q$, primary field (1) is expressed as

$$u^{pr}(\mathbf{r};\mathbf{r}_q) = 4\pi i k_q A \sum_{n=0}^{\infty}\sum_{m=-n}^{n} (-1)^m j_n(k_q r_q)\times Y_n^{-m}(\hat{\mathbf{r}}_q) h_n(k_q r) Y_n^m(\hat{\mathbf{r}}),$$

while, for $r < r_q$, as

$$u^{pr}(\mathbf{r};\mathbf{r}_q) = 4\pi i k_q A \sum_{n=0}^{\infty}\sum_{m=-n}^{n} (-1)^m h_n(k_q r_q)\times Y_n^{m}(\hat{\mathbf{r}}_q) j_n(k_q r) Y_n^{-m}(\hat{\mathbf{r}}),$$

where j_n and h_n are the n-th order spherical Bessel and first kind Hankel function and $Y_n^m(\hat{\mathbf{r}}) = Y_n^m(\theta,\phi)$ is a spherical harmonic [4].

The secondary field u^j in V_j is expanded as

$$u^j(\mathbf{r};\mathbf{r}_q) = 4\pi i k_q A \sum_{n=0}^{\infty}\sum_{m=-n}^{n} (-1)^m h_n(k_q r_q)\times Y_n^{-m}(\hat{\mathbf{r}}_q)\left(\alpha_{q,n}^j j_n(k_j r) + \beta_{q,n}^j h_n(k_j r)\right) Y_n^m(\hat{\mathbf{r}})$$

($\alpha_{q,n}^j$ and $\beta_{q,n}^j$ under determination coefficients).

By imposing the boundary conditions (2) we obtain the transformations

$$\begin{bmatrix} \alpha_{q,n}^j \\ \beta_{q,n}^j \end{bmatrix} = \mathbf{T}_n^j \begin{bmatrix} \alpha_{q,n}^{j-1} \\ \beta_{q,n}^{j-1} \end{bmatrix}, \qquad (6)$$

where $\mathbf{T}_n^j$ is the 2×2 transition matrix from V_{j-1} to V_j, which is independent of the source's location, and whose expression is given in [2].

Now, the coefficients $\alpha_{q,n}^j$ and $\beta_{q,n}^j$ are determined by applying a similar procedure to that of the successive algorithmic connection scheme of the fields coefficients, described in [2].

Moreover, the far field pattern is given by

$$g(\hat{\mathbf{r}};\mathbf{r}_q) = 4\pi i k_q A \sum_{n=0}^{\infty}\sum_{m=-n}^{n} (-1)^m (-i)^n \times h_n(k_q r_q)\beta_{q,n}^0 Y_n^{-m}(\hat{\mathbf{r}}_q) Y_n^m(\hat{\mathbf{r}}), \qquad (7)$$

while, by combining (5) with (7), we get the expression of the total cross-section

$$\sigma = 4\pi |A|^2 \frac{k_q^2}{k_0^2} \sum_{n=0}^{\infty}\sum_{m=-n}^{n} (2n+1)\frac{(n-m)!}{(n+m)!}\times |h_n(k_q r_q)\beta_{q,n}^0|^2 |P_n^m(\cos\theta_q)|^2, \qquad (8)$$

where P_n^m is the Legendre function.

4 Low-Frequency Far-Field Results

We make the low-frequency assumption $k_0 a_1 \ll 1$ for a 2-layered spherical scatterer. The (external) point-source is located at (r_0,θ_0,ϕ_0) with $r_0 > a_1$; interior excitation can be treated similarly. We define the parameters $\xi = a_1/a_2$, $\varrho = \rho_1/\rho_0$, $\eta = k_1/k_0$, $\kappa = ik_0 a_1$, $\tau = a_1/r_0$.

By using the asymptotic expressions of the spherical Bessel and Hankel functions for small arguments we obtain the expansions of $\beta_{0,n}^0$ and then calculate the far-field functions of interest. For example, the approximation of the far-field pattern, as $\kappa \to 0$, is calculated to be

$$g(\hat{\mathbf{r}};\mathbf{r}_0) = \frac{A}{r_0}\mathcal{S}_0\kappa + \frac{A}{r_0}\Big[\varrho\eta(\mathcal{S}_0)^2 + \big(P_1(\cos\theta_0)P_1(\cos\theta) + P_1^1(\cos\theta_0)P_1^1(\cos\theta)\cos(\phi-\phi_0)\big)\tau\mathcal{S}_1\Big]\kappa^2 + \mathcal{O}(\kappa^3), \qquad (9)$$

where

$$\mathcal{S}_0 = \frac{1}{(1-\xi)\varrho - 1}, \quad \mathcal{S}_1 = \frac{\xi^3(1-\varrho)+2+\varrho}{\xi^3(1+2\varrho)+2-2\varrho}.$$

In the special case $\theta_0 = 0$ (for a point source on the z-axis), (9) reduces to (4.5) of [2].

A low-frequency approximation of the cross-section can be calculated by similar techniques.

Such low-frequency approximations can be utilized in inverse algorithms determining the point-source as well as the sphere's materials.

References

[1] G. Dassios and G. Kamvyssas, Point source excitation in direct and inverse scattering: the soft and the hard small sphere, *IMA J. Appl. Math.* **55** (1995) pp. 67-84.

[2] N. L. Tsitsas and C. Athanasiadis, Point-source excitation of a layered sphere: direct and far-field inverse scattering problems, *Q. J. Mech. Appl. Math.* **61** (2008), pp. 549-580.

[3] N. L. Tsitsas and P. A. Martin, Finding a source inside a sphere, *Inverse Problems* **28** (2012), 015003 (11pp).

[4] P. A. Martin, *Multiple Scattering*, Cambridge University Press, Cambridge, 2006.

An offline/online algorithm for scattering in half-plane stochastic configurations

M. Ganesh[1], **Stuart C. Hawkins**[2,*]

[1]Department of Applied Mathematics and Statistics, Colorado School of Mines, CO 80228, USA
[2]Department of Mathematics, Macquarie University, NSW 2109, Australia

*Email: stuart.hawkins@mq.edu.au

Abstract

We develop computational statistical tools to facilitate quantification of stochastic acoustic multiple scattering in the half-plane. The plane is bounded by a sound-soft wall along the x-axis. Wave propagation in the half-plane is induced by an incident wave impinging on multiple stochastic particles in the half-plane. We develop an efficient algorithm to compute moments of certain quantities of interest (QoI). Key ingredients of our algorithm include offline computations, fast online realizations, image theory, and high-order Monte Carlo realizations.

Keywords: Half-plane scattering, Helmholtz equation, quasi-Monte Carlo, T-matrix

1 Introduction

Recently phase-stepping interferometric microscopy has been used to measure a sample material using light scattering by the material and the surface beneath it [4]. Calibration requires numerical scattering simulation in the upper half plane bounded by the underlying surface.

The half plane model requires simulation of reflections from the plane boundary as well as reflections from the scatterers. The additional boundary reflections make this problem more complicated, and more computationally expensive, than the free space model.

We present an efficient algorithm for simulating wave scattering in an uncertain configuration $S(\boldsymbol{\omega}) = \mathbb{R}^2_+ \setminus \overline{D(\boldsymbol{\omega})}$. Here, $\mathbb{R}^2_+$ denotes the upper half-plane bounded by a sound-soft wall along the x-axis and the bounded stochastic domain $D(\boldsymbol{\omega})$ comprises N distinct random scatterers located in the upper half-plane. Randomness in the scatterers with various material properties arises because of uncertainties in their location in $\mathbb{R}^2_+$ and how they are oriented.

We use the notation $\boldsymbol{\omega}$ to denote an element of the set of outcomes Ω in a probability space $(\Omega, \mathcal{F}, P)$, where $\mathcal{F}$ is a σ-algebra of Ω with P the associated probability measure. We denote by $u^\infty(\cdot;\boldsymbol{\omega})$ the far field induced by $D(\boldsymbol{\omega})$.

Our main focus is to compute the expected value of the intensity of the random far field. The offline part of the algorithm is independent of the location and orientation of the particles and hence tens of thousands of stochastic realizations of $S(\boldsymbol{\omega})$ and associated scattering simulations can be carried out efficiently.

We simulate the stochastic model problem using high-order quasi-Monte Carlo (QMC) realizations and compare its efficiency with the industrial standard low-order MC approach.

2 Mathematical model

For each realization $\boldsymbol{\omega}^*$ of the half-plane, the scattered field is induced by the incident field

$$u^{\mathrm{inc}}(\boldsymbol{x}) = e^{ik\boldsymbol{x}\cdot\boldsymbol{d}} - e^{ik\boldsymbol{x}\cdot\boldsymbol{d}^{\mathrm{R}}}, \qquad (1)$$

impinging on the N particles in $D(\boldsymbol{\omega}^*)$. Here, $k = 2\pi/\lambda$ where λ is the wavelength of the incident field and the unit direction vector $\boldsymbol{d} = (d_1, d_2)^T$ is taken with $d_2 < 0$. In (1) we have used the notation

$$\boldsymbol{d}^{\mathrm{R}} = (d_1, -d_2)^T, \qquad \boldsymbol{d} = (d_1, d_2)^T \in \mathbb{R}^2.$$

That is, $\boldsymbol{d}^{\mathrm{R}}$ is the reflection of $\boldsymbol{d}$ in the line $\partial H = \{(x, 0) \ : \ x \in \mathbb{R}\}$. The first term on the right hand side of (1) represents a standard plane wave (travelling downwards), and the second term represents the reflection of the standard plane wave in the line ∂H.

Since the half-plane is bounded by the sound-soft wall, the total field $u + u^{\mathrm{inc}}$ vanishes on ∂H:

$$u(\boldsymbol{x}) + u^{\mathrm{inc}}(\boldsymbol{x}) = 0, \qquad \boldsymbol{x} \in \partial H. \qquad (2)$$

The scattered field u is governed by the exterior Helmholtz equation

$$\triangle u(\boldsymbol{x}) + k^2 u(\boldsymbol{x}) = 0, \qquad \boldsymbol{x} \in S(\boldsymbol{\omega}^*). \qquad (3)$$

Depending on the material properties of the particles $D_1(\boldsymbol{\omega}^*), \ldots, D_N(\boldsymbol{\omega}^*)$ we impose appropriate conditions on the boundaries of these particles. Our method is readily applied with identical or different boundary conditions applied on each scatterer.

Our main focus is to compute the expected value of the intensity of the far field

$$\mathbb{E}[|u^\infty(\widehat{\boldsymbol{x}};\cdot)|^2] = \int_\Omega |u^\infty(\widehat{\boldsymbol{x}};\boldsymbol{\omega})|^2 \, dP(\boldsymbol{\omega}), \quad \widehat{\boldsymbol{x}} \in \partial B,$$

where ∂B is the unit circle, comprising all our observation direction vectors. The variance can be represented similarly. For convenience, below we drop the notation $\boldsymbol{\omega}$.

3 Brief Description of the algorithm

For each realization, obtained using MC or QMC sampling, our algorithm is based on the fact that if a field v satisfies the Helmholtz equation (3) then the field $v + \mathrm{R}v$, where $\mathrm{R}v(\boldsymbol{x}) = -v(\boldsymbol{x}^{\mathrm{R}})$, also satisfies (3). We begin by writing the scattered field as a sum of fields scattered by each scatterer

$$u = \sum_{I=1}^{N} \left(u^I + \mathrm{R}u^I\right), \tag{4}$$

where $u^I \in C(\mathbb{R}^2)$ and $u^I + \mathrm{R}u^I$ is the field scattered by D_I.

For each $I = 1, \ldots, N$, using techniques introduced and analyzed in [2], we develop a radiating wavefunction expansion of u^I with a finite number of unknown coefficients. Here each expansion is with respect to a fixed center $\boldsymbol{x}_I$, typically the center of D_I.

Ergo, for each $I = 1, \ldots, N$, we obtain an expansion of $\mathrm{R}u^I$ involving the same unknown coefficients. Similar to the image theory [1], the expansion for the reflected field $\mathrm{R}u^I$ can be considered to be radiating from a *theoretical* scatterer D_I^{R} in the lower half plane. The theoretical scatterer is the reflection of D_I in the x-axis, with local origin $\boldsymbol{x}_I^{\mathrm{R}}$.

We use similar truncated expansions for the incident field (1) with respect to various centers $\boldsymbol{x}_I$, for $I = 1, \ldots, N$ and the coefficients of such expansions are evaluated analytically [2].

Using the linearity of the Helmholtz equation, the T-matrices associated with the scatterers $D_1, \ldots, D_N$ connect these coefficients. We use the techniques in [2] to efficiently compute the T-matrix for each distinctly shaped obstacle in the configuration. The T-matrix is independent of location, orientation and the incident wave. Hence computation of each T-matrix is an offline process and is independent of the tens of thousands of stochastic realizations.

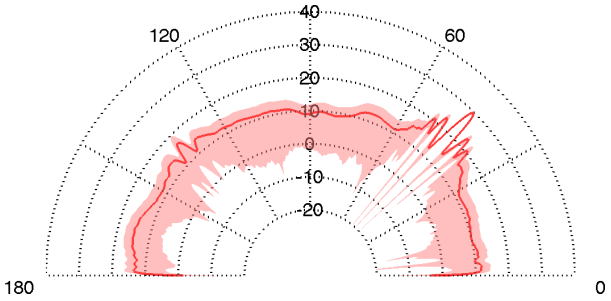

Figure 1: Visualization of the mean cross section of three scatterers with random locations simulated using more than 65 000 QMC realizations (shading indicates plus and minus one standard deviation).

For each realization $\boldsymbol{\omega}^*$, we use the translation-addition theorem and offline T-matrix to setup an N-dimensional linear system for the coefficients in the representation of the unknown scattered field in the half-plane $S(\boldsymbol{\omega}^*)$. We solve this linear system iteratively using GMRES. We develop an object-oriented framework, TMATROM [3], for the efficient offline/online simulation.

Subsequently, we combine the QMC approach with our efficient offline/online framework for tens of thousands of parallel realizations of the stochastic configurations. Figure 1 shows a visualisation of the mean cross section of a random configuration of three scatterers computed using our efficient computational framework.

References

[1] J. C. Chao et al. General formulation for light scattering by a dielectric body near a perfectly conducting surface. *J. Opt. Sci. Am.*, 13:338–344, 1996.

[2] M. Ganesh et al. Convergence analysis with parameter estimates for a reduced basis acoustic scattering T-matrix method. *IMA J. Numer. Anal.*, 32:1348–1374, 2012.

[3] M. Ganesh and S. C. Hawkins. *TMATROM user manual*, 2015 (to appear).

[4] D. J. Little et al. An exact surface-integral approach for accurate interferometric microscopy of single nanoparticles. *Optics Express*, 23:6228–6238, 2015.

Preconditioning Techniques for Local Multiple Traces Formulation for Scattering Problems

Carlos Jerez-Hanckes, José Pinto, Simon Tournier [1,*]

[1]School of Engineering, Pontificia Universidad Católica de Chile

[*]Email: simon.tournier@alumni.enseeiht.fr

Abstract

Helmholtz scattering by heterogeneous penetrable objects is solved by the local *Multiple Traces Formulation*, i.e. transmission conditions are weakly imposed and Calderón identities per subdomain are used. The resulting Fredholm first-kind formulation possesses built-in preconditioners based on Calderón-type techniques. Furthermore, the resulting block matrices possess a structure that suggests other preconditioning alternatives and/or hybridization. In this presentation, we focus on these aspects, presenting numerical results for different alternatives over a wide frequency range.

Keywords: boundary integral equations, wave scattering, multiple traces formulations, preconditioning techniques

1 Introduction

We consider so-called *high frequency* scattering problems, i.e. whenever wavelengths are much smaller than the scatterer's size. Available solution methods are based on: geometrical or physical optics [1]; Nyström approach [2]; and, hybrid numerical asymptotics [3]. Still, questions arise as to when and how these techniques should be applied and what to do in situations that require accommodating different ranges of frequencies as in heterogeneous scatterers.

Previously, we showed that the local *Multiple Traces Formulations* (MTFs) [4, 5], was capable of dealing with composite scatterers with largely varying wavenumbers. All Neumann and Dirichlet unknown traces are locally defined on sub-domain boundaries and transmission conditions are enforced weakly with also locally defined test functions. The resulting first-kind Fredholm formulation possesses a block structure hinting at its amenability to parallelization. The formulation is discretized by h- or p-element approximation, which seems well adapted for high–frequen-cy regimes. However, the convergence rate of iterative solvers, such that those based on Krylov subspaces, is poor or never occurs. Moreover, since the Helmholtz equation becomes more indefinite when the wavenumber increases, the use of preconditioning scheme is required to tackle this difficulty. We will explore and present robust and efficient preconditioning techniques for MTF.

2 Local Multiple Traces Formulation

Following [4], we consider a bounded scatterer Ω composed of two different materials with wavenumbers κ_i and such that $\overline{\Omega} := \overline{\Omega}_1 \cup \overline{\Omega}_2$ with exterior domain $\Omega_0 := \mathbb{R}^2 \setminus \overline{\Omega}$. From the integral representation formulas, we retrieve weak Calderón identities on each sub-domain boundary,

$$\langle \boldsymbol{\lambda}^i \, , \, \boldsymbol{\varphi}^i \rangle_\times = \left\langle \left(\frac{1}{2}\mathrm{Id} + \mathsf{A}_i \right) \boldsymbol{\lambda}^i \, , \, \boldsymbol{\varphi}^i \right\rangle_\times \tag{1}$$

where we have condensed the standard boundary integral operators,

$$\mathsf{A}_i := \begin{pmatrix} -\mathsf{K}_i & \mathsf{V}_i \\ \mathsf{W}_i & \mathsf{K}_i' \end{pmatrix}. \tag{2}$$

Transmission conditions are weakly enforced across each interface Γ_{ij}. This is done via local restriction and normal orientation operators $\widetilde{\mathsf{X}}_{ij}$. Finally, the system takes the form,

$$\langle \mathsf{M}\boldsymbol{\lambda} \, , \, \boldsymbol{\varphi} \rangle \quad = \langle \mathbf{g} \, , \, \boldsymbol{\varphi} \rangle_\times \tag{3}$$

where $\boldsymbol{\lambda} = (\boldsymbol{\lambda}^0, \boldsymbol{\lambda}^1, \boldsymbol{\lambda}^2)$ belongs to p.w.-interface Cauchy functions, $\boldsymbol{\varphi} = (\boldsymbol{\varphi}^0, \boldsymbol{\varphi}^1, \boldsymbol{\varphi}^2)$ in p.w.-interface dual spaces, and the MTF operator reads,

$$\mathsf{M} := \begin{pmatrix} \mathsf{A}_0 & -\frac{1}{2}\widetilde{\mathsf{X}}_{01} & -\frac{1}{2}\widetilde{\mathsf{X}}_{02} \\ -\frac{1}{2}\widetilde{\mathsf{X}}_{10} & \mathsf{A}_1 & -\frac{1}{2}\widetilde{\mathsf{X}}_{12} \\ -\frac{1}{2}\widetilde{\mathsf{X}}_{20} & -\frac{1}{2}\widetilde{\mathsf{X}}_{21} & \mathsf{A}_2 \end{pmatrix}. \tag{4}$$

3 Preconditioning techniques

Instead of solving the linear system $\mathbb{M}\mathbf{u} = \mathbf{b}$, the preconditioned linear system $\mathbb{M}\mathbb{P}\mathbf{v} = \mathbf{b}$ with $\mathbf{u} = \mathbb{P}\mathbf{v}$ is solved. The MTF matrix is rewritten as

$$\mathbb{M} = \mathbb{A} - \mathbb{X} \tag{5}$$

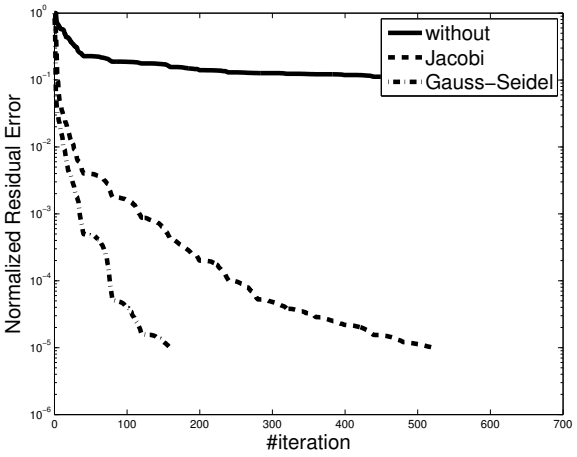

Figure 1: Normalized Residual Error in 2-norm against the number of iteration for GMRes(40). The size of the linear system is 644. The preconditioner is applied by left scheme.

where $\mathbb{A}$ is the block diagonal matrix and $\mathbb{X}$ contains the discretization of the local restriction operators $\widetilde{\mathsf{X}}_{ij}$. The Calderón identity $4\mathsf{A}_i^2 = \mathrm{Id}_i$ leads to built-in preconditioners. In [5], the Jacobi block diagonal preconditioner is proposed,

$$\mathbb{P}_J = \mathbb{M}_{\text{mass}}^{-1}\mathbb{A} \tag{6}$$

with $\mathbb{M}_{\text{mass}}$ is a mass-like matrix. Since the mass-like matrix owns a well-adapted structure, the numerical extra cost of its inverted matrix vector product is negligible compared to the dense matrix vector product by $\mathbb{A}$.

We propose the Gauss-Seidel preconditioner $(\mathbb{A} - \mathbb{U})^{-1}$ where $\mathbb{U}$ is the upper triangular part of $\mathbb{X}$. This inverted matrix vector product is approximated by the first Neumann series order,

$$\mathbb{P}_{GS} = \Big(\mathbb{I} + \mathbb{M}_{\text{mass}}^{-1}\mathbb{A}\mathbb{M}_{\text{mass}}^{-1}\mathbb{U}\Big)\mathbb{M}_{\text{mass}}^{-1}\mathbb{A} \tag{7}$$

Other methods such that SOR, SSOR schemes and specialized schemes using the properties of the matrix $\mathbb{A}$ and $\mathbb{X}$ are considered.

4 Numerical Results

The geometry considered three domains such that, $\Omega_0 = \{\mathbf{x} \in \mathbb{R}^2, \|\mathbf{x}\|_2 > 1\}$, $\Omega_1 = \{\mathbf{x} \in \mathbb{R}^2, \|\mathbf{x}\|_2 < 1, x_1 < 0\}$, $\Omega_2 = \{\mathbf{x} \in \mathbb{R}^2, \|\mathbf{x}\|_2 < 1, x_1 > 0\}$. This geometry contains all the difficulties portraying Lipschitz domains with sharp corners.

Fig. 1 shows the convergence history for the case $\kappa_0 = 10$, $\kappa_1 = 30$ and $\kappa_2 = 1$, discretized by spectral elements. The Krylov method is GMRes with a restart of 40. One can observe the no convergence of the unpreconditioned system and the improvements by the preconditioning techniques.

5 Conclusions and Future Prospects

Numerical analysis is done to evaluate the robustness and the efficiency of the proposed preconditioning techniques, and the influence of the parameters is discussed.

References

[1] P. D. Lin, *New computation methods for geometrical optics*, Vol. 178 of Springer Series in Optical Sciences, Springer, Singapore, 2014.

[2] O. P. Bruno, S. K. Lintner, *A high-order integral solver for scalar problems of diffraction by screens and apertures in three-dimensional space*, J. Comput. Phys. 252 (2013) 250–274. 1

[3] S. L. Samuel P. Groth, David P. Hewett, *Hybrid numerical-asymptotic approximation for high frequency scattering by penetrable convex polygons*, IMA J Appl Math (2013), DOI: 10.1093/imamat/hxt040.

[4] R. Hiptmair, C. Jerez-Hanckes, *Multiple traces boundary integral formulation for Helmholtz transmission problems*, Advances in Computational Mathematics 37 (1) (2012) 39–91.

[5] C. Jerez-Hanckes, J. Pinto, S. Tournier, *Local multiple traces formulation for high-frequency scattering problems*, J. Computational and Applied Mathematics (2015), DOI: 10.1016/j.cam.2014.12.045.

Boundary integral algorithms for Laplace eigenvalue problems

Eldar Akhmetgaliyev[1,*], **Oscar Bruno**[1]
[1]Applied and Computational Mathematics, Caltech, Pasadena, CA, USA
*Email: eakhmetg@caltech.edu

Abstract

We present numerical methods based on integral equation formulations that produce solutions of Laplace eigenvalue problems with mixed Dirichlet/ Neumann boundary conditions in arbitrary domains with possible corners. We characterize the solution singularities which arise at points where Dirichlet and Neumann boundary conditions meet, and employ the novel Fourier Continuation technique to approximate the integral densities. The resulting methods exhibit high-order convergence in spite of the solution singularities.

Our eigensolver searches for frequencies for which the integral equations of the problem admit non-trivial kernels. The "minimum-singular-value" objective function gives rise to a challenging nonlinear optimization problem; we put forth an improved objective functional which can be optimized by means of standard root-finding methods.

Applications and generalizations of our methods can solve variety of problems including modal analysis problem in electromagnetics, transmission eigenvalue problems, eigenproblems in multiply connected domains, time-dependent PDEs, Steklov eigenproblems, 3-dimensional eigenvalues and spectral optimization problems.

Keywords: Mixed boundary conditions, Laplace eigenvalues, integral equations

1 Introduction

The use of boundary methods for the solution of Laplace eigenproblems appears in a number of contributions, including the recent works based on boundary element method [1], method of particular solutions [2] as well as Nystrom approximation of the Fredholm determinant [3]. The presented eigenvalue solver [4] approximates solution of the Laplace eigenvalue problem

$$\begin{aligned} -\Delta u &= \lambda u, \quad x \in \Omega \\ u &= 0, \quad x \in \Gamma_D \\ \frac{\partial u}{\partial \nu} &= 0, \quad x \in \Gamma_N. \end{aligned} \tag{1}$$

Introducing the Helmholtz Green function $G_k(x,y) := \frac{i}{4} H_0^1(k|x-y|)$ with $k^2 = \lambda$ and the associated single-layer potential

$$u(x) = \int_\Gamma G_k(x,y)\psi(y)\mathrm{d}s_y, \qquad x \in \Omega \tag{2}$$

with surface density ψ the eigenvalue problem (1) is transformed into the integral equation system

$$\begin{aligned} \int_\Gamma G_k(x,y)\psi(y)\mathrm{d}s_y &= 0 \qquad x \in \Gamma_D, \\ -\frac{\psi(x)}{2} + \int_\Gamma \frac{\partial}{\partial n_x} G_k(x,y)\psi(y)\mathrm{d}s_y &= 0 \qquad x \in \Gamma_N. \end{aligned} \tag{3}$$

.

The system (3) is discretized using Nystrom method. For the approximation of the boundary integrals we developed high-order quadratures: in the case boundary Γ is smooth these quadratures rely on the novel Fourier Continuation method to account for the singular behaviour of the integral density ψ, for domains with Lipschitz boundary Γ, on the other hand, we employ graded meshes near corners and transition points.

Discretization of the integral equation system (3) leads to an approximate boundary operator in the form of the matrix A_k. The eigenvalue problem (1) is then reduced to a search for value of k for which matrix A_k is singular. To obtain these values of k, we examine the smallest singular value of A_k and solve a nonlinear optimization problem

$$\sigma_{min}(k) = 0.$$

Direct evaluation of the zeroes of $\sigma_{min}(k)$ is highly challenging. Use of a descent-based approach such as the Newton method is not appropriate in this context since the function $\sigma_{min}(k)$ is essentially constant away from its roots. A modified integral equation formulation approach and associated smallest singular values $\widetilde{\sigma}_{min}(k)$ that successfully tackle this difficulty (see Figure 1). This modified approach inspired by [2] is based on use of interior points and a stabilization method based on QR-decomposition.

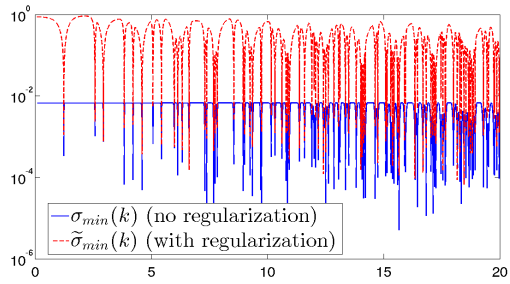

Figure 1: Comparison between $\sigma_{min}(k)$ and $\widetilde{\sigma}_{min}(k)$

2 Numerical Results

The resulting eigensolvers demonstrate high-order convergence. Figure 2 compares the convergence history for both FC-based and graded-mesh eigensolvers as they are used to obtain the Zaremba eigenvalue $\lambda_{18} = 73.1661817902$ for the unit disc.

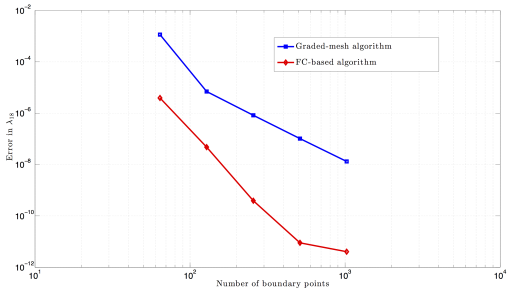

Figure 2: Convergence for FC-based and graded-mesh eigensolvers

The high-order nature of the eigensolvers enables evaluation of eigenfunctions for very high frequencies. Figure 3 shows eigenfunction for a trapezoid (that also corresponds to symmetric Laplace-Dirichlet eigenfunction for L-shaped domain corresponding to the eigenvalue $\lambda = 40013.2312203$ (left) and an eigenfunction for a unit disc corresponding to the eigenvalue λ=10005. 97294969 (right).

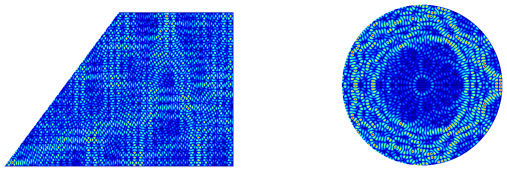

Figure 3: High frequency Zaremba eigenfunctions

References

[1] Steinbach, O., and G. Unger. "A boundary element method for the Dirichlet eigenvalue problem of the Laplace operator." *Numerische Mathematik* **113.2** (2009): 281-298.

[2] Betcke, Timo, and Lloyd N. Trefethen. "Reviving the method of particular solutions." *SIAM review* **47.3** (2005): 469-491.

[3] Zhao, Lin, and Alex Barnett. "Robust and efficient solution of the drum problem via Nostrum approximation of the Fredholm determinant." *arXiv preprint* arXiv:1406.5252 (2014).

[4] E. Akhmetgaliyev, O. Bruno, N. Nigam, A boundary integral algorithm for the Laplace Dirichlet-Neumann mixed eigenvalue problem *arXiv preprint* arXiv:1411.0071, 2014

Wednesday, July 22
Morning Session
10:30 – 12:30

Finite Elements for linear wave propagation in polygonal domains

Fabian L. Müller[1,*], **Christoph Schwab**[1]
[1]Seminar for Applied Mathematics, ETH Zürich, Rämistrasse 101, CH - 8092 Zürich
[*]Email: muelfabi@ethz.ch

Abstract

Error estimates for the space-semidiscrete Finite Element approximation of solutions to initial boundary value problems for linear, second-order hyperbolic systems in bounded polygons $\mathsf{G} \subset \mathbb{R}^2$ with straight sides are presented. Using recent results on corner asymptotics of solutions of linear wave equations with time-independent coefficients in conical domains, it is shown that continuous, simplicial Lagrangian Finite Elements of uniform polynomial degree $p \geq 1$ with either suitably graded mesh refinement or with bisection tree mesh refinement towards the corners of G, achieve the (maximal) asymptotic rate of convergence $O(N^{-p/2})$, where N denotes the number of degrees of freedom spent for the Finite Element space semi-discretization.
This research was supported by the Swiss National Science Foundation under grant no. SNF 200021_149819/1.

Keywords: Linear second-order Wave Equations, Method of lines, Finite Element Methods, Polygonal domains, Transmission problem, Corner singularities, Locally refined meshes, Convergence rates.

1 Polygonal domains

Let $\mathsf{G} \subseteq \mathbb{R}^2$ be an open, bounded two-dimensional domain. Throughout, we assume G to be a polygonal domain, i. e. its boundary consists of a finite union of $M \in \mathbb{N}$ straight line segments e_i, $i = 1, \ldots, M \in \mathbb{N}$ of positive one-dimensional measure. The vertices of the polygon are denoted by $\mathbf{c}_i := \bar{e}_i \cap \bar{e}_{i+1}$, $i = 1, \ldots M$ where the indices i are taken modulo M. For all i, the interior opening angle of the domain at $\mathbf{c}_i$ is measured in positive orientation. We denote it by $\varphi_i \in (0, 2\pi]$, $i = 1, \ldots, M$.
The set of edges on the boundary are split into two sets $\mathcal{E}_D$ and $\mathcal{E}_N$ where Dirichlet and Neumann conditions will be applied, respectively. Let $\Gamma_{D,N} := \bigcup_{e \in \mathcal{E}_{D,N}} \bar{e}$.
We introduce local conical domains G_i, $i = 1, \ldots, M$ defined by

$$\mathsf{G}_i := \{x \in \mathsf{G} \,|\, |x - \mathbf{c}_i| < R_i\} \,, \tag{1}$$

where $0 < R_i < \frac{1}{2} \min_{j=1,\ldots M} |\mathbf{c}_i - \mathbf{c}_j|$. Hence the G_i are mutually disjoint and $\partial\mathsf{G}_i \cap \partial\mathsf{G} \subset \bar{e}_i \cup \bar{e}_{i+1}$.
We also define $r_i(x) = |x - \mathbf{c}_i|$ for all $i = 1, \ldots, M$.

2 Wave equations

Let $m \in \{1, 2\}$ be the system size. We define $H := L^2(\mathsf{G})^m$, $V := \{v \in H^1(\mathsf{G})^m : v|_{\Gamma_D} \equiv 0\}$. There are material properties $a_{ij}^{kl} \in \mathcal{C}^\infty(\bar{\mathsf{G}}; \mathbb{R}_{>0})$ $(i = 1, \ldots, m)$ s. t. for all $i, j, k, l = 1, \ldots, m$:

$$a_{ij}^{kl} \equiv a_{kl}^{ij} \equiv a_{ji}^{kl} \,. \tag{2}$$

Moreover, we assume that there is a $c > 0$, s. t. for all $\mathbf{0} \neq \boldsymbol{\xi} = (\xi_{ij})_{1 \leq i,j \leq m} = (\xi_{ji})_{1 \leq i,j \leq m}$

$$\operatorname{essinf}_{x \in G} \frac{\sum_{i,j,k,l} a_{ij}^{kl}(x) \xi_{ij} \xi_{kl}}{\sum_{i,j} (\xi_{ij})^2} \geq c \,. \tag{3}$$

Given initial conditions $u_0 \in V, u_1 \in H$ and $f \in L^2(I; H)$, the continuous problem reads

$$\begin{aligned} \text{Find } u \in H^1(I; V) \cap H^2(I; V^*), \text{ s. t. } \forall\, t \in I : \\ \partial_t^2(u(\cdot, t), v) + a(u(\cdot, t), v) &= (f(\cdot, t), v)_H \\ (u(\cdot, 0), v) &= (u_0, v) \,, \\ \partial_t(u(\cdot, 0), v) &= (u_1, v) \,, \end{aligned} \tag{4}$$

for all $v \in V$, where

$$a(w, v) := \int_G \sum_{i,j,k,l=1}^{m} a_{ij}^{kl}(x) \partial_j w_i(x)\, \partial_l v_k(x)\, \mathrm{d}x \tag{5}$$

and where by $(\cdot, \cdot)$ we denote the H inner product extended to the pair of spaces $V \times V^*$ with duality taken with respect to the "pivot" space H by continuity. A standard result implies that the problem is well-posed and that

$$u \in \mathcal{C}^0(\bar{I}; V), \quad u_t \in \mathcal{C}^0(\bar{I}; H), \quad u_{tt} \in C^0(\bar{I}; V^*) \,. \tag{6}$$

3 Regularity of solutions

We assume that $u_0, u_1 \in H^{p+1}(\mathsf{G})$. The effect of polygonal corners on the regularity of $u(\cdot, t)$ has been established by Plamenevskiĭ and collaborators. The following Theorem can be deduced from their results, see [1] and [2]:

Theorem 1 *For each $s, s' \in \mathbb{N}$, the solution $u(x,t)$ of (4) admits the following decomposition into a regular and a singular part:*

$$u(x,t) = u_{reg}(x,t) + \sum_{i=1}^{M} \chi_i(x) \sum_{j=1}^{n_{i,\max}} c(t)\, u^{(i)}_{sing,j}(x)\, \Psi^{(i)}_j(\theta_i)\,, \quad (7)$$

where $u_{reg} \in H^s(I; H^{s'}(\mathsf{G}))^m$ and

1. *$\chi_i \in \mathcal{C}^\infty(\bar{\mathsf{G}})$ are smooth cut-offs such that $\mathrm{supp}(\chi_i) \in \bar{\mathsf{G}}_i$ and $\chi_i|_{\{r_i(x)<\frac{R_i}{2}\}} \equiv 1$,*
2. *$u^{(i)}_{sing,j} \in H^\sigma(\mathsf{G}_i)^m$ for any $\sigma < \Re\lambda^{(i)}_j$, but*

$$\|u^{(i)}_{sing,j}\|^2_{H^{2,p+1}_{\delta_i}(\mathsf{G}_i)} := \|u^{(i)}_{sing,j}\|^2_{H^1(\mathsf{G}_i)} + \sum_{k=2}^{p+1} \int_{\mathsf{G}_i} r_i(x)^{2(\delta_i+k-2)}\, |D^k u^{(i)}_{sing,j}|^2 \,\mathrm{d}x \quad (8)$$

   is finite for certain $\delta_i \in [0,1)$ and all i.

3. *$\theta_i \in [0, \phi_i]$ is the angular coordinate in G_i,*
4. *$(\lambda^{(i)}_j, \Psi^{(i)}_j)$ are solutions of a Sturm-Liouville eigenvalue problem associated to $a(\cdot,\cdot)$ s. t. $\Re\lambda^{(i)}_j > 0$ and $\Psi_i \in \mathcal{C}^\infty([0,\phi_i])^m$.*

4 Locally refined meshes

Hence, $u(x,t)$ is the sum of a regular function and of finitely many superpositions of functions which satisfy (8). To approximate such functions with optimal convergence order using the h-version of FEM on regular triangulations $\mathcal{T}$, it is well-known that $\mathcal{T}$ needs to be graded towards the vertices $\mathbf{c}_i$. This means that there exist grading parameters $\beta_i > 0$, $i = 1, \ldots, M$ and a constant $L > 0$ such that for all elements $K \in \mathcal{T}$ s. t. $K \subseteq \mathsf{G}_i$,

$$\begin{cases} h(\mathcal{T}) L^{-1} r_i^{\beta_i} \le h(K) \le L\, h(\mathcal{T}) r_i^{\beta_i} & \text{if } \mathbf{c}_i \notin K\,, \\ h(\mathcal{T}) L{-}1 \sup_{x\in K} r_i(x)^{\beta_i} \le h(K) & \\ \quad \le L\, h(\mathcal{T}) \sup_{x\in K} r_i(x)^{\beta_i} & \text{if } \mathbf{c}_i \in K\,. \end{cases}$$

5 Optimal rates for the semi-discretization

Let $\mathcal{T}$ be a regular triangulation and let V_N be the finite-dimensional subspace of $V \cap \mathcal{C}^0(\bar{\mathsf{G}})$ consisting of piecewise polynomials w. r. to $\mathcal{T}$ of degree $\le p \in \mathbb{N}$. We define $N := \dim(V_N)$. It is by now a standard result that for all $\delta_i \in [0,1)$ there is a choice of $\beta_i \in (0,1]$ such that the FEM interpolant I_p on a $\boldsymbol{\beta}$-graded mesh satisfies

$$\|v - I_p v\|_{H^1(\mathsf{G}_i)} \le c(u)\, N^{-p/2}\,, \quad (9)$$

for all $v \in V$ such that $v|_{(\bigcup_i \mathsf{G}_i)^{\complement}} \in H^{p+1}((\bigcup_i \mathsf{G}_i)^{\complement})$ and $v|_{\mathsf{G}_i} \in H^{p+1,2}_{\delta_i}(\mathsf{G}_i)$.
Using standard techniques in semi-discretization of the Wave equation, we obtained the following Theorem, see [1] and [2]:

Theorem 2 *Let u_N be the solution of the (in space) finite-dimensional semi-discrete problem (4) posed on V_N instead of V, which is constructed upon a triangulation $\mathcal{T}$ with "suitable" grading β_i towards all vertices $\mathbf{c}_i$. Moreover, let the semi-discrete problem be posed with initial conditions $u_{0,h}, u_{1,h}$.*
Then,

$$\|u(\cdot,t) - u_N(\cdot,t)\|_V + \|\partial_t u(\cdot,t) - \partial_t u_N(\cdot,t)\|_H \le C(u, \mathsf{G}, \boldsymbol{\beta})\, N^{-p/2}\,. \quad (10)$$

References

[1] F. L. Müller and Ch. Schwab, Finite Elements with mesh refinement for wave equations in polygons, *Accepted in Journal of Computational and Applied Mathematics* (2014)

[2] F. Müller and Ch. Schwab, Finite elements with mesh refinement for elastic wave propagation in polygons, *Accepted in Mathematical Methods in the Applied Sciences* (2014)

Interior penalty finite element methods for high-order local boundary conditions

Kersten Schmidt[1,*], **Julien Diaz**[2], **Christian Heier**[1]

[1]Research Center Matheon & Department of Mathematics, TU Berlin, Berlin, Germany
[2]Magique3D, INRIA Bordeaux Sud Ouest & IRA-LMA, U Pau et des Pays de l'Adour, Pau, France
[*]Email: kersten.schmidt@math.tu-berlin.de

Abstract

We propose a new solution methodology to incorporate symmetric local absorbing boundary conditions involving higher tangential derivatives into C^0 continuous finite element methods. For this we use discontinuous Galerkin-like bilinear forms for the discretization of differential operators of order four or higher, in which further auxilliary variables are not needed. We will present well-posedness results and *a-priori h*-convergence error estimates for uniform polynomial degrees. Numerical results show that the method does not hamper the order of convergence of the finite element method, if the polynomial degree on the boundary is sufficiently high.

Keywords: Nonconforming Galerkin methods, Local boundary conditions.

1 Introduction

Local boundary conditions are used to mimick the solution in presence of an infinite exterior in diffusion problems or time-harmonic scattering problems, in highly conducting bodies or thin layers. We consider symmetric local boundary conditions in $\mathbb{R}^2$, which take the following form of Dirichlet-to-Neumann maps [1, Eq. 3.14]

$$\partial_\nu u(x) + \sum_{j=0}^{J} (-1)^j \partial_\Gamma^j (\alpha_j \, \partial_\Gamma^j u)(x) = 0, \qquad (1)$$

where ∂_ν and ∂_Γ are the normal and tangential derivatives on the boundary Γ of the computational domain, respectively, and α_j are smooth functions on Γ. The parameter J corresponds to the order of the derivatives. If $J < 0$ then (1) is known as the (homogeneous) Neumann boundary conditon, for $J = 0$ and $J = 1$ as Robin or Wentzell boundary condition, respectively. Prominent examples of symmetric local boundary conditions are the Bayliss-Turkel-Gunzberger conditions (BGT) up to order 2 and Feng's conditions at any order for time-harmonic scattering problems.

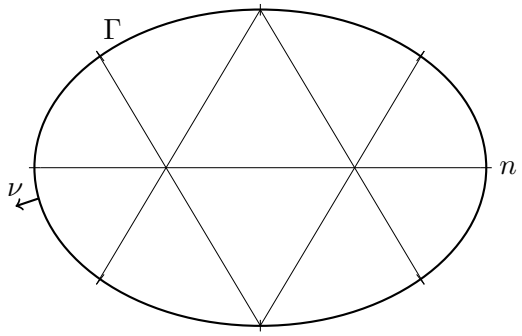

Figure 1: Triangulation $\mathcal{M}_h$ of the domain Ω with boundary Γ and unit normal vector ν. The interior penalty formulation is with additional terms on boundary nodes n.

If only second derivatives are present, *i.e.*, for the Neumann, Robin and Wentzel conditions, and the boundary is smooth enough, we can incorporate the condition in usual piecewise continuous finite element methods. After J-times integration by parts the variational formulation contains terms like

$$\int_\Gamma \alpha_j \partial_\Gamma^j u \, \partial_\Gamma^j v \, \mathrm{d}\sigma(x), \qquad (2)$$

and the natural space is

$$V_J := H^1(\Omega) \cap H^J(\Gamma).$$

Then, positivity of $\mathrm{Re}(\alpha_J)$ or nonvanishing $\mathrm{Im}(\alpha_J)$ implies well-posedness for the Helmholtz equation by the Fredholm-Riesz-Schauder theory, except for a countable set of frequencies [2]. For $J \geq 2$, the usual C^0 continuous finite element spaces V_h are not any more contained in V_J. In this case, trial and test functions with $C^{(J-1)}$-continuity (at least) along Γ [1] or auxilliary unknowns [3] may be used.

2 Interior penalty formulation

Following [4] we propose a variational formulation for the broken Sobolev space

$$V_{J,h} := H^1(\Omega) \cap H^1(\Gamma) \cap H^J(\Gamma_h)$$

where Γ_h is the boundary Γ without the boundary nodes n of a finite element mesh $\mathcal{M}_h$, which contain as a subspace the usual C^0 continuous finite element spaces V_h. Then, for each $j > 1$ each term in (2) is replaced by

$$\int_{\Gamma_h} \alpha_j \partial_\Gamma^j u \, \partial_\Gamma^j v \, \mathrm{d}\sigma(x) + \sum_{n \in \mathcal{N}(\mathcal{M}_h, \Gamma)} \left(\sum_{i=1}^{j-1} (-1)^{i+j} \{\partial_\Gamma^{j-i-1} \alpha_j \partial_\Gamma^j u\}_n [\partial_\Gamma^i v]_n + \frac{\beta_j}{h_n^{2(J-j)+1}} [\partial_\Gamma^{j-1} u]_n [\partial_\Gamma^{j-1} v]_n \right),$$

where $\{\cdot\}_n$ and $[\cdot]_n$ are mean and jump operators on the boundary nodes n. The coefficients β_j are penalty terms and h_n is the minimum of the lengthes of the two neighbouring edges of n. To obtain the symmetry or non-symmetric formulation we may add or substract the term $[\partial_\Gamma^i u]_n \{\partial_\Gamma^{j-i-1} \alpha_j \partial_\Gamma^j v\}_n$ on each boundary node n.

If β_j are large enough the so introduced interior penalty formulation is stable in $V_{J,h}$, if the original formulation in V_J is stable, and is stable in V_h, if in addition the mesh-width is small enough. In this case we can bound the discretisation error $\|u_{J,h} - u_J\|_{V_{J,h}}$ by

$$C_{J,h} \left(\inf_{v_h \in V_h} \|v_h - u_J\|_{H^1(\Omega)} + h^{p_\Gamma - J + 1} \|f_J\|_{V_J'} \right),$$

where p_Γ is the minimum polynomial order on the boundary Γ_h. This means that the discretisation error is bounded by the best-approximation error in the computational domain plus a power of the mesh-width, where the polynomial degree on the boundary has to be increased to compensate increasing derivatives J.

3 Numerical experiments

As an example we study the scattering of a plane wave with wave number k by a bounded object in a homogeneous infinite space, which is modelled by Feng-4 conditions

$$\partial_\nu u = \left(\mathrm{i}k - \tfrac{1}{2R} + \tfrac{\mathrm{i}}{8kR^2} + \tfrac{1}{8k^2R^3} - \tfrac{25\mathrm{i}}{128k^3R^4}\right) u + \left(\tfrac{\mathrm{i}}{2k} - \tfrac{1}{2k^2R} - \tfrac{13\mathrm{i}}{16k^3R^2}\right) \partial_\Gamma^2 u - \tfrac{\mathrm{i}}{k^3} \partial_\Gamma^4 u.$$

on the circular boundary of the computational domain of radius R. For this we have implemented the proposed method within the C++ library Concepts. Choosing $R = 3$ and $k = 1$ we observe optimal convergence of the discretisation error for polynomial orders $p = 1, 2, 3$.

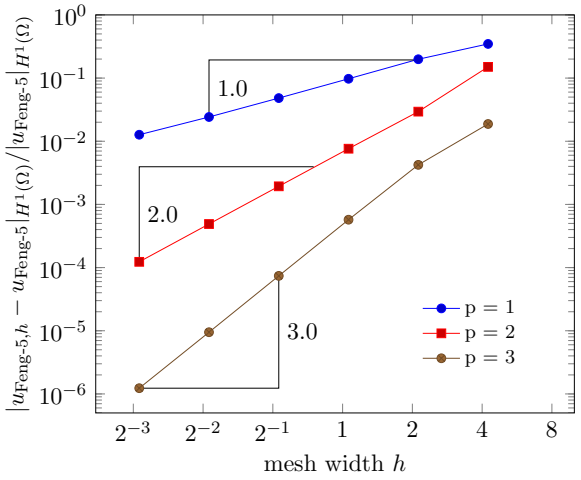

Figure 2: Convergence of the relative discretisation error for polynomial orders $p = 1$ to $p = 3$.

References

[1] Givoli, D., Patlashenko, I., and Keller, J. B. High-order boundary conditions and finite elements for infinite domains. *Comput. Methods Appl. Mech. Engrg.*, 143 (1997), pp. 13–39.

[2] Schmidt, K., and Heier, C. An analysis of Feng's and other symmetric local absorbing boundary conditions. *ESAIM: M2AN*, 49 (2015), pp. 257–274.

[3] Givoli, D. High-order local non-reflecting boundary conditions: a review. *Wave Motion*, 39 (2004), pp. 319–326.

[4] Grote, M., Schneebeli, A., and Schötzau, D. Discontinuous Galerkin finite element method for the wave equation. *SIAM J. Numer. Anal.* 44 (2006), pp. 2408–2431.

[5] Schmidt, K., Diaz, J. and Heier, C. Non-conforming Galerkin finite element method for symmetric local absorbing boundary conditions. *Preprint series of the Institute of Mathematics*, Preprint 5-2015, Technische Universität Berlin, 2015.

Locally implicit discontinuous Galerkin time domain method for electromagnetic wave propagation in dispersive media

Stéphane Descombes[1,*], **Stéphane Lanteri**[2], **Ludovic Moya**[2]

[1]Univ. Nice Sophia Antipolis, CNRS, LJAD, UMR 7351, 06100 Nice, France and INRIA Sophia Antipolis-Mediterranée Research Center, Nachos project-team, 06902 Sophia Antipolis Cedex, France

[2] INRIA Sophia Antipolis-Mediterranée Research Center, Nachos project-team, 06902 Sophia Antipolis Cedex, France

[*]Email: sdescomb@unice.fr

Abstract

We are concerned with the numerical simulation of electromagnetic wave propagation in dispersive media i.e. when the electromagnetic material characteristics depend of the frequency. In the time-domain, this translates in a time dependency of these parameters that can be taken into account through and additional differential equation for, e.g, the electric polarization, which is coupled to the system of Maxwell's equations.

More precisely we consider Maxwell's equations in a Debye dispersive medium, the magnetic field $\vec{H}$, the electric field $\vec{E}$ and the electric polarization $\vec{P}$ satisfy the following system of equations in $[0,T]$

$$\left\{\begin{array}{rcl} \mu_0 \dfrac{\partial \vec{H}}{\partial t} = & -\mathrm{curl}\left(\vec{E}\right), & \\ \varepsilon_0\varepsilon_\infty \dfrac{\partial \vec{E}}{\partial t} = & \mathrm{curl}\left(\vec{H}\right) - \dfrac{\varepsilon_0\left(\varepsilon_s-\varepsilon_\infty\right)}{\tau}\vec{E} & \\ & -\sigma\vec{E} + \dfrac{1}{\tau}\vec{P}, & \\ \dfrac{\partial \vec{P}}{\partial t} = & \dfrac{\varepsilon_0\left(\varepsilon_s-\varepsilon_\infty\right)}{\tau}\vec{E} - \dfrac{1}{\tau}\vec{P}. & \end{array}\right. \tag{1}$$

μ_0 denoting the magnetic permittivity in vacuum, ε_0 the electric permittivity in vacuum, ε_∞ the infinite frequency relative permittivity, ε_s, the static relative permittivity, the permittivity at zero frequency ($\varepsilon_s > \varepsilon_\infty$) and τ the Debye relaxation time constant, characteristic of the material. The boundary conditions are of the following type: we introduce the decomposition $\partial\Omega = \Gamma_m \cup \Gamma_a$ of the boundary of Ω on which we impose

$$\left\{\begin{array}{l} \vec{n}\times\vec{E} = 0 \quad \text{on } \Gamma_m, \\ \vec{n}\times\vec{E} - \sqrt{\dfrac{\mu}{\varepsilon}}\vec{n}\times\left(\vec{H}\times\vec{n}\right) = \\ \vec{n}\times\vec{E}^{inc} - \sqrt{\frac{\mu}{\varepsilon}}\vec{n}\times\left(\vec{H}^{inc}\times\vec{n}\right) \quad \text{on } \Gamma_a, \end{array}\right.$$

where $\vec{n}$ denotes the unit outward normal to $\partial\Omega$ and $\left(\vec{E}^{inc}, \vec{H}^{inc}\right)$ is a given incident field.

As in [2] we propose and study a locally implicit discontinuous Galerkin time-domain method formulated on an unstructured tetrahedral mesh coupled with an efficient time integration method introduced in [1] for dealing with grid induced stiffness when using non-uniform (locally refined) meshes for solving the resulting system of differential equations in the case of Debye-type media. The time integration method is a blend of the second order leap-frog scheme and the second order Crank-Nicolson scheme. We wonder whether the method retains its second-order ODE convergence under stable simultaneous space-time grid refinement $\Delta t \backsim h$, $h \to 0$ towards the exact PDE solution. This is not a priori clear due to the splitting between two different time integration methods which can introduce order reduction but it is possible to prove that splitting is not detrimental to the second-order ODE convergence of the method under stable simultaneous space-time grid refinement towards the exact underlying PDE solution.

Three-dimensional numerical simulations are presented concerning the exposure of head tissues to a localized source radiation showing the efficiency of this method.

Keywords: Maxwell's equations, discontinuous Galerkin time-domain method

References

[1] J.G. Verwer, Component splitting for semi-discrete Maxwell equations, *BIT. Numerical Mathematics* **51** (2011), pp. 427–445.

[2] S. Descombes, S. Lanteri and L. Moya, Locally implicit time integration strategies in a discontinuous Galerkin method for Maxwell's equations, *Journal of Scientific Computing* **56** (2013), pp. 190–218.

A Comparison of High-order Finite Element Method and Wave-based Discontinuous Galerkin Method for Helmholtz Problems

Alice Lieu[1,*], **Gwénaël Gabard**[1], **Hadrien Bériot**[2]

[1]ISVR, University of Southampton, Southampton, SO17 1BJ, United Kingdom
[2]Siemens PLM, Interleuvenlaan 68, Researchpark Z1, Leuven, Belgium

Abstract

In this paper, we compare the performance of the wave-based discontinuous Galerkin method against the polynomial high-order finite element method (FEM) for Helmholtz problems. Previous studies demonstrate that both methods lead to a control of the dispersion error associated with low-order FEM at high frequency. Common belief is that compared to polynomial methods, physics-based methods can provide a significant improvement in performance, at the expense of a deterioration of the conditioning. However, the results presented in this paper indicate that the differences in accuracy, efficiency and conditioning between the two approaches are more nuanced than generally assumed.

Keywords: Helmholtz Problem, Wave-based Discontinuous Galerkin Method, High-order Finite Element Method.

1 Introduction

We compare the performance of the wave-based discontinuous Galerkin method against the polynomial high-order finite element method (p-FEM). The methods were both devised to tackle the so-called pollution effect (accumulation of dispersion error) encountered by standard Finite Element Method when solving short wave problems. Another common characteristic between these two methods is that they easily allow local order refinement, which makes them suited for p-adaptive and hp-adaptive strategies.

The studied p-FEM replaces the low-order Lagrange polynomials with Lobatto shape functions [5], taking advantage of the improved interpolation properties of this family of functions. As the polynomial order P is increased, different types of shape functions appear: vertex, edge and bubble functions (and also face functions in 3D). Bubble functions have no connectivity with the neighbouring elements and can therefore be removed from the global system using static condensation which improves the conditioning and reduces the memory requirements.

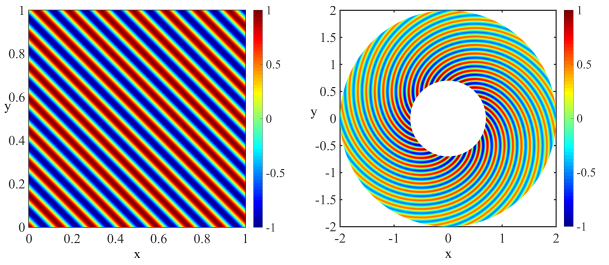

(a) Plane wave. (b) Prop. spinning waves.

Figure 1: Example of solutions.

Wave-based discontinuous Galerkin method (DGM) [1] uses plane waves to interpolate the solution in each element and the continuity between elements is weakly imposed using numerical fluxes.

Both numerical models have been identified as effective methods to address the pollution effect [2, 4] but, to the authors' knowledge, they have not been compared.

2 Description of the test cases

To assess the performance of the methods, we use four types of solutions of the Helmholtz equation. The propagating plane wave problem in figure 1(a) involves a single direction of propagation and therefore allows a detailed study of the anisotropy of the numerical models. The spinning wave problem in figure 1(b) consists of spiral-shaped waves radiating from a cylinder. All the wave directions are equally present in the domain, which is closer to a realistic problem compared to the first test case. Propagating and evanescent waves are investigated. Finally, a singular corner solution is considered. The gradient of the solution exhibits a singularity at the origin. The objective with this last test case is to investigate how the two methods behave when confronted with such solutions.

The computational domains are discretised using uniform triangular unstructured elements. To generate the solutions, an inhomogeneous Robin boundary condition is used for p-FEM and ghost cells are used for wave-based DGM [1].

3 Main results

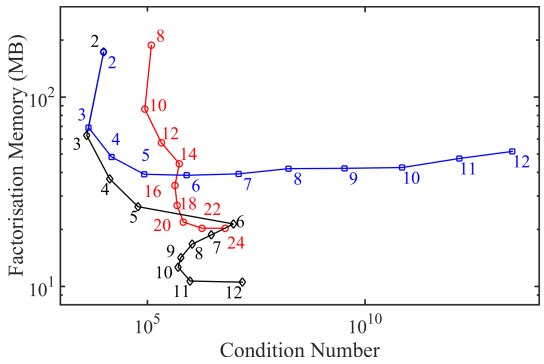

Figure 2: Propagating spinning wave problem (ka=28); factorisation memory (MB) against condition number to achieve 1% of accuracy; circles: wave-based DGM, squares: p-FEM without condensation, diamonds: p-FEM with condensation. The numbers of plane wave or polynomial order is shown next to each point.

A first part of the study is dedicated to the interpolation properties of the bases. The rest of the study focuses on the numerical models for which the following conclusions have been drawn. For the propagating wave problems, wave-based DGM and p-FEM are able to achieve the same level of accuracy and similar levels of performance. To reach the required accuracy (1% of the relative L^2-error), the wave-based systems are not ill-conditioned contrary to what is commonly assumed (figure 2). However, the studied physics-based method does not provide a step change in computational performance, even at high frequency. When dealing with evanescent waves, wave-based DGM becomes expensive compared to p-FEM which costs remained similar to that of the propagating waves. The exponential convergence of both methods for regular problems is lost when representing singular solutions. However, p-FEM is more robust and for a given mesh, the levels of accuracy reached are higher than those reached by the physics-based method.

Compared to wave-based DGM, p-FEM has a more consistent behaviour for the different types of problems. Moreover, p-FEM can directly be used on problems with non-uniform coefficients, whereas wave-based DGM would require some non-trivial developments to generalise the plane-wave basis to non-uniform media [3].

Acknowledgements

This work is performed as part of the CRANE (Community and Ramp Aircraft NoisE) project and is supported in full by European Union funding under the Framework Programme 7.

References

[1] G. Gabard, Discontinuous Galerkin methods with plane waves for time-harmonic problems, *J Comput Phys* **225** (2007), pp. 1961-1984

[2] T. Huttunen, P. Gamallo and R.J. Astley, Comparison of two wave element methods for the Helmholtz problem, *Comm Numer Meth En* **25** (2009), pp. 35-52

[3] L.-M. Imbert-Gerard and B. Després, A generalized plane-wave numerical method for smooth nonconstant coefficients, *IMA J Numer Anal* **34** (2014), pp. 1072-1103

[4] S. Petersen, D. Dreyer and O. von Estorff, Assessment of finite and spectral element shape functions for efficient iterative simulations of interior acoustics, *Comput Method Appl M* **195** (2006), pp. 6463-6478

[5] P. Solin, K. Segeth and I. Dolezel, Higher-Order Finite Element Methods, Chapman and Hall, 2004

Acoustic scattering by inhomogeneous anisotropic obstacle: Boundary-domain integral equation approach

David Natroshvili[1,*]

[1]Department of Mathematics, Georgian Technical University, Tbilisi, Georgia

[*]Email: natrosh@hotmail.com

Abstract

We consider the time-harmonic acoustic wave scattering by a bounded layered *anisotropic inhomogeneity* embedded in an unbounded *anisotropic homogeneous* medium. The material parameters and the refractive index are assumed to be discontinuous across the interfaces between inhomogeneous interior and homogeneous exterior regions. The corresponding mathematical problems are formulated as boundary-transmission problems for a second order elliptic partial differential equation of Helmholtz type with discontinuous variable coefficients.

We show that with the help of *localized potentials* the boundary-transmission problems can be reformulated as a *localized boundary-domain integral equations* (LBDIE) systems and prove that the corresponding *localized boundary-domain integral operators* (LBDIO) are invertible.

Keywords: acoustic scattering, inhomogeneous anisotropic obstacle, transmission problems, boundary-domain integral equations.

1 Uniqueness and existence results

The physical time-harmonic acoustic wave scattering problem under consideration mathematically is formulated as a transmission problem for a second order elliptic partial differential equation with variable coefficients

$$A_2(x,\partial_x)\,u(x) \equiv \partial_{x_k}\big(a_{kj}^{(2)}(x)\,\partial_{x_j}u(x)\big) + \omega^2\,\kappa(x)\,u(x) = f_2$$

in the inhomogeneous anisotropic bounded region Ω_2 and for the anisotropic Helmoltz type equation with constant coefficients

$$A_1(\partial_x)u(x) \equiv \partial_{x_k}\big(a_{kj}^{(1)}\partial_{x_j}u(x)\big) + \omega^2\kappa u(x) = f_1$$

in unbounded homogeneous region $\Omega_1 = \mathbb{R}^3 \setminus \overline{\Omega}_2$.

Since the material parameters $a_{kj}^{(q)}$ and the refractive index κ are assumed to be discontinuous across the interface $S = \partial\Omega_1 = \partial\Omega_2$ between the inhomogeneous interior and homogeneous exterior regions, on S there are given standard transmission conditions relating the interior and exterior limiting values of the sought for wave functions and their co-normal derivatives.

The similar transmission problems when $A_1(\partial_x)$ is the Helmholtz operator $\Delta+\omega^2$ and $A_2(x,\partial_x) = \Delta + \omega^2\kappa(x)$ is well investigated in the literature (see [2] and the references therein).

The acoustic scattering problem in the whole space corresponding to an *isotropic inhomogeneity*, i.e., when $a_{kj}^{(2)}(x) = a^{(2)}(x)\,\delta_{kj}$ with Kronecker's delta and $A_1(\partial_x) = \Delta+\omega^2$, by the indirect boundary-domain integral equation method is investigated by P.Werner [6], [7]. Applying the potential method based on the Helmholtz fundamental solution, he reduces the problem to the *Fredholm-Riesz integral equations* system and proves its unique solvability. Applying these results the same problem by the direct method is studied by P.Martin [4].

Werner's approach is not applicable in anisotropic case.

Our goal here is to show that the above mentioned transmission problem for a general anisotropic case with the help of *localized potentials* associated with the Laplace operator can be reformulated as a *localized boundary-domain integral equations* system and prove that the corresponding *localized boundary-domain integral operators* are invertible. Beside a pure mathematical interest these results seem to be important from the point of view of numerical analysis, since LBDIE system can be applied in constructing very convenient numerical schemes in applications.

In our analysis, we apply the localized parametrix $P_\chi(x-y)$ associated with the Laplace operator which is represented as the product of the fundamental solution $-[\,4\,\pi\,|x-y|\,]^{-1}$ of the Laplace operator and an appropriately chosen localizing cut-off function $\chi(x-y)$ supported on some neighbourhood of the origin. Evidently, the kernels of the corresponding localized po-

tentials are supported in some neighbourhood of the reference point y (assuming that x is an integration variable) and they do not solve the original differential equation. Moreover, note that the harmonic localized parametrix $P_\chi(x-y)$ is not a Levi function for the operator $A_2(x,\partial_x)$, in general.

By means of the standard and localized layer and volume potentials we reduce the transmission problem under consideration to the localized boundary-domain integral equations system. This system contains standard and localized boundary integral operators on S and a localized pseudodifferential operator of zero order (a Cauchy singular integral operator) defined on a bounded domain Ω_2. Consequently, the corresponding system does not belong to the Fredholm-Riesz class of integral operators.

Our analysis consists of several steps and is based on the results obtained in [1], [3], [5].

First we establish the equivalence between the original transmission problems and the corresponding LBDIE system which plays a crucial role in our analysis.

Afterwards, we establish that the localized boundary domain integral operator obtained belongs to the Boutet de Monvel algebra of pseudodifferential operators.

And finally, applying the Vishik-Eskin theory based on the factorization method (the Wiener-Hopf method) we investigate Fredholm properties of the LBDIO and prove its invertibility in appropriate function spaces. This invertibility property implies then, in particular, existence and uniqueness results for the LBDIE system and the corresponding original transmission problem.

The same approach is applicable when the inhomogeneous region Ω_2 contains holes (empty inclusions) with appropriate Dirichlet, Neumann or mixed type boundary conditions.

This is a joint work with Sergey Mikhailov (Brunel University of London, UK) and Otar Chkadua (Tbilisi State University, Georgia).

Acknowledgements: This research was supported by grant No. EP/H020497/1 from the EPSRC, UK, and by the Shota Rustaveli National Science Foundation (SRNSF) Grant No. FR/286/5-101/13.

References

[1] O. Chkadua, S. Mikhailov and D. Natroshvili, Localized Boundary-Domain Singular Integral Equations Based on Harmonic Parametrix for Divergence-Form Elliptic PDEs with Variable Matrix Coefficients, *Integral Equations and Operator Theory*, **76** (2013), pp. 509-547.

[2] D. Colton and R. Kress, *Inverse Acoustic and Electromagnetic Scattering Theory.* Second Edition, Springer-Verlag, Berlin, New York, Tokyo, 1998.

[3] L. Jentsch and D. Natroshvili, Interaction between thermoelastic and scalar oscillation fields, *Integral Equations and Operator Theory*, **28**(1997), pp. 261-288.

[4] P.A. Martin, Acoustic scattering by inhomogeneous obstacles, *SIAM Journal of Applied Mathematics*, **64**, No. 1 (2003), pp. 297-308.

[5] D. Natrosvili, S. Kharibegashvili and Z. Tediashvili, Direct and inverse fluid-structure interaction problems, *Rediconti di Matematica, Serie VII,* **20**(2000), pp. 57–92.

[6] P. Werner, Zur mathematischen Theorie akustischer Wellenfelder, *Arch. Ration. Mech. Anal.*, **6** (1960), pp. 231-260.

[7] P. Werner, Beugungsprobleme der mathematischen Akustik, *Arch. Ration. Mech. Anal.*, **12** (1963), pp. 155-184.

A Spectral Volumetric Integral Equation Method for Ocean Acoustics with Depth-Dependent Background Sound Speed

T. Rienmueller[1,*]

[1]ZeTeM, Zentrum für Technomathematik, Universität Bremen, Germany

[*]Email: rienmueller@uni-bremen.de

Abstract

Time-harmonic acoustic wave propagation in an ocean with depth-dependent background sound speed can be described by the Helmholtz equation. Lechleiter and Nguyen introduce in [1] a spectral volumetric integral equation method for ocean acoustics for constant background sound speed. For computations of acoustic scattering in a depth ocean and computations over large distances, however, it is necessary to have depth-depended background sound speed. We apply the idea of [1] to present fundamental ingredients for the numerical analysis for a spectral volumetric integral equation method for inhomogeneous ocean acoustics.

Keywords: Lippmann-Schwinger Equation, spectral method, ocean acoustics

1 Sound Waves in an Ocean

We consider a waveguide $\Omega = \mathbb{R}^m \times [0, h]$, where $h > 0$ is the constant depth of the ocean and $m = 2, 3$ is the dimension of the ocean. For simplicity, we assume in this work only $m = 3$. The time harmonic sound propagation for an ocean with depth-dependent background sound speed is formally governed by the Helmholtz equation

$$\Delta u + \frac{\omega^2}{c^2(x_3)} n^2 u = 0 \quad \text{in } \Omega, \tag{1}$$

where ω is the frequency and c is the speed of sound depending on the depth of the ocean. Moreover, the sound speed c is bounded by $0 < c_- \leq c \leq c_+$. Furthermore, n is the refractive index and we suppose $n = 1$ outside a bounded and open set D. Since $D \subset \Omega$ is a local perturbation in the inhomogeneous ocean characterized by refractive index n, we denote the contrast by

$$q(x) := n^2(x) - 1 \text{ for } x \in \Omega.$$

Next, the free surface of the ocean is modeled by sound soft boundary conditions (BCs)

$$u = 0 \text{ on } \Gamma_0 := \{x \in \mathbb{R}^3 : x_3 = 0\},$$

and the seabed of the ocean by sound hard BCs

$$\frac{\partial u}{\partial x_3} = 0 \text{ on } \Gamma_h := \{x \in \mathbb{R}^3 : x_3 = h\}.$$

Further, writing $x = (\tilde{x}, x_3)^T$, for $|\tilde{x}|$ large enough we expand u by separation of variables as

$$u(\tilde{x}, x_3) = \sum_{j \in \mathbb{N}} w_j(\tilde{x}) u_j(x_3). \tag{2}$$

Exploiting the Helmholtz equation (1) we have

$$\frac{\partial^2 u_j}{\partial x_3^2} - \frac{\omega^2}{c^2(x_3)} u_j = \lambda_j^2 u_j, \text{ in } (0, h), j \in \mathbb{N}, \tag{3}$$

and

$$\frac{\partial^2 w_j}{\partial x_1^2} + \frac{\partial^2 w_j}{\partial x_2^2} + \lambda_j^2 w_j = 0 \text{ in } \mathbb{R}^2, \tag{4}$$

for some constant λ_j. We investigate (3) with BCs $u_j(0) = 0$ and $\partial u_j / \partial x_3(h) = 0$ corresponding to the waveguide BCs. Since this eigenvalue problem is self-adjoint, it is well known that for $c \in L^\infty(0, h)$ the eigenvalues $\lambda_j^2 \in \mathbb{R}$ form a discrete set and corresponding eigenvectors $u_j \in H^2(0, h)$.

To obtain a radiating solution u in (2), the functions w_j need to satisfy a radiation condition for $\lambda_j (= i\sqrt{|\lambda_j|^2}$, for $\lambda_j^2 \leq 0)$. By the fact that $\lambda_j^2 \to -\infty$ $(j \to \infty)$, only finitely many λ_j are real, and for those j we prescribe the radiation condition

$$\lim_{|\tilde{x}| \to \infty} \sqrt{\tilde{x}} \Big(\frac{\partial w_j}{\partial |\tilde{x}|} - i|\lambda_j| w_j \Big) = 0, \text{ uniformly in } \frac{\tilde{x}}{|\tilde{x}|}.$$

If $\lambda_j < 0$, we prescribe that w_j must be a bounded solution to (4), yielding an evanescent mode. Note that, for a certain choice of ω, h, c we might have $\lambda_j = 0$ for some j. For simplicity, we exclude these eigenvalues in this work, however, the analysis will be influenced. For a homogeneous ocean this is discussed in [2]. Assuming $\lambda_j \neq 0$, then the Green's function can be expanded as

$$G(x, y) = \frac{i}{4} \sum_{j=1}^{\infty} \phi_j(x_3) \phi_j(y_3) H_0^{(1)}(\lambda_j |\tilde{x} - \tilde{y}|),$$

where $\tilde{x} \neq \tilde{y}$ and ϕ_j denotes the normalized eigenfunctions. Note that for an inhomogeneous ocean, computing λ_j and ϕ_j requires substantial numerical efforts, since no explicit representation is available.

2 Volumetric Integral Equation

We would like to introduce a volumetric integral equation of second kind, called Lippmann-Schwinger equation (LSE), that corresponds to solving the scattering problem (1) with BCs and radiation condition. Furthermore, we show that the volumetric integral equation $\mathcal{V}f$, formally defined for a function $f : D \to \mathbb{C}$ by

$$\mathcal{V}f = \int_D G(\cdot, y) f(y) dy \qquad \text{for } f \in L^2(\Omega),$$

is a bounded operator from $L^2(D)$ into $H^2_{loc}(\Omega)$.

Let us point out here that for analytic aspects we work later in the domain $\Lambda_\rho := \{x \in \Omega : |\tilde{x}| < \rho\}$, where $\rho > 0$ and $\tilde{\Lambda}_\rho := \{\tilde{x} \in \mathbb{R}^2 : |\tilde{x}| < \rho\}$.

Lemma 2.1 *The operator $\mathcal{V}_j$, defined by*

$$\begin{aligned} \mathcal{V}_j : & L^2(\tilde{\Lambda}_\rho) \to L^2(\tilde{\Lambda}_\rho) \\ & f \mapsto \int_{\tilde{\Lambda}_\rho} H_0^{(1)}(\lambda_j |\tilde{x} - \tilde{y}|) f(\tilde{y}) d\tilde{y}, \quad j \in \mathbb{N}, \end{aligned}$$

is bounded from $L^2(\tilde{\Lambda}_\rho)$ into $H^1(\tilde{\Lambda}_\rho)$, and

$$\|\mathcal{V}_j f\|^2_{H^1(\tilde{\Lambda}_\rho)} \leq C j^{-1} \|f\|^2_{L^2(\tilde{\Lambda}_\rho)}. \qquad (5)$$

The boundedness of $\mathcal{V}_j$ follows for fixed j directly from the weak singularity of the kernel, however, estimate (5) requires more carefully arguments to obtain an explicit dependency on j.

Fourier theory gives

$$\begin{aligned} L^2(\Lambda_\rho) = \{ & f : \Lambda_\rho \to \mathbb{C}, f(x) = \sum_{j \in \mathbb{N}} \hat{f}(j, \tilde{x}) \phi_j(x_3), \\ & \sum_{j \in \mathbb{N}} \int_{\tilde{\Lambda}\rho} |\hat{f}(j, \tilde{x})|^2 \, d\tilde{x} = \|f\|^2_{L^2(\Lambda_\rho)} < \infty \}. \end{aligned}$$

Then we have the corresponding separation in horizontal and vertical components

$$L^2(\Lambda_\rho) = L^2([0, h], L^2(\tilde{\Lambda}_\rho)).$$

In particular, we get

$$\|\mathcal{V}f\|^2_{L^2(\Lambda_\rho)} = \sum_{j \in \mathbb{N}_+} \|\mathcal{V}_j \hat{f}(j, y_1)\|^2_{L^2(\tilde{\Lambda}_\rho)} \leq C \|f\|^2_{L^2(\Lambda_\rho)}.$$

To get boundedness of $\mathcal{V}$ from $L^2(\Lambda_\rho)$ into $H^1(\Lambda_\rho)$ we use the same representation idea for $H^1(\Lambda_\rho)$.

Moreover, for every $f \in L^2(\Omega)$, with compact support, function $\mathcal{V}f \in H^2_{loc}(\Omega)$ solves $\Delta \mathcal{V}f + \omega^2/c^2(x_3)\mathcal{V}f = -f$. For an incident wave solving (1) for $n^2 \equiv 1$, with scattered field u^s is the field that satisfies the BCs and such that the total field

$$u(x) = u^i(x) + u^s(x), \quad x \in \Omega,$$

solves Helmholtz equation (1) and BCs. With these ingredients the scattering problem can be equivalently described by the LSE

$$u^s - \mathcal{V}\Big(\frac{\omega^2}{c^2(x_3)} q u^s\Big)\Big|_D = \mathcal{V}\Big(\frac{\omega^2}{c^2(x_3)} q u^i\Big)\Big|_D \text{ in } L^2(D).$$

In order to do numerically approximation to this equation, we establish a periodized LSE, then use a spectral method. Further, we present an optimization technique for this spectral method, when the height of the obstacle is small compared to the height of the inhomogeneous ocean.

References

[1] Lechleiter, A. and Nguyen, D. L., *Spectral volumetric integral equation methods for acoustic medium scattering in a 3D waveguide.* IMA Num. Anal. 2010, **32(3)**:813-844.

[2] Arens, T., Gintides D. and Lechleiter, A., *Variational formulation for scattering in a three-dimensional acoustic waveguide.* Math. Meth. App. Sci 2008, **31**:821-847.

A high-order Nyström scheme for acoustic scattering by inhomogeneous penetrable media in three dimensions

Ambuj Pandey[1,*], **Akash Anand**[1], **B.V. Rathish Kumar**[1]

[1]Department of Mathematics, Indian Institute of technology, Kanpur, India

[*]Email: ambuj@iitk.ac.in

Abstract

We present a high-order Nyström method for scattering of acoustic waves by inhomogeneous penetrable media in three dimensions where refractive index is allowed to jump across the material interface. This integral equation based approach adopts the framework of overlapping local parameterizations for describing general scattering geometries and employees a partition of unity to simplify the design of quadratures for approximation of the integral operator. A high-order convergence is achieved through analytic resolution of singularities via suitable changes of parametric variables. Accelerated evaluation of the non-singular integrals is accomplished by a method of equivalent source representations on a Cartesian grids and employing three dimensional FFTs.

Keywords: Acoustic scattering, Lippmann-Schwinger integral equation, FFTs.

1 Introduction

We present a high-order integral equation solver for acoustic scattering by three dimensional bounded penetrable inhomogeneous media with refractive index n which is assumed to be one outside the scatterer Ω. Existing fast techniques for this problem at best achieves second order convergence for discontinuous scattering configurations, e.g., [2, 5]. Although, high-order nature of the algorithm introduced in [1] is not constrained by smoothness of n across material interface, it is computationally efficient only for "thin" scatterers. Our present approach, in fact, is a nontrivial extension of the the ideas introduced in [1] to obtain a solver for general scattering configurations while retaining high-order accuracy even in the presence of material discontinuity.

2 Numerical Scheme

An equivalent integral equation formulation for scattering problem is given by the *Lippmann-Schwinger Integral Equation* [3], $u(\boldsymbol{x})+\kappa^2 K[u](\boldsymbol{x}) = u^i(\boldsymbol{x})$ where $K[u](\boldsymbol{x}) = \int_\Omega G(\boldsymbol{x},\boldsymbol{x}')m(\boldsymbol{x}')u(\boldsymbol{x}')d\boldsymbol{x}'$. Here $G(\boldsymbol{x},\boldsymbol{x}') = \exp(i\kappa|\boldsymbol{x}-\boldsymbol{x}'|)/(4\pi|\boldsymbol{x}-\boldsymbol{x}'|)$ and $m(\boldsymbol{x}) = 1-n^2(\boldsymbol{x})$.

The proposed high-order Nyström scheme is based on approximation of $K[u](\boldsymbol{x})$ by means of a high-order quadrature rule. We begin by covering the scatterer Ω by overlapping coordinate patches $\{\Omega_p\}_{p=1}^P$, where each patch Ω_p is parametrized by a smooth invertible map $\boldsymbol{x}_p = \boldsymbol{x}_p(\boldsymbol{s},t)$, $(\boldsymbol{s},t) = (s_1,s_2,t) \in (0,1)^3$. Further, with the help of a partition of unity $\{w_p(\boldsymbol{x})\}_{p=1}^P$ subordinate to this covering, we rewrite $K[u](\boldsymbol{x})$ as sum of P integrals $K[u](\boldsymbol{x}) = \sum_{p=1}^P K_p[u](\boldsymbol{x})$ where $K_p[u](\boldsymbol{x}) = \int_{[0,1]^3} G(\boldsymbol{x},\boldsymbol{x}_p)\phi_p^u(\boldsymbol{s}',t')d\boldsymbol{s}'dt'$, $\phi_p^u(\boldsymbol{s},t) = m(\boldsymbol{x}_p(\boldsymbol{s},t))u(\boldsymbol{x}_p(\boldsymbol{s},t))w_p(\boldsymbol{x}_p(\boldsymbol{s},t))$ $J_p(\boldsymbol{s},t)$ and J_p is the Jacobian of the parametric change of variable $\boldsymbol{x}_p$. Note that, w_p vanishes to high-order on the sides of those patches (referred to as "interior patches") whose closure have an empty intersection with the boundary of Ω, while this, of course, does not happen on remaining patches, (referred to as "boundary patches"). This difference, in turn, alters the behavior of integrands on the boundary of respective patches, and therefore demands specialized treatment for accurate evaluation of $K_p[u](\boldsymbol{x})$ corresponding to both groups, boundary and interior, patches – that we describe in what follows.

Integration Over Boundary Patches: We employ the strategy of splitting the kernel into two; a smooth kernel and a singular but localized kernel. The respective integrals with non-singular and singular kernels are then approximated to high-order by means of two different strategies explained below.

Non-Singular Integration: In this case the integrand is smooth in all variable and vanishes to high-order at end-points of the integration intervals in parallel coordinates $\boldsymbol{s}'$. Therefore, high-order can be attained by simply employing spectrally accurate trapezoidal rule for planar integration with respect to $\boldsymbol{s}'$ and a high-order composite Newton-Cotes quadrature in trans-

verse variable t'.

Singular Integration: More careful treatment is required for obtaining accurate approximation when kernel is singular. A change to polar coordinates (ρ, θ) centered around $\boldsymbol{s}$, the projection of $\boldsymbol{x}_p^{-1}(\boldsymbol{x})$ on to the integration plane $(\boldsymbol{s}', t')$, followed by a polynomial change of variable in ρ provides an effective resolution of kernel singularity. A high-order approximation can then be obtained by employing quadratures similar to the ones employed in the non-singular integration case. We refer the readers to [1] for a more detailed discussion on this approach.

Integration Over Interior Patches: Following an approach similar to the one adopted for integration over boundary patches, we again use two different approximation strategies for integrals with smooth and singular kernels.

Non-Singular Integration: In this case, $\phi_p^u(\boldsymbol{s}, t)$ vanishes to high order on the boundary of interior patches while the kernel is smooth. Consequently, the integrand for evaluation of $K_p[u](\boldsymbol{x})$ is smooth and compactly supported in the domain of integration and is approximated to high-order accuracy by means of Trapezoidal rule.

Singular Integration: In order to resolve the kernel singularity, a change of variables to spherical coordinates around target point $\boldsymbol{x}(\boldsymbol{s}, t)$ is employed. This procedure yields smooth and compactly supported integrand that again converges to high-order when Trapezoidal rule is employed for approximation.

Finally, the computation of non-singular integrals over boundary and interior patches is accelerated by a suitable use of two face equivalent source approximations on Cartesian grids, introduced in [4].

3 Numerical Result

We begin by comparing our approximate integral operator against the continuous operator for a spherical shaped scatterer of the size $ka = 10$ with a constant refractive index of $\sqrt{2}$. The convergence study shown in Table 1 clearly shows that our approximate operators converge to the continuous integral with expected high-order convergence. In Fig 1, we present a scattering computation for the same spherical shaped scatterer with a computational grid of $64 \times 64 \times 64$ on each patch (see Fig.1 (a)) and computed solution has a relative error of order 10^{-4} when compared to the analytic solution.

Grid	Error	Order
$3 \times 4 \times 4 \times 4$	5.25×10^{-1}	–
$3 \times 8 \times 8 \times 8$	1.70×10^{-1}	1.62
$3 \times 16 \times 16 \times 16$	3.72×10^{-2}	2.20
$3 \times 32 \times 32 \times 32$	7.31×10^{-4}	5.67
$3 \times 64 \times 64 \times 64$	2.17×10^{-5}	5.07

Table 1: Convergence for a penetrable sphere of size $ka = 10$ with $n = \sqrt{2}$.

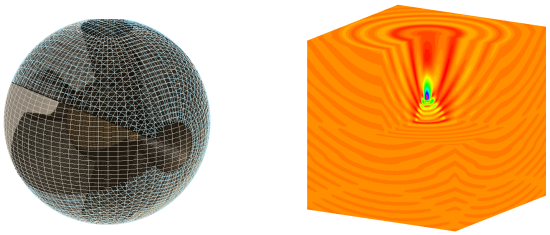

(a) Computational grid (b) Total field

Figure 1: Scattering of a plane wave by a penetrable sphere of size $ka = 20$ with $\sqrt{2}$ as its refractive index.

Acknowledgments

AA gratefully acknowledges support from DST.

References

[1] A. Anand and F. Reitich , *An efficient high-order algorithm for acoustic scattering from penetrable thin structures in three dimensions*, Journal of Acoustical Society of America, **121** (2007), pp. 2503–2514.

[2] E. M. Hyde and O. P. Bruno, *A fast, higher-order solver for scattering by penetrable bodies in three dimensions*, Journal of Computational Physics, **202** (2005), pp. 236–261.

[3] P. Martin, *Acoustic scattering by inhomogeneous obstacles*, SIAM Journal on Applied Mathematics' **64** (2003), pp. 297-308.

[4] O. P. Bruno and L. A. Kunyansky, *A Fast, High-Order Algorithm for the Solution of Surface Scattering Problems: Basic Implementation, Tests, and Applications*, Journal of Computational Physics, **169** (2001), pp. 80–110.

[5] Zhu, Aiming and Gedney, Stephen D *A quadrature-sampled precorrected FFT method for the electromagnetic scattering from inhomogeneous objects*, Antennas and Wireless Propagation Letters, IEEE, **2** (2003), pp. 50–53.

Sensitivity analysis for shape optimization of a focusing acoustic lens in lithotripsy

Vanja Nikolić[1,*], **Barbara Kaltenbacher**[1]

[1]Institute of Mathematics, University of Klagenfurt, 9020 Klagenfurt, Austria

[*]Email: vanja.nikolic@aau.at

Abstract

We are interested in shape sensitivity analysis for an optimization problem arising in medical applications of high intensity focused ultrasound. The goal is to find the optimal shape of a focusing acoustic lens so that the desired acoustic pressure at a kidney stone is achieved. We follow the variational approach to calculating the shape derivative of the cost functional, introduced in [2], which does not require computing the shape derivative of the state variable.

Keywords: nonlinear acoustics, Westervelt's equation, shape derivative

1 Introduction

In lithotripsy, the aim of obtaining a sharp focus of the acoustic pressure exactly at the desired location of a kidney stone leads to the task of optimizing the shape of the acoustic lens.

Let $\Omega \subset \mathbb{R}^d$, $d \in \{1,2,3\}$, be a fixed bounded domain with Lipschitz boundary $\partial\Omega$, and Ω_+ a subdomain, representing the lens, such that $\bar{\Omega}_+ \subset \Omega$ and Ω_+ has Lipschitz regular boundary $\partial\Omega_+ = \Gamma$ (see fig. 1). $\Omega_- = \Omega \setminus \overline{\Omega}_+$ represents the fluid region. Coupling of the acoustic lens and nonlinearly acoustic fluid region can be modeled by the Westevelt equation with nonlinear damping and piecewise constant coefficients, first introduced in [1]:

$$
(1)\quad \begin{cases} \frac{1}{\lambda(x)}(1-2k(x)u)\ddot{u} - \operatorname{div}(\frac{1}{\varrho(x)}\nabla u \\ -b(x)((1-\delta(x)) + \delta(x)|\nabla\dot{u}|^{q-1})\nabla\dot{u}) \\ = \frac{2k(x)}{\lambda(x)}(\dot{u})^2 \quad \text{in } \Omega_+ \cup \Omega_-, \\ [\![u]\!] = 0 \quad \text{on } \Gamma, \\ \Big[\!\Big[\frac{1}{\varrho(x)}\frac{\partial u}{\partial n_+} + b(x)(1-\delta(x))\frac{\partial \dot{u}}{\partial n_+} \\ \quad +b(x)\delta(x)|\nabla\dot{u}|^{q-1}\frac{\partial\dot{u}}{\partial n_+} \Big]\!\Big] = 0 \text{ on } \Gamma, \\ u = 0 \quad \text{on } \partial\Omega, \\ (u,\dot{u})|_{t=0} = (u_0,u_1). \end{cases}
$$

Here u stands for the acoustic pressure, b is related to the diffusivity, c denotes the speed of sound, $k = \beta_a/\lambda$, $\lambda = \varrho c^2$ is the bulk modulus, ϱ is the mass density, $\beta_a = 1 + B/(2A)$, and B/A represents the parameter of nonlinearity. n_+ and n_- stand for the unit outer normals to the lens Ω_+ and the fluid region Ω_- and $[\![\cdot]\!]$ denotes the jump across the interface Γ.

For brevity, we emphasize the space dependence of coefficients in (1), while omitting space and time dependence of u in the notation. We make the following assumptions on coefficients:

$$
\begin{aligned} &b_i := b|_{\Omega_i}, \varrho_i := \varrho|_{\Omega_i}, \lambda_i := \lambda|_{\Omega_i},\ \delta_i := \delta|_{\Omega_i}, \\ &k_i := k|_{\Omega_i} \text{ are constants,} \\ &b_i, \varrho_i, \lambda_i > 0,\ \delta_i \in (0,1),\ k_i \in \mathbb{R},\ i \in \{+,-\}. \end{aligned}
$$

An important feature of the Westervelt equation is possible degeneracy due to the factor $1-2ku$. This means that any analysis of the Westervelt equation has to include bounding away from zero this term or, in other words, obtaining a bound on $\|u\|_{L^\infty(0,T;L^\infty(\Omega))}$. In [1], this issue was resolved by employing the Sobolev embedding $W^{1,q+1}(\Omega) \hookrightarrow L^\infty(\Omega)$, $q > d-1$.

2 Shape optimization problem

We consider the following optimization problem

$$
\begin{aligned} &\min_{\substack{\Omega_+ \in \mathcal{O}_{\text{ad}} \\ u \in L^2(\Omega\times[0,T])}} J(u,\Omega_+) \\ &\equiv \min_{\substack{\Omega_+ \in \mathcal{O}_{\text{ad}} \\ u \in L^2(\Omega\times[0,T])}} \int_0^T \int_\Omega (u-u_{\text{d}})^2\,dx\,ds \end{aligned}
$$

subject to the constraint

$$
\begin{aligned} \int_0^T \int_\Omega \Big\{ &\frac{1}{\lambda(x)}(1-2k(x)u)\ddot{u}\phi + \frac{1}{\varrho(x)}\nabla u\cdot\nabla\phi \\ &+ b(x)(1-\delta(x))\nabla\dot{u}\cdot\nabla\phi - \frac{2k(x)}{\lambda(x)}(\dot{u})^2\phi \\ &+ b(x)\delta(x)|\nabla\dot{u}|^{q-1}\nabla\dot{u}\cdot\nabla\phi \Big\}\,dx\,ds = 0, \end{aligned}
$$

for all $\phi \in \tilde{X} = L^2(0,T;W_0^{1,q+1}(\Omega))$, with initial conditions (u_0,u_1).
$u_d \in L^2(0,T;H_0^1(\Omega))$ denotes the desired acoustic pressure. The set of admissible shapes is

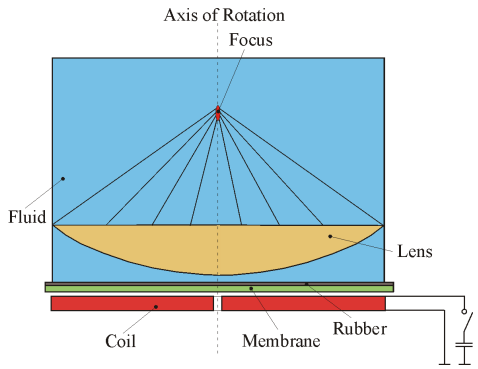

fig. 1: Schematic of a power source in lithotripsy based on the electromagnetic principle

defined as follows:

$$\mathcal{O}_{\text{ad}} = \{\Omega_+ : \overline{\Omega}_+ \subset \Omega,\ \Omega_+ \text{ is open and Lipschitz with uniform Lipschitz constant } L_{\mathcal{O}}\}.$$

The shape derivative will be obtained under the assumption that $q > 2$.

3 Challenges related to the model (1)

The present task of optimizing the shape of the acoustic lens provides us with several challenges. Not only a part of the domain boundary is optimized, but a subdomain which lies in the interior of the domain; this implies providing shape sensitivity analysis for the acoustic-acoustic interface problem (1).

Working with the state equation also implies handling the nonlinear damping term of the q-Laplace type, which is in itself a nontrivial task.

Insufficient spatial regularity of the primal (at most $W^{1,q+1}$ in space) and the adjoint state (H^1 in space) on the whole domain at first does not allow for the shape derivative to be expressed in terms of the boundary integrals. However, it turns out that the state variable exhibits H^2-regularity on each of the subdomains, provided that it is Lipschitz continuous in time and space on the whole domain. This result, together with an assumption of a slightly higher regularity of the adjoint state will allow us to obtain the desired expression in terms of the integrals over the boundary of the lens.

4 The main result

We denote by $\tau \in \mathbb{R}$ an artificial time variable which will indicate varying subdomains. If Ω_+ is the initial shape of the lens, then $\Omega_{+,\tau}$ will denote the perturbed lens obtained by moving points into the direction of some vector field $h \in C^{1,1}(\bar{\Omega}, \mathbb{R}^d)$ by some steplength τ.

The Eulerian derivative of J at Ω_+ in the direction of the vector field h is defined as

$$dJ(u, \Omega_+)h = \lim_{\tau \to 0} \frac{1}{\tau}(J(u_\tau, \Omega_{+,\tau}) - J(u, \Omega_+)),$$

where u_τ satisfies the state equation on the perturbed domain Ω_τ.

For obtaining the shape derivative, we follow the general framework introduced by Ito, Kunisch and Peichl in [2]. We employ the variational form of the state and the adjoint problem and the method of mappings. The difference quotient of the cost functional is then rearranged in an efficient manner before passing to the limit with respect to the admissible class of domain perturbations.

In our talk we will show that, under suitable and realistic assumptions on regularity of the subdomains, the primary state u and the adjoint state p on the whole domain, the strong shape derivative of J at Ω_+ in the direction of a vector field $h \in C^{1,1}(\bar{\Omega}, \mathbb{R}^d)$ is given by

$$\begin{aligned}
&dJ(u, \Omega_+)h \\
&= \int_0^T \int_\Gamma \Big[\!\Big[-\frac{1}{\lambda}(1 - 2ku)\ddot{u}p - \frac{1}{\varrho}\nabla u \cdot \nabla p \\
&\quad - b((1-\delta) + \delta|\nabla \dot{u}|^{q-1})\nabla \dot{u} \cdot \nabla p \\
&\quad + \frac{2k}{\lambda}(\dot{u})^2 p + \frac{2}{\varrho}\frac{\partial u}{\partial n_+}\frac{\partial p}{\partial n_+} \\
&\quad + 2b((1-\delta) + \delta\,|\nabla \dot{u}|^{q-1})\frac{\partial \dot{u}}{\partial n_+}\frac{\partial p}{\partial n_+} \\
&\quad + b\delta(q-1)|\nabla \dot{u}|^{q-3}(\nabla \dot{u} \cdot \nabla p)\Big|\frac{\partial \dot{u}}{\partial n_+}\Big|^2 \Big]\!\Big]\, h^T n_+ \, dx\, ds.
\end{aligned}$$

Developing and implementing an efficient steepest descent algorithm based on the obtained derivative will be the subject of future research.

References

[1] R. Brunnhuber, B. Kaltenbacher and P. Radu, Relaxation of regularity for the Westervelt equation by nonlinear damping with application in acoustic-acoustic and elastic-acoustic coupling, *Evolution Equations and Control Theory*, **3(4)**, (2014), pp. 595 – 626.

[2] K. Ito, K. Kunisch and G. Peichl, Variational approach to shape derivatives, *ESAIM: Control, Optimisation and Calculus of Variations* **14** (2008), pp. 517–539.

Nonlinear Bloch Waves in the Periodic Gross-Pitaevskii Equation in $\mathbb{R}^d$

Tomáš Dohnal[1,*], **Hannes Uecker**[2]

[1]TU Dortmund, Vogelpothsweg 87, 44221 Dortmund, Germany

[2]Carl von Ossietzky Universität Oldenburg, 26111 Oldenburg, Germany

[*]Email: tomas.dohnal@math.tu-dortmund.de

Abstract

We study the bifurcation of small nonlinear solutions, so called nonlinear Bloch waves, of the periodic Gross-Pitaevskii equation in $\mathbb{R}^d$. The bifurcation takes place in the frequency parameter from points in the linear spectrum. Asymptotically, the nonlinear Bloch waves are a linear combination of N linear Bloch waves and they retain the quasi-periodicity of these linear Bloch waves. Our method of proof requires periodic Bloch waves, i.e. those with rational wave-vectors, such that the nonlinearity generates only finitely many types of periodicity and the Lyapunov-Schmidt reduction can be directly applied. We derive an algebraic system for the amplitudes of the linear combination and prove that certain solutions of the algebraic system imply the existence of nonlinear Bloch waves. We illustrate the results with numerics and show that nonlinear Bloch waves play a central role in the delocalization of families of gap solitons entering a spectral interval from a spectral gap.

Keywords: Gross-Pitaevskii equation, nonlinear Bloch wave, bifurcation, Lyapunov-Schmidt reduction

1 Introduction

The stationary Gross-Pitaevskii equation

$$\omega\phi + \Delta\phi - V(x)\phi - \sigma|\phi|^2\phi = 0, \qquad (1)$$

for $x \in \mathbb{R}^d$ with V periodic and $\omega, \sigma \in \mathbb{R}$, models standing waves in Bose-Einstein condensates ($d = 1, 2, 3$) loaded on an optical lattice but also standing waves in one and two dimensional photonic crystals ($d = 1, 2$). For simplicity we assume $V(x + 2\pi e_m) = V(x), m = 1, \dots, d$. The corresponding linear problem ($\sigma = 0$) is fully described by the Bloch waves $\xi_n(x, k) = p_n(x, k)e^{\mathrm{i}k\cdot x}$ with $k \in \mathbb{B} := (-1/2, 1/2]^d, n \in \mathbb{N}$. The functions $p_n(\cdot, k)$ are 2π-periodic in each x_m-variable and are given as solutions of the eigenvalue problem

$$\omega_n(k)p_n(x, k) = -(\nabla+\mathrm{i}k)^2 p_n(x, k)+V(x)p_n(x, k)$$

for $x \in (-\pi, \pi]^d$. The spectrum $\sigma(-\Delta + V)$ is continuous and it is a union of possibly disjoint intervals given by the band structure $(\omega_n(k))_{n\in\mathbb{N},k\in\mathbb{B}}$.

For a given spectral point $\omega_* \in \sigma(-\Delta + V)$ the linear problem has typically more (quasi-periodic) Bloch wave solutions $\xi_n(x, k)$. The question arises about the nature of nonlinear quasi-periodic solutions (for $\sigma \neq 0$) bifurcating from the trivial solution.

2 Description of the analytical result

We prove the bifurcation in ω of solutions with the asymptotic form

$$\phi(x) \sim \sum_{j=1}^{N} \phi_j(x)$$

for $\omega \to \omega_*$ with $\phi_j(x+2\pi e_m) = e^{\mathrm{i}k^{(j)}\cdot x}\phi_j(x), m = 1, \dots, d$ and with a selected bifurcation point $\omega_* \in \sigma(-\Delta+V)$. The quasi-periodicity vectors $k^{(j)} \in \mathbb{B}$ are those belonging to a subset of the linear Bloch waves at $\omega = \omega_*$, i.e. to a subset of the ω_*-level set of the band structure.

Our approach needs several assumptions on ω_* and the vectors $k^{(j)}$ including the rationality of all components of $k^{(j)}, j = 1, \dots, N$. This rationality implies that the exact solution ϕ is, in fact, a sum of *finitely* many *periodic* functions.

We show in [1] that asymptotically (for ω close to ω_*) there are small solutions with the components ϕ_j approximated by small multiples of the Bloch waves at ω_* with the wave-vectors $k^{(j)}$. In detail, we show that for $V \in H^s_{\mathrm{loc}}(\mathbb{R}^d), s > d/2, \omega = \omega_* + \mathrm{sign}(\sigma)\varepsilon^2$ and $0 < \varepsilon$ small enough there is a solution ϕ such that

$$\left\| \phi - \varepsilon \sum_{j=1}^{N} A_j \xi_{n_j}(\cdot, k^{(j)}) \right\|_{H^s((-\pi,\pi)^d)} \leq C\varepsilon^3$$

provided the vector of the amplitudes $(A_1, \dots, A_N)$ is a symmetric solution of a simple algebraic system of equations (with constant coefficients). Moreover, the exact solution has the form $\phi =$

$\sum_{j=1}^{M} \phi_j$ with $N \le M < \infty$ and with each ϕ_j periodic.

The algebraic equations for the asymptotic envelopes are obtained by the Lyapunov-Schmidt reduction and constitute an effective system describing the bifurcation.

3 Numerical examples

We illustrate the results by numerics in 2D ($d = 2$) using the continuation package `pde2path` [2] for elliptic systems. In Figure 1 the continuation diagram is plotted for a solution with two components $N = 2$ and $k^{(1)} = (1/2, 0), k^{(2)} = (0, 1/2)$ for a bifurcation point $\omega_* \in \partial\sigma(-\Delta+V)$ and for the potential

$$V(x_1, x_2) = 1 + 4.35 W(x_1) W(x_2), \; x \in [-\pi, \pi]^2,$$
$$W(s) = \frac{1}{2}\left[\tanh\left(7\left(s + \frac{3\pi}{5}\right)\right) + \tanh\left(7\left(\frac{3\pi}{5} - s\right)\right)\right]. \tag{2}$$

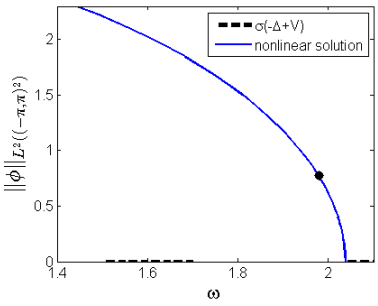

Figure 1: Continuation diagram of one nonlinear Bloch wave family with $N = 2$ for the case $d = 2$ and V in (2).

We also numerically show that nonlinear Bloch waves play a central role in the delocalization of families of gap solitons [3, 4] entering a spectral interval from a spectral gap. Upon entry into the spectrum such gap solitons develop oscillatory tails, where the oscillations perfectly match the nonlinear Bloch waves bifurcating from the entry edge of the spectrum.

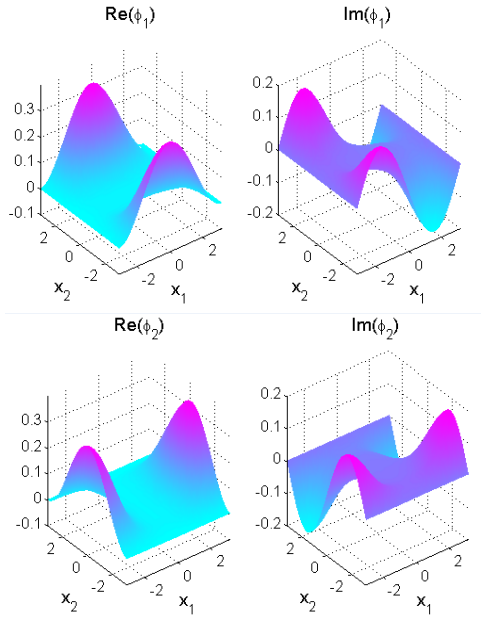

Figure 2: Nonlinear Bloch wave marked by the thick dot in Figure 1. The full solution is $\phi(x) = \phi_1(x) + \phi_2(x)$.

References

[1] T. Dohnal and H. Uecker, Bifurcation of Nonlinear Bloch Waves from the Spectrum in the Gross-Pitaevskii Equation, *submitted* (2014).

[2] T. Dohnal, J. Rademacher, H. Uecker, D. Wetzel, pde2path 2.0: multi-parameter continuation and periodic domains, in H. Ecker, A. Steindl, S. Jakubek, eds, *ENOC 2014 - Proceedings of 8th European Nonlinear Dynamics Conference.*

[3] A. Pankov, Periodic nonlinear Schrödinger equation with application to photonic crystals, *Milan J. Math.*, 2005, 73:259–287.

[4] T. Dohnal, and H. Uecker, Coupled mode equations and gap solitons for the 2D Gross-Pitaevskii equation with a non-separable periodic potential, *Physica D*, 2009, 238:860-879.

A variational approach of soliton interaction with localized $\mathcal{PT}$-symmetric potential

H. Susanto[1], **N. Karjanto**[2,*]

[1]Department of Mathematical Sciences, University of Essex, UK

[2]Department of Mathematics, Nazarbayev University, Kazakhstan

*Email: natanael@skku.edu

Abstract

Interaction of soliton in nonlinear Schrödinger equation (NLS) model with parity-time symmetric potential is investigated. An analytical approach is implemented through the variational formulation of the model equation. A basic characteristic of the scattering of the solitons is a critical velocity separating their reflection and transmission. These critical velocities are calculated numerically. An initial finding suggests that there is a good qualitative agreement between the theoretical approach and the numerical calculation.

Keywords: soliton, NLS equation, parity-time symmetry, variational formulation

1 Introduction

We employ variational approximation explained in [5], where the authors investigated the dynamics of a dark soliton in a Bose-Einstein condensate with an external magnetic trap. The method also adopts other works in coupled Bose-Einstein condensates [6, 7]. By considering the NLS equation

$$i\frac{\partial u}{\partial t}+\frac{1}{2}\frac{\partial^2 u}{\partial z^2}-a|u|^2u-\left[U_1(z)+U_2(z)\right]u=0,$$

an Ansatz is chosen as follows:

$$u(z,t)=\phi_1(z)\phi_2(z)e^{-iat}v(z,t),$$

where $\phi_1\in\mathbb{R}$, $\phi_2, v\in\mathbb{C}$ and they satisfy

$$\begin{aligned} a\phi_1+\frac{1}{2}\partial_z^2\phi_1-a\phi_1^3-U_1\phi_1 &= 0\\ a\phi_2+\frac{1}{2}\partial_z^2\phi_2-a|\phi_2|^2\phi_2-U_2\phi_2 &= 0. \end{aligned}$$

Substituting the Ansatz to the NLS equation and employing the conditions above, taking either $\phi_1=\phi$, $\phi_2=1$ or $\phi_1=1$, $\phi_2=\phi$, our derived equation should resemble the one in [5], except for the final term, which has been incorporated to the earlier condition. Furthermore, we are interested to study the NLS equation where the terms are re-arranged as follows, after taking $a=1$:

$$i\frac{\partial v}{\partial t}+\frac{1}{2}\frac{\partial^2 v}{\partial z^2}-(|v|^2-1)v=R(v)$$

where the right-hand side term $R(v)$ reads

$$\begin{aligned} R(v) &= \left[(\phi_1^2|\phi_2|^2-1)|v|^2-\phi_1^2-|\phi_2|^2+2\right]v\\ &\quad -\frac{\partial\ln\phi_1}{\partial z}\frac{\partial\ln\phi_2}{\partial z}v-\frac{\partial\ln(\phi_1\phi_2)}{\partial z}\frac{\partial v}{\partial z}. \end{aligned}$$

2 Soliton interaction

In particular, we are interested in the interaction of bright and dark NLS solitons with a strongly localized parity-time symmetric potential. Let $U_1(z)=\frac{1}{2}\Omega^2z^2$, $0<\Omega^2\ll 1$ and $U_2(z)=\epsilon\delta(z)+i\gamma\delta'(z)$, $\epsilon,\gamma>0$. Here, δ' stands for the derivative of the Dirac delta function and ϵ and γ are real, positive or negative, constants. The reason to adopt parity-time symmetry is motivated by the seminal works of Carl Bender and other scientists [1–3]. Now let also $\phi_1\cong\sqrt{1-U_1(z)}$ and ϕ_2 reads

$$\phi_2=\begin{cases}\sqrt{\mu}(\cos\theta+i\,\mathrm{sign}(z)\sin\theta)\tanh(\sqrt{\mu}(|z|+\zeta)),\\ \text{for }\ \epsilon>0\\ \sqrt{\mu}(\cos\theta+i\,\mathrm{sign}(z)\sin\theta)\coth(\sqrt{\mu}(|z|+\zeta)),\\ \text{for }\ \epsilon<0.\end{cases}$$

After taking $\mu=1$ and for $|\zeta|\gg 1$ so that $\tanh(|z|+\zeta)\approx 1-2e^{-2(|z|+\zeta)}$ and $\coth(|z|+\zeta)\approx 1+2e^{-2(|z|+\zeta)}$, we can write ϕ_2 as follows

$$\phi_2=\begin{cases}(\cos\theta+i\,\mathrm{sign}(z)\sin\theta)(1-2e^{-2(|z|+\zeta)}),\\ \text{for }\ \epsilon>0\\ (\cos\theta+i\,\mathrm{sign}(z)\sin\theta)(1+2e^{-2(|z|+\zeta)}),\\ \text{for }\ \epsilon<0.\end{cases}$$

Applying natural logarithm to ϕ_1 and ϕ_2 and implement further approximation, we obtain

$$\begin{aligned} \ln\phi_1 &= -\frac{1}{2}U_1(z)-\frac{1}{4}U_1^2(z)-\ldots\\ &= -\frac{1}{4}\Omega^2z^2-\ldots\\ \ln\phi_2 &= \ln(\cos\theta+i\,\mathrm{sign}(z)\sin\theta)\\ &\quad -2\,\mathrm{sign}(\epsilon)e^{-2(|z|+\zeta)}+\ldots \end{aligned}$$

We adopt Ansatz for v from [4]:

$$\begin{array}{lll} v(z,t) & = & B\tanh D(z-z_0)+iA \\ \text{where} & & A^2+B^2=1. \end{array}$$

3 Remark

We are interested in the corresponding Euler–Lagrange equation. For simplification of analytical computation, for some terms, we take $D=1$, and for the rest, $D=B$ is taken. A second order differential equation for z_0 depending on t obtained from the Euler-Langrange equation is studied and investigated. Furthermore, we are interested to find critical velocities that separate the reflection and transmission of the corresponding NLS solitons. Both the variational formulation approach and numerical simulation will be compared quantitatively. An initial finding suggests that there is a good qualitative agreement between the theoretical approach and the numerical calculation.

References

[1] C. M. Bender and S. Boettcher, Real spectra in non-Hermitian Hamiltonians having $\mathcal{PT}$ symmetry, *Physical Review Letters* **80** (1998), 5243.

[2] C. M. Bender and D. C. Brody and H. F. Jones, Complex extension of quantum mechanics, *Physical Review Letters* **89** (2002), 270401.

[3] C. M. Bender, Making sense of non-Hermitian Hamiltonians, *Reports on Progress in Physics* **70** (2007), 947.

[4] Y. Kivshar and W. Królikowski, Lagrangian approach for dark solitons, *Optics Communications* **114** (1995), pp. 353–362.

[5] H. Li and D. N. Wang, Effects of localized impurity on a dark soliton in a Bose-Einstein condensate with an external magnetic trap, *Chinese Physics B* **18** (2009), pp. 2659–2666.

[6] M. I. Qadir, H. Susanto and P. C. Matthews, Fluxon analogues and dark solitons in linearly coupled Bose-Einstein condensates, *Journal of Physics B: Atomic, Molecular and Optical Physics* **45** (2012), 035004: pp. 1–8.

[7] M. I. Qadir, H. Susanto and P. C. Matthews, Multiple fluxon analogues and dark solitons in linearly coupled Bose-Einstein condensates, *Progress in Optical Sciences, Photonics* (2013), pp. 485–508.

Nonlinear Standing Waves on a Periodic Array of Circular Cylinders

Lijun Yuan[1], **Ya Yan Lu**[2,*]

[1]College of Mathematics and Statistics, Chongqing Technology and Business University, China
[2]Department of Mathematics, City University of Hong Kong, Hong Kong

*Email: mayylu@cityu.edu.hk

Abstract

For a periodic array of circular dielectric cylinders surrounded by air, where the cylinders are made of a linear medium, it is well known that standing waves that are periodic along the array and decay exponentially away from the array could exist at a discrete set of frequencies, corresponding to the non-uniqueness of a related diffraction problem. We consider a periodic array of nonlinear cylinders with a Kerr nonlinearity, and show numerically that standing waves exist continuously with the frequency.

Keywords: periodic structures, standing waves, nonlinear effects, Kerr media

1 Introduction

Consider a periodic array of circular dielectric cylinders surrounded by air, where the period of the array is L and the radius of the cylinders is $a < L/2$. In the Cartesian coordinate system (x, y, z), we assume the cylinders are parallel to the z axis and their centers (in the xy plane) are located on the y axis at $y = mL$ for integers m. For the E polarization, the z component of the electric field, denoted by u here, satisfies the two-dimensional (2D) Helmholtz equation

$$\partial_x^2 u + \partial_y^2 u + k_0^2(n^2 + \gamma|u|^2)u = 0, \qquad (1)$$

where k_0 is the wavenumber, n is the refractive index function satisfying $n = n_1 > 1$ and $n = 1$ for (x, y) inside and outside the cylinders, respectively, γ is the nonlinear coefficient (for the nonlinear Kerr effect) satisfying $\gamma = \gamma_1$ and $\gamma = 0$ for the cylinders and air, respectively. If the cylinders are linear, i.e., $\gamma_1 = 0$, it is known that there could be standing waves on the periodic array which are periodic in y with period L, and decay exponentially as $|x| \to \infty$. These standing waves are non-zero solutions of the homogeneous Eq. (1) without any incident wave. They only exist at a possibly discrete sequence of frequencies, and they correspond to the non-uniqueness of a diffraction problem associated with the periodic array.

Based on an efficient computational method, we numerically show that Eq. (1) has nonlinear standing waves (when $\gamma_1 > 0$) that continuously depend on the frequency (or wavenumber k_0). These standing waves are periodic in y with the minimum period L, and localized around the array, i.e., they decay exponentially as $|x| \to \infty$. Their amplitudes depend on the frequency. As the frequency approaches the frequencies where linear standing waves exist, the amplitude approaches zero.

2 Computation method

Due to the periodicity of the array and the solution, the problem can be considered in the strip given by $|y| < L/2$, with a periodic boundary condition in the y direction. If we use transparent boundary conditions at $x = \pm L/2$, the problem can be further reduced to the square $S = \{(x, y) : |x| < L/2, |y| < L/2\}$. These boundary conditions can be written as $\partial_x u = \pm\Lambda\, u$ at $x = \pm L/2$, where Λ is an operator depending on k_0. The cross section of the cylinder in S is the disk D given by $r < a$, where r is the radial variable. In the domain outside the disk and inside the square, i.e. $Q = S\backslash\overline{D}$, the Helmholtz equation is linear and its solution can be expanded in cylindrical waves. This allows us to find a Dirichlet-to-Neumann (DtN) map $\mathcal{N}$ (it depends on k_0) for Eq. (1) in Q, and it satisfies $\mathcal{N}u = \partial_\nu u$ on ∂Q, where $\partial_\nu u$ is the normal derivative of u, ∂Q is the boundary of Q and it consists of the circle $r = a$ and the four sides of the square S. Combining these conditions, we can find an operator $\mathcal{B}$ such that

$$\partial_r u = \mathcal{B}(k_0)\, u, \quad r = a. \qquad (2)$$

Notice that $\mathcal{B}$ depends on the wavenumber k_0. With this condition, it is only necessary to solve the nonlinear Helmholtz equation on a disk. We have used similar techniques for analyzing optical bistability [2] and symmetry breaking [3] in structures with nonlinear circular cylinders.

Therefore, the nonlinear standing waves are non-trivial solutions of Eq. (1) in the disk D

with boundary condition (2). It is a nonlinear eigenvalue problem, where k_0 can be regarded as the eigenvalue, and u is the eigenfunction. To solve this problem, we discretize Eq. (1) by a mixed Fourier-Chebyshev pseudospectral method [4], with Fourier and Chebyshev methods for θ and r respectively, where θ is the polar angle, and use an iterative method.

3 Results

We consider an array of circular cylinders with radius $a = 0.3L$, refractive index $n_1 = 2.5$ and nonlinear coefficient $\gamma_1 = 2\times10^{-12}$. For the corresponding linear problem, standing waves exist at $k_0L/(2\pi) \approx 0.5502$ and 0.7800. In Fig. 1, we show the amplitudes of the standing waves

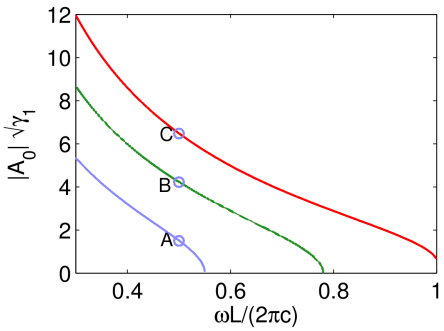

Figure 1: Amplitude-frequency relations of nonlinear standing waves on a periodic array.

as functions of the frequency. It is clear that as the frequency decreases away from those for linear standing waves, the amplitudes increases. In Fig. 2, we show the electric field patterns of the nonlinear standing waves corresponding to points A, B and C in Fig. 1.

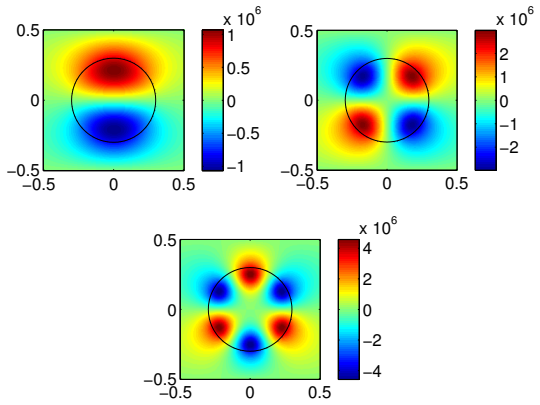

Figure 2: Electric field patterns of three nonlinear standing waves.

4 Conclusion

A periodic array of nonlinear circular cylinders with a Kerr nonlinearity is studied in the E polarization. Nontrivial solutions that are localized and periodic along the array are found numerically. These nonlinear standing waves exist continuously with the frequency, leading to the continuous non-uniqueness of a related diffraction problem of the array.

Acknowledgment

This work was supported by the National Natural Science Foundation of China (project No. 11201508), the Scientific Research Foundation of Chongqing Technology and Business University (project No. 20125605), the Scientific and Technological Research Program of Chongqing Municipal Education Commission (project No. KJ130726), and the Research Grants Council of Hong Kong Special Administrative Region, China (project CityU 11301914).

References

[1] A.-S. Bonnet-Bendhia and F. Starling, "Guided waves by electromagnetic gratings and nonuniqueness examples for the diffraction problem," *Math. Methods Appl. Sci.* **17** (1994), pp. 305–338.

[2] L. Yuan and Y. Y. Lu, "Efficient numerical method for analyzing optical bistability in photonic crystal microcavities," *Optics Express* **21** (2013), pp. 11952–11964.

[3] L. Yuan and Y. Y. Lu, "Bilateral symmetry breaking in nonlinear circular cylinders," *Optics Express* **22** (2014), pp. 30128–30136.

[4] L. N. Trefethen, *Spectral Methods in MATLAB*, Society for I ndustrial and Applied Mathematics, 2000.

Double Absorbing Boundaries for Finite Difference Time Domain Electromagnetics

John LaGrone[1,*], **Thomas Hagstrom**[1]
[1]Department of Mathematics, Southern Methodist University, Dallas, United States
[*]Email: jlagrone@smu.edu

Abstract

An important issue in the simulation of electromagnetic effects is the ability to truncate unbounded domains into regions of interest that can be simulated efficiently and accurately for long times. In order to do this, accurate artificial boundary conditions are required. In the context of finite difference time domain (FDTD) solvers, this typically takes the form of a perfectly matched layer (PML). While PMLs have proven to be effective, their performance is closely tied to the selection of parameters that can often only be found through experimentation. Instead, we use a Double Absorbing Boundary (DAB) constructed by forming a thin non-reflecting layer on which we apply the complete radiation boundary conditions (CRBC) on two parallel boundaries. A primary advantage of this DAB formulation is that there is an *a priori* error estimate and method for selecting optimized parameters. The performance of the method is demonstrated with numerical experiments.

Keywords: double absorbing boundary, absorbing boundary condition, electromagnetics, finite difference, time domain, waves

1 Introduction

Following from [2], we illustrate the (DAB) formulation for the scalar wave equation in the semi-infinite wave guide:

$$\begin{aligned} Wu &\equiv \frac{\partial^2 u}{\partial t^2} - c^2\nabla^2 u = f, \\ u(x_L, y, t) &= u(x, y_L, t) = u(x, y_R, t) = 0, \\ u(x, y, 0) &= g(x, y), \qquad \frac{\partial u}{\partial t}(x, y, 0) = \dot{g}(x, y). \end{aligned}$$

We further suppose that if $x > x_I > x_L$, the medium is homogeneous and free of sources. Additionally, we require that the initial conditions vanish so $g = \dot{g} = 0$ for $x > x_I$.

We now truncate the domain at some $x = x_R > x_I$. We can view the entire truncated domain as being divided into two sub-domains: the interior domain $\Omega_I \equiv [x_L, x_I] \times [y_L, y_R]$ and a thin layer $\Omega_L \equiv [x_I, x_R] \times [y_L, y_R]$. The goal is to use Ω_L as an absorbing layer. To do this, we introduce auxiliary variables $u_0, ..., u_{P+1}$ in Ω_L and require u_j to satisfy that same wave equation as u:

$$Wu_j \equiv \frac{\partial^2 u_j}{\partial t^2} - c^2\nabla^2 u_j = 0, \qquad \text{in } \Omega_L. \quad (1)$$

The auxiliary variables are defined to satisfy zero initial conditions and boundary conditions

$$\begin{aligned} u_j(x, y, 0) &= \frac{\partial u_j}{\partial t} = 0, \\ u_j(x, y, t) &= 0, \qquad y = y_L, y_R, \end{aligned}$$

To define the additional boundary conditions on Ω_L, we utilize the CRBC boundary recursions [1]:

$$\begin{aligned} \bar{a}_j \frac{\partial u_{j+1}}{\partial t} - \frac{\partial u_{j+1}}{\partial x} + \bar{\sigma}_j u_{j+1} \\ = a_j \frac{\partial u_j}{\partial t} + \frac{\partial u_j}{\partial x} + \sigma_j u_j, \end{aligned} \quad (2)$$

and require them to hold at $x = x_I, x_R$. Note that the parameters a_j, $\bar{a}_j$, σ_j and $\bar{\sigma}_j$ can be optimally chosen *a priori*. On $x = x_I$, we require the u and u_0 to agree in value and slope:

$$u_0 = u, \qquad \frac{\partial u_0}{\partial x} = \frac{\partial u}{\partial x}, \qquad x = x_I. \quad (3)$$

Since u and u_0 satisfy the same wave equation in Ω_L,

$$u_0 \equiv u, \qquad \text{in } \Omega_L.$$

Finally, at $x = x_R$, we require the termination condition

$$\bar{a}_{P+1} \frac{\partial u_{P+1}}{\partial t} - \frac{\partial u_{P+1}}{\partial x} + \bar{\sigma}_{P+1} u_{P+1} = 0. \quad (4)$$

2 Application to Maxwell's Equations

In a homogeneous, isotropic, dielectric material free from charges or currents, Maxwell's equations are

$$\begin{aligned} \frac{\partial \mathbf{E}}{\partial t} &= \frac{1}{\varepsilon}\nabla \times \mathbf{H}, \qquad \frac{\partial \mathbf{H}}{\partial t} = -\frac{1}{\mu}\nabla \times \mathbf{E}, \\ \nabla \cdot \mathbf{E} &= 0, \qquad \nabla \cdot \mathbf{H} = 0. \end{aligned}$$

We discretize using Yee's well known algorithm [4]. Noting that Yee's that the **E** field components in Yee's algorithm can be shown to satisfy the standard second order, centered difference approximation to the wave scalar wave equation, we introduce **a three point wide DAB layer for E alone**. Discretizing the layer using second order centered differences in space and time, we use (1) to update the center points of the layer, (3) and (2) to update the auxiliary variables on the interior side, and finally we use (4) and (2) to update the auxiliary variables on the exterior side. We apply these updates to the **E** field components required to provide a boundary condition. Edges and corners are handled similarly by introducing doubly or triply indexed auxiliary variables, respectively.

3 Numerical Results

To illustrate the effectiveness of the DAB boundaries, Fig. 1 shows a comparison between a PML with some suggested parameters from literature [3]. Although it is possible to obtain better results from the PML by modifying the parameters, we note that the DAB used here have been automatically generated.

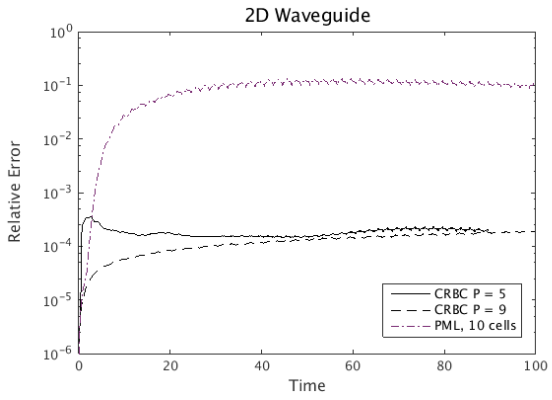

Figure 1: Comparison of relative error for a 2D waveguide simulation on a 6000×3000 grid.

In 3D, we show the results from a parallel plate simulation in Fig. 2. In particular, we want to point out that on a sufficiently refined grid, we meet our expected error tolerance from the DAB and no longer improve significantly with refinement which indicates that the boundary error dominates.

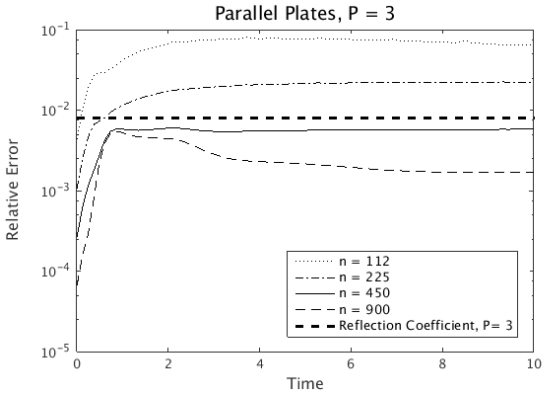

Figure 2: Relative error for a parallel plate simulation with 3 recursions.

4 Acknowledgements

This work was supported in part by ARO Grant W911NF-09-1-0344 and STTR A11A-015-0067. All conclusions in the paper are those of the authors and do not necessarily reflect the views of the ARO.

References

[1] T. Hagstrom and T. Warburton. Complete radiation boundary conditions: Minimizing the long time error growth of local methods. *SIAM Journal on Numerical Analysis*, 47(5):3678–3704, 2009.

[2] Thomas Hagstrom, Dan Givoli, Daniel Rabinovich, and Jacobo Bielak. The double absorbing boundary method. *Journal of Computational Physics*, 259(0):220 – 241, 2014.

[3] J. Alan Roden and Stephen D. Gedney. Convolution pml (cpml): An efficient fdtd implementation of the cfs–pml for arbitrary media. *Microwave and Optical Technology Letters*, 27(5):334–339, 2000.

[4] Kane Yee. Numerical solution of initial boundary value problems involving maxwell's equations in isotropic media. *Antennas and Propagation, IEEE Transactions on*, 14(3):302–307, 1966.

A DG discretization of a Double Absorbing Boundary

Fritz Juhnke[1,*], **Thomas Hagstrom**[1]

[1]Department of Mathematics, Southern Methodist University, Dallas, TX, U.S.A.

[*]Email: kjuhnke@smu.edu

Abstract

The Double Absorbing Boundary (DAB) is a recently-invented, high-order method for truncating unbounded domains of wave problems expressed in second-order form. It is a thin layer with a coefficient of reflection that can be made arbitrarily small. For discretization of the DAB, we use a recently-invented discontinuous Galerkin (DG) method. Unstable modes are suppressed by directly damping high-order basis functions. We test on the Klein-Gordon equation in one dimension.

Keywords: absorbing boundary, high-order, discontinuous Galerkin, artificial dissipation

1 Introduction

Simulating waves in an unbounded domain is a problem with, as yet, no completely satisfactory solution. Even the premier methods for artificially truncating the domain, such as a Perfectly Matched Layer (PML) or high-order Absorbing Boundary Condition (ABC), produce spurious reflections of outgoing waves. The Double Absorbing Boundary is a relatively new alternative that aims to be easier to implement than ABCs, and have better *a priori* error bounds than PMLs. [1]

For this paper, we examine a DAB in one dimension only, in the (small) interval $x_I < x < x_\Gamma$, but make radiation of waves non-trivial by simulating the Klein-Gordon equation. We use a non-standard DG discretization; success validates both the chosen discretization and the DAB itself.

2 The DAB method

The DAB comprises u_0, a continuation of the volume solution u in $(x < x_I)$, and P auxiliary solutions u_j. The boundary condition on u_0 at x_I is to match u, and the final auxiliary solution is terminated by $u_{P,t} + cu_{P,x} = 0$ at x_Γ.

In between, all the solutions satisfy $u_{j,tt} = c^2 u_{j,xx} - k^2 u_j$, and each is coupled to the one before and after on both endpoints via

$$\begin{aligned} a_j u_{j-1,t} + c u_{j-1,x} + \sigma_j u_{j-1} \\ = \bar{a}_j u_{j,t} - c u_{j,x} + \bar{\sigma}_j u_j \end{aligned} \tag{1}$$

If relationship (1) holds true throughout the DAB at time $t = 0$, enforcing it at the endpoints is sufficient for it to remain true throughout the DAB for all subsequent times. The parameters a_j, σ_j, $\bar{a}_j$ and $\bar{\sigma}_j$ are all positive, and can be optimized based on the duration of the simulation and distance of the DAB from any sources.

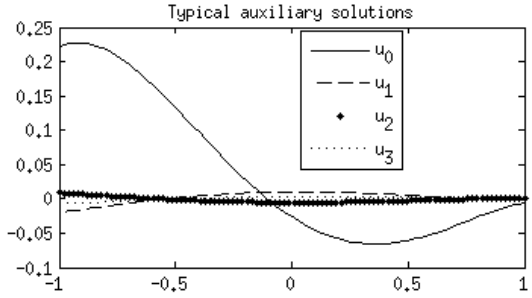

3 The new DG discretization

o

We discretize according to the method of [2]. We impose for $j = 0, \ldots, P$

$$\begin{aligned} &\int_{x_I}^{x_\Gamma} \left(k^2 \psi_{u_j} + c^2 \frac{\partial \psi_{u_j}}{\partial x} \frac{\partial}{\partial x} \right) \left(\frac{\partial u_j}{\partial t} - v_j \right) \mathrm{d}x \\ &+ \int_{x_I}^{x_\Gamma} \left(\psi_{v_j} \frac{\partial v_j}{\partial t} + c^2 \frac{\partial \psi_{v_j}}{\partial x} \frac{\partial u_j}{\partial x} + k^2 \psi_{v_j} u_j \right) \mathrm{d}x \\ &\quad = c^2 \left[\frac{\partial \psi_{u_j}}{\partial x} (v_j^* - v_j) \right]_{x_I}^{x_\Gamma} + c^2 \left[\psi_{v_j} w_j^* \right]_{x_I}^{x_\Gamma} \end{aligned}$$

Both the test and trial functions u_j and ψ_{u_j} are polynomials of degree q, and v_j and ψ_{v_j} are of degree $q-1$. As the two basis sets have different degree it is simplest to use a modal basis of Legendre polynomials.

To compactly express the fluxes and boundary conditions, is convenient to re-write our $P+1$ equations in matrix-vector notation with, e.g.,

$U = (u_0, \ldots, u_P)^T$.

$$\int_{x_I}^{x_\Gamma} \left(k^2 \Psi_u + c^2 \frac{\partial \Psi_u}{\partial x} \frac{\partial}{\partial x} \right)^T \left(\frac{\partial U}{\partial t} - V \right) \mathrm{d}x + \int_{x_I}^{x_\Gamma} \left(\Psi_v^T \frac{\partial V}{\partial t} + c^2 \frac{\partial \Psi_v^T}{\partial x} \frac{\partial U}{\partial x} + k^2 \Psi_v^T U \right) \mathrm{d}x = c^2 \left[\frac{\partial \Psi_u^T}{\partial x} (V^* - V) \right]_{x_I}^{x_\Gamma} + c^2 \left[\Psi_v^T W^* \right]_{x_I}^{x_\Gamma}$$

The boundary conditions at x_Γ become $AU_t + cDU_x + \Sigma U = 0$. Inspired by the half-space energy proven in [3], we choose the fluxes at x_Γ to be $V^* = V$ and $cW^* = -D^{-1}(AV + \Sigma U)$. Analogously, at the driven boundary x_I, we write the boundary conditions as $\tilde{A}U_t - c\tilde{D}U_x + \tilde{\Sigma}U = (u_t - cu_x)\,(1, 0, \ldots, 0)^T$, where u_t and u_x come from the boundary of the volume solution. We use fluxes $V^* = V$ and $cW^* = \tilde{D}^{-1}(\tilde{A}V + \tilde{\Sigma}U - (u_t - cu_x)\,(1, 0, \ldots, 0)^T)$. Unfortunately, the matrices in the boundary condition are not the same as on the terminal side, being now lower bidiagonal instead of upper bidiagonal. We are therefore unable to extend the half-space energy to the full layer $x_I < x < x_\Gamma$, which makes artificial dissipation necessary.

4 Artificial dissipation

We follow Chapter 5, Section 3 of [4] in reducing the magnitude of the coefficients of the basis elements of U and V after each time step. The most damping is applied to the highest-frequency basis elements, much less to lower frequencies, and none at all to the constant basis element. More precisely, each coefficient is damped by

$$e^{-\alpha(\Delta t)(j/q)^s},$$

where Δt is the size of the time step, j is the degree of the basis function being damped, s is the order of the damping, and α is a free parameter expressing the amount of damping.

We naturally wish to apply as little artificial dissipation as possible to stabilize the discretization, because excessive dissipation reduces accuracy. Unfortunately, there is no theory as to how much dissipation should suffice. In practice we have settled on fixing $\alpha = P^2/q$ and choosing the order small enough. We start with $s = 16$, calculate the eigenvalues of the timestepping scheme, and decrement s if any eigenvalue has significant positive real part.

Experiments so far indicate that choosing a larger number q of basis functions allows the order s of the artificial dissipation to be higher as well, for much better overall accuracy.

5 Numerical Results

As the number of auxiliary functions P increases, the reflection coefficient decreases exponentially. As q increases, the polynomial approximation of u converges to u spectrally. The discretization is order $q+1$ accurate in space, although we typically would not refine the DAB in space, since it does not need to be any particular width. We would instead use a single cell across the width and choose q large enough for sufficient accuracy.

Future research will investigate the computational efficiency relative to alternative methods. Preliminary results suggest that in order to allow the artificial dissipation to be sufficiently high order to not interfere with accuracy, the discretization order must be higher than otherwise necessary, and this relationship limits computational efficiency.

6 Acknowledgements

This work was supported in part by ARO Grant W911NF-09-1-0344 and STTR A11A-015-0067. All conclusions in the paper are those of the authors and do not necessarily reflect the views of the ARO.

References

[1] T. Hagstrom, D. Givoli, D. Rabinovich, and J. Bielak, *The double absorbing boundary method*, J. Comput. Phys. **259** (2014), 220-241.

[2] D. Appelö and T. Hagstrom, *A new discontinuous Galerkin formulation for wave equations in second order form*, submitted.

[3] D. Baffet, T. Hagstrom, and D. Givoli, *Double absorbing boundary formulations for acoustics and elastodynamics*, SIAM J. Sci. Comp. **36** (2014), A1277-A1312.

[4] J. Hesthaven and T. Warburton, *Nodal Discontinuous Galerkin Methods*, Springer-Verlag, New York, 2008.

Perfectly Matched Layers for dispersive Maxwell's equations

Eliane Bécache[1], **Patrick Joly**[1,*], **Valentin Vinoles**[1]
[1]POEMS (CNRS/ENSTA Paristech/INRIA), Palaiseau, France
*Email: patrick.joly@inria.fr

Abstract

We propose and analyse new Perfectly Matched Layers (PMLs) in time domain for a large class of dispersive electromagnetic media, particularly for Negative Index Metamaterials (NIMs). In such materials, "classical" PMLs lead to instabilities due to the presence of backward waves, that we overcome with the new PMLs.

Keywords: PMLs, dispersive media, stability

1 Introduction

We consider the two dimensional Maxwell's equations in the free space

$$\begin{cases} \partial_t D_x = \partial_y H \\ \partial_t D_y = -\partial_x H \\ \partial_t B = \partial_y E_x - \partial_x E_y \end{cases} \tag{1}$$

completed by the following constitutive laws, in the frequency domain

$$\begin{cases} \widehat{D_x}(\omega) = \varepsilon(\omega)\widehat{E_x}(\omega) \\ \widehat{D_y}(\omega) = \varepsilon(\omega)\widehat{E_y}(\omega) \\ \widehat{B}(\omega) = \mu(\omega)\widehat{H}(\omega) \end{cases} \tag{2}$$

where the permittivity $\varepsilon(\omega)$ and the permeability $\mu(\omega)$ are real valued functions which express the dispersion properties of the medium. A large class of representative models are given by generalized Lorentz models [4], where

$$\begin{aligned} \varepsilon(\omega) &= \varepsilon_0 \left(1 - \sum_{\ell=1}^{M_e} \frac{\omega_{e,\ell}^2}{\omega^2 - \Omega_{e,\ell}^2}\right), \\ \mu(\omega) &= \mu_0 \left(1 - \sum_{\ell=1}^{M_m} \frac{\omega_{m,\ell}^2}{\omega^2 - \Omega_{m,\ell}^2}\right). \end{aligned} \tag{3}$$

The simplest of these models is the Drude's model, that corresponds to $M_e = M_m = 1$ and $\Omega_{e,1} = \Omega_{m,1} = 0$. Writing (1, 2) in time domain leads to a coupling between standard Maxwell's equations in the vacuum with ordinary differential equations involving extra unknowns vector fields (omitted here). The well-posedness of the associated evolution problem is easily shown by means of energy conservation, which illustrates the non dissipativity of such media.

When looking at the propagation of time harmonic plane waves $e^{i(\mathbf{k}\cdot\mathbf{x}-\omega t)}$ (with frequency ω and wave vector $\mathbf{k}$), defining the function

$$\mathcal{D}(\omega) := \frac{1}{\omega}\frac{\partial}{\partial\omega}\big(\omega^2\varepsilon(\omega)\mu(\omega)\big). \tag{4}$$

as well as the set

$$\mathcal{S} := \{\omega \in \mathbb{R} \ / \ \varepsilon(\omega)\,\mu(\omega) > 0\}, \tag{5}$$

one has, for each ω, the following alternative

- $\omega \notin \mathcal{S}$: one is in a band gap and waves do not propagate ($\mathbf{k}$ is not real);
- $\omega \in \mathcal{S}$: waves propagate ($\mathbf{k}$ is real) and
  1. if $\mathcal{D}(\omega) > 0$, group and phase velocity point in the same direction : the wave is propagating forward,
  2. if $\mathcal{D}(\omega) < 0$, group and phase velocity point in opposite directions : the wave is propagating backward.

If case 2. occurs for a range of frequencies, the interesting case, one says that we have a negative index material (NIM).

In this work, we consider the construction of PML's for such media, for their use as an artificial way to bound a computational domain, typically a rectangle whose exterior is supposed to be homogeneous since the classical PMLs are known to be unstable for these media [2, 5].

This is an extension of the results of our previous work [5], which deals with Drude's model, to general dispersive models, especially to Lorentz models (3).

2 Construction and analysis of PML's

Considering a PML in the x-direction, we use the ideas of complex change of variable [3]

$$x \longrightarrow x + \frac{\chi(\omega)}{i\omega}\int_0^x \sigma(s)\,ds \tag{6}$$

where the damping function $\sigma(x)$ is non negative and the novelty lies in the introduction of the real valued function χ. The choice $\chi(\omega) = 1$ corresponds to the classical Bérenger's PML. More precisely, we consider $\chi(\omega)$ of the form:

$$\chi(\omega) = 1 + \sum_{k=1}^{N} \frac{b_k}{a_k^2 - \omega^2}, \tag{7}$$

with $(a_k, b_k) \in \mathbb{R}^2$, $b_k \neq 0$, so that, in time domain, the corresponding PML system can be written as the coupling of the original PDE system with additional ODEs through the introduction of new auxiliary unknowns.

A critical issue is the stability of the corresponding evolution system that can be studied, when σ is constant, via a modal analysis : the stability (see [1] for a definition) is related to the location in the complex plane of the solutions ω of the corresponding dispersion relation $F(\omega, \mathbf{k}) = 0$ when $\mathbf{k}$ describes $\mathbb{R}^2$.

A first necessary condition is obtained by looking at the modes which are perturbations, for $\sigma \neq 0$, of the physical modes of the original problem. This leads to the following theorem, which is the counterpart, for dispersive systems, of the main result of [1] for non dispersive ones.

Theorem 1 *A necessary condition for stability of the PML model associated to (6, 7) is*

$$\forall\, \omega \in \mathcal{S}, \quad \chi(\omega)\, \mathcal{D}(\omega) \geq 0. \tag{8}$$

Note that this implies in particular the instability of the standard PMLs for NIM's. To obtain a necessary and sufficient condition, one also has to look at the other (artificial) modes linked to the additional unknowns. This leads to the following result:

Theorem 2 *A necessary and sufficient condition for stability of the PML model associated to (6, 7) is that :*

1. *(8) holds;*
2. *for all $1 \leq k \leq N$, $b_k < 0$, $a_k \notin \mathcal{S}$ and $z_k \notin \mathcal{S}$ where the z_k are the real zeros of χ (if need be, we exclude the a_k and z_k that are poles of $\varepsilon\mu$) ;*
3. *$\chi(0) \geq 0$.*

To be complete, it remains to show that it is always possible to build a function of the form (7) that fulfills the three conditions of the Theorem 2. Here is the answer in the case where $\mathcal{D}(\omega)$ has an even number of sign changes inside $\mathcal{S}$ (a similar result holds when this number is odd).

Theorem 3 *Assume that there exists $2M$ numbers $0 < \omega_1^2 < \cdots < \omega_{2M}^2$ such that (with $\omega_0^2 = 0$ and $\omega_{2M+1}^2 = +\infty$ by convention)*

$$(-1)^\ell\, \mathcal{D}(\omega) > 0 \quad \textit{in} \quad (\omega_\ell^2, \omega_{\ell+1}^2) \,\cap\, \mathcal{S},$$

then an appropriate choice for $\chi(\omega)$ is :

$$\chi(\omega) = \prod_{\ell=1}^{M} \Big(1 - \frac{\omega_{2\ell-1}^2}{\omega^2}\Big) \prod_{\ell=1}^{M} \Big(1 - \frac{\omega_{2\ell}^2}{\omega^2}\Big)^{-1}. \tag{9}$$

3 Numerical application

We shall illustrate numerically our theoretical results in the case of the Drude's model (see (3) and below), a case already considered in [2] (with no analysis) and in our previous work [5]. We shall show the instability of the classical PMLs and the stability of the new ones with

$$\chi(\omega) = \left(1 - \frac{\omega_*^2}{\omega^2}\right)^{-1} \tag{10}$$

with ω_*^2 chosen between $\omega_{e,1}^2$ and $\omega_{m,1}^2$.

References

[1] E. Bécache, S. Fauqueux and P. Joly, Stability of perfectly matched layers, group velocities and anisotropic waves, *J. of Comp. Physics* **188** (2003), no. 2, pp. 399–433.

[2] S. A. Cummer, Perfectly matched layer behavior in negative refractive index materials, *Antennas and Wireless Propagation Letters, IEEE* (2004), no. 1, pp. 172–175.

[3] W. C. Chew and W. H. Weedon, A 3d perfectly matched medium from modified maxwell's equations with stretched coordinates, *Microwave and optical technology letters* 7 (1994), no. 13, pp. 599–604.

[4] A Tip, Linear dispersive dielectrics as limits of Drude-Lorentz systems, *Physical review. E*, 69 (2004), no. 1

[5] E. Bécache, P. Joly, M. Kachanovska and V. Vinoles, Perfectly matched layers in negative index metamaterials and plasmas, *ESAIM: Proceedings and Surveys* (2015), vol. 50, pp. 113-132

Computation of modes in embbeded helical structures with the SAFE-PML method

K.L. Nguyen[1,*], **F. Treyssède**[2]

[1]ENSTA ParisTech, 828, Boulevard des Maréchaux, 91762 Palaiseau Cedex, France

[2]IFSTTAR, Centre de Nantes, Route de Bouaye, 44344 Bouguenais Cedex, France

[*]Email: n_khaclong@yahoo.com

Abstract

Helical multi-wire cables are widely used in bridge construction and can be degraded due to corrosion and fatigue. To reveal defects inside cable structures, elastic guided waves are of interest owing to their ability to propagate over long distances. In practice, cables are often buried into a solid matrix and can be considered as open waveguides. Waves can be leaky and strongly attenuate along the guide axis, which reduces the propagating distance. Maximizing this distance is necessary for non-destructive testing. The goal of this work is to propose a numerical method for computing modes in embedded helical structures, combining the so-called semi-analytical finite element (SAFE) method and a radial perfectly matched layer (PML) technique.

Keywords: waveguide, helical, leaky modes, finite element, perfectly matched layer

1 Introduction

The numerical modeling of cable waveguides encounters three difficulties : the helical nature of the geometry, the unbounded cross-section and the exponential transverse growth of leaky modes. The helical geometry can be represented in the twisting coordinate system proposed in [1]. In order to overcome the last two difficulties, a simple method consists in using absorbing layers of artificial growing viscoelasticity [2]. An alternative approach is to use a PML technique. Such a technique has already been developed for open straight waveguides [3]. The present work consists in extending the SAFE-PML method for embedded helical structures.

2 SAFE-PML formulation

The time harmonic dependence is chosen as $e^{-i\omega t}$. Acoustic sources and external forces are discarded for computing eigenmodes. The 3D elastodynamic equations satisfied by the displacement vector $\boldsymbol{\mathcal{U}}$ are represented in Cartesian coordinates (X, Y, Z) as:

$$\nabla \cdot \sigma(\boldsymbol{\mathcal{U}}) + \omega^2 \rho \boldsymbol{\mathcal{U}} = 0 \tag{1}$$

where ρ is the material density, σ is the stress tensor related to the strain tensor $\epsilon = (\nabla\boldsymbol{\mathcal{U}} + (\nabla\boldsymbol{\mathcal{U}})^T)/2$ by the relation $\sigma = C : \epsilon$, C is the stiffness tensor and T is the matrix transpose. The tilde notation will be explained later.

For modeling of helical waveguides, Eq. (1) is rewritten in the twisting coordinate system (x, y, z) defined as $x = X\cos(\tau Z) + Y\sin(\tau Z)$, $y = -X\sin(\tau Z) + Y\cos(\tau Z)$, $z = Z$ where τ denotes the torsion of the (x, y) plane around the z axis. One considers a linearly elastic embedded helical waveguide $S \times \mathbb{R}$ whose cross-section S and material properties in the transverse (x, y) plane are invariant along the z axis.

The SAFE method is applied, which consists in assuming the solutions of the form $\boldsymbol{\mathcal{U}}(x, y, z) = \mathbf{u}(x, y)e^{ikz}$, where k is the axial wavenumber. The axial derivative $\partial/\partial z$ is replaced with product by ik. We are led to a bidimensional problem satisfied by $\mathbf{u}$ in the transverse directions (x, y) with the following variational formulation:

$$\int_S \delta\boldsymbol{\epsilon}^T \boldsymbol{\sigma} dxdy - \omega^2 \int_S \rho\delta\mathbf{u}^T \mathbf{u} dxdy = 0 \tag{2}$$

where $\boldsymbol{\sigma}$ and $\boldsymbol{\epsilon}$ denote the stress and train vectors respectively.

In addition to the SAFE technique, the radial PML method will be implemented.

The formulation (2) is now transformed in cylindrical coordinates (r, θ, z) defined from twisting coordinates (x, y, z) as $x = x_{O'} + r\cos\theta$, $y = y_{O'} + r\sin\theta$. In the (x, y) plane, the point $O' = (x_{O'}, y_{O'})$ is the center of this cylindrical system. $x_{O'}$ and $y_{O'}$ are independent of the axial coordinate z.

The radial PML defines a complex radial coordinate $r_c = \int_0^r \gamma(\xi)d\xi$ where $\gamma(r) = 1$ for $r \leq d$, $\mathrm{Im}(\gamma) > 0$ for $r > d$. d is the radius of the PML interface. The twisted radial PML is called centered if $x_{O'} = y_{O'} = 0$ and off-centered

if not. The change of variable $r_c \mapsto r$ yields for any function f :

$$\frac{\partial f}{\partial r_c} = \frac{1}{\gamma}\frac{\partial f}{\partial r},\ dr_c = \gamma dr \tag{3}$$

The variational formulation (2) must be then transformed back to the coordinates (x, y).

Finally, the FE discretization of the variation formulation (2) along the transverse directions (x, y) yields a matrix eigensystem of the following form:

$$\{\mathbf{K}_1 - \omega^2\mathbf{M} + ik(\mathbf{K}_2 - \mathbf{K}_2^T) + k^2\mathbf{K}_3\}\mathbf{U} = \mathbf{0} \tag{4}$$

where the column vector $\mathbf{U}$ contains nodal displacements. Given ω and finding k, this eigenproblem is quadratic. The linearization of this eigensystem is detailed in [3] and yields non hermitian matrices, which makes the numerical treatment of the eigensystem complicated.

3 Results

A Dirichlet condition is chosen at the exterior boundary of truncated domain. Finite elements are triangles with six nodes. Following [3], the PML layer is close to the core in order to reduce the effects of the transverse growth of leaky modes on numerical results. The PML function γ should be chosen as smooth as possible to minimize numerical reflection [3]. γ is a parabolic function in this work.

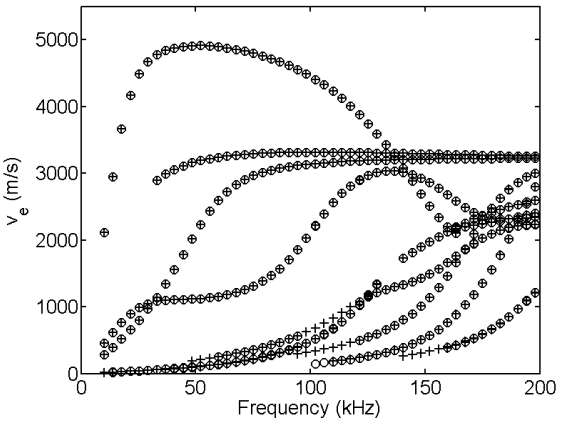

Figure 1: Energy velocity for an embedded cylindrical bar obtained by untwisted (circles) and twisted SAFE-PML (crosses) methods.

The twisted SAFE-PML method is validated with a cylinder test case owing to the fact that any arbitrary twist can be applied (a twisted cylinder remains a cylinder). The centered PML is used. Figure 1 compares the numerical results computed in twisting and untwisting coordinate systems and yields the same physical modes. However, their axial wavenumbers are translated by $\pm\tau m$ in the twisting system, where m denotes their circumferential order.

A first application consists of a steel helical wire buried in concrete. Since the computational domain with a centered PML is quite large, an off-centered PML should be preferred. The off-centered PML is validated by comparing the numerical results with those computed with the centered PML method, which has been checked in the previous test case. Results show that the twist of the helical geometry enhances the modal axial attenuation.

A second numerical example is given by a steel seven-wire buried in concrete. Compared with the results of a free strand, the modal behavior is strongly modified due to the introduction of the surrounding medium. Modes of lowest attenuation are identified, which may be of interest for inspecting cable structures.

References

[1] F. Treyssède, and L. Laguerre, Investigation of elastic modes propagating in multiwire helical waveguides, *Journal of Sound and Vibration* **329** (2010), pp. 1702–1716.

[2] M. Castaings and M. Lowe, Finite element model for waves guided along solid systems of arbitrary section coupled to infinite solid media, *Journal of the Acoustical Society of America* **123(2)** (2008), pp. 696–708.

[3] F. Treyssède, K.L. Nguyen, A.-S. Bonnet-BenDhia and C. Hazard, Finite element computation of trapped and leaky elastic waves in open stratified waveguides, *Wave Motion* **51** (2014), pp. 1093–1107.

Thursday, July 23
Morning Session
10:30 – 12:30

Statistical Inverse Problem and Numerical Simulation Related to Electromagnetic Wave Propagation

Timo Lähivaara[1,*], **Kati Niinimäki**[2]

[1]Department of Applied Physics, University of Eastern Finland, Kuopio, Finland
[2]Department of Mathematics, KTH Royal Institute of Technology, Stockholm, Sweden
[*]Email: timo.lahivaara@uef.fi

Abstract

An inverse problem of estimating the pipeline location from ground-penetrating radar data is studied in the context of Bayesian full-wave inversion. Numerical reconstructions are presented for a 2D case.

Keywords: Maxwell's equations, discontinuous Galerkin method, Bayesian inversion methods

1 Introduction

Let Ω be a bounded Lipschitz domain in $\mathbb{R}^2$ with boundary $\partial\Omega$. Let $\boldsymbol{x} = (x, y) \in \Omega$ be the spatial variables and $t \in [0, T]$ be the time. The transverse magnetic mode Maxwell's equations can be written as

$$\begin{aligned} \epsilon\partial_t E^z - \partial_x H^y + \partial_y H^x + \sigma E^z &= J^E, \\ \mu\partial_t H^x + \partial_y E^z &= 0, \\ \mu\partial_t H^y - \partial_x E^z &= 0, \end{aligned} \tag{1}$$

where $\epsilon(\boldsymbol{x})$ is the dielectric permittivity, $E^z(\boldsymbol{x}, t)$ is the electric field, $(H^x(\boldsymbol{x}, t), H^y(\boldsymbol{x}, t))$ are the magnetic field components, $\mu(\boldsymbol{x})$ is the magnetic permeability, $\sigma(\boldsymbol{x})$ is the electrical conductivity, and $J^E(\boldsymbol{x}, t)$ is the volume current source term. Zero initial and perfect electric conductor (PEC) conditions are assumed throughout this paper.

Here, the numerical results are computed using the discontinuous Galerkin (DG) and low-storage Runge-Kutta methods. For a detailed discussion of these methods, see [1,4] and references therein.

The results shown in this study are based on the work [3].

2 Statistical Inverse Problem

We consider the following observation model

$$z = K_a(\chi) + e, \quad e \sim \mathcal{N}(0, \Gamma_e), \tag{2}$$

where z is a measurement vector containing the recorded signals, K_a is the forward mapping related to (1), χ are the unknown variables, and e is the measurement noise.

In the Bayesian framework all the variables related to the model are modelled as random variables. The randomness reflects the uncertainty of the variables' true values. The solution to the inverse problem is given as summary statistics over the posterior probability distribution $\pi(\chi \,|\, z)$ which is given by Bayes' formula:

$$\pi(\chi \,|\, z) \approx \pi(z \,|\, \chi)\pi(\chi). \tag{3}$$

In (3), $\pi(z \,|\, \chi)$ is the likelihood function which measures the relative probability of observing the measurements z given χ, while $\pi(\chi)$ is the *priori* density describing the knowledge that is known prior to the measurements.

In the Bayesian approximation error method (BAE) [2], the main idea is to replace the computationally accurate forward mapping K_a by a less accurate but computationally feasible one K_r. Furthermore, the BAE may also allow for the reduction of the unknowns in the model by carrying out approximative pre-marginalization over the uninteresting unknowns. To this end, we write $\chi = (\chi_1, \chi_2)$ where χ_1 and χ_2 denote the uninteresting and interesting unknowns, respectively. In this paper, we set $\chi_1 = (\epsilon, \mu, \sigma)$ and $\chi_2 = \theta$, where $\theta \in \mathbb{R}^2$ are the parameters indicating the location of the pipeline.

For the BAE, we fix the nominal values $\chi_1 = \tilde{\chi}_1$ and rewrite (2) as follows

$$z = K_r(\tilde{\chi}_1, \theta) + \xi + e, \tag{4}$$

where $\xi = K_a(\chi_1, \theta) - K_r(\tilde{\chi}_1, \theta)$ is an *additive approximation error* term. The approximation error ξ is the discrepancy between K_a and K_r.

For the sampling of the posterior models in this paper, we employ the standard Metropolis-Hastings algorithm.

3 Numerical Experiments

The studied problem geometry is shown in Figure 1. The domain consists of four main subdomains, which are highlighted with different colors.

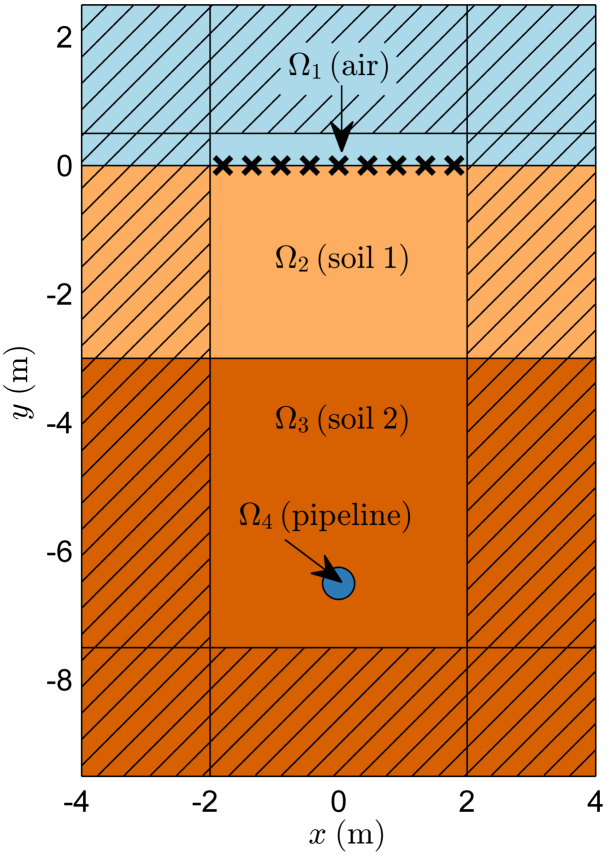

Figure 1: Problem geometry. The crosses denote the array of antennas. The shaded area denotes the perfectly matched layer.

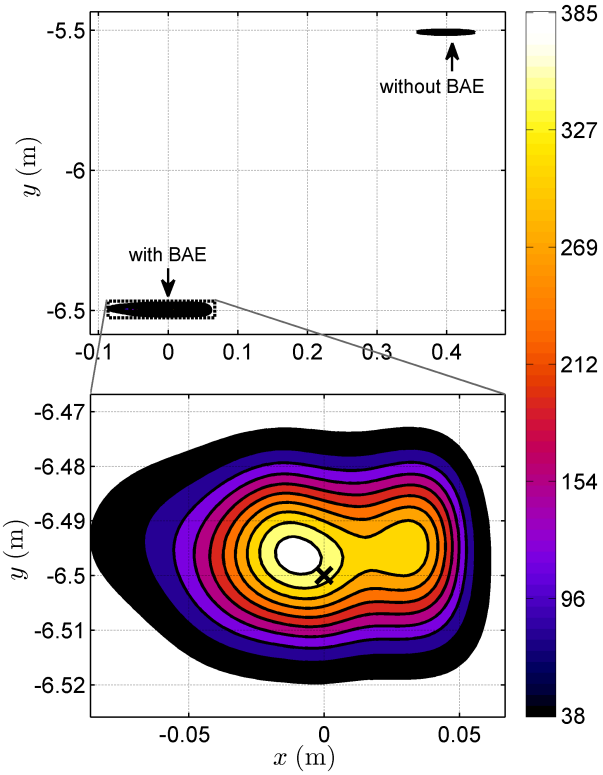

Figure 2: The posterior probability distributions $\pi(\theta \mid z)$ for the BAE model and for the model omitting ξ (see Eq. (4)), i.e. without BAE. The actual pipeline location is marked by a cross.

The variables (ϵ, μ, σ) in $\Omega_{2,3}$ are modelled as Gaussian Markov random fields (MRF). The non-homogeneous MRF's are generated using an anisotropic smoothness prior.

The prior distribution was also used to generate samples for the computation of the approximation error model. The statistics of the approximation error were estimated with 200 draws from the prior model $\pi(\epsilon, \mu, \sigma, \theta)$.

Figure 2 shows the posterior probability distributions $\pi(\theta \mid z)$ with 10% noise level.

4 Conclusions

In this work, we studied the application of radar data to the estimation of pipeline location with material parameter uncertainties. As a conclusion of the results, the application of BAE allows accurate reconstructions of the pipeline location with reduced computational burden.

Acknowledgments

This work has been supported by the Academy of Finland (projects 250215 and 257372).

References

[1] J.S. Hesthaven and T. Warburton, *Nodal Discontinuous Galerkin Methods: Algorithms, Analysis, and Applications*, Springer, 2007.

[2] J.P. Kaipio and E. Somersalo, *Statistical and Computational Inverse Problems*, Springer-Verlag, 2005.

[3] T. Lähivaara, N.F. Dudley Ward, T. Huttunen, J.P. Kaipio, and K. Niinimäki, Estimating pipeline location using ground-penetrating radar data in the presence of model uncertainties, *Inverse Problems*, **30** (2014), pp. 114006.

[4] B. Cockburn, G.E. Karniadakis, and C-W. Shu, *Discontinuous Galerkin Methods: Theory, Computation and Applications*, Springer-Verlag, 2000.

Combination of Finite Differences with Discontinuous Galerkin Method for Seismic Modeling

Vadim Lisitsa[1,*], **Vladimir Tcheverda**[2]

[1]Institute of Petroleum Geology and Geophysics SB RAS, Novosibirsk, Russia and Novosibirsk State University, Novosibirsk, Russia

[2]Inst. of Petroleum Geol. and Geophysics SB RAS, Novosibirsk, Russia

[*]Email: lisitsavv@ipgg.sbras.ru

Abstract

In this paper we present a numerical algorithm for simulation of seismic wave propagation in models with complex upper part and free surface topography. The approach is based on the combination of the discontinuous Galerkin method with finite differences. The discontinuous Galerkin is used in the upper part of the model providing accurate description of wave interaction with harp interfaces with complex topography, whereas finite differences are applied elsewhere to preserve computational efficiency of the algorithm.

Keywords: seismic wave propagation, finite differences, discontinuous Galerkin

1 Introduction

Numerical simulation of seismic wave propagation is widely used nowadays in seismic processing, acquisition design etc. Among numerical method utilized for seismic modeling finite differences (FD) are the most wide spread, as they combine high computational efficiency, robustness, applicability to models of almost arbitrary complexity with sufficient (for seismic processing) accuracy [1]. However, in presence of sharp interfaces, in particular free surface, with complex topography use of FD on regular rectangular mesh leads to stair-step approximation of the interface, thus multiple artificial diffractions appear in the simulated wavefield. On the contrary, variational methods, in particular discontinuous Galerkin (DG), can be used on polyhedral, including curvilinear, meshes which accurately follow the interfaces, significantly improving quality of numerical solution. However, use of DG require a mesh of a high quality, which can be a troublesome task for problems of a realistic size. Moreover, computational complexity of the DG is much higher, than that of FD.

In this paper we present combination of the two methods, so that centered-flux DG [2] is used in the upper part of the model ensuring high accuracy of the solution in the vicinity of free surface, whereas a standard staggered grid scheme (SSGS) [3] is applied in the main part of the modem, to preserve computational efficiency of the algorithm.

2 The algorithm

To couple the standard staggered grid scheme with the discontinuous Galerkin method we suggest introducing a transition zone combining properties of the two methods 1. Such an approach is a conventional non-staggered grid scheme (NSGS) which is equivalent to finite volume technique on a rectangular grid thus equivalent to P0 DG formulation on regular rectangular grid. Thus the problem of the combination of SSGS and DG decouples into two: combination of the P0 DG on rectangular grid with P1-P3 DG on triangular mesh, and combination of the standard staggered grid scheme with non-staggered grid scheme. The first problem is easy to solve within the frame of hp-adaptivity, which is naturally applicable in to DG. In order to solve the second problem one needs to suppress the artificial reflections, especially those connected with high-frequency (plus-minus) modes. This problem may be reduced to the coupling of the SSGS with the Lebedev scheme, presented in [4], because the conventional non-staggered grid is a combination of two partially staggered Lebedev grids. As the result the artificial reflections, caused by the combination of different numerical techniques do not exceed 0.1 for standardly used discretizations and they decay with the second order as a grid step tends to zero.

3 Numerical experiment

To illustrate applicability of the approach we simulated wave propagation in a model provided

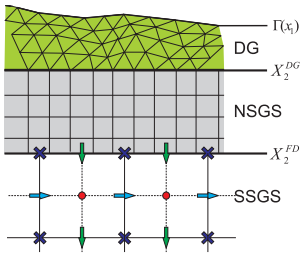

Figure 1: A sketch of the domain decomposition for the combination of the FD with DG. The DG is used in the green subdomain, the NSGS is applied in grey subdomain, and the SSGS is applied the in the white subdomain.

in fig. 2. The source and the receivers were burred by 0.5 m below surface. Ricker pulse with central frequency of 20 Hz, was used as the source wavelet. The grid step was chosen 5 m, size of the grid cell for DG was about one half of that for FD.

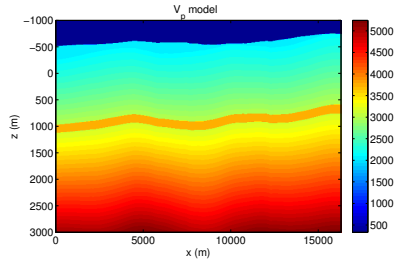

Figure 2: A model (V_p) with realistic topography.

Results of simulation, seismogramms recorded 0.5 below free surface, are presented in fig. 3. One can see that the wavefield computed by the hybrid approach is free from the artificial diffractions of the surface wave, where as FD simulated data are full of nose. If compared with the FD simulation the hybrid modeling took about twice as long (with 10 % of the model discretized by DG mesh), however pure DG simulation for the same model took about 20 times longer than the hybrid approach.

4 Conclusions

We presented the hybrid algorithm to simulate seismic wave propagation in presence of sharp interfaces with complex topography. To account for the topography DG is used in the upper part of the model. To make the algorithm computationally cheap the FD are used in the major part

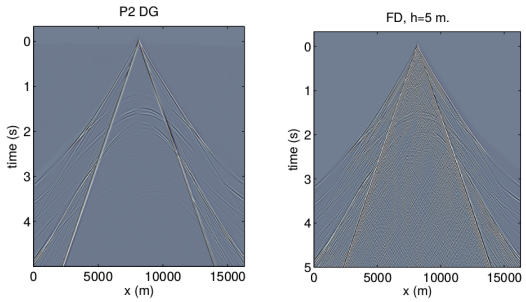

Figure 3: Seismogramms computed by hybrid approach (left) and purely by the FD (right).

of the model.

The research was supported by RFBR grants 13-05-00076, 13-05-12051, 14-05-00049, 14-05-93090, 15-05-01310, 15-35-20022.

References

[1] J. Virieux, H. Calandra and R.-E. Plessix, A review of the spectral, pseudo-spectral, finite-difference and finite-element modelling techniques for geophysical imaging, *Geophysical Prospecting* **59** (2011), pp. 794–813.

[2] V. Etienne, E. Chaljub, J. Virieux and N. Glinsky, An hpadaptive discontinuous Galerkin finite-element method for 3D elastic wave modelling, *Geophysical Journal International* **183** (2010), pp. 941–962.

[3] J. Virieux, P-SV wave propagation in heterogeneous media: Velocity-stress finite-difference method, *Geophysics* **51** (1986), pp. 889–901.

[4] V. Lisitsa, V. Tcheverda and D. Vishnevsky, Numerical simulation of seismic waves in models with anisotropic formations: coupling Virieux and Lebedev finite-difference schemes, *Computational Geosciences* **16** (2012), pp. 1135–1152.

A lumped nodal DGTD-PIC method to ensure charge conservation for the 3D Vlasov-Maxwell system on nonconforming cartesian grids

Bruno Fornet[1,*], **Alexandra Grabon**[1], **Josette Despinoy**[1]

[1]NUCLETUDES, 3 avenue du Hoggar -Les Ulis -CS 70117- 91978 Courtaboeuf Cedex, France

[*]Email: bfornet@nucletudes.com

Abstract

A critical issue in numerical computing related to plasma physics is to satisfy charge conservation. We present here a new high order approach, based on a upwind biased lumped nodal RKDG scheme combined with a PIC scheme dealing with Dirac shape functions for macroparticles, which ensures charge conservation on nonconforming grids without having to use either a correction method as in [4], [2] or curl-conforming basis functions as in [5].

Keywords: Discontinuous Galerkin, Particle in Cell, Vlasov-Maxwell system, numerical charge conservation, Dirac shape function

1 Introduction

The Vlasov-Maxwell system is used to describe collisionless plasmas. Discontinuous Galerkin Methods in Time Domain (DGTD) are promising high order methods for the efficient numerical simulation of the Maxwell system while Particle In Cell (PIC) is a powerful tool to account for the charged particles arising from Vlasov equation. We expose a new method yielding charge conservation in this framework.

2 Charge conservation and operator conforming spaces

The divergence of Maxwell-Ampère in vacuum reads: $\partial_t(\epsilon_0 \nabla.E) + \nabla.J = \nabla.(\nabla \times H)$.
Defining ρ as $\epsilon_0 \nabla.E$ (Maxwell-Gauss equation), the charge conservation can be written as:
$\nabla.(\nabla \times H) = 0$. The numerical satisfaction of these laws is a complex problem depending both of operator and data discretizations. It is the key point to check in order for a DGTD-PIC method to be suitable for practical use.

Using a Galerkin method, the fields are approximated by polynomials, the coefficients of which are called degrees of freedom (dofs). For Continuous Galerkin (CG) approximations (Finite Elements: FE) the dofs are defined globally over the mesh. If the approximated space is the Sobolev space H^1, continuity is then strongly imposed over the faces of the mesh whereas only tangential continuity holds. Using instead an adapted Galerkin approximation of $H^1(curl)$ spaces (see [3]), only the physically relevant continuity is enforced. CG approaches based on a differential geometry approach (like in [5]) lead to methods preserving charge conservation without any need of divergence cleaning. For Discontinuous Galerkin Methods (DGM), the dofs are defined locally and tangential continuity (viewed as a transmission condition between mesh elements) is weakly inforced via the numerical fluxes. DGM are of two kinds : the one with centered fluxes for which a work similar to continuous Galerkin methods (choice of Kernel-friendly spaces) has to be conducted, and the one with upwind flux for which we will show that a **well-chosen** H^1 approximation (like the ones used in divergence-cleaning correction methods) works just fine in the DGTD-PIC framework. We chose the second kind of approach which **is unique to Discontinuous Galerkin** (not inherited from FE).

3 Description of the method

We will describe here the set of all not strictly standard choices characterizing our DGTD-PIC method. We use a weak DGTD formulation with lumped Gauss-Lobatto basis functions (Q^2 and Q^3) and full upwind fluxes. Since Gauss-Lobatto quadrature points cover the boundary, they are used to perform both volumic and surface integration to estimate the scheme stiffness and fluxes matrices. The resulting mass matrix is diagonal. We also observed that lumping had a positive effect on the time constraint restriction (CFL condition since we perform an explicit time integration using a RK4 scheme). Moreover the approximation of any data in this basis can be performed in a quadrature-free manner. As in [1], the current source is deduced from macroparticles viewed as Dirac measures directly sampled as a consequence of the variational formulation, denoting by J the current resulting from N particules travelling in the con-

sidered mesh element Ω_K during the time step and by φ^K a basis function:

$$\int_{\Omega_K} J\varphi_i^K = \sum_{\alpha=1}^{N} \frac{1}{\Delta t} \int_{\tau_\alpha}^{\tau_\alpha+\Delta\tau_\alpha} qw_\alpha v(t)\varphi_i^K(x_\alpha(t))\ dt.$$

Macroparticle α of charge qw_α spans Ω_K for $t \in [\tau_\alpha, \tau_\alpha + \Delta\tau_\alpha) \subset [t_n, t_{n+1})$. The proposed method is genuinely discontinuous since no continuous quantities have to be reconstructed in order to make it work.

4 High order convergence

While considering numerical convergence for the Vlasov-Maxwell system, both mesh convergence and statistical convergence have to be considered. Given a fine enough statistical convergence, the table below shows, for different methods, the coarsest uniform cartesian meshes for which spatial convergence occurs.

Method	FDTD-PIC	Q2-PIC	Q3-PIC
Mesh	400^3	55^3	30^3

5 Numerical illustration of charge conservation

A sensitive case with respect to charge conservation (3D version of the 2D-diode tested in [4]) has been tested Figure 1. Electrons travel from y^- to y^+ in a stable manner, an equilibrium state is reached during the first nanoseconds. We validated persistance of this state for one microsecond. Silver-Müller boundary conditions are used to approximate free space.

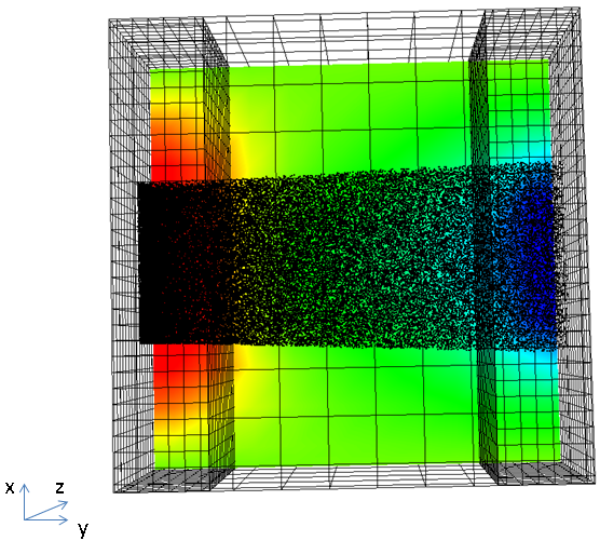

Figure 1: Diode 3D on a nonconforming mesh

6 Conclusion and outlook

Upwind flux are known to delay spurious behavior. Combined with other suitable choices involving basis functions, projector and shape functions, they are at the core of a new high order method ensuring long time charge conservation as checked on a stringent test case. Future steps to take would be to improve the computational efficiency of the method and test its flexibility to more general meshes.

Acknowledgements:
This work has been supported by DGA (Direction générale de l'armement).

References

[1] A. Crestetto and P. Helluy, Resolution of the Vlasov-Maxwell system by PIC Discontinuous Galerkin method on GPU with OpenCL, *ESAIM: PROCEEDINGS* **38** (2012), pp. 257–274.

[2] G.B. Jacobs and J.S. Hesthaven, High-order nodal discontinuous Galerkin particle-in-cell method on unstructured grid, *JCP* **214** (2006), pp. 96–121.

[3] J.C. Nédelec, Mixed Finite Elements in $\mathbb{R}^3$, *Numer. Math.* **35** (1980), pp. 315–341.

[4] A. Stock et al., Investigation of the purely hyperbolic Maxwell System for divergence cleaning in Discontinuous Galerkin based Particle-In-Cell methods, in *IV International Conference COUPLED PROBLEMS 2011.*

[5] M.L. Stowell and D. A. White, Discretizing transient current densities in the Maxwell equations, in *Proceedings of ICAP09, San Francisco, CA*, pp. 213–217.

A posteriori error estimates for discontinuous Galerkin method to the elasticity problem

DAVEAU Christian[1,*], **LUONG Thi Hong Cam**[1]

[1]Department of Mathematics, University of Cergy-Pontoise, France

[*]Email: christian.daveau@u-cergy.fr

Abstract

In this work, we derive an *a posteriori* error bounds for the discontinuous Galerkin method for the time-dependent linear elasticity problem, by making use of the *stationary reconstruction* technique which allows to estimate the error for time-dependent problem through the error estimation of the associated stationary elasticity problem. We apply the backward-Euler scheme for fully discrete scheme, and then illustrate the theory with a series of numerical experiments.

Keywords: elasticity equations, discontinuous Galerkin, a posteriori.

1 Introduction

A posteriori error estimation and adaptivity recently have become successful tools for efficient numerical computations. They have already been widely considered for solving elliptic, parabolic and first order hyperbolic problems. Howerver, there are few results for *a posteriori* error analysis of the second order evolution problems; we mention, in particular, [1] and [2] derive rigorous *a posteriori* bounds for conforming finite element methods in case of fully discretization for wave equation.

Recently, discontinuous Galerkin (DG) methods have been developped for elasticity problem. There are several approaches have been developed for stationary problem: residual type error estimators, method based on dual variables. In case of time-dependent problem, to our knowledge there is still no work for *a posteriori* error control for elasticity equation with DG method, so this is the first study about this. We here propose an *a posteriori* bound in the $L^\infty(L^2)$ norm of the error for the elasticity equation, and in case of DG method. This study is inspired from the work of [2] concerning with the wave equation in case of conforming finite element method.

2 Notations

Denote by L^p, $1 \le p \le \infty$ the space of integrable functions, and by H^s the Sobolev space and $\|\cdot\|_{s,\Omega}$ for the H^s-norm.

Denote by Ω a bounded polygonal domain in $\mathbb{R}^d$, $d = 2, 3$, let $\mathcal{T}_h$ be a subdivision of Ω into disjoint open sets $\{K\}$ such that $\overline{\Omega} = \cup_{K\in\mathcal{T}_h}\overline{K}$, and denote by $h_K := \mathrm{diam}(K)$ and by $h := \max_{K\in\mathcal{T}_h} h_K$.

Consider the DG finite element space

$$\mathbf{V}_h := \{\boldsymbol{v} \in L^2(\Omega)^d : \boldsymbol{v}|_K \in \mathbb{P}_r(K)^d,\ K \in \mathcal{T}_h\}, \tag{1}$$

here $\mathbb{P}_r(K)$ denotes the set of polynomials of total degree at most r on K. Let $\mathcal{E}_h = \mathcal{E}_h^I \cup \mathcal{E}_h^B$ with $\mathcal{E}_h^I$ the union of all interior faces (edges) of the triangulation $\mathcal{T}_h$, and $\mathcal{E}_h^B$ being the set of all boundary faces. Let K^+ and K^- be two adjacent elements of $\mathcal{T}_h$, then the average and jump at $\boldsymbol{x} \in e = \partial K^+ \cap \partial K^-$ are defined as follows:

$$\{\!\{\boldsymbol{q}\}\!\} = \frac{1}{2}(\boldsymbol{q}^+ + \boldsymbol{q}^-); \quad [\![\boldsymbol{q}]\!] = (\boldsymbol{q}^+ - \boldsymbol{q}^-).$$

Introducing the function h defined on $e \in \mathcal{E}_h$ by

$$\mathsf{h}|_e = \begin{cases} \min\{h_K, h_{K'}\}, & e \in \mathcal{E}_h^I,\ e = \partial K \cap \partial K', \\ h_K, & e \in \mathcal{E}_h^B,\ e = \partial K \cap \partial\Omega. \end{cases}$$

3 Model problem

Consider the equations of linear elasticity problem of finding the displacement vector $\boldsymbol{u} = (u_i(\boldsymbol{x}, t))_{i=1}^d$ such that

$$\begin{cases} \rho\partial_{tt}^2 u_i - \sum_{j=1}^d \dfrac{\partial\sigma_{ij}(\boldsymbol{u})}{\partial x_j} = f_i & \text{in } (0,T)\times\Omega, \\ & i = \overline{1,d}, \\ \boldsymbol{u} = \boldsymbol{0} & \text{on } \partial\Omega\times(0,T], \end{cases} \tag{2}$$

with initial conditions $\boldsymbol{u}_0 \in H_0^1(\Omega)^d$, and $\boldsymbol{u}_1 \in L^2(\Omega)^d$:

$$\begin{cases} \boldsymbol{u}(\cdot,0) = \boldsymbol{u}_0 & \text{on } \Omega\times\{0\}, \\ \partial_t\boldsymbol{u}(\cdot,0) = \boldsymbol{u}_1 & \text{on } \Omega\times\{0\}. \end{cases} \tag{3}$$

Here $\boldsymbol{\sigma}(\boldsymbol{u}) = (\sigma_{ij}(\boldsymbol{u}))_{1\le i,j\le d}$ is the stress tensor which satisfies the constitutive relationship: $\boldsymbol{\sigma}(\boldsymbol{u}) = \mathbb{C}\boldsymbol{\varepsilon}(\boldsymbol{u})$, or equivalently

$$\forall 1 \le i,j \le d, \sigma_{ij}(\boldsymbol{u}) = \sum_{k,l=1}^{d} C_{ijkl}\varepsilon_{kl}(\boldsymbol{u}),$$

where $\mathbb{C} = (C_{ijkl})_{ijkl}$ is a fourth order tensor, independent of t and satisfying some symmetry properties: $C_{ijkl} = C_{jikl} = C_{ijlk} = C_{klij}$. We assume that the stiffness tensor $\mathbb{C}$ is positive definite and piecewise constant in Ω.

4 Fully discrete error estimates

We consider a subdivision of the time interval $(0,T]$ into subintervals $(t^{n-1},t^n], n = 1,\dots,N$, with $t^0 = 0$ and $t^N = T$, with the uniform time step $\tau := t^n - t^{n-1}$. Associated with the time subdivision, let $\mathcal{T}_h^n$, $n = 0,\dots,N$ be a sequence of meshes, by $\mathbf{V}_h^n$ a DG finite element space of fixed degree r built on the partition $\mathcal{T}_h^n$, by $\mathcal{E}_h^n$ the union of all edges (or faces) of the triangulation $\mathcal{T}_h^n$, and denote by $\boldsymbol{u}_h^n$ the discrete solution at t^n.

By using the stationary reconstruction technique to obtain an error relation, then applying the special testing function as used in [3], in combination with the error estimation from the corresponding stationary problem obtained by the method of duality or *via* energy norm, we finally obain the following *a posteriori* error bound:

Theorem 1 *The following bound holds*

$$\|\boldsymbol{u} - \boldsymbol{u}_N\|_{L^\infty(0,t^N;L^2(\Omega)^d)} \le \zeta_{\rm sp} + \zeta_{\rm tp} + \zeta_{\rm IC},$$

where $\zeta_{\rm sp}$ *mainly accounts for the spatial error,* $\zeta_{\rm tp}$ *mainly accounts for the temporal error and* $\zeta_{\rm IC}$ *represents the initial conditions of the problem. They are given as follows:*

$$\zeta_{\rm sp} = \zeta_{\rm sp,1} + \zeta_{\rm sp,2} + \zeta_{\rm sp,3},$$
$$\zeta_{\rm tp} = 2\big(\zeta_{\rm MC} + \zeta_{\rm evo} + \zeta_{\rm osc} + \zeta_{\rm T.Rec}\big),$$
$$\zeta_{\rm IC} = \sqrt{2}\|\boldsymbol{u}_0 - \boldsymbol{u}_h^0\|_{0,\Omega} + 2C_{F\Omega}c_*^{-1/2}\|\boldsymbol{u}_1 - \partial\boldsymbol{u}_h^0\|_{0,\Omega},$$

where the spatial indicators are given by

$$\zeta_{\rm sp,1} = \sqrt{2}E_{IP}^0\,,$$
$$\zeta_{\rm sp,2} = 3\max_{0\le n\le N}\left(E_{IP}^n + 2C_{F\Omega}^2c_*^{-1}\|\widetilde{\boldsymbol{f}}^n - \boldsymbol{f}^n\|_{0,\Omega}\right),$$
$$\zeta_{\rm sp,3} = \sum_{n=1}^{N} 2(E_{IP}^n + E_{IP}^{n-1}) + \sum_{n=1}^{N} 4\tau C_{F\Omega}^2c_*^{-1}\|\partial\boldsymbol{f}^n - \partial\widetilde{\boldsymbol{f}}^n\|_{0,\Omega}\,.$$

and the temporal indicators are defined by

$$\zeta_{\rm MC} = \sum_{n=1}^{N}\int_{t^{n-1}}^{t^n}\|(\mathsf{I} - \Pi_h^n)\partial_t\boldsymbol{u}_N\|_{0,\Omega}{\rm d}t + \sum_{n=1}^{N-1}(t^N - t^n)\|(\Pi_h^{n+1} - \Pi_h^n)\partial\boldsymbol{u}_h^n\|_{0,\Omega}\,,$$
$$\zeta_{\rm evo} = \int_0^{t^N}\|\mathcal{G}\|_{0,\Omega}{\rm d}t\,,$$
$$\zeta_{\rm osc} = \frac{1}{2\pi}\sum_{n=1}^{N}\left(\int_{t^{n-1}}^{t^n}\tau^3\|\widetilde{\boldsymbol{f}}^n - \boldsymbol{f}\|_{0,\Omega}^2{\rm d}t\right)^{1/2},$$
$$\zeta_{\rm T.Rec} = \frac{1}{2\pi}\sum_{n=1}^{N}\left(\int_{t^{n-1}}^{t^n}\tau^3\|\mu^n\partial^2\boldsymbol{u}_h^n\|_{0,\Omega}^2{\rm d}t\right)^{1/2}.$$

where $E_{IP}^n := E_{IP}(\boldsymbol{u}_h^n, \boldsymbol{B}^n\boldsymbol{u}_h^n - \Pi_h^n\boldsymbol{f}^n + \boldsymbol{f}^n, \mathcal{T}_h^n)$, *for all* $0 \le n \le N$, *with* E_{IP} *is given by*

$$E_{IP}(\boldsymbol{z}_h,\boldsymbol{r},\mathcal{T}_h) := C\Big\{\sum_{K\in\mathcal{T}_h} h_K^4\|\boldsymbol{r} + \nabla\cdot(\boldsymbol{\sigma}(\boldsymbol{z}_h))\|_{0,K}^2 + \sum_{e\in\mathcal{E}_h^I}\mathsf{h}^3\|[\![\boldsymbol{\sigma}(\boldsymbol{z}_h)\boldsymbol{\nu}_e]\!]\|_{0,e}^2 + \sum_{e\in\mathcal{E}_h}\mathsf{h}\|[\![\boldsymbol{z}_h]\!]\|_{0,e}^2\Big\}^{1/2},$$

where C *is a positive constant independent of* $\boldsymbol{z}_h, \boldsymbol{r}, h$ *and* $\mathcal{T}_h$.

5 Numerical tests

This numerical part will be presented at the conference.

References

[1] Bernardi, C. and Süli, E., Time and space adaptivity for the second-order wave equation, *Math. Models Methods Appl. Sci.* 2005, 15, 199-225.

[2] E. H. Georgoulis, O. Lakkis , C. Makridakis, A posteriori $L_\infty(L^2)$-error bounds for finite element approximations to the wave equation, *IMA J Numer Anal* (2013) 33, 1245 - 1264.

[3] Baker G. A., Error estimates for finite element methods for second order hyperbolic equations, *SIAM J. Numer. Anal.* 1976, 13, 564-576.

Non-scattering wavenumbers and far field invisibility for a finite set of incident/scattering directions

Lucas Chesnel[1,*], **Anne-Sophie Bonnet-Ben Dhia**[2], **Sergei A. Nazarov**[3]

[1]Defi team, centre de mathématiques appliquées, École Polytechnique, Palaiseau, France
[2]Poems team, unité de mathématiques appliquées, Ensta ParisTech, Palaiseau, France
[3]Lab. of Mathematical Methods in Mechanics of Materials, IPME RAS, St. Petersburg, Russia
[*]Email: Lucas.Chesnel@cmap.polytechnique.fr

Abstract

We investigate a time harmonic acoustic scattering problem by a penetrable inclusion with compact support embedded in the free space. We consider cases where an observer can produce incident plane waves and measure the far field pattern of the resulting scattered field only in a finite set of directions. In this context, we say that a wavenumber is a non-scattering wavenumber if the associated relative scattering matrix has a non trivial kernel. Under certain assumptions on the physical coefficients of the inclusion, we show that the non-scattering wavenumbers form a (possibly empty) discrete set. Then, in a second step, for a given real wavenumber, we present a constructive technique (which provides a numerical algorithm) to prove that there exist inclusions for which the corresponding relative scattering matrix is null. These inclusions have the important property to be impossible to detect from far field measurements.

Keywords: non-scattering wavenumbers, invisibility.

1 Setting

Consider an inclusion supported in $\overline{\mathcal{D}}$, where $\mathcal{D} \subset \mathbb{R}^d$, $d = 2, 3$, is a bounded domain with Lipschitz boundary. We assume that the scattering of the incident plane wave $u_{\rm i} := e^{ik\boldsymbol{\theta}_{\rm i}\cdot\boldsymbol{x}}$, of direction of propagation $\boldsymbol{\theta}_{\rm i} \in \mathbb{S}^{d-1}$, by $\mathcal{D}$, is described by the problem

$$\left|\begin{array}{l} \text{Find } u \in \mathrm{H}^1_{\rm loc}(\mathbb{R}^d) \text{ such that} \\ -\Delta u = k^2\rho\, u \quad \text{in } \mathbb{R}^d, \\ \quad u = u_{\rm i} + u_{\rm s} \quad \text{in } \mathbb{R}^d, \\ \lim\limits_{r\to+\infty} r^{\frac{d-1}{2}}\left(\dfrac{\partial u_{\rm s}}{\partial r} - iku_{\rm s}\right) = 0. \end{array}\right. \tag{1}$$

In (1), the real valued function ρ models the properties of the inclusion and is such that $\rho - 1$ is supported in $\overline{\mathcal{D}}$. It is known that the scattered field $u_{\rm s}(\cdot, \boldsymbol{\theta}_{\rm i})$ admits the expansion

$$u_{\rm s}(\boldsymbol{x}, \boldsymbol{\theta}_{\rm i}) = e^{ikr}r^{-\frac{d-1}{2}}\Big(u^\infty_{\rm s}(\boldsymbol{\theta}_{\rm s}, \boldsymbol{\theta}_{\rm i}) + O(1/r)\Big),$$

as $r \to +\infty$, uniformly in $\boldsymbol{\theta}_{\rm s} \in \mathbb{S}^{d-1}$. Here $\boldsymbol{\theta}_{\rm s}$ is the direction of observation. We shall assume we have a finite set of emitters and receivers located at the same positions so that we can produce incident plane waves in some given directions $\boldsymbol{\theta}_1, \ldots, \boldsymbol{\theta}_N \in \mathbb{S}^{d-1}$ and measure the far field pattern of the resulting scattered field only in the directions $-\boldsymbol{\theta}_1, \ldots, -\boldsymbol{\theta}_N$ (backscattering directions). This corresponds to knowing all elements of the relative scattering matrix $\mathscr{A}(k) \in \mathbb{C}^{N\times N}$ such that

$$\mathscr{A}_{mn}(k) = u^\infty_{\rm s}(-\boldsymbol{\theta}_m, \boldsymbol{\theta}_n). \tag{2}$$

2 Discreteness of non-scattering wavenumbers

We say that $k > 0$ is a non-scattering wavenumber if $\mathscr{A}_{mn}(k)$ has a non trivial kernel. In this case, there is an incident field, combination of the plane waves of directions $\boldsymbol{\theta}_1, \ldots, \boldsymbol{\theta}_N$ whose scattered field vanishes at infinity in the directions $-\boldsymbol{\theta}_1, \ldots, -\boldsymbol{\theta}_N$. To prove that non-scattering wavenumbers form an empty or discrete set, we use the following strategy.

i) We show that $k \mapsto \mathscr{A}(k)$ can be meromorphically continued to the complex plane.

ii) For $k = i\kappa$, with $\kappa > 0$, we establish energy identities allowing to infer that $\mathscr{A}(k)$ is injective under certain assumptions on ρ.

iii) We conclude using the principle of isolated zeros.

3 Construction of invisible inclusions

Now, assume that $k > 0$, $\mathcal{D}$ and $\boldsymbol{\theta}_1, \ldots, \boldsymbol{\theta}_N$ are given. We develop a technique (introduced in [1, 3]) to build real valued functions ρ supported in $\overline{D}$ such that $\mathscr{A}(k)$ is the null matrix. For such inclusions, for all incident fields

combinations of the plane waves of directions $\boldsymbol{\theta}_1, \ldots, \boldsymbol{\theta}_N$, the scattered field vanishes at infinity in the directions $-\boldsymbol{\theta}_1, \ldots, -\boldsymbol{\theta}_N$. Below, we explain the general procedure (for details, see [2]).
Because of the reciprocity relation

$$u_{\mathrm{s}}^{\infty}(-\boldsymbol{\theta}_m, \boldsymbol{\theta}_n) = u_{\mathrm{s}}^{\infty}(-\boldsymbol{\theta}_n, \boldsymbol{\theta}_m),$$

the matrix $\mathscr{A}(k)$ is symmetric. Let us look for ρ under the form $\rho = 1 + \varepsilon\mu$ with $\varepsilon > 0$, $\mu \in \mathrm{L}^{\infty}_{\mathbb{R}}(\mathcal{D})$ (the set of real valued L^{∞} functions). Define the map $F : \mathrm{L}^{\infty}_{\mathbb{R}}(\mathcal{D}) \to \mathbb{R}^{N(N+1)}$ by

$$F(\varepsilon\mu) = \Big(\Re e(u_{\mathrm{s}}^{\infty}(-\boldsymbol{\theta}_m, \boldsymbol{\theta}_n)), \\ \Im m(u_{\mathrm{s}}^{\infty}(-\boldsymbol{\theta}_m, \boldsymbol{\theta}_n)) \Big)_{1 \le m \le n \le N}.$$

Our goal is to find $\varepsilon\mu \not\equiv 0$ such that $F(\varepsilon\mu) = 0$. Since $F(0) = 0$, for ε small enough, we obtain the following Taylor expansion

$$F(\varepsilon\mu) = \varepsilon dF(0)(\mu) + \varepsilon^2 \tilde{F}(\varepsilon, \mu).$$

Assume that there are $\mu_1, \ldots, \mu_{N(N+1)} \in \mathrm{L}^{\infty}_{\mathbb{R}}(\mathcal{D})$ such that $dF(0)(\mu_1), \ldots, dF(0)(\mu_{N(N+1)})$ is a basis of $\mathbb{R}^{N(N+1)}$. Decompose μ as

$$\mu = \mu_0 + \sum_{i=1}^{N(N+1)} \tau_i \, \mu_i, \qquad (3)$$

where the τ_i are real parameters to tune and $\mu_0 \in \ker dF(0)$. There holds $F(\varepsilon\mu) = 0$ iff $\vec{\tau} = (\tau_1, \ldots, \tau_{N(N+1)})^{\top} \in \mathbb{R}^{N(N+1)}$ verifies

$$\mathbb{D}\,\vec{\tau} = \hat{F}^{\varepsilon}(\vec{\tau}), \qquad (4)$$

where $\mathbb{D}$ is an invertible matrix and where $\hat{F}^{\varepsilon}(\vec{\tau}) = -\varepsilon\tilde{F}(\varepsilon, \mu)$. For any $\gamma > 0$, we can show that $\hat{F}^{\varepsilon}$ is a contraction of $\mathbb{B}_{\gamma} := \{\vec{\tau} \in \mathbb{R}^{N(N+1)} \,|\, |\vec{\tau}| \le \gamma\}$ for ε small enough. Therefore, the Banach fixed-point theorem guarantees the existence of some $\varepsilon_0 > 0$ such that for all $\varepsilon \in (0; \varepsilon_0]$, (4) has a unique solution $\vec{\tau}^{\,\mathrm{sol}}$ in $\mathbb{B}_{\gamma}$. Define $\rho = 1 + \varepsilon\mu$ with μ as in (3) and $\vec{\tau} = \vec{\tau}^{\,\mathrm{sol}}$. Then, for this inclusion there holds $\mathscr{A}(k) = 0$.
⋆ When the vectors of the family $\{\boldsymbol{\theta}_m + \boldsymbol{\theta}_n\}_{1 \le m \le n \le N}$ are all non null and all different, we can prove that the functions $\mu_1, \ldots, \mu_{N(N+1)}$ mentioned above exist. This allows to construct invisible inclusions in this situation.
⋆ When there holds $\boldsymbol{\theta}_m + \boldsymbol{\theta}_n = 0$ for some incident directions $\boldsymbol{\theta}_m$, $\boldsymbol{\theta}_n$, the previous procedure fails. Actually, for any given $\boldsymbol{\theta}_{\mathrm{i}}$, we can show that imposing $u_{\mathrm{s}}^{\infty}(-\boldsymbol{\theta}_{\mathrm{i}}, \boldsymbol{\theta}_{\mathrm{i}}) = 0$ requires to impose $u_{\mathrm{s}}^{\infty}(\boldsymbol{\theta}, \boldsymbol{\theta}_{\mathrm{i}}) = 0$ for all $\boldsymbol{\theta}$. As a consequence of the Rellich lemma, this means that our task consists in finding an inclusion such that the incident plane wave $e^{ik\boldsymbol{\theta}_{\mathrm{i}} \cdot \boldsymbol{x}}$ produces no scattered field outside $\mathcal{D}$. This is a much more constrained problem and we do not know if it has a solution.

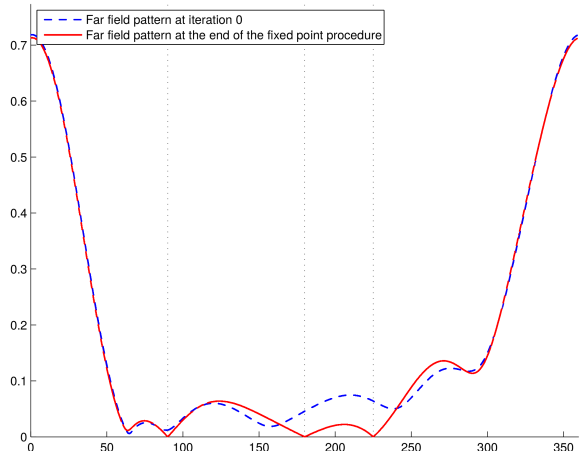

Figure 1: The fixed point problem (4) can be solved numerically. Here, we have constructed an inclusion which is invisible at infinity in the three directions indicated by the dotted lines (the solid curve represents the far field pattern at the end of the fixed point procedure).

References

[1] A.-S. Bonnet-Ben Dhia and S.A. Nazarov, Obstacles in acoustic waveguides becoming "invisible" at given frequencies, *Acoust. Phys.*, **59**(6), 2013, 633–639.

[2] A.-S. Bonnet-Ben Dhia, L. Chesnel and S.A. Nazarov, Non-scattering wavenumbers and far field invisibility for a finite set of incident/scattering directions, *Inverse Problems*, **31**(4), 2015, 045006.

[3] S.A. Nazarov, Asymptotic expansions of eigenvalues in the continuous spectrum of a regularly perturbed quantum waveguide, *Theor. Math. Phys.*, **167**(2), 2011, 606–627.

Inverse wave scattering via moment relaxation

Augustin Cosse[1,*], **Laurent Demanet**[2]
[1]Harvard, IACS and UCL, ICTEAM
[2]MIT, Department of Mathematics
[*]Email: acosse@seas.harvard.edu

Abstract

This note studies the application of moment relaxation to the acoustic inverse scattering problem. The original problem is lifted into a rank-1 matrix recovery formulation, then relaxed into a convex program by a semidefinite constraint. We introduce a low-rank-plus-sparse iteration and a rounding scheme to cope with the size of the lifted problem. The new formulation is shown to increase the basin of attraction of the nonlinear least-squares objective on a simple example.

Keywords: imaging, lifting, rounding.

1 Introduction

We aim to recover a medium $m = 1/c^2$ from the field $u(x,\omega)$ measured at receivers and generated by a source $f(x)$. We let $m(x) = \overline{m} + W(x)\mu(x)$, where $\overline{m}$ is a known constant, $W(x)$ is an indicator of the interior of the domain, and $\mu(x)$ is unknown. The imaging problem can be written

$$\begin{aligned} \text{find} \quad & \mu(x) \\ \text{s.t} \quad & \Delta u + \omega^2(\overline{m} + W\mu)u = f \\ & \mathcal{S}u = d \end{aligned} \tag{1}$$

We let $\mathcal{S}$ for sampling at the receivers, d for the vector of measurements, and u for the concatenation of the fields arising from different sources f. Following recent developments in convex algebraic geometry [1] and interferometric inversion [2], we propose to consider the following relaxation by lifting of (1):

$$\begin{aligned} \text{find} \quad & \boldsymbol{X} = \begin{pmatrix} X_{11} & X_{12} & X_{13} \\ X_{21} & X_{22} & X_{23} \\ X_{31} & X_{32} & X_{33} \end{pmatrix} \\ \text{s.t} \quad & \Delta X_{31} + \omega^2(\overline{m}X_{31} + W\,\mathrm{diag}(X_{32})) = f \\ & \mathcal{S}X_{31} = d, \quad X_{11} = 1, \quad \boldsymbol{X} \succeq 0. \end{aligned} \tag{2}$$

This convex program has many feasible points besides the expected $\boldsymbol{X}_0 = ((1 \quad \mu^T \quad u^T)^T)^{\otimes 2}$ (where $\boldsymbol{v}^{\otimes 2}$ denotes $\boldsymbol{v}\boldsymbol{v}^T$). To restore uniqueness, but breaking convexity, we further impose $\mathrm{rank}(X) = 1$. Nonetheless, we now demonstrate that an appropriate algorithm can have a larger basin of attraction for (2) than for (1).

2 Low rank plus sparse algorithm

To solve (2), we propose an alternating scheme combining a sparse projection onto the intersection of the linear subspaces $\mathcal{V}_1$, $\mathcal{V}_2$, $\mathcal{V}_3$, with

$$\mathcal{V}_1 = \left\{\boldsymbol{X} \mid \Delta X_{31} + \omega^2\overline{m}X_{31} + \omega^2 W\,\mathrm{diag}(X_{32}) = f\right\}$$
$$\mathcal{V}_2 = \{\boldsymbol{X} \mid \mathcal{S}X_{31} = d\} \quad \text{and} \quad \mathcal{V}_3 = \{\boldsymbol{X} \mid X_{11} = 1\}$$

and a low-rank-plus-sparse projection onto the manifold of rank-1 positive semidefinite matrices. We let $\mathcal{V} := \mathcal{V}_1 \cap \mathcal{V}_2 \cap \mathcal{V}_3$ and let $X = RR^T$ with $R = (R_1^T \quad R_2^T \quad R_3^T)^T$.

Algorithm 1 Low-rank-plus-sparse backward-backward splitting

Require: Rank 1 matrix $\boldsymbol{X}^{(0)} = RR^T \in \mathbb{R}^{n\times n}$

1: **Repeat**
2: Get Y_{11}, Y_{31} and Y_{32}^{diag} components via $(Y_{11}, Y_{31}, Y_{32}^{\mathrm{diag}}) \leftarrow (R_1R_1^T, R_3R_1^T, \mathrm{diag}(R_3R_2^T))$
3: Update Y_{11}, Y_{31} and Y_{32}^{diag} components through a projection onto $\mathcal{V}$ (see 2.1). $(R; Y_{11}, Y_{31}, Y_{32}^{\mathrm{diag}}) \leftarrow \mathcal{P}_{\mathcal{V}}(R; Y_{11}, Y_{31}, Y_{32}^{\mathrm{diag}})$
4: Project onto the rank-1 manifold via Arnoldi iterations. $R \leftarrow \mathcal{P}_{\mathcal{M}_k}(R; Y_{11}, Y_{31}, Y_{32}^{\mathrm{diag}})$
5: Get μ through rounding from $\boldsymbol{X} = RR^T$ (see 2.2) .

2.1 Projection onto $\mathcal{V}$

We will only detail the projection onto $\mathcal{V}_1 \cap \mathcal{V}_2$ since the projection onto $\mathcal{V}_3$ is trivial and can be carried out independently.

Let A and b help represent the intersection $\mathcal{V}_1 \cap \mathcal{V}_2$ as

$$A = \begin{pmatrix} \mathcal{D} & \omega^2 W \\ \mathcal{S} & 0 \end{pmatrix} \qquad b = \begin{pmatrix} f \\ d \end{pmatrix},$$

where $\mathcal{D} = (\Delta + \omega^2 B)$, and $B = \mathrm{diag}(\overline{m})$. If we define $\boldsymbol{x} := (X_{31}^T \quad \mathrm{diag}(X_{32})^T)^T$, then $\boldsymbol{X} \in \mathcal{V}_1 \cap \mathcal{V}_2$ iff $A\boldsymbol{x} = b$. The projector $\boldsymbol{P}_{\mathcal{V}_1 \cap \mathcal{V}_2}$ onto $Ax = b$ only requires to invert the matrix AA^*. The update
$(R; Y_{11}, Y_{31}, Y_{32}^{\mathrm{diag}}) \leftarrow \mathcal{P}_{\mathcal{V}}(R; Y_{11}, Y_{31}, Y_{32}^{\mathrm{diag}})$
is defined through $R \leftarrow R$, $Y_{11} \leftarrow 1 - Y_{11}$,

$$\begin{pmatrix} Y_{31} \\ Y_{32}^{\mathrm{diag}} \end{pmatrix} \leftarrow (\boldsymbol{P}_{\mathcal{V}_1 \cap \mathcal{V}_2} - \boldsymbol{I}) \begin{pmatrix} Y_{31} \\ Y_{32}^{\mathrm{diag}} \end{pmatrix}$$

2.2 Rounding

Since the optimization problem (2) doesn't necessarily have a unique solution, and following the work of Barak, Kelner and Steurer [3], we also propose to round the output of (2) as follows: We extract the reflectivity from the X_{31} and X_{32} components by computing the least squares solution μ to the overdetermined system of equations $\mathrm{diag}(X_{31})\mu = \mathrm{diag}(X_{32})$. This idea comes from the observation that the rank-1 algorithm converges to the solution through iterates $\boldsymbol{X}_\alpha$ defined as $\boldsymbol{X}_\alpha = ((\alpha \quad \alpha\mu^T \quad u^T/\alpha)^T)^{\otimes 2}$, for which the X_{31} and X_{32} components of the matrix $\boldsymbol{X}$ turn out to be unaffected by the weight α.

3 Numerical Results

We propose to benchmark algorithm 1 on a simple 7×7 domain including a PML of 3 grid points, with background reflectivity $\overline{m} = 1$ and constant perturbation $\mu = \overline{\mu}$. We consider 4 frequencies and 4 sources, and we measure the field at 12 receivers located all around the domain. The frequencies ω_i are taken equispaced between 4.5 and 6. $\boldsymbol{X}$ is thus of size $n \times n$ where $n = 2874$. For such a framework, FWI (full waveform inversion, i.e., gradient descent on the nonlinear least-squares objective $\|\mathcal{S}u - d\|$) converges to a wrong local minimizer for perturbations $\overline{\mu} > 4.5$. Results are shown in Fig. 1 for $\overline{\mu} = 4.7$. In practice, we observe that (2) in combination with algorithm 1, and possibly FWI as a refinement step to reduce the computation time towards the end, leads to an increase of 30% in the basin of attraction over FWI.

We anticipate that more powerful relaxations, still based on (2) but using some other closure condition than $\mathrm{rank}(X) = 1$, would help further enlarge this basin of attraction.

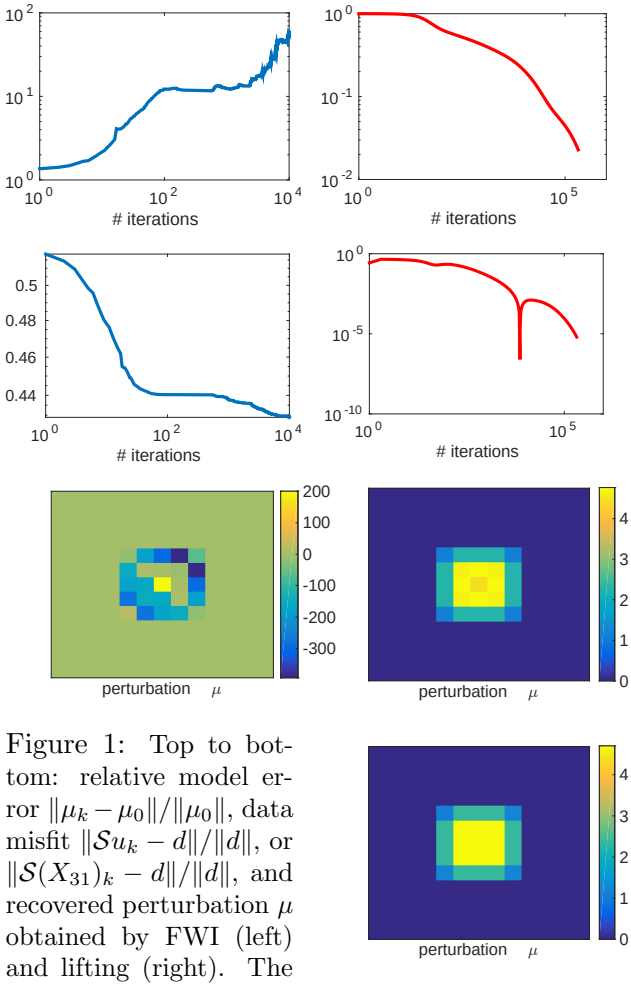

Figure 1: Top to bottom: relative model error $\|\mu_k - \mu_0\|/\|\mu_0\|$, data misfit $\|\mathcal{S}u_k - d\|/\|d\|$, or $\|\mathcal{S}(X_{31})_k - d\|/\|d\|$, and recovered perturbation μ obtained by FWI (left) and lifting (right). The last figure shows the unknown μ.

Acknowledgements

AC is funded by an FNRS grant. LD is funded by AFOSR, ONR, NSF, and Total SA.

References

[1] M. Laurent, Sums of squares, moment matrices and optimization over polynomials, *Emerging applications of algebraic geometry, Springer*, (2009), pp.157-270.

[2] L. Demanet and V. Jugnon. Convex recovery from interferometric measurements. *arXiv preprint arXiv:1307.6864*, (2013).

[3] B. Barak, J. Kelner, and D. Steurer. Rounding Sum-of-Squares Relaxations. *arXiv preprint arXiv:1312.6652*, (2013).

An Efficient FEM Model for Wave Propagation in Heterogeneous Media

M. Ganesh[1,*], C. Morgenstern [1]

[1]Department of Applied Mathematics and Statistics, Colorado School of Mines, CO 80401, USA

*Email: mganesh@mines.edu

Abstract

Propagation of acoustic waves in media containing obstacles with spatially varying interior material properties that are different to that of the exterior media can be modeled using the Helmholtz equation with non-constant refractive index coefficient, and the model is described in the unbounded media. Appropriate truncation of the exterior domain (including the heterogeneity) leads to the model problem with mixed interfaces. It is efficient to consider the artificial truncated boundary to be smooth and hence require finite element discretizations of domains with curved boundaries and in general non-smooth and non-convex interfaces. We describe and demonstrate a high-order approach to simulate such a mixed boundary heterogeneous media problem.

Keywords: Wave Propagation, Heterogeneity, Interfaces, FEM

1 Introduction

In this work we consider an efficient approach for simulation of scattered and absorbed time-harmonic acoustic waves in non-convex heterogeneous media with curved absorbing boundaries and non-smooth obstacles. Time-harmonic acoustic wave propagation, induced by a plane-wave (or a point-source) impinging on an obstacle, can be modeled using the non-constant coefficient Helmholtz partial differential equation (PDE) in an unbounded domain, see [1–3] and references therein.

The unbounded domain comprises the exterior to and also the interior of the obstacle, in case it has a penetrable boundary. The PDE is supplemented with a transmission condition at the interface in the penetrable case or the Dirichlet/Neumann condition on the boundary of the sound–soft/hard obstacle. The unbounded domain nature of the model problem requires that the unknown scattered field satisfies a radiation condition [1–3, 5].

In the case of homogeneous media, the radiation condition can be exactly satisfied using a boundary integral equation (BIE) reformulation of the constant coefficient Helmholtz PDE [3]. This is obtained by representing the scattered field using the fundamental solution and an unknown density that needs to be computed only on the bounded boundary.

Computer modeling of the inhomogeneous media problem requires truncation of the unbounded domain, using an absorbing boundary condition on the artificial truncated boundary. The absorbing boundary conditions are typically a first-order approximation of the radiation condition or its high-order variant. We refer to the recent work [1, 2, 5] and extensive references therein for further details.

For the heterogeneous obstacle media model, the literature is dominated by considering the Helmholtz PDE in a bounded domain Ω with an absorbing boundary condition and a standard (low-order) finite element method (FEM) to design a discrete computer model of the problem. For implementation of the FEM model, it is also standard to avoid mixed (comprising curved, non-smooth, and non-convex) boundaries, and simulations are based on low-order continuous ($\mathscr{C}^0$) piecewise linear FEM approximations applied to model problems with convex polygonal domains.

Further, to avoid the pollution effect in the standard FEM model, to obtain even low-order (1%) accuracy, at least 10 discretization points in each dimension per wavelength are required. This leads to large linear systems for high frequency problems, especially for the low-order FEM. Large linear systems require iterative solvers, and hence development of preconditioners is necessary. Such a development is complicated further by the fact that the standard FEM formulations of the Helmholtz problems are sign-indefinite [1, 2, 5].

The recent work [5] proposes a variational formulation to avoid the celebrated sign-indefinite issue by incorporating additional operators in the standard models. The yet to be explored FEM approximations and implementation need to be sought in finite dimensional subspaces spanned by $\mathscr{C}^1$ splines. In a future work, we shall consider computational validation of the formulation in [5] and compare with the standard sign-indefinite FEM formulation.

2 A high-order computer model

In this work, we consider the Helmholtz model problem in a bounded domain Ω that comprises mixed (curved, non-smooth, and non-convex) boundaries such as that visualized in Fig. 1. The outer curved boundary in the figure represents the artificial truncation of the unbounded domain on which we impose an absorbing boundary condition [1].

The non-smooth and non-convex boundary in the figure represents the boundary of an elongated penetrable object that induces the inhomogeneity in the media. For the general model problem, we choose the artificial boundary to be a close fit to a general non-convex and non-smooth scattering object, surrounding the inhomogeneity so that the unbounded media exterior to the curved boundary is homogeneous [2].

We develop a high-order accurate computer model of the Helmholtz problem on such domains for wide range of frequencies using spline basis functions with various smoothness properties $\mathscr{C}^\ell$ with $\ell = 0, 1, 2, \cdots$. In a future work, we shall combine the advantage of using the BIE reformation in the exterior homogeneous media with that proposed in this work for the heterogeneous media, to develop a FEM–BEM computer model that satisfies the radiation condition exactly.

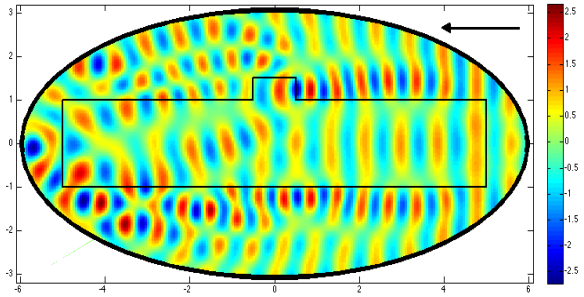

Figure 1: *The real part of the FEM approximation total field u with* 15 *wavelengths per diameter of* Ω *with an absorbing condition on the exterior curved boundary and an interface condition on the interior non-convex boundary of a penetrable object. The direction of the incident wave is shown by the arrow*

Construction of standard basis spline (B-spline) functions on a triangular mesh with various $\mathscr{C}^\ell$ smoothness properties on domains such as those in Fig. 1 is difficult. Consequently, standard FEM formulations with $\mathscr{C}^0$ smoothness are used for typical implementations that avoid mixed boundaries such as that in Fig. 1.

The meshless weight extended B-splines (WEB-splines) [4] approach provides a remedy to this situation, including construction of splines with high degree and smoothness without substantial increase in degrees of freedom (DoF).

We describe and demonstrate a WEB-spline based high-order FEM for the heterogeneous wave propagation model and show that the high-order approximations facilitate simulation of a wide range of frequencies with few DoF.

For our implementation, instead of achieving high-order accuracy by increasing the degrees of freedom in the FEM model, we increase the degree p of the WEB-spline functions to achieve high-order accuracy with relative few DoF. This allows for the DoF to be kept small enough to use a direct solve and avoids the need for iterative methods and preconditioners for the poorly conditioned Helmholtz systems which additionally have larger condition numbers when the aspect ratio of the domain and/or the frequency is large.

References

[1] M. Ganesh and C. Morgenstern, An Efficient Multigrid Algorithm for Heterogeneous Acoustic Media Sign-indefinite High-Order FEM Models, *Pre-print* (2015).

[2] M. Ganesh and C. Morgenstern, High-Order FEM-BEM Computer Models for Wave Propagation in Unbounded and Heterogeneous Media: Application to the Acoustic Horn Problem, *Pre-print* (2015).

[3] D. Colton and R. Kress, Inverse Acoustic and Electromagnetic Scattering Theory. Springer, 2012.

[4] K. Höllig, Finite Element Methods with B-Splines. Frontiers in Applied Mathematics, SIAM, 2003.

[5] A. Moiola and E.A. Spence, Is the Helmholtz Equation Really Sign-indefinite? *SIAM Review*, **56** (2014), pp. 274-312.

A nonconforming substructuring method for first-order systems of time-dependent PDEs in space-time

Johannes Ernesti[1,*], **Christian Wieners**[1]
[1]KIT, Institute of Applied and Numerical Mathematics, Karlsruhe, Germany
[*]Email: johannes.ernesti@kit.edu

Abstract

We introduce a novel substructuring discretization scheme for first order systems in space-time. It is based on a skeleton reduction procedure related to the recently introduced discontinuous Petrov-Galerkin (DPG) methods. While being applicable to a variety of problems, the substructuring approach is flexible with respect to the selection of trial and test spaces allowing for problem-specific nonconforming choices with desired approximation and conservation properties. The scheme yields a discrete equation that can be solved in two steps, where first a representation of the solution restricted to the skeleton is obtained by solving a symmetric positive definite linear system. In a second step the approximate solution on each cell is reconstructed from the skeleton values. As a model problem, we consider the linear acoustic wave equation on a bounded interval in one dimension formulated as a first order system. We compare the performance of various discretization schemes, e.g., leap-frog finite differences, space-time LSFEM of different orders, to the new substructuring approach.

Keywords: Nonconforming finite elements, space-time methods, acoustic wave equation

1 Introduction

We consider the linear acoustic wave equation described by the first-order differential operator

$$L(p,q) = (\partial_t p + \nabla \cdot q, \partial_t q + \nabla p)$$

on $Q = \Omega \times (0,T) \subset \mathbb{R}^D \times \mathbb{R}$ with domain

$$D(L) \subset \mathrm{L}_2\big((0,T),H\big) \cap \mathrm{H}^1\big((0,T),\mathrm{L}_2(\Omega)^{D+1}\big)$$

with $H \subset \mathrm{H}^1\big(\Omega\big) \times \mathrm{H}(\mathrm{div},\Omega\big)$.

Let V be the closure of $D(L)$ with respect to the graph norm $\|u\|_L = \sqrt{\|u\|_Q + \|Lu\|_Q}$, where $\|\cdot\|_Q$ denotes the norm in $\mathrm{L}_2(Q)^{D+1}$. Based on a decomposition of Q into space-time cells $R \in \mathcal{R}$, we define local discrete ansatz spaces V_R and local trace operators $\gamma_R, \gamma_R^{\mathrm{ad}}$ with

$$(Lu,v)_R - (u,L^{\mathrm{ad}}v)_R = \langle \gamma_R u, \gamma_R^{\mathrm{ad}} v\rangle\,,$$

where $L^{\mathrm{ad}} = -L$ is the adjoint operator with domain $D(L^{\mathrm{ad}})$. For acoustic waves we have on a space-time cell $R = K \times (t_{n-1},t_n)$

$$\begin{aligned}\langle \gamma_R(p,q), \gamma_R^{\mathrm{ad}}(\phi,\psi)\rangle = \\ \big((p,q),(\phi,\psi)\big)_{K\times\{t_n\}} - \big((p,q),(\phi,\psi)\big)_{K\times\{t_{n-1}\}} \\ + \big\langle (p,q\cdot n),(\psi\cdot n,\phi)\big\rangle_{\partial K\times(t_{n-1},t_n)}\,.\end{aligned}$$

We introduce a discretization with degrees of freedom on the skeleton $\Gamma = \bigcup \partial R$, where the local approximation in R is reconstructed by minimal residuals. The method is very flexible with respect to the choice of the minimal residuals functional, the local discrete ansatz spaces and the skeleton degrees of freedom. Our aim is to find a nonconforming finite element setting which is reliable and efficient also in case of weak solutions with jumps.

2 The substructuring method

Depending on a conforming approximation space $W_h \subset D(L^{\mathrm{ad}})$ we define the nonconforming space

$$V_h = \Big\{ v_h \in \prod V_R \colon \langle \gamma v_h, \gamma^{\mathrm{ad}} w\rangle = 0\,,\ w \in W_h \Big\}$$

with $\langle \gamma v_h, \gamma^{\mathrm{ad}} w_h\rangle = \sum_R \langle \gamma_R v_h|_R, \gamma_R^{\mathrm{ad}} w_h|_R\rangle$. We set $V_{\mathcal{R}} = \prod V_R$, $W_{\mathcal{R}} = \prod W_R$ with $W_R = W_h|_R$, and we define the trace $\gamma_{\mathcal{R}} \in \mathcal{L}(V_{\mathcal{R}}, W_{\mathcal{R}}')$ by

$$\langle \gamma_{\mathcal{R}} v_h, w_h\rangle = \Big(\langle \gamma_R v_h|_R, \gamma_R^{\mathrm{ad}} w_h|_R\rangle\Big)_{R\in\mathcal{R}}\,,$$

and the trace space as $\hat{V}_h = \gamma_{\mathcal{R}}(V_h)$, respectively. For given trace data $\hat{v}_h \in \hat{V}_h$ we define

$$\begin{aligned}V_R(\hat{u}_h) = \big\{ v_R \in V_R \colon \\ \langle \gamma_R v_R - \hat{u}_h|_R, \gamma_R^{\mathrm{ad}} w_R\rangle\,,\ w_R \in W_R\big\}\,.\end{aligned}$$

The nonconforming approximation on the skeleton is the minimizer $\hat{u}_h = (\hat{u}_R)_R \in \hat{V}_h$ of

$$J_h(\hat{v}_h) = \sum_R \inf_{v_R \in V_R(\hat{v}_h)} J_R(v_R) \qquad (1)$$

with, e.g., $J_R(u_R) = \frac{1}{2}\|Lu_R - f\|_R^2$.

For the solution of this problem we derive an equivalent saddle point problem. Let A_R, B_R and C_R be linear operators and ℓ_R a linear functional with

$$J_R(v_R) = \frac{1}{2}\langle A_R v_R, v_R\rangle - \langle \ell_R, v_R\rangle\,,$$
$$\langle B_R w_R, v_R\rangle = \langle \gamma_R v_R, \gamma_R^{\mathrm{ad}} w_R\rangle\,,$$
$$\langle C_R \hat{v}_h, w_R\rangle = \langle \hat{v}_R, \gamma_R^{\mathrm{ad}} w_R\rangle\,.$$

Then, the minimizer of (1) is characterized by

$$\begin{aligned} A_R u_R - \ell_R + B_R \mu_R &= 0\,, \\ B_R' u_R - C_R \hat{u}_h &= 0 \end{aligned}$$

for all R and

$$\sum_R C_R' \mu_R = 0\,.$$

This yields locally $(u_R, \mu_R) \in V_R \times W_R$ solving

$$\begin{pmatrix} A_R & B_R \\ B_R' & 0 \end{pmatrix} \begin{pmatrix} u_R \\ \mu_R \end{pmatrix} = \begin{pmatrix} \ell_R \\ C_R \hat{u}_h \end{pmatrix}$$

and the skeleton solution $\hat{u}_h \in \hat{V}_h$ of the global Schur complement problem $\hat{S}_h \hat{u}_h = \hat{\ell}_h$ with

$$\hat{S}_h = \sum_R \begin{pmatrix} 0 \\ C_R \end{pmatrix}' \begin{pmatrix} A_R & B_R \\ B_R' & 0 \end{pmatrix}^{-1} \begin{pmatrix} 0 \\ C_R \end{pmatrix},$$
$$\hat{\ell}_h = \sum_R \begin{pmatrix} 0 \\ C_R \end{pmatrix}' \begin{pmatrix} A_R & B_R \\ B_R' & 0 \end{pmatrix}^{-1} \begin{pmatrix} \ell_R \\ 0 \end{pmatrix}.$$

Provided inf-sup stability for the saddle point discretization, the Schur complement reduction is well defined.

3 Numerical results

We consider $Q = (0,1) \times (0,T)$, homogeneous boundary conditions $p(0,t) = p(1,t) = 0$, $t > 0$, and initial conditions $p(x,0) = 1$ and $q(x,0) = 0$ for $x \in (0,1)$. The exact solution is given by

$$p(x,t) = \frac{1}{2}\big(p_0(x+t) + p_0(x-t)\big)$$

with $p_0(x) = \begin{cases} 1 & x \in (0,1) + 2\mathbb{Z} \\ 0 & x \in \mathbb{Z} \\ -1 & x \in (-1,0) + 2\mathbb{Z} \end{cases}$

cf. [4]. Observe that p is piecewise constant and that $p \in \mathrm{BV}(Q)$. For this model problem, we compare standard discretization methods to the new substructuring method, see Fig. 2–4. We choose $T \approx 8$ and wave speed $c = 1$ so that the jumps are not aligned with the mesh. All discretizations shown in the figures use approximately 83500 global DoFs.

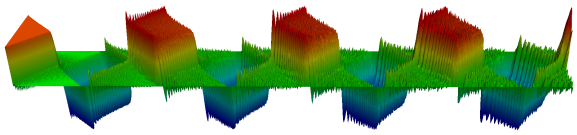

Figure 1: A simple explicit leap-frog method generates oscillations which grow in time.

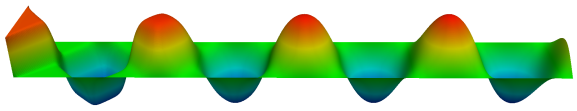

Figure 2: Simple $\mathbb{Q}_1$-space-time least-squares produces a strongly diffusive approximation.

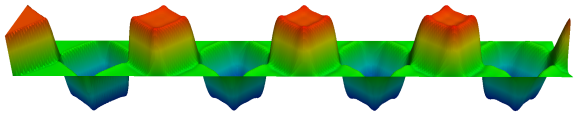

Figure 3: The $\mathbb{Q}_2$-least-squares approach shows Gibbs phenomenon at the jump while being diffusive.

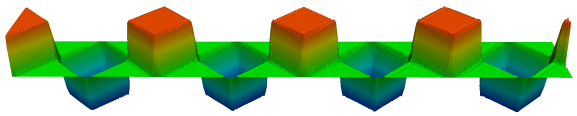

Figure 4: Using $V_R = (\mathbb{P}_3 \otimes \mathbb{P}_3) \times (\mathbb{P}_3 \otimes \mathbb{P}_3)$ and $W_R = (\mathbb{P}_3 \times \mathbb{P}_2) \times (\mathbb{P}_3 \times \mathbb{P}_2)$ in the substructuring method improves the above approximations.

References

[1] C. Wieners. A geometric data structure for parallel finite elements and the application to multigrid methods. *Comput. Vis. Sci.*, 13(4):161–175, 2010.

[2] L. F. Demkowicz, J. Gopalakrishnan. An Overview of the Discontinuous Petrov Galerkin Method. *Recent Developments in Discontinuous Galerkin Finite Element Methods for Partial Differential Equations*, pages 149–180, Springer, 2014.

[3] C. Wieners and B. Wohlmuth. Robust operator estimates and the application to substructuring methods for first-order systems. *ESAIM: Mathematical Modelling and Numerical Analysis*, 48(5):161–175, 2014.

[4] R. Leis. *Initial boundary value problems in mathematical physics.* Teubner, 1986.

Material derivatives of the boundary integral operators arising from time-harmonic electromagnetic potential theory and applications

Frédérique Le Louër[1,*]

[1]Sorbonne Université, Université de technologie de Compiègne, LMAC EA2222 Laboratoire de mathématiques appliquées de Compiègne - CS 60 319 - 60 203 Compiègne cedex, France

[*]Email: frederique.le-louer@utc.fr

Abstract

We present new results on the differentiability analysis of boundary integral operators with respect to the shape of the boundary in electromagnetism. Our approach simplifies previous investigations based on either projection operators [7] or the Hodge decomposition of the space of tangential vector fields of mixed regularity $\mathbf{H}_{\mathrm{div}}^{-\frac{1}{2}}(\Gamma)$ [2].

Keywords: Maxwell equation, boundary integral operators, Piola transform, material derivatives

1 Introduction

Consider the scattering of time-harmonic electromagnetic waves by a perfect conductor (PC) Ω in $\mathbb{R}^3$ with a smooth closed boundary Γ which is diffeomorphic to a sphere. Let Ω^c denote the exterior domain $\mathbb{R}^3\backslash\overline{\Omega}$ and $\boldsymbol{n}$ denote the outer unit normal vector to the boundary Γ. Let $\kappa > 0$ denote the exterior wavenumber. The PC problem is formulated as follows [1, 6] : Given an incident electric wave $\boldsymbol{E}^{\mathrm{inc}}$, find the scattered field $\boldsymbol{E}^{\mathrm{s}}$ satisfying the second order Maxwell equation $\mathbf{rotrot}\boldsymbol{E}^{\mathrm{s}} - \kappa^2\boldsymbol{E}^{\mathrm{s}} = 0$ in Ω^c, the boundary condition $\boldsymbol{n} \times (\boldsymbol{E}^{\mathrm{s}} + \boldsymbol{E}^{\mathrm{inc}}) = 0$ on Γ and the Silver-Müller radiation condition: $\left|\mathbf{rot}\boldsymbol{E}^{\mathrm{s}}(\mathbf{x})\times\mathbf{x} - i\kappa|\mathbf{x}|\boldsymbol{E}^{\mathrm{s}}(\mathbf{x})\right| \overset{|\mathbf{x}|\to+\infty}{\longrightarrow} 0$. This problem can be reduced in several different ways to a uniquely solvable modified combined field boundary integral equation (M-CFIE) [1].

The radiation condition implies that the scattered field $\boldsymbol{E}^s$ has an asymptotic behavior of the form $\boldsymbol{E}^s(\mathbf{x}) = \frac{e^{i\kappa|\mathbf{x}|}}{|\mathbf{x}|}\boldsymbol{E}^\infty(\widehat{\mathbf{x}}) + O\left(\frac{1}{|\mathbf{x}|}\right)$ when $|\mathbf{x}| \to \infty$, uniformly in all directions $\widehat{\mathbf{x}} = \frac{\mathbf{x}}{|\mathbf{x}|}$.

We denote by F the boundary to far-field operator that maps the boundary Γ onto the far-field pattern $\boldsymbol{E}^\infty$. The inverse PC problem is formulated as follows: Given noisy far field measurements $\boldsymbol{E}_\delta^\infty$, solve

$$\text{(IP)} \qquad F(\Gamma) = \boldsymbol{E}_\delta^\infty.$$

Here, the index δ denotes the noise level and is assumed to be known.

In the scientific litterature, one can distinguish two different approaches relying on domain derivatives to solve such an inverse problem in acoustic scattering. The first one consists in reformulating (IP) as a nonlinear equation posed on an open set of parametrized boundaries. Then, we apply an iteratively regularized Newton-type method to the nonlinear equation via first order linearization e.g. [3]. The algorithm requires the numerical solution of CFIEs at each iteration step to obtain the Fréchet derivative of F in any direction. The second one consists in reformulating (IP) as a pair of nonlinear and ill-posed integral equations for the unknown boundary representing the incoming wave and the far-field pattern e.g. [5]. Then, we follow the previous procedure to recover simultaneously the unknown parametrization of the boundary and the density. The algorithm requires the computation of the material derivatives of some boundary integral operators. The first approach has been recently applied to electromagnetism by Hohage and Le Louër [4]. The second approach has the advantage to avoid the numerical solution of CFIEs at each iteration step. Its extension to the inverse PC problem requires, before all, the differentiability analysis of the standard electromagnetic boundary integral operators with respect to the parametrization of the boundary. In Section 2 we recall the mapping properties of these operators and discuss the difficulty of the whole analysis. In Section 3, we show how to tackle the problem using the Piola transform of the parametrizations.

2 The boundary integral operators

We introduce the following Hilbert space : $\mathbf{H}_{\mathrm{div}}^{-\frac{1}{2}}(\Gamma) = \{\boldsymbol{j} \in \mathbf{H}_{\mathrm{div}}^{-\frac{1}{2}}(\Gamma);\ \boldsymbol{j}\cdot\boldsymbol{n} = 0,\ \mathrm{div}_\Gamma\,\boldsymbol{j} \in H^{-\frac{1}{2}}(\Gamma)\}$. Let $\Phi(\kappa, \mathbf{z}) = \frac{e^{i\kappa|\mathbf{z}|}}{4\pi|\mathbf{z}|}$. The single layer potential operator is defined for $\boldsymbol{j} \in \mathbf{H}_{\mathrm{div}}^{-\frac{1}{2}}(\Gamma)$ and $\mathbf{x} \in \Gamma$

by

$$C_\kappa \boldsymbol{j}(\mathbf{x}) = \frac{1}{\kappa}\int_\Gamma \boldsymbol{n}(\mathbf{x}) \times \mathbf{curl}\,\mathbf{curl}^{\mathbf{x}}\{\Phi(\kappa, \mathbf{x}-\mathbf{y})\boldsymbol{j}(\mathbf{y})\}ds(\mathbf{y}).$$

The double layer potential operator is defined by

$$M_\kappa \boldsymbol{j}(\mathbf{x}) = \int_\Gamma \boldsymbol{n}(\mathbf{x}) \times \mathbf{curl}^{\mathbf{x}}\{\Phi(\kappa, \mathbf{x}-\mathbf{y})\boldsymbol{j}(\mathbf{y})\}ds(\mathbf{y}).$$

The operator $M_\kappa : \mathbf{H}_{\mathrm{div}}^{-\frac{1}{2}}(\Gamma) \to \mathbf{H}_{\mathrm{div}}^{-\frac{1}{2}}(\Gamma)$ is compact and the operator C_κ has a hypersingular kernel but is bounded on $\mathbf{H}_{\mathrm{div}}^{-\frac{1}{2}}(\Gamma)$.

We define an open set of admissible variations $\mathcal{X} \subset \{\boldsymbol{q} \in \mathscr{C}^1(\Gamma_{\mathrm{ref}}, \mathbb{R}^3);\ \Gamma_{\boldsymbol{q}} = \boldsymbol{q}(\Gamma_{\mathrm{ref}})$ *is diffeomorphic to* $\Gamma_{\mathrm{ref}}\}$, where Γ_{ref} is a fixed reference boundary, e.g. a sphere. The operators C_κ and M_κ are now considered as operators acting from $\mathcal{X}$ to the space of linear operators $\mathscr{L}(\mathbf{H}_{\mathrm{div}}^{-\frac{1}{2}}(\Gamma_{\boldsymbol{q}}), \mathbf{H}_{\mathrm{div}}^{-\frac{1}{2}}(\Gamma_{\boldsymbol{q}}))$. Their differentiability analysis poses non trivial problems because the operators $C_\kappa(\boldsymbol{q})$ and $M_\kappa(\boldsymbol{q})$ are both defined on the $\boldsymbol{q}$-dependent space $\mathbf{H}_{\mathrm{div}}^{-\frac{1}{2}}(\Gamma_{\boldsymbol{q}})$.

3 The Piola transform

The (3×3) matrix $[\mathbf{D}_{\Gamma_{\mathrm{ref}}}\boldsymbol{q}(\mathbf{x})] = {}^{\mathsf{T}}[\boldsymbol{\nabla}_{\Gamma_{\mathrm{ref}}}\boldsymbol{q}(\mathbf{x})]$ maps the tangent plane to Γ_{ref} at the point $\mathbf{x}$ onto the tangent plane to $\Gamma_{\boldsymbol{q}}$ at the point $\boldsymbol{q}(\mathbf{x})$. We set $[\mathbf{D}_{\Gamma_{\mathrm{ref}}}\boldsymbol{q}]^{-1} = [\mathbf{D}_{\Gamma_{\boldsymbol{q}}}\boldsymbol{q}^{-1}] \circ \boldsymbol{q}$. To remove the $\boldsymbol{q}$-dependence of the operators domain, we transport these boundary integral operators on the reference boundary Γ_{ref} by means of the Piola transform of $\boldsymbol{q}$. It is an invertible and bi-continuous operator defined as follows [4, Lemma 3.1]:

$$\begin{array}{rccc} \mathcal{P}_{\boldsymbol{q}}: & \mathbf{H}_{\mathrm{div}}^{-\frac{1}{2}}(\Gamma_{\boldsymbol{q}}) & \longrightarrow & \mathbf{H}_{\mathrm{div}}^{-\frac{1}{2}}(\Gamma_{\mathrm{ref}}) \\ & \boldsymbol{j}_{\boldsymbol{q}} & \mapsto & \boldsymbol{j} = J_{\boldsymbol{q}}[\mathbf{D}_{\Gamma_{\mathrm{ref}}}\boldsymbol{q}]^{-1}(\boldsymbol{j}_{\boldsymbol{q}} \circ \boldsymbol{q}), \end{array}$$

where $J_{\boldsymbol{q}}$ is the determinant of the jacobian matrix of the change of variable $\mathbf{x} \mapsto \boldsymbol{q}(\mathbf{x})$.
This allows us to use the following identities stated in [4]: $\mathcal{P}_{\boldsymbol{q}}(\mathbf{curl}_{\Gamma_{\boldsymbol{q}}} u) = \mathbf{curl}_{\Gamma_{\mathrm{ref}}}(u \circ \boldsymbol{q})$ and $J_{\boldsymbol{q}}(\mathrm{div}_{\Gamma_{\boldsymbol{q}}} \boldsymbol{v}) \circ \boldsymbol{q} = \mathrm{div}_{\Gamma_{\mathrm{ref}}}\big(\mathcal{P}_{\boldsymbol{q}}\boldsymbol{v}\big)$. The parametrized boundary integral operators $\mathcal{M}_\kappa := \mathcal{P}_{\boldsymbol{q}} M_\kappa(\boldsymbol{q}) \mathcal{P}_{\boldsymbol{q}}^{-1}$ and $\mathcal{C}_\kappa := \mathcal{P}_{\boldsymbol{q}} C_\kappa(\boldsymbol{q}) \mathcal{P}_{\boldsymbol{q}}^{-1}$ take the form

$$\mathcal{M}_\kappa \boldsymbol{j}(\mathbf{x}) = \boldsymbol{n}(\mathbf{x}) \times \int_{\Gamma_{\mathrm{ref}}} {}^{\mathsf{T}}\mathbf{D}_{\boldsymbol{q}(\mathbf{x})}\{\boldsymbol{\nabla}\Phi(\kappa, \boldsymbol{q}(\mathbf{x}) - \boldsymbol{q}(\mathbf{y})) \times \mathbf{D}_{\boldsymbol{q}(\mathbf{y})}\boldsymbol{j}(\mathbf{y})\}ds(\mathbf{y}),$$

$$\begin{aligned} \mathcal{C}_\kappa \boldsymbol{j}(\mathbf{x}) = {} & \kappa\, \boldsymbol{n}(\mathbf{x}) \times \int_{\Gamma_{\mathrm{ref}}} {}^{\mathsf{T}}\mathbf{D}_{\boldsymbol{q}(\mathbf{x})} \Phi(\kappa, \boldsymbol{q}(\mathbf{x}) - \boldsymbol{q}(\mathbf{y})) \mathbf{D}_{\boldsymbol{q}(\mathbf{y})}\boldsymbol{j}(\mathbf{y}) ds(\mathbf{y}) \\ & - \frac{1}{\kappa}\, \mathbf{curl}_{\Gamma_{\mathrm{ref}}} \int_{\Gamma_{\mathrm{ref}}} \Phi(\kappa, \boldsymbol{q}(\mathbf{x}) - \boldsymbol{q}(\mathbf{y}))\, \mathrm{div}_{\Gamma_{\mathrm{ref}}} \boldsymbol{j}(\mathbf{y}) ds(\mathbf{y}), \end{aligned}$$

where $\boldsymbol{j} \in \mathbf{H}_{\mathrm{div}}^{-\frac{1}{2}}(\Gamma_{\mathrm{ref}})$, $\boldsymbol{n}$ is the outer unit normal vector to Γ_{ref} and $\mathbf{D}_{\boldsymbol{q}(\mathbf{x})} = [\mathbf{D}_{\Gamma_{\mathrm{ref}}}\boldsymbol{q}(\mathbf{x})]$ for any $\mathbf{x} \in \Gamma_{\mathrm{ref}}$. We are led to compute the material derivatives of some integral operators with a weakly singular kernel.

4 Conclusion and future work

Contrary to the previous investigations in [2], we do not have to compute the Fréchet derivatives of the surface differential operators [6, pp. 68-75]. Moreover, the use of the Piola transform allows us to consider regularizing operators in the M-CFIE which do not depend on the boundary $\Gamma_{\boldsymbol{q}}$. It considerably reduces the expression of the material derivatives of the integral equation operator by comparison to [7].

The application of the whole analysis to develop *a nonlinear integral equation method for solving electromagnetic inverse obstacle scattering problems* is a joint project in progress with O. Ivanyshyn Yaman from Izmir Institute of Technology.

References

[1] D. Colton and R. Kress, *Inverse acoustic and electromagnetic scattering theory*, vol. 93 of Applied Mathematical Sciences, Springer-Verlag, Berlin, second ed., 1998.

[2] M. Costabel and F. Le Louër, *Shape derivatives of boundary integral operators in electromagnetic scattering. Part II: Application to scattering by a homogeneous dielectric obstacle*, IEOT, 72 (2012), pp. 509–535.

[3] T. Hohage, *Iterative Methods in Inverse Obstacle Scattering: Regularization Theory of Linear and Nonlinear Exponentially Ill-Posed Problems*, PhD thesis, 1999.

[4] T. Hohage and F. Le Louër, *A spectrally accurate method for the dielectric obstacle scattering problem and applications to the inverse problem*, preprint, (2013).

[5] O. Ivanyshyn and T. Johansson, *Nonlinear integral equation methods for the reconstruction of an acoustically sound-soft obstacle*, JIEA, 19 (2007), pp. 289–308.

[6] J.-C. Nédélec, *Acoustic and electromagnetic equations*, vol. 144 of Applied Mathematical Sciences, Springer-Verlag, New York, 2001. Integral representations for harmonic problems.

[7] R. Potthast, *Domain derivatives in electromagnetic scattering*, M2AS, 19 (1996), pp. 1157–1175.

Matched asymptotics approach to the construction and justification of reduced graph models for 3D Maxwell's equations in networks of thin co-axial cables

Geoffrey Beck[1,*], **Sébastien Imperiale**[2], **Patrick Joly**[3]

[1]Inria, POems - CNRS:UMR7231 - ENSTA ParisTech, 828 Boulevard des Maréchaux, 91762 Palaiseau, France

[2]Inria, MΞDISIM, Alan Turing, 1 rue Honoré d'Estienne d'Orves, 91120 Palaiseau, France

[3]Inria, POems - CNRS:UMR7231 - ENSTA ParisTech

[*]Email: geoffrey.beck@ensta-paristech.fr

Abstract

We consider electromagnetic wave propagation in domains constituted by thin coaxial cables (made of a dielectric material which surrounds a metallic inner-wire) and a small junction. The goal is to trim down $3D$ Maxwell's equations in this complicated geometry to a quantum graph (see [3]) in which, along each edge, one is reduced to compute the electrical potential and current a by solving wave equations (the telegrapher's model) coupled by vertex conditions. In this work, using the method of matched asymptotics, we propose improved Kirchhoff conditions and we give a rigorous justification of such a model reduction.

Keywords: Maxwell's equations, telegrapher's equation, matched asymptotics, quantum graph.

1 The geometry

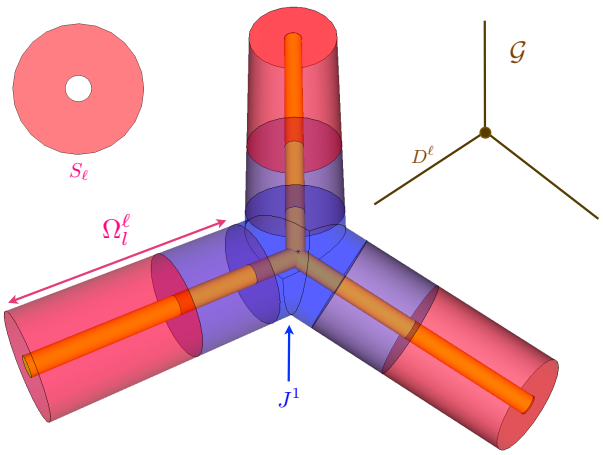

Figure 1: The refernce domain Ω^1 (center) the limit graph $\mathcal{G}$ (right) and a cross-section S_ℓ (left)

We consider a domain Ω^δ, with $\delta > 0$, which is homothetic to a (unbounded) reference domain namely

$$\Omega^\delta = \delta\, \Omega^1 \tag{1}$$

as described in Figure 1 where Ω^1 is the connected union of $(L+1)$ semi-infinite cables Ω^1_ℓ $(\ell = 0...L)$ and a bounded junction J^1 as illustrated by Figure 1. More precisely, each Ω_ℓ is isomorphic to $S^\ell \times \mathbb{R}^+$, where S_ℓ is a non simply connected bounded domain of $\mathbb{R}^2$ with one single hole. The "small" parameter δ refers to the thinness of the propagation domain. When $\delta \to 0$, Ω^δ converges to a graph $\mathcal{G}$, union of L half-lines D_ℓ. In the following, we denote $x_3^\ell \geq 0$ the abscissa along D_ℓ and $x_T^\ell = (x_1^\ell, x_T^\ell)$ associated transverse coordinates.

$$\Omega^\delta_\ell = \left\{ (\delta\, x_T^\ell, x_3^\ell) \,|\, (x_T^\ell, x_3^\ell) \in \Omega^1_\ell \right\}$$

We are interested in the solution (E^δ, H^δ) of lossy 3D-Maxwell's equations in this domain, with constant coefficients for simplicity, and perfectly conducting boundary conditions along $\partial\Omega^\delta$. More precisely we wish to describe the behavior of this solution for small δ from the solution of a 1D "effective model" on the limit graph.

2 The reduced model

We describe below only the behavior of the electromagnetic fields in the $(L+1)$ cables:

$$\begin{aligned} E^\delta(x_T^\ell, x_3^\ell, t) &\sim V_\ell^\delta(x_3^\ell, t)\, \nabla\varphi^\ell\left(\frac{x_T}{\delta}\right) \\ H^\delta(x_T^\ell, x_3^\ell, t) &\sim I_\ell^\delta(x_3^\ell, t)\, \nabla\psi^\ell\left(\frac{x_T}{\delta}\right) \end{aligned} \tag{2}$$

where the harmonic potentials φ^ℓ and ψ^ℓ are defined by elliptic problems in S^ℓ (see [1]). The electrical potential V^ℓ and current I^ℓ are solutions of the telegrapher's equation ($\partial_\ell \equiv \partial/\partial x_3^\ell$):

$$\left\{ \begin{array}{l} \left(C^\ell\, \partial_t + G^\ell\right) \mathbf{V}_\ell^\delta + \partial_\ell\, \mathbf{I}_\ell^\delta = 0, \\ \left(L^\ell\, \partial_t + R^\ell\right) \mathbf{I}_l^\delta + \partial_\ell\, \mathbf{V}_\ell^\delta = 0, \end{array} \right. \quad \text{on } D_\ell \tag{3}$$

where $C^\ell > 0, G^\ell \geq 0$ are explicity given in term of φ^ℓ, the permittivity ε and the electric conductivity σ_e while $L^\ell > 0, R^\ell \geq 0$ are explicity given in terms of ψ^ℓ, the permeability μ and the magnetic conductivity σ_m. The system has to be completed by vertex conditions.

At first order, these are the Kirchoff's laws

$$V_\ell^\delta(0,t) - V_0^\delta(0,t) = 0, \quad \sum_{\ell=0}^{L} I_\ell^\delta(0,t) = 0. \quad (4)$$

A better accuracy is obtained with second order conditions, namely **improved Kirchhoff laws**

$$\begin{aligned} &V_\ell^\delta(0,t) - V_0^\delta(0,t) = \delta \sum_{\ell'=1}^{L} Z^{\ell,\ell'}\, \mathbf{I}_{\ell'}^\delta(0,t), \\ &\sum_{\ell=1}^{L} I_\ell^\delta(0,t) + \delta\, Y\, V_0^\delta(0,t) = 0. \end{aligned} \quad (5)$$

where the coefficient Y and the $L \times L$ matrix $\mathbf{Z} = \left(Z^{\ell,\ell'}\right)$ are defined from the material properties of the medium and from 3D potentials Φ and $\{\, \Psi_\ell,\, 1 \leq \ell \leq L\}$ defined in the reference domain Ω^1. These potentials are the solutions of elliptic equations in Ω^1 that are constrained to satisfy a specific non homogeneous behavior at infinity inside each cable Ω^1 (and, concerning the Ψ_ℓ's, non homogeneous jump conditions across L artificial cuts).

Note that the condition (4) only sees the structure of the limit graph while (5) also takes into account (partly) the geometry of the junction.

3 The method of analysis

The derivation of (3) and (4) or (5) relies on a preliminary asymptotic expansion of the solution. Since the problem is of multi-scale nature, a uniform asymptotic expansion in the whole domain is not possible. We use the method of matched asymptotics, as in [2] for a simpler scalar case, which consists in looking for the electric field as follows:

- Far from the origin, for $x_3^\ell > 0$, we use the ansatz

$$E^\delta(x_T^\ell, x_3^\ell) = \sum_{p=0}^{\infty} \delta^p\, E_\ell^p\left(\frac{x_T}{\delta}, x_3^\ell\right) \quad (6)$$

  where the fields E_ℓ^p are defined in $S_\ell \times \mathbb{R}^+$.

- Close to the origin, we use the ansatz

$$E^\delta(\mathbf{x}) = \sum_{p=0}^{\infty} \delta^p\, E^p\left(\frac{\mathbf{x}}{\delta}\right) \quad (7)$$

  where the fields E^p are defined in Ω^1.

Our models are obtained only by looking at $p = 0, 1$. Using (6) leads to the construction of equation (3) (see [1]). To obtain (4) and (5), we need to express the fact that the two expansions (6) and (7) must match.

In addition, it is possible to obtain error estimates. More precisely, denoting $(E_{app}^\delta, H_{app}^\delta)$ the right hand side of (2) with (V^δ, I^δ) defined as the solution of (3, 4) or (3, 5), one can show that, in appropriate energy norms

$$\|E_{app}^\delta - E^\delta\| \leq C\, \delta^k\, \|E^\delta\| \quad (8)$$

where $k = 1$ for (3, 4) and $k = 2$ for (3, 5), modulo, in this second case, a post-treatment which consists in adding a $O(\delta)$ longitudinal component to the transverse electromanetic field defines by the right hand side of (2).

References

[1] G. Beck, S. Imperiale, P. Joly. Mathematical modelling of multi conductor cables . Discrete and Continuous Dynamical Systems - Series S, American Institute of Mathematical Sciences (AIMS), Volume 8, Issue 3, June 2015, pp.521-546.

[2] P. Joly, A. Semin, Construction and analysis of improved Kirchoff conditions for acoustic wave propagation in a junction of thin slots, ESAIM: Proc., 2008, pp. 44–67.

[3] P. Kuchment, Quantum graphs I. Some basic structures, Waves in Random Media 14, S107-S128 (2004)

Plasmonic waveguides: T-coercivity approach for Maxwell's equations

A.-S. Bonnet-Ben Dhia[1], **C. Carvalho**[1,*], **P. Ciarlet Jr.**[1]
[1]POEMS, UMR 7231 CNRS-INRIA-ENSTA, Palaiseau, France
*Email: camille.carvalho@ensta-paristech.fr

Abstract

We look for the electromagnetic guided modes in a closed waveguide made of layers of materials characterized by real permittivities of opposite signs: we will consider a dielectric and a metal at optical frequencies. Due to this sign-changing permittivity, self-adjointness can be compromised. However, under some conditions, it can be recovered thanks to the T-coercivity approach.
The T-coercivity theory has been extensively developed for scalar problems with sign-changing coefficients, then extended to Maxwell 2D (no dependence in one direction) and Maxwell 3D. We extend these results to our case, referred to as the 2.5D case. When self-adjointness is ensured, with the adapted functional framework, and for a chosen wavenumber, we can prove resolvent compactness. Then we can derive error estimates for the approximation of eigenvalues and the guided modes using edge elements.

Keywords: Maxwell's equations, sign-changing permittivity, waveguide, T-coercivity, eigenvalue approximation

1 Problem setting

Let a domain $D := \{(x, y, z) := (\mathbf{x}, z) \in \Omega \times \mathbb{R}\}$ of section $\Omega \subset \mathbb{R}^2$, such that $\Omega := \Omega_\mathrm{d} \cup \Omega_\mathrm{m}$: $\Omega_\mathrm{d} \times \mathbb{R}$ is a homogeneous domain of permittivity $\varepsilon_\mathrm{d} > 0$, permeability $\mu_\mathrm{d} > 0$, and $\Omega_\mathrm{m} \times \mathbb{R}$ a metal inclusion characterized by $\varepsilon_\mathrm{m} < 0$, and $\mu_\mathrm{m} > 0$. Assume that Ω is simply connected with Lipschitz connected boundary, and define the interface $\Sigma := \overline{\Omega_\mathrm{d}} \cap \overline{\Omega_\mathrm{m}}$.
We look for the guided modes for the electromagnetic field $(\underline{\mathbf{E}}, \underline{\mathbf{H}})$, that is solutions of Maxwell's equations of the form:

$$(\underline{\mathbf{E}}, \underline{\mathbf{H}})(\mathbf{x}, z, t) = (\mathbf{E}, \mathbf{H})(\mathbf{x}) e^{i(\beta z - \omega t)}, \quad \omega, \beta \in \mathbb{R}, \tag{1}$$

where $\omega \neq 0$ is the frequency, and β the axial wavenumber. It is well-known that, in particular for the unknown $\underline{\mathbf{H}}$, using (1), we can reduce the system into a 2D problem parametrized by β that involves the three components of $\mathbf{H}$. We define new operators indexed by β ($\mathbf{rot}_\beta$ and div_β) which are simply a rewriting of the classical operators taking into account (1). Then we get:

$$\left| \begin{array}{l} \text{Find } \mathbf{H} \in \mathbf{W}(\Omega) \text{ such that:} \\ \mathbf{rot}_\beta \left(\dfrac{1}{\varepsilon} \mathbf{rot}_\beta \mathbf{H} \right) - \omega^2 \mu \mathbf{H} = 0 \quad \text{in } \Omega \\ \dfrac{1}{\varepsilon} \mathbf{rot}_\beta \mathbf{H} \times \mathbf{n} = 0 \quad \text{on } \partial\Omega \end{array} \right. \tag{2}$$

with $\mathbf{n}$ the unit outward normal of Ω, ε and μ two piece-wise constant functions gathering the permittivity and the permeability of the two materials. Finally for all $\mathbf{F} := (\overrightarrow{F_\perp}, F_z)^t$ define

$$\mathbf{W}(\Omega) = \{\mathbf{F} / \overrightarrow{F_\perp} \in \overrightarrow{H}(\mathrm{rot}; \Omega),\ F_z \in H^1(\Omega)\}$$

where

$$\overrightarrow{H}(\mathrm{rot}; \Omega) := \{\overrightarrow{F_\perp} := (F_x, F_y)^t \in L^2(\Omega)^2 / \ \mathrm{rot}\overrightarrow{F_\perp} := \partial_x F_y - \partial_y F_x \in L^2(\Omega)\}.$$

One can show that a solution $\mathbf{H}$ of (2) also satisfies the conditions

$$\mu \mathbf{H} \cdot \mathbf{n} = 0 \text{ on } \partial\Omega,\ \mathrm{div}_\beta(\mu \mathbf{H}) = 0 \text{ in } \Omega. \tag{3}$$

To look for the guided modes, we interpret Problem (2) as an eigenvalue problem: for a chosen $\beta \in \mathbb{R}$, find $(\mathbf{H}, \omega^2) \in \mathbf{W}(\Omega) \setminus \{0\} \times \mathbb{C}$ satisfying (2). Since ε is sign-changing, well-posedness for the forward problem (that is (2) with some data at the right-hand side) is not automatically guaranteed. First we need to ensure existence and uniqueness of this forward problem then, when it is satisfied, we can study the eigenproblem, and tackle the approximation of the eigenvalues.

2 Self-adjointness

As $\mathbf{W}(\Omega)$ is not compactly embedded in $\mathbf{L}^2(\Omega)$, we will work in a subspace that takes into account the divergence free condition (3):

$$\mathbf{V}_T(\beta; \mu; \Omega) = \{\mathbf{F} \in \mathbf{W}(\Omega) / \ \mu \mathbf{F} \cdot \mathbf{n} = 0\ \partial\Omega,\ \mathrm{div}_\beta(\mu \mathbf{F}) = 0\ \Omega\},$$

and which is compactly embedded in $\mathbf{L}^2(\Omega)$. We can prove that solving (2) is equivalent to:

$$\left|\begin{array}{l}\text{Find } \mathbf{H} = (\overrightarrow{H_\perp}, H_z)^t \in \mathbf{V}_T(\beta;\mu;\Omega) \text{ such that:}\\ a(\mathbf{H},\mathbf{H}') + c(\beta;\mathbf{H},\mathbf{H}') = \omega^2(\mu\mathbf{H},\mathbf{H}')\\ \forall \mathbf{H}' \in \mathbf{V}_T(\beta;\mu;\Omega),\end{array}\right. \tag{4}$$

with

$$\begin{aligned} a(\mathbf{H},\mathbf{H}') &:= a_\perp(\overrightarrow{H_\perp},\overrightarrow{H_\perp}') + a_z(H_z,H_z')\\ &= \int_\Omega \frac{1}{\varepsilon}\mathrm{rot}\overrightarrow{H_\perp}\overline{\mathrm{rot}\overrightarrow{H_\perp'}} + \int_\Omega \frac{1}{\varepsilon}\nabla H_z\cdot\overline{\nabla H_z'},\end{aligned}$$

$$\begin{aligned} c(\beta;\mathbf{H},\mathbf{H}') &:= i\beta\int_\Omega \frac{1}{\varepsilon}\left(\nabla H_z\cdot\overline{\overrightarrow{H_\perp'}} - \overrightarrow{H_\perp}\cdot\overline{\nabla H_z'}\right)\\ &\quad + \beta^2\int_\Omega \frac{1}{\varepsilon}\overrightarrow{H_\perp}\cdot\overline{\overrightarrow{H_\perp'}}.\end{aligned}$$

Note that for $\beta \neq 0$, the functional framework and the compact part $c(\beta;\cdot,\cdot)$ depend on β, then we cannot decouple $\overrightarrow{H_\perp}$ from H_z and rewrite (4) into two problems. Due to the sign-changing permittivity, the form a is not coercive. Besides, coercivity can be recovered under some conditions on the ratio $\varepsilon_\mathrm{d}/\varepsilon_\mathrm{m}$ and the geometry of Σ, via the T-coercivity approach. Particularly it tells us that (4) (with some data at the right-hand side) is of Fredholm type if and only if there exists an isomorphism $\mathtt{T}$ of $\mathbf{V}_T(\beta;\mu;\Omega)$ such that $a(\cdot,\mathtt{T}\cdot)$ is coercive, and $c(\beta;\cdot,\cdot)$ is compact. As mentioned above, this theory has been developed for instance in [1, 2] providing *ad hoc* operators $\mathtt{T}$ (explicit for scalar problems, abstract for Maxwell's). In that case, it has been proved that the form $a_\perp$ is in fact coercive for any value of $\varepsilon < 0$, while we recover coercivity for the form a_z under some conditions.

For the 2.5D case, we extend the results coupling those from scalar and Maxwell's problems. As we cannot decouple the components of $\mathbf{H}$, the construction of the operator $\mathtt{T}$ now involves an operator $\mathtt{T}_z$ from the scalar problem, an operator $\mathtt{T}_\perp$ from Maxwell 2D problems, and we add to $\mathtt{T}_\perp$ a potential solution of an elliptic problem whose right-hand side depends on $\mathtt{T}_z$ and β.

With the Riesz representation we introduce the operator $A(\beta) \in \mathcal{L}(\mathbf{V}_T(\beta;\mu;\Omega))$ associated to the form $a(\cdot,\cdot)+c(\beta;\cdot,\cdot)$. Once we have proved that the forward problem is of Fredholm type, we can prove that $A(\beta)$ is self-adjoint and has compact resolvent, so that its spectrum is composed of a sequence of positive and negative eigenvalues.

3 Approximation of the guided modes

Finally, following [5], and in the spirit of [4] we can provide error estimates for the approximation of the eigenvalues using edge elements. To do so, we first have to state compactness of the discrete operators and norm convergence towards $A(\beta)$: this requires to transpose T-coercivity to the discrete problem and some conditions on the mesh [3].

Acknowledgments

We thank the ANR project METAMATH and the DGA for financial support.

References

[1] A.-S. Bonnet-Ben Dhia, L. Chesnel and P. Ciarlet Jr., T -coercivity for scalar interface problems between dielectrics and metamaterials, *Math. Mod. Num. Anal.* **46**(2012), pp. 1363-1387.

[2] A.-S. Bonnet-Ben Dhia, L. Chesnel and P. Ciarlet Jr., Two-dimensional Maxwell's equations with sign-changing coefficients, *Appl. Num. Math.* **79** (2014), pp. 29-41.

[3] L. Chesnel, P. Ciarlet Jr., T-coercivity and continuous Galerkin methods: application to transmission problems with sign changing coefficients, *Numer. Math.* **124** (2013), pp. 1-29.

[4] P. Joly, C. Poirier, J.-E. Roberts, P. Trouve, A new non-conforming finite element method for computation of electromagnetic guides waves, *SIAM J. Numer. Appl.* **33** (1996), pp. 1494-1525.

[5] J.E. Osborn, Spectral approximation for compact operators, *Math. Comp.* **29** (1975), pp. 712–725.

Low-Frequency Asymptotics for Time-Harmonic Maxwell Equations in Exterior Domains

Dirk Pauly[1,*]

[1]Fakultät für Mathematik, Universität Duisburg-Essen, Campus Essen, Germany

[*]Email: dirk.pauly@uni-due.de

Abstract

In this talk we will give a detailed description of the complete low-frequency asymptotics for time-harmonic Maxwell equations in exterior domains.

Keywords: Low-Frequency Asymptotics, Time-Harmonic Maxwell Equations, Exterior Domains, Electro-Magnetic Scattering, Weighted Sobolev Spaces

1 Results

We will prove the complete low-frequency asymptotics for time-harmonic Maxwell equations in exterior domains. We start with introducing the solution theory for time-harmonic electromagnetic scattering problems via a generalized Fredholm alternative using the limiting absorption principle and continue with proving an adequate corresponding electro-magneto static solution theory providing also special so-called towers of static solutions. In both cases we will work in polynomially weighted Sobolev spaces. Then a comparison with the whole space solution shows that a generalized asymptotic Neumann series gives the desired asymptotics for low frequencies up to a finite sum of degenerate operators, which can be described explicitly by strongly growing towers. Finally we compare these time-harmonic Maxwell radiation solutions with the corresponding solutions provided by the eddy-current model for low frequencies.

References

[1] P. Kuhn and D. Pauly, Regularity results for generalized electro-magnetic problems, *Analysis (Munich)* **30** 3 (2010), pp. 225–252.

[2] D. Pauly, Low Frequency Asymptotics for Time-Harmonic Generalized Maxwell Equations in Nonsmooth Exterior Domains, *Adv. Math. Sci. Appl.* **16** 2 (2006), pp. 591–622.

[3] D. Pauly, Generalized Electro-Magneto Statics in Nonsmooth Exterior Domains, *Analysis (Munich)* **27** 4 (2007), pp. 425–464.

[4] D. Pauly, Hodge-Helmholtz Decompositions of Weighted Sobolev Spaces in Irregular Exterior Domains with Inhomogeneous and Anisotropic Media, *Math. Methods Appl. Sci.* **31** (2008), pp. 1509–1543

[5] D. Pauly, Complete Low Frequency Asymptotics for Time-Harmonic Generalized Maxwell Equations in Nonsmooth Exterior Domains, *Asymptot. Anal.* **60** 3-4 (2008), pp. 125–184

[6] D. Pauly, On Polynomial and Exponential Decay of Eigen-Solutions to Exterior Boundary Value Problems for the Generalized Time-Harmonic Maxwell System, *Asymptot. Anal.* **79** 1-2 (2012), pp. 133–160

[7] D. Pauly, On Constants in Maxwell Inequalities for Bounded and Convex Domains, *Zapiski POMI*, 435:46-54, 2014*, & J. Math. Sci. (N.Y.)* (2014)

[8] D. Pauly, On Maxwell's and Poincaré's Constants, *Discrete Contin. Dyn. Syst. Ser. S* **8** 3 (2015), pp. 607–618

[9] D. Pauly, On the Maxwell Constants in 3D, *Math. Methods Appl. Sci.* (2015)

[10] R. Picard, On the low frequency asymptotics in and electromagnetic theory, *J. Reine Angew. Math.* **354** (1984), pp. 50–73

[11] R. Picard, N. Weck and K.-J. Witsch, Time-Harmonic Maxwell Equations in the Exterior of Perfectly Conducting, Irregular Obstacles, *Analysis (Munich)* **21** (2001), pp. 231–263.

[12] N. Weck, Maxwell's boundary value problems on Riemannian manifolds with nonsmooth boundaries, *J. Math. Anal. Appl.* **46** (1974), pp. 410–437.

Diffraction of Weierstrass scalar fractal waves by circular apertures: symmetry and patterns, complexity and dimension

J. M. Christian[1,*], **E. P. Woodroofe**[1], **G. S. McDonald**[1]

[1]Materials & Physics Research Centre, University of Salford, Greater Manchester M5 4WT, UK

[*]Email: j.christian@salford.ac.uk

Abstract

The diffraction of plane waves from simple hard-edged apertures constitutes a class of boundary-value problem that is well understood in optics, at least within the scalar approximation. Similarly, the diffraction of such waves from fractal apertures (amplitude or phase masks possessing structure across decades of spatial scale) has also received much attention in the literature. But the diffraction of *fractal waves* by *simple apertures* constitutes an entirely new paradigm (in optics particularly, and wave physics more generally) that remains largely unexplored.

Here, we consider the diffraction of fractal waves by a hard-edged circular aperture using a range of analytical and semi-analytical methods. Fast computational techniques are used to obtain Fresnel (near field) diffraction patterns, and specialist software assists with the investigation of their properties. Key issues to be addressed include the fractal dimension of diffraction patterns, and the asymptotic emergence of Fraunhofer (far field) predictions in an appropriate limit.

Keywords: Fresnel diffraction, fractal waves, Weierstrass function.

1 Fractal Diffraction

We have recently proposed fractal diffraction as a context of fundamental physical importance with enormous scope for potential applications [1]. Preliminary analyses investigated a Weierstrass function [2] for modelling fractal illumination of the most elementary aperture imaginable: the infinite single slit. The Weierstrass function has an intuitive interpretation, comprising a set of periodic patterns whose amplitudes and spatial frequencies are connected in a very particular way. Moreover, each constituent pattern scale can be constructed from a superposition of two interfering plane waves.

The diffraction of a uniform wavefront by a circular aperture is another classic wave-based problem that has well-known solutions, both in Fresnel and Fraunhofer regimes [3]. While we consider the optical analogue with fractal illumination, our results are expected to be readily applicable to other fields, such as acoustics [4].

2 Diffraction Integral

The diffraction of a scalar optical field $U(r)$ by a circular aperture of radius a is routinely described by the paraxial wave equation. For a hard-edged circular aperture, and where the incident wave $U_{\rm in}$ is azimuthally invariant, the diffracted wave at a distance L beyond the aperture is given by the formal solution,

$$U(r) = \frac{2\pi N_{\rm F}}{i} \exp\left(i\pi N_{\rm F} r^2\right) \times \int_0^{+1} d\rho\, \rho J_0(2\pi N_{\rm F} r\rho) \exp\left(i\pi N_{\rm F}\rho^2\right) U_{\rm in}(\rho), \quad (1)$$

where the radial coordinate r is measured in units of a. In this representation, the diffraction pattern is uniquely parametrized by the aperture Fresnel number $N_{\rm F} \equiv a^2/\lambda L$.

3 Weierstrass Illumination

Here, we consider an illuminating field that has the form of an azimuthally invariant Weierstrass wave such that

$$\frac{U_{\rm in}(r)}{U_0} = 1 + \epsilon \sum_{n=0}^{N} \frac{1}{\gamma^{(2-{\rm D}_0)n}} \cos(\kappa_n r + \phi_n), \quad (2)$$

where U_0 is a uniform plane-wave amplitude and ϵ controls the strength of the fractal modulation. The spatial frequencies in Eq. (2) form a Weierstrass spectrum given by $\kappa_n \equiv 2\pi(a/\Lambda)\gamma^n$, where $\gamma > 0$ is a free parameter, and the set of phases ϕ_n may be either deterministic or random. When $N \to \infty$, the number $1 < {\rm D}_0 \leq 2$ corresponds to the Hausdorff-Besicovich dimension of $U_{\rm in}$ with values approaching 2 giving an increasingly complex fractal curve.

The illuminating field is bandwidth-limited with a cut-off at $n = N$; the spatial scalelengths in Eq. (2) then range from the largest, Λ, to the

smallest, $\Lambda\gamma^{-N}$. Placing a restriction on the number of spatial scales in $U_{\rm in}$ is important for two principal reasons. Firstly, no physical object can possess structure down to arbitrarily-small scales (since finite-size effects will eventually come into play). Secondly, there tends to exist a high-frequency cut-off beyond which spatial scales cannot contribute to the diffracted *intensity* pattern [5] (so the basis on which one introduces finite-bandwidth considerations, and selects a value for N, are rooted in diffraction theory).

4 Diffraction of Fractal Waves

Earlier analyses focusing on infinite-slit geometries have tended to use Young's edge waves as convenient spatial structures for understanding and quantifying fractal diffraction phenomena [1]. While edge waves can be used for circular apertures and uniform illumination [3], such a formalism is not quite so readily deployed for fractal illumination (despite the one-dimensional nature of the system) and one must instead consider the diffraction integral more directly. Substitution of Eq. (2) into Eq. (1) yields a formal expression for $U(r)$ as a linear superposition of patterns with different scalelengths,

$$\frac{U(r)}{U_0} = \frac{2\pi N_{\rm F}}{i}\exp\left(i\pi N_{\rm F} r^2\right)\left[P(r;0,0) + \epsilon\sum_{n=0}^{N}\frac{1}{\gamma^{(2-{\rm D}_0)n}}P(r;\kappa_n,\phi_n)\right], \quad (3a)$$

where P is given by the integral

$$P(r;A,B) \equiv \int_0^{+1} d\rho\,\rho J_0(2\pi N_{\rm F} r\rho) \times \exp\left(i\pi N_{\rm F}\rho^2\right)\cos(A\rho + B) \quad (3b)$$

and $P(r;0,0)$ fully describes the diffraction pattern in the classic plane-wave problem [3].

A selection of new results will be discussed, with a combination of analytical methods and specialist fractal analysis software [6] identifying trends in the Fresnel patterns (see Fig. 1). Attention is paid to the role played by $N_{\rm F}$ in characterizing these patterns, and we consider different self-affine measures of *dimension* (such as roughness-length, variogram, and rescaled-range). Asymptotic emergence of classic Fraunhofer results will also be demonstrated, and a wide range of potential applications highlighted.

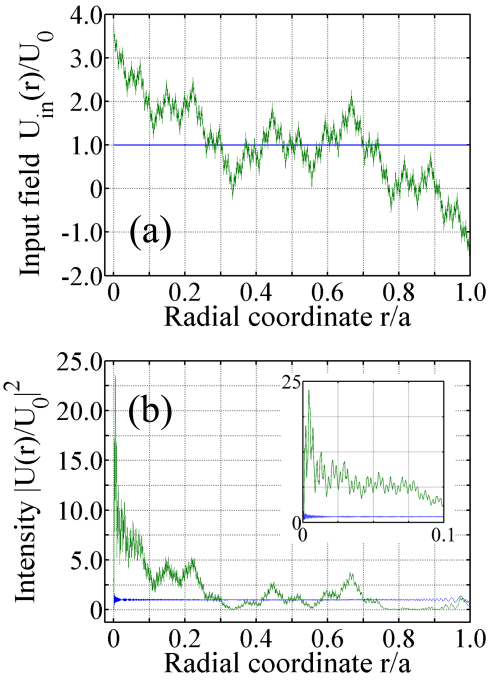

Figure 1: (a) Illumination across a circular aperture corresponding to a plane wave (blue) and a Weierstrass function with fractal dimension $\rm D_0 = 1.6$ and $\gamma = 3$ (green). (b) Diffracted intensity patterns when $N_{\rm F} = 1000$.

References

[1] J. M. Christian, M. Mylova, and G. S. McDonald, Diffraction of fractal optical fields by simple apertures, in *Proceedings of the European Optical Society Annual Meeting, Berlin, Germany, 15-19 September 2014* (online).

[2] G. H. Hardy, Weierstrass's nondifferentiable function, *Transactions of the American Mathematical Society* **17** (2006), pp. 301–325.

[3] D. S. Burch, Fresnel diffraction by a circular aperture, *American Journal of Physics* **53** (1985), pp. 255–260.

[4] R. D. Spence, The diffraction of sound by circular disks and apertures, *Journal of the Acoustical Society of America* **20** (1948), pp. 380–386.

[5] G. H. C. New and T. Albaho, Spatial spectrum of intensity profiles diffracted by a slit, *Journal of Modern Optics* **50** (2003), pp. 155–160.

[6] BENOIT 1.3, TruSoft International Inc., www.trusoft-international.com.

Unstable resonators with polygon and von Koch-type boundary conditions: virtual source modelling of fractal eigenmodes

J. M. Christian[1,*], **I. Begleris**[2], **S. J. Wickham**[1], **G. S. McDonald**[1], **J. G. Huang**[3]

[1]Materials & Physics Research Centre, University of Salford, Greater Manchester M5 4WT, UK

[2]Computational Modelling Group, University of Southampton, Highfield SO17 1BJ, UK

[3]Faculty of Advanced Technology, University of South Wales, Pontypridd CF37 1DL, UK

[*]Email: j.christian@salford.ac.uk

Abstract

We will report on our latest research into modelling fractal lasers (linear systems that involve geometrically-unstable resonators with inherent magnification), and propose two new classes of cavity configuration. These devices are of fundamental theoretical interest as table-top generators of tunable fractal light that can be used in a wide range of applications. Moreover, we expect them to play a pivotal role in new Nature-inspired optical architectures and designs.

The virtual source theory of classic kaleidoscope lasers will be reviewed, and we show how that semi-analytical method can be applied to novel cavity designs which incorporate a feedback mirror whose outer boundary corresponds to iterations of the von Koch *snowflake* (an iterated function system involving self-similar sequences of equilateral triangles) and its isosceles counterpart, the von Koch *pentaflake* . A range of new numerical results will be given, including calculations of mode patterns, eigenvalue spectra, and detailed computations of fractal dimension measures.

Keywords: Unstable resonators, virtual source theory, snowflake, pentaflake.

1 Fractal Lasers

Unstable cavity lasers involve linear resonators with inherent magnification whose eigenmodes possess fractal characteristics (that is, proportional level of details spanning decades of spatial scale). The physical origin of such multi-scale patterns in strip resonators (systems comprising a single transverse dimension) has been explained by considering repeated diffraction of the circulating cavity field at the feedback mirror (which subsequently plays a key role in determining mode properties) [1].

The term *kaleidoscope laser* has been coined to describe similar systems with two transverse dimensions where the feedback mirror has the shape of a regular polygon (e.g., an equilateral triangle) [2]. This complicated boundary-value problem (which involves non-orthogonal edges in the aperturing element) gives rise to mode patterns that have a remarkable beauty and complexity [3]. Here, we propose two new classes of unstable resonator that involve fractal (rather than regular) boundary conditions: *snowflake* and *pentaflake* systems.

2 Virtual Source Modelling

A confocal unstable resonator is fully described by two parameters: the equivalent Fresnel number $N_{\rm eq}$ and the round-trip magnification M. Southwell's virtual source (VS) method unfolds the cavity into a plane wave diffracting through a sequence of $N_{\rm S} = \log(250N_{\rm eq})/\log M$ apertures, each of which has a characteristic size [4]. The modes of the cavity correspond to a linear superposition of the edge waves from each of these fictitious apertures.

Previously, we have applied a two dimensional (2D) VS approach to find the empty-cavity eigenmodes $V(\mathbf{X})$ of kaleidoscope lasers across the feedback mirror, where

$$V(\mathbf{X}) = \epsilon \left[\frac{E_{N_{\rm S}+1}(\mathbf{X_C})}{\alpha^{N_{\rm S}}(\alpha-1)} - \sum_{m=1}^{N_{\rm S}} \alpha^{-m} E_m(\mathbf{X}) \right], \tag{1a}$$

$E_m(\mathbf{X})$ is the edge-wave pattern from virtual aperture m, $\mathbf{X_C}$ is an arbitrary point on the boundary of the feedback mirror (typically a vertex), and ϵ is a Heaviside function (equal to 1 in the domain of the feedback mirror, and 0 otherwise). The mode eigenvalue α, obtained by solving the high-order polynomial equation

$$\alpha^{N_{\rm S}+1} + \sum_{m=0}^{N_{\rm S}} \left[E_m(\mathbf{X_C}) - E_{m+1}(\mathbf{X_C}) \right] \alpha^{N_{\rm S}-m} = 0, \tag{1b}$$

plays the role of a formal expansion parameter. Each individual root of Eq. (1b) thus describes

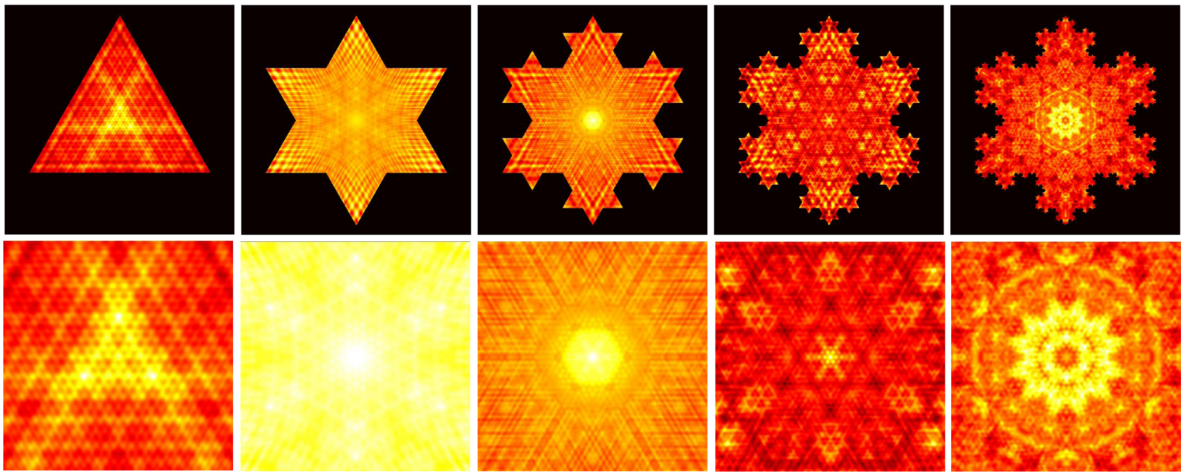

Figure 1: Snowflake laser modes (top row) and corresponding magnification of the central portion (bottom row). For iteration number $n = 0, 1, 2, 3$ and 4 (left to right), there are $N = 3 \times 4^n = 3, 12, 48, 192$, and 768 edges to the feedback mirror (a computationally-intensive problem).

an eigenmode of the unstable resonator. In this way, the virtual source formalism provides a hierarchy of solutions whose round-trip losses are related to $|\alpha|$ (and where the lowest-loss mode corresponds to the largest value of $|\alpha|$). In contrast, $ABCD$ (paraxial) matrix modelling in combination with fast Fourier transforms computes only a single mode per application.

In this presentation, we show how our 2D-VS theory can also be applied to find the modes of snowflake (see Fig. 1) and pentaflake resonators. The approach requires detailed knowledge of the constituent edge waves, which are typically found using a line-integral method [5].

3 Modes & Fractal Dimension

A key issue to be addressed in detail is the fractal dimension of unstable-resonator modes for cavities with arbitrary N_{eq} and M parameters. Previously, Berry [6] has made similar considerations but only for the lowest-loss modes of kaleidoscope cavities, and in the limit $N_{\text{eq}} \to \infty$ (where asymptotic approximations may be deployed). We will conclude with a summary of results from the first detailed exploration of fractal dimension in kaleidoscope systems. Specialist software [7] has been deployed in parallel with our suite of 2D-VS codes to investigate potential anisotropy in the dimension using various different measures. Cross-sections through the lowest-loss (and a set of higher-order) mode patterns are computed, and direct comparisons with a strip resonator for the same cavity parameters [1] uncover some intriguing results.

References

[1] G. H. C. New, M. A. Yates, J. P. Woerdman, and G. S. McDonald, Diffractive origin of unstable resonator modes, *Optics Communications* **193** (2001), pp. 261–266.

[2] G. P. Karman, G. S. McDonald, G. H. C. New, and J. P. Woerdman, Fractal modes in unstable resonators, *Nature* **402** (1999), p. 138.

[3] G. S. McDonald, G. P. Karman, G. H. C. New, and J. P. Woerdman, The kaleidoscope laser, *Journal of the Optical Society of America B* **17** (2000), pp. 524–529.

[4] W. H. Southwell, Virtual-source theory of unstable resonator modes, *Optics Letters* **6** (1981), pp. 487–489.

[5] J. G. Huang, J. M. Christian, and G. S. McDonald, Fresnel diffraction and fractal patterns from polygonal apertures, *Journal of the Optical Society of America A* **23** (2006), pp. 2768–2774.

[6] M. V. Berry, Fractal modes of unstable lasers with polygonal and circular mirrors, *Optics Communications* **200** (2001), pp. 321–330.

[7] BENOIT 1.3, TruSoft International Inc., www.trusoft-international.com.

Boundary Conditions for Hyperbolic Systems of Equations on Curved Erroneous Domains

Samira Nikkar[1,*], **Jan Nordström**[1]

[1]Department of Mathematics, Linköping University, Sweden

[*]Email: samira.nikkar@liu.se

Abstract

In this paper, we discuss the potential consequences of having an erroneous computational domain for hyperbolic problems. We validate our findings by solving the linearized Euler equations using a high order finite difference method in space and time.

Keywords: hyperbolic problem, initial boundary value problems, erroneous computational domains

1 Introdcution

A non-perfect mesh generator often results in an inaccurate geometry description. The errors by the inaccurate geometry will affect the global accuracy of all discretization techniques used. In this paper, we quantify that effect by considering the error induced by applying boundary conditions at the wrong position and/or with an incorrect normal, see Figure 1.

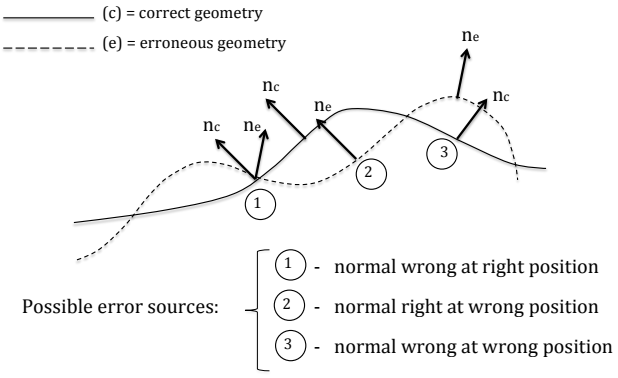

Figure 1: A schematic of the erroneous and correct (nc = correct normal, ne = erroneous normal) boundary definitions.

2 Correct geometries

Consider the following constant coefficient symmetric system of size M,

$$\begin{aligned} V_t+(\hat{A}V)_x+(\hat{B}V)_y = 0, \;\; (x,y)\in\Omega, \quad t\in[0,T] \\ LV = g, \;\; (x,y)\in\delta\Omega, \;\; t\in(0,T] \\ V = f, \;\; (x,y)\in\Omega, \quad t=0, \end{aligned} \tag{1}$$

in which $V = V(x,y,t)$ is the solution, Ω is the spatial domain with the boundary $\delta\Omega$, L is the boundary operator and $f(x,y)$ and $g(x,y,t)$ are data to the problem. $\hat{A}$ and $\hat{B}$ are constant symmetric matrices.

By imposing boundary conditions of the form

$$LV = (X_-^T - RX_+^T)V = g, \qquad (x,y)\in\delta\Omega, \tag{2}$$

where the matrix R is of appropriate size, and

$$\Lambda^+ + R^T\Lambda^- R^T \geq 0 \tag{3}$$

it can be shown that the energy is bounded.

We consider the transformation

$$x(\xi,\ \eta)\leftrightarrow\xi(x,\ y),\ \ y(\xi,\ \eta)\leftrightarrow\eta(x,\ y)$$

which takes (1) to

$$\begin{aligned} JV_t+(\hat{A}V)_\xi+(\hat{B}V)_\eta = 0, \;\; (\xi,\eta)\in\Phi, \quad t\in[0,T] \\ LV = g, \;\; (\xi,\eta)\in\delta\Phi, \;\; t\in(0,T] \\ V = f, \;\; (\xi,\eta)\in\Phi, \quad t=0. \end{aligned} \tag{4}$$

In (4), $A = J\xi_x\hat{A}+J\xi_y\hat{B}$ and $B = J\eta_x\hat{A}+J\eta_y\hat{B}$.

The energy method together with the use of Geometric Conservation Law (GCL), see [1], and also Green's theorem lead to

$$\frac{d}{dt}||V||_J^2 = -\oint_{\delta\Phi} V^T \underbrace{(A,\ B)\cdot n}_{\tilde{\mathcal{A}}}\ V\ ds, \tag{5}$$

in which $n=(n_1,\ n_2)$, $\tilde{\mathcal{A}} = n_1A+n_2B$ and the norm is defined by $||V||_J^2 = \iint_\Phi V^T J\ V\ d\xi\ d\eta$. By the use of (2) we can show that (5) leads to a bounded energy and well-posedness, see more details in [1].

3 Erroneous geometries

Consider two hyperbolic problems

$$U_t + \hat{A}U_x + \hat{B}U_y = 0, \qquad (x, y) \in \Omega_c \qquad (6)$$
$$V_t + \hat{A}V_x + \hat{B}V_y = 0, \qquad (x, y) \in \Omega_e \qquad (7)$$

posed on two nearby domains (c and e denote correct and erroneous respectively). The two domains are both transformed to the unit square, see Figure 2.

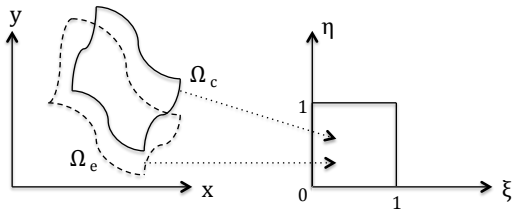

Figure 2: A schematic of correct and erroneous geometries both mapped to the unit square.

We apply energy method on the transformed version of (6) and (7) and we get

$$\frac{d}{dt}||W||^2_{J^i} = -\oint_{\delta\Phi} W^T \underbrace{(A^i,\ B^i) \cdot n^i}_{\tilde{\mathcal{A}}^i}\ W\ ds^i, \quad (8)$$

for $W \in \{U,\ V\}$ and $i \in \{c,\ e\}$.

The relations (6), (7) and (8) lead directly to the conclusion that i) the wave speeds given by the eigenvalues of the matrices will differ. Moreover, ii) wrong normals may lead to either wrong number of boundary conditions or imposition of the wrong data at the boundary. Finally, iii) boundary conditions with data for $\delta\Omega_c$ may be imposed at $\delta\Omega_e$. Consequently, the erroneous boundary description can lead to an ill-posed problem and inaccurate results. The errors induced by the wrong position and form of the boundary might be more important than the order of accuracy and specific discretization technique one is using.

4 Numerical experiments

We consider the two-dimensional constant coefficient symmetrized Euler equations. The correct and erroneous computational domains are chosen as shown in Figures 3 and 4 (Note that the erroneous computational domain here is exaggerated).

We solve the fully discrete problem and expect third order accuracy in the space. The convergence rates for the correct and erroneous geometries are shown in Figures 5 and 6. As seen in Figure 6, the erroneous geometry affects the global accuracy of the discretization technique used (only first order accuracy is obtained).

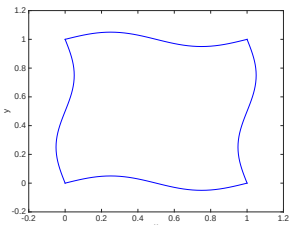

Figure 3: The correct computational domain, Ω_c.

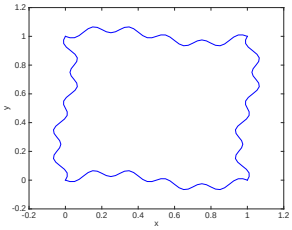

Figure 4: The erroneous computational domain, Ω_e.

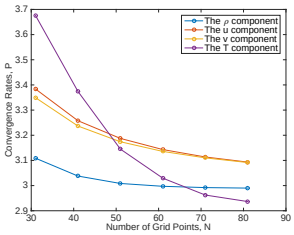

Figure 5: 3rd order accurate, convergence rate, Ω_c.

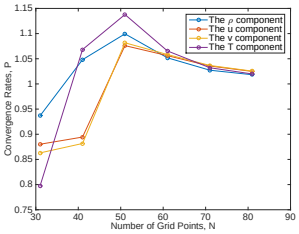

Figure 6: 1st order accurate, convergence rate, Ω_e.

5 Summary and conclusions

We discussed the effect of erroneous boundary description. We showed that the errors caused by an erroneous geometry description affects the solution more than the accuracy of the discretization technique using Euler's equation and 3rd order SBP operators. In the presentation we will discuss these issues more in detail.

References

[1] S. Nikkar, J. Nordström, Fully Discrete Energy Stable High Order Finite Difference Methods for Hyperbolic Problems in Deforming Domains, in *LiTH-MAT-R; 2014:15, Department of Mathematics, Linköping University.*

Thursday, July 23
First Afternoon Session
15:30 – 17:00

Verification of a Variational Source Condition for Inverse Medium Scattering Problems

Thorsten Hohage[1], **Frederic Weidling**[1,*]
[1]Institute for Numerical and Applied Mathematics, University of Goettingen, Germany
[*]Email: f.weidling@math.uni-goettingen.de

Abstract

In this talk, see [5], we consider the inverse scattering problem to recover the *contrast* f of a medium given either near or far field measurements of acoustic waves. Using geometrical optics solution we show that the contrast satisfies a logarithmic source condition if it belongs to a Sobolev ball. This yields the first rigorous proof of logarithmic convergence rates of Tikhonov regularization applied to inverse medium scattering.

Keywords: inverse medium scattering, convergence rates, variational source condition

1 Statement of the inverse problem

We consider scattering of time-harmonic acoustic waves by a medium characterized by its contrast $f \in L^\infty(\mathbb{R}^3)$, assuming that $\operatorname{Re} f \le 1$, $\operatorname{Im} f \le 0$, $\operatorname{supp} f \subset B(\pi) := \{x \in \mathbb{R}^3 \colon |x| \le \pi\}$, and $\kappa > 0$. The forward problem is then given by finding the *total field* $u = u^{\mathrm{i}} + u^{\mathrm{s}}$ solving the differential equation

$$\Delta u + \kappa^2 u = \kappa^2 f u \quad \text{in } \mathbb{R}^3 \tag{1}$$

where the *incident field* u^{i} solves the Helmholtz equation $\Delta u^{\mathrm{i}} + \kappa^2 u^{\mathrm{i}} = 0$ and the *scattered field* u^{s} fulfills the Sommerfeld radiation condition (RC).

We will consider two inverse problems corresponding to two kinds of incident fields u^{i}. Incident point source waves are of the form

$$u^{\mathrm{i}}_y(x) = \frac{1}{4\pi} \frac{\mathrm{e}^{\mathrm{i}\kappa|x-y|}}{|x-y|}.$$

For a fixed radius $R > \pi$ we want to reconstruct f using *near field data* $w(x,y) = u_y(x)|_{|x|=R}$ for all y with $|y| = R$, which is the Green function of the problem. Here u_y is the total field for the incident point source wave u^{i}_y.

Another inverse problem occurs if we use incident plane waves $u^{\mathrm{i}}_{d,\infty}(x) = \mathrm{e}^{\mathrm{i}\kappa d\cdot x}$ traveling in direction d with $|d| = 1$ and the asymptotic behavior of solutions to (1) and (RC)

$$u(x) = u^{\mathrm{i}}(x) + \frac{\mathrm{e}^{\mathrm{i}\kappa|x|}}{|x|} u^\infty(\hat{x}) + \mathcal{O}\left(\frac{1}{|x|^2}\right)$$

uniformly for all directions $\hat{x} := x/|x|$ where u^∞ is the *far field pattern* of u. The inverse problems is to reconstruct f from measurements $u^\infty(\hat{x}, d)$ for all directions $\hat{x}$ and d with $u^\infty(\cdot, d)$ given by the far field pattern corresponding to $u^{\mathrm{i}}_{d,\infty}$.

2 Regularization and convergence rates

The problems above can be formulated as operator equation $F(f) = g$ where F is either the near field operator

$$F_{\mathrm{n}} \colon \mathcal{D} \to L^2(\partial B(R) \times \partial B(R)), f \mapsto w$$

for $R > 1$ or the far field operator

$$F_{\mathrm{f}} \colon \mathcal{D} \to L^2(\partial B(1) \times \partial B(1)), f \mapsto u^\infty$$

with domain $\mathcal{D} := \{f \in L^\infty(\mathbb{R}^3) \colon \operatorname{supp}(f) \subset B(\pi), \operatorname{Re} f \le 1, \operatorname{Im} f \le 0\}$. Both operators are injective but their inverses are not continuous (see [6]). To obtain a stable reconstruction we use nonlinear Tikhonov regularization

$$f^\delta_\alpha \in \operatorname{argmin}_f \left[\left\| F(f) - g^\delta \right\|^2_Y + \frac{\alpha}{2} \|f\|^2_X \right] \tag{2}$$

where F is either F_{n} or F_{f}, $X \subset \mathcal{D}$ is a Hilbert space and Y the corresponding image space containing the data g^δ, which is assumed to satisfy $\|g^\delta - F(f^\dagger)\|_Y \le \delta$. If the operator is weakly closed (2) is a regularization method that is the worst case error tends to 0 as $\delta \to 0$ if the regularization parameter α is chosen appropriately though the convergence is in general arbitrarily slow (see [1]).

One way to obtain convergence rate is by requiring that a *variational source condition* (VSC)

$$\frac{\beta}{2} \left\| f - f^\dagger \right\|^2_X \le \frac{1}{2} \|f\|^2_X - \frac{1}{2} \|f^\dagger\|^2_X + \psi\left(\left\| F(f^\dagger) - g^\delta \right\|^2_Y \right) \tag{3}$$

holds true for $f^\dagger$ and all $f \in X$ with $\beta \in (0,1]$ and a concave index function ψ, that is $\psi : [0,\infty) \to [0,\infty)$ is continuous, monotonically increasing and $\psi(0) = 0$. Then (2) converges with rate

$$\frac{\beta}{2} \left\| f^\dagger - f_{\bar{\alpha}}^\delta \right\|_X^2 \leq 4\psi(\delta^2) \tag{4}$$

for the optimal choice $\bar{\alpha}$ of the regularization parameter, which is given by $1/(2\bar{\alpha}) = \psi'(4\delta^2)$. VSCs, proposed in [4] and further developed in [2], have become popular in regularization theory due to several advantages over classical spectral source conditions. They simplify proofs, allow generalizations to Banach spaces and do not require further conditions on F'. In the case of linear operators they are also necessary for certain convergence rates. However only a few results on the verification of such conditions exists so far, except via spectral source conditions. Note that if (3) holds true for all $f^\dagger \in K \subset X$, then the *conditional stability estimate*

$$\|f_1 - f_2\|_X^2 \leq \psi\left(\|F(f_1) - F(f_2)\|_Y^2 \right)$$

for all $f_1, f_2 \in K$ is satisfied whereas the reverse implication is not obvious. For the described problems such stability estimates have been established with

$$\psi(t) = C\left(\ln(t^{-1})\right)^{-p} \tag{5}$$

for some $p > 0$ starting with [7]. In [3] K was chosen as a ball in a Sobolev space and an explicit exponent p depending on the order of the Sobolev space was derived. The key tool in the stability proofs are *geometrical optics solutions*.

3 Results

We choose X as the Sobolev space $H_0^m(B(\pi))$. For $m > 3/2$ we have that $H^m \subset L^\infty$ with continuous embedding, so $H^m \cap \mathcal{D} \subset H^m$ is a closed subset.

Theorem 1 *Let $3/2 < m < s$, $s \neq 2m + 3/2$ and $\pi < R$. Assume that the true contrast $f^\dagger \subset \mathcal{D}$ fulfills and $\|f^\dagger\|_{H_0^s(B(\pi))} \leq C_s$ for some $C_s > 0$. Then for all $f \in H_0^m(B(\pi)) \cap \mathcal{D}$ a VSC (3) is fulfilled with $F = F_{\mathrm{n}}$, $\beta = 1/2$ and ψ as in (5) with $p = 2\mu$ and $\mu := \min(1, (s-m)/(m+3/2))$.*

Hence using (4) one obtains:

Corollary 2 *Under the assumptions of Theorem 1 the convergence rate*

$$\left\| f^\dagger - f_{\bar{\alpha}}^\delta \right\|_X^2 \leq c\left(\ln(\delta^{-2})\right)^{-2\mu}.$$

for (2) holds true.

To extend the result to far field data we use a technique proposed in [3].

Theorem 3 *Under the assumptions of Theorem 1 for all $0 < \theta < 1$ a VSC (3) is fulfilled with $F = F_{\mathrm{f}}$, $\beta = 1/2$ and ψ being of the form (5) and $p = 2\mu\theta$.*

References

[1] H. Engl, M. Hanke and A. Neubauer, *Regularization of inverse problems*, Kluwer, 1996.

[2] M. Grasmair, Generalized Bregman distances and convergence rates for non-convex regularization methods, *Inverse Problems* **26** (2010), pp. 115014.

[3] P. Hähner and T. Hohage, New stability estimates for the inverse acoustic inhomogeneous medium problem and applications, *SIAM Journal on Mathematical Analysis*, **33** (2001), pp. 670–685.

[4] B. Hofmann, B. Kaltenbacher, C. Pöschl and O. Scherzer, A convergence rates result for Tikhonov regularization in Banach spaces with non-smooth operators, *Inverse Problems* **23**, (2007), pp. 987–1010.

[5] T. Hohage, F. Weidling, Verification of a variational source condition for acoustic inverse medium scattering problems, arXiv:1503.05763.

[6] A. Kirsch, *An Introduction to the Mathematical Theory of Inverse Problems*, 2nd Edition, Springer Verlag, 2011.

[7] P. Stefanov, Stability of the inverse problem in potential scattering at fixed energy, *Annales de l'institut Fourier*, **40** (1990), pp. 867–884.

Regularization Techniques for Inverse Scattering Problems with Sparsity Constraints

Marcel Rennoch[1,*], **Florian Bürgel**[1]
[1]Center for Industrial Mathematics, University of Bremen, Germany
*Email: mrennoch@math.uni-bremen.de

Abstract

Considering time-harmonic inverse scattering of either electromagnetic waves or of acoustic waves from an inhomogeneous (anisotropic) medium, it is sometimes reasonable to assume that the contrast of the scatterer can be described by few non-zero coefficients for a chosen basis. Such contrasts are called sparse. Although regularization techniques involving sparsity constraints are widely accepted in e.g. image processing, they are rarely used in inverse scattering theory. Because of that we generalize first results from [1] on some iterated soft-shrinkage regularization methods.

Keywords: inverse medium scattering, regularization, sparsity

1 The scattering problem

An incident time-harmonic wave u^i with time-dependence $\mathrm{e}^{-\mathrm{i}\omega t}$ solving the Helmholtz equation $\Delta u^i + k^2 u^i = 0$ illuminates the scattering object $D \subset \mathbb{R}^d$, $d = 2, 3$, so that the total field u solves

$$\Delta u + k^2 n^2 u = 0 \quad \text{in } \mathbb{R}^d, \tag{1}$$

and so that the scattered wave $u^s = u - u^i$ satisfies Sommerfeld's radiation condition

$$\lim_{|x|\to\infty} |x|^{\frac{d-1}{2}} \left(\frac{\mathrm{d}}{\mathrm{d}|x|} - \mathrm{i}k \right) u^s(x) = 0 \tag{2}$$

uniformly in all directions $\hat{x} = x/|x|$. Here we suppose the wave number k to be positiv and the refractive index n to equal one outside the open and bounded set D while it differs from one from the inside. By that a contrast function $q\colon \mathbb{R}^d \to \mathbb{C}$, with $\operatorname{supp}(q) = \overline{D}$, defines through $q := n^2 - 1$ in $\mathbb{R}^d$.

Denoting by Φ the radiating fundamental solution of the Helmholtz equation, it is well known that u^s is a solution to the Lippmann-Schwinger integral equation

$$u^s - k^2 V(qu^s) = k^2 V(qu^i) \quad \text{in } D, \tag{3}$$

where we defined the radiating volume potential by

$$V(f)(x) := \int_D \Phi(x,y) f(y)\, \mathrm{d}y, \quad x \in \mathbb{R}^d.$$

Both the classical inverse scattering solution theory for (3) and the extension to the Banach space setting seen in [1], provides an unique solution of the scattering problem (1, 2).

2 The inverse problem

Representing either near- or far-field measurements due to a contrast q by $\mathcal{F}(q)$ with a non-linear operator $\mathcal{F}$ gives rise to the inverse problem to determine q from measurements $\mathcal{F}(q)$:

$$\mathcal{F}(q) = \mathrm{F}_{q^\dagger}\,. \tag{4}$$

Thus, $\mathcal{F}$ maps the contrast to a linear integral operator F with a kernel given by measurements depending on q and the incident fields. Here q is locally ill-posed about the searched-for exact contrast $q^\dagger$, so that the inversion has to be regularized for noisy measurements $\mathrm{F}^\varepsilon_{\mathrm{meas}}$, i.e.

$$\|\mathcal{F}(q^\dagger) - \mathrm{F}^\varepsilon_{\mathrm{meas}}\| \leqslant \varepsilon.$$

By the aid of variational methods one derives the Tikhonov functional

$$\mathcal{J}^\varepsilon_\alpha(q) := \frac{1}{t}\|\mathcal{F}(q) - \mathrm{F}^\varepsilon_{\mathrm{meas}}\|^t + \alpha\mathcal{R}(q), \quad t \geqslant 1,$$

with some appropriate discrepancy-norm, a convex functional $\mathcal{R}$ and regularization parameter $\alpha > 0$.
Now instead of considering $q \in L^\infty(D)$ penalty terms in L^p-norm for small p coincide quite better with given a-priori information, stating the contrast is supported only in a small region.

Therefore Lechleiter et al. [1] presented convergence of such non-linear Tikhonov regularization for pointwise near-field measurements of scattered fields. We show that it is also possible to extend the analysis to the far-field setting or to a different kind of penalty terms, e.g. BV-norms.

3 Further generalizations

To prove convergence results for variational regularization methods one has to ensure that the solution $q^\dagger$ to (4) is unique. Since in [1] uniqueness in dimension $d = 3$ was only shown for $q \in L^p$ with $p > d$, we show that the classical uniqueness proof generalizes to $p > d/2$.

The techniques from [1] can partly be extended to scattering problems for penetrable anisotropic media, where the contrast Q of the scatterer is matrix-valued, so that the Helmholtz equation for the total field $u = u^i + u^s$ becomes

$$\operatorname{div}(A\nabla u) + k^2 u = 0 \quad \text{in } \mathbb{R}^d, \tag{5}$$

for a material parameter $A = Id + Q$. To this end, we transfer several of the results from [2] to the scattering problem (5).

References

[1] A. Lechleiter, K. S. Kazimierski and M. Karamehmedović, Tikhonov regularization in L^p applied to inverse medium scattering, *Inverse Problems* **29** (2013), 075003.

[2] B. Jin and P. Maass, An Analysis of Electrical Impedance Tomography with Applications to Tikhonov Regularization, *ESAIM:COCV* **18** (2012), pp.1027–1048.

Higher-order expansion of misfit functional for defect identification in elastic solids

Marc Bonnet[1], **Rémi Cornaggia**[1,*]
[1]Poems (UMR 7231 CNRS-INRIA-ENSTA), Palaiseau, France
*Email: remi.cornaggia@ensta-paristech.fr

Abstract. In this work, least-squares functionals commonly used for defect identification are expanded in powers of the small radius of a trial inclusion, in the context of time-harmonic elastodynamics, generalizing to higher orders the concept of topological derivative. Such expansion, whose derivation and evaluation are facilitated by using an adjoint state, provides a basis for the quantitative estimation of flaws whereby a region of interest may be exhaustively probed at reasonable computational cost.

Keywords: Topological derivative, identification, elastodynamics, asymptotic analysis

Problem statement. We consider a reference (i.e defect-free) 3D elastic solid Ω characterized by Hooke's tensor $\boldsymbol{\mathcal{C}}$ and mass density ρ. The time-harmonic background displacement $\boldsymbol{u}$ then solves

$$\langle \boldsymbol{u}, \boldsymbol{w}\rangle_\Omega^{\mathcal{C}} - \omega^2 (\boldsymbol{u}, \boldsymbol{w})_\Omega^{\rho} = \mathcal{F}(\boldsymbol{w}) \ \forall \boldsymbol{w} \in \mathcal{W}, \quad (1)$$

where $\langle .,. \rangle_D^{\mathcal{C}}$ and $(.,.)_D^{\rho}$ denote the stiffness and mass bilinear forms associated to a given domain D characterized by $(\boldsymbol{\mathcal{C}}, \rho)$, $\mathcal{W} \subset H^1(\Omega)$ is the function space incorporating the relevant essential boundary conditions (if any), the linear form $\mathcal{F} \in \mathcal{W}'$ defines the applied time-harmonic loading and ω is the angular frequency.

Assuming the presence of a defect inside Ω, and that we can measure the resulting displacement $\boldsymbol{u}^{\text{ex}}$ on a surface Γ, we define the least-squares cost functional $J(\boldsymbol{w})$, with the elastodynamic displacement $\boldsymbol{w}$ associated to the given excitation and a known trial defect, by:

$$J(\boldsymbol{w}) = \frac{1}{2} \int_\Gamma |\boldsymbol{w}(\boldsymbol{x}) - \boldsymbol{u}^{\text{ex}}(\boldsymbol{x})|^2 \, \mathrm{d}S_{\boldsymbol{x}} \quad (2)$$

We now consider a specific trial defect $B_a = \boldsymbol{z} + a\mathcal{B}$ (Fig 1), centered at $\boldsymbol{z} \in \Omega$, of small size a and reference shape $\mathcal{B}$. It is a perfectly bonded inclusion filled with a material characterized by its Hooke tensor $\boldsymbol{\mathcal{C}}^\star = \boldsymbol{\mathcal{C}} + \Delta\boldsymbol{\mathcal{C}}$ and mass density $\rho^\star = \rho + \Delta\rho$. We denote $\boldsymbol{u}_a$ the displacement in the perturbed domain, and $\boldsymbol{v}_a = \boldsymbol{u}_a - \boldsymbol{u}$ the displacement perturbation. $J(\boldsymbol{u}_a)$ admits the exact expansion about $\boldsymbol{u}$:

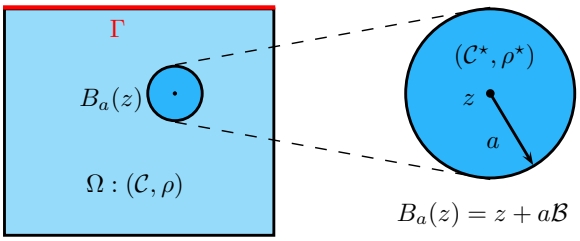

Figure 1: Computational domain and inclusion.

$$\begin{aligned} J(\boldsymbol{u}_a) &= J(\boldsymbol{u}) + J'(\boldsymbol{u}; \boldsymbol{v}_a) + J''(\boldsymbol{u}; \boldsymbol{v}_a, \boldsymbol{v}_a) \\ &= J(\boldsymbol{u}) + \Re \int_\Gamma \overline{(\boldsymbol{u} - \boldsymbol{u}^{\text{ex}})} \cdot \boldsymbol{v}_a + \frac{1}{2} \int_\Gamma |\boldsymbol{v}_a|^2 \end{aligned} \quad (3)$$

The goal is now to expand $J(\boldsymbol{u}_a)$ in powers of a. Similar expansions have been studied in e.g. [2] for rigid obstacles in 3D acoustic media and [5] for holes in 2D elastic bodies.

Define the adjoint field $\boldsymbol{p}$ as the solution of

$$\langle \boldsymbol{p}, \boldsymbol{w}\rangle_\Omega^{\mathcal{C}} - \omega^2 (\boldsymbol{p}, \boldsymbol{w})_\Omega^{\rho} = J'(\boldsymbol{u}; \boldsymbol{w}) \ \forall \boldsymbol{w} \in \mathcal{W}. \quad (4)$$

We can then compute $J'(\boldsymbol{u}; \boldsymbol{v}_a)$ as

$$J'(\boldsymbol{u}; \boldsymbol{v}_a) = -\langle \boldsymbol{p}, \boldsymbol{u}_a\rangle_{B_a}^{\Delta\mathcal{C}} + \omega^2 (\boldsymbol{p}, \boldsymbol{u}_a)_{B_a}^{\Delta\rho} \quad (5)$$

Expanding $\boldsymbol{v}_a$ in powers of a is now needed. As we will see, $J''(\boldsymbol{u}; \boldsymbol{v}_a, \boldsymbol{v}_a)$ requires only the leading contribution of $\boldsymbol{v}_a|_\Gamma$ whereas a higher-order expansion of $\boldsymbol{v}_a|_{B_a}$ is needed for evaluating (5).

Expansion of the solution perturbation. Following e.g. [3], $\boldsymbol{v}_a$ solves the integro-differential Lippmann-Schwinger equation:

$$\mathcal{L}_a[\boldsymbol{v}_a](\boldsymbol{x}) = -\langle \boldsymbol{u}, \boldsymbol{G}\rangle_{B_a}^{\Delta\mathcal{C}} + \omega^2 (\boldsymbol{u}, \boldsymbol{G})_{B_a}^{\Delta\rho} \quad (6)$$

with $\mathcal{L}_a[\boldsymbol{v}](\boldsymbol{x}) := \boldsymbol{v}(\boldsymbol{x}) + \langle \boldsymbol{v}, \boldsymbol{G}\rangle_{B_a}^{\Delta\mathcal{C}} - \omega^2 (\boldsymbol{v}, \boldsymbol{G})_{B_a}^{\Delta\rho}$ and $\boldsymbol{G} = \boldsymbol{G}(\cdot, \boldsymbol{x})$ is the elastodynamic Green's tensor for a unit point force applied at $\boldsymbol{x}$ and satisfying homogeneous boundary conditions consistent with problem (1) on $\partial\Omega$. Substituting the ansatz

$$\begin{aligned} \boldsymbol{v}_a(\boldsymbol{x}) = a\boldsymbol{V}_1(\bar{\boldsymbol{x}}) + a^2\boldsymbol{V}_2(\bar{\boldsymbol{x}}) + \tfrac{1}{2}a^3\boldsymbol{V}_3(\bar{\boldsymbol{x}}) \\ + \tfrac{1}{6}a^4\boldsymbol{V}_4(\bar{\boldsymbol{x}}) + \boldsymbol{\delta}_a(\boldsymbol{x}), \qquad \boldsymbol{x} \in B_a \end{aligned} \quad (7)$$

(with $\bar{\boldsymbol{x}} := (\boldsymbol{x}-\boldsymbol{z})/a \in \mathcal{B}$) into (6) and expanding the resulting equation in powers of a (in particular using that $\boldsymbol{G}(\boldsymbol{\xi},\boldsymbol{x}) = a^{-1}\boldsymbol{G}_\infty(\bar{\boldsymbol{\xi}}-\bar{\boldsymbol{x}})+O(1)$, with $\boldsymbol{G}_\infty$ denoting the *static* full-space Kelvin fundamental solution) yields a sequence of integral equations for the $\boldsymbol{V}_j$. These equations correspond to *elastostatic* problems for the normalized inclusion $\mathcal{B}$ embedded in an unbounded reference medium, and are solved with the help of Eshelby's equivalent inclusion method [4].

The remainder $\boldsymbol{\delta}_a$ in (7) solves an integro-differential equation of the form $\mathcal{L}_a[\boldsymbol{\delta}_a] = \boldsymbol{\gamma}_a$. The operator $\mathcal{L}_a : H^1(B_a) \to H^1(B_a)$ is shown to be invertible with bounded inverse, while $\boldsymbol{\gamma}_a$ can be estimated as $\|\boldsymbol{\gamma}_a\|_{H^1(B_a)} = O(a^{11/2})$. Consequently, there exists a constant $C > 0$ independent of a such that

$$\|\boldsymbol{\delta}_a\|_{H^1(B_a)} \leq C a^{11/2}. \tag{8}$$

For $\boldsymbol{x} \notin B_a$, plugging (7) in the form $\boldsymbol{v}_a(\boldsymbol{x}) \approx a\boldsymbol{V}_1(\bar{\boldsymbol{x}})$ into (6) yields the outer expansion

$$\begin{aligned}\boldsymbol{v}_a(\boldsymbol{x}) = -a^3\big[\,&\boldsymbol{\nabla}\boldsymbol{u}(\boldsymbol{z}):\boldsymbol{\mathcal{A}}:\boldsymbol{\nabla}\boldsymbol{G}(\boldsymbol{z},\boldsymbol{x}) \\ &- \omega^2\Delta\rho|\mathcal{B}|\boldsymbol{u}(\boldsymbol{z})\cdot\boldsymbol{G}(\boldsymbol{z},\boldsymbol{x})\,\big] + o(a^3),\end{aligned} \tag{9}$$

$\boldsymbol{\mathcal{A}}$ being the elastic moment tensor associated to $\mathcal{B}$, $\boldsymbol{\mathcal{C}}$ and $\Delta\boldsymbol{\mathcal{C}}$ [1,3].

Cost functional expansion. Substituting (7) into (5) and (9) into (3), $J(\boldsymbol{u}_a)$ is finally found to have an expansion of the form:

$$J(\boldsymbol{u}_a) = J_6(a,\boldsymbol{z}) + o(a^6) \tag{10}$$

$$\begin{aligned}\text{with}\quad J_6(a,\boldsymbol{z}) = J(\boldsymbol{u}) &+ a^3\mathcal{T}_3(\boldsymbol{z}) + a^4\mathcal{T}_4(\boldsymbol{z}) \\ &+ a^5\mathcal{T}_5(\boldsymbol{z}) + a^6\mathcal{T}_6(\boldsymbol{z}),\end{aligned}$$

the $o(a^6)$ estimate resulting from (8) and (9).

The $\mathcal{T}_j(\boldsymbol{z})$ are found to be given in terms of (i) the background field $\boldsymbol{u}$ and its derivatives at $\boldsymbol{z}$, (ii) the adjoint field $\boldsymbol{p}$ and its derivatives at $\boldsymbol{z}$, (iii) $\boldsymbol{\mathcal{A}}$ and other elastic moment tensors that involve the material parameters, the shape $\mathcal{B}$ and the angular frequency ω, and (iv) the complementary part of $\boldsymbol{G}$, i.e. $\boldsymbol{G} - \boldsymbol{G}_\infty = (\boldsymbol{G}_{\infty,\omega}-\boldsymbol{G}_\infty)+\boldsymbol{G}_C$, where $\boldsymbol{G}_{\infty,\omega}$ is the elastodynamic full-space fundamental solution and $\boldsymbol{G}_C$ accounts for the boundedness of Ω. In particular, $\mathcal{T}_3(\boldsymbol{z})$ is the well-known topological derivative:

$$\mathcal{T}_3(\boldsymbol{z}) = -\big[\,\boldsymbol{\nabla}\boldsymbol{u}:\boldsymbol{\mathcal{A}}:\boldsymbol{\nabla}\boldsymbol{p} - \omega^2\Delta\rho|\mathcal{B}|\boldsymbol{u}\cdot\boldsymbol{p}\,\big](\boldsymbol{z}).$$

Moreover, $\mathcal{T}_4(\boldsymbol{z}) = 0$ for any centrally-symmetric shape $\mathcal{B}$. The complementary part $\boldsymbol{G}_{\infty,\omega} - \boldsymbol{G}_\infty$ (known analytically) is involved in $\mathcal{T}_5(\boldsymbol{z})$ and $\mathcal{T}_6(\boldsymbol{z})$, while $\boldsymbol{G}_C$ appears in $\mathcal{T}_6(\boldsymbol{z})$ only. Since the exact computation of $\boldsymbol{G}_C$ would require solving an elastodynamic problem on Ω for each trial location $\boldsymbol{z}$, we plan to use an approximation method to save computational time.

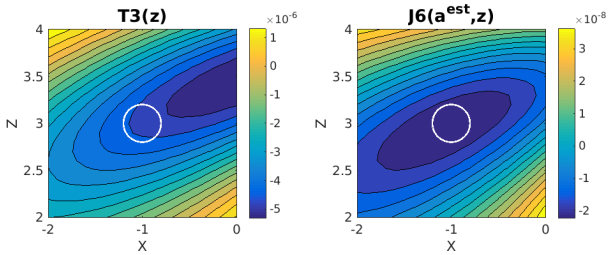

Figure 2: $\mathcal{T}_3(\boldsymbol{z})$ and $J_6(a^{\text{est}},\boldsymbol{z})$ plotted in the (XZ) plane around the obstacle (in white).

Closed-form formulae for the $\mathcal{T}_j$ can be obtained when $\mathcal{B}$ is spherical (for which case we provide explicit expressions) or ellipsoidal.

Identification. Following [2], estimates of the location $\boldsymbol{z}^{\text{est}}$ and size a^{est} of the real defect can then be sought as minimizers of $J_6(a,\boldsymbol{z})$, with $\boldsymbol{z}$ spanning a predefined sampling grid. This entails computing the $\mathcal{T}_j(\boldsymbol{z})$ over the sampling grid and minimizing $a \mapsto J_6(a,\boldsymbol{z})$ for each $\boldsymbol{z}$, the latter step being very fast and straightforward

A preliminary example is set in free space (so that $\boldsymbol{G}_C = 0$) for a spherical scatterer of radius $0.1\lambda_S$ illuminated by a plane P-wave travelling along the positive x-direction, with a discrete array of displacement sensors lying behind the scatterer. The above procedure yields the size estimate $a^{\text{est}} \approx 0.105\lambda_S$; moreover, the estimated location $\boldsymbol{z}^{\text{est}}$ is found to be very close to the true center of the scatterer. The contour plot of $J_6(a^{\text{est}},\boldsymbol{z})$ (Fig 2) shows improved localisation (relative to the topological derivative $\mathcal{T}_3(\boldsymbol{z})$) for this partial-aperture configuration.

References

[1] H. Ammari and H. Kang. *Polarization and moment tensors.* Springer, 2007.

[2] M. Bonnet. Inverse acoustic scattering by small-obstacle expansion of a misfit function. *Inverse Problems*, 24(3):035022, 2008.

[3] M. Bonnet and G. Delgado. The topological derivative in anisotropic elasticity. *Quart. J. Mech. Appl. Math.*, 66:557–586, 2013.

[4] T. Mura. *Micromechanics of defects in solids.* M. Nijhoff Publishers, 1982.

[5] M. Silva, M. Matalon, and D. A. Tortorelli. Higher order topological derivatives in elasticity. *Int J Solids Struct.*, 47:3053 – 3066, 2010.

High order asymptotic expansion for thin periodic layers in polygonal domains

Bérangère Delourme[1,*], **Kersten Schmidt**[2], **Adrien Semin**[3]

[1]Université Paris 13, Sorbonne Paris Cité, LAGA, UMR 7539, F-93430 Villetaneuse, France
[2]Research center Matheon & Department of Mathematics, TU Berlin, Berlin, Germany
[3]Department of Mathematics, TU Berlin, Berlin, Germany
[*]Email: delourme@math.univ-paris13.fr

Abstract

The present work deals with the resolution of the Poisson equation in a bounded domain made of a thin and periodic layer of finite length placed into an homogeneous medium. We provide a high order asymptotic expansion which takes into account the boundary layer effect occurring in the vicinity of the periodic layer as well as the corner singularities appearing in the neighborhood of the extremities of the layer. Our approach mixes the method of matched asymptotic expansions and the method of surface homogenization for periodic layers.

Keywords: asymptotic analysis, surface periodic homogenization, singular asymptotic expansions.

1 Introduction

We consider a bounded domain Ω^δ (see Fig. 1) that consists of the union of two rectangular domains $\Omega_\pm$ minus the set $\Omega^\delta_{\rm hole}$ made of similar small holes equi-spaced along the interface $\Gamma = \partial\Omega_+ \cap \partial\Omega_-$. The distance between two consecutive holes and the diameter of the holes are supposed to be of the same order of magnitude δ, which is supposed to be small. We are interested in the solution $u^\delta \in H^1(\Omega^\delta)$ of the Poisson equation

$$-\Delta u^\delta = f \text{ in } \Omega^\delta, f \in L^2(\Omega^\delta), \tag{1}$$

homogenous Neumann boundary conditions on the small holes,

$$\partial_n u^\delta = 0 \text{ on } \partial\Omega^\delta_{\rm hole}, \tag{2}$$

together with homogeneous Dirichlet boundary conditions on the remaining part of the boundary:

$$u^\delta = 0 \text{ on } \partial\Omega^\delta \setminus \partial\Omega^\delta_{\rm hole}. \tag{3}$$

It is well known that Problem (1-2-3) is well posed.
Our aim is to understand the behavior of u^δ as δ tends to 0. The layer of small holes generates two different kinds of singular behaviors.

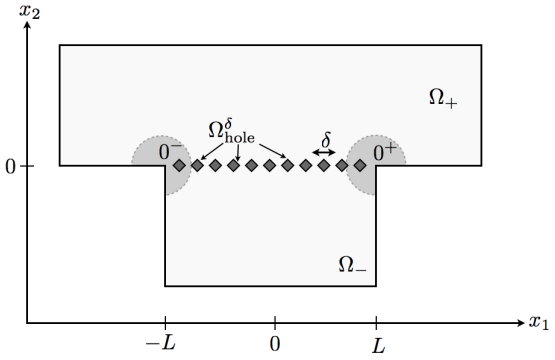

Figure 1: The domain Ω^δ.

First, there is an exponentially decaying boundary layer effect in the vicinity of the periodic layer (see e.g. [1], [2] and references therein). In addition, as mentioned (and investigated) in the case of an homogeneous thin layer in [3], corner singularities appear in the neighborhood of the vertices $0^\pm = (\pm L, 0)$ (see Fig. 1) of the two reentrant corners of angle $\frac{3\pi}{2}$, *i.e.*, at the extremities of the periodic layer.

2 Asymptotic expansion

In this part, for the sake of simplicity, we assume that f is compactly supported in Ω_+. Based on the previous remark, we construct an asymptotic expansion of u^δ using the method of matched asymptotic expansion. In the present context, following [3] and [4], we distinguish a far field area, located far from the reentrant corners (light grey on Fig. 1) from two near field areas located in the vicinity of them (dark grey on Fig. 1).

2.1 Far field area

For $|x_1| < L$, the solution u^δ takes the form

$$\sum_{(n,q)\in\mathbb{N}^2} \delta^{\frac{2}{3}n+q} \left(u^\delta_{n,q}(\mathbf{x})\chi(\frac{x_2}{\delta}) + \Pi^\delta_{n,q}(x_1, \frac{\mathbf{x}}{\delta}) \right), \tag{4}$$

where $\mathbf{x} = (x_1, x_2) \in \mathbb{R}^2$. For $|x_1| > L$, the solution u^δ takes the form

$$\sum_{(n,q)\in\mathbb{N}^2} \delta^{\frac{2}{3}n+q} u^\delta_{n,q}(\mathbf{x}). \tag{5}$$

The macroscopic terms $u^\delta_{n,q}$ are defined in the limit domain $\Omega_+ \cup \Omega_-$. They might jump across Γ. The periodic correctors $\Pi^\delta_{n,q}(x_1, X_1, X_2)$ are defined in the periodicity cell $\mathcal{B}$ (see Fig. 2 (left)). They are 1-periodic with respect to X_1 and exponentially decaying as $|X_2|$ tends to $+\infty$. The function $\chi(t)$ is a smooth cut-off function equal to 1 for $|t| > 2$ and 0 for $|t| < 1$. Both macroscopic and boundary layer correctors might have a polynomial dependance on $\ln \delta$.

The appearance of the terms $\delta^{\frac{2}{3}n}$ in the asymptotic expansion is strongly linked to the existence of a set of functions $s_n = r^{\frac{2}{3}n} \sin(\frac{2n}{3}\theta)$, $n \in \mathbb{Z} \setminus \{0\}$, satisfying $\Delta s_n = 0$ in the angular sector of angle $\frac{3\pi}{2}$ and vanishing on its boundary (homogeneous Dirichlet boundary conditions).

2.2 Near field areas

In the vicinity of the two reentrant corners, we construct an expansion of the form

$$\sum_{(n,q)\in\mathbb{N}^2} \delta^{\frac{2}{3}n+q} U^\delta_{n,q}(\mathbf{x}). \tag{6}$$

The near field terms $U^\delta_{n,q}$ are defined in the normalized unbounded domain $\hat{\Omega}$ represented in Figure 2 (right). Here again, the near field terms might have a polynomial dependance on $\ln \delta$. Near field terms satisfy Laplace problems in $\hat{\Omega}$. These problems require a careful analysis (cf. [5]).

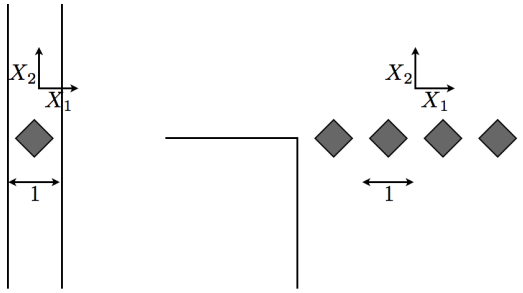

Figure 2: The periodicity cell $\mathcal{B}$ (left) and the normalized domain $\hat{\Omega}$ (right).

2.3 Matching procedure

As usual for the matched asymptotic method, we assume that near field expansion and far field expansion coincide in an intermediate zone, which is called matching area. The matching procedure plays a crucial role in the definition of the terms of the far and near field expansions.

References

[1] J. R. Poirier, A. Bendali and P. Borderies, Impedance boundary conditions for the scattering of time-harmonic waves by rapidly varying surfaces, *IEEE Trans. Antennas and Propagation* **54** (2006), pp. 995-1005.

[2] X. Claeys and B. Delourme, High order asymptotics for wave propagation across thin periodic interfaces, *Asymptot. Anal.* **83** (2013), pp. 35-82.

[3] G. Caloz, M. Costabel, M. Dauge and G. Vial, Asymptotic expansion of the solution of an interface problem in a polygonal domain with thin layer, *Asymptot. Anal.* **50** (2006), pp. 121-173.

[4] S. A. Nazarov, Dirichlet problem in an angular domain with rapidly oscillating boundary: modeling of the problem and asymptotic of the solution, *St. Petersburg. Math. J.* **19** (2008), pp. 297-326.

[5] S. A. Nazarov, The Neumann problem in angular domains with periodic and parabolic perturbations of the boundary, *Tr. Mosk. Mat. Obs.* **69** (2008), pp. 182-241.

Error estimates for an Helmholtz transmission problem with a perforated thin structure and corner singularities

Bérangère Delourme[1], **Kersten Schmidt**[2], **Adrien Semin**[3,*]

[1]LAGA, Université Paris 13, Villetaneuse, France
[2]Research center Matheon & Institute of Mathematics, TU Berlin, Berlin, Germany
[3]Institute of Mathematics, TU Berlin, Berlin, Germany
*Email: adrien.semin@math.tu-berlin.de

Abstract

This paper is dedicated to the analysis of the time-harmonic wave equation in a perforated polygonal domain. We construct and justify an asymptotic expansion that extends the results obtained for the Poisson problem (presented in another talk by the authors) to the Helmholtz equation. We pay particular attention to the resolution of near field problems and we prove error estimates. In addition, we present some numerical results.

Keywords: surface homogenization, matched asymptotic expansions, corner singularities

1 Setting of the problem

In this paper, we are interested in the resolution of the Helmholtz equation in the polygonal bounded domain Ω^δ represented on Fig. 1, which consists of the union of two rectangular domains $\Omega_\pm$ minus the set $\Omega^\delta_{\text{hole}}$ made of similar small holes equi-spaced along the interface $\Gamma = \partial\Omega_+ \cap \partial\Omega_-$. The distance between two consecutive holes and the diameter of the holes are supposed to be of the same order of small magnitude δ. We are interested in the solution $u^\delta \in H^1(\Omega^\delta)$ of the Helmholtz equation

$$-\Delta u^\delta - k^2 u^\delta = f \text{ in } \Omega^\delta, f \in L^2(\Omega^\delta), \qquad (1)$$

where the wavenumber k differs from a constant value k_0 on the domain $(-L, L) \times (-\delta, \delta)$ by a function $\widehat{k}(\cdot/\delta)$, which is 1-periodic with respect to X_1. We complete problem (1) with homogenous Neumann boundary conditions on the small holes

$$\partial_{\mathbf{n}} u^\delta = 0 \text{ on } \partial\Omega^\delta_{\text{hole}}, \qquad (2)$$

first order absorbing boundary conditions on the left and right boundaries Γ_- and Γ_+, and homogeneous Neumann boundary conditions on the remaining part of the boundary:

$$\begin{aligned} \partial_{\mathbf{n}} u^\delta - \mathrm{i}k_0 u^\delta = 0 \text{ on } \Gamma_\pm, \\ \partial_{\mathbf{n}} u^\delta = 0 \text{ on } \partial\Omega^\delta \setminus \{\partial\Omega^\delta_{\text{hole}} \cup \Gamma_\pm\}. \end{aligned} \qquad (3)$$

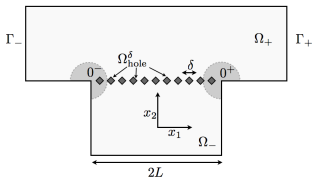

Figure 1: The domain Ω^δ.

The objective of this work is to construct an asymptotic expansion of the solution u^δ as δ tends to 0. To do so, we use the method of matched asymptotic expansion, which yields in the present case to consider two distincts areas where the asymptotics expansion are different. Far from the two corners, we use an 'ansatz' based on the method of periodic surface homogenization (see *e.g* [2] and references therein): u^δ is given by

$$\sum_{(n,q)\in\mathbb{N}^2} \delta^{\frac{2n}{3}+q} \left(u^\delta_{n,q}(\mathbf{x}) \chi\left(\frac{x_2}{\delta}\right) + \Pi^\delta_{n,q}\left(x_1, \frac{\mathbf{x}}{\delta}\right)\right), \qquad (4)$$

where χ is a cut-off function, $\Pi_{n,q}$ are periodic with respect to $X_1 = \frac{x_1}{\delta}$ and exponentially decaying functions with respect to x_2/δ. In the vicinity of the two reentrant corners, we make the local variable change $\mathbf{X} = (\mathbf{x} - 0^-)/\delta$ (and, similarly for the right corner), and we construct an expansion of the form

$$u^\delta(\mathbf{x}) = \sum_{(n,q)\in\mathbb{N}^2} \delta^{\frac{2n}{3}+q} U^\delta_{n,q}(\mathbf{X}), \qquad (5)$$

where the functions $U^\delta_{n,q}$ are defined on the unbounded domain $\hat{\Omega}_-$ (see Fig. 2).

2 Embedded Laplace equations

The near field functions $U^\delta_{n,q}$ satisfy the following collection of Laplace equations posed in the

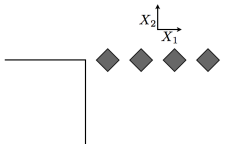

Figure 2: The normalized domain $\hat{\Omega}_-$.

unbounded domain $\hat{\Omega}_-$ (similar for $\hat{\Omega}_+$):

$$\begin{cases} -\Delta U^\delta_{n,q} = \widehat{k}^2 U^\delta_{n,q-2} \text{ in } \hat{\Omega}_-, \\ \partial_{\mathbf{n}} U^\delta_{n,q} = 0 \text{ on } \partial\hat{\Omega}_-, \\ U^\delta_{n,0} \sim R^{\frac{2n}{3}} \cos\left(\frac{2n}{3}\left(\theta+\frac{\pi}{2}\right)\right) \text{ for large } R, \end{cases} \tag{6}$$

where (R,θ) are polar coordinates centered at 0^-. If $\widehat{k} = k_0$ and there were no holes, the terms $U_{n,q}$ can be explicitly determined. Indeed, the first terms are given by

$$\begin{aligned} &U^\delta_{n,0} = R^{\frac{2n}{3}} \cos\left(\frac{2n}{3}\left(\theta+\frac{\pi}{2}\right)\right), U^\delta_{n,1} = 0, \\ &U^\delta_{n,2} = \frac{3k_0^2}{4(2n+3)} R^{\frac{2n}{3}+2} \cos\left(\frac{2n}{3}\left(\theta+\frac{\pi}{2}\right)\right), \end{aligned} \tag{7}$$

and hence the sum

$$\sum_{q=0}^{\infty} \delta^q U^\delta_{n,q} = \Gamma\left(\frac{5}{3}\right) 2^{\frac{2}{3}} \cos\left(\frac{2n}{3}\left(\theta+\frac{\pi}{2}\right)\right) J_{\frac{2n}{3}}(\delta k_0 R)$$

satisfies $(\Delta + \delta^2 k_0^2)U = 0$. The natural spaces to describe the behaviour of the functions $U^\delta_{n,q}$ are the Kondratiev spaces $\mathrm{V}^\ell_\beta(\Omega_-)$ (see *e.g* [1]), for which the norm

$$\|v\|^2_{\mathrm{V}^\ell_\beta(\Omega_-)} = \sum_{m=0}^{\ell} \left\|(1+R)^{\beta-\ell+m} \nabla^m_{\mathbf{X}} v\right\|^2_{\mathrm{L}^2(\Omega)}$$

is finite.

If now $\widehat{k} \neq k_0$ and if there were still no holes, then the function $U^\delta_{n,2}$ in (7) is now given by

$$\begin{aligned} U^\delta_{n,2} = &\frac{3k_0^2}{4(2n+3)} R^{\frac{2n}{3}+2} \cos\left(\frac{2n}{3}\left(\theta+\frac{\pi}{2}\right)\right) \\ &+ X_1^{\frac{2n}{3}+2} \Psi(X_1, X_2) + O(R^{\frac{2n}{3}+1}) \end{aligned}$$

where $\Psi(X_1, X_2)$ is a 1-periodic function in X_1 and exponentially decaying in X_2. If $\widehat{k}$ is constant in the layer, then Ψ does not depend on X_1 and $U_{n,2}$ can still be described using the Kondratiev spaces as done in [1] for the case of a thin layer surrounding a polygonal domain.

However, if $\widehat{k}$ depends on X_1, then Ψ depends on X_1 as well. Then, when differentiating $U^\delta_{n,2}$, the exponents in R decrease by 1 for each derivative far away from the layer, where inside and close to the layer the exponents remain the same. Then, the description of $U_{n,2}$ and the solution theory of (6) requires the introduction on the weighted spaces $\mathbf{V}^\ell_{\beta,\gamma}(\hat{\Omega}_-)$ (see [3]) for which the norm

$$\|v\|^2_{\mathbf{V}^\ell_{\beta,\gamma}(\hat{\Omega}_-)} = \sum_{m=0}^{\ell} \left\|(1+R)^{\beta-\ell+m} \rho^{\gamma-\ell+m} \nabla^m_{\mathbf{X}} v\right\|^2_{\mathrm{L}^2(\hat{\Omega}_-)}$$

is finite, and the weight ρ is given by

$$\rho(R,\theta) = \sqrt{(1+R^2)^{-1} + \theta^2}.$$

3 Error estimates

Let N be a real number such that $3N \in \mathbb{N}$. The existence of the terms of the expansion being proved, we can build a global approximation $u^{\delta,N}$ of the solution by taking a finite number of terms in (4, 5) corresponding to the indices (n,k) such that $\frac{2n}{3} + q \leqslant N$. We prove the following result:

Theorem 1 *For δ sufficiently small, the error between u^δ and $u^{\delta,N}$ in H^1-norm is bounded by $\delta^{N+\frac{1}{3}}$.*

References

[1] G. Caloz, M. Costabel, M. Dauge and G. Vial, Asymptotic expansion of the solution of an interface problem in a polygonal domain with thin layer, *Asymptot. Anal.*, **50** (2006), pp. 121–173.

[2] X. Claeys and B. Delourme, High order asymptotics for wave propagation across thin periodic interfaces, *Asymptot. Anal.*, **83** (2013), pp. 35–82.

[3] S.A. Nazarov, The Neumann problem in angular domains with periodic and parabolic perturbations of the boundary, *Tr. Mosk. Mat. Obs.*, **69** (2008), pp. 182–241.

Study of spoof plasmons in an array of sound hard to sound soft inclusions

Jean-Francois Mercier[1,*], **Agnès Maurel**[2]
[1]POEMS, CNRS-INRIA-ENSTA, Palaiseau, France
[2]Institut Langevin, CNRS, ESPCI ParisTech, Paris, France
[*]Email: jean-francois.mercier@ensta.fr

Abstract

It is nowadays possible to design materials with tunable acoustic properties. While classical plasmon have been proposed for periodic arrays of sound hard inclusions, we show that penetrable inclusions allows to produce plasmon with wavelengths tuned by the relative densities between the inclusion material and the surrounding medium. Plasmons are solutions of an eigenvalue problem in which the plasmons frequencies are the eigenvalues. Thanks to the Min-Max principle, general estimates on the eigenvalues are found. Moreover it is demonstrated that sound soft materials are able to increase the efficiency in the generation of sub-wavelength plasmons, with much lower values of the wavelength than with sound hard materials.

Keywords: plasmon, homogenization, Min-Max

1 Geometry and equation

We consider the acoustic propagation through an array of inclusions of width ℓ, of filling fraction φ, of constant density ρ_1 and sound celerity c_1 ($B_1 = \rho_1 c_1^2$) (Fig. 1 (a)). The outside

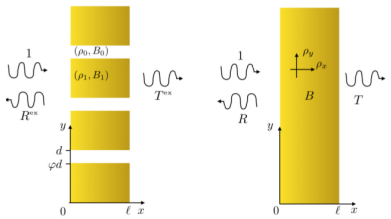

(a) (b)

Figure 1: (a) Geometry of the array (b) equivalent birefringent layer.

medium is the air indexed by 0. At low frequencies ($kd \ll 1$ where $k = \omega/c_0$ is the wavenumber in the air), the homogenization theory enables us to approximate the layered medium by an homogeneous but anisotropic medium (Fig. 1 (b)). In time harmonic regime $e^{-i\omega t}$, it leads to the wave equation for the pressure $P(x, y)$:

$$\frac{\partial}{\partial x}\left(\tilde{a}\frac{\partial P}{\partial x}\right) + \tilde{b}\frac{\partial^2 P}{\partial y^2} + k^2\tilde{c}P = 0.$$

$\tilde{a}(x)$, $\tilde{b}(x)$ and $\tilde{c}(x)$ are equal to 1 outside $[0, \ell]$ (the air is the reference medium) and are defined for $x \in [0, \ell]$ by $\tilde{a} = a = (\varphi\alpha/q) + 1 - \varphi$, $\tilde{b} = b = 1/[(\varphi q/\alpha) + 1 - \varphi]$ and $\tilde{c} = c = (\varphi/\alpha q) + 1 - \varphi$. $q = \alpha\rho_1/\rho_0$ is the ratio of impedances with $\alpha = c_1/c_0$ the ratio of celerities. In the following, our aim is to determine the spoof plasmons (or guided waves) propagating at low frequencies in this anisotropic homogenized medium for a fixed value of α and for q going from infinity (hard or heavy material) to zero (soft or light material).

2 The eigenvalue problem

We look for a solution of the form $P(x, y) = p(x)e^{i\beta y}$ with $p(x) \in L^2(\mathbb{R})$. For a fixed value of β, we introduce the unbounded operator A

$$A : p \;\rightarrow\; \frac{1}{\tilde{c}}\left[-\frac{d}{dx}\left(\tilde{a}\frac{dp}{dx}\right) + \beta^2\tilde{b}p\right],$$

of $L^2(\mathbb{R})$ with domain

$$D(A) = \left\{p \in L^2(\mathbb{R}); \frac{d}{dx}\left(\tilde{a}\frac{dp}{dx}\right) \in L^2(\mathbb{R})\right\}.$$

We are lead to solve the eigenvalue problem:

For $\beta \in \mathbb{R}^+$, find $(p, \lambda) \in D(A) \times \mathbb{R}^+$ such that $Ap = \lambda p$. To each eigenvalue λ_n corresponds the plasmon frequency $k_n = \sqrt{\lambda_n}$.

3 General results

The spectrum of A satisfies $\sigma(A) \subset [(\beta/n)^2, \infty[$, where $n^2 = c/b$ is the slab index. The essential spectrum is $\sigma_{ess}(A) = [\beta^2, \infty[$. We take $\alpha < 1$ (slow inclusions) which ensures that $n > 1$ for all q and $\varphi \in [0, 1]$ values. Therefore, if the discrete spectrum σ_d exists, it is located in $[(\beta/n)^2, \beta^2[$.

Let us characterize the discrete spectrum of A. We note γ_m, $m \geq 1$, the Min-Max values of

A [1]. The Min-Max principle indicates that if $\gamma_m < \beta^2$, then γ_m is an eigenvalue, noted λ_m, $m = 1, \cdots, \mathcal{N}$ with $\mathcal{N}$ the number of eigenvalues. Using the usual Dirichlet and Neumann comparison principles [1], we get the eigenvalues control: $\min[\lambda_m^N, \beta^2] \leq \gamma_m \leq \lambda_m^D$, where

$$\lambda_m^D = \frac{a}{c}\left(\frac{m\pi}{\ell}\right)^2 + \left(\frac{\beta}{n}\right)^2 \quad \text{and} \quad \lambda_m^N = \lambda_{m-1}^D.$$

λ_m^D and λ_m^N are simply the eigenvalues of A restricted to $]0, \ell[$ with respectively Dirichlet or Neumann boundary conditions at $x = 0, \ell$.

4 Some limit cases

• If $q \to \infty$ (sound hard inclusions): then $n \to \infty$ and $a/c \sim 1$. Thus $\lambda_m^D = (m\pi/\ell)^2$ and $\mathcal{N} \sim \beta\ell/\pi$. It is possible to prove that $\lambda_1 \sim \lambda_1^D$ when $\beta \to \infty$ [1]. This means that a plasmon with a small wavelength (large β) for a small frequency k is not possible ($k \sim \pi/\ell$ for $\beta \to \infty$).
• If $q \to 0$ (sound soft inclusions): then $n \to \infty$ and $a/c \sim \alpha^2$ which leads to $\lambda_m^D = (\alpha m\pi/\ell)^2$ and to the estimation $\mathcal{N} \sim \beta\ell/\alpha\pi$.

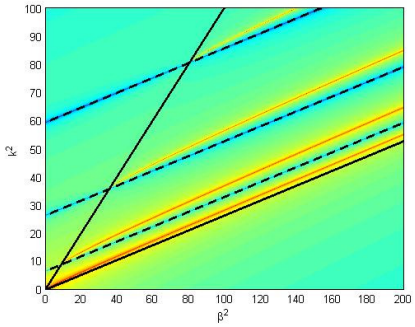

Figure 2: For $q = 10^{-1}$ and for $m = 1, 2, 3$, $\lambda_m(\beta^2)$ in red, λ_m^D in dashed lines, $k^2 = \beta^2$ and $k^2 = \beta^2/n^2$ in solid lines.

Eigenvalues and upper and lower bounds of the eigenvalues are plotted in Fig. 2 for the small value $q = 10^{-1}$. $\lambda_1(\beta^2)$ is found close to the slab light line $k^2 = \beta^2/n^2$ (bottom line).

5 Behavior of λ_1 when $q \to 0$

Here we prove that for any $\beta > 0$, the first eigenvalue tends to zero when the inclusions become soft. This is achieved by using the Min-Max principle: $\gamma_1 \leq R(p)$ for any $p \in H^1(\mathbb{R})$ where

$$R(p) = \int_{\mathbb{R}} a \left|\frac{dp}{dx}\right|^2 + \beta^2 b|p|^2 / \int_{\mathbb{R}} c|p|^2,$$

is the Rayleigh quotient. We consider the test field $p_0(x) = e^{\beta x}$ for $x \leq 0$, $p_0(x) = 1$ for $0 \leq x \leq \ell$, $p_0(x) = e^{-\beta(x-\ell)}$ for $\ell \leq x$. A simple calculation leads for small values of q to

$$\lambda_1^N = \frac{\alpha q \beta^2}{\varphi(1-\varphi)} \leq \lambda_1 \leq \frac{\alpha q}{\varphi(1-\varphi)}\left[\beta^2 + \frac{2\beta(1-\varphi)}{\ell}\right].$$

Therefore, $\lambda_1(q)$ tends to zero for a soft material. This result is confirmed numerically in Fig. 3 (λ_1 is the lowest red curve).

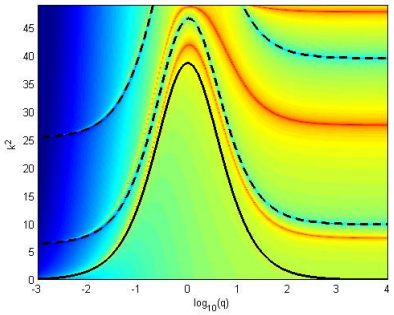

Figure 3: For $\beta = 7$, $m = 1, 2$, $\lambda_m(q)$ in red, $\lambda_m^D(q)$ in dashed lines, $\lambda_1^N(q) = \beta^2/n(q)^2$ in solid line.

This leads to an interesting consequence for the lowest plasmon frequency given by $k^2 = \lambda_1(\beta, q)$. For practical applications in imaging, it is important to have k small and β large, which corresponds to produce a small wavelength plasmon λ_{pl} (of the size of the defect to image) with a large external wavelength λ. This is possible: for $\varphi = 0.7$, we have found $\lambda/\lambda_{pl} = 2.6 \to 18$ when $q = 10^4 \to 10^{-3}$. These analytical results have been compared to direct calculations to check the validity of the homogenized approach.

References

[1] A. S. Bonnet, G. Caloz, and F. Mahé, Guided modes of integrated optical guides. A mathematical study, *IMA journal of applied mathematics*, **60** 3 (1998), pp.225–261.

Numerical Approximation of Solitary waves in Some Internal Wave Systems

Angel Duran[1,*], **Dimitrios Mitsotakis**[2]

[1]Department of Applied Mathematics, University of Valladolid, Valladolid, Spain
[2]Victoria University of Wellington School of Mathematics, Statistics and Operations Research, Wellington, New Zealand

[*]Email: angel@mac.uva.es

Abstract

We consider the Benjamin-Ono and the Intermediate Long Wave systems of [1] that model two-way propagation of long internal waves of small amplitude along the interface of two fluid layers under the effects of gravity. After reviewing some theoretical properties of the models at hand, we present numerical evidence of the existence of solitary waves. Some properties of the waves, suggested by the numerical experiments, are discussed including the speed-amplitude relation and their asymptotic decay rate. We also present some numerical studies concerning the dynamics of the waves which involve experiments about their interactions, stability properties along with comparisons with their unidirectional counterparts.

Keywords: Benjamin-Ono system, Intermediate Long wave system, Internal solitary waves

1 Introduction

The idealized model in [1] consists of two inviscid, homogeneous fluids of depths $d_j, j = 1, 2$ and densities $\rho_j, j = 1, 2$ with $\rho_2 > \rho_1$. The upper layer is bounded above by a horizontal rigid lid while the lower layer is bounded below by an impermeable, horizontal, flat bottom. The deviation of the interface, denoted by ζ, is assumed to be a graph over the bottom and surface tension effects are not considered.

The approach in [1] is based on the reformulation of the Euler system with two nonlocal operators. Then, different asymptotic models, consistent with the Euler system, are derived. The systems considered here correspond to the assumptions for which the interfacial wave is of small amplitude with respect to the upper fluid layer, which is shallow. In the ILW regime, the amplitude of the interface is also small compared to the lower layer, while in the BO regime the lower layer is of infinite depth (i.e. $d_2 = \infty$). We will consider the corresponding one-dimensional versions of the systems, which have the form

$$\begin{aligned}\left[1+\sqrt{\mu}\frac{\alpha}{\gamma}\mathcal{H}\right]\zeta_t+\frac{1}{\gamma}\left((1-\varepsilon\zeta)u\right)_x & \\ -(1-\alpha)\frac{\sqrt{\mu}}{\gamma^2}\mathcal{H}u_x &= 0,\\ u_t+(1-\gamma)\zeta_x-\frac{\varepsilon}{2\gamma}(u^2)_x &= 0,\end{aligned}$$

where u is the horizontal velocity, a is a typical wave amplitude and λ is a typical wavelength, $\varepsilon = a/d_1$ and $\mu = d_1^2/\lambda^2$ denote, respectively, the amplitude and long-wavelength parameters for the upper fluid, $\gamma = \rho_1/\rho_2 < 1$ is the density ratio and α is a positive parameter. The Benjamin-Ono regime assumes $\mu \sim \varepsilon^2 \ll 1$. Finally, $\mathcal{H}$ is a nonlocal operator with Fourier symbol $\widehat{\mathcal{H}f}(k) = |k|\coth(\sqrt{\mu_2}|k|)\widehat{f}(k)$, $k \in \mathbb{R}$ in the ILW case and $\widehat{\mathcal{H}f}(k) = |k|\widehat{f}(k)$, $k \in \mathbb{R}$ in the BO case.

2 Main Goals

Our purpose is to study, by numerical means, the existence and dynamics of solitary wave solutions for these systems. The existence of solitary wave profiles is analyzed by different computational techniques and some properties of the waves are suggested. From these computed profiles, a numerical study of the dynamics of the solitary waves is carried out. This involves comparisons with related unidirectional models, interactions and stability under small perturbations.

3 References

References

[1] J.L. Bona, D. Lannes and J.-C. Saut, Asymptotic models for internal waves, *J. Math. Pures Appl.*, **89** (2008), pp. 538-566.

Application of the Entropy Viscosity Method to Hermite Methods for Shock Problems

Adeline Kornelus[1,*], **Daniel Appelö**[1]

[1]Department of Mathematics and Statistics, The University of New Mexico

[*]Email: kornelus@unm.edu

Abstract

Hermite methods are polynomial based methods of arbitrary order whose degrees of freedom are the solution and its m first derivatives at each vertex. The convergence and stability theory of the methods were developed in [1] for smooth solutions to hyperbolic partial differential equations. The methods work well for linear advection of discontinuities, as decribed in [2], but does not have sufficient built-in dissipation to handle solutions with shocks. Moreover, they are not in flux conservative form.

In this paper, we show how the entropy viscosity method [3], which constructs a local artificial nonlinear viscosity based on the entropy residual, can be adopted to the Hermite framework. We also extend the methods to be conservative. We discuss implementational details and present numerical experiments illustrating the effectiveness and accuracy of the resulting methods.

Keywords: Shock, Hermite method, Entropy Viscosity, artificial viscosity, high order method

1 Introduction

In computational fluid dynamics, we typically have to compute the solution to conservation laws

$$\partial_t u(\mathbf{x},t) + \nabla \cdot f(u(\mathbf{x},t)) = 0, \mathbf{x} \in D, t \geq 0, \quad (1)$$

where D denotes the spatial domain. We are interested in solutions to Eq. (1) that involve shocks and also small amplitude smooth waves. While high order methods work well for the latter, they generally do not have enough natural dissipation to break the shocks. To accommodate the lack of viscosity, we add an artificial viscosity term on the right hand side of Eq. (1), so the PDE becomes

$$\partial_t u(\mathbf{x},t) + \nabla \cdot f(u(\mathbf{x},t)) = \nu \Delta u(\mathbf{x},t), \quad (2)$$

where the viscosity coefficient, ν, is found using the entropy viscosity method as outlined in [3]. In this paper, we use Hermite methods as a building block to solve the PDE, and then integrate the entropy viscosity method into Hermite methods for shock capturing capability.

2 Description of Methods

We will describe Hermite methods only in 1-dimension as the extension to higher dimension is straightforward. We then introduce a number of significant concepts in the entropy viscosity method.

2.1 Hermite Methods

Hermite methods are polynomial based methods of arbitrary degree whose Degrees of Freedom (DoF) are the solution and its m first derivatives at each vertex. For a domain $D = [x_L, x_R]$, we generate a mesh with a primal and a dual grid. Let $\mathcal{G}^p$ be the primal grid and $\mathcal{G}^d$ be the dual grid defined by

$$\mathcal{G}^p = \{x_j\} = x_L + jh_x,\ j = 0, ..., N, \quad (3)$$

$$\mathcal{G}^d = \{x_{j+1/2}\} = x_L + \left(j + \frac{1}{2}\right) h_x, j = 0, ..., N-1, \quad (4)$$

where $h_x = \frac{x_R - x_L}{N}$ is the distance between two adjacent nodes and N is the number of cells. Time is discretized by $t_n = t_0 + n\Delta t$, where t_0 denotes the initial time.

The structure of the methods primarily consists of two steps:

- Interpolation, compute a degree $(2m + 1)$ Hermite interpolant at each cell, using $(m + 1)$ DoF from two adjacent vertices. The resulting polynomial is piecewise C^m, and can be expressed locally as a (truncated) Taylor series approximation centered at the midpoint of the cell,

$$\begin{aligned} u(x,t_n) &\approx p_{j+1/2}(x,t_n) \\ &= \sum_{k=0}^{2m+1} c_k(t_n) \left(x - x_{j+1/2}\right)^k, \\ x &\in [x_j, x_{j+1}],\ j = 0, ..., N-1. \end{aligned} \quad (5)$$

- Evolution, evolve the coefficients $c_k(t)$, $k = 0, ..., 2m + 1$ which represents the discrete solution and its derivatives, according to the PDE, using an ODE solver.

The original Hermite methods, as in [1], are not flux conservative. Here, we discuss a conservative way of computing flux, which guarantees that the numerical solution does not converge to the wrong solutions.

2.2 The Entropy Viscosity Method

The entropy viscosity method introduces a nonlinear dissipation function based on the residual of the entropy inequality associated with the PDE. This entropy residual is large near shocks and practically zero everywhere else so it serves as a great shock detector. Now consider again Eq. (2) with $\nu = \mathcal{S}[\min(\nu_E, \nu_{max})]$, where ν_E is proportional to the entropy residual and ν_{max} is a linear viscosity aimed at limiting viscosity near shocks, and $\mathcal{S}$ is a smoothing operator. We discuss different scalings α for $\nu_E \propto h_x^\alpha$ and its impact on convergence.

3 Experiment

As an illustration of the results[1] obtained with the Hermite-EV method, we solve the Euler equations in one dimension with the initial data

$$(\rho, u, p)^T = \begin{cases} (1, 0, 1)^T & x \in [-5, 0), \\ (0.125, 0, 0.1)^T & x \in [0, 5], \end{cases}$$

corresponding to Sod's problem.

We obtained a numerical solution at time $T = 2$, as shown in Fig. 1. The wave structures (rarefaction, contact discontinuity, and shock) are preserved by the Hermite-Entropy Viscosity method. Particularly, the shock and contact discontinuity have been replaced by sharp gradient regions. Moreover, oscillations near the jump have been eliminated.

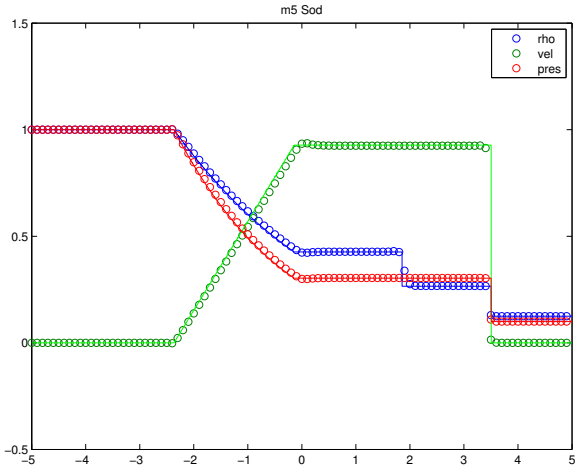

Figure 1: Solution to Sod's shock tube problem with $nx = 100$, $m = 5$. The numerical solution is shown in circles while the exact solution is plotted in solid lines.

References

[1] J.Goodrich, T.Hagstrom and J. Lorenz, Hermite Methods for Hyperbolic Initial-Boundary Value Problem, *Math. Comp.* **75** 2006, pp. 595–630.

[2] D.Appelö and T.Hagstrom, On Advection by Hermite Methods, *Pacific Journal of Aplied Mathematics* **4** 2011, pp. 125–139.

[3] J.L.Guermond and R.Pasquetti, Entropy Viscosity Method for Higher Order Approximations of Conservation Laws, *Lecture Notes in Computational Science and Engineering* **76** 2011, pp. 411–418.

[1] more results will be presented in the actual talk.

4 Acknowledgement

This work was supported in part by NSF Grant DMS-1319054. Any conclusions or recommendations expressed in this paper are those of the author and do not necessarily reflect the views of NSF.

Uncertainty Quantification for High Frequency Waves

Gabriela Malenová[1,*], **Mohammad Motamed**[2], **Olof Runborg**[3]

[1]Department of Mathematics, KTH, Sweden

[2]Department of Mathematics and Statistics, The University of New Mexico, USA

[3]Department of Mathematics and Swedish e-Science Research Center, KTH, Sweden

[*]Email: malenova@kth.se

Abstract

We present a stochastic spectral asymptotic method for the uncertainty quantification of high frequency waves subject to stochastic uncertainty. The method consists of Gaussian beam superposition in the deterministic space and collocation on sparse grids in the stochastic space. In the presence of stochastic regularity, the method exhibits a faster rate of convergence compared to the current Monte Carlo techniques.

Keywords: uncertainty quantification, high frequency waves, Gaussian beams

1 Introduction

We consider the scalar wave equation with highly oscillatory initial conditions where the wave speed and/or the initial data are stochastic:

$$u^\varepsilon_{tt}(t,\mathbf{x},\mathbf{y}) = c(\mathbf{x},\mathbf{y})^2\,\Delta u^\varepsilon(t,\mathbf{x},\mathbf{y}), \qquad (t,\mathbf{x},\mathbf{y})\in\mathbb{R}^+\times\mathbb{R}^n\times\Gamma, \tag{1a}$$

$$u^\varepsilon(0,\mathbf{x},\mathbf{y}) = A_0(\mathbf{x},\mathbf{y})e^{i\Phi(\mathbf{x},\mathbf{y})/\varepsilon}, \tag{1b}$$

$$u^\varepsilon_t(0,\mathbf{x},\mathbf{y}) = \frac{1}{\varepsilon}B_0(\mathbf{x},\mathbf{y})e^{i\Phi(\mathbf{x},\mathbf{y})/\varepsilon}. \tag{1c}$$

Here, $\varepsilon \ll 1$ is the wavelength, c is the wave speed, Φ is the initial phase, and A_0, B_0 are amplitude parameters. The uncertainty is described by a random vector $\mathbf{y}\in\Gamma\subset\mathbb{R}^N$, consisting of N independent random variables. The functions A_0, B_0 and Φ are real-valued, compactly supported and smooth, with $|\nabla\Phi|$ bounded away from zero, $\forall\mathbf{y}\in\Gamma$.

The goal is to predict the statistics of some quantities of interest (QoI), such as

$$Q^\varepsilon(\mathbf{y}) = \int_{\mathbb{R}^n} |u^\varepsilon(T,\mathbf{x},\mathbf{y})|^2\,\psi(\mathbf{x})\,d\mathbf{x},\ \psi\in C_c(\mathbb{R}^n). \tag{2}$$

The problem (1) is a stochastic multiscale problem with uncertain and highly oscillatory solutions. Two major difficulties have to be addressed. First, for high frequencies the computational cost to solve (1) grows rapidly, and when $\varepsilon\to 0$ the numerical solution becomes too expensive [5]. Second, for computing the statistics of (2), Monte Carlo and classical quadrature methods for large N, suffer from slow rate of convergence in the number of collocation points. We remedy this by employing *Gaussian beam summation* for propagating high frequency waves, and *sparse stochastic collocation* for approximating the statistics of (2). The proposed method requires a systematic coupling of the two components.

2 Gaussian beam approximation

The Gaussian beam method describes high frequency waves in a way closely related to geometrical optics and ray tracing, where the solution of (1) is assumed to be of the form

$$u^\varepsilon(t,\mathbf{x},\mathbf{y}) = a(t,\mathbf{x},\mathbf{y})e^{i\phi(t,\mathbf{x},\mathbf{y})/\varepsilon}. \tag{3}$$

In the limit $\varepsilon\to 0$, ϕ and a satisfy the *eikonal* and *transport equations*, respectively. The geometrical optics rays are bicharacteristics of the eikonal equation and satisfy the ODEs

$$\frac{d\mathbf{q}}{dt} = c(\mathbf{q},\mathbf{y})\frac{\mathbf{p}}{|\mathbf{p}|}, \qquad \frac{d\mathbf{p}}{dt} = -\nabla c(\mathbf{q},\mathbf{y})\,|\mathbf{p}|\,.$$

The main drawback of geometrical optics is that the approximation breaks down at caustics.

The Gaussian beam method is another type of high frequency approximation [4]. Unlike geometrical optics, it is locally defined everywhere and performs well even at caustics. A Gaussian beam v^ε has the same form as (3):

$$v^\varepsilon(t,\mathbf{x},\mathbf{y}) = A(t,\mathbf{x},\mathbf{y})e^{i\Phi(t,\mathbf{x},\mathbf{y})/\varepsilon},$$

but the phase Φ and amplitude A are centered around the geometrical optics ray $\mathbf{q}(t,\mathbf{y})$:

$$A(t,\mathbf{x},\mathbf{y}) = a(t,\mathbf{x}-\mathbf{q}(t,\mathbf{y}),\mathbf{y}),$$
$$\Phi(t,\mathbf{x},\mathbf{y}) = \phi(t,\mathbf{x}-\mathbf{q}(t,\mathbf{y}),\mathbf{y}).$$

For the first order Gaussian beams, a and ϕ read

$$a(t,\mathbf{x},\mathbf{y}) = a_0(t,\mathbf{y}),$$
$$\phi(t,\mathbf{x},\mathbf{y}) = \phi_0(t,\mathbf{y}) + \mathbf{x}\cdot\mathbf{p}(t,\mathbf{y}) + \frac{1}{2}\mathbf{x}\cdot M(t,\mathbf{y})\mathbf{x}.$$

Like $\mathbf{q}$ and $\mathbf{p}$, the coefficients ϕ_0, M, a_0 also obey ODEs; see [4]. In this setting, $\mathrm{Im}(\Phi) > 0$ away from the ray, and therefore the shape of v^ε is Gaussian. To obtain more general solutions, we use superpositions of Gaussian beams [1, 2],

$$u^\varepsilon(t, \mathbf{x}, \mathbf{y}) = \frac{1}{(2\pi\varepsilon)^{n/2}} \int_{K_0} v^\varepsilon(t, \mathbf{x}, \mathbf{y}; \mathbf{z}) d\mathbf{z},$$

where $v^\varepsilon(t, \mathbf{x}, \mathbf{y}; \mathbf{z})$ is a beam starting at $\mathbf{x} = \mathbf{z}$ and $K_0 \subset \mathbb{R}^n$ is the compact support of the initial data. The superposition integral is numerically approximated by quadrature. The computational cost of Gaussian beam method is much less than that of a direct solver.

3 Stochastic collocation

Current non-intrusive techniques for the uncertainty propagation of stochastic high frequency waves are based on Monte Carlo sampling, which feature a slow rate of convergence. We show that under certain conditions, sparse stochastic collocation can be employed to speed up convergence.

In stochastic collocation, the semi-discrete asymptotic solution is collocated on a sparse grid $\{\mathbf{y}^{(k)}\}_{k=1}^M \in \Gamma$, see [3]. From the solutions at the collocation points, one can build a quadrature formula to compute e.g. the mean of (2):

$$\mathbb{E}[Q^\varepsilon(\mathbf{y})] = \int_\Gamma Q^\epsilon(\mathbf{y}) d\mathbf{y} \approx \sum_{k=1}^M \alpha_k \, Q^\varepsilon(\mathbf{y}^{(k)}), \quad (5)$$

where α_k are the weights associated with the interpolation points used. The number of collocation points M grows slowly with respect to the dimension N. The computational cost for sparse grids is therefore lower than for classical quadrature methods on full tensor grids.

In order to obtain fast convergence rates at high frequencies, a high stochastic regularity of the QoI is required, independent of the wave length. In other words, we need to have bounds of the derivatives $\left| d_{\mathbf{y}}^{\mathbf{m}} Q^\varepsilon(\mathbf{y}) \right|$, which are *uniform* in ε, for all multi-indices $\mathbf{m} \in \mathbb{N}^N$ and $|\mathbf{m}| \leq m_0$, with m_0 large. This property has been verified numerically, under proper assumptions on the data. Moreover, for simplified model problems, we can derive theoretical bounds.

4 Numerical example

We consider two wave packets, which are initially separated but overlap at time $T > 0$. The initial position of one packet and the wave speed are stochastic, described by $N = 3$ uniform random variables. Figure 1 shows the error in the expected value of (2), computed by the proposed method, versus the number of collocation points M, for four different ε. While Monte Carlo shows a slow convergence, the convergence of the proposed method is exponential, uniformly in ε.

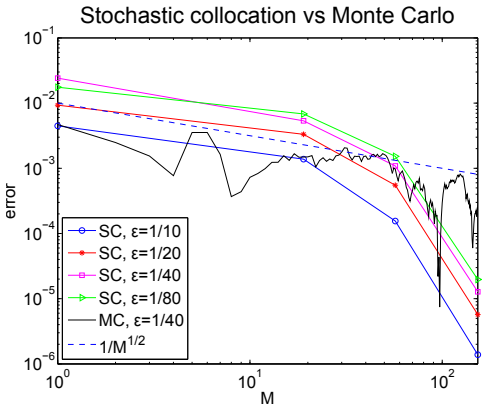

Figure 1: Error in the approximation (5) versus the number of collocation points.

References

[1] V. C. Červený, M. M. Popov, and I. Pšenčík, *Geophys. J. R. Astr. Soc.*, 70: 109–128, 1982.

[2] H. Liu, O. Runborg, and N. M. Tanushev, *Math. of Comput.* Vol. 82, No. 282, pp 919–952, 2012.

[3] F. Nobile, R. Tempone, and C. G Webster, *SIAM J. on Num. An.*, 46(5):2309–2345, 2008.

[4] J. Ralston, *Studies in Part. Diff. Eq.*, Vol. 23 of MAA Stud. Math., pp 206–248. Math. Assoc. America, 1982.

[5] O. Runborg, *Commun. Comput. Phys.*, 2:827–880, 2007.

Reflection of waves by a fractional interface

Laurent Demanet[1], **Olivier Lafitte**[2,*]

[1]MIT Math Department, 99, Massachusetts Avenue, Cambridge, MA 02139, USA

[2]LAGA, UMR 7539, Université Paris 13, Sorbonne Paris Cité, 99 av J.B. Clement, 93430 Villetaneuse and DM2S/DIR, CEA Saclay, 91191 Gif sur Yvette Cedex

[*]Email: lafitte@math.univ-paris13.fr

Abstract

We estimate the reflection coefficient generated by a fractional singularity of order $\alpha > 0$ in the acoustic wave velocity across a planar interface. The leading order term of this reflection coefficient for a velocity model of the form $c^{-2}(z) = c_0^{-2}\,(1+\lambda(z_+)^\alpha)$ is given by $c_\alpha \lambda(\frac{\omega}{c_0})^{-\alpha}$ $(\cos\theta_0)^{-\alpha-2}$ where θ_0 is the angle of incidence.

Keywords: fractional reflector, wave reflection

1 Introduction and main result

Let $c(z)$ as in the abstract. The propagation of acoustic waves in a layered medium with z-dependent wave speed $c(z)$, at fixed frequency ω, is governed by the ordinary differential equation

$$\frac{d^2u}{dz^2} + \omega^2(c^{-2}(z) - \eta^2 c_0^{-2})u = 0, \qquad (1)$$

where $\eta = \sin\theta_0$ is the sine of the wave's angle of incidence in $z < 0$. The general solution in $z < 0$ is $u(z) = A\,e^{-i\omega c_0^{-1}(1-\eta^2)^{\frac{1}{2}}z} + B\,e^{i\omega c_0^{-1}(1-\eta^2)^{\frac{1}{2}}z}$. From $c^{-2} \in C^0(\mathbb{R})$, one deduces $u \in C^2(\mathbb{R})$ and $u(0_+) = u(0_-) = A + B$, $u'(0_+) = u'(0_-) = i\omega c_0^{-1}(1-\eta^2)^{\frac{1}{2}}(B - A)$, hence the solution in $z > 0$ is entirely determined from A and B.

In the next section, we will see that there is a one-parameter family, called $\mathcal{U}^>$, of solutions that obey an outgoing condition at $z = +\infty$. For any such solution we view $A\,e^{-i\omega c_0^{-1}(1-\eta^2)^{\frac{1}{2}}z}$ as the incident wave (incoming from $z = -\infty$), $B\,e^{i\omega c_0^{-1}(1-\eta^2)^{\frac{1}{2}}z}$ as the reflected wave (outgoing to $z = -\infty$), and the corresponding $u(z)$ for $z > 0$ as the transmitted wave (outgoing to $z = +\infty$). The reflection coefficient is then (uniquely) defined as $R = B/A$ for any such nonzero solution.

When $\eta^2 < 1$ (nongrazing waves), we further change variables to nondimensionalize the ODE as

$$\frac{d^2u}{dx^2} + (1 + \theta(x_+)^\alpha)u = 0, \qquad (2)$$

where

$$\theta = \lambda\omega^{-\alpha}c_0^\alpha(1-\eta^2)^{-\frac{\alpha+2}{2}}.$$

The reflection coefficient is unchanged by this operation. We respectively define the WKB right-going and left-going solutions as $v^>(x) = b(x)e^{-i\phi(x)}$ and $v^<(x) = b(x)e^{i\phi(x)}$, where $\phi'(x) = (1+\theta x^\alpha)^{\frac{1}{2}}$, $\phi(0) = 0$, and $b^2(x)\phi'(x) = 1$. These WKB solutions solve the modified equation

$$\frac{d^2v}{dx^2} + (1 + \theta x^\alpha)v = M(x)v, \quad x > 0,$$

where $M(x) = b(x)b''(x)$. For $\alpha > 1$, $M \in L^1([0,+\infty[)$ and $M_\infty := \int_0^{+\infty} |M(x)|dx = O(\theta^{\frac{1}{\alpha}})$.

Our main result is as follows.

Theorem 1 *Under the assumption $M_\infty < 2$, the reflection coefficient R obeys, when $\theta \to 0$ (or equivalently when $M_\infty \to 0$)*

$$R - \theta c_\alpha = o(\theta),$$

where c_α is an explicit constant in terms of α.

2 Outgoing solutions

Outgoing and incoming solutions are defined from a limiting absorbtion principle. Consider

$$\frac{d^2u}{dx^2} + (1 + i\sigma)^2(1 + \theta x^\alpha)u = 0, \quad x > 0. \qquad (3)$$

One defines the limiting absorption WKB solutions as $v_\sigma^>(x) = b(x)e^{-i(1+i\sigma)\phi(x)}$ and $v_\sigma^<(x) = b(x)e^{i(1+i\sigma)\phi(x)}$

Definition 2 *A nonzero solution u of (2) is said to be*

- *outgoing to $+\infty$ ($\in \mathcal{U}^>$), if there exists a sequence of solutions $u(x;\sigma)$ of (3) with $\sigma < 0$ such that*[1] $\lim_{\sigma\to 0^-} u(x;\sigma) = u(x), \lim_{x\to+\infty} u(x;\sigma) = 0$.

[1]The $\sigma \to 0$ limits are all understood to converge uniformly over compact sets of $x \in \mathbb{R}$.

- *incoming from* $+\infty$ ($\in \mathcal{U}^<$)*, if there exists a sequence of solutions* $u(x;\sigma)$ *of (3) with* $\sigma > 0$ *such that* $\lim_{\sigma\to 0^+} u(x;\sigma) = u(x), \lim_{x\to+\infty} u(x;\sigma) = 0$.

Theorem 3 *Any solution of (2) can be written uniquely as the sum of an element of* $\mathcal{U}^<$ *and of* $\mathcal{U}^>$*, each being of dimension 1.*

A first step of the proof relies on Theorem 8.1 of Chapter 3 of Coddington-Levinson and the change of variable $y = \phi(x)$. Equation (3) is equivalent, with $W(y) = (U(y), U'(y))^T$, and $U(y) = \frac{u}{b}(x(y))$, to

$$W' = \begin{pmatrix} 0 & 1 \\ (\sigma - i)^2 + \epsilon(y) & 0 \end{pmatrix} W,$$

with $\epsilon(y)$ an L^1 function linked to M and $y'(x)$.

The two eigenvalues of the above matrix tend to $\pm(\sigma - i)$ as $y \to \infty$. Since $\sigma \neq 0$, one deduces that there exists a unique $W^\sigma_\pm(y)$ solving the above equation and such that $W^\sigma_\pm(y)e^{\pm(\sigma-i)y} \to (1, \pm(\sigma - i))^T$. Undo the transformation from u to W to obtain $u^>_\sigma(x)$ in the minus case, and $u^<_\sigma(x)$ in the plus case. Any solution of (3) is decomposed uniquely as a linear combination of $u^>_\sigma$ and $u^<_\sigma$. In the case $\sigma < 0$, the limit as $\sigma \to 0$ of $u^>_\sigma(x)$ is an element $u^>$ of $\mathcal{U}^>$. In the case $\sigma > 0$, the limit as $\sigma \to 0$ of $u^<_\sigma(x)$ is an element $u^<$ of $\mathcal{U}^<$.

3 Expression for the outgoing solution

Let us set $\sigma < 0$ and further characterize $u^>_\sigma(x)$. Using Duhamel's principle, i.e.,

$$u^>_\sigma(x) = A^\sigma(x)v^>_\sigma(x) + B^\sigma(x)v^<_\sigma(x),$$

one finds an integral equation for $S^>_\sigma(x)$ such that $u^>_\sigma(x) = S^>_\sigma(x)v^<_\sigma(x)$. This is not an error, one expresses the outgoing solution in terms of the incoming WKB solution. Calculations show that

$$(I - K)S^>_\sigma(x) = A^\sigma(0)e^{-2i(1+i\sigma)\phi(x)}$$

where, for $f \in L^\infty([0, +\infty[)$,

$$K(f)(x) = \frac{1}{2i(1 + i\sigma)} \int_0^{+\infty} R(x, y)M(y)f(y)dy,$$

$R(x, y) = e^{-2i(1+i\sigma)(\phi(x)-\phi(y)}$ for $y \geq x$, and $R(x, y) = 1$ for $y \leq x$. Under the assumption $M_\infty < 2$, the Volterra series of general term $K^n(e^{-2i(1+i\sigma)\phi(x)})$ converges uniformly in $x \in \mathbb{R}_+$, for all $\sigma < 0$ towards a quantity $S^>_\sigma$ (the one associated with $A^\sigma(0) = 1$). Its limit is not 0 as $x \to \infty$, as we saw in the previous section when dealing with $W^\sigma_-(x)$.

4 Reflection coefficient

Consider a solution u of the equation on $\mathbb{R}$ that belongs to $\mathcal{U}^>$. Since the coefficients of the equation are continuous on $\mathbb{R}$, and $u(x) = e^{-ix} + Re^{ix}$, $x < 0$, one obtains $u(x) = A(x)v^>(x) + B(x)v^<(x)$, with $A(0) = 1$ and $B(0) = R$. As $u \in \mathcal{U}^>$, there exists $u(x;\sigma)$ such that $u(x;\sigma)$ goes to 0 when $x \to +\infty$ and $u(x, \sigma) \to u(x)$ when $\sigma \to 0_-$. One can prove that $u'(x;\sigma) \to u'(x)$, and A^σ, B^σ converge to a limit when $\sigma \to 0_-$. Finally,

$$B^\sigma(0) + \frac{1}{2i(1 + i\sigma)} A^\sigma(0) \int_0^{+\infty} M(y)S^>_\sigma(y)dy = 0,$$

which allows to pass to the limit. One thus deduces that

$$R = -\frac{1}{2i} \int_0^{+\infty} M(y)S^>_0(y)dy.$$

To obtain Theorem 1, we show successively that
$\int_0^{+\infty} M(y)[S^0_+(y) - (Id + K + ... + K^{[\alpha]-1})(e^{-2i\phi(y)})]dy = o(\theta)$,
$\int_0^{+\infty} M(y)e^{-2i\phi(y)}dy = c_\alpha\theta + o(\theta)$,
$\int_0^{+\infty} M(y)(K + ... + K^{[\alpha]-1})(e^{-2i\phi(y)})dy = o(\theta)$.
This completes the proof of Theorem 1.

References

[1] L.M. Brekhovskikh O.A. Godin, *Acoustics of layered media*, 2nd edition, Springer-Verlag, 1998.

[2] Coddington and Levinson, *Theory of ordinary differential equation* McGraw Hill Books, London, 1955.

[3] L. Demanet and O. Lafitte, in preparation

Role of Special Functions in Multiple-Edge Diffraction

Wonju Jeon[1,*]

[1]Department of Mechanical Engineering, Korea Advanced Institute of Science and Technology, 305-701 Daejeon, South Korea

[*]Email: wonju.jeon@kaist.ac.kr

Abstract

Wave diffraction by sharp edges has been reduced to the calculus of special functions such as Whittaker function and Kobayashi's generalized gamma function, which are essentially equivalent to the confluent hypergeometric function ${}_1F_1$. In this paper, we examine the expansions of the generalized gamma function occurring in diffraction theory. By deriving an exact and closed-form formula of the generalized gamma function, we show that the generalized gamma function consists of polynomial, exponential function and incomplete gamma function. By comparing the present formula with the existing ${}_1F_1$ formula, we discuss the computational availability of the formulas for the practical applications to acoustics and electromagnetism. Finally, we emphasize the role of the incomplete gamma function in mathemtical theory of wave diffraction.

Keywords: confluent hypergeometric function, wave diffraction, singular integral equation

1 Introduction

After the diffraction by a semi-infinite strip having a single edge was approximately solved by Poincaré [1], Sommerfeld [2] obtained an exact solution expressed by Fresnel integral [3] which is an important special function in mathematical theory of diffraction. As studied in recent articles [4, 5], the Fresnel integral also played an important role in finite diffraction as well as in semi-infinite diffraction. The scattering of wave impinging on sharp edges has been reduced to the calculus of special functions such as Whittaker function [7] and Kobayashi's generalized gamma function [8], which are substantially equivalent to the confluent hypergeometric function [9]. In this paper, the author revisits the generalized gamma function for a specific argument occurring in finite diffraction theory.

2 An exact and closed-form formula of generalized gamma function

The generalized gamma function in Eq.(1) was formally introduced in 1991 by Kobayashi who emphasized the role of this special function in mathematical theory of diffraction.

$$\Gamma_m(u,v)=\int_0^\infty \frac{t^{u-1}e^{-t}}{(t+v)^m}dt. \tag{1}$$

As shown in the previous paper [5], the argument u have a specific form of u=non-negative integer+1/2 in the solution procedure by using Taylor series expansion of the unknown function in singular integral equation [4]. Now, we introduce an exact and closed-form formula of Eq.(1) for arbitrary interger m and u=n+1/2 where n is a non-negative integer [6].

Theorem 1 *For arbitrary integers $n \geq m \geq 1$, an exact and closed-form formula of the generalized gamma function is derived by Eq.(2). For $m > n$, the first summation symbol in Eq.(2) is set to be zero. For m=1, $\sum_{i=1}^{0}(\ \ )$ is set to be zero.*

$$\begin{aligned}\Gamma_m(n+1/2,v)=&\\ &\sum_{k=0}^{n-m}(-1)^{n+m-k}\frac{\Gamma(n-k)\Gamma(k+1/2)}{\Gamma(m)\Gamma(n-m-k+1)}v^{n-m-k}\\ &+\sum_{j=0}^{m-1}\frac{(-1)^{n+m-1}\pi\Gamma\left(n+\frac{1}{2}\right)}{\Gamma(m-j)\Gamma(j+1)\Gamma\left(n-j+\frac{1}{2}\right)}\\ &\left(\frac{v^{n-j-1/2}}{\Gamma\left(j+\frac{1}{2}\right)}e^v\Gamma\left(j+\frac{1}{2},v\right)-\sum_{i=1}^{m-1}\frac{v^{n-i}}{\Gamma\left(j-i+\frac{3}{2}\right)}\right)\end{aligned} \tag{2}$$

where

$$\Gamma(a,x)=\int_x^\infty t^{a-1}e^{-t}dt$$

which is an upper incomplete gamma function.

3 Discussion

3.1 Comparison of Three Formulas

Now, we have at least three different formulas of the generalized gamma function. The first one

is the Kobayashi's asymptotic formula which is adequate to large values of argument v.

$$\Gamma(u,v) \sim \sum_{j=0}^{\infty}(-m,j)\frac{\Gamma(u+j)}{v^{m+1}} \qquad (3)$$

where

$$(m,j) = \frac{m(m-1)\times\cdots(m-j+1)}{j!}$$

The second one is Srivastava's formula expressed by the confluent hypergeometric series ${}_1F_1$.

$$\Gamma_m(u,v) = \Gamma(u)\Big[\frac{\Gamma(u-m)}{\Gamma(u)}\ {}_1F_1(m,1-u+m;v) + v^{u-m}\frac{\Gamma(m-u)}{\Gamma(m)}\ {}_1F_1(u,u-m+1;v)\Big] \qquad (4)$$

where

$${}_1F_1(a,c;z) = \sum_{n=0}^{\infty}\frac{(a)_n}{(c)_n}\frac{z^n}{n!}$$

and

$$(a)_n = a(a+1)(a+2)...(a+n-1).$$

And, the third one is the author's formula Eq.(2). As compared in the previous article [5] for m=1, the asymptotic formula Eq.(3) was only valid for large value of argument v. In Fig.(1), the Srivastava's exact formula Eq.(4) is compared to the author's formula Eq.(2) for m=1 and u=7/2. Srivastava's formula expressed by two confluent hypergeometric series shows large computational error due to the finite number of significant figure.

3.2 Role of Incomplete Gamma Function in Finite Diffraction Theory

Equation (5) shows the relation between the Fresnel integral and the error function.

$$\mathrm{erfc}(e^{-i\pi/4}x) = \sqrt{2}e^{-i\pi/4}F(\sqrt{2/\pi}x) \qquad (5)$$

where

$$F(x) = \int_x^{\infty} e^{i\frac{\pi}{2}q^2}dq$$

And, Eq.(6) shows that the error function is a special case of the incomplete gamma function.

$$\mathrm{erfc}(\sqrt{v}) = \frac{1}{\sqrt{\pi}}\Gamma\left(\frac{1}{2},v\right) \qquad (6)$$

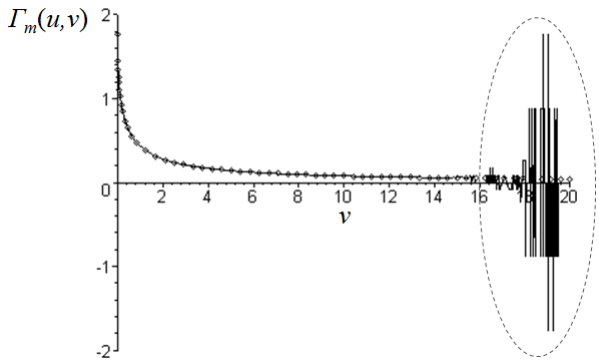

Figure 1: Comparison of Srivastava's formula (line) with the present formula (circle) for m=1 and u=7/2.

where

$$\Gamma(a,x) = \int_x^{\infty} t^{a-1}e^{-t}dt$$

As a concluding remark, we emphasize the role of incomplete gamma function in multiple-edge diffraction by summarizing the previous [5, 7, 10] and the present works as written below.

(i) In our previous work [5], Fresnel integral played an important role in finite diffraction as well as in semi-infinite diffraction.

(ii) Noble [7] and Kobayashi [10] showed that their zeroth-order solutions were sufficiently accurate for high-frequency diffraction.

(iii) Their asymptotic solutions [7, 10] were described by the Fresnel integral.

(iv) From the Eqs.(5,6), the Fresnel integral is a special case of the incomplete gamma function, $\Gamma(j+1/2,v)$, for j=0.

(v) Accurate series solution for low-frequency diffraction can be obtained in the form of incomplete gamma functions, $\Gamma(j+1/2,v)$, for $j \geq 0$.

From (i) to (iv), the sentence (i) can be rewritten such that the incomplete gamma function, $\Gamma(j+1/2,v)$, for j=0 plays an important role in finite diffraction theory, only for high-frequency waves. By including (v), we conclude that the incomplete gamma functions, $\Gamma(j+1/2,v)$ for $j \geq 0$, plays a significant role in finite diffraction theory, especially for low-frequency ranges.

References

[1] H. Poincaré, Sur la Polarisation par Diffraction , *Acta Math.* 16 (1982) pp. 297-338.

[2] A. Sommerfeld, Mathematische Theorie der Diffraction, *Math. Ann.* 47 (1896) pp. 317-374.

[3] M. Abramowitz and I. A. Stegun, *Handbook of Mathematical Functions*, Dover Publications, New York, 1970.

[4] W. Jeon and D.-J. Lee, Acoustic diffraction by a finite airfoil in uniform flow, *AIAA Journal*, 46 (2008) pp. 2977-2986.

[5] W. Jeon and D.-J. Lee, Exact and useful formulas of generalized gamma functions occurring in finite diffraction theory, *Integral Transforms Spec. Funct.* 19 (2008) pp. 735-745.

[6] W. Jeon, Expansions of generalized gamma function and a mixed boundary value problem in wave scattering, *12th International Symposium on Orthogonal Polynomials, Special Functions and Applications, Sousse, Tunisia, 25-29 March 2013*

[7] B. Noble, *Methods Based on the Wiener-Hopf Technique*, Pergamon Press, Oxford, 1958.

[8] K. Kobayashi, On generalized gamma functions occurring in diffraction theory, *J. Phys. Soc. Jpn.* 60 (1991) pp. 1501-1512.

[9] H. M. Srivastava, R. K. Saxena and Chena Ram, "A unified presentation of the gamma-type functions occurring in diffraction theory and associated probability distributions", *Appl. Math. Comput.* 162 (2005) pp. 931-947.

[10] K. Kobayashi, Plane wave diffraction by a strip: exact and asymptotic solutions, *J. Phys. Soc. Jpn.* 60 (1991) pp. 1891-1905.

Thursday, July 23
Second Afternoon Session
17:15 – 18:15

A robust inversion method for quantitative 3D shape reconstruction from coaxial eddy-current measurements

Houssem Haddar[1], **Zixian Jiang**[2], **Mohamed Kamel RIAHI**[3,*]

[1]CMAP, Ecole Polytechnique, Route de Saclay, 91128 Palaiseau Cedex FRANCE.
[2]Centre for Industrial Mathmatics, Universitaet Bremen, Germany.
[3]Department of mathematical science, New Jersey Institute of Technology, University Heights Newark, New Jersey, USA.
[*]Email: riahi@njit.edu

Abstract

This work [3] is motivated by the monitoring of conductive clogging deposits in steam generator at the level of support plates of steam generator in nuclear power plant. One would like to use monoaxial coils measurements to obtain estimates on the clogging volume. We propose a 3D shape optimization technique based on simplified parametrization of the geometry adapted to the impedance measurements and resolution.

Keywords: Inverse problem, Shape identification, Eddy current approximation of Maxwell's equations.

1 Industrial problem

In eddy current testing (ECT), we introduce in the stream generator (SG) tube a probe composed of two coils $\{k, l\}$. The generator coil creates an electromagnetic field which in turn induces a current flow in the conductive material nearby. The default distorts the flow and change the current in the receiver coil, which is measured as ECT signals, from which we will estimate the shape of deposits with known electromagnetic parameters.

2 The direct eddy current problem

The eddy current approximation of the harmonic Maxwell's equations reads: $\mathbf{curl}\mathbf{H} - \sigma\mathbf{E} = \mathbf{J}$ in Ω and $\mathbf{curl}\mathbf{E} - i\omega\mu\mathbf{H} = 0$ in Ω, where $\mathbf{H}$ and $\mathbf{E}$ are the magnetic and the electric field respectively. $\mathbf{J}$ is the the source term representing the current density (located on the probe). In order to solve the eddy current problem we use the mixed formulation on $(\mathbf{A}, \mathbf{V}_c)$, where $\mathbf{A}$ represents the magnetic vector potential and $\mathbf{V}_c$ the scalar electric potential only defined on $\Omega_c \subset \Omega$ where $\sigma \neq 0$. The region where $\sigma = 0$ is called $\Omega_I \subset \Omega$. We have $\mathbf{E} = i\omega\mathbf{A} + \nabla\mathbf{V}_c$ in Ω and $\mu\mathbf{H} = \mathbf{curl}\mathbf{A}$ on Ω (see the complet monograph [1]). We are thus concerned with the strong formulation:

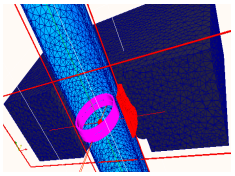

Figure 1: Probing the TSP in steam generator.

$$\begin{cases} \mathbf{curl}\left(\frac{1}{\mu}\mathbf{curl}\mathbf{A}\right) - \frac{1}{\tilde{\mu}}\nabla\mathbf{div}\mathbf{A} - \sigma i\omega\mathbf{A} - \sigma\nabla\mathbf{V}_c = \mathbf{J} & \text{on } \Omega, \\ \mathbf{div}\left(i\omega\sigma\mathbf{A} + \sigma\nabla\mathbf{V}_c\right) = \mathbf{div}\mathbf{J} = 0 & \text{on } \Omega_c, \\ \left(\sigma i\omega\mathbf{A} + \sigma\nabla\mathbf{V}_c\right)\cdot\boldsymbol{\nu} = \mathbf{J}\cdot\boldsymbol{\nu} & \text{on } \partial\Omega_I \cap \partial\Omega_c, \\ \mathbf{A}\cdot\boldsymbol{\nu} = 0 & \text{on } \partial\Omega, \\ \left(\frac{1}{\mu}\mathbf{curl}\mathbf{A}\right)\times\boldsymbol{\nu} = 0 & \text{on } \partial\Omega, \end{cases} \tag{1}$$

The ECT is based on the analysis and processing of impedance signal $\mathbf{Z}(\Omega_D)$ measured during a scan procedure of SG tube. Numerically the impedance measured for the coil k in the electromagnetic field induced by the coil l is computed as follows (see [2] for more details):

$$\Delta\mathbf{Z}_{kl} = \frac{1}{|\mathbf{J}|}\left(\frac{\mu_0 - \mu_d}{i\omega\mu_d\mu_0}\int_{\Omega_d}\left(\mathbf{curl}\mathbf{E}_k\cdot\mathbf{curl}\mathbf{E}_l^0\right)\delta v + (\sigma_0 - \sigma_d)\int_{\Omega_d}\mathbf{E}_k\cdot\mathbf{E}_l^0\,\delta v\right). \tag{2}$$

where $\Omega_d \subset \Omega_c$ defining the support of the deposit in term of conductivity. The notation of the electric field $\mathbf{E}_l^0$ means a solution to (1) with a source term located on the coil l and the calculation correspond to the case of deposit free. Industrial applications, consider different combinations of $\Delta\mathbf{Z}_{kl}$ with a given frequency $\omega = 100kHz$. We give in Figure 2 a validation of the direct 3D vs 2D solvers (in the axisymmetric case) by comparing two frequently used combinations $\mathbf{Z}_{FA}$ and $\mathbf{Z}_{F3}$.

3 The inverse problem

The inverse problem aims at minimizing the misfit cost function

$$\mathcal{J}(\Omega_d) = \int_{z_{\min}}^{z_{\max}} |\mathbf{Z}(\Omega_d;\zeta) - \mathbf{Z}_{mes}(\zeta)|^2 d\zeta,$$

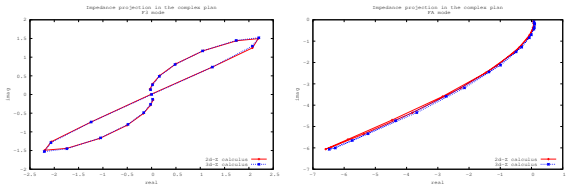

Figure 2: Complex-plan 3D-vs-2D comparison of the Impedance **Z**-F3 and **Z**-FA.

where $\mathbf{Z}$ is either $\mathbf{Z}_{FA}$ or $\mathbf{Z}_{F3}$. The algorithm is based on steepest gradient descent, where the shape gradient is $\mathcal{J}'(\Omega_d)(\boldsymbol{\theta}) = -\frac{\omega}{I^2}\int_{\Gamma_0}(\boldsymbol{\nu}^t\boldsymbol{\theta})g\,\delta s$ where the computation of the the function g involves the solution of the direct and the adjoint problem. In the shape gradient formulae, θ represents the transformation field and $\boldsymbol{\nu}$ is stands for the outward normal.

4 Numerical tests

We consider deposits with conductivity ($\sigma = 1.e{+}4S/m$) and constant permeability ($\mu_r = 1$). We present a series of impedance signal measurements, with respect to the iteration of the inversion algorithm, in Figure 3 and we give corresponding snapshots of the reconstruction of the noisy shaped deposit in Figure 4.

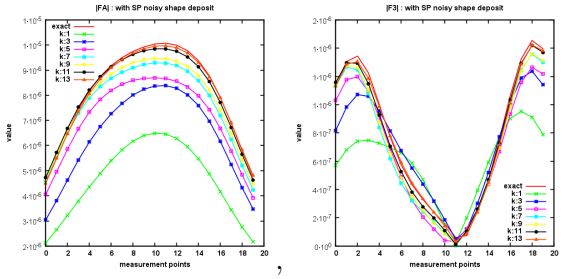

Figure 3: History of the impedances in the case of noisy shaped deposit: $|FA|$ measurement (left) and $|F3|$ measurement (right).

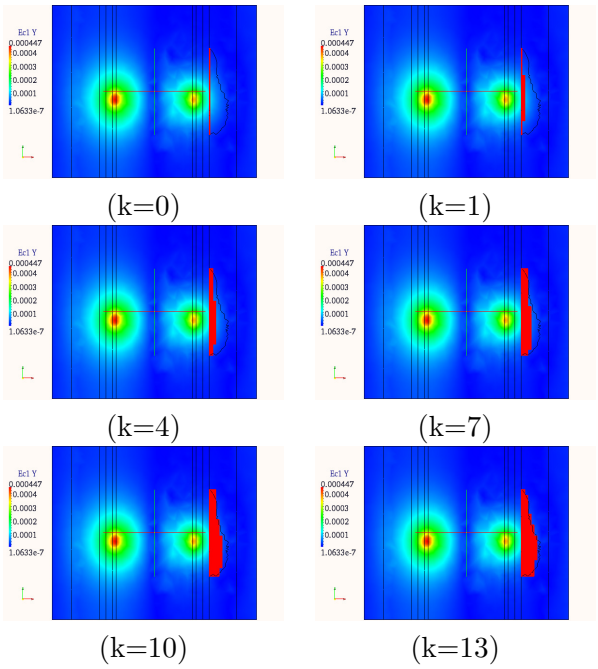

Figure 4: Snapshots of the reconstruction with respect to the iteration of the inversion algorithm. The red part corresponds to the deposits reconstruction.

References

[1] Ana Alonso Rodriguez and Alberto Valli.Eddy current approximation of Maxwell equations, volume 4 of MS&A. Modeling, Simulation and Applications. *Springer-Verlag Italia, Milan, 2010.* Theory, algorithms and applications.

[2] B. A Auld, J. C. Moulder. Review of Advance in Quantitative Eddy Current Nondestructive Evaluation. Journal of Nondestructive Evaluation, Vol. 18, No.1 1999.

[3] H. Haddar, Z. Jiang and M.-K. Riahi. .A robust inversion method for quantitative 3D shape reconstruction from coaxial eddy-current measurements. submitted 2014.

Reflection Full Waveform Inversion in MBTT formulation

Guy Chavent[1], **Kirill Gadylshin**[2,*], **Vladimir Tcheverda**[2]
[1]Inria-Rocquencourt, Domaine de Voluceau, France
[2]Institute of Petroleum Geology and Geophysics, Novosibirsk, Russia
*Email: GadylshinKG@ipgg.sbras.ru

Abstract

We present Reflection FWI algorithm in Migration Based Travel Time (MBTT). This approach is based on decomposition of the velocity model for two constituents: smooth propagator and rough depth reflector. Subsequent reformulation of the data misfit function leads to a new FWI statement. Numerical experiments prove the feasibility of reflection FWI in MBTT formulation for macro velocity model reconstruction in case of absence low frequencies in the input data.

Keywords: Macro velocity reconstruction, FWI, inverse problems

1 Introduction

Macro velocity reconstruction is the main challenge of the seismic data processing. Full waveform inversion (FWI) of reflection seismic data is characterized by extremely poor behaviour of the least- squares data misfit with respect to the slow varying in space components of the velocity model. There are a lot of approaches to overcome this hardship and among them the reflection FWI in Migration Based Travel-Time Formulation (MBTT).

2 Method

Seismic inverse problem can be treated as a nonlinear operator equation:

$$F(m) = d,$$

where $F : M \to D$ is a nonlinear forward map, which transforms model space M into data space D. In order to simplify the mathematics in what follows we deal with Helmholtz equation:

$$\triangle u + \frac{\omega^2}{c(x)^2} u = f(\omega)\delta(x - x_s),$$

with data d being its solution computed at receivers position.

In the contrast to the standard non-linear least-squares FWI formulation (*Tarantola, 1984; Virieux and Operto, 2009*), when unknown velocity model m(x) is searched as

$$m^* = argmin\|F(m) - d\|_D^2,$$

reflection FWI in MBTT formulation uses decomposition of the model m (*Chavent et. al, 2001*) for two constituents:

$$m = p + r = m + \mathcal{M}(p) < s > .$$

Here p –**propagator**, which describes smooth macro velocity, r-**depth reflector** describing rough perturbations of the model. The key moment in this decomposition is propagator-reflector interrelation $r = \mathcal{M}(p) < s >$, where s - unknown **time reflectivity** (preimage of depth reflector in data space D for a given propagator p), $\mathcal{M}(p)$ - a true amplitude prestack migration operator with linear reweighting W (true-amplitude imaging):

$$\mathcal{M}(p) < s >= W \circ Re\left\{\left(\frac{\delta F}{\delta m}(p)\right)^* < s >\right\},$$

where $*$ denotes adjoint operator in application to Frechet derivative of nonlinear forward map F.

Such decomposition of the model leads to the following *modified non-linear least squares FWI formulation*:

$$(p^*, s^*) = argmin\|F(p + \mathcal{M}(p) < s >) - d\|_D^2.$$

The minimization with respect to the new variables (p and s) is performed independently and is implemented by the standard local optimization techniques, such as the modified Newton method.

3 Numerical experiments

As a demonstrative example we consider the 2D velocity model presented in Figure 1.

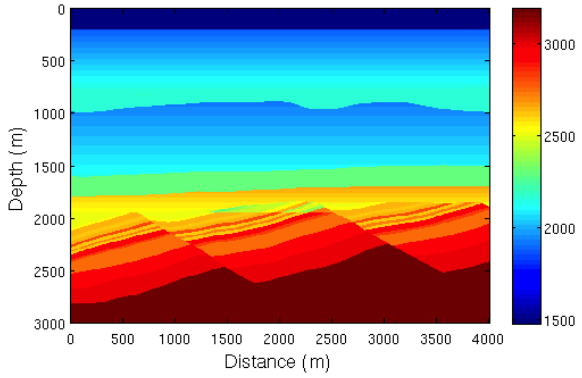

Figure 1: True velocity model for inversion

Input data are synthesized for the set of uniform 18 frequencies [5:0.88:20] Hz. Vertically inhomogeneous model (see Fig. 2) were used as an initial model to start iterations for inversion.

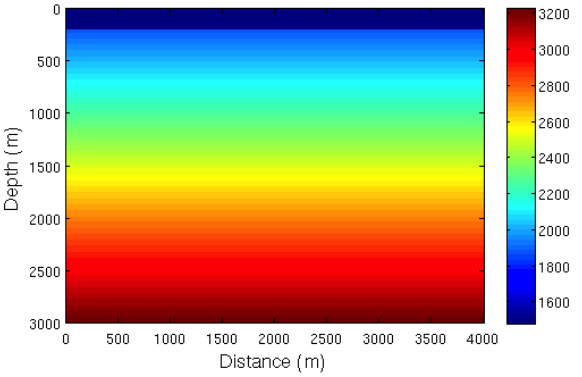

Figure 2: Start model for inversion

The results of conventional simultaneous inversion for 18 frequencies can be seen in Figure 3. As it can be clear observed, the standard non-linear FWI fails to reconstruct smooth velocity model for chosen frequency range in input data. Recovered model contains mainly the reflectivity component of the solution, but location of target horizons is reconstructed with a sizeable error. Alternatively, we present the results of reflection FWI in MBTT formulation in Figure 4. As an initial guess for the time reflectivity variable s were used the observed data itself, starting propagator model p was the same as for conventional inversion (see Fig. 2). 2D B-Splines functions of order 3 were used as the basis of the smooth propagator space.During the minimization process are simultaneously updated both the smooth model and depth reflector. As a result, if propagator is close to the true macro velocity model, then reflectors appears at the correct positions. The final velocity model, obtained by MBTT formulation of FWI is presented on Figure 4.

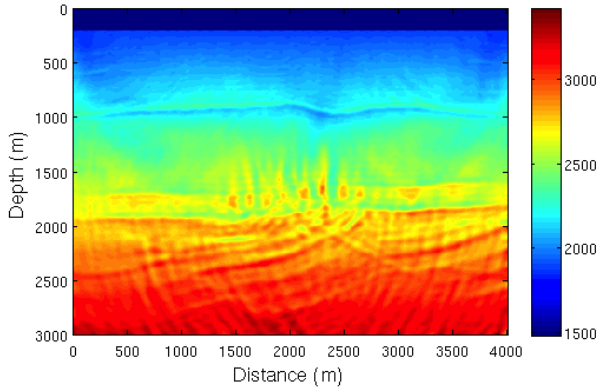

Figure 3: Conventional FWI results

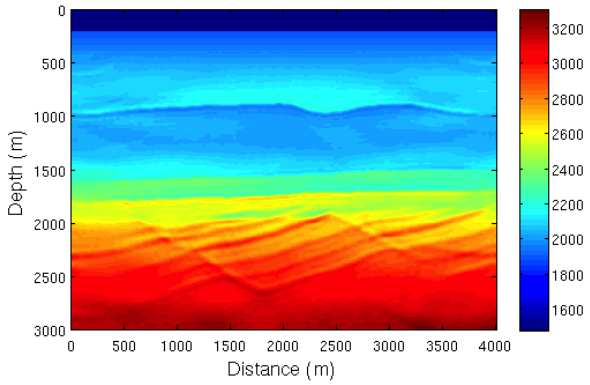

Figure 4: MBTT FWI results

References

[1] Clement F., Chavent G. and Gomez S., Migration-based traveltime waveform inversion of 2-D simple structures: A synthetic example *Geophysics* **66** (2001), pp. 845–860.

[2] Tarantola A., Inversion of seismic reflection data in the acoustic approximation *Geophysics* **49(8)** (1984), pp. 1259–1266.

[3] Virieux J. and Operto S., An overview of full-waveform inversion in exploration geophysics *Geophysics* **74(6)** (2009), WCC1–WCC26.

Periodic quantum graphs with asymptotically predefined spectral gaps

Diana Barseghyan[1], **Andrii Khrabustovskyi**[2,*]

[1]Nuclear Physics Institute of ASCR, Řež near Prague; Department of Mathematics, University of Ostrava, Czech Republic

[2]Institute of Analysis, Karlsruhe Institute of Technology, Germany

[*]Email: andrii.khrabustovskyi@kit.edu

Abstract

Quantum graph is a pair consisting of a metric graph and a second order self-adjoint differential operator on it, which is determined by differential operations on the edges and interface conditions at the vertices. Quantum graphs have been studied intensively during last years due to a number of applications in nanotechnology, optics and other areas. The paper deals with some spectral properties of a class of periodic quantum graphs. The main peculiarity of the graphs under investigation is that their spectral gaps can be nicely controlled via a suitable choice of the graph geometry and of coupling constants involved in interface conditions at its vertices.

Keywords: periodic quantum graphs, spectral gaps, δ'-type conditions

1 Introduction

The name "quantum graph" is usually used for a pair $(\Gamma, \mathcal{A})$, where Γ is a network-shaped structure of vertices connected by edges ("metric graph") and $\mathcal{A}$ is a second order self-adjoint differential operator ("Hamiltonian") on it, which is determined by differential operations on the edges and certain interface conditions at the vertices. Quantum graphs arise naturally in mathematics, physics, chemistry and engineering as models of wave propagation in quasi-one-dimensional systems looking like a narrow neighbourhood of a graph. We refer to recent book [3] containing a comprehensive bibliography on this topic.

In many applications (for example, to graphen and carbon nano-structures) periodic infinite graphs are studied. The metric graph Γ is called *periodic* ($\mathbb{Z}^n$*-periodic*) if there is a group $G \simeq \mathbb{Z}^n$ acting isometrically, properly discontinuously and co-compactly on Γ. Roughly speaking, it means that Γ is glued from countably many copies of a certain compact graph Y ("period cell") and each $g \in G$ maps Y to one of these copies. In what follows, in order to simplify the presentation, we will assume that Γ is embedded into $\mathbb{R}^d$ (with some $d \in \mathbb{N}$). Its $\mathbb{Z}^n$-periodicity means that Γ is invariant under translations through linearly independent vectors $e_1, \dots, e_n$, i.e.

$$\Gamma = \Gamma + e_j, \ j = 1, \dots, n. \tag{1}$$

These vectors produce an action of $\mathbb{Z}^n$ on Γ.

The Hamiltonian $\mathcal{A}$ on a metric graph Γ satisfying (1) is said to be periodic if it commutes with the shifts on the vectors $e_1, \dots, e_n$. It is well-known (see, e.g., [3, Chapter 4]) that the spectrum of such operators has a band structure, i.e. it is a locally finite union of compact intervals called *bands*. In general the neighbouring bands may overlap. A bounded open interval is called a *gap* if it has an empty intersection with the spectrum, but its edges belong to it.

In general the presence of gaps in the spectrum is not guaranteed – for example if Γ is a rectangular lattice and $\mathcal{A}$ is defined by the operation $-\mathrm{d}^2/\mathrm{d}x^2$ on its edges and the Kirchhoff conditions at the vertices then the spectrum $\sigma(\mathcal{A})$ of the operator $\mathcal{A}$ has no gaps, namely $\sigma(\mathcal{A}) = [0, \infty)$. Existence of spectral gaps is important because of various applications, for example in physics of photonic crystals.

Various mechanisms leading to the creation of gaps in the spectra of periodic quantum graphs are described, for example, in [4, 8, 9].

2 Outline of the results

The goal of the current work is to study some specific class of periodic quantum graphs whose spectral gaps can be nicely controlled – via a suitable choice of the graph geometry and of coupling constants involved in interface conditions at its vertices.

Our main result is as follows.

Theorem 1 *For arbitrary finite intervals* $(\alpha_j, \beta_j) \subset [0, \infty)$ $(j = 1, \dots, m)$ *whose closures*

are pairwise disjoint and for arbitrary $n \in \mathbb{N}$ we construct a family of $\mathbb{Z}^n$-periodic quantum graphs $\{(\Gamma, \mathcal{A}^\varepsilon)\}_{\varepsilon>0}$ such that the spectrum of $\mathcal{A}^\varepsilon$ has at least m gaps when ε is small enough, moreover the first m gaps tend to the intervals (α_j, β_j) as $\varepsilon \to 0$.

The family $\{(\Gamma, \mathcal{A}^\varepsilon)\}_{\varepsilon>0}$ is constructed in the following way. We take an arbitrary $\mathbb{Z}^n$-periodic graph $\Gamma_0 \subset \mathbb{R}^d$ with vectors $e_1, \dots, e_n$ producing an action of $\mathbb{Z}^n$ on it and attach to Γ_0 a family of compact graphs Y_{ij}, $i = (i_1, \dots, i_n) \in \mathbb{Z}^n$, $j = 1, \dots, m$ satisfying $Y_{0j} + \sum_{k=1}^{n} i_k e_k = Y_{ij}$. We denote by Γ the obtained graph and consider on it the Hamiltonian $\mathcal{A}^\varepsilon$ defined by the operation

$$-\varepsilon^{-1} \frac{d^2}{dx^2}$$

on its edges and the Kirchhoff conditions in all its vertices except the points of attachment of Y_{ij} to Γ_0. In these points we pose δ'-type conditions (in the case of vertex with two incoming edges they coincide with the usual δ' conditions on the line – see [1, Sec. I.4]). The required structure for the spectrum of $\mathcal{A}^\varepsilon$ is achieved via a suitable choice of coupling constants involved in δ'-type conditions and of "sizes" of attached graphs.

The example of Γ for the case $m = 2$ is presented on the figure. Here the initial graph Γ_0 is highlighted in bold lines and two families of compact graphs $\{Y_{i1}\}_{i\in\mathbb{Z}^n}$ (triangular graphs) and $\{Y_{i2}\}_{i\in\mathbb{Z}^n}$ ("flower"-like graphs) are attached.

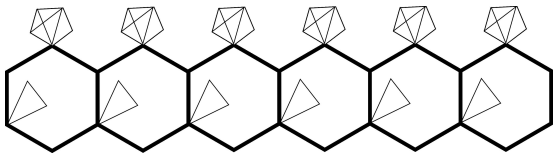

The result are published in [2]. Close results for other periodic differential operators were obtained in [5–7].

The work was supported by the Czech Science Foundation (GACR), the project 14-02476S "Variations, geometry and physics", by the project "Support of Research in the Moravian-Silesian Region 2013" and by the University of Ostrava.

References

[1] S. Albeverio, F. Gesztesy, R. Høegh-Krohn, H. Holden, *Solvable Models in Quantum Mechanics*, 2nd edition, with an appendix by P. Exner, AMS Chelsea, New York, 2005.

[2] D. Barseghyan, A. Khrabustovskyi, Gaps in the spectrum of a periodic quantum graph with periodically distributed δ'-type interactions, *J. Phys A* **48** (2015), 255201.

[3] G. Berkolaiko and P. Kuchment, *Introduction to quantum graphs*, American Mathematical Society, Providence, RI, 2013.

[4] P. Exner, Lattice Kronig-Penney models, *Phys. Rev. Lett.* **74** (1995), pp. 3503–3506.

[5] A. Khrabustovsky, Periodic Riemannian manifold with preassigned gaps in spectrum of Laplace-Beltrami operator, *J. Differ. Equ.* **252** (2012), pp. 2339–2369.

[6] A. Khrabustovskyi, Periodic elliptic operators with asymptotically preassigned spectrum, *Asymp. Anal.* **82** (2013), pp. 1–37.

[7] A. Khrabustovskyi, Opening up and control of spectral gaps of the Laplacian in periodic domains, *J. Math. Phys.* **55** (2014), p. 121502.

[8] P. Kuchment, Quantum graphs. II. Some spectral properties of quantum and combinatorial graphs, *J. Phys. A* **38** (2005), pp. 4887–4900.

[9] B.-S. Ong, *Spectral Problems of Optical Waveguides and Quantum Graphs*, PhD thesis, Texas A&M University, 2006.

Guided modes in ladder-like open periodic waveguides

Bérangère Delourme[1], Sonia Fliss[2], Patrick Joly[2], Elizaveta Vasilevskaya[1,*]
[1]LAGA, University Paris 13, Villetaneuse, France
[2]POEMS (CNRS/ENSTA Paristech/INRIA), Palaiseau France
[*]Email: vasilevs@math.univ-paris13.fr

Abstract

We consider the theoretical and numerical aspects of the wave propagation in ladder-like periodic structures. We exhibit situations where the introduction of a lineic defect into the geometry of the domain leads to the appearance of guided modes and we provide numerical simulations to illustrate the results.

Keywords: open waveguides, periodic media, quantum graphs, asymptotic analysis

1 Introduction

We consider the propagation of acoustic waves in a particular periodic medium that consists of the plane $\mathbb{R}^2$ minus an infinite set of equispaced perfect conductor rectangular obstacles with Neumann boundary conditions. The parameter ε represents the distance between the obstacles. We introduce a lineic defect in this perfectly periodic domain by changing the distance between two consecutive columns of obstacles from ε to $\mu\varepsilon$, where $\mu > 0$ (cf. fig. 1 for $\mu \in (0,1)$).

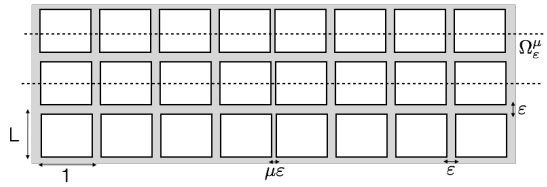

Figure 1: Periodic and perturbed domains

Our aim is to find guided modes, that is to say solutions of the homogeneous wave equation propagating along the defect. It is well-known that this problem can be reformulated as an eigenvalue problem for the Laplacian in the periodicity band Ω_ε^μ with β-quasi-periodic boundary conditions in the $y-$direction (cf. fig. 2). More precisely, we seek the couples $(u_\varepsilon, \lambda^\varepsilon) \in H^1(\Omega_\varepsilon^\mu) \times \mathbb{R}^+$ satisfying

$$-\Delta u^\varepsilon = \lambda_\varepsilon^2\, u^\varepsilon \quad \text{in} \quad \Omega_\varepsilon^\mu, \tag{1}$$

together with β-quasi-periodicity boundary conditions on $\Sigma^\pm = \partial\Omega_\varepsilon^\mu \cap \{y = \pm L/2\}$ ($\beta \in [0, 2\pi]$),

$$v|_{\Sigma^+} = e^{i\beta}\, v|_{\Sigma^-}\,, \quad \partial_y v|_{\Sigma^+} = e^{i\beta}\, \partial_y v|_{\Sigma^-}\,, \tag{2}$$

and homogeneous Neumann boundary conditions on the remaining part of the boundary:

$$\partial_n u^\varepsilon = 0 \quad \text{on} \quad \partial\Omega_\varepsilon^\mu \setminus (\Sigma^+ \cup \Sigma^-). \tag{3}$$

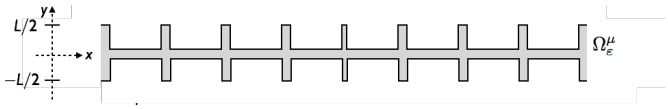

Figure 2: The periodicity band Ω_ε^μ

Problem (1-2-3) turns out to be an eigenvalue problem for a selfadjoint operator $A_\varepsilon^\mu(\beta)$ in $L^2(\Omega_\varepsilon^\mu)$. For $\mu = 1$, there is no eigenvalue. We investigate the possibility of creating eigenvalues by playing with the parameter μ.

2 Limit problem

The investigation of the spectral problem (1-2-3) is based on its asymptotic analysis as ε tends to zero. First, we identify the limit spectral problem. This problem is posed on the graph $\mathcal{G}$ obtained by taking the geometrical limit of the domain Ω_ε^μ when its thickness tends to zero (cf. fig. 3). More precisely, we look for the eigenpairs (u, λ), where, for any edge e of $\mathcal{G}$, the restriction u_e of u to e is solution of

$$-u_e'' = \lambda\, u_e,$$

u is β-quasi periodic in the $y-$direction, and, at each "interior" vertex M of the graph, u is continuous and satisfies the so-called Kirchhoff transmission conditions

$$\sum_{e \in \mathcal{E}(M)} w^\mu(e)\, u_e'(M) = 0, \tag{4}$$

$u_e'(M)$ being defined outward. In (4), $\mathcal{E}(M)$ denotes the set of the edges sharing M as a common vertex, $w^\mu(e) = 1$ for any unperturbed

edge and $w^\mu(e) = \mu$ for the two perturbed edges.

The spectrum of the operator $\mathcal{A}^\mu(\beta)$ associated with this limit spectral problem can be characterized explicitly and we have in particular the following result:

Theorem 1 *For any $\beta \in [0, 2\pi)$, the spectrum of $\mathcal{A}^\mu(\beta)$ has infinitely many gaps of the form (a_0^n, b_0^n), $n \in \mathbb{N}$, where, a_0^n and b_0^n go to $+\infty$ as n tends to $+\infty$, and $b_0^{n-1} < a_0^n$. Moreover, if $\mu \geq 1$, the discrete spectrum of $\mathcal{A}^\mu(\beta)$ is empty, while if $\mu < 1$ it contains one or two eigenvalue(s) in each gap.*

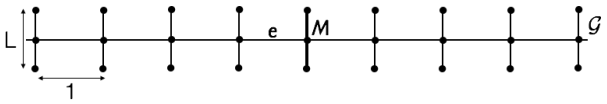

Figure 3: Limit graph

3 Asymptotic analysis

In this section, we restrict ourselves to the case $\mu \in (0, 1)$. It is known that the spectrum of the operator $A_\varepsilon^\mu(\beta)$ approaches in some sense the spectrum of the operator $\mathcal{A}^\mu(\beta)$ as ε is small enough (see [2,3] for more details). Using matched asymptotics expansions (cf. [1]), we can obtain a more precise result:

Theorem 2 *Let (a_0, b_0) (i.e (a_0^n, b_0^n) for some n, see Theorem 1) be a gap of the limit operator $\mathcal{A}^\mu(\beta)$ for some $\beta \in [0, 2\pi)$. Then, for ε small enough, there is a gap $(a_\varepsilon, b_\varepsilon)$ in the spectrum of $A_\varepsilon^\mu(\beta)$ with*

$$a_\varepsilon = a_0 + O(\varepsilon), \quad b_\varepsilon = b_0 + O(\varepsilon), \quad \varepsilon \to 0.$$

Moreover, if $\lambda_0 \in (a_0, b_0)$ is an eigenvalue of the limit operator (see Theorem 1), then, for ε small enough, the operator $A_\varepsilon^\mu(\beta)$ has an eigenvalue λ_ε inside the gap $(a_\varepsilon, b_\varepsilon)$ having the following asymptotic expansion:

$$\forall\, n \in \mathbb{N}, \quad \lambda_\varepsilon = \lambda_0 + \sum_{k=1}^{n} \lambda_k\, \varepsilon^k + O\left(\varepsilon^{n+1}\right).$$

The coefficients $\{\lambda_k\}_{k\in\mathbb{N}}$ can be computed by an explicit recurrence procedure which involves the computation of profile functions defined in two reference junctions (see Figure 4)

We illustrate the theoretical results described above by numerical simulations obtained using

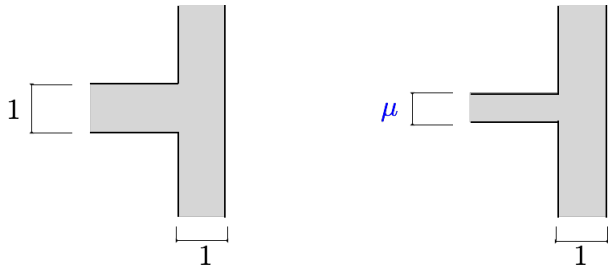

Figure 4: The two reference junctions

a numerical method dedicated to periodic media (see [4]). This method relies on the reduction of the initial (linear) eigenvalue problem (posed on the unbounded domain), to a non-linear one posed on a bounded domain, by means of an exact Dirichlet-to-Neumann operator.

References

[1] P. Joly and A. Semin, Construction and analysis of improved Kirchhoff conditions for acoustic wave propagation in a junction of thin slots, vol. **25** of *ESAIM Proc.,* pp. 44–67, 2008.

[2] P. Kuchment and H. Zeng, Convergence of spectra of mesoscopic systems collapsing onto a graph, *J. Math. Anal. Appl.* **258**, 2001.

[3] O. Post, Spectral convergence of quasi-one-dimensional spaces, *Ann. Henri Poincaré* **7**, 2006.

[4] S. Fliss, A Dirichlet-to-Neumann approach for the exact computation of guided modes in photonic crystal waveguides, *SIAM J. Sci. Comp.*, vol. **35(2)**, 2013.

Friday, July 24
Morning Session
10:30 – 12:30

Recovering the initial state of the wave equation in unbounded domain using observers

S. Fliss[1], **S. Imperiale**[2,*], **P. Moireau**[2]
[1]POEMS (CNRS/ENSTA Paristech/Inria), Palaiseau France
[2]Inria Saclay-Ile de France, Team MΞDISIM, France
[*]Email: sebastien.imperiale@inria.fr

Abstract

We consider the problem of recovering compactly supported initial data of a scalar wave equation set in the whole space, when the time derivative of the solution is known on a domain surrounding the data. We prove the exponential convergence of an iterative back and forth nudging strategy and proposes a numerical framework that reduces computations in a bounded domain.

Keywords: Initial state recovery, Observers, Open domains

1 An open domain configuration

In this work we consider the problem of recovering the initial data of

$$\partial_t^2 u - \Delta u = 0 \quad [0,T]\times\mathbb{R}^d,$$

with unknown initial data $u(0)=u_0$ and $\partial_t u(0) = u_1$ supported in a bounded domain B compactly included in Ω. The only available informations is $\partial_t u$, up to a given time T, on a non degenerating subdomain ω such that $\partial\Omega \subset \partial\omega$ (see Figure 1 or Figure 2). In [1] is introduced an iterative back and forth observer that uses the data at hand to reconstruct the initial condition. The exponential convergence is ensure for bounded domain in [1] and an extension is envisioned for unbounded domain in [2] but with only a polynomial convergence. Our objective here is to justify the exponential convergence and proposed a strategy to restrict the formulation and computation around the initial condition.

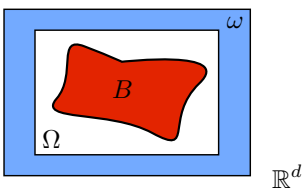

Figure 1: B is the support of the initial data, ω is the observation domain.

2 Iterative reconstruction strategy

Following [1] and [2] an iterative strategy is presented. A sequence $\{\widehat{u}_n, \widehat{u}_{\flat,n}\}$, $n \geq 0$, of solutions of wave equations is constructed recursively. At iteration n the *forward* observer $\widehat{u}_n$ is defined as the solution over $[0,T]\times\mathbb{R}^d$ of

$$\partial_t^2 \widehat{u}_n - \Delta \widehat{u} + \gamma\, \mathbb{1}_\omega\, \partial_t\big(\widehat{u}_n - u(t)\big) = 0, \quad (1)$$

with γ is a positive scalar. We also define the *backward* observer $\widehat{u}_\flat$ as the solution over $[0,T]\times\mathbb{R}^d$ of a *backward* wave equation using again the available observations

$$\partial_t^2 \widehat{u}_{\flat,n} - \Delta \widehat{u}_{\flat,n} + \gamma\, \mathbb{1}_\omega\, \partial_t\big(\widehat{u}_{\flat,n} - u(T-t)\big) = 0, \quad (2)$$

The initial conditions for (1) and (2) are chosen as follows: $\widehat{u}_0(0)$ and $\partial_t\widehat{u}_0(0)$ are initial guess compactly supported in Ω. The initial conditions for the *backward* observer are given using the *forward* observer at final time of propagation

$$\widehat{u}_{n,\flat}(0) = \widehat{u}_n(T), \quad \partial_t\widehat{u}_{n,\flat}(0) = -\partial_t\widehat{u}_n(T), \quad n \geq 0.$$

The initial conditions for the *forward* observer, for $n \geq 1$, are computed using the *backward* observer at final time of propagation but adequately truncated:

$$\begin{cases} \widehat{u}_n(0) = \Delta_\Omega^{-1}\,(\nabla\cdot\chi\,\nabla)\widehat{u}_{\flat,n-1}(T), \\ \partial_t\widehat{u}_n(0) = -\chi\,\partial_t\widehat{u}_{\flat,n-1}(T), \end{cases} \quad (3)$$

where χ is a smooth positive cut-off function that equals 1 over B and 0 outside Ω, Δ_Ω^{-1} is the inverse Laplace operator in $H_0^1(\Omega)$. We emphasize that the truncation, not present in [2], is necessary to ensure the exponential convergence.

Theorem 1 *For T sufficiently large and for all $(u_0,u_1)\in H_0^1(B)\times L^2(B)$ there exists $0<\delta<1$ such that for all $n\geq 1$*

$$|\widehat{u}_n(0) - u_0|^2_{H^1(\Omega)} + \|\partial_t\widehat{u}_n(0) - u_1\|^2_{L^2(\Omega)}$$
$$\leq \delta^n \left(|u_0 - \widehat{u}_0(0)|^2_{H^1(\Omega)} + \|u_1 - \partial_t\widehat{u}_0(0)\|^2_{L^2(\Omega)}\right).$$

For the proof we use, at each forth and back stages, stabilization results for the wave equation with localized initial data and standard energy analysis. Between each stage we have to show that the truncation procedure defined by (3), does not deteriorate the approximation. This is obvious for the approximation of u_1 and for u_0 one can show

$$|\widehat{u}_{n+1}(0) - u_0|_{H^1(\Omega)} \leq |\widehat{u}_{\flat,n}(T) - u_0|_{H^1(\mathbb{R}^d)}.$$

3 Restriction to a bounded domain

A natural idea to restrict the computation in a bounded is to use a large enough computation domain so that we can impose homogeneous Dirichlet condition at its boundary. In order to restrict the computational cost we want here to use transparent boundary condition. Denoting $\Gamma = \partial\omega \setminus \partial\Omega$, we introduce the DtN operator

$$\mathcal{T}_t : C^1\big([0,t]; H^{1/2}(\Gamma)\big) \to H^{-1/2}(\Gamma),$$

such that $\widehat{u}_n$ solution (1) over $[0,T]\times\mathbb{R}^d$ satisfies

$$\nabla\widehat{u}_n \cdot \mathbf{n} + \mathcal{T}_t(\widehat{u}_n) = 0, \quad [0,T] \times \Gamma.$$

We recall that in a one-dimensional setting we have $\mathcal{T}_t \equiv \partial_t$. With such DtN operator at hand, solving problem (2) is equivalent to solve the same equations in $\overline{\Omega \cup \omega}$ with the following boundary condition on $[0,T] \times \Gamma$,

$$\nabla\widehat{u}_{\flat,n} \cdot \mathbf{n} + \mathcal{T}_t(\widehat{u}_{\flat,n}) = \mathcal{T}_t(\widehat{u}_n(T-t)) - \mathcal{T}_t(\widehat{u}_n)(T-t).$$

We point out that an inhomogeneous boundary condition is used on Γ which depends only on the *forward* observer and not the observations.

The quality of the discretization process in space and time, in particular of the DtN condition, is of fundamental importance to ensure – using well-developed strategies in bounded domain such as [3] – that the exponential convergence can hold at the discretized level. However, low order approximation of DtN condition or adapted perfectly match layers may introduce some spurious phenomena. In this respect, we propose an adapted semi-discretization in time of the DtN condition in 1D with possible extension to higher dimension and anisotropic media.

4 Instructive 1D numerical results

Preliminary numerical results (see Figure 2) are computed using, in space, first order finite element, in time, a second order implicit theta-schemes. The imposed approximate DtN condition is exact for the semi-discrete problem in time. Finally classical numerical vanishing viscosity are added to damped the classical high frequencies spurious modes associated with the observer discretization (see [3]), convergence results are given figure 3 .

Figure 2: Parameters of the simulation: $T = 1$, $\gamma = 1, u_1 = \partial_t\widehat{u}_0(0) \equiv 0, \Delta t = 10^{-2}, \Delta x = 10^{-3}$.

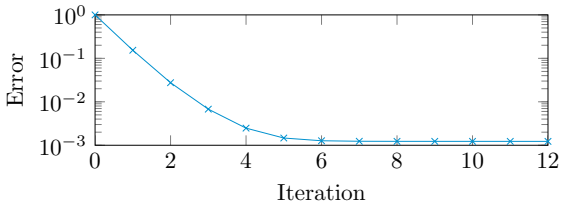

Figure 3: Convergence of the algorithm in the $H^1(\Omega)$ semi-norm.

References

[1] K. Ito, K. Ramdani, M. Tucsnak. A time reversal based algorithm for solving initial data inverse problems. *Discrete Contin. Dyn. Sys. Ser. S*, **4**(3), (2011).

[2] G. Haine, Recovering the observable part of the initial data of an infinite-dimensional linear system with skew-adjoint generator. *Math. Control Signal*, **26**(3), (2014).

[3] S. Ervedoza, E. Zuazua, Uniformly exponentially stable approximations for a class of damped systems. *Journal De Mathématiques Pures Et Appliqués*, **91**(1), (2009).

DORT Method For The Detection Of Small Moving Disks In A Fluid

Karim Ramdani[1,*], **Alexandre Munnier**[2]

[1]Inria, Villers-lès-Nancy, F-54600, France

[2]Institut Élie Cartan de Lorraine (UMR 7502), Université de Lorraine, Vandœuvre-lès-Nancy, F-54506, France

[*]Email: karim.ramdani@inria.fr

Abstract

We are interested in determining the positions and the velocities of small rigid disks moving in a bounded cavity filled with a perfect fluid. Using an integral formulation, we first derive the asymptotic expansion of the DtN map of the problem as the diameters of the disks tend to zero. Then, combining a suitable choice of exponential type data and the DORT[1] technique, we propose a reconstruction method for the unknown positions and velocities.

Keywords: Inverse problems, perfect fluid, integral equations, asymptotic analysis, DtN operator, time reversal, DORT Method

Geometric inverse problems of detecting moving solids in a fluid appear in many applications. However, the associated literature is quite limited, as most contributions deal with motionless solids. For moving obstacles, Conca *et al.* show in [3] that the position and the velocity for a single disk moving in a perfect fluid can be recovered from one measurement of the velocity on part of the boundary. In Conca *et al.* [4], the authors consider a moving rigid solid immersed in a potential fluid and provide examples of detectable (ellipses for instance) and undetectable shapes. Finally, Conca *et al.* obtained in [5] an identifiability result in the case of a rigid solid immersed in a viscous fluid.

1 Statement of the problem

In this paper, we investigate the inverse problem of determining the positions and the velocities of small rigid solids slowly moving in a cavity filled with a perfect fluid by using actuators and sensors located on the outer boundary of the cavity. More precisely, let Ω be an open and simply connected bounded domain of $\mathbb{R}^2$ with smooth boundary $\Gamma := \partial\Omega$. The domain Ω, which is supposed to be filled with a perfect fluid, contains M rigid solids D_m^ε, $m = 1, \dots, M$, where $D_m^\varepsilon \subset \Omega$ is a closed disk with boundary γ_m^ε (see Figure 1). We assume that D_m^ε is the disk centered at r_m and of radius εR_m, where the parameter ε tends to 0. The domain occupied by the fluid is denoted by $\mathcal{F}^\varepsilon := \Omega \setminus \left(\sum_{m=1}^M D_m^\varepsilon\right)$. We denote by n the unit normal to $\partial\mathcal{F}^\varepsilon$ directed towards the exterior of the fluid and by τ the unit tangent vector to $\partial\mathcal{F}^\varepsilon$ such that $\tau = n^\perp$ (where $x^\perp := (-x_2, x_1)$ for all $x = (x_1, x_2) \in \mathbb{R}^2$). Let $\mathbf{U}^\varepsilon(x)$ denote the Eulerian velocity field of the fluid and let $\psi^\varepsilon : \mathcal{F}^\varepsilon \to \mathbb{R}$ be the corresponding stream function (i.e. $\mathbf{U}^\varepsilon = -\nabla^\perp\psi^\varepsilon$ in $\mathcal{F}^\varepsilon$).

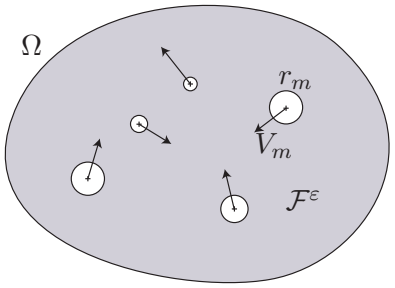

Figure 1: The cavity Ω containing M small rigid disks and filled with a perfect fluid in $\mathcal{F}^\varepsilon$.

Assuming that the flow is irrotational and circulation free and that we can impose the normal velocity of the fluid on Γ, we can show that the stream function ψ^ε satisfies

$$\begin{array}{rcll} -\Delta\psi^\varepsilon & = & 0 & \text{in } \mathcal{F}^\varepsilon, \\ \psi^\varepsilon & = & V_m^\perp \cdot x + c_m^\varepsilon & \text{on } \gamma_m^\varepsilon, \\ \psi^\varepsilon & = & f & \text{on } \Gamma, \end{array} \qquad (1)$$

where $V_m \in \mathbb{R}^2$ denotes the velocity of the $m-$th disk and where the constants $c_m^\varepsilon \in \mathbb{R}$ are such that

$$\int_{\gamma_m^\varepsilon} \partial_n\psi^\varepsilon(s)\,\mathrm{d}s = 0, \quad m = 1, \dots, M. \qquad (2)$$

Considering that the available measurement is $\partial_n\psi^\varepsilon$, our detection problem reads: *Knowing*

[1]DORT is the French acronym for Decomposition of the Time-Reversal Operator.

the DtN map

$$\Lambda^\varepsilon : f \in H^{1/2}(\Gamma) \longmapsto \partial_n \psi^\varepsilon \in H^{-1/2}(\Gamma),$$

where ψ^ε solves (1)-(2)*, is it possible, and if so how, to recover the positions r_m ($m = 1, \dots, M$), the radii R_m and the velocities V_m of the moving disks?*

2 Results

In this contribution, we answer this question in two steps. First, using a boundary integral formulation, we obtain the following asymptotic expansion of the DtN operator Λ^ε as $\varepsilon \to 0^+$.

Theorem 1 *For every $f \in H^{1/2}(\Gamma)$, we denote by $U^f \in H^1(\Omega)$ the solution of the boundary value problem*

$$\left\{ \begin{array}{rcl} -\Delta U^f & = & 0, \quad in\ \Omega, \\ U^f & = & f, \quad on\ \Gamma. \end{array} \right.$$

Let $\Lambda^0 \in \mathcal{L}(H^{1/2}(\Gamma), H^{-1/2}(\Gamma))$ denote the DtN map $\Lambda^0 : f \longmapsto \partial_n U^f$. Then, as $\varepsilon \to 0^+$, the DtN map $\Lambda^\varepsilon \in \mathcal{L}(H^{1/2}(\Gamma), H^{-1/2}(\Gamma))$ admits the asymptotic expansion:

$$\Lambda^\varepsilon = \Lambda^0 + \varepsilon^2 \Lambda^2 + O(\varepsilon^3),$$

where for every $f, g \in H^{1/2}(\Gamma)$:

$$\langle \Lambda^2 f, g \rangle_{H^{-1/2}(\Gamma), H^{1/2}(\Gamma)} = 2\pi \sum_{m=1}^{M} R_m^2 \Big\{ \nabla U^f(r_m) \cdot \nabla U^g(r_m) - \nabla U^g(r_m) \cdot V_m^\perp \Big\}.$$

Next, we combine this expansion with the DORT method to recover the number of disks and their positions (provided they are distant enough). Initially introduced by Fink and Prada [6], this method has been justified mathematically and used in the framework of wave systems for the detection of distant point-like scatterers in acoustics [1,7]. Here, following an idea introduced by Calderón [2], we apply this approach after a suitable choice of excitations f and test functions g of exponential type. More precisely, we choose for every given $\eta \in \mathbb{R}^2$:

$$f(x) = e^{i(\eta + i\eta^\perp)\cdot x}, \qquad g(x) = e^{i(\eta - i\eta^\perp)\cdot x}.$$

This allows us to recover the unknown positions r_m using the eigenfunctions of a suitably chosen (non physical) time reversal operator. Once the positions have been determined, the velocities and rescaled radii can be easily recovered using suitably chosen data.

References

[1] C. Burkard, A. Minut, and K. Ramdani, *Far field model for time reversal and application to selective focusing on small dielectric inhomogeneities*, Inverse Probl. Imaging, 7 (2013), pp. 445–470.

[2] A.-P. Calderón, *On an inverse boundary value problem*, in Seminar on Numerical Analysis and its Applications to Continuum Physics (Rio de Janeiro, 1980), Soc. Brasil. Mat., Rio de Janeiro, 1980, pp. 65–73.

[3] ——, *On the detection of a moving obstacle in an ideal fluid by a boundary measurement*, Inverse Problems, 24 (2008), pp. 045001, 18.

[4] C. Conca, M. Malik, and A. Munnier, *Detection of a moving rigid solid in a perfect fluid*, Inverse Problems, 26 (2010), pp. 095010, 18.

[5] C. Conca, E. L. Schwindt, and T. Takahashi, *On the identifiability of a rigid body moving in a stationary viscous fluid*, Inverse Problems, 28 (2012), pp. 015005, 22.

[6] M. Fink and C. Prada, *Eigenmodes of the time-reversal operator: A solution to selective focusing in multiple-target media*, Wave Motion, 20 (1994), pp. 151–163.

[7] C. Hazard and K. Ramdani, *Selective acoustic focusing using time-harmonic reversal mirrors*, SIAM J. Appl. Math., 64 (2004), pp. 1057–1076.

A dispersion minimizing finite difference scheme and Multifrontal Hierarchically Solver for the 3D Helmholtz equation

Sergey Solovyev[1,*], **Dmitry Vishnevsky**[1]
[1]Institute of Petroleum Geology and Geophysics SB RAS, Novosibirsk, Russia
[*]Email: solovevsa@ipgg.sbras.ru

Abstract

In this paper we present algorithm of solving 3D Helmholtz problem. It based on two features: 1) construction of 27-point approximation scheme to minimize the dispersion error; 2) using low-rank approximation technique and hierarchically semiseparable (HSS) structure in the multifrontal direct solvers to decrease computational resources. Quality of low-rank compression is improved by using cross approximation (CA) approach. Numerical experiments show that current implementation of algorithm requires less than 3 times computational resources compared with sparse direct solvers.

Keywords: 27-point finite-difference scheme, numerical dispersion, Low-rank approximation, hierarchically semi-separable (HSS) structure, Cross Approximation (CA)

1 Introduction

The dispersion error of the Helmholtz solution leads to the using huge computational grid and increasing computational time. There are different approachs for decreasing this error, like increasing the approximation order or developing various rotation schemes [3].

In this paper we present the optimal 27-point scheme which is easier than proposed ones and provides the same quality. To decrease memory and performance issues we develop supernodal multifrontal method based on direct solver and low-rank/HSS technique.

2 Methods

The Helmholtz equation has a form:

$$\Delta u + \frac{(2\pi\nu)^2}{V^2} u = \delta(\overline{r} - \overline{r}_s) f \qquad (1)$$

where ν – frequency, V – velocity, $\overline{r}_s$ – source coordinates, f – source. Using the 7-point stencil is the standard way of finite difference 2-nd order approximation on the parallelepipedal grid.

This approach gives the dispersion solution error demonstrated in Fig.1. Dispersion analysis shows that should to be at least 15 points per wavelength to have suitable error (less than 1%).

To handle with this issue we propose the 27-point 2-nd order scheme. To approximate Laplace operator we use combination of the three schemes (Fig. 3) with coefficients $\gamma_1, \gamma_2, \gamma_3$.

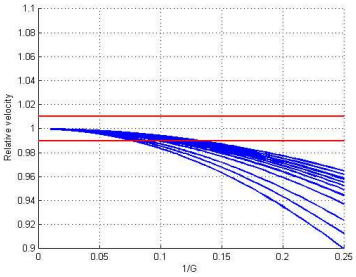

Figure 1: The dispersion curves of the 2-nd order approximation for the 7-point scheme. Numerical phase velocity V_{ph} are normalized with respect to the true velocity V and plotted versus $1/G$, where G is the number of grid points per wavelength.

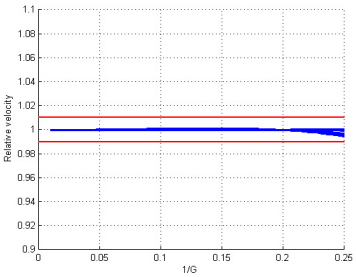

Figure 2: The dispersion curves of the 2-nd order approximation for the optimized 27-point scheme.

To approximate wave number we use combination of four schemes with coefficients (w_1, w_2,-w_3, w_4). The first scheme uses the center point of parallelepiped, the second – center of faces (6 points), the third – center of edges (12 points) and the fouth scheme uses the corner points (8

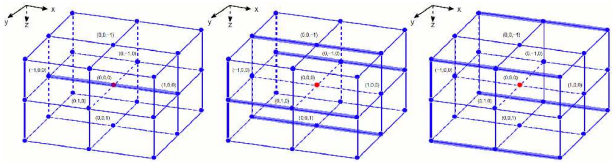

Figure 3: Three stencils of approximation the second order derivation along X axis.

ones). After dispersion analysis, minimization the functional $J(\overline{\gamma w})$ (2) gives the scheme with optimal parameters $\overline{\gamma w} = (\gamma_1, \gamma_2, \gamma_3, w_1, w_2, w_3, w_4)$ in terms of phase velocity V_{ph}.

$$J(\overline{\gamma w}) = \iiint_{G=[G_{min},G_{max}];\varphi=[0,\pi/2];\theta=[0,\pi/4]} \left(V_{ph}(\overline{\gamma w})/V - 1\right)^2 dG d\varphi d\theta \quad (2)$$

Analyse of dispersion curves (Fig.2) shows that 4 points per wavelength are enough to achieve 0.5% dispersion error in wave propagation velocity.

The proposed scheme, jointly with the Perfect Matching Layer (PML), gives the complex sparse symmetric (not Hermitian) 27-diagonal matrix. Solving such system of linear algebraic equations (SLAE) is based on the direct approach (LDL^t decomposition of the matrix A), Nested Dissection algorithm and low-rank/HSS technique. The large off-diagonal blocks efficiently approximated by low-rank matrices [1] while diagonal blocks effectively represented in hierarchically semiseparable (HSS) format [4]. To compress dense blocks into low-rank or HSS structures, we use the panel modification of cross approximation (CA) approach [2]. To additionally increasing the accuracy, the LDL^t inversion step uses the iterative refinement process.

3 Numerical experiments

To validate the algorithm we compare numerical solution both with analytic one (homogenous medium) and with solution, computed in time domain on realistic model. Frequency is varied from 1Hz to 8Hz. Computational grid contains about 24×10^6 points. Results of testing show that using standard 7-point scheme with 10 grid points per wavelength produces large dispersion error, while optimized 27-point scheme shows better results, i.e. relative error less than 1% in analytic tests and 5% for realistic model).

Memory measurements show that: 1) memory usage of L-factors are the similar despite of number of nonzero elements in matrix A for 7-point stencil is more than 3 times than for 7-point one; 2) HSS compressing allows us to use 3-4x times memory less than for exact arithmetic.

Moreover, using 27-point scheme insignificantly (less than 10%) increases the factorization time in compare with 7-point scheme.

The research was supported by CRDF grant RUE1-30034-NO-13 and by RFBR grants 14-01-31340, 14-05-31222, 14-05-93090, 14-05-00049, 15-35-20022.

References

[1] Dewilde P. Gu M. Somasunderam N. Chandrasekaran, S. On the numerical rank of the off-diagonal blocks of schur complements of discretized elliptic pdes. *SIAM J. Matrix Anal. Appl.*, 31(5):2261–2290, 2010.

[2] Rjasanow S. Adaptive cross approximation of dense matrices. In *IABEM 2002, International Association for Boundary Element Methods*, UT Austin, TX, USA, May 28-30, 2002.

[3] J. Xia S. Wang, M.V. de Hoop and X.S. Li. Massively parallel structured multifrontal solver for time-harmonic elastic waves in 3D anisotropic media. In *Project Review, Geo-Mathematical Imaging Group*, volume 1, pages 97–121. Purdue University, West Lafayette IN, 2012.

[4] Hackbusch W. A sparse matrix arithmetic based on H-matrices. part I: Introduction to H-matrices. *Computing*, 62(2):89 – 108, 1999.

A Nitsche-type Method for Helmholtz Equation with an Embedded Acoustically Permeable Interface

Esubalewe Lakie Yedeg[1,*], **Eddie Wadbro**[1], **Peter Hansbo**[2], **Mats G. Larson**[3], **Martin Berggren**[1]

[1]Department of Computing Science, Umeå University, Sweden
[2]Department of Mechanical Engineering, Jönköping University, Sweden
[3]Department of Mathematics and Mathematical Statistics, Umeå University, Sweden
[*]Email: yedegl@cs.umu.se

Abstract

We propose a new finite element method for Helmholtz equation in the situation where an acoustically permeable interface is embedded in the computational domain. A variant of Nitsche's method enforces weakly the impedance conditions on the interface. As opposed to a standard finite-element discretization of the problem, the proposed method can stably handle a vanishing acoustic impedance.

Keywords: Helmholtz equation, Nitsche-type method, interface problem, acoustic impedance

1 Problem Formulation

Let Ω_0 be the union of two disjoint, open, and connected regions Ω^1 and Ω^2 ($\Omega_0 = \Omega^1 \cup \Omega^2$) such that the closures of Ω^1 and Ω^2 intersect at an interface Γ_I ($\Gamma_\mathrm{I} = \overline{\Omega}^1 \cap \overline{\Omega}^2$) of codimension one with positive measure. We consider Helmholtz equation for the acoustic pressure in Ω_0,

$$\Delta p + \kappa^2 p = 0 \qquad \text{in } \Omega^l,\ l = 1,2 \tag{1a}$$

$$\mathrm{i}\kappa p + \frac{\partial p}{\partial n} = 2\mathrm{i}\kappa g \qquad \text{on } \Gamma_\mathrm{io}, \tag{1b}$$

$$\frac{\partial p}{\partial n} = 0 \qquad \text{on } \Gamma_\mathrm{s}, \tag{1c}$$

where κ is the wavenumber, Γ_io is inlet and outlet boundaries, and Γ_s is sound hard boundaries of Ω_0.

Moreover, we assume that the flux across the interface is continuous and related to the pressure jump $[\![p]\!] = p^1 - p^2$ through a complex acoustic impedance ζ,

$$-\frac{\partial p^1}{\partial n_1} = \frac{\partial p^2}{\partial n_2} = \frac{\mathrm{i}\kappa}{\zeta}[\![p]\!] \qquad \text{on } \Gamma_\mathrm{I}. \tag{2}$$

Here p^l is the trace on Γ_I of the acoustic pressure in Ω^l, and n_l is the normal vector on Γ_I, directed outward from Ω^l. The impedance $\zeta = 0$ stands for no interface, the limit $|\zeta| \to \infty$ represents sound-hard (rigid) material, and intermediate values model acoustically permeable materials. We assume that the interface is acoustically passive, that is, $\mathrm{Re}(\zeta) \geq 0$. The acoustic properties of, for instance, a perforated plate can be modeled by condition (2) [1].

2 Formulation of the method

We will consider weak solutions to problem (1), (2) in $H^1(\Omega_0)$; $p \in H^1(\Omega_0)$ means $p|_{\Omega^l} \in H^1(\Omega^l)$, for $l = 1, 2$. Note that elements in $H^1(\Omega_0)$ may be discontinuous across the interface Γ_I. A variational problem associated with equation (1) is

$$\begin{aligned} &\text{find } p \in H^1(\Omega_0) \text{ such that} \\ &a(p,q) = \ell(q) \quad \forall q \in H^1(\Omega_0), \end{aligned} \tag{3}$$

where

$$\ell(q) = 2\mathrm{i}\kappa \int_{\Gamma_\mathrm{io}} g\overline{q} \tag{4}$$

and

$$a(p,q) = a_0(p,q) + \mathrm{i}\kappa \int_\Gamma \frac{1}{\zeta}[\![p]\!][\![\overline{q}]\!], \tag{5}$$

with

$$a_0(p,q) = \int_{\Omega_0} \nabla p \cdot \nabla \overline{q} - \kappa^2 \int_{\Omega_0} p\overline{q} + \mathrm{i}\kappa \int_{\Gamma_\mathrm{io}} p\overline{q}. \tag{6}$$

Sesquilinear form (5) satisfies the following uniqueness property.

Lemma 1. *For each $\kappa \in \mathbb{R}$, if $p \in H^1(\Omega_0)$ such that $a(p,q) = 0$, $\forall q \in H^1(\Omega_0)$ then $p \equiv 0$.*

In addition, the real part of $a(\cdot,\cdot)$ satisfies a Gårding inequality. Variational problem (3) thus has a unique solution for each κ [2, Theorem 6.5.15].

A finite element discretisation of sesquilinear form (5) leads to an ill-conditioned system matrix as $\zeta \to 0$. To incorporate the limit case

without a blowup of the interface condition, we propose a new variational form based on a version of Nitsche's method first proposed for compliant interfaces in solid mechanics [3].

We introduce the finite element space V_h, where for $l = 1, 2$, $V_h|_{\Omega^l} \subset H^1(\Omega^l)$ is the space of continuous functions that are piecewise polynomials on a triangulation of Ω^l. The method does *not* require that the mesh nodes associated with $V_h|_{\Omega^1}$ and $V_h|_{\Omega^2}$ match at the interface.

The proposed method is defined by the following variational problem:

$$\begin{aligned} &\text{find } p_h \in V_h \text{ such that} \\ &a_\lambda(p_h, q_h) = \ell(q_h) \quad \forall q_h \in V_h, \end{aligned} \tag{7}$$

where

$$\begin{aligned} a_\lambda(p_h, q_h) = a_0(p_h, q_h) &- \int_\Gamma (1 - \lambda \frac{\zeta}{\mathrm{i}\kappa}) [\![\overline{q_h}]\!] \left\{ \frac{\partial p_h}{\partial n} \right\} \\ &- \int_\Gamma \left(1 - \lambda \frac{\zeta}{\mathrm{i}\kappa}\right) [\![p_h]\!] \left\{ \overline{\frac{\partial q_h}{\partial n}} \right\} \\ &- \int_\Gamma \frac{\zeta}{\mathrm{i}\kappa} \left(1 - \lambda \frac{\zeta}{\mathrm{i}\kappa}\right) \left\{ \frac{\partial p_h}{\partial n} \right\} \left\{ \overline{\frac{\partial q_h}{\partial n}} \right\} + \int_\Gamma \lambda [\![p_h]\!] [\![\overline{q_h}]\!]. \end{aligned}$$

Here, $2\{\partial p_h/\partial n\} = \partial p_h^1/\partial n_1 - \partial p_h^2/\partial n_2$, and parameter λ is a function of the acoustical impedance ζ, the wavenumber κ, the mesh size h, and a sufficiently large real penalty parameter γ (see Theorem 3 below).

For $\zeta = 0$, our method reduces to the standard symmetric interior penalty method for imposing continuity across the interface [4]. Consistency of our method follows from Lemma 2.

Lemma 2. *If $p \in H^1(\Omega_0) \cap H^2(\Omega_0)$ solves problem (3), then*

$$a_\lambda(p, q_h) = \ell(q_h) \quad \forall q_h \in V_h.$$

Following theorem ensures stability of the method.

Theorem 3. *If $Im(\zeta) \geq 0$, then a_λ satisfies the Gårding inequality*

$$\mathrm{Re}\, a_\lambda(p_h, p_h) + \alpha \|p_h\|_{L^2}^2 \geq C |||p_h|||_{k,h}^2 \quad \forall p_h \in V_h$$

for $\lambda = \left(h/\gamma + \zeta/(\mathrm{i}\kappa)\right)^{-1}$, for some $\alpha > 0$, some $C > 0$, and for

$$\begin{aligned} |||p_h|||_{\kappa,h}^2 = &\int_{\Omega_0} |\nabla p_h|^2 + \kappa^2 \int_{\Omega_0} |p_h|^2 \\ &+ \frac{1}{\gamma} \int_\Gamma h \left| \left\{ \frac{\partial p_h}{\partial n} \right\} \right|^2 + \int_\Gamma \left| \lambda [\![p_h]\!] \right|^2. \end{aligned}$$

3 Numerical Experiments

We solve boundary value problem (1) in a waveguide of length 2 and height 0.1. The interface is placed vertically at the middle of the waveguide. We use $\kappa = 1.83$ and study two acoustic impedances $\zeta = 1 + 0.37\mathrm{i}$ and $\zeta = 0$. Bilinear elements on separate square meshes on each side of the interface are used for the finite element discretization.

Figure 1 shows the convergence rates. The lines with square and asterisk marks show second order L^2-convergence of the standard finite element method based on variational form (3) and our method for $\zeta = 1 + 0.37\mathrm{i}$, respectively, while lines with diamond and dot marks illustrate first-order H^1-convergence. Thus the proposed method behaves as the standard finite element method for ζ not close to zero. The lines with triangle marks show L^2 and H^1-convergence of the new method for $\zeta = 0$, which verifies optimal convergence of the proposed method also in the limit case.

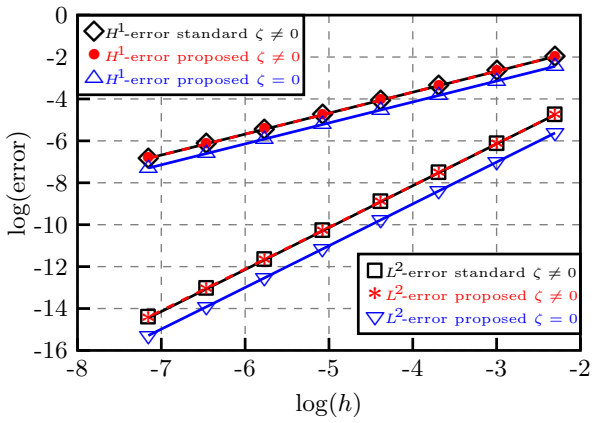

Figure 1: Convergence rates of the standard finite element and the proposed method for the interface problem; $\zeta \neq 0$ stands for $\zeta = 1 + 0.37\mathrm{i}$.

References

[1] R. Kirby and A. Cummings, *J. Sound Vib.* **217** (1998), pp. 619–636.

[2] W. Hackbusch, *Elliptic Differential Equations: Theory and Numerical Treatment*, Springer, 1992.

[3] A. Hansbo and P. Hansbo, *Comput. Methods in Appl. Mech. Engrg.* **193** (2004), pp. 3523–3540.

[4] R. Becker, P. Hansbo and R. Stenberg, *ESAIM: Math. Model. Num. Anal.* **37** (2003) pp. 209–225.

A Fictitious Domain Approximation of Hard Scatterers Free from Spurious Resonances

Martin Berggren[1,*], **Fotios Kasolis**[1], **Eddie Wadbro**[1]
[1]Department of Computing Science, Umeå University, Sweden
[*]Email: martin.berggren@cs.umu.se

Abstract

A sound-hard scatterer can be modeled in a fictitious-domain manner by an almost vanishing coefficient in the governing Helmholtz equation. We observe that this approach results in spurious resonances at certain frequencies inside the scatterer and generates ill-conditioned system matrices after discretization. We present a stabilization strategy to remove these resonances, and we prove that the solution to the stabilized problem converges linearly in the vanishing coefficient to the solution to the problem with an exactly modeled scatterer.

Keywords: Helmholtz equation, hard scatterers, fictitious domain method

1 Introduction

A sound-hard scatterer of acoustic waves is characterized, in frequency domain, by a homogeneous Neumann condition for the acoustic pressure at the boundary of the scatterer. In the context of design optimization, it may be advantageous to avoid tracking of boundaries by using a fictitious-domain approach and approximately represent the scatterer through a varying coefficient α in the Helmholtz equation

$$\nabla \cdot \alpha \nabla p + k^2 \alpha p = 0, \tag{1}$$

where $\alpha = 1$ in the wave medium and $\alpha = \epsilon$ inside the scatterer, where ϵ is a small positive number. This fictitious domain approach is particularly well established for so-called topology optimization of static load-bearing elastic structures, but the approach is also increasingly used for wave propagation problems [1]. We have recently observed an issue with this approach in the context of the Helmholtz equation, namely that spurious resonances occur inside the sound-hard region at certain frequencies, and that the system matrix after discretization becomes ill-conditioned around these frequencies. This phenomenon is analogous to the non uniqueness problem for certain formulations of the boundary-element method for the exterior Helmholtz problem [2] and occurs when k^2 is in the vicinity of the eigenvalues for the Dirichlet problem associated with the Laplacian in the sound hard region.

2 Preventing the Spurious Resonances

We propose to replace problem statement (1) with

$$\nabla \cdot \alpha \nabla p + k^2 \eta(\alpha) \alpha p = 0, \tag{2}$$

where η is a continuous function on the $[0, 1]$ interval such that $\eta(0) = 0$ and $\eta(1) = 1$; in the numerical experiments, we typically use $\eta(\alpha) = \alpha$. In regions of approximate sound-hard material, that is, when $\alpha = \epsilon$ for some small positive ϵ, the effective wavenumber will then be decreased to $k\sqrt{\eta(\epsilon)}$. The effective wavenumber in the scatterer will therefore, at least with a reasonable choice of function η, be way below values that can generate resonances.

3 Stability and convergence results

We consider a setup with a single scatterer Ω surrounded by a bounded domain D. The exact solution p^D solves the boundary-value problem

$$\begin{aligned} \Delta p^D + k^2 p^D &= 0 && \text{in } D, \\ \mathrm{i}k p^D + \frac{\partial p^D}{\partial n} &= 2\mathrm{i}k g && \text{on } \Gamma_{\text{io}}, \\ \frac{\partial p^D}{\partial n} &= 0 && \text{on } \partial D \setminus \Gamma_{\text{io}}. \end{aligned} \tag{3}$$

The radiation boundary condition on Γ_{io} specifies an incoming wave of amplitude g and absorbs outgoing waves.

In the fictitious domain approach, scattering problem (3) is approximated by solving equation (2) in $\widehat{D} = D \cup \overline{\Omega}$ where α equals 1 in D and ϵ in Ω. The associated bilinear form will then take the form

$$\begin{aligned} a_\epsilon(q, p) = &\int_D \nabla q \cdot \nabla p - k^2 \int_D qp + \mathrm{i}k \int_{\Gamma_{\text{io}}} qp \\ &+ \epsilon \left(\int_\Omega \nabla q \cdot \nabla p - \eta(\epsilon) k^2 \int_\Omega qp \right) \end{aligned} \tag{4}$$

We show that no resonances can occur within Ω if

$$\eta(\epsilon) < 2/(k^2(\operatorname{diam}\Omega)^2). \tag{5}$$

In addition, the following stability condition holds for bilinear form (4).

Theorem 1 *There is an $\alpha > 0$ such that, for each $\epsilon \in (0, 1/2]$ and each $p \in H^1(\widehat{D})$,*

$$\alpha\|p\|_\epsilon \leq \sup_{q\in H^1(\widehat{D})\setminus\{0\}} \frac{\operatorname{Re} a_\epsilon(q,p)}{\|q\|_\epsilon}, \tag{6}$$

where $\|p\|_\epsilon^2 = \|p\|_{H^1(D)}^2 + \epsilon\|p\|_{H^1(\Omega)}^2$.

Note that inf–sup condition (6) holds uniformly in ϵ.

Let $p_\epsilon \in H^1(\widehat{D})$ such that $p_\epsilon\big|_D = p^D$ and $p_\epsilon\big|_\Omega = p_\epsilon^\Omega$, where p_ϵ^Ω is the continuous extension of p^D into Ω such that $\Delta p_\epsilon^\Omega + \eta(\epsilon)k^2 p_\epsilon^\Omega = 0$. This extension is uniquely defined under condition (5).

With the help of p_ϵ, we can formulate the following inconsistency estimate between the fictitious domain solution using bilinear form (4) and the weak solution to problem (3),

Lemma 2 *Let $\widehat{p}_\epsilon$ be the fictitious domain solution using bilinear form (4), and p_ϵ the extended weak solution to problem (3). Then,*

$$a_\epsilon(q, \widehat{p}_\epsilon - p_\epsilon) = \epsilon\left\langle \partial_n p_\epsilon^\Omega, \gamma q\right\rangle \quad \forall q \in H^1(\widehat{D}), \tag{7}$$

where $\gamma : H^1(\Omega) \to H^{1/2}(\partial\Omega)$ is the trace operator and $\langle\cdot,\cdot\rangle$ the duality pairing on $H^{-1/2}(\partial\Omega)\times H^{1/2}(\partial\Omega)$.

Stability property (6) and estimate (7) yield the following bound of the error invoked by the approximate handling of the scatterer,

$$\|p_\epsilon - p^D\|_{H^1(D)} \leq \epsilon C\|p^D\|_{H^1(D)}. \tag{8}$$

The above analysis is carried out in the infinite-dimensional case. However, numerical experience suggests an analogous behavior also in the discrete case, after finite-element discretization.

Figure 1 shows a numerical example in 2D. The scatterer is a disk with radius 0.2, $\epsilon = 10^{-8}$, and $k = 12$. This wavenumber corresponds to the first eigenmode of the Dirichlet problem for the Laplacian inside the scatterer.

The unstabilized case ($\eta = 1$) is illustrated in the upper picture. We notice a resonance

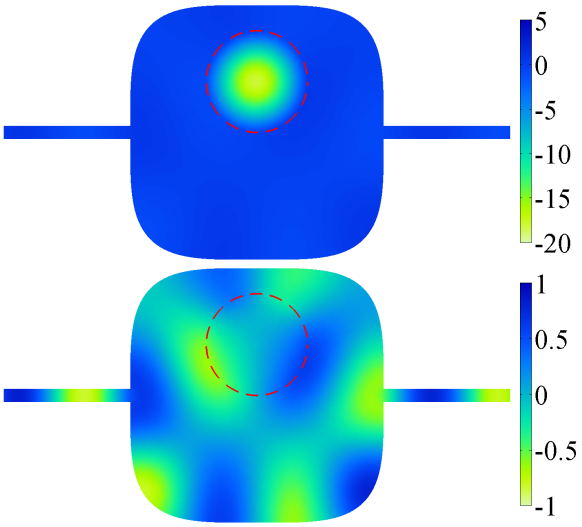

Figure 1: Re(p) without and with stabilization

in the scatterer that completely dominates the solution. However, when using $\eta = \epsilon$, the resonance goes away as we see in the lower picture. The stabilized problem is free from resonances up to about $k = 12 \times 10^4$ ($\epsilon^{-1/2}$ times the first unstable mode) for the choice $\eta = \epsilon$.

References

[1] M. P. Bendsøe and O. Sigmund. *Topology optimization: theory, methods and applications*. Springer, 2003.

[2] H. A. Schenck. Improved integral formulation for acoustic radiation problems. *J. Acoust. Soc. Am.*, 44(1):41–58, 1968.

Approximate computation of the time-dependent magnetic and electric Green's functions in a rectangular parallelepiped

Valery Yakhno[1,*], **Sengul Ersoy**[2]

[1] Electrical and Electronics Engineering Department, Dokuz Eylul University, Izmir, TURKEY
[2]Graduate School of Natural and Applied Sciences, Dokuz Eylul University Izmir, TURKEY
[*]Email: valery.yakhno@deu.edu.tr

Abstract

A method for the approximate computation of the time-dependent magnetic and electric matrix Green's functions in a parallelepiped with the perfect conducting boundary is suggested. The method consists of the following. The equations for the magnetic Green's function are written in the form of the initial boundary value problem for a vector wave equation. Applying the Fourier series expansion approach, an explicit formula for an approximate solution of this problem is constructed. Using this formula the elements of an approximate electric Green's function are found explicitly.

Keywords: Maxwell's equations, perfect conducting boundary, Green's function, analytical method, simulation

1 Introduction

In [1] the frequency dependent dyadic electric and magnetic Green's functions corresponding to the elementary electric and magnetic current point sources have been presented inside the cavity with the perfect conducting boundary by the eigenvalues and eigenmodes. The computation of the frequency dependent Green's functions in the rectangular parallelepiped with the perfect conducting boundary by the Fourier series meta-approach has been worked out in [2]. Several approaches for the computation of the time-dependent electric and magnetic Green's functions have been developed in [3] (see also the references of [3]) for unbounded three dimensional electrically and magnetically anisotropic media by the Fourier transform with respect to space variables and matrix transformations. But the computation of the time dependent electric and magnetic Green's functions has not been achieved so far for the bounded domain with perfect conducting conditions. We note that there exists a connection between the time dependent Green's functions and frequency dependent Green's functions which can be expressed by the Fourier transform with respect to the time variable. Moreover the time-dependent Green's function, for example, of the wave equation in a whole space can be derived explicitly by the application of the Fourier transform to the Green's function of the Helmholtz equation. The Fourier transform and inverse Fourier transform are defined here in the class of the generalized functions (tempered distributions) and for some scalar hyperbolic differential equations the application of the Fourier transform can be done explicitly. Unfortunately the explicit or approximate computation of the inverse Fourier transform, applied to the frequency dependent electric and magnetic Green's functions in a bounded domain of the three dimensional space, is unknown. This computation requires knowledge of the frequency dependent Green's functions for all frequencies that is difficult to realize in practice. Moreover the time dependent electric and magnetic Green's functions are singular generalized functions and numerical methods in the space of generalized functions are not developed yet. To overcome these difficulties we suggest the adaptation of the Fourier series approach for the direct computation of the approximate (regularized) time dependent electric and magnetic Green's functions in a rectangular parallelepiped with the perfect conducting boundary which does not use the frequency dependent Green's functions.

2 The time-dependent magnetic and electric Green's functions

Let b_1, b_2, b_3 be given positive numbers, $x = (x_1, x_2, x_3)$ be a 3D variable from $\mathbf{R}^3$; V be a rectangular parallelepiped defined as the set of points $x = (x_1, x_2, x_3)$ from $\mathbf{R}^3$ satisfying $0 < x_1 < b_1$, $0 < x_2 < b_2$, $0 < x_3 < b_3$; Γ be the boundary of V; t be the time variable; $\vec{e^s}$ be the basis vectors of $\mathbf{R}^3$ ($\vec{e^1} = (1,0,0)^T$, $\vec{e^2} = (0,1,0)^T$, $\vec{e^3} = (0,0,1))^T$ (the superscript "T" means "transpose"). The 3×3 matrices $\mathbf{G}^H$,

$\mathbf{G}^E$ whose s-column ($s = 1, 2, 3$)

$$\mathbf{H}^s = \begin{pmatrix} H_1^s \\ H_2^s \\ H_3^s \end{pmatrix}, \quad \mathbf{E}^s = \begin{pmatrix} E_1^s \\ E_2^s \\ E_3^s \end{pmatrix},$$

satisfy for $x \in V, \quad t \in \mathbf{R}$

$$curl_x \mathbf{H}^s = \epsilon \frac{\partial \mathbf{E}^s}{\partial t} + \vec{e^s}\delta(x - x^0, t),$$
$$curl_x \mathbf{E}^s = -\mu \frac{\partial \mathbf{H}^s}{\partial t},$$
$$\mathbf{E}^s\big|_{t\le 0} = 0, \quad \mathbf{H}^s\big|_{t\le 0} = 0,$$
$$(\mathbf{E}^s \times \vec{n})\big|_\Gamma = 0, \quad (\mathbf{H}^s \cdot \vec{n})\big|_\Gamma = 0, \quad s = 1, 2, 3,$$

are called the magnetic Green's function (matrix) and the electric Green's function (matrix), respectively. Here the positive constants ϵ and μ are the electric permittivity and magnetic permeability, respectively; $\vec{n}$ is the unit normal to the boundary Γ of the parallelepiped V;
$x^0 = (x_1^0, x_2^0, x_3^0)$ is a 3D parameter from V;
$\delta(x - x^0, t) = \delta(x_1 - x_1^0)\delta(x_2 - x_2^0)\delta(x_3 - x_3^0)\delta(t)$,
$\delta(x_j - x_j^0)$ is the Dirac delta function considered at $x_j = x_j^0$, $j = 1, 2, 3$; $\delta(t)$ is the Dirac delta function at $t = 0$.

The suggested method for the approximate computation of the magnetic and electric matrix Green's functions $\mathbf{G}^H(x, t, x^0)$, $\mathbf{G}^E(x, t, x^0)$ consists of the following. The equations for the magnetic Green's function are written in a special form which does not contain elements of the electric Green's function. These equations are partial differential equations of the hyperbolic type and our method is based on the standard Fourier series expansion approach for solving the initial boundary value problem for the hyperbolic partial differential equations in the bounded region. The elements of the approximate Green's function for the magnetic field are found by explicit formulae. These formulae have the form of the partial sums of the Fourier series with a finite number of terms. This finite number (denoted as N) is a parameter of regularization (approximation). Using these explicit formulae we derive explicitly the approximate elements of the electric Green's matrix by integration with respect to time variable. The simple implementation of our method for computing the Green's functions in a rectangular parallelepiped is based on the obtained presentations and does not contain any type of discretization. Numerical computation of the time-dependent magnetic and electric Green's functions has been implemented in MATLAB. The computational experiments confirm robustness of the method. To obtain the reasonable accuracy and time for the computation of approximate Green's functions for electric and magnetic fields in MATLAB by a personal computer it is necessary to find a parameter of the regularization N. The elements of the regularized (approximate) matrix Green's function for the magnetic field (computed by our method) are classical differentiable and integrable functions over V with the values at the fixed points. These classical functions define the regular distributions. The comparison of the distributions can be made by the comparison of their integral characteristics. Some integral characteristics of the elements of the matrix Green's function of the magnetic field can be found explicitly. These characteristics have been compared with integral characteristics of the approximate Green's function for different parameter of the approximation N to select reasonable one. The results of the computational experiments can be found in [4].

References

[1] G. Dolmans, Electromagnetic Fields Inside a Large Room with Perfectly Conducting Walls, *EUT Report 95-E-286, Eindhoven University of Technology, Faculty of Electrical Engineering*, 1995.

[2] V. Yakhno and S. Ersoy, Computing the electric and magnetic matrix Greens functions in a rectangular parallelepiped with a perfect conducting boundary, *Absract and Applied Analysis*, Article ID **586370** (2014), pp. 1–13.

[3] V. Yakhno and T. Yakhno, Computation of the time-dependent Greens functions for non-dispersive magnetoelectric materials, *International Journal of Engineering Science* **54** (2012), pp. 1–14.

[4] V. Yakhno, S. Ersoy, The computation of the time-dependent magnetic and electric matrix Green's functions in a parallelepiped,*Applied Mathematical Modelling*, (2015), http://dx.doi.org/10.1016/j.apm.2015.01.057

Huygens-Fresnel wavefront tracing in non-uniform media

F.A. Volpe[1,*], **P.-D. Létourneau**[1], **A. Zhao**[1]

[1]Dept of Applied Physics and Applied Mathematics, Columbia University, New York, NY, USA

*Email: fvolpe@columbia.edu

Abstract

A new numerical method for wave propagation, inspired by Huygens' principle and deploying a zero-search method, accounts for diffraction and refraction in slowly varying and discontinuous 2D isotropic media, but can be extended to 3D anisotropic media by means of anisotropically expanding ellipsoidal wavelets.

Keywords: Huygens-Fresnel principle, wavefront tracing

1 Introduction

Huygens' model of the wavefront as an array of wavelet emitters [1], combined with Huygens' principle that wavelets interfere [2] is an important principle in the theory of diffraction [3]. Not surprisingly, it was used in pedagogical widgets illustrating diffraction [4] and refraction [5], and was recently invoked in the design of new metamaterials [6]. Numerical applications to wave propagation, however, are relatively limited. This is surprising, considering that Huygens' original drawings basically outlined an iterative graphical solver, suggestive of a modern iterative solver on a computer.

Wavefront tracing are cited in seismic modeling, but rarely include diffraction [7]. An interesting and elegant exception [8, 9] manipulates the eikonal equation into an expression describing a small expanding sphere centered in a generic point on the wavefront. The analogy with Huygens' construction is evident. Diffraction is also partly included: differentiation of that expression leads to an explicit finite-difference scheme in which each point on the new wavefront is constructed by three or five points on the previous one, respectively in 2D and 3D. However, all point-sources are assumed of equal strength. Also, despite high numerical stability [8, 9], small phase-increments might be required for the restriction to three or five neighboring points to be a good approximation.

The simple technique presented here retains diffraction effects. It was originally intended for electromagnetic and electrostatic waves in plasmas, but has much broader applicability. Cpu-time and physics content are intermediate between ray-tracing [10, 11] and full-wave solvers [12].

2 Numerical Method

Huygens-Fresnel formula for the field amplitude $\mathbf{E}$ in a point $\mathbf{x}'$ can be written as follows [13]:

$$\mathbf{E}(\mathbf{x}') = \frac{1}{4\pi}\int\left[\frac{\cos\theta}{r} - ik(1+\cos\theta)\right]\frac{e^{ikr}}{r}\mathbf{E}(\mathbf{x})dS$$

This form is valid *also* in the near-field, thanks to the $\cos\theta/r$ dipole term that makes it consistent with Kirchhoff theorem [14]. Here θ is the angle between the local wavefront-normal and vector $\mathbf{x}' - \mathbf{x}$, of norm r. In 2D, the surface integral is replaced by a line integral, and the denominator by $\sqrt{r}$.

Our objective is to compute the integral to identify a set of points $\mathbf{x'}_{ab}$ where $\mathbf{E}$ has equal phase, or, without losing generality, $\Re(\mathbf{E})$=0. This is easily generalized by shifting all sources in the integrand by a phase ϕ.

The points found form the new wavefront. The same integral should be recalculated in those points again, but with all sources phase-shifted so that $\mathbf{E} \neq 0$. This permits to attribute proper amplitudes and treat the points $\mathbf{x'}_{ab}$ as emitters in the following iteration.

Equivalently, one could search for the locus of points where $\arctan[\Im(\mathbf{E})/\Re(\mathbf{E})]=\phi$.

To fix the ideas, consider now a 2D problem in Cartesian coordinates x and y, and let us search the new points in the x direction. The existence of multiple solutions is prevented by restricting the search to intervals of length $\lambda/2$, where λ is the wavelength in the medium. We avoid placing such intervals too closely ($\ll \lambda$) to the original wavefront. This is to discard the dipole correction, for simplicity. Let us call $\mathbf{x'}_{Ac}$ the generic point on the search interval, where A is a specific a and c denotes an iteration index in the zero-search, conducted in our case by bisection. The electric field amplitude in $\mathbf{x'}_{Ac}$ is obtained by interference of point-sources, each

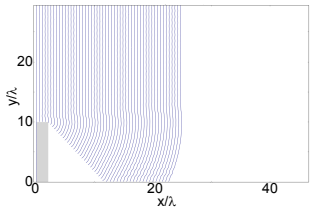

Figure 1: Traced initially planar wavefront, diffracting around obstacle as expected.

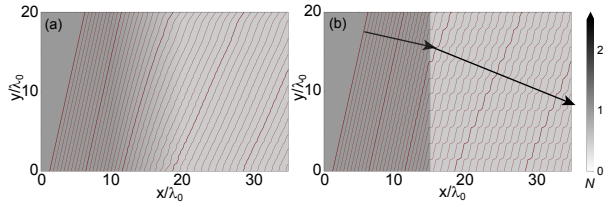

Figure 2: Wavefronts refracting in a medium of refractive index N (a) varying over ten wavelengths or (b) discontinuous.

one of amplitude $\mathbf{E}_a$, distance $r_{Ac,a}$ from the target and inclination $\theta_{Ac,a}$. Repeated evaluation of

$$\mathbf{E}_{Ac} = -\sum_{a=1}^{m} \frac{ik}{4\pi}(1+\cos\theta_{Ac,a})\frac{e^{ikr_{Ac,a}}}{\sqrt{r_{Ac,a}}}\mathbf{E}_a$$

in various $\mathbf{x'}_{ac}$ suggested by bisection (or other search method) eventually localizes the point $\mathbf{x'}_A$ (or actually its x component, as y is fixed) where $\Re(\mathbf{E})$=0.

The 2D algorithm is easily generalized to 3D by adding a subscript $_b$ and summing over it, and replacing the denominator $\sqrt{r_{ac}}$ with r_{abc}.

3 Numerical examples

The results for plane waves (not shown), diffraction around an obstacle (Fig.1) and refraction in a medium whose refractive index varies slowly with space (Fig.2a) are all as expected.

The wavefront bends as expected from Snell's law even in the case of discontinuity (Fig.2b), which, however, requires special care: if $\mathbf{E}$ is being evaluated in medium 2, the contributions from points in medium 1 will travel at different inclinations in the two media. Therefore, instead of a single Green's function, two propagators are actually needed, from the emitter to a proper point on the boundary (uniquely defined by Snell's law), and then to the observer.

Moderately focused Gaussian beams (Fig. 3a) agree with theory [15]. The geometrical optics solution is also shown and, as expected, is a good approximation away from the waist.

The zero-search can be subject to errors where the electric field is very small, comparable

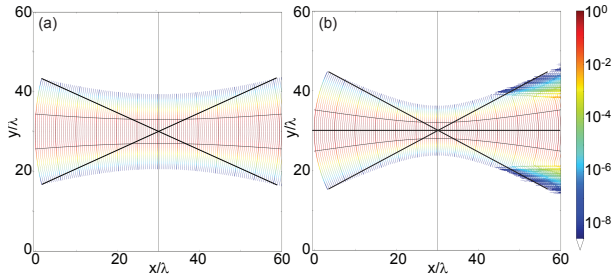

Figure 3: Wavefronts for (a) moderately and (b) strongly focused Gaussian beam, colored according to intensity normalized to on-axis value.

with machine precision, or if the search interval is chosen incorrectly, which can occur in regions of strong refraction or diffraction. In the latter case, the zero can be mistakenly located on the "next" wavefront, as if the corresponding wavefront portion "jumps" too far ahead. This is sometimes observed for strongly focused beams (Fig.3b) and could be solved by an adaptive definition of the zero-search interval.

References

[1] C. Huygens, *Traité de la Lumiere*, Leyden, 1690.
[2] A. Fresnel, *Ann. Chem. Phys.* **1** (1816) 239.
[3] M. Born, E. Wolf, *Principles of Optics*, Cambridge University Press, 2006.
[4] P. Falstad, http://www.falstad.com/ripple/ (2014).
[5] W. Fendt, http://www.walter-fendt.de/ph14e/huygenspr.htm (2010).
[6] C. Pfeiffer, A. Grbic, *Phys. Rev. Lett.* **110** (2013) 197401.
[7] N. Rawlinson, J. Hauser, M. Sambridge, *Advances in Geophys.* **49** (2008) 203.
[8] P. Sava, S. Formel, *SEP Report* **95** (1997) 101.
[9] P. Sava, S. Formel, *Geophysics* **66** (2001) 883.
[10] E. Tracy, A. Brizard, A. Kaufman, A. Richardson, *Ray Tracing and Beyond* Cambridge Univ. Press, 2014.
[11] F. Volpe, H. Laqua, *Rev. Sci. Instrum.* **74** (2003) 1409.
[12] M. Brambilla, *Plasma Phys. Control. Fusion* **41** (1999) 1.
[13] K. Makris, D. Psaltis, *Optics Communications* **284** (2011) 1686.
[14] D. Miller, *Optics Lett.* **16** (1991) 1370.
[15] P.F. Goldsmith, *Quasioptical Systems*, WIley 1998

Convergence of Krylov subspace solvers with Schwarz' preconditioner for Maxwell exterior problem

Eric Darrigrand[1,*], **Nabil Gmati**[2], **Rania Rais**[2,3]

[1]Université de Rennes 1, IRMAR, Campus de Beaulieu, 35042 Rennes, France
[2]Ecole Nationale d'Ingénieurs de Tunis, LAMSIN, B.P. 37, 1002 Le Belvédère, Tunisia
[3]Université de Kairouan, ISSAT, 3100 Kairouan, Tunisia
[*]Email: eric.darrigrand-lacarrieu@univ-rennes1.fr

Abstract

The use of integral representations as an exact boundary condition for the finite elements resolution of wave propagation problems in exterior domain induces algorithm difficulties. We focus on the resolution of 3D Maxwell equations by a coupling of finite elements and integral representation (CEFRI). The justification of an algorithm described in literature, using an interpretation as a Schwarz method, reveals the finite element term of Schwarz method as a preconditioner for Krylov iterative solvers. An analytical study of the case of a spherical perfect conductor indicates the efficiency of such approach. The application of the preconditioner leads to a superlinear convergence of the GMRES predicted by the analytical study and verified numerically.

Keywords: Maxwell equations, finite elements, integral representation, Schwarz preconditioner

1 Introduction to CEFRI

We focus on the resolution of the regularized Maxwell equations in exterior domain by a coupling of finite elements and an integral representation as derived by Hazard and Lenoir (see [3]). To this aim, we consider a bounded domain Ω_i of boundary Γ. The exterior domain is delimited by an artificial boundary Σ on which the integral representation is applied as an exact boundary condition. In the case of a perfect conductor, the problem reduces equivalently to the one defined as follows on the bounded domain Ω delimited by Γ and Σ:

$$\begin{cases} (\operatorname{curl}\operatorname{curl} - t^{-1}\nabla\operatorname{div} - k_s^2)E = 0 \text{ in } \Omega, \\ E \times n_\gamma = 0, \operatorname{div} E = 0 \text{ on } \Gamma, \\ T_{\nu_1}(E) = T_{\nu_1}(E^{inc} - \mathcal{I}_\Gamma^{\mathcal{R}}(E)) \text{ on } \Sigma, \\ N_{\nu_2}(E) = N_{\nu_2}(E^{inc} - \mathcal{I}_\Gamma^{\mathcal{R}}(E)) \text{ on } \Sigma, \end{cases} \tag{1}$$

where k_s is the wavenumber, t^{-1} is the regularization parameter, $t \in \mathbb{R}_+^*$, and n_γ is the exterior unit normal of the domain Ω_i on Γ. ν_1 and ν_2 are complex numbers which have a negative imaginary part to ensure well-posedness. The two differential operators T_{ν_1} and N_{ν_2} are defined by $T_{\nu_1}E = \operatorname{curl} E \times n_\sigma + \nu_1\, n_\sigma \times (E \times n_\sigma)$ and $N_{\nu_2}E = \operatorname{div} E + \nu_2 E \cdot n_\sigma$ with n_σ the exterior unit normal of the domain Ω on Σ. The integral operator is identified by: for $x \in \Sigma$,

$$\begin{aligned} &\mathcal{I}_\Gamma^{\mathcal{R}}(E)(x) = \\ &-k_s^2 \int_\Omega (\mathcal{R}\mathcal{G}_t(x,.)E + \operatorname{curl}\mathcal{R}\mathcal{G}_t(x,.)\operatorname{curl} E) d\Omega \\ &+t^{-1}\int_\Omega \operatorname{div}\mathcal{R}\mathcal{G}_t(x,.)^T \operatorname{div} E\, d\Omega \\ &-t^{-1}\int_\Gamma \operatorname{div}\mathcal{G}_t(x,.)^T (E \cdot n_\gamma) d\gamma\,, \end{aligned}$$

where $\mathcal{G}_t = G_{k_s} I + \dfrac{1}{k_s^2}\operatorname{Hess}(G_{k_s} - G_{k_p})$ is the outgoing Green tensor associated with the differential operator $\operatorname{curl}\operatorname{curl} - t^{-1}\nabla(\operatorname{div}) - k_s^2 I$ of the regularized Maxwell equation; I is the identity matrix in $\mathbb{R}^3$; Hess stands for Hessian operator; $k_p = \sqrt{t}k_s$; G_k is the fundamental solution of Helmholtz equation. The linear operator $\mathcal{R}$ maps every regular function φ defined on Γ into a regular function $\mathcal{R}\varphi$ defined on Ω that satisfies $\mathcal{R}\varphi = \varphi$ on Γ and $\mathcal{R}\varphi = 0$ on Σ.

Let us introduce the Hilbert functional space

$$\begin{aligned} \mathcal{H}_t = \big\{ &E \in H(\operatorname{curl},\Omega)/\operatorname{div} E \in L^2(\Omega), E \times n_\gamma = 0, \\ &E \times n_\sigma \in L^2(\Sigma)^3,\ E \cdot n_\sigma \in L^2(\Sigma) \big\}, \end{aligned}$$

and $(.,.)_t$ the scalar product associated to $\mathcal{H}_t$,

The variational formulation of Problem (1) is: Find $E \in \mathcal{H}_t$ such that

$$(\mathcal{A}_t + \mathcal{C}_t)E = F_t, \tag{2}$$

where $\mathcal{A}_t$ and $\mathcal{C}_t : \mathcal{H}_t \to \mathcal{H}_t$ are defined by

$$\begin{aligned}(\mathcal{A}_t E, E')_t &= t^{-1} \int_\Omega \operatorname{div} E \operatorname{div} E' d\Omega \\ &+ \int_\Omega (\operatorname{curl} E \cdot \operatorname{curl} E' - k_s^2 E \cdot E') d\Omega \\ &+ \nu_1 \int_\Sigma (n_\sigma \times E) \cdot (n_\sigma \times E') d\sigma \\ &+ t^{-1} \nu_2 \int_\Sigma (n_\sigma \cdot E)(n_\sigma \cdot E')) d\sigma,\end{aligned} \tag{3}$$

$$\begin{aligned}\text{and } (\mathcal{C}_t E, E')_t &= \int_\Sigma T_{\nu_1}(\mathcal{I}_\Gamma^{\mathcal{R}}(E)) \cdot E' d\sigma \\ &+ t^{-1} \int_\Sigma N_{\nu_2}(\mathcal{I}_\Gamma^{\mathcal{R}}(E))(n_\sigma \cdot E') d\sigma.\end{aligned} \tag{4}$$

2 Resolution of the system

To solve System (2), Jin and Liu [4] suggested to consider $\mathcal{C}_t$, the term containing the integral representation, in the right hand side. An application of the fixed point algorithm leads to finding E_{n+1} such that $\mathcal{A}_t E^{n+1} = -\mathcal{C}_t E^n + F_t$. The invertibility of $\mathcal{A}_t$ is ensured by the well-posedness of Maxwell equations, on the bounded domain Ω, together with the corresponding boundary conditions. Such an algorithm as been justified and analyzed as a total overlapping Schwarz method (see [1]). The study leads to the following statements (see [2]): the convergence is linear but conditioned by the distance between Γ and Σ; the scheme shows $\mathcal{A}_t$ as a natural preconditioning of Schwarz method and motivate the name of Schwarz' preconditioner.

An interesting alternative to Jin and Liu algorithm consists then in solving System (2) with a Krylov subspace solver preconditioned by the operator $\mathcal{A}_t$, equivalently solving

$$(\mathcal{I} + (\mathcal{A}_t)^{-1}\mathcal{C}_t)E = (\mathcal{A}_t)^{-1} F_t$$

by a Krylov solver. An analysis of the convergence in the spherical case indicates a superlinear convergence for the GMRES.

3 Numerical illustration

The numerical results illustrate the superlinear convergence of Krylov solvers in the spherical configuration. The theoretical convergence estimation is numerically observed for the GMRES (Figure 1). The results were obtained considering an incident plane wave with the direction (0,0,1) and the polarization (1,0,0), choosing $\nu_1 = \nu_2 = -ik_s$, and the regularization parameter $t = 1$. The essential condition is penalized with a penalty parameter $\varepsilon_p = 10^{-4}$. The meshes were built such that the average mesh length and the distance between the boundaries are proportional to the wavelength. In Figure 1, we show the residuals of GMRES at every restart. The study is done for the wavenumbers $k_s = 1.25, 2.5, 5$.

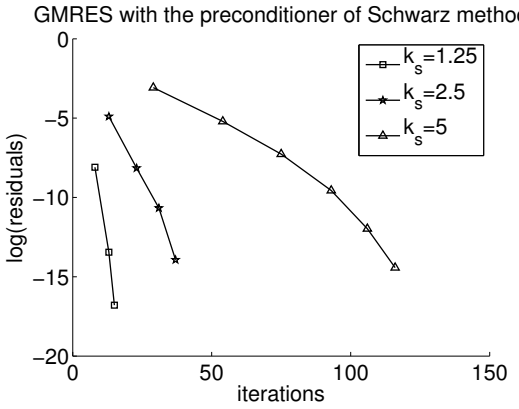

Figure 1: GMRES residuals

References

[1] F. Ben Belgacem, M. Fournié, N. Gmati and F. Jelassi, On the Schwarz algorithms for the elliptic exterior boundary value problems, *M2AN Math. Model. Numer. Anal.*, **39** (2005), pp. 693–714.

[2] E. Darrigrand, N. Gmati and R. Rais, Schwarz method justification of a coupling between finite elements and integral representation for Maxwell exterior problem, *C. R. Math. Acad. Sci. Paris*, **352** (2014), pp 311–315.

[3] C. Hazard and M. Lenoir, On the solution of time-harmonic scattering problems for Maxwell's equations, *SIAM J. Math. Anal.*, **27** (1996), pp. 1597–1630.

[4] J-M. Jin and J. Liu, A novel hybridization of higher order finite element and boundary integral methods for electromagnetic scattering and radiation Problems, *IEEE Trans. Antennas and Propagation*, **49** (2001), pp. 1794–1806.

High-quality meshes for exact controllability method in electromagnetics

Jukka Räbinä[1], **Sanna Mönkölä**[2,*], **Tuomo Rossi**[3]

[1,2,3] University of Jyvaskyla, Department of Mathematical Information Technology, P.O. Box 35 (Agora), FI-40014 University of Jyvaskyla, Finland

*Email: sanna.monkola@jyu.fi

Abstract

In this paper, we apply high-quality meshes and exact time integration for simulating time-harmonic electromagnetic scattering. We follow the exact controllability concept, and solve the time-harmonic scattering problem by using the model presented in time domain. Essentially, the approach is a controlled variation of the asymptotic approach with periodic constraints, in which the time-dependent equation is simulated in time until the time-harmonic solution is reached.

Keywords: computational electromagnetics, discrete exterior calculus, exact controllability

1 Introduction

We consider the Maxwell system,

$$\varepsilon \frac{\partial \mathbf{E}}{\partial t} - \nabla \times \mathbf{H} = -\mathbf{J}, \tag{1}$$

$$\mu \frac{\partial \mathbf{H}}{\partial t} + \nabla \times \mathbf{E} = -\mathbf{J}^*, \tag{2}$$

where $\mathbf{E}$ and $\mathbf{H}$ are the electric and magnetic fields, ε is the electric permittivity, μ is the magnetic permeability, and $\mathbf{J}$ and $\mathbf{J}^*$ are the source functions. The properties of the discretization mesh play a fundamental role in the quality of the coupling between the electric and magnetic fields. The efficiency of the computational method can not be improved by simply developing the discretization of one field variable corresponding to, e.g., the primal formulation. Instead, high-quality meshes both at the primal and the dual level are needed to obtain accurate results.

2 Discretization

The traditional way of solving electromagnetic scattering problems is to use the finite difference time domain method (FDTD) introduced by Yee [1]. Originally, the method is restricted to cubic elements. Since the simple cubic mesh is a relatively rare construction in the natural crystals, we concentrate on the structures based on more natural space lattices. In particular, we consider the constructions of computational meshes based on the natural crystal structures, i.e., the mesh structures imitating the geometry of the close packing in crystal lattices which is a typical structure for elemental metals and inter-metallic compounds.

The discrete exterior calculus (DEC) provides the properties and calculus of differential forms in a natural way at the discretization stage. With this framework, developed by Bossavit and Kettunen [2], we associate the degrees of freedom of the electric and magnetic fields to the primal and dual mesh structures, respectively. The diagonal Hodge operators, mapping between the primal and dual mesh, are obtained by constructing the dual elements that are orthogonal to the corresponding primal elements. The orthogonality of the primal and dual elements implies diagonal Hodge operators providing a significant saving in computing time. The formulation works on unstructured grids, and it covers both the classical Yee's FDTD scheme and the Bossavit-Kettunen approach.

3 Time-harmonic simulations

In principle, the time-harmonic solution can be reached by simple time integration (asymptotic approach), but we accelerate the convergence rate by using the exact controllability technique pioneered by Bristeau, Glowinski, and Périaux, see, e.g., [3]. Essentially, the approach is a controlled variation of the asymptotic approach with periodic constraints, in which the time-dependent equation is simulated in time until the time-harmonic solution is reached. A natural quadratic error functional is the squared energy norm of the system, allowing the minimization by the conjugate gradient (CG) method operating in Hilbert spaces. Combining the exact controllability method with the DEC gives a reasonable method for solving electromagnetic problems. The early stage numerical results are presented in [4]. Thereafter, we have improved the

approach by, e.g., applying a wave frequency - based correction term to the time-stepping.

4 Numerical experiments

We consider electromagnetic scattering by a spherical obstacle of radius 2.5, discretized by simple cubic, face-centered cubic (FCC), body-centered cubic (BCC), A15, C15, or Z elements (see, [5]), and centered in a spherical computational domain of radius 2.7. Inside the scatterer, the material parameters are $\epsilon = 2.5599 + 0.032\mathrm{i}$ and $\mu = 1$, whereas $\epsilon = 1$ and $\mu = 1$ in the rest of the computational domain. The source functions are $\mathbf{J} = (0, 2\pi(\epsilon - 1)\sin(2\pi(x - t)), 0)^T$ and $\mathbf{J}^* = (0, 2\pi(\mu - 1)\sin(2\pi(x - t)), 0)^T$, presenting a wave of angular frequency $\omega = 2\pi$ and time period $T = 1$ propagating in the direction of the positive x-axis.

The boundary of the scatterer is discretized by triangles, and the space between the boundary and the interior grid is constructed by the Voronoi tessellation. Then, the boundary elements are optimized by the HOT method [6]. The boundary surface is stretched in radial direction, such that a 1.7 thick layer is generated outside the scatterer. The domain is truncated by a 1.5 thick perfectly matched layer [7].

The algorithm is implemented in C++ programming language. The simulations are initialized by $\mathbf{E} = \mathbf{H} = (0, 0, 0)^T$, carried out on an 16 Intel Xeon E5-2670 processors at 2.6 GHz, and stopped after 100 CG iterations. By following [8], the near-field solution is used to form the Mueller matrix [9] including the scattering intensities and polarization in all scattering directions. The relative error, compared to the exact solution computed by the Mie scattering code [10], is presented in Figure 1.

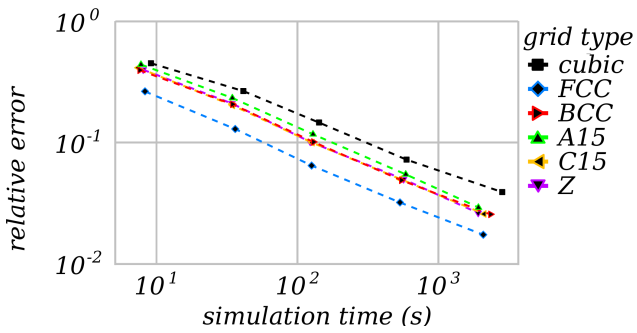

Figure 1: Relative error of the Mueller matrix.

Acknowledgements

This project has been funded by the Academy of Finland, grants 259925 and 260076.

References

[1] K. S. Yee, Numerical solution of initial boundary value problems involving Maxwell's equations in isotropic media, IEEE Trans. Antennas Propag. 14 (3) (1966) 302–307.

[2] A. Bossavit, L. Kettunen, Yee-like schemes on a tetrahedral mesh, with diagonal lumping, Int. J. Numer. Model. 12 (1–2) (1999) 129–142.

[3] M. O. Bristeau, R. Glowinski, J. Périaux, Controllability methods for the computation of time-periodic solutions; Application to scattering, J. Comput. Phys. 147 (2) (1998) 265–292.

[4] J. Räbinä, S. Mönkölä, T. Rossi, A. Penttilä, K. Muinonen, Comparison of discrete exterior calculus and discrete-dipole approximation for electromagnetic scattering, J. Quant. Spectrosc. RA 146 (2014) 417–423.

[5] J. M. Sullivan, New tetrahedrally close-packed structures, in: Foams, emulsions and applications; Eurofoam 2000, Verlag MIT, Bremen, 2000, pp. 111–119.

[6] P. Mullen, P. Memari, F. de Goes, M. Desbrun, HOT: Hodge-optimized triangulations, ACM T. Graphic 30 (4) (2011) 103.

[7] J.-P. Berenger, A perfectly matched layer for the absorption of electromagnetic waves, J. Comput. Phys. 114 (2) (1994) 185–200.

[8] K. Umashankar, A. Taflove, A novel method to analyse electromagnetic scattering of complex object, IEEE Trans. Electromagn. Compat. 24 (4) (1982) 397–405.

[9] C. F. Bohren, D. R. Huffman, Absorption and Scattering of Light by Small Particles, Wiley & Sons, New York, 1983.

[10] C. Mätzler, MATLAB functions for Mie scattering and absorption. version 2, Tech. Rep. 2002–11, Institute of Applied Physics, University of Bern (August 2002).

Local absorbing boundary conditions for 2d open waveguides

Dirk Klindworth[1], **Kersten Schmidt**[1]
[1]Research Center Matheon & Department of Mathematics, TU Berlin, Berlin, Germany

Abstract

Based on an asymptotic expansion we present local absorbing boundary conditions for the radiative field in 2d open waveguides with a defect. While the boundary conditions in the surrounding material are equivalent to Feng's boundary conditions for homogeneous media, the boundary conditions in the waveguide respect the larger decay rate in the guide.

Keywords: open waveguide, absorbing boundary conditions, asymptotic expansions, Helmholtz equation

1 Introduction

The scattering of waves by a defect in 2d open waveguides can be studied using, e.g., the modal radiation condition [1]. We shall consider the *radiative field* in this work, i.e., the scattered field without guided modes. The asymptotic behaviour of the radiative field in 3d open waveguides was discussed in [3] and it can be shown that the radiative field in 2d behaves like $\mathcal{O}(r^{-3/2})$ in the waveguide while it shows a Sommerfeld behaviour of $\mathcal{O}(r^{-1/2})$ in the surrounding material. This can also be seen from numerical results obtained by using perfectly matched layers (PML), see Figure 1. In this work we present an asymptotic expansion of the radiative field. This expansion has the expected decay behaviour and allows for the derivation of local absorbing boundary conditions.

Let us consider a waveguide $\Omega_1 = \{\mathbf{x} \in \mathbb{R}^2 : |x_2| < \frac{h}{2}\}$ of height h centered at the x_1-axis. The waveguide is characterized by constant material coefficients $a_1, b_1 \in \mathbb{R}$ and surrounded by homogeneous media $\Omega_\pm = \{\mathbf{x} \in \mathbb{R}^2 : \pm x_2 > \frac{h}{2}\}$ with coefficients $a_0, b_0 \in \mathbb{R}$. Implicitly taking the defect of the waveguide into account, the scattered field and in particular the radiative field satisfy the inhomogeneous Helmholtz equation

$$-\nabla \cdot a\nabla u - \omega^2 b\, u = f \qquad \text{in } \mathbb{R}^2 \tag{1}$$

with angular frequency ω and source term f, that is assumed to have compact support in Ω_1. Considering that the coefficient functions a and b are piecewise constant and introducing $k_i^2 = \omega^2 \frac{b_i}{a_i}$, $i = 0, 1$, and $f_1 \equiv \frac{1}{a_1} f|_{\Omega_1}$, we may rewrite Eq. (1) in the form

$$-\Delta u_\pm - k_0^2 u_\pm = 0 \qquad \text{in } \Omega_\pm, \tag{2a}$$
$$-\Delta u_1 - k_1^2 u_1 = f_1 \qquad \text{in } \Omega_1, \tag{2b}$$

with continuity conditions

$$u_\pm(\pm\tfrac{h}{2}) - u_1(\pm\tfrac{h}{2}) = 0, \tag{2c}$$
$$a_0 \tfrac{\partial}{\partial x_2} u_\pm(\pm\tfrac{h}{2}) - a_1 \tfrac{\partial}{\partial x_2} u_1(\pm\tfrac{h}{2}) = 0. \tag{2d}$$

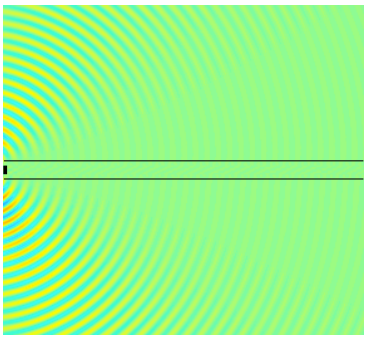

Figure 1: Radiative field of a 2d open waveguide with defect computed by J. Chabassier (INRIA Bordeaux Sud Ouest) using PML.

2 Asymptotic expansion

We introduce a new coordinate system with polar coordinates $(r, \varphi) \in \mathbb{R}_0^+ \times]-\pi, 0[$ in Ω_- and $(r, \varphi) \in \mathbb{R}_0^+ \times]0, \pi[$ in Ω_+, that satisfy $x_1 = r\cos\varphi$ and $x_2 \mp \frac{h}{2} = r\sin\varphi$, and Cartesian coordinates $(x_1, x_2) \in \mathbb{R} \times]-\frac{h}{2}, \frac{h}{2}[$ in Ω_1.

For simplicity of notation let us focus on the right half plane $\{\mathbf{x} \in \mathbb{R}^2 : x_1 > 0\}$. The compact support of f implies that for large $|\mathbf{x}|$ the solution u_1 in the waveguide Ω_1 also satisfies a homogeneous Helmholtz equation. This motivates the ansatz for the radiative field

$$u_\pm(r, \theta) = \sum\nolimits_{j \in \mathbb{N}_0} \Theta_\pm^{(j)}(\theta) r^{-1/2-j} \mathrm{e}^{\mathrm{i}k_0 r}, \tag{3a}$$
$$u_1(x_1, x_2) = \sum\nolimits_{j \in \mathbb{N}_0} \Theta_1^{(j)}(x_2) x_1^{-1/2-j} \mathrm{e}^{\mathrm{i}k_0 x_1}, \tag{3b}$$

where $u_\pm^{(m)}(r, \theta) = \sum_{j=0}^m \Theta_\pm^{(j)}(\theta) r^{-1/2-j} \mathrm{e}^{\mathrm{i}k_0 r}$ and $u_1^{(m)}(x_1, x_2) = \sum_{j=0}^m \Theta_1^{(j)}(x_2) x_1^{-1/2-j} \mathrm{e}^{\mathrm{i}k_0 x_1}$ sat-

isfy

$$-\Delta u_\pm^{(m)} - k_0^2 u_\pm^{(m)} = \mathcal{O}(r^{-3/2-m}) \quad \text{in } \Omega_\pm, \quad (4a)$$
$$-\Delta u_1^{(m)} - k_1^2 u_1^{(m)} = \mathcal{O}(x_1^{-3/2-m}) \quad \text{in } \Omega_1, \quad (4b)$$

with continuity conditions

$$u_\pm^{(m)}(\pm\tfrac{h}{2}) - u_1^{(m)}(\pm\tfrac{h}{2}) = 0, \quad (4c)$$
$$a_0 \tfrac{\partial}{\partial x_2} u_\pm^{(m)}(\pm\tfrac{h}{2}) - a_1 \tfrac{\partial}{\partial x_2} u_1^{(m)}(\pm\tfrac{h}{2}) = 0, \quad (4d)$$

for all $m \in \mathbb{N}_0 := \mathbb{N} \cup \{0\}$, $\mathbb{N} := \{1, 2, \dots\}$.

We can easily verify that the zeroth order solutions $u_\pm^{(0)}$ in $\Omega_\pm$ satisfy (4a). However, using the ansatz (3b) for the zeroth order solution $u_1^{(0)}$ in Ω_1 shows that (4b) can only be satisfied if

$$\Theta_1^{(0)\prime\prime} + \big(k_1^2 - k_0^2\big)\Theta_1^{(0)} = 0.$$

Due to our special coordinate system, the continuity conditions (4d) of the Neumann traces yield $\Theta_1^{(0)\prime}(\pm\frac{h}{2}) = 0$. Assuming $k_1^2 > k_0^2$, which is a necessary condition for guided modes to exist [3], and $\sqrt{k_1^2 - k_0^2}\frac{h}{4\pi} \notin \mathbb{N}$, we find that $\Theta_1^{(0)} \equiv 0$, i.e., there do not exist any radiative modes behaving like $x_1^{-1/2}$ in the waveguide Ω_1, which corresponds to the 2d analogon of the results in [3].

Now let us consider the expansions of arbitrary order $m \in \mathbb{N}$. Neglecting terms of order $\mathcal{O}(r^{-3/2-m})$ or smaller, we conclude that (4a) can only be satisfied if

$$\Theta_\pm^{(j+1)} = \frac{-\mathrm{i}}{2(j+1)k_0}\Big(\Theta_\pm^{(j)\prime\prime} + (\tfrac{1}{2}+j)^2\Theta_\pm^{(j)}\Big)$$

for all $j = 0, \dots, m-2$. And in Ω_1 we require

$$\begin{aligned}
\Theta_1^{(1)\prime\prime} + \big(k_1^2 - k_0^2\big)\Theta_1^{(1)} &= 0,\\
\Theta_1^{(2)\prime\prime} + \big(k_1^2 - k_0^2\big)\Theta_1^{(2)} &= 3\mathrm{i}k_0\Theta_1^{(1)},\\
\Theta_1^{(j)\prime\prime} + \big(k_1^2 - k_0^2\big)\Theta_1^{(j)} &= (2j-1)\mathrm{i}k_0\Theta_1^{(j-1)}\\
&\quad - (j-\tfrac{3}{2})(j-\tfrac{1}{2})\Theta_1^{(j-2)}
\end{aligned}$$

for all $j = 3, \dots, m$, such that (4b) is satisfied.

3 Absorbing boundary conditions

With these expansions and the equations for $\Theta_\pm^{(j)}$ and $\Theta_1^{(j)}$, $j \in \mathbb{N}_0$, we can derive local absorbing boundary conditions at artificial boundaries $\Sigma_\pm(R) = \{\mathbf{x} \in \Omega_\pm : |\mathbf{x}| = R\}$ and $\Sigma_1(R) = \{\mathbf{x} \in \Omega_1 : x_1 = R\}$.

Due to the standard expansion (3a) in the top and bottom half-planes $\Omega_\pm$, we find that the boundary conditions on $\Sigma_\pm(R)$ are equivalent to Feng's absorbing boundary conditions for homogeneous media [2], i.e., we have $(\frac{\partial}{\partial r} - \mathcal{A}_0^{(m)})u_\pm = \mathcal{O}(R^{-3/2-m})$ on $\Sigma_\pm(R)$ for all $m \in \mathbb{N}_0$ with, e.g.,

$$\begin{aligned}
\mathcal{A}_0^{(1)} &= \mathrm{i}k_0 - \tfrac{1}{2R},\\
\mathcal{A}_0^{(2)} &= \mathcal{A}_0^{(1)} + \tfrac{\mathrm{i}}{2k_0R^2}\Big(\tfrac{1}{4} + \tfrac{\partial^2}{\partial\theta^2}\Big),\\
\mathcal{A}_0^{(3)} &= \mathcal{A}_0^{(2)} + \tfrac{1}{2k_0^2R^3}\Big(\tfrac{1}{4} + \tfrac{\partial^2}{\partial\theta^2}\Big).
\end{aligned}$$

In the waveguide, however, the expansion (3b) is non-standard and we obtain $(\frac{\partial}{\partial x_1} - \mathcal{A}_1^{(m)})u_1 = \mathcal{O}(R^{-3/2-m})$ on $\Sigma_1(R)$ for all $m \in \mathbb{N}_0$ with, e.g.,

$$\begin{aligned}
\mathcal{A}_1^{(1)} &= \mathrm{i}k_0,\\
\mathcal{A}_1^{(2)} &= \mathrm{i}k_0 - \tfrac{3}{2R},\\
\mathcal{A}_1^{(3)} &= \mathrm{i}k_0 + \tfrac{\mathrm{i}}{2k_0}\Big(\big(k_1^2 - k_0^2\big) + \tfrac{15}{4R^2} + \tfrac{\partial^2}{\partial x_2^2}\Big).
\end{aligned}$$

These conditions for the radiative field can be used to derive boundary conditions for the scattered field by explicitly taking the guided modes into account.

References

[1] A.-S. Bonnet-BenDhia, G. Dakhia, C. Hazard and L. Chorfi, Diffraction by a defect in an open waveguide: a mathematical analysis based on a modal radiation condition, *SIAM J. Appl. Math.*, **70** (2009), pp. 677–693.

[2] K. Feng, Finite element method and natural boundary reduction, *Proceedings of the International Congress of Mathematicians, Warsaw, Poland, 16-24 August 1983,* pp. 1439–1453.

[3] C. Jerez-Hanckes and J.-C. Nédélec, Asymptotics for Helmholtz and Maxwell solutions in 3-d open waveguides, *Commun. Comput. Phys.* **11** (2012), pp. 629–646.

Local High-Order Absorbing Boundary Condition for Multiple Scattering of Time-Harmonic Waves

Sebastian Acosta[1], **Vianey Villamizar**[2,*]

[1]Department of Pediatric Cardiology, Baylor College of Medicine, Houston, TX

[2]Department of Mathematics, Brigham Young University, Provo, UT 84602

[*]Email: vianey@mathematics.byu.edu

Abstract

In this work we construct a local absorbing boundary condition (ABCs) for multiple scattering of time-harmonic waves. Inspired in a recent work of Grote and Sim [1] for the time-dependent multiple scattering, the scattered field is decomposed as the superposition of purely outgoing wave fields in the exterior of appropriate artificial boundaries. Then, we employ a truncated Atkinson-Wilcox expansion as an evaluation formula for the scattered field in the exterior region to the artificial boundaries. Finally by matching the exterior scattered field with the interior one at the artificial boundaries, we obtain our local absorbing boundary condition (ABC) for multiple scattering. Several computational advantages by applying this technique have already been discussed in previous works cited below. An additional advantage of our approach is its simplicity. For instance, there is no need of deriving an exterior evaluation formula. Also, no new auxiliary functions other than the terms in the Atkinson-Wilcox expansion are required.

Keywords: Multiple scattering, Local absorbing boundary condition, Helmholtz equation

1 Introduction

There are major challenges when numerically solving multiple scattering problems defined in unbounded regions using volume discretization methods. One of this consists of the use of appropriate ABCs on artificial boundaries that reduce the original unbounded problem to an equivalent boundary value problem in a bounded computational domain. Normally, the scatterer is formed by several obstacles that may be distant from each other. A common practice consists of choosing an artificial boundary large enough to enclose all the obstacles. This practice leads to a large computational domain that may require huge amount of storage and computer time. In this paper, we derive a new high-order local absorbing boundary condition for multiple scattering of time-harmonic waves. As our first step in the derivation process, we adopt a technique, first introduced by Grote-Kirsch [3]. This consists of defining artificial boundaries that only enclose the immediate vicinity of each obstacle. Then, ABCs are imposed at each artificial boundary which leads to a dramatic reduction of the discretization region. As a consequence, the computational cost is greatly reduced. In [2] Acosta and Villamizar used this approach for scattering from multiple obstacles of arbitrary shape. As in [3], they imposed a nonlocal Dirichlet-to-Neumann (DtN) ABC for each artificial boundary enclosing each obstacle. A disadvantage of this approach is that the matrix that results from the discretization is partially dense at boundary points due to the nonlocal nature of the DtN condition.

The main objective of this work is to derive a high-order computationally efficient local ABC for multiple-scattering problems of time-harmonic waves. Our procedure is similar to recent work by Grote and Sim [1] for time-dependent multiple scattering which is based on an exact local ABC first introduced by Hagstrom and Hariharan [4]. We maintain the definition of the computational domain used in [2]. Then, the novel local ABC is obtained by decomposing the scattered field in the exterior of the artificial boundaries as the superposition of purely-outgoing fields which are approximated by truncated Atkinson-Wilcox expansions [5]. This is followed by matching the scattered fields inside the artificial boundary with the one outside, at the interface. As a result, a new local ABC, which effectively accounts for the outgoing behavior of the scattered field, as well as its interaction with the obstacles, is obtained. Some of the advantages of this approach are that the matrix that results applying volume discretization methods to the scattering problem is sparse, contrary to the partially dense matrices obtained using the DtN approach. Also, improving the order of approximation of the local ABC is simple. It only requires to incorporate as many terms of the Atkinson-Wilcox expansion as needed to reach the desired order.

2 Statement of the problem

We consider J disjoint obstacles each occupying a simply connected and bounded domain whose bound-

ary is denoted by Γ_j for $j = 1, 2, ..., J$. The open unbounded region in the exterior of Γ_j is denoted by Ω_j. Now, we assume that the obstacles are sufficiently separated from each other as to enclose each one with disjoint artificial boundaries $\mathbb{S}_j$ for $j = 1, ..., J$. These artificial boundaries are assumed to be spheres. We define Ω_j^- as the open region bounded internally by the obstacle boundary Γ_j and externally by the artificial boundary $\mathbb{S}_j$. It will become clear in the following sections, that Ω_j^- is the computational region to be discretized. The open unbounded region in the exterior of $\mathbb{S}_j$ is denoted by Ω_j^+ so that $\mathbb{S}_j$ is precisely the interface between Ω_j^- and Ω_j^+. Also consider the following definitions,

$$\Omega = \bigcap_{j=1}^{J} \Omega_j, \quad \Omega^- = \bigcup_{j=1}^{J} \Omega_j^-,$$
$$\Omega^+ = \bigcap_{j=1}^{J} \Omega_j^+ \quad \text{and} \quad \Gamma = \bigcup_{j=1}^{J} \Gamma_j.$$

An incident wave u_{inc} impinges upon the J obstacles. This incident field is assumed to satisfy the governing Helmholtz equation in Ω with wavenumber $k > 0$. The total field u_{t} is decomposed as $u_{\text{t}} = u_{\text{inc}} + u_{\text{sc}}$ in Ω^+ where u_{sc} represents the wave field scattered by the obstacles. For sake of simplicity, we assume a Dirichlet condition $u_{\text{t}} = 0$ on Γ but a Neumann condition or Robin-type condition can also be considered without any obstruction. For clarity in the presentation, we replace the usual exterior boundary value problem of the scattered field u_{sc} by an equivalent interface problem where the artificial surfaces $\mathbb{S}_j$ become the interface boundaries. By defining $u_{\text{sc}}^- = u_{\text{sc}}|_{\Omega^-}$ and $u_{\text{sc}}^+ = u_{\text{sc}}|_{\Omega^+}$, we arrive to the following interface problem,

$$\Delta u_{\text{sc}}^- + k^2 u_{\text{sc}}^- = 0 \qquad \text{in } \Omega^-, \tag{1}$$
$$\Delta u_{\text{sc}}^+ + k^2 u_{\text{sc}}^+ = 0 \qquad \text{in } \Omega^+, \tag{2}$$
$$u_{\text{sc}}^- = -u_{\text{inc}} \qquad \text{on } \Gamma, \tag{3}$$
$$\lim_{r\to\infty} r\left(\partial_r u_{\text{sc}}^+ - \mathrm{i}k u_{\text{sc}}^+\right) = 0,\ r = |x|,\ x \in \mathbb{R}^3 \tag{4}$$

with the interface conditions, $u_{\text{sc}}^- = u_{\text{sc}}^+$, and $\partial_\nu u_{\text{sc}}^- = \partial_\nu u_{\text{sc}}^+$ on $\bigcup_{j=1}^{J} \mathbb{S}_j$, where ∂_ν denotes the derivative in the outer normal direction on each artificial boundary $\mathbb{S}_j$. The usual unbounded scattering problem for u_{sc} and the above interface problem are equivalent as shown in [2, Thm 1] .

3 The local ABC for multiple scattering

Our derivation of the multiple absorbing condition rests upon the following fundamental decomposition theorem of u_{sc} for multiple scattering problems. Proofs and application of this theorem are found in various recent works.

Theorem 1. *Let u_{sc}^+ solve the above interface BVP. Then, u_{sc}^+ can be uniquely decomposed in Ω^+ into purely-outgoing wave fields u_j for $j = 1, 2, ..., J$ such that*

$$u_{\text{sc}}^+ = \sum_{j=1}^{J} u_j, \qquad \text{in } \overline{\Omega^+}, \tag{5}$$

where u_j radiates purely from $\mathbb{S}_j$, that is,

$$\Delta u_j + k^2 u_j = 0 \quad \text{in } \Omega_j^+, \tag{6}$$
$$\lim_{r\to\infty} r\ (\partial_r u_j - \mathrm{i}k u_j) = 0. \tag{7}$$

First of all, notice from (7) that by *purely-outgoing* field u_j, we mean a radiating solution to the Helmholtz equation on all of Ω_j^+, including the interior of all the other obstacles. This suggests a representation of u_{sc} in the exterior region Ω^+ by means of a well-known infinite series described in the next theorem.

Theorem 2 (Atkinson-Wilcox [5])**.** *Let u_j for $j = 1, 2, ..., J$ be the purely-outgoing wave fields defined in Theorem 1. Then,*

$$u_j(x) = \frac{e^{\mathrm{i}k|x_j|}}{|x_j|} \sum_{n=0}^{\infty} \frac{F_{j,n}(\hat{x}_j)}{|x_j|^n}, \qquad x_j = x - c_j \tag{8}$$

where c_j is the center of the sphere $\mathbb{S}_j$, and $\hat{x}_j = x_j/|x_j|$. If we assume that $\mathbb{S}_j$ and Γ_j are disjoint, (implying that they are separated by a positive distance) then the series converges for all x in the region $\overline{\Omega_j^+}$. The series may be differentiated (any number of times) term-by-term with respect to x in this region, and the resulting series all converge absolutely and uniformly.

Moreover, the coefficients $F_{j,n}$ satisfy the following recursive relation,

$$2\mathrm{i}knF_{j,n} = n(n-1)F_{j,n-1} + \Delta_{\mathbb{S}} F_{j,n-1}, \qquad n \geq 1, \tag{9}$$

where $\Delta_{\mathbb{S}}$ is the Laplace-Beltrami operator on the unit-sphere $\mathbb{S}$.

The numerical computation requires to use only a finite number of N terms of the Atkinson-Wilcox series. By replacing this truncated infinite series in our interface problem (1)-(4) and its corresponding interface conditions, we are lead to the following BVP in the bounded region Ω^-,

$$\Delta u_{\text{sc}}^N + k^2 u_{\text{sc}}^N = 0 \qquad \text{in } \Omega^-, \tag{10}$$
$$u_{\text{sc}}^N = -u_{\text{inc}} \qquad \text{on } \Gamma, \tag{11}$$

along with the local ABC,

$$u_{\rm sc}^N = \sum_{j=1}^{J}\sum_{n=0}^{N} P_{ij}^n[F_{jn}], \quad \text{and} \tag{12}$$

$$\partial_\nu u_{\rm sc}^N = \sum_{j=1}^{J}\sum_{n=0}^{N} T_{ij}^n[F_{jn}], \quad \text{on } \mathbb{S}_i, \tag{13}$$

for $i = 1, 2, ..., J$, which also includes the recursive formulas

$$2{\rm i}knF_{j,n} = n(n-1)F_{j,n-1} + \Delta_{\mathbb{S}}F_{j,n-1}, \tag{14}$$

The *propagation* P_{ij}^n and *transfer* T_{ij}^n operators are defined as follows

$$P_{ij}^n[F_{jn}](x) = \frac{e^{{\rm i}k|x_j|}}{|x_j|}\frac{F_{jn}(\hat{x}_j)}{|x_j|^n},$$

$$T_{ij}^n[F_{jn}](x) = {\rm grad}_x\left(\frac{e^{{\rm i}k|x_j|}}{|x_j|}\frac{F_{jn}(\hat{x}_j)}{|x_j|^n}\right)\cdot\nu_i(x),$$

for each $n = 0, 1, ..., N$ where c_j is the center of the sphere $\mathbb{S}_j$, $x_j = x - c_j$ for $x \in \mathbb{S}_i$, $\hat{x}_j = x_j/|x_j|$, and $\nu_i(x)$ is the outer normal vector on the artificial boundary $\mathbb{S}_i$. Due to the spherical separability of each term in the Atkinson-Wilcox expansion, it is convenient in practice to express the gradient in the above formula in spherical coordinates centered at c_j. Hence, if we let (r, θ, ϕ) be the spherical coordinates centered at c_j, we obtain

$$\begin{aligned} T_{ij}^n[F_{jn}](r,\theta,\phi) &= \frac{e^{{\rm i}kr}}{r}\frac{1}{r^n}\left[\left({\rm i}k - \frac{n+1}{r}\right)F_{jn}(\theta,\phi)\,(\nu_i\cdot\hat{r})\right. \\ &+ \left.\frac{1}{r}\frac{\partial F_{jn}(\theta,\phi)}{\partial\theta}(\nu_i\cdot\hat{\theta}) + \frac{1}{r\sin\theta}\frac{\partial F_{jn}(\theta,\phi)}{\partial\phi}(\nu_i\cdot\hat{\phi})\right], \qquad (r,\theta,\phi)\in\mathbb{S}_i. \end{aligned}$$

Notice that when $i = j$, the above formula reduces to

$$T_{jj}^n[F_{jn}](r,\theta,\phi) = \frac{e^{{\rm i}kr}}{r}\frac{1}{r^n}\left({\rm i}k - \frac{n+1}{r}\right)F_{jn}(\theta,\phi), \qquad (r,\theta,\phi)\in\mathbb{S}_j.$$

4 Final Remarks

By truncating the Atkinson-Wilcox expansion at N terms, an error is introduced. This truncation error can be easily controlled by including more terms in the series (8). This is a more convenient procedure than using the computationally expensive one of enlarging the radius of the artificial boundary. The new unknowns introduced also satisfy the recursive formula (9) which leads to a well-determined system of equations.

In the presentation, we will discuss our numerical results for various shapes and configuration of multiple obstacles.

References

[1] M. Grote, I. Sim, Local nonreflecting boundary condition for time-dependent multiple scattering, *J. Comput. Phys.* **230** (2011), pp. 3135–3154.

[2] S. Acosta, V. Villamizar, Coupling of Dirichlet-to-Neumann boundary condition and finite difference methods in curvilinear coordinates for multiple scattering, *J. Comput. Phys.* **229** (2010), pp. 5498–5517.

[3] M. Grote, C. Kirsch, Dirichlet-to-Neumann boundary conditions for multiple scattering problems,, *J. Comput. Phys.* **201** (2004), pp. 630–650.

[4] T. Hagstrom, S. Hariharan, A formulation of asymptotic and exact boundary conditions using local operators, *Appl. Num. Math.* **27** (1998), pp. 403–416.

[5] C.Wilcox, A generalization of theorems of Rellich and Atkinson, *Proc. Am. Math. Soc.* **7** (1956), pp. 271–276.

PML for Time-Dependent Wave Equation with Highly Oscillating Coefficients

Imbo Sim[1,*], **Ohsung Kwon**[1]
[1]National Institute for Mathematical Sciences, Republic of Korea
[*]Email: imbosim@nims.re.kr

Abstract

We consider a perfectly matched layers (PML) method for the wave equation with highly oscillating coefficients in unbounded domain. The PML approach has proved a flexible and accurate method for the simulation of waves in unbounded media. We propose a finite element heterogeneous multiscale method (HMM), which can be efficiently combined with PML formulation. HMM is based on a finite element discretization of an effective wave equation at the macro scale, whose a priori unknown effective coefficients are computed on sampling domains at the micro scale within each macro finite element. The computational work is independent of the highly heterogeneous nature of the medium at the smallest scale. Various numerical examples illustrate the accuracy and robustness of our method.

Keywords:perfectly matched layers, heterogeneous multiscale method, finite element

1 Model Problem

We consider a time dependent wave field p^ε propagating through unbounded space and assume that all sources and initial disturbances are confined to the rectangular domain $\Omega = [-\ell_1, \ell_1] \times [-\ell_2, \ell_2]$, $\ell_1, \ell_2 > 0$. The waves are purely outgoing in the unbounded exterior $\mathbb{R}^2 \backslash \Omega$. Inside Ω, the wave field $p^\varepsilon(x,t)$ satisfies

$$\begin{aligned} p^\varepsilon_{tt} - \nabla \cdot (\, a^\varepsilon(x)\, \nabla p^\varepsilon) &= f \qquad \text{in}\, \Omega \times]0,T[, \\ p^\varepsilon(x,0) &= p_0(x) \quad \text{in}\, \Omega, \\ p^\varepsilon_t(x,0) &= p_1(x) \quad \text{in}\, \Omega, \end{aligned}$$

where $a^\varepsilon \in L^\infty(\Omega)^{d\times d}$ is symmetric and uniformly elliptic and bounded, i.e., $\exists \lambda, \Lambda > 0$ such that

$$\lambda |\xi|^2 \le a^\varepsilon(x)\xi \cdot \xi \le \Lambda |\xi|^2,\ \forall \xi \in \mathbb{R}^d \text{ and } \forall \varepsilon > 0.$$

Here ε represents a small scale, which characterizes the multiscale nature of $a^\varepsilon(x)$. We assume that the source term f lies in $L^2(]0,T[; L^2(\Omega))$, while $p_0 \in H^1_0(\Omega)$ and $p_1 \in L^2(\Omega)$ are prescribed initial conditions.

2 Finite element HMM with PML

Our PML formulation for wave equation with highly oscillating coefficients is constructed as follows:

$$\begin{aligned} p_{tt} + (\zeta_1 + \zeta_2)\, p_t + \zeta_1\, \zeta_2\, p &= \nabla \cdot (\, a^\varepsilon\, \nabla p) + \nabla \cdot \boldsymbol{\phi} \\ &\quad + f, \\ \boldsymbol{\phi}_t + \Gamma_1\, \boldsymbol{\phi} &= a^\varepsilon\, \Gamma_2\, \nabla p, \end{aligned} \tag{1}$$

where the damping matrices, for $\zeta_1,\, \zeta_2 \ge 0$,

$$\Gamma_1 = \mathrm{diag}\,(\zeta_1,\, \zeta_2)\,,\ \Gamma_2 = \mathrm{diag}\,(\zeta_2 - \zeta_1,\, \zeta_1 - \zeta_2)\,.$$

We turn to the finite element heterogeneous multiscale method [1]. Let $\mathcal{T}_H$ be a (macro) partition of Ω in simplicial or quadrilateral elements K of diameter H_K with $H = \max_{K\in\mathcal{T}_H} H_K$. In each macro partition, the mesh size H could be much bigger than the scaling factor ε. For this partition we define a macro FE space $S^\ell_0(\Omega, \mathcal{T}_H) = \{v^H \in H^1_0(\Omega); v^H|_K \in \mathcal{R}^\ell(K),\, \forall K \in \mathcal{T}_H\}$, where $R^\ell(K)$ is the space $\mathcal{P}^\ell(K)$ of polynomials on K of total degree at most ℓ, if K is a simplex, or the space $\mathcal{Q}^\ell(K)$ of polynomials on K of degree at most ℓ in each variable, if K a rectangle. Next we consider a (micro) partition $\mathcal{T}_h$ of each sampling domain K_{δ_j} in simplicial or quadrilateral elements Q of diameter h_Q and let $h = \max_{Q\in\mathcal{T}_h} h_Q$. For this partition we define a micro FE space $S^q(K_\delta, \mathcal{T}_h) = \{z_h \in W(K_{\delta_j}); z_h|Q \in \mathcal{R}^r(Q),\, Q \in \mathcal{T}_h\}$, where $W(K_{\delta_j})$ is a Sobolev space whose choice sets the boundary conditions for the micro problems and thus determines the type of coupling between micro and macro problems. Furthermore, we introduce the following variables inside each macro element $K \in \mathcal{T}_H$, that each number are given by number of quadrature points J: quadrature points $x_{j,K} \in K$, quadrature weights $w_{j,K}$, and sampling domains $K_{\delta_j} = x_{j,K} + \delta\, I$, where $I = (-0.5,\, 0.5)^d$ and $\delta \ge \varepsilon$.
The heterogeneous multiscale Galerkin form for solving the equation (1) is constructed as follows:

Find $p^H \in C^0([0,T]; S_0^\ell(\Omega, \mathcal{T}_H))$ such that, for $v^H \in S_0^\ell(\Omega, \mathcal{T}_H)$,

$$\begin{aligned}&\left(p_{tt}^H, v^H\right) + \left((\zeta_1+\zeta_2)\, p_t^H, v^H\right) + (\zeta_1\,\zeta_2\, p^H, v^H)\\ &= - B_H(p^H, v^H) + (\nabla\cdot\boldsymbol{\phi}^H, v^H).\end{aligned}$$

Here we define the discrete bilinear form as

$$\begin{aligned}&B_H\left(p^H,\, v^H\right)\\ &= \sum_{K\in\mathcal{T}_H}\sum_{j=1}^{J} \frac{w_{j,K}}{|K_{\delta_j}|}\int_{K_{\delta_j}} a^\varepsilon(x)\,\nabla p_{K_j}^h\cdot\nabla v_{K_j}^h\,\mathrm{dx},\end{aligned} \tag{2}$$

where $p_{K_j}^h$, $v_{K_j}^h$ are micro functions defined on sampling domains K_{δ_j} as in the reference [1] and $|K_{\delta_j}|$ is the measure of the sampling domains K_{δ_j}.

We now need to compute the microfunctions $p_{K_j}^h$ on each sampling domain K_{δ_j} for completing the discretization (2) on every macro element $K \in \mathcal{T}_h$. The discrete micro problem is to find $p_{K_j}^h$ such that $p_{K_j}^h - p_{\mathrm{lin},K_j}^H \in S_h^q(K_{\delta_j}, \mathcal{T}_h)$ and

$$\int_{K_{\delta_j}} a^\varepsilon(x)\,\nabla p_{K_j}^h\cdot\nabla z^h\,\mathrm{dx} = 0,\ z^h \in S_h^q(K_{\delta_j}, \mathcal{T}_h),$$

where $S_h^q(K_{\delta_j}, \mathcal{T}_h)$ is the micro FE space defined above and

$$p_{\mathrm{lin},K_j}^H(\boldsymbol{x}) = p^H(x_{j,K}) + (x - x_{j,K})\cdot\nabla p^H(x_{j,K})$$

is a piecewise linearization of the macro function $p^H \in S_0^\ell(\Omega, \mathcal{T}_H)$ at the quadrature point $x_{j,K}$.

References

[1] A. Abdulle, On A Priori Error Analysis of Fully Discrete Heterogeneous Multiscale FEM, *SIAM Multiscale Model. Simul.* **4** (2005), pp. 447–459.

[2] J. P. Bérenger, A Perfectly Matched Layer for the Absorption of Electromagnetic Waves, *J. Comput. Phys.* **114** (1994), pp.185–200.

[3] B. Kaltenbacher, M. Kaltenbacher, and I. Sim, A Modified and Stable Version of a Perfectly Matched Layer Technique for the 3-d Second Order Wave Equation in Time Domain with an Application to Aeroacoustics, *J. Comput. Phys.* **235** (2013), pp. 407–422.

High Order Absorbing Boundary Conditions for the 2D Helmholtz Equation

H. Barucq[1], **M. Bergot**[2,*], **J. Chabassier**[1]

[1]Magique 3d team, Inria Sud Ouest, Talence, France

[2]Institut Camille Jordan, Université Lyon 1, Villeurbanne, France

*Email: bergot@math.univ-lyon1.fr

Abstract

We present high order absorbing boundary conditions (ABC) for the 2D Helmholtz equation that can adapt to any regular shaped surface. The new ABCs are derived by using the technique of micro-diagonalisation to approximate the Dirichlet-to-Neumann map. Numerical results on different shapes illustrate the behavior of the new ABCs along with high-order finite elements.

Keywords: absorbing boundary conditions, Helmholtz equation, high-order approximation.

1 Introduction

Local boundary conditions called "absorbing boundary conditions" (ABC) are often used to simulate outgoing waves in a artificially truncated numerical domain. The aim of the present work is to develop high order ABCs for the Helmholtz equation that can adapt to regular shaped surfaces.

To obtain efficient conditions, Taylor's micro-diagonalisation method (see [1]) can be used for hyperbolic systems (see [2]). The use of this technique is followed by an asymptotic truncation to make the ABC local. During the process, while increasing the degree of the pseudo differential operator decomposition along with the order of asymptotic truncation, we retrieve classical ABCs that have been found with other techniques by other authors (see [3]).

2 General Approach

The Helmholtz equation in local coordinates system near the artificial boundary Σ reads:

$$\partial_r U = LU \tag{1}$$

where $U = (u, v)^t$ is the vectorial unknown, and the symbol of the pseudo-differential operator L is given by

$$\mathcal{L} = \sigma(L) = \begin{pmatrix} 0 & -i\omega \\ -\dfrac{i\omega}{c^2} - \dfrac{\partial_s h}{h^3}\dfrac{\xi}{\omega} - \dfrac{\xi^2}{i\omega h^2} & -\kappa_r \end{pmatrix} \tag{2}$$

where ξ is the dual variables associated to the tangent coordinate s, $\kappa(s)$ is the curvature of Σ, $h = 1 + r\,\kappa(s)$ and $\kappa_r = \kappa(s)/h$, r being the radial coordinate.

For a given $m \in \mathbb{N}$, our aim is to find a diagonal pseudo-differential operator Λ such that

$$\Lambda = \Lambda_1 + \Lambda_0 + \Lambda_{-1} + \ldots + \Lambda_{-m}$$

where $\sigma(\Lambda_j) = \mathcal{D}_j$ is homogeneous of degree exactly j, and a pseudo-differential operator P such that

$$P = P_0 + P_{-1} + P_{-2} + \ldots + P_{-m-1}$$

where $\sigma(P_j) = \mathcal{P}_j$ is homogeneous of degree j, so that

$$\begin{cases} V = PU \\ (1) \Longleftrightarrow \partial_r V = \Lambda V \end{cases}$$

When all the operators have an explicit expression, we end up with a diagonal system. As the first component of V corresponds to the ingoing wave, and the second component stands for the outgoing wave, we state that the first component of V must vanish on the boundary. To obtain a local ABC, we take a Taylor expansion up to an order n with two possible asymptotics: small "angle of incidence" ($\delta = \xi/\omega \to 0$) or "high frequency" ($\omega \to \infty$).

3 Obtained ABCs

The non-local ABC for $m = 1$ writes

$$\left[1 + \frac{\gamma}{\lambda_1}\right]\left(\frac{\lambda_1}{i\omega}\hat{u} + \frac{\partial_r \hat{u}}{i\omega}\right) + \frac{\kappa\omega}{4i\lambda_1^2 c^2}\left(\frac{\partial_r \hat{u}}{\lambda_1} - \hat{u}\right) = 0 \tag{3}$$

where $\lambda_1 = i\sqrt{k^2 - \xi^2/h^2}$, $k = \omega/c$ and γ is a parameter that can be arbitrarily fixed.

– Taking the Taylor expansion of order $n = 1$ in δ, we obtain the following local ABC

$$(\partial_r \hat{u} + ik\,\hat{u}) + \left(\gamma + \frac{\kappa}{4}\right)\,\hat{u} + \left(\gamma - \frac{\kappa}{4}\right)\,\frac{\partial_r \hat{u}}{ik} = 0 \tag{4}$$

We notice that for the specific value $\gamma = \kappa/4$, we retrieve the classical C-ABC.

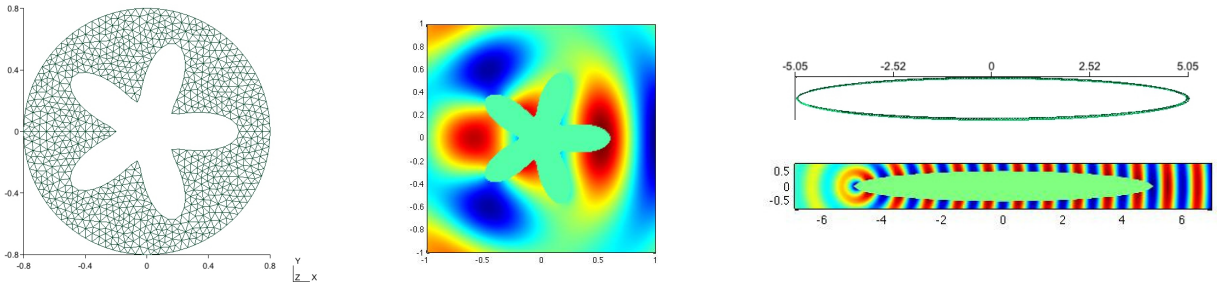

Figure 1: Mesh and reference solution for the star-shaped case (left) and the ellipse case (right)

– Taking the Taylor expansion of order $n = 1$ in $1/\omega$, we obtain the following local ABC

$$\left[1 + \frac{\gamma - \frac{\kappa}{4}}{ik}\right] \partial_r \hat{u} + \left[ik + \gamma + \frac{\kappa}{4}\right] \hat{u} + \frac{\xi^2}{2\,ik} \hat{u} = 0 \quad (5)$$

We notice that only the specific value $\gamma(s) = \kappa(s)/4$ leads to a symmetric ABC that can be used in a variational context.

More generally, all the obtained ABCs for $m = 1, 2$ and $n = 0, 1, 2$ can be written under the following form:

$$\begin{aligned} &\left[a_0(ik) + a_1(ik)\, i\xi + a_2(ik)\, \xi^2\right] \partial_r u \\ &+ \left[b_0(ik) + b_1(ik)\, i\xi + b_2(ik)\, \xi^2\right] u = 0 \end{aligned} \quad (6)$$

where the coefficients a_j and b_j contains parameters that have to be fixed. When need is and when it is possible, specific parameters are used so that the ABC can be used in a variational context. A particular choice of the other parameters may optimize the ABC in terms of L^2 error, but a thorough study of their impact has to be done.

4 Numerical Illustrations

We consider an obstacle in a convex domain with different ABCs placed on the boundary. In Fig. 1, two geometries tested are displayed: a star-shaped obstacle in a circular domain and an elliptic obstacle placed in an elliptic domain. Frequency is taken equal to 1Hz. Solutions are computed with with Galerkin finite elements $\mathbb{Q}_8$. The reference solution displayed on Fig. 1 is computed with Galerkin finite elements $\mathbb{Q}_8$ and with an artificial boundary carrying a transparent condition far from the obstacle. Only variational ABCs are tested and the remaining parameters are all set equal to $\frac{\kappa(s)}{4}$. Tab. 1 summarizes the relative L^2 error of the Dirichlet trace between the reference solution and each solution obtained with different ABCs placed on the boundary.

Table 1: Relative L^2-error of the Dirichlet trace for the ellipse and the star-shaped obstacle

(m,n) asymptotic	Ellipse	Star
$(1,1)$ δ	12,70%	8,55%
$(1,1)$ ω	5,56%	3,03%
$(2,1)$ δ	12,69%	8,49 %
$(2,1)$ ω	7,15%	3,31 %
$(2,2)$ ω	7,31%	1,62 %

References

[1] M.E. Taylor, Reflection of Singularities of Solutions to Systems of Differential Equations, *Comm. Pure and Appl. Math.*, vol 28(4), pp 457–478, 1975.

[2] B. Engquist and A. Majda, Absorbing Boundary Conditions for the Numerical Simulation of Waves, *Math. Comp.* ,vol 31, pp 629–651, 1977.

[3] H. Barucq, M. Bergot, J. Chabassier and E. Estecahandy, Derivation of high order absorbing boundary conditions for the Helmholtz equation in 2D, *Research Report RR-8632 Inria Bordeaux*, hal-01085180, 2014.

Index of Authors